UNIVERSITY OF ILORIN
FACULTY OF ENGINEERING AND TECHNOLOGY

2nd Faculty of Engineering and Technology
INTERNATIONAL CONFERENCE
(FETICON 2024)

THEME:
LEVERAGING ARTIFICIAL INTELLIGENCE TO ACHIEVE UNITED NATIONS SUSTAINABLE DEVELOPMENT GOALS

CONFERENCE PROCEEDINGS

IHS Towers of strength

matrix

2nd-6th June, 2024 University of Ilorin Main Auditorium, University of Ilorin, Ilorin, Nigeria

SPONSORS

PARTICIPANT COUNTRIES

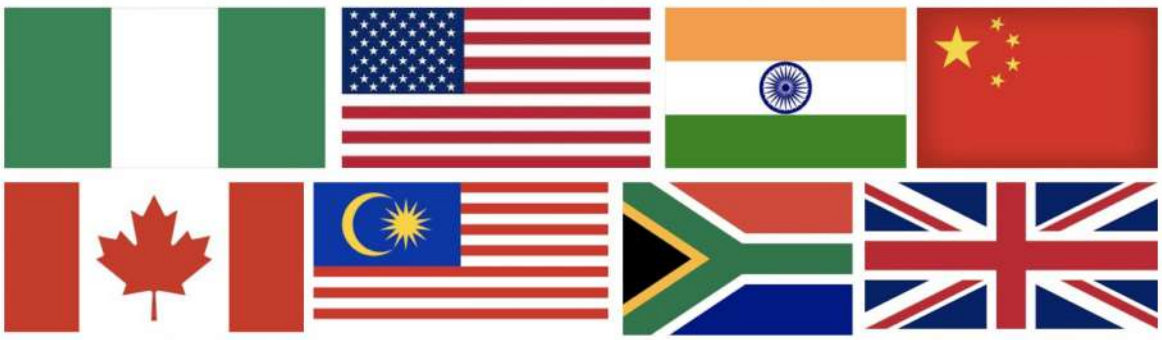

ORGANISING COMMITTEE

Prof. Nazmat T. Surajudeen-Bakinde (Chairman) – Department of Electrical and Electronics Engineering, University of Ilorin, Nigeria

Prof. J. K. Odusote (Co-Chair) – Department of Materials and Metallurgical Engineering, University of Ilorin, Nigeria

Dr. S. A. Yahaya (Secretary) – Department of Biomedical Engineering, University of Ilorin, Nigeria

Dr. H. U.Hambali (Member)- Department of Chemical Engineering, University of Ilorin, Nigeria

Dr. Esther O. Babatunde (Member) – Department of Chemical Engineering, University of Ilorin, Nigeria

Dr. J. A. Adebisi (Member) – Department of Materials and Metallurgical Engineering, University of Ilorin, Nigeria

Dr A. S. Afolabi (Member) – Department of Electrical and Electronics Engineering, University of Ilorin, Nigeria

Dr. P. Omoniyi (Member) – Department of Mechanical Engineering, University of Ilorin, Nigeria

Dr. S. I. Mustapha (Member)- Department of Chemical Engineering, University of Ilorin, Nigeria

Dr. O. O. Mohammed (Member) – Department of Electrical and Electronics Engineering, University of Ilorin, Nigeria

Dr T. Akpenpuun (Member) – Department of Agric and Biosystems Engineering, University of Ilorin, Nigeria

Dr. M. S. Sanusi (Member) – Food Engineering, University of Ilorin, Nigeria

Dr. Olubunmi Mokuolu (Member) – Water Resources and Environmental Engineering, University of Ilorin, Nigeria

Dr K.O. Abdulrahman (Member) – Department of Mechanical Engineering, University of Ilorin, Nigeria

Dr O. A. Otuoze (Member) – Department of Electrical and Electronics Engineering, University of Ilorin, Nigeria

Dr S. O. Zakarriya (Member) – Department of Electrical and Electronics Engineering, University of Ilorin, Nigeria

Dr Temitope Fajemilehin (Member), Department of Electrical and Electronics Engineering, University of Ilorin, Nigeria.

Dr Y.O. Babatunde (Member) – Department of Civil Engineering, University of Ilorin, Nigeria

Engr. I. B. Ibrahim (Member) – Department of Mechanical Engineering, University of Ilorin, Nigeria

PUBLICATIONS COMMITTEE

Dr. T. Akpenpun, Department of Food Engineering, University of Ilorin, Nigeria – Chair

Dr. P. Omoniyi, Department of Mechanical Engineering, University of Ilorin, Nigeria – Co-chair

Dr. Esther O. Babatunde, Department of Chemical Engineering, University of Ilorin, Nigeria – Member

Dr. Temitope Fajemilehin, Department of Electrical and Electronics Engineering, University of Ilorin, Nigeria – Member

Dr. O. Mohammad, Department of Electrical and Electronics Engineering, University of Ilorin, Nigeria – Member

Dr. B. Yusuf, Department of Civil Engineering, University of Ilorin, Nigeria – Member

PUBLICITY COMMITTEE

Dr. M. S. Sanusi, Food Engineering, University of Ilorin, Nigeria – Chair

Engr. S. Ajao, Materials and Metallurgical Engineering, University of Ilorin, Nigeria – Member

Engr. M. Amoloye, Chemical Engineering, University of Ilorin, Nigeria – Member

Engr. A. Bello, Food Engineering, University of Ilorin, Nigeria – Member

Zainab Yaqub, Chemical Engineering, University of Ilorin, Nigeria – Member

Engr. Ndagi Mustapha – Mechanical Engineering, University of Ilorin, Nigeria – Member

PUBLICATIONS COMMITTEE

Dr. T. Akpenpun, Department of Food Engineering, University of Ilorin, Nigeria – Chair

Dr. P. Omoniyi, Department of Mechanical Engineering, University of Ilorin, Nigeria – Co-chair

Dr. Esther O. Babatunde, Department of Chemical Engineering, University of Ilorin, Nigeria – Member

Dr. Temitope Fajemilehin, Department of Electrical and Electronics Engineering, University of Ilorin, Nigeria – Member

Dr. O. Mohammad, Department of Electrical and Electronics Engineering, University of Ilorin, Nigeria – Member

Dr. B. Yusuf, Department of Civil Engineering, University of Ilorin, Nigeria – Member

EXHIBITION COMMITTEE

Dr. Esther O. Babatunde, Department of Chemical Engineering, University of Ilorin, Nigeria – Chair

A. M. Usman, Department of Electrical and Electronic Engineering, Stellenbosch University, South Africa – Co- chair

Engr. I. Tijani, Department of Chemical Engineering, University of Ilorin, Nigeria – Member

Engr. Victoria O. Ajiboye, Department of Agric & Biosystem Engineering, University of Ilorin, Nigeria – Member

TECHNICAL PROGRAM COMMITTEE

Dr. S. A. Yahaya, Department of Biomedical Engineering, University of Ilorin, Nigeria – Chair

Dr. H. U. Hambali, Department of Chemical Engineering, University of Ilorin, Nigeria – Co-chair

Mr I. O. Munir, Department of Biomedical Engineering, University of Ilorin, Nigeria – Member

Dr. K. O. Abdulrahman, Department of Mechanical Engineering, University of Ilorin, Nigeria – Member

Dr. S. A. Afolabi, Department of Electrical and Electronics Engineering, University of Ilorin, Nigeria – Member

Dr. J. A..Adebisi, Department of Materials and Metallurgical Engineering, University of Ilorin, Nigeria – Member

Dr. S. O. Zakarriya, Department of Electrical and Electronics Engineering, University of Ilorin, Nigeria

Engr I. Ibrahim, Department of Mechanical Engineering, University of Ilorin, Nigeria – Member

FINANCE COMMITTEE

Dr. Olubunmi A. Mokuolu, Water Resources and Environmental Engineering, University of Ilorin, Nigeria – Chair

Dr A. S. Afolabi, Department of Electrical and Electronics Engineering, University of Ilorin, Nigeria – Member

Dr Esther O. Babatunde, Department of Chemical Engineering, University of Ilorin, Nigeria – Member

Dr. Hambali U. Hambali, Department of Chemical Engineering, University of Ilorin, Nigeria – Member

LOGISTICS COMMITTEE

Dr J. A. Adebisi, Department of Materials and Metallurgical Engineering, University of Ilorin, Nigeria – Chair

Dr S. O. Zakariyyah, Department of Electrical and Electronics Engineering, University of Ilorin, Nigeria – Co-chair

Engr. M. A. Amoloye, Chemical Engineering, University of Ilorin, Nigeria – Member

Engr. H. K. IBRAHIM Mechanical Engineering, University of Ilorin, Nigeria – Member

Engr. I. B. Ibrahim, Department of Mechanical Engineering, University of Ilorin, Nigeria – Member

Mr. A. D. Abdulraheem, Department of Materials and Metallurgical Engineering, University of Ilorin, Nigeria

Mr. R. K. Abdulrazaq, Department of Materials and Metallurgical Engineering, University of Ilorin, Nigeria

INTERNATIONAL ADVISORY COMMITTEE

Prof J. O. Ojo, Tennessee Technological University, Cookeville, USA

Prof. C. J. Hogan JR, Department of Mechanical Engineering, University of Minnesota, USA

Prof. W. Northrop, Department of Mechanical Engineering, University of Minnesota, USA

Prof. James Katende, Namibia University of Science and Technology

Prof. Yusuf Isa Makarfi, University of the Witwatersrand, Johannesburg, South Africa

Prof. Pandolfelli Victor Carlos, Federal University of São Carlos, Brazil.

Prof. Adnan Rasheed, Kyungpook National University Daegu, South Korea

Prof. Esther T. Ososanya, University of the District of Columbia, Washington DC

Prof. Sadhan K. Ghosh, Department of Mechanical Engineering and Coordinator, Centre for QMS, Jadavpur University, India.

Prof. A. M. Zungeru, Botswana University of Science and Technology, Botswana

LOCAL ADVISORY COMMITTEE

Prof O. A. Lasode, Department of Mechanical Engineering, University of Ilorin, Nigeria

Prof K. R. Ajao, Department of Mechanical Engineering, University of Ilorin, Nigeria

Prof. Omodele A. A. Eletta, Department of Chemical Engineering, University of Ilorin, Nigeria

Prof T. K. Ajiboye, Department of Mechanical Engineering, University of Ilorin, Nigeria

PREFACE

It is with immense pleasure and a profound sense of accomplishment that we present the Book of Proceedings for the University of Ilorin 2nd Faculty of Engineering International Conference (FETiCON 2024). This collection represents the culmination of a remarkable event that took place between 2nd and 6th June 20234, bringing together brilliant minds from diverse disciplines within the realm of engineering and technological development. The theme of the conference is **Leveraging Artificial Intelligence to Achieve the United Nations Sustainable Development Goals**,

During FETICON 2024, explored the boundless possibilities of leveraging artificial intelligence to achieve the United Nations Sustainable Development Goals. It was indeed a journey of innovation, collaboration, and sustainable impact.

Within these pages, we present a compilation of research papers, presentations, and insights that encapsulate the rich tapestry of ideas and advancements shared during the conference. The contributions come from a diverse array of professionals and scholars who have dedicated their expertise to addressing some of the most pressing challenges facing our world today, most especially harnessing the power of AI to create a brighter, more equitable future for all.

The thematic areas covered in this book encompass a wide spectrum of engineering disciplines, including Aeronautic Engineering, Agricultural and Biosystems Engineering, Biomedical Engineering, Chemical Engineering, Civil Engineering, Computer Engineering, Electrical and Electronics Engineering, Food Engineering, Materials and Metallurgical Engineering, Mechanical Engineering, and Water Resources and Environmental Engineering. Each contribution reflects the dedication and passion of its respective authors, whose commitment to their fields of study is commendable.

This Book of Proceedings also serves as a testament to the invaluable support we have received from numerous individuals and organizations. We extend our deepest gratitude to our sponsors, whose generous contributions made this conference possible. Their commitment to promoting knowledge exchange and technological advancement is truly commendable.

We are equally indebted to our keynote speaker, plenary presenters, and all the presenters who enriched the conference with their insightful contributions. Their expertise and thought-provoking ideas have set new benchmarks for future research endeavours.

Our heartfelt appreciation also goes to our Vice Chancellor, Professor Wahab Olasupo Egbewole and all principal officers, our Dean, Professor Jamiu Kolawole Odusote, the faculty members, students, and dedicated conference planning committee who worked tirelessly to ensure the smooth organization and seamless execution of FETiCON 2024. Your efforts have left an indelible mark on the success of this conference.

Lastly, we express our gratitude to the University of Ilorin and all supporting institutions for their unwavering support and encouragement. Their commitment to promoting excellence in engineering and technology education has been the bedrock of our endeavours.

In conclusion, we hope that this Book of Proceedings will serve as a source of inspiration, knowledge, and collaboration for researchers, students, policymakers, and industry leaders alike. We are confident that the research and ideas presented here will contribute significantly to the advancement of engineering knowledge and the attainment of sustainable development goals.

Thank you for being a part of FETiCON 2024, and we look forward to future collaborations and endeavours that will continue to shape the landscape of engineering and technological development.

Prof. Nazmat T. Surajudeen-Bakinde

General Chair

Table of Content

PAPER 2- SOLID WASTE CHARACTERIZATION IN THE STAFF RESIDENTIAL AREA OF A UNIVERSITY FOR SUSTAINABLE MANAGEMENT PRACTICE

M.N.O. Yusuf[1,2*], J.A. Adeniran[1], R.O. Yusuf[1], K.A. Abdulraheem[3], H.M. Adedoyin[4]

[1]Environmental Research Laboratory, Department of Chemical Engineering, University of Ilorin, Ilorin
[2]Scientific Equipment Development Institute, Minna, National Agency for Science and Engineering Infrastructure (NASENI)
[3]Department of Civil Engineering, Ahmadu Bello University, Zaria
[4]Department of Public Health, University of Ilorin, Ilorin

**Email: najeeb77yusuf@gmail.com*

ABSTRACT

The continuous expansion of academic programs across the tertiary institutions in Nigeria has led to the growing need for the services of extra academic and non-academic staff. With this increase, many staff prefer to reside in the institution's estates due to its proximity and basic social amenities provided for them. It has consequently led to a rise in the quantity of solid wastes generated amongst residents, whilst its management is becoming a key challenge faced by the local waste management authorities. This study aims to expose the inadequacies found in the management of solid wastes generated in the municipality of Unilorin Staff Quarters. This was achieved by assessing the existing status of waste generation and management via the determination of the mean quantity of solid waste generated, characterization of its various compositions and estimation of the recyclable potential of the wastes. An average of 10.77 kg of solid waste by weight was estimated to be generated daily with a mean of 0.83 kg per site and capita waste generation of 0.056 kg/day. Organic and polythene wastes represented the largest portion in all the sampled sites, except in three. The study revealed the high recoverability potential of waste generation particularly from organic wastes and polythene. Hence, composting at household levels would be most appropriate as it would divert more than 50% of the wastes from organic sources and the implementation of the 3Rs (reduce, reuse and recycle) in the case of polythene and other wastes to significantly limit the amounts of waste generated. Comprehensive community involvement and willingness to change individual orientation to an organized system are some of the required actions for reduction from sources. The adoption of these sustainable strategies after having understood the characteristics of solid wastes typical of a developing municipality would provide an incentive for similar studies in other Staff residential areas of Nigerian institutions.

KEYWORDS: Staff Quarters, solid waste, waste generation, recyclable potentials

1. INTRODUCTION

As the world evolves through industrialization and advancement in technology, university communities are rapidly bridging the gap between 'town-and-gown', by integrating knowledge delivery with citified activities and diverse human settlement. Many Nigerian universities are becoming independent municipalities through the various functions that tend to affect both the environment and socio-economy of their immediate and extended communities (Adeniran *et al.*, 2017). Housing has been a challenge faced across all sectors of the civil service in Nigeria. The University is not left out of this welfare deficit, as the housing stock in most universities is not adequately met to cater for the increasing demands of the members of staff (Akinsanya and Adewusi, 2017). The increasing population of students due to the continuous expansion of academic programs needs the services of additional academic and non-academic staff, inflated

real estate values outside the university community, and the worsening security situation of the country are some of the known factors that have forced many staff to seek haven within the reserved quarters (Alufohai, 2013; Najib and Yusof, 2009). To address this issue, the management in collaboration with the various institutional unions provides affordable housing units for their Senior and Junior staff.

The standard of living alongside some specific socioeconomic indices can greatly influence municipal solid waste generation (MSWG) (Mian *et al.*, 2017; Namlis and Komilis, 2019). Thus, the per capita GDP is found to be a strong driving force in the amounts and types of solid wastes generated within a specific region (Estay-Ossandon and Mena-Nieto, 2018). Although the wage and salary administration for public university workers by their employers have been a controvertible subject over the years (Odoziobodo, 2015), nonetheless, this category of workers has enjoyed fairer benefits when compared to their counterparts' shares in other sectors of the labour organization (Agburu, 2012; Anazodo *et al.*, 2012). As a result, they have been able to meet their necessities of food, clothing, and other sundries.

Solid waste management is a key challenge faced by the local management team of the University of Ilorin Senior Staff Quarters and by extension, the waste management authorities of the University. As supported by Malik *et al.* (2015), the complexity and system multi-dimensionality of managing these solid wastes from their generation to disposal are the main challenges faced by every stakeholder.

The source and composition of solid wastes generated in a typical residential area of an urban community in Nigeria satisfy the definition of solid wastes by Al-Khatib *et al.* (2007) and Ephantus *et al.* (2021). Sustainable development is thus required to overcome this challenge. Given this, the development and implementation of Integrated Solid Waste Management (ISWM) first requires comprehensive data on existing and anticipated waste situations in an area (Aich and Ghosh, 2019). Integrated Solid Waste Management (ISWM) is a systematic approach to waste management in a sanitary and environmentally friendly manner (Asefi and Lim, 2017). According to USEPA (2001), ISWM prioritizes waste processing methods in the order of reduction, reuse, recycling and ultimate disposal of solid waste.

This study aims to expose the weakness in the management of solid wastes generated in the municipality of Unilorin Staff Quarters. The data obtained from this study will propose efficient management alternatives for the MSW in Unilorin Senior Staff Quarters. Ultimately, this study intends to fill the void created from the marginal information currently available in the literature for the affected University, and in general, the residential staff Quarters in all Nigeria tertiary institutions. To achieve this, the average amounts of solid waste generated in the study area would be estimated; characterization of its various compositions would be carried out via sorting; the recyclable potential of the waste generated in the residential area would thence be estimated; and lastly, the per capita waste generation would be compared with those generated from prominent tertiary institutions' Staff Quarters within the State, to help discuss possible collaborations amongst the institutions' waste management authorities for economic gains.

Hence, the efficient management of solid wastes in the study area is inevitable, to control the filths and malodorous emissions from the designated dumping sites in a bid to limit the risks on the environment, and public health as well as the potential economic benefits to be derived therefrom. There is a need to develop robust solid waste storage, collection and sanitary disposal plans, to overcome the use of unsophisticated methods such as open dumps. Insufficient information about regulations and in some cases, financial restrictions have often

brought a setback in the organization and proper planning in waste management by many tertiary institutions in Nigeria.

2. THEORETICAL FRAMEWORK

Effective management of solid wastes is important for promoting environmental sustainability within the University of Ilorin staff residential areas. Waste characterization in the study area will allow us to develop targeted strategies to reduce environmental impact and improve waste management practices amongst the residents. Mathematical models involved in the characterization of solid wastes generated include descriptive statistics to calculate mean and standard deviation used to summarize waste data collected.

The mean is the average value of the number of waste samples collected from all the study sites and is calculated as:

$$\bar{n} = \frac{\sum_{i=1}^{n} n_i}{n} \quad (1)$$

where,

$\bar{n}$ – mean

n_i – waste site i

n – number of waste sites

The standard deviation is the square root of the variance (a measure of the spread of the waste volume around the mean);

$$\sigma = \sqrt{\sigma^2} \quad (2)$$

3. MATERIALS AND METHOD

3.1 Sampling Area

The University of Ilorin is located in the southern region of the ancient city of Ilorin, Kwara state. The University of Ilorin Senior Staff Quarters (study area) is located within the premises of the University Permanent Site- which serves as the main campus of the tertiary institution. The study area has an estimated land area of 238,108 square metres, hosting a total number of 115 apartments. It is suitably divided into two parts- the Old and New Quarters, where the former and latter accommodate 82 and 63 apartments, respectively. The Old Quarters is typical of three-bedroom detached bungalows, while the New Quarters is characteristic of storeys (Block of flats), semi-detached bungalows (G-Blocks) and duplexes (F-Blocks). There is a Pro-chancellor lodge and a community mosque that is centrally situated within the entire area (Figure 1). Each apartment has an extended building that is mainly used as Boys Quarters. The Boys Quarters is an allotted room for every apartment, except for the F-Blocks which have four rooms allotted to each building. It is assumed that there is an average of six people in every household and an average of two persons in each Boys Quarters. Based on this, the estimated population of the study area is set as 1,184.

Figure 1: Google Earth Imagery showing the location of the study area

3.2 The Waste Disposal Site and Collection System

In total, there are thirteen (13) waste disposal sites within the study area, each provided with at least three large waste bins for collection; depending on the number of households given to the particular site (Figure 2).

Figure 2: Site images of some designated waste sites within the study area

Each designated site is meant to serve the nearby residents. Table 1 shows the general description of each dumpsite.

Table 1: Description of each dump site

Waste Site	Coordinates		Number of containers	Average number of houses frequent at the site	Average weight of wastes before collection (kg)
	Latitude	Longitude			
A	8.462901	4.646812	5	22	8.76
B	8.468787	4.653948	5	5	7.92
C	8.463737	4.643274	2	5	1.62
D	8.463737	4.643274	1	7	2.10
E	8.464308	4.643072	5	22	6.66
F	8.466919	4.642832	4	16	5.82
G	8.471026	4.643387	4	23	5.82
H	8.472374	4.642634	3	11	4.98
I	8.473473	4.643684	1	5	2.10
J	8.472961	4.644141	1	2	2.10
K	8.471666	4.644653	2	2	2.94
L	8.470159	4.644161	2	4	2.94
M	8.464470	4.645004	7	19	10.86

The collection of the solid wastes is managed by workers employed by the University management. This is done every 6-7 days with a waste truck. The waste is disposed of at a landfilling site located within the University campus where they are sorted for either recycling or burning.

3.3 Waste Grouping and Determination of Recycling Potentials

A four-week sampling period was used to determine the types of waste that are commonly generated within the study area. The grouping pattern that was considered suitable for the sampling exercise was adopted from the study of Adeniran *et al.* (2017). They were classified into major categories with little modifications to accommodate peculiar waste streams that are generated locally (Table 2). The recycling potential of each waste was determined based on the availability of recycling markets for each waste material within Kwara State.

Table 2: Waste classification by type

Waste Category	Items Description
Organic	Food waste, fruit rinds, vegetable stalks, eggshells, yam/potato peels, hairs, yard wastes, etc.
Plastics	Polystyrene, polyethylene (LDPE and HDPE), Polypropylene, PET bottles, etc.
Polyethene	Nylons, packaging bags, etc.
e-waste	Computer parts, radio components, gaming accessories, electric cables, etc.
Glass	Glass materials
Paper	Printing materials, cartons, writing materials, newsprints
Metals	Aluminium cans, tins and jars, stainless steel rails, iron nails, etc.
Wood	Planks
Textile	Clothes, wigs, diapers, napkins, curtains, etc.
Leather and skin	Shoes, bags, etc.
Rubber	Tyres, machine belts, etc.
Inert	rocks, soil, etc.

3.4 Sampling Procedure

ASTM D5231-92 testing method for calculating the composition of unprocessed wastes was applied to the study. The requirements expected by this standard sampling method are that; statistical analyses of the sampling should be performed to determine the number of samples; sampling should be random and performed over a 5- to 7-day period and; the representative sample should weigh approximately four times the subsample that is to be sorted (Abd Alqader and Hamad, 2012; Abdulredha *et al.*, 2017; Adeniran *et al.*, 2017). The containers for sampling were selected randomly during each day of the four-week sampling period at each waste site, which is representative of the total waste stream. According to ASTM D5231-92, for a weekly sampling period of k days, the number of containers sampled each day should be approximately n/k, where n is the total number of containers to be selected for the determination of waste composition (ASTM, 2008). In this study, a weekly period is defined as 6 days, which is the average number of days used before the solid wastes are collected. According to the Standard's recommendation, each unprocessed solid waste sample collected for sorting should weigh 91–136 kg (200–300 lb) (ASTM, 2008). However, since sorting was conducted at the dumpsites as applicable in this study, the average sample size was between 2-10kg. Each sample was properly prepared by thoroughly mixing from each discharged MSW container using a shovel poured into a 0.0026 m^3 bucket. After sampling, hand sorting was applied for the classification of MSW into twelve waste categories. Each material category is then weighed and registered in the datasheet. The fraction of each waste component was evaluated in percentage. The sampling operation was carried out between September 15, 2021, and October 21, 2021.

For precision, an equation proposed by the standard was used to calculate the number of samples required (Equation 1).

$$n = \left(\frac{T^* \times S}{E \times X}\right)^2 \quad (3)$$

where,

T^*- student's t-test corresponding to the desired level of confidence,

S- the estimated standard deviation,

E- the desired level of precision, and

X- the estimated mean

Polyethylene wastes were selected as the governing component of the waste to calculate the standard deviation (S) and mean (X). Therefore, the number of samples to be collected was statistically determined using the student T^* value at 90% confidence level and 10% precision level. A total of 26 samples were collected based on Eq. (1) (S = 0.52, X = 0.95). Based on this requirement, two samples were collected from thirteen waste sites. Sampling was carried out once every week, especially at the peak period before the collection day was due.

3.5 Estimation of the amounts of waste generated daily

The average solid waste generated daily (type/kg/day) on each disposal site was determined by estimating the overflowing capacity of the waste bins used for collecting the waste. In events when the containers provided at a particular site are filled quickly beyond capacity, additional containers are assumed in essence, to accommodate for the overflow, depending on the waste density per area.

The estimation was achieved by measuring the dimension of the waste bins at 90% of their capacity- to accommodate loading errors that could be associated with non-compactor waste containers. The waste volumes (m^3) were converted to weight (in kg) using the NALAS Municipal Solid Waste Information System (SWIS) management software for municipal waste (NALAS, 2009).

4. RESULTS AND DISCUSSION

4.1 Rate of waste generation

The University of Ilorin Senior Staff Quarters generated an estimated average of 10.77 kg of solid wastes by weight daily during the four-week study period (Figure 3). The mean weight of solid wastes generated in all the waste sites is estimated as 0.83kg. Site C generated the least solid waste by weight (0.27kg) while Site M dominated the areas where solid waste was disposed of. This affected site was frequently visited because it was mutually used by residents of other dominated areas due to its proximity and accessibility. In addition, outsiders who visit the staff Quarters use this particular dump site to avoid waste tax levied on them by their communities.

The total amounts of solid wastes generated in all the waste sites present in the study area during the period of sampling are relatively higher than the amounts generated in the study locations (Ugwu *et al.*, 2020). It is approximately 4 times and 2 times higher than the solid wastes generated in the staff residential area (82.42kg) and student hostel (146.66kg) of the University of Nsukka, respectively over a six-month sampling period. The difference in population, waste types, and consumption patterns are some probable factors that could affect the high amounts of waste generated in this study.

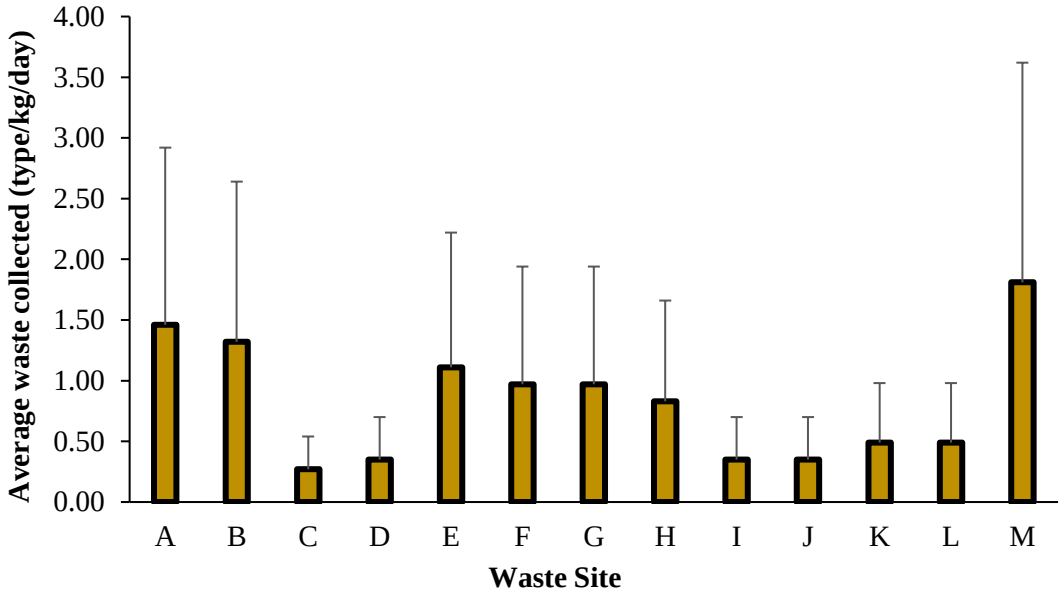

Figure 3: Average weights of solid waste generated (kg/day)

The per capita waste generated in the University of Ilorin Staff Quarters is 0.025 kg/day. This is lower when compared to the 0.06 kg/day reported by Ugwu *et al.* (2020) for the University of Nsukka; 0.34 kg/day reported by Adeniran *et al.* (2017) for the University of Lagos; and 0.06 kg/day reported by Okeniyi *et al.* (2012) for a model community. The superior populations of these Universities and their socioeconomic distributions make the per capita wastes generated in this study area lower. In addition, higher income is found to be a strong driver to

the generation of household waste. The per capita waste determined in this study is found to be relatively lower than the 0.5-0.9 kg/capita/day of solid wastes generated by 74 households enumerated in the survey of Ogwueleka (2013) in a highly developed area of Abuja; a city in the Federal Capital Territory of Nigeria.

4.2 Characterization of waste at each disposal site

Figure 4 shows the average percentage of the composition of solid wastes generated in each waste site of the University of Ilorin Staff Quarters. Compostable wastes that comprise putrefiable food materials and other organics were found to be the major constituents of the waste in all waste sites, except for Waste Sites H, I, and J, where polythene is the most dominant constituent. The reason for the exception is likely due to how the reachability of these sites could be hard for the residents allocated to these sites. They found other mutually used sites to be more accessible. In addition, the adherence to modern waste management practices by these sets of residents could also be attributed to the lower generation of compostable wastes.

In the category of non-compostable wastes, polythene and plastic wastes were predominant among the waste types. Site L had the highest composition of 32.2%, which is closely followed by Sites M and A having an average composition of 30.9 and 30.7%, respectively for polyethylene waste material. For plastics, Sites J, H, and E had the highest average compositions of 23.1, 21.3, and 19.3%, respectively. Papers and other wastes were moderately high amongst the waste constituents in all the sample sites. Paper had an average composition of 14.5, 12.1, and 11.9% in Sites C, I, and D, respectively. Wastes classified as others comprise; e-wastes, leather and skins, textiles, wood, rubber, and inert materials (stones and soils). They are grouped due to their lower compositions, or in some cases, their nonexistence in some sample sites. However, textiles and e-waste were more frequent than the other types of waste. Sites B and M had the highest average composition of 3.3 and 1.6% of textiles and e-waste types, respectively.

The average percentage compositions of solid wastes were determined by Ajadi and Tunde (2010) for similar municipalities within the city of Ilorin. The analyses of the solid wastes revealed from their studies indicated a high percentage of food and paper waste generated in all the study locations. In Magaji Ngeri, food wastes, papers and nylons, bottles and tins, and human faeces constituted 28.2, 27.3, 11.5, and 11.5% respectively. For the waste sampled at Oko-Erin Ward, the average compositions of solid wastes were obtained as; 27.8, 25.0, 26.1, and 6.5%, for papers, food wastes, leaves/nylons, and human faeces, respectively. However, the Government Reservation Area (G.R.A.), which closely matched the demographic characteristics of the area considered in this study had an average composition of the waste generated as; 30.9, 23.0, 15.0, 14.1%, for food waste, papers, nylons, and tins/bottles, respectively. No human faeces were found amongst the wastes in this particular area.

Table 3 shows the overall weights of the solid wastes generated in each waste site during the entire study period;

Table 3: Overall weights of the waste categories at each site during the sampling period

Waste Site	**W**eight of each waste category (kg)					
	Organic	**Plastics**	**Polyethene**	**e-waste**	**Glass**	**Papers**
A	0.51	1.77	0.03	6.39	4.92	0.45
B	0.81	1.22	0.19	0	4.18	0.05
C	0.65	1.85	0.13	0.72	9.18	0.20
D	2.43	2.87	0.02	0.11	1.27	0.33

E	0.22	9.08	0.01	9.48	1.13	0.12
F	0.73	7.69	0.06	0.24	3.86	0.54
G	1.03	6.82	0.28	0.68	4.35	0.54
H	0.29	6.55	0.01	12.86	4.95	0.81
I	0.39	2.76	0.32	1.23	1.52	0.39
J	0.28	2.88	0.11	0.68	2.26	0.08
K	1.74	4.16	0.29	0	1.22	0.49
L	2.64	4.42	0.36	0.17	1.06	0.38
M	1.70	2.28	0.90	1.67	5.07	0.17
Σ	13.42	54.35	2.71	34.23	44.97	4.55

Waste Site	**Weight of each waste category (kg)**					
	Metals/can	**Wood**	**Textile**	**Leather and skin**	**Rubber**	**Inert**
A	3.72	13.57	0.86	0.16	0	0.04
B	2.99	1.15	1.37	0.63	0	0.78
C	1.10	7.11	0.11	0.05	0	0.14
D	1.67	1.03	0	0	0.01	1.11
E	15.66	6.00	0.44	0.37	0.03	0
F	2.50	0	0.43	0.33	0.22	0.03
G	2.80	18.70	0.68	0.35	0.27	0
H	3.70	10.13	0.51	0.07	0.02	0
I	1.19	5.72	0.21	0.25	0.27	0.04
J	1.18	5.80	0.28	0.03	0.25	0
K	1.36	1.29	0.23	0	0.05	0
L	1.54	9.20	0.07	0.01	0.03	0
M	12.55	4.53	0.15	0.10	0.15	0
Σ	**51.96**	**84.23**	**5.34**	**2.35**	**1.30**	**2.14**

From Table 3, 301.55 kg is estimated as the total amounts of solid wastes generated in all the waste sites during the four weeks sampling period. About 13.42kg of organic waste was across the entire site. Site L generated the highest amounts of organic waste (2.64kg), while Site E was the site that received the least amounts of organic waste (0.22kg). Wood, plastics, and metals weighed the highest, with overall weights of 84.23, 54.35, and 51.96kg, respectively; which is more attributed to their bulk density. Commercial wastes which include, nylons for packaging and polyethylene bags for sachet water were predominant at Site M, with an overall weight of 2.71kg during the study period. Site H had the highest weight of e-waste (12.86kg). This was due to a computer screen that was disposed of on the site. The types of e-waste that were frequently seen at most of the waste sites were electrical cables and household appliances. Writing materials and package boxes dominated the constituents in the paper category, with Site H (0.81kg) being the site that had the highest amounts of the type of waste during the study period.

The characteristics of solid wastes revealed in this study are closely related to those reported in similar studies. They are typical for developing municipalities as organic wastes are found to be the dominant constituent of the total waste generated. Organic wastes and polythene were the predominant wastes revealed by Adeniran *et al.* (2017) and Ugwu *et al.* (2020) in two Nigerian universities. From both studies, the average composition of organic wastes and polythene is 34.29 and 22.0%; 32.36 and 13%, respectively.

Sujauddin *et al.* (2008) recorded the highest percentage of organic waste constituents (72.8%) in their study, which are closely followed by polythene and metals, having values of 6.2% and 6.0%, respectively. Topanou *et al.* (2011) and Bichi and Amatobi (2013) revealed the MSW composition generated in a municipality dominated by households in their respective West African countries. Organic and plastic wastes were more frequently disposed of than other waste types; with an average composition of 48.26 and 57.5% (organic wastes); and 2.68 and 17.6% (plastics) respectively. In the study of Olukanni and Mnenga (2015), food wastes and papers were prevalent among the waste samples, having an average composition of 14.0% and 11.5%, respectively.

Figure 5 shows the average percentage compositions of the dominant waste types selected from this study and compared with other related literature.

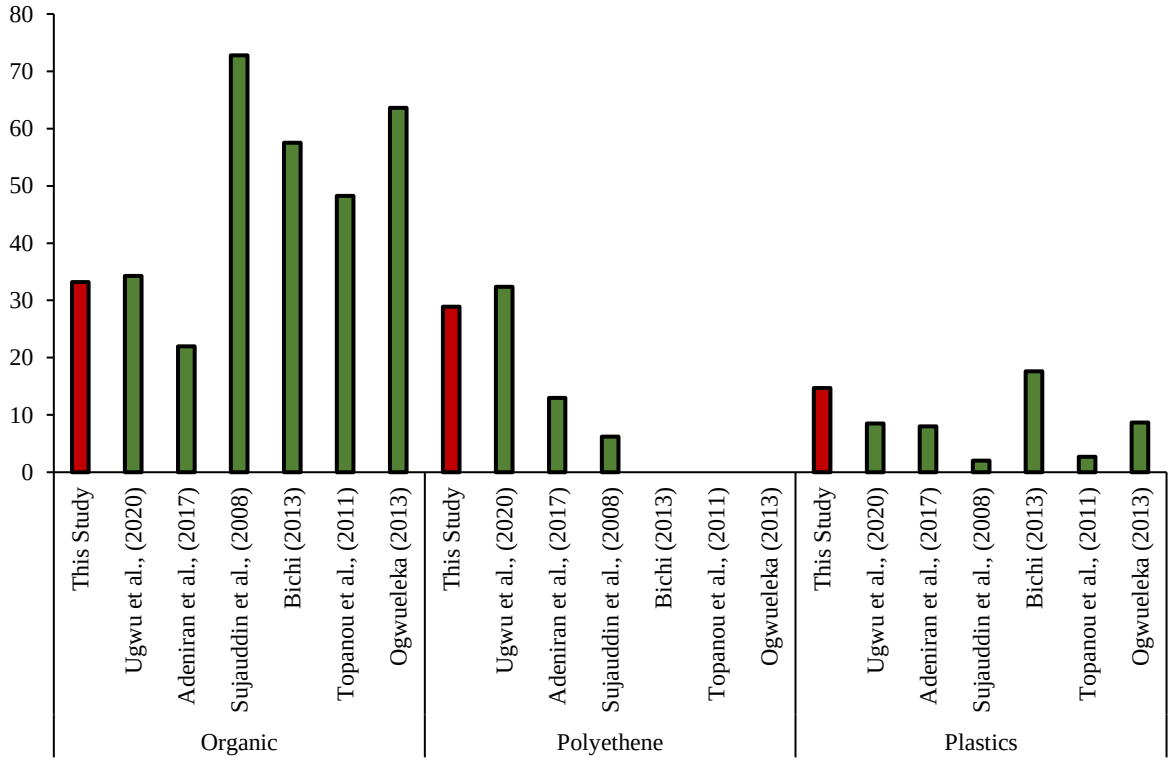

Figure 5: Comparability of the average percentage composition of selected waste types

The amounts of solid waste generated in all the waste sites are seemingly high. The characterization of the waste categories has been established, which is the most paramount when setting up a sustainable and efficient waste management plan. From the proportions of the waste constituents revealed, it is found that the solid wastes generated in the study area have a high recoverability potential as illustrated in Figure 4. Proper composting of the putrefiable wastes would lead to a significant reduction in greenhouse emissions. Composting at household levels would be most appropriate as it would divert more than 50% of the waste from the waste streams by which the manure could be used to enrich soils in the local gardens (Mohee, 2002).

The recycling option is also highly achievable from the entire waste category. Small-scale plastic recycling markets are springing up across many areas of Kwara state. There exists a plastic production company in the State, where this type of waste can be collected, washed, pelletised and extruded, to form a new product. Waste scavenging is economically viable in the city of Ilorin, where the study area is located. In the study of Adeyemi *et al.* (2001), it is

suggested that waste scavengers could be incorporated formally into the recycling process. From their findings, it is reported that despite the limited formal education possessed by all of the waste scavengers interviewed in their survey, they had an appreciable knowledge of the waste categories during collection. Iron materials were reported to be the most common wastes collected by the scavengers, most probably due to the broad market available. Bottles were much more variable, depending on factors such as; the availability of unbroken bottles, their size and weight. The type of waste is sold to where they are utilised.

Energy recovery from solid wastes is a prospective technology that can be applied to solve the problem of MSW generation. According to Yusuf *et al.* (2019), Nigeria's annual waste generation is aimed to reach 36,250Gg per year by 2030, with revenue to be derived from the electricity production from methane emissions estimated at US$473.82×10^6 by 2030.

The continuous development of new models as a result of technological advancements has made Electrical/Electronic wastes quickly become technologically obsolete (Adediran and Abdulkarim, 2012). Waste electronic products should be disposed of separately from other household wastes, with a special disposal facility provided to reduce the possibility of a radioactive leak of hazardous electronic components.

The transportation system of the local authorities responsible for the collection of waste on a periodic basis also needs to be improved. The turnaround time and the provision of an impactor vehicle will lead to an efficient waste management system. To solve the extreme excess of polythene and plastic litter, potable water should be provided for the residents. In addition, reorientation of existing customs that will conform to modern waste management practices will help in reducing wastes from their sources, through a well-planned reduction, reuse and recycling of some of these wastes.

5.0 CONCLUSION

The University of Ilorin Senior Staff Quarters serves as a residential area for a group of people characterized by a superior economic status. To this effect, there has been an increased generation of solid wastes in the area. An estimated average of 10.77 kg of solid wastes by weight is generated daily during the four-week study period in all the thirteen designated waste sites. The per capita waste generated in the study area is gotten as 0.056 kg/day. Organic and polythene wastes represented the largest portion of all the sample sites, except for Sites H, I, and J. It was recommended that an efficient solid waste management plan should be developed. The implementation of the 3Rs (reduce, reuse, and recycle) is imperative to significantly limit the amounts of solid waste generated in the study area. Comprehensive community involvement and willingness to change individual orientation to a controlled waste generation are some of the required actions for reduction from sources. The reuse of resources would also decrease the purchasing power of the residents on new items so that the existing ones could be alternatively used for other purposes. The adoption of these sustainable strategies after having understood the characteristics of solid wastes typical of a developing municipality would provide an incentive for similar studies in other Staff residential areas in Nigeria tertiary institutions.

Declarations

Authors' contributions:

All authors contributed to the conception of ideas presented here and to drafting the article and approved the final version

Funding statement

This research was not funded by a specific grant from agencies in the public, private, or non-profit sectors.

Competing interest statement

The authors declare no conflict of interest.

Acknowledgement

We sincerely appreciate the University of Ilorin Senior Staff Quarters ExCo members for their cooperation and the supports they rendered to the actualization of this Project

REFERENCES

Abd Alqader, Ahmad, and Hamad, Jehad. (2012). Municipal solid waste composition determination supporting the integrated solid waste management in the Gaza strip. *International Journal of Environmental Science and Development, 3*(2), 172.

Abdulredha, Muhammad, Rafid, AL, Jordan, David, and Hashim, Khalid. (2017). The development of a waste management system in Kerbala during major pilgrimage events: determination of solid waste composition. *Procedia Engineering, 196*, 779-784.

Adediran, Yinusa Ademola, and Abdulkarim, A. (2012). Challenges of electronic waste management in Nigeria. *International Journal of Advances in Engineering and Technology, 4*(1), 640.

Adeniran, AE, Nubi, AT, and Adelopo, AO. (2017). Solid waste generation and characterization in the University of Lagos for sustainable waste management. *Waste management, 67*, 3-10.

Adeyemi, AS, Olorunfemi, JF, and Adewoye, TO. (2001). Waste scavenging in Third World cities: A case study in Ilorin, Nigeria. *Environmentalist, 21*(2), 93-96.

Agburu, John I. (2012). Recent trends in wage and salary administration in Nigeria: A synopsis on theoretical and empirical challenges.

Aich, A, and Ghosh, Sadhan Kumar. (2019). Conceptual framework for municipal solid waste processing and disposal system in India *Waste management and resource efficiency* (pp. 91-107): Springer.

Ajadi, BS, and Tunde, AM. (2010). Spatial variation in solid waste composition and management in Ilorin Metropolis, Nigeria. *Journal of Human Ecology, 32*(2), 101-108.

Akinsanya, GM, and Adewusi, AO. (2017). Staff Housing Needs of Nigerian University: A Case of Obafemi Awolowo Univeristy, Ile-Ife. *International Journal of Geography and Environmental Managemen, 3*(1), 38-52.

Al-Khatib, Issam A, Arafat, Hassan A, Basheer, Thabet, Shawahneh, Hadeel, Salahat, Ammar, Eid, Jaafar, and Ali, Wasif. (2007). Trends and problems of solid waste management in developing countries: A case study in seven Palestinian districts. *Waste management, 27*(12), 1910-1919.

Alufohai, AGELE J. (2013). *The Lagos State 2010 Mortgage Law (LAGOSHOMS) and the Supply of Housing.* Paper presented at the FIG Working Week.

Anazodo, Rosemary O, Okoye, Joseph C, and Chukwuemeka, Emma EO. (2012). Civil service reforms in Nigeria: The journey so far in service delivery. *American journal of social and management sciences, 3*(1), 17-29.

Asefi, Hossein, and Lim, Samsung. (2017). A novel multi-dimensional modeling approach to integrated municipal solid waste management. *Journal of Cleaner Production, 166*, 1131-1143.

ASTM. (2008). *Standard test method for determination of the composition of unprocessed municipal solid waste*: ASTM International.

Bichi, MH, and Amatobi, DA. (2013). Characterization of household solid wastes generated in Sabon-gari area of Kano in Northern Nigeria. *American Journal of Research Communication, 1*(4), 165-171.

Ephantus, Mugo, Robert, Kinyua, and Paul, Njogu. (2021). An analysis of solid waste generation and characterization in thika municipality of Kiambu County, Kenya.

Estay-Ossandon, Charles, and Mena-Nieto, Angel. (2018). Modelling the driving forces of the municipal solid waste generation in touristic islands. A case study of the Balearic Islands (2000–2030). *Waste management, 75*, 70-81.

Malik, Nur Khaliesah Abdul, Abdullah, Sabrina Ho, and Abd Manaf, Latifah. (2015). Community participation on solid waste segregation through recycling programmes in Putrajaya. *Procedia Environmental Sciences, 30*, 10-14.

Mian, Md Manik, Zeng, Xiaolan, Nasry, Allama al Naim Bin, and Al-Hamadani, Sulala MZF. (2017). Municipal solid waste management in China: a comparative analysis. *Journal of material cycles and waste management, 19*(3), 1127-1135.

Mohee, Romeela. (2002). Assessing the recovery potential of solid waste in Mauritius. *Resources, conservation and Recycling, 36*(1), 33-43.

Najib, NU, and Yusof, NA. (2009). *A review of student housing facilities in higher learning institutions.* Paper presented at the Proceeding of the 3rd International Conference on Built Environment in Developing Countries (ICBEDC 2009), Dec.

Namlis, Konstantinos-Georgios, and Komilis, Dimitrios. (2019). Influence of four socioeconomic indices and the impact of the economic crisis on solid waste generation in Europe. *Waste management, 89*, 190-200.

Odoziobodo, Severus Ifeanyi. (2015). Integrity and conflict resolution in Nigeria: An analysis of trade disputes between the Federal Government of Nigeria and the academic staff union of universities, ASUU. *European Scientific Journal, 11*(22).

Ogwueleka, Toochukwu Chibueze. (2013). Survey of household waste composition and quantities in Abuja, Nigeria. *Resources, conservation and Recycling, 77*, 52-60.

Okeniyi, Joshua Olusegun, Anwan, EU, and Okeniyi, ET. (2012). Waste characterisation and recoverable energy potential using waste generated in a model community in Nigeria. *Journal of Environmental Science and Technology, 5*(4), 232-240.

Olukanni, David O, and Mnenga, Myem U. (2015). Municipal solid waste generation and characterization: A case study of Ota, Nigeria. *International Journal of Environmental Science and Toxicology Research, 3*(1), 1-8.

Sujauddin, Mohammad, Huda, SMS, and Hoque, ATM Rafiqul. (2008). Household solid waste characteristics and management in Chittagong, Bangladesh. *Waste management, 28*(9), 1688-1695.

Topanou, Nikita, Domeizel, Mariane, Fatombi, Jacques, Josse, Roger Gérard, and Aminou, Taofiki. (2011). Characterization of household solid waste in the town of Abomey-Calavi in Benin. *Journal of Environmental Protection, 2*(06), 692.

Ugwu, Collins O, Ozoegwu, Chigbogu G, and Ozor, Paul A. (2020). Solid waste quantification and characterization in university of Nigeria, Nsukka campus, and recommendations for sustainable management. *Heliyon, 6*(6), e04255.

USEPA. (2001). United States environmental protection agency. *Quality Assurance Guidance Document-Model Quality Assurance Project Plan for the PM Ambient Air, 2*.

Yusuf, RO, Adeniran, JA, Mustapha, SI, and Sonibare, JA. (2019). Energy recovery from municipal solid waste in Nigeria and its economic and environmental implications. *Environmental Quality Management, 28*(3), 33-43.

PAPER 3 - CONTEMPORARY ISSUES OF POSTHARVEST ACTIVITIES VIS-A'-VIS IMPLICATION ON FOOD SECURITY IN NIGERIA

S.E. Chukwu[1], A.I. Oyebanji[1], O.P. Akomolafe[1], A.O. Usman[1], F.O. Raji[1], U. B. Umar[1] and J.B. Akpotaire[2]

[1]Department of Postharvest Engineering Research, Nigerian Stored Products Research Institute, Ilorin, Nigeria.
[2]Department of History and International Studies, University of Ilorin, Nigeria
Email: obanjiometer87@gmail.com and sechukwu6@gmail.com

Abstract
Nigeria is highly food insecure, as the losses are replicated in fruits, vegetables, nuts, grains and fish, among others. Nigeria received a paltry 48.4 per cent overall score on the Economist Intelligence Unit's 2019 Global Food Security Index, a mere 0.7 per cent improvement from the 47.7 per cent score it received in 2018. Equally relevant to food production in Nigeria is the development of infrastructure that will promote production, circulation and storage. As iterated by the Central Bank of Nigeria (CBN) (1994) increased food production cannot satisfy the increasing food demand unless attention is focused on reducing postharvest losses. However, it is disheartening that much of the products is lost due to improper or lack of postharvest handling methods. It is recommended, that state, local, and federal governments, private investors, and non-governmental organisation should embrace action or robust techniques that will ultimately reduce post-harvest losses. This research has successfully provided insight into the prevailing issues that face postharvest in Nigeria as well as food insecurity. Hence, leveraging state-of-the-art technologies and experienced extension services will adequately communicate innovative and research findings to the surmised beneficiaries.
Keywords: Storage, Techniques, Fruits, Vegetables, Postharvest

1. Introduction

The quality and safety of food at the time of harvest, potential damages during harvest, and the need for further processing of the harvested foods have continually been a contemporary issue in pre- and post-harvest with its concomitant effect, which cut across product market value, deterioration during storage, cost of postharvest technology, connotation of emerging technologies as well as regulatory flux all these constitute issues that may mare or promote postharvest activities (Gimba *et al.,* 2017). Developing countries have been reported to have lost roughly 40% of their food harvest, especially fruits and vegetables, to spoilage and infestations in transit to the consumer (Kitinoja *et al.,* 2011). In developing countries, such as Nigeria, where tropical weather and poorly developed infrastructure contribute to the problem, losses are sometimes of shocking proportions if equated to the Naira equivalent. Losses occur in all facets of agriculture productivity from preharvesting to postharvest via handling, storage, processing and marketing. Accrued losses are technically proportional to the influence of mixed factors such as the perishability of the commodity, ambient temperature and relative humidity which determine the natural course of deterioration, bacterial and fungal attack, damage by pests (insects), rodents and birds, the length of time between harvesting and consumption, and practices of postharvest handling, storage and processing. It is important to note that reducing postharvest losses of already produced food is more sustainable than increasing production to compensate for those losses (Kitinoja, *et al*., 2011). Increasing investments in postharvest technology is long overdue in Nigeria, and can have a major impact on reducing waste and increasing food supply, leading to improved incomes without increasing production while reducing expenditures on all farm inputs.

Evidently, in developed nations, fruits and vegetables are packaged in Hammock packs and polyethylene to reduce moisture loss, fresh meat is sold in vacuum packs to extend its shelf life, and cereals are distributed in Polyethylene and other suitable packages (Cantwell 2011). This is to contain and present these foodstuffs to consumers safely and to prevent food contamination in the distribution chain (Cantwell 2011). Conversely, in Nigeria, foodstuffs are still sold in the markets without any packaging exposing them to all sorts of organisms (pathogenic and non-pathogenic) and other damaging environmental factors, such as sunlight, dust, flies and human activities (Serbranek *et al*., 2013). In addition, in developed nations, farmers and traders of food are fully aware that it is a collective responsibility to ensure food safety and quality in the food supply chain (FAO 2006). The time has come when such a system has to be embraced in Nigeria. This is because the market is becoming competitive; also educated and probing customers are demanding fresh and processed foods that are safe for consumption. Also, if Nigerian foods must be accepted for international trading, a robust National Food Control System (NFCS) must be put in place, and monitored by suitable and qualified personnel, which is the major approach that could ensure accommodation of our local produce into the international food supply chain (Kitinoja *et al.,* 2011).

Consequently, a contending issue that has steadily been a challenge is that of postharvest activities as well as that of postharvest research and extension (PR&E) that have long ago been downplayed in Nigeria. For instance, the surmised function of PR&E which was saddled with the responsibility of carrying out quantitative and qualitative surveys of the current human, physical, and financial resources accruable to individuals in society via robust agriculture, has been damped. Proposed findings and observations, from the spelt engagement will be the basis for the development of an action plan for postharvest activities. In most instances, solutions to existing problems in the postharvest handling system require the use of available information supposedly gotten from PR&E which will help in the implementation of existing appropriate traditional and modern technological innovation tilted toward solving the postharvest problem. Sadly, this has not been the case.

Kitinoja *et al.* (2010) submitted that most of the articulated post-harvest studies were centric on post-harvest microbiology and food technology, primarily for the reduction of losses in quality, quantity, and safety at the consumption level of the distribution chain. However, it places less emphasis on the empirical relationship between postharvest loss and food security in Nigeria. In a related development, Mohammed *et al*. (2017) opined that for quality and safety to be guaranteed, good practices must be employed from growing, harvesting and postharvest handling of foods, to the processing, packaging, distribution, during storage and preparation before consumption. This has become imperative because foodstuffs undergo progressive deterioration in quality and safety after being harvested, gathered, caught, or slaughtered. Microbes such as bacteria, yeasts, molds, insects, and rodents are in endless competition with humans for the food supply. Mohammed *et al*. (2017) recommended an advanced technological approach for curbing pre- and post-harvest losses. In fact, in line with the findings of FAO (2006), most technical literature has not adequately given comprehensive overviews of the magnitude of post-harvest losses in Nigeria nor its related linkages. This subtle gap constituted missing linking in which this research was hinged on.

2. RESULTS AND DISCUSSION

2.1 Perspectives on Postharvest Loss in Nigeria

Postharvest loss (PHL) is a large and increasingly urgent problem and is particularly acute in developing countries where loss reduces income by at least 15% for 470 million smallholder farmers and downstream value chain actors. It was estimated that 1.2 billion people are food insecure (Cite a source). The world population will reach 9 billion by 2050, and with 2 billion more mouths to feed, if PHL is not curtailed, food production in developing countries will need to increase by an estimated 70% and this requires an investment of $83 billion per year to meet the growing demand (FAO, 2006). Together, crop foods (e.g., grains, fruits, vegetables, tubers, pulses) and dairy comprise 92% of developing world losses, with the remaining 8% occurring in meat (4%) and fish (4%). Meat and fish are a small part of overall food loss and are comparable to other crops as a percentage of production in their category. In developing countries, the root causes of food loss are interlinked and complex, but the primary drivers include a lack of extension services to build skills in handling, packaging, and storage; insufficient postharvest storage facilities or on-farm storage technologies; and poor market access that leads to spoilage before sale (FAO,2006).

For instance, the Central Bank of Nigeria (CBN) (1994), observed that increased food production cannot satisfy the increasing food demand unless attention is focused on reducing postharvest losses. This will create an opportunity for providing a substantial amount of food for consumption and other uses. However, it is disheartening that much of the products is lost due to improper or lack of postharvest handling methods. Adebooye (1997) classified postharvest losses of fruits and vegetables in Nigeria into (1) damaged but marketable and (2) damaged but unmarketable. He concluded that most of the losses are due principally to mechanical damage which often gives room for further damage by pathogens. In transit from northern to southern Nigeria, they found that tomatoes recorded higher damage than onions, while in transit from southern to northern Nigeria, oranges recorded higher losses than kola nut.

Estimation of postharvest losses calculations as opined by Adebooye (1997) were based on postharvest losses of 20-33% reported by FAO (1986). Therefore, five percentages were chosen between 20% and i.e. 20 %, 25 %, 30 %, 35% and losses were calculated per hectare (Adebooye, 1997). As shown in Tables 1 and 2 show the estimated postharvest losses in fruits and leaf vegetables that are consumed in Nigeria. It can be suggested that the longer the products stay after harvest the more the degree of biodeterioration sets in. There is no doubt that losses can reach 100 %, especially in tomatoes if there is a glut in the market. The amount/quantity of products lost between 20 is so high that efforts have to be made to stern this loss.

Table 1: Estimation of postharvest losses in fruit vegetables

Fruit Vegetable	Region	Fruit Yield (tons/ha)	Estimated Losses (tons/ha)				
			20%	25%	30%	35%	40%
Tomato	SN*	5.00	1.00	1.25	1.50	1.75	2.00
	NN*	20.00	4.00	5.00	5.00	7.00	8.00
Pepper	SN	2.50	0.50	0.63	0.75	0.88	1.00
	NN	3.09	0.62	0.77	0.93	1.08	1.24
Okra	SN	4.80	0.96	1.20	1.44	1.68	1.92
	NN	5.20	1.04	1.30	1.56	1.82	2.08

Source: Adebooye (1997); SN = Southern Nigeria; NN = Northern Nigeria

Table 2: Estimation of postharvest losses in leaf vegetables

Leaf Vegetable	Leaf Yield (tons /ha)	Estimated Losses (tons/ha)				
		20%	25%	30%	35%	40%
Amaranth	26.80	5.36	6.70	8.04	9.38	10.72
Celosia	24.60	4.92	6.15	7.38	8.61	9.84
Solarium	27.20	5.44	6.8	8.16	9.52	10.88
Telfaria	40.40	8.08	10.1	12.12	14.14	16.16

Source: Adebooye (1997)

2.2 Trends and Innovations in Postharvest Activities in Developing Countries

There are several initiatives designed to reduce post-harvest loss in Africa. As highlighted in Table 3. In Nigeria a number of approaches have been introduced to reduce PHL, for instances, Hazard Analysis and Critical Control Point (HACCP) was articulated to implement an effective food safety management system (FSMS) which is critical to the production of safe food from farm to fork (Mortimore and Wallace, 2013). HACCP systems build upon effectively designed and implemented prerequisite food safety programmes and focus on three major key concepts: (a) Identifying significant food safety hazards, (b) Controlling these significant hazards, and (c) Documenting the system (Mortimore and Wallace, 2013). Therefore, HACCP is the process of identifying and assessing product and production-related chemical, microbial and physical hazards and the process of controlling and monitoring them. Proper implementation of the HACCP system provides the framework to produce foods safely and to prove they were produced safely through proper process documentation (Mortimore and Wallace, 2013).

Table 3: Selected post-harvest loss interventions in Africa

Name of intervention	Description	Number of people reached	Quantification of impact
Cowpea Storage Project (Purdue University)	Gates Foundation developed and sold improved bags for cowpeas, amounting to $11.4M in five years from 2007-2011.	1 million bags sold since 2007, out of a projected 1.7 million goals for West and Central Africa. No estimates are available on an actual number of people reached.	Expecting annual income increases of $150 per farmer.
Poverty reduction and women's empowerment project (UNDP)	$19M over four years (2008-2011) was used to establish 600 rural agro enterprises in Burkina Faso, Mali and Senegal.	The goal was to directly impact 0.9 million people in rural areas through improving off-farm livelihoods.	Butter processing Increased household income.
Yam Improvement for Income and Food Security in West Africa (IITA, AGRA)	$12M from the Gates The foundation will engage the International	The goal is to reach 200,000 yam farmers in Ghana and Nigeria.	Overall yam income

	Institute for Tropical Agriculture to improve yam varieties and lower postharvest losses.		Is expected to double.
Hybrid seed and postharvest storage program (USAID, Ethiopia, DuPont)	$3M from DuPont over three years (2013-2015) will distribute improved seeds and increase access to improved postharvest storage.	The goal is to reach 32,000 maize farmers in Ethiopia.	Yields are expected to rise by up to 50% and losses decrease by 20%.
Rwanda Post-Harvest Handling& Storage Project(CARANA,ACDI/VOCA)	USAID is spending $8.6M on a five-year program to support farmers' acquisition of storage and processing equipment, training in postharvest handling, and access to finance.	Supported 37,500 farmers to acquire storage and processing technology; trained 40,000 farmers in Postharvest handling.	Unmeasured.

Source: UK Cooperative Extension Service (2010).

3.2 Post-Harvest Losses Verse Food Security in Nigeria

Nigeria's food insecurity is being aggravated by acute post-harvest losses, which the Federal Government estimates at $12 billion annually (PUNCH, 2020). For a country labelled as the poverty capital of the world, this adds an extremely staggering burden to Nigeria's predicament. Achieving the government's goal of snapping the losses in half will test the country's broken structure to the limits. According to the 2019 Global Hunger Index, Nigeria's case is progressing from a "serious to alarming level" as it scored 29.2 per cent, placing 98 out of 107 countries assessed. It means Nigeria fares better than only nine countries. Take a tomato, a national staple, Nigeria is Africa's second-largest producer with nearly 2.3 million tonnes annually. That makes the country the 14th largest tomato producer globally, but between 40 and 60 per cent of the crop rots away before reaching the market. A 2019 report by the Raw Materials Research and Development Council stated that Nigeria's annual c**o**nsumption is 2.4 million tonnes. To augment the deficit, Nigeria has become the 13th largest importer of tomato products, including canned tomato paste, tomato ketchup and various sauces and canned tomato fruit estimated at $360 million annually.

In essence, Nigeria is highly food insecure, as the losses are replicated in fruits, vegetables, nuts, grains and fish, among others. The Global Food Security Index compiled by the Economist Intelligence Unit ranked Nigeria a lowly 94 out of 113 countries in 2019 with an overall score of 48.4 per cent, a mere 0.7 per cent upgrade from the 2018 score of 47.7 per cent. In contrast, the study puts Singapore, Ireland and the United States as the first three most secure food nations in 2019, scoring 87.4, 84.0 and 83.7 per cent respectively. The agricultural sector is sector contributed 24.6 per cent of the GDP in the second quarter of 2020 (Abacha, 1997). If the current trend of post-harvest losses persists, Nigeria, with an annual population growth rate of 2.58 per cent, faces imminent peril. A report by the United Nations Food and Agriculture Organisation states that around 1.3 billion metric tonnes of food, which is 33 per cent of the total produce, is lost in the post-harvest stage globally; it predicts that if the current practices continue, the loss would be around 2.1 billion metric tonnes in 10 years.

Factors driving increases in food prices in Nigeria are numerous and still very much debated. These include the hike in the price of oil with ripple effects on transportation, fertilizers and processing costs. Improve living standards and urbanisation increase food consumption and demand for meat, fruits and cereals. Decades of under-investment and declining yield in agriculture led to increased demand for food supplies. The state attributed soaring food prices and crisis in 2008 to poor weather affecting major food items such as rice, beans, fruits and cereals. Corporate farmers like Obasanjo Farms Limited attributed the crisis to low productivity and the diversion of food items to industrial purposes.

In bide to understand the intricacy of the supposed existing empirical relationship between PHL and food security, Ewah, (2011) investigated contributorily impact of PHL on food security in an agrarian society of Yakurr, Abi, Obubra, Ikom, Etung, Boki, Ogoja, Yala, Bekwara, Obudu and Odukpani Local Government Areas of Cross River State is in the production and distribution of rice, yam, cassava, plantain banana and fruits grown in commercial quantities. Within this identified region, farmers unanimously affirmed that post-harvest losses are the greatest

challenge to optimum production and income. In major centres of rice production and processing, it has been confirmed that post-harvest losses and leakages are more grievous than other problems experienced by producers as farmers report that at least two out of every ten bags of rice are lost to rodents, birds, pests, locust and through manual harvest (Ewah, 2011)). In addition, rice and yam production and distribution are common within the region, produced in commercial quantity, PHL is largely attributed to poor storage and high incidence of road accidents on badly maintained inter-city highways. Ewah (2011) and Ayantunji (2009) observed that farmer's income has been reduced and labour wasted because of rot. About 30% of yams, cocoyam and fruits rot away because of poor storage facilities, chemicals and technology to prevent rot. Indigenous knowledge systems of preservation cannot withstand existing pressure from cultivation and preservation. Ewah, (2011) reiterated that the high cost of limited transport facilities to convey products from farmlands to local and intercity markets increases overhead costs as shown in Table 4. As observed in 2008 after 15 years, Table 4 underestimates the current situation in Nigeria.

Table 4: Average cost of transportation and distribution of yams between Cross River and Benue States regions of Nigeria (September–December 2008).

Destination Market	**Purchasing Price quantity per ten-tonne lorry (₦)**	**Carriage cost per ten-tonne lorry (₦)**	**Produce tax (₦)**	**Wholesale price (N)**	**Surplus value (₦)**
Zaki Biam to Calabar	150,000.00	80,000.00	20,000.00	300,000.00	50,000.00
Ogoja to Portharcourt	110,000.00	100,000.00	14,000.00	271,000.00	56,000.00

Source: Ewah, (2011)

3.2 .1 Food Security and the Challenges of Post-Harvest Losses in Nigeria

Sawyer (2009) opined that policymakers must make sure that post-harvest losses are drastically reduced. Unless this is achieved, the export of cassava chips will further induce soaring food prices and insecurity in Nigeria. Equally proximate to soaring food prices in Nigeria, is the lack of storage facilities to preserve garri and akpu. The prices of cassava products are unstable and ever-increasing because demand is higher than supply. The absence of silos to preserve garri and cassava chips promotes losses and reduces production targets. In Nigeria, existing eleven national silos are often restricted to grain storage. Most silos have been abandoned since 1983.

Food stuff such as yams, bananas, plantains, carrots, onions, tomatoes and others are largely wasted because of the absence of storage facilities. The lack of adequate planning and financing to purchase and preserve surplus to last throughout the off-season periods. This scenario creates scarcity during off-season periods and largely explains seasonal and sustained increases in prices often beyond the reach of ordinary Nigerians. From the above examination of production, exchange and preservation of food items in Nigeria, it is clear that post-harvest loss is the greatest challenge to food security rather than climatic conditions and diversion of food items for industrial purposes as alleged by the state and some nascent farmers in Nigeria (Table 5).

Table 5: Post Harvest Losses of Food Items in Nigeria.

S/No	**Crops Staples**	**Botanical Name**	**Percentage of Post Harvest Losses**
Grains			
1	Rice	Oryza sativa	30%
2	Beans		30%
3	Maize	Zea maize	30%
4	Groundnut		30%
5	Beneseed		30%
6	Suya Beans	Glycie max	30%
7		Anacardium occidentiate	
Fibre/Root Crops			
8	Yams	Dioscoria	25%
9	Cassava	Manihot esculentia	25%
10	Bananas		30%
11	Plantains		30%
12	Carrots		30%
13			40%
FRUITS			
14	Tomatoes	Lycopesicum Esculentum	
15	Onions	Alum Cepa	40%

16	Oranges		70%
17	Mangoes	Magnifera Indica	70%
18	Paw-Paw		70%
19	Apple		10%
20	Bush-mango		10%
20	Coconut	Coco nucifera	20%

Sources: Ekpu (2009)

4.0 Conclusion

This review has successfully gained insight into prevailing issues that face postharvest as well as food insecurity in Nigeria. The absence of silos to preserve garri and cassava chips promotes losses and reduces production targets. In Nigeria, existing eleven national silos are often restricted to grain storage. In the light of the aforementioned submission, it is clearer that post-harvest loss is the greatest challenge to food security rather than climatic conditions and diversion of food items for industrial purposes as alleged by the state and some nascent farmers in Nigeria**.** In essence, Nigeria is highly food insecure, as the losses are replicated in fruits, vegetables, nuts, grains and fish, among others. The Global Food Security Index compiled by the Economist Intelligence Unit ranked Nigeria a lowly 94 out of 113 countries in 2019 with an overall score of 48.4 per cent, a mere 0.7 per cent upgrade from the 2018 score of 47.7 per cent. Equally relevant to food production in Nigeria is the development of infrastructure that will promote production, circulation and storage. Infrastructure relevant to agricultural production includes roads, silos, energy and transportation. The improved transport system will help to evacuate food crops from production centres to exchange and storage centres. To achieve these results An efficient transport system must be put in place and this will consequently improve the profit margins of farmers and processors. To boost economic growth in Nigeria, the State should key into the Yokohama action plan of 2008 which encouraged building, roads, ports, energy, water systems, and other infrastructure vital for expanding the Nigerian economy. Millennium Development Goals (MDGs) was adopted by world leaders in 2008 to reduce global poverty and promote the well-being of humankind (Harsch 2008).

REFERENCES

Abacha, S., General (1997), National budget of the Federal Republic of Nigeria, *The Guardian Newspaper,* Jan. 14, 1997, Lagos, 20 -22

Adebooye, O. C. (1997). Proximate Composition and Nutrient Analysis of Six Selected Leaf

Ayantunji, O. (2009, December 23). Why garri is costly. The Nation Newspaper.

Batholomew, S. (2003). Reducing global hunger. *In Cross River Newsletter* Vol. 10 No. 9. United States Embassy, Nigeria.

Cantwell, M. (2011). Postharvest Handling Maintaining Quality and Safety for Farmers' and other Local Markets. Available from http://postharvest.ucdavis.edu (accessed 9/11/2013).

Central Bank of Nigeria (CBN) (1994). Major Agricultural Products of Nigeria. *Annual Report,* December 1994. 142 p.

Ekpu, R. (2009, August 3). The looming food crises. Newswatch Special Colloquium Edition

Ewah, J. O. (2011). Food Security and the Challenges of Post Harvest Waste in Nigeria. *A Journal of Contemporary Research,* 8(3), 292-305, 2011.

Ewah, J. O. (1992). The Development of Banana Trade in Boki Society of Upper Cross River Region of Nigeria 1970 – 1990. Unpublished M.A Thesis Department of History, University of Calabar.

FAO (1986). World Agricultural Production, Food and Agricultural Organisation of the United

FAO (2006). Strengthening National Food Control Systems: Guidelines to Assess Capacity Building Needs. Available from *ftp://ftp.fao.org/docrep/fao/009/a0601e/a0601e00*.pdf (accessed 14/11/2013).

FAO (2006). Strengthening National Food Control Systems: Guidelines to Assess Capacity Building Needs. Available from ftp://ftp.fao.org/docrep/fao/009/a0601e/a0601e00.pdf (accessed 14/11/2013).

Grebitus, C., Jehsen, H. E., Roosen, J. and Serbranek, J. G. (2013). Fresh Meat Packaging: Consumer Acceptance of Modified Atmosphere Packaging Including Carbon Monoxide. *Journal of Food Protection*, 76, 99-107.

Harsch, E. (2008). Japan summit promotes vibrant Africa. Africa Renewal Vol. 22 No. 2.

Kitinoja, L., Saran, S., Royb, S. K and Kaderc A. A. (2011). Postharvest Technology for Developing Countries: Challenges and Opportunities in Research, Outreach and Advocacy Perspective. *Journal of Science and Food Agriculture,* 91 (597–603).

Mohammed, S. F., Ismail, B. B. and Gimba, K. I. (2017). Postharvest and Food Safety: Contemporary Issues and a Future Direction for the Nigerian Food Supply Chain. Annals. *Food Science and Technology*. www.afst.valahia.ro.

Mortimore, S. and Wallace, C. (2013). HACCP: a Practical Approach (3rd ed.) UK: *Springer Publishers Ltd.* Nations, Rome, Italy.

Sani, M. (2003). With RUSEP: Garri turns money spinner in Abia State. *Cross River News Letter*. Vol. 10 No. 9. United States Embassy, Nigeria.

Sawyer, S. (2009). Averting looming food crises. *Tell News Magazine.*

UK Cooperative Extension Service (2010). Good Agricultural Practices (GAP) Available from *http://www.uky.edu/Ag/CCD/gap.pdf* (accessed 9/11/2013).

Vegetables of South West Nigeria, *Ife J. Agric*. 18 (1 & 2): 56 -62.

PAPER 5 - EFFECT OF CERAMIC WASTE TILES ON SOIL STRENGTH AND INDEX PROPERTIES OF LATERITIC SOIL

E. A. Nyebe[1*], J. E Sani[2], G. Moses[3], I. Ibrahim[4] B. Aniekpeno[5], M. Yusuf[6]

[1,] Department of Civil Engineering, Ahmadu Bello University, Zaria, Kaduna, Nigeria.
[2, 3, and 6] Department of Civil Engineering, Nigerian Defence Academy, Kaduna, Nigeria
[5] Engineering Unit, Tectonics Engineering, and Consult Limited, Nigeria

[*]Email: esther.nyebe31@gmail.com

ABSTRACT
Lateritic soil strength and index properties are crucial in selecting construction materials. examination of the effect of ceramic waste tile (CWT) on lateritic soil was conducted. Lateritic soil combined with CWT ranged from 0 to 8% by increments of 2%. Atterberg limit tests were conducted to determine the index properties, whereas compaction, California bearing ratio (CBR), and unconfined compressive strength (UCS) tests were carried out to assess this effect on the strength properties of the modified soil. Results indicate that the plasticity index (PI) and liquid limit (LL) are 18.65% and 44.47%, respectively. For the compaction test, when 6% CWT-lateritic soil, optimum moisture content (OMC) increased to a peak value of 24.7 and 19.75%, utilising British Standard Light (BSL) and British Standard Heavy (BSH) compaction effort, respectively. An increase in CWT resulted in a decrease in maximum dry density (MDD). When applying BSL and BSH compaction efforts, the MDD of the lateritic soil was 1.68 and 1.87 mg/m3, respectively. With the addition of 6% CWT, the MDD values dropped to 1.32 and 1.67 mg/m3, respectively. Based on the findings, lateritic soil can be strengthened to be used as a sub-base material by adding 6% of CWT.

KEYWORDS: Ceramic tile, Clay, Lateritic soil, Strength, Waste

1. INTRODUCTION

The world population is expanding, especially in emerging countries, which has increased demand for infrastructure such as housing complexes, railroads, and roads. The weight of large constructions requires soil with a higher degree of stability; in theory, any construction relies on soil stability, either directly or indirectly. One of these types of soils that is frequently found in Nigeria is the lateritic soil (Obianyo *et al.*, 2021).

Lateritic soils, which are typically covered in concretions rich in sesquioxide, are created as byproducts of tropical weathering processes and are typically found in the leached soils of the humid tropics (Adedokun, and Oluremi, 2019; Ayoola & Agbude, 2023). According to Nichiri and Adetayo (2019), soils with a silica-to-sesquioxide ratio (SiO_2/ (Fe_2O_3 + Al_2 O_3)) of less than 1.33 are classified as laterites, those with a ratio between 1.33 and 2.00 are classified as lateritic soil, and soils with a ratio over 2.00 are defined as non-lateritic soils. Quartz, kaolinite, and iron-magnesium-manganese (the amphibole group) comprise most lateritic soil. Since it is readily available in many tropical areas and is inexpensive to buy and transport, lateritic soil is frequently used in road construction projects. However, these soils might need to be stronger in their natural state to build highways, dams, and foundations. Therefore, lateritic soils should be stabilised to achieve the necessary geotechnical specifications for the intended engineering application (Obianyo *et al.*, 2021).

In the correction of the soil's poor engineering qualities or the maintenance of the stability of the soil mass, soil stabilisation helps to ensure enhanced soil performance. It transforms the soil into an improved construction material (Adeboje *et al.*, 2020). The transformation process frequently results from applying stabilisers such as lime, sawdust ash, ceramic dust, regular Portland cement, or a mixture of these. These additives can stabilise the soil efficiently, producing an acceptable outcome. Research has demonstrated that the efficacious application of various additives, such as fly ash, coconut husk ash, rice husk, sawdust, and Portland cement, enhances the soil's engineering characteristics for construction (Onakunle *et al.*, 2019; Consoli *et al.*, 2021; Etim *et al.*, 2021).

However, several investigations and studies have revealed that lateritic soils can be improved by using inexpensive, locally accessible materials derived from industrial and agricultural wastes. This aims to lower stabilisation expenses associated with traditional stabilising agents like cement and CO_2 emissions associated with the stability of the cement manufacturing process (Consoli *et al.*, 2021).

It has been demonstrated that using recycled solid waste materials in crushed or amorphous forms as geomaterials is a technically reliable practice in geotechnical and materials engineering (Consoli *et al.*, 2021). Waste materials are used to stabilise or treat clay soils to improve their mechanical, structural, geotechnical, and physical properties. To improve poor soils so that engineering infrastructures can be built, various methods and quantities of ash obtained from the direct combustion of the parent solid waste materials—palm bunch-, palm kernel shell-, bagasse-, periwinkle shell-, paper-, eggshell-, and rice husk- ash—have been applied (Onyelowe *et al.*, 2019).

Due to the high generation rate of these waste products, industrial waste management is a critical issue. Industrial wastes may be readily utilised to stabilise soil, which solves the issue of disposing of them safely for the environment. One such waste item that can be utilised to improve the qualities of weak lateritic soils is stabilisation using ceramic waste tiles. Ceramic waste materials are widely accessible in various manufacturing facilities and building sites. Utilising ceramic waste thus addresses the issue of their disposal while also improving the quality of the soil (Onakunle *et al.*, 2019; Onyelowe *et al.*, 2019; Saber & Iravanian, 2022).
Ceramics can be recycled, ground, or broken down into its original clay form with a flat tamping instrument or a heavy hammer. The waste ceramic particles are pozzolanic and not dangerous (Onyelowe *et al.*, 2019; Saber & Iravanian, 2022). Ceramic dust has the advantages of being an inexpensive, ecologically friendly technique of collection and processing, as well as a robust, sustainable material that can be used in highway construction facilities. In addition, a lot of tile and ceramic trash is produced during the destruction of different buildings, and this garbage needs to be disposed of properly. Using ceramic waste as stabilising admixtures for clay soils during construction can be an environmentally appropriate means of disposing of the waste (Consoli *et al.*, 2021; Saber & Iravanian, 2022).
This study aims to evaluate the effect of CWT on the strength and index properties of lateritic soil.

2. THEORETICAL ANALYSIS

Construction and demolition waste account for a significant amount of pollution worldwide, and ceramic products contribute a substantial proportion of this waste (Saber & Iravanian, 2022). In Nigeria, most landfills are littered with enormous quantities of broken ceramics generated during the production, installation, and demolition phases (Adeboje *et al.*, 2020). Several studies in the literature have reported using ceramic wastes as admixtures for stabilisation (Cabalar *et al.*, 2017; Meepon *et al.*, 2019; Arya & Soorya, 2020; Mahmud, 2021).

In the analysis of ceramic waste use in road applications, Cabalar *et al.* (2017) mixed ceramic waste at different concentrations ranging from 5% to 30% at 5% increments and found that this increased CBR and MDD. Because of an observed reduction in UCS and swelling potential, researchers advocated using ceramic waste as a substitute soil stabiliser. Meepon *et al.* (2019) used ceramic waste to boost the laterite soil properties for the suburban road by enhancing it by 3%. According to the researchers, the plasticity index (PI), swelling percent, LL, and PL all declined. On the other hand, the MDD and CBR values were found to have increased.
The impact of ceramic dust on the strength characteristics of clayey soil was investigated by Arya and Soorya (2020). According to the test results, there was a noticeable difference in the Atterberg limits when varying the quantity of ceramic dust added to the clayey soil under study. As a result, the Atterberg limits fell. The percentage of ceramic dust increases with a fall in the liquid limit, plastic limit, and plasticity index. The percentage of ceramic dust increases along with the UCS. Conversely, a rise of up to 20% in ceramic dust was associated with an increase in the unconfined compressive strength value. They suggested using up to 20% of ceramic dust to improve the geotechnical characteristics of clayey soil and maximise stabilisation.

Mahmud (2021) studied how cement and CW worked together to affect the geotechnical properties of clayey soil. After curing for 90 days, it concluded that the maximum UCS in a clay composite is 30% ceramic waste and 6% cement. The increase in UCS is attributed to the generation of cementation compounds and cation exchange, reducing the porosity of treated soil.

3. MATERIALS AND METHODS

3.1 Materials

This study uses lateralitic soil and ceramic waste tiles. Both materials were obtained locally in Nigeria.
CWT was used in powdered form with particle sizes between 20 and 45 μm.

3.2 Methods

3.2.1 Soil Preparation

The preparation process of the CWT stabilised lateritic soil involves sieving the soil through a 0.425 mm sieve for the Atterberg limits test. In contrast, compaction, CBR, and UCS were sieved through 4.76 sieves. The modified soil samples were mixed with CWT by replacing 2%, 4%, 6%, and 8% of its weight with CWT.

3.2.2 Index Properties and Atterberg Limits Test

Index tests were performed on untreated soil using the specifications given in BS 1377: Part 2 (1990). While Atterberg limit test determines the LL, PL, and PI for each of the untreated and modified soils. The test was conducted according to the guidelines outlined in BS 1377: Part 2 (1990).

3.2.3 Compaction Test

A compaction experiment was conducted for both natural and modified soil (i.e., at differing CWT content), using BSL and BSH compaction energy, all by BS 1377: Part 4 (1990) and BS 1924 (1990), respectively.
3 kg of soil was utilised with 5% water introduced at each step to compact the natural soil. A 2.5 kg rammer dropping over a height of 300 mm (BSL energy) and a 4.5 kg rammer dropping over a height of 450 mm (BSH energy) were used to compact the material into a 1000 cm^3 (of mass ml); in three layers of each receiving 27 blows. After compacting, the collar is removed, and the compacted soil is levelled with the top section of the mould using a straight edge and weighed. After that, two tiny samples were removed from the mould and cut open to extract a tiny soil sample for measuring the moisture content. After that, the sample was removed from the mould, crumbled, and another five per cent of water was added. This process was repeated until at least five samples were obtained, each with a moisture content sample collected. Afterwards, each compacted layer's bulk density in mg/m^3 was determined using (1):

$$\rho = \frac{m_2 - m_1}{1000} \quad (1)$$

Where ρ is the bulk density, m_1 is the mass of the mould, and m_2 is the mass of the mould with the compacted sample.

The dry density was also calculated using (2):

$$\rho d = 100\rho/(100 + w) \quad (2)$$

Where *w* is the moisture content of each compacted layer?

The dry density values derived from (2) were plotted against their corresponding moisture contents, and the MDD was calculated as the peak point on the resulting curves.

The optimum moisture content (OMC) is determined by deducing the value corresponding to moisture contents at MDD from the plot of dry density against moisture contents.

3.2.4 California Bearing Ratio (CBR) Test

The CBR tests assessed the lateritic soil samples' strength and bearing capacity in compliance with BS 1377: Part 4 (1990) specification. The soil's capacity to support weight was assessed using the CBR test, which was used to evaluate the soil's suitability as a building material for roads. The degree of strength enhancement can be assessed using CBR to support the use of loose or deficient soil material for the construction of roads.

3.2.5 Unconfined Compressive Strength (UCS) Test

The soil sample was subjected to UCS tests using the BSL and BSH energy levels following BS 1377: Part 4 (1990). To replicate field conditions during the construction of roads, the control and enhanced soil samples (sample with CWT) were compacted in a 1000 cm^3 mould at a moisture content compared to the OMC of the control sample. After removing the specimens from the mould, the cylinder's top was appropriately trimmed to create a cylinder that measured 38 mm in diameter and 76 mm in height. After being cured for 7-, 14- and 28 days at a temperature of 26°C, the specimens from the compaction mould were crushed using the machine. A compressive force was applied to the specimen at a strain-controlled rate of 0.10 %/min. Results of the axial deformation and failure modes were recorded simultaneously at fixed intervals until the specimen was crushed. Using (3), the UCS was obtained.

$$UCS\ (\delta) = PCr\frac{(100 - \varepsilon\%)\ \text{x}\ 10^3}{100\text{Ao}} \quad (3)$$

4. RESULTS AND DISCUSSION

4.1 Mineralogy of Soil Sample

The oxide composition of lateritic soil and CWT carried out at Crossroads Scientific Laboratories Centre Kaduna are presented in Table I. The result of the oxide composition shows that the lateritic soil contains a higher percentage of SiO_2(41.05%) and very low CaO (0.23%). In comparison, CWT, on the other hand, which is used to stabilise the lateritic soil, contains a high percentage of CaO (72.773%), which, on reaction to lateritic soil, will undergo hydration and form $Ca(OH)_2$, leading to the formation of cementitious compounds such as calcium silicates and aluminates binding the soil particles together to improve cohesion and strength thereby enhancing the problematic soil by AASHTO classification of Soils, the lateritic soil falls under the A-6 category based on results obtained from the Atterberg limits test.

Table I: Oxide Composition of the Lateritic Soil and CWT

Oxide Composition	Lateritic (%)	CWT (%)
SiO_2	41.05	11.713
Al_2O_3	24.16	5.740

MgO	0.21	1.843
K_2O	0.34	0.824
CaO	0.23	72.773
TiO_2	0.39	0.397
P_2O_5	1.32	0.000
SO_3	1.04	1.000
V_2O_5	0.098	0.045
Fe_2O_3	10.16	4.321
MnO	ND	0.055
NiO	0.008	0.003
Cr_2O_3	0.02	0.000
Na_2O_3	11.872	0.000
LOI	19.35	

4.2 *Atterberg Limits Test*

Fig. 1 shows the variation of the Atterberg limits of the control and the CWT-stabilised lateritic soil. The LL was reduced as the CWT content increased. This could be attributed to flocculation and agglomeration caused by cation exchange reactions in which additive cations reacted with laterite ions of lower valence (Yohanna *et al.*, 2022). The LL was reduced by 14.6% at 8% CWT content compared to the control sample.

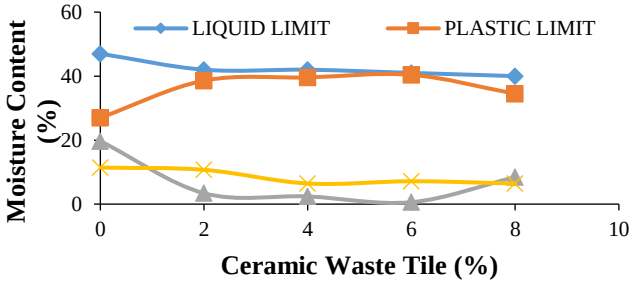

Fig. 1 Variation of CWT Content for Atterberg limits

A maximum PL value of 41% was observed for soils with CWT content of 6% before dropping to 35% at 8% CWT content. Fig. 1 also displays the PI of lateritic soil with CWT content. The PI generally declined with an increase in CWT content. The linear shrinkage trended similarly to the LL, showing a general decline as the CWT content increased. The shrinkage limit and PI show a declining trend, suggesting that the CWT-modified soils are less prone to shrinking and swelling (Adeboje *et al.*, 2020). Also, CaO reduces the plasticity of the lateritic soil by modifying its mineralogy and improving soil structure. The findings for the Atterberg limits in this study are consistent with (Onakunle *et al.*, 2019 Adeboje *et al.*, 2020; Saber & Iravanian, 2022).

4.3 Compaction Test

4.3.1 Optimum Moisture Content (OMC)

The variation of OMC of the CWT stabilised lateritic soil from 0 - 8% is shown in Fig. 2. For BSL and BSH compaction effort, the OMC of the control sample (0%) was 20.2% and 14.2%, respectively. It was observed that there was an increase in the OMC with an increase in CWT content for the modified soil. Peak OMC values of 24.7% and 19.75% using BSL and BSH compaction effort were obtained at 6% CWT content. The presence of CaO in the CWT aids in enhancing particle bonding. It reduces voids within the soil matrix, resulting in moisture absorption by the waste tile during the compaction process. As the CWT content in the soil increased, more water was needed to lubricate the soil surface, increasing the OMC. This suggests that the CWT has a high water absorption capacity, thereby influencing the increase in OMC.

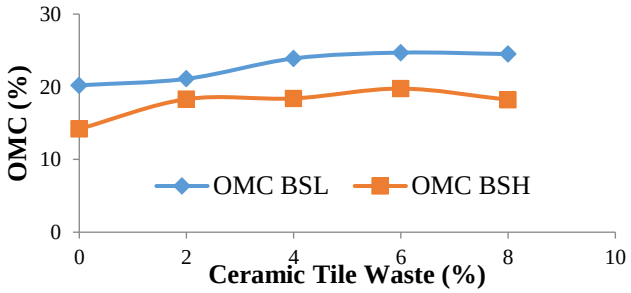

Fig. 2 Variation of CWT Content for OMC

4.3.2 Maximum Dry Density (MDD)

The variation of the MDD of the control and the CWT stabilised lateritic soil is seen in Fig. 3. The BSL and BSH compaction effort indicate that the MDD of 0% CWT lateritic soil was 1.68Mg/m^3 and 1.87g/cm^3 respectively. At the same time, a decrease was observed as CWT increased for the modified soil until the modified samples had 8% CWT content, where a slight increase was recorded. Peak MDD values of 1.62 Mg/m^3 and 1.77 Mg/cm^3 using BSL and BSH compaction effort were obtained at 2% CWT content before decreasing subsequently. The general decrease in MDD, with an increase in CWT content, could result from an increase in voids, thereby reducing the density of the compacted soil mass. This decrease can also result from the physiochemical reaction between the increasing moisture content and the CWT content in the CWT-stabilised lateritic soil matrix. A similar trend was observed in Fatoye (2021).

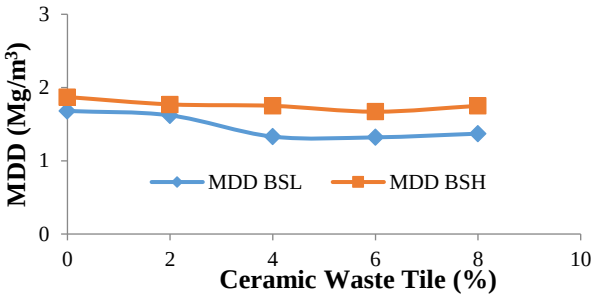

Fig. 3 Variation of CWT Content for MDD

4.4 California Bearing Ratio Test

The variation of the CBR for the 0% CWT and the CWT stabilised lateritic soil is illustrated in Fig. 4 and Fig. 5, respectively. For Fig. 4, BSL compaction effort, an increase in the CBR value, with an increase in CWT content, was observed until a peak value of 19% at 4% CWT content and then a decline afterwards. However, for the BSH compaction effort, peak values of 30% were recorded at 6% CWT content. A similar trend was observed for the soaked CBR samples, as seen in Fig. 5. The reason for this increase can be attributed to the improvement in the intergranular matrix of the compacted soil mass as a result of an enhanced interaction between the soil grains and the CWT (Akrawi, 2023). Other reasons for the increase can be attributed to the increase in the stiffness of the stabilised soil due to the higher stiffness of CWT and a decrease in the plasticity index resulting from the addition of CWT (Adeboje *et al.*,2020).

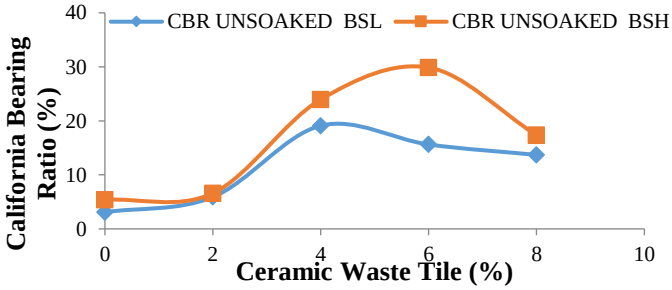

Fig. 4 Variation of CWT Content for Unsoaked CBR

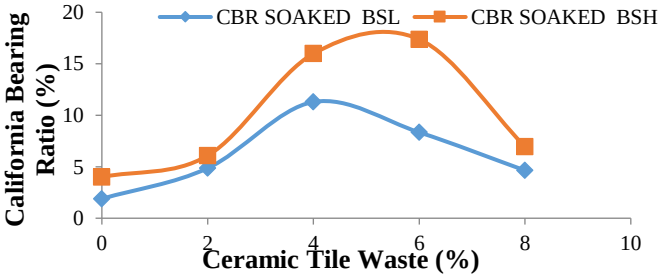

Fig. 5 Variation of CWT Content for Soaked CBR

4.5 Unconfined Compressive Strength Test

The variation of the UCS for the control and the CWT stabilised lateritic soil after the 7-, 14-, and 28-day curing period is shown in Fig. 6, 7, and 8, respectively. For seven days of curing, an increase in the UCS

strength was observed from 337 kN/m^3 and 653 kN/m^3 for the control samples, and subsequently, for 14 and 28 days, an increase for BSL and BSH were 418 and 810 kN/m^3 and 601 and 1007 kN/m^3 respectively. This can be attributed to strength development due to curing and compaction effort. Meanwhile, in the CWT-modified samples, the highest UCS value was noticed when the percentage of CWT was 6%, 368 and 753 kN/m^3, using BSL and BSH compaction effort, respectively. A similar increment in USC values was recorded for the specimens subjected to 14- and 28-day curing duration at 6% CWT content for BSL and BSH as 438 and 907 kN/m^3 and 913 and 1008 kN/m^3, respectively. The increase in the UCS with the addition of CWT can be attributed to the production of pozzolanic compounds and the exchange of cations, which resulted in the enhancement of the UCS strength of CWT-modified lateritic samples (Rathore & Tiwari, 2023). A similar trend of improved UCS values for CWT-modified clay soils has been reported by (Al-Bared *et al.*, 2018a Al-Bared *et al.*, 2018a Rathore & Tiwari, 2023). Based on results obtained for the UCS for BSH, 6% CWT meets the requirement for a sub-base of 687 kN/m2, as reported by (Ingles & Metcalf, 1990).

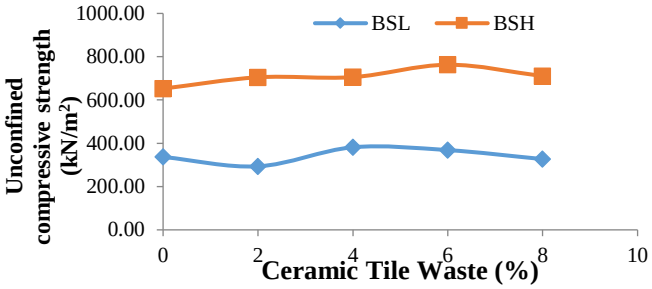

Fig. 6 Variation of CWT Content for UCS values after 7 days curing period

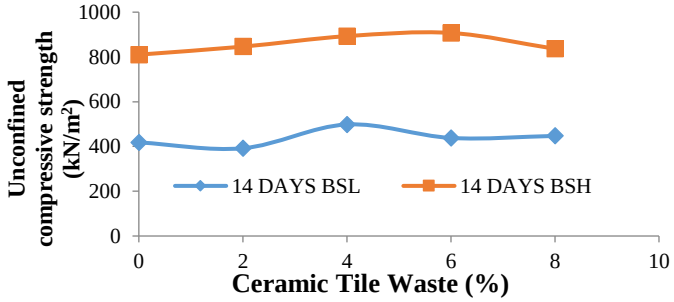

Fig. 7 Variation of UCS for UCS values after 14 days curing period

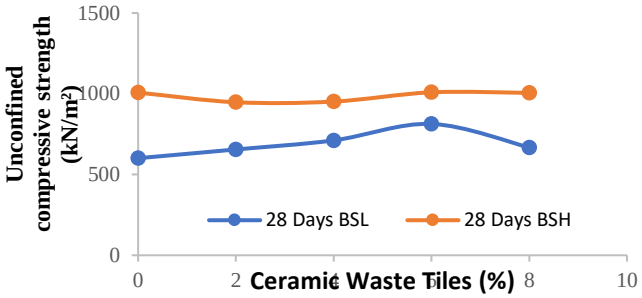

Fig. 8 Variation of UCS with CWT Content for UCS values after 28 days curing period

The failure plane pattern is observed in Fig 9, where the bulging shape indicates that of the untreated lateritic soil samples, whereas the pattern obtained for the CWT-modified samples is sheared in a different pattern. This is consistent with research conducted by (Wahab et al., 2021).

Fig. 9 Failure plane for 14-day curing a) shearing axially deformation b) bulging shape

5. CONCLUSION

This study investigated the effect of ceramic waste tiles (CWT) on lateritic soil's strength and index properties. The study indicates that CWT can improve lateritic soil's strength and index properties. It was observed from the study that the parameters (Liquid Limit, Plasticity index, and Shrinkage index) of the Atterberg limits of lateritic soil modified with CWT generally decreased with an increase in CWT content, except for the plastic limit, which increased with higher CWT content. For the compaction characteristics, it was observed that the OMC increased with an increase in CWT content, while a corresponding decrease was recorded for the MDD with an increase in CWT content. Improvements were also recorded in the strength properties of CWT-modified lateritic soils. The study has shown that adding CWT to lateritic soil strengthens and improves it to prevent potential adverse effects from water. The results indicate that including 6% CWT significantly improves the quality of lateritic soil, making it suitable for building a subbase pavement layer on roads with low traffic volumes. Further research is needed to determine how adding CWT in combination with other elements affects the strength and index of lateritic soil, mainly when used for road construction.

REFERENCES

Adeboje, A. O., Kupolati, W. K., Sadiku, E. R., Ndambuki, J. M., Owolabi, A. O., & Kambole, C. (2020). Stabilisation of lateritic soil with pulverised ceramic waste for road construction. *International Journal of Environmental Engineering*, *10*(3), 221-242.

Adedokun, S. I., & Oluremi, J. R. (2019). A Review of The Stabilization of Lateritic Soils with Some Agricultural Waste Products. *Acta Technica Corviniensis-Bulletin of Engineering*, *12*(2).

Akrawi, M. S. Y. (2023). Utilising ceramic dust to improve soil geotechnical properties. *Nasaq*, *39*(7).

Al-Bared, M. A. M., Harahap, I. S. H., & Marto, A. (2018). Sustainable strength improvement of soft clay stabilised with two sizes of recycled additive. *GEOMATE Journal*, *15*(51), 39-46.

Al-Bared, M. A. M., Marto, A., Latifi, N., & Horpibulsuk, S. (2018). Sustainable improvement of marine clay using recycled blended tiles. *Geotechnical and Geological Engineering*, *36*, 3135-3147.

Ayoola, A., & Philip, A. (2023). Stabilisation of Lateritic Soil for Road Application Using Lime and Cow Bone Ash. *Journal of Engineering Research and Reports*, *25*(6), 109–121.

B. S. 1377:1990. Methods of Test for Soils for Civil Engineering Properties: Classification tests and determination of geotechnical properties. British Standard Institution: London, UK.

B. S. 1377:1990. Methods of Test for Soils for Civil Engineering Properties: Compaction-related tests. British Standard Institution: London, UK.

B. S. 1924:1990. Methods of Testing for Stabilized Soils. British Standards Institute: London.

Cabalar, A. F., Hassan, D. I., & Abdulnafaa, M. D. (2017). Waste ceramic tiles are used for road pavement subgrade. *Road Materials and Pavement Design*, *18*(4), 882-896.

Consoli, N. C., Párraga Morales, D., & Saldanha, R. B. (2021). A new approach for stabilisation of lateritic soil with Portland cement and sand: strength and durability. *Acta Geotechnica*, *16*, 1473-1486.

Etim, R. K., Ekpo, D. U., Udofia, G. E., & Attah, I. C. (2022). Evaluation of lateritic soil stabilised with lime and periwinkle shell ash (PSA) admixture bound for sustainable road materials. *Innovative Infrastructure Solutions*, *7*, 1-17.

Fatoye, J. A. (2021). *Evaluation of Strength Characteristics of Low Plastic Clay Soil Treated with Ceramic Dust* (Doctoral dissertation).

Ingles, O.G., & Metcalf, J.B. (1990). Soil stabilisation: principles and practice.

Mahmud, M. B. (2021). *Effect of Ceramic Waste on Geotechnical Properties of Cement Stabilized Clay Soil* (Doctoral dissertation).

Meepon, I., Voottipruex, P., & Teerawattanasuk, C. (2019). Marginal lateritic soil treated using ceramic waste for rural road application. *GEOMATE Journal*, *16*(53), 70-77.

Nnochiri, E. S., and Adetayo, O. A. (2019). Geotechnical properties of lateritic soil stabilised with corn cob ash. *Acta Technica Corviniensis-Bulletin of Engineering*, *12*(1), 73-76.

Obianyo, Ifeyinwa Ijeoma, Assia Aboubakar Mahamat, Esther Nneka Anosike-Francis, Tido Tiwa Stanislas, Yang Geng, Kennedy Chibuzor Onyelowe, Shola Odusanya, Azikiwe Peter Onwualu, Alfred B. O. Soboyejo, and Ramon Fernando Colmenares. (2021). *Performance of Lateritic Soil Stabilized with Combination of Bone and Palm Bunch Ash for Sustainable Building Applications* Cogent Engineering, 8(1), 1921673.

Onakunle, O., Omole, D. O., & Ogbiye, A. S. (2019). Stabilisation of lateritic soil from Agbara Nigeria with ceramic waste dust. *Cogent Engineering*, *6*(1), 1710087.

Onyelowe, K. C., Bui Van, D., Nguyen Van, M., Ezugwu, C., Amhadi, T., Sosa, F., ... & Alaneme, G. (2019). Experimental assessment of subgrade stiffness of lateritic soils treated with crushed waste plastics and ceramics for pavement foundation. *International Journal of Low-Carbon Technologies*, *14*(2), 187–204.

Rathore, P., & Tiwari, S. K. (2023). Soil Stabilisation using Ceramic Waste: An Experimental Study. *Journal of Mining and Environment*, *14*(1), 47-65.

Saber, S.A., & Iravanian, A. (2022). Using Waste Ceramic Dust in Stabilization of Clay Soils. *International Journal of Sustainable Construction Engineering and Technology*, *13*(1), 68-80.

Arya, S.M., & Soorya, S. R. (2020). Improvement of Strength of Clayey Soil Using Ceramic Dust. *International Journal of Scientific Research and Engineering Development*, *3*.

Wahab, N.A.; Roshan, M.J.; Rashid, A.S.A.; Hezmi, M.A.; Jusoh, S.N.; Nik Norsyahariati, N.D.; Tamassoki, S. (2021). Strength and Durability of Cement-Treated Lateritic Soil. Sustainability, 13, 6430

Yohanna, P., Johnson, P., Victor, B. P., Badamasi, A., Mije, F. G., Ako, T., & Bassey, A. B. (2022). Evaluation of Geotechnical Properties of Black Cotton Soil Reinforced with Sisal Fibre for Waste Containment Application. *Engineering Science & Technology*, 151-168.

PAPER 6 - OPTIMIZATION OF THE EXTRACTION OF KERNEL OIL FROM TWO SPECIES OF MANGO (*MANGIFERA INDICA*) AND ITS CHARATERIZATION FOR POTENTIAL AS BIODIESEL

Ugwoke A. O.[1]*, K. I. Omoniyi[2] and S. S. Dalhatu[3]

[1]Department of Chemistry, Nigeria Police Academy, Wudil, P.M.B. 3474, Kano State, Nigeria
[2]Department of Chemistry, Ahmadu Bello University, P.M.B. 06, Zaria, Nigeria
[3]Department of Pure and Industrial Chemistry, Bayero University, Kano, Nigeria
*Email: augustinaaroh@yahoo.com

ABSTRACT
The paper presents the optimization of the extraction of kernel oil from two species of mango (*Mangifera indica*) and their physico-chemical analysis, towards serving as potential biodiesel in the clamour for renewable energy sources. The mix-ratio, operating temperature and heating time were optimized using One Factor at A Time (OFAT) with n-hexane as solvent by Soxhlet extraction. The ratio of kernel : n-hexane of 1:3 had the highest percentage oil yield (6.67±0.009 – 9.60±0.012%) compared to the 1:1 and 1:2 ratios, for the two mango species (Cherry and Peach) at 6 hrs and 60 ºC. At the optimized mix-ratio, increasing the heating time from 4 to 8 hrs generally resulted to steady increase in the % (w/w) oil yield from 4.00±0.002 – 13.01±0.006% for the Cherry cultivar and 3.93±0.004 – 12.60±0.009% in Peach. Heating temperature significantly elevated the oil extraction process at $p < 0.05$ (One way ANOVA); with the optimum taken as 70ºC. The kernel of Cherry mango had higher % oil yield; though not significantly higher than the counterpart. The studied kernel oil has pale colour, pH 5.9 – 6.1, melting point 31.5±0.5 (Cherry) and 31.7±0.3 (Peach), flash point 263.0 ºC, refractive index 1.440 - 1.445, specific gravity at 20ºC of 0.900 – 0.908, solidification temperature 24 ºC, pleasant odour, acid value 6.90 mgKOH/g, viscosity at 40ºC was 39.25 MPa, saponification value 205.0 – 207.5 mg KOH/g, iodine value 40.1 gI/100g oil and ester value of 198.0 – 202.2 mg KOH/g. Generally, Cherry mango had higher oil yield than Peach. The result showed that mango tree plantation aside meeting the nutritional and medicinal needs can serve as a potential source of biodiesel for ameliorating global warming.

***KEYWORDS*:** Renewable energy, mango curtivar, mango kernel oil , global warming

1. INTRODUCTION

Mango (*Mangifera indica*) is a member of the *Anacardiaceae* group. Mangos are commonly consumed in the seasons of harvest, though the hybrid cultivars elongate their availability. However, consumers of the peels and pulps and mango processing sector usually discard the endocarp (seed kernel) (Kittiphoom et al., 2013). Depending on the cultivar, mango seed makes up 35–55 percent of the fruit (Bhalerao et al., 1989). The quest for quality oils that can serve as renewable energy sources is in line with the shared blueprint for an urgent call for action on "no povert" (SDG 1), "affordable and clean energy" (SDG 7) and "climate action" (SDG 13). The world energy system is heavily dependent on fossil fuels, but the current cost of production, environmental menace and stringent restrictions by regulatory bodies on application of fossil fuel gave way for the growing interest in renewable energy sources (Bórawski et al., 2023). Fossil fuels currently dominate global energy consumption, accounting for more than 80% of the global energy consumption. These energy sources contribute to greenhouse gas emissions, climate change and rising temperatures (Daniyanto and Budiman, 2015). The economy of a developing country, like Nigeria, is heavily influenced by fossil fuel exploration and over-dependence on advanced countries, making the production of renewable energy from alternative sources highly significant.

Mango kernel oil (MKO) can have the extracted oil being nearly 15% oil (Nzikou et al., 2010). According to research, mango kernel is a possible future source of a variety of antioxidants and bioactive substances. Biodiesel is a mono alkyl ester of fatty acids derived from vegetable oils and animal fats; it is a clean and renewable fuel (Demirbas, 2009); an eco-friendly alternative to petroleum-based diesel fuel (Atabani et al., 2012). Biodiesel is known to be non-toxic, biodegradable and emits less amount of carbon monoxide (CO), polyaromatic hydrocarbons, smoke and particulate matter when compared to petroleum diesel (Egwim et al., 2015).

The work of Karunanithi et al. (2015) asserted that at the operating temperatures between 40 – 70 ºC, the optimum percentage oil extracted from an Indian mango seed kernel was 12% by solvent extraction, with minimum n-

hexane requirement of 200 ml for 20 g of mango kernel, at heating time of 3 hrs. Further, Musa et al. (2014) carried out transesterification, for production of biodiesel from MKO using various catalyst.

Therefore, this paper aimed at optimizing the percentage yield of extracted kernel oil from two species of mango and characterize the oils, for assessment of the specie with better parametric quality that will place mango kernel as a domestic source for potential biodiesel or blend with fossil diesel.

2. MATERIALS AND METHODS

2.1 Sample collection and pre-treatment

Two species of Mango, Cherry (an indigenous specie) in their matured and riped stage presented in Figure I and Peach (an hybrid specie) presented in Figure II were purchased from markets in Zaria, Kaduna State, Nigeria in June 2021. The two species were then taken to Botany Department, Ahmadu Bello University, Zaria for identification and were given voucher numbers.

Following the removal of the peels and pumps by consuming them. The seeds (Figure III) were sun-dried for two months and later in an oven at 70 ^{o}C for 8 hrs; until constant weight was obtained.

The seeds were then dehulled mechanically and the dried kernels of each mango specie were ground using an agate mortar and pestle. These were then ground using a mechanical blender to particle size less than 2000 microns.

2.2 Extraction of oil

The oil from each kernel type (500 g) was extracted using a Soxhlet apparatus and a heating mantle. As the diagram shows (Figure IV), the kernel powder encapsulated in filter paper was placed in the extractor. The organic solvent used for extraction being n-hexane, was placed in the flask. The solvent vapourized and rose to the condenser where it was condensed. The condensed organic solvent then dripped on the kernel powder. The kernel powder upon contact with the hot organic solvent began to extract the oil. When the oil and solvent mixture had risen high enough (higher than the siphon tube, the mixture flowed through the siphon tube back into the flask. The oil was then recovered from the organic solvent by heating the mixture with a condenser coupled to the flask. The organic solvent vapourized and was then condensed back into another container. The oil was then recovered by evaporating off the solvent using a rotary evaporator (Model no. TT107R; Techmel and Techmel, USA).

2.3 OFAT optimization of the extraction of Mango Kernel Oil (MKO)

The factors considered and the responses (% MKO extracted) were:
1) Mix-ratio of kernel cake : n-hexane (C_6H_{14}); of 1:1, 1:2 and 1:3. This was carried out at heating time of 6 hrs and at a temperature of 60 ^{o}C. The optimum mix ratio obtained was then used to optimize the heating time.
2) Effect of heating time (4 – 10 hrs) at the optimum mix-ratio at temperature 60 ^{o}C. The optimum heating time obtained was then used to optimize the heating temperature.
3) Effect of heating temperature (40 – 70 ^{o}C) was considered at the optimum mix-ratio, time and temperature obtained.

The percentage oil yield in each case was determined as:

$$\text{Percentage Yield} = \frac{mass of oil extracted}{Initial mass of sample used} \times 100$$

Figure I: Cherry mango

Figure II: Peach mango

Figure III: Cherry mango seed

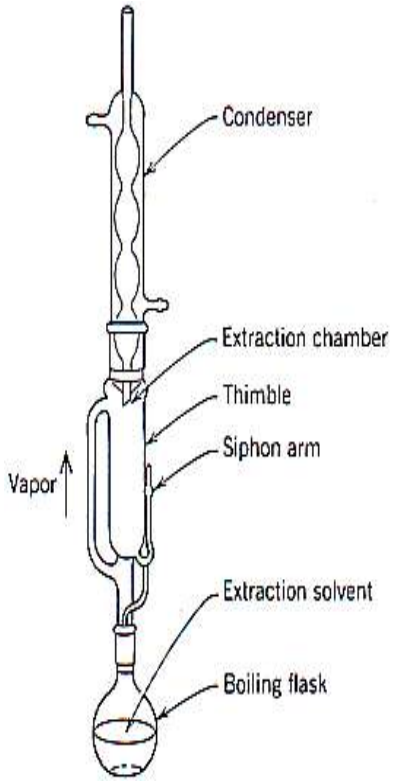

Figure IV: Soxhelet apparatus

Figure V: Mango kernel oil

2.4 Physical properties of the mango kernel oil

The colour and odour of the oil was observed with Lovibond comparator and panel of analysts respectively. The melting point of the MKO was determined using a capillary tube. pH was assessed with a pH meter.

2.5 Determination of refractive index

The refractive index of the oil was measured at 42 ^{o}C using a Refractometer (Bellingham and Stanley Ltd No 909271). Droplets of MKO were added to the measuring prism and were thoroughly spread out using a disposable pipette. It was then closed and tightened for about 2 minutes to allow the oil attain the required temperature. The

instrument was set and the reading was taken. The measurement prism was cleaned using a non-abrasive wipe (Dhellot et al., 2011). The specific gravity and flash point were determined according to Yuan et al. (2004) and AOAC (1990) standards.

2.6 Determination of viscosity value of MKO

The viscosity of the oil samples was measured by using a glass capillary U-tube viscometer (Ostwald viscometer) in which 60 ml of the MKO oil was poured into the suction tube, until it reached the start position indicated on the side, the suction was then released allowing the sample to flow back through the tube under gravity. The capillary section of the tube controls the oil's flow rate (AOAC, 1990).

The kinetic viscosity was calculated using the equation 1 reported by Yerima (2018).

$$\text{Kinetics Viscosity (Centistokes)} = \text{Time (minutes)} \times \text{Standard factor} \quad \text{----------1}$$

$$= 73 \times 0.755 = 55.155 \text{ mPa.s}$$

2.7 Chemical properties of mango kernel oil

The determination of acid value followed AOCS Official Method Cd 3d-63 (2017), while saponification value determination adhered to AOCS Official Method Cd 3-25 (2017). For iodine value determination, the method outlined in AOCS Official Method Cd 1d-92 (2017) was followed. These standardized methods ensure accuracy, reliability, and comparability of results across different laboratories and industries.

The acid value was calculated using the formula:

$$Acid\ value = \frac{TD\ x\ M\ x\ 56.1}{G} \quad \text{---------- 2}$$

Where: TD = Titre Difference = B – S; B = Titre value blank; S = Titre value with sample
M = Molarity of titrating solution (KOH used herein); G = Mass of oil sample (g)

The saponification value was calculated using:

$$\text{S.V} = \frac{\text{volume of acid required to neutralised remaining KoH} \times \text{Equivalent factor X 1000}}{\text{Weight of the oil used}} \quad \text{---------- 3}$$

The Iodine Value was calculated using:

$$Iodine\ value = \frac{TD\ x\ 1.269}{M} \quad \text{---------- 4}$$

Where: TD = Titre Difference = B – S B = Titre value blank;

S = Titre value with sample N = Molarity of titrating solution (KOH used herein)

M = Mass of oil sample (g).

The ester value was determined as the difference between the saponification value and acid value (Amira, 2014).

2.8 Statistical analysis

Statistical difference in the percentage oil yield during the optimization process and in the physicochemical parameters of the mango kernel oil as a function of specie was considered at $p < 0.005$ using One-way ANOVA.

3. RESULTS AND DISCUSSION

3.1 Optimization of the extraction of mango kernel oil (MKO)

The mango kernel: n-hexane of ratio 1:3 gave the highest percentage oil yield (6.67±0.009 – 9.60±0.012%) at 6 hrs heating duration and temperature of 60 ^{o}C; closely followed by the 1:2 ratio. This could be attributed to steric

hinderance at the higher mix-ratio, which limits diffusivity of the oil into the organic phase. So, at the optimized mix-ratio, increasing the heating time from 4 to 10 hr at 60 ^{o}C, generally resulted to steady increase in the % oil yield from 3.85±0.004 – 11.01±0.005% for the Cherry cultivar and 3.11±0.006 – 10.35±0.007% in Peach. The optimum heating time was taken as 8 hrs.

By carrying out extraction of oil from kernel at the temperatures 40 – 70 ^{o}C, under the optimum mix-ratio and time obtained, it was observed that heating temperature significantly elevated the oil extraction process at $p < 0.05$ (One way ANOVA; 95% degree of freedom); with the optimum % oil extracted being at 70 ^{o}C for both species of mango. The kernel of Cherry mango had higher % oil yield; though not significantly higher than the counterpart. The better yield of oil from the kernel of Cherry mango could be accounted for by higher lipid content in the cultivar. Therefore, the optimum condition for extraction of MKO is 1:3 mix ratio, 8 hours heating time and 70 ^{o}C heating temperature.

3.2 Extraction of Mango Kernel Oil (MKO) at the Optimum Condition

As presented in Tables 1 and 2, heating time resulted to steady increase in the percentage of oil extracted from both of the Cherry and Peach kernels. The percentage oil yield range was 4.00±0.002 – 13.01±0.006% for the Cherry cultivar and 3.93±0.004 – 12.60±0.009% for Peach cultivar; with the use of 500 g of each mango kernels. The kernel of Cherry mango had higher percentage oil yield; though not significantly higher than the counterpart.

Table 1: Yield of oil from Cherry mango at optimum condition

Heating time	Mean weight of oil (g)	Yield (% w/w)
4	1.20	4.00±0.002
5	2.00	6.67±0.007
6	2.90	9.67±0.012
7	3.70	12.33±0.009
8	3.90	13.00±0.007

Table 2: Yield of oil from Peach mango at optimum condition

Heating time	Mean weight of oil (g)	Yield (% w/w)
4	1.18	3.93±0.004
5	1.56	5.20±0.009
6	2.00	6.67±0.019
7	3.03	0.11±0.011
8	3.78	12.60±0.010

This work had higher percentage oil yield compared to that of Sani (2014) that reported mean of 8.27% for mango kernel; though the specie of mango used was not reported. However, at 8 hours the value obtained in this study is lower than the value of 14.00% oil yield reported in the work of Musa (2014) for mango kernel.

Mango kernel is therefore lower in oil yield compared to sesame seed (55 – 60%), palm kernel oil (46 – 50%) and water melon seed (35 – 40%). However, research about the physical and chemical properties of mango kernel oil is crucial due to its abundant availability and a waste being channeled to wealth.

3.3 Physical Properties of MKO

The kernel oil has pale colour, pleasant odour, pH 5.9 – 6.1, melting point 31.5±0.5 for the one from Cherry specie and 31.7±0.3 for Peach. The MKO from both cultivars had the flash point of 263.0^{o}C; the refractive index ranged

from 1.440 - 1.445; and the specific gravity at 20ºC was in the range 0.900-0.908. Further, the semi-liquid oils obtained have solidification temperature 24.0 – 24.5^{0}C, and mean viscosity at 40ºC was 39.25 – 39.45 MPa.

The physical properties observed in this study, such as colour and odour, align with findings from other studies, regardless of the mango species examined. The melting point of mango kernel oil (MKO) in our study is lower than the range of 38.93 to 39.33°C reported by Gurjar (2022) and Saiprabha et al. (2011). Similarly, the flash point of MKO obtained via solvent extraction method falls within the range of 261.66 to 265°C as reported by Gurjar (2022), which is consistent with our findings.

The ASTM recommended flash point range of a minimum of 130 °C ensures safety by reducing the risk of fire outbreaks in case of accidents, and it also aligns with the flash point of >100°C recommended by SNI 04 (Sulistyo et al., 2006). Furthermore, the specific gravity and refractive index of MKO obtained in our study are similar to those reported in previous research (Saiprabha et al., 2011; Gurjar, 2022). These parameters are crucial for assessing the degree of unsaturation and are commonly used to differentiate fats and oils that may be adulterated (Abdelaziz, 2018).

3.4 Chemical properties of MKO

The study revealed that mango kernel oil (MKO) has a saponification value (SV) of 205.0 – 207.5 mg KOH/g, which aligns with values found in existing literature. A low SV indicates the presence of long-chain fatty acids on the glycerol backbone of the oil. Compared to common oils/fats from vegetable or animal sources (such as sunflower, soybean, rapeseed, and pork lard), which typically contain only long-chain fatty acids (C18 and C16) with SV values ranging from 168 to 196 mg KOH/g oil (Li et al., 2001), coconut and palm kernel oils exhibit higher SV values ranging from 235 to 260 mg KOH/g oil (Toscano et al., 2012; Naksuk et al., 2009). Thus, although MKO has a lower SV than oils like coconut oil, it still shows potential as a biodiesel. However, biodiesel derived from oils with high saponification values can lead to exhaust emissions during engine combustion and pose challenges in product separation during biodiesel production, resulting in very low methyl ester yields.

The iodine value (IV) measures the degree of unsaturation of a specific vegetable oil, a crucial factor in assessing its biodiesel potential. In our study, the IV of MKO was found to be 40.1 gI/100g oil, closely resembling values reported by Gurja and John (43.05-44.33 gI/100g) and those obtained by Mohamed and Girgis (2005)

and Kittiphoom and Sutasinee (2013) for MKO. IV also indicates the quality of biodiesel by assessing its oxidative stability, with a required limit of 120 g I2/100 g according to standard EN 14214 for biodiesel. Both species of mango kernel oil analyzed in our study have IV values below this specification limit, indicating their potential as diesel sources. Soybean and sunflower biodiesels, in contrast, have IV values above this limit. IV helps classify oils based on unsaturation degree into drying oils (IV > 150), semi-drying oils (IV: 125 – 150), and non-drying oils (IV < 125), with lower IV indicating better stability (Saiprabha and Goswami-Giri, 2011).

The study on the kernel oils of Cherry and Peach mango species revealed an ester value of 198.0 – 202.2 mg KOH/g. Adel et al. (2018) reported a much lower ester value of 20.81 mg KOH/g for sunflower oil. Though not part of biodiesel standards, the fatty ester components of biodiesel, influenced by the ester moiety derived from the alcohol, can impact fuel properties such as cetane number (CN), viscosity, and oxidation stability (Knothe, 2005). Hence, assessing ester value is critical for biodiesel evaluation.

4. CONCLUSION

The optimized condition for obtaining % oil yield of 13.01±0.006% for the Cherry cutivar and 12.60±0.009% in Peach mango was mango kernel : n-hexane of ratio 1:3, at 70 ºC for 6hr heating. The physico-chemical properties of the oil did not differ significantly.

Some properties of the feedstock obtained that signals its potential as an efficient biodiesel are saponification value (SV) 205.0 – 207.5 mg KOH/g; indicating tendency to cause less exhaust emissions during burning in the engine. The iodine value 40.1 gI/100g oil obtained is far below the required limit of 120 g I_2/100 g standard for biodiesel. The oxidative and thermal stability of mango kernel oil should be investigated further, and compared to the esterified oil. This targets proffering environmental and energy solutions in line with the Sustainable Development Goals.

REFERENCES

Abdelaziz, S.A. (2018). Physico-chemical characteristics of mango kernel oil and meal. *Middle East Journal of Applied Sciences*, 08(01), 01-06.

Adel, I. A., Sherami, F.E. & Mohamed, A.E. (2018). Acid, peroxide, ester and saponification values for some vegetable oils before and after frying. *AASCIT Journal of Materials,* 4(2), 43-47.

Amira, P.O., Babalola O. & Oyediran, A.M. (2014). Physicochemical properties of palm kernel oil. *Current Research Journal of Biological Sciences*,

Association of Official Agricultural Chemists, AOAC. (1990). Official Methods of Analysis. 15th edition. Association of Official Analytical chemists, Washington. DC.

AOCS Official Method Cd 3d-63: American Oil Chemists' Society (AOCS). (2017). Official methods and recommended practices of the AOCS (7th ed.). AOCS Press.

AOCS Official Method Cd 3-25: American Oil Chemists' Society (AOCS). (2017). Official methods and recommended practices of the AOCS (7th ed.). AOCS Press.

AOCS Official Method Cd 1d-92: American Oil Chemists' Society (AOCS). (2017). Official methods and recommended practices of the AOCS (7th ed.). AOCS Press.

Atabani, A.E., Silitonga, A.S., Badruddin, I.A., Mahlia, T.M.I., Masjuki, H.H. & Mekhilef S. (2012). A comprehensive review on biodiesel as an alternative energy resource and its characteristics, *Renewable and Sustainable Energy Reviews*, 16, 2070-2093.

Bhalerao, S.D., Mulmuley, G.V., Anathakrishna, S.M. & Potty, V.H. (1989). Wash and wastewater management in the food industry. Fruit Veg. Process. Indian Food Pack. 43, 5–11.

Demirbas, A. (2009). Characterization of biodiesel fuels. *Energy Source,* Part A 31 889 – 896.

Dhellot, J.R., Matouba, E., Maloumbi, M.G., Nzikou, J.N., Safou-Ngoma, D.G., Linda, M. & Desobey, S. (2011). Parmentier extraction, chemical composition and nutritional characterization of vegetable oil in case of Amaranthushybridus (Varl and 2) of Congo Brazzaville. *African Journal of Biotechnology*, 5(11),1096-1101.

Egwim, E.C., Isege, S. I., Stephen O.S. & Akpan, G. (2015). Production and characterization of biodiesel from Allamanda (*Allamanda cathartica*) oil using lipase as catalyst. *An International Journal of the Nigerian Society for Experimental Biology*, 27 (4), 153–158.

Gurjar, H.R. & Raj, J.D. (2022). Extraction of mango kernel (*Magnifera indica*) Oil. *Asian Journal of Dairy and Food Research*, 41(3), 361-364.

Karunanithi, B., Bogeshwaran, K., Manasa T. & Krishna R. S. (2015). Extraction of mango seed oil from mango kernel. *International Journal of Engineering Research and Development***,** 11 (11), 32-41.

Kittiphoom, S. & Sutasinee, S. (2013). Mango seed kernel oil and its physicochemical properties. *International Food Research Journal,* 20, 1145.

Knothe, G. (2005). Dependence of biodiesel fuel properties on the structure of fatty acid alkyl esters. *Fuel Process Technology,* 86, 1059 - 1070.

Knothe, G. (2008). Designer biodiesel: Optimizing fatty ester composition to improve fuel properties. *Energy & Fuels,* 22: 1358-1364.

Knothe, G. (2009). Improving Biodiesel Fuel properties by modifying fatty esters composition. *Journal of Energy and Environmental Science,* 10, 1039-1054.

Knothe, G. (2003). Structure indices in FA chemistry. How relevant is the iodine value? *Journal of the American Oil Chemists' Society*, 79(9), 847-854.

Li, Y. & Watkins, B.A. (2001). Oil quality indices. In: Wrolstad R.E., editor. Current Protocols in Food Analytical Chemistry. John Wiley & Sons, Inc.; New York, NY, USA

Mohamed, E.M. & Girgis, A.Y. (2005). Utilization of mango seed kernels for improving stability of some oils and biscuit production. *Journal of Agriculture and Science*, 30, 4625-4636.

Musa, U., Mohammed, I. A., Sadiq, M. M., Aliyu, A. M., Suleiman, B. & Talabi, S. (2014). Production and characterization of biodiesel from Nigerian mango seed oil. Proceedings of the World Congress on Engineering, July 2 - 4, 2014, London, U.K. London, Volume 1.

Naksuk, A., Sabatini, D.A. & Tongcumpou, C. (2009). Microemulsion-based palm kernel oil extraction using mixed surfactant solutions. *Industrial Crops Production*, 30, 194–198.

Nzikou, J.M., Kimbonguila, A., Matos, L., Loumouamou, B., Pambou-Tobi, N.P.G., Ndangui, C.B., Abena, A.A., Silou, T.H., Scher, J. & Desobry, S. (2010). Extraction and characteristics of seed kernel oil from mango (Mangifera indica). *Research Journal of Environmental Earth Science*, 2, 31–35.

Puravankara, D., Boghra, V. & Sharma, R.S. (2000). Effect of antioxidant principles isolated from mango (*Mangifera indica L.*) seed kernels on oxidative stability of buffalo ghee (butter-fat). *Journal of Science Food Agriculture*, 80, 522–526.

Ramos, M.J., Carmen, M.F, Abraham, C., Lourdes, R. & Angel, P. (2009). Influence of fatty acid composition of raw materials on biodiesel properties. *Bioresources Technology,* 100, 261-268.

Saiprabha M. M. & Goswami-Giri, A.S. (2011). Composition and characterization of refined oil compared with its crude oil from waste obtained from Mangifera indica. *Asian Journal Research Chemistry*, 4, 1415-1419.

Sani, I. (2014). Soxhlet extraction and physicochemical characterization of *Mangifera indica* L. seed kernel oil. *Research and Reviews: Journal of Food and Dairy Technology*, 2(1), 20 – 24.

Sulistyo, H., Suardjaja, I. M. & Rahayu, S. S. (2006). Transesterification of candlenut oil with ethanol to biodiesel, in: *Proceeding on Regional Symposium on Chemical Engineering (RSCE '06)*, Singapore, December 2006.

Toscano, G., Riva, G., Foppa, P.E. & Duca, D. (2012). Vegetable oil and fat viscosity forecast models based on iodine number and saponification number. *Biomass Bioenergy*, 46, 511–516.

Yerima, E.A., Yebpella, G.G. & Ogah, E., Longbap, B.D. & Johnson, S.N. (2018). Effect of extraction methods on the physicochemical properties of palm kernel oil. *International Journal of Modern Chemistry*, 10(1), 104-116.

Yuan, Y., Hansen, A. & Zhang, Q. (2004). The Specific Gravity of Biodiesel Fuels and Their Blends With Diesel Fuel. Agricultural Engineering International: the CIGR Journal of Scientific Research and Development. Manuscript EE 04 004. Vol. VI, 1-11.

PAPER 7- DEVELOPMENT AND DEPLOYMENT OF A NEURAL NETWORK-BASED REMOTE TRACKING SYSTEM FOR POULTRY BIRDS

G. K. Raji[1], K. E. Jack[1*], T. A. Folorunso[1], J. C. Anunuso[1],
J. G. Kolo[1], J. G. Ambafi[2], A. B. Garba[3], E. M. Nwanga[4]

[1]Department of Mechatronics Engineering, Federal University of Technology Minna, Nigeria.
[2]Department of Electrical and Electronics Engineering, Federal University of Technology Minna, Nigeria.
[3]Department of Mechanical Engineering, Federal University of Technology Minna, Nigeria.
[4]Department of Software Engineering, Federal University of Technology Owerri, Nigeria.

[*]Email: Kufre@futminna.edu.ng

ABSTRACT
Poultry farmers are experts charged with catering for the well-being of the poultry livestock to improve yields. This operation requires physical presence most times and can be labourious and highly cost intensive. Furthermore, the inability of farmers to detect predators early in the flock causes a high mortality rate. This study tracks poultry birds' conditions using a neural network to reduce mortality and other causes of losses in the poultry system. The proposed methodology uses the yoloV5 model to detect poultry birds and predators in poultry housing and track the movement of birds using the DeepSort tracking algorithm. The proposition also incorporates using Raspberry Pi and Pi cameras to obtain and process information on poultry 'birds' movement on the farm. The live video stream of the poultry housing is deployed on the local host, providing a means to monitor the poultry bird in the poultry housing from a remote location. The implementation shows promising results in the ability of the model to detect poultry birds, and predators as well as monitor the welfare of the entire livestock in the system.

KEYWORDS: Artificial Intelligence; Poultry Farming; tracking; Deep-Sort; Neural Network; Biosecurity

1. INTRODUCTION

In Animal Husbandry, the word poultry refers to birds, chickens, turkeys and other related animals. The rearing of poultry has been a source of income for poultry farmers. Poultry farmers are experts charged with catering to the well-being of the livestock in poultry housing by focusing on ensuring proper welfare for the livestock to improve farming yields. The agricultural industry is related to the rearing of this species of animals for egg and meat purposes (Abd *et al*., 2021).

Globally, there has been increased demand for livestock production, which has increased the tasks of the farmers. This creates a need for there to be a balance between quantity and quality in their production. Amongst the 69 billion chickens reared for human consumption every year, a million die during the rearing process and even some of the livestock that gets to the slaughterhouse is rejected due to the presence of disease, bruises or any sign that shows poor living conditions (Neethirajan, 2022a). This increase in the demand for poultry farming products is attributed to the need for humans to consume food with high protein but low cholesterol. To meet these demands, there is a need for constant and active monitoring of the livestock in the poultry housing, which requires high-cost labour (Ojo *et al*., 2022a).

To ensure the welfare of the poultry, different methods are considered. Of all these methods, the behavioural assessment of poultry is one with the utmost relevance. The presence of a predator and disease in livestock affects the behaviour of animals, thereby reflecting their living and physiological conditions. Focusing on the behavioural activities of the livestock helps livestock's growth and increases productivity, protecting the animal, improving the livestock's growth, and increasing productivity in poultry farming (Li *et al*., 2020). To ensure a high profit and a very productive poultry industry, there is a need to constantly monitor poultry housing. In ancient times, this task was done manually, which increased the intensity the poultry farmers needed to work to ensure the proper welfare of the poultry. With the help of emerging technologies, different methods such as monitoring certain environmental conditions like temperature, pressure, water level and so on, have been developed to reduce manual labour. Some other methods can also measure the poultry's behaviour and activities (Mazunga *et al*., 2023).

Mostly, not all poultry farmers are equipped with the knowledge of poultry health. When these farmers are faced with a challenge concerning the poultry's health, they tend to seek the consultation of a veterinary doctor. Sometimes, the doctors may not be available, which means there would be a high risk for those farmers because they won't be able to diagnose their livestock early and properly. However, if the farmers and doctors can view the

pictorial footage of these livestock remotely, the health and safety of the livestock can be assured (Balachandar and Chinnaiyan, 2020).

Thus, with the advancement of technology especially in the field of Artificial Intelligence and Embedded Systems, a wide range of solutions exist for managing livestock systems. Such solutions include but are not limited to monitoring the climatic condition of livestock and their environment (Pereira *et al*., 2020; Mcloughlin *et al*., 2019), Detection and Monitoring of welfare conditions using varying techniques (Achour *et al*., 2020; Mcloughlin *et al*., 2019; Marsot *et al*., 2020; Fang *et al*., 2021) and the acquisition and transmission of vital livestock parameters (Pereira *et al*., 2020; Neethirajan and Kemp, 2021; Aziz *et al*., 2021b; Razman *et al*., 2022). A summarized review table is presented in Tables 1 and 2, highlighting some of these past approaches.

Furthermore, based on the review and the importance of monitoring the welfare condition of poultry birds concerning health conditions and the influx of predators, this work proposes the development and integration of an Artificial intelligence-based technique (YOLOV5) to detect, monitor and predict the welfare conditions and influx of predator.

The remaining section of the work is divided into the following sections: Section 2 presents the Methodology adopted in the development of the proposed system, detailing the description of the dataset, neural network model, and the metric of evaluation. The results of the performance of the developed system are presented in Section 3 and Section 4 concludes the work and highlights the achievements as well as the direction for future research.

Table 1. Research on Chicken Detections Based on Neural Networks for Animal Welfare Monitoring

Reference	**Neural Network Model (Algorithm)**	**Applications**	**Dataset Volume**	**Accuracy**
(Thenmozhi *et al*., 2020)	Custom Sequential model on SSD algorithm	To increase the accuracy of predicting strange or abnormal behaviour in poultry animals	444 images	91.1%
(Nasirahmadi *et al*., 2020)	Convolutional neural network (CNN) model	Real-time tracking of turkey pecking patterns	13,100 sound clips	96.8%
(Fang *et al*., 2021)	A Resnet-50 deep neural in conjunction with a Naïve Bayesian model	To recognize chickens while they are standing, walking, running, eating, resting, and preening	28 broiler chicken videos with multiple behaviours	75.12% (standing), 51.35% (walking), 62.7% (running), 93.61% (eating), 96.23% (resting), and 92.58% (preening).
(Zhang and Chen, 2020)	ResNet residual network	To create an automated system for the detection of sick chickens	5000 sick chicken images	93.7%

Table 2. Research on Existing Remote Monitoring Methods of Poultry Conditions

References	Existing Remote Monitoring methods	Sensors	Applications
(Balachandar and Chinnaiyan, 2020)	Imagery analytics and machine learning are used to detect bird diseases early and reduce mortality rates by analysing images and videos of poultry farms and birds. This is done by using CCTV cameras and body cameras to collect data, which is then ingested into a data lake and analysed with algorithmic	• Camera	-Detect bird diseases early and accurately reduce bird mortality rates improve the overall health and well-being of their birds make informed decisions about treatment

	imagery models to detect any abnormalities in the birds' appearance, such as changes in colour, stains, or abnormal droppings. Once the system detects a disease, it sends alerts and precautionary messages to the farmer through a mobile application, along with personalized recommendations for medicine dosage based on the bird's individual needs.		
(Pereira *et al*., 2020)	A low-cost IoT system to monitor the poultry farm environment in real-time, using sensors to collect data on temperature, humidity, ammonia concentration, and light intensity was presented. This data can be used to identify potential problems that could lead to health problems in the birds.	• DHT22 sensor (temperature and relative humidity) • MQ-137 (ammonia concentration in the air) • LDR (light-dependent resistor) sensor	• Graphical view of environmental data in real-time and over time. • Identification of potential problems that could lead to health problems in the birds
(Neethirajan and Kemp, 2021)	Use of biometric sensors to monitor an individual 'animal's health and behaviour in real-time, process and integrate the data using big data analytics systems, and enable secure and guaranteed traceability of animal products from farm to table using blockchain technology It also discusses the use of big data analytics to inform management about nutritional needs, reproductive status, declining trends in productivity, and detect abnormalities that may affect animals	• Thermometers • Accelerometers • Radio-frequency identification • Thermal infrared imaging sensors	Digitalizing animal agriculture to: • improve efficiency • animal welfare • environmental sustainability • public health

2. RESEARCH METHODOLOGY

2.1 *Materials Components*

In this section, the key components used for the realisation of the prototype welfare monitoring system are highlighted and discussed.

a. Raspberry Pi

The choice of microcontroller used was the Raspberry Pi 4 model with 8 GB RAM because of its high computational power and the ability to run deep learning programs at a faster rate.

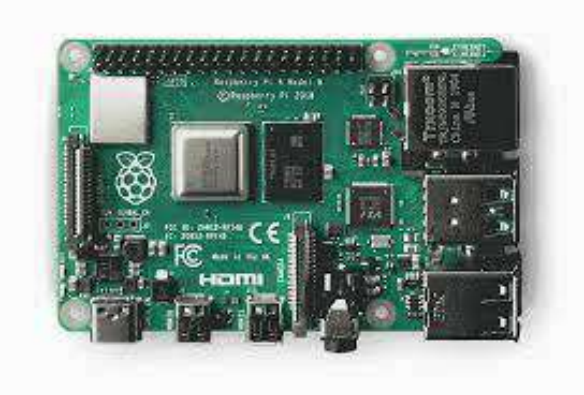

Plate 1: Raspberry PI Model 4B

b. Raspberry PI Camera Module

The Raspberry Pi camera module is a camera which is compatible with the Raspberry Pi microcontroller. The version of the camera series chosen for this project was Pi Camera version 3 because it produces images and videos of higher quality than other camera modules.

Plate 2: Raspberry Pi CSI camera module

In the quest to capture the live feed on the poultry in situ. The pi camera and the pi controllers are connected to form a complete circuitry as depicted in Figure 1. This complete circuitry can acquire and transmit the acquired images of the poultry system, thus, leading to the remote poultry monitoring system.

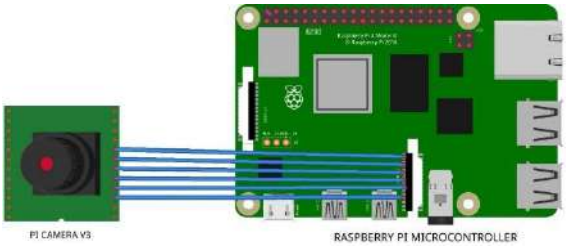

Figure 1: Circuit diagram for the remote poultry monitoring system.

The process of monitoring the poultry system starts at the point when the camera module begins to capture the video coverage of the poultry housing. This video is then sent to the Raspberry Pi in which the Raspberry Pi takes each frame of the video and runs it through the poultry detection model in other to detect poultry birds and snakes in the frame. For each poultry bird detected, a boundary box is drawn around the bird and an ID is attached to that bird. The detection model also monitors for the presence of snakes. Following this process is a tracking algorithm that follows the motion of each bird detected. The output of this tracking algorithm can then be viewed from a remote location by connecting to the same local host as the system. The processes taken are represented in Figure 2 and the flow in Figure 3.

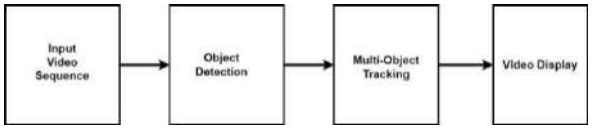

Figure 2: Block diagram of the remote poultry birds' conditions tracking system

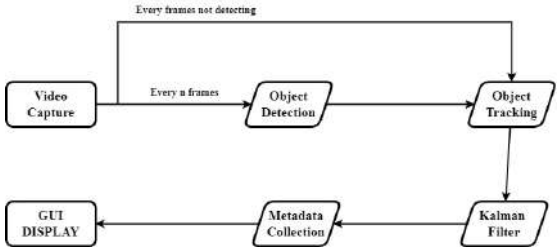

Figure 3: Flow chart of the remote poultry animal conditions tracking system.

2.2 *Datasets Characteristics*

The dataset used consists of chicken and chick images collected from open sources; Unsplash, pexels, and Flickr. about 461 images were collected, which were divided in a ratio of 7:3 representing the training and validation datasets respectively. The training dataset comprises about 325 images, utilized for training the model, while the validation dataset includes around 136 images used to evaluate the model. For better model performance, the images were of diverse backgrounds and included different unrelated random objects. These images were annotated using the open-source graphical annotation tool known as LabelImg, which was used to mark the object boundary boxes within the images, as shown in Figure 4. As a result, the dataset then contains images and their corresponding .txt files containing the class name and boundary box coordinates.

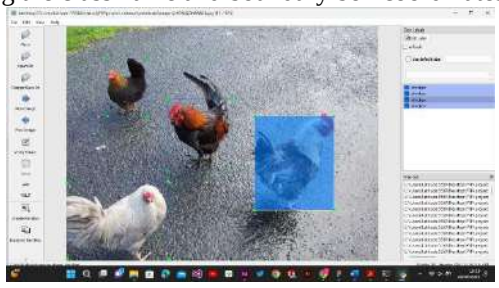

Figure 4: Dataset Annotation using LabelImg

2.3 *Detector Model and Architecture*

This work leveraged the advantages of employing transfer learning when training the Convolutional Neural Networks (CNN) based model. Specifically, the You Only Look Once model version 5 (Yolov5) was adopted for the chicken detection. YOLO represents a unique approach in neural network-based algorithms as it employs a single convolutional network to directly predict bounding boxes and class probabilities from entire images in a single evaluation. This differs from traditional detection systems, which typically involve separate networks for generating region proposals and classifying those proposals (Menaka *et al*., 2020). Consequently, YOLO offers both speed and accuracy advantages over traditional methods. The trained Yolov5 model utilized in this project consists of 157 layers and leverages class probabilities for chicken recognition and bounding box coordinates for trajectory path measurement between video frames.

For the training and testing of the proposed model, a high-computation-power computer system was used. The model framework was embedded in logistic regression, incorporating a convolutional neural network with three major multi-scale modules. The detector module utilizes the Yolov5 architecture to employ deep neural networks for detection across different scale kernels, which is then followed by the tracking modules. The YOLOv5 model was also trained to detect snakes as predators. About 800 images of snakes were used to train the model. The

dataset was labelled using labelling, and it was trained using 157 layers of the yoloV5 model. To adjust the model parameters, about 300 images containing snakes were used to validate the model performance.

2.4 Tracking Movement and Motion

To track the movement and motion of the birds, a computer-based tracking technique called the DeepSort in combination with the video stream acquired from the monitoring infrastructure was adopted. DeepSort is a clever method made for super-accurate, real-time object tracking in videos. It uses both deep learning and old tracking ways to do it well. The process starts by using a deep learning model to spot things in each part of a video, shown as boxes that connect. Special things that help us tell apart objects as they change between pictures are then taken out. To guess where an object will be in the next picture, a special tool called the Kalman filter is used. It thinks about what state the thing was earlier and how much time passed between pictures.

Subsequently, the algorithm employs nearest neighbour tracking based on Mahalanobis distance to associate detected objects with existing object tracks, thereby ensuring objects are correctly matched over time. It maintains a record of all active tracks and their corresponding objects, assigning new detections to existing tracks or initiating new tracks for newly detected objects.

Finally, the algorithm conducts track validation by applying specific criteria, such as having a minimum number of consecutive detections, to ensure the reliability of the created tracks. Figure 5 shows all the sub-systems of the DeepSort tracking algorithm.

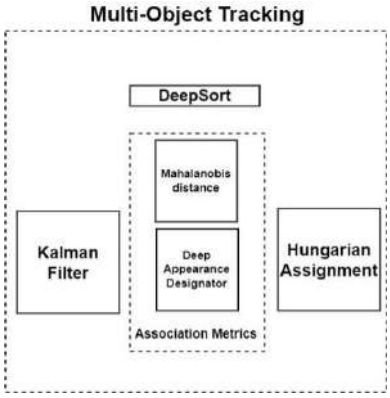

Figure 5: Block Diagram of Tracking Algorithm

2.5 *Evaluation of the performance*

The performance of the model was evaluated based on the precision, recall, f1_score, and mean absolute precision metrics.

a. Precision: Precision is a term that defines the accuracy of the model's prediction related to falsely accepted positive cases. It is the proportion of correct positive predictions to all actual positives. False positives will be less if precision levels are high.

$$Precision = \frac{True\ Positives}{True\ Positives + False\ Positives}$$

b. Recall (Sensitivity): It is a measurement that is obtained by taking true positives and dividing them by the total count of real positive situations. Recall is a way to see if important information is found accurately.

$$Recall = \frac{True\ Positives}{True\ Positives + False\ Negatives}$$

c. F1 Score: It is also called F-scores. The F1-score is the balanced middle between recall and precision. A good reading has both wrong conclusions and correct positives. This score is the space below the Precision-Recall Curve. If a model has a better F1 score, it means the overall work of that model is good.

$$F1\ Score = \frac{2\ (precision\ \times recall)}{(precision + recall)}$$

d. Mean Average Precision (mAP): mAP provides an overall assessment of a model's performance by averaging the AP values for all object categories. It is widely used for evaluating object detection models on datasets with multiple object classes.

3 RESULTS AND DISCUSSIONS

The results obtained from the implementation and the deployment of the developed system are presented herewith.

3.1 Detection of Poultry birds

On the ability to detect poultry birds, the developed system was tested using different types of birds in comparison with the poultry birds. In addition to the use of images of other birds, the system was also subjected to testing using random images of other livestock. This test procedure depicts an accuracy of 68%, Precision of 83% and Recall of 74%. The metrics of evaluation are depicted in Table 3. This performance shows a high level of precision and recall depicting a good performance of the model.

Table 3: Detection of Poultry Metrics

Precision	*Recall*	*mAP_0.5*	*mAP_0.5:0.95*
83%	74%	76%	48%

3.2 Tracking Movement and Motion

The system was evaluated using numerous video recordings of various habitats with different bird populations. It demonstrated the capability to accurately assign tracking numbers to identified poultry birds and effectively monitor their movements within the footage. Additionally, the system successfully updated the tracking numbers whenever new poultry birds appeared in the videos. This setup performed reliably under varying lighting conditions, whether bright or dim. Figure 6 illustrates several video feed frames, highlighting the system's proficiency in tracking the movements of the detected poultry birds. Figure 7 shows the prototype design of the remote poultry animal conditions tracking system.

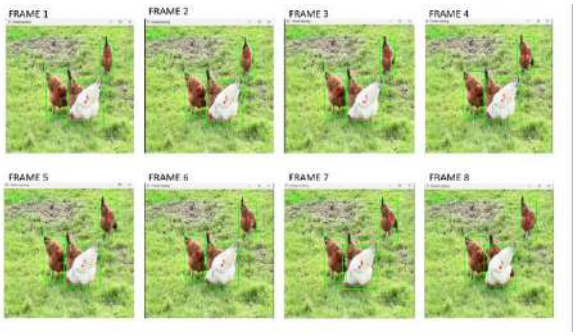

Figure 6: Frame by frame as the tracking algorithm tracks the movement of the poultry bird

Figure 7: Prototype design of remote poultry animal conditions tracking system

3.3 Predator Detection

The system underwent rigorous testing with a diverse set of images containing snakes, encompassing various lighting conditions and background settings. This comprehensive evaluation was designed to assess the system's ability to accurately detect the presence of snakes in different environments. The results demonstrated that the system was capable of correctly identifying snakes within these images, despite the variability in lighting and backgrounds. Table 4 provides a detailed overview of the model's performance in detecting snakes on poultry farms. According to the data, the system achieved a success rate of 48% in identifying snakes within these specific contexts. This indicates a moderate level of accuracy, suggesting that while the system is somewhat effective at detecting snakes, there is still room for improvement to enhance its reliability in diverse environmental conditions.

Table 4: Evaluation metrics of the snake detection model

Precision	*Recall*	*mAP_0.5*	*mAP_0.5:0.95*
90%	94%	94%	68%

3.4 Condition Monitoring

The system was designed to provide live video streaming capabilities, wherein detected chickens were highlighted with a rectangular box, enabling the tracking of their movements within their habitat. This functionality was integrated into a locally hosted webpage, developed using HTML, ensuring that the live feed could be accessed and monitored effectively. The webpage was designed to be user-friendly and accessible, allowing users to monitor the poultry remotely.

To facilitate remote monitoring, the system was set up to enable access from distant locations, provided that the remote user was connected to the same network as the poultry tracking system. This network connectivity ensured that the live feed could be viewed in real-time, allowing for comprehensive monitoring of the poultry birds' activities and movements.

Figure 8 illustrates the HTML webpage that displays the live video feed of the remote poultry monitoring system. The figure shows the video stream with a boundary box and an assigned ID for each poultry bird, categorizing them based on their age. Specifically, it includes one-month-old poultry birds (a), two-week-old poultry birds (b), four-week-old poultry birds (c), and four-month-old poultry birds (d).

This categorization allows for detailed monitoring and management of the poultry at different stages of development, ensuring that the tracking system provides valuable insights into the behaviour and well-being of the birds.

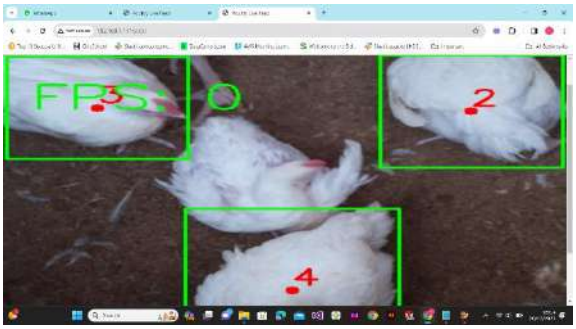

Figure 8: Web page displaying the video feed of the remote poultry monitoring system.

3.5 Overall Performance Evaluation

The entire system was subjected to a thorough evaluation on a poultry farm to assess its real-time monitoring capabilities. The system processed video feeds at a rate of approximately 25 frames per minute, closely resembling the frame rate experienced in real-life observation. During these video analyses, the system effectively identified poultry birds, enclosing each detected bird within a bounding box and assigning a unique identification number. This enabled accurate tracking and monitoring of individual birds within the farm environment.

Table 5 presents a comprehensive overview of the primary detection system's performance metrics, which include precision, recall, and mean Average Precision (mAP) scores. The system demonstrated a slightly above-average performance, achieving an accuracy of 58%. These metrics are crucial in evaluating the system's overall effectiveness in detecting and tracking poultry birds.

Table 5: Evaluation metrics of the overall detection system

Precision	*Recall*	*mAP_0.5*	*mAP_0.5:0.95*
87%	84%	86%	58%

Furthermore, Figure 9 provides a detailed depiction of the F1-Confidence curve, which illustrates the relationship between the F1 score and the confidence score. This curve is essential for understanding the system's performance across different confidence thresholds, helping to optimize its detection capabilities.

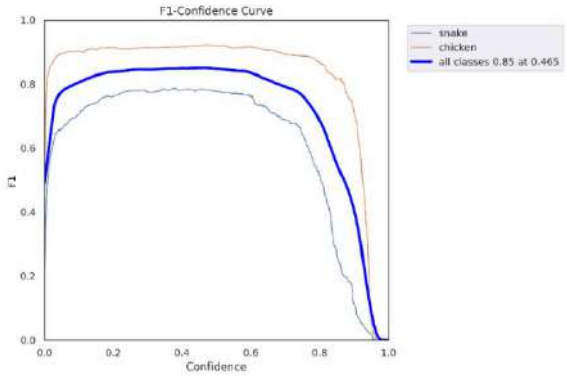

Figure 9: F1_score-Confidence curve

In addition, Figure 10 showcases the Precision-Recall curve, highlighting the detection model's efficacy in identifying chickens compared to snakes during testing. This curve is indicative of the model's precision and recall at various thresholds, offering insights into its strengths and areas for improvement.

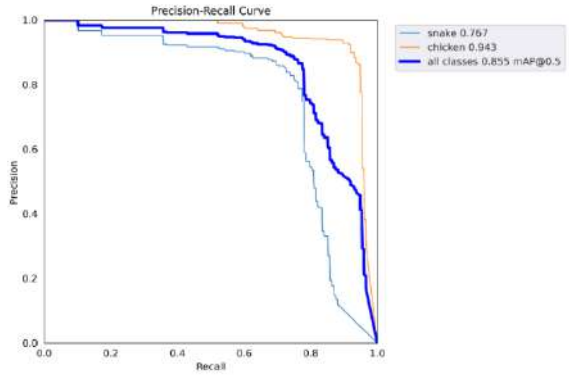

Figure 10: Precision-Recall Curve

The results elaborate on the outcomes of implementing the remote poultry monitoring system, discussing its performance in meeting the defined objectives. The system demonstrated its capability to effectively detect poultry birds in a variety of images, ensuring comprehensive monitoring of the poultry housing environment, including the identification of potential snake intrusions. With a mAP_0.5:0.95 score of 58%, the system showcased its accuracy and reliability in real-world conditions. Additionally, the system's ability to track the movement of birds across successive video frames further underscores its utility in dynamic monitoring scenarios. This continuous tracking is vital for maintaining an up-to-date understanding of the poultry's behaviour and movement patterns. The system also proved capable of streaming live video feeds to an HTML webpage hosted locally. This webpage could be accessed remotely within the same network, facilitating remote monitoring and management of the poultry farm. The live streaming feature is particularly beneficial for farm managers and stakeholders who need real-time insights into the farm's operations without being physically present. During the evaluation of the poultry farm, the system consistently produced approximately 25 frames per minute, demonstrating its efficiency in both detection and tracking tasks. This frame rate ensures that the monitoring system can keep pace with the rapid movements of poultry birds, providing accurate and timely data for decision-making.

4 CONCLUSION AND FUTURE DIRECTIONS

This work canvassed the necessity of integrating advanced systems to monitor the welfare of poultry birds, leading to the proposition of a more robust solution to the challenges associated with poultry welfare monitoring. A simplified methodology was adopted, incorporating embedded systems and a CNN-based neural network (YOLO v5) for the development of the poultry monitoring system. The proposed system was evaluated using various metrics, including precision, recall, and accuracy, with promising results demonstrating its efficiency in addressing the challenges of poultry system monitoring. The findings indicate that an automated bird detection system utilizing computer vision and deep learning techniques is a highly effective tool for detecting the presence of poultry birds within their housing. Additionally, the system proved capable of accurately and efficiently monitoring poultry housing for the presence of predators. By enabling effective remote monitoring of poultry birds' health and welfare, the system enhances biosecurity and minimizes the need for human presence. This advancement in poultry farm management ensures better oversight and care of the birds, promoting overall farm productivity and biosecurity.

REFERENCES

Abd Aziz, N. S. N., Mohd Daud, S., Dziyauddin, R. A., Adam, M. Z., and Azizan, A. (2021a). A Review on Computer Vision Technology for Monitoring Poultry Farm - Application, Hardware, and Software. IEEE Access, 9, 12431–12445. https://doi.org/10.1109/ACCESS.2020.3047818

Abd Aziz, N. S. N., Mohd Daud, S., Dziyauddin, R. A., Adam, M. Z., and Azizan, A. (2021b). A Review on Computer Vision Technology for Monitoring Poultry Farm - Application, Hardware, and Software. In

IEEE Access (Vol. 9, pp. 12431–12445). Institute of Electrical and Electronics Engineers Inc. https://doi.org/10.1109/ACCESS.2020.3047818

Achour, B., Belkadi, M., Filali, I., Laghrouche, M., and Lahdir, M. (2020). Image analysis for individual identification and feeding behaviour monitoring of dairy cows based on Convolutional Neural Networks (CNN). Biosystems Engineering, 198, 31–49. https://doi.org/10.1016/J.BIOSYSTEMSENG.2020.07.019

Astill, J., Dara, R. A., Fraser, E. D. G., Roberts, B., and Sharif, S. (2020). Smart poultry management: Smart sensors, big data, and the internet of things. In Computers and Electronics in Agriculture (Vol. 170). Elsevier B.V. https://doi.org/10.1016/j.compag.2020.105291

Aydin, A. (2017). Development of an early detection system for the lameness of broilers using computer vision. Computers and Electronics in Agriculture, 136, 140–146. https://doi.org/10.1016/J.COMPAG.2017.02.019

Balachandar, S., and Chinnaiyan, R. (2020). Internet of Things Based Reliable Real-Time Disease Monitoring of Poultry Farming Imagery Analytics. In Lecture Notes on Data Engineering and Communications Technologies (Vol. 31, pp. 615–620). Springer Science and Business Media Deutschland GmbH. https://doi.org/10.1007/978-3-030-24643-3_73

Bauer, E. A., and Jagusiak, W. (2022). The Use of Multilayer Perceptron Artificial Neural Networks to Detect Dairy Cows at Risk of Ketosis. Animals, 12(3). https://doi.org/10.3390/ani12030332

Bhatt, D., Patel, C., Talsania, H., Patel, J., Vaghela, R., Pandya, S., Modi, K., and Ghayvat, H. (2021). Cnn variants for computer vision: History, architecture, application, challenges and future scope. In Electronics (Switzerland) (Vol. 10, Issue 20). MDPI. https://doi.org/10.3390/electronics10202470

Cai, L., and Zhu, Y. (2015). The challenges of data quality and data quality assessment in the big data era. Data Science Journal, 14. https://doi.org/10.5334/dsj-2015-002

Chatterjee, R. N., and Rajkumar, U. (2015). An Overview of Poultry Production in India. In Anim. Hlth 54(2).

Coble, K. H., Mishra, A. K., Ferrell, S., and Griffin, T. (2018). Big data in agriculture: A challenge for the future. Applied Economic Perspectives and Policy, 40(1), 79–96. https://doi.org/10.1093/aepp/ppx056

da Silva, I. N., Hernane Spatti, D., Andrade Flauzino, R., Liboni, L. H. B., and dos Reis Alves, S. F. (2017). Artificial Neural Network Architectures and Training Processes. In Artificial Neural Networks (pp. 21–28). Springer International Publishing. https://doi.org/10.1007/978-3-319-43162-8_2

Edwan, E., Qassem, M. A., Al-Roos, S. A., Elnaggar, M., Ahmed, G., Ahmed, A. S., and Zaqout, A. (2020). Design and implementation of a monitoring and control system for a poultry farm. Proceedings - 2020 International Conference on Promising Electronic Technologies, ICPET 2020, 44–49. https://doi.org/10.1109/ICPET51420.2020.00017

Escamilla-García, A., Soto-Zarazúa, G. M., Toledano-Ayala, M., Rivas-Araiza, E., and Gastélum-Barrios, A. (2020). Applications of artificial neural networks in greenhouse technology and overview for smart agriculture development. In Applied Sciences (Switzerland) (Vol. 10, Issue 11). MDPI AG. https://doi.org/10.3390/app10113835

Fang, C., Zhang, T., Zheng, H., Huang, J., and Cuan, K. (2021). Pose estimation and behaviour classification of broiler chickens based on deep neural networks. Computers and Electronics in Agriculture, 180. https://doi.org/10.1016/j.compag.2020.105863

Isaac Abiodun, O., Jantan, A., Esther Omolara, A., Victoria Dada, K., AbdElatif Mohamed, N., and Arshad, H. (2018). State-of-the-art in artificial neural network applications: A survey. Heliyon, 4, 938. https://doi.org/10.1016/j.heliyon.2018

Karcher, D. M., and Mench, J. A. (2017). Overview of commercial poultry production systems and their main welfare challenges. In Advances in Poultry Welfare (pp. 3–25). Elsevier. https://doi.org/10.1016/B978-0-08-100915-4.00001-4

Kujawa, S., and Niedbała, G. (2021). Artificial neural networks in agriculture. In Agriculture (Switzerland) (Vol. 11, Issue 6). MDPI AG. https://doi.org/10.3390/agriculture11060497

Li, G., Hui, X., Lin, F., and Zhao, Y. (2020). Developing and evaluating poultry preening behaviour detectors via mask region-based convolutional neural network. Animals, 10(10), 1–18. https://doi.org/10.3390/ani10101762

Li, N., Ren, Z., Li, D., and Zeng, L. (2020). Review: Automated techniques for monitoring the behaviour and welfare of broilers and laying hens: towards the goal of precision livestock farming. In Animal (Vol. 14, Issue 3, pp. 617–625). Elsevier B.V. https://doi.org/10.1017/S1751731119002155

Lufyagila, B., Machuve, D., and Clemen, T. (2022). IoT-powered system for environmental conditions monitoring in poultry house: A case of Tanzania. African Journal of Science, Technology, Innovation and Development, 14(4), 1020–1031. https://doi.org/10.1080/20421338.2021.1924348

Marsot, M., Mei, J., Shan, X., Ye, L., Feng, P., Yan, X., Li, C., and Zhao, Y. (2020). An adaptive pig face recognition approach using Convolutional Neural Networks. Computers and Electronics in Agriculture, 173. https://doi.org/10.1016/j.compag.2020.105386

Mazunga, F., Mzikamwi, T., Mazunga, G., Mashasha, M., and Mazheke, V. (2023). IoT Based Remote Poultry Monitoring Systems for Improving Food Security and Nutrition: Recent Trends and Issues. Journal of Agriculture Science and Technology JAGST, 22(2), 4–21. https://doi.org/10.4314/jagst.v22i2.2

Mcloughlin, M. P., Stewart, R., and McElligott, A. G. (2019). Automated bioacoustics: Methods in ecology and conservation and their potential for animal welfare monitoring. In Journal of the Royal Society Interface (Vol. 16, Issue 155). Royal Society Publishing. https://doi.org/10.1098/rsif.2019.0225

Md. Mahfujul Islam, Shaharya Sourov Tonmoy, Sazzad Quayum, Al Russel Sarker, Sumaiya Umme Hani, and Mohammad Abdul Mannan. (2019). Smart Poultry Farm Incorporating GSM and IoT.

Mohammad Naim Elham, Mohammad Sadegh Sabeghi, Faris Salim Al-Rasbi, Salwani Mohd Daud, Nur Qamarina Noor, Rohilah Sahak, and Ahmad Akmaluddin Mazlan. (2019). ISCAIE 2020 : IEEE 10th Symposium on Computer Applications and Industrial Electronics : Malaysia, 18-19 April 2020.

Nasirahmadi, A., Gonzalez, J., Sturm, B., Hensel, O., and Knierim, U. (2020). Pecking activity detection in group-housed turkeys using acoustic data and a deep learning technique. Biosystems Engineering, 194, 40–48. https://doi.org/10.1016/j.biosystemseng.2020.03.015

Neethirajan, S. (2022a). Automated Tracking Systems for the Assessment of Farmed Poultry. Animals, 12(3). https://doi.org/10.3390/ani12030232

Neethirajan, S. (2022b). ChickTrack – A quantitative tracking tool for measuring chicken activity. Measurement: Journal of the International Measurement Confederation, 191. https://doi.org/10.1016/j.measurement.2022.110819

Neethirajan, S., and Kemp, B. (2021). Digital Livestock Farming. In Sensing and Bio-Sensing Research (Vol. 32). Elsevier B.V. https://doi.org/10.1016/j.sbsr.2021.100408

Ojo, R. O., Ajayi, A. O., Owolabi, H. A., Oyedele, L. O., and Akanbi, L. A. (2022a). Internet of Things and Machine Learning techniques in poultry health and welfare management: A systematic literature review. Computers and Electronics in Agriculture, 200. https://doi.org/10.1016/j.compag.2022.107266

Ojo, R. O., Ajayi, A. O., Owolabi, H. A., Oyedele, L. O., and Akanbi, L. A. (2022b). Internet of Things and Machine Learning techniques in poultry health and welfare management: A systematic literature review. In Computers and Electronics in Agriculture (Vol. 200). Elsevier B.V. https://doi.org/10.1016/j.compag.2022.107266

Olejnik, K., Popiela, E., and Opaliński, S. (2022). Emerging Precision Management Methods in the Poultry Sector. In Agriculture (Switzerland) (Vol. 12, Issue 5). MDPI. https://doi.org/10.3390/agriculture12050718

Patel, H., Samad, A., Hamza, M., Muazzam, A., and Harahap, M. K. (2022). Role of Artificial Intelligence in Livestock and Poultry Farming. Sinkron, 7(4), 2425–2429. https://doi.org/10.33395/sinkron.v7i4.11837

Pereira, W. F., Fonseca, L. da S., Putti, F. F., Góes, B. C., and Naves, L. de P. (2020). Environmental monitoring in a poultry farm using an instrument developed with the Internet of Things concept. Computers and Electronics in Agriculture, 170. https://doi.org/10.1016/j.compag.2020.105257

Philion, J., Kar, A., and Fidler, S. (2020). Learning to Evaluate Perception Models using Planner-Centric Metrics. https://nv-tlabs.github.io/detection-relevance.

Ramaprasad Poojary, and Akul Pai. (2019). 2019 International Conference on Electrical and Computing Technologies and Applications (ICECTA).

Razman, N. A., Ismail, W. Z. W., Kamil, N. A. I. M., Zainurin, S. N., Ismail, I., Jamaludin, J., Sahrim, M., Ariffin, K. N. Z., and Balakrishnan, S. R. (2022). A Review of Water Quality Monitoring Methods Based on Electronics and Optical Sensing. Journal of Advanced Research in Applied Sciences and Engineering Technology, 26(2), 1–7. https://doi.org/10.37934/araset.26.2.17

Sakamoto, K. S., Benincasa, N. C., da Silva, I. J. O., and Lobos, C. M. V. (2020). The challenges of animal welfare in modern Brazilian poultry farming. In Journal of Animal Behaviour and Biometeorology (Vol. 8, pp. 131–135). Malque Publishing. https://doi.org/10.31893/JABB.20018

Shafiur, M., Chowdhury, R., and Chowdhury, M. M. (2015). Profitability Analysis of Poultry Farming in Bangladesh: A Case Study on Trishal Upazilla in Mymensingh District. 5(19). www.iiste.org

Sinclair, M., Zhang, Y., Descovich, K., and Phillips, C. J. C. (2020). Farm animal welfare science in China—A bibliometric review of Chinese literature. Animals, 10(3). https://doi.org/10.3390/ani10030540

Sinduja, K., Jenifer, S. S., Abishek, M. S., and Sivasankari, B. (2016). Automated Control System for Poultry Farm Based On Embedded System. In International Research Journal of Engineering and Technology. www.irjet.net

Thenmozhi, M., Saravanan, M., Kumar, K. P. M., Suseela, S., and Deepan, S. (2020). Improving the prediction rate of unusual behaviours of animals in poultry using deep learning techniques. Soft Computing, 24(19), 14491–14502. https://doi.org/10.1007/s00500-020-04801-2

Wang, K., Liu, K., Xin, H., Chai, L., Wang, Y., Fei, T., Oliveira, J., Pan, J., and Ying, Y. (2019). An RFID-based automated individual perching monitoring system for group-housed poultry. Transactions of the ASABE, 62(3), 695–704. https://doi.org/10.13031/trans.13105

Wang, T., Xu, X., Wang, C., Li, Z., and Li, D. (2021). From smart farming towards unmanned farms: A new mode of agricultural production. Agriculture (Switzerland), 11(2), 1–26. https://doi.org/10.3390/agriculture11020145

Wu, D., Cui, D., Zhou, M., and Ying, Y. (2022). Information perception in modern poultry farming: A review. Computers and Electronics in Agriculture, 199, 107131. https://doi.org/10.1016/J.COMPAG.2022.107131

Wu, Y. chen, and Feng, J. wen. (2018). Development and Application of Artificial Neural Network. Wireless Personal Communications, 102(2), 1645–1656. https://doi.org/10.1007/s11277-017-5224-x

Yang, X., Chai, L., Bist, R. B., Subedi, S., and Wu, Z. (2022). A Deep Learning Model for Detecting Cage-Free Hens on the Litter Floor. Animals, 12(15). https://doi.org/10.3390/ani12151983

Yaw Kusi, L., Agbeblewu, S., Kwadwo Anim, I., and Minta Nyarku, K. (2015). The Challenges and Prospects of the Commercial Poultry Industry in Ghana: A Synthesis of Literature. In International Journal of Management Sciences (Vol. 5, Issue 6). http://www.rassweb.com

Zhang, F. Y., Hu, Y. M., Chen, L. C., Guo, L. H., Duan, W. J., and Wang, L. (2016). Monitoring the behaviour of poultry based on RFID radio frequency network. International Journal of Agricultural and Biological Engineering, 9(6), 139–147. https://doi.org/10.3965/j.ijabe.20160906.1568

Zhang, H., and Chen, changxi. (2020). Design of Sick Chicken Automatic Detection System Based on Improved Residual Network. In 2020 IEEE 4th Information Technology, Networking, Electronic and Automation Control Conference (ITNEC) (Vol. 1).

Zheng, K., Zhao, S., Yang, Z., Xiong, X., and Xiang, W. (2016). Design and Implementation of LPWA-Based Air Quality Monitoring System. IEEE Access, 4, 3238–3245. https://doi.org/10.1109/ACCESS.2016.2582153

PAPER 8 - DEFINING INTERACTION GROUPS AMONG INVERTER-BASED GENERATORS FOR SYSTEM STRENGTH ASSESSMENT IN POWER GRIDS

S. O. Sanni[1,2*], A. I. Abdullateef[1], O. O. Mohammed[1], F. I. Bawonda[3]

[1]Department of Electrical and Electronics Engineering, University of Ilorin, Ilorin, Nigeria
[2]Department of Electrical and Electronics Engineering, Federal University Oye Ekiti, Nigeria
[3]Department of Electrical and Electronics Engineering, Kogi State Polytechnic Lokoja, Nigeria

[*]Email: shereefdeen.sanni@fuoye.edu.ng

ABSTRACT
As inverter-based generation (IBG) proliferates in power grids, there are concerns about grid strength, particularly due to interactions among closely clustered IBGs. This study proposes a novel approach to identifying potential interactions between IBGs in power grids. The concept of "Relative Electrical Distance" (RED), derived from the network admittance matrix, is utilised to assess the likelihood of interaction between different points of interconnection (PoIs). The methodology involves iteratively converting each PoI into a synchronous generator and calculating the RED between this generator and all other PoIs. The resulting interaction matrix reveals potential interacting groups based on their RED values (0 signifies high interaction, while 1 indicates no interaction). The effectiveness of the proposed approach is demonstrated on two modified test systems: the IEEE 39-bus and the IEEE 57-bus system. The results show that the RED-based method successfully identifies interacting IBG groups within the network. This approach offers significant benefits for power grid operators and planners by simplifying the classification of interacting groups, identifying potential areas of concern, and eliminating the need for repetitive power flow studies. Further research will explore the application of the new approach in real-world scenarios, including simulations of actual control interaction scenarios.

KEYWORDS: Inverter-based generation, Short-circuit ratio, Synchronous condenser, System strength,

1. INTRODUCTION

In recent years, research has increasingly stressed the importance of system strength in the global transition of power grids to renewable energy sources (RES). This is due to the presence of inverter interfaces in the RES integration, leading to their categorisation as inverter-based generation (IBG) (Sanni *et al*., 2023). Moreover, in many cases, these IBGs are located in regions where the availability of resources such as wind energy and solar irradiance is guaranteed. However, the locations also allow the IBGs to exhibit weak characteristics due to their remote location from most synchronous generators (Arraño-Vargas *et al*., 2023; Sanni *et al*., 2024). This increases the IBG's system parameter sensitivity to disturbances, which is influenced by its strength. The short-circuit ratio (SCR) serves as a metric for measuring system strength (North American Electric Reliability Corporation (NERC), 2018). SCR quantifies the potential risks attributed to large-scale IBG integration within a power network, by defining the voltage response at the point of interconnection (PoI) (AEMO, 2020; Dozein *et al*., 2018). Weak systems, characterised by lower SCRs, experience substantial voltage fluctuations and other disturbances, leading to adverse effects like over-voltages, control instability, and low-frequency resonances (Schmall *et al*., 2015).
The control systems of IBGs can interact in ways that negatively impact grid stability, particularly in weak grids with high IBG penetration (Zhou *et al*., 2013). These interactions can trigger undesirable oscillations that threaten grid stability (Fernandes *et al*., 2015). Under these conditions, the SCR metric will provide an inadequate assessment of system strength since it does not account for these interactions. While alternative metrics that capture IBG interactions, such as the weighted short-circuit ratio (WSCR) and composite short-circuit ratio (CSCR), have been proposed, they do not consider the electrical connections of a power grid and thus assume full interaction between all IBGs, regardless of their physical location, which misrepresents the system's true strength at specific PoIs (Sanni *et al*., 2022; Wu *et al*., 2018). Additionally, these methods offer no guidance on defining the extent of interaction among IBGs within a network. Utilities such as the Australian Energy Market Operator (AEMO) already suggest limiting interaction assessment to within three buses surrounding the PoI (Australian Energy Market Operator (AEMO), 2020). However, the specific selection criteria for which bus is to be selected becomes ambiguous if several multiple buses fit the criteria for selection. This is also highlighted by the Electric Reliability Council of Texas (ERCOT), which expresses concern about how increasing numbers of IBGs complicate interaction boundary determination (Dissanayaka *et al*., 2018). In addition, the application of a power flow tracing strategy has been proposed as an alternative (Choi *et al*., 2021), though their results can be unreliable if network-

changing conditions are considered. Therefore, establishing clear and reliable boundaries to accurately assess IBG interaction and system strength remains a critical challenge.

Many power grid issues stem from the network's connectivity of the different components. This information is stored in the grid's network's admittance matrix which can be harnessed to solve network problems, particularly for nodes without the need for power flow solutions (Sanni *et al*., 2022). Studies have shown this approach is effective for tasks like identifying critical lines, weak nodes, and optimal locations for new generation, all without requiring power flow solutions (Aldaoudeyeh *et al*., 2019; Dhadbanjan and Chintamani, 2009; Ekic *et al*., 2018). Additionally, the RED concept based on this approach has proven useful in calculating reactive power contributions and allocating transmission charges, leading to improved efficiency and stability (Thukaram and Vyjayanthi, 2009; Visakha *et al*., 2004a). Overall, this structural analysis approach offers valuable tools for addressing various grid challenges without relying on computationally intensive methods.

Existing literature highlights the increased complexity of control interactions caused by the proliferation of IBGs, especially in weak grids, but struggles to define the precise "interaction zone" among them. This study addresses this gap by proposing the RED method, which uses network topology and line parameters to establish the interaction relationship between any two points in the grid, independent of changing conditions. The following sections explore the relationship between system strength and control interactions (Section 2). Sections 3 and 4 present the methodology, case study results, and discussions, respectively. Finally, Section 5 concludes the analysis.

2. SYSTEM STRENGTH AND CONTROL INTERACTIONS IN IBGS

Effective planning of the integration of IBG by grid operators requires assessing grid strength at the PoI. The SCR, which represents the ratio of the short-circuit capacity at a PoI to the connected IBG capacity, plays a vital role in this assessment (IEEE Standards Board, 1997). For a simple power system illustrated in Figure 1, an IBG is situated remotely and connected to a 'stiff' grid via a long transmission line, maintaining a constant voltage via synchronous generators (SGs). The SCR at bus *i* can be expressed as:

$$SCR_i = \frac{|S_{AC,i}|}{P_{\mathrm{IBG},i}} = \frac{|V_i|^2}{P_{\mathrm{IBG},i}} \cdot \frac{1}{Z_i} \tag{1}$$

where S_{ACi} is the short-circuit capacity of the AC system at bus I; P_{IBDGi} is the rated power of the inverter-based distributed generator; V_i is the voltage at the bus I; Z_i Thevenin equivalent impedance of the grid.

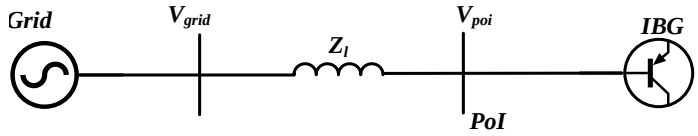

Figure 1: Simple representation of an IBG-grid system

To support grid voltage at the PoI, IBGs in voltage-control mode can inject or absorb reactive power (Q) as described by Equation (2) (Hu *et al*., 2019).

$$Q = \frac{V_{PoI}^2 - V_{PoI} V_{grid} \cos\delta}{Z_l} \tag{2}$$

The sensitivity of this reactive power injection to the PoI voltage is further explained by Equation (3) as:

$$\frac{dQ}{dV_{PoI}} = \frac{2V_{PoI} - V_{grid} \cos\delta}{Z_l} \tag{3}$$

Given a grid voltage of $V_{grid} = 1.0\ pu$ and $\delta = 0$, the sensitivity of the PoI's *depot/dQ* is represented in Equation (4) as:

$$\frac{dV_{PoI}}{dQ} = \frac{Z_l}{2V_{PoI} - 1} \tag{4}$$

Equations (1) and (4) both show how the electrical distance from the grid (Z_i or Z_l) affects system strength and IBG reactive power response at the PoI. This underscores the importance of impedance as a common factor in both system strength assessment and control system interactions within interconnected power grids. Thus, a weak grid (high impedance), characterised by low strength, experiences significant interactions due to increased sensitivity to

network changes. In contrast, strong grid (low impedance) exhibits minimal sensitivity due to their inherent resilience, even with high IBG penetration.

In other words, the network topology and impedances are critical factors in determining the effect of changing voltage at one PoI over the others (Troncia *et al*., 2021). Moreover, the rapid response of IBG controllers in scenarios with high penetration of closely connected PoIs and high sensitivity can exacerbate grid instability. For example, a voltage dip at one PoI triggers reactive power injection, but the sensitive controllers may overreact, causing an excessive voltage rise. This leads to reactive power absorption, creating a cycle of "hunting" that propagates to nearby IBGs and induces sustained oscillations, potentially leading to grid instability (North American Electric Reliability Corporation, 2017).

3. METHODOLOGY

In this section, the Relative Electrical Distance (RED) concept, derived from the network's admittance matrix, is extended to identify the boundaries of interaction between IBGs in power grids. Conventionally, it offers an indication of the relative position of a load bus to a synchronous generator bus for proportional resource allocation (Visakha *et al*., 2004b).

3.1 Formulation of Relative Electrical Distance Concept

An interconnected power system with IBG integration represented with *n* buses. Among these, buses 1, *2, 3, ..., g,* are conventional synchronous generator buses. The remaining *(n - g)* buses are categorised as composite load buses, incorporating both actual loads and IBG PoIs. The network Equation for this system is:

$$\begin{bmatrix} I_G \\ I_L \end{bmatrix} = \begin{bmatrix} Y_{GG} & Y_{GL} \\ Y_{LG} & Y_{LL} \end{bmatrix} \begin{bmatrix} V_G \\ V_L \end{bmatrix} \tag{5}$$

Where $[I_G] = [I_1, \cdots, I_g]^T$ and $[V_G] = [V_1, \cdots, V_g]^T$ are the vector of injected current and voltage of synchronous generators; $[I_L] = [I_{g+1}, \cdots, I_n]^T$ and $[V_L] = [V_{g+1}, \cdots, V_n]^T$ are the vector of injected current from the composite load buses. $[Y_{GG}]$, $[Y_{GL}]$, $[Y_{LG}]$, and $[Y_{LL}]$ are the corresponding part of the Y-bus admittance matrix. Rearranging (5) in terms of $[I_L]$ and $[V_G]$, we get,

$$\begin{bmatrix} V_L \\ I_G \end{bmatrix} = \begin{bmatrix} {Y_{LL}}^{-1} & -{Y_{LL}}^{-1}Y_{LG} \\ Y_{GL}{Y_{LL}}^{-1} & Y_{GG} - Y_{GL}{Y_{LL}}^{-1}Y_{LG} \end{bmatrix} \begin{bmatrix} I_L \\ V_G \end{bmatrix} \tag{6}$$

A compact representation of Equation (6) yields Equation (7) as:

$$\begin{bmatrix} V_L \\ I_G \end{bmatrix} = \begin{bmatrix} Z_{LL} & F_{LG} \\ K_{GL} & H_{GG} \end{bmatrix} \begin{bmatrix} I_L \\ V_G \end{bmatrix} \tag{7}$$

The vector for voltage and current is given as $V_L = [V_D \quad V_\Omega]^T$ and $I_L = [I_D \quad I_\Omega]^T$ respectively. subscripts "*D*" represents IBG PoI, and "*Ω*" represent load buses. The desired contributions of IBG injection to conventional generator buses can be derived from

$$[F_{LG}] = -[Y_{LL}]^{-1}[Y_{LG}] \tag{8}$$

The RED between composite load nodes and synchronous generator nodes is given as (Visakha *et al*., 2004b):

$$[RED] = [D] - abs[F_{LG}]] \tag{9}$$

Where [*D*] is an L x G unity matrix, representing the composite load buses (L rows) and synchronous generator buses (G columns).

Pre-multiplying row 1 of (7) by the conjugate of the diagonal IBG current matrix $[{I_D}^*]$, we have,

$$[{I_D}^*][V_D] = [{I_D}^*][Z_{LL}][I_D] + [{I_D}^*][F_{LG}][V_G] \tag{10}$$

Interpreting Equation (10) with respect to complex power injection as:

$$[S_{DG}] = [S_{DG}^L] + [S_{DG}^C] \tag{11}$$

If only the real part of Equation (11) is considered, we have:

$$[P_{DG}] = [P_{DG}^L] + [P_{DG}^C] \tag{12}$$

The ideal contribution of IBG injection interacting with synchronous generator buses is provided by $[P_{DG}^C]$.

3.2 Approach for Identifying the Boundary of Interaction

To assess potential interactions among PoIs, this study establishes an "interaction matrix". This matrix is built by iteratively converting each PoI into a synchronous generator. During each iteration, RED is calculated between this

converted PoI and all other PoIs, forming a new column in the interaction matrix. This process allows us to identify potential interactions based on their relative electrical distance as determined by the RED. The steps involved are outlined in Algorithm 1.

Algorithm 1: Defining interaction between IBG points of interconnection

Step 1. **Initialise:** Create an empty interaction matrix to store potential interactions between different PoIs.

Step 2. **Partition Network:** Based on the number of generators and composite load buses, the network is divided into different zones using Equation (5).

Step 3. **Calculate Reference Matrices:** Calculate two reference matrices **[F_{LG}], and [*RED*]** for the initial structure of the network using Equation (8) and (9) respectively. These matrices will be used as a reference point.

Step 4. **Iterate through PoIs:** For each PoI in the provided list:

a. Temporarily convert this specific PoI into a synchronous generator bus.

b. Re-partition the network equations (5) to account for the newly added generator and recalculate the **[F_{LG}] matrix**.

c. Based on the updated **[F_{LG}] matrix**, recalculate the ***[RED]* matrix**.

d. Extract the last column of the updated ***[RED]* matrix** and store it in the interaction matrix. This column represents the RED values between the generator (the current PoI) and all other PoIs.

Step 5. **Identify Interactions:** Loop through each column (representing a PoI) in the interaction matrix:

a. For each row (representing another PoI) in the current column, if the RED value is less than 1, it indicates a potential interaction.

b. If there is an interaction, add both PoIs (represented by the row and column indexes) to the same interaction group.

4. CASE STUDY RESULTS AND DISCUSSION

The effectiveness of the proposed RED method in identifying interaction boundaries among IBGs is examined through two case studies: the IEEE 39-bus and IEEE 57-bus systems. The case studies investigate the interaction potential between IBGs within each system using the RED concept. Python scripts were utilised to perform simulations and validate the approach.

4.1 Case 1: Modified IEEE 39 bus system

The single-line diagram of the modified IEEE 39 bus test system, comprising 39 buses with six conventional generators, 4 IBGs, and 17 loads, is shown in Figure 2. Other detailed parameters of the IEEE 39 bus system are available (Conto, 2015) and (Sanni *et al*., 2022).

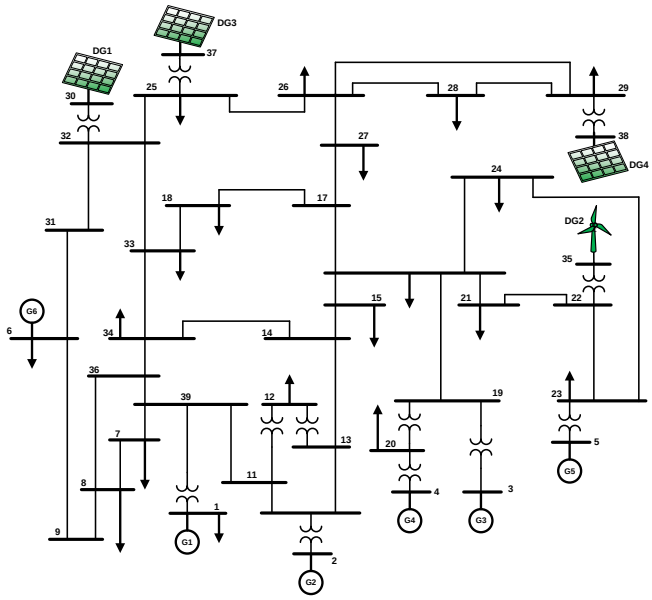

Figure 2: Single-line diagram of the modified IEEE 39-bus test system

Applying Algorithm 1 (described in Section 3.2) to this test system yields the resulting interaction matrix, visualised as a heatmap correlation plot in Figure 3. Based on the interpretation guidelines outlined in Section 3.2, all elements

in each row of the interaction matrix have values less than 1 for every column considered as the PoI. This implies that all IBG within the network units form a single interacting group. The heatmap also reveals the degree of interaction between specific IBGs. Bus 29, with the lowest RED value of 0.628, exhibits the strongest interaction with bus 22, as shown in column 1. In contrast, buses 32 and 25 show comparable interaction levels with bus 22. Moving to column 2, while bus 22 with a RED value of 0.818 indicates a lower level of interaction, buses 29 and 32 display similar values, suggesting similar interaction strengths with bus 25. However, bus 29's lower RED value (0.215) indicates a slightly stronger interaction compared to bus 32. Column 3 demonstrates that bus 22 experiences the least level of interaction with bus 29 among the three analysed buses. Column 4 reveals that bus 25 exerts the most significant influence on bus 32, evidenced by the lowest RED value of 0.055. This aligns with the network diagram, showing a direct connection between these two buses thus validating the result of the RED concept.

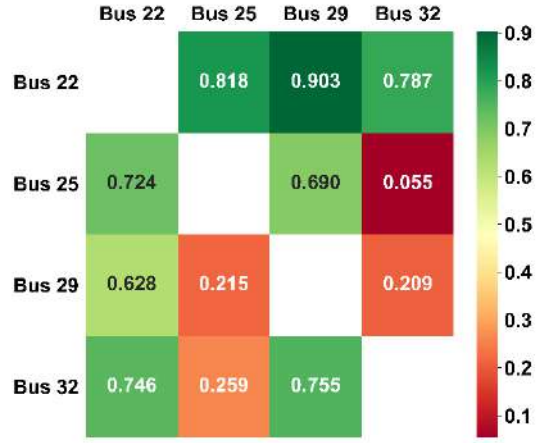

Figure 3: Heatmap correlation of the RED interaction matrix for the IEEE 39-bus system

4.2 Case 2: Modified IEEE 57 bus system

This section analyses the IEEE 57-bus system, illustrated by the single-line diagram in Figure 4. The original network with seven conventional generators was modified to include four IBGs dispersed across a wider area. In such scenarios, identifying the interaction boundary helps understand potential IBG risk areas within the grid.

Figure 4: Single-line diagram of the modified IEEE 57-bus test system

The proposed method was applied to the network, and the resulting heat map correlation plot of the RED interaction matrix is presented in Figure 5. Two distinct groups of interacting IBGs are identified: group 1 which includes IBGs

at buses 31, 34, and 36; and group 2 consisting solely of the IBG at bus 16. Within Group 1, considering bus 31 as the PoI (column 1), bus 34 (with a RED value of 0.792) will interact more closely compared to bus 36 (with a RED value of 0.865). Also, within this group, IBGs at buses 31 and 36 will have a similar level of interaction with bus 34 (column 2), although bus 36 will exert a slightly greater influence. When bus 36 is the PoI (column 3), the IBG at bus 34 (with a RED value of 0.034) will interact significantly more closely than bus 31. This highlights that the level of interaction is not symmetrical between any two buses. While one bus may significantly influence another, the reverse may not hold true. A review of column 4 for bus 16 shows that all RED values are 1, indicating that none of the other IBG PoIs in the network will interact with it. This explains why bus 16 forms the sole member of group 2. The isolated topological location of the IBG at bus 16 aligns with this finding, suggesting minimal influence on, or from, other IBGs in terms of interaction patterns. This demonstrates one of the advantages of the RED approach: its ability to efficiently identify limited interaction scenarios. This shows that the RED approach offers several advantages. Firstly, it simplifies the classification of IBG groups likely to interact with each other. Secondly, it serves as a valuable tool during IBG integration planning. By quickly identifying potential interacting IBGs that might impact system operation, the RED method eliminates the need for repetitive power flow studies. This becomes particularly beneficial for larger networks, where numerous components can influence network operation.

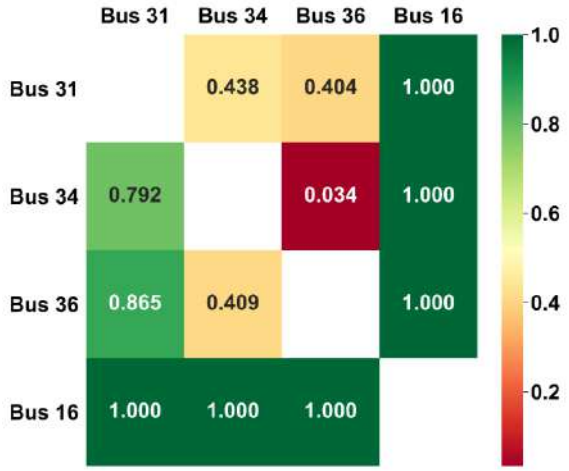

Figure 5: Heatmap correlation of the RED interaction matrix for the IEEE 57 bus system

4. CONCLUSION

This study has presented a novel and effective method for identifying interacting IBGs in power grids using the RED concept. The proposed method was implemented on two modified IEEE test systems: the 39-bus and 57-bus systems. Both systems included the integration of IBGs at various locations within the network. In the 39-bus system, all IBGs formed a single interaction group due to network size and their proximity within the network. The heatmap visualisation of the interaction matrix revealed the strength of interaction between specific IBG pairs, with buses 25 and 29 exhibiting the strongest interaction on bus 32. The 57-bus system presented a more complex scenario with geographically dispersed IBGs. The proposed method successfully identified two distinct interaction groups: one consisting of IBGs at buses 31, 34, and 36, and another solely comprising the IBG at bus 16. This result aligned with the network topology, where bus 16's location isolated it from the other IBGs. The heatmap further demonstrated the varying degrees of interaction within each group, while also highlighting the non-symmetrical nature of these interactions between any PoI pair. This approach offers significant benefits for power grid operators and planners by simplifying the classification of interacting groups, identifying potential areas of concern, and without the need for repetitive power flow studies. Further research will validate the new approach in real-world practical power grids by validating it with actual control interaction phenomena.

REFERENCES

AEMO. (2020). System Strength in the NEM explained. In *Australian Energy Market Operator (AEMO)*.

Aldaoudeyeh, A. M., Wu, D., and Jiang, J. J. (2019, August). Identification of Critical Branches for Improving Weak Grid with Large-scale Integration of Inverter-based Resources. *2019 IEEE Power and Energy Society General Meeting (PESGM)*. https://doi.org/10.1109/pesgm40551.2019.8974106

Arraño-Vargas, F., Jiang, S., Bennett, B., and Konstantinou, G. (2023). Mitigation of power system oscillations in weak grids with battery energy storage systems: A real-world case study. *Energy*, *283*, 128648. https://doi.org/10.1016/j.energy.2023.128648

Australian Energy Market Operator (AEMO). (2020). System Strength in the NEM explained. In *System Strength*.

Choi, N., Lee, B., Kim, D., and Nam, S. (2021). Interaction Boundary Determination of Renewable Energy Sources to Estimate System Strength Using the Power Flow Tracing Strategy. *Sustainability 2021, Vol. 13, Page 1569*, *13*(3), 1569. https://doi.org/10.3390/SU13031569

Conto, J. (2015). *Dynamics Networks 4 PSSe - Google Drive*. https://drive.google.com/drive/folders/0B7uS9L2Woq_7fmd4YXVxMEZKT3dJV2FleGkzS2FzVmd1RHhBNVdUTGpvdldkMnl2bXRLM1k?resourcekey=0-nuCqXu2XJ0_fxBzwHcmCGg

Dhadbanjan, T., and Chintamani, V. (2009). Evaluation of Suitable Locations for Generation Expansion in Restructured Power Systems: A Novel Concept of T-index. *International Journal of Emerging Electric Power Systems*, *10*(1). https://doi.org/10.2202/1553-779x.2023

Dissanayaka, A., Wiebe, J., and Isaacs, A. (2018). Panhandle and South Texas stability and system strength assessment. In *ERCOT, Tech. Rep*.

Dozein, M. G., Mancarella, P., Saha, T. K., and Yan, R. (2018, November). System Strength and Weak Grids: Fundamentals, Challenges, and Mitigation Strategies. *2018 Australasian Universities Power Engineering Conference (AUPEC)*. https://doi.org/10.1109/aupec.2018.8757997

Ekic, A., Fischer, A., Eisenbeisz, A., Lind, G., Aldaoudeyeh, A. M., and Wu, D. (2018, September). Impact Analysis of Power Network Structure on Grid Strength. *2018 North American Power Symposium (NAPS)*. https://doi.org/10.1109/naps.2018.8600573

Fernandes, R., Achilles, S., and MacDowell, J. (2015). *Report to NERC ERSTF for Composite Short Circuit Ratio (CSCR) Estimation Guideline*.

Hu, S., Xiang, Y., Zhang, X., Liu, J., Wang, R., and Hong, B. (2019). Reactive power operability of distributed energy resources for voltage stability of distribution networks. *Journal of Modern Power Systems and Clean Energy*, *7*(4), 851–861.

IEEE Standards Board. (1997). *IEEE Guide for Planning DC Links Terminating at AC Locations Having Low Short-Circuit Capacities* (IEEE Standard 1204-1997). IEEE. https://doi.org/10.1109/ieeestd.1997.85949

North American Electric Reliability Corporation. (2017). *Integrating Inverter-Based Resources into Low Short Circuit Strength Systems*.

North American Electric Reliability Corporation (NERC). (2018). Short-Circuit Modeling and System Strength. *White Paper, February*.

Sanni, S. O., Abdullateef, A. I., and Mohammed, O. O. (2023). The Implications of Low Short-Circuit Capacity on the Strength of Power Grid : A Nigerian Case Study. *1st Faculty of Engineering and Technology Conference (FETiCON 2023), Jun. 5 - 7, 2023, University of Ilorin, Nigeria*, *1*, 652–658.

Sanni, S. O., Abdullateef, A. I., Mohammed, O. O., Aman, M. N., Raji, A. K., and Fajuke, I. D. (2024). Investigating the Impact of Solar PV and Wind Energy Systems on the Strength of a Longitudinal Power Grid. *E-Prime - Advances in Electrical Engineering , Electronics and Energy*, *8*(May), 100593. https://doi.org/10.1016/j.prime.2024.100593

Sanni, S. O., Akorede, M. F., and Olarinoye, G. A. (2022). Strength assessment of electric power systems containing inverter-based distributed generation. *Electric Power Systems Research*, *207*. https://doi.org/10.1016/j.epsr.2022.107825

Schmall, J., Huang, S.-H., Li, Y., Billo, J., Conto, J., and Zhang, Y. (2015, July). Voltage stability of large-scale wind plants integrated in weak networks: An ERCOT case study. *2015 IEEE Power and Energy Society General Meeting*. https://doi.org/10.1109/pesgm.2015.7286224

Thukaram, D., and Vyjayanthi, C. (2009). Relative electrical distance concept for evaluation of network reactive power and loss contributions in a deregulated system. *IET Generation, Transmission and Distribution*, *3*(11), 1000–1019. https://doi.org/10.1049/iet-gtd.2009.0154

Troncia, M., Ávila, J. P. C., Pilo, F., and San Román, T. G. (2021). Remuneration mechanisms for investment in reactive power flexibility. *Sustainable Energy, Grids and Networks*, *27*, 100507.

Visakha, K., Thukaram, D., and Jenkins, L. (2004a). Transmission charges of power contracts based on relative electrical distances in open access. *Electric Power Systems Research*. https://doi.org/10.1016/j.epsr.2003.12.003

Visakha, K., Thukaram, D., and Jenkins, L. (2004b). Transmission charges of power contracts based on relative electrical distances in open access. *Electric Power Systems Research*. https://doi.org/10.1016/j.epsr.2003.12.003

Wu, D., Li, G., Javadi, M., Malyscheff, A. M., Hong, M., and Jiang, J. N. (2018). Assessing Impact of Renewable Energy Integration on System Strength Using Site-Dependent Short Circuit Ratio. *IEEE Transactions on Sustainable Energy*, *9*(3), 1072–1080.

Zhou, Y., Nguyen, D. D., Kjaer, P. C., and Saylors, S. (2013). Connecting wind power plant with weak grid - Challenges and solutions. *2013 IEEE Power and Energy Society General Meeting*. https://doi.org/10.1109/pesmg.2013.6672755

PAPER 9- EFFECT OF MULTIPLE OPERATIONAL FACTORS ON PUSH FORCE IN A PUSH BEHIND LAWNMOWER

J. I. Ayanlade[1*], L. O. Akomolafe[1], S. M. Adedayo[1]

[1]Department of Mechanical Engineering, University of Ilorin, Ilorin, Nigeria.

[*]Email: 17-30gd024@students.unilorin.edu.ng

ABSTRACT

Push force is an indicator for making various design and optimization decisions when developing lawnmowers. This study aims to develop a model that can be used to estimate push force during mowing operations. Prediction models were developed through regression analysis using key factors affecting push force. The push speed, cutter height, and grass height were selected as explanatory variables. Push force readings were obtained using a horizontally positioned weighing balance, while push speeds were obtained from the distances covered and time taken. A total of four push force prediction regression models were proposed using 50 experimental data. The adjusted coefficient of determination (R^2) of the proposed regression model showed a range of 0.252 to 0.660 and a mean absolute percentage error of 4.9 to 8.12. Models C (which accounts for the push speed and the cutter height) and D (which accounts for the push speed, cutter height and grass height) satisfy all the basic assumptions of the regression analysis. Model D has the least MAPE and the highest R2 values, making it suitable for push force prediction.

KEYWORDS: Big wheels, Cutter height, Grass height, Lawnmower, Push force, Push speed, Regression model.

1. INTRODUCTION

A lawnmower is a machine that uses a revolving blade to cut a lawn to an even height (Duniyan *et al*., 2020). Reel mowers and rotary mowers are the two basic types of lawnmowers. The axis of rotation of blades distinguishes the reel and rotary mower. While the blade rotates along the horizontal axis in the former, the blade rotation is along the vertical axis in the latter (Adubika and Adebayo, 2021; Tanaji *et al*., 2018). As opposed to self-propelled lawnmowers, rotary mowers are often powered by internal combustion engines or electric motors, and they are navigated by hand with the engine configured to simply spin the cutting blades (Tanaji *et al*., 2018). The cutting blade is made of a variety of materials; however, stainless steel is typically utilized in applications where resistance to corrosion, weight and strength are crucial (Ajetunmobi *et al*., 2022).

As noted by Tanaji *et al*. (2018), the force required to cut the lawn depends on the height, density, and area of the grass. Also, vibration, grass height, soil moisture, terrain smoothness, and push speed have been identified to affect the efficiency of a lawnmower and, by extension, affect the push force and comfort of the user (Abolarinwa and Adedayo, 2018; Ajetunmobi *et al*., 2022; Okokpujie *et al*., 2017; Olaoye *et al*., 2012).

There are different methods used in measuring force; a load cell was used by Garg *et al*. (1988) to obtain the static pulling strength when evaluating the one-handed dynamic pulling strength of lawn mower users, while an electromagnetic dynamometer was used to obtain the dynamic pulling strengths. When studying the effect of the angle of the mower handle on the manoeuvrability of a simple self-powered lawn mower, Okafor (2013) used the relation $P = Wsin\theta$ to determine the force required to move the mower, where W is the weight of the mower and P is the push force.

In order to predict the tractor axle torque during tillage operation, Kim *et al*. (2020) developed a model using regression analysis by considering operational factors which include engine torque, engine speed, tillage depth, slip ratio, and travel speed.

This work aims to study the effect of multiple operational factors on push force in a locally fabricated push-behind lawnmower using a regression analysis and to develop a push force prediction model based on the relationship between these factors and the push force. The factors taken into consideration are the cutter height, grass height, and push speed. Regression analysis would be used to examine the relationship between these variables. The push force is the response variable, otherwise known as the dependent variable, while the cutter height, grass height, and push speed are the explanatory variables (independent variables).

2. METHODOLOGY

.

2.1 Mower description and specification

The large-sized wheeled lawn mower (as shown in Fig. 1) is an indigenous mower, both in conception and development (Salami, 2021). Its major components include a 5.5 Hp spark ignition I.C engine, orthogonal drive bevel gearbox, 700 mm diameter wheels, a locally fabricated cutter, and adjustable height brackets. The maximum weight is 35 kg. The large wheels, located around the center of gravity of the machine, serve to reduce horizontal push force and enable easy movement along rough terrains. The handle is adjustable in height, and it features a fixture to which the push force measurement device is attached. The weighing scale used for measuring the horizontal push force is a "Camry" weighing scale with dimensions of 258 x 258 x 320 mm, which has an accuracy of 50 grams and can measure weights up to 20 kg.

2.2 Experimental field demarcation

The experiments were carried out on a demarcated 10 x 5 m buffalo grass (*Stenoaphrum secundatum*) field at 8°29'0.8"N 4°40'28.5"E. The field length was further divided into three equal sections, each measuring 2.5 m with clearance of 1.25 m at extreme ends, as shown in Figure 2. The experiment started from the point labelled "S," and push force and time taken were recorded at Points X, Y, and Z, providing a total of three sets of push force and time readings for each experiment. The experiment was repeated until a total of 7.5 m x 4.5 m cut area was covered, resulting in a total of 15 data per experimental field. The area covered during the first experiment is depicted by the labelled portion "F".

Figure 1. The locally-made lawnmower.

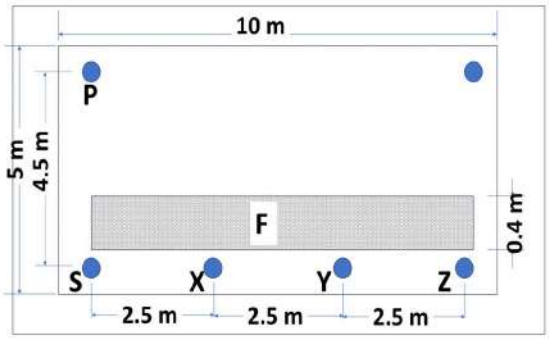

Figure 2. Demarcation of Experimental field.

2.3 Measurement of Push Force and Push Speed

The push force is the force required to move the lawnmower across the lawn. A weighing scale was used to measure this force. A weighing scale designed for measuring the mass of an object placed vertically on it was fixed horizontally by a metallic frame as shown in Figure 1. The values obtained directly on this device were multiplied by a factor of 9.8 to get the corresponding force values in Newton.

The push speed was obtained by measuring the time taken in seconds for the mower to cover a fixed distance of 10 m during operation. To achieve a better reading, the experiment was carried out 3 times for the same walking pace and in the same environmental conditions, the average of these values was used for the analysis.

2.4 Regression Model Development

Using the data obtained from the experiment, a simple regression was developed for the push force and each of the explanatory variables, as represented in the equations below;

$$P_f = \beta_0 + \beta_1 P_s + \varepsilon \quad (4)$$

$$P_f = \beta_0 + \beta_2 C_h + \varepsilon \quad (5)$$

$$P_f = \beta_0 + \beta_3 G_h + \varepsilon \quad (6)$$

The multiple regression model was developed for a combination of explanatory variables and is represented in the equations below;

$$P_f = \beta_0 + \beta_1 P_s + \beta_2 C_h + \varepsilon \quad (7)$$

$$P_f = \beta_0 + \beta_1 P_s + \beta_2 C_h + \beta_3 G_h + \varepsilon \quad (8)$$

From equations 4-8, P_f is the push force (N), P_s is the push speed (m/s), G_h is the grass height (m), C_h is the cutter height (m), β_0 is the intercept, $\beta_1, \beta_2, \beta_3$ are the coefficients of the regression models, ε is the model error.
Based on the above equations, the prediction model was developed, with a total of three variable conditions, which include push speed, cutter height, and grass height, using the following Python packages*; sklearn, pandas, numpy, matplotlib, seaborn, and statsmodels. scipy.* The following basic assumptions were made; linearity, normality, independence, homoscedasticity, and multicollinearity.

.

2.5 Verification of Regression Models

The predictive ability of the developed model was evaluated using R^2, mean absolute percentage error (MAPE), root mean square error (RMSE), and relative deviation (RD), which are given in the equation below (Kim *et al*., 2020):

$$R^2 = \frac{\sum_{j=1}^{j=N}(y_j - \bar{y}) - \sum_{j=1}^{j=N}(y_j - \hat{y}_j)}{\sum_{j=1}^{j=N}(y_j - \bar{y})} \quad (9)$$

$$MAPE = \frac{1}{N}\sum_{j=1}^{j=N}\left|\frac{1}{y_j}(y_j - \hat{y}_j)\right| x\ 100(\%) \quad (10)$$

$$RMSE = \sqrt{\frac{1}{N}\sum_{j=1}^{j=N}(\hat{y}_j - y_j)^2} \quad (11)$$

$$RD = \frac{RMSE}{Mean}\ x\ 100 \quad (12)$$

where $\bar{y}$ is the mean push force, y_j is the j[th] actual push force, and $\hat{y}_j$ is the jth predicted push force.

3. RESULTS AND DISCUSSION

3.1 Correlation Analysis

For all the independent variables under investigation, three experimental fields were used, and a total of 50 data were obtained after removing the data obtained at the start of each experiment. These data were not considered during analysis because of the large deviation of these values relative to subsequent readings obtained, owing to the high static friction that must be overcome to move the mower from rest in contrast to the kinetic friction.
Table 1 shows the results of the correlation analysis for the factors taken into consideration. The average push force, which is the dependent variable, had a moderate correlation with the average push speed (r = 0.502), a negative relationship with the cutter height (r = -0.651), and a very low correlation with the average grass height (r = 0.058). This suggests that the cutter height and average push speed are the main factors that affect the push force value.

Table 1. Pearson correlation coefficient matrix for variables predicting push force

	Avg Push Speed, P_s	**Avg Grass Height, G_h**	**Cutter Height, C_h**	**Avg Push Force, P_f**
P_s	1.00			
G_h	0.115	1.000		
C_h	-0.145	0.378	1.00	
P_f	0.502	0.058	-0.651	1.00

3.3 Prediction Model

3.3.1 Development of the Regression Model

Four regression models were developed, which include both single regression models and multiple regression models. Each explanatory variable was considered in developing the single regression models, while one of the multiple regression models was developed using the combined data of push speed and cutter height, and the other was developed using the combined data of the three independent variables. Table 2 shows the R^2, adjusted R^2, and standardized error (S.E.) for each regression model. The R^2 values indicate the accuracy with which each developed model can predict the actual push force.

Table 2. Regression model for prediction of Push force

Model	Regression Model	R^2	R^2 adj	S.E
A	$23.741P_s + 80.04$	0.252	0.236	10.76
B	$-4.764C_h + 132.461$	0.424	0.412	9.439
C	$19.690P_s - 4.323C_h + 108.92$	0.594	0.577	8.01
D	$17.371P_s + 0.776G_h - 5.156C_h + 105.80$	0.660	0.638	7.41

The degrees of freedom (Df), sum square (SS), mean square (MS), F-value, and p-value for each model were calculated using ANOVA. Table 3 presents the results of the ANOVA regression analysis for each model. All regression models are significant and can be used to predict push force using their input parameters because their F-significant values are less than 0.05 at the 95% confidence level. Model B had the highest F-value (35.381), which is a measure of the extent to which the regression model's results were more than the average prediction. This implied that the addition of only the cutter height variable to the prediction model improved the model's fit the most. Models C (34.373), D (29.739), and A (16.160) had the next highest F-values.

Table 3. Analysis of variance (ANOVA) for each prediction regression model

Model		Df	SS	MS	F-Value	F-significant
	Regression	1	1871.351	1871.352	16.160	0.0002045
A	Residual	48	5558.423	115.800		
	Total	49	7429.774			
	Regression	1	3152.661	3152.661	35.381	3.008E-07
B	Residual	48	4277.113	89.107		
	Total	49	7429.774			
	Regression	2	4412.823	2206.411	34.373	6.337E-10
C	Residual	47	3016.951	64.190		
	Total	49	7429.774			
	Regression	3	4902.198	1634.066	29.739	7.66E-11
D	Residual	46	2527.577	54.947		
	Total	49	7429.774			

3.3.2 Normality Test of Residuals

One of the assumptions of the regression analysis is that the data must be normally distributed. Therefore, it was crucial to confirm this presumption. For each prediction model (A–D), Figure 3 displays the distribution of the

regression-standardized residuals. It shows a normal distribution with constant variance and zero as the mean of the regression standardized residuals. The outcome showed that the residuals in each model satisfied normality and followed a normal distribution.

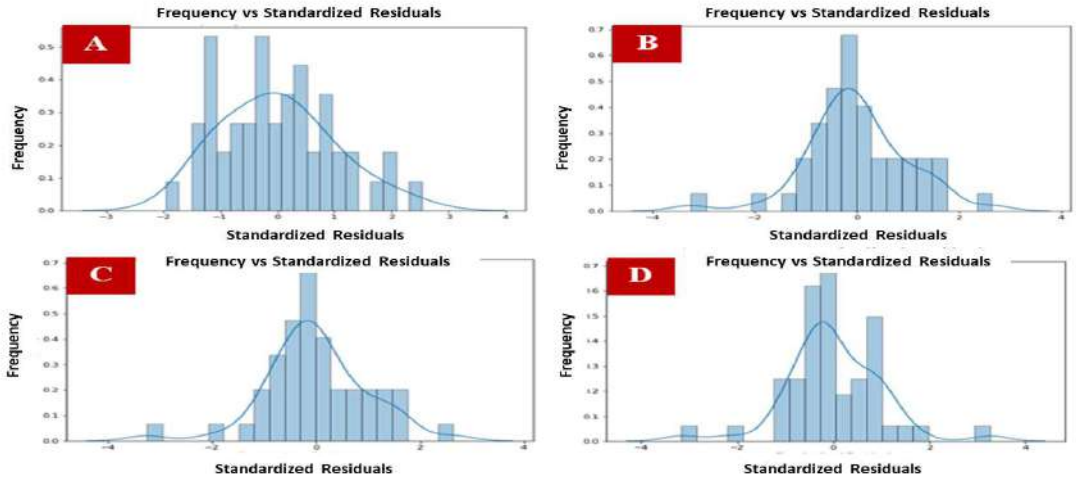

Figure 3. The distribution of the regression's standardized residuals for each prediction. Model (A–D).

Model A represents push force as a linear function of push speed; Model B represents push force as a linear function of cutter height; Model C represents push force as a linear function of push speed and cutter height; and Model D represents push force as a linear function of push speed, grass height, and cutter height.

3.3.3 Test of Multicollinearity

Tolerances and variance inflation factors (VIFs) are used to evaluate the collinearity problems of the developed linear regression models. As presented in Table 5, all the regression models showed a VIF of less than 10, with the highest being 1.218. According to Gujarati (2012) and Ayinde *et al*.(2020), when the VIF is greater than 10, it shows that the model suffers from collinearity. Since the VIFs are well below 10, it can be said that the developed regression model is usable.

3.4 Model Verification

The measured data was used to validate the four prediction models. Figure 4 shows the relationship between the predicted push force and the actual push force for each prediction model. The comparison of the results was done using a 1:1 line. The distribution of the actual push force and the predicted push force deviates from a 1:1 line, and there is some vertical deviation (i.e., error) from the 1:1 line, according to prediction Model A. Other models also exhibit this, though not to the same extent as model A. The 1:1 line and the prediction model D have a close distribution, making it possible to predict the actual push force.

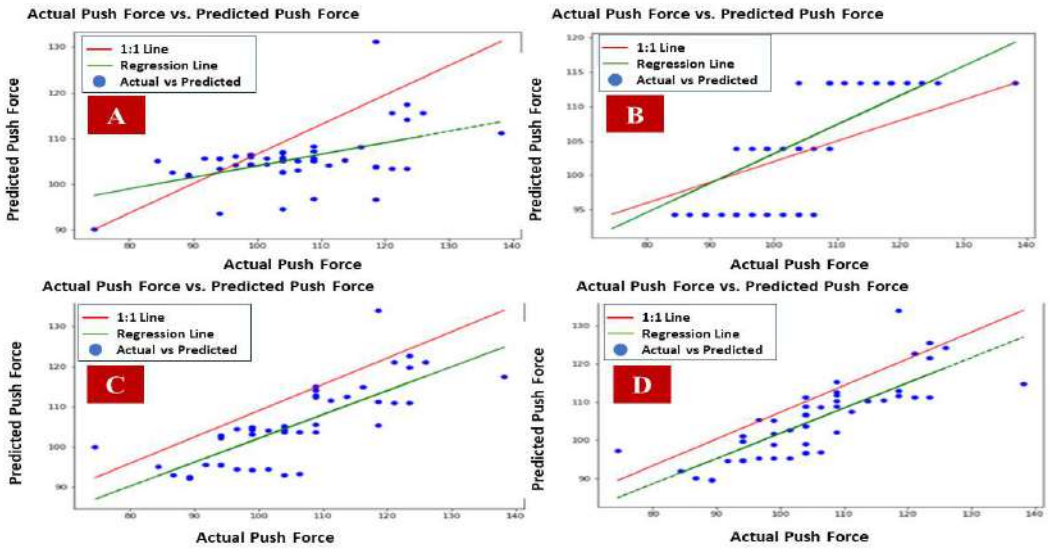

Figure 4. Relationships between the predicted and measured push force for each regression. Model (A–D). Model A represents push force as a linear function of push speed; Model B represents push force as a linear function of cutter height; Model C represents push force as a linear function of push speed and cutter height; and Model D represents push force as a linear function of push speed, grass height, and cutter height.

The results of the actual push force prediction performance evaluation are shown in Table 4 for each prediction regression mode. It was discovered that for all regression models, the MAPE was less than 9% and the R^2 ranged from 0.252-0.660. Additionally, the RMSE and RD showed respective ranges of 7.11 to 10.54 N and 6.75 to 10%. With a MAPE of 8.12%, Model A showed the lowest level of accuracy. With an R^2 of 0.66, MAPE of 4.9%, RSME of 7.11 N, and RD of 6.75%, Model D performed the best. Thus, it was discovered that three explanatory variables—push speed, cutter height, and grass height—could describe the push force in the best way.

Table 4. Regression models' actual push force prediction performance result

Model	R^2	MAPE (%)	RMSE(N)	RD (%)
A	0.252	8.12	10.54	10.00
B	0.424	6.24	9.25	8.78
C	0.594	5.49	7.77	7.37
D	0.660	4.90	7.11	6.75

3.5 Discussion

A model for predicting a locally designed and developed lawnmower push force is presented. The cutter height, average push speed, and average grass height were the three factors used to develop the push force prediction models. These three variables had Pearson correlation coefficients in increasing order: cutter height, average push speed, and average grass height. The developed models A and B had low adjusted R^2 values of 0.252 and 0.424, respectively, making them unsuitable for use as models to forecast push force. Models C and D both had R^2 values above 0.5, indicating that by combining the explanatory factors, the prediction model's accuracy can be increased. Models C and D satisfied the assumptions of regression analysis, including linearity, normality, independence, homoscedasticity, and multicollinearity. For the developed locally-made lawnmower, model D is more suitable for push force prediction because it has the lowest MAPE (4.9%) and RMSE (7.11 N), the highest R^2 (66%), and satisfies all fundamental regression analysis assumptions.

4. CONCLUSION

In this study, a model for predicting push force during lawn-mowing operations was developed. Three variables that have an impact on push force were taken into account. The push force is the dependent variable, and the push speed, cutter height, and grass height were chosen as independent variables. The range of the proposed regression model's adjusted R^2 was 0.252 to 0.66, with model D (which includes the independent variables push speed, grass height, and cutter) having the greatest R2 value. Model D has the least MAPE and the highest R2 value and is considered suitable for push force prediction.

REFERENCES

Abolarinwa, E., and Adedayo, S. (2018). Design, development and testing of an orthogonal shaft transmission lawn mowing machine. *Leonardo Electronic Journal of Practices and Technologies*, *32*, 173–182.

Adubika, O. A., and Adebayo, S. D. (2021). Design and Fabrication of Solar Operated Car. *International Journal for Research in Applied Science and Engineering Technology*, *9*(VII), 1177–1180. https://doi.org/10.22214/ijraset.2021.36307

Ajetunmobi, O.; Ajetunmobi, D. T., Odede, M. M., and Bello, T. (2022). Development of an Improved Solar-Powered Lawnmower. *International Journal of Women in Technical Education and Employment (IJOWITED)*, *3*(1), 12–18. https://fpiwitedjournal.federalpolyilaro.edu.ng

Ayinde, K., Lukman, A., and Olusegun, A. O. (2020). A New Approach of Principal Component Regression Estimator with Applications to Collinear Data. *International Journal of Engineering Research and Technology*, *13*(7), 1616–1622. https://doi.org/10.37624/IJERT/13.7.2020.1616-1622

Daniyan, I., Balogun, V., Adeodu, A., Oladapo, B., Kayode, J., Balogun, V., and Kayode, J. (2020). Development and Performance Evaluation of a Robot for Lawn Mowing. *Procedia Manufacturing*, *49*(2019), 42–48. https://doi.org/10.1016/j.promfg.2020.06.009

Garg, A., Funke, S., and Janisch, D. (1988). One-handed dynamic pulling strength with special application to lawnmowers. *Ergonomics*, *31*(8), 1139–1153. https://doi.org/10.1080/00140138808966753

Gujarati, D. N. (2012). *Basic Econometric* (4th ed.). McGraw-Hill Higher Education.

Kim, W., Kim, Y., Baek, S., Baek, S., Kim, Y., and Park, S. (2020). Development of a Prediction Model for Tractor Axle Torque during Tillage Operation. *Applied Sciences*, *10*(12), 4195–4214.

Okafor, B. (2013). Simple Design of Self-Powered Lawn Mower. *International Journal of Engineering and Technology*, *3*(10), 933–938.

Okokpujie, P. I., Okokpujie, K. O., Ajayi, O. O., and Joseph, A. (2017). Design, Construction and Evaluation of a Cylinder Lawn Mower. *Journal of Engineering and Applied Sciences*, *12*(5), 1254–1260.

Olaoye, J. O., Samuel, O. D., Adekanye, T. A., Campus, I., State, O., and Author, C. (2012). Performance Evaluation of an Indigenous Rotary Power Weeder. *Energy and Environmental Engineering Journal*, *1*(2), 1–4.

Tanaji, S. V., Chandrakant, C. S., Shashikant, P. S., Raju, G. O., and Bhalchandra, G. S. (2018). Automated mower robot. *International Research Journal of Engineering and Technology*, *5*(1), 343–346.

PAPER 10- HARMONIC DISTORTION IN PV SYSTEMS: A COMPARATIVE STUDY OF PID AND ANN CONTROLLERS

A. J. Aliyu*[1], N. A. Iliyasu[1], D. E. Abah[1]

[1]Department of Electrical Engineering, Ahmadu Bello University

*Email: aminujaliyu@gmail.com

ABSTRACT

This paper presents a comparative analysis of Total Harmonic Distortion (THD) in grid-connected Photovoltaic (PV) systems controlled by Proportional Integral Derivative (PID) and Artificial Neural Network (ANN) strategies. THD is a critical factor affecting power quality, and managing it is crucial. While PID controllers are traditionally used for their simplicity and effectiveness, their performance can be limited under varying conditions. ANNs, on the other hand, offer adaptability and robustness, making them a promising alternative. Through rigorous simulations and real-world testing, this paper evaluates the performance of both control strategies under different operating conditions. The findings provide valuable insights into the choice of control strategy for grid-connected PV systems, contributing to the broader goal of enhancing the reliability and efficiency of renewable energy systems.

KEYWORDS: Harmonic Distortion, ANN, PID, THD, PV, MATLAB

1. INTRODUCTION

The advent of renewable energy sources has revolutionized the energy sector, with Photovoltaic (PV) systems emerging as a promising and sustainable solution. PV systems convert sunlight directly into electricity, offering a clean, renewable, and abundant source of power. However, the integration of these systems into the grid poses several challenges, particularly in terms of power quality. One of the critical factors affecting power quality is Total Harmonic Distortion (THD). THD is a measure of the distortion of the electrical signal and can have significant implications for both the performance and lifespan of the system (Keerthana and Sathyan, 2018). High levels of THD can lead to a variety of problems. These include a reduced power factor, which can result in increased electricity costs; increased heating in equipment, which can shorten the lifespan of the equipment and increase maintenance costs; and malfunctioning of sensitive electronics, which can lead to operational inefficiencies (Kamel, 2016; Rana *et al*., 2022). Therefore, managing THD is of paramount importance in grid-connected PV systems.

Traditionally, Proportional Integral (PID) controllers have been widely used to manage THD. PID controllers are a type of feedback controller where the error (difference between the desired and actual output) is processed and used to adjust the system's control inputs (M. Hassan *et al*., 2023). The PID controller is simple in design and effective in eliminating steady-state errors, making it a popular choice in many control systems (Harrag and Messalti, 2015; A. Hassan *et al*., 2023; Karami *et al*., 2017).

However, with the increasing complexity and non-linearity of power systems, the limitations of PID controllers are becoming more apparent. For instance, PID controllers may not perform optimally under varying operating conditions or in the presence of noise. Furthermore, they require accurate knowledge of the system's dynamics, which may not always be available or easy to obtain (Senthilkumar *et al*., 2022).

In light of these challenges, there is a growing interest in exploring more advanced control strategies. One such strategy is the use of Artificial Neural Networks (ANNs). ANNs are computing systems inspired by the human brain's neural networks. They consist of interconnected processing elements, or "neurons," that work together to solve specific problems. ANNs can learn and improve their performance over time, making them highly adaptable. They are also robust to noise and can handle non-linear systems, making them a promising alternative to traditional PID controllers (Mohapatra *et al*., 2017).

This paper presents a comparative analysis of the THD between PID and ANN control of a grid-connected PV system. Our results highlight valuable insights into their performance in managing THD in grid-connected PV systems.

By understanding the performance of different control strategies in managing THD, we can make informed decisions about the design and operation of grid-connected PV systems. This not only improves the power quality but also maximizes the return on investment, paving the way for a sustainable energy future.
The rest of the paper is organized as follows: Section II presents the methodology used for the comparative analysis. Section III discusses the results and findings, and finally, Section IV concludes the paper with key takeaways and future research directions.

2. MATERIALS AND METHODS

This study is centred around a comparative analysis of the Total Harmonic Distortion (THD) between Proportional Integral Derivative (PID) and Artificial Neural Network (ANN) control of a grid-connected Photovoltaic (PV) system. The analysis is conducted through simulations, which are designed to mimic real-world conditions as closely as possible.

2.1 PID Control Strategy

The PID controller is tuned to enhance the performance of the grid-connected Photovoltaic system. Tuning is a critical process that entails adjusting the three key parameters: proportional, integral, and derivative gains. This adjustment aims to attain the desired system response and optimize the controller's effectiveness.

2.2 ANN Control Strategy

The ANN is trained using a backpropagation algorithm with data from the PV system under various operating conditions. The backpropagation algorithm is a supervised learning algorithm that adjusts the weights of the ANN based on the error between the ANN's output and the desired output. The training process involves presenting the ANN with input-output pairs and adjusting the weights to minimize the error. Once trained, the ANN can be used to control the PV system. The ANN's ability to learn and adapt makes it a robust control strategy, especially for non-linear systems like PV systems.

2.3 Simulations

The simulations were conducted using MATLAB/Simulink, a popular platform for modelling and simulating dynamic systems. The PV system is modelled in Simulink using the SimPowerSystems toolbox, which provides models of electrical power systems and components. The model includes the PV array, the power electronic converter, the control system, and the grid. The model is parameterized based on typical values for a grid-connected PV system.
ANN control loop is proposed to track the MPP. To create the ANN controller, Matlab/Simulink was used. A total of 5 hidden for the MPPT controller, was used. The combination of "tansig" and "purelin" activation functions for hidden and output layers, respectively, along with the optimization of weights and biases using the Particle Swarm Optimization (PSO) algorithm, was used to train and fine-tune the neural network.

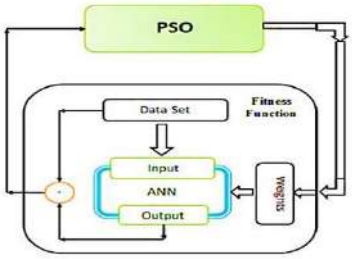

Figure 1: ANN training using PSO (Matrood and Sedeeq, 2020)

The performance of the PID and ANN control strategies is evaluated under varying levels of solar irradiance and temperature. These conditions are chosen to represent the range of conditions that a grid-connected PV system might encounter in the real world. The primary metric for comparison is the THD. As such, only the THD results are compared.

2.4 Scenario One

In this scenario, the MPPT algorithm used was the perturbed and observe (P&O) while the PI controller was used for the inverter side control

2.5 Scenario Two

In this scenario, ANN was used to track the MPP while ANN controller was also used for the inverter side control.

3.6 Simulation Parameters

Parameters	**Value**
PV array power (rated)	100kW
PV panel power (rated)	213.15W
open circuit voltage of PV panel	36.3V
short circuit current of PV panel	7.84A
MPP voltage of PV panel	29.00 V
MPP current of PV panel	7.36 A
quantity per string of connected panels in series	10
quantity of PV strings	47
MPPT PID Controller Parameters	Kp = 1.2366; Ki=0.0062637; Kd=10.986

3. RESULTS AND DISCUSSION

3.1 Current THD Analysis

The THD analysis of scenarios one and two was carried out after running the simulations. For irradiance of 800W/m2, scenario one showed a THD of 8.74% while scenario two showed a THD of 3.25%. Also, for irradiance of 1000W/m2 scenario, one showed a THD of 5.45% while scenario two showed a THD of 1.61%. in both scenarios, it can be observed that the ANN outperforms the PI controller. The results are presented in Figure 2-5.

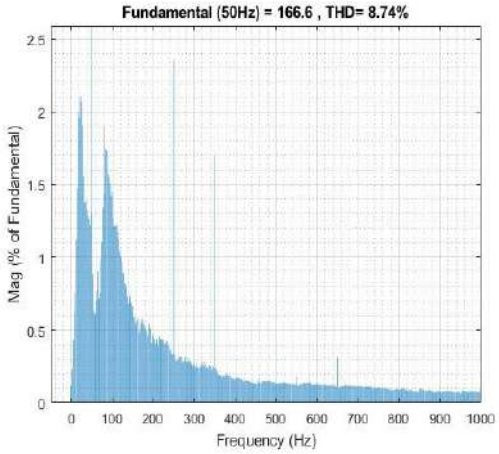

Figure 2: Scenario One THD result for 800W/m2

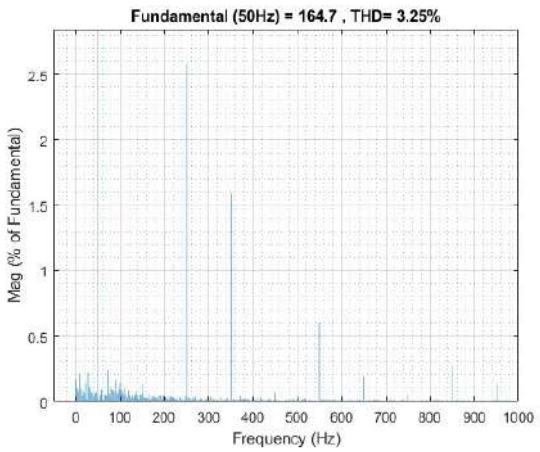

Figure 3: Scenario Two THD result for 800W/m2

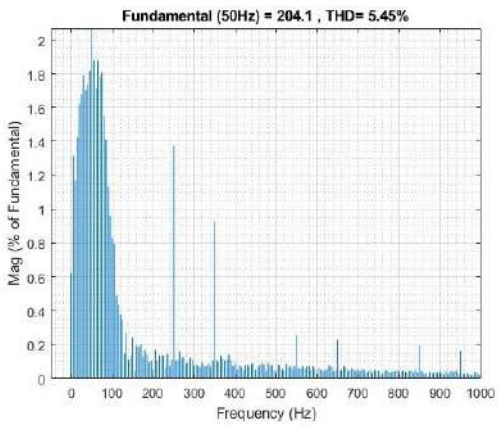

Figure 4: Scenario Two THD result for 1000W/m2

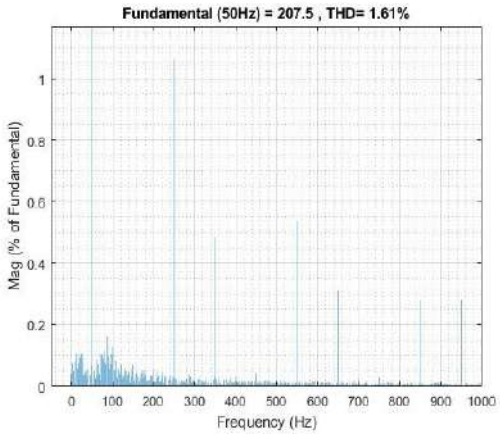

Figure 5: Scenario Two THD result for 1000W/m2

3.2 PV Output Analysis

The results shown in Figure 6 indicate the success of the ANN control strategy. More precisely, the Artificial Neural Network (ANN) approach effectively optimized the power output of the solar system. As depicted in Figure 6, the system consistently kept the solar panel current at its optimal level, demonstrating the effectiveness of the ANN technique in controlling the panel current to attain the maximum value associated with peak power.

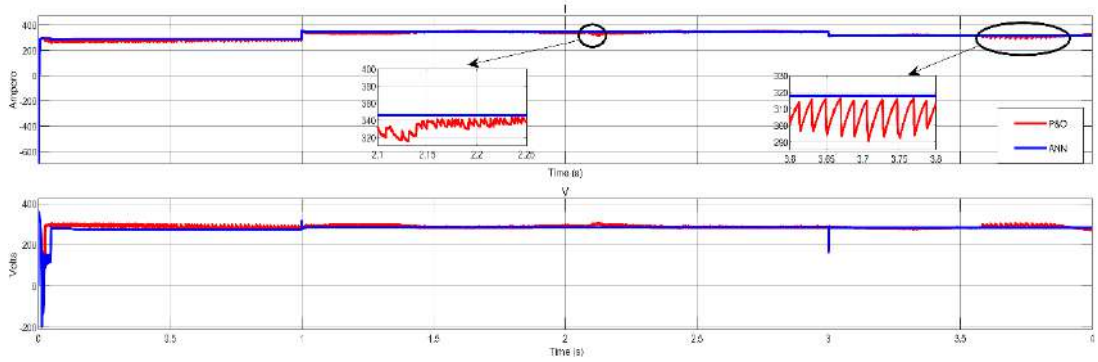

Figure 6: PV Current and Voltage

Additionally, it can be observed in Figure 6 that within the period 2.1 to 2.25, the ANN technique showed a stable output as compared to the P&O technique.

4. CONCLUSION

The implementation of the ANN-MPPT technique aided the extraction of the maximum power output of the PV system, leading to improved efficiency. Also, the ANN control of the inverter enables the further reduction in the system's THD. Furthermore, it can be concluded that the harmonics are dependent on the amount of irradiance as demonstrated in Figure 2-5. Future work can focus on the relationship between irradiance and harmonics and how to maintain a lower THD even with a reduction in irradiance.

REFERENCES

Harrag, A., and Messalti, S. (2015). Variable step size modified P&O MPPT algorithm using GA-based hybrid offline/online PID controller. *Renewable and Sustainable Energy Reviews*, *49*, 1247–1260. https://doi.org/https://doi.org/10.1016/j.rser.2015.05.003

Hassan, A., Bass, O., and Masoum, M. A. S. (2023). An improved genetic algorithm-based fractional open circuit voltage MPPT for solar PV systems. *Energy Reports*, *9*, 1535–1548. https://doi.org/https://doi.org/10.1016/j.egyr.2022.12.088

Hassan, M., Abubakar, A. S., Salisu, S., Aliyu, A., and Almustapha, M. (2023). *Modeling and Implementation of a Self-Tuning Adaptive Controller of an Inverter in a Grid-Connected Microgrid*.

Kamel, R. M. (2016). New inverter control for balancing standalone micro-grid phase voltages: A review on MG power quality improvement. *Renewable and Sustainable Energy Reviews*, *63*, 520–532. https://doi.org/https://doi.org/10.1016/j.rser.2016.05.074

Karami, N., Moubayed, N., and Outbib, R. (2017). General review and classification of different MPPT Techniques. *Renewable and Sustainable Energy Reviews*, *68*, 1–18. https://doi.org/https://doi.org/10.1016/j.rser.2016.09.132

Keerthana, D. M. S., and Sathyan, S. (2018). Comparison of Control Methods For Single Stage 3-Phase Grid Connected PV System. *2018 International Conference on Inventive Research in Computing Applications (ICIRCA)*, 1004–1007. https://doi.org/10.1109/ICIRCA.2018.8597330

Matrood, D., and Sedeeq, M. (2020). PSO Swarm intelligence technique to optimized ANN for demand forecasting. *Proceedings of the Proceedings of the 1st International Multi-Disciplinary Conference Theme: Sustainable Development and Smart Planning, IMDC-SDSP 2020, Cyberspace, 28-30 June 2020*. https://doi.org/10.4108/eai.28-6-2020.2297944

Mohapatra, A., Nayak, B., Das, P., and Mohanty, K. B. (2017). A review on MPPT techniques of PV system under partial shading condition. *Renewable and Sustainable Energy Reviews*, *80*, 854–867. https://doi.org/https://doi.org/10.1016/j.rser.2017.05.083

Rana, M. M., Uddin, M., Sarkar, M. R., Shafiullah, G. M., Mo, H., and Atef, M. (2022). A review on hybrid photovoltaic – Battery energy storage system: Current status, challenges, and future directions. *Journal of Energy Storage*, *51*, 104597. https://doi.org/https://doi.org/10.1016/j.est.2022.104597

Senthilkumar, S., Mohan, V., Mangaiyarkarasi, S. P., and Karthikeyan, M. (2022). Analysis of Single-Diode PV Model and Optimized MPPT Model for Different Environmental Conditions. *International Transactions on Electrical Energy Systems*, *2022*, 4980843. https://doi.org/10.1155/2022/4980843

PAPER 13- DEVELOPMENT OF AN AUTOMATIC PILL DISPENSING AND HEALTH VITALS MEASURING SYSTEM FOR HYPERTENSIVE PATIENTS

N. Ismail*, F.O Anafi, A. A. Sabur

Department of Mechatronics Engineering, Ahmadu Bello University, Zaria, Nigeria.

*Email: mnasir6887@gmail.com

ABSTRACT

Medication non-adherence is a significant issue for patients who require regular medication, especially those with complex schedules or multiple daily doses. This problem is particularly severe in hospitals where doctors are scarce, and monitoring hypertensive patients can be challenging. To address this problem, a proposed system has been developed that integrates automatic pill dispensers and health monitoring systems to help patients manage their condition effectively and reduce the need for constant doctor checkups. The system uses an ESP32 microcontroller and MYSQL database for data storage. DC and servo motors are utilized for dispensing medication mechanisms, and the real-time clock ensures that it only dispenses when required. The health monitoring system can measure temperature and blood pressure and has shown promising results when compared to other devices. The system has been tested with ten different people, and the overall reading error is within the acceptable range, with blood pressure reading error of < 10mmHg and temperature of <2.0°C indicating that it is an effective tool for managing medication adherence and monitoring health vitals. The system was able to transmit all the measured data, and the web can display the recorded data correctly.

KEYWORDS: ESP32 microcontroller, DC motor, Health vitals, HTML, MCU, MYSQL, PHP

1. INTRODUCTION

Hypertension is the most common chronic health condition, affecting 1.4 billion (31%) adults globally (Ostchega, *et al* 2020). With long-term manifestations including cardiovascular, cerebrovascular and chronic kidney disease and stroke, hypertension has been identified by WHO (World Health Organization) as a leading risk factor for morbidity and mortality, responsible for the death of one in six adults annually (Allison, *et al*, 2021). Despite the availability of effective antihypertensive medications and lifestyle interventions, hypertension remains poorly-controlled in many patients. One of the primary reasons for this is the lack of continuous monitoring and medication management. Despite significant evidence demonstrating the benefits of antihypertensive treatment, hypertension remains underdiagnosed and undertreated, with an estimated 11 million hypertensive adults unaware of their disease and, of those aware, half surpassing guideline-recommended blood pressure targets (Kario, 2020).

In recent years, there has been an increasing demand for innovative healthcare technologies that can help improve the quality of life for patients (Amine, *et al,* 2020). It significantly impacted various aspects of healthcare, and the integration of health monitoring and medication management systems holds tremendous potential to improve patient outcomes and enhance healthcare management. This system has the potential to revolutionize the way patients manage their medication by automating the dispensing process and providing real-time monitoring of their health vitals (Moh., *et al* 2019).

Managing multiple medications can be particularly challenging, especially when patients are taking several different drugs that need to be taken at different times of the day. In addition, coordinating medication refills to ensure that patients never run out of their prescribed medications can be time-consuming and requires careful planning.

Proper medication management is crucial for hypertensive patients, and caregivers play a vital role in ensuring that patients receive their prescribed medications as directed. To achieve this, caregivers must not only administer medications on time but also oversee a range of other tasks, including coordinating refills, managing side effects, and adjusting medication dosages as needed. (Sanjay, 2021).

The responsibilities of caregivers can often be overwhelming, leaving them with limited time and resources to adequately monitor patients who have been admitted to the hospital. This can be particularly challenging for patients requiring intensive and frequent check-ups, as inadequate monitoring can lead to serious health complications. The advancement of technology has the potential

to transform medication management and enhance health outcomes for patients with hypertension. This innovation could aid in reducing medication errors, enhancing medication adherence, and providing monitoring of a patient's health parameters. It can be particularly advantageous for patients with chronic diseases such as hypertension, elderly patients, and disabled patients, who require long-term medication management and monitoring. It can also diminish the workload of healthcare professionals, enabling them to concentrate on providing more personalized care to their patients. The proposed system tends to develop an automatic pill dispenser that stores and dispenses antihypertensive and related medications integrating it with a health vitals measuring system capable of measuring a patient's blood pressure, temperature and heart rate. Also, the proposed system proposed a web application that caregivers will use to access the patient's information and schedule medication for patients.

1.1 Existing work

Vishaal et al. 2019, have developed a system that uses a line-following robot and obstacle avoidance to deliver medication to patients in their respective hospital rooms. To ensure only authorized patients receive their medication, the patient is required to scan their finger for authentication. Additionally, the system notifies the caregiver via text message if the patient has taken or has not taken their medication. The system was built using an Arduino Mega and a GSM module.

Diaa et al, 2018 developed a smart healthcare and monitoring system that uses Arduino and ESP8266 microcontrollers to improve the medication process. The system comes with an Android app which connects to the system via Wi-Fi, allowing users to schedule medication dispense time and view their previous medication history. The system can automatically sort and dispense medication according to the pre-set schedule.

Samhitha and Srinath, 2018 have designed a portable pill dispenser that can hold up to 7 different medications. The dispenser is scheduled to release the medication at the appropriate times. The system is built using NodeMCU, which is connected to the internet to send data to the Firebase database that records the patient's intake status as either taken or missed. To configure the device and view the saved records online, an Android app was developed that allows the user to connect to the device.

Ajaegbu et al., 2020 developed a patient monitoring system that uses the Internet of Things to measure a patient's body temperature and heart rate. The system was created using Arduino Uno and ESP8266 microcontrollers to process the raw data from the sensors and convert it into user-readable values. The ESP8266 was utilized to connect the system to the internet, enabling data transfer from the system to cloud storage. Users can access the readings on the ThingSpeak platform over the internet.

Rao et al., 2020 developed a health monitoring system for patients using IoT. The system uses a NodeMCU and MCP3008 microcontroller to measure the patient's pulse rate, body temperature, and ECG using sensors. Since it is difficult to monitor patients around the clock, the system uses the ThingSpeak cloud platform to receive the collected data and save it. Caregivers can access this data throughout the day, enabling them to keep track of the patient's condition.

2. THEORETICAL ANALYSIS

Designing an automatic pill dispensing and vital measuring system for hypertensive patients is a complex task that requires careful component selection. The dispensing mechanism includes a medication compartment operated by a DC and servo motor, a good microcontroller with better processing power and memory is required, which processes and controls every component in the system.

The equations and theories adopted in this study are given in table 1 below:

Table 1 Parts calculations

SN	Item	Equation	Parameters
1	Compartment	$v = \pi r^2 h$	h = 4.5 cm, r = 3.15cm, v = 140 cm^3
2	Pill	$v = w * h * b$	h = 2.5cm, b = 1.2cm, w = 1.0 cm volume = 3.0 cm^3
3	DC motor torque	$\tau = F * r$	τ = 0.023Nm, F = 7.848N, r = 0.029m
4	DC motor power	$P = \tau x \omega$	P = 0.23 watt, τ = 0.023Nm, ω = 10 rpm
5	Power consumption	Power = V * I	v = 5.0 V, I = 1,882.505mA, P = 16,328.5025mW
6	Battery rating	$Time\ in\ hours = \frac{battery\ rating\ (Ah)}{total\ current\ drawn\ by\ the\ system\ (Amp}$	T = 3 hrs., battery rating (Ah) = 5,565mAh

The blood pressure monitor was developed using a non-inversive method as shown in the figure below

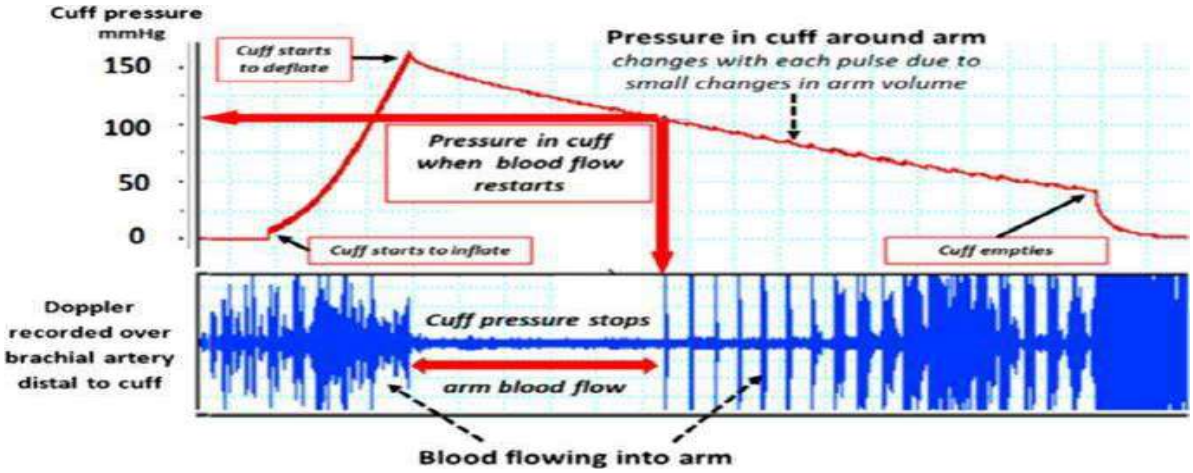

Fig 1 The relationship between the pressure in an automated machine cuff and the flow of blood into the underlying arm (Lewis, 2019)

3. MATERIALS AND METHODS

Designing an automatic pill dispensing and health vital measuring system for hypertensive patients is a complex process that requires the integration of both software and hardware components. These components include microcontrollers, sensors, actuators, and display units, among others. For the software part, it involves developing web-based applications and firmware source code for the microcontroller.

3.1 Body temperature sensor

The DS18B20 is a highly reliable temperature sensor that can precisely measure human body temperature within the range of -55°C to +125°C with an accuracy of ±5°C. It can be placed on various parts of the body such as the forehead, under the arms, and even under the tongue as it is waterproof. This temperature sensor has three wires, namely VCC, GND, and DATA, all connected to a single wire. It is connected to the Nodemcu and since every DS18B20 has a unique silicon serial number, multiple DS18B20s can be connected to the same wire. This sensor is ideal for use in thermostat control systems, industries for temperature measurement, and as a thermometer (Rao, et al., 2020).

Fig 2 Temperature sensor (Rao, et al., 2020)

3.2 Microcontroller

The ESP32 microcontroller is a popular and versatile microcontroller module developed by Espressif Systems. It is based on the Xtensa LX6 dual-core processor architecture and is designed specifically for IoT (Internet of Things) applications (Ravi, 2021). The ESP32 offers a wide range of features and capabilities, making it a popular choice for various projects (Rishit, 2019). The ESP32 microcontroller is widely used in IoT projects, home automation, wearable devices, robotics, industrial applications, and many other domains. Its combination of processing power, wireless connectivity, and a rich set of peripherals makes it a versatile platform for developing a wide range of applications (Mischianti, 2021).

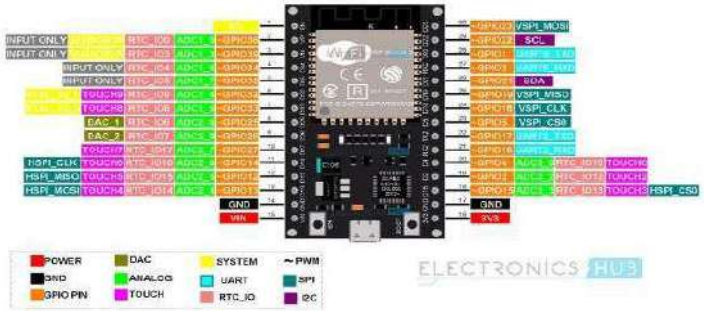

Fig 3 ESP32 microcontroller (Rishit, 2019)

3.3 Pressure sensor

A pressure sensor, also known as a pressure transducer or pressure transmitter, is a device used to measure the pressure of gases or liquids. It converts the applied pressure into an electrical signal that can be measured and analyzed (Mohammad, 2020).

Fig 4 Pressure sensor (Mohammad, 2020)

3.4 Stepper motor

A stepper motor is a type of electric motor that converts digital pulses into precise mechanical movements. It is designed to move in discrete steps or increments, hence the name "stepper" motor. Stepper motors are commonly used in various applications that require precise position control, such as robotics, 3D printers, CNC machines, disk drives, and more (Odhiambo, 2023).

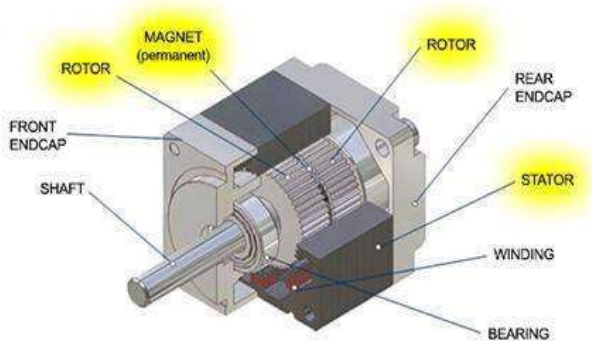

Fig 5 Stepper motor (Odhiambo, 2023)

3.5 Methodology

The system development methodology refers to the structured approach used to design, develop, test, and deploy the automatic pill dispensing and health vitals measuring system for hypertensive patients. The development of the system would have the following steps as described in Fig 6 below.

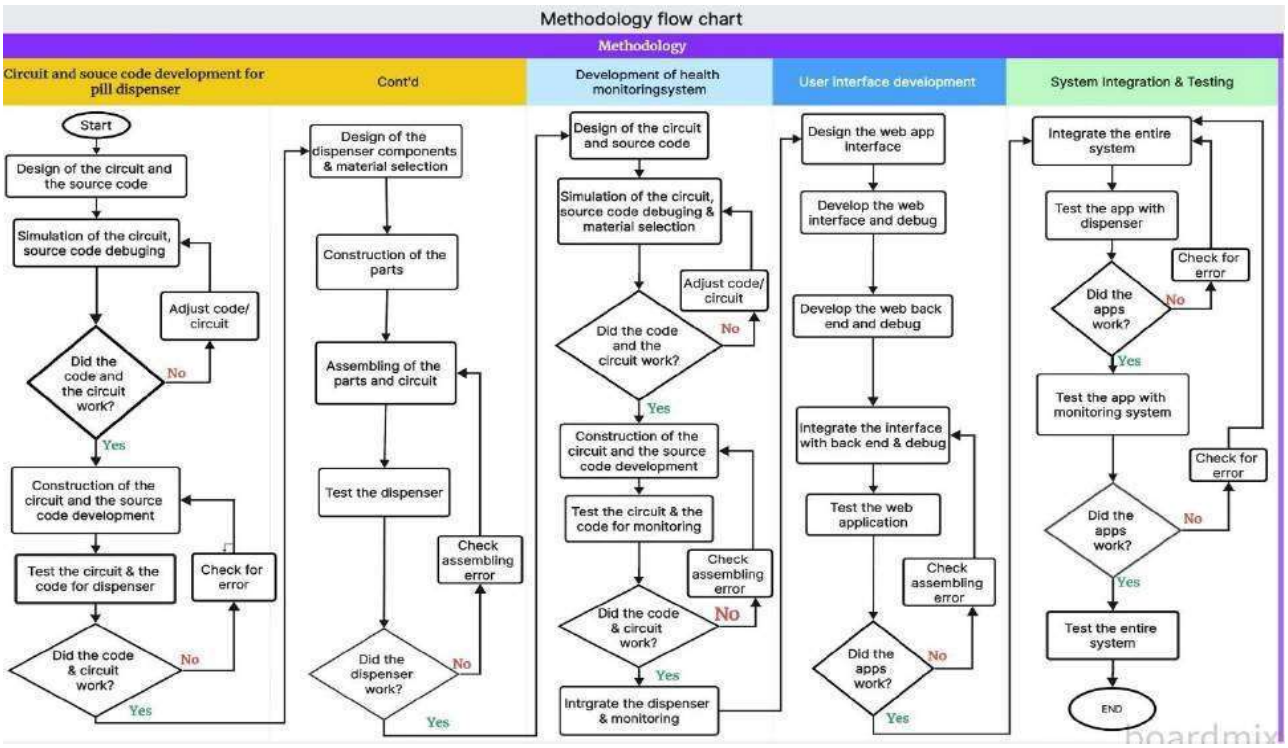

Fig 6 System development methodology flowchart

The system development process followed the steps outlined in Fig 6. An online tool was used to create the circuit design and source code, which the code was simulated and debugged to check and fix any errors. The system uses a web application as a user interface for the doctors to interact with the system. The web application allows them to prescribe medications to patients, view their vitals readings and a lot more. The application was developed using HTML (Hypertext Markup Language) and PHP (Hypertext Preprocessor) was used as the back-end script. After that, the construction of the circuit and assembling the necessary components were done. The design of the pill dispenser was carefully done and materials with the best performance were selected. The

parts were assembled and enclosed them in a plastic case to protect the mechanism. The final construction is shown in Fig 7 below.

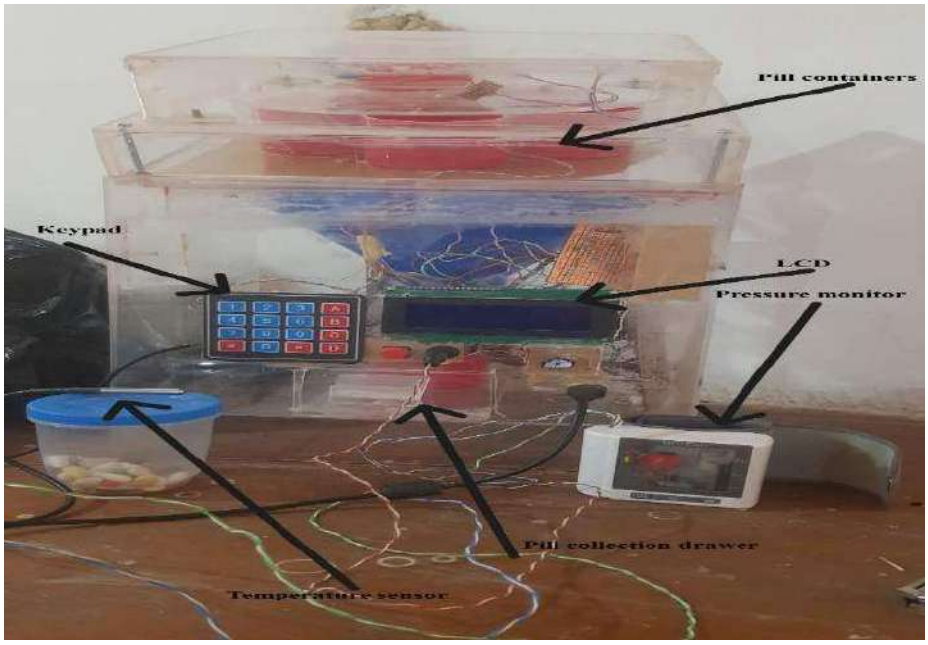

Fig 7 Developed system

4. RESULTS AND DISCUSSION

The developed system went through several intensive tests to ensure reliability on the system which revealed a good positive result.

4.1 WEB APPLICATION TEST

To access the dashboard of the web application, the user must input their login credentials to check if they are a registered user or not. Authenticated users can access patient data through the web application, which also enables doctors to prescribe medication and view vitals. See the figures below for the web app pages.

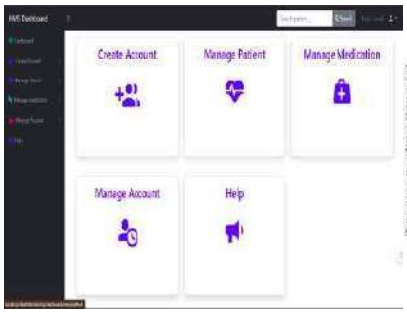

Fig 8 Dashboard

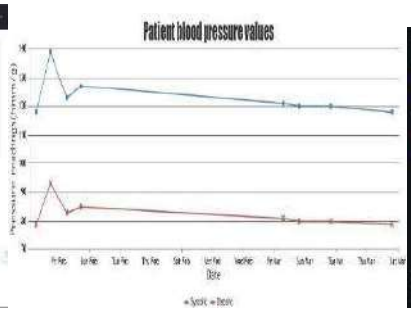

Fig 9 Blood pressure readings

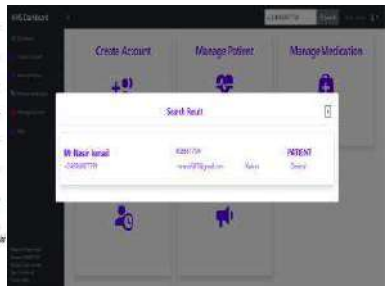

Fig 10 Patient search result

4.2 HEALTH VITAL MEASURING TEST

The health vitals measuring system consists of a blood pressure and temperature monitor. The blood pressure monitor measures the patient's blood pressure and sends the reading directly to his account on the database. Fig 11 shows the image captured during measurement.

Fig 11 Pressure readings

Table 2 Blood pressure readings between developed and Motech blood pressure monitoring device.

SN	Systolic pressure		Error (mmHg)	% Error	Diastolic pressure		Error (mmHg)	% Error
	Measured value (mmHg)	Actual value (mmHg)			Measured value (mmHg)	Actual value (mmHg)		
1	129	121	8	6.20%	86	79	7	8.14%
2	121	125	4	3.31%	81	84	3	3.71%
3	139	136	2	1.44%	93	87	6	6.45%
4	127	122	5	3.94%	85	82	2	2.35%
5	130	127	3	2.31%	87	84	3	3.45%
6	139	136	2	1.44%	93	86	7	6.45%
7	105	110	5	4.80%	72	69	3	4.20%
8	118	111	7	5.93%	71	69	2	2.82%
9	115	110	5	4.35%	75	71	4	5.33%

Table 2 above shows the readings obtained from the newly developed blood pressure measuring device in comparison to those obtained from the Motech blood pressure monitor. The readings obtained from the developed device were found to be close to those obtained from the Motech monitor, with percentage errors ranging from 1.44% to 6.20% (2 - 8 mmHg) in systolic readings and 2.35% to 8.14% (2 - 7 mmHg) in diastolic readings. These errors are within the acceptable range of ≤10 mmHg as per the current ANSI/AAMI/ISO requirements (Stergiou, *et al*., 2018).

4.3 Temperature monitor test

The temperature measurement device was tested multiple times, and the system was found to be working correctly, delivering accurate readings as required, as depicted in Table 3. The system was also compared to an infrared laser thermometer, and the results showed a negligible percentage error, ranging from 0.85% to 3.5%.

Table 3 Temperature measuring device test

SN	Developed temperature monitor (°C)	Infrared thermometer (°C)	Error (°C)	%Error
1	28.0	29.0	1.0	3.5%
2	30.0	29.6	0.4	1.4%
3	30.0	29.5	0.5	1.7%
4	30.0	29.2	0.8	2.7%
5	32.0	32.5	0.5	1.5%
6	34.0	35.0	1.0	2.9%
7	35.0	34.7	0.3	0.9%
8	34.0	35.0	1.0	2.9%
9	34.2	35.2	1.0	2.9%
10	35.2	35.3	0.3	0.85%

Fig 12 Temperature reading

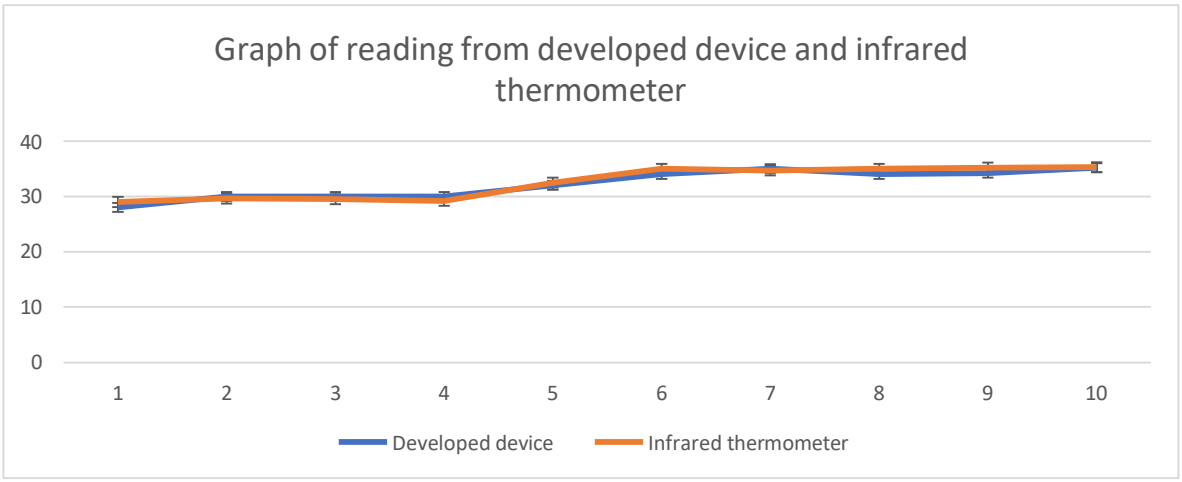

Fig 13 Temperature reading against developed and infrared thermometer

The graph provided above depicts the readings obtained from the temperature-measuring device and the infrared thermometer. As per the graph, the readings indicate a negligible variation and a high level of accuracy, with a percentage error ranging from 0.85% to 3.5%. The results obtained from the device seem to be satisfactory and reliable.

4.4 PILL DISPENSER TEST

The main central unit of the system responsible for dispensing medication to patients as per the doctor's prescription on the web app is the pill dispenser. It comes with a keypad that accepts user input and responds accordingly. The figure below illustrates the functionality of the dispenser that was tested.

Fig 14 Home and menu screen

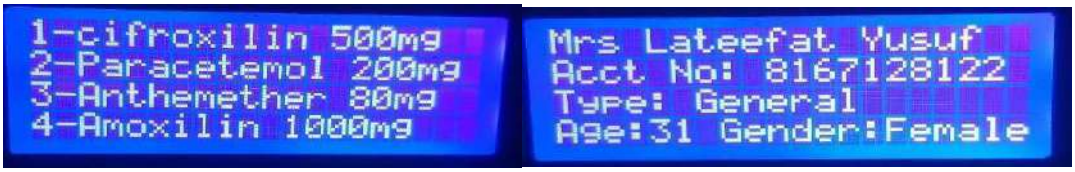

Fig 15 Prescribed medication and patient account information

Table 4 Pill dispenser test

Test	Container	Morning dosage				Afternoon dosage				Evening dosage				Night dosage			
		Expected dose	Dose dispensed	Error	Pill detection	Expected dose	Dose dispensed	Error	Pill detection	Expected dose	Dose dispensed	Error	Pill detection	Expected dose	Dose dispensed	Error	Pill detection
Day one	One	1	1	0		0	0	0		0	0	0		0	0	0	
	Two	2	2	0		2	2	0		2	2	0		0	0	0	
	Three	1	1	0		1	1	0		1	1	0		0	0	0	
	Four	3	3	0		3	3	0		3	3	0		0	0	0	
Day two	One	1	1	0		0	0	0		0	0	0		0	0	0	
	Two	2	2	0		2	2	0		2	2	0		0	0	0	
	Three	1	1	0		1	1	0		1	1	0		0	0	0	
	Four	3	3	0		3	3	0		3	3	0		0	0	0	
Day three	One	1	1	0		0	0	0		0	0	0		0	0	0	
	Two	2	2	0		2	2	0		2	2	0		0	0	0	
	Three	1	1	0		1	1	0		1	1	0		0	0	0	
	Four	3	3	0		3	3	0		3	3	0		0	0	0	
Day four	One	1	1	0		0	0	0		0	0	0		0	0	0	
	Two	2	2	0		2	2	0		2	2	0		0	0	0	
	Three	1	1	0		1	1	0		1	1	0		0	0	0	
	Four	3	3	0		3	3	0		3	3	0		0	0	0	
Day five	One	1	1	0		0	0	0		0	0	0		0	0	0	
	Two	2	2	0		2	2	0		2	2	0		0	0	0	
	Three	1	1	0		1	1	0		1	1	0		0	0	0	
	Four	3	3	0		3	3	0		3	3	0		0	0	0	

The table labelled as Table 4 displays the results obtained from the pill dispenser test that was conducted over five days with different prescriptions as mentioned in the table. The pill dispenser is an incredibly efficient device that ensures the accurate dispensation of prescribed medication at the scheduled time and in the exact dosage. This is made possible by the pill detection mechanism, which eliminates the possibility of any dosage errors by ensuring that the pills are dispensed and accurately counted, thereby eliminating any possibility of dosage errors.

5 CONCLUSION

The system that automatically dispenses pills and measures health vitals for hypertensive patients is a great example of how the Internet of Things technology can be integrated into healthcare services. This system helps doctors and nurses manage patients remotely, making it easier and more convenient for everyone involved. With this technology, healthcare professionals no longer need to go from bed to bed to perform check-ups or administer medication. It's a practical solution that solves an existing problem in hospitals.

A new health vital measuring system has been developed and tested. It consists of sensors that measure blood pressure and temperature accurately. The readings are within the range stated by ANSI/AAMI/ISO requirements of <10mmHg. The measured readings are transmitted to the database for record-keeping purposes. The device has been developed to help regulate the health condition of individuals by keeping track of their vitals and improving medication adherence. Additionally, it assists in connecting the individual to their doctor and reducing the workload on caregivers. The web application, as an interface capable of displaying the information to doctors, was tested and found to be functioning correctly, displaying the right information on each page.

6 ACKNOWLEDGEMENT

I would like to express my sincere gratitude to Professor F.O. Anafi, Dr Alim A. Sabur, Dr Y.S. Danbatta, PTDF, Ahmadu Bello University Zaria, and my family and friends for their invaluable guidance, support, funding, resources, and encouragement throughout my research work.

REFERENCES

Ajaegbu, C., Nwaocha, O. V., Nzenwata, J. U., & Oreoluwa, A. A. (2020). A Patient Monitoring System Using Internet of Things Technology. *nternational Information and Engineering Technology Association*, 351-357.

Allison, J. H., Chokshi, N., & Adusumalli, S. (2021). Novel Digital Technologies for Blood Pressure Monitoring and Hypertension Management. *TECHNOLOGY AND CARDIOVASCULAR HEALTH*, 1-9.

Amine, R., Jaime, L., Mohamed, H., & Abdelmajid, O. (2020). A Smart Glucose Monitoring System for Diabetic Patient. *Electronics*, 768-786.

Diaa, S. A., & Mohamed, A.-E. (2018). Smart drugs:Improving healthcare using Smart Pill Box for Medicine Reminder and Monitoring System. *Future Computing and Informatics Journal*, 443-456.

George S. Stergiou, B. A. (2018). A Universal Standard for the Validation of Blood Pressure Measuring Devices. *Association for the Advancement of Medical Instrumentation/European Society of Hypertension/International Organization for Standardization (AAMI/ESH/ISO) Collaboration Statement*, 368-374.

Kario, K. (2020). Management of Hypertension in the Digital Era Small Wearable Monitoring Devices for Remote Blood Pressure Monitoring. *AHA Journals*, 640-650.

Lewis, P. S. (2019). Oscillometric measurement of blood pressure: a simplified explanation. A technical note on behalf of the British and Irish Hypertension Society. *Journal of Human Hypertension* , 349-351.

Mischianti, R. (2021, February 17). *DOIT ESP32 DEV KIT v1 high resolution pinout and specs*. Retrieved from MISCHIANTI: https://mischianti.org/2021/02/17/doit-esp32-dev-kit-v1-high-resolution-pinout-and-specs/

Moh., K. H., Md., S., Mostafa, Z. C., & Yeong, M. J. (2019). Real-Time Healthcare Data Transmission for Remote Patient Monitoring in Patch-Based Hybrid OCC/BLE Networks. *Multidisciplinary Digital Publishing Institute (MSPI)*, 1-23.

Mohammad, D. (2020, November 16). *Interfacing MPS20N0040D Barometric Pressure Sensor with Arduino*. Retrieved from Electro Peak: https://electropeak.com/learn/interfacing-mps20n0040d-barometric-pressure-sensor-with-arduino/

Odhiambo, B. (2023, May 09). *Stepper Motors Part 1: An Overview*. Retrieved from EEPower: https://eepower.com/technical-articles/stepper-motors-part-1-an-overview/#

Ostchega, Y., Fryar, C. D., Nwankwo, T., & Nguyen, D. T. (2020). *Hypertension Prevalence Among Adults Aged 18 and Over: United States, 2017–2018.* USA: National Center for Health Statistics Data Brief, no 364. Hyattsville, MD: National Center for Health Statistics. 2020.

Rao, G. J., Karthik, P., Kumar, G. S., Ajay, N., Kumar, K. A., & Prasad, J. D. (2020). Health Monitoring System of Patient Using IoT. *International Journal of Scientific Research in Science, Engineering and Technology*, 56-65.

Ravi, T. (2021, February 17). *Getting Started with ESP32 | Introduction to ESP32*. Retrieved from ElectronicsHub: https://www.electronicshub.org/getting-started-with-esp32/

Rishit, D. (2019). Design and Implementation of Medicine Dispenser. *International Advanced Research Journal in Science, Engineering and Technology*, 42 - 48.

Samhitha, S., & Srinath, N. (2019). Design and development of Portable Smart Medicine Dispenser. *International Journal of Scientific Research in Computer Science, Engineering and Information Technology*, 147-152.

Sanjay, K. R. (2021, March 24). *How Medication Non-adherence Impacts Brand Management*. Retrieved from pharmexec: https://www.pharmexec.com/view/how-medication-non-adherence-impacts-brand-management

Vishaal, M., Vishwa, B., Sri, V., & Usha, A. (2019). AUTOMATED MEDICAL DISPENSING SYSTEM USING ROBOTICS. *INTERNATIONAL JOURNAL OF CURRENT ENGINEERING AND SCIENTIFIC RESEARCH (IJCESR)*, 15-1

PAPER 15- POTENTIAL OF CALCIUM CARBIDE RESIDUE MODIFIED SANDCRETE BLOCKS IN ENHANCING THERMAL AND ENERGY EFFICIENCY FOR SUSTAINABLE BUILDING DESIGN

M. Ibrahim[1], M. Abubakar[2*], A. Abdullahi[2], B. A. Abbas[3]

[1]Department of Civil Engineering, Federal University of Technology, Minna, Nigeria.

[*]Email: mibrahim2294@gmail.com

ABSTRACT

Sustainability has increasingly become a prominent topic in the field of construction, and as such, it is necessary to explore means of reducing the overdependence on the use of cement in construction works**.** This study investigated the effects of calcium carbide residue (CCR) as a partial substitute for cement in sandcrete blocks. Due to the high pH value of calcium carbide residue, its disposal in landfills increases the alkalinity of the environment. From raw material extraction through final product disposal, the construction industry is integrally involved in every stage of the lifecycle of greenhouse gas emissions. In this study, cement was partially substituted using CCR at 0% and 12% by weight replacement. The sandcrete blocks were of 450 mm × 225 mm × 225 mm dimensions and made from a Cement-CRR mix ratio of 1:6 and water-cement ratio of 0.6. Preliminary tests such as consistency, setting times, soundness, and specific gravity tests were carried out on cement and cement + 12% CCR. The thermal properties, which include thermal conductivity (k), heat transfer coefficient (U), specific heat capacity (C_p) and diffusivity (α) of the sandcrete blocks were determined. The thermal tests were carried out after the 28th day of curing. The result showed that CCR increased the water demand by the sandcrete blocks, hence reducing its workability. The sandcrete block samples made with 12% CCR replacement showed improved compressive strength. The k for 0% and 12% replacement was 0.5497 W/mK and 0.3978 W/mK, respectively, while the U was 54.974 W/m^{2}K and 39.784 W/m^{2}K, respectively for the 0% and 12% replacement. On the other hand, the C_p for 0% and 12% was 0.0003364 J/kg°C and 0.0001598 J/kg°C, respectively, while the diffusivity was 636.54m^2/s and 1113.94m^2/s for 0% and 12% replacement, respectively. As such, we can infer that 12% CCR replacement of cement gives more energy-efficient and sustainable sandcrete blocks.

KEYWORDS: Calcium Carbide Residue (CCR), sandcrete block, Fine aggregates, Thermal properties, Energy.

1. INTRODUCTION

Buildings consume roughly 40% of the world's energy, and a significant portion of this energy is required to create thermal comfort conditions, both in heating and cooling, which results in large carbon dioxide (CO_2) emissions from buildings. Given that thermal comfort accounts for over 65% of a building's energy use and since effective energy management is one method of lowering CO_2 emissions, it should be one of the top concerns (Bio Intelligence Services *et al*, 2013). A wall envelope is another approach to storing energy inside a building. Heat naturally moves from a warmer to a colder space because of the temperature difference. Heat is transferred from the outside to the building during the summer, and vice versa during the winter. To ensure thermal comfort at a reasonable cost, the excess heat in the summer and the heat losses in the winter need to be regulated. The daily and seasonal fluctuations in external temperature also add to the heating and cooling burdens (Victor *et al*., 2014).

The wall envelope is a significant contributor to reducing heating and cooling loads in buildings. The thermal demand under various weather conditions has been studied in some scientific publications, using novel techniques like the incorporation of cellulose, expanded polystyrene, or vegetation as rooftop layers in the walls, to better utilize the thermal energy. Other studies document the use of thermal energy storage systems (TES) to incorporate fluid-based heat exchange circuits within the construction. To restrict energy flow and delay thermal load on the building while also achieving the optimum internal temperature, a microencapsulated PCM is placed in concrete walls to substantially reduce and delay the thermal load on the building, trying to minimize the energy flow and, at the same time, reach the desired indoor temperature (Uribe *et al*., 2015). The main aim of Cunha et. al., (2023) consists of a perspective of the evolution of the development and application of thermal storage technology through the incorporation of PCM in the construction sector, focusing on the last 10 years of research, showing the most recent developments of its application in construction materials, such as mortars, concrete, incorporation in porous aggregates, naturally based materials, carbon-based materials, boards, blocks and solar thermal systems**.**

Cement-based materials are the most used for wall construction in urban areas, representing about 52% of buildings. Cement-based materials have worse energy efficiency than earthen materials, and in addition, the process of production of cement-based materials is very polluting, without mention their relatively high cost. In recent decades, some studies tried to evaluate the thermal comfort in buildings gained from construction with cement, which has posed limited satisfaction and as such the introduction of other Cementous materials to improve both strength, thermal efficiency and sustainability has been suggested (Hassane *et al*., 2019).

Recently, the introduction of calcium carbide residue (CCR) as a partial/full replacement of cement in the production of unfired clay bricks reveals its benefits for improving the thermal efficiency, compressive strength, and sustainability of buildings due to its good qualities such as improving the consistency of mortar mixture, convenient storage, high strength, improved workability, easy accessibility and transportation, and good thermal insulation properties (Banjo *et al*., 2021).

Sandcrete blocks have been the predominant walling material in both residential and commercial buildings in West Africa for over fifty years (Onwuka *et al*., 2013). They are used extensively due to the availability of raw materials used in their production (Yusuf *et al*., 2017). Sandcrete blocks are produced with a mixture of cement and sand mixed with a varying percentage of water. In the production of sandcrete blocks, the materials are mixed thoroughly until a homogenous mix with uniform colour is obtained. The mixture is placed in a mould which is removed immediately after compaction and levelling of the top and it is then left to harden. The compaction is either done manually or by machine vibration. The strength of the resulting hardened sandcrete blocks is to a great extent affected by the mix composition, production method, method and duration of curing and properties of the constituent materials (Ambrose *et al*., 2019).

The waste product is frequently disposed of in landfills and presents a threat to the environment for both the surrounding air and subsurface water. It is very alkaline in nature and contains 92% calcium hydroxide (Kampala *et al*., 2013). With a recent study indicating that there is anticipated to be an increase of 6.49% in the calcium carbide residue (CCR) market globally (Banjo et al., 2021), the availability of CCR as a substitute in cement applications is guaranteed on a global scale. In several studies, CCR has been heavily utilized to enhance and stabilize construction materials to boost their strength and durability.

It has good qualities such as; improving the consistency of mortar mixture, convenient storage, high strength, improved workability, easy transportation, and good thermal insulation properties. These properties make it a suitable material that can be used to improve sustainability in construction (Banjo *et al*., 2021).

The construction industry is encountering the challenges of incorporating sustainability into the production processes, either by searching for or incorporating raw materials or waste by-products that are more environmentally friendly and/or contributing toward the reduction of CO_2 emissions into the atmosphere. The possibility of incorporating waste from industrial or agricultural activities in their production processes can help to achieve this goal. (Hardjito *et al*., 2012).

To reduce environmental pollution, attempts have been made to utilize Calcium Carbide Residue (CCR) in a better way, especially for building material applications. Since the dominant component of CCR is $Ca(OH)_2$, it provides a potential application in the cement manufacturing industry and can be used as a cement replacement material (Chen *et al*., 2010)

In the recent past, some researchers used CCR as a substitute for limestone to produce clinker which was also mixed with fly ash or waste ash to produce cementitious materials. Researchers and scientists are still searching for new approaches to recycle CCR. The purpose of this research is to use CCR as a partial substitute for cement by investigating the potential of Revit for energy-efficient sustainable building design and construction.

Recent studies have shown that infrastructure plays a crucial role in the social and economic development of every nation. It also shapes and builds the environment making it a crucial aspect of human life. As the world's population expands, urbanization accelerates, and countries demand more services, depicting the need for infrastructure (The Economist Intelligence Unit, 2019). The safety and reliability of infrastructure entities have been a great concern to engineers as construction materials are contributing greatly to global warming. The construction industry consumes approximately 40% of total energy resources worldwide, accounting for nearly 36% of global emissions (Mathur *et al*., 2021). The methods involved in the production of constituent materials and construction of infrastructures consume a great amount of energy which in turn contributes to the emission of greenhouse gases such as CO_2 (Namutebi *et al*., 2017).

In the context of sustainable construction, there is a need to evaluate and enhance energy efficiency in building materials and practices. Calcium carbide residue, as a potential alternative material, holds promise for

reducing energy consumption in construction. However, there is a research gap regarding the comprehensive understanding of the energy efficiency potential of calcium carbide residue. This study aims to address this research gap by investigating the energy efficiency characteristics of calcium carbide residue and its suitability as a partial replacement for cement in construction materials. The research also aims to quantify the energy savings achieved by incorporating calcium carbide residue and provide valuable insights for sustainable building design and construction practices.

2. THEORETICAL ANALYSIS

The mathematical principles used should be included as follows.

The thermal conductivity, k, of the sample, is derived from the equation

$$k = \frac{Q * X}{A\,(T2 - T1)} \quad (1)$$

where;

k; Thermal conductivity of sample [W/mK]
Q; generated heat per unit length of sample/time [W/m^{2}K]
X; Thickness of sample [m]
A; Area [m^2]
T0 and T5; Temperature at t0 and t5 [K]
t1 and t2; measured time length [second, s]

The heat transfer is obtained from the equation

$$U = \frac{Q}{A * \Delta T} \quad (2)$$

Where;
Q: heat flux, W/m^2;
U: heat transfer coefficient, W/ (m^2•K)
ΔT: difference in temperature between the solid surface and surrounding fluid area, K
The specific heat capacity,

$$C_p = \frac{Q}{m\Delta T} \quad (3)$$

Unit of C is J/kg* $^{\circ}$C, M is the Mass (kg), Q changes in energy (J), and ΔT is Temperature change (^{O}C)

The thermal diffusivity α (m^2/s)

$$\alpha = \frac{k}{\rho Cp} \quad (4)$$

Where;
k; Thermal conductivity of sample [W/mK]
ρ is the density of the material
Cp is the specific heat capacity (J/gK)

3. MATERIALS AND METHODS/METHODOLOGY/EXPERIMENTAL PROCEDURE

3.1 Materials

The experimental materials utilized in the study encompassed cement, fine aggregate (sand), and calcium carbide residue (CCR). Ordinary Portland cement with a strength of 42.5 N was selected for its finely powdered, greyish appearance and adhesive properties. The CCR, obtained from the welding process of automotive body repair technicians, underwent drying and sieving to eliminate impurities. Similarly, the fine aggregate, sourced locally in Minna, underwent a rigorous preparatory process involving washing, drying, and sieving to eliminate foreign particles retained on a 4.76 mm sieve.

3.2 Methods

Using the mix ratio 1:6 (1-part cement and 6-part fine aggregate) with a water-cement ratio of 0.6, the absolute volume method was used to determine the mix volume of each constituent material used in moulding the sandcrete block. Sandcrete blocks with dimensions 450 × 225 × 225 mm were moulded for 0% as control and 12% cement replacement with CCR. The sandcrete blocks were cured consecutively for 28 days. After which, the Armfield HT10XC heat transfer service unit and Armfield IFDC interface console shown in plate 1, were used to determining the thermal properties (thermal conductivity (k), heat transfer coefficient (U), specific heat capacity (C_p) and thermal diffusivity (α)) by measuring the steady-state heat transfer through the samples cut out from the respective sandcrete blocks shown in plate 2.

Plate 1:Armfield heat transfer service unit

Plate 2: 12% CCR sandcrete block

4. RESULTS AND DISCUSSION

Table 1: Final and initial settings time

	Initial setting time (mins)	Final setting time (mins)
OPC	125	205
OPC + CCR	75	183

BS EN197-1(2000) requires that the initial setting time of an OPC should be greater than 45 mins, while the final setting time should be less than 10 hours. From Table 1, the initial and final setting times are 125 and 205 mins respectively, these values are in correspondence with the requirement and therefore this cement can be used for masonry and concrete works.

Also from Table 1, the initial and final setting times of OPC + CCR were gotten to be 75 and 183 mins respectively, this shows that the mixture of OPC + CCR hardens faster than OPC alone. These values are also within the specified range required; hence the mix percentage can be used for masonry and concrete works. Table 2 shows the determined thermal conductivity, heat transfer coefficient, specific heat capacity and the thermal diffusivity of each sample.

Thermal properties of sandcrete blocks

Table 2: Thermal conductivity, heat transfer coefficient, specific heat and diffusivity

S/N	ID	k = Q * x/(A*ΔT)	U = Q/(A*ΔT)	C_p = Q/(m*ΔT)	α = λ/(ρ*cp)
1	0%	0.549736705	54.97367	0.000336372	636.53724
2	12%	0.397835773	39.78358	0.000159847	1113.9402

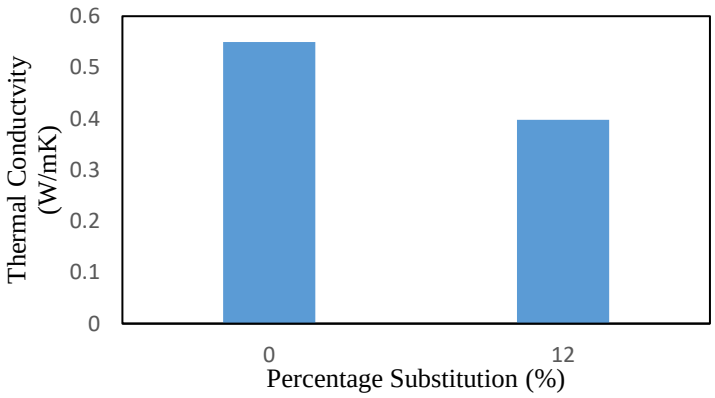

Figure 1: Thermal conductivity results for 0% and 12%

From Figure 1, it can be seen that the thermal conductivity of the conventional sandcrete block i.e. 0% substitution is 0.5497 W/mK, while that of the 12% substitution is 0.3978 W/mK. A valuable method of reducing the amount of heat transfer and energy consumption of buildings is using materials with lower k-values as the building envelope (Iman *et al, 2018)*.

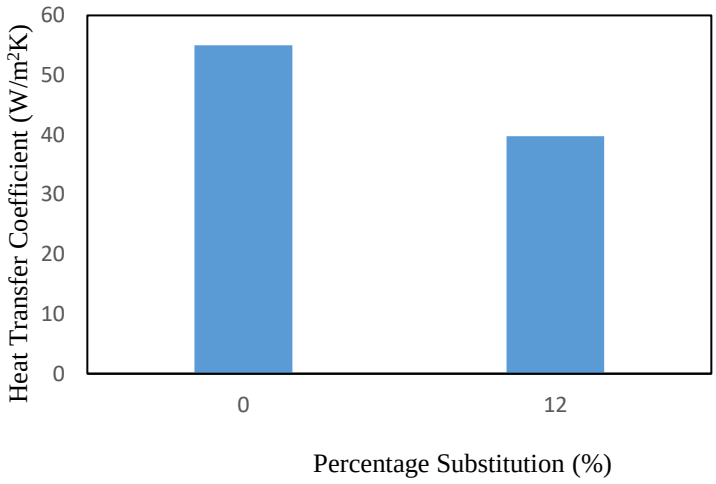

Figure 2: Heat transfer coefficient result

From Figure 2, it can be seen that the heat transfer coefficient is higher with the conventional concrete i.e. 0% substitution with a value of 54.974 W/m^{2}K. The larger the heat transfer coefficient, the more heat transfer occurs. In general, the larger the thermal conductivity, the larger the heat transfer coefficient.

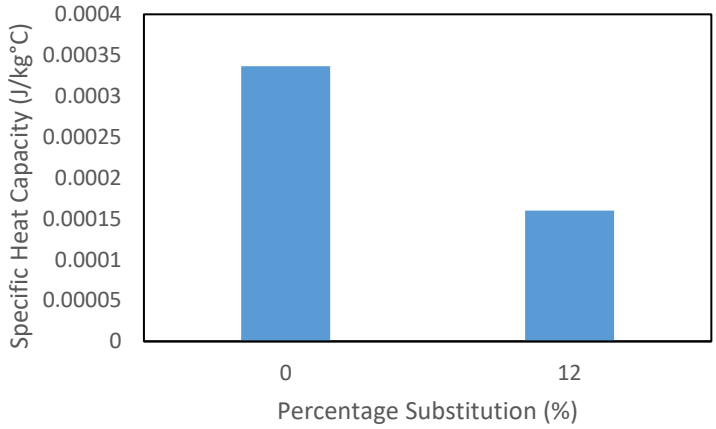

Figure 3: Specific heat capacity results

From Figure 3, it can be seen that the specific heat capacity is higher with the conventional concrete i.e. 0% replacement of cement by CCR. A higher value means that it takes more energy to raise or lower its temperature. We can infer that 12% CCR replacement of cement gives a more sustainable building in terms of thermal energy.

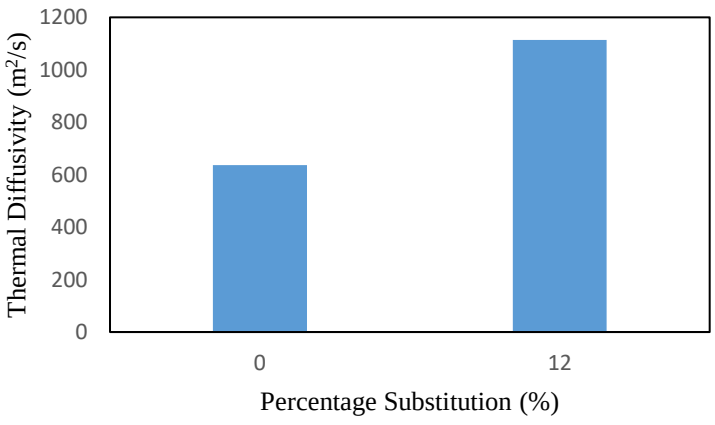

Figure 4: Thermal diffusivity

Thermal diffusivity measures the ability of a material to conduct thermal energy relative to its ability to store thermal energy. Sandcrete block with 0% CCR which has higher thermal diffusivity will heat up or cool down quickly, conversely, Sandcrete block with 12% CCR will heat up or cool down more slowly.

5. CONCLUSION (10 point)

The effects of calcium carbide residue (CCR) on the thermal properties of sandcrete have been carried out and the results have been presented, analysed and discussed. From this study, the following conclusions were drawn:

i. the presence of calcium carbide residue in mortar decreases its workability and thereby requires more water-cement ratio to mix.
ii. the optimum compressive strength of the sandcrete block was obtained at 12% replacement of cement by CCR with a value of approximately 3.919 Mpa, this corresponds with the mix ratio 1:7 and w/c of 0.5.
iii. the thermal properties of the CCR sandcrete block used in this research showed that the highest thermal conductivity of 0.5497 W/mK and 0.3978W/mK were obtained on the 28th day of curing, respectively for 0% and12% replacement, while the corresponding heat transfer coefficient was 54.974W/m^{2}K and 39.784W/m^{2}K respectively 0% for 12% cement replacement.
iv. Inputting the thermal properties from the two samples, Revit generates resistance and thermal mass as 0.1819 (m^{2}K)/W, 6.40 kJ/K for 0% and 0.2514 (m^{2}K)/W, 3.04 kJ/K for 12% respectively.
v. Despite this difference in thermal properties obtained, Insight gives the same thermal energy demand for the buildings modelled using the two sandcrete blocks.

ACKNOWLEDGEMENT

The authors are especially grateful to the Department of Civil Engineering, Kaduna Polytechnic, Kaduna for providing the laboratory and equipment for carrying out this research.

REFERENCES (10 point)

Ambrose E. E., Etim R. K., & Koffi E. N., (2019). Quality Assessment of Commercial Produced Sandcrete Blocks in Part of Akwa Ibom State, Nigeria. *Nigerian Journal of Technology*. 38(2), 586-593, doi: 10.4314/njt.v38i3.7

Banjo, A. A., Blessing O. O., & Chukwunonyenim W. O., (2021). The potential of calcium carbide waste and termite mound soil as materials in the production of unfired clay bricks. *Cleaner Production*, *279*(123693). doi:10.1016/j.jclepro.2020.123693

Bio Intelligence Services, Ronan L., & IEEP (2013). Energy Performance Certificates in Buildings and Their Impact on Transaction Prices and Rents in Selected EU Countries. Retrieved from European Union Website: https://energy.ec.europa.eu/publications/energy-performance-certificates-buildings-and-their-impact-transaction-prices-and-rents-selected-eu_en 19th April 2013.

BS EN 197-1 (2000): *Cement assessment and verification of consistency of performance.* https://www.en-standard.eu/bs-en-197-1-2011-cement-composition-specifications-and-conformity-criteria-for-common-cements/

Chen, C. H., Lee, C. M., Tung, W. C., Wang, J. H., Hung, C. H., Hu, T. H., Wang, J. C., Lu, S. N., & Changchien, C. S. (2010). Evolution of full-length HBV sequences in chronic hepatitis B patients with sequential lamivudine and adefovir dipivoxil resistance. *Journal of Hepatology*, *52*(4), 478–485. doi:10.1016/J.JHEP.2010.01.006

Cunha, S., Sarcinella, A., Aguiar, J., & Frigione, M., (2023). Perspective on the Development of Energy Storage Technology Using Phase Change Materials in the Construction Industry: A Review, *Energies*, 16(12), 4806, doi: 10.3390/en16124806

Hardjito, D., Antoni, Wibowo, G. M., & Christianto, D. (2012). Pozzolanic activity assessment of LUSI (Lumpur SIdoarjo) mud in semi-high volume pozzolanic mortar. *Materials*, *5*, 1654–1660. doi: 10.3390/a5091654

Hassane, S., Nshimiyimana, P., Hema, C., Zoungrana, O., Messan, A., & Courard, L., (2019). Comparative Study of Thermal Comfort Induced from Masonry Made of Stabilized Compressed Earth Block vs Conventional Cementitious Material. *Journal of Mineral and Materials Characterization and Engineering*, *7*(6). 385-403, doi: 10.4236/jmmce.2019.76026

Kampala A., Horpibulsuk S. B., Chinkullijniwat A., & Shen S. L., (2013). Engineering properties of recycled Calcium Carbide Residue stabilized clay as fill and pavement materials. *Construction and Building Materials*, 46, 203–210, doi: 10.1016/j.conbuildmat.2013.04.037.

Mathur, V. S., Farouq, M. M., & Labaran, Y. H. (2021). The carbon footprint of the construction industry: A review of direct and indirect emission. *Journal of Sustainable Construction Materials and Technologies*, *6*(3), 101–115. doi: 10.29187/jscmt.2021.66

Namutebi, M., Birgisson, B., Guarin, A., & Jelagin, D. (2017). An exploratory study on bitumen content determination for foamed bitumen mixes based on porosity and indirect tensile strength. *Journal of Traffic and Transportation Engineering (English Edition)*, *4*(2), 131–144. https://doi.org/10.1016/j.jtte.2016.11.002

Onwuka, D. O., Osadebe, N. N., & Okere, C. E. (2019). Structural characteristics of sandcrete blocks produced in South-east Nigeria Structural characteristics of sandcrete blocks produced in South-East Nigeria, *Journal of Innovative Research in Engineering and Science, 4(3),* 483-490. http://www.grpjournal.org/Journal/Category/JOIRES.aspx

Sergey, P. Z., Elena, V. I., & Irina, A. Z., (2016). The organization of Autodesk Revit Software Interaction with Applications for Structural Analysis. *Procedia Engineering*, *153*, 915–919, doi: 10.1016/j.proeng.2016.08.225

Shetty, M.S & Jain, A.K. (2019). *Concrete Technology: Theory and Practice*, Uttar Pradesh, India, S. Chand Publishing

Sun, H., Li, Z., Bai, J., Memon, S. A., Dong, B., Fang, Y., Xu, W., & Xing, F. (2015a). Properties of chemically combusted calcium carbide residue and its influence on cement properties. *Materials*, *8*(2), 638–651, doi: 10.3390/ma8020638

Suryakanta, P., (2016). What are the properties of aggregates for concrete. Retrieved from Civilblog website: civilblog.org/2016/10/01/properties-aggregates-concrete/ 1st October, 2016.

Taylor, H. F. W., (1997). *Cement chemistry*. London. Thomas Telford Publishing.

The economist intelligence unit, 2019. The critical role of infrastructure for the SDGs_EN. Retrieved from UNOPS website: https://content.unops.org/publications/The-critical-role-of-infrastructure-for-the-SDGs_EN.pdf, 2019.

Uribe, O. H., Martin, J. P. S., Garcia-Alegre, M. C., Santos, M., & Guinea, D. (2015). Smart building: Decision-making architecture for thermal energy management. *Sensors (Switzerland)*, *15*(11), 27543–27568, doi: 10.3390/s151127543

Victor, D.G., Zhou, D., Ahmed, E. H. M., Dadhich, P. K., Olivier, J., Rogner, H., Sheikho, K., & Yamaguchi, M., (2014). *Mitigation of Climate Change, Contribution of Working Group III to the Fifth Assessment Report of the IPCC.* Cambridge, University Press.

Yusuf A, Aminulai, H. O., Abdullahi, A, Alhaji, B Alalade, A. (2017). *Dimensional Compliance and Compressive Strength of Sandcrete Hollow Blocks Produced in Minna Metropolis*. Proceedings of 2nd International Engineering Conference, School of Engineering and Engineering Technology, Federal University of Technology, Minna, Niger state 2017 (pp. 11-16).

PAPER 19- DURABILITY OF BIO-CEMENTED SOIL AGAINST WIND EROSION: A CASE STUDY OF SEMI-ARID SOIL TREATED WITH BACILLUS *MEGATERIUM*-CEMENTATION REAGENT MIX

M. A. Oyelakin[1*], M. I. Kanyi[2], K. J. Osinubi[3], A. O. Eberemu[4], T. S. Ijimdiya[5]

[1]Ph.D. Student, Department of Civil Engineering, Ahmadu Bello University, Zaria, Nigeria.
[2]Department of Civil Engineering, Joseph Sarwuan Tarka University, Makurdi, Nigeria
[3]Professor of Civil Engineering, Ahmadu Bello University, Zaria, Nigeria
[4]Civil Engineering and Researcher at Africa Center of Excellence on New Pedagogies in Engineering Education (ACENPEE), Ahmadu Bello University, Zaria, Nigeria
[5]Professor of Civil Engineering, Ahmadu Bello University, Zaria, Nigeria

*Email: m_coonloy@yahoo.com

ABSTRACT

Semi-arid zone soils are vulnerable to wind erosion which causes sand movement, destruction of agroforestry and dust storms. To mitigate these effects, the impacts of ageing and rain scour on bio-cemented semi-arid zone soil of North-eastern Nigeria were investigated. The soil was treated with varying non-pathogenic urease-positive Bacillus *megaterium* (*B. megaterium*) suspension densities (i.e., 1.5 x 10^8, 6.0 x 10^8, 1.2 x 10^9, 1.8 x 10^9, and 2.4 x 10^9 cells/ml) and cementation reagent concentrations (i.e., 0.25, 0.5, 0.75, and 1 M) in 3 treatment cycles using 50% (B. *megaterium*): 50% (Cementation reagent) mix ratio. With 1.8 x 10^9 cells/ml *B. megaterium* suspension density and 1 M cementation reagent treatment, the bulk density of the natural soil increased from 1964 kgm^{-3} to 2187 kgm^{-3}; the sediment flux values of the natural soil reduced from 3.4, 3.7 and 4.2 $kgm^{-2}s^{-1}$ to 0.09, 0.19 and 0.23 $kgm^{-2}s^{-1}$ at wind speeds of 8, 11 and 14 ms^{-1}, respectively; and for the rain scour effects, the sediment flux value of samples cured for 7 days increased from 0.45, 0.83 and 1.17 $kgm^{-2}s^{-1}$ to 0.54, 0.97 and 1.35 $kgm^{-2}s^{-1}$ after 3 days at wind speeds of 8, 11 and 14 ms^{-1}, respectively. Based on the ageing and rain scour impacts, the bio-cemented soil has good potential in mitigating wind erosion.

Keywords: Ageing, bio-cementation, mitigation, rain scour, sediment flux, wind erosion.

1. INTRODUCTION

The major impact of wind erosion is land desertification (Kheirabadi *et al*., 2018) which leads to a shortage of land availability for engineering and agricultural uses (Gomes *et al*., 2003; Mendez and Buschiazzo, 2010; Lee *et al*., 2019). This also causes blockage of waterways and ditches with transported sediments (Pan *et al*., 2023); it produces aerosol (Li *et al*., 2023) and exacerbates aeolian desertification and dust storms (Haouzi *et al*., 2019). In Nigeria, it is reported that the country's annual loss to desertification is a large amount of 300,000 hectares of land (Olagunju, 2015a; Pona *et al*., 2021). The USDA (2009) survey of the World's desertification vulnerability shows that northern Nigeria was generally highly vulnerable to desertification while the vulnerability of parts of Jigawa, Yobe and Borno States was revealed to be very high (see Plate I).

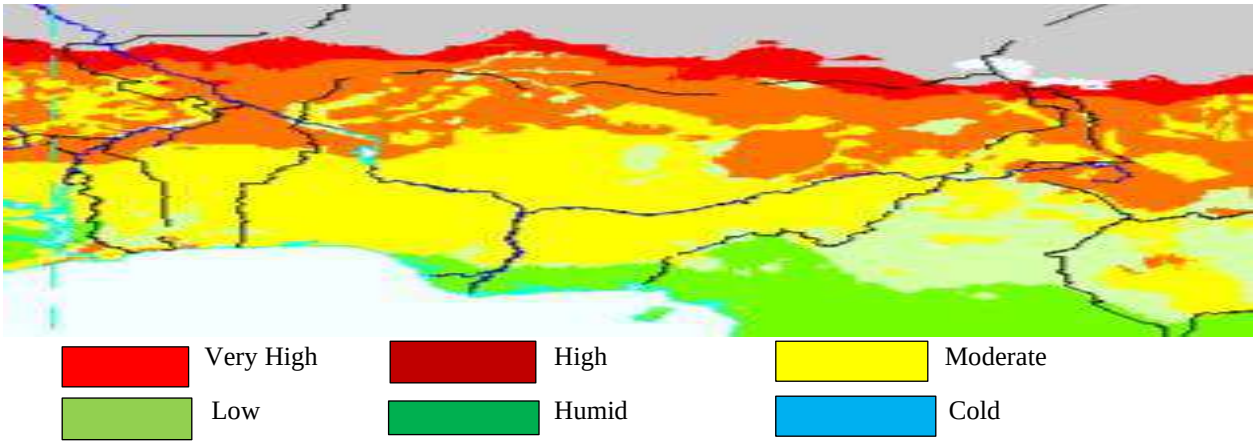

Plate I: Map showing desertification vulnerability in Nigeria (Source: USDA, 2009)

The majority of traditional control methods have either been chemical or mechanical, resulting in certain degrees of health hazard on frequent applications (Anderson *et al*., 2014). A relatively green and eco-friendly soil improvement technique also known as Microbially Induced Calcite Precipitation (MICP) was introduced by Kantzas *et al*. (1992) as alternative to traditional soil improvement methods and it had gained prominence in soil improvement, as reported in different studies (e.g. DeJong *et al*. 2006; Whiffin *et al*. 2007; Mitchell *et al*. 2008; van Paassen *et al*. 2010; Shanahan and Montoya, 2016; Fattahi *et al.*, 2020a; b; c; Osinubi *et al.*, 2023a; b).

Microbial Induced Calcite Precipitation (MICP), a bacterial soil treatment, is a sustainable soil improvement technique that involves the use of microbes. Its novelty is in its use of natural soil bacteria to induce cementation in situ in an innocuous manner (Montaya *et al*., 2012; Goswami *et al.*, 2018; Zomorodian *et al.*, 2019) which promotes sustainability and eco-friendliness (Rebata-Landa, 2007; Ivanov and Chu, 2008; Osinubi *et al*., 2019a, b, c). The precipitation of calcite in the MICP process is a biochemical depositional process that resembles the formation of natural cementation (Molenaar and Venmans, 1993; Tian *et al*., 2018).

Recent studies (e.g., Tian *et al*., 2018; Wang *et al*., 2018; Fattahi *et al*., 2020a, b, c; Lajevard and Shafiei, 2023) have all adopted the use of biotechnology in the mitigation of desertification with tremendous improvement in the amount of sediment flux (q_s) under the action of wind flow. However, the studies did not consider the durable resistance to rain scour and ageing on the reduced sediment flux. This study presents the sediment mass flux of loose sand treated with bacteria and its durability effects to suppress dust.

2. MATERIALS AND SAMPLES PREPARATION

2.1 Soil

A semi-arid soil obtained from Maigatari town, 12º48’25” N and 9º26’34” E, located in the Sahel along Niger - Nigeria border in Jigawa State, North-Eastern Nigeria, was used for the study.

2.2 Bacteria / Cementation reagents

A non-pathogenic urease-positive Bacillus *megaterium* (B. *megaterium*), classified by the American Type Culture Collection (ATCC) as ATCC 14581, was used for the study. The bacterium strains were cultured and prepared in different suspension densities of 1.50×10^8, 6.0×10^8, 1.20×10^9, 1.80×10^9 and 2.40×10^9 cells/ml for the study. The cementation reagent was prepared according to Stocks-Fischer *et al*., (1999) where mass concentrations of urea and calcium chloride were varied to obtain different concentrations of 0.25, 0.5, 0.75 and 1.0 M.

2.3 Specimen Preparation

A 50 % B. megaterium (B): 50 % cementation reagents (C) mix ratio was used for the treatment of the soil. Injection of the samples in three (3) cycles was also adopted as the best treatment from the strength results of the different treatment cycles used by Osinubi *et al*. (2023a). The samples were treated with various B. *megaterium* suspension densities and the cementation reagents, corresponding to the optimum moisture content (OMC) of the soil, as determined by Osinubi *et. al.* (2023a), in the ratio of 50 B: 50 C.

For the determination of bulk density, twenty-five (25) specimens were prepared in a 235 mm diameter by 33 mm deep pan (see Plate II) and each air-dried for 7, 42 and 84 days while twenty-four (24) specimens were prepared for the sediment flux determination, also in the same dimension of the pan, air-dried for 7, 42, 84 days as well as 3 days of soaking and exposed to 3 different wind speeds of 8, 11 and 14 m/s for 20 seconds. The specimens were prepared at a temperature of 21º C and a relative humidity of 70 %. The dimension of the pan was considered such that the circumference is wide enough to depict the flat terrain of semi-arid lands, deep enough to contain a substantial mass of sand and not too deep to block off wind blows.

Plate II: Samples prepared for the determination of density and sediment flux.

2.4 Bulk Density

A pan of 235 mm diameter by 33 mm deep with a volume of 1.4 x 10^6 mm^3 and weighing 650 g were used for the test. The same quantity of soil samples was used to fill each of the twenty-five (25) pans, treated and cured for 7, 42 and 84 days before weighing. Twenty (20) specimens were treated with various B. megaterium suspension densities and the cementation reagents corresponding to the optimum moisture content (OMC) of the soil in the ratio of 50B:50C; four (4) specimens were treated with the cementation reagents alone at 100% OMC as control and the remaining one (1) specimen was treated with water. A total number of 75 specimens were prepared for the bulk density which was calculated as the ratio of soil mass in the pan to the volume of the pan.

2.5 Sediment Flux

Sediment mass flux is the rate of sediment transport per unit area of material. It gives the measure of a soil's susceptibility to transportation under the influence of wind. The experiment was performed using a wind tunnel (TQ AF100 Subsonic Wind Tunnel) to simulate the effect of wind on soil (see Plate III). For ageing effects, the samples of soil were weighed in a pan of surface area 4.34 x 10^{-2} m^2, treated with various B. *megaterium* suspension densities and the cementation reagents corresponding to the OMC of the soil in the ratio of 50B:50C when cured for 7, 42 and 84 days.

Plate III: A TQ AF100 Subsonic Wind Tunnel used for the determination of sediment flux.

The rain scour effects were determined by spraying water, equivalent to the OMC of the soil, onto the 7-day cured sample and allowed to dry for 24 hours and the procedure was repeated for 2 more days (cycles). The strength on the 10^{th} day (after 3 days of water soaking) was considered as the effect of rain scour. At the end of durability check periods, the samples were levelled-placed at 500 mm away from the wind outlet and exposed to 8, 11 and 14 m/s wind speeds for 20 seconds. A total number of 288 specimens were prepared for the sediment flux which was calculated as the ratio of the soil loss to the product of the surface area of the pan and the time taken by the wind action.

3. RESULTS AND DISCUSSIONS

3.1 Bulk Density

The variation of the bulk density of soil-cementation reagent mixture with B. *megaterium* suspension density when cured for 7, 42 and 84 days, are presented in Figure 1. The bulk density of the natural soil increased from a value of 1964 to 2100 kgm^{-3} when cured for 7 days (see Figure 1) at 1.8 x 10^9 cells/ml bacteria and 1 M cementation reagent treatment. The bulk density values decreased at 2.4 x 10^9 cells/ml - 1 M treatment because the bacteria density had reached its optimum and the cementation reagents available could not supply the higher required nutrients needed for precipitation reaction. Further increments were recorded for samples cured for 42 and 84 days (see also Figure 1) with peak bulk density values of 2170 and 2187 kgm^{-3} at 2.4 x 10^9 cells/ml bacteria and 1 M cementation and 1.8 x 10^9 cells/ml bacteria and 1 M cementation reagent, respectively. This incremental trend, with respect to curing age, was observed by Wang *et al.* (2018) who concluded that the bulk density of bio-treated samples increased as the concentration of treatment and curing period increased.

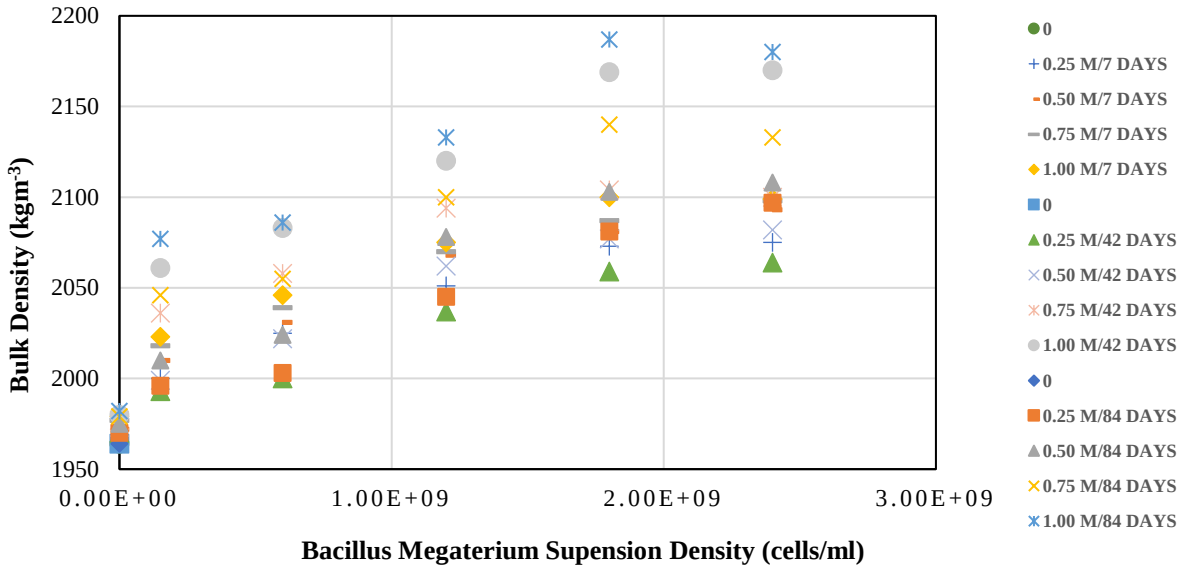

Figure 1. Variation of bulk density of soil-cementation reagent mixture with B. *megaterium* suspension density cured for 7, 42 and 84 days.

3.2 Sediment Flux

The sediment flux values of various soil-cementation reagent mixtures with B. *megaterium* suspension density are presented in Figures 2, 3 and 4 for wind speeds of 8, 11 and 14 ms^{-1} respectively. For the ageing effect and at 8 ms^{-1} wind speed (see figure 2), the sediment flux values decreased from 3.4 $kgm^{-2}s^{-1}$ value for the natural soil to 0.45, 0.22 and 0.09 $kgm^{-2}s^{-1}$ for 7, 42 and 84 days, respectively, at 1.8 x 10^9 cells/ml B. *megaterium* suspension density and 1 M cementation reagent. It was observed that the more the concentration of treatment and curing age, the lower the values of the sediment flux; and hence, the better the resistance against wind erosion. These values, however, increased slightly on soaking with water for 3 days (10th day) to record a least value of 0.54 $kgm^{-2}s^{-1}$ (see Figure 2) at 1.8 x 10^9 cells/ml B. *megaterium* suspension density and 1 M cementation reagent.

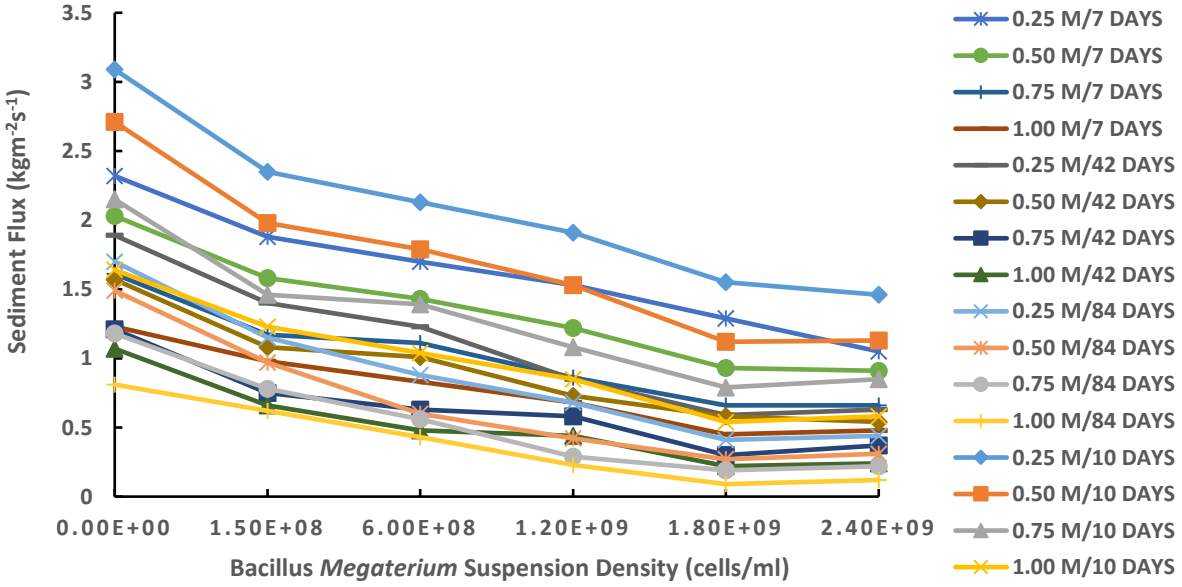

Figure 2: Variation of sediment flux of soil-cementation reagent mixture with B. *megaterium* suspension density at 8 ms^{-1} speed for 7, 42, 84 days of curing and 3 days of soaking.

The recorded sediment flux values of samples exposed to 11 ms^{-1} (see Figure 3) were 0.83, 0.53 and 0.19 $kgm^{-2}s^{-1}$ when treated with 1.8 x 10^9 cells/ml bacteria and 1 M cementation reagent at 7, 42 and 84 days, respectively. The values decreased with higher concentrations of treatment due to the bonding effects of calcite precipitation within the soil matrix but increased compared to the samples exposed to 8 ms^{-1}. Similar trends have been reported by previous studies (e.g. Agereh *et al.*, 2019; Fattahi *et al.*, 2020b; c; as well as Zhang *et al.*, 2023) where they observed that the higher the wind speed, the more the agitation within the soil particles and thus, the sediments transport. For the rain scour effect, the observed sediment flux value of 0.97 $kgm^{-2}s^{-1}$ recorded a 12 % increment with respect to the 7-day curing value which is attributed to the hydrolysis of water within the calcite precipitated (see Figure 3).

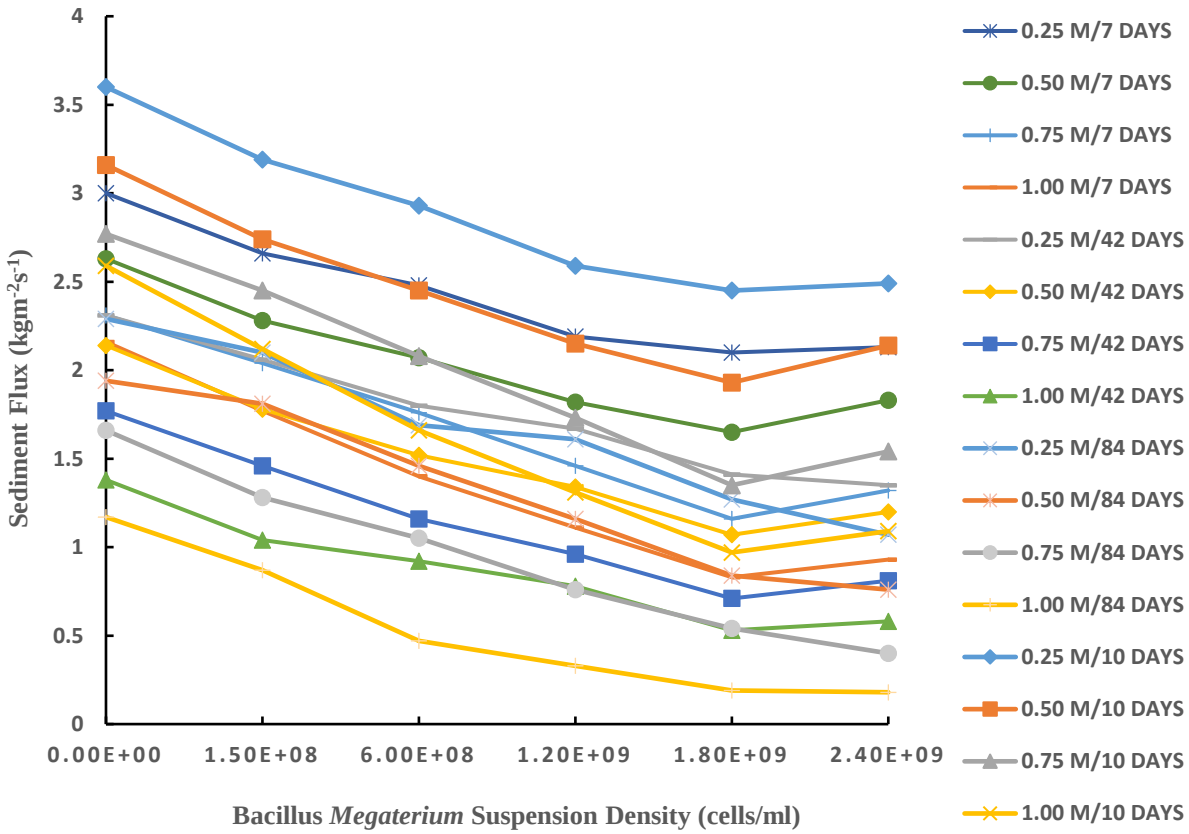

Figure 3: Variation of sediment flux of soil-cementation reagent mixture with B. *megaterium* suspension density at 11 ms^{-1} speed for 7, 42, 84 days of curing and 3 days of soaking.

For sediment flux of samples exposed to 14 ms^{-1} speed, the results showed further agitation of the soil particles compared to the lower speeds. However, the values were reduced with respect to higher treatment concentration and curing age which is attributed to the longer exposure to air which aided higher reactions for calcite precipitation (Palmén, 2012). The values obtained (see Figure 4) were 1.17, 0.85 and 0.23 $kgm^{-2}s^{-1}$ for 7, 42- and 84-days curing, respectively, at 1.8 x 10^9 cells/ml bacteria and 1 M cementation reagent treatment compared to 4.2 $kgm^{-2}s^{-1}$ obtained when the natural soil was exposed to the same speed. A similar trend was also reported by different studies (e.g. Wang *et al.*, 2018; Tian *et al.*, 2020; Lajevard and Shafiei, 2023 as well as Osinubi *et al.*, 2023a) where they observed that the longer the curing age of the bio-treated sample, the higher the strength of the sample. The water soaking effect reduced the 7-day curing value of 1.17 to 1.35 $kgm^{-2}s^{-1}$ on the 10th day which represents about a 15 % loss.

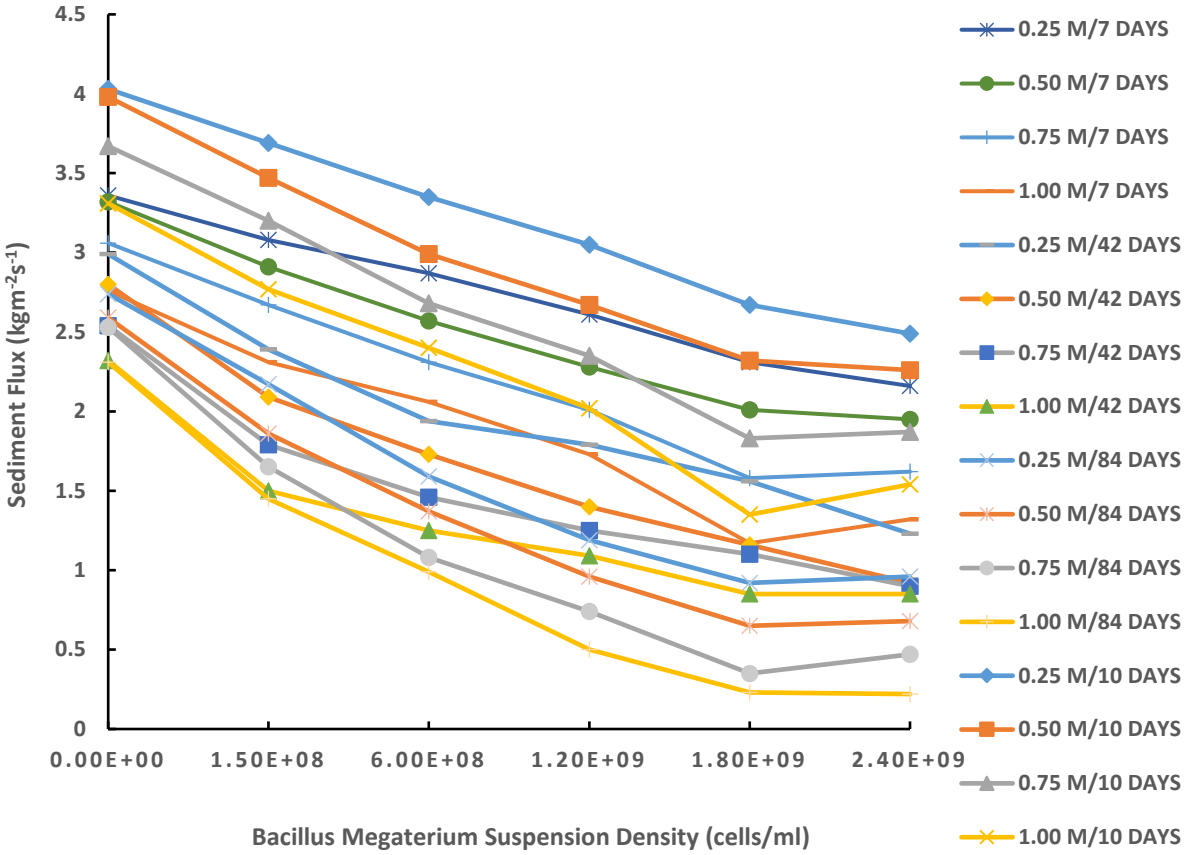

Figure 4: Variation of sediment flux of soil-cementation reagent mixture with B. *megaterium* suspension density at 14 ms^{-1} speed for 7, 42, 84 days of curing and 3 days of soaking.

4. CONCLUSIONS

Effects of durability of ageing and rain scour were investigated on various concentrations of cementation solutions on soil-bacteria mix on wind erosion resistance of a semi-arid sand. The results demonstrated that the 3 cycles injection method used and the 50:50 mix ratio can mitigate the soil against wind erosion. Specific conclusions are outlined as follows:

i. The bulk density of the treated samples increased with curing age, the suspension density of B. *megaterium* and the molar concentration of the cementation reagent. A peak value of 2187 kgm^{-3} was recorded for the bulk density.

ii. The sediment flux values decreased with the concentration of treatment and curing age but increased with wind speed. Least sediment flux values of 0.09, 0.19 and 0.23 kgm^{-2}s^{-1} were recorded for 8, 11 and 14 ms^{-1} speed, respectively, at 1.8 x 10^{9} cells/ml bacteria and 1 M cementation reagent. The sediment flux value also recorded a 15 % loss on soaking but the increment was not as significant as to break the bonds within the soil particles already established by the precipitation of calcites.

5. RECOMMENDATION

Based on the results obtained from the study, the semi-arid zone soil considered bio-treated with B. *megaterium* suspension density of 1.8 x 10^{9} cells/ml and 1 M cementation reagent concentration applied in 3 cycles using 50B:50C mix ratio can mitigate wind erosion.

REFERENCES

Agereh, S. R, Kiani, F, Khavazi, K, Rouhipour, H and Khormali, F. (2019) "An Environmentally Friendly Soil Improvement Technology for Sand and Dust Control". *Environmental Health Engineering and Management Journal*, Vol. 6, No. 1, pp. 63-71

Anderson J., Bang S., Sookie P. E., Bang S., Lee S. J., Choi S. R., Dho N. Y. (2014) "Reduction of Wind Erosion Potential Using Microbial Calcite and Soil Fibers" *Geo-Congress 2014 Technical Papers, GSP 234*, pp. 1664-1673

ATCC (2013). *American Type Culture Collection*. PO Box 1549 Manassas, VA 20108 USA

DeJong J. T., Fritzges M. B., and Nüsslein K., (2006)."Microbially Induced Cementation to Control Sand Response to Undrained Shear." *Journal of Geotechnics and Geoenvironmental Engineerin*g, Vol. 132, pp. 1381-1392.

Fattahi, S.M., Soroush, A., Huang, N., Zhang, J., Abbasi, S.J., Yu, Y. (2020a). "Laboratory Study on Biophysicochemical Improvement of Desert Sand." *Catena* Vol. 190, 104531.

Fattahi, S.M., Soroush, A., Huang, N. (2020b). "Wind Erosion Control Using Inoculation of Aeolian Sand with Cyanobacteria." *Land Degradation & Development*.

Fattahi, S.M., Soroush, A., Huang, N. (2020c). "Biocementation Control of Sand Against Wind Erosion." Journal of Geotechnical and *Geoenvironmental* Engineering, Vol. 146, No. 6, 04020045.

Gomez MG, Anderson CM, Dejong JT, Nelson DC, Lau XH. (2018) "Stimulating *in-situ* Soil Bacteria for Bio-Cementation of Sands." *Geotechnical Special Publication*. Vol. 2, No. 234, pp. 1674-82.

Goswami, G., Panda, D., and Samanta, R. (2018) "Bacillus *Megaterium* Adapts to Acid Stress Condition Through A Network of Genes: Insight from a Genome-wide Transcriptome Analysis" *Scientific Reports* 8, 16105

Haouzi, F., Filet, A. E. and Courcelles, B. (2019) "Performance Studies of Microbial Induced Calcite Precipitation to Prevent the Erosion of Internally Unstable Granular Soils". *Proceedings of the 5th GeoChina International Conferences 2018 – Civil Infrastructures Confronting Severe Weathers and Climate Changes: From Failure to Sustainability*, held on July 23 – 25, 2018 in Hangzhou, China, pp. 37-49

Ivanov, V. and Chu J. (2008)."Applications of Microorganisms to Geotechnical Engineering for Bioclogging and Biocementation of Soil *In-Situ*." *Reviews in Environmental Science and Bio-Technology*, Vol. 7, pp. 139 – 153

Kantzas, A., Ferris, F. G., Stehmeier, L., Marentette, D. F., Jha, K. N., and Mourits, F. M. (1992). "A Novel Method of Sand Consolidation Through Bacteriogenic Mineral Plugging," CIM 92-46, *Proceedings of the CIM 1992 Annual Technical Conference, Society of Canadian Institute of Mining, Metallurgy, and Petroleum.* Calgary, Canada. 2. 1-15.

Kheirabadi, H. Majid Mahmoodabadi, Vahidreza Jalali, Hormozd Naghavi (2018) "Sediment flux, wind erosion and net erosion influenced by soil bed length, wind velocity and aggregate size distribution" *Geoderma*, Volume 323, pp. 22-30

Lee M, Gomez MG, San Pablo ACM et al (2019) "Investigating ammonium by-product removal for ureolytic bio-cementation using meter-scale experiments." *Sci Rep* 9:18313. https:// doi. org/ 10. 1038/ s41598- 019- 54666-1

Li, J. W., He, B. Y., Hui, H. Y., Zhang, X. X., Li, C., & Han, G. D. (2023). "Effects of abnormal precipitations on plant species richness and dominance under different stocking rates". *Chinese Journal of Ecology*, Vol 42, pp. 1610–1617

Lajevardi, S. H., and Shafiele, H. (2023) "Investigating the Biological Treatment Effects on Fine grained Soil Resistance Against Wind Erosion." *Aeolian Research*, Vol. 60, No. 1

Mendez, M. J., Buschiazzo, D. E. (2015) "Soil coverage evolution and wind erosion risk on summer crops under contrasting tillage systems." *Aeolian Research*, Vol. 16, pp. 117–124

Mitchell, A. C., A. J. Phillips, J. P. Kaszuba,W. Hollis, A. B. Cunningham and R. Gerlach. (2008) "Microbially enhanced carbonate mineralization and the geologic containment of CO2." *Geochimica Cosmochim. Acta*, Vol. 72 No. 12 pp. A636. https://doi.org/10.1016/j.gca.2008.05.016.

Molenaar, N., and Venmans, A. A. M. (1993). "Calcium carbonate cementation of sand: A method for producing artificially cemented samples for geotechnical testing and a comparison with natural cementation processes." *Engineering Geology*., Vol. 35, No. 1, pp. 103–122

Olagunju, T. E. (2015a). "Impacts of Human-induced Deforestation, Forest Degradation and Fragmentation on Food Security" *New York Science Journal*, Vol. 8, No. 1, pp. 4-16

Osinubi, K. J., Yohanna, P., Eberemu, A. O. and Ijimdiya, T. S. (2019a) "Evaluation of Hydraulic Conductivity of Lateritic Soil Treated with Bacillus Coagulans For Use In Waste Containment Applications". *Proceedings of the 8th international congress on Environmental Geotechnics*. Vol. 3, pp. 401-409

Osinubi, K. J., Sani, J. E., Eberemu, A. O., Ijimdiya, T. S. and Yakubu, S. E. (2019b) "Unconfined Compressive Strength of Bacillus *Pumilus* Treated Lateritic Soil". *Proceedings of the 8th International Congress on Environmental Geotechnics*. Vol. 3, pp. 410-418

Osinubi, K. J., Gadzama, E. W., Eberemu, A. O., Ijimdiya, T. S. and Yakubu, S. E. (2019c) "Evaluation of The Strength of Compacted Lateritic Soil Treated With Sporosarcina *Pasteurii*". *Proceedings of the 8th international congress of Environmental Geotechnics*. Vol. 3, pp. 419-428.

Osinubi, K. J., Eberemu, A. O., Ijimdiya, T. S. and Oyelakin, M. A (2023a) "The Impact of Biocalcification on Strength of Semi-Arid Zone Sand of Northeastern Nigeria." *Geo-Congress 2023*, ASCE GSP 339. Los Angeles, California

Osinubi, K. J., Ijimdiya, T. S., Eberemu, A. O., and Kanyi, I. M. (2023b). Effect of Curing and Treatment Method on Ultrasonic Pulse Velocity of Compacted Lateritic Soil Treated with *Bacillus Thuringiensis*. *Proceedings of the 1st Faculty of Engineering and Technology Conference (FETiCON 2023)*. Theme: Advances in Technological Innovations in Nation Building and Attainment of Sustainable development Goals. Jun. 5 - 7, 2023, University of Ilorin, Nigeria pp 163-170

Palmén, A. (2012) "Stabilization of Frictional Soil Through Injection Using CIPS (Calcite In-situ Precipitation System)" PhD thesis, *KTH Royal Institute of Technology, Stockholm*, Sweden

Pan, X., Chu, J., Cheng, L. (2023) "Reduction of rainfall infiltration in soil slope using a controllable biocementation method" *Biogeotechnics*. http://creativecommons.org/licenses/by-nc-nd/4.0/

Pona, H. T., Xiaoli, D., Ayantobo, O. O., Tetteh, N. D. (2021) "Environmental Health Situation in Nigeria: Current Status and Future Needs" *Heliyon*, Vol. 7, No. 3, e06330

Rebata-Landa, V. & Santamarina, J.C. (2007). Mechanical limits to microbial activity in deep sediments. *Geochemistry Geophysics Geosystems*, Vol. 7, No. 11, pp. 1–12.

Shanahan, C. and Montoya, B. M. (2016). "Erosion Reduction of Coastal Sands Using Microbial Induced Calcite Precipitation". In: *Geo Journal*, Chicago Press, pp. 42-51

Stocks-Fisher, S., Galinat, J. K. and Bang, S. S. (1999) "Microbial Precipitation of CaCO3. *SoilBiology and Biochemistry*, -Elsevier, Vol. 31, No. 11, pp. 1563-1571.

Tian, K., Wu, Y., Zhang, H., Li, D., Nie, K., Zhang, S., (2018) "Increasing wind erosion resistance of aeolian sandy soil by microbially induced calcium carbonate precipitation." *Land Degradation*. & *Development*. Vol. 29, No 12, pp. 4271–4281. https://doi.org/10.1002/ldr.3176

Tian, K.L.; Wang, X.D.; Zhang, S.C.; Zhang, H.L.; Zhang, F.; Yang, A.Q. (2020) "Effect ofreactant injection rate on solidifying aeolian sand via microbially induced calcite precipitation. *Journal of Materials in Civil Engineering*, Vol. 32, No. 10,

US Department of Agriculture, Natural Resources Conservation Service (USDA NRCS). (2009) Web Soil Survey. http://Www.Websoilsurvey. Ncsc.Usda.Gov/App

van Paassen, L. A., R. Ghose, T. J. van der Linden, W. R. van der Star, and M. C. van Loosdrecht. (2010). "Quantifying biomediated ground improvement by ureolysis: large-scale biogrout experiment." *Journal of Geotechnical and Geoenvironmental Engineering*, Vol. 136, No 12, pp.1721-1728.

Wang, Z, Zhang, N, Ding, J, Lu, C and Jin, Y (2018). "Experimental Study on Wind Erosion Resistance and Strength of Sands Treated with Microbial Induced Calcite Precipitation."*Advances in Materials Science and Engineering*,. https://doi.org/10.1155/2018/3463298

Whiffin VS, Van Paassen LV, Harkes MP. Microbial carbonate precipitation as a soil improvement technique. Geomicrobiol J 2007; 24(5): 417-23. doi: 10.1080/01490450701436505

Zhang, B., Qu, Z., Lv, S., Han, G., Gao, C., Wilkes, A., Li, J., Li, Z., Wang, S., Wang, R., Wang, X., & Bai, Y. (2023). "Grazing effects on total carbon and nitrogen content of wind-eroded soils in desert steppe." *Land Degradation & Development*, pp. 1–15. https://doi.org/10.1002/ldr.4847

Zomorodian, S.M.A., Ghaffari, H., O'Kelly, B.C. (2019). "Stabilisation of crustal sand layer using biocementation technique for wind erosion control." *Aeolian Research,* Vol. 40, pp. 34–41.

PAPER 21 - REVIEWING THE SAFETY, BENEFITS, AND IMPLEMENTATION OF CNG AND CBG ADOPTION AS ENERGY AND TRANSPORT FUELS IN NIGERIA

E.I Muhibbu-Din [1]*

[1]Clean Energy and Environmental Research Laboratory (CE^2RL), Department Of Chemical Engineering, University Of Ilorin, Nigeria

*Email: muhibbudin.ei@unilorin.edu.ng

ABSTRACT

The removal of fuel subsidies in Nigeria highlights inefficiencies in the country's energy mix, resulting in a significant increase in energy and transportation costs. This has led to higher prices for goods and services across the board, worsening the country's economic situation. Consequently, the adoption of alternative fuel sources such as Compressed Natural Gas (CNG) and Compressed Biomethane Gas (CBG) becomes imperative. This review article explores the safety considerations, economic benefits, and energy security implications associated with replacing traditional fossil fuels like petrol and diesel with CNG and CBG in both the energy and transportation sectors. It offers a comprehensive analysis of the advantages, potential challenges, and the current state of adoption of CNG/CBG in Nigeria and other parts of the world, underscoring the urgency and importance of embracing these alternative fuel options. Drawing from a diverse range of academic and scientific sources, this review provides a thorough and robust examination of this critical subject and its implementation.

KEYWORDS: Compressed Natural Gas (CNG), Compressed Biomethane Gas (CBG), Energy Security, Energy Sustainability, Clean Environment, Nigeria

1. INTRODUCTION

The utilization of Compressed Natural Gas (CNG) and Compressed Biomethane Gas (CBG) as alternative fuels in the energy and transportation sectors has garnered significant attention due to their potential availability, affordability, emissions reduction, and enhanced fuel efficiency. Both CNG and CBG represent gaseous forms of natural gas compressed for use in internal combustion engines (Kaushik,*et al*., 2022), offering substantial benefits over traditional gasoline and diesel fuel (Okoro *et al.*, 2024).

CNG, akin to gasoline, is sourced from underground reserves and primarily consists of compressed methane gas, typically extracted from natural gas wells or obtained as a byproduct of oil extraction (Dam et al., 2022). It is mainly composed of methane with trace amounts of other gases such as ethane, propane, and butane. Production involves compressing natural gas to pressures ranging from 200 to 250 bars to reduce its volume for storage and transportation. Commonly employed in vehicles like buses, trucks, and cars, CNG is celebrated for its reduced carbon content and lower emissions of pollutants like nitrogen oxides and particulate matter, making it an environmentally favorable alternative (Trivedi *et al*., 2020).

In contrast, CBG is derived from organic materials like agricultural waste, food waste, sewage, or landfill gas through anaerobic digestion or biomethanation processes. This involves breaking down organic matter by bacteria in the absence of oxygen to produce biogas, which is then purified and compressed to form CBG. This renewable fuel not only offers a sustainable alternative to fossil fuels but also aids in mitigating greenhouse gas emissions by utilizing organic waste that would otherwise release methane into the atmosphere (Lucas *et al.*, 2023).

Both CNG and CBG are methane-based gases that can be interchangeably used with diesel or petrol engines upon conversion. While both offer clean-burning properties and a reduction in particulate matter emissions, they differ in their sources and production processes, with CNG primarily derived from natural gas wells and CBG produced from organic waste through anaerobic digestion and purification (Miroslaw *et al*., 2023).

Extensive research has underscored the advantages of CNG and CBG, including their potential to enhance fuel consumption, reduce exhaust emissions, and improve energy security. Moreover, advancements in storage technology have further bolstered their application as transport fuels, showcasing their viability as sustainable and cost-effective alternatives to traditional fuels. The versatility of CNG and CBG in various engine types, including dual-fuel compression-ignition engines, and their feasibility for marine transportation further emphasizes their potential role in mitigating environmental impact and addressing energy needs (Jamrozik *et al*., 2019; Ibeneme & Ighalo, 2020).

2. THE CHEMICAL COMPOSITION OF COMPRESSED NATURAL GAS (CNG) AND COMPRESSED BIOMETHANE GAS (CBG)

The chemical composition of Compressed Natural Gas (CNG) and Compressed Biomethane Gas (CBG) is a subject of significant interest due to their diverse applications across various sectors. While both gases share similarities in their major gaseous compounds, the production processes for biomethane involve additional steps such as methane content upgrading and cleaning to eliminate various impurities, distinguishing it from natural gas (Abanades *et a*l., 2021; Tonrangklang *et a*l., 2021).

Biomethane, chemically identical to methane, holds promise as a renewable resource for vehicle fuel or injection into natural gas grids, offering potential to replace fossil fuel natural gas and contributing to sustainable energy transitions (Kabeyi & Olanrewaju, 2022). It can also be utilized as compressed biomethane gas for vehicle and engine fuel, and distributed through natural gas or local biogas grids (Tanat *et a*l., 2021).

In terms of production, biomethane is often incentivized in European countries for grid injection or as a biofuel for vehicles, with processes including anaerobic digestion, methanation, and upgrading to ensure high methane content (Caposciutti *et a*l., 2020). Its chemical potential enables direct use as a vehicle fuel or conversion into electricity and heat in cogeneration units, emphasizing its versatility and sustainability (Kamalimeera & Kirubakaran, 2021). Regarding purification processes, both CNG and CBG undergo various methods to remove impurities and meet quality standards for compression and transportation. Membrane technology and adsorption processes are commonly employed for natural gas purification, with advancements such as Metal-Organic Frameworks (MOFs) showing promise in enhancing purification efficiency (Imtiaz *et al*., 2022; Tan *et al*., 2022). Additionally, optimization of purification processes is essential to reduce energy consumption and ensure gas quality meets required standards (Shi et al., 2020). For biogas purification, several techniques are utilized, including chemical absorption, adsorption, and biological removal of impurities, aimed at enhancing biogas composition and quality for various applications (Nevzorova & Karakaya, 2020). Innovative approaches such as enzymatic pretreatment and thermal techniques have shown potential in improving biogas production and quality (Nevzorova & Karakaya, 2020). The purification of both natural gas and biogas involves a range of techniques and processes aimed at removing impurities, enhancing gas quality, and maximizing yield, contributing to sustainable energy applications and environmental conservation efforts.

3. SAFETY AND BENEFITS OF ADOPTION OF CNG AND CBG AS ENERGY AND TRANSPORT FUEL

3.1 ENVIRONMENTAL IMPACT ASSESSMENT

Decreased Greenhouse Gas Emissions: Both CNG and CBG are acknowledged for their low carbon content, positioning them as cleaner alternatives to traditional fossil fuels. Research conducted by Trivedi et al., (2020) revealed that CNG vehicles emit substantially fewer greenhouse gases (GHGs) compared to their gasoline or diesel counterparts. This finding has spurred the adoption of CNG/CBG as a means to address air pollution and combat climate change.

3.2 ENHANCED AIR QUALITY

Incorporating CNG/CBG in engines and vehicles leads to diminished particulate matter emissions, decreased nitrogen oxide (NOx) emissions, and reduced volatile organic compounds. This decrease in air pollutants significantly benefits local air quality, particularly in urban regions. Research conducted by Tong *et a*l. (2020) showcased the enhancements in air quality attributed to CNG/CBG vehicles and combustion engines.

3.3 ENHANCING ENERGY SECURITY

Minimized Reliance on Imported Oil: Numerous nations, such as Nigeria, rely heavily on imported oil to fulfill their energy and transportation requirements, rendering them susceptible to global oil price fluctuations and supply interruptions. Transitioning to domestically sourced natural gas (CNG) or biomass (CBG) for transportation fuel and electricity generation can break this dependency on refined crude oil, thereby bolstering energy security. Research conducted by Rotman *et al.* (2019) highlights the geopolitical benefits of reducing crude oil dependence, leading to a bolstered national economy.

3.4 ECONOMIC CONSIDERATIONS

Financial Benefits: Natural gas (CNG) and biomass (CBG) are readily accessible and generally cheaper than gasoline or diesel when compared on an energy-equivalent basis (Drielli *et al.,* 2023). This economic advantage,

combined with governmental incentives and tax benefits for CNG/CBG engines and vehicles, has the potential to result in substantial savings for both consumers and fleet operators. A study conducted by the U.S. Department of Energy (DOE) details the cost-effectiveness of CNG (Kagiri, 2019).

3.5 DOMESTIC NATURAL GAS RESERVES AND ORGANIC WASTE

In nations endowed with ample natural gas reservoirs and significant organic waste resources, such as Nigeria, adopting CNG/CBG for transportation and electricity offers an opportunity to capitalize on domestic energy reservoirs. The report by Nwogu *et al.* (2020) underlines the economic advantages of utilizing domestic natural gas and organic waste. The prospect of oil serving as a sustainable long-term source of foreign exchange appears increasingly dim. Consequently, the Nigerian government must prioritize the development and integration of CNG and CBG technologies with other renewable energy.

4. CHALLENGES AND BARRIERS TO CNG AND CBG ADOPTION

4.1 INFRASTRUCTURE DEVELOPMENT

4.1.1 AVAILABILITY OF DISPENSING STATIONS

A notable hurdle hindering the widespread acceptance of CNG and CBG as energy and automotive fuels is the scarcity of CNG/CBG dispensing stations (Nouni *et al.*, 2021). Building a dependable network of CNG/CBG refueling stations is pivotal to assist owners of CNG/CBG engines/vehicles (Mustafi & Agarwal, 2020). The growth of CNG/CBG infrastructure differs across regions and is frequently shaped by governmental regulations and incentives. Guaranteeing a sufficient quantity of conveniently located CNG stations is vital in overcoming this obstacle (Philipp *et al*., 2020).

4.1.2 PIPELINE INFRASTRUCTURE

CNG distribution often relies on pipelines to transport natural gas from production facilities to refueling stations (Hryhoriy *et al*., 2021). The availability and capacity of these pipelines are vital considerations for the growth of the CNG market. The development and maintenance of an efficient pipeline infrastructure are essential to ensure a consistent and reliable supply of CNG to dispensing stations (Igbojionu, *et al*., 2019).

4.2 ENGINE RANGE AND REFUELING TIME

4.2.1 LIMITATIONS OF CNG/CBG VEHICLES

CNG/CBG engine/vehicles may have limitations in terms of their driving range compared to traditional gasoline or diesel engines/vehicles. This is due to the need for larger CNG/CBG storage tanks to achieve an adequate range. For some applications, such as long-haul trucking, this limitation may be a barrier to adoption. Manufacturers and researchers are continually working on improving CNG/CBG engine or vehicle efficiency to extend their range (Dahlgren, 2022).

4.2.2 TECHNOLOGICAL ADVANCES

Overcoming the limitations of CNG/CBG engines often requires technological advancements in storage tank design, engine efficiency, and fueling infrastructure (Suroto *et al.*, 2020). Research and development in these areas are ongoing to enhance the range and reduce refueling times. Innovations such as lightweight composite CNG/CBG tanks and faster refueling methods have the potential to address these challenges.

4.3 AWARENESS CAMPAIGNS

Awareness campaigns play a significant role in overcoming barriers related to public perception. These campaigns can provide information about the safety, environmental, and economic benefits of CNG/CBG, dispelling myths and misconceptions. Government agencies, environmental organizations, and industry stakeholders often collaborate on campaigns to promote CNG/CBG as a viable and safe alternative energy fuel.

5. CASE STUDIES OF COUNTRIES THAT HAVE ADOPTED CNG AND CBG AS ENERGY AND TRANSPORT FUEL

5.1 EXPERIENCES FROM COUNTRIES LEADING IN CNG/CBG ADOPTION

5.1.1. INDIA

India stands out as a notable example of successful adoption of CNG/CBG in the energy and transport sector. Recognizing the environmental and economic advantages of CNG/CBG, the Indian government has implemented policies and regulations to promote its usage (Tapas *et al*., 2020). Major cities like Delhi, Mumbai, and Ahmedabad have established extensive networks of CNG/CBG refueling stations to cater to both public and private transportation and domestic needs (Suverna *et al*., 2020). Delhi, in particular, boasts one of the world's largest CNG/CBG bus fleets. This transition has not only resulted in reduced emissions but has also enhanced air quality in these urban areas (Trivedi, *et al*.,2020).). India's experience underscores the potential for widespread adoption of CNG/CBG on a large scale, especially when bolstered by governmental initiatives and infrastructure development.

5.1.2 PAKISTAN

Pakistan has made notable advancements in utilizing CNG/CBG as a transportation fuel (Muhammad *et al*., 2022). The nation confronted substantial energy and environmental obstacles, with air pollution emerging as a significant issue. In response, Pakistan directed investments towards CNG/CBG infrastructure and encouraged the conversion of gasoline and diesel vehicles to CNG/CBG (Rafiq *et al*., 2022). This initiative markedly decreased dependence on conventional fossil fuels and mitigated greenhouse gas emissions. The success of CNG in Pakistan serves as a model demonstrating how the adoption of alternative fuels can effectively tackle environmental concerns and enhance energy security in developing countries (Muhammad *et al.,* 2022).

5.1.3. ARGENTINA

Argentina has enthusiastically embraced CNG/CBG for both public and private transportation ((Nikas, *et al.*, 2022). The Argentine government has introduced incentives to promote CNG/CBG usage, leading to a significant rise in the number of CNG-fueled vehicles on the streets ((Nikas, *et al*., 2022). The integration of CNG has not only diminished the carbon footprint but has also provided financial savings to consumers owing to the lower cost of CNG/CBG compared to gasoline (Grassi *et al.,* 2021)). Argentina's experience highlights the economic and environmental advantages of shifting towards CNG/CBG.

6. IMPLEMENTATION OF CNG AND CBG AS ENERGY FUEL

Implementing CNG and CBG as alternative energy fuels involves several key steps and considerations. The following implementation strategies are proposed to expand, encourage, and enhance the adoption of CNG and CBG as alternative energy fuels in Nigeria.

6.1 POLICY SUPPORT AND REGULATORY FRAMEWORK

It is essential for governments to formulate supportive policies and regulatory frameworks to encourage the adoption of CNG and CBG as energy fuels (Sirothiya & Chavadi, 2020). For instance, in India, the government has implemented initiatives such as the Pradhan Mantri Ujjwala Yojana to promote clean cooking fuel, including CBG and CNG (Breitenmoser *et al.,* 2019).

6.2 INFRASTRUCTURE DEVELOPMENT

Creating a sturdy infrastructure for distributing CNG and CBG is essential, encompassing the establishment of refueling stations and transportation pipelines (Takman & Andersson-Sköld, 2021). Investments in infrastructure development are vital to guarantee accessibility and convenience for consumers (Akther, 2023).

6.3 TECHNOLOGICAL DEVELOPMENT AND INNOVATION

Continuous research and development play a pivotal role in enhancing the efficiency of CNG and CBG production, storage, and utilization technologies (Sawale & Kulkarni, 2022). Nigerian universities, particularly federal universities, could be instrumental in this aspect, focusing on research and development of Compressed Natural Gas (CNG) and Compressed Biomethane Gas (CBG) in various forms. Each Nigerian university should establish a center for the conversion of petrol and diesel engines/vehicles to CNG/CBG engines/vehicles. These centers should be mandatory for acquiring skills, where students learn about CNG/CBG, their applications, and the conversion of petrol and diesel engines to CNG/CBG engines. The government must ensure that conversion kits are affordable and readily available. This initiative will create numerous job opportunities for Nigerians and foster a heightened interest in energy security and sustainability. Furthermore, innovation in gas compression and purification technologies has the potential to improve the feasibility and scalability of CNG and CBG as energy fuels (Jagtap & Dalvi, 2021).

6.4 FINANCIAL INCENTIVES AND SUBSIDIES

To stimulate investment in CNG and CBG infrastructure and vehicles, governments may offer financial incentives and subsidies (Schipfer, *et al.*, 2022). Subsidizing equipment such as biogas plants and CNG conversion kits can incentivize consumers to adopt these fuels (Patterson *et al.*, 2011).

6.5 AWARENESS AND EDUCATION

Public awareness campaigns emphasizing the environmental and economic advantages of CNG and CBG can foster consumer acceptance (Sawale *et al*., 2020). Educational initiatives targeting vehicle manufacturers, fleet operators, and consumers can enhance comprehension and acceptance of CNG and CBG technologies.

6.6 COLLABORATION AND PARTNERSHIPS

Collaboration among government agencies, private sector stakeholders, and research institutions is vital for the effective execution of CNG and CBG adoption efforts (Bhatia *et al.*, 2020). Public-private partnerships can expedite the deployment of CNG and CBG infrastructure and facilitate technology transfer and knowledge exchange .By implementing these measures, policymakers and industry stakeholders can promote the widespread adoption of CNG and CBG as sustainable energy fuels, thereby reducing greenhouse gas emissions and bolstering energy security.

7. CONCLUSION

The adoption of Compressed Natural Gas (CNG) and Compressed Biomethane Gas (CBG) in engines and automotive applications presents numerous environmental benefits, including reduced greenhouse gas emissions, lower levels of particulate and NOx emissions, and quieter engine operation. These benefits contribute to improved air quality and noise pollution reduction in urban areas. With its environmental advantages and widespread availability, CNG/CBG emerges as a promising alternative fuel option for a more sustainable and healthier energy and transportation future. Furthermore, the growing interest in CNG/CBG as an energy fuel is stimulated by its multifaceted advantages, including environmental sustainability, enhanced energy security, and economic viability. These factors collectively underscore the importance of considering CNG/CBG as a practical and sustainable solution in the transportation and energy sectors. By embracing CNG and CBG technologies, Nigeria has the potential to shield the country from global crude oil crises by accelerating its transition towards a more sustainable and resilient energy future while fostering economic development and improving public health.

REFERENCES

1 Kaushik, H. K., Rani, A., & Sarna, N. (2022). Assessment of CNG & CBG Composition Variation on CO_2 Emissions, Engine Performance and Durability for a Small Size PFI Engine (No. 2022-28-0020). SAE Technical Paper.

.2. Okoro, E. E., Aimikhe, V. J., Sanni, S. E., & Ogali, O. I. (2024). Compressed natural gas storage and transmission. In Advances in Natural Gas: Formation, Processing, and Applications. Volume 6: Natural Gas Transportation and Storage (pp. 81-106). Elsevier.

3. Dam, Leonardo., Semin. (2022). Effect of CNG Engine Conversion on Performance Characteristic: A Review. IOP Conference Series: Earth and Environmental Science, doi: 10.1088/1755-1315/972/1/012028

4. Trivedi, S., Prasad, R., Mishra, A., Kalam, A., & Yadav, P. (2020). Current scenario of CNG vehicular pollution and their possible abatement technologies: an overview. Environmental Science and Pollution Research, 27, 39977-40000. https://doi.org/10.1007/s11356-020-10361-7

5. Lucas, Xan, Pimienta. (2023). Biogas Energy from Animal Waste. doi: 10.1007/978-981-19-8774-8_20

6. Mirosław, Karczewski., Grzegorz, Szamrej. (2023). Experimental Evaluation of the Effect of Replacing Diesel Fuel by CNG on the Emission of Harmful Exhaust Gas Components and Emission Changes in a Dual-Fuel Engine. Energies, doi: 10.3390/en16010475

7. Jamrozik, A., Tutak, W., & Grab-Rogaliński, K. (2019). An experimental study on the performance and emission of the diesel/cng dual-fuel combustion mode in a stationary ci engine. Energies, 12(20), 3857. https://doi.org/10.3390/en12203857

8. Ibeneme, I. O. and Ighalo, J. O. (2020). Implementation of cng as an alternative fuel for automobiles in nigeria: benefits and recommendations. International Journal of Engineering Research And, V9(07). https://doi.org/10.17577/ijertv9is070654

9. Abanades, S., Abbaspour, H., Ahmadi, A., Das, B., Ehyaei, M., Esmaeilion, F., & Bani-Hani, E. H. (2021). A critical review of biogas production and usage with legislations framework across the globe. International Journal of Environmental Science and Technology, 19(4), 3377-3400. https://doi.org/10.1007/s13762-021-03301-6

10. Tonrangklang, P., Theryothin, A., & Preechawuttipong, I. (2021). Promotion and potential analysis of biogas plants to produce compressed biomethane gas for transportation in thailand.. https://doi.org/10.21203/rs.3.rs-302979/v1

11. Kabeyi, M. J. B., & Olanrewaju, O. A. (2022). Biogas production and applications in the sustainable energy transition. Journal of Energy, 2022, 1-43.

12. Tanat, Limpachoti., Kampanart, Theinnoi. (2021). The Comparative Study on Compressed Natural Gas (CNG) and Compressed Biomethane Gas (CBG) Fueled in a Spark Ignition Engine. doi: 10.1051/E3SCONF/202130201005

13. Caposciutti, G., Baccioli, A., Ferrari, L., & Desideri, U. (2020). Biogas from anaerobic digestion: power generation or biomethane production?. Energies, 13(3), 743. https://doi.org/10.3390/en13030743

14. Kamalimeera, N., & Kirubakaran, V. (2021). Prospects and restraints in biogas fed SOFC for rural energization: a critical review in Indian perspective. Renewable and Sustainable Energy Reviews, 143, 110914.

15. Imtiaz, A., Othman, M. H. D., Jilani, A., Khan, I. U., Kamaludin, R., Iqbal, J., … & Al-Sehemi, A. G. (2022). Challenges, opportunities and future directions of membrane technology for natural gas purification: a critical review. Membranes, 12(7), 646. https://doi.org/10.3390/membranes12070646

16. Tan, B., Liu, X., Wang, H., Yang, G., & Zhang, J. (2022). A charge-decorated porous framework with polar pores and open o donor sites for co2/ch4 and c2h2/c2h4 separations. Dalton Transactions, 51(35), 13419-13425. https://doi.org/10.1039/d2dt01961b

17. Shi, B., Pan, J., Guo, X., Zhang, X., Wu, L., Li, K., … & Zhang, Y. (2020). Optimization of the natural gas purification process based on exergy analysis. Geofluids, 2020, 1-9. https://doi.org/10.1155/2020/8830402

18. Nevzorova, T., & Karakaya, E. (2020). Explaining the drivers of technological innovation systems: The case of biogas technologies in mature markets. Journal of Cleaner Production, 259, 120819

19. Tong, Y., Wang, C., Zhang, Y., & Yao, H. (2020). Environmental benefits of compressed natural gas in the urban public transportation system of Xi'an, China. Environmental Pollution, 266, 115309

20. Rotman, D., Paltsev, S., & Jacoby, H. D. (2019). Energy security implications of switch to natural gas in road transport. Energy Policy, 134, 110977

21. Drielli, Peyerl., André, Bergsten, Mendes. (2023). The economic and environmental benefits of adopting natural gas in isolated systems of Amazonas state, Brazil. Environmental development, doi: 10.1016/j.envdev.2023.100889

. 22. Kagiri, C. M. (2019). Optimal Approach to Energy Management and Gas Delivery of a Compressed Natural Gas Station. University of Pretoria (South Africa

23. Nwogu, Ngozi, Claribelle., Izuwa, Nkemakolam, Chinedu., Ohia, Princewill, Nnaemeka., Ekwueme, Stanley, Toochukwu. (2020). Production of Electricity from Human Waste as a Strategy for Curbing Electricity Generation Problem in Nigeria. International Journal of Literature and Arts, doi: 10.11648/J.IJRSE.20200904.12
24. Nouni, M. R., Jha, P., Sarkhel, R., Banerjee, C., Tripathi, A. K., & Manna, J. (2021). Alternative fuels for decarbonisation of road transport sector in India: Options, present status, opportunities, and challenges. Fuel, 305, 121583.
25. Mustafi, N. N., & Agarwal, A. K. (2020). Biogas for transport sector: current status, barriers, and path forward for large-scale adaptation. Alternative Fuels and Their Utilization Strategies in Internal Combustion Engines, 229-271

26. Philipp, K., Rose., Rizqi, Nugroho., Till, Gnann., Patrick, Plötz., Martin, Wietschel., Melanie, Reuter-Oppermann. (2020). Optimal development of alternative fuel station networks considering node capacity restrictions. Transportation Research Part D-transport and Environment, doi: 10.1016/J.TRD.2019.11.018

27. Hryhoriy, Nykyforchyn., Leonid, Unigovskyi., Olha, Zvirko., O., T., Tsyrul'nyk., H., V., Krechkovs'ka. (2021). Pipeline durability and integrity issues at hydrogen transport via natural gas distribution network. Procedia structural integrity, doi: 10.1016/J.PROSTR.2021.10.071
28. Igbojionu, A., Anyadiegwu, C., Anyanwu, E., Obah, B., & Muonagor, C. (2019). Technical and economic evaluation of the use of CNG as potential public transport fuel in Nigeria. Scientific African, 6, e00212.

29. Dahlgren, S. (2022). Biogas-based fuels as renewable energy in the transport sector: an overview of the potential of using CBG, LBG and other vehicle fuels produced from biogas. Biofuels, 13(5), 587-599.
30. Suroto, Munahar., Muji, Setiyo., Madihah, Mohd, Saudi., Azuan, Ahmad., Dori, Yuvenda. (2022). Modelling Fuel Cut Off Controller on CNG Engines Using Fuzzy Logic: A Prototype. International Journal on Advanced Science, Engineering and Information Technology, doi: 10.18517/ijaseit.12.5.16849
31. Tapas, Peshin., Inês, Azevedo., Shayak, Sengupta. (2020). Life-cycle greenhouse gas emissions of alternative and conventional fuel vehicles in India. doi: 10.1109/VPPC49601.2020.9330819

32. Suverna, Trivedi., Ram, Prasad., Ashuthosh, Mishra., Ashuthosh, Mishra., Abul, Kalam., Abul, Kalam., Pankaj, Yadav. (2020). Current scenario of CNG vehicular pollution and their possible abatement technologies: an overview.. Environmental Science and Pollution Research, doi: 10.1007/S11356-020-10361-7

33. Muhammad, Asim., Adnan, Qamar., Ammara, Kanwal., Ghulam, Moeen, Uddin., Muhammad, Abbas., Muhammad, Farooq., M.A., Kalam., Mohamed, Mousa., Kiran, Shahapurkar. (2022). Opportunities and Challenges for Renewable Energy Utilization in Pakistan. Sustainability, doi: 10.3390/su141710947

34. Rafiq, Asghar., Mohd, Herwan, Sulaiman., Zuriani, Mustaffa., Nasim, Ullah., W., Hassan. (2022). The important contribution of renewable energy technologies in overcoming Pakistan's energy crisis: Present challenges and potential opportunities. doi: 10.1177/0958305x221134110

35. Nikas, A., Koasidis, K., Köberle, A. C., Kourtesi, G., & Doukas, H. (2022). A comparative study of biodiesel in Brazil and Argentina: An integrated systems of innovation perspective. Renewable and Sustainable Energy Reviews, 156, 112022

36. Grassi, Y. S., Brignole, N. B., & Díaz, M. F. (2021). Vehicular fleet characterisation and assessment of the on-road mobile source emission inventory of a Latin American intermediate city. Science of the Total Environment, 792, 148255

37. Sirothiya, M., & Chavadi, C. (2020). Role of compressed biogas to assess the effects of perceived value on customer satisfaction and customer loyalty. BIMTECH Bus. Perspect, 1, 70-89.
38. Breitenmoser, L., Gross, T., Huesch, R., Rau, J., Dhar, H., Kumar, S., ... & Wintgens, T. (2019). Anaerobic digestion of biowastes in India: Opportunities, challenges and research needs. Journal of environmental management, 236, 396-412.
39. Takman, J., & Andersson-Sköld, Y. (2021). A framework for barriers, opportunities, and potential solutions for renewable energy diffusion: Exemplified by liquefied biogas for heavy trucks. Transport Policy, 110, 150-160.

40. Akther, F. (2023). E-commerce in India: Trends, Hurdles, and Growth Opportunities. Formosa Journal of Science and Technology, 2(10), 2871-2880.
41. Sawale, S. D., & Kulkarni, A. A. (2022). Current technical advancement in biogas production and Indian status. In Advanced Biofuel Technologies (pp. 501-532). Elsevier.
42. Jagtap, N. J., & Dalvi, V. H. (2021). Feasibility study of bio-methane economy in India. Biomass and Bioenergy, 149, 106059.
43. Schipfer, F., Mäki, E., Schmieder, U., Lange, N., Schildhauer, T., Hennig, C., & Thrän, D. (2022). Status of and expectations for flexible bioenergy to support resource efficiency and to accelerate the energy transition. Renewable and Sustainable Energy Reviews, 158, 112094.
44. Patterson, T., Esteves, S., Dinsdale, R., & Guwy, A. (2011). An evaluation of the policy and techno-economic factors affecting the potential for biogas upgrading for transport fuel use in the UK. Energy policy, 39(3), 1806-1816.
45. Sawale, S., Patil, D., Joshi, C., Rachappanavar, B., Mishra, D., & Kulkarni, A. (2020). Biogas commercialization: commercial players, key business drivers, potential market, and fostering investment. Biogas Production: From Anaerobic Digestion to a Sustainable Bioenergy Industry, 343-387.
46. Bhatia, R. K., Ramadoss, G., Jain, A. K., Dhiman, R. K., Bhatia, S. K., & Bhatt, A. K. (2020). Conversion of waste biomass into gaseous fuel: present status and challenges in India. BioEnergy Research, 13, 1046-1068.

PAPER 22 - OPTIMIZATION OF OIL EXPRESSION FROM TRUNK FISH (*MORMYRUS RUME*) BY RESPONSE SURFACE METHODOLOGY USING EXTRUDER

A. B. Ayuba[1]*, T. K. Ajiboye[2], K. O. Abdulrahman[2], & Sunmonu[3] M. O.

[1] Department of Product Development and Engineering, National Institute for Freshwater Fisheries Research, New Bussa, Niger State. Nigeria
[2]Department of Mechanical Engineering, University of Ilorin. Ilorin, Kwara State, Nigeria.
[3]Department of Agriculture and Food Engineering, University of Ilorin. Ilorin, Kwara State, Nigeria.
*E-mail: aababanna@gmail.com

ABSTRACT
Oily fish have always been associated with numerous health benefits like improvement in mental ability and lowering the risk of heart diseases. The health benefits of fish oil are linked to its fatty acids, docosahexaenoic acid (DHA) and eicosapentaenoic acid (EPA) that are of immense benefits to the cardiovascular system. Despite the benefit of fish oil, its expression has been challenging. Fish oil expression is usually achieved using an extruder. The desire for less harmful oil from freshwater fish species is of importance to this study. In the current investigation, Response Surface Methodology (RSM) was used to optimize oil expression from Trunk fish. Screw diameter was varied from 32.5 to 42.5 mm, Screw Speed from 25 to 85 rpm, applied pressure from 5 to 45 N/mm^2, and pitch height from 10 to 30 mm to study their effects on fish oil yield with the aid of a two-level, four-factor central composite design (CCD). The second-order model developed accurately predicts the optimum oil yield. Optimum oil yield was obtained from the empirical model as 27.8% at a screw diameter of 42.5mm, screw speed of 55rpm, applied pressure of 40N/mm^2 and pitch height of 20mm. It was observed that the optimum oil yield of 27.8% is higher than the maximum oil yield of 27.1% obtained when experiment was conducted. Screw diameter, screw speed, applied pressure and pitch height substantially influence the optimum oil yield.

KEYWORDS: Extruder, Fish oil, Mormyrus rume, Optimization, Shaft.

INTRODUCTION

The fish samples considered in this study is Trunk fish (*Mormyrus rume)*, with local name Miligi in Hausa, Dwangwa in Yoruba and Ugbala in Igbo, the fish can grow up-to 1meter in size. The fish have Trunk-like snout and small terminal mouth 72-95 dorsal fin rays, 92-115 lateral lines scales with widespread distribution across water bodies.

The fish are radially available in freshwater bodies and feed on insects larvae. They are also bottom dwellers**.** Mechanical process of expression is highly needed in food value addition like fish oil in developing country like Nigeria. Mechanical extraction is the oldest unit operation used for oil extraction from solid matrix containing oil. Expression is the process of mechanically pressing liquid out of liquid containing solid (Brennan, 2009). Solid/liquid separator (mechanical expression) is popularly employed in the expression of oil from fish. According to Saravacos & Kostaropoulos (2002), mechanical expression of a liquid from a solid matrix is possible only if the solid is compressible and can be used in screening, sedimentation, filtration and centrifugation of oil.

The screw power system shows the characteristic of metals and provides a very positive and rigid medium of power transmission to press the fish product under a high pressure inside the barrel. As the screw shaft is increasing in diameter, the screw system is also decreasing in pitch height, this give a combination that is essential for obtaining maximum pressure for oil expression and fish extract extrusion process (Olaniyan, 2011).

Oil recovery from fish, seeds or other materials are affected by some parameters classified as follows, screw parameters, which involves combined effect of screw speed and screw diameter, Oleaginous material parameters: restriction size and Process parameter: machine speed, moisture content, cooking time, temperature and pressure (Lonescu *et al*., 2014).

Heat treatment of oil seed breaks the oil-bearing cells of the seed, clot the protein in the cake, adjust the moisture level of the cake to optimum level for oil expression, lower the viscosity and increase the fluidity of the oil to be expelled, thereby facilitate oil expression from the material. Effect of different processing factors on yield or recovery and quality of oil from oil bearing seed have been investigated by various authors. These seeds include groundnut oil (Ajao *et al.*, 2010), castor seed (Dairo *et al.*, 2011), and neem seed oil (Orhevba *et al.,* 2018). The main objective of the study was the optimization of oil expression from Trunk fish (*Mormyrus rume*) by response surface methodology using extruder.

2.0 MATERIALS AND METHODS/METHODOLOGY/EXPERIMENTAL PROCEDURE

2.1 Sample Preparation

Fresh fish sample Trunk fish was obtained from kainji lake basin, New Bussa, Niger State, Nigeria. The fishes were thoroughly washed manually to remove dirt that might get stuck to the body after undergoing a de-freezing process. The internal organs of the fishes were removed using stainless steel knife. The remaining part of the fish are cut into strips, to enhance a speedy preheating process as shown in (Plate I and II) before oil expression (Ayuba *et al*., 2018).

Figure I Whole Trunk fish (*Mormyrus rume*)

Figure II: Cut fish ready for pre-heating

2.2 Oil Expression

The oil was expressed using modified fish oil extruder, the extruder is made up of three main units namely the feeding unit, the compression and melting unit all fabricated using locally available materials. The capacity of the extruder raged from 17–20 kg/h and was powered by a 5.0 hp, 3–phase electric motor connected to a reducing gear. All component through which the feed material (fish) will pass were made of stainless steel to prevent contamination and to withstand frictional wear. The experimental procedure was by running the machine for about 5 minutes on no load before loading the pre-heated sample as described by Akinoso (2006). As the screw pitch decreases along the screw shaft and pitch height, it provides the compressing force needed to squeeze out the entrapped oil from the pre-heated fish. Oil expressed and the cake from the sample were collected separately, At the end of the experiment, the expressed oil and the extract (cake) were collected and weighed separately. From the value obtained, oil yield is calculated as follow

$$\% \text{ Oil yield} = \frac{weight\ of\ oil}{weight\ of\ expressed\ fish}\ x\ 100 \quad (1)$$

2.3 Experimental Design for Oil Expression

Two level four factorial designs was used to fit the second-order polynomial. The setting of the design of experiment type (CCD) was implemented in Design Expert Software Package (Stat-Ease, Inc., Version 13.0 Minneapolis, USA) according to Dean and Voss (1999) was used to select the parameters that influence and maximize the oil yield in the continuous expression press with an extruder. The design points were determined by this expression as presented in Equation (2)

$$N = 2^n + 2n + k. \quad (2)$$

The independent variables selected for this study were (i) screw diameter; (ii) screw speed (iii) pitch height and (iv) applied pressure. A statistical optimization was conducted using a 2^4 full factorial CCD for the four variables, consisting of 16 factorial points, 8 axial points and 4 at the centre points were employed, implied 28 experiments were required. The variables and levels were fixed based on information from the literature and trial experiments (Olaoye *et al.*, 2018). The operating parameters selected for screw diameter (32.5, 35, 37.5, 40 and 42.5mm), screw speed (25, 40, 55, 70 and 85rpm), pitch height (10, 15, 20, 25 and 30mm) applied pressure (5, 15, 25,35 and 45kN/mm^2) while responses were actual oil yield and predicted oil yield. The correlation between the operating parameters (independent variables) and the dependent response (oil yield) was determined using a quadratic model of a second-order polynomial as shown in Equation. (3).

$$Y = \beta_0 + \sum_{i=1}^{2} \beta_i\ x_i^1 + \sum_{i}^{2} \beta_{ii}\ x_i^2 + \sum_{i=1}^{n-1} \sum_{j=2}^{2} \beta_{ij}\ x_i\ x_j \quad (3)$$

Where Y is the response, x_i and x_j are the un-coded independent variables

b_0, b_i, b_{ii} and b_{ij} are intercepts, linear, quadratic and interaction coefficients respectively.

3.0 RESULTS AND DISCUSSION

The central composite design is shown below in Table 1

Table 1 Shows the experimental ranges and levels of independent variables

Factors	Level				
	$-\alpha$	-1	0	+1	$+\alpha$
Screw diameter (mm)	32.5	35	37.5	40	42.5
Screw speed (rpm)	25	40	55	70	85
Pitch height (mm)	10	15	20	25	30
Applied pressure (N/mm^2)	5	15	25	35	45

3.1 Percentage Oil Yield of *Mormyrus rume* Fish Species

The oil yield obtained in this study ranges between 24-27.1% as shown in Table 2.

Table 2: Experimental design for variables and the response using CCD

Std	Run	Factor 1 A:Screw diameter mm	Factor 2 B:Screw speed rpm	Factor 3 C:Pitch height Mm	Factor 4 D:Applied pressure N/m^2	Response 1 Actual oil yield %	Response 2 Predicted oil yield %	Response 3 Residual %
28	1	37.5	55	20	25	24.5	26.9	-2.4
1	2	35	40	15	15	25.9	26	-0.1
14	3	40	40	25	35	27.6	26.6	1
16	4	40	70	25	35	26.6	25	-0.2
25	5	37.5	55	20	25	24.6	24.6	-0.4
27	6	37.5	55	20	25	24.5	25.4	-0.8
10	7	40	40	15	35	24.9	25	-0.1
13	8	35	40	25	35	25.8	26.3	-0.5
12	9	40	70	15	35	25.4	25.9	-0.5
26	10	37.5	55	20	25	24.4	24.6	-0.4
21	11	37.5	55	10	25	25.4	25.3	0.1
19	12	37.5	25	20	25	25.6	24.9	0.7
15	13	35	70	25	35	26.1	26.8	-0.7
4	14	40	70	15	15	26.5	26.7	-0.2
24	15	37.5	55	20	45	25.9	26.4	-0.5
22	16	37.5	55	30	25	25.7	25	0.7
7	17	35	70	25	15	25.6	25.9	-0.3

23	18	37.5	55	20	5	26.1	25.3	0.8
9	19	35	40	15	35	25.8	26.2	-0.4
6	20	40	40	25	15	24.5	25.8	-1.6
17	21	32.5	55	20	25	25.1	25	0.1
11	22	35	70	15	35	26.2	27.8	-0.7
3	23	35	70	15	15	25.6	25.9	-0.3
8	24	40	70	25	15	26.1	27	-0.9
20	25	37.5	85	20	25	25.7	26.1	-0.4
18	26	42.5	55	20	25	27.1	27.7	-0.6
2	27	40	40	15	15	26	27.4	-0.4
5	28	35	40	25	15	25.5	25.9	-0.4

3.2 Analysis of variance (ANOVA) and significant factor of oil yield

The results from regression analysis of the developed process model and response are presented in Table 3.

Table 3: ANOVA for Reduce Quadratic Model Response for Oil Yield:

Source	Sum of Squares	Df	Mean Square	F-value	p-value	
Model	35.51	14	2.54	9.94	< 0.0001	significant
A-Screw diameter	12.76	1	12.76	49.99	< 0.0001	
B-Screw Speed	0.0504	1	0.0504	0.1975	0.6640	
C-Pitch height	0.4537	1	0.4537	1.78	0.2053	
D-Applied Presure	18.20	1	18.20	71.30	< 0.0001	
AB	0.6006	1	0.6006	2.35	0.1490	
AC	0.0756	1	0.0756	0.2963	0.5954	
AD	0.1406	1	0.1406	0.5509	0.4711	
BC	0.7656	1	0.7656	3.00	0.1069	
BD	0.1406	1	0.1406	0.5509	0.4711	
CD	0.0056	1	0.0056	0.0220	0.8843	
A^2	1.07	1	1.07	4.20	0.0611	
B^2	0.0044	1	0.0044	0.0172	0.8975	
C^2	0.0319	1	0.0319	0.1250	0.7294	
D^2	0.6419	1	0.6419	2.51	0.1368	
Residual	3.32	13	0.2553			
Lack of Fit	3.27	10	0.3271	20.66	0.0149	significant
Pure Error	0.0475	3	0.0158			
Cor Total	38.82	27				

R Squared = 0.9145, Adjusted R Squared = 0.8225, 5% Level of Significance
A=screw diameter, B=screw speed, C=pitch height, D=applied pressure

The fitness of the regression model was checked with the coefficient of determination having an R^2 value of 0.9145. The maximum oil yield of 27.1% (at corresponding screw diameter, screw speed pitch height and applied pressure of 42.5mm, 55rpm, 20mm and 40N/m^2, respectively) and minimum oil yield of 23,2% (at corresponding screw diameter, screw speed, pitch height and applied pressure of 35.0mm, 70rpm, 25mm and 15N/mm^2, respectively) were obtained. The result showed that the three independent variables were relevant

to the fish oil yield in the mechanical expression process, as different levels of process parameters gave different oil yield of fish.

4.0 Model Relating Process Parameter and Process Output

The coefficient of determination, R^2 for the response, oil yield was 0.9145. the model relating the process parameters and output is stated in equation (4)

4.1 Oil Yield

The result of the comparison on oil yield at various process conditions reveal that maximum oil yield at different process condition are significantly different from each other. Table 2 above showed that oil expressed with interaction between screw diameter, applied pressure yielded more oil (Fasina & Ajibola 2009). Ajibola *et al*. **(**1999) have reported that finely ground samples yielded more oil when compared with coarsely ground samples. The reason for this was attributed to the increased surface area of oil-bearing cells exposed to heat treatment and subsequent pressure application. This expressed more oil from cells of finely ground samples than in the coarsely ground samples. Olaniyan, (2011) reported that maximum oil yield was extracted from groundnut at 20min with screw diameter of 35mm and oil yield of 24.5% oil was obtained. Tunde *et al* (2001) reported that oil yield of mechanically expressed soya beans oil increase with increased in applied pressure from 50 to 70 N/mm^2; the author observed that the oil yield of 27.9% was obtained when the sample were pressed with a screw diameter of 32.5, screw speed of 60rpm. This trend compared favourably with previous researcher on oil expression by Adejumo *et al*. (2013).

$$OY = 27.0 + 6.84x10^{-1}\text{A} - 4.47x10^{-2}\text{B} + 1.63x10^{-1}\text{C} + 8.66x10^{-1}\text{D} + 1.95x10^{-1}\text{AB} + 1.07x10^{-1}\text{AC} + 7.86x10^{-2}\text{AD} - 2.17x10^{-1}\text{BC} + 1.30x10^{-1}\text{BD} - 1.78x10^{-1}\text{CD} + 1.21x10^{-1}A^2 + 3.04x10^{-3}B^2 + 5.30x10^{-2}C^2 - 1.70x10^{-1}D^2 \qquad R^2 = 91.8\% \qquad (4)$$

OY = Oil yield A = Screw diameter, B = Screw speed, C = Pitch height D = Applied pressure

4.2 Effect of Input Variables on percentage oil yield of Trunk Fish (*Momyrus rume)*

The interaction effects of screw diameter, screw speed, pitch height and applied pressure on the oil expression yield were studied using the interaction plot and 3D surface plot of response surface methodology

It was obvious that an increase in oil yield was observed with the decrease in shaft diameter and increase pitch height. The oil yield was maximum at 27.1% when the pitch height was 20 mm and screw diameter of 42.5 mm while the minimum yield was achieved at 23.2.0% when the pitch height was 25mm and the shaft diameter was 35 mm These imply that as pitch height increase more fish tissue was broken and resulted in more oil yield.

The effect of screw diameter and screw speed was studied using the 3D surface plot in Figure 4.1 which shows the interaction between screw diameter and screw speed. Increase in oil yield was observed with the decrease pitch height and increase in screw diameter. These imply that as pitch height increases more tissue were broken and resulted to more oil yield. Minimum oil yield of 23.5 % was recorded at screw diameter of 35 mm when the screw speed was 70rpm. while maximum oil yield of 24.47% was achieved at screw diameter of 35.0 mm when the screw speed was 70rpm. Figure 4.2 presents the effects of screw diameter and applied pressure on oil yield. From the figure, it was obvious that an increase in oil yield was observed with the increase in screw diameter and pitch height at first, and then the trend was reversed when pitch height reached 15mm. and screw diameter of 42.5 mm. It can be deduced from the analysis of variance (ANOVA) results from figures 4.1-4.3 that the combined effects of screw diameter, screw speed, pitch height and applied pressure have a significant effect on the oil yield from Trunk fish species. Therefore, the reduction in the size of the fish in order to expose a greater area of the fish tissue to rupture prior to heating before mechanical oil expression can improve the oil yield as found by Adeeko & Ajibola (1994), Olajide, (2000), Sayyar *et al*. (2009), and Adesina & Bankole (2013).

From the results of the Analysis of variance for oil yield presented in Table 2 above, it can be seen that screw diameter and its interaction with other variables had significant effect on oil yield at 5% level of significance. Bako *et al.* (2018) also reported that the screw speed is an important factor that affects the yield of the oil extracted, and that oil is obtained from fish with high choke clearances, screw shaft clearances and screw speeds. The decrease in oil yield with an increase in cooking time also corresponds to the findings of Tanko *et al*. (2020) in the criteria for the extraction of fish oil. Akinoso, (2006) on the effect of heating duration, and temperature on the yield and quality of palm kernel; Olaomi, (2008) and Ajao *et al*. (2010) stated that peanut expresses their optimum oil only when the peanut is pre-treated. The fish used for the study was pre-heated in a closed pan heating method for 15 minutes at 100^{0}C with oil yield of 27.1%. Other studies with similar

findings include Ajibola *et al*. (2013), Orhevba *et al*. (2013), Ogunsina *et al*. (2014), Adejumo *et al*. (2015), and Bamgboye & Adejumo (2015) Figure 4.1-4.3 present 3-D response surface plots for the effect of input variables on oil yield of *Mormyrus rume*.

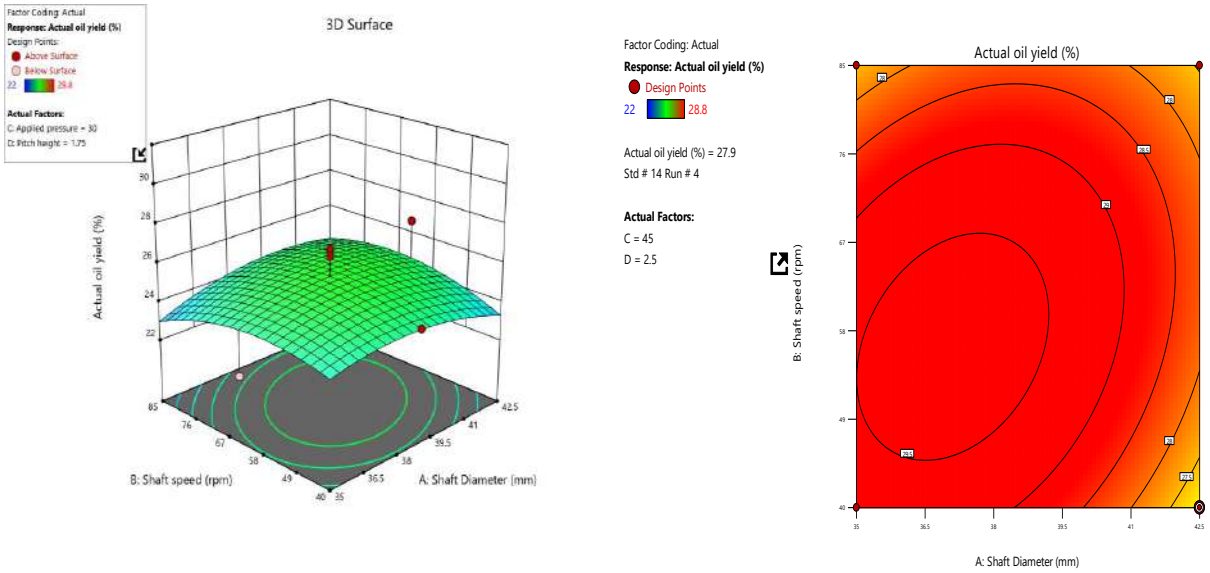

Figure 4.1. 3D surface plot and contour plot of screw diameter and screw speed interactions on oil yield

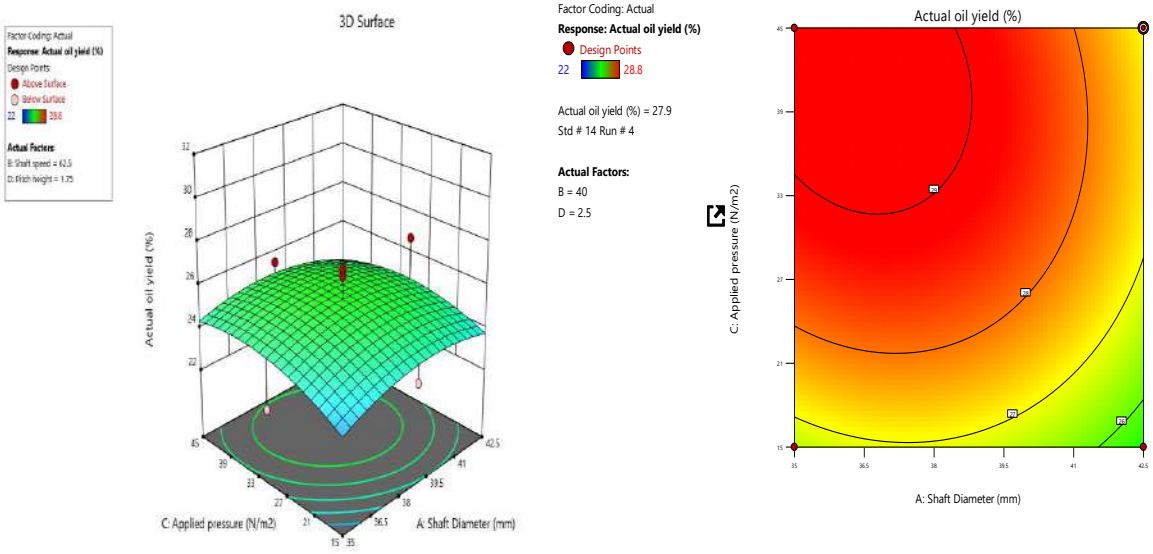

Figure 4.2. 3D surface plot and contour plot of screw diameter and applied pressure interactions on oil yield

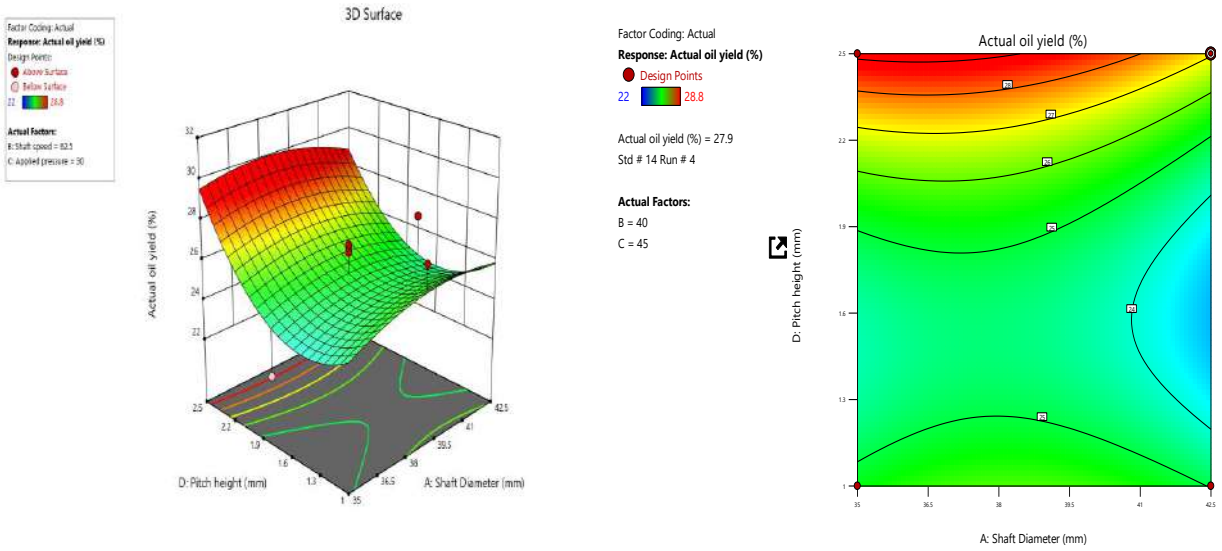

Figure 4.3. 3D surface plot and contour plot of screw diameter and pitch height interactions on oil yield.

5.0 CONCLUSION

The oil expression process from fish was optimized using Response Surface Methodology (RSM) with fractional factorial design (2^4) model of Central Composite Design (CCD). From this study, it was observed that all four factors affect the oil yield of fish during expression but the most significant is applied pressure which has the highest influence in regression model with highest F-value followed by screw diameter, pitch height and screw speed. This means that applied pressure has significant influence in oil expression from fish and other oil-bearing materials. The result obtained show optimum values of 42.5 mm, 40 N/mm^2, 20 mm and 55 rpm at a corresponding optimal oil yield of 27.1%. While predicted oil yield was 27.8%, with coefficient of variation of 2.06 and the percentage error of 0.6. Hence, this methodology could, therefore be effectively used in any process where an analysis of the optimum, effects and interaction of many experimental factors are studied.

ACKNOWLEDGEMENT

The authors gratefully acknowledge the support and contribution received from National Institute for Freshwater Fisheries Research, New Bussa through teaching and easy access to their facilities at the discretion of the Head of Department, Product Development and Engineering who assisted me during the processing stage of the material used for the experiment and fabrication.

REFERENCES

Adeeko, K. A., & Ajibola, O. O. (1999). Factors affecting the expression of oil fromgroundnut. *Journal of Agricutural EngineeringResearch, 45*(2), 45-53.

Adejumo, B. A., Alakowe, A.T., & Obi, D.E., (2013). Effect of heat treatment on the characteristic and oil yield of moringa Olifera Seed. The international journal of engineering Science (IJES): 2(1) 232-239

Ajao, K. R., Ajimotokan, H. A., Olaomi, J., & Akande, H. F. (2010). Design and development of a groundnut oil expelling machine. *Journal of Agricultural Technology, 6*(4), 643-648. Retrieved from http://www.ijat-rmutto.com

Akinoso, R. (2006a). Modeling of Oil Expression from Palm Kernel (ElaeisguineensisJacq.). *Agricultural Engineering International, 8*, 1-7.

Ayuba, A. B., Amina, I. M., Okouzi, S. A., & Olugbenga, B. O. (2018). Design and Fabrication of an Extruder for the Extraction of Fish Oil from Cat fish. *International Journal of Latest Technology in Engineering Management and Applied Science, 7*(8), 53-55.

Bako, T., Umogbai, V. I., & Garba, A. J. (2018). Optimization of Crude Fish Oil Extraction using Mechanical Screw Expeller Validated by Response Surface Methodology. *Journal of Postharvest Technology, 6*(1), 69-82.

Brennan. (2009). *Food Engineering Operations Second Edition,* (5 th ed.). London: Uk Publising Limited.

Dairo, O. U., Olayonju, T. M., Ajisegri, E. S., Awoniran, S. O., & Alamu, O. J. (2011). Effect of Temperature and Percentage of initial Catalyst on the in-situ production of Bio-diesel from Castor oil Bean Seed Using response surface Methodology. *Journal of Natural Science Engineering Tehnology, 10*(1), 163-177.

Dean, A. M., & Voss, D. T. (1999). *Design and Analysis of Experiments.* New York: Springer-Verlag.

Fasina, O. O., & Ajibola, O. O. (1998). Mechanical expression of oil from camphor (Tetracarpidiim conophom). *Journal of Agricultural Engineering Research, 44*(10), 278-285.

Lim, S., Hoong, S. S., Teong, L. K., & Bhatia, S. (2010). Supercritical fluid reactive extraction of Jatropha Curcas Seeds with Methanol. *Bioresources Technol, 102*, 7169-7172.

Lonescu, M., Voicu, G., Barris, S., Covaliu, C., Dinca, M., & Ungureanu, N. (2014). Parameter influencing the screw pressing process of oilseed materials. *Journal of Agricultural Sciences*, 234-248.

Olaniyan, A. M. (2011). Design, development and testing of a screw press expeller for palm kernel oil extraction. *Journal of Agricultural Engineering Technology*, 56-59.

Olaoye, J. O., & Busari, R. A. (2018). Optimisation of Mechanical Expression of Castor Seeds Oil (Ricinus Communis) Using Response Surface Methodology. *Arid Zone Journal of Engineering, Technology and Engineering and Enviroment, 13*(6), 878-887. Retrieved from www.azojetete.com.ng

Openshaw, K. (2000). Areview of Jatropha Curcus; an oil plant of unfulfilled promise. *Biomas Bioenerg, 19*, 1-15.

Orhevba, B. A., Chukwu, O., Zinash, D., & Sunmonu, M. O. (2018). Statistical Modelling of oil from Neem Seed using a Screw Press. *Journal of Engineering Technology and Enviroment, 14*(3), 45-48.

Saravacos, G. D., & Kostaropoulos, A. E. (2002). *Handbook of Food Processing Equipment.* (3rd ed.). New York: Springer Science Business Media.

Sayyar, S., Abidin, Z. Z., Yunus, R., & Muhammad, A. (2009). Extraction of oil from jatrpha seeds-optimisation and kinetics. *American Journal os Applied Science*, 1390-1395.

Tanko, B., Samuel, E. O., & Vivtor, I. U. (2020). Mathematical modeling of mechanical horizontal screw oil extractor. *Agricultural EngineeringInternational: CIGR Journal, 22*(2), 244-254. Retrieved from http://www.cigrjournal.org

Tunde-Akintunde, T. Y., Akintunde, B.O. & Igbeka, J.C,. (2001). Effects of Processing Factors on Yield and Quality of Mechanically Expressed Soya beans Oil. Journal of Agricultural Engineering Technology, 55, 86-92.

PAPER 23 - DEVELOPMENT OF A SOLAR-BASED SYSTEM FOR AGRICULTURAL PRODUCTS DRYING IN SOKOTO STATE, NIGERIA.

K. A. Ibrahim[1*], K. O. Lawal[2], I. K. Muritala[3]

[1]Department of Electrical & Electronics Technology, Federal College of Education, Gidan Madi, Sokoto, Nigeria.
[2]Department of Electrical & Electronics Engineering, Abubakar Tafawa Balewa University, Bauchi, Nigeria.
[3]Department of Technology Development, Research & Innovation, Afridat Research and Innovation, GmbH, Duisburg, Germany.
[*]Email: ibrahimkafayatsubomi@gmail.com

ABSTRACT
Agricultural product drying systems play a vital role in preserving the quality and extending the shelf life of harvested crops. This study investigates the fundamentals underlying operation, functionality, and design of a solar-based drying system. The solar-based drying system emphasizes the interplay of temperature, humidity, airflow dynamics, and drying kinetics to achieve optimal drying conditions for farm produce. Proper airflow within the drying chamber was considered to ensure uniform drying. The study highlights the engineering principles in designing an efficient drying system tailored to local crop characteristics and ambient conditions. From this work, the adoption of solar drying technologies reduces reliance on traditional methods, which often contribute to deforestation and environmental degradation. This work presents a sustainable method for preserving agricultural produce, and helps in improving food security, thereby reducing post-harvest losses. Additionally, it explores emerging trends such as renewable energy sources, automation technologies, and sensor-based monitoring systems which enhance efficiency and sustainability. The research provides valuable insights for advancing post-harvest processing, food preservation techniques, and food hygiene in line with the Sustainable Development Goals (SDGs): 2, 7, 9, 12 and 13 for Sokoto State's agriculture industry, which could be replicated across the nation and the continent.

KEYWORDS: Agricultural Produce, Drying Technology, Food Quality, Smart System, Solar Radiation

1. INTRODUCTION

Food security is a fundamental concern for Nigeria, Africa's most populous nation. It refers to the ability of all citizens to access safe, nutritious food at all times (FAO-UN, 2015). However, achieving food security remains a significant challenge since Nigeria's population is projected to reach 400 million by 2050, placing a growing strain on food production resources (United Nations Population Fund, 2021). Erratic weather patterns and extreme weather events can disrupt agricultural production and lead to crop failures (Intergovernmental Panel on Climate Change, 2022).

Sokoto State, in Nigeria, has significant potential for solar energy due to its location in the Sahel region with abundant sunshine throughout the year, with agriculture playing a huge role in the economic activity of the state, and contributing significantly to the state's Gross Domestic Product (GDP), providing employment opportunities for most of the population. However, the state's agriculture sector faces several challenges, including inadequate infrastructure for processing and storage, resulting in post-harvest losses. The state also faces significant energy challenges, with inadequate access to electricity hindering economic development (Sokoto State Government, 2021).

The loss of edible food products after harvest due to inadequate storage, handling, and processing techniques (post-harvest losses), is the major bottleneck, which has a devastating effect on food security and is estimated to be as high as 50% for some crops. It leads to reduced food availability, economic losses and environmental impact. Since the post-harvest losses posing a significant threat to food security in Nigeria, a promising solution lies in harnessing the sun's power. Solar dryers offer a sustainable and cost-effective method for preserving food products by utilizing renewable solar energy to gently dehydrate crops, extending their shelf life and reducing spoilage unlike traditional drying methods that rely on firewood or fossil fuels, solar dryers (Aregbesola et al., 2021). The solar dryer system have emerged as a promising solution preservation which requires minimal operating costs, helps in empowering farmers and households to preserve their harvest without significant financial burdens, and can help retain essential nutrients in food products, promoting a more nutritious diet, as compared to other traditional methods (Ozturk et al.2009 & Koua et al,.2009).

Studies have shown that solar dryers can significantly decrease post-harvest losses by effectively dehydrating food items and extending their shelf life (Oladejo et al., 2016), and, because of its gentler drying process, it can help retain essential nutrients in food products, leading to a more nutritious diet (Alibassi and Madani, 2012). From related reviewed literatures, the drying system can be grouped into different methods which includes:

Traditional Drying Methods: This method uses direct sun heat for dehydration which makes the product exposed to the element and is vulnerable to dust, insects and contamination. Unpredictable weather patterns can also disrupt the drying process leading to spoilage or inconsistent results (FAO-UN, 2015). It is mostly considered because it requires little or no finances (Oluyi, 2023).

Solar Dryer: This method can be classified into two (2) which are direct solar and indirect solar dryer. Solar dryer uses solar radiation but the difference between itself and traditional drying method is that is not vulnerable to dust, insects, contamination and the unpredictable weather condition has lesser effect on it because is protected with a transparent cover.

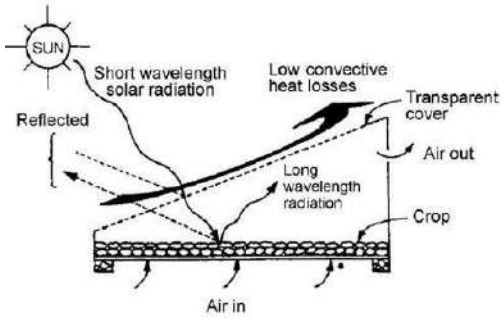

Figure 1: Direct Solar Dryer (Shittu et al 2018)

It is also crucial to acknowledge the limitations of solar dryers. Drying efficiency heavily relies on sunlight availability, while cloudy or rainy weather can significantly extend drying times (Essam and Rafea, 2007). The initial cost of purchasing and installing a solar drying system can be a barrier for some users, particularly small-scale farmers (Jannot et al., 1994). Traditional solar dryer designs may have limited capacity, making them unsuitable for large-scale drying applications (Singh et al, 2007). Figure 2 is the diagram for the indirect solar dryer

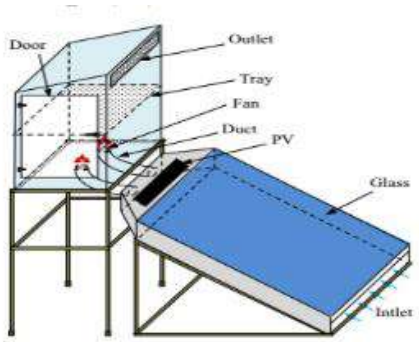

Figure 2: Indirect Solar Dryer (Jain & Bala.2017).

Smart Solar Dryer: Smart solar drying systems represent a significant advancement in food preservation technology. Their ability to leverage sensors and automated controls paves the way for more efficient and reliable drying solutions, contributing to improved food security and sustainability.

Figure 2: Smart Solar Dryer (Princewill et al, 2023).

1.1 Aim and Objectives

The development of a solar-based system for Agricultural products drying in Sokoto State is the aim of this work. The following are the set objectives:

a) To design a prototype solar-based drying system for agriculture farm produce in Sokoto State to achieve a faster and more controlled drying.
b) To conduct a comprehensive need assessment to understand the specific challenges and requirements of farmers in Sokoto State
c) To develop an algorithm in C++ language used for the smart control of the drying system
d) To understand the relationship between the different units involved in the smart control of the drying system

2. THEORETICAL ANALYSIS

Sokoto State, Nigeria is located in the country's North-western region, experiences a hot and dry climate with abundant sunshine throughout the year (Aliyu & Iloeeje, 2011). This makes it an ideal location to explore solar drying as a sustainable and energy-efficient method for preserving agricultural products. Traditional sun drying, a widely used practice, suffers from drawbacks such as weather dependence, slow drying times, and vulnerability to pest infestation and spoilage (Singh & Manikantan 2008). The analysis considered various factors influencing the design, which includes: solar radiation, collector design, drying chamber design, heat transfer, targeted agricultural products, drying technology, system capacity with economic feasibility, and the control method.

2.1 Solar Radiation Analysis

Characterizing the average daily and seasonal solar radiation levels in Sokoto State is crucial for determining the system's collector size and drying capacity (Duffie & Beckman 2013). Solar radiation data is essential for estimating the energy available for drying. This involves utilizing solar radiation models to predict the solar irradiance incident on the drying system. One commonly used model is the Hargreaves-Samani method, which estimates solar radiation based on temperature data. Equation (1) is the Hargreaves-Samani method equation (Sane et.al., 2014):

$$H = H_0 * (1 + 0.33 * sin^2\theta) \quad \ldots (1)$$

where H is the estimated daily solar radiation on a horizontal surface (MJ/m^2/day), H_0 is the extraterrestrial radiation on a horizontal surface (MJ/m^2/day), and θ is the solar elevation angle

2.2 Collector Design Analysis

The analysis here involves the designing of the solar collector to maximize solar energy absorption. This includes determining the collector area, orientation, tilt angle, and absorber plate material. The efficiency of the collector can be calculated using equation (2):

$$\mu_{collector} = \frac{(m*C_p*\Delta T)}{(A*G)} * 100\% \quad \ldots (2)$$

where $\mu_{collector}$ is the collector efficiency (%), m is the mass flow rate of air (kg/s), C_p is the specific heat of air (kJ/kg°C) $\triangle$T is the temperature difference across the collector (°C), A is the collector area (m^2), and G is the solar radiation (W/m^2) (Matavel et al., 2021).

2.3 Drying Chamber Analysis

This involves the designing the drying chamber to facilitate efficient heat and mass transfer. Here the chamber volume, airflow rate, and insulation thickness will be determined. The drying rate equation was used to predict the drying kinetics, as can be seen in equation (3).

$$\frac{dX}{dt} = k * (X_{wet} - X_{dry}) \quad \ldots (3)$$

where $\frac{dX}{dt}$ is the drying rate (kg/s), k is the drying rate constant (1/s), X_{wet} is the moisture content of the wet product (kg water/kg dry solid), and X_{dry} is the moisture content of the dry product (kg water/kg dry solid). (Matavel et al., 2021).

2.4 Heat Transfer Analysis

The heat transfer mechanisms within the drying system were evaluated, including conduction, convection, and radiation. Equations such as Fourier's Law and Newton's Law of Cooling are used to calculate heat transfer rates. This can be seen in equations (4) and (5) respectively:

$$q = -k\frac{dT}{dx} \quad \ldots (4)$$

$$q = h * A * (T_{surface} - T_{Ambient}) \quad \ldots (5)$$

where q is the heat transfer rate (W), k is the thermal conductivity (W/m°C), $\frac{dT}{dx}$ is the temperature gradient (°C/m), h is the convective heat transfer coefficient (W/m^2°C), A is the surface area in m^2, $T_{surface}$ is the surface temperature (°C) and $T_{ambient}$ is the ambient temperature in °C (Matavel et.al., 2021).

2.5 Targeted Agricultural Product

The drying requirements of different agricultural products (e.g., fruits, vegetables, grains) vary significantly in terms of temperature, humidity and drying time. The system's design will accommodate the specific needs of the products intended for drying (Kinsley et. al. 2007).

2.6 Drying Technology Selection

Several solar drying technologies exist, each with its advantages and limitations. This analysis will evaluate options such as direct solar dryers, indirect solar dryers, and mixed-mode dryers to determine the most suitable technology for the targeted products and local context (Kumar et al, 2016).

2.7 System Capacity

The optimal system size will be determined based on factors like the volume of agricultural products to be dried, desired drying times, and economic considerations. The analysis will assess the system's life-cycle cost and potential return on investment for farmers in Sokoto State (Janja and McCann, 2017).

2.8 Control Analysis

This involves the designing of a control system to maintain optimal drying conditions within the drying chamber. This includes the development and the implementation of the algorithms to regulate the parameters such as temperature and humidity. Arduino ATMEGA328 was used to control the drying process to achieve precise drying

3. MATERIALS AND METHODS

The methodology for the development of the solar-based system for agricultural products drying in Sokoto State, Nigeria encompasses two key stages: needs assessment analysis (data collection), and the development of the solar-based drying system.

An assessment of the predominant agricultural products in Sokoto State was carried out using a questionnaire and short structured interviews, to determine their specific drying requirements needed. This assessment included valuable insights into the specific needs and challenges related to agricultural product drying. These include product details, drying challenges, post-drying handling, and drying improvement. The interviews underscored the importance of engaging with local stakeholders and tailoring of a solar-based system to meet the specific requirements of Sokoto State's agricultural sector.

Based on the findings from the needs assessment of different locations in the state, a customized solar-based drying system was conceptualized and designed. The system incorporates elements such as solar collectors, drying trays, ventilation mechanisms, and monitoring/control devices to ensure efficient and uniform drying of agricultural products.

3.1 Materials

The materials that were used in the construction of the solar-based system for agricultural products drying for Sokoto State Nigeria are presented below:

(i) Metal Sheet: A dark, heat-absorbing metal sheet, that acts as the absorber plate, with a selective coating that maximizes solar energy absorption and minimizes heat radiation outwards.

(ii) Transparent Glass: A transparent glass (5mm thick) traps heat inside the collector while allowing sunlight to pass through.

(iii) MBF Wood**:** Two sheets of MBF wood were used for the drying chamber construction

(iv) Malena Wood: The solar collector is made of Malena wood, to prevent outdoor weather conditions, especially the action of solar radiation. The collector will face south to receive maximum direct sunlight throughout the day. The tilt angle of 15^0 was used in the design should be seasonally adjustable to optimize sun exposure based on location and time of year. In the collector is also a foam for proper insulation and to minimize heat loss to the surroundings. The design ensures proper airflow without excessive heat loss.

(v) ARDUINO ATMEGA 328: This is the brain of the smart system. It controls the system's intelligence which facilitates sensor readings (Fan, heater control and user interface functionality)

(vi) DHT-22 **Sensor:** Temperature and humidity sensors (DHT-22) are embedded in the drying chamber to monitor temperature and humidity levels respectively, with the help of a microcontroller. The microcontroller will be powered by a solar panel. There will be a keypad to key in a particular temperature for optimum performance.

(vii) Heater: It provides another option for drying if there is no solar radiation. It can also be used with the conventional dryer to reduce the drying time of some farm produce.

(viii) DC Fan (12V): This is used for heat circulation in the drying chamber.

3.2 System Description

Central to the operation of the dryer are the DHT 22 sensors strategically placed within the drying compartment to monitor both temperature and humidity levels. This dual-sensor setup allows for precise control over the dying environment, essential for maintaining optimal conditions during the drying process. The temperature sensor captures overall temperature, while the humidity sensor gauges moisture content in the air providing critical data for regulating the drying process. Figure 4 is the block diagram of the solar-based drying system.

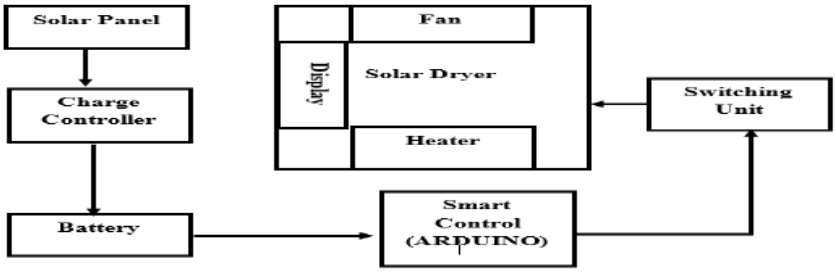

Figure 3: Block Diagram of the System

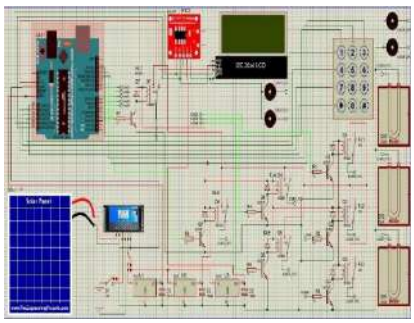

Figure 4: Circuit Diagram of the Solar-based Dryer

The system integrates 12V DC fans and heaters to facilitate airflow and heat distribution in the drying compartment. Fans ensure consistent air circulation, while heaters provide the necessary warmth for even onion drying. Strategic placement of fans and heaters ensures uniform heat distribution, optimizing the drying process and enhancing preservation quality. Four fans were strategically positioned to enhance system performance, with a 12VDC/220o dry heater as the temperature source. A 9VDC voltage regulator powered the Arduino

board, while 5VDC was used for the LCD and sensor. The DC heater, relays, and fan were directly powered by the 12V/18AH battery.

An Arduino ATmega 328 microcontroller unit controls the system's intelligence, managing sensor readings, fan and heater control, and user interface functions. The microcontroller adjusts fan and heater operation based on real-time sensor data through a developed control algorithm to maintain desired temperature and humidity levels. A user interface with a Keypad and LCD allows users to input desired settings and view real-time readings.

Integration of a real-time clock module ensures accurate timekeeping for scheduling and logging purposes. The onion preservation drier system offers precise control, efficient operation, and superior onion preservation outcomes with these capabilities. Figures 5 and 6 are the flow chart and the circuit diagram of the solar-based dryer.

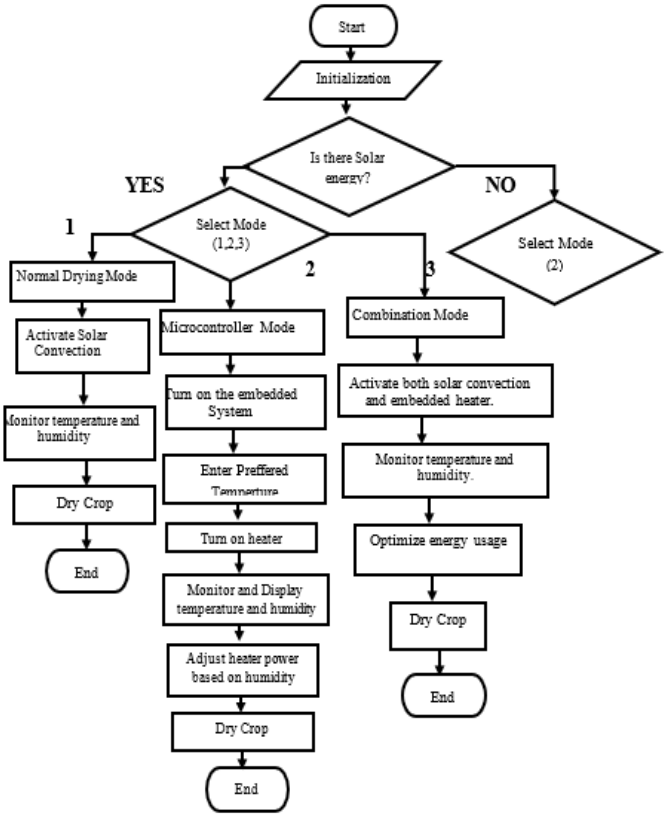

Figure 5: Flow Chart of the Solar-based Dryer

4. RESULTS AND DISCUSSION

This section discusses the outcomes and analysis of designing a solar-based drying system for agricultural products. Figures 7 show the diagram of the solar-based dryer prototype with dimensions. Figure 8 is the 3-D diagram of the system.

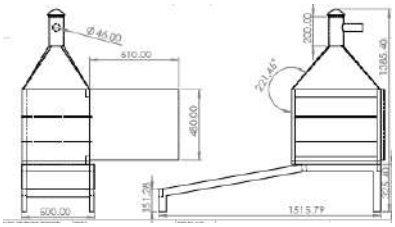

Figure 6: Front and Side View of the Pilot Smart Solar Dryer

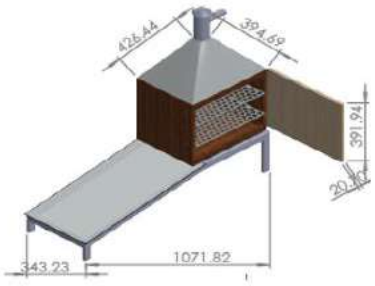

Figure 7: 3D Diagram Side of the Dryer.

Figure 9: Designed Solar-based Dryer (Prototype)

Figure 9 is the prototype of the designed solar-based dryer.

The results from the needs assessment indicated that the farmers expressed the desire for reliable, affordable and efficient drying methods that would enable them to preserve the quality of their farm produce and reduce losses. This can be buttressed with the following points:

(i) There was no drying equipment, method or technology in place, except drying directly from the solar radiation. According to the responses from the needs assessment 59.5% confirmed the absence of any drying technology, while 82.9% confirmed that the only available method was the direct sun drying. This can be seen in Figure 10 and 11 respectively. The direct solar drying makes farm produce take longer times (days) for the farm product to get dried. This was justified in Figure 12.

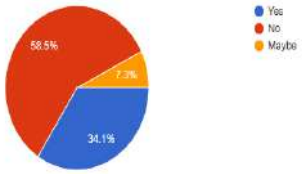

Figure 10: Drying Equipment Available in Sokoto State

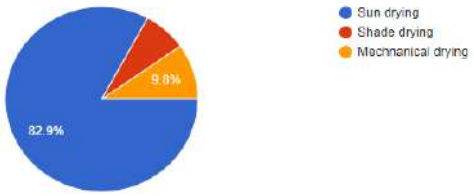

Figure 11: Methods of Drying in Sokoto State

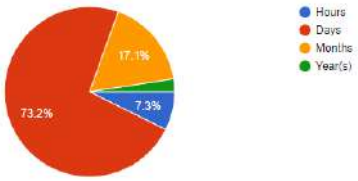

Figure 12: Drying Time for Farm Produce in Sokoto State.

(ii) Lack of appropriate drying equipment, pests and insects are some of the challenges faced post harvest in Sokoto State. This was validated in Figure 13, with 26.8% each.

(iii) Absence of existing drying structure is another challenge faced by farmers in the state. This can be confirmed by the distribution in Figure 14, with approximately 77%.

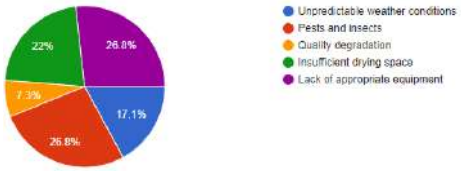

Figure 13: Pictogram Showing Lack of Appropriate Drying Equipment in Sokoto State.

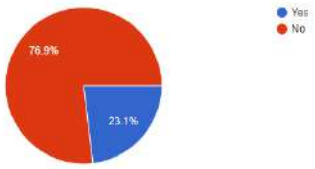

Figure 14: Pictogram Showing Absence of Drying Structures in Sokoto State.

5. CONCLUSION

The solar-based drying system has been successfully designed and effectively adapted through the need assessment and understanding the requirements of the agricultural context of Sokoto State. The system operation was made possible by developing an algorithm using C++ programming language, which was embedded in Arduino ATMEGA328 interface, for smart monitoring and control. This presented an opportunity to address the challenges faced by local farmers and other stakeholders during the post-harvest period in the State.

ACKNOWLEDGEMENT

This research was funded by The Tertiary Education Trust Fund (TETFUND) under the Institution-Based Research (IBR) Annual Intervention. The support of TETFUND in making this work a reality is hereby acknowledged and appreciated. We also appreciate the Federal College of Education, Gidan Madi, Sokoto State, for finding the research worthy of selection.

REFERENCES

Alibassi, H. A. & Madani, M. H. (2012). The Influence of Drying Methods on the Physicochemical Properties of Carrot Slices. International Journal of Food Science & Technology, 47(1), 172-178

Aliyu, O. M., & Iloeje, O. C. (2011). Seasonal Variations in Solar Radiation Components at Gusau, Nigeria. Renewable Energy, 36(2), 716-722.: https://doi.org/10.1016/j.renene.2010.08.020

Aregbesola, O.A., Ogundipe, O.O., & Abegunde, K.O. (2021), Post-harvest Losses in the Nigerian Food Supply Chain: Causes and Solutions. Food Reviews ,55,542-553:https://doi.org/10/1016/j.ser.2021.11.077

Duffie, J. A., & Beckman, W. A. (2013), Solar Engineering of Thermal Processes (Vol. 3). John Wiley & Sons.

Essam, M. R. & Rafea, A. A. (2007). Solar dryers: Fundamentals, Types, and Applications. Renewable Energy, 32 (8), 1221-1243.

Food and Agriculture Organization of the United Nations. (2015). The State of Food Insecurity in the World 2015. Strengthening the Enabling Environment for Food Security and Nutrition: https://www.fao.org/3/a-i4030e.pdf

Intergovernmental Panel on Climate Change (2022) Climate Change 2022: Impacts, Adaptation, and Vulnerability.

International, 37:5,2062–2080. https://www.tandfonline.com/journals/timp20.

Jain, I. J., & Bala, K. (2017), A Review on Solar Drying: Potential, Applications and Advancements. Renewable and Sustainable Energy Reviews, 76, 792-810. https://doi.org/10.1016/j.rser.2017.03.112

Jannot, M. A., Buckles, D. S., & Lawson, T. L. (1994) Solar Food Drying for Developing Countries. Renewable Energy, 5(1-4), 417-425.

Janjai, D. D., & McCann, L. M. (2017). Techno-economic feasibility analysis of solar drying technologies for food preservation in rural developing countries. Renewable and Sustainable Energy Reviews, 74, 123-134.: https://doi.org/10.1016/j.rser.2017.03.012

Kingsly, A. R., Manikantan, M. R., & Jain, S. K. (2007). Design and development of a natural convection solar dryer for drying of agricultural produce. Journal of Agricultural Engineering Research, 91(1), 69-76.

Koua, E., Finkenstadt, A., Muller, B., Sanders, S. & Lucas, D. B. (2009) Low-cost Solar Dryers for Developing Countries. Drying Technology, 27(6), 797-802. DOI: 10.1080/07373930802642321

Kumar, M., Kumar, A., & Kothari, S. (2016). A Review on Recent Advancements in Solar Dryer Technologies. Renewable and Sustainable Energy Reviews, 55, 378-399.

Matavel, C. E., Hoffmann, H., Rybak, C., Hafner, J. M., Salavessa, J., Eshetu, S. B., & Sieber, S. (2021). Experimental evaluation of a passive indirect solar dryer for agricultural products in Central Mozambique. *Journal of Food Processing and Preservation*, *45*(11), e15975. https://doi.org/10.1111/jfpp.15975

Oladejo, E. I., Abegunde, O. A., Ogundipe, O. O. & Akinlabi, A. A. (2016) Performance Evaluation of a Mixed-mode Solar Dryer for Drying Pepper Fruits. Journal of Stored Products Research, 66, 129-135. DOI: 10.1016/j.jspr.2016.03.006

Oluyi Isaac (2023): Exploring Food Processing Techniques in Nigeria for Sustainable Health. https://sciencenigeria.com/exploring-food-processing-techniques-in-nigeria-for-sustainable-health/

Ozturk, S., Colak, H. & Dincer, A. (2009) Performance Analysis of a Solar Dryer for Drying of Apricots. Energy Conversion and Management, 50(4), 1057-1063. DOI: 10.1016/j.enconman.2008.10.012 https://doi.org/10.1016/j.enconman.2008.10.012

Princewill, Nwadinobi Chibundo l, Nwaiwu Uchechukwu, Awani Victor Toju, & Ogbu Kosiso Michelangelo (2023), Development of an Improved Smart Solar Post-harvest Dryer. Int.J.Adv.Sci.Eng.Vol.9, No.3, 2998-3005, E-ISSN: 2349 5359; P-ISSN: 2454-9967. https://doi.org/10.29294/IJASE.9.3.2023.2998-3005

Sane, J.S., Suleiman, M. S. & Afolabi, U.I (2014), Design, Construction and Performance Evaluation of a Prototype Natural Convection Solar Dryer for Drying Pepper Fruits. Nigerian Journal of Solar Energy, 25(1), 127-134.

Shitu Abubakar, Samaila Umaru, Fatai O. Anafi, Aminu S. Abubakar & Dangana M. Kulla (2018), Design And Performance Evaluation Of A Mixed-Mode Solar Crop Dryer. FUOYE Journal of Engineering and Technology,V(3),Issue1,ISSN: 2579-0625, 2579-0617.https://doi.org/10.46792/fuoyejet.v3i1.133

Singh, B., Goyal, R. K., & Marwaha, S. K. (2007). A Review of Solar Drying Technology. Drying Technology, 25(12), 1595-1601.

Singh, K. K., & Manikantan, M. R. (2008). Potential applications of solar energy for agricultural drying: A review. Energy Conversion and Management, 49(5), 1011-1021.

Sokoto State Government. (2021), Sokoto State. Retrieved from http://www.sokotostate.gov.ng/

United Nations Population Fund. (2021). World Population Prospects 2021.

PAPER 24 - Development of an Intelligent Evaporative Cooling System for Post-harvest Storage of Tomato

O. R. Isah[1]*, S. E. Adebayo[2], B. K. Nuhu[3], B. U. Umar[4], D. Maliki[5], I. M. Abdullahi[6], E. M. Dogo[7], O. M. Olaniyi[8], J. Agajo[9]
[1,2,3,4,5,6,7,8,9]Department of Computer Engineering, Federal University of Technology, Minna
*Email: isah.rabiu@futminna.edu.ng

ABSTRACT
This research developed an intelligent evaporative cooling system for post-harvest tomato preservation that adapts to its suitable temperature, humidity, and CO_2 states to store, preserve quality, and increase the shelf life of the fruits. This was accomplished through the use of transfer learning for fruit classification, the Internet of Things (IoT) for remote monitoring and shelf life tracking, and the integration of the evaporative cooling system with a CO_2 sensor, a temperature sensor, a humidity sensor, an Arduino Uno, and a Raspberry Pi 4b. The system can classify tomato fruit status as ripe or overripe with a prediction accuracy of 87.5% and a receiver operating characteristic (ROC) value of 88.89%. The developed evaporative cooling system extended the shelf life of ripe tomatoes from 5 to 14-17 days at 20℃ and 90% relative humidity and overripe tomatoes from 3 to 9-11 days at 18℃ and 95% relative humidity. These results emphasize the crucial function of evaporative cooling in fruit and vegetable storage, as it extends the shelf life of tomatoes by 180–200%, hence minimizing post-harvest loss as it also increases the farmers' income, thereby contributing positively to the economy.

KEYWORDS: Intelligent, Evaporative, Cooling system, Tomato, post-harvest, Transfer Learning

1. INTRODUCTION

The word "tomato" is derived from the Nahuatl word tomato, which means "swelling fruit" (Online Etymology Dictionary). After potato (*Solanum tuberosum L.*), tomato (*Solanum lycopersicum L.*) is the second most important fruit or vegetable crop, with around 182.3 million tons of tomato fruits grown on 4.85 million ha each year [1]. Asia produces 61.1 percent of the world's tomatoes, while Europe, America, and Africa each contributed 13.5 percent, 13.4 percent, and 11.8 percent of the total tomato harvest [1]. Deterioration of food products after harvest is a severe issue in underdeveloped countries, such as Nigeria. It results in considerable reductions in socioeconomic well-being, including decreased household income and the likelihood of hunger [2]. Tomatoes are essential vegetable crop but are naturally perishable, resulting in post-harvest losses before the produce is consumed [3]. In Nigeria, approximately 1.8 million tonnes of fresh tomatoes are produced annually, but over half of these are lost due to insufficient storage, transportation, and processing facilities [4]. Due to its great importance as a source of livelihood for farmers and food for consumers, these losses are detrimental and must be reduced to the barest minimum.

Evaporative cooling is a heat and mass transfer method that uses water evaporation to cool the air, transferring a considerable quantity of heat from the air to the water and lowering the air temperature [5]. Evaporative cooling has many advantages, including significant energy and cost savings, the absence of CFCs, lower CO_2, enhanced indoor air quality, and increased life-cycle cost-effectiveness [6].

One in every nine persons lacks enough food to live a healthy life. However, one-third of all food produced globally is lost or squandered. Food loss occurs owing to factors beyond the farmers' control, such as weather, market volatility, storage facilities, and post-harvest technology [8]. Numerous approaches have been applied to reduce post-harvest loss, including cold storage systems, which have been shown to maintain fruit quality and characteristics better than chemical and biological methods. Additionally, the evaporative cooling approach has been shown to extend shelf life and preserve average fruit quality over time when combined with high relative humidity, low temperature, and enough cooling [3, 7]. Some post-harvest storage systems use fuzzy logic [9, 10], while other evaporative cooling systems require manual operation [11, 12]. However, none of these systems coupled transfer fruit classification using transfer learning, remote monitoring, and shelf life tracking using IOT into an evaporative cooling system [17, 18 and 19]. These characteristics improve the efficacy of the evaporative cooling system used for tomato post-harvest storage, necessitating the design and development of an intelligent evaporative cooling system.

1.1 REVIEW OF RELATED WORKS

The purpose of this project is to develop an intelligent evaporative cooling system. There have been several developments in the evaporative cooling system. Still, none have included tomato fruit image classification, adaptive evaporative cooling, remote monitoring, automated control of temperature and humidity, and fruit shelf-life tracking. To this effect, the reviews of related works are presented thus:

A cost-effective tomato maturity grading system for farmers was developed [13]. This system used an inexpensive material and image processing algorithms to identify the six essential stages of tomato ripening. The algorithms were designed using Simulink, a part of MATLAB 2011b, on a 2.5GHz GPU. This system had an overall 98% accuracy concerning maturity grade detection. The execution speed of the system was 7.6 times greater than other popular methodologies. The limitation of this system was that it did not have a storage facility for the tomato.

A system that measures the ripeness and grading of tomatoes using an image analysis on a Raspberry Pi was developed [14]. This system used the tomato's size, shape, and degree of ripeness to determine its quality. An edge detection algorithm was used to estimate the size and shape. In contrast, a colour-detecting algorithm was used to determine its degree of ripeness, and all these were implemented on a Rasberry Pi development board. This system, however, did not provide storage for classified tomatoes.

Researchers [15] worked on a computer vision system for defect discrimination and grading in tomatoes using Machine Learning and image processing. This research presented a Red, Green, and Blue (RGB) image-based tomato grading machine. A Radial Basis Function-Support Vector Machine (RBF-SVM) classifier was used to detect infected regions using LAB colour-space pixel values. This system had an overall accuracy of 98.9%. This system did not handle the storage of the tomato after successful sorting.

Machine learning techniques were used [16] for evaluating tomato ripeness. This article described an automatic multi-class classification method for measuring and assessing tomato ripeness by examining and classifying the various maturity/ripeness levels. For feature extraction and classification, the method presented in this article employed Principal Components Analysis (PCA), as well as Support Vector Machines (SVMs) and Linear Discriminant Analysis (LDA) algorithms. The suggested classification solution achieved a ripeness classification accuracy of 90.80% using a one-against-one (OAO) multi-class SVMs algorithm with linear kernel function, a ripeness classification accuracy of 84.80% using a one-against-all (OAA) multi-class SVM algorithm with linear kernel function, and ripeness classification accuracy of 84 percent using one-against-all (OAA) multi-class SVMs algorithm with a linear kernel function. This system, however, did not provide storage for classified tomatoes.

Other researchers [20] worked on Tomato volume and mass estimation using computer vision and machine learning algorithms: Cherry Tomato model. A prediction method of mass and volume of cherry tomatoes based on a computer vision system and machine learning algorithms was introduced in this study. The relation between tomato mass and volume was established as M=1.312, V=0.9551, and was used to estimate mass on a test dataset at an R2 of 0.9824 and RMSE of 15.84g. The RBF-SVM outperformed all explored models with an accuracy of 0.9706 (only 2D features) and 0.9694 (all features) in mass and volume estimation, respectively. This system did not classify good or bad tomatoes.

The study [12] developed an effective evaporative charcoal cooler for the post-harvest preservation of tomatoes and kale. The air temperature and relative humidity were measured to examine the cooler microclimate and outdoor temperatures. The mean temperature differential between the cooler and the outside was 9.2 °C during the study period, while the maximum relative humidity difference was 36.8%. Temperature and relative humidity variations were significantly decreased due to the effects of light rain and low solar radiation. Despite the light rain, the cooler still had a maximum relative humidity of 83.5 percent and a maximum cooling performance of 91.5 percent. The limitation of this system was that it did not sort the tomatoes before they were stored in the cooler.

The quality of tomatoes stored in the Zero Energy Cool Chamber (ZECC) was studied [11]. The ZECC is an environmentally friendly and low-cost post-harvest technology for storing fruits and vegetables. Vitamin C content 39.95 mg / 100g, pH 4.15, total acid 0.40, total soluble solids 5.40Brix, and weight loss 4.66 grams were the chemical analysis results of tomato deposited in ZECC. Tomatoes can be stored for 20 days in ZECC, 15 days at cool temperatures, and ten days at room temperature. Although this system increases the shelf life of the tomato, it does not classify the tomato-based on its ripeness.

Another research work [21] proposed some tomato post-harvest handling practices and treatment methods for tomato handlers in developing countries revealed that the tomatoes' post-harvest quality and shelf life would depend on the practices and treatments carried out after harvest, like precooling, grading, packaging, storing, and transportation. A conclusion was made that by using specific post-harvest techniques, there could be an extension in the shelf life of the tomatoes, and failure to adopt such practices would result in a high level of wastage of tomatoes.

The incidence of post-harvest diseases can affect the quality and restrict the shelf life of horticultural fresh produce [22]. Since some countries have limited the amount of pesticide residue left on imported farm produce, some fungal pathogens have been reported to have developed resistance to synthetic fungicides. Therefore, this review summarises the use of essential oils to control post-harvest diseases of horticultural commodities, their mode of action, their effects on the defense mechanism, and the quality of fresh fruit.

A technique using a Metal Oxide Semiconductor (MOS) electronic nose and Extreme Learning Machine (ELM) to predict the post-harvest quality of cherry tomato fruit treated with high-pressure argon was developed [23]. The purpose was to investigate the reliability and validity of using electronic nose (e-nose) technology to evaluate the quality and freshness of cherry tomatoes after high-pressure argon treatments. The results showed that the freshness of the tomatoes based on flavour over the time of storage was categorized into four groups (fresh, acceptable, stale, and very stale, respectively). Pressure argon at 0.8 MPa maintained the freshness and quality of cherry tomatoes during cold storage.

Recent advances in modeling and predicting quality parameters of fruits and vegetables during post-harvest storage was studied [24]. The study stated that ANN, genetic algorithm, fuzzy logic, and an adaptive nervously inference system (ANFIS) have been applied in every aspect of food science in recent years. These models are valuable tools for fruit and vegetable monitoring, grading and classification, sorting, predicting the food and modeling properties, modeling microbial growth, and forecasting chemical, physical, and sensory characteristics during post-harvest storage processing. Also, these models were used for different fruit and vegetable storage process modeling, detecting chilling injury, detecting defects, controlling various drying processes, and improving climate control.

2. THEORETICAL ANALYSIS

2.1 Control Unit Design Calculation.

Equations (1 and 2) compute the power rating, ampere-hour rating, and how long the control unit can continuously run before recharging.

$$P_T = I_{op} \times V_{op} \quad (1)$$

$$Ampere\ hour = \frac{power \times time}{voltage} \quad (2)$$

Where,

P_T represents the total power of the control unit

V_{op} represents the operating voltage of the control unit

I_{op} represents the operating current of the control unit

T_c represents the total lasting time of the control unit

$I_{op} = 3.0A$, $V_{op} = 5V$, $P_T = 3.0 \times 5$, $P_T = 15.0W$. Calculating the control unit ampere-hour rating

$Amphr = \frac{15.0 \times T_c}{5}$, $Amphr = 3.0T_c\ Ahr$. A 10000mAh 5V battery will power the ECS for T_c hours, $10000Ahr = 3.0T_cAhr$, $T_c = 3.33hrs$, $T_c = 3hr\ 20mins$

2.2 Evaporative Cooling System Calculations

Volume of the Storage System: The capacity of the storage system was determined using Equation (3);

$$V_s = L_S \times B_S \times H_S \quad (3)$$

$V_s = 0.4 \times 0.5 \times 0.8 = 0.16m^3$

Where; V_s = volume of the storage system, L_s = Length of the storage system, B_s = Breadth of the storage system, H_s = height of the storage system

The volume of Reservoir:

The volume of the reservoir was determined using Equation (4);

$$V_c = \pi r^2 h \quad (4)$$

$V_c = 3.14 \times 0.16^2 \times 0.3 = 0.024m^2 = 24litres$

Where; V_c = volume of reservoir, $\pi = 3.142$ r= radius of reservoir, H_c = height of the reservoir

2.3 Heat Transfer Analysis of the System

The heat gain by the aluminum material used for the cabinet construction was estimated using Fourier's law of heat conduction.

$$Q_h = \frac{-cA\Delta T}{l} \quad (5)$$

$$Q_h = \frac{-204 \times 1.418 \times 10}{0.001} = 2892720w$$

Where; Q_h = Quantity of heat gained by the material (W), A = Area of the material (m), c = Thermal conductivity of the material $(W/m\ K)$, ΔT = Temperature difference of thermal $(°C)$, l = Thickness of the material (m).

3. MATERIALS AND METHODS/METHODOLOGY/EXPERIMENTAL PROCEDURE

The system is made up of two modules, namely hardware and software. The hardware module is made up of various units that are used to build the evaporative cooling system. In contrast, the software module contains the deep learning model for sorting the tomato and the mobile app for feedback.

3.1 System Hardware

The evaporative cooling system, a Raspberry Pi 4, an Arduino Uno, sensors, a servo motor, and a pump comprise the system hardware components. Figure 1 shows the 3-D model of the developed system.

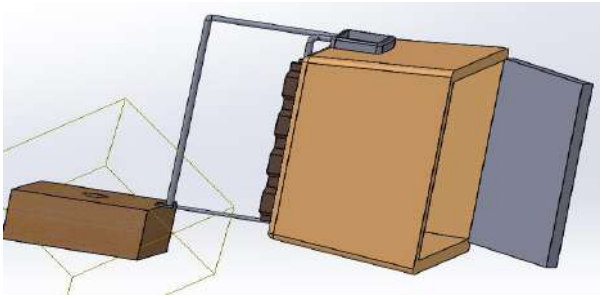

Figure 1: 3-D model of the system

3.2 System Block Diagram

The sensing unit monitors the state of critical components that contribute to the tomato's health; the Arduino, a control unit member, then retrieves these values. This unit is in charge of the overall system's operation. The Arduino shows the parameters on the LCD and sends them to the Raspberry Pi, which uploads them to the database and finally sends them to the mobile application. The automation unit comprises two DC fans and a DC pump connected to a robotic switch that operates via signals from the Arduino. Additionally, the Raspberry Pi is responsible for photographing and submitting photos to the web server for fruit classification, as shown in Figure 2.

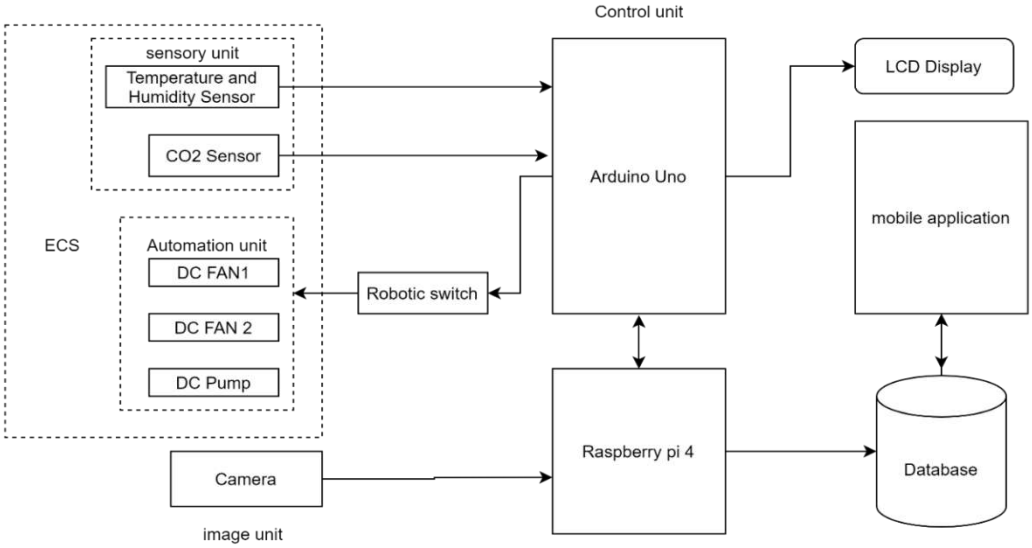

Figure 2: System Block Diagram.

When the system is turned on for the first time, it initializes the parameter monitoring unit consisting of temperature, humidity, and CO_2 sensors. It then captures the camera's image for classification. After classifying the image as ripe or unripe, the evaporative cooling system's parameters are adjusted according to the classification result. The parameters are then monitored continuously to verify that the system is acceptable for the stored tomato by maintaining the conditions and, if not, by lowering or increasing the temperature and relative humidity. The shelf life is calculated and communicated to the mobile application for user feedback.

3.3 The System Flowchart

The system shows the operational flow of the Evaporative cooling system sequence in steps. The flow sequences are explained and shown in Figure 3.

Figure 3 shows the flowchart of the system. Once switched on, the parameter monitoring unit, which consists of temperature, humidity, and CO_2 sensors, is initialized. It then captures the camera's image for classification. After classifying the image as ripe or unripe, the evaporative cooling system's parameters are adjusted according to the classification result. The parameters are then monitored continuously to verify that the system is acceptable for the stored tomato by maintaining the conditions and, if not, by lowering or increasing the temperature and relative humidity. The shelf life is calculated and communicated to the mobile application for user feedback.

3.4 Software Design Consideration

The design of the software is concerned with the development of an online server and a mobile application. The classification model was programmed using Python on the Tensor Flow machine learning platform with Keras Library. These are flexible, efficient, easily understandable machine learning tools. The Firebase cloud server holds feedback information from the Raspberry Pi 4, where a get request from the mobile application could fetch it. Firebase provides fast and flexible real-time data.

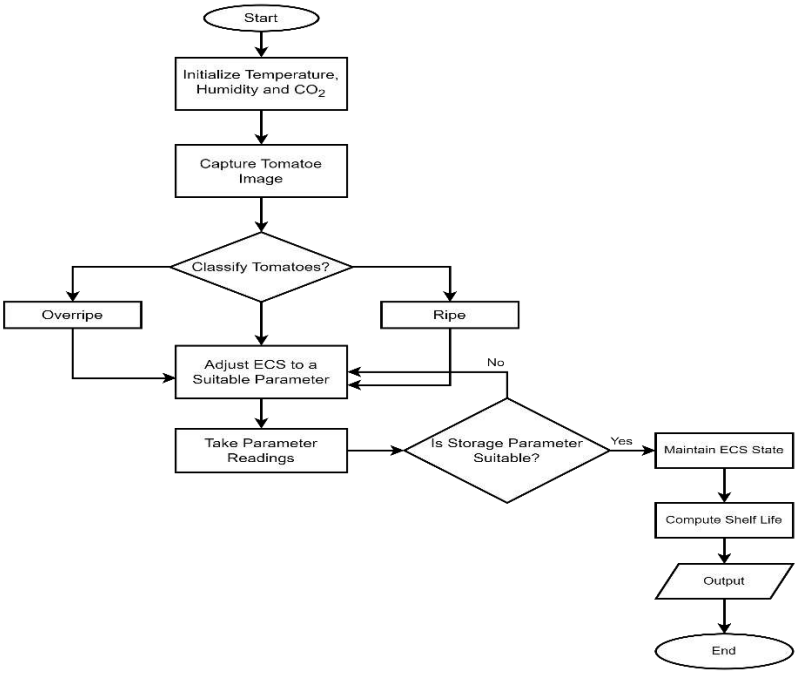

Figure 3: Flowchart of the system

The communication protocol between the cloud server and the Raspberry Pi is an HTTP POST request. In contrast, communication between mobile applications is done through HTTP GET requests to fetch real-time data. Figure 4 shows the user interface of the mobile application.

Figure 4: Mobile App for monitoring parameters

4. RESULTS AND DISCUSSION

This section discusses the results obtained after designing, developing, and testing the intelligent evaporative cooling system. It will include hardware development, software development, and system performance evaluation.

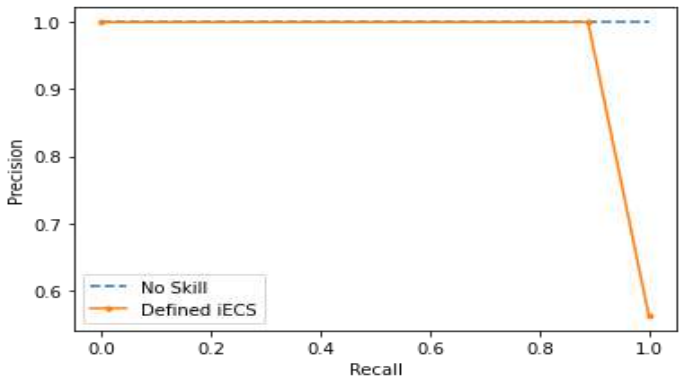

Figure 6: Precision-Recall curve

Furthermore, the software model (deep learning) had a precision value of 1, as shown in Figure 6, with a recall value of 0.888889. The F1 Score calculates the harmonic mean of the precision and the recall rates. It also signifies a summary of the model skill for a specific probability threshold. This model has an F1-Score of 0.941176. These results depict the efficacy of the deep learning model in its prediction.

4.1 Average Shelf Life

One of the performance metrics of the evaporative cooling system is the increased shelf life of the stored fruits. Table 2 shows the average shelf life at room temperature and after storage of tomatoes using an evaporative cooling system. At 25 degrees Celsius, which is the room temperature of the system, ripe tomatoes could stay for a shelf-life of 5 days, after which they start to deteriorate, while overripe tomatoes have about three days of shelf-life, however, after being subjected to the evaporative cooling system at 20 degrees Celsius, the ripe tomatoes have an increased shelf-life within the range of 14-17 days and the overripe within 9-11 days.

Shelf-life performance was calculated using equation 6:

$$S_I = \frac{y_2 - y_1}{y_1} \times 100\% \quad (6)$$

where,

y_2 denote shelf-life after storage in iIECS,

y_1 denotes shelf life at room temperature.

Table 2: The Shelf Life Performance Result of the Evaporative Cooling System

	Ripe (days)	Overripe (days)
Temperature (Ambient condition)	5	3
Temperature (20℃) and 90% RH in iECS	14-17	__
Temperature (18℃) and 95% RH iECS	__	9-11
Percentage increase in shelf-life	180%	200%

4.2 Percentage Weight Loss of Tomato

Fresh fruits and vegetables contain high levels of water (80-90 percent), making them highly perishable. Accordingly, to find the system's efficiency, we must measure the percentage weight loss of the tomato. Table 3 shows the weight loss recorded in the tomato stored in the evaporative cooling system and at ambient temperature.

Table 3: Weight Loss Relationship between Tomatoes in ECS and Ambient Temperature Measured In Grams

	Weight in iECS (g)	Weight in Ambient Temperature (g)
Day 1	1.7	9.7
Day 2	3.2	14.2

Day 3	4.7	18.8
Day 4	5.2	14.1
Day 5	5.8	11.9
Day 6	5.9	10
Day 7	6.2	8.3
Average Weight Loss	4.67	12.43

Over seven days (1 week), tomato fruits were stored in two conditions: inside the intelligent evaporative cooling system and in a container with ambient conditions. The loss of weight measured daily is as follows;
The tomatoes stored in IECS exhibit an average weight loss of 4.67, while the traditional cooling system depicts an average weight loss of 12.43. These results were due to the ability of the IECS to optimally adjust its temperature and humidity suitable for the stored fruits.
It is a fact that there were weight losses in both conditions; however, as illustrated, there is a slow and steady increase in the weight loss in tomatoes that were stored in the Intelligent Evaporative Cooling System, while for those stored in ambient temperature, there was a high and Rapid loss in the weight in the first three days, followed by a gradual decrease in the weight loss. These results denote that the Intelligent Evaporative Cooling system helps reduce the loss in weight while preserving the fruit quality over time compared to when stored at ambient temperature.

5. CONCLUSION

This research developed an intelligent evaporative cooling system that reduces the post-harvest wastage of tomatoes while increasing the food security potential. The designed system classifies stored fruits and adapts to temperature and humidity states suitable for storing, preserving quality, and improving the shelf life of the fruits, thus providing enough market time for the farmer to get his fruits to the customers. Intelligent storage, automatic control, and remote monitoring were achieved after the implementation of this research.

ACKNOWLEDGMENT

The authors appreciate TETFund for funding this research. They are also grateful to the management of the Federal University of Technology, Minna, for providing the enabling environment for the execution of the study.

REFERENCES

[1] "FAOSTAT." http://www.fao.org/faostat/en/#home (accessed Aug. 17, 2021).

[2] Balana, B.B., Aghadi, C.N., Ogunniyi, A.I. (2021). Improving livelihoods through postharvest loss management: evidence from Nigeria. In: *Food Secur.*, 1-17, doi: 10.1007/s12571-021-01196-2.

[3] Nkolisa, N., Magwaza, L.S., Workneh, T.S, and Chimpango, A. (2018). Evaluating evaporative cooling system as an energy- free and cost- effective method for postharvest storage of tomatoes (Solanum lycopersicum L.) for smallholder farmers. In: *Sci. Hortic. (Amsterdam).*, *241*(1), 131-143, doi: 10.1016/j.scienta.2018.06.079.

[4] Ugonna, C., Jolaoso, M., and Onwualu, A. (2015). Tomato value chain in nigeria: issues, challenges and strategies. In: *J. Sci. Res. Reports*, *7*(7), 501-515, doi: 10.9734/jsrr/2015/16921.

[5] Amer, O., Boukhanouf, R., and Ibrahim, H.G. (2015). A review of evaporative cooling technologies. In: *Int. J. Environ. Sci. Dev.*, *6*(2), 111-117, doi: 10.7763/ijesd.2015.v6.571.

[6] Yang, Y., Cui, G., and Lan, C.Q. (2019). Developments in evaporative cooling and enhanced evaporative cooling - A review. In: *Renew. Sustain. Energy Rev.*, 113 doi: 10.1016/j.rser.2019.06.037.

[7] Adekanye, T., Babaremu, K., and Okunola, A. (2021). Evaluation of an active evaporative cooling device for storage of fruits and vegetables. In: *Agric. Eng. Int. CIGR J.*, *21*(1), 203-208,. Available: http://cigrjournal.org/index.php/Ejounral/article/view/5126.

[8] Srivastava, R., and Ayyagari, A. (2021). Moving towards an environmentally sustainable food sector through mitigation of food losses and wastage-a possibilitarian's approach. In: *Invertis J. Renew. Energy*, *11*(1), 42-50, doi: 10.5958/2454-7611.2021.00007.2.

[9] Oluwo, A., Khan, M.R., and SalamI, M.J.E. (2015). Intelligent temperature control of a tropical post-harvest storage system. In: *2015 10th Asian Control Conf. Emerg. Control Tech. a Sustain. World, ASCC*

2015, doi: 10.1109/ASCC.2015.7244749.

[10] Babawuro, A. Y., Umar, S. A., Fatai, S., Salami, M. J. E., & Sidek, S. N. (2015). Fuzzy logic based intelligent temperature controller for cassava post-harvest storage system. *International Conference on Artificial Intelligence, Electrical & Electronics Engineering (AIEE '15).*

[11] Dirpan, A. (2019). The quality of tomato (lycopersicum esculentum mill.) stored on zecc (zero energy cool chamber). In *IOP Conference Series: Earth and Environmental Science*, 270(1), 012012. IOP Publishing.

[12] Ronoh, E. K., Kanali, C. L., & Ndirangu, S. N. (2020). Effectiveness of an evaporative charcoal cooler for the postharvest preservation of tomatoes and kales. Res. *Agric. Eng*, *66*(2), 66-71.

[13] Rupanagudi, S. R., Ranjani, B. S., Nagaraj, P., & Bhat, V. G. (2014). A cost effective tomato maturity grading system using image processing for farmers. In *2014 International Conference on Contemporary Computing and Informatics (IC3I)* 7-12. IEEE.

[14] Mhaski, R. R., Chopade, P. B., & Dale, M. P. (2015). Determination of ripeness and grading of tomato using image analysis on Raspberry Pi. In *2015 communication, control and intelligent systems (CCIS)*, 214-220. IEEE.

[15] Ireri, D., Belal, E., Okinda, C., Makange, N., & Ji, C. (2019). A computer vision system for defect discrimination and grading in tomatoes using machine learning and image processing. *Artificial Intelligence in Agriculture*, *2*, 28-37.

[16] El-Bendary, N., El Hariri, E., Hassanien, A. E., & Badr, A. (2015). Using machine learning techniques for evaluating tomato ripeness. *Expert Systems with Applications*, *42*(4), 1892-1905.

[17] Pacheco, W. D. N., & López, F. R. J. (2019). Tomato classification according to organoleptic maturity (coloration) using machine learning algorithms K-NN, MLP, and K-Means Clustering. In *2019 XXII symposium on image, signal processing and artificial vision (STSIVA)*, 1-5. IEEE.

[18] Taofik, A., Ismail, N., Gerhana, Y. A., Komarujaman, K., & Ramdhani, M. A. (2018). Design of smart system to detect ripeness of tomato and chili with new approach in data acquisition. In *IOP Conference Series: Materials Science and Engineering*, 288, 012-018. IOP Publishing.

[19] Kumar, S. D., Esakkirajan, S., Bama, S., & Keerthiveena, B. (2020). A microcontroller based machine vision approach for tomato grading and sorting using SVM classifier. *Microprocessors and Microsystems*, *76*, 103090.

[20] Nyalala, I., Okinda, C., Nyalala, L., Makange, N., Chao, Q., Chao, L., ... & Chen, K. (2019). Tomato volume and mass estimation using computer vision and machine learning algorithms: Cherry tomato model. *Journal of Food Engineering*, *263*, 288-298.

[21] Arah, I. K., Ahorbo, G. K., Anku, E. K., Kumah, E. K., & Amaglo, H. (2016). Postharvest handling practices and treatment methods for tomato handlers in developing countries: A mini review. *Advances in Agriculture*, *2016*.

[22] Sivakumar, D., & Bautista-Baños, S. (2014). A review on the use of essential oils for postharvest decay control and maintenance of fruit quality during storage. *Crop protection*, *64*, 27-37.

[23] Feng, L., Zhang, M., Bhandari, B., & Guo, Z. (2018). A novel method using MOS electronic nose and ELM for predicting postharvest quality of cherry tomato fruit treated with high pressure argon. *Computers and electronics in agriculture*, *154*, 411-419.

[24] Salehi, F. (2020). Recent advances in the modeling and predicting quality parameters of fruits and vegetables during postharvest storage: A review. *International Journal of Fruit Science*, *20*(3), 506-520.

PAPER 25 - A REVIEW ON THE METHODS OF CRUDE OIL SPILL POLLUTION CONTROL

I. A. Joseph[1,2*], E. O. Ajala [1], A. A. El-Imam [3], M. A. Ajala [1], C. T. Are[4], E. O. Babatunde[1]
[1]Department of Chemical Engineering, University of Ilorin, Ilorin Nigeria
[2]Department of Chemical Engineering, Confluence University of Science and Technology, Osara, Nigeria
[3]Department of Microbiology, University of Ilorin, Ilorin Nigeria
[4]Department of Pure and Industrial Chemistry, Prince Abubakar Audu University, Anyigba, Nigeria
* Email: isaacchemeng@yahoo.com

ABSTRACT
Crude oil is a naturally occurring accumulation of petroleum products due to geological formations over a long time under the Earth's surface and is primarily composed of organic materials and hydrocarbons. Globally, crude oil has been the main driving force in the energy sector. On the other hand, this natural resource has plagued both the terrestrial and the aquatic habitats due to its indiscriminate disposal which is commonly referred to as oil spill. Impacts of crude oil spills range from interruption of the food chain due to contamination of agricultural lands and water bodies to human population which suffers several debilitating diseases. Methods of combating this crude oil spill involve physical, chemical, and biological techniques. Among these methods of remediation, the biological method has been proven to be the best approach especially the use of microorganisms such as fungi and bacteria. This is because it is more eco-friendly and also more efficient.

KEYWORDS: Crude oil spill, Contamination, Eco-friendly, Microorganisms, Remediation

1. INTRODUCTION

The global community has continued to raise increasing concern over the devastating effect of increasing cases of oil spills (Chorom *et al.*, 2010; Nwadinigwe and Onyeidu, 2012; Pongcharoenand *et al.,* 2012; Ugwoha and Oweh, 2020). An oil spill is an illegal discharge of hydrocarbons into the environment either by intended or unintended human actions (Abii and Nwosu 2009; Saleh *et al.,* 2017; Al-Dhabaan *et al.,* 2020; Ugwoha and Oweh, 2020). The causes of oil spills range from continuous stealing of crude oil by vandals via damaging and sabotage of pipelines, human failure resulting from corrosion of oil installations and pipelines, poor maintenance of oil facilities, indiscriminate discharge of oil from offshore platforms, runoff from processing plants, oil wells and drilling rigs (Abii and Nwosu 2009; Pongcharoenand *et al.,* 2012; Nwilo and Badejo, 2015; Saleh *et al.,* 2017; Li *et al.,* 2019).
The Niger Delta area of Nigeria has been adversely affected by the oil spill (Abii and Nwosu 2009). These negative effects of crude oil spills include loss of revenue, disruptions of the food chain, loss of soil fertility, loss of aquatic life, severe diseases to humans such as cancer and irregular heartbeat, the inability of plants to undergo photosynthesis and damage to vital organs such as the intestines, lungs, liver, and kidney (Abii and Nwosu 2009; Kriti and Shubash, 2014, Saleh *et al.,* 2017; Wang *et al.,* 2017). To overcome these challenges of oil spillage, there is need to investigate on efficient, effective, environmentally friendly and viable means of remediation. This review paper is aimed at providing useful information on the remediation of crude oil spills.

1.1 CRUDE OIL SPILL IN NIGERIA

Nigeria's crude oil spills are majorly concentrated within the Niger Delta which is an oil-producing area, a large proportion of the oil spill within this region are left uncleaned (Kadafa, 2012; Watts and Zalik, 2020). According to Kadafa (2012), a crude oil spill of not less than 1.5 million tons has been recorded within the last five decades of petroleum industry operating in the Niger Delta region of Nigeria. Nwilo and Badejo (2015) reported the occurrence of the crude oil spill of more than 200,000 barrels between 1991 and 1996 to swamp, land, and offshore environments. However, less than 23 % of the crude oil was successfully recovered. Similarly, more than 264,000 barrels of crude oil spill occurred between the year 1997 to 2001 with only a small fraction of recovery. Ogbonna (2018) reported that 127,467.96 barrels of oil spilled between 2006 and 2012, out of which Ogoni crude oil spill accounted for about 100,000 barrels of oil as of 2010 (Vanguard Newspaper, 2018). Wattas and Zalik (2020) reported that 692 barrels of crude oil spill occurred between 2006 to March 2020. Premium Times of Nigeria (2021) reported the loss of 235,206 barrels of crude oil spill between 2015 and 2021.

3. CRUDE OIL SPILL REMEDIATION

Crude oil is a low water-soluble, highly hydrophobic and low polar organic substance. It forms a protective layer on water and it also binds strongly to soil thereby limiting oxygen access to both microorganisms and other aquatic lives to render them inactive or eliminate them, this leads to a reduction in the rate of biodegradation (Tewari and Sirvaiya, 2015; Wang *et al.,* 2019). Due to the negative health impacts on humans and the environmental damages resulting from the crude oil spill, several remediation types of research approaches had been conducted (Wang *et al.,* 2019). Crude oil spill remediation involves processes and activities leading to the restoration of crude oil spill polluted environment to its original state. Methods such as physical, chemical, and biological means of remediation have been investigated (Yang *et al.,* 2016; Wang *et al.,* 2019). However, no single technique is capable of completely eliminating petroleum contaminants due to its compositional complexity (Wang *et al.,* 2017). Crude oil has been considered to the most complex organic compounds with more than seventeen thousand different chemical compounds (Koshalaf and Ball, 2017).

3.1 CHEMICAL METHOD OF CRUDE OIL SPILL REMEDIATION

The use of chemical techniques in oil spillage remediation involves the application of chemical substances that can easily interact with the molecules of crude oil to break it down to a less harmful substance to both humans and the biophysical environment. However, the chemical method has low remediation efficiency and is time-consuming (Wang *et al.,* 2017; Al-Dhabaan *et al.,* 2020). The chemical technique is subdivided into the oxidation process, the extraction process, photochemical oxidation process.

3.1.1 EXTRACTION PROCESS

Extraction process is a method of chemical treatment that can either be in the presence or absence of heat. Crude oil remediation via heat treatment employs the application of heat energy in recovering crude oil from contaminated soil (Wang *et al.,* 2019; Ossai *et al.,* 2020). When heat is applied to crude oil contaminated soil, the binding force between the molecules of the crude oil and that of the soil becomes weaken. The molecules of the crude oil will gain kinetic energy to move freely and the viscosity becomes lower. To ensure high separation between the molecule of the crude oil and the soil, solvents that are cable of dissolving the crude oil are introduced during the heat treatment process which helps in extracting the oil effectively. When crude oil remediation is carried out via solvent extraction in the absence of heat it is called soil-washing (Wang *et al.,* 2019). Examples of soil-washing reagents are surfactants, short-chain organic acid, and chelating agents. Surfactants are amphiphilic substances made up of both hydrophobic (lipophilic i.e lipid dissolving) and hydrophilic groups. The role of surfactants in soil washing is to solubilize the crude oil and also make the hydrophobic conterminal fraction mobile. The mechanism of operation of the surfactant in soil-washing is that the hydrophobic tail interacts with the organic pollutants while the hydrophilic head interacts with the lipid phase (Bolan *et al.,* 2023; Wang *et al.,* 2019). The concentration of the surfactant plays a very important role in the remediation process. A higher concentration of the surfactant helps to display the interfacial solvent and subsequently results in a reduction of the interfacial tension with low polarity at the solid-liquid interface. Lower concentration of the surfactant results in no activity by causing molecular build-up at the solid-liquid interface (Kékicheff, and Contal, 2019; Mambwe *et al.,* 2021). However, this can be overcome by increasing the surfactant concentration above the critical micelles concentration to increase the solubility of the organic pollutant which will now help in the significant transport of the pollutants from the solid environment to an aqueous environment (Wang *et al.,* 2019; Mambwe *et al.,* 2021). The major setback to this method is that it is time-consuming with low extraction efficiency. However, Wang *et al.,* (2019) achieved 97 % extraction efficiency at a higher concentration of a mixture of organic solvents (toluene, methanol, and acetone) and surfactant for the remediation of crude oil-contaminated soil.

3.1.2 CRUDE OIL SPILL REMEDIATION BY OXIDATION METHOD

This is a chemical process in which a harmful organic component in crude oil interacts with a reactive oxidizing agent and is converted into a less harmful one. Examples of such oxidizing agents are persulphate ($S_2O_8^{2-}$), hydrogen peroxide, (H_2O_2), permanganate (MnO_4^-), ozone (O_3), chlorine dioxide (Mambwe *et al.,* 2021; Oil and Gas Portal 2021). Crude oil remediation by oxidation is carried out in situ treatment through injection of gaseous, colloidal reactive chemicals and liquid on subsurface aquifers/soils. However, the major setback for in situ treatment is poor mass transfer of chemicals, poor distribution and poor delivery to the affected subsurface environment (Oil and Gas Portal 2021). Another important simple and powerful high oxidative process for site remediation is the Fenton's oxidation in which an iron ion combine with H_2O_2 to form an hydroxyl radical that is capable of destroying bio-refractory organic compounds in soil, aqueous waste, and groundwater (Ershadi *et al.,* 2011; Pongcharoenand *et al.,* 2012). Ershadi *et al.* (2011) reported the application of the Fenton process for crude oil remediation, this involved the use of both hydrogen peroxide and nano zero-valent Iron at a molar ratio of 33.7:1 and reaction time of 4 hours for the remediation of clay polluted hydrocarbons contaminant, 91 % total petroleum hydrocarbon removal was achieved. Pongcharoenand *et al.* (2012), reported 96 % total petroleum hydrocarbon recovery using of Fenton oxidation process at a molar ratio of H_2O_2:Fe^{3+} of 200:1, the pH of 4.0, and the reaction time of 7 hours.

3.2 PHYSICAL METHOD OF CRUDE OIL SPILL REMEDIATION

The physical methods of treatment of crude oil contaminants are the various techniques used for the recovery or remediating crude contaminant in which the chemical composition of crude oil remain unchanged most of the time after recovery or remediation. There are various physical methods of remediating crude oil contamination such as sonication, soil flushing, low-temperature thermal treatment, capping, cementations waste forms, incineration, soil vapor extraction, air separation. However, the physical method has low remediation efficiency and is time-consuming (Wang *et al.,* 2017; Al-Dhabaan *et al.,* 2020).

3.2.1 INCINERATION

Incineration involves processes where crude oil contaminated soil is collected and subjected to a high temperature by pyrolysis at about 800 ^oC to vaporize the crude oil fractions (Mishra *et al.,* 2021; Mambwe *et al.,* 2021). This method is a very effective means of remediating crude oil but could result in serious air pollution owning to vapourized crude oil fractions. Some of the challenges associated with this method include the cost and time to transport the contaminated soil to the incinerator, presence of heavy metals in the crude oil and soil that form residues requiring further treatment and onsite remediation may be difficult over large polluted areas (Mambwe *et al.,* 2021; Oil and Gas Portal, 2021).

3.2.2 EXCAVATION

This method of crude oil spill remediation involves the removal of contaminated soil either for further treatment or dumped to another location with no human activities. Excavation is an efficient and fast way of treating both inorganic and organic contaminants (Ahmad *et al.,* 2020, Mambwe *et al.,* 2021). However, the cost of excavation and transportation may not be economical. Another major disadvantage of this method is that dumping of contaminated soil to areas with less human activity at the moment may constitute a major environmental problem when human activities and settlement develop in such areas in the nearest future (Al-Dhabaan *et al.,* 2020; Mambwe *et al.,* 2021).

3.3 BIOLOGICAL METHOD FOR CRUDE OIL SPILL REMEDIATION

This method of remediation employs the activity of a living organism to feed or breakdown the organic component of the crude oil while the inorganic component is converted to a less toxic form, living behind by-products such as water, carbon dioxide, cell protein and heat (Koshlaf and Ball, 2019; Olowomofe *et al.,* 2019; Al-Dhabaan, 2020; Tewari and Sirvaiya, 2015; Ogbonna, 2018). Different microorganisms such as bacteria and fungi utilize the pollutants as an energy source (Ogbonna, 2018) during the metabolic process of crude oil degradation (Tewari and Sirvaiya, 2015; Al-Dhabaan, 2020). The different categorizes of microorganisms that are capable of degrading petroleum are categorized into bacteria, fungi, yeast, and algae (Oudot *et al.,* 1993; Chaillan *et al.,* 2004; El-Sheekh *et al.,* 2009; Sheekh *et al.,* 2013; Singh and Chandra, 2014).

Algae are groups of nucleus-bearing organisms with no identifiable true leaves, stems and roots but are capable of undergoing photosynthesis to produce their own food (Adesalu and Olugbemi, 2015). Some species of algae have the ability of surviving in a crude oil polluted environments by degrading the organic contaminants. Walker *et al.* (1975) in a study reported that Prototheca zopfii, an achlorophyllous alga, degraded 10 % motor oil and 40 % crude oil. In another study conducted by Sheekh *et al.* (2013), two green microalgae *Scenedesmus obliquus and Chlorella vulgaris* were reported to be more suitable for degrading of both n-alkane and petroleum aromatic hydrocarbon component in a crude oil contamination.

The use of fungi in the biodegradation of hydrocarbon is called mycoremediation. Previous research findings have established certain fungi species to be effective and efficient in the degradation of crude oil. Notable ones among them are *Trichophyton ajelloi, Alternata fungal strains, Aspergillus flavus, Curvularia lunata, Ulocladium atrum, Fusarium solani, penicillium notatum and Mucor racemosum* (Al-Dhabaan, 2020). In a mycoremediation study conducted on crude oil from Dhahran in Saudi Arabia, Al-Dhabaan, (2020) reported that *Aspergillus polyporicola* has only 47 % crude oil degradation ability followed *by Aspergillus spelaeus* with 51 % crude oil degradation ability and *Aspergillus niger* recorded 58 % crude degradation ability. A high proportion of crude oil contaminants are degraded in situ by a consortium of microorganisms which involves the combined use of different species of microbial as a replacement for the catabolic capacity of individual species. No less than 200 bacteria species have been reported for biodegradation of crude oil, among them are *Proteus, Flavobacterium, Rhodotorula, Arthrobacter, Thiobacillus, Neurospora, Sporobolomyces, Articulosporium, Micrococcus, Halomonas, Achromobacter, Brevibacterium, Acinetobacter, Pseudomonas, Penicillium, Aspergillus, Lactobacter, Corynebacterium, Klebsiella, Nocardia, Bacillus, Aeromonas, Candida, Mucor, Trichoderma, Vibrio Staphylococcus, Rhizopus.*

Based on biological activity, petroleum degrading bacteria can be classified as fermentation bacteria, Iron III reducing bacteria, sulphate reducing bacteria, and methanogenic Achaea (Wolicka *et al.,* 2010; Victor *et al.,* 2020).

3.3.1 NATURAL ATTENUATION

Natural attenuation is a bioremediation method in which a natural degradation of soil pollutants occurs via the activities of soil microorganisms in the absence of human involvement (Ogbonna, 2018). Bioremediation involves the biochemical conversion harmful substance into a non-harmful one. The two main categories of bioremediation are bioaugmentation and bio-stimulation. The addition of an external microbial population (endogenous or exogenous) to a contaminated site is known as bioaugmentation (Nwadinigwe and Onyeidu, 2012; Ogbonna, 2018). The most prevalent bioaugmentation species are bacteria. The main disadvantages of bioaugmentation are that it requires extensive long-term monitoring and it is not always effective (Kriti and Shubash, 2014; Koshlaf and Ball, 2019). The supply of appropriate microbial nutrients to a polluted environment to stimulate the metabolic activity of indigenous microbial flora is known as bio-stimulation (Nwadinigwe and Onyeidu, 2012; Kriti and Shubash, 2014; Ugwoha and Oweh, 2020). There is ongoing research into the bio-stimulation of crude oil spills (Adenipekun and Fasidi, 2005; Koshlaf and Ball, 2019). High concentrations of magnesium and calcium sulphate solutions (> 1,000 mg/l) can be used to stimulate the biodegradation of crude oil spills under field conditions at different sites (Cuthbertson, 2010).

Ugwoha and Oweh (2020), investigated the use of pig droppings and bone char for the bio-stimulation of simulated crude oil-polluted soil. Loamy soil of 500 g weight was contaminated with 3 % (w/w) crude oil then treated with different proportions of pig droppings and bone char for six weeks. Optimum bio-stimulation efficiency of 95.74 % was achieved at 50 % pig droppings and 50 % bone char.

In another study conducted by Ofoegbu *et al.* (2015), 6 % of crude oil contamination by mass of soil was bio-stimulated with cow dung (organic fertilizer), inorganic fertilizer (NPK), and palm kernel ash (organic fertilizer) for 40 days. Optimum biodegradation efficiency of 58.83 and 58.60 % were reported for inorganic fertilizer only and a combination of cow dung and inorganic fertilizer. Similarly, optimum biodegradation efficiency of 50.90 and 45.31% were also reported for cow dung and a combination of palm kernel husk ash and cow dung, while the least optimum biodegradation efficiency of 41.50% was reported for the use of palm kernel hush ash only.

The limitation of the studies above is that where there is a large crude oil spill, it may be difficult to get enough inorganic fertilizer, animal dung, and poultry droppings for biodegradation because they are also used by farmers as manures. Another limitation identified by Ofoegbu *et al.* (2015) is that the degree of degradation of total hydrocarbon content decreases with an increase in the volume of the crude oil spill, this also confirms that bioremediation by animal dungs and inorganic fertilizer may not give the desired result under field conditions, hence, alternative bio-stimulant that is readily available, more efficient and can be used for large crude oil spill should be in the lookout for.

The population of microorganisms and the degree of their bioremediation ability of crude oil contaminated soil depend mainly on the balance in oxygen content, acidity, and temperature of the soil (Tewari and Sirvaiya, 2015).
Crude oil bioremediation offers several benefits over other remediation methods. These include the cheap operational cost of clean-up, no harmful environmental contaminants are left behind after the process, a wide range of land can be covered over a short period, and it is an effective method (Al-Hawash *et al.*, 2018; Ogbonna, 2018; Li *et al.*, 2019). Beyond crude oil spill remediation, it can also be used in treatment of contaminants such as halogenated organic solvents and compounds, metals (lead, mercury, chromium), and non-chlorinated pesticides and herbicides (Ogbonna, 2018).

3.3.2 MECHANISM OF CRUDE OIL DEGRADATION

Microbes play about 80 % to 90 % active roles in soil processes which include organic matter transformation, nutrient cycling, and soil structure maintenance, with microbial degrader accounting for more than 90 % of the energy flow in the soil (Condron *et al.*, 2010; Victor *et al.*, 2020) . A large diversity of microorganisms, including bacteria, algae, viruses, and protozoa, live in soil, which is a major component of the environment. Bacteria in the soil are the soil's major digestive system, with their activity accounting for about 90 % of all biological and chemical processes (Victor *et al.*, 2020). Microorganisms exploit chemical contaminants in the soil as an energy source (Ogbonna, 2018; Victor *et al.*, 2020) and metabolize the target contaminant into usable energy for the microbes through oxidation-reduction reactions during bioremediation. By-products (metabolites) are often less harmful than the primary pollutants when released into the environment. Microorganisms can, for example, destroy petroleum hydrocarbons by aerobic respiration in the presence of oxygen. The hydrocarbon is oxidized via electron losses, whilst oxygen is reduced via electrons gains leading to the releases of carbon dioxide and water. When oxygen is scarce or unavailable, such as in saturated or anaerobic soils or lake silt, anaerobic (oxygen-free) respiration takes over. To aid biodegradation, inorganic chemicals such as nitrate, sulphate, ferric iron, manganese, or carbon dioxide are commonly used as terminal electron acceptors (Widdel and Musat, 2010; Ogbonna, 2018; Victor *et al.*, 2020).
Several physicochemical parameters in the environment such as nutrition and oxygen availability, light, temperature, pressure, salinity, and pH influence bacterial breakdown of petroleum hydrocarbons (Maier, 2015; Victor *et al.*, 2020).

5. CONCLUSION

Crude oil spill has continued to have a deleterious effect on both the physical and the biophysical environment. The negative effect such as interruption of the food chain due to loss of farmland and aquatic lives as well as the negative health implication on humans have prompted researchers into finding a viable solution to this problem. Remediation of crude oil polluted land and water bodies had been carried out through physical, chemical, and biological means. Among the three methods, biological means of remediation could be more effective, environmentally friendly, and advantageous if an appropriate bioremediation process is employed. Microorganisms such as bacteria (*Proteus, Flavobacterium, Rhodotorula, Arthrobacter, Thiobacillus, Neurospora, Sporobolomyces, Articulosporium* among others*)* and fungi (*Aspergillus polyporicola, Aspergillus spelaeus, Aspergillus niger* among others) poses the ability to break down crude oil in a polluted environment to less harmful products. Research findings have shown that bacteria are the best microorganisms suitable for bioremediation of crude oil pollution.

REFERENCE

Abii, T. A., and Nwosu, P. C. (2009). The effect of oil-spillage on the soil of Eleme in Rivers State of the Niger-Delta Area of Nigeria. *Research journal of environmental sciences*, *3*(3), 316-320.

Adesalu, T. A. and Olugbemi, O. M. (2015). Soil Algae: A Case Study of Two Vegetable Farmlands in Lagos and Ogun States, Southwest Nigeria. *Ife Journal of Science.* 17(3), 765-772

Ahmad, A. A., Muhammad, I., Shah, T., Kalwar, Q., Zhang, J., Liang, Z., and Rui-Jun, L. (2020). Remediation methods of crude oil contaminated soil. *World Journal of Agriculture and Soil Science*, *4*(3), 8.

Al-Dhabaan, F. A. (2021). Mycoremediation of crude oil contaminated soil by specific fungi isolated from Dhahran in Saudi Arabia. *Saudi Journal of Biological Sciences*, *28*(1), 73-77.

Bolan, S., Padhye, L. P., Mulligan, C. N., Alonso, E. R., Saint-Fort, R., Jasemizad, T., and Bolan, N. (2023). Surfactant-enhanced mobilization of persistent organic pollutants: potential for soil and sediment remediation and unintended consequences. *Journal of Hazardous Materials*, *443*, 130189.

Chorom M., Sharifi H. S., and Motamedi H. (2010). Bioremediation of A Crude Oil - Polluted Soil by Application of Fertilizers. *Iranian. Journal Environmental Health Science and Engineering 7, (4).* 319-326.

Condron, L., Stark, C., O'Callaghan, M., Clinton, P., and Huang, Z. (2010). The role of microbial communities in the formation and decomposition of soil organic matter. *Soil microbiology and sustainable crop production*, 81-118.

El-Sheekh M. M., Hamouda R. A. and Nizam A. A. (2013). Biodegradation of crude oil by *Scenedesmus obliquus* and *Chlorella vulgaris* growing under heterotrophic conditions. *International Biodeterioration and Biodegradation.* 82, 67-72

Ershadi, L., Ebadi, T., Ershadi, V., and Rabbani, A. R. (2011, February). Chemical oxidation of crude oil in oil contaminated soil by Fenton process using nano zero valent Iron. In *Proceedings of the 2nd international conference on environmental science and technology, Singapore* (pp. 26-28).

Kadafa, A. A. (2012). Oil exploration and spillage in the Niger Delta of Nigeria. *Civil and Environmental Research*, *2*(3), 38-51.

Koshlaf E. and Ball S. A. (2019). Soil bioremediation approaches for petroleum hydrocarbon polluted environments. AIMS Microbiology, 3, (1), 25-49.

Kriti S. and Subhash C. (2014). Treatment of Petroleum Hydrocarbon Polluted Environment through Bioremediation: A Review. *Pakistan Journal of Biological Sciences.* 17(1), 1-8

Li, X., Li, H., and Qu, C. (2019, March). A review of the mechanism of microbial degradation of petroleum pollution. In *IOP Conference Series: Materials Science and Engineering* (Vol. 484, No. 1, p. 012060). IOP Publishing.

Nwadinigwe A. O. and Onyeidu E. G. (2012). Bioremediation of Crude Oil-Polluted Soil Using Bacteria and Poultry Manure Monitored through Soybean Productivity. *Pollution Journal and. Environmental. Study. 21 (1) 171-176.*

Nwilo P.C. and Badejo O.T. (2015). Oil Spill Problems and Management in the Niger Delta. International Oil Spill Conference Proceedings. DOI: 10.7901/2169-3358-2005-1-567

Mambwe, M., Kalebaila, K. K., and Johnson, T. (2021). Remediation technologies for oil contaminated soil. *Global Journal of Environmental Science and Management*, 7(3), 419- 438.

Maier, R. M., and Gentry, T. J. (2015). Microorganisms and organic pollutants. In *Environmental Microbiology* (377-413). Academic Press.

Mishra, A., Siddiqi, H., Kumari, U., Behera, I. D., Mukherjee, S., and Meikap, B. C. (2021). Pyrolysis of waste lubricating oil/waste motor oil to generate high-grade fuel oil: A comprehensive review. *Renewable and Sustainable Energy Reviews*, *150*, 111446.

Ofoegbu, R. U., Momoh, Y. O., and Nwaogazie, I. L. (2015). Bioremediation of crude oil contaminated soil using organic and inorganic fertilizers. *Journal of Petroleum and Environmental Biotechnology*, *6*(1), 1.

Ogbonna, D. N. (2018). Application of biological methods in the remediation of oil polluted environment in Nigeria. *Journal of Advances in Biology and Biotechnology*, 1-10.

Oil and Gas Portal (2021). http://www.oil-gasportal.com/environmental-issues/petroleum-contaminated-soils-remediation-technologies/

Olowomofe T. O., Oluyege J. O., Aderiye B.I. and Oluwole O. A. (2019). Degradation of poly aromatic fractions of crude oil and detection of catabolic genes in hydrocarbon- degrading bacteria isolated from Agbabu bitumen sediments in Ondo State. *AIMS Microbiology.* 5(4), 308–323.

Ossai, I. C., Ahmed, A., Hassan, A., and Hamid, F. S. (2020). Remediation of soil and water contaminated with petroleum hydrocarbon: A review. *Environmental Technology and Innovation*, *17*, 100526.

Oudot, J., Dupont, J., Haloui, S., Roquebert, M.F., 1993. Biodegradation Potential of Hydrocarbon-Assimilating Tropical Fungi. *Soil Biology and Biochemistry*. 25, 1167-1173

Pongcharoen, C., and Satapanajaru, K. K. T. (2012, September). Remediation of petroleum hydrocarbon-contaminated soil slurry by Fenton oxidation. In *proceedings of world academy of science, engineering and technology*.

Saleh M. A., Ashiru M. A., Sanni J. E., Ahmed T. A., and Muhammad S. (2017). Risk and Environmental Implications of Oil Spillage in Nigeria (Niger-Delta Region). International Journal of Geography and Environmental Management. 3 (2) 44-59.

Tewari, S., and Sirvaiya, A. (2015). Oil spill remediation and its regulation. *International Journal of Engineering Research and General Science*, *1*(6), 1-7.

Ugwoha, E., Amah, V. E., and Oweh, G. O. (2020). Bioremediation of Crude Oil Contaminated Soil Using Pig Droppings and Bone Char. *Journal of Advances in Biology and Biotechnology*, 13-24.

Vanguard Newspaper, 2018

Victor, I. A., Iwok, E. O., Archibong, I. A., Effiom, O. E., Okon, E., and Andem, A. B. (2020). The biochemical mechanisms of petroleum degradation by bacteria. *Int. J. Sci. Eng. Res*, *11*, 1258-1275.

Wang, S., Xu, Y., Lin, Z., Zhang, J., Norbu, N., and Liu, W. (2017, August). The harm of petroleum-polluted soil and its remediation research. In *AIP Conference proceedings* (Vol. 1864, No. 1, p. 020222). AIP Publishing LLC.

Watts, M., and Zalik, A. (2020). Consistently unreliable: Oil spill data and transparency discourse. *The extractive industries and society*, *7*(3), 790-795.

Widdel, F, and Musat, F. (2010). Diversity and common principles in enzymatic activation of hydrocarbons. In: K. N. Timmis (Ed.) *Handbook of Hydrocarbon and Lipid Micro- biology*. Berlin, Heidelberg: Springer Berlin Heidelberg.

Wolicka, D., Borkowski, A., and Dobrzyński, D. (2010). Interactions between microorganisms, crude oil and formation waters. *Geomicrobiology Journal*, *27*(1), 43-52.

Yang, S., Wen, X., Shi, Y., Liebner, S., Jin, H., and Perfumo, A. (2016). Hydrocarbon degraders establish at the costs of microbial richness, abundance and keystone taxa after crude oil contamination in permafrost environments. *Scientific reports*, *6*(1), 1-13.

PAPER 27 - DESIGN MODIFICATION AND PERFORMANCE EVALUATION OF SOLAR PV SYSTEM AT AUTOCAD LABORATORY

H. M. Usman[1,3*], M. S. Yahaya[2,4], S. Saminu[5], M. Muhammad[1], S. Ibrahim[6], B. I. Sani[1], M. Sulaiman[7]
[1]Department of Electrical Engineering, Ahmadu Bello University, Zaria, Nigeria
[2]Department of Mechanical Engineering Aliko Dangote University of Science and Technology Wudil, Kano, Nigeria
[3]Department of Electrical Engineering, Mewar University, Chittorgarh, Rajathan, India
[4]Department of Mechanical Engineering, Mewar University, Chittorgarh, Rajathan, India
[5]Department of Biomedical Engineering, University of Ilorin, Ilorin, Nigeria
[6]Department of Electrical Engineering, Waziru Umaru Federal Polytechnic, Birnin Kebbi, Nigeria
[7]Department of Chemistry, Mewar University, Chittorgarh, Rajathan, India
[*]Email: habibusman015@gmail.com

ABSTRACT

The AutoCAD Laboratory at Faculty of Engineering at Kano University of Science and Technology, Wudil (KUST Wudil) faced power supply issues due to an inadequate photovoltaic (PV) system. This paper presents a comprehensive overhaul, dimensioning, and implementation of an amended PV system in the Laboratory. A load analysis was carried out, revealing a daily requirement of 275.97 Wh, significantly surpassing the average power output achievable with the current PV system. Consequently, the PV system components were meticulously tailored to power the load adequately, with a surplus. The Ampere Hour Load Method guided the sizing, resulting in the inclusion of eight batteries (100 Ah, 12 V), ten PV panels (100 W, 12 V), one 80 A charge controller, and one 1.5 kW inverter, which collectively meet the load demand. Evaluation of both systems' performance from January to December 2022 revealed that the old system's struggle to generate sufficient power, with monthly averages ranging from 1750 to 2200 Watts, falling short of load requirements varying from 3800 to 4050 Watts. Conversely, the modified PV system consistently outperformed expectations, generating monthly averages ranging from 3850 to 4220 Watts, surpassing the load requirements and ensuring uninterrupted equipment operation. This success emphasizes the significance of appropriately sizing and designing renewable energy systems.

***KEYWORDS*:** Photovoltaic (PV) system, load analysis, renewable energy, sizing of battery, inverter, charge controller.

1. INTRODUCTION

Energy is a necessity like food and water. Everything around us requires energy. Over the years there has been an increase in the earth's population which is directly proportional to the energy used as well. All the possible gadgets and equipment need some or the other kind of energy to function. With depleting fossil fuel reserves it becomes necessary to identify viable renewable energy resources that can decrease the dependency on fossil fuels (Bosshard, 2006; Seger, 2016). Solar energy is the most abundant form of energy available to us. It is approximated that 10000 TW worth of solar energy is incident on earth's surface in a day (Bosshard, 2006). According to a report, the world energy consumption in 2015 was 17.4 TW altogether (Seger, 2016). There has been a minimal increase in the energy consumption every year, approximately 1-1.5% annual growth.

The world's total energy consumption is expected to grow by 56% by the year 2040 (U.S. Energy Information Administration, 2013). To guarantee maximum performance and efficiency, PV system design incorporates a number of components and factors. Solar irradiance, panel orientation, tilt angle, shading analysis, battery storage, and system sizing are examples of design elements (Feng et al., 2017). To meet energy demand and maximize the use of solar resources, proper sizing and configuration are essential (Alghoul et al., 2019). Furthermore, new developments in PV technology, such as bifacial panels and smart inverters, present chances to raise system dependability and efficiency (Bashir et al., 2020).

The adoption of PV systems is influenced by a range of socio-economic, institutional, and policy factors. Studies have identified factors such as affordability, access to financing, awareness, technical expertise, and government incentives as critical determinants of adoption (Aderamo et al., 2020; Oseni et al., 2018). Additionally, community perceptions, cultural norms, and trust in technology play significant roles in shaping adoption behaviour (Adefila et al., 2019). The abundant solar resource in the region presents an opportunity for PV system adoption to diversify the energy mix and enhance energy access, especially in rural and underserved communities (Balogun et al., 2021). Studies have shown the economic viability of PV systems in Kano State, with potential benefits including

cost savings, job creation, and environmental sustainability (Abdulaziz et al., 2019). However, challenges such as limited infrastructure, regulatory barriers, and market fragmentation need to be addressed to unlock the full potential of PV adoption in the region (Oladejo et al., 2020).

The contribution of this work lies in its specific focus on addressing the challenges posed by an inadequate power supply in the AutoCAD Lab through the modification and optimization of a photovoltaic (PV) system. While there exists a considerable volume of related works on PV system design and implementation, this study offers a unique perspective by presenting a comprehensive redesign, sizing, and installation tailored specifically to the energy needs of the AutoCAD Lab at Kano University of Science and Technology, Wudil (KUST Wudil). By conducting load analysis and employing the Ampere Hour Load Method for sizing, this research ensures that the modified PV system effectively meets the lab's energy demands, thereby enabling uninterrupted operation of essential equipment for learning, teaching, and research activities. Furthermore, the evaluation of system performance over an entire year provides valuable insights into the effectiveness and reliability of the modified PV system compared to the previous setup. This detailed and context-specific approach adds significant value to the existing body of research on renewable energy systems, highlighting the importance of tailored solutions for addressing energy challenges in educational and research environments.

2. MATERIALS AND METHOD

The materials and methods used in this work are explained in this section. The materials used involved:

i. Mono-crystalline Panel: these panels are made from a single crystal. Specifications: brand name: PRIME SOLAR, capacity: 100W/12V, size: $1200 \times 540 \times 30mm$ mm, quantity: 10
ii. Deep Cycle Lead-acid Battery: Specifications: brand name: GSR Power Company India, capacity: 100AH 12V, quantity: 8
iii. Inverter: Specifications: capacity: 1.5KW, quantity: 1
iv. Charge controller: Specifications: capacity: 80A 12V/24V, quantity: 1
v. Wire cable (solar cable 23 yards and electric cable 10 yards)
vi. Change over switch
vii. Circuit breaker

Moreover, the method adopted in this study was Amphere Hour Load, designed procedures and sizing of stand-alone system are detailed in this section. It also outlines the design process that must be completed before the purchase and installation of any PV system component. The process includes the following steps:

- Assessment /Evaluation of the Existing PV System Design in the Laboratory
- Design Consideration for the Modified PV system
- Sizing of PV System Components using Ampere Hour Load Method

2.1. Assessment /Evaluation of the Existing PV System Design in the Laboratory

Table 1. Shows Load evaluation and power consumption for existing PV System in the laboratory

Table 1. Load evaluation and power consumption for existing PV System in the laboratory

Appliances	AC (W)	DC (W)	Quantity (Number)	Wattage $AC \times 1.15$ (W)	Hours/Day	Days/Week	Daily Consumption of load (Wh)	Average Wh/day (Wh)
Projector	100	0	1	115	4	6	76.67	98.57
Fan	20	0	6	23	4	6	15.33	19.7
Computer	65	0	5	74.75	3	6	37.375	64.07
Bulbs	11	0	6	12.65	2	6	4.22	10.84

Highest AC loads in watts =100 W

Total AC connected in wattage at a time = $100 + (20 \times 6) + (65 \times 5) + (11 \times 6) = 611\ W$

Total watt-hour per day = 98.57+19.7+64.07+10.84 =193.18 Wh/day

Corrected watt-hour per day $= \frac{\text{Total watt−hour per day}}{\text{correction factor}} = \frac{193.18}{0.7} = 275.97\ \text{Wh/day}$

Total daily consumption of a load =76.67+15.33+37.375+4.22 =133.595 Wh/day

The existing solar PV system uses sun hours as 10 hours, whereas the actual sun hours in Kano was highest in October with average sun hours of 9 hours 48 minutes daily, and lowest in August with average sun hours of 6 hours daily. Hence the sun hours in Wudil is averagely 8 hours (Oladosu & Adegbuluge, 1994).

2.2. Design Consideration for the Modified PV system

The system design tried to minimize the initial system costs by maximizing the system's energy efficiency. Efficient energy use lowers initial system cost. For example, reducing the electric lighting load by 75 percent, perhaps by shifting from incandescent to fluorescent lights, will reduce the number of modules and batteries needed for the system. Eliminating module shading by relocating the mounting system doesn't cost money and can increase the system's efficiency. Inefficiency caused by excessive voltage drop in the system's wiring can be reduced with proper wire sizing. In general, the design consider the some factors in order to optimize the PV system in the laboratory (Weis, 2013).

2.3. Sizing of PV System Components using Ampere Hour Load Method

Figure 1 illustrates the PV system, comprising components such as PV modules, charge controller, battery, inverter, and the load. Each component is meticulously sized to ensure optimal performance.

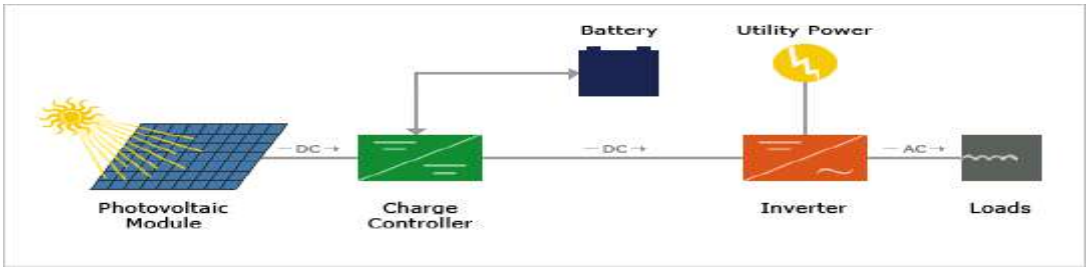

Figure 1. Schematic arrangement of the system

2.4. Electric Load Estimation

First of all, complete electric load was estimated by inputting the load, volts, amps, and usage information for each of the loads in a system. Upon completion total connected watts (AC and/or DC) and the average daily load (AC and/or DC) was determined. If the loads vary significantly on a seasonal or monthly basis or are of a critical nature, use the highest values in designing the system (Hankins, 2010).

$$A.D.L = \frac{PR \times Daily\ Use \times Weekly\ Use}{Total\ weekly\ days} \quad (1)$$

Where A.D.L is the Average Daily Load for each appliance, PR is the power rating of the appliances

For Projector $A.D.L = \frac{320 \times 4 \times 5}{7} = 914.28\ Wh$

For Computers $A.D.L = \frac{130 \times 4 \times 5}{7} = 371.43\ Wh$

For Fans $A.D.L = \frac{160 \times 4 \times 5}{7} = 457.14\ Wh$

For Bulbs $A.D.L = \frac{60 \times 4 \times 5}{7} = 141.43\ Wh$

$$A.D.L_{TOTAL} = \sum A.D.L \quad (2)$$

Where,

$A.D.L_{TOTAL}$ Is the appliances total Average Daily Load for the for AC load

$$A.D.L_{TOTAL} = \sum A.D.L = (914.28 + 371.43 + 457.14 + 141.43)$$

$$= 1884.28\ Wh$$

$$PR_{TOTAL} = \sum PR \quad (3)$$

$PR_{TOTAL} = \sum PR = (320 + 130 + 160 + 60)$= 670 Watt

2.5. Battery Sizing

The average ampere hours per day of battery is determined using the equations below (Shankar et al., 2008):

$$A.A.H\ Per\ day = \frac{A.D.L_{TOTAL}}{Battery\ Nominal\ voltage} \quad (4)$$

A.A.H per day is the average ampere hours per day of battery.

$$A.A.H\ Per\ day = \frac{1884.28}{12} = 157.02\ Ah/day$$

Now that the average amp-hour per day load has been determined, the next step is designing an adequate battery bank.

The battery capacity required was determined using equation below;

$$Battery\ Capacity = \frac{A.A.H\ Per\ day \times \text{Days of Autonomy}}{\text{Battery Discharge limit}} \quad (5)$$

Where discharge limit, or the battery's maximum depth of discharge is a number less than 1.0. Battery Discharge limit is 50% for lead acid battery and 80% for lihium ion battery, (Bala et al., 2019).

Days of Autonomy is 1 day

$Battery\ Capacity = \frac{157.02 \times 1}{0.5} = 314.05\ Ah$

The number of batteries in parallel is calculated using:

$$No\ of\ parallel\ batteries = \frac{Battery\ Capacity}{\text{Battery Ampere hour Capacity}} \quad (6)$$

$$No\ of\ parallel\ batteries = \frac{314.05}{100} = 3.14 \quad Say\ 4\ Battery$$

The number of batteries in series is calculated using:

$$No\ of\ Series\ battery = \frac{\text{DC System Voltage}}{\text{Battery Norminal Voltage}} \quad (7)$$

$$No\ of\ Series\ battery = \frac{24}{12} = 2\ Battery$$

The total numbers of batteries required by the system were obtained using equation below;

$$Total\ No\ of\ batteries = No.of\ parallel\ batteries \times No.of\ Series\ battery \quad (8)$$

$$Total\ No.of\ batteries = 4 \times 2 = 8$$

2.6. Sizing of Solar Array

To begin sizing the array, you must increase the average daily load (amp-hour) to account for the inefficiency of the batteries and controller that have been selected (Hankins, 2010).

$$A.P.A = \frac{A.A.H\ Per\ day}{\text{Battery efficiency}} \tag{9}$$

Where,

A.P.A is the Average Peak Ampere, Battery Efficiency is commonly considered as 0.8

$$A.P.A = \frac{157.02}{0.8} = 196.275\ Ah/day$$

The Average Peak Ampere of Array is calculated using:

$$A.P.A\ of\ array = \frac{A.P.A}{\text{Peak Sun Hours per day}} \tag{10}$$

Peak sun hours $per\ day\ in\ kano\ is\ 8\ hours$

$$A.P.A\ of\ array = \frac{196.275}{8} = 24.53$$

$$No\ of\ parallel\ module = \frac{A.P.A\ of\ array}{\text{Peak Ampere per module}} \tag{11}$$

Peak Ampere per module is 5.62 for 100Watt panels

$$No\ of parallel\ module = \frac{24.53}{5.62} = 4.36\ Say\ 5$$

$$No.of\ Series\ module = \frac{\text{DC System Voltage}}{\text{Module Nominal Voltage}} \tag{12}$$

DC System Voltage is 24V

$$No.of\ Series\ module = \frac{24}{12} = 2$$

$$Total\ No.of\ module = No.of\ parallel\ module \times No\ of\ series\ module \tag{13}$$

$$Total\ No.of\ module = 5 \times 2 = 10\ modules$$

2.7. Charge Controller Sizing

The charge controller sizing can be determined using equations below (Hankins, 2010);

$$ASC = MSP \times No\ of\ parallel\ module \tag{14}$$

Where ASC is the array short circuit and

MSC is the module short circuit and its 6.06A for 100W 12V panel

$$ASC = 6.06 \times 10 = 60.6A$$

The design controller capacity was obtained using equation

$$Controller\ capacity = (1 + 25\%) \times ASC = 1.25ASC \tag{15}$$
$$Controller\ capacity = 1.25 \times 60.6 = 75.75\ A\ Say\ 80\ A$$

3. Inverter Sizing

In general, inverter should be over sized by 25% of the load to increase reliability and life time.

Inverter rating was obtained using equations below (Hankins, 2010).

$$Total\ energy\ demanded = \frac{PR_{TOTAL}}{0.8} \quad (16)$$

$$Total\ energy\ demanded = \frac{PR_{TOTAL}}{0.8} = \frac{670}{0.8} = 837.5\ Watt$$

$$\text{Inverter rating } = 1.25 \times \text{Total energy demanded} \quad (17)$$

$$\text{Inverter rating } = 1.25 \times 837.5 = 1046.875\ W\ Say\ 1500\ W$$

Table 2. Summary of quantity of the components needed.

Component	Designed parameters	Quantity	Selected component
Battery	314.05 Ah capacity 4pieces parallel connection 2pieces series connection	8	100 Ah, 12V
Array/ Panels	24.53A Av. Peak Ampere of array 5 parallel connection module 2 series connection module	10	100W 12V
Controller	75.75A Controller capacity	1	80A
Inverter	1046.875W Rating	1	1.5KW 12V

4. RESULT AND DISCUSSION

The results obtained in this work are presented, and the discussion of these results is well explained in this section.

4.1. Result Analysis

The monthly average load demand over a year was quantified and tabulated as shown in Table 3, alongside the average power output recorded by the existing PV system throughout the entirety of 2021, as monitored by the intelligent charge controller. Furthermore, the average power output of the modified PV system per month was assessed for the entire duration of 2022. Notably, it's pertinent to mention that the prevailing environmental conditions governing sunlight in Kano State remained relatively consistent over this period. All pertinent data points are summarized within Table 3 for comprehensive analysis.

Table 3: power generated by old and modified PV over the year 2021 and 2022

	Jan	Feb	March	April	May	June	July	Aug	Sep	Oct	Nov	Dec
Average Power generated by old PV system monthly (Watt)	1950	2000	2050	2060	2060	2200	2200	2000	2000	1900	1800	1750
Average Power generated by modified system PV monthly (Watt)	4000	4150	4200	4200	4220	4220	4220	4200	4200	4100	3900	3850

Load requirement (Watt)	3900	4020	4040	4050	4050	4100	4100	4030	4010	4000	3800	3800

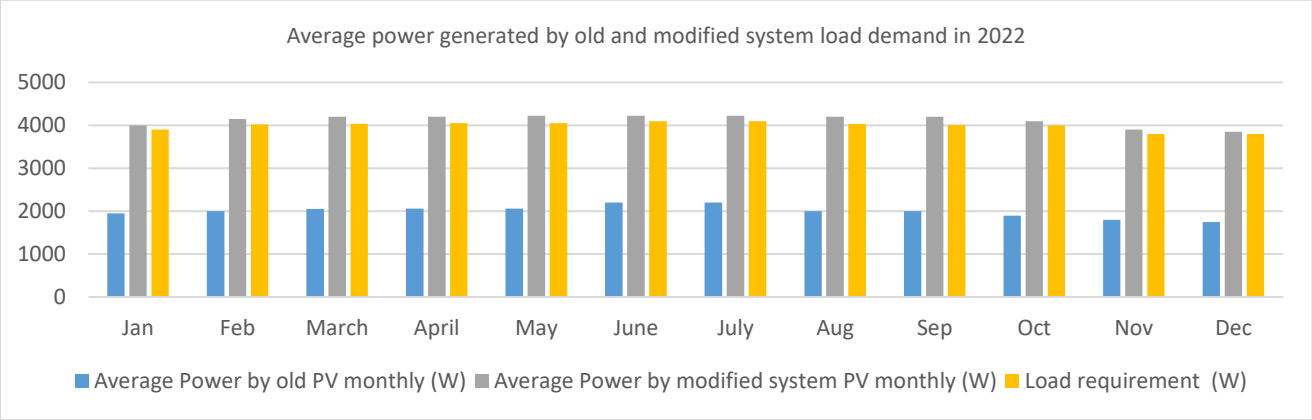

Figure 2: Power generated from old and modified PV system with respect to load demand

4.2. Result Discussion

The sizing of PV system components using the Ampere Hour Load Method involved meticulous calculations to ensure optimal performance. Electric load estimation yielded a total Average Daily Load (A.D.L) of 1884.28 Wh, with a cumulative power rating (PR_TOTAL) of 670 Watts. Battery sizing calculations determined a required capacity of 314.05 Ah, necessitating the installation of 8 batteries in total, arranged in 4 parallel connections and 2 series connections. The solar array was sized to deliver an Average Peak Ampere (A.P.A) of 196.275 Ah/day, leading to the configuration of 5 parallel modules and 2 series modules, totalling 10 modules. Charge controller sizing resulted in a designed capacity of 80 A, ensuring efficient regulation of the solar array output. The inverter was sized at 1500 W, 25% larger than the total energy demanded of 837.5 Watts, to enhance reliability and accommodate potential load variations.

The current PV system in the AutoCAD Lab at KUST Wudil is insufficient for effective power supply, causing disruptions in learning, teaching, and research. Despite efforts, it fails to sustain essential equipment operation simultaneously, resulting in frequent disruptions. Load requirement ranges from 3800 to 4050 Watts monthly, while the old PV system generates only 1750 to 2200 Watts per month, consistently falling short. A comprehensive redesign and installation of a modified PV system were undertaken to address this issue. The modified system's performance from January to December 2022 shows significant improvement, consistently exceeding load requirements with monthly average power ranging from 3850 to 4220 Watts. This ensures uninterrupted operation of equipment, enhancing learning, teaching, and research activities. The success of the modified system underscores the importance of appropriately sizing and designing renewable energy systems for educational and research facilities, especially in energy-shortage-prone regions.

5. CONCLUSION

In conclusion, this study has effectively addressed the deficiencies of the existing photovoltaic (PV) system in the AutoCAD Lab, where insufficient power hindered the operation of essential equipment. Through comprehensive redesign, sizing, and installation efforts, the modified PV system has demonstrated significant improvements. For example, the average monthly power generation increased from 1950 to 2200 Watts in 2021 with the old system to a range of 3850 to 4220 Watts in 2022 with the modified system, consistently surpassing the load requirements, which varied from 3800 to 4050 Watts. This enhancement has ensured uninterrupted operation, facilitating improved learning environments and research activities. The success of this endeavour underscores the necessity of tailored renewable energy system design. Moving forward, ongoing monitoring will be vital for ensuring optimal performance and meeting evolving energy demands. Future directions could include further optimization of the PV system, exploration of additional renewable energy sources, and integration of smart energy management technologies to enhance efficiency and sustainability.

ACKNOWLEDGMENT

We extend our sincere gratitude to the Department of Electrical and Mechanical Engineering, Aliko Dangote University of Science and Technology, Wudil, Kano, Nigeria, for their invaluable support throughout the duration of this study. Their provision of support, instruments, and assistance with data collection has been instrumental in the completion of our research.

REFERENCES

Abdulaziz, D. Y., Mohammed, Y. S., & Gandu, M. A. (2019). Economic feasibility of residential grid-connected photovoltaic systems in Kano, Nigeria. Cogent Engineering, 6(1), 1625782.

Adefila, K., Adekunle, A., & Olayiwola, K. (2019). Socio-cultural drivers of solar photovoltaic technology adoption in selected communities in Nigeria. Energy Reports, 5, 268-277.

Aderamo, A. J., Oyedepo, S. O., & Fagbenle, R. O. (2020). Barriers to the adoption of photovoltaic energy systems in Nigeria. Heliyon, 6(4), 37-63.

Alghoul, M. A., Khatib, T., & Othman, A. K. (2019). A review of photovoltaic systems: Classifications, components and sizing methods. Renewable and Sustainable Energy Reviews, 101, 545-556.

Bala, A. Saidu, B. A. Nura, M. M. Al-Dadah, R. K. Mahmoud, S. (2019). Optimum Tilt angle for Solar Collectors used in Kano, Nigeria. Journal of Advanced Research in Fluid Mechanics and Thermal Sciences, 56(1), 31-42.

Balogun, A. L., Suleiman, H., & Ahmad, F. (2021). Solar energy prospects in Kano State, Nigeria: A review. Renewable and Sustainable Energy Reviews, 137, 110553.

Bashir, N., Saidur, R., Jameel, M., & Mekhilef, S. (2020). Recent progress and emerging trends in solar energy: A bibliometric study. Renewable and Sustainable Energy Reviews, 119, 109537.

Feng, C., Li, X., & Ma, T. (2017). Optimal design and techno-economic analysis of standalone photovoltaic systems for applications in Nigeria. Applied Energy, 187, 36-52.

Hankins, M. (2010). Stand-alone Solar PV Systems, The earth expert handbook for Planning, How Solar Panels Work. www.wholesalesolar.com

Oladejo, N. K., Mustafa, M. W., Bashir, N., & Jamel, M. (2020). A review on solar photovoltaic systems in Nigeria: Policies, challenges and prospects. Journal of Cleaner Production, 262, 121354.

Oladosu, G. A., & Adegbuluge, A. O. (1994). Nigeria's Energy Sector: Issues and Supply/Demand Frontiers. Energy Policy, 22(6), 538-549.

Oseni, M. O., Nwanya, S. C., & Ohunakin, O. S. (2018). Determinants of solar photovoltaic technology adoption among households in Nigeria. Cogent Engineering, 5(1), 1536273.

Shankar, K. H. R., Aithal, R. S., Singh, P. K., Ashis, K. S., & Danak, A. R. (2008). Modelling of Photovoltaic Array and Maximum Power Point Tracker using ANN. Journal of Engineering Sciences

Weis, C. (2013, January). Considerations for Off-Grid PV Systems. Retrieved from Home Power: https://www.homepower.com/articles/solar-electricity/designinstallation/considerations-grid-pv-systems

PAPER 29 - EXPERIMENTAL STUDY ON THE COMPRESSIVE STRENGTH OF CEMENT MORTAR WITH TERNARY BLENDS OF METAKAOLIN AND IRON ORE TAILINGS

O. K. YUSUF[1*], S. M. Adeniran-Bakare[2], A. Alhassan[1], A. A. Abdulazeez[1]

[1] Department Civil Engineering, Kogi State polytechnic, Lokoja
[2] Department Civil Engineering, Yaba College of Technology, Lagos State
*Email: kudiratoziyusuf@yahoo.com

ABSTRACT

The addition of alternative materials as a replacement for cement has been researchers' main focus for sustainable development, to reduce the quantity of cement usage as construction materials thereby reducing the carbon dioxide (CO_2) emission into the atmosphere during its production and also for waste management. Metakaolin (MK) and Iron Ore Tailing (IOT) have been considered as a good alternative material in cement individually or in combination with other materials for better mortar or concrete performance. This study is carried out to investigate the behaviour of ternary blends of MK and IOT as partial replacement of cement in mortar. The compressive strength was carried out by following the standard specification on the mortar cube size of 70.6 mm^3 prepared by partially replacing cement by weight with MK and IOT each in the ratio of 0, 5, 10, 15, and 20%. The two materials were blended by varying MK from 0 to 20% while keeping IOT constant at each percentage replacement of MK. The prepared samples were cured in the water tank for 7 and 28 days. The x-ray fluorescence conducted shows that MK and IOT are both pozzolanas since the sum of their oxide composition of SiO_2, Al_2O_3, and Fe_2O_3 in MK and IOT gives 91.14% and 95.58% respectively which is higher than the minimum value of 70% specified by ASTMC618. Optimum compressive strength was at mix sample M10T10, that is, 10% of metakaolin and 10% of Iron Ore Tailings, with values at 26 N/mm^2 and 34 N/mm^2 for 7 and 28 curing days respectively. Generally, 20% of the blends can be recommended for cement replacement in cement mortar.

***KEYWORDS*:** Metakaolin, Iron Ore Tailings, Ternary Blends, Cement Mortar, Compressive Strength

1. INTRODUCTION

The extensive use of mortar or concrete in the construction industry has given way to high demands for cement, which is one of the major constituents of mortar or concrete because of its binding properties. With the present urbanization and civilization in the developing countries, the rate of infrastructure development will be very high leading to the possibility of mortar or concrete being used globally to likely increase from 10 billion tons to about 18 billion tons yearly by the year 2050 due to its numerous roles in construction works. This means, there will likely be high cement consumption in today's world (Ajay et al., 2012).

Over time, Cement as a binder has gotten so much attention due to its more expensive and the environmental issues it creates during its production such as the emission of CO_2 and other greenhouse gases and it is also more expensive in terms of its high energy consumption. The need to complement cement by adding alternative materials known as supplementary cementitious materials (SCMs) which tend to show good binding properties obtained from either industrial or agricultural wastes now becomes very important in the construction industry. Presently, most SCMs used in cement are mainly byproducts of other industries, such as blast furnace slag, fly ash, and pozzolans (Usman, et. al., 2013; Yao et al., 2020).

Metakaolin is obtained from kaolin clay through a process that involves heating the clay at a temperature ranging from 500^0C to 950^0C. It is widely recognized for its positive impact on enhancing concrete performance through its reaction with existing portlandite to form a secondary calcium silicate hydrate gel and several other gels (Zeljkovic, 2009). Researchers such as (Basu, 2003; Khatib, 2008; Patil and Kumbhar, 2012) as well as Poon et.al., (2001), also documented these observations. Most studies that have investigated the use of MK as a pozzolan in mortar or concrete as cement replacement proved that it has shown significant improvement (El-din., et al., 2017; Salimi, et al., 2019; Shafiq, et al., 2019). According to some researchers, their investigations show that the incorporation of 15% MK replacement in cement concrete gives a significant improvement (Dianakar, 2012; Jagtap et al., 2008; and Fezzioui, et al., 2021). Other researchers such as (Rajender and Samanta, 2023; Dinakar et al., 2013) also specified other optimum percentage of MK to be 10% for compressive strength.

The global objective to reduce the high cost of waste disposal and also minimize environmental hazards associated with this waste materials which are mostly stockpiled in the dam, has led to great researchers' interest in the economic use of waste for engineering purposes most especially iron ore tailings (IOT). Iron ore tailings (IOTs) are generally considered by-products that are generated from the processing of Iron ore. With increasing mining

activities, more minerals are being demanded for economic development. One such place where mining activities are being carried out is in Itakpe-Okene, Kogi State in Nigeria. being carried which amounts to an average of one billion metric tons of raw ore produced in the world annually (Lasisi *et al.*, 2010; Ugama *et al.* 2014). Over the years, IOT has been considered to contain high quartz content in their composition and also relatively inert in particle sizes which makes it mostly used for fine aggregate replacement in the construction industry (Zhao et al., 2014; Li et al., 2023). The fact remains that any SCMs considered as being perfect for cement replacement are either pozzolanic, cementitious or possess both properties. However, due to the poor cementitious property of tailing, there is a need to subject it to treatment before utilization. The need for researchers to explore more trending SCMs leads to researchers finding ways to use IOT as cement replacement through activation or pretreatment. According to (Gou et al., (2019), this treatment can be done by drying, grinding, and/or calcining. The grinding decreases the particle size thereby increasing the specific surface area. During calcination, some of the minerals in tailings are decomposed and the crystal structure of minerals is destroyed, which gives room for amorphous minerals which have high pozzolanic activity (Guo, et al., 2016). Chen, et al., (2016) found that the mechanochemical activation decreases the crystallinity of silicon dioxide (SiO_2) in tailings and causes a hydration reaction between IOT and calcium hydroxide to produce C-S-H gel. Wei et al., (2017) reports showed that mechanical activation was an effective way to promote the reactivity of the tailings. In the course of this study, thermal and mechanical activation was use in tailings activation or treatment, which made the IOT to be ball milled and calcined at 650^0C for 3 hours.

For sustainability and reusability, intensive research and development efforts have been directed toward finding a better way to minimize and utilize the waste produced in iron ore mining operations (Bandopadhyay *et al.*, 2002; Ugama, *et al.*, 2014), addressing the negative effect of stockpiling the tailings in the tailing dam which could lead which causes environmental degradation. Cui et al., (2022) reutilize waste Iron tailing powders in mortar as cement reduction and strength enhancement, and their result shows that 20% of these tailing powders give a significant improvement in the developing strength and the nucleation effect as well as the pozzolanic effect of tailings powders demonstrated its ability to promote cement hydration while effectively optimizes pore structure. Largeau, et al., (2018), studied the effect of Iron powder (Fe_2O_3) on concrete strength in the ratio of 1.5%, 2.5%, 3.5%, and 5% of cement replacement, although, in a nano form, their result shows that strength improvement was at 2.5% Iron powder.

The possibility of extending the range of SCMs or combining more than one SCM in cement mortar and concrete is called ternary blends. This is due to their physical and chemical properties, which can, in turn, improve some mortar or concrete properties in terms of performance (Jozwiak, 2015; Acordi et al., 2020; Vargas and Lopez, 2018). Adel Al Menhosh et al. (2016) studied the effect of metakaolin additive and polymer admixture on the concrete strength properties. They found that the addition of 5% optimized polymer and 15% cement replacement using metakaolin generates an optimized concrete mixture for both strength and durability. Kandasamy et al., (2024)investigated blended MK and Ground pound ash (PA) for reduced carbon footprint emission and improved mechanical properties in cement and were able to see the significant compressive strength enhancement at MK and PA 6% (MK_6PA_6) mix. Whether incorporating MK with flyash (Sujjavanich et al., 2017), Mk with Silica fume (Ambroise et al., (2012), MK with rice husk ash (Khan et al., 2012), MK with ground granulated blast furnace slag(GGBS) (Mohd Nasir et al., 2014), MK with sugarcane bagasse ash (Chi, 2012), MK with Alccofine (Bhat., 2023), MK with nano-silica (Sousa and Rego, 2021), MK with dolomites powders (Ye, 2020). All demonstrated enhanced mechanical properties and reduced pore spaces in ternary blended cement.
It is well observed from the literature that a lot of research had been directed towards the investigation of the effect of binary blend and ternary blend of MK and IOT as SCMs in either cement mortar or concrete, but limited research is being carried out in the investigation of MK with IOT as ternary blended cement, hence, the motivation for this research. The primary goal of this study is to investigate the behavior of a ternary blend of MK with IOT as SCMs in Mortar considering the percentage of replacement to cement weight to be 0, 5, 10, 15, and 20% for each SCM.

3. MATERIALS AND METHODS

Preliminary tests were conducted on Iron Ore Tailings, Metakaolin, cement, and fine aggregates in the Department of Civil Engineering, Ahmadu Bello University, Zaria.

3.1 Materials

Materials used for this study are Iron Ore tailings, Metakaolin, cement, and fine aggregates.
The fine aggregate was collected from dredged river sand in Zaria, Kaduna State; while cement was purchased from a local depot in Samaru, Zaria, Kaduna State.

The Iron Ore Tailings were collected from the tailing dam in Itakpe, Kogi State, ball milled and calcined at 650 ^{0}C for 3 hours, as treatment or activating method as stated in some works of literature.

Kaolin which was collected from KanKara L.G.A in Kastina State was beneficiated manually, sieved with cloth mesh, and allowed to air dry. It was ball milled, then calcined at 850 ^{0}C for 3 hours to obtain metakaolin, which was later sieved with a 75-micron size sieve.

X-ray Fluorescence (XRF) test was carried out on cement, Iron Ore Tailings, and Metakaolin to determine their oxide composition. The samples were taken for elemental analysis at the National Geoscience Research Laboratory (NGRL) in Kaduna and the result is shown in Table 3.

Plates I and 2 below show the image of the metakaolin and the Heaps of Iron Ore tailings waste in the dam site at Itakpe yard in Okene-Kogi State.

Plate 1: Metakaolin

Plate2: Heaps of Iron ore Tailings waste in Itakpe yard

3.2. Method

3.2.1. Experimental procedure

The mixed proportion of the MK-IOT blend using 1:3 mix ratios is presented in Table 1

Table 1: Mixed Proportion of MK-IOT with Cement

S/N	LABEL	Cement	MK	IOT	SAND
1	M0T0	747	0	0	2240
2	M5T0	710	37	0	2240
3	M10T0	672	75	0	2240
4	M15T0	635	112	0	2240
5	M20T0	597	150	0	2240
6	M0T5	710	0	37	2240
7	M5T5	672	37	37	2240
8	M10T5	635	75	37	2240
9	M15T5	597	112	37	2240
10	M20T5	560	150	37	2240
11	M0T10	672	0	75	2240
12	M5T10	635	37	75	2240
13	M10T10	597	72	75	2240
14	M15T10	560	112	75	2240
15	M20T10	522	150	75	2240
16	M0T15	635	0	112	2240
17	M5T15	597	37	112	2240
18	M10T15	560	75	112	2240
19	M15T15	522	112	112	2240
20	M20T15	485	150	112	2240
21	M0T20	447	0	150	2240
22	M5T20	560	37	150	2240
23	M10T20	522	75	150	2240
24	M15T20	485	112	150	2240
25	M20T20	447	150	150	2240

3.2.2. Compressive Strength of Mortar

The compressive strength of cement mortar for the various mixes was determined according to IS: 10080-1982. Mortar was prepared by partially replacing cement with Metakaolin and Iron ore Tailings in the ratios 0, 5, 10, 15, and 20%. Each MK and IOT were blended by varying MK and keeping IOT constant as shown in Table 1. The combination gave 25 mixes including the control (M0T0) which is 100% cement with no metakaolin and Iron Ore Tailings. The mortar cubes were prepared with a mould size of 70.6 mm^3 and cured for 7 and 28 days inside the water tank.

4. RESULTS AND DISCUSSION

4.1 Physical Property of Materials

The fine aggregate used falls within the zone I envelope according to BS 882: 1992 limits for grading, which indicate it is coarse with a silt content of 4% and a specific gravity of 2.63. Table 2 presents the physical properties of the material

Table 2: Physical Properties of Cement, MK, and IOT

Property	Cement	MK	IOT	
Specific Gravity	3.15	2.31	3.40	
Colour		Dark Grey	whitish Pink	Dark Ash

4.2. Test result on Oxide Composition of Cement, MK, and IOT

The result of the X-ray fluorescence (XRF) test on cement, MK, and IOT is presented in Table 2. MK has a high content of silica (45.73%) followed by Alumina (44.62). While IOT has a high content of ferric oxide (55.90%) followed by Alumina (35.85%). The combined oxide composition of SiO_2, Al_2O_3, and Fe_2O_3 in MK and IOT is 91.14 and 95.58% respectively which is more than the minimum value of 70% specified by ASTM C 618 for pozzolana. This observation conforms to that of Elinwa and Maichibi, (2014).

Table 3: Chemical composition of materials

Oxide Composition	SiO_2	Al_2O_3	Fe_2O_3	K_2O	SO_3	Ti_2O	MnO	CaO
Cement (%)	18.71	2.654	0.745	0.459	1.047	0.042	0.044	68.87
Metakaolin (%)	45.73	44.62	0.788	0.319	0.046	0.266	0.178	0.128
Iron Ore Tailing (%)	35.85	3.83	55.90	0.5	0.052	0.187	0.219	0.534

Oxide Composition	MgO	P_2O_5	Cl	Na_2O	CeO_2	ZnO	LOI
Cement (%)	0.67	0.113	0.036	0.232	0.091	0.003	1.81
Metakaolin (%)	2.9	0.162	0.014	0.161	0.838	0.012	2.9
Iron Ore Tailing (%)	1.1	0.398	0.046	0.211	0.11	0.003	1.2

4.3. Test results on compressive strength of MK-IOT mortar blends

The results of the compressive strength of Mortar prepared with the blends for 7 and 28 days of curing are presented in Figures 1 and 2 respectively. Where; M0, M5, M10, M15, M20 represent 0%, 5%, 10%, 15%, 20% of Metakaolin as well as T0,T5, T10, T15 and T20 represent 0%, 5%, 10%, 15%, 20% of Tailings.

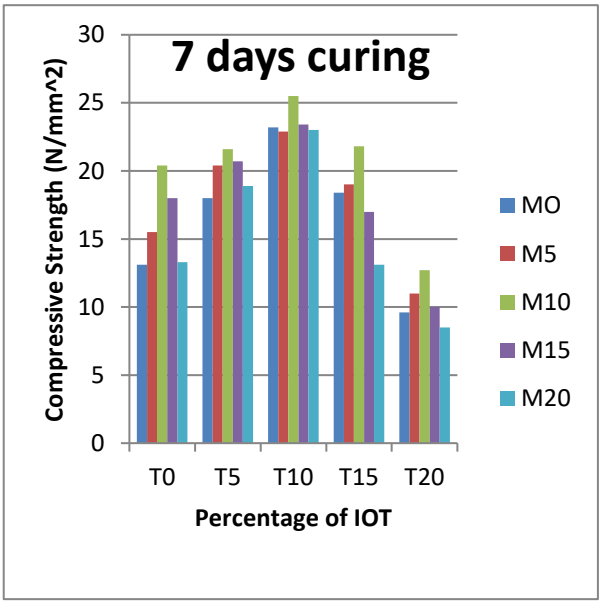

Fig 1: Compressive Strength of MK-IOT at 7 days curing

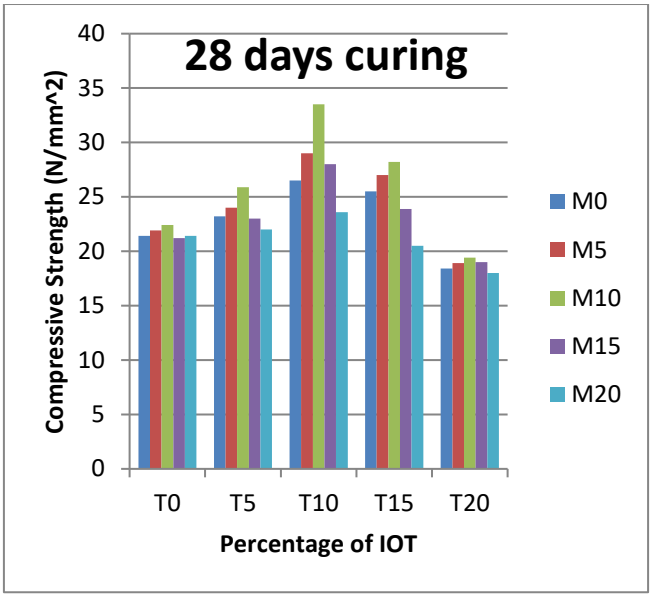

Fig 2: Compressive Strength of MK-IOT blends at 28 days curing

From Figures 1 and 2, It can be observed that an increase in the blends increases the compressive strength at all curing ages as compared to the control sample (M0T0). The high improvement of compressive strength most especially at an early age could be attributed to the rapid consumption of portlandite ($Ca(OH)_2$) formed during cement hydration as related to high reactivity of Fe_2O_3 present in the matrix. This similar observation was seen by Largeau et al., (2018).

The optimum strength was observed at M10T10, which shows an exceptional increase. This could be attributed to the large proportion of silica content present in MK and IOT which undergo a reaction with excess portlandite produced during hydration to form secondary C-S-H gel which contributes to the increased strength. The more reason a denser cement matrix is generated through the pozzolanic reaction as observed by Elinwa and Maichibi (2014) and Frias and Cabrera (2000). The reduction at M20T20 could be attributed to the fact that at the increased proportion of MK and IOT present in the matrix, it's now likely to be higher than the required amount to combine with the portlandite liberated during the hydration process, which could translate to excess silica leaching out thereby causing deficiency in strength. A similar approach was tested by Kandasamy et al., (2024).

5. CONCLUSIONS

The following conclusions were drawn from the results obtained;

i. MK and IOT are both pozzolanas given the sum of SiO_2, Al_2O_3, and Fe_2O_3 greater than 70% as specified by ASTM C618.
ii. The compressive strength increases as the curing age increases and the percentage of blends increases as compared to the control (conventional mortar with cement only). However Optimum compressive strength was at M10T10 (MK was at 10% and IOT was at 10%).

REFERENCES

Acordi, J.; Luza, A.; Fabris, D.C.N.; Raupp-Pereira, F.; De Noni, A., Jr. and Montedo, O.R.K. (2020), "New Waste-Based Supplementary Cementitious Materials: Mortars And Concrete Formulations." Constr. Build. Mater., 240, 117877.

Abdulwahab, R., Olalekan, S., & Temitope, H. (2021). *Effects of metakaolin and treated rice husk ash on the compressive strength of concrete Effects of metakaolin and treated rice husk ash on the compressive strength of concrete*. *January*. https://doi.org/10.17515/resm2020.223ma1014

Ajay, V., Rajeev, C., & Yadav, R. K. (2012). *Effect of Micro Silica on The Strength of Concrete with Ordinary Portland Cement*. *1*(3), 1–4.

Cui, L., Chen, P., Wang, L., Xu, Y., & Wang, H. (2022). Reutilizing Waste Iron Tailing Powders as Filler in Mortar to Realize Cement Reduction and Strength Enhancement. *Materials*, *15*(2). https://doi.org/10.3390/ma15020541

Dinakar, P., Sahoo, P. K., & Sriram, G. (2013). Effect of Metakaolin Content on the Properties of High Strength Concrete. *International Journal of Concrete Structures and Materials*, *7*(3), 215–223. https://doi.org/10.1007/s40069-013-0045-0

Fezzioui, N., Amrane, B., Souici, K., Hami, B., Kennouche, S., Safi, B., & Nadir, M. (2021). Effect of metakaolin as partially cement replacement on the compressive strength of standard mortars. *Revista Romana de Inginerie Civila/Romanian Journal of Civil Engineering*, *12*(2), 268–280. https://doi.org/10.37789/rjce.2021.12.2.6

Gou, M., Zhou, L., Wei, N., & Then, Y. (2019). *Utilization of tailings in cement and concrete : A review*. 449–464.

Jagtap, S. A., Shirsath, M. N., & Karpe, Sambhaji L, I. (2008). Effect of Metakaolin on the Properties of Concrete. *International Research Journal of Engineering and Technology*, *4*(07), 643–645. www.irjet.net

Kandasamy, Y., Kumarasamy, V., Murugan, S., & Singaraj, R. (2024). Utilizing binary ternary blended metakaolin and ground pond ash for reduced carbon footprint emissions and improved mechanical properties in concrete. *Revista Materia*, *29*(1). https://doi.org/10.1590/1517-7076-RMAT-2023-0335

Largeau, M. A., Mutuku, R., & Thuo, J. (2018). Effect of Iron Powder (Fe₂O₃) on Strength, Workability, and Porosity of the Binary Blended Concrete. *Open Journal of Civil Engineering*, *08*(04), 411–425. https://doi.org/10.4236/ojce.2018.84029

Li, J., Ren, W., Zhang, A., Li, S., Tan, J., & Liu, H. (2023). *Mechanical Properties and Microstructure Analysis of Cement Mortar Mixed with Iron Ore Tailings*.

Yao, G., Wang, Q., Wang, Z., Wang, J., & Lyu, X. (2020). Activation of hydration properties of iron ore tailings and their application as supplementary cementitious materials in cement. *Powder Technology*, *360*, 863–871. https://doi.org/10.1016/j.powtec.2019.11.002

Zhao, S., Fan, J., & Sun, W. (2014). Utilization of iron ore tailings as fine aggregate in ultra-high performance concrete. *Construction and Building Materials*, *50*, 540–548. https://doi.org/10.1016/j.conbuildmat.2013.10.019

Józwiak-Niedzwiedzka, D. (2015), "Microscopic Observations of Self-Healing Products in Calcareous Fly Ash Mortars." Microsc. Res. Tech., 78, 22–29.

Mehta, P. K. and Monterio, P. J. M. (2006). Concrete: Microstructure, Properties and Materials., 3rd ed McGraw-Hill: New York.

Oey T., Kumar A., Bullard J.W., Neithalath N., Sant G., Scherer G. (2013). The Filler Effect: The Influence of Filler Content and Surface Area on Cementitious Reaction Rates. J. Am. Ceram. Soc; 96: Pg 1978–1990

Ugama, T.I., Ejeh, S.P. and Amartey, D.Y. (2014), "Effect of Iron Ore Tailings on the Properties of Concrete", Civil and Environmental Research, 6, (10), pg. 7-13,

Usman, J., Mohd Sam, A. R., & Radin Sumadi, S. (2013). Strength and Porosity of Cement Mortar Blended with Metakaolin. Advanced Materials Research, 838-841, 142-147.

Vargas, F., and Lopez, V. (2018). "Development of a new supplementary cementitiousmaterial from the activation of copper tailings: Mechanical performance and analysis of factors." Journal of Cleaner Production 182, Pg.427-436.

Rajender, A. and Samanta, A.K. (2023) "Compressive strength prediction of metakaolin based high-performance concrete with machine learning", Materials Today: Proceedings, 2023.

Zeljkovic, M. (2009) "Metakaolin effects on concrete durability", M.Sc. Thesis, University of Toronto,Toronto.

Khatib, J.M.(2008) "Metakaolin concrete at a low water to binder ratio", Construction & Building Materials, v. 22, n. 8, pp. 1691–1700.

Patil, B.B. and Kumbhar, P.D., (2012) "Strength and durability properties of high performance concrete incorporating high reactivity metakaolin", Journal of Engineering Research, v. 2, pp. 1099–1104.

Poon, C.S., Lam, L., Kou, S.C., (2001) "Rate of pozzolanic reaction of metakaolin in high-performance cement pastes", Cement and Concrete Research, v. 31, n. 9, pp. 1301–1306.

El-Din, H.K.S., Eisa, A.S., Aziz, B.H.A., (2017) "Mechanical performance of high strength concrete made from high volume of Metakaolin and hybrid fibers", Construction & Building Materials, v. 140, pp. 203–209.

Salimi, J., Ramezaninaianpour, A.M., Moradi, M.J. (2020) "Studying the effect of low reactivity metakaolin on free and restrained shrinkage of high performance concrete", Journal of Building Engineering, v. 28, pp. 101053, 2020.

Shafiq, N., Kumar, R., Zahid, M., (2019) "Effects of modified metakaolin using nano-silica on the mechanical properties and durability of concrete", Materials (Basel), v. 12, n. 14, pp. 2291, 2019.

Dinakar, P., (2012) "Design of self compacting concrete with fly ash", Magazine of Concrete Research, v. 64, n. 5, pp. 401–409.

Adel Al Menhosh, YanWang and YuWang, (2016), The Mechanical Properties of the Concrete Using Metakaolin Additive and Polymer Admixture, journal of Engineering, Pg 1- 6

Guo, Z., Feng, Q. M, Wang, W. Q., Huang, Y., Deng, J., Xu, Z. H., (2016) Study on Flotation Tailings of Kaolinite-type Pyrite when Used as CementAdmixture and Concrete Admixture, Procedia Environmental Sciences 31, Pg. 644-652

Cheng, Y., Huang, F., Li, W., Liu, R., Li, G., Wei, J., (2016) Test research on the effects of mechanochemically activated iron tailings on the compressive strength of concrete, Constr. Build. Mater. 118, Pg 164–170

Wei, B., Zhang, Y., Bao, S., (2017) Preparation of geopolymers from vanadium tailings by mechanical activation, Constr. Build. Mater. 145, Pg 236–242.

Sujjavanich, S., Suwanvitaya, P., Chaysuwan, D., (2017) "Synergistic effect of metakaolin and fly ash on properties of concrete", *Construction & Building Materials*, v. 155, pp. 830–837.

Ambroise, J., Maximilien, S., Pera, J., (2012) "Properties of metakaolin blended cements", *Advanced Cement Based Materials*, vol.1, n. 4, pp. 161–168,

Khan, R., Jabbar, A., Ahmad, I.,(2012) "Reduction in environmental problems using rice-husk ash in concrete", *Construction & Building Materials*, v. 30, pp. 360–365

Mohd Nasir, N.A. and Mccarthy, M.J., (2014)"Effect of metakaolin on early strength of GGBS ternary concrete", *Applied Mechanics and Materials*, v. 584, pp. 1551–1557,

Chi, M.C., "Effects of sugar cane bagasse ash as a cement replacement on properties of mortars", *Science and Engineering of Composite Materials*, v. 19, n. 3, pp. 279–285, 2012.

Sousa, M.I.C.and Rêgo, J.H.S., (2021) "Effect of nanosilica/metakaolin ratio on the calcium alumina silicate hydrate (CASH) formed in ternary cement pastes", *Journal of Building Engineering*, v. 38, pp. 102226,

Yao, G., Wang, Q., Wang, Z., Wang, J., & Lyu, X. (2020). Activation of hydration properties of iron ore tailings and their application as supplementary cementitious materials in cement. *Powder Technology*, *360*, 863–871.

Ye, H., (2020) "Autogenous formation and smart behaviors of nitrite-and nitrate-intercalated layered double hydroxides (LDHs) in Portland cement-metakaolin-dolomite blends", *Cement and Concrete Research*, v. 139, pp. 106267.

Zhao, S., Fan, J., & Sun, W. (2014). Utilization of iron ore tailings as fine aggregate in ultra-high performance concrete. *Construction and Building Materials*, *50*, 540–548

PAPER 31 - CONCENTRATION LEVELS AND HEALTH RISKS ASSESSMENT METALS IN BEAUTY SALONS

A. S. Atanda [1*], J. A. Adeniran[1], T. L. Adewoye[1], A. K. Abdulraheem[2]

[1]Department of Chemical Engineering, University of Ilorin, Ilorin, Nigeria.
[2]Department of Water Resources, Ahmadu Bello University, Zaria
[*]Email: sarat.morenikeji@gmail.com

ABSTRACT
Heavy metals are one of the main components of indoor air pollution which has detrimental effects on human health. This study investigated the concentration levels and health risks of heavy metals in the ambient air of beauty salons. Fourteen (14) beauty salons were sampled and deposited air samples were taken from the breathing zone of workers and customers at 1.5 m above the ground level with Sorbent-impregnated polyurethane foam (SIP-PUF) disk for 30 days. Concentrations of Pb, As, Cd, Zn, Cu, Mn, Fe, Cr, Co, and Ni were analyzed with the Atomic Absorption Spectrophotometer (AAS). The mean concentrations of the selected metals ranged between 0.0968-0.5867 mg/kg, which exceeded indoor air guidelines, and workplace limit levels set by the United States Environmental Protection Agency (USEPA). The average hazard index for all the heavy metals was obtained to be lower than the statutory limit. The cancer risk estimated for Pb, As, Cr, Cd, and Ni for a child and adult ranged between $1.22 - 2.91 \times 10^{-4}$ and $1.47 - 7.55 \times 10^{-7}$, respectively. These values were above the limits set by the USEPA and World Health Organization (WHO). Findings from this study have a potential influence on workplace air pollution regulations and would provide insights for policies regarding air pollution prevention in indoor spaces and product safety standards.

KEYWORDS*:* Ambient air, beauty salon, heavy metals, cancer and Hazard index

1. INTRODUCTION

Reducing indoor air pollution is a global challenge that needs concerted efforts, to protect the environment and human health. The indoor environment is a crucial component of the human habitat and the contaminations associated with these closed boundaries must be brought to their minimum concentration levels, for the safer inhabitation of the dwellers (Capíková et al., 2019). Most people spend 85-90% of their time in indoor environments such as homes, offices, schools, and others (Adeniran et al., 2015; Almeida et al., 2011; Capíková et al., 2019; Năstase & Șerban, 2019; Zhou et al., 2019). Poor indoor air quality affects productivity, health (Moya et al., 2019), and even death in severe cases. About 4.5 million annual death reported globally are as a result of indoor air pollution owing to stroke (34%), pneumonia (12%), heart disease (26%), pulmonary disease (22%), and cancer (%) (Shi & Wang, 2021). It is therefore imperative to find suitable ways to lower the concentrations of harmful air pollutants in indoor areas.

Beauty salons offer a wide range of services from skin treatment and hair styling to manicures, make-ups, and hair treatment. Numerous cosmetic products are used for hairstyling, treatments, and pigmentation among others in the beauty salons contain pollutants which have detrimental effects on the health of the workers and the environment (Hadei *et al*., 2018). Hairdressers and their customers are frequently exposed to high concentrations of toxic air pollutants such as heavy metals and VOCs (Blessy *et al*., 2023). These pollutants are emitted from many of the cosmetic products used which are unregulated and may contain carcinogens (Okereke et al., 2020). Heavy metals such as lead (Pb), cadmium (Cd), arsenic (As), Iron (Fe), Cadmium(Cd), Cobalt (Co), Zinc (Zn), and nickel (Ni) are commonly incorporated in most hairdressing cosmetics (Eneh, 2021). These heavy metals have a detrimental effect on human health especially children (Al-Swadi *et al*., 2022; Shi & Wang, 2021) and the environment.

Heavy metals do not degrade easily because their half-lives can be as high as 30 years as such are persistent in the environment (Zhou *et al*., 2019) and are subjected to bioaccumulation in the food chain. Heavy metals can get absorbed into the human system through dermal, inhalation, and ingestion. Pb poisoning was attributed to about 1.06 million deaths in 2017 and 2016, it accounted for 63.2% of intellectual disability, 10.3% of hypertension, 5.6% of heart disease, and 6.2% of stroke (Eneh, 2021). Cadmium (Cd) has been attributed to infertility, high concentration of As can cause diarrhea, vomiting, vomiting blood, blood in the urine, cramping muscles, hair loss, stomach pain, and more convulsions and Nickel (Ni) has been attributed to headaches, nausea, vomiting, dizziness, irritability, and difficulty sleeping (Eneh, 2021).

The wide range of harmful effects of heavy metals from beauty products on human health and the environment, calls for in-depth investigation. Hence, this study aims to examine heavy metal concentration levels in the air of these beauty shops to determine the extent to which customers and workers are exposed to heavy metals and the health risks associated with human exposure to heavy metals in the ambient air of beauty salons.

2. THEORETICAL ANALYSIS

Exposure pathways for heavy metals are mainly through three pathways, which include inhalation, ingestion, and dermal contact. Assessments of human exposure to heavy metals were estimated for non-carcinogenic and carcinogenic risk assessment. The non-carcinogenic risk of the heavy metals was estimated with the hazard quotient (HQ) which is computed from the average daily dose. The average daily dose of heavy metals for children and adults in $mg/(kgday)$ via the three exposure paths of ingestion (ADD_{ing}), inhalation (ADD_{inh}) and dermal contact (ADD_{derma}) were estimated using Equations 1, 2, and 3, respectively (USEPA, 2001). The exposure risk factors and parameters for health risk assessment are presented in Table S1.

$$ADD_{ing} = \frac{C \times \mathrm{IngR} \times \mathrm{EF} \times \mathrm{ED}}{\mathrm{BW} \times \mathrm{AT}} \times 10^{-6} \quad (1)$$

$$ADD_{inh} = \frac{\mathrm{C} \times \mathrm{InhR} \times \mathrm{EF} \times \mathrm{ED}}{\mathrm{PEF} \times \mathrm{BW} \times \mathrm{AT}} \quad (2)$$

$$ADD_{derm} = \frac{\mathrm{C} \times \mathrm{ESA} \times \mathrm{SAF} \times \mathrm{DAF} \times \mathrm{EF} \times \mathrm{ED}}{\mathrm{BW} \times \mathrm{AT}} \times 10^{-6} \quad (3)$$

Where, C_{ing}= concentration of ingested pollutant; C_{inh}= concentration of inhaled pollutant; C_{derm}= concentration from dermal contact; IngR = ingestion rate; EF = exposure frequency; ED = exposure duration; BW = body weight; AT = average exposure time; ESA = Exposed skin area; SAF = skin adherence factor; DAF= dermal adsorption factor.

The calculation methods of potential non-carcinogenic risk and cancer risk for the heavy metals are calculated using Equations (4 – 7) (Abdulraheem *et al*., 2022; Odediran *et al*., 2021; Zhou *et al*., 2019)

$$HQ = \frac{ADD}{RfD} \quad (4)$$

$$HI = \sum HQ \quad (5)$$

The cancer risk was estimated with Equations 6 and 7

$$\mathrm{IL}CR = ADD \times SF \quad (6)$$

$$CR = \sum ILCR \quad (7)$$

The RfD is the homologous reference dose and SF is the homologous slope factor. In this study, the values of RfD and SF for heavy metals used in (Odediran *et al*., 2021) were adopted.

If the average daily dose (ADD) value is lower than the reference dose, it indicates that there would not be any adverse health effects; otherwise, if the ADD value is higher than the RfD, the exposure pathway will likely cause adverse human health effects. The Hazard index (HI) is the non-carcinogenic risk from various routes. HI is equal to the addition of HQ for all exposure pathways. When $\mathrm{HI} > 1$, there is a possibility that the non-carcinogenic risk is significant, but when $\mathrm{HI} < 1$, it shows there is an insignificant non-carcinogenic risk (Senthong & Wittayasilp, 2021). For regulatory purposes, the international threshold limits permitted by the USEPA and the International Agency for Research on Cancer (IARC) were followed (Du et al., 2013; IARC, 2011; Men et al., 2018; USEPA, 2011).

3. METHODOLOGY

3.1 *Study area and sampling location*

Samples were collected from fourteen (14) beauty shops in Ilorin as shown by the red dots on the map depicted in Figure 1. Ilorin is the capital city of Kwara State in Nigeria, located between latitudes 8º30'00''N and 8º50'00''N and longitudes 4º20'00''E and 4º35'00''E. The city occupies a land area of about 468 km^2 and it is

situated in the transitional zone within the forest and the Guinea savannah regions of Nigeria. It is the most populated town in Kwara state with a population of about 908,490 (Khairat et al., 2023). It serves as a major trade Centre between the Hausa of the north and the Yoruba of the south (Damilare, 2021). The economy in Ilorin is rapidly growing, the service industry developing, consumer culture is becoming more sophisticated and so are hairdressing and beauty businesses. The fourteen beauty shops selected were selected based on their proximity to a commercial area and higher institution.

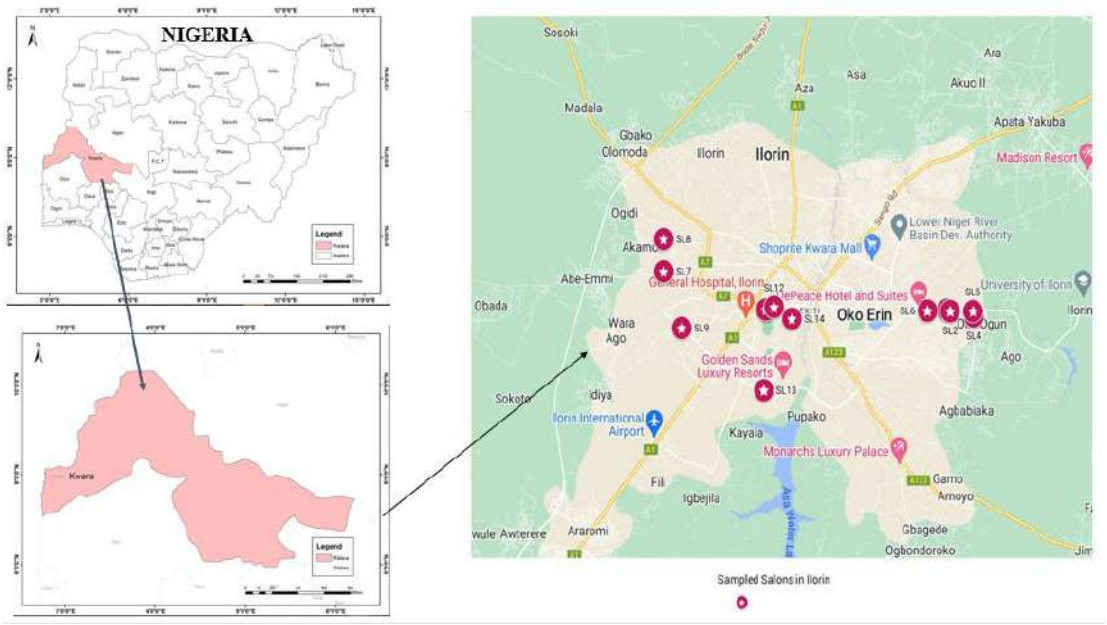

Figure 1: Map showing locations of sample collection

3.2 Sample collection

The indoor air samples were collected using a Polyurethane Foam (PUF) passive sampler as described by Strandberg *et al*., (2018). The PUFs were impregnated with XAD-4/hexane slurry (6.4 g/L) to improve the absorptive capacity for VOCs (Shoeib et al., 2008). The air samples were taken from fourteen beauty shops in the Ilorin metropolis of Kwara State, Nigeria. Beauty shops were chosen because hairdressers are exposed to numerous VOCs contained in hair styling products in their work environment, often without the use of personal protective equipment such as aprons, appropriate hand gloves, and respiratory masks within a short period (Ana et al., 2019). The measurement of emission rate and concentration involved the preparation of a sorbent-impregnated PUF disk. The samplers were placed in beauty shops for 30 days for the collection of samples and health risk assessment of the VOCs.

3.2.1 Preparation of sorbent-impregnated polyurethane foam (SIP-PUFs) disk

PUF disk was cut to 7 cm diameter and a thickness of 1 cm (99 cm^2 surface area and density of 0.0104 g/cm^3) (Liu *et al*., 2016) and then washed with distilled water. This was followed by a Soxhlet extraction with acetone for 6 hours at a temperature of 56 °C. 20 g of Amberlite XAD-4 resin was cleaned with a water bath shaker with 30 ml each of methanol, dichloromethane (DCM), and hexane for 30 min each. The wet XAD-4 was blown under a stream of N_2 and then dehydrated for 3 days in a vacuum desiccator containing a molecular sieve of 0.75 µm. 6.4 g of XAD-4 powder was mixed with one litre of hexane in a glass beaker to give a homogenous emulsion. A homogenizer was used for further mixing to ensure a thorough mixture of XAD-4/ Hexane slurry. The XAD-4 resin was impregnated onto the PUF disks dipping it into XAD-hexane slurry three times to deposit onto the porous surface of PUFs. The coated PUFs were placed in a vacuum desiccator for 24 hours to dry and then stored in a zip lock to avoid capture of untargeted pollutants.

3.2.2 Deployment of samplers

All parts of the Passive Air Samplers (PAS) were pre-cleaned with hexane and acetone solvents in sequence before assembly to ensure that it is free from the targeted pollutants. The SIP-PUFs were connected with a hinge to avoid

contact with the stainless bowls in the supplementary material. The samplers were hung at a height of 1.5 m above the ground in 14 beauty shops within the Ilorin metropolis for 30 days. Field blank was collected and treated as exposed dirt.

3.2.3 Sample digestion and heavy metal extraction

The heavy metal in the PUF was digested by dissolving 1g of the PUF in 100 ml 1M solution of the nitric acid (HNO_3) and then heated for 30 minutes on a hot plate at 70 °C. The solution was allowed to cool down for 5 minutes and then filtered in a Whatman filter paper of 157 mm diameter. The filtrate was transferred into a sample bottle and transferred to the Atomic Absorption Spectrophotometer (AAS) AA320N model to check the heavy metals present.

Atomic Absorption Spectrophotometer (AAS) with model number AA320N was used to analyze digested samples and obtain the concentrations of ten (10) heavy metals (iron (Fe), lead (Pb), zinc (Zn) arsenic (As), cobalt (Co) chromium (Cr), copper (Cu), cadmium (Cd), manganese (Mn), and nickel (Ni)] that were potentially toxic elements in urban environments (Odediran *et al*., 2021). Aqua-regia was prepared with analytical reagent (AR) grade (HCl and HNO3), and all solutions were prepared with deionized distilled water (DDW). 1000 mg/L of standard stock solution of each metal were prepared using their corresponding AR grade metallic salts while the pure solid forms of Cu, Ni, and Zn were used to prepare their 1000 mg/L of standard solutions by dissolving in either HCI or HNO3 with distilled water.

3.2.4 Quality control

For quality control, Standard reference material (GSS-1/RDMIB2019), method blanks, and replicate samples were analyzed to verify the determination accuracy of elements. No heavy metals were detected in blank samples. The PTEs recoveries ranged between 94% and 112%, and the relative standard deviations of replicate samples did not exceed 5%. The method detection limits (MDL) for Fe, Pb, Zn, As, Co, Cr, Cu, Cd, Mn, and Ni were 0.0005, 0.25, 0.12, 0.0017, 0.00009, 0.04, 0.04, 0.01, 0.04 and 0.05, respectively.

4. RESULTS AND DISCUSSION

4.1 Distribution of heavy metals in the Salon ambient air

The mean, max, median, and SD concentrations of heavy metals (mg/kg) in fourteen (14) beauty salons in the Ilorin metropolis are summarized and presented in Table 1. The concentration of the heavy metals ranged from 0.460±0.10 - 1.137 ±0.10 mg/kg in all the salons considered. The mean concentration of each metal decreases in the order Fe (0.6689 ±0.2322)>As (0.5942±0.4354) > Cd (0.5967±0.1521) > Cu (0.4520±0.1044) > Zn (0.4127±0.2405) > Pb (0.3685±0.2237) > Ni (0.3581±0.1421) > Cr (0.1034±0.0688) > Mn (0.0753±0.0332). The arsenic (As) concentration for SL01, SL02, SL07, SL11, and Nickel (Ni) for SL12 was below the detection limit. Detailed results of the concentration distribution of the heavy metals in the beauty shops are shown in Figure S1.

Table 1: Descriptive statistics of heavy metals concentration in salon ambient

Heavy metals (mg/kg)	Pb	As	Cd	Zn	Cu	Mn	Fe	Cr	Co	Ni
Mean	0.3685	0.5942	0.5867	0.4127	0.4520	0.0753	0.6689	0.1034	0.0968	0.3581
Minimum	0.1230	0	0.3360	0.0420	0.2530	0.0160	0.3070	0	0	0
Maximum	1.0060	1.1370	0.9110	0.7950	0.6220	0.1490	1.1200	0.2730	0.2500	0.5510
Median	0.3120	0.8120	0.5930	0.3985	0.4665	0.0825	0.6420	0.0740	0.0965	0.3500
SD	0.2237	0.4354	0.1521	0.2405	0.1044	0.0332	0.2322	0.0688	0.0686	0.1421

The average heavy metals concentrations for Pb, As, Cd, Cu, and Co were above the permissible exposure limit by the Occupational Safety and Health Organization (OSHA) (Safety & Administration, 2018) by 62.4, 3.6, 539.5, 1.2, and 2.3 folds. The USEPA (Geiger & Cooper, 2010) limit and the National Environmental Standards and Regulation Enforcement Agency (NESREA, 2009) were exceeded by all the heavy metals considered as presented in Table 2. The heavy metals found in the salon ambient find their way from the airborne dust either from the outdoors or from the activities carried out within the salon. Activities carried out in the surrounding area or vicinity also contribute to the indoor heavy metal concentration and the type of heavy metal found in the shop. The presence of Pb can be attributed to the location of the beauty shop, which is close to the main road with high traffic density, and it is therefore expected to contain Pb from the combustion of petroleum products.

Table 2: Comparison of heavy metals concentration and statutory limit

		Standards		
Heavy metals	**Mean concentration (ppm)**	**OSHA**	**USEPA**	**NESREA**
Pb	0.3685	62	78071	3
As	0.5942	4	91135	5
Cd	0.5867	539	337185	3
Zn	0.4127	0	10714	83
Cu	0.452	1	4195	80
Mn	0.0753	0	8459	0
Fe	0.6689	0	955	0
Cr	0.1034	0	137417	0
Co	0.0968	2	466620	372

3.2.1 Non-carcinogenic risk

The risk associated with exposure to heavy metals was evaluated using the Average Daily Dose (ADD) of the metals. The three major pathways of exposure, which include, inhalation via the nose, ingestion through the mouth, and adsorption through the skin are considered. The estimated value for the average daily dose is shown in Table S3. The ADD via ingestion for a child ranged between 3.08×10^{-6} to 1.12×10^{-6}, 4.16×10^{-6} to 1.14×10^{-5}, 3.37×10^{-6} to 9.14×10^{-6}, 1.63×10^{-6} to 8.20×10^{-6}, 2.54×10^{-6} to 6.24×10^{-6}, 1.61×10^{-7} to 1.50×10^{-6}, 1.87×10^{-6} to 1.01×10^{-5}, 4.01×10^{-6} to 2.74×10^{-6}, 4.01×10^{-8} to 9.69×10^{-6} and 1.83×10^{-6} to 5.53×10^{-6} mg/kg/day for Fe, As, Cd, Zn, Mn, Pb, Cr, Co, and Ni respectively. The values obtained are similar to what was reported by (Arshad et al., 2020). The hazard index obtained is presented in Figure 2. SLO7 had the highest hazard index which could be attributed to the fact that it is located close to a road construction site. The lowest hazard index was obtained in SL12 because the salon was well-ventilated.

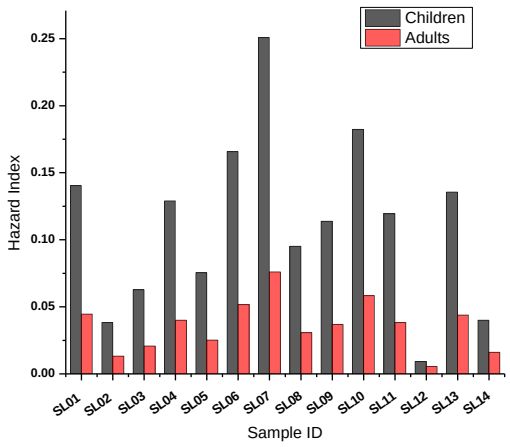

Figure 2: Non-carcinogenic risk of heavy metals in the salon ambient

3.2.2 Lifetime Cancer Risk

Lifetime cancer risk is the estimation of the cancer risk to humans exposed to heavy metals. The three major pathways of exposure to heavy metals were considered in the calculation of cancer risk associated with exposure to this toxic element IARC (2012) identified chromiun (Cr), lead (Pb), Nickel (Ni), and cadmium (Cd) as carcinogenic heavy metals (Odediran et al., 2021; Olawoyin et al., 2018). As, Cd, Cr (vi), and Ni are classified as class 1 carcinogens, whereas Pb is classified as a class 2a carcinogen (Olawoyin *et al*., 2018). Using the statutory limits set by USEPA and IARC, the ILCR for the five heavy metals studied, for children was a little bit higher than 10^{-4} and for adults either between 10^{-5} – 10^{-6}. The result depicts that exposure in beauty shops is likely to cause cancer in a child this is because children are more sensitive to the pollutants.

Total excess cancer risks (that is, the sum of the individual elemental ILCR) obtained for children ranged from 1.36 to 2.92 $\times 10^{-4}$ indicating a potential cancer risk according to AIRC. The contribution of each of the exposure pathways increased in the order: inhalation < dermal < ingestion. However, values of total cancer risk (CR) range between 10^{-6} and 10^{-4} are considered as an acceptable range. Moderate risk level (ILCR>10^{-3}) and (ILCR>10^{-2}) that is above 1 in 1000 and 1 in 100, respectively are considered unacceptable and the health safety of the public is of concern (Isegen et al., 2021; Odediran et al., 2021; Olawoyin et al., 2018).

The CR obtained for adults varied from 1.47 to 7.55 $\times 10^{-6}$ as presented in Figure 3 which shows an acceptable cancer risk. The ILCR increased from inhalation < ingestion < dermal. It has been determined that lung cancer and other related cancerous health conditions may develop, due to chronic inhalation exposures to Cr (Olawoyin *et al*., 2018). Cr has the highest contribution to the cancer risk (Odediran et al., 2021). Therefore, the carcinogenic impacts through ingestion should be of special concern to the children around the salon area and children should be monitored in the vicinity. Also of importance is the high probability of children developing both non-carcinogenic and carcinogenic health effects in the beauty shop, therefore mitigation policies should be considered for the sustainability of the environment and protection of people living and working in such an environment.

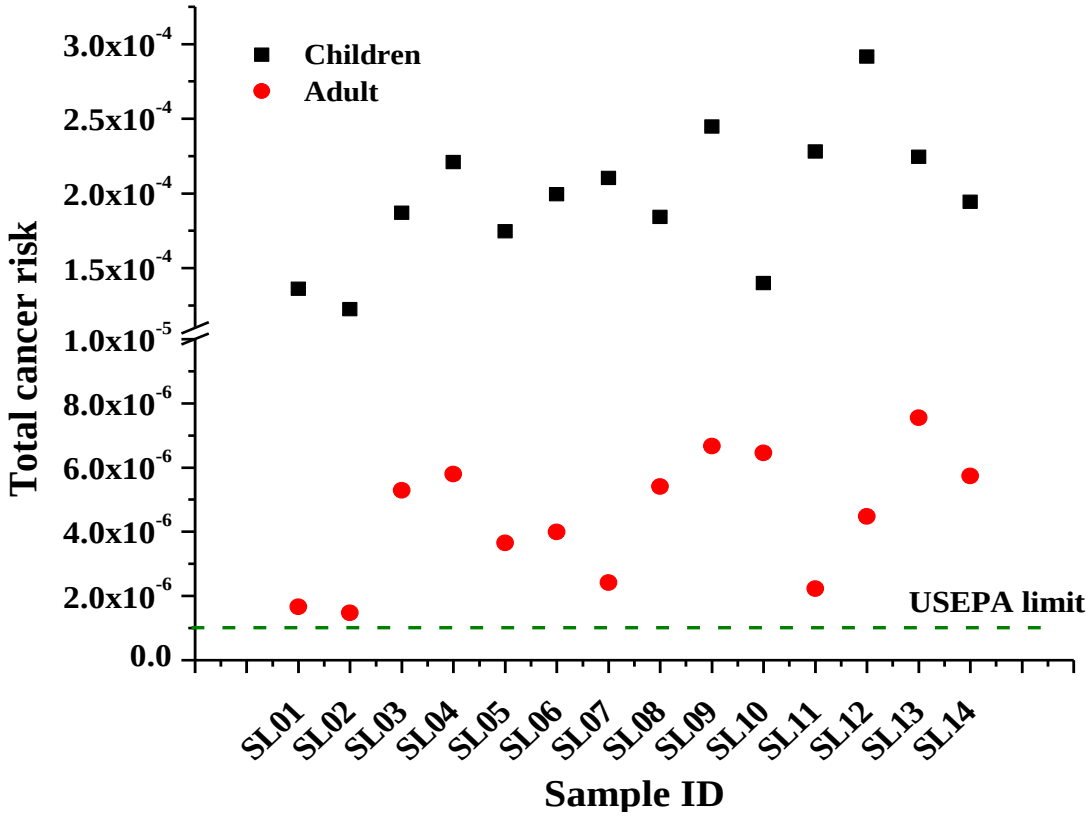

Figure 3: Total cancer risk of heavy metals

5. CONCLUSION

The analysis of passively sampled beauty salon ambient air showed the concentration and distribution of heavy metals within the study area. The mean concentrations of Pb, As, Cd, Zn, Cu, Mn, Fe, Cr, Co, and Ni in fourteen (14) beauty shops were obtained to be 0.3685, 0.5942, 0.5867, 0.4127, 0.4520, 0.0753, 0.6689, 0.1034, 0.0968, 0.3581 mg/kg respectively. The ranking of the heavy metals in decreasing concentrations in the indoor air of the beauty salons is Fe > As > Cd >Cu> Zn > Pb >Ni > Cr > Co > Mn. The non-carcinogenic risks for both adults and children were in the acceptable range while the carcinogenic risks were above the permissible limit in which Cd was a major contributor to the expected risk. As such, stricter regulations are needed to limit using these kinds of products to reduce the potential health effects on the workers.

ACKNOWLEDGEMENT

We would like to express our gratitude to all those who have contributed to this research paper. Without your hard work, expertise, and dedication, this research would not have been possible.

REFERENCES

Abdulraheem, M. O., Adeniran, J. A., Ameen, H. A., Odediran, E. T., Yusuf, M.-N. O., & Abdulraheem, K. A. (2022). Source identification and health risk assessments of heavy metals in indoor dusts of Ilorin, North central Nigeria. *Journal of Environmental Health Science and Engineering*, *20*(1), 315-330.

Adeniran, J. A., Sonibare, J. A., & Jimoda, L. A. (2015). Statistical approach for determining the effects of microclimatic parameters on household spray products aerosol deposition. *Atmospheric Pollution Research*, *6*(1), 21-28.

Al-Swadi, H. A., Usman, A. R., Al-Farraj, A. S., Al-Wabel, M. I., Ahmad, M., & Al-Faraj, A. (2022). Sources, toxicity potential, and human health risk assessment of heavy metals-laden soil and dust of urban and suburban areas as affected by industrial and mining activities. *Scientific reports*, *12*(1), 8972.

Almeida, S. M., Canha, N., Silva, A., do Carmo Freitas, M., Pegas, P., Alves, C., . . . Pio, C. A. (2011). Children exposure to atmospheric particles in indoor of Lisbon primary schools. *Atmospheric Environment*, *45*(40), 7594-7599.

Ana, G. R., Alli, A. S., Uhiara, D. C., & Shendell, D. G. (2019). Indoor air quality and reported health symptoms among hair dressers in salons in Ibadan, Nigeria. *Journal of Chemical Health & Safety*, *1*(1), 1-8.

Arshad, H., Mehmood, M. Z., Shah, M. H., & Abbasi, A. M. (2020). Evaluation of heavy metals in cosmetic products and their health risk assessment. *Saudi Pharmaceutical Journal*, *28*(7), 779-790.

Capíková, A., Tesařová, D., Hlavaty, J., Ekielski, A., & Mishra, P. K. (2019). Estimation of Volatile Organic Compounds (VOCs) and Human Health Risk Assessment of Simulated Indoor Environment Consisting of Upholstered Furniture Made of Commercially Available Foams. *Advances in Polymer Technology*, 1-10.

Damilare, O. T. (2021). *Assessment of domestic solid waste recycling in ilorin south LGA, Kwara state* Unilversity of Ilorin]. ilorin.

Du, Y., Gao, B., Zhou, H., Ju, X., Hao, H., & Yin, S. (2013). Health risk assessment of heavy metals in road dusts in urban parks of Beijing, China. *Procedia Environmental Sciences*, *18*, 299-309. https://doi.org/10.1016/j.proenv.2013.04.039

Eneh, O. C. (2021). Health effects of selected trace elements in hairdressing cosmetics on hairdressers in Enugu, Nigeria. *Scientific reports*, *11*(1), 20352.

Geiger, A., & Cooper, J. (2010). Overview of airborne metals regulations, exposure limits, health effects, and contemporary research. *Environmental Protection Agency, Portland*, 1-56.

Hadei, M., Hopke, P. K., Shahsavani, A., Moradi, M., Yarahmadi, M., Emam, B., & Rastkari, N. (2018). Indoor concentrations of VOCs in beauty salons; association with cosmetic practices and health risk assessment. *Journal of Occupational Medicine and Toxicology*, *13*, 1-9.

IARC. (2011). *International Agency for Research on Cancer Agent Classified by the IARC Monograph*.

IARC. (2012). Pharmaceuticals. Volume 100 A. A review of human carcinogens. *IARC monographs on the evaluation of carcinogenic risks to humans*, *100*(PT A), 1.

Isegen, W., Asomugha, R., Amendu, J., & Asomugha, A. (2021). Risk assessment of some heavy metals and polycyclic aromatic hydrocarbons in selected cosmetics locally produced. *World Journal of Pharmaceutical Research*, *11*(2), 122-142.

Khairat, K., Ayinde, M., Dangana, A., Favour, I., Pius, O., Daniel, H., & Onoja, O. (2023). Assessments of viral load and haematological parameters in HIV patients on HAART in Ilorin, Kwara State. *international Journal of Science and Research Archive*, *10*(01), 366-373.

Liu, R., Lin, Y., Liu, R., Hu, F., Ruan, T., & Jiang, u. (2016). Evaluation of two passive samplers for the analysis of organophosphate esters in the ambient air. *Talanta*, *147*, 69-75.

Men, C., Liu, R., Xu, F., Wang, Q., Guo, L., & Shen, Z. (2018). Pollution characteristics, risk assessment, and source apportionment of heavy metals in road dust in Beijing, China. *Science of The Total Environment*, *612*, 138-147.

Moya, T. A., Dobbelsteen, A. v. d., Ottele, M., & Bluyssen, P. M. (2019). A review of green systems within the indoor environment. *Indoor and built environment*, *28*(3), 298-308.

Năstase, G., & Șerban, A. (2019). Experimental study on CO_2 capture in a residential space. *Environmental Engineering & Management Journal (EEMJ)*, *18*(5).

NESREA. (2009). Federal Republic of Nigeria. In.

Odediran, E. T., Adeniran, J. A., Yusuf, R. O., Abdulraheem, K. A., Adesina, O. A., Sonibare, J. A., & Du, M. (2021). Contamination levels, health risks and source apportionment of potentially toxic elements in road dusts of a densely populated African City. *Environmental Nanotechnology, Monitoring & Management*, *15*, 100445.

Okereke, J., Dike Ijere, N., Ukaoma, A., & Ezejiofor, T. (2020). Genotoxicity of Hairdressing Salon Effluent Using Allium cepa. *World Journal of Innovative Research*, *9*, 6-12.

Olawoyin, R., Schweitzer, L., Zhang, K., Okareh, O., & Slates, K. (2018). Index analysis and human health risk model application for evaluating ambient air-heavy metal contamination in Chemical Valley Sarnia. *Ecotoxicology and environmental safety*, *148*, 72-81.

Safety, O., & Administration, H. (2018). Permissible exposure limits: OSHA annotated table Z-1. *Washington, DC: Occupational Safety and Health Administration*.

Senthong, P., & Wittayasilp, S. (2021). Working Conditions and Health Risk Assessment in Hair Salons. *Environmental Health Insights*, *15*, 11786302211026772.

Shi, T., & Wang, Y. (2021). Heavy metals in indoor dust: Spatial distribution, influencing factors, and potential health risks. *Science of the Total Environment*, *755*, 142367.

Shoeib, M., Harner, T., Lee, S. C., Lane, D., & Zhu, J. (2008). Sorbent-Impregnated Polyurethane Foam Disk for Passive Air Sampling of Volatile Fluorinated Chemicals. *Analytical Chemistry*, *80*(3), 675-682.

USEPA. (2001). Risk assessment guidance for superfund (RAGS), vol III—Part A, process for conducting probabilistic risk assessment. *Office of emergency and remedial response, Washington, DC*.

USEPA. (2011). Exposure factors handbook: 2011 edition. In: USEPA Office of Research and Development Washington.

WHO. (2018). Indoor Air Pollution. *Geneva, swizerland*.

Zhou, L., Liu, G., Shen, M., Hu, R., Sun, M., & Liu, Y. (2019). Characteristics and health risk assessment of heavy metals in indoor dust from different functional areas in Hefei, China. *Environmental pollution*, *251*, 839-849.

PAPER 32- A REVIEW OF WATER RESOURCES EVALUATION USING GIS AND REMOTE SENSING TECHNIQUES

A.T. Baker[1], O.O. Olla[2], L.A. Bello[3], O.O. Ilevbaoje[4], S.I. Salman[5], H. Nurudeen[6]

[1]Department of Land and Water Engineering.
National Centre for Agricultural Mechanization, Ilorin, Nigeria.
[*]Email:bakeradebayour@gmail.com

ABSTRACT
Water resource management is crucial for sustainable development and environmental conservation. Geographic Information Systems (GIS) and Remote Sensing (RS) technologies have revolutionized the assessment and management of water resources by providing valuable tools for data analysis, visualization, and decision-making. This paper reviews the application of GIS and RS techniques in evaluating water resources, focusing on their contributions to hydrological modeling, water quality assessment, and monitoring of water availability. The paper also discusses challenges and future directions in the field, highlighting the importance of integrating these technologies with traditional methods for comprehensive water resource management.

KEYWORDS: Water resources, GIS, Remote Sensing, Hydrological modelling, water quality assessment.

1. INTRODUCTION

Water is a fundamental resource essential for various human activities, ecosystem functioning, and agricultural production (Fisher *et al*., 2017). Sustainable management of water resources is critical to ensure availability for current and future generations while preserving environmental integrity. However, the increasing demand for water coupled with climate change and environmental degradation, poses significant challenges to water resource management. According to Evsahibloglu (2015), Geographic Information Systems (GIS) and Remote Sensing (RS) technologies offer powerful tools for assessing and managing water resources by providing spatially explicit data, analysis capabilities, and decision support systems. This paper aims to evaluate the effectiveness of GIS and RS techniques in water resource management, focusing on their applications in hydrological modeling, water quality assessment, and monitoring of water availability. Geographic Information Systems (GIS) and remote sensing technologies have revolutionized the way water resources are assessed, monitored, and managed.

Applications of GIS in Water Resources Evaluation: GIS facilitates the integration of spatial data related to hydrology, topography, land use, and climate, enabling comprehensive analysis and visualization of water resources. Key applications include watershed delineation, hydrological modeling, flood mapping, and groundwater assessment. GIS-based decision support systems aid in optimal water allocation, infrastructure planning, and disaster management.

Remote Sensing Techniques for Water Resources Assessment: Remote sensing platforms, such as satellites and aerial drones, provide valuable data for monitoring water bodies, land cover changes, and hydrological processes. Remote sensing imagery is utilized for mapping surface water extent, detecting water quality parameters, and assessing vegetation health. Advanced sensors, including multispectral and hyperspectral imagers, enhance the capability to monitor water resources with high spatial and temporal resolutions.

Integration of GIS and Remote Sensing: The synergy between GIS and remote sensing enables comprehensive analysis and monitoring of water resources at various spatial and temporal scales. Remote sensing data serve as inputs for GIS-based models, improving the accuracy of hydrological simulations and water resource assessments. Furthermore, GIS facilitates the visualization and dissemination of remote sensing-derived information to stakeholders, policymakers, and the public. Despite their immense potential, the application of GIS and remote sensing techniques in water resources evaluation faces several challenges, including data availability, processing complexities, and the need for skilled manpower. Future research should focus on developing advanced algorithms for automated feature extraction, enhancing data fusion techniques, and improving the accessibility of remote sensing data. Additionally, integrating emerging technologies such as machine learning and artificial intelligence with GIS and remote sensing can further enhance the accuracy and efficiency of water resource assessments.

Figure 1 shows the image of GIS vs Remote Sensing as applicable to assessment of water resource management.

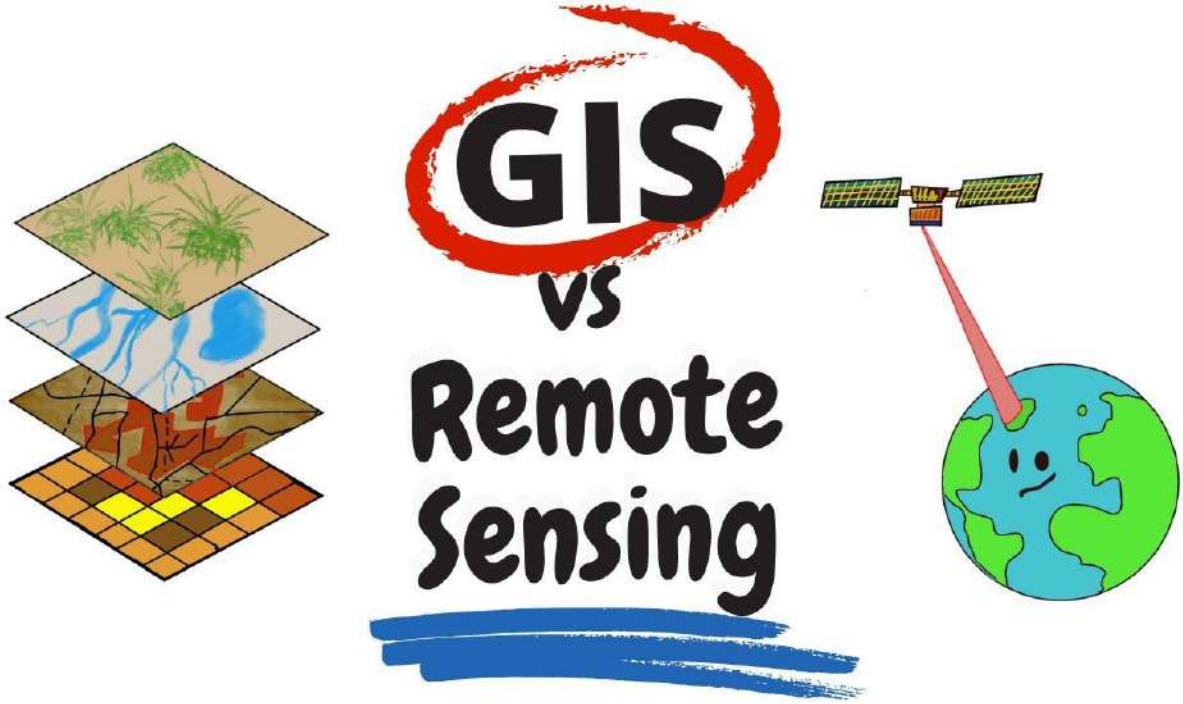

Figure 1: Image of Remote sensing vs GIS **Source:** ACGS India

2. HYDROLOGICAL MODELLING

Hydrological modeling plays a crucial role in understanding the behavior of water systems, predicting water availability, and assessing the impacts of land use and climate change on water resources (Dwarakish and Ganasri, 2015). GIS-based hydrological models integrate spatial data on terrain, land cover, soil properties, and precipitation to simulate the movement of water through the landscape. Remote sensing data, such as satellite imagery and aerial photographs, provide valuable inputs for model calibration, validation, and scenario analysis. Viljoen (2007) gave examples of GIS-based hydrological models to include the Soil and Water Assessment Tool (SWAT), the Hydrological Simulation Program-FORTRAN (HSPF), and the Distributed Hydrology Soil Vegetation Model (DHSVM). These models enable researchers and water managers to simulate streamflow, groundwater recharge, sediment transport, and pollutant loading under different land management practices and climate scenarios.

3. WATER QUALITY ASSESSMENT

Water quality study is the process of determining the chemical, physical and biological characteristics of waterbodies and identifying the possible contamination sources that degrade the quality of water (Vasistha and Ganguly, 2020). Degradation of the quality of water resources may result from waste discharges, pesticides, heavy metals, nutrients, microorganisms, and sediments.

Maintaining water quality is essential for human health, ecosystem integrity, and sustainable development. GIS and RS techniques facilitate the assessment of water quality by integrating spatial data on land use, land cover, topography, and hydrology with in-situ measurements and water quality parameters obtained from satellite sensors (Hall and Hossain, 2020).

Gholizadeh *et al.,* (2016) reported that remote sensing imagery, such as multispectral and hyperspectral data, can detect changes in water quality indicators, including chlorophyll-a concentration, turbidity, dissolved oxygen, and nutrient levels.

4. MONITORING OF WATER AVAILABILITY

Monitoring water availability is essential for water resource planning, drought management, and disaster response (Vargas and Paneque, 2019). GIS and RS technologies offer cost-effective solutions for monitoring surface water bodies, groundwater levels, snow cover, and soil moisture content over large spatial extents and temporal scales. Satellite-based remote sensing platforms provide synoptic views of water bodies, allowing for the estimation of surface area, volume, and changes in water levels. Microwave remote sensing techniques, such as Synthetic Aperture Radar (SAR), can penetrate cloud cover and vegetation to monitor soil moisture and groundwater dynamics (Wagner *et al.,*2007).

5. CHALLENGES AND FUTURE DIRECTIONS

Wilson *et al.,* (2000) reported that despite their numerous benefits, GIS and RS techniques face several challenges in the evaluation of water resources. These include data availability and quality issues, technical limitations, and the need for capacity building and interdisciplinary collaboration. Future research directions include the integration of advanced modeling techniques, such as machine learning and artificial intelligence, the development of standardized protocols for data collection and analysis, and the enhancement of spatial resolution and temporal frequency of remote sensing data.

6. CONCLUSION

In conclusion, GIS and RS technologies play a vital role in evaluating water resources by providing valuable tools for hydrological modeling, water quality assessment, and monitoring of water availability. These techniques enable researchers and water managers to make informed decisions and implement sustainable management practices for the conservation and equitable distribution of water resources. However, addressing existing challenges and embracing emerging technologies are essential to enhance the effectiveness and applicability of GIS and RS in water resource management. Furthermore, GIS and remote sensing have emerged as indispensable tools for water resources evaluation, offering unprecedented capabilities for data analysis, monitoring, and decision-making. By leveraging these technologies, stakeholders can better understand hydrological processes, mitigate water-related risks, and promote sustainable water management practices. Continued research and innovation are essential to overcome existing challenges and unlock the full potential of GIS and remote sensing in water resources assessment.

REFERENCES

Dwarakish, G.S., Ganasri, B.P. (2015). Impact of land use change on hydrological system: a review of current modelling approaches, article 1115691. Cogent Geoscience vol. 1, Issue 1 https://doi.10.1080/23312041

Evsahibloglu, A.N. (2015). Integration of remote sensing technology to geographic information system for sustainable planning of water resources. Fourth international conference on agro-geoinformatics pp. 25-87

Fisher, J.B, Melton, F., Middleton, E. (2017). The future of evapotranspiration: global requirements for ecosystem functioning, carbon and climate feedback, water resource research. Advancing Earth and Space Science https://doi.org/10.1002/2016WR020175.

Gholizadeh, M.H., Melesse, A.M., Reddi, L. (2016). A comprehensive review on water quality parameters estimation using remote sensing techniques. Sensors 16 (8) 2016. https://doi.org/10.3390/S16081298

Hall, J., Hossain, A.K.M.A. (2020.) Mapping urbanization and evaluating its possible impacts on stream water quality in Tennessee using GIS and remote sensing. Sustainability volume 12, issue 5, https://doi.org/10.3390/SU12051980;

Vargas, J., Paneque, P. (2019). Challenges for the integration of water resource and drought-risk management in Spain-sustainability volume 11, issue 2: https://doi.org/10.3390/SU11020308

Vasistha, P., Ganguly, R. (2020). Water quality assessment of natural lakes and its importance: an overview-volume 32 part 4, 2020, pages 544-552. Materials today proceeding.

Viljoen, S.J. (2007). Creation of a hydrological modelling environment to assist in the decision-making of water-related activities. Central University of Technology, Free State. Faculty of engineering and information technology; https://hdel.handle.net/11462/96

Wagner, W., Bloschl, G., Pampaloni, P., Calvet, J.C. (2007). Operational readiness of microwave remote sensing of soil moisture for hydrologic applications. Hydrology research journal volume 33, issue 38(1) 1-20; https://doi.org/10.2166/nh.2007.029

Wilson, J.P., Mitasova, H., Wright, D. (2000). Water resource applications of geographic information systems pp. 61-73 volume 12 number 2. Spring 2000 journal of the urban and regional information systems association.

PAPER 34 - Adaptive and Personalised VARK E-Learning System Design Based on Open-Source Applications

A. M. Abdelaziz[1], S. A. Darma[1*], M. K. Abubakar[1]

[1]Department of Computer Science and Information Technology, Al-Qalam University, Katsina, Nigeria.
[*]Email: sanusiabudarma69@gmail.com

ABSTRACT
For students who struggle with more conventional forms of instruction, there are a variety of freely accessible resources that can be used to create comprehensive, intelligent learning environments. This study investigates the adaptability of e-learning platforms and builds a flexible learning system to aid in the evaluation of users' learning preferences through the use of VARK questions, which stand for Visual, Auditory, Read/Write, and Kinesthetic. In order to facilitate the development of modules to assist in the learning process of adaptable and individualised e-learning systems, the system has extracted materials from an online free source while keeping in mind the usability viewpoint and a broad variety of criteria. The data extraction procedure was improved and optimized with ontology. The development of various models has encouraged the incorporation of adaptability and personalisation features. One such model is the learner's model, which incorporates the student's needs, details, and study domains into the system. This model is based on learning style theories, which are used to identify users and enhance their online learning experience. By efficiently delivering personalised learning materials to users from the vast array of open-source apps on the web or through search engines, the system provided a groundbreaking addition to adaptive e-learning systems. The system has improved with the use of evaluation and feedback provided at the beginning of each learning session, providing a more tailored experience for each learner's style.

KEYWORDS: Adaptive Learning System, Personalized Learning, Learning Style, E-Learning, Open-Source

1. INTRODUCTION

Online education, on the other hand, is defined as the process of influencing education via the use of information and communication technology and contemporary digital media. Online courses make higher education accessible to individuals who struggle with or are unable to participate in more conventional classroom settings (Billett and Choy, 2013). The adaptable and individualized e-learning platform gives students access to educational materials by facilitating an information transfer process (Aeiad & Meziane, 2018). Currently, e-learning platforms do not offer personalized learning alternatives to learners, as identical knowledge and practices are available to all users. Personalisation is defined as providing learning content to various learners based on an assessment of their talents, knowledge, and learning priorities (Bittencourt et al., 2008). The fundamental objective of personalised learning approaches is to adapt the instruction according to the particular skills and needs of the learner. Certain barriers, like distance, time, etc., to accessing education are eradicated by the tailored learning technique (Karagiannidis & Sampson, 2002).

Adaptable e-learning systems have been used by many people all across the world. However, the considerable diversity of learners on the internet raises further issues for the traditional "one-size-fits-all" learning method, in which a single set of learning resources is supplied to all learners (Li & Chang, 2005). As a result, an adaptive and personalised e-learning system will be introduced to enhance the present comprehension and usage of conventional e-learning resources by applying free, open educational resources on the web to build and deliver content for individual learners. The system can be employed by individual learners, colleges that may not have the funds and skills to produce learning tools, and anyone who wishes to learn a certain field. The system will enable users to design custom learning content based on internationally recognised courses and materials. Using regular search engines to locate learning content suitable for specific learners is time-consuming and may not lead to an acceptable outcome. The fundamental impact of this project is to develop an intelligent system to aid with online course creation, testing, and assessment based solely on existing open-source software on the web.

Furthermore, the system has handled three key concerns. The first challenge is the identification of the learner's requirements, such as learning style and field of interest. The user can then specify a particular model to allow the system to give the exact information sought. The second challenge is defining the knowledge domain of a pre-selected area using an ontology to get appropriate learning resources from the web. Furthermore, this system will address the primary resemblance between the learning outcomes specified by conventional curricula and the content gathered from relevant websites to enable appropriate learning of the subject. The last issue is the ability

of the adaptive and personalised learning system to update and adjust the material and learning style based on the interactions of the users with the system over time.

2. MATERIALS AND METHODS

2.1. Research Methodology

This study uses quantitative and qualitative approaches to obtain all the relevant information for this analysis based on the research objectives. Moreover, when both quantitative and qualitative research techniques are employed, it simply suggests that data has been collected and assessed in a mixed research method manner to have a comprehensive knowledge of the study problems that may not be known using only one method (Morse, 2016). Quantitative and qualitative applications in this study complemented each other by delivering thorough and clear knowledge of analysing the research problems (Palinkas et al., 2013).

2.1.1. Research Process

Research is studied in different definitions by numerous writers; the importance of the research process is supplied by Saunders et al. (2009), as it indicates that research provides a platform on which the research approach can be built. However, research onions might go with almost different research techniques. The research onion highlights the layers and discusses the functions carried out in every stage of the layers. The layers include the research philosophy, research strategies, research techniques, research choice, research processes, data collection, and time zone, as depicted in Figure 1 below.

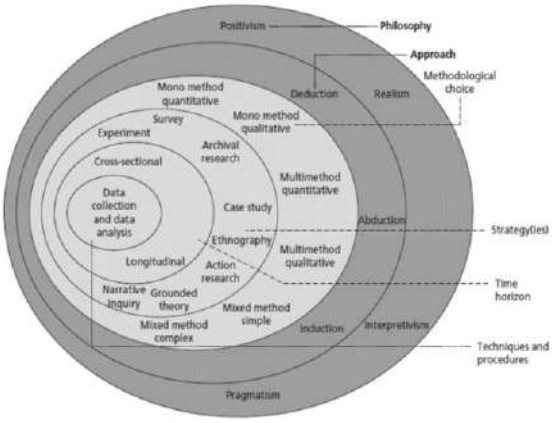

Figure 1: Research Onion (Dudovskiy, 2019)

2.1.2. Research Philosophy

Research philosophy is a system of assumptions and beliefs about the development of knowledge (Saunders et al., 2016). The study methodology and approaches were selected based on these assumptions. It also helps the researcher analyse and recognise the most relevant approaches to be applied in the entire research process by encouraging the researchers to be more creative in adjusting the required research approach. Research philosophy is separated into three: interpretivism, positivism, and pragmatics, as depicted in Figure 2 below.

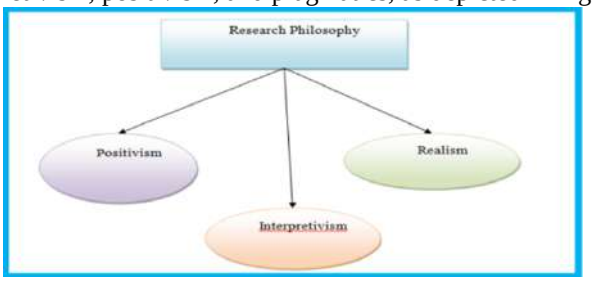

Figure 2: Research Philosophy

Research philosophy comprises three essential assumptions about how we interpret the world (Saunders et al., 2016). They include;

- Ontology: assumptions about the nature of reality.

- Axiology: techniques and nature of how academics evaluate their research.
- Epistemology: assumptions that create accurate knowledge.

Table 1 below outlines these philosophical concepts of positivism and interpretivism.

Table 1: Philosophical Views of Positivism and Interpretivism Assumptions

Philosophical Assumptions	Positivism	Interpretivism
Ontology	Social reality is objective to the researcher	Social reality is subjective to the researcher
Axiology	Objective posture is maintained by the researcher	Subjective posture is maintained by the researcher
	The findings are valuable and unbiased	The findings are prejudiced and not that valuable
Epistemology	Objective evidence supplies the knowledge	Subjective evidence arises from participants
Methods of Assumptions	Larger Samples, Quantitative Analysis, Deductive Research Approach	Smaller Samples, Qualitative Analysis, Inductive Research Approach

2.1.3. Research Approach

The research approach aims to provide a researcher with a platform to serve as a guide for selecting the most appropriate research methods and planning and defining data collection and analysis procedures based on the study objectives (Saunders et al., 2016). The research approach is classified into inductive and deductive approaches, as shown in Figure 2 above.

2.1.4. Research Strategy

The research strategy adopted for this research is the survey strategy, which satisfies the research objectives by allowing the researcher to examine the quantitative and qualitative data using inferential statistics and descriptions (Saunders et al., 2016). The questionnaire is the survey strategy to be employed, as it is extensively used in collecting standardized information from a large population in a very accommodating way of establishing comparisons (Bryman, 2016).

A questionnaire was designed and delivered to learners to gather information or data about their learning preferences. Moreover, the questionnaire is based on the VARK learning style, which comprises questions about learners' preferences in verbal, aural, read/write, and kinesthetic modes of learning. The questionnaire is based on the research technique (deductive), philosophy, and methodological way of acquiring data.

2.2. Data Collection Techniques

Data collection is seen as a significant and critical component of research outcomes, as it supports the research's claim with strong evidence to make the theoretical model more applicable (Xian & Meng-Lewis, 2018). Data collecting approaches are classified into primary and secondary tactics used to gain data for this research.

2.2.1. Primary Data

Primary data is a collection of original data that has yet to be analysed, reviewed, or summarised by other researchers' work (Zikmund et al., 2010). Researchers gather a range of data according to their needs (Xian & Meng-Lewis, 2018). The main techniques by which primary data can be obtained include focus groups, interviews, and questionnaires (Xian & Meng-Lewis, 2018). The questionnaire was used in this study to collect primary data.

2.2.1.1. Questionnaire

According to Oppenheim (2000), questionnaires are the most effective strategy, accessible to respondents, and cost-efficient compared to interviews. The Bristol Online Survey (BOS)/JISC Online Survey is used to administer the questionnaire for this survey.
The questionnaire was designed based on the VARK learning style questionnaire and the literature review (Xian & Meng-Lewis, 2018). The VARK learning approach is applied in this study, as indicated by Saunders et al. (2015), where the quality of the research data depends on the valid questions used by the researchers.

2.2.2. Secondary Data
These are the data gathered by prior researchers for various purposes (Xian & Meng-Lewis, 2018). This means that the secondary data can be summarised, published, or re-analysed based on the objectives of other researchers. For this project, secondary data is used to examine:

- Adaptability in e-learning systems
- Using open-source software to create an adaptable system framework
- Benefits of using e-learning technologies for adaptation
- Theories of learning, the learning model, and the adaptation model process
- Learners' or students' learning style
- How adaptable systems will assist in applying VARK for learning reasons

3. RESULTS AND DISCUSSION

3.1. Data Presentation and Analysis
Data analysis is the act or process of gathering, investigating, analysing, and comparing obtained data (Saunders et al., 2016). Qualitative and quantitative data analysis were used in this study, with the qualitative data shown descriptively and the quantitative data presented thematically. As a result, the statistical mechanism (BOS-Jisc Online Survey) was used to apply the research VARK questionnaire, which contains 101 respondents. In this research, the responses from the users are used for quantitative data analysis of the VARK learning style in adaptable and personalized system design using open-source apps.

3.1.1. Learning Profile Responses
The respondent's e-learning profile is the first phase of the questionnaire, which focuses on finding the features of the respondent's preferences during learning. This phase analysis reveals how learners wish to study, hours spent on computers, preferred methods of acquiring learning materials to know whether students previously utilised e-learning, and the learners' requirement to construct the learning support system. The following are the questionnaire data presentation and analysis based on the questions in the respondents' learning profiles.

Figure 3 below indicates that 38 (37.6%) of the respondents always choose to use computer displays to study, 23 (22.8%) prefer computer monitors, and 35 (34.7%) and 5 (5%) are neutral and do not prefer computer monitors to study, respectively. Generally, most learners choose computer monitors to learn.

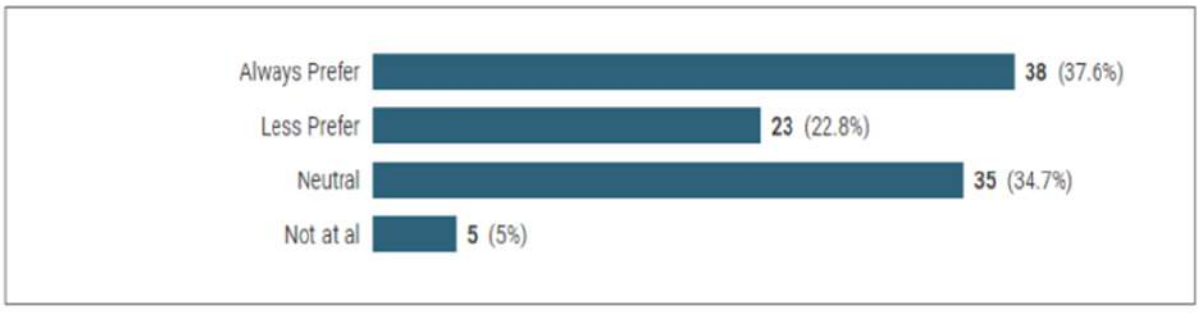

Figure 3: Question 1 - Respondents' Learning Profile

Figure 4 below shows that 20 (19.8%) of the respondents spent less than two hours on a computer, 36 (35.6%) spent three to four hours on a computer, 18 (17.8%) spent four to six hours on a computer, and 27 (26.7%) spent more than six hours on a computer. The majority of the learners spent three to four hours on a computer.

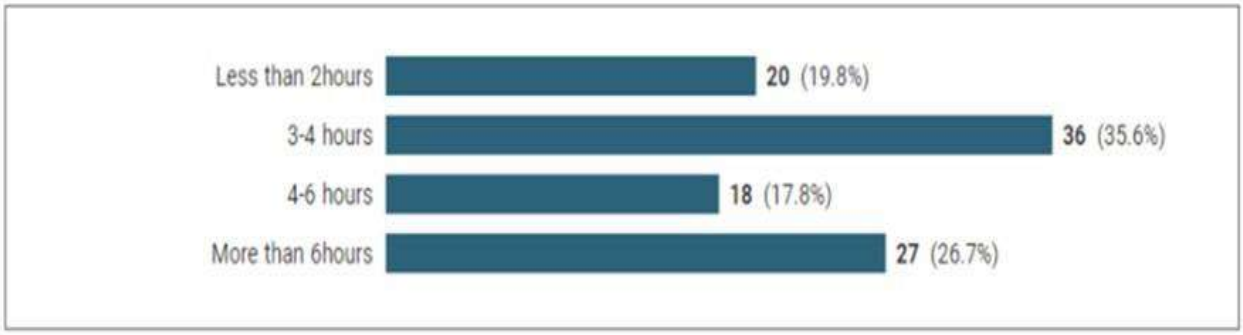

Figure 4: Question 2 - Respondents' Learning Profile

Figure 5 below shows that 28 (27.7%) of the respondents prefer the electronic way, 2 (2%) prefer the traditional technique, and 71 (70.3%) prefer both the conventional and electronic means of accessing learning materials. Most learners enjoy both traditional and technological means of accessing learning materials.

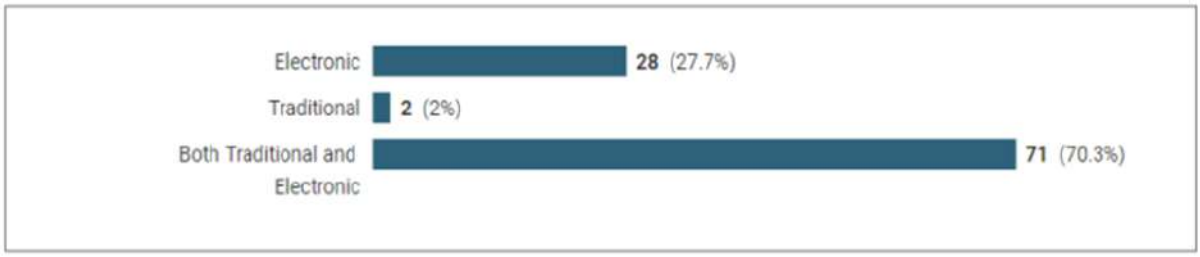

Figure 5: Question 3 - Respondents' Learning Profile

Figure 6 below shows that 23 (22.8%) of the respondents once used the e-learning system, and 53 (51.5%) commonly use the e-learning system in their day-to-day activities. It also reveals that 14 (13.9) and 12 (11.9) always utilise e-learning, and some have yet to use e-learning. Based on the survey responses, learners frequently use the e-learning system.

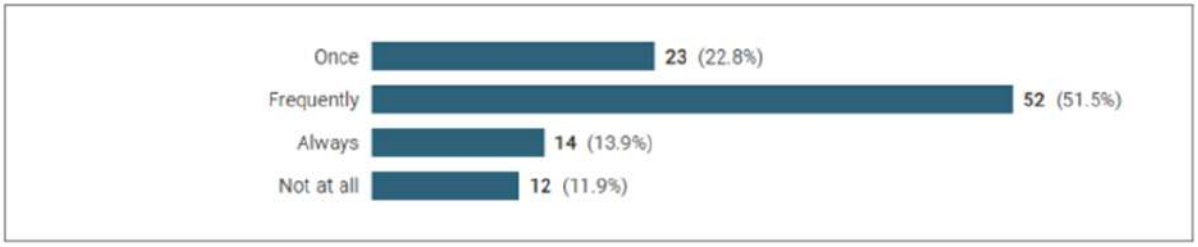

Figure 6: Question 4 - Respondents' Learning Profile

Figure 7 below reveals that 40 (39.6) of the respondents strongly agreed with the need for a learning support system, 46 (45.5) agreed to the essential requirement for a learning support system, and 12 (11%) and 3 (3%) were neutral and disagreed with the demand for a learning support system. The majority of respondents agreed that a learning support system was necessary to allow users to learn better.

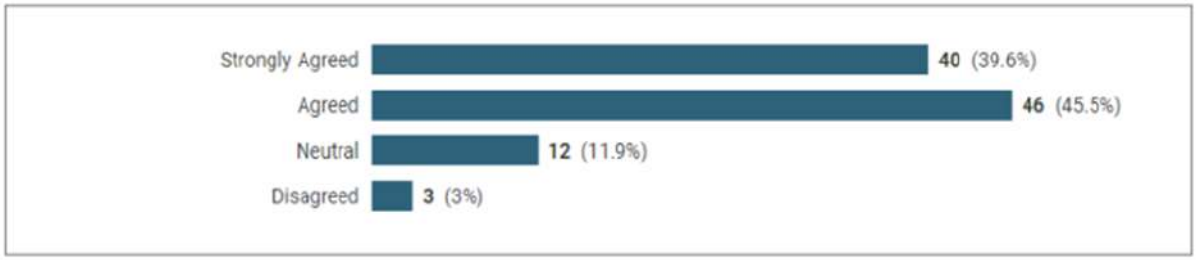

Figure 7: Question 5 - Respondents' Learning Profile

3.1.2. VARK Learning Style Responses

The VARK learning style responses reveal the most consistent findings about varied learning preferences (Lohri-Posey, 2003). VARK is essential because learners realize they are instinctively fit to practice. Learning preferences differ from strengths (Alkhasawneh et al., 2008). The cumulative scores for each VARK question reveal how the respondents prefer to learn. For improved understanding, learners with the multi-dimensional model set of the VARK learning style need to analyze facts in different modalities. The following questionnaire responses are based on the VARK questionnaire used in this research to examine learners' preferences in e-learning.

3.2. Discussion and Evaluation of the Vark Questionnaire

Peter et al. (2008) undertakes a study on certain regularly utilised learning styles and the approaches they are applying in the field of adaptive e-learning. Suitable learning styles were assessed using the Karagiannidis & Sampson (2002) criteria to identify the right learning methodology for the e-learning domain. Evaluation criteria for flexible learning styles were established in terms of descriptiveness, measurability, and time effectiveness (Karagiannidis & Sampson, 2002). In this research, the most relevant learning styles offered to the learner to promote customization and flexibility were based on the prior criterion.

Measurability: In order to determine whether a personalised and flexible learning environment is most suited to a student's needs, it is necessary to determine whether the learning style model is measurable (Karagiannidis & Sampson, 2002). There is an appropriate and pertinent questionnaire for the type of learning used and evaluated in this study.

Time Effectiveness: The amount of time it would take the student to complete the questionnaire, and how well the questions related to the desired customization were used to evaluate the learning styles. Using the most time-efficient strategy yields high results for this class, whereas using the least time-efficient technique yields low results (Alkhasawneh et al., 2008). The learning style assessment was determined by the learner's perceived necessity to complete the survey and the relevance of the questions to the desired level of customisation were the determinants of the learning style assessment.

Descriptiveness: In this section, we'll go over the system's learner classifications and the method for changing a student's specific learning category. The Felder-Silverman tools classify people based on their preferred method of learning, which can be sequential or global, sensory or intuitive, active or introspective, or visual or verbal.

3.2.1. Validity

This study investigated the dimensionality of the VARK learning styles inventory. The VARK measures four perceptual preferences: visual (V), aural (A), read/write (R), and kinesthetic (K). VARK questions can be referred to as testlets because respondents can select a large number of items within a single question. The correlations between items inside testlets are a type of method effect. To determine the VARK's dimensionality, four multitrait-multimethod confirmatory factor analysis models were tested. For the VARK scores, the correlated trait-correlated method model provided the best fit. The estimated reliability coefficients were sufficient. The study discovered preliminary evidence for the validity of the VARK scores. Potential issues with item wording and the scale's scoring algorithm were identified, and cautions about using the VARK in research were highlighted.

3.2.2. Reliability

This study also shows that Cronbach's alpha underestimates the dependability of VARK scores because it assumes that all items are parallel measures of the construct, which is not the case with VARK. As a result, they estimated dependability using confirmatory factor analysis. The VARK subscale scores had reliability estimates of .85, .82, .84, and .77, respectively, which is considered good given that the VARK is not used for high-stakes selections.

Table 2: Evaluation of the Vark Questionnaire

	Learning Style Preference Responses by %			
Questions	**V**	**A**	**R**	**K**
Q1	25.7%	49.5%	7.9%	16.8%
Q2	29.7%	18.8%	9.9%	41.6%
Q3	30.7%	10.9%	16.8%	41.6%
Q4	39.6%	11.9%	18.8%	29.7%

Q5	11.9%	51.5%	16.8%	19.8%
Q6	5%	73.3%	9.9%	11.9%
Q7	18.8%	9.9%	9.9%	61.4%
Q8	14.9%	29.7%	19.8%	35.6%
Q9	15.8%	47.5%	29.7%	6.9%
Q10	10.9%	34.7%	31.7%	22.8%
Q11	38.6%	26.7%	22.8%	11.9%
Q12	14.9%	28.7%	28.7%	27.7%
Q13	60.4%	27.7%	7.9%	4%
Q14	16.8%	13.9%	26.7%	42.6%
Q15	53.5%	6.9%	16.8%	22.8%
Q16	16.8%	26.7%	34.7%	21.8%
Overall Style% = Sum of Percentage / Number of Questions	404 / 16 = 25.25%	468.3 / 16 = 29.26%	308.8 / 16 = 19.25%	418.9 / 16 = 26.125%
Total	25.25% + 29.26% + 19.25% + 26.125% = 99.885 ~ 100%			

4. CONCLUSION

The findings are given and discussed in the earlier sections, leading to the system's effective development based on the aim, research questions, and objectives. E-learning is one of the primary parts of information technology widely employed globally. These research findings have presented a background for an adjustable and customisable system design employing open-source software. The research examines the theories of learning, adaptability in learning systems, flexible system components, and comparative evaluation of learning systems. Moreover, after reviewing numerous approaches, the right method is picked. The system design and implementation deliver adaptability based on the learners' feedback from the VARK questions answered to establish the preferred learning style. The implemented system is built based on the VARK learning style, which stands for visual, auditory, read/write, and kinesthetic (VARK) learning tools for various future learning domains. The recommendation will assist improve the flexible and personalized e-learning system design functions based on open-source software but will require future work or study. Conformance to specification, system evaluation by some learners, project sample technique, and time horizon were examined with the social, ethical, and legal concerns associated to the research and the system development.

ACKNOWLEDGEMENT

The authors would like to offer their gratitude to all respondents who participated in the study. Also, thank the Dean of the College of Computing and Information Science for his maximum support and direction. The entire community of Al-Qalam University, Katsina, for all the support. They would like to express their appreciation to the editor and the reviewers for their useful comments.

REFERENCES

Aeiad, E., & Meziane, F. (2018, November 28). An adaptable and personalised E-learning system applied to computer science Programmes design. Education and Information Technologies. https://doi.org/10.1007/s10639-018-9836-x

Alkhasawneh, I. M., Mrayyan, M. T., Docherty, C., Alashram, S., & Yousef, H. Y. (2008, July). Problem-based learning (PBL): Assessing students' learning preferences using vark. Nurse Education Today, 28(5), 572–579. https://doi.org/10.1016/j.nedt.2007.09.012

Bittencourt, I.I., Isotani, S., Costa, E.D., & Mizoguchi, R. (2008). Research Directions on Semantic Web and Education. https://api.semanticscholar.org/CorpusID:16459129

Bryman, A. (2016). Social Research Methods (5th ed.). London: Oxford University Press.

Chang, Y. C., Li, J. W., & Huang, D. Y. (2022). A Personalized Learning Service Compatible with Moodle E-Learning Management System. Applied Sciences (Switzerland), 12(7). https://doi.org/10.3390/app12073562

Diaz, F. S., Rubilar, T. P., Figueroa, C. C., & Silva, R. M. (2018, March). An Adaptive E-Learning Platform with VARK Learning Styles to Support the Learning of Object Orientation. 2018 IEEE World Engineering Education Conference (EDUNINE). https://doi.org/10.1109/edunine.2018.8450990

El-Sabagh, H. A. (2021). Adaptive e-learning environment based on learning styles and its impact on development students' engagement. International Journal of Educational Technology in Higher Education, 18(1). https://doi.org/10.1186/s41239-021-00289-4

Karagiannidis, C., & Sampson, D. (2002). Personalised Learning. Dialnet. https://dialnet.unirioja.es/servlet/articulo?codigo=1229979

Li, X., & Chang, S. (2005). A Personalized E-Learning System Based on User Profile Constructed Using Information Fusion. Distributed Multimedia Systems. https://dblp.org/rec/conf/dms/LiC05.bib

Lohri-Posey, B. (2003, March). Determining Learning Style Preferences of Students. Nurse Educator, 28(2), 54. https://doi.org/10.1097/00006223-200303000-00002

Murtaza, M., Ahmed, Y., Shamsi, J. A., Sherwani, F., & Usman, M. (2022). AI-Based Personalized E-Learning Systems: Issues, Challenges, and Solutions. IEEE Access, 10, 81323–81342. https://doi.org/10.1109/access.2022.3193938

Morse, J.M. (2016) Mixed Method Design: Principles and Procedures. Routledge.

Oppenheim, A.N. (2000) Questionnaire Design, Interviewing and Attitude Measurement. Bloomsbury Publishing.

Palinkas, L. A., Horwitz, S. M., Green, C. A., Wisdom, J. P., Duan, N., & Hoagwood, K. (2013, November 6). Purposeful Sampling for Qualitative Data Collection and Analysis in Mixed Method Implementation Research. Administration and Policy in Mental Health and Mental Health Services Research, 42(5), 533–544. https://doi.org/10.1007/s10488-013-0528-y

Peter, S., Dastbaz, M., & Bacon, L. (2008, June 30). Personalised e-learning, Semantic Web and Learning Ontologies. Learning & Technology Library (LearnTechLib). https://www.learntechlib.org/primary/p/28621

Ristić, I., Runić-Ristić, M., Savić Tot, T., Tot, V., & Bajac, M. (2023). The Effects and Effectiveness of An Adaptive E-Learning System on The Learning Process and Performance of Students. International Journal of Cognitive Research in Science, Engineering and Education, 11(1), 77–92. https://doi.org/10.23947/2334-8496-2023-11-1-77-92

Saunders, M., Lewis, P., & Thornhill, A. (2009, January 1). Research Methods for Business Students. Pearson Education. http://books.google.ie/books?id=u-txtfaCFiEC&pg=PA95&dq=0273716867&hl=&cd=1&source=gbs_api

Saunders, M. N. K., Lewis, P., & Thornhill, A. (2015, July 15). Research Methods for Business Students PDF eBook. Pearson Higher Ed. http://books.google.ie/books?id=vUdOCgAAQBAJ&dq=1292016647&hl=&cd=1&source=gbs_api

Saunders, M., Lewis, P. and Thornhill, A. (2016) Research Methods for Business Students. 7th Edition, Pearson, Harlow. http://books.google.ie/books?id=vUdOCgAAQBAJ&dq=1292016620&hl=&cd=1&source=gbs_api

Tsolis, D., Stamou, S., Christia, P., Kampana, S., Rapakoulia, T., Skouta, M., & Tsakalidis, A. (2010). An adaptive and personalized open-source e-learning platform. Procedia - Social and Behavioral Sciences, 9 (May 2014), 38–43. https://doi.org/10.1016/j.sbspro.2010.12.112

Urdan, T. A., & Weggen C. C. (2000). Corporate e-Learning: Exploring a New Frontier. WR Hambrecht + Co.

Xian, H., & Meng-Lewis, Y. (2018, March 19). Business Research Methods for Chinese Students. SAGE.

Zikmund, W. G., Babin, B. J., Griffin, M., & Carr, J. C. (2010, January 1). Business Research Methods. Cengage Learning. http://books.google.ie/books?id=pexMPgAACAAJ&dq=1111826927&hl=&cd=1&source=gbs_api

PAPER 35 - MODELING OF CRITERIA AIR POLLUTANT EMISSIONS IN AND AROUND CASSAVA GRANULES PROCESSING IN OYO STATE, NIGERIA.

J.A Adeniran, R. O. Yusuf, N. G. Aremu*, A. S. Atanda, E. T. Odediran

Department of Chemical Engineering, University of Ilorin, Ilorin, Nigeria.

*Email: Aremuola01@yahoo.com

ABSTRACT

The processing of cassava leads to an elevation in atmospheric air pollutants, consequently affecting the surrounding communities. This study modelled the dispersion of NOx, CO, SO_2, VOCs, and PM_{10} from cassava processing in Oyo town, Nigeria using American Meteorological Society/Environmental Protection Agency Regulatory Model (AERMOD). Emissions from 10-point sources were considered with 5 different scenarios. One year of hourly meteorological observations was used for the investigation of dispersion. The daily NOx Federal Ministry of Environment - Nigeria (FMEnv) limits were exceeded in all sampling locations and each of the scenarios respectively. Particulates were detected in all the sampling locations. The cumulative gaseous pollutants resulting from simultaneous operations of all the identified air emissions from the worst-case scenario are 19.9–301.3% of their respective 24-hour limits. However, the 24-h SO_2 and VOCs are breaching the limits at scenarios 1, 3, and 5 respectively with value ranges from 18.88-37.8% for SO_2 and 9.97-19.95% for VOCs respectively. This emission inventory information is expected to guide researchers and policymakers to know the fate and effects of aerosol emission in the area for adequate air quality management.

KEYWORDS: Air quality, Cassava processing, Modeling criteria, ParticulaPollutant monitoring

1 INTRODUCTION

Air quality degradation has been observed in several areas of the world due to rapid industrialization, urbanization, population growth, and increased vehicular emissions (Carley and Christie, 2017). Rapid industrialization in the urban areas of Nigeria is of great threat to air quality (Adeniran *et al.*, 2016). Different industrial activities are degrading various environmental components like water, air, soil, and vegetation (Lohan *et al.*, 2018). The World Health Organization has estimated that air pollution is responsible for seven million premature deaths per year in the world (Murray *et al.*, 1996). Gaseous emissions and particulate matter can be regarded as the most abundant harmful air pollutant found in the ambient air of industrialized environments (Wagner *et al.*, 2018).

Cassava plays a major role in increasing African food supplies because of its efficient food production, availability, tolerance to extreme stress conditions, and suitability to present farming (Oyegbami *et al.*, 2010). It was estimated that over 70% of cassava yield in Nigeria is processed into 7- 10 million tons of garri (cassava flour) annually (Ozoegwu *et al.*, 2017). People engage in the local processing of the product in many towns in southwestern Nigeria (Teye *et al.*, 2017). The processing of cassava to garri after harvesting is intensive during the dry season which contributes significantly to the ambient air pollution (Abass *et al.*, 2019). Open frying is the most common method used by garri processors (Bechoff *et al.*, 2019). Firewood is the major source of fuel in this industry (Parmar *et al.*, 2019). Cassava is now being processed into flour in industries due to the Federal Government of Nigeria's policy of 10% inclusion of Cassava flour into bread making (Saranraj *et al.*, 2019). However, along with the positive effect of cassava flour production, some negative impacts on the environment have also arisen (Adepoju *et al.*, 2019). Cassava processing, especially in areas where the industry is highly concentrated is regarded as pollution and a burden on natural resources (Parmar *et al.*, 2019).

The processing of cassava flour is divided into eight unit operations and the steps are: peeling, washing, grating, dewatering or pressing, agitation, roasting or frying, sieving, and finally packing for sales (CAMPUS, 2010). Hazards arising from cassava processing are associated with different processing steps that lead to food products (Olaniran *et al.*, 2017). The most widely adopted method (traditional method) of cassava processing has also led to various high emissions of pollutants generated due to smoke in the roasting environment (Escobar *et al.*, 2018).

The major air emissions are carbon monoxide (CO), oxides of nitrogen (NOx), carbon dioxide (CO2), particulate matter of 10.0 microns in diameter (PM10), sulphur dioxide (SO2), particulate matter of 2.5 microns in diameter (PM2.5) and volatile organic compounds (VOCs) which comes from cassava processing industries (Stewart, 2017). Pollutants are released from grating, dewatering, agitation, frying, sieving, and packaging of the final product (Shittu *et al.*, 2016). Air pollutants released from cassava processing industries can have a negative impact on the environment and health (Kolawole, 2014). Adeniran *et al.*, 2019 showed that pollutants emitted from processing industries

increased morbidity and premature mortality of people living in the nearby receptor locations. A wide range of health challenges ranging from infertility, cancer, respiratory diseases, pulmonary and cardiovascular diseases have been attributed to exposure to PM and gaseous fuel (Balakrishnan *et al.*, 2019).

Information about air quality status and modeling of air pollutant concentration levels in Nigerian industrial areas is limited in the literature. Dispersion modeling tools that have proven useful in estimating the air quality impact of industrial activities on receptor environments include CALPUFF, AERMOD, and HYSPLIT (Adeniran *et al.*, 2019). AERMOD has been described as a more refined dispersion model in complex and simple terrain for determining the impact of air pollutants emanating from industrial sources on receptors (Moharreri *et al.*, 2019). The AERMOD View modeling system is the current EPA (Environmental Protection Agency)-approved model for regulatory compliance applications and is recommended for field impacts up to 50 km from a facility (emission source). Determination of concentration levels of pollutants transported to the nearby communities is important. This will assist in the evaluation of associated potential risks and the formulation of relevant policies and control measures. The prime objective of this study is to investigate the concentration levels of pollutants associated with the operations of the industries to ambient air quality.

2. Methodology

2.1. Description of the sampling location

Oyo is a town in Oyo State, Nigeria. The town has a population of 442,699 people, located within longitudes 3o 54‟11.48‟ E and 3o 57‟33.46‟ and latitudes 7o 48‟18.79‟ N and 7o 52‟41.07‟ N (Njoku and Alagbe, 2015). It is about 52km north of Ibadan, 166km to Lagos, and 480km to Abuja (Isibor, 2016). Oyo town and her suburbs are located in three (3) Local Government Areas (LGAs) namely: Atiba, Oyo East, and Oyo West Local Government Areas (Ogunseye *et al.*, 2015). It has an equatorial climate notably with dry and wet seasons, average daily temperature ranging between 25℃ and 35℃ (ODUDU, 2019). Notable cassava granule processing factories were chosen as study locations. These include Ilora, Irepo, Ajonibadi, Sabo Oke Oranyan, Sabo Sakutu Agbo Ogede, Iwanikan School of Science, Olomowewe Amulekanwo, Isale Oyo Commercial, Ajegunle and Elere. The selected sampling locations' characteristics are presented in Table 1 while Figures 1 and 2 show a map of the selected sampling locations.

Table 1: Sampling locations

Sampling location	LGA	Latitude	Longitude	FP	Milling machine	Population
GR1	Afijio	7˚ 48˙5”	3˚ 55’ 0”	600	200	7400
GR2	Oyo West	7˚ 50’ 53”	3˚ 54’ 18”	560	80	1200
GR3	Atiba	7˚ 86’74”	3˚ 93’ 52”	76	25	529
GR4	Atiba	7˚ 85’ 01”	3˚ 90’ 75”	30	8	332
GR5	Atiba	7˚86’ 636”	3˚ 93’ 142”	200	40	1680
GR6	Atiba	7˚ 86’ 849”	3˚ 93’ 524”	288	72	4320
GR7	Oyo	7˚ 86’ 77”	3˚ 92’ 367”	24	4	58
GR8	Atiba	7˚ 87’ 236”	3˚ 91’ 044”	420	84	2100
GR9	Oyo East	7˚ 85’ 12”	3˚ 95’ 585”	195	65	2405
GR10	Oyo East	7˚ 88’ 353”	3˚ 94’ 398”	750	250	9250

2.2. Air Quality Assessment

2.2.1. Particulate matter (PM) monitoring

Particulate matter (PM) was measured during this survey with an AEROCET 531S Particle Count Monitor, supplied by Met One Instruments. It contains a 6V self-contained battery pack, a vacuum pump, an isokinetic probe, an electronics microprocessor with a computer interface, and an LCD all in one small package. Its PM_{10} of the total particulates was the focus of these measurements.

2.2.2. Gaseous pollutants monitoring

All the gaseous pollutants were monitored with the Aeroqual Series 200 monitor analyzer, an environmental air monitoring equipment. It is embedded with a WinCE® computer that runs GrayWolf's WolfSense® 2009 application software for displaying, documenting, and logging key parameters. It is composed of two main components, a Series 200 monitor and a sensor head. The equipment monitors up to 20 sensors and simultaneously generates 30 readings and runs on a rechargeable battery that can last 15 h of continuous measurements. It has a facility for Short-Term Exposure Limit (STEL) from which the carbon monoxide concentration for the last 15 min can be determined; the Time Weighted Average (TWA) from which the accumulated reading of the gas concentration since the monitor was turned on is divided by 8 h; and the Peak Reading, which is the highest reading since the monitor was turned on. Its resolution for NO, NO_2, and O_3 is 0.01 ppm and 0.1 ppm for SO_2, NH_3, VOCs, and CO. Concentration of SO_2 less than 0.1 ppm may not be detectable because of the detection limit of the SO_2 sensor.

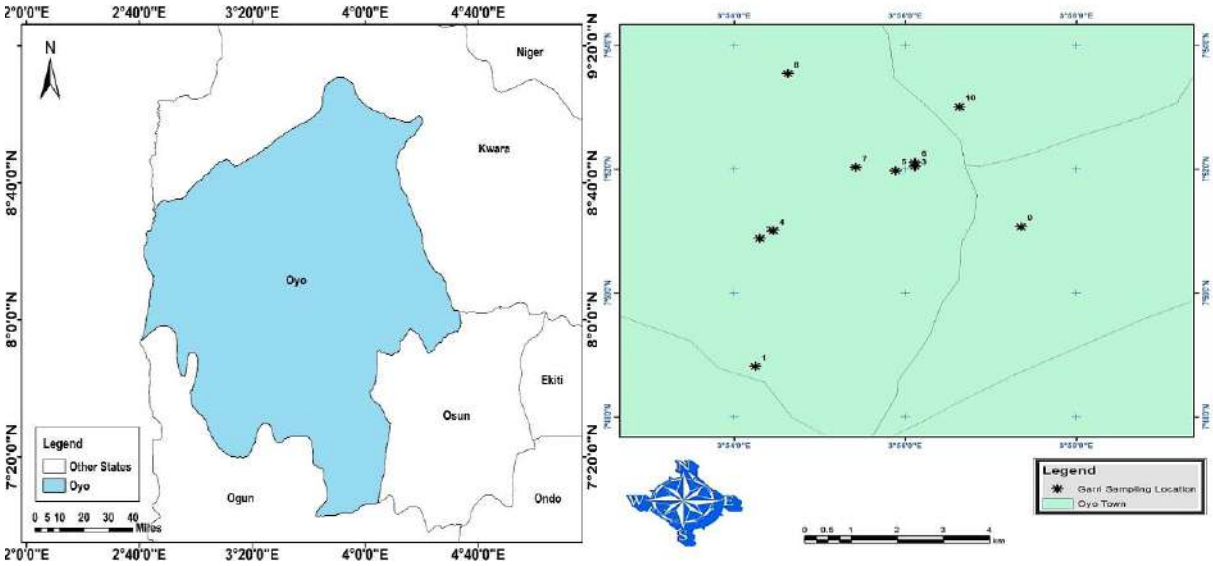

Figure 1: Map of the study area

2.2.3. Air Quality Assessment

Several approaches were employed to assess the present air quality status in cassava processing industries in Oyo Township. These are comparisons with the Ambient Air Quality Standards (AAQS) and the use of air emission dispersion modeling.

2.2.4. Comparison with Ambient Air Quality Standards (AAQS)

The present air quality status of cassava processing industries and their host Communities was investigated by determining their level of compliance with the National and World Bank Ambient Air Quality Standards as shown in Table 3.

2.3. Air pollutants contribution determination

The air pollutant from the factory to ambient levels in the communities was determined using the ISC-AERMOD View version 16216. The major sources of air emissions from the factories include grating, agitation, frying, sieving, and packing.

2.4. Emission modeling protocol

This air emission modeling exercise used the AERMOD View emission dispersion modeling software version 16216. It uses pathways that compose the run stream file as the basis for its functional organization. These pathways include the Control Pathway (CO) where the modeling scenario and the overall control of the modeling run are specified; the Source Pathway (SO), where the sources of pollutant emissions are defined; the Receptor Pathway (RE), where the receptors to determine the air quality impact at specific locations are defined; Meteorology Pathway (ME), where the atmospheric conditions of the area being modeled are defined, so it can be taken into account when determining the distribution of air pollution impacts for the area; Terrain Grid Pathway (TG), where the option of a gridded terrain data to be used in calculating dry depletion in elevated or complex terrain are taken; Output Pathway (OU), where the

output results necessary to meet the needs of the air quality modeling analyses are determined. Modeling parameters are shown in Table 4.

2.5 Emission sources input scenarios

Five operational scenarios of air emission from the identified sources at the factory were considered in this study. The scenarios estimated the ground level concentrations of air pollutants associated with the operation scenarios within the factory and at it host communities for the prevailing meteorological conditions. The five operational scenarios investigated are as summarized in Table 2 with worst case scenario from scenario 1 where all the frying point and milling machine were fully working.

Table 2: Operational scenario

Scenario	Operation
1	All milling and frying point were working
2	100% milling machine is working
3	100% wood burning (frying point) is working
4	50% milling is working
5	50% wood burning (frying point) is working

Table 3: Standards of ambient air quality

Pollutants	Average Time	NAAQS	WB	WHO
CO	24-Hr	11,400	-	-
NO_x	24-Hr	113	150	-
SO_2	24-Hr	26	-	20
PM_{10}	24-Hr	250	80	50
VOCs	24-Hr	20	-	-

Table 4: Modeling parameter

SP/Characteristics	GR1	GR2	GR3	GR4	GR5	GR6	GR7	GR8	GR9	GR10
Frying Point	600	560	76	30	200	288	12	420	195	750
Garri production(tons/day)	500	160	57	15	50	40	5	252	9.75	150
Milling Machine	200	80	25	8	40	72		84	65	250
Diesel Consumption(liters)	3000	800	300	40	480	720	10	1680	650	250
Wood Consumption(tons/day)	1800	1600	228	90	600	1080	36	252	195	1875
POPULATION	7400	1200	529	332	1680	4320	58	2100	1430	6250
Area (m^2)	103124.51	94823.28	5074.92	13014.96	33863.00	48768.00	2026.92	71025.08	33020.50	12699.4
X-cord	12218.78	12231.31	12447.51	12253.64	12447.48	12476.77	12381.94	12273.16	12651.09	12554.87
Y-cord	12243.16	12462.43	12580.97	12476.34	12580.97	12590.73	12586.55	12749.71	12481.95	12692.54

2.5.2. Receptors locations

The cassava processing industries are located close to communities and settlements. Both the immediate and distant environments of the factory were considered as receptors to air pollutants in this study. All the significant receptors in a 50 km radius within the plant location were considered in this study to have a better understanding of the air pollutants emission impact of the processing industrial operations on the wider receptor environments.

2.5.3. Meteorological data

An essential input requirement of ISC-AERMOD View air dispersion modeling is the meteorological information. Surface and upper air observations of cassava processing industries host community, were compiled using data from Lakes Environmental observations (MET 134283) and the project acquired surface meteorological data on-site. The data obtained include temperature, wind speed, wind direction, relative humidity, sun intensity, air pressure, and dew point temperature. The data were incorporated in a format needed for the modeling software.

2.5.4 Emission Rate Calculation

The emission rate was calculated from Eq. 1 and 2 for milling machine and wood consumption respectively using Emission factors of the food production industrial approach as shown in Table 5 from AP-42 of the United States EPA (1995).

E_{is} = P * operating hours * E_f * $(\frac{100-ERi}{100})$ 1

E_{is} = quantity of fuel * $(\frac{100-ERi}{100})$ * E_f 2

Where, ERi = emission reduction efficiency, E_f = emission factor of substances in (g/Kg), P = engine power capacity rating

Table 5: Emission factors used in emission computation

Parameter	Emission factor
CO	180
NO_x	301
PM	6.78
SO_2	3.45
VOCs	2.09

Source: USEPA (1995)

3. Results and Discussion

3.1 Ambient air quality status in cassava processing industrial operations

The measured air quality parameters in Cassava processing industrial during the study are presented in table 5. The pollutants monitored in cassava processing industries were SO_2, NO_2, CO, PM_{10} and VOCs. The 24–hour average of the pollutant concentrations measured are indicated in Table 5. The daily SO_2 of the NAAQS limit was exceeded in all the sampling locations. The daily NO limit was breached in all sampling location. The highest value was recorded at GR4 while the lowest was recorded at GR2 as shown in Table 6. However, the daily PM_{10} breached the limit in four sampling locations including the GR2, GR3, GR4 and GR8. In all the sampling locations, the daily CO 11400µg/m^3 of the NAAQS limit was breached and the daily VOCs 20µg/m^3 NAAQS limit was breached in GR2, GR7, GR8 and GR10 during the study. The detected gaseous pollutants from cassava processing industries are combustion products, their sources could include the grating, frying and packing.

3.2. Ambient air quality in the host communities

The measured ambient air quality parameters in the communities during the study are summarized in Table 4. Air quality impact on Cassava processing is important to assess the impacts of emissions from Cassava processing industrial operations on their environment. Table 3 shows the dispersion model parameters for Cassava processing industries these include the emission estimate of criteria pollutants from area sources. The dispersion modeling outputs from the ISC-AERMOD View for 24-hour averaging periods for the criteria pollutants are shown in Figure 3 and Figure 3.2, while Tables 4.1 showing the results of maximum ground level concentration of air pollutant within 50 km for each of the scenarios obtained. The ground level concentration of the criteria pollutants from the sampling location was compared with the set limits of National Ambient Air Quality Standard (NAAQS), the results predicted the total emissions of criteria pollutant emitted per day in each scenario. For garri processing industries, ground-level concentrations of CO, NO_x, SO_2, PM and VOC for an averaging period of 24 h were established in the study as presented in Table 4.1. Figures 1–5 show the surface plots of the maximum predicted 24-h concentration of the pollutants in worst case scenario which has the highest number of wood consumption. The maximum daily ground-level concentrations of CO from garri processing industries were 58.7–568025 µg/m3. While the maximum daily ground-level concentrations of NOx from the industries were 160– 3750 µg/m3 with a mean of 75.33 µg/m3 , the maximum PM_{10} daily were 11.3–75323 µg/m3 with a mean of 2.0 µg/m3 . The maximum daily ground level concentrations of SO_2 were 0-038– 982 µg/m3 with a mean of 0.82 µg/m3 and the maximum VOCs daily were 11.8–119.618 µg/m3 with a mean of 0.64 µg/m3. From garri processing industries, the minimum of the maximum concentrations was obtained in scenario 4 and the maximum in scenario 1. All these ground-level concentrations were obtained at about 0.5 km and 2.5 km from the source. In scenario 1, daily CO was 568025µg/m3 while NOx was

3750µg/m3 with PM_{10} of 75323µg/m3, SO_2 levels of 982µg/m3, and VOC levels of 119618µg/m3. Scenario 2 daily levels of CO, NOx, PM, SO_2, and VOC were 71, 320, 22.6, 0.075, and 23.5µg/m3, respectively. The daily concentrations of CO, NOx, PM, SO2, and VOC in the scenario 3 were 567957, 2890, 75301, 982, and 119596µg/m3, respectively. The maximum daily predicted for CO, NOx, PM, SO2, and VOC in scenario 4 were 58.7, 160, 11.3, 0.038 and 11.8µg/m3, respectively and 283979µg/m3, 1285µg/m3, 37651µg/m3, 491µg/m3 and 59798µg/m3 were obtained respectively for CO, NOx, PM, SO_2, and VOC in scenario 5. The impacts of garri processing industries air emissions on ambient air quality were investigated by comparing the daily maximum ground-level concentrations of each of the investigated air pollutants with their National Ambient Air Quality Standard (NAAQS) recommended limits, the daily maximum emitted CO from garri processing industries activities in the country investigated was 50% of the 11,400 µg/m3 daily limit. While the daily maximum NOx was 33.12% of the 113 µg/m^3 limit, the daily maximum PM was 301% of the 250 µg/m^3 limit. The daily maximum SO2 from the garri processing industries was 37.8% of the 26 µg/m^3 limit and VOCs was 6% of 20 µg/m3. In scenario 1, 3 and 5 the pollutants exceeded the set standard, while scenario 2 and 4 where below the set standard except NOx and VOCs. Since emissions are directly proportional to the generation capacities, the higher the generation capacities the higher the volume of wood and diesel consumption hence, the higher the ground-level concentration predicted.

Table 6: Ambient air quality status in cassava processing industrial operations

S P	SO_2	NO_2	CO	VOCS	H_2S	NH_3	O_3	TSP	PM_{10}	$PM_{2.5}$
GR1	1883.74	4355.28	46717.08	0.96	537.31	5532.110	471.63	458.26	167.04	37.23
GR2	366.26	1406.60	27547.17	75.58	771.16	35796.48	395.080	663.21	252.32	37.18
GR3	1880.87	3290.66	35012.48	1.20	780.22	5408.10	277.53	1175.96	453.44	80.12
GR4	7112.76	5261.83	65896.42	8.27	4341.05	168697.10	1333.09	383.80	218.48	87.66
GR5	565.55	2445.41	24589.80	0.55	203.16	12690.44	506.57	300.16	111.26	35.19
GR6	1874.41	3481.26	39565.19	1.13	346.49	2861.43	216.53	209.18	107.93	60.17
GR7	1077.25	1019.46	19275.95	39.83	447.10	53866.4	135.33	98.75	52.45	27.80
GR8	3836.07	5858.66	66735.33	22.44	1203.52	68903.21	743.80	1399.02	595.97	53.41
GR9	2925.80	4316.57	57945.68	0.96	366.26	30903.43	133.58	448.08	234.93	49.38
GR10	1218.37	7194 .28	56272.58	22.65	376.56	44495.22	567.25	235.58	96.03	44.65

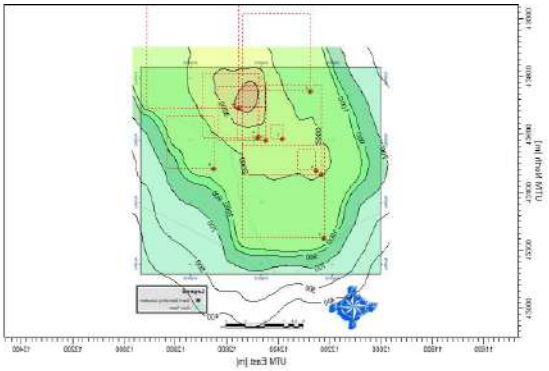

Figure 2: Isopleths of Ambient Pollutants Levels for 24-h NOx at the cassava processing industries for scenario 1 (Area Sources).

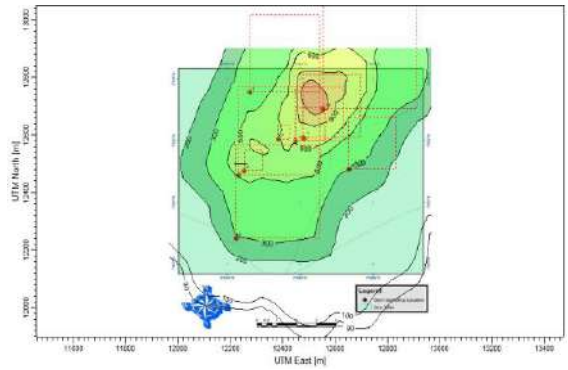

Figure 3: Isopleths of Ambient Pollutants Levels for 24-h SO_2 at the cassava processing industries for scenario 1 (Area Sources).

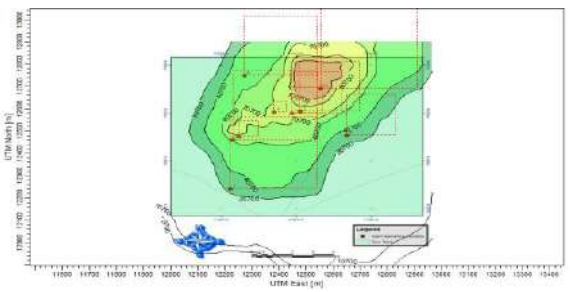

Figure 4: Isopleths of Ambient Pollutants Levels for 24-h VOCs at the cassava processing industries for scenario 1 (Area Sources).

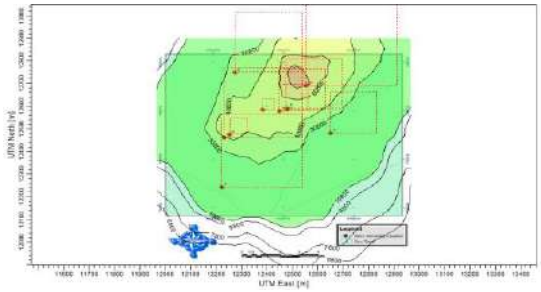

Figure 5: Isopleths of Ambient Pollutants Levels for 24-h PM_{10} at the cassava processing industries for scenario 1 (Area Sources).

4. CONCLUSION

The AERMOD dispersion model has been used in this study to evaluate the ground level concentration of pollutants from cassava processing industries in Nigeria to predict the air quality impact. Emissions for five operating scenarios were considered for area sources. The 24-hour averaging period of ground level concentration was measured and compared with Nigeria's ambient air quality set by the National Ambient Air Quality Standard (NAAQS), World Bank and World Health Organization (WHO) within 50 km receptor locations.

The modeling outputs in all scenarios, NOx exceeded the set limit, thereby causing harmful effects to the environment while CO, SO_2, PM_{10}, $PM_{2.5}$, and VOCs were all within the set standard for scenarios 2 and 3 and it shows that diesel consumption by milling machine is not major contributing factor to the air pollution in and around cassava processing industries in Nigeria. Scenarios 1, 3, and 5 exceeded the set limit for all the pollutants examined and it shows that firewood is the major source of air pollution for the industries. The study reveals that the contribution of emissions from criteria pollutant to its ambient air is significant. Possible impacts of anticipated emissions of criteria pollutants on humans, vegetation, soil and water are strong enough for necessary control measures to be implemented in cassava processing industries. Hence, the air quality standards guiding food production industrial emissions must be strictly considered, in order to ensure that the ground level concentrations do not exceed the required standard limits and prevent the adverse effect of air pollution in the Nigeria air shed.

Reference

Abass, A., Awoyale, W. and Alamu, E. (2019). Assessment of the chemical and trace metal composition of dried cassava products from Nigeria. *Quality Assurance and Safety of Crops & Foods, 11*(1), 43-52.

Adeniran, J., Yusuf, R., Jimoda, L., Fakinle, B. and Sonibare, J. (2016). Airborne Particulate Matter in the Atmospheric Environment of a Tobacco Manufacturing Plant. *UMUDIKE JOURNAL OF ENGINEERING AND TECHNOLOGY, 2*(2), 129-138.

Adeniran, J. A., Yusuf, R. O., Fakinle, B. S. and Sonibare, J. A. (2019). Air quality assessment and modelling of pollutants emission from a major cement plant complex in Nigeria. *Atmospheric pollution research, 10*(1), 257-266.

Adepoju, A., Oladeebo, J. and Toromade, A. (2019). Analysis of Occupational Hazards and Poverty Profile among Cassava Processors in Oyo State, Nigeria. *Asian Journal of Advances in Agricultural Research*, 1-13.

Balakrishnan, K., Dey, S., Gupta, T., Dhaliwal, R., Brauer, M., Cohen, A. J., Stanaway, J. D., Beig, G., Joshi, T. K. and Aggarwal, A. N. (2019). The impact of air pollution on deaths, disease burden, and life expectancy across the states of India: the Global Burden of Disease Study 2017. *The Lancet Planetary Health, 3*(1), e26-e39.

Bechoff, A., Tomlins, K., Bennett, B. and Westby, A. (2019). Variability in traditional processing of garri-a major food security product from cassava. *Food Chain*.

CAMPUS, E. (2010). *AN EMPIRICAL ASSESSMENT OF THE PRESIDENTIAL INITIATIVE ON CASSAVA CROP PRODUCTION AND USE AS SUBSITITUTE IN BREAD PRODUCTION IN ENUGU STATE.* UNIVERSITY OF NIGERIA, ENUGU CAMPUS.

Carley, M. and Christie, I. (2017). *Managing sustainable development*: Routledge.

Denton, O., Aduramigba-Modupe, V., Ojo, A., Adeoyolanu, O., Are, K., Adelana, A., Oyedele, A., Adetayo, A. and Oke, A. (2017). Assessment of spatial variability and mapping of soil properties for sustainable agricultural production using geographic information system techniques (GIS). *Cogent Food & Agriculture, 3*(1), 1279366.

Escobar, A., Dahdouh, L., Rondet, E., Ricci, J., Dufour, D., Tran, T., Cuq, B. and Delalonde, M. (2018). Development of a novel integrated approach to monitor processing of cassava roots into garri: Macroscopic and microscopic scales. *Food and bioprocess technology, 11*(7), 1370-1380.

Isibor, R. A. (2016). Assessment of trace metals contamination of soils around some automobile mechanic workshops in Oyo South-Western Nigeria. *Global Journal of Pure and Applied Sciences, 22*(1), 115-128.

Jackson, J., Chiwona-Karltun, L. and Gordon, A. (2020). Food safety and quality considerations for cassava, a major staple containing a natural toxicant *Food Safety and Quality Systems in Developing Countries* (pp. 343-366): Elsevier.

Kolawole, O. P. (2014). *Cassava processing and the environmental effect.* Paper presented at the World Sustainability Forum.

Lohan, S. K., Jat, H., Yadav, A. K., Sidhu, H., Jat, M., Choudhary, M., Peter, J. K. and Sharma, P. (2018). Burning issues of paddy residue management in north-west states of India. *Renewable and Sustainable Energy Reviews, 81*, 693-706.

Moharreri, M. A., Arkian, F., Lari, K. and Salehi, G. R. (2019). PM10 and CO Dispersion Modeling of Emissions from the Four Thermal Power Plants in Mashhad-Iran. *Scientia Iranica*.

Murray, C. J., Lopez, A. D. and Organization, W. H. (1996). The global burden of disease: a comprehensive assessment of mortality and disability from diseases, injuries, and risk factors in 1990 and projected to 2020: summary.

Njoku, C. G. and Alagbe, A. (2015). Site Suitability Assessment of Petrol Filling Stations (PFS) in Oyo Town, Oyo State, Nigeria: A Geographic Information System (GIS) Approach. *ISOR Journal of Environmental Science, Technology and food Technology (IOSR-JESTFT) e-ISSN*, 2319-2402.

ODUDU, C. (2019). URBAN FARMING IN VACANT LANDS IN TERTIARY INSTITUTIONS: A STUDY OF GREENHOUSE FARMING IN AJAYI CROWTHER UNIVERSITY, OYO TOWN, NIGERIA. *Ethiopian Journal of Environmental Studies & Management, 12*(5).

Ogunseye, T., Olurin, O., Adekunle, G. and Olowofela, J. (2015). Estimation of Magnetic Basement Depth of Oyo Area from Aeromagnetic Data. *Journal of the Nigerian Association of Mathematical Physics, 30*, 181–186.

Olaniran, J., Jekayinfa, S. and Agbarha, H. (2017). Life cycle assessment of cassava flour production: A case study in Southwest Nigeria. *Journal of Engineering and Technology Research, 9*(1), 6-13.

Oyegbami, A., Oboh, G. and Omueti, O. (2010). Cassava processors' awareness of occupational and environmental hazards associated with cassava processing in south-western Nigeria. *African Journal of Food, Agriculture, Nutrition and Development, 10*(2).

Ozoegwu, C., Eze, C., Onwosi, C., Mgbemene, C. and Ozor, P. (2017). Biomass and bioenergy potential of cassava waste in Nigeria: Estimations based partly on rural-level garri processing case studies. *Renewable and Sustainable Energy Reviews, 72*, 625-638.

Parmar, A., Tomlins, K., Sanni, L., Omohimi, C., Thomas, F. and Tran, T. (2019). Exposure to air pollutants and heat stress among resource-poor women entrepreneurs in small-scale cassava processing. *Environmental monitoring and assessment, 191*(11), 693.

Plucknett, D. (2019). *Small-scale processing and storage of tropical root crops*: CRC Press.

Saranraj, P., Behera, S. S. and Ray, R. C. (2019). Traditional Foods From Tropical Root and Tuber Crops: Innovations and Challenges *Innovations in traditional foods* (pp. 159-191): Elsevier.

Seiyaboh, E. and Izah, S. (2019). Impacts of soil pollution on air quality under Nigerian setting. *Journal of Soil and Water Science, 3*(1).

Shittu, T. A., Alimi, B. A., Wahab, B., Sanni, L. O. and Abass, A. B. (2016). Cassava flour and starch: Processing technology and utilization. *Tropical Roots and Tubers: Production, Processing, and Technology*, 415-450.

Stewart, D. R. (2017). *Air Quality Modeling and Health and Economic Assessment of Projected Particulate Matter and Ozone Response to Varying Reductions of Oxides of Nitrogen and Volatile Organic Compound Emissions in the South Coast Air Basin.* Howard University.

Teye, E., Amoah, R. S., Adu, M. O. and Darko, D. (2017). Evaluation and Developing Simple Techniques for Assessing Garri Adulteration. *Journal of Food Security, 5*(5), 162-168.

Wagner, S., Hüffer, T., Klöckner, P., Wehrhahn, M., Hofmann, T. and Reemtsma, T. (2018). Tire wear particles in the aquatic environment-A review on generation, analysis, occurrence, fate and effects. *Water research, 139*, 83-100.

PAPER 36 - Parametric Investigation into Electromechanical Coupling Factor for Nanostructured PVDF-ZnO-TiO_2 Piezoelectric Hybrids Materials

Oluwafemi K. Ajewole[1], Ojo Sunday Isaac Fayomi[2,3], Olamide O. Olusanya[4]

[1]Department of Mechatronics Engineering Department, Bells University of Technology, Ota, Nigeria.
[2]Department of Mechanical Engineering Department, Bells University of Technology, Ota, Nigeria.
[3]Department of Mechanical Engineering Science, University of Johannesburg, Auckland Park Kingsway Campus, Johannesburg.
[4]Department of Computer Engineering Department, Bells University of Technology, Ota, Nigeria
[*]Email: okajewole@bellsuniversity.edu.ng; ajewole_kehinde@outlook.com

ABSTRACT
This study aims to enhance energy conversion efficiency in flexible materials through investigating the electromechanical properties of PVDF-ZnO-TiO_2 piezoelectric hybrids. Methodologically, ZnO nanoparticles and TiO_2 were integrated into the PVDF solution to fabricate piezoelectric ZnO-TiO_2 nanorods within the matrix, followed by parametric analysis on samples S1-S10. Findings highlight Sample S5 as an exceptional performer, boasting the highest recorded values for both electromechanical coupling factor (k) at 1.54E-06 and coefficient for energy transmission (λmax) at 2.37E-12 compared to S1-S10, indicating superior energy conversion efficiency. Acknowledged limitations include a focus on specific hybrid compositions and the necessity for further research on scalability and long-term stability. The study's originality lies in offering novel insights into the electromechanical properties of nanostructured PVDF-ZnO-TiO_2 piezoelectric hybrids, underscoring their potential for transducer design and energy harvesting technologies. The practical implications include advancements in flexible piezoelectric technologies, with potential applications in energy-efficient transducer design and sustainable energy harvesting.

KEYWORDS: Coefficient for Energy Transmission λmax, Electrospinning, Nanofabrication, Piezoelectric Electromechanical Coupling Factor (k), Piezoelectric materials, Renewable energy harvesting, Transducer design

1. INTRODUCTION

Flexible piezoelectric materials have gained significant attention in recent years due to their potential applications in energy harvesting, sensing, and actuation. These materials can convert mechanical deformation or vibrations into electrical energy, and vice versa, through the piezoelectric effect. The electromechanical coupling factor (k) and coefficient (λmax) for energy transmission in flexible piezoelectric developments have been extensively studied in the literature. The efficiency of this energy conversion is quantified by various parameters, including the electromechanical coupling factor (k) and the coefficient λ_{max} for energy transmission. This article here shall discuss these concepts extensively.

Several papers provide insights into these factors. Fan *et al*., (2018) proposed a novel metric called the wave electromechanical coupling factor (WEMCF) to quantify the coupling strength between the mechanical and electric fields in piezoelectric composites. Additionally, Nabawy and Crowther in (Nabawy & Crowther, 2016) analyzed the dynamic electromechanical coupling factor (dynamic EMCF) for cantilever-based piezoelectric actuators and derived explicit expressions for its calculation based on various design parameters. Hang Lu in (Lu *et al*., 2023) presented an acoustic wireless energy transmission system using a piezoelectric cantilever-based transmitter and receiver, achieving high efficiency and robustness. Moreover, Rodríguez and Chong-Quero in (Rodríguez & Chong-Quero, 2021) reviewed the derivation of the electromechanical coupling factor (k) in dynamic regime for different piezoelectric resonators. Furthermore, Yaguang Wu in (WU *et al*., 2023) introduced the concept of the nonlinear modal electromechanical coupling factor (NMEMCF) and proposed a numerical method to evaluate the electromechanical coupling capability of nonlinear piezoelectric structures. These five critical figures of merit in piezoelectrics, which form the Key consideration factors in piezoelectric fabrications shall be discussed such as the piezoelectric strain constant d, piezoelectric voltage constant g, acoustic impedance Z moreover, with special focus on electromechanical coupling factor K, mechanical quality factor Q_m of the fabricated samples shall be charachterised.

1.1 *Literature reviews of Electromechanical coupling factor (k) and coefficient (λmax)*

Electromechanical coupling factor (k) and coefficient (λmax) are important parameters in the field of flexible piezoelectric developments. These parameters determine the efficiency and effectiveness of energy transmission in flexible piezoelectric devices. The electromechanical coupling factor (k) and coefficient (λmax) are important parameters for energy transmission in flexible piezoelectric developments. The electromechanical coupling factor

(k) denotes the conversion competence between electrical and mechanical energy, while the coefficient (λmax) is a measure of the piezoelectric response of the material.

In the field of flexible piezoelectric developments, there have been significant advancements in achieving large electromechanical coupling factors and coefficients. For example, in (Pei *et al*., 2022) reported a molecular ferroelectric crystal, TMCM-CdCl3, with a large electromechanical coupling factor (k_{33}) of 0.483, which is comparable to that of barium titanate (BTO). This indicates that TMCM-CdCl3 has a high conversion efficiency between electrical and mechanical energy. Additionally, Dai *et al*., (2019) discussed the use of two-dimensional van der Waals materials with aligned in-plane polarization, which showed large piezoelectric effects and excellent mechanical durability. These materials have the potential to be used in self-powered piezoelectric sensors. The electromechanical coupling factor (k) represents the efficiency of energy conversion between mechanical and electrical forms in a piezoelectric material. It is a dimensionless quantity that ranges from 0 to 1. A higher value of k indicates a higher efficiency of energy conversion. The coefficient (λmax) represents the maximum strain generated in a piezoelectric material under an applied electric field. It is a measure of the piezoelectric response of the material.

Several studies have investigated the electromechanical coupling factor (k) and coefficient (λmax) in flexible piezoelectric developments. Dai and other authors studied two-dimensional van der Waals materials with aligned in-plane polarization and large piezoelectric effect for self-powered piezoelectric sensors. They found that the piezoelectric coefficients (e_{22}) of these materials intensification with layer quantity, allowing for the fabrication of flexible piezotronic devices with large piezoelectric responsivity. The piezoelectric outputs can reach up to 0.363 V for a 7-layer α-In2Se. This indicates a high value of k and λmax in these materials (Dai *et al*., 2019). Hao, in (Hao *et al*., 2023) developed flexible 1-3 piezoelectric composites with soft embedded conductive interconnects for underwater acoustic transducers. They combined a soft silicone rubber polymer with flexible embedded island-bridge conductive interconnects to enable the flexibility of both the piezoelectric sensing core and the electrical layer. The flexible, wide bond structure entrenched in the polymer can handle with large bending deformations. Although this study does not directly mention the values of k and λmax, the use of flexible materials and the ability to withstand large bending deformation suggest that these composites have high values of k and λmax.

In addition to these specific studies, there are general references that discuss the electromechanical coupling factor (k) and coefficient (λmax) in the context of flexible piezoelectric developments. Dia, in (Dai *et al*., 2019) mentioned that piezoelectric ceramics such as PZT and barium titanate (BTO) are widely used due to their excellent electromechanical conversion. Chen *et al*., (2021) discussed the high degrees of electromechanical coupling exhibited by polyvinylidene fluoride) (PVDF)-based piezoelectric films, which are widely applied as flexible piezoelectric sensors, soft robotics, energy harvesters, and actuators.

Furthermore, Lv *et al*., (2022) highlighted the importance of the electromechanical coupling factor (k) for various piezoelectric applications, such as ultrasonic transducers and actuators. They emphasized that although the piezoelectric coefficient (d_{33}) of molecular ferroelectrics has achieved great progress, the electromechanical coupling factor (k) is still an essential parameter that needs to be explored further.

In addition to molecular ferroelectrics and ceramics, other materials have also been investigated for their electromechanical coupling properties. (Zhao *et al*., 2007), discussed the use of lead-free piezoceramics based on (Na, K)NbO_3, which exhibited a large planar electromechanical coupling coefficient (kp) and the piezoelectric charge coefficient (d_{33}) but a small increase in dielectric constant $\frac{\varepsilon T33}{\varepsilon 0}$ values. This indicates that these materials have a high conversion efficiency between electrical and mechanical energy.

To evaluate the performance of piezoelectric materials, the figure of merit (FOM) is often used. FOM, which is calculated as $\left[\frac{k^2 \times Qm}{sE}\right]$, where k represents the electromechanical coupling factor, Qm represents the mechanical quality factor, and sE represents the elastic compliance of the material. This FOM provides a measure of the power output of piezoelectric devices at resonance frequency (Kang *et al*., 2016; Lv *et al*., 2022).
Hence, it is safe to say, in the realm of flexible piezoelectric developments, the electromechanical coupling factor (k) and coefficient (λmax) are pivotal factors influencing energy transmission. These parameters can vary depending on the materials and structures employed in these devices, but recent research highlights the potential of materials like molecular ferroelectrics and lead-free piezoceramics in achieving substantial coupling factors.

Additionally, the figure of merit (FOM) serves as a crucial metric for evaluating piezoelectric material performance. Continued research and development in this area hold promise for advancing flexible piezoelectric technologies and improving their energy conversion and transmission capabilities.

1.2 *Key points to consider:*

1.3 Material Properties

Piezoelectric materials are essential for efficient energy conversion, relying on properties like d_{33}, g_{33}, c_{33}, and ϵ_{33}. These intrinsic material attributes are influenced by factors such as composition and microstructure, with lead zirconate titanate (PZT) ceramics exemplifying enhanced properties through modifications like crystal phase structure, grain characteristics, and the introduction of dopants like Sb_2O_3 and $MnCO_3$ (Fei *et al*., 2023). Biological materials, such as peptides and proteins, offer robust piezoelectricity with unique advantages despite lower dielectric constants, hinging on their molecular organization, which can be probed using atomic force microscopy (AFM) (Kim, 2022). Polymer-based piezoelectric materials like polyvinylidene fluoride (PVDF) and polycaprolactone (PCL) exhibit piezoelectricity when combined with other substances, allowing for tailored properties, especially when PCL is employed as a core layer material within PVDF sheath layers, while nanoparticle doping further enhances their performance (Feng *et al*., 2023). Additionally, control over poling direction, including tuning techniques, plays a pivotal role in optimizing piezoelectric coefficients and shape control in applications like piezolaminated structures (Sharma *et al*., 2022). In essence, piezoelectric material efficiency depends on various factors, and these citations underscore the significance of material engineering, molecular structure, and control techniques in achieving desired properties and performance.

1.1.1 Strain Conditions

Both k and $\lambda_{max}$are influenced by the strain conditions applied to the piezoelectric material. Piezoelectric materials' performance and properties, influenced by strain conditions, have significant implications (Zhang *et al*., 2023). Understanding strain effects is vital for optimizing energy harvesting and actuation performance, with some conditions, like quasi-static and low-frequency excitation, having distinct impacts. Strain engineering modulates semiconductor properties effectively. In piezoelectric device design, strain conditions affect vibration modes and coupling (Li *et al*., 2021), and materials with high strain constants and low permittivity are preferred for energy harvesting (Aldahiry *et al*., 2022). Developing stretchable piezoelectric materials is crucial for applications like health monitoring (Sun *et al*., 2019), and optimizing material placement in devices improves performance (Kelley *et al*., 2021). In summary, strain conditions are pivotal in optimizing piezoelectric material performance and applications.

1.1.2 Device Design

The design of the energy harvesting or actuation device also plays a significant role in determining the overall efficiency. The performance and applications of piezoelectric elements depend on their shape, size, and arrangement, which influence the coupling of mechanical and electrical domains. Accurate modeling considers both direct and converse piezoelectric effects, with the electromechanical coupling factor "k" playing a key role. Enhanced coupling can be achieved through textured ceramics and multilayered structures. Size and shape affect performance, including natural frequency and non-linear behavior. Three-dimensional modeling is essential for complex configurations, and size-dependent response can be effectively modeled using the consistent couple stress theory (Covaci & Gontean, 2020; Hajesfandiari, 2021; Haugen *et al*., 2020; Ishihara *et al*., 2023; Min *et al*., 2021; Rathnam & Deepak, 2022; Yan *et al*., 2022).

1.1.3 Nonlinear Effects

The relationship between mechanical stress/strain and electrical output can exhibit nonlinear behavior under certain conditions. Nonlinear effects in the relationship between mechanical stress/strain and electrical output are crucial in device design. (Wang *et al*., 2022) studied lead zirconate titanate (PZT) under high-pressure stress, finding nonlinear behavior. (Dong *et al*., 2023) observed strain rate effects in cement-based piezoelectric composites. (Zhou *et al*., 2020) explored nonlinear Hall effects in strained materials. (Akhlaq *et al*., 2023) considered piezoelectric nonlinearity in smart laminated composites, and (Roscow *et al*., 2019) examined mechanical compliance in piezoceramics. These studies emphasize the need to account for nonlinear effects to optimize device and material performance.

1.2 Key Considerations: Figure of Merits (FOM) in the development of Flexible Piezoelectric Devices

1.2.1 Piezoelectric figure of merit parameters

Piezoelectric Strain Constant d, is essential for actuator applications, represents the size of the induced strain x by an external electric field E:

$$x = dE \tag{1}$$

Piezoelectric Voltage Constant g. Through the piezoelectric voltage constant g, generated electric field E is connected to an external stress X:

$$E = gX \tag{2}$$

Taking into account the relation, $P = dX$, we obtain an essential relation between g and d:

$$g = {}^{d}/_{\varepsilon_0 \varepsilon} \tag{3}$$

(ε: relative permittivity)

Electromechanical Coupling Factor k measures how well a piezoelectric material converts electrical energy to mechanical energy. Sometimes the phrases electromechanical coupling factor, energy transfer coefficient, and efficiency interchangeably (Uchino, 2019), are concerned with electrical to mechanical energy conversion rate, although their definitions vary(Nabawy & Crowther, 2016). It also defines the ratio of electrical and mechanical energy exchanged during a flexure cycle of a piezoelectric actuator. The electromechanical coupling factor (k) is a crucial parameter that characterizes the efficiency of energy conversion between mechanical and electrical domains in piezoelectric materials. It represents the fraction of mechanical energy that is effectively converted into electrical energy, and vice versa. A high k-value indicates a more efficient conversion process. Mathematically, the electromechanical coupling factor (k) is defined as:

$$k = \left\{\frac{(d_{33} \cdot g_{33})}{(c_{33} \cdot \epsilon_{33})}\right\} \tag{4}$$

Where:
d_{33} is the piezoelectric charge constant (in C/N or m/V).
g_{33} is the piezoelectric voltage constant (in Vm/N or Vm/V).
c_{33} is the elastic compliance constant (in m^2/N).
ϵ_{33} is the permittivity constant (in F/m).

$$K^2 = \left(\frac{Stored\ mechanical\ energy}{(Input\ electrical\ energy)}\right) \tag{5}$$

$$K^2 = \frac{(Stored\ electrical\ energy)}{(Input\ Mechanical\ energy)} \tag{6}$$

The difference between Equations (5) and (6) is "stored" or "spent."

1.2.2 Coefficient for Energy Transmission λ_{max}

The coefficient for energy transmission λ_{max} is a parameter that relates to the maximum amount of energy that can be efficiently transmitted from the mechanical domain to the electrical domain or vice versa. It represents the ability of a flexible piezoelectric material to effectively convert and transmit energy under specific mechanical deformation conditions. Mathematically, the coefficient for energy transmission λ_{max} can be defined in terms of the k-value as:

$$\lambda_{max} = \frac{2k^2}{1+k^2} \tag{7}$$

It is important to note that λ_{max} is dimensionless, and its value ranges between 0 and 1. A higher λ_{max} indicates a better energy conversion efficiency. Not all the stored energy are be used, and the work done depends on the mechanical load. No output work is done with zero mechanical loads or a complete clamp (no strain). The energy transmission coefficient is defined by

$$\lambda_{max} = \left(\frac{Output\ mechanical\ energy}{Input\ electrical\ energy}\right) max \tag{8}$$

or equivalently,

$$\lambda_{max} = \left(\frac{Output\ electrical\ energy}{Input\ mechanical\ energy}\right) max \tag{9}$$

The efficiency η

$$\eta = \frac{Output\ mechanical\ energy}{Consumed\ electrical\ energy} \tag{10}$$

Or

$$\eta = \frac{Output\ electrical\ energy}{Consumed\ mechanical\ energy} \quad (11)$$

For a typical dielectric and elastic losses in PZT, η are about 1%–3% (Uchino, 2017)

Mechanical Quality Factor Q_M

The mechanical quality factor, Q_M is a characteristic that describes the sharpness of the electromechanical resonance spectrum. When the motional admittance Y_M is plotted around the resonance frequency ω_0, the mechanical quality factor Q_M is specified to the whole width [2Δω] at $\frac{Ym}{\sqrt{2}}$ (or 3 dB-down) as

$$Q_M = \frac{\omega_0}{2\Delta\omega} \quad (12)$$

Another important note: $Q_m^{-1} = (tan\emptyset m)$nerates the heat primarily in the piezo-sample when driven at its resonance mode.

Acoustic Impedance Z

The acoustic impedance Z parameter evaluates the acoustic energy transfer between two materials. It is defined, in general, by

$$Z^2 = \left(\frac{pressure}{volume\ velocity}\right) \quad (13)$$

It is expressed as below in a solid material, where ρ is the density and c, the elastic stiffness of the material.

$$Z = \sqrt{\rho c} \quad (14)$$

2 MATERIALS AND METHODS

2.1 Demonstration of Electromechanical coupling factor (k) and coefficient (λmax)

2.1.1 Fabrication of Nano-Flexible Piezoelectric fiber

In the course of this material characterization of the fabricated electro-spun flexible piezoelectric nanocomposites (Polyvinylidene Fluoride-Zinc Oxide and Titanium Dioxide, (PVDF-ZnO-TiO_2). To create PVDF-ZnO-TiO_2 composite nanofibers, ZnO nanoparticles are added to the PVDF solution. The electrostatic force was extended during the preparation process, and ZnO nanorods were produced, allowing the piezoelectric phase of PVDF to form. To boost the material's piezoelectric properties, the PVDF fiber is combined with piezoelectric ZnO nanorods at the same time. PVDF-ZnO composite fiber membrane has softness, flexibility, low weight, and easy and controlled preparation, making it a good choice for developing flexible electronics (Wu *et al.*, 2021).

Figure 1: (a) Weighing substrates (b) Magnetic Mixing stage (c) 15K Volts Electrospinning device with collector wall, (d) Piezonanofiber (e) Electrospinning Prototype (f) Electrospinning Model available in Bells Biomedical laboratory (g) 50K Volts Electrospinning collector wall, (h) Electro-spun Nanofiber for Piezoelectric Fabrication.

2.1.2 Electromechanical Characterisation

The piezoelectric materials' sensing and transduction capabilities are essential in the proper functioning of any smart hybrid piezoelectric applications device. When subjected to the required test, piezoelectric materials should provide the strain amplitude and dynamic information (electrical potential, voltage-pressure, frequency, acoustic response and respective wave pattern associated with each sample. The laboratory was set up as shown with on

the listed materials, the samples fabricated from the flexible electro-spun piezoelectric fiber were dimensioned and subjected to loads Vs electrical response protocol. This test aims at the determination of direct piezoelectric response in order to determine the Electromechanical Coupling Factor k for each sample. Each of the samples S1 to S11 fabricated were subjected to an average loading there were significant voltage response for each of the samples. Individual sample pressure voltage responses were recorded as shown on the Table 1. By obtaining this kind of information from piezoelectric materials, we can continuously monitor the system performance and detect various loads or pressure interference.

2.1.3 List of Apparatus

The list of the equipment required for this study includes the listed below

(i) Signal Function Generator SFG 1000 Series
(ii) Digital Storage Oscilloscope DSO 5000P
(iii) Portable Volt meter
(iv) DC Power supply Unit
(v) TH2811D LCR Bench Meter
(vi) Decade Variable Resistance Box
(vii) Static Load 5N

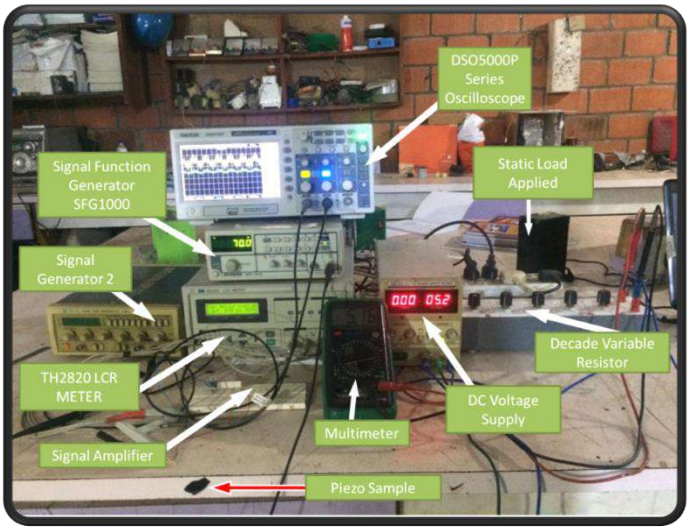

Figure 2: Laboratory Setup for Tests

Table 1: Direct Piezoelectric Moving Pressure –Voltage Response Comparative Analysis for samples S1-S11

Weight (g) Force (N)	Force (N)	Pressure (Nsm)	Voltage S1(Volts)	Voltage S2 (Volts)	Voltage S3 (Volts)	Voltage S4 (Volts)	Voltage S5 (Volts)	Voltage S6 (Volts)	Voltage S7 (Volts)	Voltage S8 (Volts)	Voltage S9 (Volts)	Voltage S10 (Volts)	Voltage S11 (Volts)
100	0.98	12251.25	0.00	0.07	0.04	0.06	0.07	0.06	0.04	0.04	0.04	0.04	0.03
200	1.96	24516.25	0.03	0.10	0.07	0.09	0.10	0.09	0.06	0.07	0.07	0.07	0.06
300	2.94	36781.25	0.03	0.10	0.07	0.09	0.10	0.09	0.07	0.07	0.07	0.07	0.06
400	3.92	49046.25	0.03	0.10	0.08	0.09	0.10	0.09	0.07	0.07	0.07	0.07	0.06
500	4.90	61311.25	0.03	0.10	0.08	0.09	0.10	0.10	0.07	0.08	0.07	0.07	0.06
600	5.89	73576.25	0.04	0.11	0.08	0.10	0.11	0.10	0.07	0.08	0.08	0.08	0.07
700	6.87	85841.25	0.04	0.11	0.08	0.10	0.11	0.10	0.08	0.08	0.08	0.08	0.07
800	7.85	98106.25	0.04	0.11	0.08	0.10	0.11	0.10	0.08	0.08	0.08	0.08	0.07
900	8.83	110371.25	0.04	0.11	0.08	0.10	0.11	0.10	0.08	0.08	0.08	0.08	0.07
1000	9.81	122636.25	0.05	0.12	0.09	0.11	0.12	0.11	0.09	0.09	0.09	0.09	0.08

3. RESULTS AND DISCUSSION

2.2 Direct Piezoelectic Moving Pressure Voltage Direct Piezoelectric Response for Samples S1-S11 Graph

The plot reveals in
Figure 3 the direct piezoelectric effect behavior of the sensor. The internal perturbation of the nano crystals causes the pooling electron when the nanocrystal is within the internal matrix of the sensor. From the graph, we can see that the pristine PVDF shows the least voltage generation. However, the sample with the highest voltage response is sample 5, while sample 2, sample 6 and sample 4 show favorable responses. So, from the above, it could be computed for each sample specimen where the consumed electrical energy is the input voltage, and the output mechanical energy is the pressure.

Nanofiller fills increased the piezoelectric effect by enhancing the piezoelectric phase development in the PVDF film. This indicates that when the w percent of ZnO increases, so do the corresponding output signals, which complements the increase in the piezoelectric coefficient d_{31} value, indicating a more intense piezoelectric action. A larger electric voltage output may be attained even when the material is subjected to increased loading. This is a major benefit of using a substance as a sensor. The data and graph showed that increasing the porosity of the PVDF sensor with TiO_2 enhanced the d_{31} value, signaling a more piezoelectric sensor (Azimi *et al*., 2020).

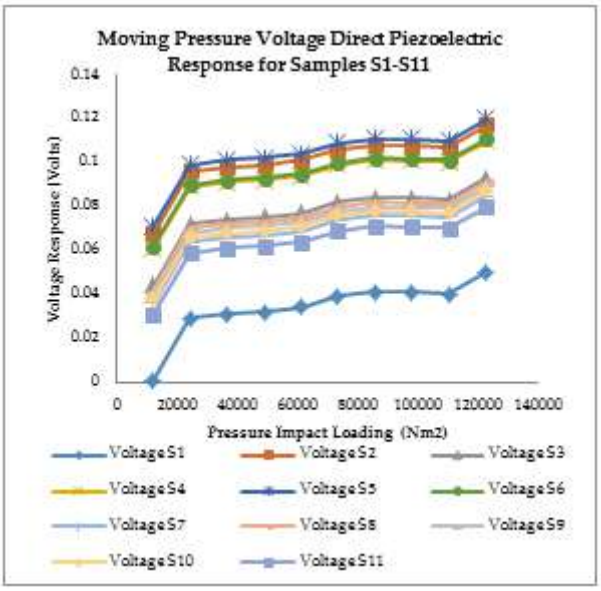

Figure 3: Voltage (Volts) Vs Pressure (N/m^2) Chart

2.3 Electromechanical Coupling Factor for samples S1- S10

From the experiment result in Table 1, we can determine the Electromechanical Coupling Factor k as expressed in equations (5)and (6), respectively. Also, it is possible to determine the coefficient λ_{max} for energy transmission for each of the samples S1- S10. The results of these values are given in Table.2 the Sample S5 also shows the highest vales 1.54E-06 and 2.37E-12. (All values are dimensionless)

Table.2: Electromechanical Coupling Factor k and coefficient λmax for energy transmission

Sample	Avg Volt-(Volts)	Mech (Pressure N/m^2)	Coff λ_{max}	K^2	K
S1	0.03379	67443.75	5.01E-07	2.51E-13	5.0101E-07
S2	0.10079	67443.75	1.49E-06	2.23E-12	1.49443E-06
S3	0.07679	67443.75	1.14E-06	1.30E-12	1.13858E-06
S4	0.09379	67443.75	1.39E-06	1.93E-12	1.39064E-06
S5	0.10379	67443.75	1.54E-06	2.37E-12	1.53891E-06
S6	0.09479	67443.75	1.41E-06	1.98E-12	1.40547E-06
S7	0.06879	67443.75	1.02E-06	1.04E-12	1.01996E-06
S8	0.07479	67443.75	1.11E-06	1.23E-12	1.10892E-06

S9	0.07279	67443.75	1.08E-06	1.16E-12	1.07927E-06
S10	0.06379	67443.75	9.46E-07	8.95E-13	9.45825E-07

3 Novelty

This research breaks new ground by delving into the electromechanical coupling factor of nanostructured PVDF-ZnO-TiO_2 piezoelectric hybrids, a topic rarely explored before. What sets this work apart is its introduction of the nonlinear modal electromechanical coupling factor (NMEMCF), offering a fresh perspective on evaluating the electromechanical capabilities of nonlinear piezoelectric structures. Furthermore, it does not just stop at theory, as it also discusses the real-world applications of PVDF-based piezoelectric films in flexible sensors, robotics, energy harvesting, and actuators, providing practical insights. Additionally, the inclusion of experimental characterization adds tangible value, offering concrete data on properties like piezoelectric strain and voltage constants. In essence, this work stands out for its blend of novel research, innovative methodology, practical relevance, and hands-on experimentation in the realm of piezoelectric materials' electromechanical coupling factors.

4. CONCLUSIONS

In conclusion, the experimental results presented in Table 2 provide valuable insights into the Electromechanical Coupling Factor (k) and the coefficient λmax for energy transmission for a range of samples (S1-S10). These dimensionless values are crucial in characterizing the efficiency and effectiveness of electromechanical energy conversion within the studied materials. Upon analysis, it is evident that Sample S5 stands out with the highest values for both k (1.54E-06) and λmax (2.37E-12), indicating its superior ability to convert electrical energy into mechanical energy and transmit energy efficiently. These findings could have significant implications in various applications, such as transducer design and energy harvesting technologies.

Furthermore, the comprehensive dataset presented in this report allows for a comparative study of the different samples' performance, enabling researchers and engineers to make informed decisions regarding material selection and optimization in electromechanical systems.

In summary, the results of this experiment shed light on the electromechanical coupling behavior of the tested samples and provided a foundation for further research in the field of energy conversion and transmission. These findings hold promise for advancing the development of more efficient and sustainable electromechanical devices.

Funding: This research received no external funding

Acknowledgments: Oluwafemi Kehinde Ajewole https://orcid.org/0009-0006-2381-3241

Conflicts of Interest: The authors declare no conflict of interest.

4 REFERENCES

Akhlaq, A., Shaik Dawood, M. S. I., Jaffar Syed, M. A. and Sulaeman, E. (2023). A Study on the Effect of Piezoelectric Nonlinearity on the Bending Behaviour of Smart Laminated Composite Beam. *Materials*, *16*(7), 2839. https://doi.org/10.3390/ma16072839

Aldahiry, D. A., Bajaba, D. A., Basalamah, N. M. and Ahmed, M. M. (2022). Piezoelectric Transducer as an Energy Harvester: A Review. *Yanbu Journal of Engineering and Science*, *19*(1). https://doi.org/10.53370/001c.33771

Azimi, B., Milazzo, M., Lazzeri, A., Berrettini, S., Uddin, M. J., Qin, Z., Buehler, M. J. and Danti, S. (2020). Electrospinning Piezoelectric Fibers for Biocompatible Devices. *Advanced Healthcare Materials*, *9*(1), 139–148. https://doi.org/10.1002/adhm.201901287

Chen, Y., Zhang, M., Su, Y. and Zhou, Z.-D. (2021). Coupling Analysis of Flexoelectric Effect on Functionally Graded Piezoelectric Cantilever Nanobeams. *Micromachines*. https://doi.org/10.3390/mi12060595

Covaci, C. and Gontean, A. (2020). Piezoelectric Energy Harvesting Solutions: A Review. *Sensors*, *20*(12), 3512. https://doi.org/10.3390/s20123512

Dai, M., Wang, Z., Wang, F., Qiu, Y., Zhang, J., Xu, C.-Y., Zhai, T., Cao, W., Fu, Y., Jia, D., Zhou, Y. and Hu, P.-A. (2019). Two-Dimensional van der Waals Materials with Aligned In-Plane

Polarization and Large Piezoelectric Effect for Self-Powered Piezoelectric Sensors. *Nano Letters*, *19*(8), 5410–5416. https://doi.org/10.1021/acs.nanolett.9b01907

Dong, H., Li, Z., Zhu, Z., Li, Y., Cheng, W. and Chen, J. (2023). Construction of 2-2 Type Cement-Based Piezoelectric Composites' Mechanic–Electric Relationship Based on Strain Rate Dependence. *Materials*, *16*(7), 2702. https://doi.org/10.3390/ma16072702

Fan, Y., Collet, M., Ichchou, M., Bareille, O. and Li, L. (2018). Wave Electromechanical Coupling Factor for the Guided Waves in Piezoelectric Composites. *Materials*, *11*(8), 1406. https://doi.org/10.3390/ma11081406

Fei, X., Lin, X., Wang, C., Li, W., Yu, F., Yang, C. and Huang, S. (2023). Sb_2O_3 -modified lead zirconate titanate piezoelectric ceramics with enhancing piezoelectricity and low loss. *Journal of the American Ceramic Society*, *106*(1), 501–512. https://doi.org/10.1111/jace.18771

Feng, Z., Wang, K., Liu, Y., Han, B. and Yu, D.-G. (2023). Piezoelectric Enhancement of Piezoceramic Nanoparticle-Doped PVDF/PCL Core-Sheath Fibers. *Nanomaterials*, *13*(7), 1243. https://doi.org/10.3390/nano13071243

Hajesfandiari, A. (2021). Boundary Element Solution to Size-Dependent Piezoelectric Bimaterials. *14th WCCM-ECCOMAS Congress*. https://doi.org/10.23967/wccm-eccomas.2020.077

Hao, S., Zhong, C., Zhang, Y., Chen, Y., Wang, L. and Qin, L. (2023). Flexible 1-3 Piezoelectric Composites with Soft Embedded Conductive Interconnects for Underwater Acoustic Transducers. *ACS Applied Electronic Materials*, *5*(5), 2686–2695. https://doi.org/10.1021/acsaelm.3c00155

Haugen, A. B., Ringgaard, E. and Levassort, F. (2020). Textured multilayered piezoelectric structures for energy conversion. *Journal of Physics: Energy*, *2*(1), 015002. https://doi.org/10.1088/2515-7655/ab5f30

Ishihara, D., Chigahalli Ramegowda, P., Aikawa, S. and Iwamaru, N. (2023). Importance of Three-Dimensional Piezoelectric Coupling Modeling in Quantitative Analysis of Piezoelectric Actuators. *Computer Modeling in Engineering & Sciences*, *136*(2), 1187–1206. https://doi.org/10.32604/cmes.2023.024614

Kang, M.-G., Jung, W.-S., Kang, C.-Y. and Yoon, S.-J. (2016). Recent Progress on PZT Based Piezoelectric Energy Harvesting Technologies. *Actuators*, *5*(1), 5. https://doi.org/10.3390/act5010005

Kelley, C. R., Lopp, G. K. and Kauffman, J. L. (2021). Optimizing Piezoelectric Material Location and Size for Multiple-Mode Vibration Reduction of Turbomachinery Blades. *Journal of Vibration and Acoustics*, *143*(2). https://doi.org/10.1115/1.4048263

Kim, K. (2022). Advances in Atomic Force Microscopy for the Electromechanical Characterization of Piezoelectric and Ferroelectric Nanomaterials. *Korean Journal of Metals and Materials*, *60*(9), 629–643. https://doi.org/10.3365/KJMM.2022.60.9.629

Li, Z., Yi, X., Yang, J., Bian, L., Yu, Z. and Dong, S. (2021). Designing Artificial Vibration Modes of Piezoelectric Devices Using Programmable, 3D Ordered Structure With Piezoceramic Strain Units. *Advanced Materials*. https://doi.org/10.1002/adma.202107236

Lu, H., Xu, J. and Yan, R. (2023). A high-efficient piezoelectric wireless energy transmission system based on magnetic force coupling. *Review of Scientific Instruments*, *94*(2), 025007. https://doi.org/10.1063/5.0103915

Lv, H.-P., Liao, W.-Q., You, Y.-M. and Xiong, R.-G. (2022). Inch-Size Molecular Ferroelectric Crystal with a Large Electromechanical Coupling Factor on Par with Barium Titanate. *Journal of the American Chemical Society*, *144*(48), 22325–22331. https://doi.org/10.1021/jacs.2c11213

Min, H., Zhang, J. and Fan, M. (2021). Size Effect of a Piezoelectric Patch on a Rectangular Plate with the Neural Network Model. *Materials*, *14*(12), 3240. https://doi.org/10.3390/ma14123240

Nabawy, M. and Crowther, W. (2016). Dynamic Electromechanical Coupling of Piezoelectric Bending Actuators. *Micromachines*, *7*(1), 12. https://doi.org/10.3390/mi7010012

Mani Rathnam, P. and Deepak N. R. M (2022). Shape Control of Composite Structure with Suitably Placed Piezoelectric Sensors Under Electro-Thermo-Mechanical Condition with Non-linear Analysis. *INTERANTIONAL JOURNAL OF SCIENTIFIC RESEARCH IN ENGINEERING AND MANAGEMENT*, *06*(06). https://doi.org/10.55041/IJSREM14376

Pei, H., Shi, S., Chen, Y., Xiong, Y. and Lv, Q. (2022). Combining Solid-State Shear Milling and FFF 3d-Printing Strategy to Fabricate High-Performance Biomimetic Wearable Fish-Scale PVDF-Based Piezoelectric Energy Harvesters. *Acs Applied Materials & Interfaces*. https://doi.org/10.1021/acsami.2c02491

Rodríguez, O. and Chong-Quero, J. E. (2021). Uniform behavior of the electromechanical coupling factor in piezoelectric resonators. *Materials Research Express*, *8*(4), 046303. https://doi.org/10.1088/2053-1591/abf2f1

Roscow, J. I., Pearce, H., Khanbareh, H., Kar-Narayan, S. and Bowen, C. R. (2019). Modified energy harvesting figures of merit for stress- and strain-driven piezoelectric systems. *The European Physical Journal Special Topics*, *228*(7), 1537–1554. https://doi.org/10.1140/epjst/e2019-800143-7

Sharma, S., Kumar, R., Talha, M. and Narain, V. (2022). *Shape Control of Piezolaminated Structure Using Poling Tuned Piezoelectric Actuators* (pp. 1765–1776). https://doi.org/10.1007/978-981-16-0550-5_170

Sun, R., Carreira, S. C., Chen, Y., Xiang, C., Xu, L., Zhang, B., Chen, M., Farrow, I., Scarpa, F. and Rossiter, J. (2019). Stretchable Piezoelectric Sensing Systems for Self-Powered and Wireless Health Monitoring. *Advanced Materials Technologies*, *4*(5), 1900100. https://doi.org/10.1002/admt.201900100

Uchino, K. (2017). The Development of Piezoelectric Materials and the New Perspective. In *Advanced Piezoelectric Materials* (pp. 1–92). Elsevier. https://doi.org/10.1016/b978-0-08-102135-4.00001-1

Uchino, K. (2019). Micro Mechatronics. In *VDI Berichte* (Issue 1971, pp. 1–12). CRC Press. https://doi.org/10.1201/9780429260308

Wang, R., Tang, E., Yang, G., Han, Y., Chen, C., Chang, M., Guo, K. and He, L. (2022). Electrical properties of PZT under high-pressure stress pulse: Effects of loading frequency and circuit load. *Ceramics International*, *48*(2), 2421–2430. https://doi.org/10.1016/j.ceramint.2021.10.023

WU, Y., FAN, Y. and LI, L. (2023). Nonlinear modal electromechanical coupling factor for piezoelectric structures containing nonlinearities. *Chinese Journal of Aeronautics*, *36*(2), 100–110. https://doi.org/10.1016/j.cja.2022.06.020

Wu, Y., Ma, Y., Zheng, H. and Ramakrishna, S. (2021). Piezoelectric materials for flexible and wearable electronics: A review. *Materials & Design*, *211*, 110164. https://doi.org/10.1016/j.matdes.2021.110164

Yan, Y., Geng, L. D., Liu, H., Leng, H., Li, X., Wang, Y. U. and Priya, S. (2022). Near-ideal electromechanical coupling in textured piezoelectric ceramics. *Nature Communications*, *13*(1), 3565. https://doi.org/10.1038/s41467-022-31165-y

Zhang, H., Gao, H., Geng, J., Meng, X. and Xie, H. (2023). In Situ Quantification of Strain-Induced Piezoelectric Potential of Dynamically Bending ZnO Microwires. *Small Methods*, *7*(3). https://doi.org/10.1002/smtd.202201342

Zhao, P., Zhang, B. P. and Li, J. F. (2007). High piezoelectric d33 coefficient in Li-modified lead-free (Na,K)NbO3 ceramics sintered at optimal temperature. *Applied Physics Letters*, *90*(24), 242909. https://doi.org/10.1063/1.2748088

Zhou, B. T., Zhang, C.-P. and Law, K. T. (2020). Highly Tunable Nonlinear Hall Effects Induced by Spin-Orbit Couplings in Strained Polar Transition-Metal Dichalcogenides. *Physical Review Applied*, *13*(2), 024053. https://doi.org/10.1103/PhysRevApplied.13.024053

PAPER 37 - CASTING SIMULATIONS FOR ALSI$_7$MG ALLOY WHEEL FOR PROCESS PERFORMANCE AND OPTIMIZATION

S.O. Tanimowo[1], J.K. Odusote[2], N.S.Tiedje[3]

[1]Department of Mechanical Engineering, University of Ilorin, Ilorin, Nigeria
[2]Department of Materials and Metallurgical Engineering, University of Ilorin, Ilorin, Nigeria
[3]Department of Mechanical Engineering, Technical University of Denmark,Lyngby, Denmark

[*]Email: 92-032141@students.unilorin.edu.ng

ABSTRACT
The molten fluid flow of materials, process parameters, solidification, shrinkage formation and residual stress is essential for the quality performance of a metal cast product. While various FEM and VEM methods have been analyzed in automotive wheel rims, casting simulation has not been explored using the finite volume method. This study investigates the transformation solidification and mould filling processes of aluminium silicon magnesium (AlSi7Mg) alloy wheels for process performance and optimization. MAGMASOFT software examined the phase change during the cast AlSi7Mg alloy wheel rim simulation in low pressure sand casting (LPSC). During the phase transition in the solidification process of the alloy wheel, a large amount of hidden heat was released. The location of the transition front between the molten and solid state is a strong function of the casting flow and the cooling rate in the mould.

KEYWORDS**:** Simulation, Gate design, Feeder design, Low pressure sand casting

1. INTRODUCTION

Metal casting is widely used for producing intricate automobile parts (Campbell, 2011). Still, issues arise due to poor control of parameters leading to defects like shrinkage, porosity and incomplete filling. While aluminum alloys are favoured for their cost-effectiveness and strength-to-weight ratio, defects such as oxide films and porosity impact mechanical properties. Research on alloying elements like copper and zinc reveals their influence on defects and mechanical properties in recycled sand-cast aluminium (Odusote and Ajayi, 2016). Advancements in computer simulations, exemplified by (Dučić *et al*., 2017) optimization of gating systems, facilitate defect prediction and reduction.

Majidi and Beckermann (2019) reiterated that oxide inclusions are among casting defects that are difficult to casting performance, which can be controlled by minimizing the head height and pouring time and adding a nozzle extension. Recently, it was reported that appropriate applications of feeders and chills through simulation technology could be used to solve internal casting defects in ductile cast iron (Takemoto *et al*., 2021). This is important because it is economical and eliminates trial and error in shop floor casting, which can also be extended to cast aluminium alloy. However, limited information exists on predicting defects in AlSi7Mg alloy wheel rims, highlighting a research gap.

This paper pioneers the investigation of Low Pressure Sand Casting (LPSC) for producing automotive AlSi7 alloy wheel rims to predict casting defects, an approach not previously explored in the available literature. While existing studies have focused on other casting methods like Low Pressure Die Casting (LPDC) and High Pressure Die Casting (HPDC) (Zhang *et al*., 2005), LPSC offers distinct advantages for large aluminum castings. Design calculations for LPSC are conducted alongside empirical and casting simulations using Magmasoft software, underscoring the potential of LPSC in aluminum alloy wheel rim production and defect prediction.

2. THEORETICAL ANALYSIS

Laminar fluid flow is considered by describing the fluid velocity, u, and the pressure, p, according to Equations 1 to 3 (Ravi, 2005)

(1) Continuity Equation (mass conservation equation):

$$D = \frac{\partial u}{\partial x} + \frac{\partial v}{\partial y} + \frac{\partial w}{\partial z} = 0 \qquad \textbf{(1)}$$

Where D is divergence; u, v, w are components of the velocity vector in x, y, z direction, m/s;

(2) N-S equation (momentum conservation equation):

$$\frac{\partial u}{\partial \tau}+u\frac{\partial u}{\partial x}+v\frac{\partial u}{\partial y}+w\frac{\partial u}{\partial z}=-\frac{1}{\rho}\frac{\partial p}{\partial x}+\gamma\left[\frac{\partial^2 u}{\partial x^2}+\frac{\partial^2 u}{\partial y^2}+\frac{\partial^2 u}{\partial z^2}\right]+g_x$$

$$\frac{\partial v}{\partial \tau}+u\frac{\partial v}{\partial x}+v\frac{\partial v}{\partial y}+w\frac{\partial v}{\partial z}=-\frac{1}{\rho}\frac{\partial p}{\partial y}+\gamma\left[\frac{\partial^2 v}{\partial x^2}+\frac{\partial^2 v}{\partial y^2}+\frac{\partial^2 v}{\partial z^2}\right]+g_y \quad \textbf{(2)}$$

$$\frac{\partial w}{\partial \tau}+u\frac{\partial w}{\partial x}+v\frac{\partial w}{\partial y}+w\frac{\partial w}{\partial z}=-\frac{1}{\rho}\frac{\partial p}{\partial z}+\gamma\left[\frac{\partial^2 w}{\partial x^2}+\frac{\partial^2 w}{\partial y^2}+\frac{\partial^2 w}{\partial z^2}\right]+g_z$$

Where p is the pressure of unit density, Pa; γ is dynamic viscosity, Pas; g is the acceleration due to gravity, m/s^2; ρ is density of the fluid, kg/m^3; τ is filling time, s.

(3) Energy Equation:

$$\frac{\partial T}{\partial \tau}+u\frac{\partial T}{\partial x}+v\frac{\partial T}{\partial y}+z\frac{\partial T}{\partial z}=\frac{K}{\rho C_v}\left[\frac{\partial^2 T}{\partial x^2}+\frac{\partial^2 T}{\partial y^2}+\frac{\partial^2 T}{\partial z^2}\right]+Q \quad \textbf{(3)}$$

Where C_v is specific heat capacity, J/ (kg-K); Q is heat which results from the liquid surface stress applying work for liquid, J; T is the temperature of liquid, k; K is the thermal conductivity of liquid, W/(m-K).

3.0 METHODOLOGY

3.1 Solid modelling of casting

The part selected for this study is wheel rim casting.3D CAD model of the as-cast part is created with the following steps: sketching the front view, extruding the section and setting the depth, adding a boss at the central front plane, and extruding the hole using SolidWorks [http://www.solidworks.com/] as shown Figure 1.

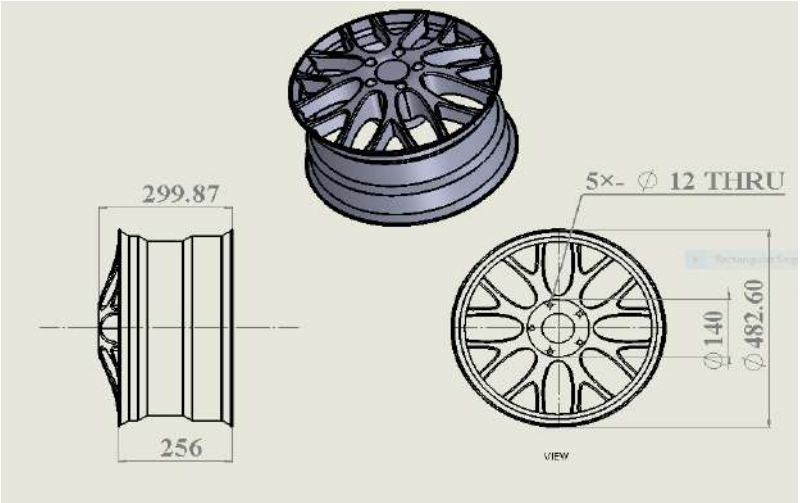

Figure 1: CAD drawing of design of wheel casting (all dimensions are in mm)

Geometric properties such as part volume, part bounding box volume, part weight, part surface area, hole volume, minimum and maximum section thickness, and maximum thickness gradient is computed accurately from the software as shown in Table 1. These are required for product design and tooling development.

Table 1: Geometric properties of the aluminium wheel casting

Properties	**Value**	**Unit**	**Symbol**
Volume	5689921.79	mm^3	V
Density	2700	Kg/m^3	ρ_{cast}
Weight	15.362	Kg	W_c
Surface area	1182464.81× 10^{-6}	Kg/m^3	A
Wall thickness – minimum	10	mm	t
Wall thickness – maximum	20	mm	t

Next, the wheel is exported as still file format for downstream software. Then, the wheel model is converted to wheel casting by importing it into an integrated casting design and simulation software for rigging design.

3.2 Material selection

The data of AlSi12 and AlSi7Mg are collected using Cambridge Engineering Selector (CES) Edupack 2019 and compared to select the optimum. The material selected is AlSi7Mg alloy because of its excellent thermophysical properties, as shown in Table 2. Similarly, the sand mould material properties used during the simulation are selected from Table 4.

Table 2: Typical Properties of Aluminium Alloy Casting and Mould Material (Ravi, 2005)

Material	**Property**	**Symbol**	**Value**	**Unit**
Aluminium Casting	Thermal conductivity of liquid	k_l	160	W/(mK)
	Thermal conductivity of solid	k_s	210	W(mK)
	Specific heat of liquid	C_l	820	J/(KgK)
	Specific heat of solid	C_s	900	J/(KgK)
	Surface tension coefficient of liquid	σ	0.5	N/m
	Dynamic viscosity	μ	0.002	Ns/m^2
	Density of liquid	ρ_l	2385	Kg/m^3
	Density of solid	ρ_s	2700	Kg/m^3
	Latent heat of fusion	L	390	kJ/Kg
	Liquidus temperature	T_l	660	K
	solidus temperature	T_s	660	K
Sand mould	Density (ambient)	ρ	1600	Kg/m^3
	Thermal conductivity	k_m	0.61	W/(mK)
	Volumetric specific heat	ρ^C	1130	J/(KgK)

4. RESULTS AND DISCUSSION

In this study, simulations are performed to analyze gating sizes for the required filling time, filling temperature, solidification processes for solidification temperature, and feeder size for the desired quality.

4.1 Mould filling Analysis

Figure 2 shows the major elements of the casting system. The casting is made in a sand mould with 470 mm diameter by 350 mm length. During the casting process, the liquid melt is poured into the mould through a gravity-controlled gating system comprising an inlet, sprue, runner, and ingates. The inlet accepts the molten metal from the ladle. The sprue with

a circular cross-section leads the molten metal, changing its direction at the right angle and sending it to the runner that slows down the molten. The casting system is set up using the process parameters.

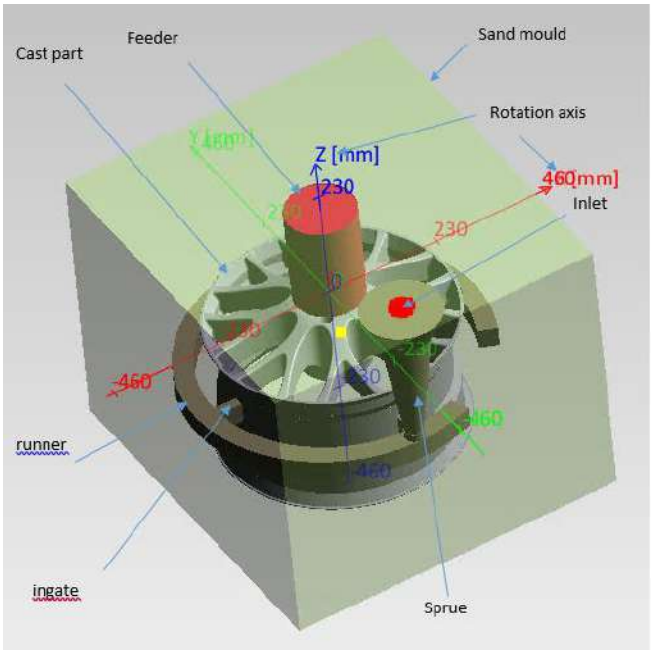

Figure 2: Major elements of the casting system

4.2 Filling time

The melt velocities during filling at different intervals are shown in Figures 4 to 6. The results revealed that for every 0.35 seconds, 5% of the total volume (comprising of gating systems, casting, and feeder) will be filled up. This is based on the magma default value setting assumption for boundary conditions in Table 3.

Table 3: Process parameters

Cast part material	Core	Mould	Mesh	Heat transfer metal/mould	Heat transfer core/mould
AlSi7 with T_{init} = 650°C	"Cold box" with T_{init} = 20°C	"Green_sand" with T_{init} = 20°C	Auto – 200,0000 cells	1000 W/ m^2K	"Mergematerials"

Figure 3a shows that the down sprue is not filled, which results in turbulent flow as the melt plunges to the bottom of the sprue and splashes back up (see arrow). At 5% filled, high velocities are still present at the down sprue region, resulting in a similar melt splash and turbulent flow. This indicates incomplete filling in the mould cavity caused by poor molten metal fluidity. In addition, the temperature distribution in the mould is not uniform after the solidification rate due to the splashing and turbulence. The uniform solidification rate reduces shrinkage cavities because of the low dissimilar cooling rate. In Figure 4b, at 10% filled, high velocities are still present at the down sprue region, resulting in a similar melt splash and turbulent flow. Filling of the gating system proceeds with less turbulent

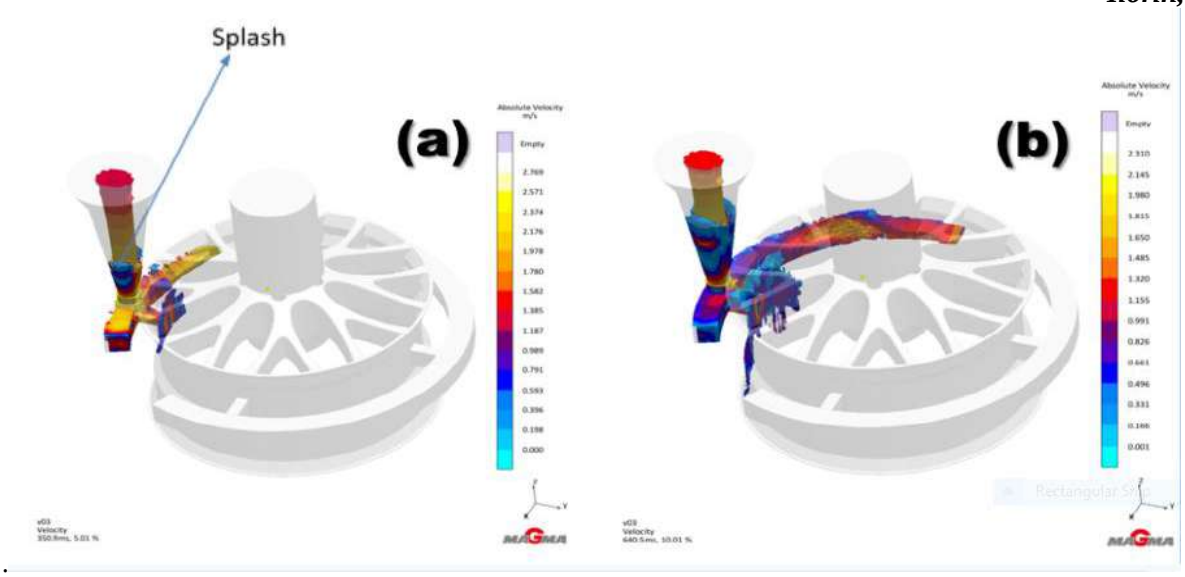

.

Figure 3: (a) 0.35 seconds, 5% filled (b) 0.64 seconds, 10% filled

In Figure 5a, at 20% filled, the sprue is still unfilled while the melt starts flowing into the part at the two inlets nearest the down sprue. At the inlets to the part, the melt velocities are much lower than the down sprue region; thus, a less turbulent flow is present. Upon entrance of the melt into the sand mould, it was observed that the two ingates nearest to the down sprue delivered the melt first. However, 40% filled the melt flowed unevenly into the sand mould from all four ingates, as shown in Figure 6b. It is similarly observed that the melt is agitated as it flows directly into the inner surface of the sand mould. This results in the oxidation of the little droplets, which could lead to "cold shuts". Reducing the melt flow velocity minimizes this turbulence. In addition, moving the ingates slightly further down the sand mould could reduce the free flow as contact with the bottom of the sand mould is maintained.

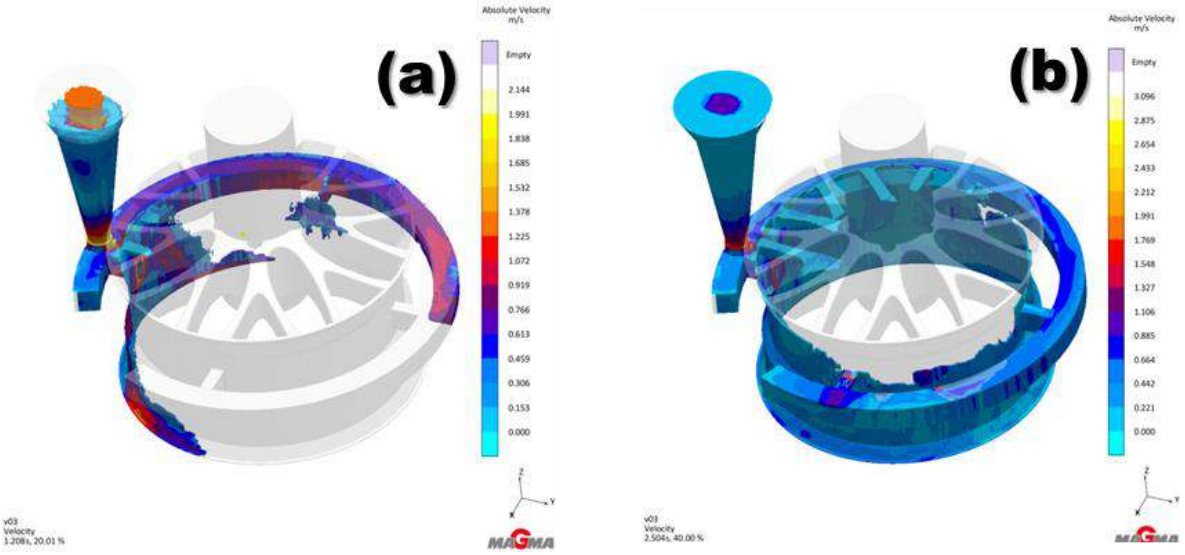

Figure 4: (a) 0.92 seconds, 20% filled (b) 0.92 seconds, 40% filled

4.3 Filling temperature

The filling temperature (solidus-liquidus scale is enabled) at 100% fill is shown in Figure 5. It is observed that some premature solidification exists along the sand mould sides. The results are generally positive except for the uneven sand cast filling, melt flow at the sprue, and gating system. Turbulent melt flow should be reduced.

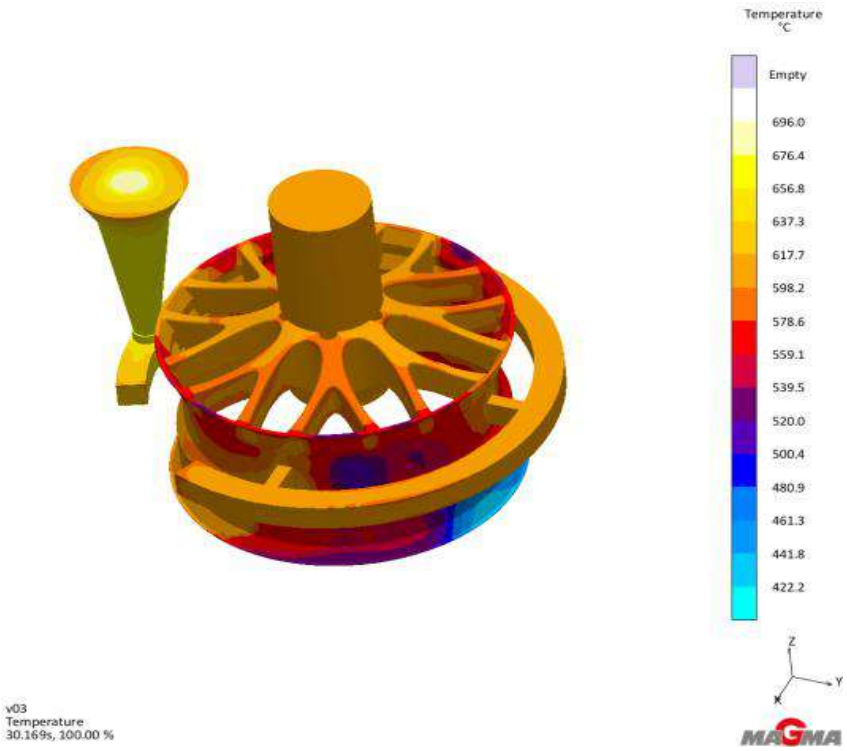

Figure 5: 100% fill temperature

4.4 Solidification temperature

When the temperature falls below 422.2°C, solidification for the cast material AlSi7Mg begins and is finished below 696°C. Figure 7 shows the contour plots of the solidification temperatures at 30%, 60%, and 90%.

Figure 6 (a) shows that at 30% solidification, the feeder is still molten. At the same time, the material in the sand mould and gating system is semi-solid (in the region between liquidus and solidus.) Liquidus is the temperature above which the alloy is completely liquid, whereas solidus is the temperature below which the alloy is completely solid. At 60% solidification, most of the gating system and sand mould is still undergoing solidification, as shown in Figure 6 (b). At 100% solidification, the whole gating system and sand mould are not yet fully solidified as shown in Figure 6 (c). The feeder is between solidus and liquidus temperature and will solidify last. The feeder design is appropriate because it is free of shrinkage porosity. However, it may require a core to produce an undercut at its neck.

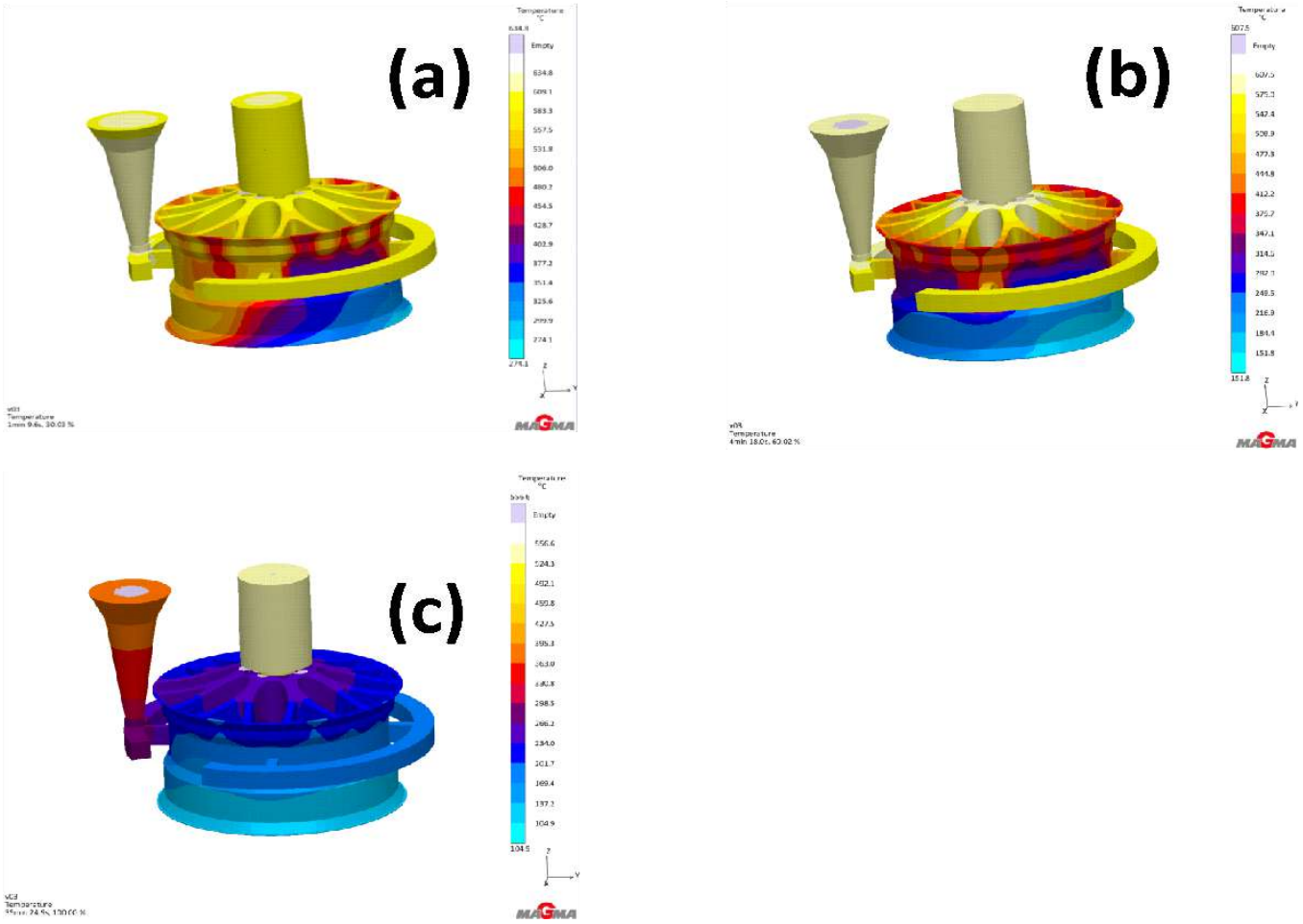

Figure 6: Temperature contour at (a) 30% (b) 60% (c) 100% solidification

The casting after the final solidification time is shown in Figure 7. It is more likely that directional solidification is achieved at the feeding system. The feeder takes approximately 360.9 seconds to solidify, four times greater than the thickest region of the sand mould. This indicates that the feeder size is appropriate based on the solidification time. This is following Chvorinov's principles, which state that solidification time should be proportional to the ratio of the volume of casting to the surface area (Campbell, 2011). The mould cavity, which is in the centre of the sand mould has relatively the longest solidification time. The sand casting model took about 360.9 seconds to solidify at the centre of the wheel casting. This observation satisfies Fourier's law of conduction that thermal resistance increases with thickness across which heat is conducted (Fredriksson and Åkerlind, 2006).

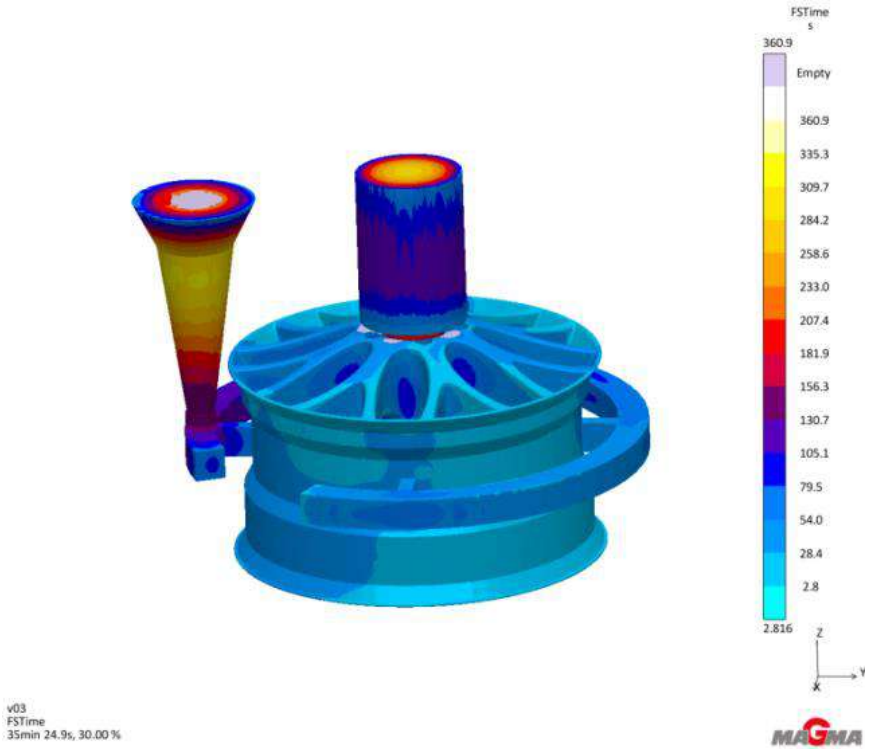

Figure 7: The cast after the final solidification time

4.5 Casting defects

Hotspots in the casting are shown in Figure 8a, while porosities are shown in Figure 8b. Hotspot regions solidify last and are most susceptible to shrinkage cavity formation. As shown in the figure, hotspots exist in the sand mould region, which is good as the feeder and gating system are eventually cut off during machining and after casting. Shrinkage at the hot spot is also the cause of localized contraction stresses, which will prevail as residual stresses at room temperature. Porosities in the wheel casting are very few. The x-ray function is enabled where porosities between 0-1% are hidden. It was observed that no porosities above 1% are present in the sand mould which indicates that the cast is good. In general, the solidification of the casting proceeds acceptably. The feeder size should be slightly increased by 25 % to reduce the overall solidification time.

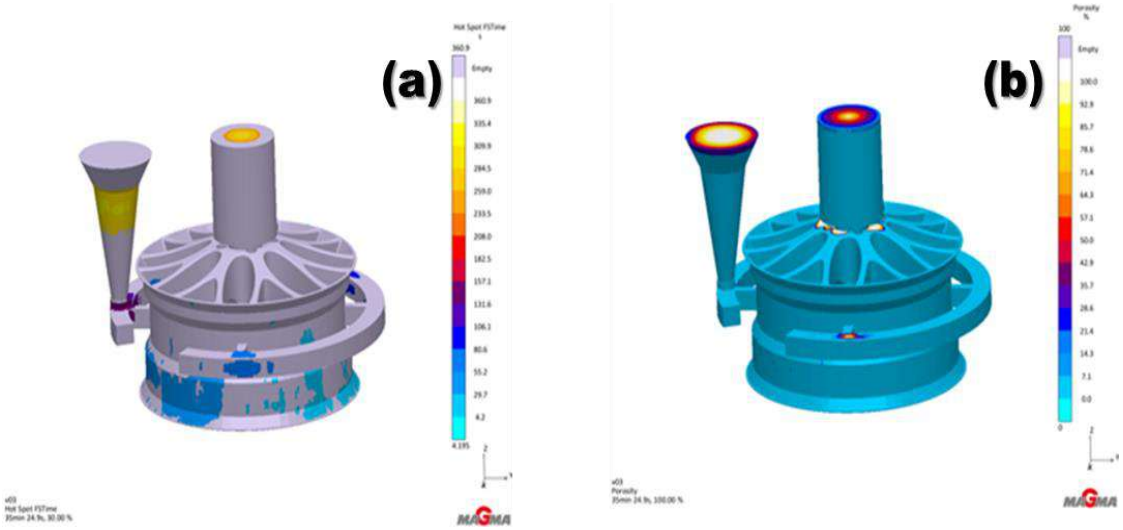

Figure 8: (a) Hotspots (b) Porosities

4. CONCLUSION

This study emphasizes the significance of understanding geometry, material, tool design parameters, and casting simulation for optimizing casting quality. It focuses on LPSC (Low-Pressure Sand Casting) of wheel castings, involving calculations of casting design parameters and simulations using Magmasoft software. The simulations analyze filling analysis, gating sizes, filling time, solidification processes, and feeder size, highlighting the necessity of using a chilled mold for controlled progressive directional solidification. Evaluation of casting defects reveals hotspots in the wheel rim, emphasizing the importance of proper riser placement to avoid porosity, cavities, and surface defects. The analysis and simulations provide valuable insights for designing molds, feeders, and gating systems to achieve high-quality wheel castings with minimal defects.

ACKNOWLEDGEMENTS

The authors thank the Department of Mechanical Engineering, Technical University of Denmark (DTU), for granting permission to use their MAGMASOFT package to simulate.

REFERENCES

Campbell, J. (2011). *Complete casting handbook: Metal casting processes, metallurgy, techniques and design* (1st ed). Elsevier Butterworth-Heinemann.

Dučić, N., Ćojbašić, Ž., Manasijević, S., Radiša, R., Slavković, R., and Milićević, I. (2017). Optimization of the Gating System for Sand Casting Using Genetic Algorithm. *International Journal of Metalcasting*, *11*(2), 255–265. https://doi.org/10.1007/s40962-016-0040-8

Fredriksson, H., and Åkerlind, U. (2006). *Materials Processing during Casting* (1st ed.). Wiley. https://doi.org/10.1002/9780470017920

Majidi, S. H., and Beckermann, C. (2019). Effect of Pouring Conditions and Gating System Design on Air Entrainment During Mold Filling. *International Journal of Metalcasting*, *13*(2), 255–272. https://doi.org/10.1007/s40962-018-0272-x

Odusote, J. K., and Ajayi, P. A. (2016). Mechanical Properties and Microstructure of Recycled Aluminum Cast with Zinc and Copper Additions. *International Journal of Metalcasting*, *10*(4), 483–490. https://doi.org/10.1007/s40962-016-0060-4

Ravi, B. (2005). *Metal casting: Computer-aided design and analysis*. PHI Learning Pvt. Ltd. https://books.google.com/books?hl=enandlr=andid=_AZ-kckukGwCandoi=fndandpg=PR3anddq=B.+Ravi,+Metal+casting:+Computer-Aide+Design+and+Analysis,+1st+ed.+New+Delhi:+PHI+Learning+Private+Limited,+2005.andots=l_gxzUSs5bandsig=DnqeBs9FefSvdMJMpmmHAQjg6og

Takemoto, Y., Mizumoto, M., and Kinno, K. (2021). Internal Porosity Defects in Ductile Cast Irons. *International Journal of Metalcasting*, *15*(3), 916–929. https://doi.org/10.1007/s40962-020-00527-x

Zhang, X.-P., Chen, G., Xiong, S.-M., and Xu, Q.-Y. (2005). Computer simulation of the solidification of cast titanium dental prostheses. *Journal of Materials Science*, *40*(18), 4911–4916. https://doi.org/10.1007/s10853-005-0418-0

PAPER 38 - IMPACT EVAPOTRANSPIRATION VARIABILITY ON IRRIGATION WATER REQUIREMENT OF HADEJIA VALLEY IRRIGATION PROJECT, NIGERIA

Nura I. Abdullahi*, Adamu A. Dandajeh, Al-Amin D. Bello[1], Abdullahi S. Argungu[1], and Khadijat A. Abdulraheem

Department of Water Resources and Environmental Engineering; Ahmadu Bello University Zaria, Nigeria
*Email: nurafbg@gmail.com

ABSTRACT

There is established evidence on impact of climate change on irrigation. This study therefore examines how changes in evapotranspiration affect the irrigation needs of the Hadejia Valley Irrigation Project. Using meteorological data spanning 39 years (1976-2015), a CROPWAT programme was employed to calculate the reference evapotranspiration and irrigation requirements of the study area. Mann-Kendal and Sen's slope estimates were applied to investigate the trend of the series. Results indicated that the reference evapotranspiration ranged from 4.3 mm/day to 6.70 mm/day, with an average of 5.41 mm/day. Variability in evapotranspiration was observed across the months, with an annual increasing trend of 0.0027 mm/year. The irrigation requirements ranged from 2.2 mm/month to 337 mm/month. Time series analysis showed variability in the monthly series, with an annual increasing trend of 0.140 mm/year, resulting in an annual increase of 7420m^3 of irrigation requirement. The study concludes that the variability of irrigation water requirement poses a challenge for the valley and recommends that irrigation managers and policymakers consider this variability while planning for irrigation.

KEYWORDS*:* CROPWAT, Evapotranspiration, Irrigation, Penman-Monteith, Water

1.0 INTRODUCTION

A 2009 report by the FAO projected that the global population would reach 9.1 billion by 2050, and feeding everyone would require a 70% increase in global food production. Global water resources are under strain due to climate change and variability, which is expected to worsen aridity and increase water requirements in affected areas, (Hargreaves *et al.,* 1993). Research has shown that climate change has already impacted irrigation requirements in different regions. For example, studies have projected an increase in irrigation water demand in Indonesia, Nepal, and Nigeria among other regions, (Saputra *et al.,* 2021; Kaini *et al*., 2022; Ofordu *et al*. 2022). These findings highlight the importance of understanding how evapotranspiration variability affects irrigation and agriculture for sustainable food security. Thus, this study aims to assess the impact of evapotranspiration variability on the irrigation requirement of Hadejia Valley Irrigation Project (HVIP) in Nigeria.

2.0 MATERIALS AND METHODS

2.1 About the Study Area

Hadejia Valley Irrigation Project (HVIP) is a formal irrigation project in the Hadejia-Jama'are River Basin Development Authority, Nigeria lyingalong the Hadejia River. It is designed with a 2.9 km long feeder canal (FC) that maintains the same cross-section over its entire length. The FC receives water from the storage pond at Hadejia Barrage through the fifteen (15) gates and delivers the same to Main Canals (MCs). Hadejia Barrage is a homogeneous earth-fill embankment dam on the Hadejia River, built between 1981 and 1983 as part of the Hadejia Valley Irrigation Project. The earth-fill embankment is about 2.2 km long and is bounded by the north and south dykes each 12 km long. Its maximum height above natural ground level is 9 m. Its design capacity is 11.4 x 106 m³, intended to act as a weekly buffer for HVIP irrigation, possibly needed when upstream dam releases would fail for a week. Due to the current area under irrigation (5,300 ha) as compared to the designed area (12,500ha), only about 2-4 gates are opened at a time to supply the FC. Fig. 1 presents the map of River Hadejia showing the study area.

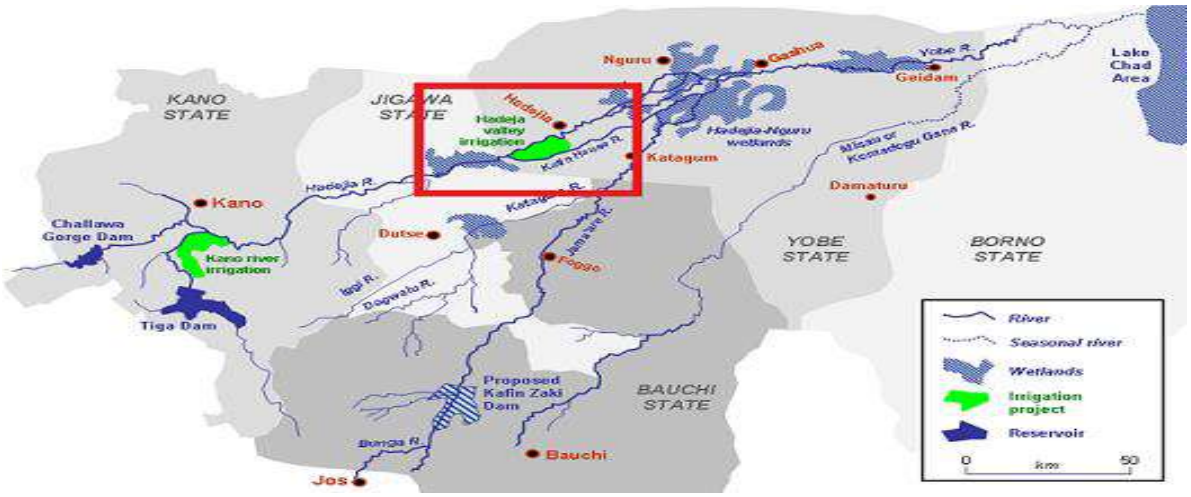

Fig: 1: Map of Hadejia River Showing HVIP

Adopted from Wikipedia, 2024

2.2 Reference evapotranspiration (ETo) and Irrigation requirement

To determine the reference evapotranspiration (ETo) and net irrigation requirement (NIR) of the HVIP scheme, the study employed CROPWAT 8.0. Data on minimum and maximum temperatures, humidity, and wind speed from Nguru Meteorological Station spanning 39 years (1976-2015) were collected on a monthly basis. The Penman-Monteith method (Eq. 1) was used to calculate the ETo of the area. Information on crop coefficients, yield response, and developmental stages was obtained from FAO Irrigation and Drainage Paper No. 56 (Allen *et al.*, 1998). Soil water properties and cropping pattern data (for the year 2016) of HVIP were sourced from Abdullahi (2019). The soil of the study area was found to be sandy clay loam with sand being the dominant soil with 47%, silt 27%, and clay 26%. The average water holding capacity of the soil was found to be 47.26%m^3m^{-3}. The adopted cropping pattern is 85% rice, 10% wheat, and 5% onion.

$$ET_o = \frac{0.408\Delta(R_n - G + \gamma \frac{900}{T_{min} + 273} U_2(e_s - e_a)}{\Delta + \gamma(1 + 0.34U_2)} \quad 1$$

Where:

ETo = reference evapotranspiration [mm day-1], Rn = net radiation at the crop surface [MJ/m2/day1], G = soil heat flux density [MJ/m2/day-1], Tmean = Mean air temperature [°C], u2 = wind speed at 2 m height [ms-1], es = saturation vapour pressure [kPa], ea = actual vapour pressure [kPa], es-ea = saturation vapour pressure deficit [kPa], Δ = slope vapour pressure curve [kPa/ °C], γ = psychrometric constant [kPa/°C].

2.2.1 Variability analysis of reference evapotranspiration and irrigation requirements

The generated program produced a monthly time series spanning 39 years for ETo and NIR, which was utilized to evaluate the variability within the time series data. To analyze the time series, the Mann-Kendall and Sen's Slope Estimate methods were employed as described by (Abdullahi *et.* al., 2017*)*. The resulting change per period (annually) was then utilized to calculate the increase in net irrigation requirement per period, using Equation 2.

$$NIR_{change} = (X(mm/year)/1000) * A * 10000 \quad 2$$

3.0 RESULTS AND DISCUSSION

3.1 Reference Evapotranspiration

Based on the analysis, it was determined that the yearly mean reference evapotranspiration (ETo) in the study area was 5.41 mm/day (1976 mm). The highest average ETo was observed in April at 6.70 mm/day, while the lowest was in January at 4.3 mm/day. Figure 2 displays the average monthly temperature and ETo. These findings align with the research conducted by FMWR-IUCN-NCF (2006), which identified the average ETo in the basin to range from 3.7 mm/day to 8.2 mm/day.

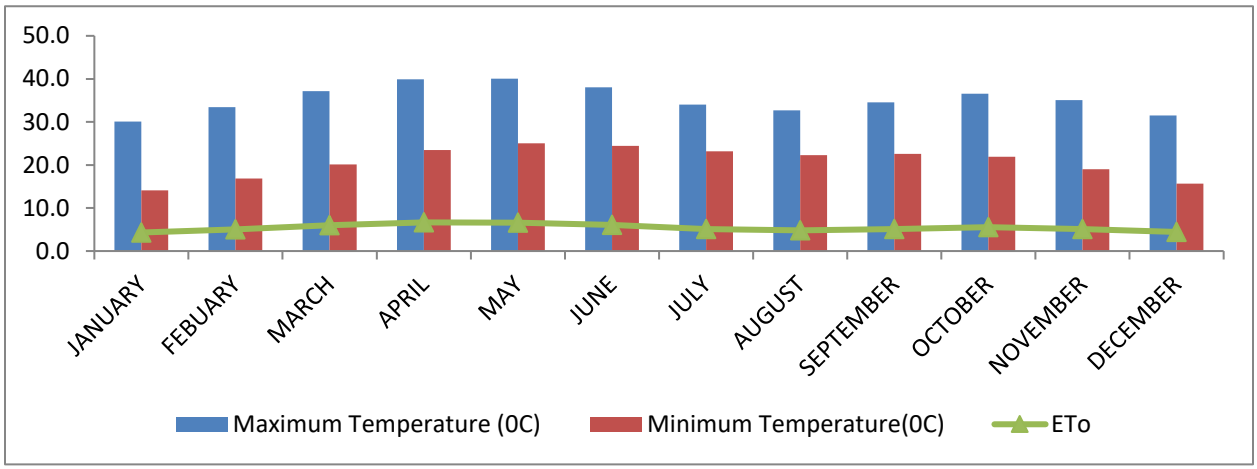

Fig. 2: Mean Monthly Temperatures and ETo

The study's time series analysis revealed that the monthly ETo displayed a varying trend over the study period. The months of January, February, March, July, November, and December showed an increasing trend with rates of 0.0034 mm/year, 0.0060 mm/year, 0.0043 mm/year, 0.0030 mm/year, 0.0106 mm/year, and 0.0075 mm/year, respectively. Conversely, the months of April, May, June, August, September, and October showed a decreasing trend with rates of -0.0002 mm/year, -0.0015 mm/year, -0.0036 mm/year, -0.0050 mm/year, -0.0109 mm/year, and -0.0030 mm/year, respectively. Appendix 1 displays the trend statistic showing the rate of change of ETo per period. Overall, the study observed an annual increasing trend of 0.0027 mm/year (Fig. 3).

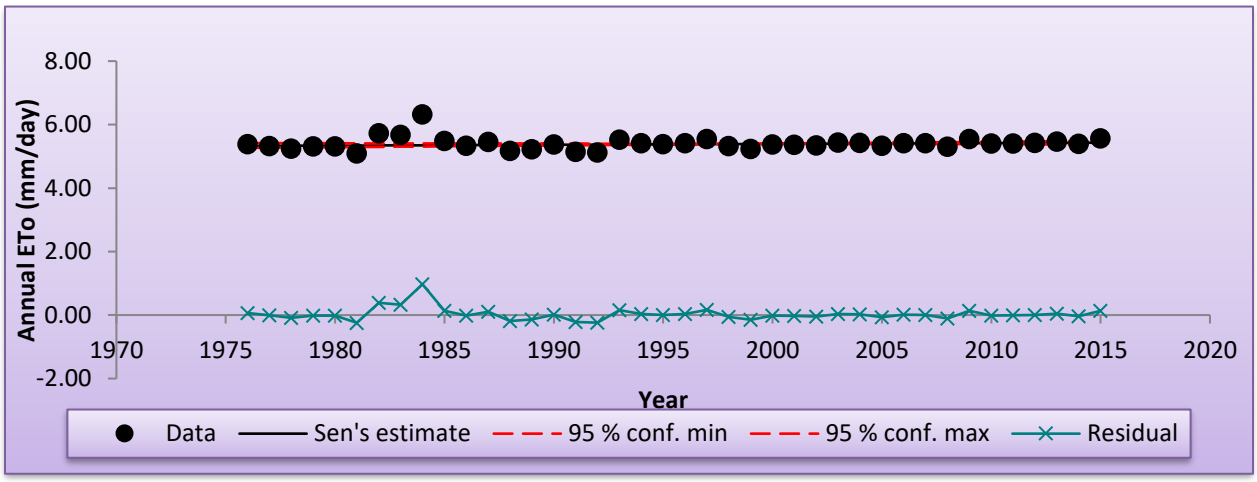

Fig. 3: Annual Tend of Evapotranspiration of HVIP

3.2 Net Irrigation Requirement

Based on our calculations, it seems that the HVIP does not require irrigation during the months of June, July, August, and September. This is because the rainfall during these months is sufficient to compensate for any water loss due to evapotranspiration. In comparison, the month preceding these months, May, has the lowest net irrigation requirement (NIR) across the study period, ranging from 2.2 mm/month to 6.2 mm/month (Fig. 4), with an average of 5.08 mm/month (Fig. 5). On the other hand, the maximum NIR was observed in November, ranging from 231.6 mm/month to 337 mm/month (1984) (Fig. 4), with an average of 302.16 mm/month (Fig. 5). This is likely due to the planting period of the scheme, where evapotranspiration is expected to be higher. This is possibly a result of a relatively higher fraction of solar radiation reaching the soil surface, leading to more evaporation from the cropped soil. As the crops grow and form a canopy that covers a larger percentage of the soil, evaporation tends to decrease, and transpiration becomes the main process of water loss.

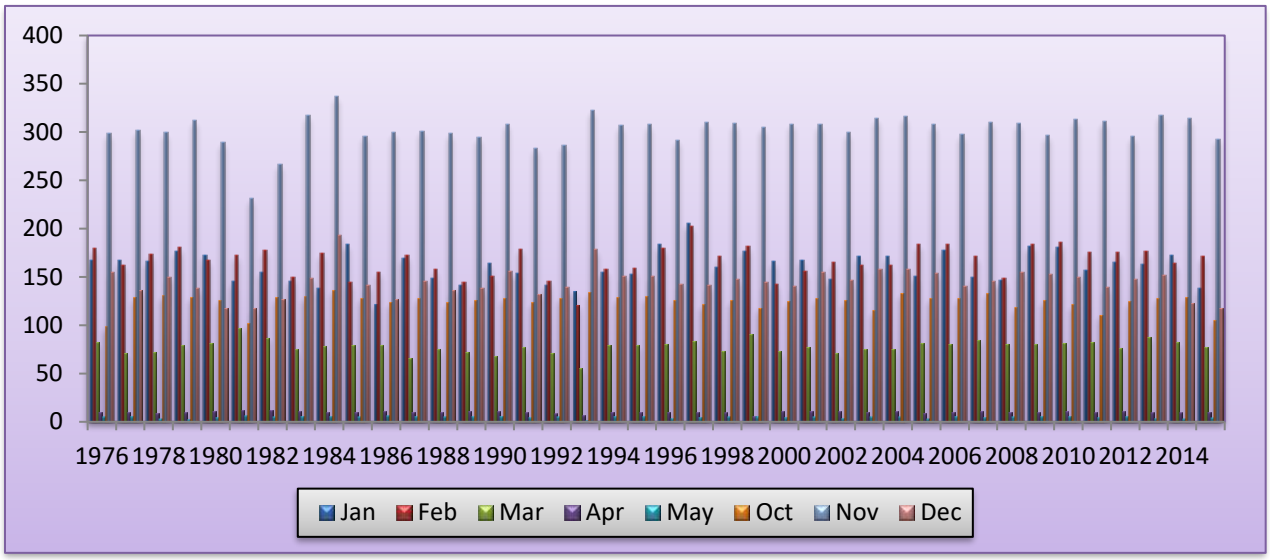

Fig. 4: Net Irrigation Water Requirement of HVIP

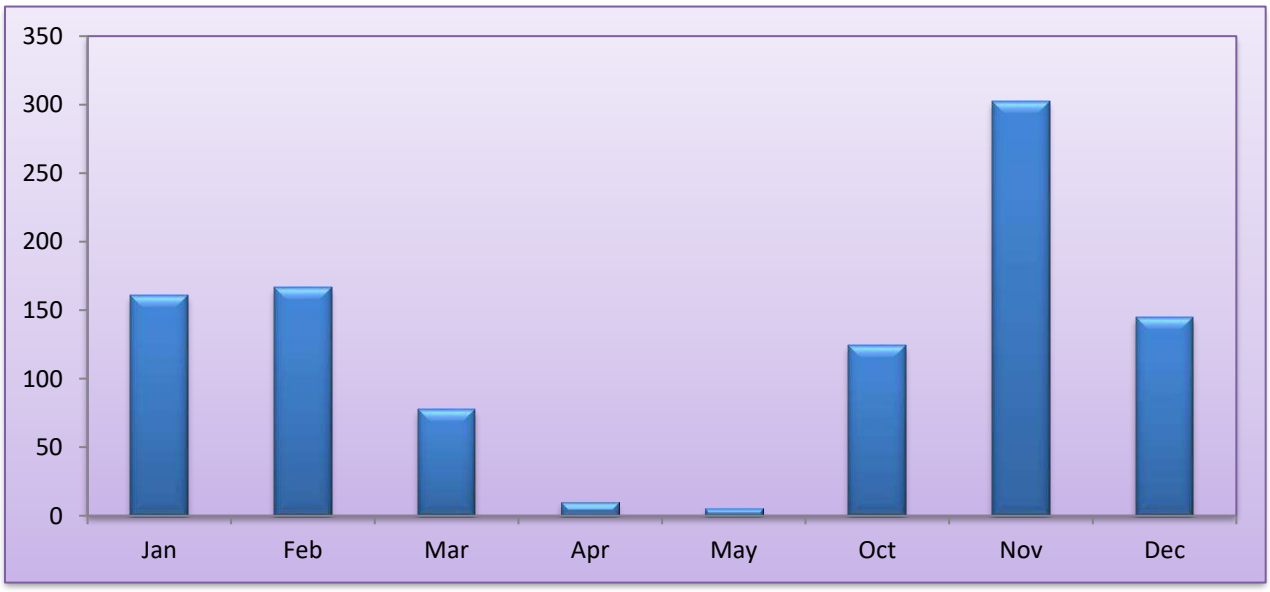

Fig. 5: Monthly Average Net Irrigation Requirement

The study's findings on time series analysis indicate a variation in the monthly NIR trend over the observed period. January, February, March, November, and December showed an upward trend at 0.127 mm/year, 0.231 mm/year,

0.118 mm/year, 0.345 mm/year, and 0.195 mm/year, respectively. Conversely, April, May, and October showed a downward trend at -0.007 mm/year, -0.014 mm/year, and -0.067 mm/year, respectively. To view the rate of NIR change per period, please refer to Appendix 1. Overall, the results showed an annual increase of 0.140 mm/year (Fig. 6, Appendix 1). Given the cultivation area of 5300 ha within the scheme, the change would lead to an average increase of 7420 m^3 per year.

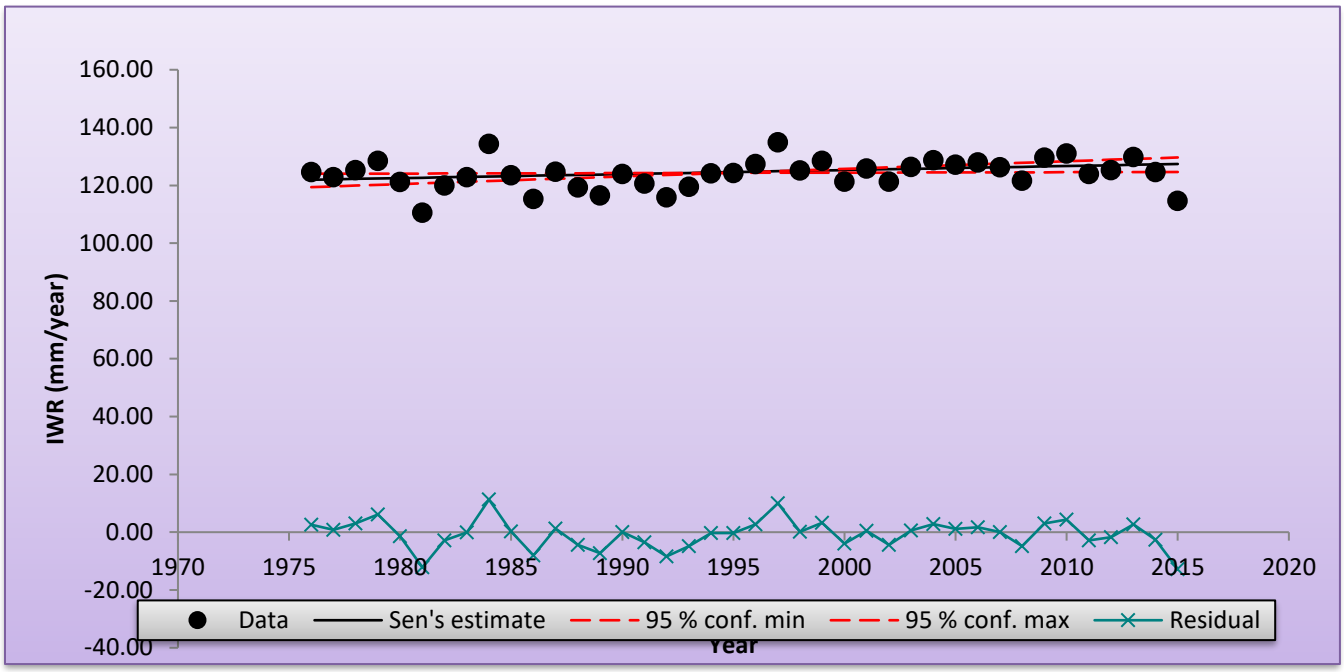

Fig. 6: Annual Tend of Net Irrigation Requirement of HVIP

4.0 CONCLUSION AND RECOMMENDATION

This study utilized the FAO computer programme for the calculation of crop water requirements and irrigation requirements (CROPWAT 8.0) and models for reference evapotranspiration and net irrigation requirement of HVIP between the periods of 1976-2015. The output from the programme was further subject to trend analysis using Man-Kendall and Sen's Slope method to analyze the variability within the time series. The following results were drawn from the study.

- A monthly upward trend of reference evapotranspiration was observed in January, February, March, July, November and December at the rate of 0.0034 mm/year, 0.0060 mm/year, 0.0043 mm/year, 0.0030 mm/year, 0.0106 mm/year, and 0.0075 mm/year respectively
- A monthly downward trend of reference evapotranspiration was observed in April, May, June, August, September, and October at the rate of -0.0002 mm/year, -0.0015 mm/year, -0.0036 mm/year, -0.0050 mm/year, -0.0109 mm/year, and -0.0030 mm/year respectively
- An annual upward trend of evapotranspiration at the rate of 0.0027 mm/year
- A monthly upward trend of net irrigation requirement was observed in January, February, March, November, and December at the rate of 0.1268 mm/year, 0.2311 mm/year, 0.1179 mm/year, 0.3481 mm/year, and 0.1950 mm/year respectively
- A monthly downward trend of net irrigation requirement was observed in April, May, and October at the rate of -0.0068 mm/year, -0.0143 mm/year, and -0.0667 respectively
- An annual upward trend of net irrigation requirement at the rate of 0.140 mm/year
- The study finally established an annual increase of net irrigation requirement of 7420m^3 in the study area

The study therefore recommends for irrigation managers and policymakers consider this variability while planning for irrigation.

REFERENCES

Abdullahi N.I. (2019). Assessment and Planning of Surface Water Resources Management of Hadejia-Jama'are River Basin, Nigeria. Department of Water Resources and Environmental Engineering, Ahmadu Bello University Zaria. Nigeria. Unpublished Thesis

Abdullahi, N.I., A. Ismail, Adie, D.B. and Ajibike, M.A., (2017). Trends Analysis of Monthly Wind Speed and Relative Humidity of Hadejia, A Watershed Of Komadugu-Yobe Basin, Nigeria. *Nigerian Journal of Scientific Research, 16(4)*:524-530.

Allen, R. G. and Pereira, L. S. (1998). Crop Evapotranspiration *(guidelines for computing crop water requirements)*. FAO Irrigation and Drainage Paper No. 56

FAO (2009). Global Agriculture Towards 2050 (*High-Level Expert Forum - How to Feed the World in 2050*) Food and Agriculture Organization

FMWR-IUCN-NCF. (2006). Water Audit for Komadugu-Yobe Basin. *Nigeria's Federal Ministry of Water Resources, International Union for Conservation of Nature, Nigerian Conservation Foundation*.

Hargreaves, G. H., Paul Riley, J. and Sikka, A. (1993). Influence of Climate on Irrigation. *Canadian Water Resources Journal*, *18*(1), 53–59. https://doi.org/10.4296/cwrj1801053

Kaini, S., Harrison, M. T., Gardner, T., Nepal, S. and Sharma, A. K. (2022). The Impacts of Climate Change on the Irrigation Water Demand, Grain Yield, and Biomass Yield of Wheat Crop in Nepal. *Water (Switzerland)*, *14*(17). https://doi.org/10.3390/w14172728

Ofordu, C. S., Okoro, E. O., Aigbokhan, E.O. and And Mba, O. J. (2012.). Impact of Climate Variability on Irrigation Water Needs and Irrigation Schedules of Maize and Cucumber in Aba, Abia State. In *Nigerian Agricultural Journal* (Vol. 53, Issue 2). http://www.ajol.info/index.php/najhttps://www.naj.asn.org.ng

Saputra, A. W. W., Zakaria, N. A., and Chan, N. W. (2021). Assessing Effects of Climate Change on Irrigation Water Demand in the Lombok River Basin, Indonesia. *IOP Conference Series: Earth and Environmental Science*, *930*(1). https://doi.org/10.1088/1755-1315/930/1/012061

Wikipedia (2004): https://en.wikipedia.org/wiki/Yobe_River assessed on 8th March, 2014

Appendix 1: Trend Statistics of Reference Evapotranspiration and Net Irrigation Requirement of HVIP Site

			Reference Evapotranspiration		**Net Irrigation Requirement**	
Time series	First-year	Last Year	Test Z	Change per Year, mm/year (Q)	Test Z	Change per Year, mm/year (Q)
January	1976	2015	0.4895	0.0034	0.5476	0.1268
February	1976	2015	0.9440	0.0060	1.1303	0.2311
March	1976	2015	0.7225	0.0043	1.5034	0.1179
April	1976	2015	-0.1517	-0.0002	-0.8300	-0.0068
May	1976	2015	-0.2681	-0.0015	-1.2843	-0.0143
June	1976	2015	-0.6410	-0.0036	N/A*	N/A
July	1976	2015	0.7228	0.0030	N/A	N/A
August	1976	2015	-0.5943	-0.0050	N/A	N/A
September	1976	2015	-1.6902	-0.0109	N/A	N/A
October	1976	2015	-0.6063	-0.0030	-1.3986	-0.0667
November	1976	2015	2.0865	0.0106	1.8876	0.3481
December	1976	2015	1.1660	0.0075	1.1535	0.1950
ANNUAL	**1976**	**2015**	**1.5496**	**0.0027**	**2.1554**	**0.140**

PAPER 39 - PARAMETRIC STUDY OF A SUITABLE VOLUME FRACTION OF AGGREGATE FOR THE COMPRESSIVE STRENGTH OF CONCRETE IN MESOSCALE MODEL

O. T. Fatai[1], Y. O. Babatunde[1*]

[1]Department of Civil Engineering, University of Ilorin, Ilorin, Nigeria.
[*]Email: babatunde.oy@unilorin.edu.ng

ABSTRACT
Concrete is a composite material with a heterogeneous internal structure.It is represented in multi-phase composite material at the macro, meso, micro, and nano levels. The mesolevel appears to be the most practicable approach for evaluating the composite behaviour of concrete. The mesostructure of concrete is mainly consist of mortar, coarse aggregate, and interfacial transition zones. This structure can be represented in 2D or 3D. Most previous works adopted the trial and error method to determine a suitable volume fraction of aggregates (between 30-50%) to predict the compressive strength of concrete. This paper proposes a suitable volume fraction of aggregates in the mesoscale modelling of normal-strength concrete. The Monte Carlo random sampling principle was used to generate the mesostructure using a Python random aggregate generator (RAG). The volume fraction was varied and the mesostructure was meshed using a tetrahedral element in ABAQUS. The mechanical behaviour was modelled using concrete damage plasticity, present in ABAQUS, under uniaxial compression.The results showed that 30%, 35%, and 40% volume fractions of aggregate gave compressive strengths of 27.8 MPa, 30.8 MPa, and 34.5 MPa, respectively.A 35% volume fraction of aggregate is proposed in predicting the compressive strength of concrete in mesoscale model and should be used in studying crack initiation and propagation of normal-strength concrete.

KEYWORDS: Mesoscale , Volume-Fraction, Mesh, FEA.

1. INTRODUCTION

The innovative interest in exceeding the limits of building structures has led to the construction of taller, lighter, or longer structures. One of the challenges engineers face is developing construction materials that can resist greater loads or withstand unfavorable environmental conditions experienced by these structures. Modern construction materials are expected to be light, have high resistance, and posses high durability in a corrosive environment, humidity, and severe thermal change. Material design requires not only laboratory experiments but also numerical simulations. Although data from real experiments are invaluable for constitutive model development and validation, such experiments are limited by cost, complexity, and inability to physically replicate certain experiments(Okereke and Akpoyomare, 2013). Concrete is a composite material with complex microstructure used in the structural design which spans several length scales. In structural design, concrete is often assumed to be a linear elastic homogeneous material. However, a closer view reveals that concrete exhibits a complex behaviour even when subjected to normal loading conditions(Thakur *et al*., 2023). Therefore, concrete possesses a heterogeneous internal material structure and is not homogeneous as assumed from the structural design viewpoint. Concrete has a nonlinear behaviour characterized by initiation, propagation, and accumulation of micro cracks within its internal structure(Ansari, 2020). Consequently, concrete failure is a multiscale phenomenon- its behaviour is greatly influenced by its multiphase materials rather than a single phase (Unger *et al*., 2011).The main three length scales of concrete are macroscale, mesoscale, and microscale(Wang and Jivkov, 2015). Macroscale models treat concrete as an isotropic homogeneous continuum, lumping the constituent materials of concrete together as a single phase. This approach ignores the material heterogeneity, limiting its ability to predict the macroscopic behavior of concrete. In contrast, mesoscale and microscale models consider concrete's heterogeneity. Among these length scales, mesoscale provides a practical method to predict the macroscopic properties of concrete from the heterogeneity of the underlying structure. Understanding the mesoscale fracture behavior of concrete materials has significant implications for macroscopic structural performance. Mesoscale simulations reveal crack propagation patterns and interactions, enabling the design of more robust structures with improved resistance to failure. This knowledge enhances load-carrying capacity and strength by optimizing concrete mix designs and reinforcing vulnerable areas. These insights also guide material selection and optimization, evaluating different compositions to meet specific performance requirements. These applications advance concrete engineering practices, ensuring safer and more durable structures in various practical engineering scenarios. Meso-structure of concrete is mainly composed

of mortar, coarse aggregate, and interfacial transition zones (ITZ) and the structure can be represented in 2D or 3D. Based on the size distribution and spatial arrangement of aggregates, concrete mesostructure can be generated using either Image-based modelling or parameterization modelling (Zhang *et al.,* 2023).Image-based modelling employed digital image acquisition, such as X-ray computed tomography (XCT), of the practical size and location of aggregates in generating the mesostructure of concrete. In this approach, the 2D images produced from XCT can be analysed and reconfigured into a 3D model, which can then be further meshed using either a self-created algorithm or commercial software (Wang *et al.,* 2022) . On the other hand, parameterization modelling generates mesostructure by random generation of aggregate sizes and spatial distribution of aggregates of given shapes with a specific size distribution. The former approach gave a realistic representation of the mesostructure, accurate geometry and voids can be generated. However, it is very expensive, and the generation of adequate scanned images from samples to make reasonable statistical analysis is time-consuming (Wang *et al.,* 2016). Direct parameterization modelling has the advantage of varying independent parameters of mesostructure, such as shape, volume fractions, size, and spatial distribution of voids/pores and aggregates (Wang *et al.,* 2016). This advantage makes parameterization modelling suitable for statistical analysis of failure and damage of concrete, hence, it's widely used by several researchers in modelling the mesostructure of concrete.Several different methods have been developed in generating the mesoscopic structure that represents the real concrete in parameterization modelling (Wang *et al.,* 2016). Take-and-place method, divide-and-fill method, stochastic-heuristic algorithm, random particle drop method, and distinct element method are methods proposed by different researchers (Wriggers and Moftah, 2006). Among all these methods, the take-and-place method offers a simple and straightforward approach to randomly generating and placing aggregates in a concrete specimen (Maleki *et al.,* 2020). Particle shape, size distribution and volume fraction are main parameters used in the take-and-place method. Spherical, ellipsoidal, and polyhedral shapes have been employed in representing the shape of aggregates in past studies. The volume fraction of normal-strength concrete aggregate is between 30 to 50% based on mixed design (Naderi *et al.,* 2021). Most of the previous work on mesoscale modelling only gave a range of volume fractions of aggregate which led to different researchers using different volume fractions within the range or using trial and error until a volume fraction yielded a result closer to the experimental result, even though they were working on the same type of concrete (normal strength concrete). It is then deemed necessary to propose a unified or an average volume fraction within the range of normal strength concrete which produces a result closer to the experimental results, thereby saving the time that would have been wasted on trying different volume fractions until obtaining a volume fraction that produces a closer compressive strength value when compared to the experimental result. This is achieved by varying the volume fraction of aggregates, generating the mesostructure for each volume fraction, and conducting Finite Element Analysis (FEA) on each of the generated mesostructure samples to determine their compressive strengths. The predicted compressive strengths will then be compared with the experimental result. The volume fraction aggregate that closely aligns with the experimental result will then be proposed as the unified or average volume fraction.

2. THEORETICAL ANALYSIS

2.1 Particle Size Distribution

The particle size distribution is modelled using a fuller curve. Concrete is typically modelled after the Fuller curve, which depicts a grading of aggregate particles and produces the best density and strength of the concrete mixture. An easy equation can be used to describe a fuller curve.

$$P(d) = 100\left(\frac{d}{d_{\max}}\right)^{n} \tag{2.1}$$

Where $p(d)$ is the cumulative percentage passing a sieve of diameter d , $d_{\max}$ is the maximum size of aggregate particles and n is the exponent of the equation (n = 0.45–0.70), which is taken as 0.5 in this study.

The particle size distribution of aggregate is divided into segments and the volume of each segment was computed using the modified fuller curve formula written below:

$$V_p[d_s, d_{s+1}] = \frac{P(d_s) - P(d_{s+1})}{P(d_{\max}) - P(d_{\min})} \times v_p \times V \tag{2.2}$$

Where $V_p[d_s, d_{s+1}]$ is the volume of aggregate within the grading segment $[d_s, d_{s+1}]$, d is the aperture size of the sieve, $d_{\max}$ and $d_{\min}$ are the maximum and minimum sizes of coarse aggregate, respectively. v_p is the volume fraction of the aggregate and V is the volume of the concrete cube specimen.

2.2 Concrete Damage Plasticity

The Concrete damage plasticity (CDP) is used to model the mechanical behaviour of the meshed mesoscale model of the cubic specimen. The CDP models the mechanical behaviour of mortar since the aggregate is assumed to be elastic. As reported by (Wang *et al*., 2022), the tensile behaviour of concrete is linear elastic up to the peak stress, which follows equation (2) in the post peak region:

$$\frac{\sigma_t}{f_t} = \frac{\frac{\varepsilon_t}{\varepsilon_{t0}}}{\alpha_t\left(\frac{\varepsilon_t}{\varepsilon_{t0}} - 1\right)^{1.7} + \frac{\varepsilon_t}{\varepsilon_{t0}}} \tag{2.3}$$

Where σ_t is the current tensile stress, ε_t is the current tensile strain, σ_{t0} is the peak stress, ε_{t0} is the corresponding strain, and α_t is the coefficient obtained by $\alpha_t = 0.312\sigma_{t0}^2$

The full compressive behaviour is given:

where ε_{cu} is the strain at damage initiation, α_a is a coefficient calculated by $\alpha_a = 2.4 - 0.0125\,\sigma_{cu}$, and α_d is a coefficient given by $\alpha_d = 0.157\,\sigma_{cu}^{0.785} - 0.905$. The initial behaviour of concrete is linear elastic. This is followed by a brief hardening plasticity with limited damage until peak stress, and increasing damage leading to strain softening(Wang *et al*., 2022).

$$\frac{\sigma_c}{f_c} = \begin{cases} \frac{E_0\varepsilon_c}{f_c}, \frac{\sigma_c}{f_c} \le 0.4 \\ \alpha_a\frac{\varepsilon_c}{\varepsilon_{cu}} + (3-2\alpha_a)\left(\frac{\varepsilon_c}{\varepsilon_{cu}}\right)^2 + (\alpha_a - 2)\left(\frac{\varepsilon_c}{\varepsilon_{cu}}\right)^3, \frac{\sigma_c}{f_c} \ge 0.4 \;\&\; \frac{\varepsilon_c}{\varepsilon_{cu}} \le 1 \\ \frac{\frac{\varepsilon_c}{\varepsilon_{cu}}}{\alpha_d\left(\frac{\varepsilon_c}{\varepsilon_{cu}} - 1\right)^2 + \frac{\varepsilon_c}{\varepsilon_{cu}}}, \frac{\varepsilon_c}{\varepsilon_{cu}} \ge 1 \end{cases} \tag{2.4}$$

The remaining parameter such as inelastic strain and crack strain for compressive and tensile data were generated using the formula.

$$\varepsilon_c^{in} = \varepsilon_c - \frac{\sigma_c}{\mathrm{E}_o} \tag{2.5}$$

$$\varepsilon_t^{cr} = \varepsilon_t - \frac{\sigma_t}{\mathrm{E}_o} \tag{2.6}$$

Where ε_c^{in}, ε_c, ε_t^{cr}, ε_t, and E_o are the inelastic strain, total compressive strain, cracking strain , total tensile strain , and young's modulus, respectively.

Damaged parameter for the CDP model was also calculated using the formula below:

$$d_c = 1 - \frac{\sigma_c}{\sigma_{cu}} \tag{2.7}$$

$$d_t = 1 - \frac{\sigma_t}{\sigma_{to}} \tag{2.8}$$

Where d_c, σ_c, and σ_{cu} are damage parameter, compressive strength and maximum compressive strength respectively.

3. MATERIALS AND METHODS

The controlling parameters of the 3D mesoscale model such as particle size distribution, volume fraction of aggregates, Representative Volume Element (RVE) size, and shape of aggregates were inputted as the input parameters.

3.1 Particle Size Distribution

Table 3.1: Particle size distribution of coarse aggregate in concrete (Wang *et al*.,2016)

Sieve size (mm)	Total percentage retained (%)	Total percentage passing (%)
9.5	39	61
4.75	90	10
2.36	98.6	1.4

RVE size of 50mm was used as the concrete cube size and spherical shape was taken as the aggregate shape for simplicity. The volume fraction of aggregates were varied using 30, 35, and 40 percent volume fractions, respectively. The volume of each segment in the particle size distribution was generated based on the cube size, aggregate shape, volume fraction and particle size distribution of aggregate.

3.2. Take And Place Method

On generating the volume of each segment in the particle size distribution the take and place method was employed in generating the 3D meso-structure of the model.

3.2.1 Taking Process

A Python program was developed in implementing the following steps:

1. Calculate the volume of aggregate to be generated in the grading segment using equation(1)
2. Generate a random number defining the size of an aggregate particle. Assuming that the size d has a uniform distribution between d_s and d_{s+1}, it may be calculated using the following expression:

   $$d = d_s + \eta\left(d_{s+1} - d_s\right) \tag{3.1}$$

   Where η is a random number uniformly distributed between 0 and 1.
3. Calculate the volume of the generated aggregate particle and subtract it from the volume of aggregate within the grading segment.
4. Repeat steps 2 and 3 until the volume of aggregate left to be generated is less than $\frac{4}{3}\pi\left(\frac{d_{s+1}}{2}\right)^3$, i.e not enough for generating another particle. The remaining volume of aggregate to be generated is then transferred to the next grading segment.

Repeat all the above steps for the next smaller size grading segment and then again for successively smaller size grading segment, until the last particle of the smallest size has been generated.

3.2.2 Placing Process

The generated particles are placed inside the cube with a random position describe by the formula below:

$$X = X_{\min} + \eta\left(X_{\max} - X_{\min}\right) \tag{3.2}$$

Where X is the coordinate of each particle generated, $X_{\min}$ and $X_{\max}$ are the minimum and maximum coordinates of the concrete cube.

The following steps is employed while placing individual aggregate

1. Random numbers that represent the coordinate of the particle are generated
2. The generated coordinate is checked against the placing conditions.
   Distance between particle is calculated using the formula below

$$\sqrt{\left(x_0^{'}-x_0\right)^2+\left(y_0^{'}-y_0\right)^2+\left(z_0^{'}-z_0\right)^2} \le r+r^{'} \tag{3.3}$$

where $x_0^{'}$, $y_0^{'}$ and $z_0^{'}$ are the coordinates of centre of the newly generated sphere; $r_0^{'}$ is the radius of the new sphere.

3. The coordinate is rejected if any of the placing conditions is not satisfied. If the failed condition is due to overlapping of aggregates, a translation-rotation algorithm will be used as proposed by (Wriggers and Moftah, 2006).

The size of each aggregate and its corresponding position in the RVE is saved in a CSV file, as shown below:

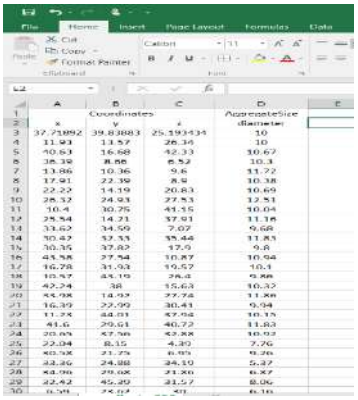

(a) 30% Volume fraction

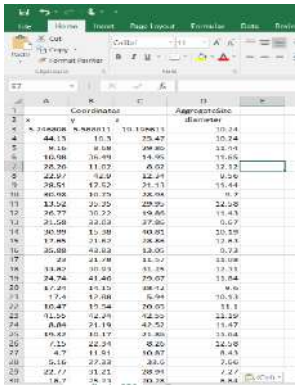

(b) 35% Volume fraction

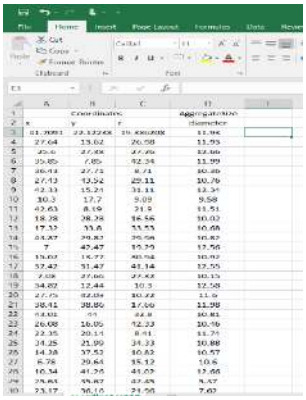

(c) 40% Volume fraction

Figure 3.1: Sizes and coordinates of aggregate particles of different volume fractions.

3.3 Importation Of Generated Mesosrtucture Into Abaqus

The coarse aggregate sizes were employed to create the spherical aggregates, and their respective positions were utilized to accurately place these aggregates within the representative volume element (RVE). Boolean operations available in the software were then applied to create the mortar phase by subtracting the volume occupied by aggregates from that of the RVE, utilizing the cut/merge option in Abaqus. To ensure accurate meshing, tetrahedral elements were used to mesh both the generated mortar and aggregates, specifically chosen to accommodate the spherical aggregates.

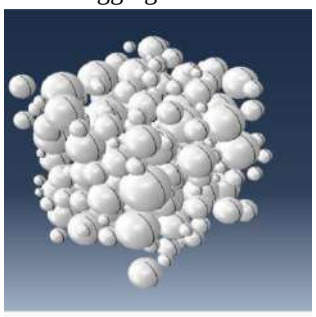

(a) 30% volume fraction

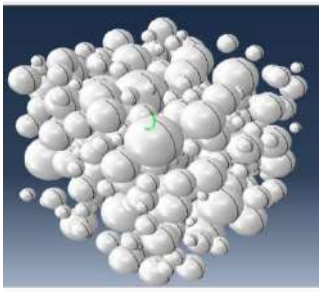

(b) 35% Volume fraction

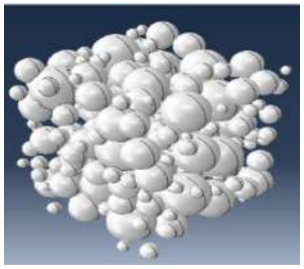

(c) 40% Volume Fraction

Figure 3.2: Generated Aggregate particles of different volume fractions.

3.4 Mechanical Property

3.4.1 Coarse Aggregate

Coarse aggregate is modelled as an elastic material because its resistance is higher than that of mortar. It is also assumed that the stress causing crack initiation is less than the strength of aggregates, therefore cracks are attributed to mortar. The Young's modulus, poison ratio, and density of coarse aggregate are obtained from available literature.

Table 3.2: Material Properties	Mortar	Aggregate
Young's modulus(MPa)	25000	60000
poison's ratio, v	0.2	0.2
Density ,ρ(kg/m^3)	2200	2600

3.4.2 Mortar

Mortar is described as an elastoplastic material. The following properties of mortar were considered while modelling: Young's modulus of mortar was obtained from the compressive strength test results carried out in the laboratory on mortar, and its density was determined before the test. Parameters such as dilation angle, flow potential eccentricity, biaxial/uniaxial compression plastic strain ratio, invariant stress ratio, and viscosity parameter have default values in Abaqus CAE.

Mortar is described as an elastoplastic material. The following properties of mortar were considered while modelling: Young's modulus of mortar was obtained from the compressive strength test results carried out in the laboratory on mortar, and its density was determined before the test. Parameters such as dilation angle, flow potential eccentricity, biaxial/uniaxial compression plastic strain ratio, invariant stress ratio, and viscosity parameter have default values in Abaqus CAE.

3.5 Multi Scale Model

The CDP models the mechanical behaviour of mortar since the aggregate is assumed to be elastic. A uniaxial compression behaviour is modelled which will give a compressive stress-strain curve. The discussion of the CDP model is present in Abaqus manual, however the parameters of importance are the yield stress, in-elastic strain for compressive behaviour or cracking strain for tensile, damage parameter for both compressive and tensile cases.The parameters need for the CDP model for uniaxial compressive strength test are the mortar compressive strength σ_{cu}, corresponding strain ε_{cu} .These parameters were obtained from the compressive strength test result. CDP requires both tensile and compressive strength data. Equation 2.5 is used to generate tensile strength data and 2.6 was used to generate compressive strength data.

3.6 Loading

A displacement load was applied only in the vertical direction at the top of the concrete cube until failure occurred. This was modelled using displacement boundary condition at the upper part of the cube, while the bottom of the cube was given zero displacement in all directions.

4. RESULTS AND DISCUSSION

The compressive strengths(which are represented by the peak stresses in the graphs) of concrete predicted by 30%, 35%, and 40% aggregate volume fractions, as shown in Figure 4. (a) to (c), were 27.8 MPa, 30.8 MPa, and 34.5 MPa, respectively. The experimental result of the compressive strength of concrete tested using a Universal Testing Machine (UTM) was 30 MPa. Figure 4 (d) shows a comparison between the experimental result and the predicted results of the varied volume fractions. The predicted compressive strength of the 30% volume fraction is less than the experimental result. This is due to the large volume of mortar compared to aggregates since mortar and aggregates collectively contribute to the strength of concrete. Mortar is weaker than aggregates in compression; this is supported by the assumption that crack initiation and propagation occur in mortar since the stress causing cracks in concrete is less than the compressive strength of aggregates(Naderi and Zhang, 2021). The lower predicted strength is attributable to the large volume of weak mortar compared to aggregates. The compressive strength predicted by the 35% volume fraction is closely aligned with experimental results. This can be associated with increased aggregate contents in the model, which represents, on average, a realistic volume fraction of aggregates present in concrete of any mix design. The compressive strength predicted by the 40% volume fraction of aggregates was far higher than the experimental compressive strength. The high strength was due to the volume of aggregates compared to other volume fractions since the strength of aggregates is higher than mortar. It over-predicted the compressive strength of concrete.

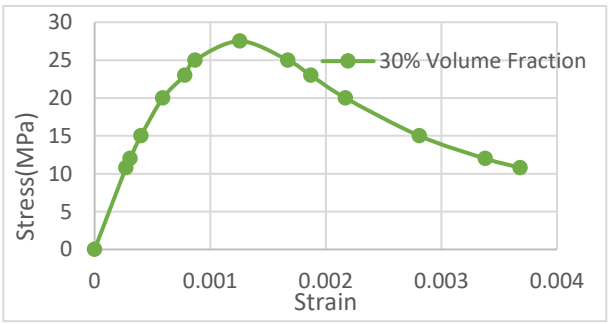

(a)

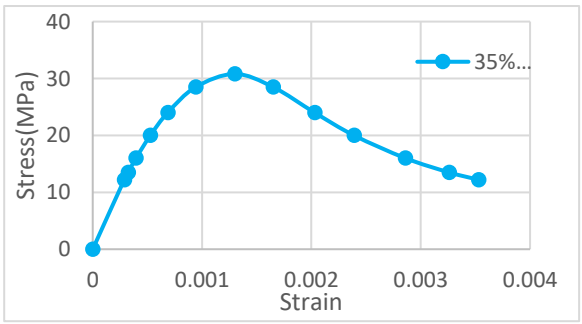

(b)

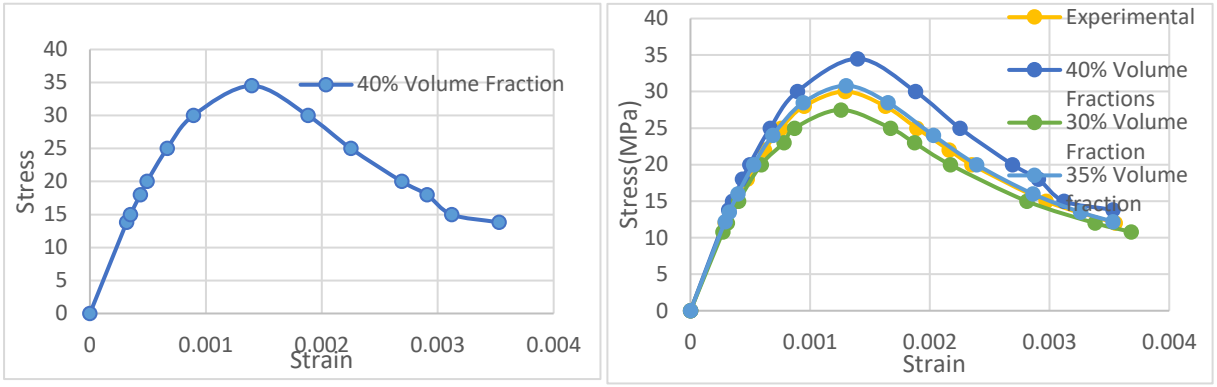

(c) *(d)*

Figure 4: (a) Predicted Stress-strain curve of 30% volume fraction, (b) Predicted Stress-strain curve of 35% volume fraction, (c) Predicted Stress-strain curve of 40% volume fraction (d) Comparison of the experimental stress-strain curve with the predicted stress-strain curve of aggregate volume fraction of 30%,35%, and 40%.

5. CONCLUSION

The volume fraction of coarse aggregate that correctly predicted the compressive strength of aggregate when validated with the experimental result is 35% volume fraction. The implemented algorithm gave a valid representation of the meso-structure of concrete.

Based on this study, the following recommendations will be made;

i. The 35% volume fraction of coarse aggregates should be used to study the crack initiation and propagation in normal-strength concrete.
ii. There should be a generalized or average value of coarse aggregate Young's modulus in the absence of experimental value.

REFERENCES

Ansari M. (2020). Simulation methods for functional and microstructured composite materials.

Hu L. S. and Chen, S. F. (2011). 3-D Numerical Modelling of Mesoscopic Configuration and Cracking of Concrete. Paper presented at the Advanced Materials Research.

Liu L., Shen D., Chen H., and Xu W. (2014). Aggregate shape effect on the diffusivity of mortar: A 3D numerical investigation by random packing models of ellipsoidal particles and of convex polyhedral particles. *Computers and structures*, 144, 40-51.

Maleki M., Rasoolan I., Khajehdezfuly I., and Jivkov A. P. (2020). On the effect of ITZ thickness in meso-scale models of concrete. *Construction and Building Materials*, 258, 119639.

Naderi Sadjad, Tu W., and Zhang, M. (2021). Meso-scale modelling of compressive fracture in concrete with irregularly shaped aggregates. *Cement and concrete research*, 140, 106317.

Okereke M.I., and Akpoyomare, A.I. (2013). A virtual framework for prediction of full-field elastic response of unidirectional composites. *Computational materials science*, 70, 82-99.

Thakur M. M., Henningsson, N. A., Engqvist, J., A., Pierre-Olivier, W., Jonathan P., and Hurley, R. C. (2023). On mesoscale modeling of concrete: Role of heterogeneities on local stresses, strains, and representative volume element. *Cement and Concrete Research*, 163, 107031.

Unger J. F., and Eckardt, S.. (2011). Multiscale modeling of concrete: from mesoscale to macroscale. *Archives of computational Methods in Engineering*, 18, 341-393.

Wang J., Jivkov, A. P., Engelberg, D. L., and Li, Q. (2022). Image-Based vs. Parametric Modelling of Concrete Meso-Structures. *Materials*, 15(3), 704.

Wang, Xiaofeng, and Jivkov, Andrey P. (2015). Combined numerical-statistical analyses of damage and failure of 2D and 3D mesoscale heterogeneous concrete. *Mathematical Problems in Engineering*.

Wang X., Zhang, M., and Jivkov A. P. (2016). Computational technology for analysis of 3D meso-structure effects on damage and failure of concrete. *International Journal of Solids and Structures*, 80, 310-333.

PAPER 40 - SYNTHESIS AND EFFICIENCY EVALUATION OF SODIUM ALGINATE-CHITOSAN HYDROGEL POLYELECTROLYTE COMPLEX FILTER FOR TREATMENT OF OIL SPILLAGE

M. Baba Saje[1*], T. O. Uthman[2]

[1]Department of Chemistry, Nile University of Nigeria, Abuja, Nigeria.
[2]Department of Biochemistry, Nile University of Nigeria, Abuja, Nigeria.
*Email: MBabaSaja@outlook.com

ABSTRACT
Crude oil spills pose considerable environmental concerns thereby demanding the development of effective, sustainable, and eco-friendly remediation solutions. This study aims to synthesize and evaluate the efficiency of a biodegradable polymer filter using sodium alginate and chitosan for the treatment of oil spillage. The sodium alginate-chitosan hydrogel polyelectrolyte complex (SACHPC) filter was synthesised based on dipping method using a layer-by-layer self-assembly technique integrated with cotton wool as the filter medium. The efficiency of the filter was evaluated based on the flow rate of recovered oil and the reusability of the filter. Simulated oil spillage of 0.5 M was subjected to filtration using the SACHPC filter. The flow rate was determined based on the time taken for 1 L of oil to pass through the filter. The SACHPC filter exhibited underwater superoleophobic behaviour with exceptional filtration efficiency (> 98.3%) across various scenarios (pH 3, 7 and 11). The flow rate of the filter was 25 x 10^5 m/s, while the re-used filter exhibited an increased flow rate of 2 x 10^6 m/s. Moreover, the filter achieved an impressive crude oil recovery rate of 85%. X-ray diffraction analysis confirmed crude oil adsorption under the presence of an amorphous phase while scanning electron microscopy analysis revealed the structural morphology of the SACPHC filter. Overall, the SACHPC filter maintained high filtration efficiency without compromising biodegradability, offering a sustainable strategy for oily wastewater purification and oil spill clean-up.

***KEYWORDS*:** Oil spillage, Polyelectrolyte, Filter, Chitosan, Hydrogel, Sodium Alginate

1. INTRODUCTION

Oil spills pose a significant threat to marine ecosystems and human health. It is a common occurrence world over with one of the most recent ones occurring off the coast of Huntington Beach in October of 2021. It was caused by a rupture in an underwater pipeline resulting in the release of over 378,541 litres of crude oil into nearby water bodies (Huntington, 2022). This unfortunate event caused significant environmental concerns with long-term impacts on marine ecosystems and human well-being (Huntington, 2022). Therefore, it is crucial to develop effective treatment strategies to combat such environmental disasters. The overall goal is to provide a preliminary solution that can ultimately lead to the development of a highly reproducible and user-friendly oil/seawater filter. Although, there are advanced devices such as oil spill emergency treatment systems equipped with sensors and oil-water separating units which can aid swift and efficient clean-up operations, as well as minimize ecological damages, they are very expensive to employ (Budiman *et al.,* 2023; Yue *et al*., 2022). On the other hand, the traditional oil cleanup methods are generally slow, ineffective, and may introduce harmful contaminants into water sources (Ross *et al.*, 2022). Therefore, to clean up oil spills, many techniques have been developed including bioremediation, mechanical cleaning, chemical dispersants, and *in situ* burning.

Bioremediation is a promising and eco-friendly technique that utilizes targeted microbes to efficiently break down the oil (Singla *et al.*, 2023). It involves breaking down of spilled oil by bacteria and microorganisms into harmless substances like fatty acids and carbon dioxide. Usually, the process is accelerated by introducing nutrients like nitrogen and phosphorus to the affected area to boost the cleaning process. Mechanical cleaning is considered one of the most effective methods because it physically removes oil from the environment. The method typically involves the use of equipment such as oil booms and skimmers to contain and collect the spilled oil, booms to surround the slick and skimmers to remove the oil from the water surface. Skimming is a technique that uses booms to encircle and collect the oil-water mixture. Skimmers then store the extracted material in a recovery tank, separating gallons of oil and water from the spill site (Ross *et al.,* 2022). Another viable approach is dispersion. Chemical dispersants are substances used to break up oil slicks, allowing the oil to mix into the water and reduce its immediate impact on wildlife and coastlines. These dispersants work by reducing the surface tension between oil and water, forming smaller oil droplets that can disperse more easily. This involves using aircraft to disperse chemical agents that break down oil into tiny particles (Grechishcheva *et al.,* 2022). Although this technique benefits surface-dwelling creatures, it can negatively affect marine wildlife due to the toxic nature of dispersants used (Onokare *et al.,* 2022; Protocol, 2023). Chemical dispersants are usually employed to mitigate

the spread of the oil in cases where rough seas or high winds make mechanical cleanup difficult. *In-situ* burning involves controlled burning of spilled oil, which can be effective in open water or remote land areas with limited access. While it is a relatively inexpensive and rapid method, its application is constrained by weather conditions and the proximity of the spill to populated areas. Additionally, this technique releases harmful carbon emissions and leaves behind charred oil residue (Huntington, 2022). To minimise harm to humans and wildlife, favourable meteorological conditions such as gentle breezes and calm seas are necessary for a controlled burn (Response, 2022).

Arising from the limitations experienced with the use of traditional and conventional methods, attention is currently focused on the use of adsorbent alternative resources like polysaccharides and proteins for developing biomaterials based on their desirable properties and benefits (Sood *et al.,* 2021). Application of adsorbents offers a promising solution to address the shortcomings experienced with erstwhile cleanup methods. The approach, which involves using materials to absorb oil from water surfaces, presents a novel and environmentally friendly alternative. The method employs natural substances like peat moss or synthetic materials like activated carbon, and it is particularly useful in sensitive ecosystems or areas with limited access. Additionally, adsorbents can be reusable, making them cost-effective and environmentally friendly (Okeke *et al*., 2022). Among the available biomaterials, hydrogels (HGs) have garnered considerable attention owing to their intrinsic properties such as biocompatibility, biodegradability, mechanical strength, and responsiveness (Pella *et al.,* 2018). HGs are soft materials that comprise three-dimensional networks of hydrophilic polymers that can swell in water and biological fluids (Rao *et al.,* 2021). Depending on the preparation method, HGs can be classified as physical or chemical gels. In physical gels, the polymeric chains are held together by molecular entanglements and secondary interactions, including ionic cross-links, hydrogen bonds, and hydrophobic interactions (Bashir *et al.,* 2020) On the other hand, chemical gels feature polymeric chains held together by covalent bonds.

In a recent study, the sodium alginate-chitosan hydrogel polyelectrolyte complex demonstrated the potential to disperse oil with zero negative environmental impact, making it a potentially preferred polymer for experimentation (George and Shrivastav, 2023). However, a limited selection of adsorbents is currently available for treating oil spills on water bodies. Chitosan-alginate combination has numerous physical and chemical properties making it a viable option for this study. Apart from being a cationic polyamine, it has a high positive charge density at lower pH, and adheres sodium alginate to negatively charged surfaces with the ability to form hydrogels with polyanions. Additionally, chitosan is highly hydrophobic at neutral and higher pH, insoluble in water and most organic solvents, soluble in dilute acids and forms highly viscous solutions (Melo *et al.,* 2018). The compound also has a high molecular weight with reactive amino/hydroxyl groups that readily undergo chemical modification. Being a natural polymer, chitosan has several biological properties including biocompatibility, bio-adsorbability, and biodegradability making it relatively non-toxic and safe (Melo *et al.,* 2018).

Building upon the adsorbent method, innovative solutions such as filters with hydrophilic and oleophobic coatings represent a significant advancement in oil spill cleanup. By enhancing traditional filtration techniques, these solutions aim to improve efficiency and reduce environmental impact. The innovative solution aims to revolutionize traditional oil collection methods by implementing filters that are enhanced with a unique hydrophilic and oleophobic coating. The coating enables the filter to attract polar water molecules while simultaneously repelling nonpolar oil molecules, resulting in a more efficient and cost-effective oil collection process (Ross *et al*., 2022). Significant progress has been made in the area of oil-water separation to address the adverse effects of oil spills. Cutting-edge advancements such as super-hydrophilic membranes and specialised filters equipped with residue treatment mechanisms have been developed to reduce maintenance needs and prevent pollution and waste during oil extraction operations (Baig *et al.,* 2021) Natural or synthetic materials of different varieties can be utilized, such as cotton, polyester, or polyamide, to construct the filters, which can be reinforced with a stainless steel mesh for added durability and strength. When the filter is pulled through water, it successfully captures surface oil while allowing water to pass through. The present study demonstrates the potential of sodium alginate-chitosan hydrogel-polyelectrolyte complex (SACHPC) filter as an effective and eco-friendly solution for oil spill cleanup.

2. THEORETICAL ANALYSIS

Layer-by-layer (LbL) techniques are a precise and versatile method for creating functional nanomaterials by sequentially depositing nanoscale units (Lee *et al.,* 2023). This approach allows for exact control over coating thickness, content, and structure, making it scalable and effective for producing nanostructured thin films **(**Guzmán *et al.,* 2022). LbL techniques have found numerous applications in various fields, including drug delivery systems, hollow capsules, and gelatin nanostructures **(**Miyazaki *et al.,* 2022). They are also capable of producing fluorescent microspheres with core-shell structures, highlighting their adaptability in creating different material designs and functionalities (Lipton *et al.,* 2020). Widely used in materials science and engineering, LbL processes are cost-effective, scalable, and flexible, making them an ideal choice for generating functional materials (Vitorino *et al.,* 2017). In the realm of oil spill treatment, LbL procedures employ biocompatible

materials such as sodium alginate, chitosan, and cotton wool, which have exceptional oil absorption capacities. This makes them suitable for use in industrial oil spill cleanup and wastewater treatment.

3. MATERIALS AND METHODS

3.1 Chemicals and Reagents

Bonny light crude oil sample was obtained from Kaduna Refinery and Petrochemical Company (KRPC), chitosan flakes with chitolytic lot No.: 251716 and deacetylation level of ≥ 95%, sodium alginate and acetic acid were procured from Fluke Chemical Company. Other chemicals and reagents used were of analytical grade.

3.2 Preparation of filter

The sodium alginate-chitosan hydrogel-polyelectrolyte complex (SACHPC) was produced using ionotropic gelation process developed by (Pedroso-Santana *et al.*, 2020). Chitosan (20 g) and sodium alginate (80 g) were dissolved in 1 L of 2% acetic acid and agitated using a homogenizer for six hours to obtain a homogeneous mixture. To produce the filter, sodium alginate-chitosan (1:3) was incorporated into the SACHPC solution. The process involved using a 5 g strip of cotton wool, which was initially washed and rinsed with a NaOH solution to eliminate impurities. The cotton wool strip was treated, dried, and repeatedly dipped in the SACHPC solution to achieve the desired layers (self-assembly techniques). The filter was then allowed to dry naturally at room temperature.

3.3 Determination of porosity

The porosity of the cotton wool strip and coated cotton strip was determined by calculating their ratio. Two strips of filters with identical dimensions were utilized for this purpose. The strips were completely immersed in hexane for 20 seconds and then taken out. The variation in the mass of the hexane before and after immersion was recorded. The porosity ratio was then obtained using equation (1).

$$\frac{\Phi \text{ Coated filter}}{\Phi \text{ Cotton}} = \frac{\text{V pore, coated}}{\text{V pore,cotton}} \left(\frac{V\ Cotton\ sample}{V\ coated\ sample}\right) = \frac{\text{m−soaked hexane,coated}}{\text{m−soaked hexane cotton}} = \left(\frac{\delta \text{ coated}}{\delta \text{ cotton}}\right) \approx \frac{\text{m−soaked hexane,coated}}{\text{m−soaked hexane,cotton}} \quad \dots \textbf{(1)}$$

In the above equation, φ represents porosity, m represents mass of material, and δ represents thickness of material. Since the thickness is much smaller than the surface area of the samples, the volume ratio of the sample can be assumed to be equal to the surface area ratio, which was controlled to be 1. Therefore, the porosity ratio between the cotton strip and coated strip filter material could be determined as the mass ratio of the mass difference of the hexane (Ross *et al.*, 2022).

3.4 Mass distribution

To determine the mass distribution of sodium alginate-chitosan hydrogel-polyelectrolyte complex (SACHPC) on the coated filter, the mass per unit surface area was calculated. The filter was prepared with precise dimensions (70 length X 76 width mm) and the pre-weighed sample was coated before undergoing the drying process and then weighed again (Ross *et al.*, 2022). To determine mass distribution, the variance between the pre and post-coating weights was divided by the surface area of the substrate (equation 2).

$$\text{Mass distribution} = \frac{Mass\ Difference}{Surface\ area\ of\ the\ substrate} \quad \dots \textbf{(2)}$$

3.5 Flow Rate Determination

Flow rate was determined according to the method described by Ghimici *et al.* (2018) to evaluate the performance of the filter. Crude oil solutions of 0.5 M concentrations was prepared in 1000 mL beakers and the pH was adjusted to 3. Filtration test was conducted using a funnel with the coated filter set atop a graduated cylinder to evaluate its performance. The experiment recorded the time taken for 1 L of spillage to pass through the filter (Figure 1). Using Equation 3, the flow rate was calculated by dividing the volume by the discharge time (Ross *et al.*, 2022).

$$Q = \frac{v}{t} \quad \dots (\textbf{3})$$

Where;
Q = velocity flow rate
v = volume of oil
t = discharge time

Figure 1: Filtration of crude oil spillage using SACHPC filter

3.6 Crude oil recovery and filter re-use

The filtered oil was transferred into a measuring cylinder and the amount of crude oil recovered was measured. The oil retained in the SACHPC filter was further extracted using Soxhlet extraction with toluene as the solvent (Figure 2). It was then separated using a rotatory evaporator. The SACHPC filter was cleaned and rinsed thoroughly with toluene and water to eliminate any impurities and excess oil. Finally, another batch of oil spillage was run through the used filter to test its effectiveness.

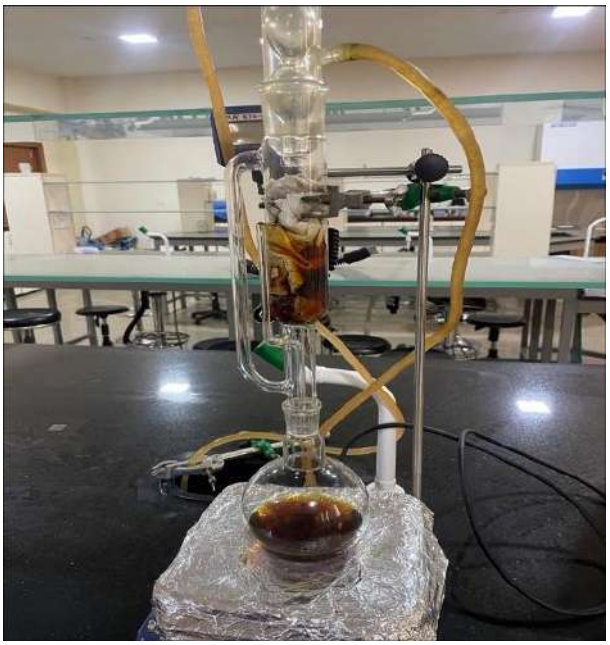

Figure 2: Extraction of crude oil from SACHPC Filter

3.7 Characterization of the filter

X-ray diffraction (XRD) and scanning electron microscopy (SEM) were employed to study the composition and morphology of the SACHPC filter before and after use. To conduct XRD, liquid samples of the treated spillage on the SACHPC filter were dried in a sealed environment with silica gel.

3.8 Statistical analysis

The data obtained were subjected to statistical analysis using one-way analysis of variance (ANOVA) with Tukey's post hoc test for single factor comparison and variance analysis (two-way ANOVA) with Bonferroni post hoc test for multifactorial comparisons. Statistical significance was determined at a confidence level of 95%, considering differences to be significant when $p < 0.05$. Additionally, a maximum acceptable coefficient of variation was predefined at 25%.

4. RESULTS AND DISCUSSION

Motivated by devastating environmental and socio-economic effects of oil spills, researchers are actively exploring different techniques for oil spill cleanup. Sodium alginate-chitosan hydrogel-polyelectrolyte complex (SACHPC) has emerged as a promising alternative, demonstrating effectiveness in dispersing oil while minimizing negative environmental impact. The SACHPC filter, developed in this study, demonstrated remarkable efficiency in adsorbing and separating crude oil from water, offering a promising solution for oil spillage. Its unique composition and structure enable effective oil capture while allowing water to pass through, resulting in superior filtration performance.

4.1 Porosity, mass distribution and flow rate

A cotton strip of 0.254 g and a coated strip of 0.156 g gave an overall porosity ratio of 0.612 g and the mass distribution of SACHPC on the coated filter was calculated to be 77.76 g/m^2. The flow rate of the filter was 25 x 10^5 m/s, whereas the reused filter showed an increased flow rate of 2 x 10^6 m/s giving a net flow of 5 x 10^5 m/s. The increased porosity enhanced the capacity of the filter to adsorb and retain oil, making it more effective in oil spill cleanup efforts (Wolok *et al.,* 2020). The consistency of the coating across the filter surface is essential for its effectiveness in oil spill cleanup. A uniform coating ensures that all areas of the filter are capable of absorbing oil efficiently, thereby maximizing the cleanup process. The mass distribution of SACHPC on the coated filter was found to be higher than 70 g/m^2, suggesting uniformity and consistency of the coating across the filter surface (Ross *et al.,* 2022). The high flow rate exhibited by SACHPC filter is an indication of its ability to efficiently filter large volumes of water contaminated with crude oil under different conditions.

4.2 Oil recovery and reusability

SACHPC filter proved to be highly effective in separating 85% of crude oil from the spillage under the different conditions employed in the study. The filter also allowed extraction of adsorbed oil with great efficiency. By combining both separation and extraction processes, the filter produced an impressive crude oil recovery rate of 97%. The oil recovery ability and reusability demonstrated by the filter agree with previous study where chitosan produced an effective performance (> 99.4%) even after multiple cycles of testing (Xiong *et al.,* 2023). This emphasizes the practicality and cost-effectiveness of using SACHPC filter for oil spill cleanup operations.

4.3 X-ray diffraction (XRD) results

The X-ray diffractogram of SACHPC filter before and after use is presented in Figures 3 and 4. XRD analysis revealed the composition of SACHPC filter before and after it encountered crude oil. The diffractogram revealed that polyelectrolyte complex (PEC) and chitosan hydrogel (C_h) appeared at position 2θ degree angle of 15.20^O and 22.20^O in the filter before use. The diffractogram of the filter after use further revealed higher intensity that shows the PEC peak moved to 17.20^O and boarding while C_h has a reduced intensive peak. The distinct peaks observed in the diffractogram confirmed the structural integrity of SACHPC filter before use. However, the slight shift observed in the peaks after use is an indication of change in the crystalline structure of the filter due to oil exposure (Tsade *et al.,* 2021). Additionally, the reduction in intensity of the Ch peak suggests that SACHPC filter significantly absorbed crude oil. The observed reduction Ch peak also confirmed absence of impurities in the samples **(**Jha *et al.,* 2022**).**

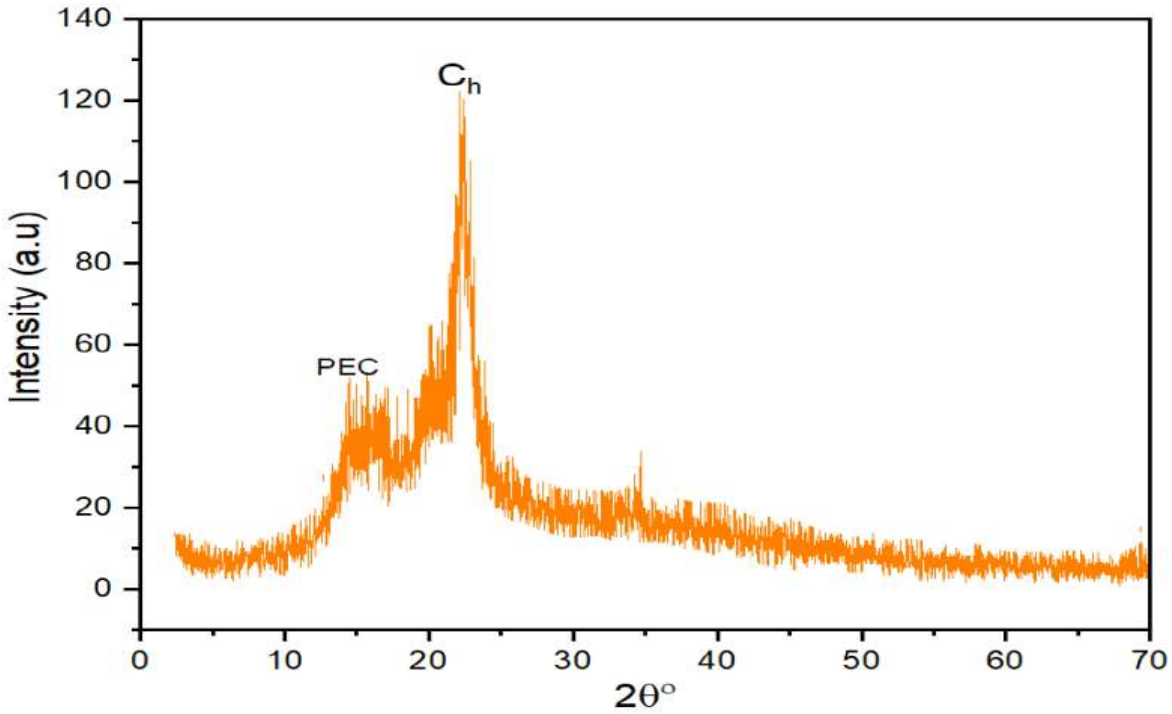

Figure 3: X-ray diffractogram of SACHPC filter before use

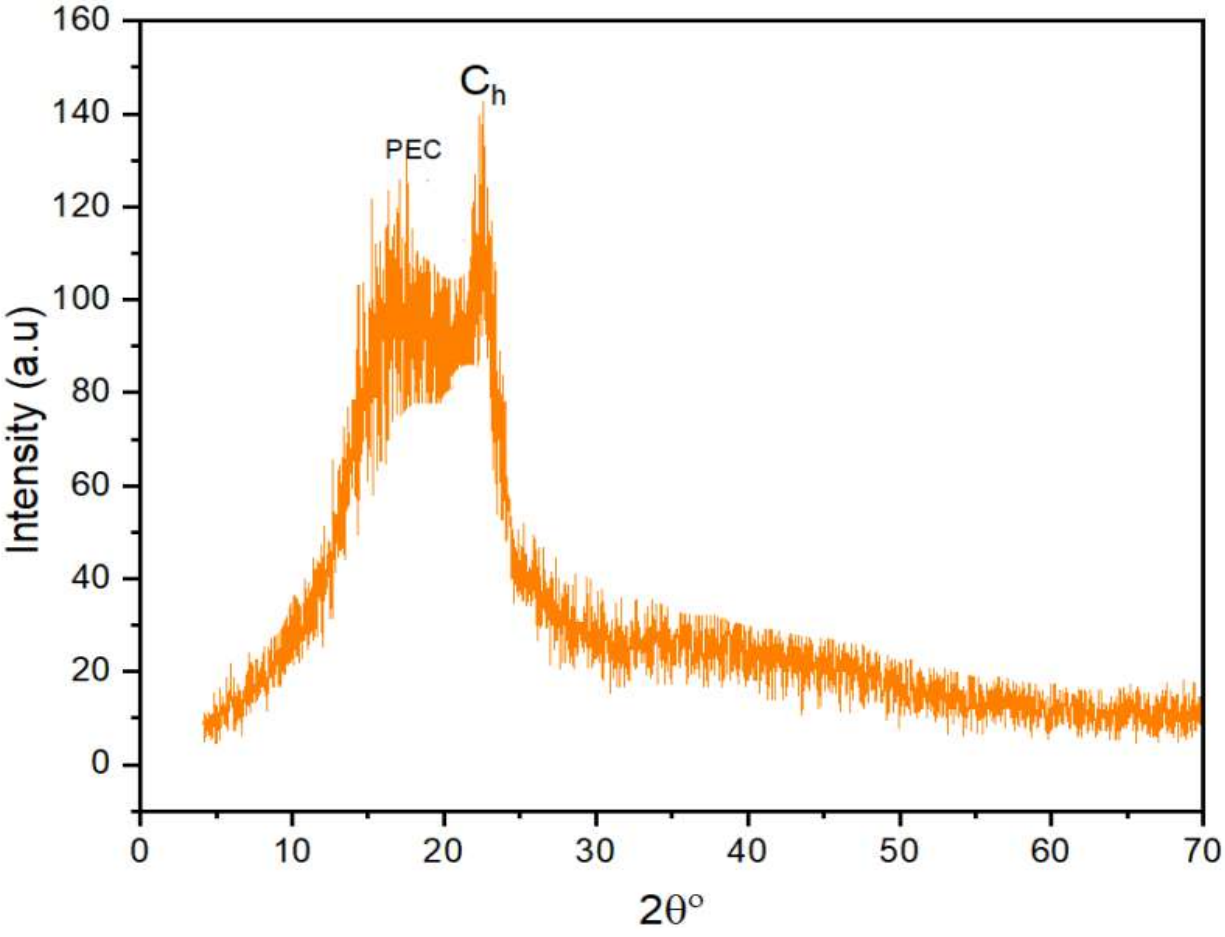

Figure 4: X-ray diffractogram of SACHPC filter after use

4.4 Scanning electron microscopy (SEM) result

Figures 5 and 6 depict the morphological features of SACHPC filter before and after crude oil absorption. Before use, the filter had a relatively smaller pore size with a cellulose diameter of 50.6 microns when compared to the pore size of the filter after use with a cellulose diameter of 60.1 microns. The increase in pore size may be attributed to random dispersion of nano-cellulose in the filter following contact with crude oil. The increase in pore size may be responsible for the enhanced crude oil absorption capacity demonstrated by the used filter by virtue of its ability to retain more oil in the pores. The images of the filter before exposure to crude oil revealed a complex surface morphology characterized by irregularly shaped particles due to incorporation of nano-cellulose into the filter structure. However, after contact with crude oil, the cellulose particles in the filter were freely aligned and showed a regular pattern of arrangement. These observations are consistent with previous studies (Escudero-Oñate *et al.,* 2018; Guarnizo-Herrero *et al.,* 2021), further supporting the applicability of PEC filters in crude oil spillage cleanup.

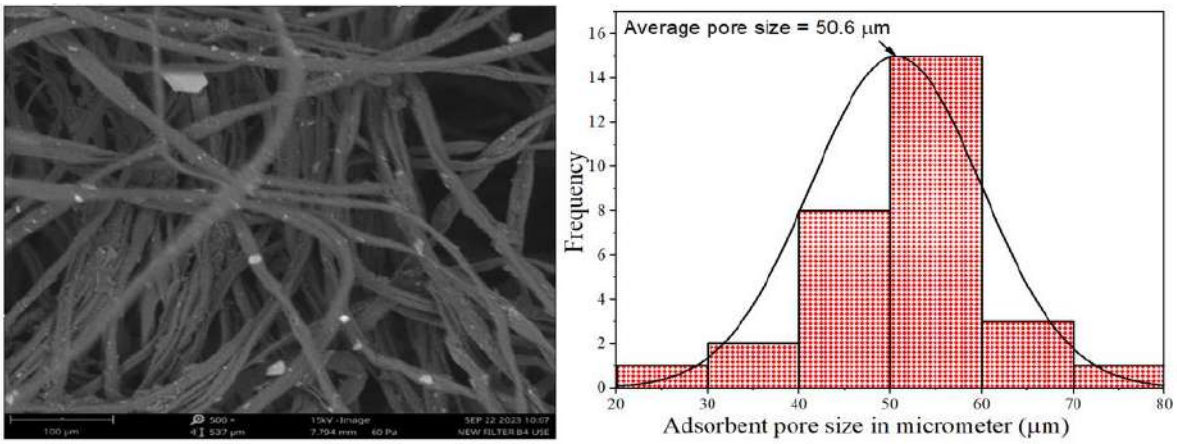

Figure 5: SEM Image of the SACHPC filter and the histogram of pore size (magnification 100 μm)

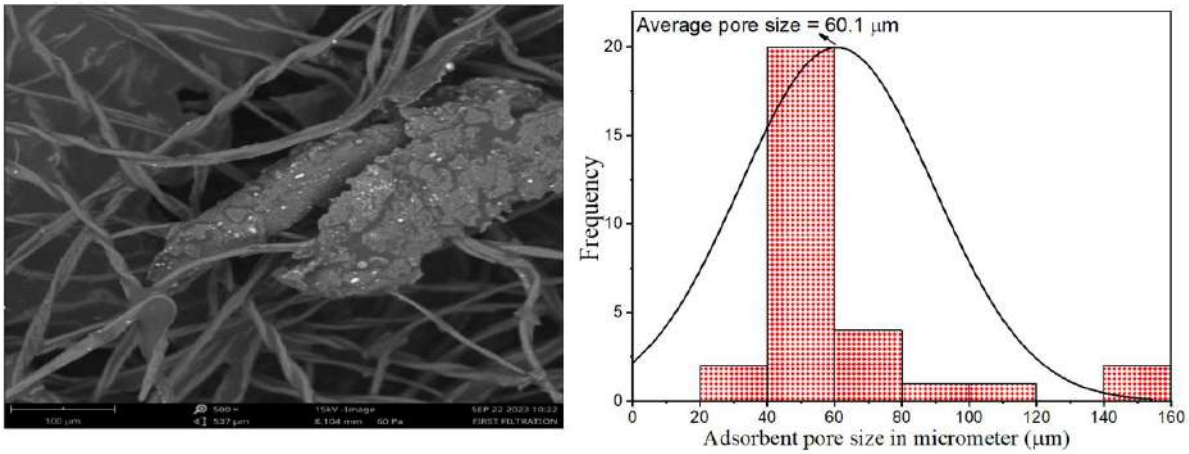

Figure 6: SEM image of SACHPC filter after filtration and the histogram of pore size

5. CONCLUSION

The study underscores the efficiency and adaptability of SACHPC filter as a promising solution for oil spill cleanup. The utilization of biocompatible materials and innovative filtration techniques represents a significant step forward in the development of sustainable strategies for oil spill management. Structural analyses using XRD and SEM techniques revealed the integrity of the filter even after exposure to crude oil, indicating its robustness and reliability in oil spill treatment. Overall, the eco-friendly nature, reusability and stability of the SACHPC filter, coupled with its high oil recovery efficiency, positioned it as a preferred solution for addressing oil spills with minimal environmental impact. Further research and development are crucial to optimize the performance and scalability of SACHPC filtration systems for practical deployment in real-world scenarios.

REFERENCES

Baig, N., and Saleh, T. A. (2021). A facile development of superhydrophobic and superoleophilic micro-textured functionalized mesh membrane for fast and efficient separation of oil from water. *Journal of Environmental Chemical Engineering*, *9*(5), 105825.

Bashir, S., Hina, M., Iqbal, J., Rajpar, A. H., Mujtaba, M. A., Alghamdi, N. A., ... and Ramesh, S. (2020). Fundamental concepts of hydrogels: Synthesis, properties, and their applications. *Polymers*, *12*(11), 2702.

Budiman, F., Ismardi, A., Hardinah, T., Muhammad, R., Hartaman, A., Nurhidayat, A., ... and Sutapa, I. D. (2023). Strengthening oil pollution monitoring system in aquatic environment through development of IoT-based Oil-Water Separator Device. *Ecohydrology and Hydrobiology*.

Escudero-Oñate, C., and Martínez-Francés, E. (2018). A review of chitosan-based materials for the removal of organic pollution from water and bioaugmentation. *Chitin-Chitosan-Myriad Functionalities in Science and Technology*, *1*.

George, A., and Shrivastav, P. S. (2023). Preparation and evaluation of chitosan-alginate/carrageenan hydrogel for oral drug delivery in the treatment of diabetes. *Journal of Bioactive and Compatible Polymers*, *38*(5), 368-386.

Ghimici, L., and Nichifor, M. (2018). Dextran derivatives application as flocculants. *Carbohydrate polymers*, *190*, 162-174.

Grechishcheva, N., Kuchierskaya, A., Semenov, A., Kuryashov, D., Meritsidi, I., and Mingazov, R. (2022). Evaluation of the dispersants effectiveness using the baffled flask test. *Journal of Environmental Engineering and Landscape Management*, *30*(1), 106-113.

Guarnizo-Herrero, V., Torrado-Salmerón, C., Torres Pabon, N. S., Torrado Durán, G., Morales, J., and Torrado-Santiago, S. (2021). Study of different chitosan/sodium carboxymethyl cellulose proportions in the development of polyelectrolyte complexes for the sustained release of clarithromycin from matrix tablets. *Polymers*, *13*(16), 2813.

Guzmán, E., Ortega, F., and Rubio, R. G. (2022). Layer-by-layer materials for the fabrication of devices with electrochemical applications. *Energies*, *15*(9), 3399.

Huntington Beach 2022 Water Quality Report. City of Huntington Beach, California. Available online: https://huntingtonbeachca. gov/files/users/public_works/2022-Drinking-Water-Quality-Report.pdf (accessed on 16 August 2022).

Jha, D., Narayanachari, K. V. L. V., Zhang, R., Liao, J., Keane, D. T., Liao, W. K., ... and Agrawal, A. (2022). An Incremental Phase Mapping Approach for X-ray Diffraction Patterns using Binary Peak Representations. *arXiv preprint arXiv:2211.04011*.

Lee, W., Fernandez-Mulligan, S., Tan, H., Yan, C., Guan, Y., Lee, S. H., ... and Yang, S. (2023). Layer-by-layer disentanglement of Bloch states. *Nature physics*, *19*(7), 950-955.

Lipton, J., Weng, G. M., Röhr, J. A., Wang, H., and Taylor, A. D. (2020). Layer-by-layer assembly of two-dimensional materials: meticulous control on the nanoscale. *Matter*, *2*(5), 1148-1165.

Melo, B. C., Paulino, F. A., Cardoso, V. A., Pereira, A. G., Fajardo, A. R., and Rodrigues, F. H. (2018). Cellulose nanowhiskers improve the methylene blue adsorption capacity of chitosan-g-poly (acrylic acid) hydrogel. *Carbohydrate polymers*, *181*, 358-367.

Miyazaki, C. M., Shimizu, F. M., and Ferreira, M. (2022). Layer-by-layer nanostructured films for electrochemical sensors fabrication. In *Functionalized Nanomaterial-Based Electrochemical Sensors* (pp. 407-441). Woodhead Publishing.

Office of Emergency and Remedial Response, Agency Response PB2000-963401 Oil Program Center Understanding Oil. United States Environmental Protection Agency. Available online: https://www.epa.gov/sites/default/files/2018-01/documents/ ospguide99.pdf (accessed on 16 August 2022).

Office of Response and Restoration. How Do Oil Spills out at Sea Typically Get Cleaned Up? National Oceanic and Atmospheric Administration. Available online: https://response.restoration.noaa.gov/about/media/how-do-oil-spills-out-sea-typically- get-cleaned.html (accessed on 15 August 2022).

Okeke, E. S., Okoye, C. O., Ezeorba, T. P. C., Mao, G., Chen, Y., Xu, H., ... and Wu, X. (2022). Emerging bio-dispersant and bioremediation technologies as environmentally friendly management responses toward marine oil spill: A comprehensive review. *Journal of Environmental Management*, *322*, 116123.

Onokare, E. P., Tesi, G. O., Odokuma, L. O., and Sikoki, F. D. (2022). Effectiveness and toxicity of chemical dispersant in oil spill aquatic environment. *Asian Journal of Water, Environment and Pollution*, *19*(2), 41-46.

Pedroso-Santana, S., Arcia, E. L., Fleitas-Salazar, N., Guevara, M. G., Mansilla, R., Gómez-Gaete, C., ... and Alonso, J. R. T. (2020). Polymeric nanoencapsulation of alpha interferon increases drug bioavailability and induces a sustained antiviral response in vivo. *Materials Science and Engineering: C*, *116*, 111260.

Pellá, M. C., Lima-Tenório, M. K., Tenório-Neto, E. T., Guilherme, M. R., Muniz, E. C., and Rubira, A. F. (2018). Chitosan-based hydrogels: From preparation to biomedical applications. *Carbohydrate polymers*, *196*, 233-245.

Rao, T., Chvs, P. H. A. N. I. N. D. R. A., Yamini, M., and Prasad, C. H. (2021). Hydrogels the three dimensional networks: a review. *Int J Curr Pharm Res*, *13*(1), 12-17.

Ross, H., Nguyen, H., Nguyen, B., Foster, A., Salud, J., Patino, M., ... and Li, M. (2022). Filter modified with hydrophilic and oleophobic coating for efficient and affordable oil/water separation. *Separations*, *9*(10), 269.

Singal, N., and Kaur, S. (2023). Bioremediation: Sustainable Approach for Pollution Control. *Asian Journal of Environment and Ecology*, *20*(4), 1-18.

Sood, A., Gupta, A., and Agrawal, G. (2021). Recent advances in polysaccharides based biomaterials for drug delivery and tissue engineering applications. *Carbohydrate Polymer Technologies and Applications*, *2*, 100067.

Tsade, H., Anshebo, S. T., and Sabir, F. K. (2021). Preparation and characterization of functionalized cellulose nanomaterials (CNMs) for Pb (II) ions removal from wastewater. *Journal of Chemistry*, *2021*, 1-18.

Vitorino, L. S., and Oréfice, R. L. (2017). Layer-by-Layer technique employed to construct multitask interfaces in polymer composites. *Polímeros*, *27*, 330-338.

Wolok, E., Barafi, J., Joshi, N., Girimonte, R., and Chakraborty, S. (2020). Study of bio-materials for removal of the oil spill. *Arabian Journal of Geosciences*, *13*(23), 1244.

Xiong, F., Wang, X., Liu, Y., Zhang, Z., Zhang, T., Gao, H., ... and Zhang, S. (2023). Sandwich structured chitosan-aerogel nonwoven filter with asymmetric wettability and pore size differences for high-efficient oil-mist filtration. *Journal of Environmental Chemical Engineering*, *11*(5), 110443.

Yue, R., An, C., Ye, Z., Bi, H., Chen, Z., Liu, X., ... and Lee, K. (2022). Cleanup of oiled shorelines using a dual responsive nanoclay/sodium alginate surface washing agent. *Environmental Research*, *205*, 112531.

PAPER 41 - DEVELOPMENT OF A SELF-POWERED GENERATOR

Gideon. O, Okegbile O.J

[1]Department of Mechanical Engineering, Federal University of Technology Minna Niger State Nigeria.
Email: gideonobhiye2013@gmail.com

ABSTRACT
Self-powered generator is a new source of power that is completely safe and efficient, the durability and design is top notch. This generator, unlike every other generator doesn't have an engine which consumes fuel/gas. Instead of an engine, it has a DC motor which is powered by a 12 volts 75 Ah rechargeable battery that recharges self while operating. Other materials used are, speed-controller, speed up gear, AC to DC charger, Ac alternator, couplings, Shafts and Gear. The alternator armature shaft was coupled directly with DC motor powered by the rechargeable battery. The DC motor rotates the armature of the alternator in the field coil at high speed when activated from the starting switch which results in alternating current output voltages of 220V. This generator generates 1KVA which can be used to power basic home appliances, office or shop. The system is designed such that an in-built battery charger recharges the battery at the same rate as the DC discharges the battery when drawing battery current. The system could be designed to any limit contingent upon the capacity of the planned load. Minimum maintenance is required. Several tests were carried out using different loads at a particular time internal, results revealed an overall efficiency of 96.30% on a load of 500W and 89.10% on a load of 700walts respectively. The results demonstrated that the generator can operate at the efficiency of 97 to 100% if permanent magn*et al*ternator is used.

KEYWORDS: Alternator, Dc motor, Gear, Shaft, Charger, capacitor.

1. INTRODUCTION

Despite the growth and advancement in power and energy production, access to constant electricity in some countries is almost unachievable. It is believed that 25-30% of the developing world has no accessible domestic power (Adewumi and Adelekan, 2016). Several research works and initiatives are in place to ensure sustainable power source frameworks, for example, wind, sun oriented, and geothermal generators to control provincial African territories. The pace of development and industrialization of any nation relies upon their capacity to deliver satisfactory electric power and ensure viable distribution to power homes, offices, banks, industries, health care, etc (Adegoke *et al*., 2020). and this is evident in Nigeria as the power sector has over the years struggled to meet required demand regardless of its bounty of sustainable power source, for example, biomass, wind, hydro control and so on whose exploitation and utilization are negligible. This inconsistent power supply has caused a surge of the search for alternative forms of power source with minimal operating costs. Industries adapted the use of natural gas generators as much saving was made compared to the traditional petrol or diesel-run generators (Ajav and Adewunmi, 2014). And considering the effect of gasoline generators, which emit toxic fumes and pollutant like carbon monoxide, and particulate matter which make it uncomfortable to humans and animals. With the increasing demand for natural gas and the subsequent increases in prices there is need for continuous improvement on existing design. Abdullah *et al*. (2012) has observed that at present, the importance of alternative energy source has become even more crucial matter not only due to the continuous depletion of limited fossil fuel stock but also for the safe, better and greener environment. Ajav and Adewumi (2014) has noticed that power generation, transmission and distribution has been an indispensable factor in the progress of an economy, ranging from manufacturing, banking, media, health care, aviation, etc. It has however been proved that power skyrocket the productivity of a country. Environmental pollution which leads to degradation or depletion of ozone layer is one of the major problems caused by the use of generator with fossil fuels (Ajav and Adewunmi, 2014). Other problem includes land and water pollution, noise pollution, increase in price of fossil fuel year in year out, among others. Recently, increase in energy demand and limited energy sources in the world caused the researchers to make effort to provide new and renewable energy sources for the usage in an economical and safe way. Besides being clean and of low running cost, renewable energy possesses the privilege of abundance and can be used wherever available (Ibrahim and Serag, 2011). The self-excited induction generators (SEIG) have been found suitable for energy conversion for remote locations. Self-excited induction generators (SEIG) are frequently considered as the most economical solution for powering costumers isolated from the utility grid. SEIG has many advantages such as simple construction, absence of DC power supply for excitation, reduced maintenance cost, good over speed capability, and self-short-circuit protection capability. Just like most undeveloped countries in the world, we are faced with the challenges of light disruption. Continuous spending on fuelling and maintenance of our fuel generator, increase in the purchase of generating sets, maintenance cost and among others, hence the need for an alternative of power sources. Converting a fuel generator into a self- powered generator becomes

important. Self-powered generator was created to address problem of conserving or storing energy that is then released to be used during the failure periods, improving uninterruptible power supply and reducing energy losses experienced by many energy generating methods, such as wind turbines and photovoltaic cells, when operating at their peak intensity. Additionally, in various denominations, such as academic institutions and churches, there are bound to be abrupt failures in power supply. The combination of an internal combustion engine with an electrical generator makes up a fuelled generator. It makes use of various fossil fuels such as diesel, gasoline, propane (in liquefied or gaseous form), or natural gas. As air is compressed in the cylinder at high pressure, fuel is injected into the compressed air chamber causing combustion and subsequently rotation of the prime mover. The mechanical rotation from the prime mover spins the alternator which in turn generates electricity. However, the alternator can be set in motion by other means to generate electricity. Otulana *et al*. (2015) used a locally sourced material to develop a 1 kVA fuelless generator with a driving mechanism of 1hp DC motor to spines a 0.95 kW alternator. The DC motor was powered by a 12 V rechargeable battery which recharges through a rectifying diode. Dipali *et al*. (2017) worked on a simple and efficient means of generating electricity with readily and easily available materials. The authors revealed that the system can be built to any capacity depending on the load requirement, and the system does not require frequent mechanical maintenance. A 2.5 kVA self-induced fuelless generator was constructed by Adewumi and Adelekan (2016) using a self-induced engine as an alternative to isolated power generation from renewable energy sources because of its low cost of purchase and maintenance, as well as the reliability. The component used for the construction includes DC motor, 12V 100Ah battery, AVR panel, and charging panel. The performance evaluation was performed using loads ranging between 0 W and 2 kW for 300 seconds. The outcome of the research shows that the self-induced power generating set must make use of a new direct current motor and alternator for future study and reliability and better performance of the system.

2. THEORETICAL ANALYSIS

The evaluation of the machine will be calculated using Equation 1-5 as stated by Tunde-Akintunde and Akintunde, (2004);

$$\text{Input Power} = \text{Input Voltage} \times \text{Input Current} \quad (1)$$

$$\text{Output Power} = \text{Out Voltage} \times \text{Output Current} \quad (2)$$

$$\text{Efficiency} = \frac{\text{Output power}}{\text{Input power}} \times 100 \quad (3)$$

$$\text{Power} = \text{Current} \times \text{Voltage} \quad (4)$$

$$\text{Battery capacity (H)} = \frac{\text{Battery Capacity in Ah or mAh}}{\text{Total Average Current in A or } \mu\text{A}} \quad (5)$$

With the use of a multi-meter as a measuring device, the input voltage, and output voltage, and output current, input current were determined.

3. MATERIALS AND METHODS

DC motor, Speed-up gear, Speed controller, Ac to Dc charger, Battery, Ac alternator, Couplings, Shafts and gears.

The design constraints were all analysed by studying the literature survey carefully and choosing the best possible design for the most efficient outcomes in order to enhance workability of the project.

METHOD

The Dc motor is connected to the speed-up gear, the connection was through coupling, and the speed-up gear is connected to the Ac alternator that produces light. The output of the AC alternator that produces light is connected from AC to Dc charger that charges the battery of the Dc motor. The speed controller is connected to the DC motor and the battery to regulate the speed of the motor. The body is made up of flat iron plate of 2mm thickness. The gear is made of cast iron which consists of input and output gear, the Dc motor is 12V, 2HP, 30arms and has a speed of 3000rpm, the shaft of the speed-up gears and the dc motor are 8mm each, the output shaft from the speed-up gear is 10mm.

3.1 CONCEPTUAL DESIGN.

The generator using battery, gear and couplings consist majorly of five major units, which includes the following; The power supply Unit, Conversion Unit, Control Unit, Output Unit and Charging Unit.

3.1.1THE POWER SUPPLY UNIT

12 volts battery was used as source of power supply unit to the D.C motor in order to induce electromotive force (e.m.f). Lead acid battery is highly recommended for DC generating system. This serves as storage device for the direct current which is to be induced.

3.1.2 CONVERSION UNIT

This unit is the unit that distinguished the DC generator from the popular fuelled generating set. The unit makes use of DC motor, which will be responsible for all voltage, current and power conversion.

3.1.3 CONTROL UNIT

This unit performs the following work; converts direct current (DC) to alternating current (AC), removal of ripples, and rectification. The size of the alternator been used, will determine the capacity of the generating set. The alternator which is a small domestic generator has three output lead cables which supplies, the load, capacitor and the diode.

4. RESULTS AND DISCUSSION

In order to ascertain the workability, reliability, and operating characteristics of the self-powered generator, tests were carried out severally on both unloaded and loaded conditions. The results of these tests were then use to validate the self-powered generator with the already existing ones. Also tests were carried out on the individual components that make up the self-powered generator in order to know their behaviour under working condition. Also, to ensure that the system is not running on the battery, a 12V 75Ah fully charged dip cycle battery was subjected to a load of 300W and 400W respectively. This was to determine the battery life when carrying a certain load; it was on the basis of these that the choices of load and time on the tables were determined using Eq. (4-6)

Mathematically;

$$\text{Battery capacity (H)} = \frac{\text{Battery Capacity in Ah or mAh}}{\text{Total Average Current in A or } \mu\text{A}} \quad (5)$$

$$\text{Power} = \text{Current} \times \text{Voltage} \quad (4)$$

$$I = \frac{p}{V}$$

$$I = \frac{300W}{12V} = 25 \text{ A}$$

Applying battery life formula,

$$\text{Battery life} = \frac{75\text{Ah}}{25\text{A}} = 3 \text{ hours} \quad (6)$$

For a load of 400W, the current can be calculated by employing Eq. 4

$$I = \frac{400W}{12V} = 33.33 \text{ A}$$

Applying Battery life formula from equation 6,

$$\text{Battery life} = \frac{75\text{Ah}}{33.33\text{A}} = 2.25 \text{ hours}$$

This was also done practically before using the battery life formula. 12V 75Ah battery was seen to have lasted for two hours fifty three minutes on a load of 300W, and a load of 400W for two hours ten minutes. The differences may be due to some loses in the discharge. This was repeated for other load; it was on the basis of these that we conclude that the system was sustainable.

4.1 OUTPUT EFFICIENCY

For self-powered Power Generator Table 1, Table 2, Table 3 and Table 4 in Appendix shows the result of performance evaluation for the 1000W (1KVA) self-powered power generating set. The load bank was connected to the self-powered generator in order to power the light bulbs on the bank, which was connected to the extension wire. Stop watch was used to record the time at interval of 60 minutes for five different runs. While the multi-meter was used to read the voltage output in Volts with Current in Ampere and the mean voltage with current result was computed in the Table 1, Table 2, Table 3 and Table 4 in the Appendix page.

Output efficiency was computed using the data obtained after testing, according to Institute of Electrical and Electronics Engineers (IEEE, 1997) reported by Sandia Inverter (2004) as shown in the Appendix Table 1, Table 2, Table 3 and Table 4. Load capacity used for this research work ranges from 0 watt to1000 watts; that is from 0% to 100% loading.

4.2 CAPACITY OF THE DC MOTOR

The output capacity of the self-powered engine is determined mainly by output capacity of the dc motor. The dc motor capacity must exceed that of the alternator coupled to the dc motor in order to produce maximum alternator output capacity. Many dc motors of different output capacities are on sale throughout the world markets from 2hp (1.5kwatts) to 500hp (373kwatts). The development of the dc motor has been on for more than a century since these dc motors of smaller capacities are used in cars, tape recorders, pump machines, fans, winders, etc. The ultimate focus is to couple dc motor whose output capacity is more than that of alternator in order to drive the alternator maximally. The dc motor used for this work is 2Hp and the alternator is 1KVA.

4.3 RELATIONSHIP BETWEEN GENERATOR SPEED AND LOAD

The generator speed depends on the amount of load of which the system is subjected to. It was observed that when more loads are continuously added to the system, it has a back effect on the system by reducing its speed. At the point where the load was zero, the generator speed was maximum and then reduces accordingly when the system is subjected to more loads.

5. CONCLUSION

The self-powered generator has been developed with local materials available, however, in the future, if the technology is further developed and embraced, the costs will reduce reasonably when commercial production is being employed. The following conclusions were drawn from the design, development of 1000W (1KVA) self-powered power generating set; It can be deduced that the machine (self-powered power generating set) had the peak efficiency of 102.09% at a load of 300W and the lowest efficiency of 89.10% at a load of 700W with voltage output of 207V. It was also revealed that there is a decrease in the output of the machine when there is a high increase in the load. After proper statistical analysis, the machine is said to have an average efficiency of 92.5%. Future Prospects of self-powered Generator When D.C motors of higher capacity than 500hp are coupled to the alternator whose capacities are lower than that of the D.C motors, then maximal output capacity of the alternator could be obtained. Self-powered engines can be incorporated into automobiles in order to have fuel less automobiles that would run without fuel. Based on the design, construction and performance evaluation test conducted on this 1KVA self-powered generating set, the following recommendations were made for further study; In order to obtain a good performance characteristic, a voltage well above 12V battery voltage should be used to power the power generator design of special DC motor, alternator and transformer for the purpose of construction of self-powered power generating set has to be encouraged in order to have clean and renewable energy especially for solving the epileptic power supply been experienced in Nigeria currently. The appliance can be adopted and made available for use in Electrical and Power establishments to enhance its value. Incorporation of battery, rectifier and an inverter for subsequent project works in order to enhance its self-sustainability. The project work is subject to further research in order to improve its existing limitations.

ACKNOWLEDGEMENT

I want to sincerely thank my project supervisor and my PG coordinator; Professor Olawale James Okegbile and Dr. Bori Ige, for their contribution to the success of this work. Am also indebted to Professor Nicolas Musa for the correction and continues encouragement. I must acknowledge the incredible and inestimable effort of everyone who has in one way or the other contributed to the success of this project work. thanks you so much for been there for me.

REFERENCES

Adegoke, A. (2020). Design and construction of a 2KVA fuelless generator. An Unpublished B.Tech

Adewumi, I., and Adelekan, B. (2016). Fuelless Power Generating Set and Power Inverter System: Analysis of Load and Efficiency Appraisal. *British Journal of Applied Science & Technology*, *15*(6), 1-7.

Ajav, E. A., and Adewumi, I. O. (2014). Fuelless generating set: Design, construction and performance evaluation. In *3rd International Conference Proceedings on Engineering and Technology Research at Ladoke Akintola University of Technology, Ogbomosho* (Vol. 3, pp. 258-269).

Dipali, S., Rutuja, S., and Shital, M. (2017). Fuel less Generator: Review. *International Journal for Research in Applied Science and Engineering Technology (IJRASET)*, *5*, 1375-1378.

Ibrahim, H. E., and Serag, M. F. (2011). Analysis of self-excited induction generator using particle swarm optimization. *International Journal of Electrical and Computer Engineering*, *5*(9), 1199-1203.

Otulana, J. O., Akinwunmi, A. A., Awoyemi, J. A., Adeleke, M. B., and EfunboteOrelaja, M. I. (2015). Construction of a Fuel less Generator. *International Journal of Recent Research in Civil and Mechanical Engineering*, *2*(1), 285-289.

Tunde-Akintunde, T. Y., and Akintunde, B. O. (2004). Some physical properties of sesame seed. *Biosystems Engineering*, *88*(1), 127-129.

APPENDICES

Table 1, at 60 minute, 120, 180, 240 and 300 minute on zero load, the input and output voltage was measured with a multi-meter the input power, output power and efficiency was zero. This was because the system is operating on no load.

Time (m)	Load (w)	Input voltage (V)	Output voltage (V)	Input current (A)	Output current (A)	Input power (W)	Output power (W)	Efficiency (%)
60	**0**	**12.40**	**220**	**0**	**0**	**0**	**0**	**0**
120	**0**	**12.46**	**225**	**0**	**0**	**0**	**0**	**0**
180	**0**	**12.35**	**230**	**0**	**0**	**0**	**0**	**0**
240	**0**	**12.45**	**225**	**0**	**0**	**0**	**0**	**0**
300	**0**	**12.35**	**230**	**0**	**0**	**0**	**0**	**0**

Table 2, at 120 minute,180, 240, 300 and 360 Minutes interval a load of 300w was used, the input voltage, output voltage, input current, output current was measured with a multi-meter, result revealed an average efficiency of 100.94 percent. It therefore means that the system in its highest efficiency.

Time (m)	Load (w)	Input voltage (V)	Output voltage (V)	Input current (A)	Output current (A)	Input power (W)	Output power (W)	Efficiency (%)
120	**300**	**12.48**	**220**	**8.00**	**0.46**	**99.84**	**101.2**	**101.36**
180	**300**	**12.40**	**220**	**7.90**	**0.45**	**97.96**	**99.00**	**101.06**
240	**300**	**12.42**	**224**	**7.68**	**0.46**	**99.11**	**103.04**	**103.90**
300	**300**	**12.45**	**225**	**7.50**	**0.43**	**93.37**	**96.75**	**103.60**
360	**300**	**12.40**	**7.3**	**7.30**	**0.40**	**90.52**	**88.00**	**97.20**
							Average	**100.94**

Table 3, at 60 minutes,120, 180,240 and 300 minutes interval a load of 400w was used, the input voltage, output voltage, input current, output current was measured with a multi-meter, result revealed an average efficiency of 99.64 percent. The test was repeated to minimized errors.

Time (m)	Load (w)	Input voltage (V)	Output voltage (V)	Input current (A)	Output current (A)	Input power (W)	Output power (W)	Efficiency (%)
120	400	12.40	220	7.80	0.44	96.72	96.80	100.08
180	400	12.40	217	7.77	0.45	96.35	97.65	101.34
240	400	12.38	215	7.70	0.44	95.33	94.60	99.23
300	400	12.35	216	7.65	0.44	94.48	95.04	100.60
360	400	12.30	213	7.5	0.39	92.25	89.46	96.97
							Average	99.64

Table 4, Different loads was applied after some time interval ranging from 300W, 400W to 1000W respectively, the input voltage, output voltage, input current, output current was measured with a multi-meter; result revealed a dropped or decline in input power, out power and efficiency as the load increases. We can conclude that the maximum permissible load for the system to operate at a good efficiency is 800W TO 850W.

Trials	Load (w)	Input voltage (V)	Output voltage (V)	Input current (A)	Output current (A)	Input power (W)	Output power (W)	Efficiency (%)
1	0	12.40	220	0	0	0	0	0
2	300	12.48	220	8.00	0.46	99.84	101.2	101.36
3	400	12.40	220	7.80	0.44	96.72	96.80	100.08
4	500	12.20	215	7.32	0.40	89.30	86.00	96.30
5	600	12.20	208	7.28	0.39	88.82	81.12	91.33
6	700	12.16	207	7.26	0.38	88.28	78.60	89.10
7	800	12.14	205	7.25	0.36	88.02	73.80	83.80
8	850	12.10	200	7.20	0.35	87.12	70.00	80.35
9	900	12.00	190	7.10	0.32	85.20	60.80	71.36
10	950	11.30	170	6.80	0.26	76.84	54.02	57.50
11	1000	11.10	110	5.2	0.20	57.72	22.00	38.12

PICTORIAL VIEW OF THE PROJECT WORK

PAPER 42 - OPTIMIZATION ANALYSIS OF DUAL-MODE RENEWABLE HYBRID POWER SYSTEMS: A REVIEW

B.O. Ariyo[1,2], L.M. Adesina[1], A. Musa[1,3], O. Ogunbiyi[1], B.J. Ojuolape[1], M.O. Balogun[1]

[1]Department of Electrical and Computer Engineering, Kwara State University Malete, Nigeria
[2]Department of Electrical and Electronics Engineering, University of Ilorin, Nigeria
[3]Institute for Intelligent Systems, University of Johannesburg, South Africa
Corresponding author email: ariy@unilorin.edu.ng, +2348102227761

ABSTRACT
The escalating threat of global warming necessitates a significant shift towards clean energy production. Renewable energy sources have emerged as a promising solution to meet the growing demand for sustainable electricity generation. However, the intermittent nature of renewable resources calls for the development of hybrid systems to ensure a consistent and reliable power supply. This review investigates the current state-of-the-art optimization analysis of dual-mode renewable hybrid power systems. Dual mode refers to grid-connected and autonomous operational modes, enabling the system to adapt to varying demands and grid availability. The paper delves into the critical challenges associated with optimizing the power output from these systems, including appropriate optimization techniques. A meticulous review of recent advancements in architecture sizing, energy management strategies, and economic evaluations of dual-mode hybrid systems is presented. The paper also explores a comprehensive classification of optimization objectives and methods employed to enhance the performance of these systems. By critically evaluating the existing body of research, this review aims to provide a roadmap for advancing the optimization of dual-mode renewable hybrid power systems. This paves the way for the development of more efficient, reliable, and cost-effective renewable energy solutions for a sustainable future.
KEYWORDS**:** Hybrid energy sources, optimization techniques, minimization, modeling, grid integration

1. INTRODUCTION

Energy is a basic necessity for all aspects of human progress, including food, health, infrastructure, prosperity, education, and civilization; as such, its supply should be secure, ample, and freely available [(Roy *et al*., 2022)]. Alternative energy solutions are required due to massive population growth, quick urbanization and industrialization, the depletion of fossil fuel energy reserves, the detrimental effects of greenhouse gas emissions, and the production of energy from non-renewable sources [(Gulzar *et al*., 2022)]. The numerous benefits of renewable energy systems (RESs), which include being cheap, safe, clean, and readily available, have made them seem like a very promising alternative [(He *et al*., 2021),(Come Zebra *et al*., 2021)]. The main issue facing renewable energy solutions is that, because they are so dependent on the environment, location, and state of operation, they fluctuate in voltage and frequency [(Cuesta *et al*., 2020)].

Reviewing the configuration of renewable hybrid systems has become essential because, in comparison to single renewable energy systems, they enable the integration of various energy generation, storage facilities, and conversion technologies to improve system performance, efficiency, and stability. The most common hybrid system designs are Wind-Hydro, Hydro-Solar, Solar-Wind, Solar-Wind-Biomass, and Solar-Wind-Battery with a diesel generator as a backup in case the required load demand is not satisfied.

Hybrid Renewable Energy Systems (HRESs)

A hybrid renewable energy system (HRESs) combines multiple energy generation and storage methods, or it uses multiple fuel types to power a generator. The transition away from economies dependent on fossil fuels requires HRESs. Renewable energy sources are configured as hybrid systems to maximize energy generation from each resource while reducing the tendency of individual energy sources to drift due to their reliance only on climate for operation. Figure 1 presents a typical hybrid system configuration that combines solar and wind energies with the capacity to operate in both grids integrated and autonomous.

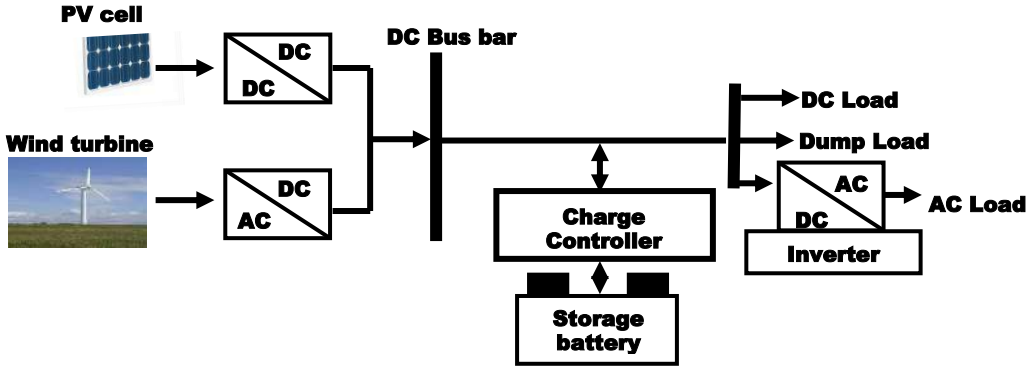

Fig 1. Schematic diagram of a renewable hybrid

The above hybrid system configuration can supply both DC and AC loads. The inverter helps to convert the DC energy to AC to power AC loads. Available DC loads can be fed directly through a direct connection to the DC bus bar. The dumped loads are supplied from the excess energy generated by the hybrid power systems.

Figure 2 gives a summary of the benefits offered by hybrid renewable energy systems. Integrating various energy sources (PV, Wind, Hydro, etc.) improves the overall system configuration's robustness, particularly in the event of climate change. This results in an output power supply that is better and of higher quality without frequency drift, which would otherwise cause sensitive loads to hum inconveniently. The ability of renewable energy sources to compensate for each other's shortcomings ensures the reliability of the hybrid grid system.

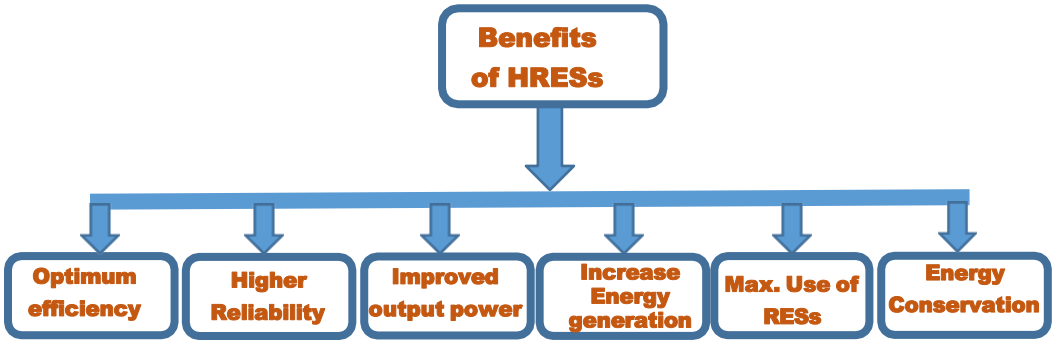

Fig 2. Merits of Renewable Hybrid power systems

2. THEORETICAL ANALYSIS

2.1 The HRES Optimization Objectives:

The capacity of various renewable energy sources to generate energy varies. To build and implement the power grid effectively, the government and utility corporations must be aware of the precise capacity of various renewable energy sources at various places. The cost of operating and maintaining energy-producing units will eventually decrease with the appropriate deployment of renewable energy sources.

When preparing for the implementation of renewable energy sources, minimizing costs and optimizing power generation are the two key goals. Various optimization methods have been suggested to accomplish these two goals. Numerous optimization models are available in the literature, including control models for the effective use of renewable energy sources, system capital cost optimization objectives, emission minimization objectives, energy optimization objectives, profit maximization objectives for Distribution Companies, and energy forecasting objectives. A thorough analysis of optimization techniques used with renewable energy sources can be found in [(Okundamiya, 2021)], however, there are always new optimization techniques being presented in this area. Consequently, an updated assessment of optimization techniques being applied to various issues about the installation and operation of electricity-generating units based on renewable energy sources is presented in this study.

2.2 Hybrid System's Optimal Sizing:

Different methods for optimal sizing of HRES in the literature include the graphical construction method [(Elmelegi *et al*., 2021)], Probabilistic methods [(Fernández-Guillamón *et al*., 2022)], Iterative methods [(Lazaroiu *et al*., 2020)], Analytical methods, and Artificial intelligence methods [(Hoarcă *et al*., 2023)], these approaches use computer models to characterize the various HRES components, enabling system designers to evaluate the performance of various HRES configurations and determine the techno-economic viability of the system. Currently, several computer software tools have been created to evaluate HRES performance, most famous of them are the hybrid optimization model for electric renewables (HOMER), iHOGA / MHOGA, Hybrid2, Hybrid Designer, iGRHYSO, SOMES, SOLSTOR, RETScreen, and SOLSIM. [(Chisale *et al*., 2023), (Arif *et al*., 2023), (Liu and Rodriguez, 2021)].

The following features set these software categories—among many others—apart: they offer remarkably precise simulation results for analysis, evaluation, and optimization, lowering initial capital cost, figuring out a renewable system's ideal capacity, predicting long-term system performance, and swiftly solving numerous system configurations, which makes it simple to compare thousands of options in a single run. The following are some of the major shortcomings of these software packages: certain solutions require lengthy and sluggish processes; some software packages, like HOMER, cannot perform thermal analysis of systems; and some software packages cannot guess key values of sizes in the event that they are absent. Moreover, some software packages necessitate the use of experienced-based criteria in order to produce a satisfactory result.

3. MATERIALS AND METHODS

3.1 Hybrid system modeling:

To model any proposed renewable hybrid power system and meet its design objectives, the main focus is on identifying all system variables and components using appropriate techniques. The next step is to create an objective function that includes all necessary restrictions and variables, as well as components, to make sure that the load requirement is met economically and consistently. The objective function of the optimization problem with its overall system components can thus be determined if the following three requirements are satisfied:

1- Formulating an objective function that, if the anticipated energy generation from the renewable hybrid systems is not fulfilled, that is, optimizing the system's capital cost and minimizing the kilogram of CO_2 emissions. Then, a diesel generator is considered in the configuration to augment energy deficiency.

2- Selecting the hybrid system configuration's ideal renewable energy mix.

3- Evaluating the ideal system configuration to ascertain the financial and technological prerequisites for implementing the suggested system configuration for any case study.

Considering figure 1 as a case study, the effective modeling of the Solar-Wind-Battery system configuration is presented as follows:

3.1.1 The Hybrid System's Total Capital Cost:

This is represented by the symbol (C^{TC}) and represents the total of the expenses associated with each of the following parts of the hybrid system:

a- **The cost price of wind energy conversion system:** This covers the wind turbine's capital cost as well as installation, inverter, and replacement costs. This is according to equation (1).

$$CP_{WT} = \sum_{i=1}^{M_{WT}} C_i^{C_{WT}} + \sum_{i=1}^{M_{WT}} C_i^{I_{WT}} + C^{V_{WT}} + C^{R_{WT}} \quad (1)$$

b- **The solar system's purchase price:** This includes the capital cost of the solar system as well as the costs associated with installation, replacement, and inverters. Equation (2) provides this.

$$C^{PV} = \sum_{i=1}^{M_{PV}} C_i^{C_{PV}} + \sum_{i=1}^{M_{PV}} C_i^{I_{PV}} + C^{V_{PV}} + C^{R_{PV}} \quad (2)$$

c- **The battery bank's overall cost:** Equation (3) provides the value as the total of the battery bank's capital cost and replacement cost.

$$C^{BB} = \sum_{i=1}^{M_{BB}} C_i^{C_{BB}} + C^{R_{BB}} \quad (3)$$

Equation (4) provides the hybrid system's total capital cost, which may be obtained from equations (1) - (3).

$$C^{TC} = C^{WT} + C^{PV} + C^{BB} \quad (4)$$

3.1.2 Replacement cost:

This gives the annual cost value of replacing any system component (s) over the project's duration, as shown in equation (5). [(S. Singh *et al*., 2020)]:

$$C^{RP} = C^{CC}.\delta(r, y) \quad (5)$$

where:

C^{CC} = Capital cost of each component,

δ = The sinking fund factors

r = Annual interest rate, y = the system component's lifespan. It is important to note that, as shown in equation (6), the sinking fund factor depends on the system life time and yearly interest rate.

$$\delta = \frac{1}{(1+r)^{y} - 1} \quad (6)$$

3.1.3 Estimation of Output Energy

The energy production from each hybrid system component is provided as:

(a) Photovoltaic System: Equations and manufacturer specifications can be used to calculate a photovoltaic panel's power output. Equation (7) provides the power output from the PV panel:

$$P^{PV} = G^{R} + A^{PV} + \eta^{PV} \quad (7)$$

where:

P^{PV} = Power generated by solar panels

G^{R} = Global solar irradiance (kW/m^2)

A^{PV} = The solar panel's surface area measured in (m^2)

η^{PV} = PV module efficiency

Equation (13) provides the annual energy generated by the photovoltaic cells.

$$J^{PV} = P^{PV}\, x \frac{9\ hrs}{day} x\ 365\ days\ [kWh] \quad (8)$$

where:

9 *hrs / day* = Average assumed sunshine hours per day at the case study site within West Africans.

(b) Wind Energy Conversion System: The wind energy system's hourly power output is represented by equ. (9) [(Rommel *et al*., 2020), (Wang *et al*., 2022)]:

$$P^{WEC} = \begin{cases} 0 & V^{W} < V^{ci}\ or\ V^{W} \geq V^{co} \\ P_R \dfrac{V^{W} - V^{ci}}{V^{r} - V^{ci}} & V^{ci} \leq V^{W} \leq V^{r} \\ P_R & V^{r} \leq V^{W} < V^{co} \end{cases} \quad (9)$$

where:

P^{WEC} = The total power produced by the wind energy conversion systems

P_R = Wind turbine rated power

V^{W} = The wind turbine speed of at hub height

V^{ci} = The wind turbine Cut-in speed

V^{co} = The wind turbine Cut-out speed

V^{r} = The wind turbine rated speed

Expression (10) [(Khan *et al*., 2022), (Alham *et al*., 2023)] provides the wind turbine's wind speed using a power law equation at the hub height, h, and reference height, h_{ref}.

$$V^{W} = V^{r}\left\{\frac{h}{h_{ref}}\right\}^{\alpha} \quad (10)$$

where:

$\propto$ = The range of the shear coefficient is 0.10 to 0.40 [(Kim *et al*., 2021), (Finnah, 2022)].

Equation (16) expresses the annual energy generated by the wind turbine.

$$J^{GWT} = P^{WEC}\, x\, 8760\ (h/yr)[kWh] \quad (11)$$

(C) Battery Bank: The battery bank's state of charge can be ascertained using the following formula, which considers the energy balance relationship between the battery bank and the hybrid system's overall energy demand:

i- Charging state of the battery bank: The process of charging the battery banks begins when the energy produced by alternative energy sources, such as solar, wind, and distributed generation (DG), exceeds the demand for power. This excess energy must be stored in the battery banks for later use. Equation (12) provides an expression for the battery bank's available capacity at hour (h).

$$J^{G_{BB}}(h) = J^{G_{BB}\,(h-1)} x\,(1-\sigma) + \left[J^{G}(h) - \frac{J^{D_M\,(h)}}{\eta^{inv}}\right] x\,\eta^{BB} \quad (12)$$

ii- Battery bank's state of discharge: On the other hand, when the total energy produced by the several sources is not enough to fulfill the load requirement, the battery bank comes in to provide the remaining energy needed. During this process, the battery bank depleted. The battery bank's available capacity at any given hour (h) can be found using equation (13).

$$J^{G_{BB}}(h) = J^{G_{BB}\,(h-1)} x\,(1-\sigma) + \left[\frac{J^{D_M\,(h)}}{\eta^{inv}} - J^{G}\,(h)\right] \quad (13)$$

where:

$J^{G_{BB}\,(h)}$ = Energy produced by the battery bank in hour (h) expressed in kWh. $J^{G_{BB}\,(h-1)}$ = The battery bank's energy production in hours (h -1), measured in kWh.

σ = Battery bank's rate of self-discharge.

$J^{G}\,(h)$ = Energy generated in kWh by the renewable hybrid system.

$J^{D_M\,(h)}$ = Hourly hybrid system energy demand, expressed in kWh

η^{inv} = Inverter efficiency

η^{BB} = Charge efficiency of the battery bank

The total energy produced in an hour by the renewable energy system is estimated as given in eqn. (14)

$$J_{G_{RES}}(h) = \sum_{i=1}^{NPV} J_i^{G_{PV}} + \sum_{i=1}^{NWEC} J_i^{G_{WEC}} \quad (14)$$

where:

$J_i^{G_{PV}}$ = Energy produced by the photovoltaic modules

$J_i^{G_{WEC}}$ = Energy supply by wind energy conversion devices

3.2 Some Research Works on Optimization of HRESs

This review paper discusses many works that explore the optimization of HRES utilizing various nature-inspired computational intelligence techniques and simulation tools as a substitute for conventional energy. Table 1 lists pertinent studies in these fields:

Table 1: Research works on Optimization Hybrid Renewable Energy Systems

Ref.	Title	Year	Objective	Optimization Method	Contribution
14	Optimal Sizing of Hybrid Renewable Energy System Using Two-Stage Stochastic Programming	2024	To address problems arising from the unpredictability of renewable energy resources	Two-stage stochastic programming	The approach safe about 8.16 % capital cost, as well out perform monte Carlo method, in term of CPU time and cost function evaluations.
15	Optimization of Solar Hybrid Power Generation Using Conductance-Fuzzy Dual-Mode Control Method	2022	To investigate how a solar hybrid power system functions using a unique fuzzy control technique.	Conductance Fuzzy Dual-mode Control Strategy	The technique effectively boosts the electrical output power of hybrid energy systems using renewable energy sources.
16	Mixed-integer linear programming-based optimization strategies for renewable energy communities	2021	To ensure that distributed energy technologies are used effectively at the regional level for both local and renewable energy communities	A planning strategy based on mixed-integer linear programming	reduction of 34% in total carbon dioxide emissions and 15% in energy expenses.
17	Microgrid Operation Optimization Using Hybrid System Modeling and Switched Model Predictive Control	2022	To optimize the financial performance of the microgrids powered by renewables.	Switched hybrid model predictive control	It is guaranteed that storage capacity and renewable energy will be used satisfactorily under shifting grid connection conditions.
18	Techno-economic optimization for isolated hybrid PV/wind/battery/ diesel generator microgrid using improved salp swarm algorithm	2024	to create a novel approach to an isolated renewable microgrid system's techno-economic optimization issue.	Improved Salp Swarm Algorithm (ISSA) with a position adaptation	By comparison with other popular algorithms, the suggested ISSA technique yields better results.
19	Hybrid Renewable Production Scheduling for a PV–Wind-EV- Battery Architecture Using Sequential Quadratic Programming and Long Short-Term Memory–K-Nearest Neighbors Learning for Smart Buildings	2024	To solve non-linear programming optimization problems by predicting the Long Short-Term Memory (LSTM) model.	Sequential Quadratic Programming and Long Short-Term Memory–K- Nearest Neighbors Learning for Smart Buildings	Using the LSTM and KNN algorithms, the prediction yielded accuracy of approximately 95% and 83%, respectively.

4. RESULTS AND DISCUSSION

4.1. HRES's limitations and Future Demands

Even though producing electricity from renewable energy sources is environmentally benign and sustainable, there are still some obstacles to overcome. Listed below are some significant obstacles and areas of potential future research:
1. Due to their high capital cost and lengthy payback period, renewable energy sources require a major reduction in production costs. The industry and buoyant individuals will be encouraged to adopt such technologies by cost savings.
2. Because the adoption of HRES raises some protection concerns, appropriate safety devices must be provided. Furthermore, the current protection mechanisms will need to be upgraded in order to incorporate these dispersed generators.
3. Because autonomous systems are less flexible in response to changes in load, a significant shift in load could cause the system as a whole to fail.
4. The creation of intelligent mini-grids that are made up of multiple generators that communicate with one another and distribute power based on demand is necessary.
5. To ensure reliable communication between the different system components, real-time management in IRES using IEEE Standard 1547 and IEC 61850 is required [(Kosai and Cravioto, 2020)].
6-As HRES is deployed in the form of separate microgrids, there is a growing demand for real-time energy management of these systems and strong communication between the microgrid's different energy sources. As such, these activities are crucial and warrant additional attention.
7- Future research should also focus on hydrogen production and the hydrogen economy. A significant advancement in this field might completely bring a new outlook to human living style.
8-Transient study of the system, involving step changes in the variable parameters such as solar radiation, wind speed, voltage, frequency, and load demand, is necessary to address stability issues with HRES.
9- The state and federal governments must offer the necessary subsidies on renewable energy products to facilitate the widespread deployment of HRES.
10- The use of silicon carbide and gallium nitride semiconductors in robust electronic power switching technology is developing quickly. These materials allow for significantly higher frequency functioning of devices, which can result in smaller inverters, choppers, and other interface systems that improve HRES performance. Research is needed to integrate these gadgets into the developing hybrid systems as they become available.

4.2 Mitigating Renewable Hybrid Energy Crisis

The increasing need for energy and the finite supply of non-renewable energy sources, including fossil fuels, are referred to as the "energy crisis." Concerns over environmental damage, economic instability, and energy security have grown because of this situation. The growing population is one of the main causes of the energy issue. Does the demand for energy increase in tandem with the growth of the world population? The population of the globe is predicted to reach 9.7 billion people by 2050 according to the United Nation [(K. M. Singh and Gope, 2021)] which will raise the need for energy to meet necessities like heating, lighting, and transportation.
Economic expansion is one of the main causes of the energy issue. Growing economies are frequently linked to rising energy prices. Energy demand rises as nations continue to industrialize and modernize. The International Energy Agency projects that by 2040, the world's energy consumption will have grown by 30 % because of population and economic expansion [(Soares *et al*., 2023)]. Economic expansion is a significant contributing factor to the energy dilemma. Increased energy use is frequently linked to economic growth.
Renewable energy sources, such as solar, wind, hydro, geothermal, biomass, and tidal energy, offer a practical solution to the energy crisis by increasing the availability of clean, sustainable, and reliable energy. Solar energy is among the most promising forms of renewable energy. It might potentially help the globe reduce its dependency on fossil fuels while meeting a significant portion of its energy needs. According to the International Energy Agency (IEA), 2021c forecasts, solar energy might provide up to 16% of global electricity needs by 2050 [(S. Singh *et al*., 2024)].

4.3 Research Gap Analysis

Several researchers have used various approaches to determine the ideal size of an autonomous renewable HES that consists of diesel generators, PV arrays, wind turbines, and battery banks at various points in time. There have been many studies on optimizing hybrid energy systems using various computational intelligence techniques, including stochastic and deterministic approaches. However, there have been few comparisons between simulation tools and strategies inspired by nature. Additionally, there haven't been many attempts to create a hybrid approach for maximizing renewable energy systems using various resources to suit rural society's energy needs. Therefore, academia and researchers are urged to focus into these subject areas and beyond just determining the variables and parameters appropriate for a given problem [(Ramesh *et al*., 2022)].

5. CONCLUSION

Energy optimization has been a global challenge for researchers and stakeholders at different levels. This work has provided the needed solution to mitigate energy crises using effective optimized renewable hybrid systems. The major contribution of this work can be summarized as follows:

- Comprehensive procedure to optimize renewable hybrid system's configuration.
- A practical approach to model HRESs for different system configurations.
- Various optimization models that can be adopted to improve renewable output power are discussed in the work.
- Applicable solutions to mitigate global energy crises were presented.
- Research gaps that needed to be covered in the future to further add values to the work were itemized.

Conclusively, the content of this work provides the technical expertise needed to realize optimized hybrid system configuration and power output.

REFERENCES

Alham, M. H., Fathy Gad, M., and Khalil Ibrahim, D. (2023). Potential of wind energy and economic assessment in Egypt considering optimal hub height by equilibrium optimizer. *Ain Shams Engineering Journal*, *14*(1), 101816. https://doi.org/10.1016/j.asej.2022.101816

Arif, R., Arief, Y. Z., Wilyanti, S., Pangestu, A., and Al-Hakim, R. R. (2023). *Using HOMER Simulation Method for Renewable Energy Power Generation Design in South Sumatra Indonesia*. *1*(2), 73–92. https://www.researchgate.net/profile/Rosyid-Ridlo-Al-Hakim-2/publication/373900510_Using_HOMER_Simulation_Method_for_Renewable_Energy_Power_Generation_Design_in_South_Sumatra_Indonesia/links/6502b8758d6da36cc877ecf9/Using-HOMER-Simulation-Method-for-Renew

Belboul, Z., Toual, B., Bensalem, A., Ghenai, C., Khan, B., and Kamel, S. (2024). Techno-economic optimization for isolated hybrid PV/wind/battery/diesel generator microgrid using improved salp swarm algorithm. *Scientific Reports*, *14*(1), 1–29. https://doi.org/10.1038/s41598-024-52232-y

Chakir, A., and Tabaa, M. (2024). Hybrid Renewable Production Scheduling for a PV–Wind-EV-Battery Architecture Using Sequential Quadratic Programming and Long Short-Term Memory–K-Nearest Neighbors Learning for Smart Buildings. *Sustainability (Switzerland)* , *16*(5). https://doi.org/10.3390/su16052218

Chisale, S. W., Eliya, S., and Taulo, J. (2023). Optimization and design of hybrid power system using HOMER pro and integrated CRITIC-PROMETHEE II approaches. *Green Technologies and Sustainability*, *1*(1), 100005. https://doi.org/10.1016/j.grets.2022.100005

Come Zebra, E. I., van der Windt, H. J., Nhumaio, G., and Faaij, A. P. C. (2021). A review of hybrid renewable energy systems in mini-grids for off-grid electrification in developing countries. *Renewable and Sustainable Energy Reviews*, *144*(2021), 1–23. https://doi.org/10.1016/j.rser.2021.111036

Cosic, A., Stadler, M., Mansoor, M., and Zellinger, M. (2021). Mixed-integer linear programming based optimization strategies for renewable energy communities. *Energy*, *237*(121559), 1–16. https://doi.org/10.1016/j.energy.2021.121559

Cuesta, M. A., Castillo-Calzadilla, T., and Borges, C. E. (2020). A critical analysis on hybrid renewable energy modeling tools: An emerging opportunity to include social indicators to optimise systems in small communities. *Renewable and Sustainable Energy Reviews*, *122*(109691), 1–13. https://doi.org/10.1016/j.rser.2019.109691

Elmelegi, A., Mohamed, E. A., Aly, M., Ahmed, E. M., Mohamed, A. A. A., and Elbaksawi, O. (2021). Optimized Tilt Fractional Order Cooperative Controllers for Preserving Frequency Stability in Renewable Energy-Based Power Systems. *IEEE Access*, *9*, 8261–8277. https://doi.org/10.1109/ACCESS.2021.3049782

Fernández-Guillamón, A., Muljadi, E., and Molina-García, A. (2022). Frequency control studies: A review of power system, conventional and renewable generation unit modeling. *Electric Power Systems Research*,

211(108191), 1–15. https://doi.org/10.1016/j.epsr.2022.108191

Finnah, B. (2022). Optimal bidding functions for renewable energies in sequential electricity markets. *OR Spectrum*, *44*(1), 1–25. https://doi.org/10.1007/s00291-021-00646-9

Gulzar, M. M., Iqbal, M., Shahzad, S., Muqeet, H. A., Shahzad, M., and Hussain, M. M. (2022). Load Frequency Control (LFC) Strategies in Renewable Energy-Based Hybrid Power Systems: A Review. *Energies*, *15*(10), 1–23. https://doi.org/10.3390/en15103488

He, W., Tao, L., Han, L., Sun, Y., Campana, E. Pietro, and Yan, J. (2021). Optimal analysis of a hybrid renewable power system for a remote island. *Renewable Energy*, *179*, 96–104. https://doi.org/10.1016/j.renene.2021.07.034

Hoarcă, I. C., Bizon, N., Șorlei, I. S., and Thounthong, P. (2023). Sizing Design for a Hybrid Renewable Power System Using HOMER and iHOGA Simulators. *Energies*, *16*(4). https://doi.org/10.3390/en16041926

Khan, A. A., Minai, A. F., Pachauri, R. K., and Malik, H. (2022). Optimal Sizing, Control, and Management Strategies for Hybrid Renewable Energy Systems: A Comprehensive Review. *Energies*, *15*(17), 1–29. https://doi.org/10.3390/en15176249

Kim, D. Y., Kim, Y. H., and Kim, B. S. (2021). Changes in wind turbine power characteristics and annual energy production due to atmospheric stability, turbulence intensity, and wind shear. *Energy*, *214*, 119051. https://doi.org/10.1016/j.energy.2020.119051

Kosai, S., and Cravioto, J. (2020). Resilience of standalone hybrid renewable energy systems: The role of storage capacity. *Energy*, *196*(117133), 1–13. https://doi.org/10.1016/j.energy.2020.117133

Lazaroiu, G., Ciupageanu, D. A., Hazmoune, M., and Vatuiu, T. (2020). Design of an enhanced performance hybrid autonomous system. *International Multidisciplinary Scientific GeoConference Surveying Geology and Mining Ecology Management, SGEM*, *2020-Augus*(4.1), 45–52. https://doi.org/10.5593/sgem2020/4.1/s17.006

Liu, B., and Rodriguez, D. (2021). Renewable energy systems optimization by a new multi-objective optimization technique: A residential building. *Journal of Building Engineering*, *35*(102094), 1–32. https://doi.org/10.1016/j.jobe.2020.102094

Maślak, G., and Orłowski, P. (2022). Microgrid Operation Optimization Using Hybrid System Modeling and Switched Model Predictive Control. *Energies*, *15*(3). https://doi.org/10.3390/en15030833

Mohammed, N., and Ali, M. M. (2024). Optimal Sizing of Hybrid Renewable Energy System Using Two-Stage Stochastic Programming. *International Journal of Energy Research*, *2024*. https://doi.org/10.1155/2024/2361858

Okundamiya, M. S. (2021). Size optimization of a hybrid photovoltaic/fuel cell grid connected power system including hydrogen storage. *International Journal of Hydrogen Energy*, *46*(59), 30539–30546. https://doi.org/10.1016/j.ijhydene.2020.11.185

Ramesh, S., Seetha, J., Ramkumar, G., Sahoo, S., Amirthalakshmi, T. M., Ranjith, A., Seikh, A. H., Khan Mohammed, S. M. A., and Subbiah, R. (2022). Optimization of Solar Hybrid Power Generation Using Conductance-Fuzzy Dual-Mode Control Method. *International Journal of Photoenergy*, *2022*. https://doi.org/10.1155/2022/7756261

Rommel, D. P., Di Maio, D., and Tinga, T. (2020). Calculating wind turbine component loads for improved life prediction. *Renewable Energy*, *146*, 223–241. https://doi.org/10.1016/j.renene.2019.06.131

Roy, P., He, J., Zhao, T., and Singh, Y. V. (2022). Recent Advances of Wind-Solar Hybrid Renewable Energy Systems for Power Generation: A Review. *IEEE Open Journal of the Industrial Electronics Society*, *3*(February), 81–104. https://doi.org/10.1109/OJIES.2022.3144093

Singh, K. M., and Gope, S. (2021). Renewable energy integrated multi-microgrid load frequency control using grey wolf optimization algorithm. *Materials Today: Proceedings*, *46*, 2572–2579.

https://doi.org/10.1016/j.matpr.2021.02.035

Singh, S., Chauhan, P., Aftab, M. A., Ali, I., Suhail Hussain, S. M., and Ustun, T. S. (2020). Cost optimization of a stand-alone hybrid energy system with fuel cell and PV. *Energies*, *13*(5), 1–23. https://doi.org/10.3390/en13051295

Singh, S., Subburaj, V., Sivakumar, K., Anil Kumar, R., Muthuramam, M. S., Rastogi, R., Ratansing Patil, V., and Rajaram, A. (2024). Optimum Power Forecasting Technique for Hybrid Renewable Energy Systems Using Deep Learning. *Electric Power Components and Systems*, *0*(0), 1–18. https://doi.org/10.1080/15325008.2024.2316251

Soares, I., Alves, M. J., and Antunes, C. H. (2023). A deterministic bounding algorithm vs. a hybrid meta-heuristic to deal with a bilevel mixed-integer nonlinear optimization model for electricity dynamic pricing. *Computers and Operations Research*, *155*(January). https://doi.org/10.1016/j.cor.2023.106195

Wang, S., Moan, T., and Jiang, Z. (2022). Influence of variability and uncertainty of wind and waves on fatigue damage of a floating wind turbine drivetrain. *Renewable Energy*, *181*, 870–897. https://doi.org/10.1016/j.renene.2021.09.090

PAPER 43 - DESIGN OF AN IMPROVED MICROSTRIP ANTENNA OPERATING AT A FREQUENCY BAND OF 28 GHZ

S. O. Zakariyya[1*], V. O. Omole[1], B. O. Sadiq[2,3], R. A. Alao[1], J. A. Adesina[4], E. Obi[5]

[1]Electrical and Electronics Engineering Department, University of Ilorin, Ilorin, Nigeria.
[2]Electrical and Computer Engineering, Kampala International University, Uganda
[3]Computer Engineering Department, Ahmadu Bello University, Zaria, Nigeria
[4]Computer Engineering Department, University of Ilorin, Ilorin, Nigeria.
[5]Electronics and Telecommunication Engineering Department, Ahmadu Bello University, Zaria, Nigeria
*Email: zakariyya.os@unilorin.edu.ng

ABSTRACT
The design of an improved microstrip antenna operating in the 28 GHz frequency spectrum is the main goal of this work. The design used a Roger RT 5880 LZ substrate with a thickness and permittivity of 0.762mm and 1.96, respectively. The antenna was simulated in CST Microwave Studio. As the antenna feed, a quarter-wave transformer was used to provide an impedance match of 50 ohms. To improve the antenna's performance, a U-shaped element was added to the ground plane. The antenna resonated at 28 GHz frequency, according to simulation data, with a return loss of -21.4 dB, VSWR of 1.18, bandwidth of 2.026 GHz, and gain of 8.19 dB. The proposed antenna exhibits a performance improvement in terms of gain and bandwidth due to the addition of U-shaped element when benchmarked with existing designs in the literature work.

KEYWORDS: 5G communication, Microstrip, Antenna, quarter-wave transformer, CST microwave studio

1. INTRODUCTION

The evolution of mobile and cellular networks has experienced remarkable progress over recent decades, evolving through various generations that each introduced enhanced features surpassing their predecessors. Demand for bandwidth and mobile broadband has surged exponentially in the last decade, resulting in a significant increase in data traffic that largely outpaced the capabilities of prior generations, most notably 4G. This burgeoning demand, particularly for data-intensive applications, necessitated a shift towards higher frequencies beyond the traditionally used sub-6 GHz range before the advent of 5G. These earlier frequencies, though sufficient for past needs, began to experience congestion issues and network capacity limitations, underscoring the imperative for higher bandwidth and data rates to support the emerging landscape of digital consumption and services (Zakariyya *et al*., 2019).

5G technology has been designed to address these challenges by not only utilizing the existing sub-6 GHz frequency bands but also expanding into the millimeter-wave spectrum, which ranges from 24 GHz to 100 GHz. This shift to higher frequencies is a cornerstone of 5G's ability to provide higher data rates, reduced latency, and increased capacity and the ability to connect numerous devices simultaneously. The millimeter waves frequencies, despite their limited propagation range and higher susceptibility to both attenuation and environmental obstructions, unlocks the potential for significantly expanded bandwidth and capacity. Among the existing millimeter waves spectrum, 28-GHz is notably preferred for 5G applications due to its lower atmospheric absorptions and attenuations rates (Larsson *et al*, 2014; Hu *et al*, 2018).

The design of antennas, especially Microstrip Patch Antennas (MPAs), is crucial in overcoming the limitations of the millimeter wave band and maximizing the use of this wider frequency range. MPAs offer significant advantages due to their compact size, design flexibility, and seamless integration with diverse devices and network setups (Zakariyya *et al*., 2015; Zakariyya *et al*., 2016; Salami *et al*., 2018). However, traditional patch antennas often suffer from low gain and limited bandwidth. To address these shortcomings, this study introduces an improved patch antenna tailored for 5G communication.

Rahman *et al*. (2016) presented an antenna operating at 28 GHz with a bandwidth of 2.66 GHz. However, this design lacked compactness and had a low gain. Przesmycki *et al*. (2020) designed a rectangular patch antenna operating at 28 GHz, utilizing RT/duroid substrate. This antenna achieved notable metrics. However, the gain did not meet the requirements for 5G applications. Awan *et al*. (2021) discussed a microstrip antenna with a defective ground structure (DGS) at 28 GHz. While this design exhibited good bandwidth and return loss, its gain may still be insufficient to overcome the path and absorption losses in the millimeter-wave spectrum. Kamal *et al*. (2021)

introduced a single-band hook-shaped antenna at 28 GHz. This antenna demonstrated a good return and wide bandwidth. However, its size was not compact, and its gain was relatively low. Additionally, Raheel *et al*. (2021) proposed a microstrip patch antenna operating at 28/38 GHz. This design achieved a gain of 7.1 dBi and an impedance bandwidth of 1 GHz (27.6 GHz - 28.6 GHz). Hussain *et al*. (2022) attempted a circular microstrip patch antenna with two rectangular slots, showcasing a good impedance bandwidth. However, this antenna was relatively large and had a modest gain. Furthermore, Farahat and Hussein (2022) introduced a patch antenna operating in the 28/38 GHz bands, achieving a gain of 6.6 dB and a bandwidth of 1.23 GHz in the 28 GHz range. Gaid *et al*, 2024 proposed a microstrip patch antenna operating at 28/38 GHz. This design achieved a gain of 8.1 dB and an impedance bandwidth of 1.43 GHz.

These discussed antennas exhibit various strengths and weaknesses, such as wide bandwidths, high gains, or compact sizes. However, their performance can be improved by adding a U shape element on the ground plane. Hence, this research aims to strike a balance between antenna size, impedance bandwidth, and gain by designing a small-size antenna with high gain, optimal impedance bandwidth, and coverage of the 28 GHz band.

2. ANTENNA DESIGN

The initial step in creating a patch antenna involves selecting the substrate, as its properties, like thickness and dielectric constant, significantly impact the antenna's characteristics. In this particular design, a Roger RT 5880LZ substrate was chosen with a thickness of 0.762mm and a relative dielectric constant of 1.96. Copper was used for both the patch conductor and ground plane. These materials were chosen due to their high conductivity. The dimensions of the patch element are calculated using transmission line model accordingly (Zakariyya *et al*., 2016; Balanis, 2005):

$$w_{pc} = \frac{v}{2f_r}\sqrt{\frac{2}{\varepsilon_{r\_l}+1}} \tag{1}$$

The patch width is w_{pc}, ε_{r_l} is the relative dielectric constant and f_r represents the frequency at which the antenna resonates and v is the speed of light.

The effective dielectric constant is expressed as where $h_{\_s}$ is substrate height:

$$\varepsilon_{r\_eff} = \frac{\varepsilon_{r\_l}+1}{2} + \frac{\varepsilon_{r\_l}-1}{2}\left(1+\frac{12h_{\_s}}{w_{pc}}\right)^{\frac{-1}{2}} \tag{2}$$

As a result of fringing, the length of the patch is extended by a distance equal to:

$$\Delta L_{\_p} = 0.412h_{\_s}\frac{(\varepsilon_{r\_eff}+0.3)(^{w_{pc}}/_{h_{\_s}}+0.264)}{(\varepsilon_{r\_eff}-0.258)(^{w_{pc}}/_{h_{\_s}}+0.8)} \tag{3}$$

The length is determined by:

$$L_{\_p} = L_{\_eff}\text{-}2\Delta L_{\_p} \tag{4}$$

$$L_{\_eff} = \frac{v}{2f_r\sqrt{\varepsilon_{r\_eff}}} \tag{5}$$

The edge impedance $Z_{in} = 90\frac{\varepsilon_{r\_l}^2}{\varepsilon_{r\_l}-1}\left(\frac{L_{\_p}}{w_{pc}}\right)^2$ (6)

Where $L_{\_p}$ is the patch length

The line impedance of the quarter wave is given by:

$$Z_T = \sqrt{Z_0 Z_{in}} \tag{7}$$

The length ($L_{\_p}$) and width (w_{pc}) of the radiating patch for the design was calculated to be 3.2 mm and 4.4 mm using the mathematical equations described in (1-4). The load impedance at the edge of the patch is calculated to be approximately 190.5 ohms using Eq. (6). A simulation model for the single element antenna implemented in

CST-MWS is shown in Figure 1. For enhancement of the antenna performance, a U shape element is created on the ground plane to serve as parasitic element.

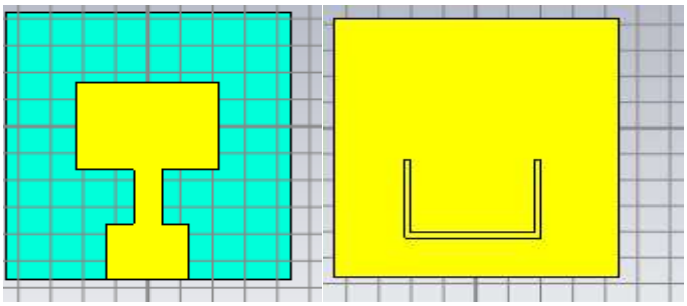

Figure 1: Front and back view of the designed antenna

3. RESULTS AND DISCUSSION

3.1. Return Loss

Figure 2 shows the return loss of the proposed MPA. For mobile communication systems, a standard value of -10 dB is acceptable as the baseline for good performance. The proposed MPA has a return loss of -21.4 dB, resonating at the desired resonant frequency of 28 GHz and covering a frequency band of 27.185 GHz – 29.211 GHz with a bandwidth of 2.026 GHz.

3.2. Voltage Standing Wave Ratio

Figure 3 shows the Voltage Standing Wave Ratio (VSWR) of the proposed MPA design. For mobile communication systems, the value of VSWR should be small (not more than 2.5 and close to 1.0) in order to ensure proper impedance matching and little amount of reflected power. The proposed MPA design achieved a VSWR of 1.18 at a resonant frequency of 28 GHz which indicates good matching between the feeding line and the radiating patch element.

3.3. Radiation Pattern

Figure 4a and Figure 4b shows the 2D and 3D radiation pattern plot of the proposed MPA design. As observed from the 3D plot, the proposed patch antenna design has a gain of 8.19 dBi which is considered acceptable in this scenario of compact antenna design.

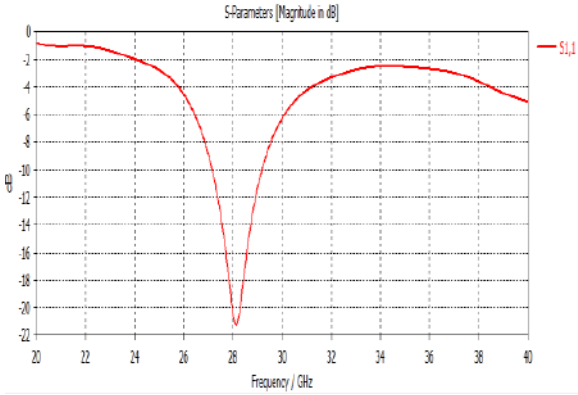

Figure 2: Return loss plot

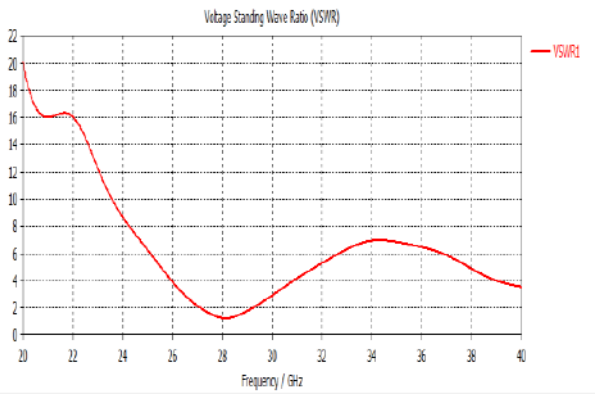

Figure 3: voltage standing wave ratio

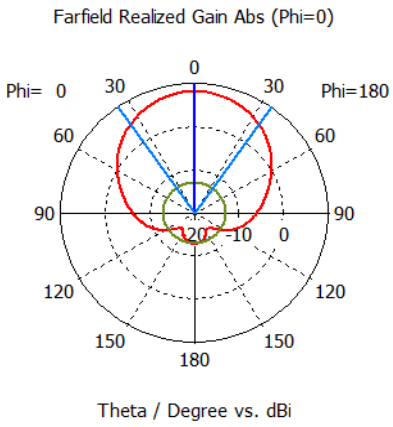

Figure 4a: 2D Radiation pattern plot

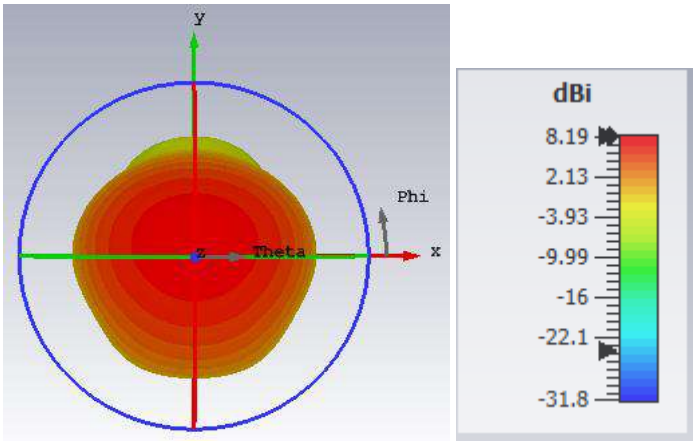

Figure 4b: 3D Radiation pattern plot

Table 1 is a summary of the comparison between the proposed design and other reported 5G antennas. From the table, the proposed 5G antenna antenna is found to perform better than the majority of the counterparts in terms of the bandwidth and gain.

Table 1: Comparison between the Proposed Design and Other Reported Antennas

Reference Antennas	S11(dB)	Bandwidth (GHz)	Gain (dB)
Proposed design	-21.4	2.02	8.19
Gaid *et al*., 2024	-45	1.43	8.1
Farahat and Hussein, 2022	-34.5	1.23	6.6
Raheel *et al*., 2021	-25	1	7.1

4. CONCLUSION

A microstrip patch antenna has been designed for 5G applications in mobile communication. The antenna was designed to resonate at 28 GHz. A U-shape structure was added to the ground plane with the aim of enhancing the antenna's performance. The proposed MPA simulation results show that the return loss, bandwidth, gain and VSWR are -21.4 dB, 2.02 GHz, 8.19 dB, and 1.18, respectively. The proposed antenna offers highly competitive performance when compared to other designs. The suggested structure is a good candidate for 28 GHz band applications due to its simplicity, good radiation properties, and compactness

REFERENCES

Awan, W. A., Naqvi, S. I., Hussain Naqvi, A., Abbas, S. M., Zaidi, A., and Hussain, N. (2021). Design and characterization of wideband printed antenna based on DGS for 28 GHz 5G applications. Journal of Electromagnetic Engineering and Science, 21(3), 177–183. https://doi.org/ 10.26866/jees.2021.3.r.24

Farahat, A. E., and Hussein, K. F. A. (2022). Dual-Band (28/38 GHz) Wideband MIMO Antenna for 5G Mobile Applications. IEEE Access, 10, 32213–32223. https://doi. org/10.1109/ACCESS.2022.3160724

Gaid, A. S. A., Ali, A. M., Saif A., and Mohammed, W. A. A. (2024). Design and analysis of a low profile, high gain rectangular microstrip patch antenna for 28 GHz applications, Cogent Engineering, 11:1, 2322827, DOI: 10.1080/23311916.2024.2322827

Hu, S., Rusek, F., and Edfors, O. (2018). Beyond Massive MIMO: The Potential of Data Transmission With Large Intelligent Surfaces. IEEE Transactions on Signal Processing, 66(10), 2746–2758. doi:10.1109/tsp.2018.2816577

Hussain, M., Mousa Ali, E., Jarchavi, S. M. R., Zaidi, A., Najam, A. I., Alotaibi, A. A., Althobaiti, A., and Ghoneim, S. S. M. (2022). Design and characterization of compact broadband antenna and its MIMO configuration for 28 GHz 5G applications. Electronics, 11(4), 523. https:// doi.org/10.3390/electronics11040523

Kamal, M. M., Yang, S., Kiani, S. H., Sehrai, D. A., Alibakhshikenari, M., Abdullah, M., Falcone, F., Limiti, E., and Munir, M. (2021). A novel hook-shaped antenna operating at 28 GHz for future 5G mmwave applications. Electronics, 10(6), 673. https://doi.org/10.3390/electronics10060673

Larsson, E., Edfors, O., Tufvesson, F., and Marzetta, T. (2014). Massive MIMO for next generation wireless systems. IEEE Communications Magazine, 52(2), 186–195. doi:10.1109/mcom.2014.6736761

Przesmycki, R., Bugaj, M., and Nowosielski, L. (2020). Broadband microstrip antenna for 5G wireless systems operating at 28 GHz. Electronics, 10(1), 1. https://doi.org/ 10.3390/electronics10010001

Raheel, K., Altaf, A., Waheed, A., Kiani, S. H., Sehrai, D. A., TuBBal, F., and Raad, R. (2021). E-shaped H-slotted dual band mmWave antenna for 5G technology. Electronics, 10(9), 1019. https://doi.org/10.3390/electronics10091019

Rahman, A., Yi, N. M., Ahmed, A. U., Alam, T., Singh, M. J., and Islam, Moha. M. M. T. (2016). A compact 5G antenna printed on manganese zinc ferrite substrate material. IEICE Electronics Express, 13(11), 20160377–20160377. https://doi.org/10.1587/elex.13.20160377

Salami, A. F., Zakariyya, O. S., Sadiq B. O., and Abdulrahman, O. A. (2018). Evaluative Assessment of an X-band Microstrip Patch Antenna for Wireless Systems. ABUAD Journal of Engineering Research and Development (AJERD), 1(2) , 264-272.

Zakariyya, O. S., Sadiq B. O., Abdulrahman, O. A., and Salami, A. F. (2016). Modified edge fed Sierpinski carpet miniaturized microstrip Patch antenna. Nigeria Journal of Technology, 35(3), 637-641.

Zakariyya, O. S., Sadiq B. O., Olaniyan, A. A., and Salami, A. F. (2016). Dual Band Fractal Antenna Design for Wireless Application. Computer Engineering and Applications Journal, 5(3), 101-108.

Zakariyya, S. O. (2015). Modeling of Miniaturized, Multiband and Ultra-Wideband Fractal antenna. M.Sc. Thesis, Institute of Graduate studies and research, Eastern Mediterranean University, Gazimagusa, North Cyprus.

Zakariyya, S. O., Sadiq, B. O., Adebayo, M. A., Salami, A. F., Usman, A. M., and Afolayan, M. A. (2019). A High Gain Patch Antenna Array for 5G Communication. 2nd International Conference of the IEEE Nigeria Computer Chapter (NigeriaComputConf), pp. 1-6.

PAPER 44- INVESTIGATING THE EFFECTS OF COCONUT SHELLS ON THE HARDNESS, DENSITY AND WEAR RESISTANCE OF ALUMINIUM

A.C Igwe[12], N.H. Ononiwu[12*], C.N Achebe[1]

[1] Department of Mechanical Engineering, University of Nigeria Nsukka Nigeria
[2] African Centre of Excellence; Sustainable Energy and Power Development, University of Nigeria Nsukka.
[*]Email: ndudim.ononiwu@unn.edu.ng

ABSTRACT
Aluminium matrix composites have grown to become a staple in materials engineering. This is due to its combination of properties including improved mechanical properties, wear and corrosion resistance and reduced weight. This research was conducted to investigate the effect of coconut shells on the hardness, density and wear resistance of aluminium. The selected fabrication route was stir casting. The composites were reinforced with coconut shells at 2 wt.% to 10 wt. % in increments of 2 wt.% bringing the reinforced aluminium samples to a total of 6. The microstructure of the investigated samples was characterised by a fairly uniform dispersal of the reinforcements with minimal segregation and agglomeration of the particles. The hardness of the samples was shown to improve up to 43.26%. The density of the samples was shown to decrease with increasing wt.% of the reinforcements which indicates the production of lightweight materials. The wear resistance was investigated and the results showed that the wear rate decreased with increasing weight fraction of the reinforcements owing to the presence of the hard brittle particles that work to improve the wear resistance. The results of this study will contribute to the ever-growing body of knowledge in aluminium matrix composite research.

KEYWORDS: aluminium matrix composites, reinforcements, coconut shells, hardness, wear resistance

1. INTRODUCTION

Industrial applications of aluminium matrix composites not limited to automotive and aerospace industries have been shown to prefer materials with a high strength-to-weight ratio, superior corrosion and wear resistance. This need has over time been met with the use of metals reinforced with sustainable materials. Sustainable materials for composite applications have been shown to improve the properties of the matrix material while ensuring environmental cost savings and overall cost reduction [1, 2]. Sustainable reinforcing materials used in the fabrication of aluminium matrix composites are either sourced from agricultural and industrial waste [3]. Several researches have shown that sustainable materials can be used to fabricate composites with properties which include high strength, high corrosion and wear resistance, and reduced densities [4–6]. In addition, researchers such as Moona *et al.* [2] have highlighted the need for environmental cost savings as a rationale behind the use of these categories of reinforcement for the fabrication of composite materials. Such sustainable materials include fly ash, egg shells, coconut shells, red mud, bagasse, and palm kernel shells among others. The positive results emanating from the research into these materials have shown that they can be put to good use thereby reducing their indiscriminate disposal. Dwivedi and Mishra [5], highlighted relative fabrication cost as a factor for the adoption of sustainable reinforcing materials compared to conventional reinforcing particles. The conventional reinforcing particles are synthetic materials which can be used to improve the properties of aluminium matrix composites through several mechanisms such as load transfer and grain refinement [7, 8]. Such materials include SiC, Al_2O_3, B_4C, TiC and carbon nanotubes. While these materials have been used successfully to improve the properties of the aluminium matrix, cost is a factor that tends to limit their use [9]. This issue can be solved through the utilization of sustainable materials which can be procured at little to no cost.

Donald *et al.* [10], fabricated a hybrid composite by reinforcing coconut shells with silicon carbide. The results showed an improvement in the hardness and tensile strength by 23.55% and 44.18% respectively. Ononiwu et al [11], successfully reinforced aluminium with eggshells and investigated selected properties. The results of the experiment showed a reduction in the density with increasing weight fraction of the eggshells. Further analysis revealed an improvement of 9.10% in the tensile strength while improvements in hardness were reported. Prakash *et al.* [12], investigated the effect of rock dust on the hardness of aluminium. The hardness increased with increasing weight fraction of the reinforcements from 39 BHN for the unreinforced aluminium to 78 BHN for the sample with 15 wt.% of the rock dust particles. Vinod *et al* [13], reinforced Al-7Si-0.3Mg with fly ash and rice husk ash and reported an improvement in the microhardness from 61 HV for the unreinforced alloy to 82 HV for

the sample reinforced with 7.5 wt.% rice husk and fly ash. The study also reported a 4.54% improvement in the compressive strength. The wear studies revealed that the wear resistance of the fly ash and rice husk ash reinforced samples improved compared to the unreinforced sample. Singh *et al*. [14], produced a hybrid aluminium matrix composite reinforced with Al_2O_3 and rice husk ash. The results showed that the tensile strength improved by 42.5% and 72.5% for the Al 6063 base metal.

The reviewed literature has shown that sustainable reinforcements are capable of improving the properties of aluminium. This study therefore aims to investigate the microstructure, hardness, density and wear resistance of aluminium reinforced with coconut shell particles.

2. MATERIALS AND METHODS

The new aluminium ingot was sourced from Nsukka, Enugu State Nigeria. The procured aluminium ingot has 4 kg. The elemental composition of the aluminium ingots is summarised in Table 1.

Table 1: Elemental composition of the aluminium matrix

Composition	Si	Fe	Mg	Cu	Al
%	0.5	0.18	0.6	0.01	98.71

Coconuts were sourced from the Ogige local Market in Nsukka Nigeria. From the coconuts, the shells were extracted for the study. The coconut shells were washed in running water to remove any contaminants that might taint the fabrication process and by extension, the results of the experiments. The washed coconut shells were subsequently dried in open air for 3 days. Further drying took place in an electric oven set at 80 °C to further remove any residual moisture. Milling of the coconut shells was done using a ball milling machine rotating at 180 rpm. The ball milling was carried out for 7 hours to ensure the samples were in the nano range. The milled samples weighed 5.47 kg. The milled samples were afterwards calcinated in the open air to reduce them to ash. The ash was in turn carbonised at a temperature of 800 °C. The carbonization is important to improve the wettability between the matrix and reinforcements, increase the carbonaceous content of the reinforcements and improve the interfacial bonding of the reinforcements with the matrix [15, 16]. The samples were passed through a sieved with mesh size of 50 µm. All particles that passed through the sieve were retained and used for the study. The composition of the coconut shell particles is shown in Table 2.

Table 2: Chemical composition of the coconut shell particles [17]

Composition	SiO_2	Al_2O_3	MgO	Fe_2O_3		CaO	Na_2O	MnO	ZnO	LOI
%	41.26	21.84	12.37	18.45		0.67	0.72	0.23	0.36	4.1

Figure 1: (a) Milled coconut shells (b) Carbonized coconut shell particles.

Fabrication of the composites was achieved through the stir-casting route. In addition to its simplicity, stir casting is a cost-effective method of fabricating aluminium matrix composites. The aluminium was cut and weighted based on the weight fractions shown in Table 3.

Table 3: Designation of the fabricated samples

Samples	Aluminium matrix wt%	Coconut shell reinforcements wt%
A	100	0
B	98	2
C	96	4
D	94	6
E	92	8
F	90	10

For proper fabrication, the coconut shell reinforcements were weighed and preheated at 400 °C. An electric furnace was heated to 750 °C while the graphite crucible was preheated at 750 °C. The graphite crucible was preheated gradually to the temperature required for the casting process to avoid the effects of thermal shock. Prior to being charged into the crucible, the aluminium was cleaned, cut and weighted based on the designations in Table 3. Melting of the aluminium was followed by the degassing of the molten metal using hexachloroethane tablets which was important to eliminate hydrogen and oxidized slag. The resulting slag was removed from the surface of the molten aluminium. The preheated reinforcements were charged into the molten aluminium, followed by 1 wt.% magnesium powder of 100% purity. The magnesium is important to further improve the wettability between the composite constituents. Mechanical stirring was carried out for 10 minutes to ensure uniform dispersal of the reinforcements in the aluminium matrix. The resulting molten composite was poured into a predetermined sand mould as shown in Figure 2(a) for the solidification and cooling process to commence. The fabricated samples are shown in Figure 2(b).

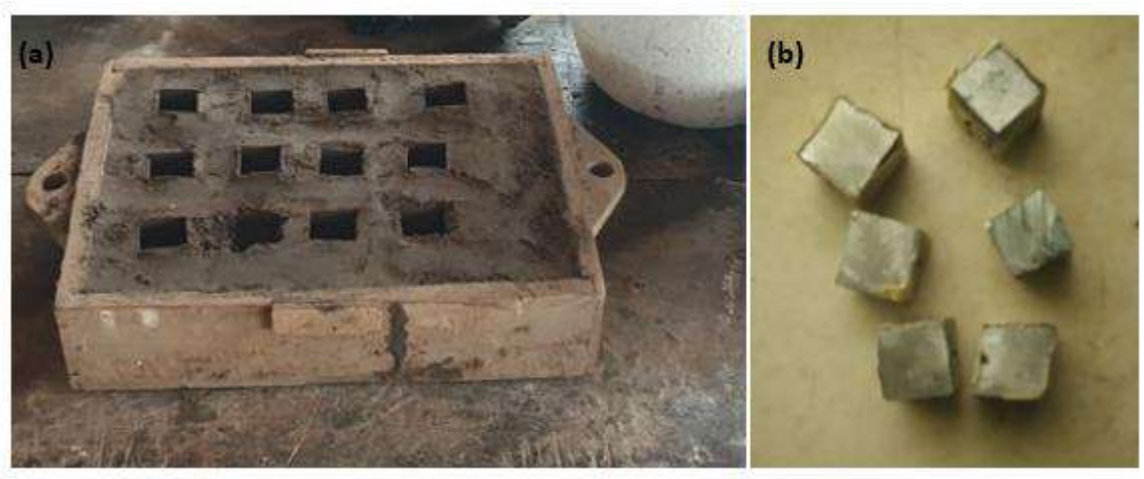

Figure 2: (a) Sand mould (b) Cast samples

The hardness of the cast samples was determined using the Vickers hardness tester. This test was conducted at room temperature. Five indentations were made with a load of 200 N for a dwell time of 15 seconds for each. The average hardness value was reported in this study.

Using Archimedes' principle of volume displacement shown in equation (1), the density of the cast samples was determined.

$$\rho_s = \frac{m}{v} \tag{1}$$

where ρ_s is the density of the sample in g/cm^3, m is the mass of the sample, v is volume displacement.

The wear resistance was conducted using a pin-on-disc tribometer with a load of 20 N for 20 cycles under dry sliding conditions. Using the expressions in equations (2) and (3), the volumetric wear loss and specific wear rates were computed respectively.

$$\Delta V = \frac{(w_1 - w_2)}{\rho} \quad (2)$$

where ΔV is the volumetric wear loss in cm^3, w_1 and w_2 is the initial and final weight respectively in g and ρ is the density of the sample.

The specific wear rate was calculated to give information on the rate of wear at the given load and sliding distance. This was obtained mathematically using the expression in equation (3).

$$W_s = \frac{\Delta V}{F \times S} \quad (3)$$

Where *Ws* is the specific wear rate in g/Nm, *F* is the applied load in N, and *S* is the sliding distance in m.

3. RESULTS AND DISCUSSION

3.1 Hardness

The hardness of the investigated samples was characterised by a steady increase up to 8 wt.% coconut shell reinforcement as evident in Figure 3. This accounted for a 43.26% increase in the hardness compared to the unreinforced aluminium. A decline from 30.80 HV for the 8 wt.% sample to 28.40 HV for the 10 wt.% sample was recorded from the experiment. The decline can be attributed to the increased viscosity of the molten which is responsible for the segregation and agglomeration of the reinforcing particles. Improvement in the hardness of the composites is due to strong interfacial bonding and proper wettability between the reinforcing particles and the aluminium matrix. Another reason for the improved hardness is due to the grain refinement brought about by the coconut shell reinforcements. The improvement in the hardness of the cast composites was also attributed to the formation of dislocations which increased the dislocation density of the samples. The increased dislocation density is a direct consequence of the difference in the coefficient of thermal expansion of the matrix and the coconut shell particles. Additionally, the improved hardness is due to the presence of hard brittle reinforcing particles that work by restricting the relative motion between individual grains during the application of localized load [18].

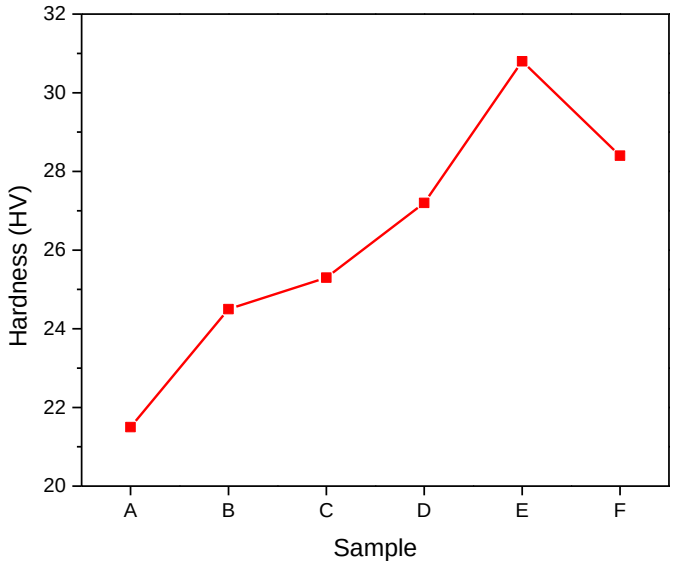

Figure 3: Results for the hardness

3.2 Density

With reference to Figure 4, it can be seen that the incorporation of the coconut shell particles was responsible for the decreased density of the reinforced samples. The relatively lower density of the coconut shell was responsible

for the reduced density of the overall composites. It was gathered from the investigation that the density of the cast aluminium composite samples decreased with increasing weight fraction of the coconut reinforcing samples up to 10 wt.%. Similar trends were reported in [19, 20]. The density of the reinforcements decreased by 12.5% for the 10 wt.% coconut shell reinforced sample. The highlighted result is an indication that the coconut shell particles are capable of producing lightweight aluminium matrix composites.

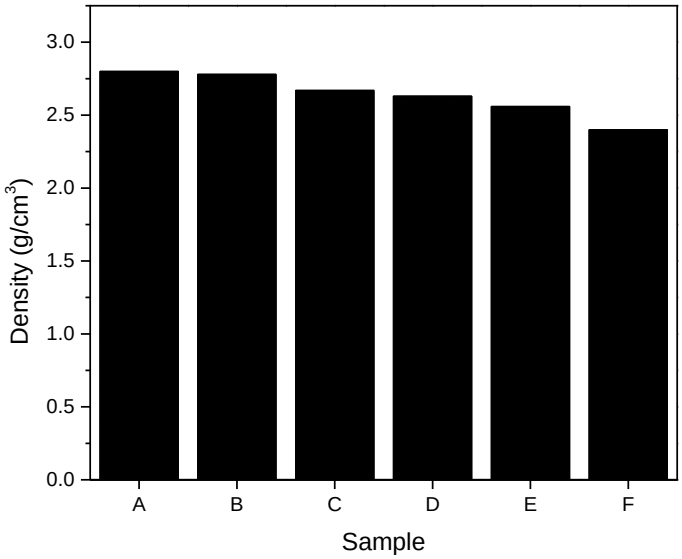

Figure 4: Hardness of the cast samples

3.3 Microstructure

The microstructure of the cast samples is shown in Figure 5. The micrographs of the matrix show the presence of the α-phase with the formation of a dendritic structure which is formed during the solidification of the aluminium metal post-casting. The microstructure of the investigated samples showed no presence of casting defects associated with sand casting which is an indication of a proper casting process. The microstructure of the cast composites reveals a fairly uniform dispersal of the reinforcing particles. The increased weight fraction of the reinforcements of sample F (10 wt.%) samples as shown in Figure 5(c) is evident by the increased cluster of the reinforcing particles. Both reinforced samples (samples C and F) showed minimal indications of agglomeration and segregation which is usually present in sustainable reinforced aluminium composites. The formation of pores as a result of trapped gases or air bubbles formed during cooling was not recorded during the microstructural examination of the fabricated samples.

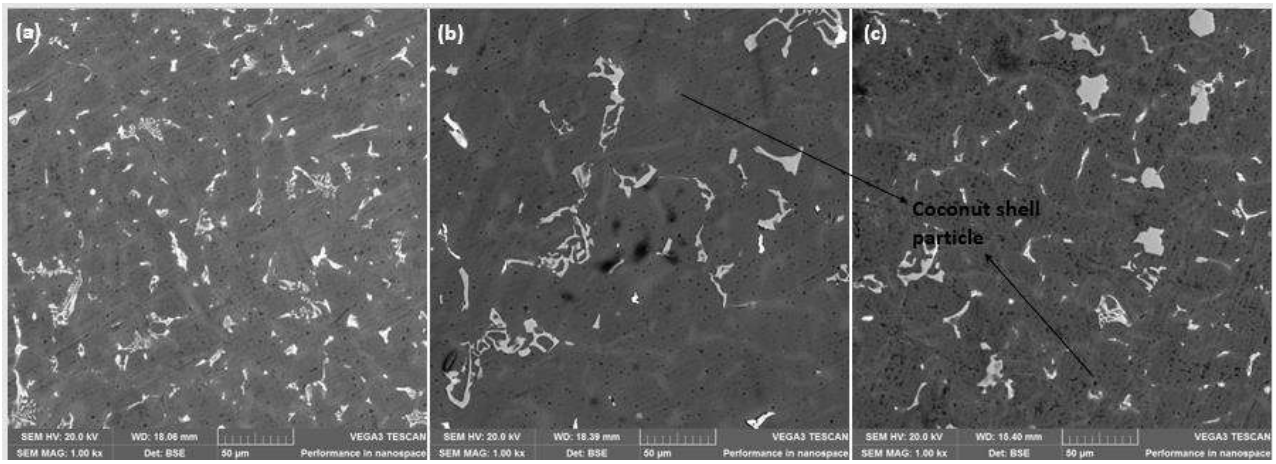

Figure 5: Micrographs of (a) Sample A, (b) Sample C and (c) Sample F

3.4 Wear studies

Figure 6 is a depiction of the wear rate of the cast samples. From the results of the wear resistance study, it can be seen that the wear rate of the samples decreased with increasing coconut shell particles. The decrease in the wear rate was 9.61%, 14.82%, 28.31%, 41.80% and 55.29% for the 2 wt.%, 4 wt.%, 6 wt.%, 8 wt.% and 10 wt.%

respectively. The improvement can be attributed to a list of factors. Such factors include the uniform dispersal of the reinforcing phase in the aluminium matrix which works to decrease the impact of the applied load from the wear propagation by acting as load-bearing members of the composite material. In addition, proper interfacial bonding between the reinforcing particles and the matrix could have also improved the wear resistance of composites by ensuring little to no particle pull-out during the dry sliding between the 2 contacting surfaces. The coconut shell particles also improved the wear resistance of the composites by the reduced contact area during the sliding wear process thereby limiting direct contact between the abrasive disc and the surface of the composite [8].

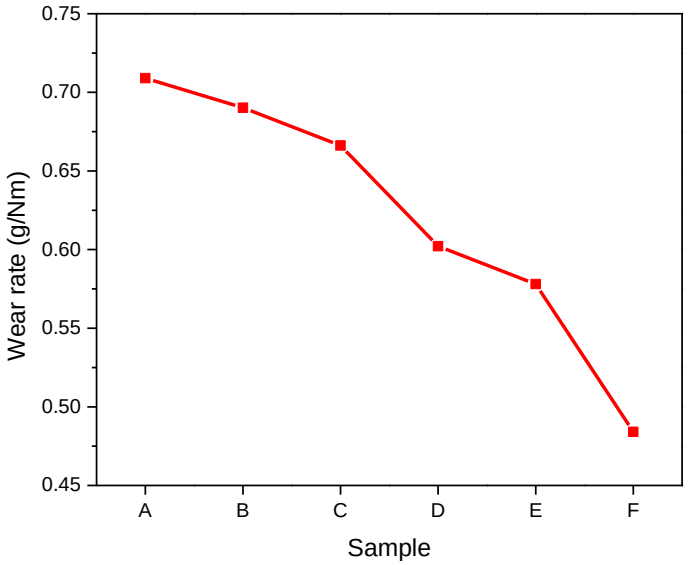

Figure 6: Results of the wear rate

4. CONCLUSION

The study was conducted to investigate the effect of coconut shells on the hardness, density and wear resistance of aluminium. From the experiments conducted, it was gathered that the hardness of the composites improved relative to the unreinforced aluminium matrix. The hardness was maximum at 30.80 HV. The density was shown to decrease with increasing weight fraction of the reinforcing particles which is an indication that the coconut shell reinforcing particles successfully decreased the weight of the samples. The wear resistance of the samples was shown to improve with increasing weight faction of the reinforcing particles up to 10 wt.%. The wear rate was shown to decrease by 55.29% for the 10 wt.% sample. The experimental studies show that reinforcing aluminium with coconut shells is capable of producing materials with an attractive mix of properties that can be applied to a variety of industrial applications.

ACKNOWLEDGEMENT

The authors acknowledge the TETFund Research grant with reference number: TETF/DR&D/CE/UNI/NSUKKA/BR/2020/VOL.I for funding this research.

REFERENCES

[1] Dwivedi SP, Dwivedi G (2019) Utilization of Organic Waste and Inorganic Waste in Development of Green Hybrid Composite Material. Materials Performance and Characterization 8:20190023. https://doi.org/10.1520/mpc20190023

[2] Moona G, Walia RS, Rastogi V, Sharma R (2019) Parameter optimization and characterization of environmental friendly aluminium hybrid metal matrix composites. Materials Research Express 6. https://doi.org/10.1088/2053-1591/ab4fb4

[3] Henry Ononiwu N, Akinlabi ET, Ozoegwu CG (2019) Sustainability in Production and Selection of Reinforcement particles in Aluminium Alloy Metal Matrix Composites: A Review. Journal of Physics:

Conference Series 1378:1–10. https://doi.org/10.1088/1742-6596/1378/4/042015

[4] Hima Gireesh C, Durga Prasad K, Ramji K (2018) Experimental Investigation on Mechanical Properties of an Al6061 Hybrid Metal Matrix Composite. Journal of Composites Science 2:1–10. https://doi.org/10.3390/jcs2030049

[5] Dwivedi SP, Mishra VR (2019) Physico-Chemical, Mechanical and Thermal Behaviour of Agro-waste RHA-Reinforced Green Emerging Composite Material. Arabian Journal for Science and Engineering 44:8129–8142. https://doi.org/10.1007/s13369-019-03784-z

[6] Kurapati VB, Kommineni R (2017) Effect of wear parameters on dry sliding behavior of Fly Ash/SiC particles reinforced AA 2024 hybrid composites. Materials Research Express 4:1–9. https://doi.org/10.1088/2053-1591/aa8a3e

[7] Lahiri D, Hadjikhani A, Zhang C, et al (2013) Boron nitride nanotubes reinforced aluminum composites prepared by spark plasma sintering: Microstructure, mechanical properties and deformation behavior. Materials Science and Engineering A 574:149–156. https://doi.org/10.1016/j.msea.2013.03.022

[8] Dinaharan I, Nelson R, Vijay SJ, Akinlabi ET (2016) Microstructure and wear characterization of aluminum matrix composites reinforced with industrial waste fly ash particulates synthesized by friction stir processing. Materials Characterization 118:149–158. https://doi.org/10.1016/j.matchar.2016.05.017

[9] Mahanta S, Chandrasekaran M, Samanta S, Arunachalam R (2019) Multi-response ANN modelling and analysis on sliding wear behavior of Al7075/B4C/fly ash hybrid nanocomposites. Materials Research Express 6:1–19. https://doi.org/10.1088/2053-1591/ab28d8

[10] Donald AO, Hassan MA, Hamza S, et al (2018) Development and Characterization of Aluminum Matrix Composites Reinforced with Carbonized Coconut Shell and Silicon Carbide Particle for Automobile Piston Application. Global Scientific Journals 6:390–398

[11] Ononiwu NH, Ozoegwu CG, Madushele N, Akinlabi T (2021) Effects of carbonised eggshells on the mechanical properties , microstructure and corrosion resistance of AA1050 of metal matrix composites. Advances in Materials and Processing Technologies 00:1–12. https://doi.org/10.1080/2374068X.2021.1959103

[12] Prakash KS, Gopal PM, Karthik S (2020) Multi-objective optimization using Taguchi based grey relational analysis in turning of Rock dust reinforced Aluminum MMC. Measurement 157. https://doi.org/10.1016/j.measurement.2020.107664

[13] Vinod B, Ramanathan S, Anandajothi M (2019) A novel approach for utilization of agro-industrial waste materials as reinforcement with Al–7Si–0.3Mg matrix hybrid composite on tribological behaviour. SN Applied Sciences 1:62. https://doi.org/10.1007/s42452-018-0066-z

[14] Singh CV, Pachauri P, Dwivedi SP, et al (2019) Formation of functionally graded hybrid composite materials with Al 2 O 3 and RHA reinforcements using friction stir process. Australian Journal of Mechanical Engineering 00:1–14. https://doi.org/10.1080/14484846.2019.1679583

[15] Oghenevweta JE, Aigbodion VS, Nyior GB, Asuke F (2014) Mechanical properties and microstructural analysis of Al–Si–Mg/carbonized maize stalk waste particulate composites. Journal of King Saud University - Engineering Sciences 28:222–229. https://doi.org/10.1016/j.jksues.2014.03.009

[16] Ononiwu NH, Ozoegwu CG, Madushele N, Akinlabi ET (2021) Carbonization temperature and its effect on the mechanical properties, wear and corrosion resistance of aluminum reinforced with eggshell. Journal of Composites Science 5:1–12. https://doi.org/10.3390/jcs5100262

[17] Ravi Kumar K, Pridhar T, Sree Balaji VS (2018) Mechanical properties and characterization of zirconium oxide (ZrO_2) and coconut shell ash (CSA) reinforced aluminium (Al 6082) matrix hybrid composite. Journal of Alloys and Compounds 765:171–179. https://doi.org/10.1016/j.jallcom.2018.06.177

[18] Ononiwu NH, Ozoegwu CG, Madushele N, Akinlabi ET (2021) Characterization, machinability studies and multi-response optimization of AA 6082 hybrid metal matrix composite. The International Journal of Advanced Manufacturing Technology 116:1–19. https://doi.org/https://doi.org/10.1007/s00170-021-07549-7

[19] Ononiwu NH, Jacobs IO, Nwachukwu VC, Akinlabi ET (2022) The influence of sustainable reinforcing particulates on the density, hardness and corrosion resistance of AA 6063 matrix composites. Frattura ed Integrità Strutturale 16:510–518. https://doi.org/10.3221/IGF-ESIS.61.34

[20] Vijaybabu G, PrasadRaju K, Raju VVMK, Sunilkumar K (2019) Studies on effect of ash in aluminium hybrid metal matrix composites. Materials Today: Proceedings 18:2132–2136. https://doi.org/10.1016/j.matpr.2019.06.640

PAPER 45 - HARNESSING ARTIFICIAL INTELLIGENCE TOOLS FOR RENEWABLE BIOENERGY OPTIMIZATION: PROSPECTS AND CHALLENGES

Mariam I Adeoba[1] Thanyani Pandelani[1] Harry Ngwagwa[1] Tracy Masebe[12]

[1] Unisa Biomechanics Research Group, Department of Mechanical, Biomedical and Bioresources Engineering, College of Science Engineering and Technology (CSET) University of South Africa, Florida 1710, South Africa, South Africa

[2] Department of Life and Consumer Sciences, College of Agriculture and Environmental Sciences, University of South Africa (UNISA), Florida 1710, South Africa

[*]Email: (mariamadedayo76@gmail.com; adeobmi@unisa.ac.za)

ABSTRACT

Transitioning to a low-carbon economy, focusing on renewable bioenergy, is crucial for meeting increasing energy demands sustainably. Bioenergy is a more reliable form of renewable energy than solar and wind energy, as it can achieve carbon neutrality and significantly impact employment. Artificial intelligence (AI) techniques are necessary to optimize energy efficiency, sustainability, and resource utilization in renewable bioenergy systems. This paper analyzes the possibilities and challenges of using AI to enhance the effectiveness of renewable bioenergy production processes. It highlights the growing importance of renewable bioenergy in addressing climate change mitigation and energy security objectives, focusing on the limitations of traditional optimization techniques. The study investigates the influence of AI technologies, including machine learning, neural networks, and optimization algorithms, on improving biomass feedstock selection, optimizing processes, and integrating systems. The potential benefits of AI include improved resource allocation, increased energy generation, and reduced costs. However, challenges such as lack of readily available data, complex model complexity, computational requirements, and ethical considerations pose significant obstacles to widespread application. The paper proposes potential areas for future investigation in driving forward innovation in renewable bioenergy. It also offers recommendations to policymakers, researchers, and industry stakeholders.

KEYWORDS: Renewable Bioenergy, Optimization, low-carbon economy, Artificial Intelligence, feedstock selection, sustainability

1.0. INTRODUCTION

Renewable bioenergy is crucial in transitioning towards a sustainable energy future, providing a practical substitute for fossil fuels. However, the efficient and optimal utilization of bioenergy resources presents complex challenges. Artificial Intelligence (AI) is a powerful tool that has the potential to significantly improve the effectiveness and environmental impact of bioenergy systems (Ahmad *et al*., 2021; Ahmad *et al*., 2022). AI encompasses a variety of technologies that empower machines to carry out tasks that usually necessitate human intelligence, such as acquiring knowledge, solving problems, and making decisions (Dwivedi et. al., 2021; Sarker, 2022). In the context of renewable bioenergy, AI algorithms can analyze complex datasets, identify patterns, and optimize processes to maximize energy output and minimize environmental impact. The energy sector is currently experiencing a substantial overhaul, primarily motivated by the imperative to decrease carbon emissions and address the challenges posed by climate change. AI provides a means to accomplish these objectives by facilitating the more effective utilization of renewable resources, enhancing the dependability of energy systems, and bolstering overall sustainability.

Renewable bioenergy, obtained from organic matter like biomass, provides a sustainable substitute for fossil fuels, thereby enhancing energy security and aiding in the prevention of climate change (Rather *et al*., 2022; Rial, 2024). However, the efficient utilization of bioenergy resources poses several challenges, including biomass availability, logistical constraints, and variability in feedstock composition. To tackle these challenges, it is necessary to employ inventive strategies that maximize the efficiency of the complete bioenergy supply chain, encompassing biomass cultivation and processing, energy conversion, and distribution. Artificial intelligence (AI) has become a potent tool for enhancing the efficiency of intricate systems, and its utilization in renewable bioenergy shows significant potential. Artificial intelligence algorithms can examine extensive datasets to detect patterns and enhance processes in previously unachievable ways (Allal *et al*., 2024; Rane, 2023). For example, AI can predict biomass yields, optimize biorefinery operations, and manage energy storage and distribution networks. Furthermore, artificial intelligence (AI)

can facilitate incorporating bioenergy systems with other forms of renewable energy, like wind and solar power, to establish hybrid energy systems characterized by enhanced dependability and efficiency. By leveraging AI, bioenergy systems can be dynamically optimized in response to changing environmental conditions and energy demands, maximizing their contribution to a sustainable energy future. Despite these opportunities, harnessing AI for renewable bioenergy optimization also presents several challenges. These factors encompass the intricacy of bioenergy systems, the necessity for accurate and reliable data, and the demand for interdisciplinary cooperation. Furthermore, there are apprehensions regarding AI's ethical and societal ramifications, such as job displacement and algorithmic bias, necessitating thorough consideration and resolution.

AI holds immense potential to revolutionize renewable bioenergy optimization, offering new possibilities for enhancing efficiency, sustainability, and resilience in the energy sector (Chakrapani *et al*., 2023; Hassan *et al*., 2023). However, harnessing this potential will necessitate collaborative endeavors from researchers, policymakers, industry stakeholders, and the public to surmount technical, regulatory, and societal obstacles. This paper aims to explore these issues in depth, providing insights and recommendations for advancing the use of AI in renewable bioenergy optimization. This paper examines the prospects and challenges of harnessing AI tools for renewable bioenergy optimization, aiming to provide insights into the role of AI in shaping the future of bioenergy. It further explores the potential of AI to revolutionize renewable bioenergy optimization, examining its role in improving efficiency, reducing costs, and enhancing environmental sustainability. Through a comprehensive review of current research and case studies, the paper aims to provide insights into the challenges and opportunities associated with harnessing AI for bioenergy optimization, offering recommendations for future research and implementation.

2.0 REVIEW OF EXISTING WORK AND RESEARCH GAP

Artificial Intelligence (AI) tools have demonstrated potential in optimizing renewable bioenergy systems. Current research emphasizes the necessity for standardized procedures in selecting AI techniques and training data samples to improve data collection and sharing across bioenergy-related areas (Ming-yang and Yao, 2021). Efforts are essential to explore AI's potential in supporting sustainable development from a holistic perspective (Ming-yang and Yao, 2021). Integrating AI techniques in bioenergy systems can enable automatic optimization based on existing experimental and numerical data, facilitating more effective progress (Chu *et al*., 2022). Furthermore, the role of renewable energy and AI in promoting environmental sustainability and achieving net-zero goals has been highlighted (Hassan *et al*., 2023). AI can significantly reduce greenhouse gas emissions, enhance energy efficiency, and foster sustainable development (Hassan *et al*., 2023). The application of AI in bioenergy optimization can help address research gaps, such as resilience capability in forest biomass and bioenergy supply chains (Dashtpeyma and Ghodsi, 2021).

Moreover, when combined with metaheuristic algorithms, AI has been utilized to address bioenergy supply chain problems, providing insights into theory, challenges, and future directions (Castillo-Villar, 2014). AI, particularly artificial neural networks, has been identified as an efficient tool for modeling and optimizing biofuel production processes (Sewsynker-Sukai *et al*., 2016). These technologies can assist in overcoming challenges and optimizing the biomass-to-bioenergy supply chain (Manyoma-Velásquez and Manotas-Duque, 2019). Tools like SMARTbioGO have been developed to transparently assess imaginative bioenergy concepts (Szarka *et al*., 2022). Innovative bioenergy generation and utilization are crucial for delivering sustainable, efficient, and flexible renewable energy (Szarka *et al*., 2020). The potential of AI in advancing the renewable energy sector, particularly in Europe, is recognized, underscoring the need for further development to position the sector as a leader in the energy industry (Șerban and Lytras, 2020). Existing research underscores the importance of AI tools in optimizing renewable bioenergy systems. Future research directions should standardize procedures, enhance data sharing, explore AI's potential from holistic perspectives, and address specific challenges in bioenergy supply chains through AI technologies.

Table 1 outlines critical existing works on the application of AI in renewable bioenergy optimization, highlighting their contributions, merits, and demerits, along with complete references. It provides a comprehensive view of the contributions and limitations of AI in the renewable bioenergy sector, offering precise citation details for further investigation or academic referencing.

Table 1. Summary of Key Existing Work on the Application of AI in Renewable Energy Optimization

Authors and Year	**Title**	**Key Contribution**	**Merits**	**Demerits**	**Complete Reference**
Castillo-Villar, K. (2014)	Metaheuristic algorithms applied to bioenergy supply chain problems: theory, review, challenges, and future	Reviewed the application of metaheuristic algorithms in bioenergy supply chain optimization.	Provides a comprehensive overview and identifies key challenges and future research directions.	Focuses mainly on theoretical aspects with limited practical implementation examples.	Castillo-Villar, K. (2014). Metaheuristic algorithms applied to bioenergy supply chain problems: theory, review, challenges, and future. Energies, 7(11), 7640-7672. https://doi.org/10.3390/en7117640
Chu, W., *et al.* (2022)	Recent advances in technologies, methods, and economic analysis for sustainable development of energy, water, and environment systems	Provided an extensive review of recent advances in technologies and methods for sustainable energy systems.	Offers a broad perspective on technological and economic aspects, aiding in holistic understanding.	Lacks focus on specific AI applications in bioenergy.	Chu, W., Vicidomini, M., Calise, F., Duić, N., Østergaard, P., Wang, Q., … and Carvalho, M. (2022). Recent advances in technologies, methods, and economic analysis for sustainable development of energy, water, and environment systems. Energies, 15(19), 7129. https://doi.org/10.3390/en15197129
Dashtpeyma, M., and Ghodsi, R. (2021)	Forest biomass and bioenergy supply chain resilience: a systematic literature review on the barriers and enablers	Systematic literature review on the resilience of forest biomass and bioenergy supply chains.	Identifies key barriers and enablers for enhancing supply chain resilience.	Primarily, it focuses on forest biomass with less emphasis on AI tools.	Dashtpeyma, M. and Ghodsi, R. (2021). Forest biomass and bioenergy supply chain resilience: a systematic literature review on the barriers and enablers. Sustainability, 13(12), 6964. https://doi.org/10.3390/su13126964
Hassan, Q., *et al.* (2023)	The role of renewable energy and artificial intelligence towards environmen	Discussed the role of AI and renewable energy in achieving environmen	Highlights the potential of AI to significantly contribute to environmental	Lacks detailed case studies or practical implementation examples.	Hassan, Q., Sameen, A., Salman, H., Al-Jiboory, A., and Jaszczur, M. (2023). The role of renewable energy and artificial intelligence towards environmental sustainability and net zero.. https://doi.org/10.21203/rs.3.rs-2970234/v1

	tal sustainability and net zero	tal sustainability and net zero emissions.	sustainability goals.		
Manyoma-Velásquez, P., and Manotas-Duque, D. (2019)	Supply chain optimization for energy cogeneration using sugarcane crop residues (scr)	Developed optimization models for the energy cogeneration supply chain using sugarcane crop residues.	Demonstrates practical applications of optimization models in bioenergy supply chains.	Limited generalizability to other types of bioenergy feedstocks.	Manyoma-Velásquez, P. and Manotas-Duque, D. (2019). Supply chain optimization for energy cogeneration using sugarcane crop residues (scr). Sustainability, 11(23), 6565. https://doi.org/10.3390/su11236565
Ming-yang, L., and Yao, Y. (2021)	Applications of artificial intelligence-based modeling for bioenergy systems: a review	Reviewed AI-based modeling applications for bioenergy systems, focusing on optimization and predictive capabilities.	Provides a comprehensive overview of AI applications in bioenergy.	Review lacks detailed insights into practical challenges and implementation barriers.	Ming-yang, L. and Yao, Y. (2021). Applications of artificial intelligence-based modeling for bioenergy systems: a review. GCB Bioenergy, 13(5), 774-802. https://doi.org/10.1111/gcbb.12816
Sewsynker-Sukai, Y., *et al*. (2016)	Artificial neural networks: an efficient tool for modelling and optimization of biofuel production (a mini review)	Reviewed the use of artificial neural networks (ANN) in biofuel production modeling and optimization.	Highlights the efficiency and accuracy of ANN in biofuel optimization.	Limited scope of review and mainly focuses on theoretical aspects.	Sewsynker-Sukai, Y., Faloye, F., and Kana, E. (2016). Artificial neural networks: an efficient tool for modelling and optimization of biofuel production (a mini review). Biotechnology and Biotechnological Equipment, 31(2), 221-235. https://doi.org/10.1080/13102818.2016.1269616
Szarka, N., *et al*. (2020)	All in one: a comprehensive goal and indicator system for smart bioenergy	Developed a comprehensive goal and indicator system for smart bioenergy optimization.	Provides a structured framework for evaluating bioenergy systems.	Implementation complexity due to the comprehensive nature of the framework.	Szarka, N., Schmid, C., Pfeiffer, D., and Thrän, D. (2020). All in one: a comprehensive goal and indicator system for smart bioenergy. Chemical Engineering and Technology, 43(8), 1554-1563. https://doi.org/10.1002/ceat.202000033

Szarka, N., *et al*. (2022)	The system role of smart bioenergy: a multicriteria assessment	Conducted a multicriteria assessment of the role of smart bioenergy systems in the energy landscape.	Comprehensive assessment covers multiple criteria, providing a holistic view.	Limited to conceptual discussions with minimal empirical data.	Szarka, N., Schmid, C., Pfeiffer, D., and Thrän, D. (2022). The system role of smart bioenergy: a multicriteria assessment. Chemical Engineering and Technology, 46(3), 550-558. https://doi.org/10.1002/ceat.202100069
Șerban, A., and Lytras, M. (2020)	Artificial intelligence for smart renewable energy sector in Europe—smart energy infrastructures for next generation smart cities	Discussed the role of AI in developing smart energy infrastructures for renewable energy in European smart cities.	Emphasizes the integration of AI in smart city infrastructure, providing futuristic insights.	Geographically limited focus on Europe, lacking global applicability.	Șerban, A. and Lytras, M. (2020). Artificial intelligence for smart renewable energy sector in Europe—smart energy infrastructures for next generation smart cities. Ieee Access, 8, 77364-77377. https://doi.org/10.1109/access.2020.2990123

2.1. Merits of Existing Works

AI models enhance the efficiency of bioenergy production processes by providing accurate predictions and optimization strategies. Reviews and theoretical studies broadly understand AI applications, identifying current trends and future research directions. Leveraging advanced AI techniques, such as neural networks and deep learning, enables tackling complex problems in bioenergy optimization that are not feasible with traditional methods.

2.2. Demerits of Existing Works

Many AI models require large datasets for training, which are often unavailable or incomplete in the bioenergy sector. Implementing sophisticated AI models often requires substantial computational resources and specialized knowledge, limiting their accessibility. Integrating AI with IoT introduces security and privacy issues that must be addressed. Many studies focus on theoretical aspects without providing practical implementation examples or addressing real-world challenges.

3. PROSPECTS OF AI IN RENEWABLE BIOENERGY OPTIMIZATION

Renewable bioenergy has garnered considerable interest as a viable substitute for fossil fuels, decreasing greenhouse gas emissions and addressing climate change (Rather *et al*., 2022; Rial, 2024). Artificial Intelligence (AI) is a powerful tool for optimizing renewable bioenergy systems and overcoming challenges like biomass availability and feedstock variability. By analyzing large datasets, AI can identify patterns and optimize process parameters, maximizing energy output while minimizing resource consumption and waste generation. It can also optimize biorefineries by adjusting processing parameters to match feedstock characteristics and meet market requirements, enhancing efficiency, environmental sustainability, and energy output. This article explores the potential of AI in renewable bioenergy optimization, highlighting its potential for enhanced efficiency and environmental sustainability (Li *et al*., 2023; Mohammad and Mahjabeen, 2023). AI can optimize bioenergy systems, leading to cost savings and increased profitability while improving environmental sustainability and reducing carbon emissions through data analysis and sustainable biomass supply chains (Ohalete *et al*., 2023; Wang *et al*., 2022). By analyzing historical data on energy

production, feedstock characteristics, and process parameters, AI can identify opportunities for optimizing energy output. For example, AI can predict the optimal timing for harvesting biomass based on weather forecasts and crop growth models, ensuring a steady feedstock supply for bioenergy production. Kanase-Patil *et al*. (2020) developed a framework for determining the appropriate dimensions of integrated renewable energy systems in smart cities, as illustrated in Figure 1.

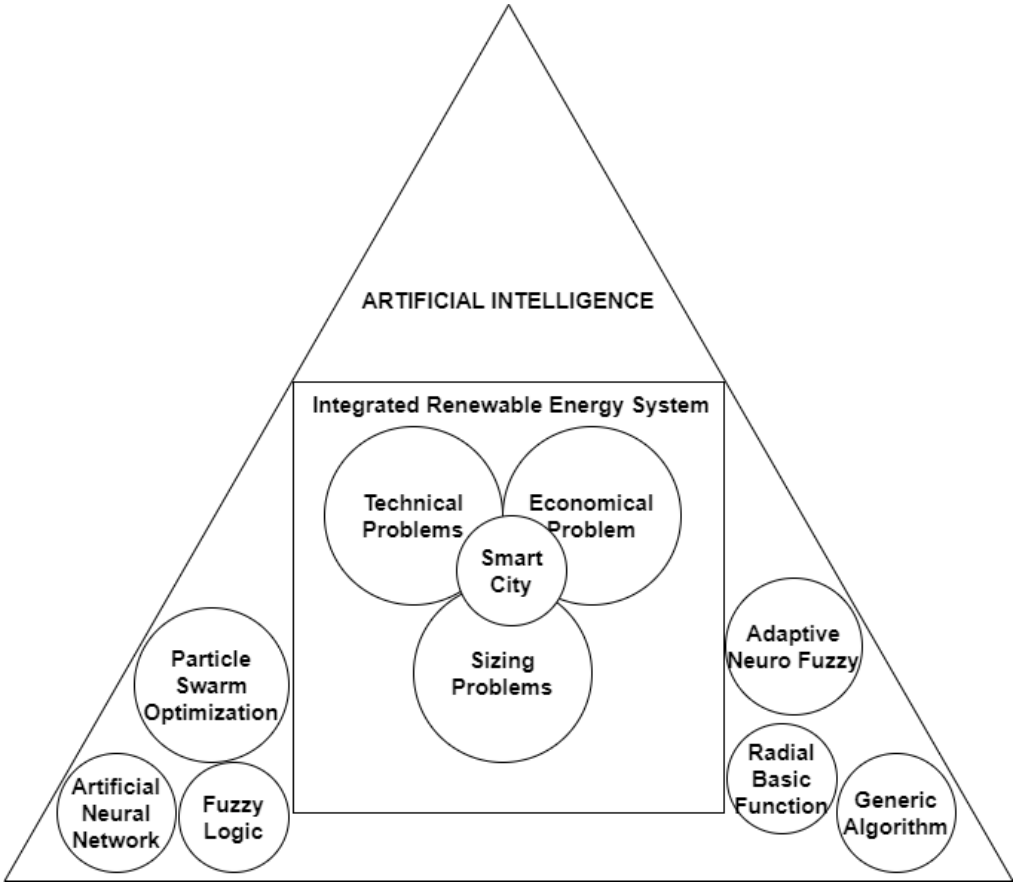

Figure 1: Framework for sizing integrated renewable energy systems in smart cities (Kanase-Patil *et al*., 2020).

AI holds great promise for optimizing renewable bioenergy systems, offering opportunities for enhanced efficiency, improved environmental sustainability, and increased energy output (Soudagar *et al*., 2024; Thirunavukkarasu *et al*., 2023). Further research is needed to address technical challenges and integrate AI technologies responsibly in the bioenergy sector. AI can optimize biomass conversion by analyzing feedstock properties and conversion processes, achieving maximum energy output. This can result in enhanced utilization of biomass resources and decreased dependence on fossil fuels. In 2022, Ahmad *et al*. (2022) and colleagues illustrated the integration of renewable energy.

Thus, three distinct classes of emerging technologies are further studied: (1) IoT and data generation, (2) decision-making and AI, and (3) blockchain and transactions, as shown in Figure 2.

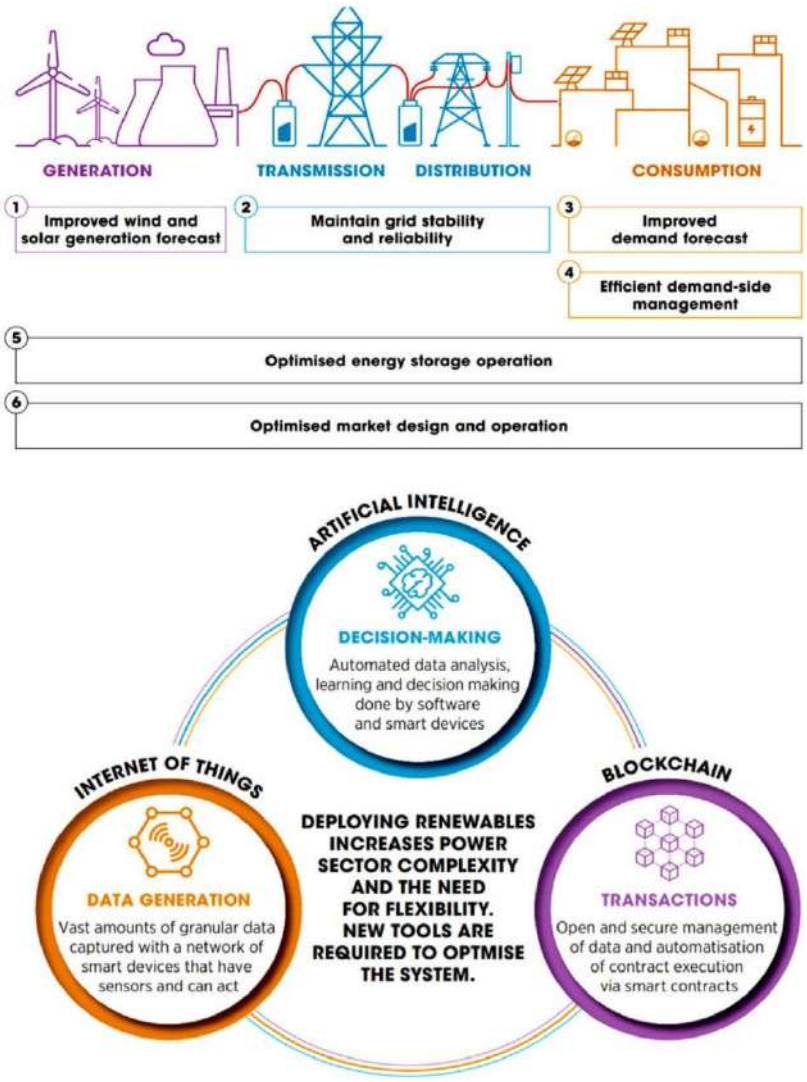

Figure 2. Emerging AI technologies for integration into variable renewable energy and digital innovations (Ahmad *et al*., 2022)

AI-driven systems can offer immediate monitoring and regulation of renewable bioenergy production processes, guaranteeing optimal performance and efficiency (Venkateswaran *et al*., 2023; Wicaksono *et al*., 2024). Additional research is required to tackle technical obstacles and responsibly incorporate AI technologies in the bioenergy industry. Artificial intelligence can enhance biomass conversion efficiency by analyzing the characteristics of the raw materials and the processes involved, resulting in the highest possible energy production. Artificial intelligence can optimize renewable energy integration by analyzing energy demand patterns and weather forecasts, ensuring the efficient utilization of solar, wind, and other renewable energy sources (Ahmad *et al*., 2021; Ahmad *et al*., 2022). Artificial intelligence can improve renewable energy systems reliability and consistency, offering opportunities for real-time monitoring, technological advancements, and integration with other forms. However, ongoing research and collaboration are needed.

4. THE DIFFICULTIES ASSOCIATED WITH IMPLEMENTING ARTIFICIAL INTELLIGENCE IN OPTIMIZING RENEWABLE BIOENERGY

A significant obstacle to utilizing AI to optimize renewable bioenergy is the adequacy and accessibility of data. Bioenergy systems produce substantial data from diverse sources, including sensors, equipment, and processes (Liao and Yao, 2021; Rangel-Martinez *et al*., 2021). However, this data is often heterogeneous, incomplete, and noisy, making it challenging to extract meaningful insights. Moreover, limited historical data may be available for training AI models, especially for emerging bioenergy technologies. Addressing these challenges requires implementing data collection and management strategies to ensure data quality and availability. Renewable bioenergy systems are inherently complex, involving multiple interconnected processes and variables. This complexity poses challenges for AI algorithms, as they must account for various factors, such as biomass composition, conversion technologies, and environmental conditions (Groundstroem and Juhola, 2021; Kakodkar *et al*., 2022). Furthermore, bioenergy systems exhibit dynamic and nonlinear behavior, which challenges developing precise predictive models. To overcome these challenges, it is necessary to develop AI algorithms that can effectively manage the intricacies of bioenergy systems and readily adjust to dynamic circumstances.

Implementing AI in renewable bioenergy optimization requires specialized expertise in AI development and implementation (Franki *et al*., 2023; Vyas *et al*., 2022). This includes knowledge of machine learning algorithms, data science, and domain-specific knowledge of bioenergy systems. However, a shortage of professionals with these skills makes it challenging for organizations to implement AI solutions effectively (Dwivedi *et al*., 2021). In addressing this challenge, it is necessary to allocate resources toward training and educational initiatives to develop a highly skilled workforce capable of effectively utilizing artificial intelligence to optimize renewable bioenergy. The regulatory and policy environment surrounding renewable bioenergy can pose challenges for AI implementation. Regulations related to biomass sourcing, environmental impact, and energy production standards can impact the feasibility and optimization of bioenergy systems (Al-Shetwi, 2022; Onu *et al*., 2023). Furthermore, data privacy and security policies can influence the gathering and utilization of data for artificial intelligence (AI) applications. To tackle these challenges, policymakers, industry stakeholders, and AI experts must work together to create regulations and policies that facilitate the efficient utilization of AI in optimizing renewable bioenergy.

While AI holds great potential for optimizing renewable bioenergy systems, several challenges must be addressed to realize these benefits. These challenges include data quality and availability, the complexity of bioenergy systems, the need for specialized expertise, and regulatory and policy challenges. Addressing these challenges will require collaboration between industry, academia, and government agencies to develop solutions that enable the effective use of AI in renewable bioenergy optimization. AI models developed for renewable bioenergy optimization often face challenges related to scalability and generalization (Ciesielski *et al*., 2021; Del Ser *et al*., 2022). While a model may perform well under specific conditions or for a particular bioenergy system, scaling it to larger systems or different environments may prove difficult. This is because the factors influencing bioenergy production can vary widely, requiring AI models to be adaptable and generalizable across different scenarios. Ensuring the scalability and generalization of AI models for renewable bioenergy optimization requires robust testing and validation procedures to assess their performance under various conditions. Optimizing renewable bioenergy systems requires collaboration between experts from various disciplines, including biology, chemistry, engineering, and computer science. However, fostering effective interdisciplinary collaboration can be challenging, as experts from different fields may have divergent perspectives, methodologies, and priorities. This can lead to communication barriers and misunderstandings, hindering the development and implementation of AI solutions for renewable bioenergy optimization. Overcoming these challenges requires creating interdisciplinary teams with diverse expertise and facilitating effective communication and collaboration among team members. Implementing AI solutions for renewable bioenergy optimization can be costly, requiring investments in technology, infrastructure, and human resources (Maghami and Mutambara, 2023; Pahwa *et al*., 2022). Small-scale bioenergy producers may face challenges in adopting AI due to limited financial resources and technical expertise. Additionally, the data-intensive nature of AI models for renewable bioenergy optimization can require significant computing power and storage capacity, which may be beyond the reach of some organizations. Addressing these challenges requires exploring cost-effective AI solutions and providing support and incentives for small-scale bioenergy producers to adopt AI technologies. The application of artificial intelligence (AI) in optimizing renewable bioenergy raises ethical and societal concerns regarding data privacy, security, and fairness (Corrigan and Ikonnikova, 2024; Kaur *et al*., 2024). There are apprehensions regarding the gathering and utilization of personal data for AI models, as well as the possibility for AI to worsen pre-existing disparities in the availability of renewable bioenergy resources. Furthermore, concerns arise regarding the responsibility and openness of AI algorithms in decision-making procedures. To tackle these challenges, it is necessary to create ethical guidelines and frameworks for utilizing AI to optimize renewable bioenergy. Additionally, it is crucial

to ensure that AI applications prioritize society's well-being and the environment's sustainability. It is essential to address these challenges to fully realize AI's potential in optimizing renewable bioenergy systems. By surmounting these obstacles, individuals with a vested interest can utilize the potential of artificial intelligence to enhance the effectiveness, durability, and availability of renewable bioenergy resources.

4.1. Addressing challenges and overcoming barriers

Artificial intelligence (AI) has significant potential for optimizing renewable bioenergy systems, providing opportunities to enhance efficiency, lower expenses, and improve sustainability (Saheb *et al*., 2022; Sayed *et al*., 2023). However, AI's potential in optimizing renewable bioenergy faces challenges, including overcoming obstacles through collaborative research, robust AI algorithms, and policy support. This can lead to novel solutions and the utilization of diverse expertise, resulting in more comprehensive and practical solutions (Bertello *et al*., 2022; Elia *et al*., 2020). Research partnerships can concentrate on creating AI algorithms that combine data from various sources, including weather forecasts, biomass availability, and energy demand, to enhance the efficiency of bioenergy production and distribution.

Robust AI algorithms and data management systems are crucial for overcoming obstacles to adopting AI in optimizing renewable bioenergy. AI algorithms must efficiently and accurately process substantial data to produce significant insights and recommendations. Data management systems must prioritize the security, integrity, and accessibility of data, particularly when handling sensitive information like biomass composition or energy consumption patterns (Martin del Campo *et al*., 2023; SaberiKamarposhti *et al*., 2024). Allocating resources to the advancement of AI algorithms and data management systems can effectively tackle these obstacles and facilitate the extensive implementation of AI in optimizing renewable bioenergy. Policy support and regulatory frameworks are crucial in addressing obstacles to implementing AI to optimize renewable bioenergy. Governments and regulatory bodies can facilitate the adoption of AI by offering incentives for research and development, financial support for pilot projects, and regulatory directives regarding data privacy and security. Furthermore, implementing policies promoting open data sharing and collaboration can expedite the progress and acceptance of artificial intelligence solutions in the renewable bioenergy industry. Policymakers can foster an environment conducive to AI innovation in optimizing renewable bioenergy by implementing well-defined policies and regulations (Danish and Senjyu, 2023; Shelare *et al*., 2023). Adopting a collaborative and multidisciplinary approach to address the challenges and overcome the barriers is necessary to effectively utilize AI tools for optimizing renewable bioenergy. To fully leverage the benefits of AI in optimizing renewable bioenergy systems, stakeholders should allocate resources to research and innovation, develop advanced AI algorithms and data management systems, and establish favorable policies and regulatory frameworks. A practical approach involves the creation of sophisticated AI algorithms capable of managing the intricacy and diversity of bioenergy systems. This encompasses algorithms that efficiently amalgamate data from various sources, such as biomass composition, weather conditions, and energy demand, to optimize bioenergy production and distribution. Machine learning algorithms, including neural networks and genetic algorithms, can be employed to analyze extensive datasets and detect patterns that can enhance the effectiveness of bioenergy systems (Alagumalai *et al*., 2023; Ifaei *et al*., 2023). Another approach involves employing sophisticated sensing and monitoring technologies to gather up-to-the-minute data on bioenergy systems. This encompasses sensors capable of quantifying biomass composition, the energy generated, and the prevailing environmental conditions, thereby furnishing valuable data for AI algorithms to scrutinize and enhance the efficiency of bioenergy operations. For instance, unmanned aerial vehicles equipped with sensors can monitor biomass fields and evaluate crop health, aiding bioenergy producers in optimizing their harvests and minimizing waste.

Furthermore, it is crucial to establish robust data management systems to guarantee the security and accuracy of data in AI-powered bioenergy optimization. This entails employing blockchain technology to establish data records that are secure, transparent, and resistant to tampering. This can effectively guarantee the traceability and genuineness of bioenergy products. Blockchain technology can also simplify transactions and agreements among various participants in the bioenergy supply chain, optimizing operations and cutting down expenses (Gawusu *et al*., 2022; Zhang *et al*., 2023). Moreover, it is essential to establish policy and regulatory frameworks that facilitate the integration of AI in renewable bioenergy. This encompasses policies that facilitate data sharing and cooperation among individuals and organizations involved, along with regulations that guarantee the ethical application of artificial intelligence in optimizing bioenergy. Policymakers can expedite the advancement and acceptance of AI technologies in the bioenergy industry by establishing a regulatory framework that promotes support and encouragement. Ahmad *et al*. (2022)

introduced a framework for constructing Machine Learning models specifically for energy materials, as depicted in Figure 3.

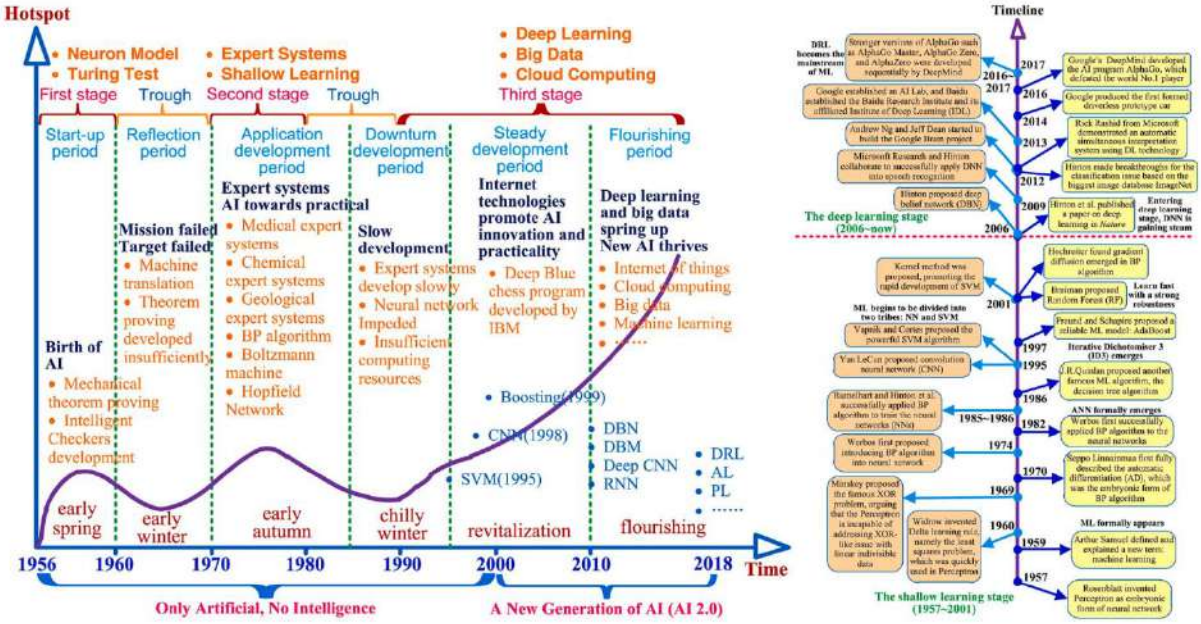

Figure 3. A new AI generation: A technology perspective for ML application to intelligent energy and control systems and the evolution of ML from 1957 to today (Cheng and Yu, 2019)

Overall, addressing the challenges of AI in renewable bioenergy optimization requires a combination of technological innovation, data management strategies, and supportive policy frameworks. By implementing these strategies, stakeholders can unlock the full potential of AI to optimize bioenergy systems and contribute to a more sustainable energy future.

4.2. Future directions and recommendations

One emerging trend is using machine learning algorithms for the predictive maintenance of bioenergy production equipment (Strielkowski *et al*., 2023; Yang *et al*., 2023). Machine learning models can predict maintenance needs based on historical data, reducing downtime and costs. AI can optimize biomass conversion into biofuels, improving efficiency and reducing waste. Integrating AI with IoT devices can optimize bioenergy production processes by analyzing real-time data (Ibegbulam *et al*., 2023; Stecyk and Miciuła, 2023). AI can significantly improve bioenergy production efficiency and sustainability by optimizing processes, reducing waste, and improving resource utilization. Governments can support this adoption by providing regulatory support and incentives, making bioenergy a more competitive renewable energy source. Using AI in bioenergy optimization can also help reduce production costs (Banerjee, 2023; Naveenkumar *et al*., 2023). AI can help bioenergy producers lower operating costs and improve profitability by identifying inefficiencies and optimizing processes. AI can also help to make bioenergy production more scalable and reliable. By optimizing production processes and predicting equipment failures, AI can help bioenergy producers scale up their operations and ensure a consistent supply of renewable energy (Franki *et al*., 2023; Pomeroy *et al*., 2022). AI advancements in renewable bioenergy can optimize production and transition to sustainable energy and can be harnessed through research, collaboration, and regulatory support. One prominent trend is the integration of AI with renewable energy systems to enhance overall efficiency (Khanal, Tarafdar and You, 2023; Stecyk and Miciuła, 2023). By optimizing the use of biomass resources and reducing waste, AI can help minimize the environmental impact of bioenergy production (Culaba *et al*., 2022; Fajobi *et al*., 2022). This includes optimizing agricultural residues, such as crop residues and animal manure, for bioenergy production, reducing the need for fossil fuels in agriculture. Continued research and development are essential to advancing AI's integration in renewable

bioenergy optimization. This includes techniques and more advanced AI algorithms, improving data collection and analysis techniques, and exploring new applications of AI in bioenergy production (Nwankwo *et al*., 2022).

5. CONCLUSION

In conclusion, harnessing artificial intelligence (AI) tools for renewable bioenergy optimization holds immense promise for the future of sustainable energy production. The prospects are bright, with AI offering the potential to enhance efficiency, reduce costs, and improve environmental sustainability in bioenergy systems. This paper highlights the key challenges and opportunities associated with AI in renewable bioenergy optimization. We have discussed the importance of collaborative research and innovation, the development of robust AI algorithms, and the need for supportive policy frameworks to overcome these challenges and realize the full potential of AI in bioenergy optimization. The significance of AI in renewable bioenergy optimization cannot be overstated. AI has the potential to revolutionize the way we produce and consume energy, paving the way for a more sustainable future. By optimizing bioenergy production processes, reducing waste, and enhancing efficiency, AI can help reduce our reliance on fossil fuels and mitigate the impact of climate change. Therefore, we call on stakeholders across the energy sector to embrace AI and invest in its development and implementation. This includes researchers, industry stakeholders, and policymakers who play a crucial role in driving the adoption of AI in bioenergy production. Together, we can harness the power of AI to accelerate the transition to a sustainable energy future and ensure a cleaner, greener planet for future generations.

REFERENCES

Ahmad, T., Zhang, D., Huang, C., Zhang, H., Dai, N., Song, Y., and Chen, H. (2021). Artificial intelligence in sustainable energy industry: Status Quo, challenges and opportunities. *Journal of Cleaner Production*, *289*, 125834.

Ahmad, T., Zhu, H., Zhang, D., Tariq, R., Bassam, A., Ullah, F. and Alshamrani, S. S. (2022). Energetics Systems and artificial intelligence: Applications of industry 4.0. *Energy Reports*, *8*, 334-361.

Alagumalai, A., Devarajan, B., Song, H., Wongwises, S., Ledesma-Amaro, R., Mahian, O. and Lichtfouse, E. (2023). Machine learning in biohydrogen production: a review. *Biofuel Research Journal*, *10*(2), 1844-1858.

Allal, Z., Noura, H. N., Salman, O. and Chahine, K. (2024). Machine learning solutions for renewable energy systems: Applications, challenges, limitations, and future directions. *Journal of Environmental Management*, *354*, 120392.

Al-Shetwi, A. Q. (2022). Sustainable development of renewable energy integrated power sector: Trends, environmental impacts, and recent challenges. *Science of The Total Environment*, *822*, 153645.

Banerjee, N. (2023). Biomass to energy—an analysis of current technologies, prospects, and challenges. *BioEnergy Research*, *16*(2), 683-716.

Bertello, A., Bogers, M. L. and De Bernardi, P. (2022). Open innovation in the face of the COVID-19 grand challenge: insights from the Pan-European hackathon 'EUvsVirus'. *R*and*d Management*, *52*(2), 178-192.

Bibri, S. E., Krogstie, J., Kaboli, A. and Alahi, A. (2024). Smarter eco-cities and their leading-edge artificial intelligence of things solutions for environmental sustainability: A comprehensive systematic review. *Environmental Science and Ecotechnology*, *19*, 100330.

Booth, M. S. (2022). "Sustainable" biomass: A paper tiger when it comes to reducing carbon emissions. *Bulletin of the Atomic Scientists*, *78*(3), 139-147.

Cabrera, E. and de Sousa, J. M. M. (2022). Use of sustainable fuels in aviation—a review. *Energies*, *15*(7), 2440.

Castillo-Villar, K. (2014). Metaheuristic algorithms applied to bioenergy supply chain problems: theory, review, challenges, and future. Energies, 7(11), 7640-7672. https://doi.org/10.3390/en7117640

Chakrapani, K., Kavitha, T., Safa, M. I., Kempanna, M. and Chakrapani, B. (2023). Applications of Artificial Intelligence in Intelligent Combustion and Energy Storage Technologies. In *Applications of Big Data and Artificial Intelligence in Smart Energy Systems* (pp. 27-45). River Publishers.

Chelliah, P. R., Jayasankar, V., Agerstam, M., Sundaravadivazhagan, B. and Cyriac, R. (2023). *The Power of Artificial Intelligence for the Next-Generation Oil and Gas Industry: Envisaging AI-inspired Intelligent Energy Systems and Environments*. John Wiley and Sons.

Cheng, L. and Yu, T., 2019. A new generation of AI: A review and perspective on machine learning technologies applied to smart energy and electric power systems. *International Journal of Energy Research*, *43*(6), pp.1928-1973.

Chu, W., Vicidomini, M., Calise, F., Duić, N., Østergaard, P., Wang, Q. and Carvalho, M. (2022). Recent advances in technologies, methods, and economic analysis for sustainable development of energy, water, and environment systems. Energies, 15(19), 7129. https://doi.org/10.3390/en15197129

Ciesielski, P. N., Pecha, M. B., Thornburg, N. E., Crowley, M. F., Gao, X., Oyedeji, O. and Brunhart-Lupo, N. (2021). Bridging scales in bioenergy and catalysis: a review of mesoscale modeling applications, methods, and future directions. *Energy* and *Fuels*, *35*(18), 14382-14400.

Corrigan, C. C. and Ikonnikova, S. A. (2024). A review of the use of AI in the mining industry: Insights and ethical considerations for multi-objective optimization. *The Extractive Industries and Society*, *17*, 101440.

Culaba, A. B., Mayol, A. P., San Juan, J. L. G., Vinoya, C. L., Concepcion II, R. S., Bandala, A. A. and Chang, J. S. (2022). Smart sustainable biorefineries for lignocellulosic biomass. *Bioresource technology*, *344*, 126215.

Danish, M. S. S. and Senjyu, T. (2023). Shaping the future of sustainable energy through AI-enabled circular economy policies. *Circular Economy*, *2*(2), 100040.

Dashtpeyma, M. and Ghodsi, R. (2021). Forest biomass and bioenergy supply chain resilience: a systematic literature review on the barriers and enablers. Sustainability, 13(12), 6964. https://doi.org/10.3390/su13126964

Del Ser, J., Casillas-Perez, D., Cornejo-Bueno, L., Prieto-Godino, L., Sanz-Justo, J., Casanova-Mateo, C. and Salcedo-Sanz, S. (2022). Randomization-based machine learning in renewable energy prediction problems: critical literature review, new results and perspectives. *Applied Soft Computing*, *118*, 108526.

Dwivedi, Y. K., Hughes, L., Ismagilova, E., Aarts, G., Coombs, C., Crick, T. and Williams, M. D. (2021). Artificial Intelligence (AI): Multidisciplinary perspectives on emerging challenges, opportunities, and agenda for research, practice and policy. *International Journal of Information Management*, *57*, 101994.

Elia, G., Margherita, A. and Passiante, G. (2020). Digital entrepreneurship ecosystem: How digital technologies and collective intelligence are reshaping the entrepreneurial process. *Technological forecasting and social change*, *150*, 119791.

Energy, A. W. (2024). Edge driven Digital Twins in distributed energy systems.

Fajobi, M. O., Lasode, O. A., Adeleke, A. A., Ikubanni, P. P. and Balogun, A. O. (2022). Effect of biomass co-digestion and application of artificial intelligence in biogas production: A review. *Energy Sources, Part a: Recovery, Utilization, and Environmental Effects*, *44*(2), 5314-5339.

Franki, V., Majnarić, D. and Višković, A. (2023). A comprehensive review of artificial intelligence (AI) companies in the power sector. *Energies*, *16*(3), 1077.

Gawusu, S., Zhang, X., Ahmed, A., Jamatutu, S. A., Miensah, E. D., Amadu, A. A. and Osei, F. A. J. (2022). Renewable energy sources from the perspective of blockchain integration: From theory to application. *Sustainable Energy Technologies and Assessments*, *52*, 102108.

Groundstroem, F. and Juhola, S. (2021). Using systems thinking and causal loop diagrams to identify cascading climate change impacts on bioenergy supply systems. *Mitigation and Adaptation Strategies for Global Change*, *26*(7), 29.

Gurawalia, H., Shinde, P. B. and Sharma, K. K. (2024). Embracing Industry 4.0 Ingredients in Synthetic Biology for the Development of Carbon–Neutral Economy. In *Biorefinery and Industry 4.0: Empowering Sustainability* (pp. 215-252). Cham: Springer Nature Switzerland.

Hassan, Q., Sameen, A. Z., Salman, H. M., Al-Jiboory, A. K. and Jaszczur, M. (2023). The role of renewable energy and artificial intelligence towards environmental sustainability and net zero.

Hassan, Q., Sameen, A., Salman, H., Al-Jiboory, A. and Jaszczur, M. (2023). The role of renewable energy and artificial intelligence towards environmental sustainability and net zero. https://doi.org/10.21203/rs.3.rs-2970234/v1

Holzinger, A., Keiblinger, K., Holub, P., Zatloukal, K. and Müller, H. (2023). AI for life: Trends in artificial intelligence for biotechnology. *New Biotechnology*, *74*, 16-24.

Ibegbulam, C. M., Aigbovbiosa, O. J., Olowonubi, J. A. and Fatounde, S. A. (2023). Role of artificial intelligence in electrification of Africa. *Engineering Science* and *Technology Journal*, *4*(6), 456-472.

Ifaei, P., Nazari-Heris, M., Charmchi, A. S. T., Asadi, S. and Yoo, C. (2023). Sustainable energies and machine learning: An organized review of recent applications and challenges. *Energy*, *266*, 126432.

Ilić, N., Milić, M., Beluhan, S. and Dimitrijević-Branković, S. (2023). Cellulases: from lignocellulosic biomass to improved production. *Energies*, *16*(8), 3598.

Kakodkar, R., He, G., Demirhan, C. D., Arbabzadeh, M., Baratsas, S. G., Avraamidou, S. and Pistikopoulos, E. N. (2022). A review of analytical and optimization methodologies for transitions in multi-scale energy systems. *Renewable and Sustainable Energy Reviews*, *160*, 112277.

Kanase-Patil, A. B., Kaldate, A. P., Lokhande, S. D., Panchal, H., Suresh, M. and Priya, V. (2020). A review of artificial intelligence-based optimization techniques for the sizing of integrated renewable energy systems in smart cities. *Environmental technology reviews*, *9*(1), 111-136.

Katarina, M., Ilić, N. and Milić, M. (2024). The Realm of Smart Biomass Degrading Enzymes in Low-Carbon Fuels and Chemicals Production. In *Biorefinery and Industry 4.0: Empowering Sustainability* (pp. 113-179). Cham: Springer Nature Switzerland.

Kaur, S., Kumar, R., Singh, K. and Huang, Y. L. (2024). Leveraging artificial Intelligence for enhanced sustainable energy management. *J. Sustain. Energy*, *3*(1), 1-20.

Khanal, S. K., Tarafdar, A. and You, S. (2023). Artificial intelligence and machine learning for smart bioprocesses. *Bioresource Technology*, *375*, 128826.

Li, J., Herdem, M. S., Nathwani, J. and Wen, J. Z. (2023). Methods and applications for Artificial Intelligence, Big Data, Internet of Things, and Blockchain in smart energy management. *Energy and AI*, *11*, 100208.

Liao, M. and Yao, Y. (2021). Applications of artificial intelligence-based modeling for bioenergy systems: A review. *GCB Bioenergy*, *13*(5), 774-802.

Maghami, M. R. and Mutambara, A. G. O. (2023). Challenges associated with Hybrid Energy Systems: An artificial intelligence solution. *Energy Reports*, *9*, 924-940.

Makepa, D. C., Chihobo, C. H., Ruziwa, W. R. and Musademba, D. (2023). A systematic review of the techno-economic assessment and biomass supply chain uncertainties of biofuels production from fast pyrolysis of lignocellulosic biomass. *Fuel Communications*, *14*, 100086.

Manyoma-Velásquez, P. and Manotas-Duque, D. (2019). Supply chain optimization for energy cogeneration using sugarcane crop residues (scr). Sustainability, 11(23), 6565. https://doi.org/10.3390/su11236565

Martin del Campo, F., Singh, S. J., Fishman, T., Thomas, A., Noll, D., and Drescher, M. (2023). Can a small island nation build resilience? The significance of resource-use patterns and socio-metabolic risks in The Bahamas. *Journal of Industrial Ecology*, *27*(2), 491-507.

Ming-yang, L. and Yao, Y. (2021). Applications of artificial intelligence-based modeling for bioenergy systems: a review. GCB Bioenergy, 13(5), 774-802. https://doi.org/10.1111/gcbb.12816

Mohammad, A., and Mahjabeen, F. (2023). Revolutionizing solar energy with AI-driven enhancements in photovoltaic technology. *BULLET: Jurnal Multidisiplin Ilmu*, *2*(4), 1174-1187.

Naveenkumar, R., Iyyappan, J., Pravin, R., Kadry, S., Han, J., Sindhu, R. and Baskar, G. (2023). A strategic review on sustainable approaches in municipal solid waste management and energy recovery: Role of artificial intelligence, economic stability and life cycle assessment. *Bioresource Technology*, 129044.

Nwankwo, W., Nwankwo, C. P. and Wilfred, A. (2022). Leveraging on Artificial Intelligence to Accelerate Sustainable Bioeconomy. *IUP Journal of Knowledge Management*, *20*(2).

Ohalete, N. C., Aderibigbe, A. O., Ani, E. C., Ohenhen, P. E., Daraojimba, D. O. and Odulaja, B. A. (2023). AI-driven solutions in renewable energy: A review of data science applications in solar and wind energy optimization. *World Journal of Advanced Research and Reviews*, *20*(3), 401-417.

Onu, P., Pradhan, A. and Mbohwa, C. (2023). The potential of Industry 4.0 for renewable energy and materials development–The case of multinational energy companies. *Heliyon*, *9*(10).

Pahwa, M. S., Dadhich, M., Saini, J. S. and Saini, D. K. (2022). Use of artificial intelligence (AI) in the optimization of production of biodiesel energy. *Artificial intelligence for renewable energy systems*, 229-238.

Peters, M. A., Alves, C. T. and Onwudili, J. A. (2023). A review of current and emerging production technologies for biomass-derived sustainable aviation fuels. *Energies*, *16*(16), 6100.

Pomeroy, B., Grilc, M. and Likozar, B. (2022). Artificial neural networks for bio-based chemical production or biorefining: A review. *Renewable and Sustainable Energy Reviews*, *153*, 111748.

Rane, N. (2023). Contribution of ChatGPT and other generative artificial intelligence (AI) in renewable and sustainable energy. *Available at SSRN 4597674*.

Rangel-Martinez, D., Nigam, K. D. P. and Ricardez-Sandoval, L. A. (2021). Machine learning on sustainable energy: A review and outlook on renewable energy systems, catalysis, smart grid and energy storage. *Chemical Engineering Research and Design*, *174*, 414-441.

Rather, R. A., Wani, A. W., Mumtaz, S., Padder, S. A., Khan, A. H., Almohana, A. I. and Baba, T. R. (2022). Bioenergy: a foundation to environmental sustainability in a changing global climate scenario. *Journal of King Saud University-Science*, *34*(1), 101734.

Rial, R. C. (2024). Biofuels versus climate change: Exploring potentials and challenges in the energy transition. *Renewable and Sustainable Energy Reviews*, *196*, 114369.

Rodriguez Franco, C. (2022). Forest biomass potential for wood pellets production in the United States of America for exportation: a review. *Biofuels*, *13*(8), 983-994.

SaberiKamarposhti, M., Kamyab, H., Krishnan, S., Yusuf, M., Rezania, S., Chelliapan, S. and Khorami, M. (2024). A comprehensive review of AI-enhanced smart grid integration for hydrogen energy: Advances, challenges, and future prospects. *International Journal of Hydrogen Energy*.

Saheb, T., Dehghani, M. and Saheb, T. (2022). Artificial intelligence for sustainable energy: A contextual topic modeling and content analysis. *Sustainable Computing: Informatics and Systems*, *35*, 100699.

Sarker, I. H. (2022). AI-based modeling: techniques, applications and research issues towards automation, intelligent and smart systems. *SN Computer Science*, *3*(2), 158.

Sayed, E. T., Olabi, A. G., Elsaid, K., Al Radi, M., Semeraro, C., Doranehgard, M. H., ... and Abdelkareem, M. A. (2023). Application of artificial intelligence techniques for modeling, optimizing, and controlling desalination systems powered by renewable energy resources. *Journal of Cleaner Production*, *413*, 137486.

Șerban, A. and Lytras, M. (2020). Artificial intelligence for smart renewable energy sector in europe—smart energy infrastructures for next generation smart cities. Ieee Access, 8, 77364-77377. https://doi.org/10.1109/access.2020.2990123

Sewsynker-Sukai, Y., Faloye, F., and Kana, E. (2016). Artificial neural networks: an efficient tool for modelling and optimization of biofuel production (a mini review). Biotechnology and Biotechnological Equipment, 31(2), 221-235. https://doi.org/10.1080/13102818.2016.1269616

Sharma, V., Tsai, M. L., Chen, C. W., Sun, P. P., Nargotra, P., and Dong, C. D. (2023). Advances in machine learning technology for sustainable advanced biofuel production systems in lignocellulosic biorefineries. *Science of The Total Environment*, 163972.

Shelare, S. D., Belkhode, P. N., Nikam, K. C., Jathar, L. D., Shahapurkar, K., Soudagar, M. E. M., ... and Rehan, M. (2023). Biofuels for a sustainable future: Examining the role of nano-additives, economics, policy, internet of things, artificial intelligence and machine learning technology in biodiesel production. *Energy*, 128874.

Soudagar, M. E. M., Shelare, S., Marghade, D., Belkhode, P., Nur-E-Alam, M., Kiong, T. S. and Fattah, I. M. R. (2024). Optimizing IC engine efficiency: A comprehensive review on biodiesel, nanofluid, and the role of artificial intelligence and machine learning. *Energy Conversion and Management*, *307*, 118337.

Stecyk, A. and Miciuła, I. (2023). Harnessing the Power of Artificial Intelligence for Collaborative Energy Optimization Platforms. *Energies*, *16*(13), 5210.

Strielkowski, W., Vlasov, A., Selivanov, K., Muraviev, K. and Shakhnov, V. (2023). Prospects and challenges of the machine learning and data-driven methods for the predictive analysis of power systems: A review. *Energies*, *16*(10), 4025.

Szarka, N., Schmid, C., Pfeiffer, D. and Thrän, D. (2020). All in one: a comprehensive goal and indicator system for smart bioenergy. Chemical Engineering and Technology, 43(8), 1554-1563. https://doi.org/10.1002/ceat.202000033

Szarka, N., Schmid, C., Pfeiffer, D. and Thrän, D. (2022). The system role of smart bioenergy: a multicriteria assessment. Chemical Engineering and Technology, 46(3), 550-558. https://doi.org/10.1002/ceat.202100069

Thirunavukkarasu, M., Sawle, Y. and Lala, H. (2023). A comprehensive review on optimization of hybrid renewable energy systems using various optimization techniques. *Renewable and Sustainable Energy Reviews*, *176*, 113192.

Usman, M., Jamil, M. K., Ashraf, W. M., Saqib, S., Ahmad, T., Fouad, Y. and Pervaiz, A. (2023). AI-driven optimization of ethanol-powered internal combustion engines in alignment with multiple SDGs: A sustainable energy transition. *Energy Conversion and Management: X*, *20*, 100438.

Venkateswaran, N., Kumar, S. S., Diwakar, G., Gnanasangeetha, D. and Boopathi, S. (2023). Synthetic Biology for Wastewater to Energy Conversion: IoT and AI Approaches. *Applications of Synthetic Biology in Health, Energy, and Environment*, 360-384.

Vyas, A. K., Balamurugan, S., Hiran, K. K. and Dhiman, H. S. (Eds.). (2022). *Artificial Intelligence for Renewable Energy Systems*. John Wiley and Sons.

Wang, Z., Peng, X., Xia, A., Shah, A. A., Huang, Y., Zhu, X. and Liao, Q. (2022). The role of machine learning to boost the bioenergy and biofuels conversion. *Bioresource Technology*, *343*, 126099.

Wicaksono, H., Trat, M., Bashyal, A., Boroukhian, T., Felder, M., Ahrens, M. and Zoerner, T. (2024). Artificial-intelligence-enabled dynamic demand response system for maximizing the use of renewable electricity in production processes. *The International Journal of Advanced Manufacturing Technology*, 1-25.

Yang, C. T., Kristiani, E., Leong, Y. K. and Chang, J. S. (2023). Big data and machine learning driven bioprocessing–recent trends and critical analysis. *Bioresource technology*, *372*, 128625.

Zhang, X., Feng, X., Jiang, Z., Gong, Q. and Wang, Y. (2023). A blockchain-enabled framework for reverse supply chain management of power batteries. *Journal of Cleaner Production*, *415*, 137823.

PAPER 47 - DEVELOPMENT OF A GSM MODULE CONTROLLED SECURITY DEVICE IN A FOREST ENVIRONMENT

Ademola, T. O., Fadele, O. K., Haruna, A. Z., Suleiman, R. T. Oni B.O., Blessing Usman and Otiwa Godwin

Federal College of Forestry Mechanization Afaka Kaduna, Forestry Research Institute of Nigeria.

* fadeleseyi@yahoo.com, +2348064487957

ABSTRACT

There has been incessant increase in the rate of banditry, kidnapping and terrorism in the North-Western part of the country especially in forest prone environment. In recent times forest environments have become hideout for these bad elements. Tree planting and afforestation programme being one of the measures to combat climate change; it is important that the forest environments need to be protected. Warning system is one of the ways of alarming a community in the event of any unpleasant intrusion by criminals. In this project a GSM module-controlled security alarm was developed. The system consists of various components such as contactor, alarm, timer, power supply unit, SIM card, and a GSM Module. The GSM module-controlled alarm system applies telephone network to relay electrical impulse to the alarm when a call is put forward to it. The GSM module allows the passage of electrical impulse to the alarm system for the period at which it is set. The security device was tested and found to be effective in sounding alarm to Afaka campus community in the event of criminal intrusion.

***KEYWORDS*:** GSM-module, security alarm, forest environment, banditry

1.0 INTRODUCTION

Security entails the condition of not being threatened, especially; physically, psychologically or emotionally. A security system is a system designed to detect intrusion or unauthorized entry into a building or an area. They are used in residential, commercial, military, and industrial properties for protection against burglary (theft) or property damage, as well as personal protection against intruders. Some security systems serve a single purpose of burglary protection. Combination of systems provides protection for a number of threats and not just a single threat. The 'modern and smart' security systems which do in fact cover other potential threats and do function smartly by incorporating other forms of alarms notably phone-based alarms for remote monitoring, costs a fortune to set up, operate and maintain, owing to the nature of software design, type of materials used etc (Xu, 2013). This design signifies a major improvement in terms of using cheaper materials, easier to maintain components and cheaper operating cost than other systems of the same kind, as notifications via text messages and calls are only made when owner is actually away. The GSM based smart security system using Arduino can be adopted at home, offices, institutions (educational, military, commercial or industrial use etc.) and forest environment in combating insecurity. The application of Arduino cut across different areas such as home security (Falohun *et al.*, 2021; Okafor, *et al*., 2024); GPS/GSM birth alarm device (Calcante *et al.*, 2014); GSM based fire alarm security device (Tang *et al.*, 2011; Odonkor *et al.*, 2020). In the recent time there has been increase in the rate of banditry and criminal activities in Kaduna state. This has affected every sector of the society viz. education, economy, infrastructural development to mention but a few. The Federal College of Forestry Mechanization is not left out in the recent attacks by the bandits on schools. The Federal College of Forestry Mechanisation was attacked on March 11, 2021 by some bandits in the night; kidnapping about 39 students. The event slowed down the academic and research activities on the campus and thus leading to temporary relocation of the College. This has resulted to setback in the academic and research activities in the college. The menace of insecurity needs to be addressed in schools in order to avert the falling standard of education especially in the northern part of Nigeria. The study focused on development of a GSM module-controlled alarm system within the Federal College of Forestry Mechanization campus community and research forest, Afaka Kaduna Nigeria.

2.0 MATERIALS AND METHODS

2.1 Materials

The hardware circuit is mainly composed of four parts; GSM communication module interface circuit, the alarm (siren), the AC contactor and an IC timer relay control circuit. The schematic diagram of hardware circuit is shown in Figure 1.

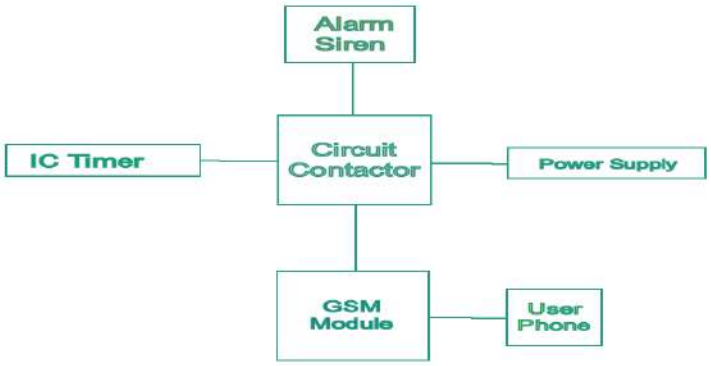

Figure 1: Circuit diagram

2.1.1 GSM Module

A GSM module is a hardware device that uses GSM mobile telephone technology to provide a data link to a remote network. From the view of the mobile phone network, they are essentially identical to an ordinary mobile phone; it has a port for SIM card. The SIM card works in two modes of operation; an internal mode and an external operation mode. On power up, the system after initialization and successful attempt of the GSM module to log on to a network provider's network, switches itself to a default internal mode. The module activates the siren through a text message or dial from authorized user number. The siren is also switch off through a dial or text message from authorized user number. Charges for text messages and call depends on the network selected for the GSM module. It also rejects calls and text messages from unauthorized number or unregistered numbers. The GSM module can also be used in places which require turning ON/OFF your system, machines, and equipment remotely with a FREE call from your mobile phone. The default Password is 1234. The RTU5024 module can be programmed with SMS commands using your phone. Figures 2a and 2b show the pictorial views of the GSM module.

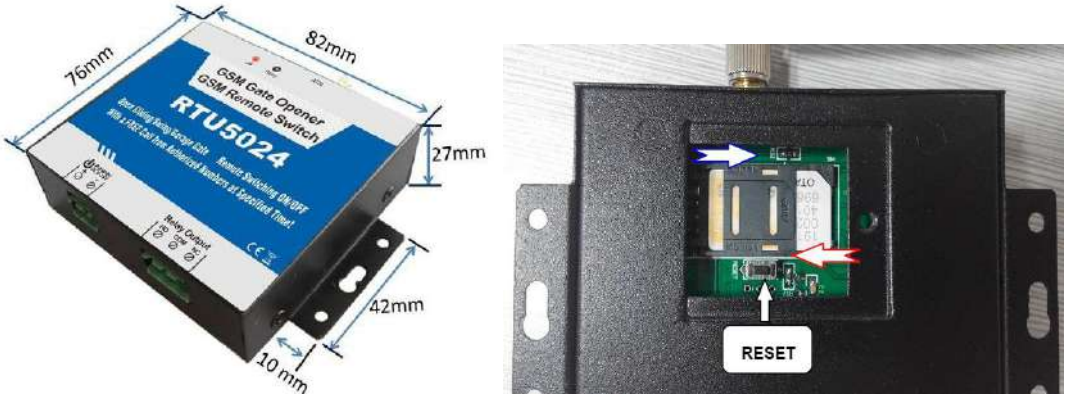

Figures 2a and 2b: GSM module with dimension and backside of the GSM module

2.1.2 Siren

The simplest version of a siren is a mechanical device that pushes an air stream against a rotating perforated disk. As the disk spins, the airflow will be alternately interrupted and allowed to pass. The ensuing fluctuation in air pressure produces a series of regular pressure waves that we perceive as sound.

2.1.3 Contactor

The AC contactor is an electromagnetic device with a NO main contact, three poles, and air as the arc extinguishing medium. Its components include: coil, short-circuit ring, static iron core, moving iron core, moving contact, static contact, auxiliary NO contact, auxiliary NC contact, pressure spring sheet, reaction spring, buffer spring, arc extinguishing. It is safety device which prevent overloading of other electrical components of equipment. Figure 3 shows the pictorial view of AC contactor.

Figure 3: A contactor

2.1.4 IC Timer

An IC timer relay is a combination of an electromechanical output relay and a control circuit. The contacts will open or close before or after a pre-selected, time interval. Time delay relays are initiated or triggered by one of two methods. Application of input voltage/auxiliary supply will either initiate the unit or make it ready to initiate when a trigger signal is applied. Applying a trigger signal is used to initiate the unit after input voltage has been applied. This trigger signal can either be a control switch (dry contact switch) or a power trigger (voltage). Figure 4 shows the diagram of a timer. The timers are installed to trigger on and off the siren to generate an intermittent sound.

Figure 4: Timers for the siren operation

2.1.5 Power Supply Unit

The power supply unit comprises of a switch, junction box, adaptor for the GSM module and plug to the mains. The main was sourced from solar photovoltaic power system to facilitate uninterrupted power supply the security device.

2.1.6 SIM Card

Subscriber Identity Module is one of the key features of GSM. The SIM is a detachable smart card containing user information and phone book. This also allows the user to retain information after switching the GSM module on.

3.0 RESULTS AND DISCUSSION

3.1 Description of the GSM Module Manned Alarm System

The *GSM Module Manned Alarm System* was constructed using components like GSM module, Siren, Timer Relay, Circuit Contactor, and power switch. All these components were fixed on plywood as shown in Figure 5. The security device works with GSM network which implies that it can be operated from any part of the world regardless of its location as long as network is available. It is designed in such a way that it can only be operated with pre-registered phone numbers. In the event of banditry or armed robbers' invasion within the college premises; the security personnel on ground can alert his colleagues from afar by calling the device to send out alarm. It can also be switched off by returning a second call to the device.

Figure 5: A GSM manned alarm system

3.2 Advantages of the System

The design and implementation of the automated GSM based manned alarm system is cost effective and reliable. The alarm system can be used in areas that require remote alarm or emergency situation like banks, residential quarters, warehouses, hospitals, schools in event of banditry and so on. Its phone call switching makes the system more secure and classy. It makes use of any type of mobile subscriber network.

- The design and implementation of the automated GSM based manned alarm system is cost effective and reliable
- The alarm system can be used in areas that require remote alarm or emergency situation like banks, residential quarters, warehouses, hospitals and so on.
- Its phone call switching makes the system more secure and classy and makes use of any type of mobile subscriber network.
- The alarm can buzz 500m long (half a kilometer).

The menace of insecurity in the Northern Nigeria has virtually affected all facets of life of people in this region. In this project a GSM module manned alarm system was developed in a bid to enhance security situation in Federal of College Forestry Mechanisation campus community. The GSM module alarm system was tested and found to be effective in alarming the campus community within a distance range of 500m. It is recommended that the alarm system should be upgraded to a bigger one for wider coverage and further research should be conducted on effects of forest trees on the alarm sound coverage.

REFERENCES

Calcante, A., Tangorra, F.M., Marchesi, G. and Lazzari, M. (2014). GPS/GSM based birth alarm system for grazing cows. Computers and Electronics in Agriculture, Vol.100:123–130.

Falohun, A.S., Makinde, B.O., Akinleye, F.W., Kehinde, O.P. and Oyelami, T.M. (2021). Design and construction of a door security alarm system based on SMS verification and voice recognition. International Journal of Advance Research in Computer Science, Vol.12(3): 23 – 37.

Odonkor, E.N., Ofosu, W.K. and Nunoo, K. (2020). Using GSM SMS controller alarm configurator to develop cost effective intelligent fire safety system in a developing country. International Journal of Computer Science, Engineering and Applications, Vol.10 (3):1 – 8.

Okafor, J.U., Akande, A.O. and Agubor, C.K. (2024). Design and implementation of domestic dual-SIM telesecurity alarm system using voice code recognition. Journal of Electrical Systems and Information Technology, Vol.11(14): 1 – 21.

Tang, Z., Shuai, W. and Luojun, A. (2011). Remote alarm monitor system based on GSM and ARM. Advanced in Control Engineering and Information Science, Procedia Engineering, Vol.15:65 – 69.

Xu, S.Q. (2013). Design of intelligent alarm system based on GSM network. Applied Mechanics and Materials, Vol. 373-375:1578 – 1582.

PAPER 48- COMPARATIVE ANALYSIS OF SUN, SOLAR, AND OVEN DRYING TECHNIQUES ON SELECTED ATTRIBUTES OF HONEY-TREATED BANANA FRUIT SLICES

A. L. Adepoju[1*], Z.D. Osunde[2]

[1]Department of Food Engineering, University of Ilorin, Ilorin, Nigeria.
[2]Department of Agricultural and Bioresources Engineering, Federal University of Technology, Minna, Nigeria.
[*]E-mail: adepoju.al@unilorin.edu.ng

ABSTRACT
This study investigated the effects of three drying methods (sun, solar, and oven drying) on the proximate and vitamin qualities of dried honey-treated ripe banana slices. Samples of 5mm-sized, firmly-ripe banana slices were soaked in 0.25% v/v honey solution for 4 minutes, drained, and divided into three groups. The samples were subjected to sun drying, solar drying, and oven drying (at 65°C) until constant moisture content was reached. The results showed that the banana sample dried in the oven has the highest values of 5.00%, 2.14%, and 5.60% for fat, protein, and ash respectively. However, both sun and solar drying methods recorded slightly lower moisture content (5.20%) than oven drying (5.40%). Also, higher vitamin C (81.70 mg/100g) and β-carotene (1361.16 ug/100g) contents were observed in the oven-dried banana sample. The results suggest that honey treatment, coupled with oven drying, is an effective combination for preserving the quality of banana slices. Oven drying demonstrated superiority in terms of vitamin C, β-carotene, and some proximate retention. The findings emphasize the potential of honey as a natural preservative and oven drying as an efficient method for producing high-quality dried banana slices. This research provides valuable insights for the food industry, offering an alternative approach for reducing postharvest losses of ripe bananas and enhancing the quality of dried banana slices through honey pre-treatment and oven drying.

KEYWORDS: Banana, Drying methods, Honey-treated, Proximate qualities, Vitamin C, β-carotene.

1. INTRODUCTION

Banana (Musa spp.) is among the major tropical fruits that are commonly consumed in many countries of the world. Bananas are golden yellow with smooth, thin skin when fully ripe and they possess an extremely sweet and fragrant aroma. The typical fruit's length is an average of 6–12 cm with a diameter ranging between 3-4 cm and has contributed to food security and income generation in many communities around the globe (Maseko *et al.*, 2024; Wong *et al.*, 2017). Bananas are full of a whole lot of nutritional goodness because it is a rich source of dietary fiber, carbohydrates, vitamins (A, B, C, E, β-carotene), minerals, oligosaccharides, and phenolic compounds such as catechin, epicatechin, epigallocatechin, gallic acid, lignin, tannins, and anthocyanins (Ghimire *et al.*, 2021; Guiné *et al.*, 2015). The presence of these compounds makes the consumption of banana fruit beneficial to the human body and helps to prevent various disorders such as bad breath, colon cancer, diabetes, intestinal disorders constipation, morning sickness, hemorrhoids, obesity, high blood pressure, broken capillaries, and lots more (Ghimire *et al.*, 2021; Puangsuwan *et al.*, 2021). However, with all the benefits of banana fruit, it has a short shelf-life and is highly perishable. In fact, (Elangovan and Natarajan, 2021) stated that the average shelf-life of bananas is 2 to 9 days when stored in a refrigerator, 2 to 3 months in a freezer, and 6 to 12 months when dried. Therefore, to preserve the bioactivity of banana fruit and enhance its shelf-stability, drying is paramount.

Drying, reported to be one of the oldest and most widely used methods of preserving fruits, is the reduction in the moisture level of a biomaterial to a level that hinders the activities of spoilage microorganisms through the application and circulation of heated air (Citra *et al.*, 2021; Radojčin *et al.*, 2021). Drying prevents microbial spoilage, reduces packaging and transportation costs, facilitates product handling, enhances versatility, and ensures the stability of fruits during storage. It also helps in tackling the problem of perishability and seasonality of fruits, making them available for consumption all year round (Ghasemi-Varnamkhasti and Aghbashlo, 2014). Several drying methods have been reported by different researchers for the preservation of banana fruits and these include superheated steam drying (Hamawand *et al.*, 2014), Osmotic dehydration (Kumari and Samsher, 2015), microwave vacuum drying, microwave multi-flash drying and freeze-drying (Monteiro and Carcio, 2016), spray drying (Wong *et al.*, 2017), thin-layer convective drying (Seyedabadi *et al.*, 2018), fixed-bed tray drying (Ferreira

and Freitas, 2019), foam mat drying (Noordia *et al.*, 2020), hybrid infrared-hot air drying (Puangsuwan *et al.*, 2021), infrared/convection drying (Badr *et al.*, 2022) and solar drying (Nguyen *et al.*, 2023).

Oftentimes before the drying process, many researchers carry out pre-drying treatments on biomaterials especially fruits to inhibit enzymatic browning and prevent undesirable chemical reactions that cause many adverse changes during and after drying. For instance, 0.5% sodium metabisulfite and 0.5% calcium chloride were used as pretreatments for tomato (Mwende *et al.*, 2018), ultrasound pretreatment for garlic slices (Bozkir *et al.*, 2019), lemon juice, salt solution dips, and hot water blanching were used by (Dereje and Abera, 2020) as pretreatments for mango, osmotic pretreatment for African star apple (Bolarinwa and Ajetunmobi, 2020), ascorbic acid dip, honey dip, and steam blanching were used for pawpaw (Adepoju *et al.*, 2021), blanching, citric acid solution, lemon juice, brine solution, and rice rinse water for banana flower powder (Jha *et al.*, 2021), soaking, blanching for mango kernel (Zikri *et al.*, 2022). These pretreatments have been observed to have some desirable effects on the qualities of dried food products, to shorten the drying time, and to reduce the energy consumption of the drying process (Radojčin *et al.*, 2021). To this end, therefore, this study aimed to investigate the influence of sun, solar, and oven drying methods on proximate and vitamin contents of dried honey-treated banana fruit slices.

2. MATERIALS AND METHODS

2.1 Materials and Pretreatment

Fresh firmly ripe banana fruits and the honey used for the pretreatment of the fruit slices were procured from a local fruit market and a pharmaceutical outfit respectively, both in Minna, Niger State. The banana fruits were inspected, sorted, washed, hand-peeled, and cut into about 5 mm thick slices to enhance fast and uniform drying. The sliced fruit samples were pretreated with a honey solution of 0.25% v/v (one part honey to four parts water) by dipping the fruit slices into the solution immediately after slicing and left for 4 minutes and afterward drained well before drying. The honey-treated fruit samples were then subdivided into three, 400 g each. There were three samples of untreated banana slices, 400g each, to serve as the control for the three drying methods.

2.2 Drying procedure

Sun drying of the fruits was carried out by placing the honey-treated sliced banana fruits on netted drying trays in a thin layer. The trays were placed on a raised platform, which helped to facilitate adequate air circulation around the slices, and left in the sun to dry. The slices were weighed at 1-hour intervals until a constant weight was obtained after 15 hours. Solar drying was carried out with the aid of a solar dryer (in the Department of Agric and Bioresources Engineering Lab) consisting of a wooden cabinet with trays on which the treated sliced fruit were placed. The dryer was put in the sun and solar rays were trapped with the help of the solar collector of the dryer. The samples were weighed at intervals until a constant weight was obtained after 12 hours. Oven drying experiments were done using a fan-aerated (Galen Kamp) oven. The oven was preheated and calibrated to a temperature of 65 $^{\circ}$C before the banana slices were placed into it and the fruit were weighed at 1-hour intervals until constant weight was obtained after 9 hours.

2.3 Quality Analysis

Proximate analysis for the dried banana fruit samples was determined according to AOAC standard procedures. Moisture content was calculated using the oven dry method, ash content was determined with the use of a Muffle furnace; the Kjedahl method was used for protein content determination, Soxhlet fat extraction method, and Hennenberg, Stohmann, and Rantenberg method was used to determine fat and fibre contents respectively while carbohydrate content was calculated by difference. Vitamin C and β-carotene contents of the dried fruit were determined by the titration method of Osborne and Voost and the spectrophotometric method based on Ultraviolent (UV) inactivation respectively, as outlined in (AOAC, 2005).

2.4 Statistical Analysis

SPSS 20.0 software was used to carry out the Analysis of Variance (ANOVA) tests for all experiments at a 0.05% level of significance and the Duncan Multiple Range Test (DMRT) was used to determine the differences in the

mean of the treatments. Also, drying curves that show the rate of drying of the fruit samples were plotted using the Excel software.

3. RESULTS AND DISCUSSIONS

3.1 Drying curve for dried honey-treated banana fruit

The moisture content of the dried fruits was plotted against the time of drying to generate the drying curves for honey-treated (Figure 1) and untreated (Figure 2) banana slices dried with different drying methods. The results showed that as the drying time increased, the moisture content of the fruit slices decreased until a constant moisture content is reached. It was deduced from the drying curve that the moisture content of fruit slices dried in the oven reduced and reached a constant moisture content faster than the other two drying methods. This certainly was because the oven drying method is dependent on a power source other than the sun, as in the case of sun and solar drying methods. Also, the honey pretreatment applied to the banana slice did not affect the drying time, as both the treated and untreated samples had the same drying time. However, a little difference was observed in the drying curves, especially at the initial stage of the drying process. A similar trend of moisture content/ratio-drying time curves was reported for different drying air temperatures for dried banana (Cristina Pagliari Braga *et al.*, 2021; Macedo *et al.*, 2020) and for different pre-treatments on the qualities and storage life of a dried banana (Nguyen *et al.*, 2023).

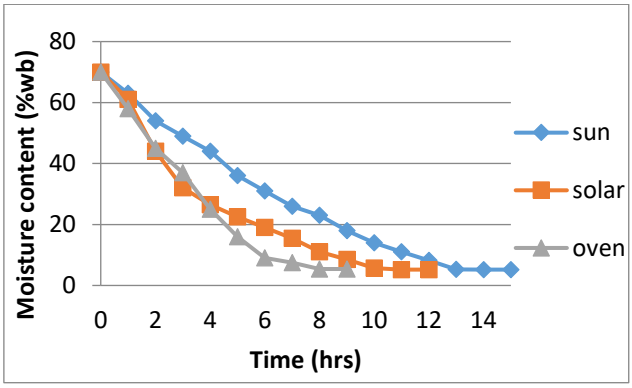

Figure 1: Drying curves of dried honey-treated banana samples across the three drying methods

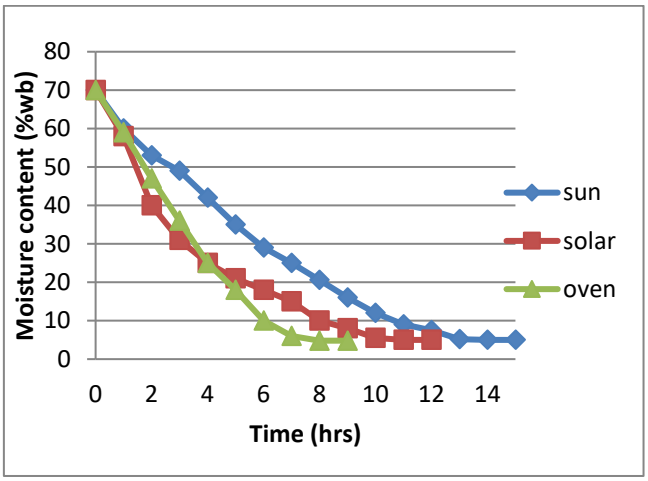

Figure 2: Drying curves of dried untreated (control) banana samples

3.2 Proximate qualities of samples as influenced by drying methods

The proximate qualities of the dried honey-treated banana samples were analysed and the results are shown in Table 1. Slightly lower values of moisture contents were obtained in the sun and solar drying methods than in the

oven drying method. This may be because oven-dried samples are hygroscopic and have gained moisture from the environment when exposed. However, these moisture contents were not significantly different and were still within the safe level for dried fruits. (Hussain *et al.*, 2020) reported 4.6% and 4.81% moisture content for 5mm and 7mm thick dried banana slices pretreated with honey juice, which is lower than the ones obtained in this study. However, higher values of moisture contents were reported for bananas dried with different air temperatures (Macedo *et al.*, 2020) and dried banana pretreated with food additive and antioxidant solution (Ferreira and Freitas, 2019). The fat contents of the dried honey-treated banana slices increased in the order: sun dried<solar dried<oven dried banana slices. This implies that the banana sample dried in the oven had the highest fat content (5.00%.) compared to the other drying methods. The values of fat obtained in this study are higher than those recorded for pretreated dried mango (Dereje and Abera, 2020) and dried stinging nettle leaves (Shonte *et al.*, 2020). Banana slices dried in the oven recorded the highest protein content of 2.14% when compared with 1.13% and 1.16% respectively for sun and solar-dried slices. (Dereje and Abera, 2020) reported 2.71% for oven-dried mango whereas (Shonte *et al.*, 2020) reported 28.8% for dried stinging nettle leaves. The oven-drying method had the highest ash content with a value of 5.60%. This value is higher than the 1.26% reported for oven-dried malbhog banana slices and pulp (Dadhaneeya *et al.*, 2023) and 2.50% for keitt mango sliced chips (Techane, 2022). The highest value of crude fibre (0.43%) and carbohydrate (86.06%) were recorded in solar-dried and sun-dried banana samples respectively. However, (Shonte *et al.*, 2020) reported a higher value of crude fibre (28.8%) but a lower value of carbohydrate (26.1%) in their research on the effect of drying methods on the chemical composition and antioxidant activity of underutilized stinging nettle leaves.

Table 1: Proximate Qualities of Honey-Treated Dried Banana Samples

Samples	MC (%)	Fat (%)	Protein (%)	Ash (%)	Fibre (%)	Carbohydrate (%)
SUC	5.00^{a}	3.50^{a}	1.33^{a}	3.20^{a}	0.36^{a}	86.61^{b}
SUD	5.20^{b}	4.00^{a}	1.13^{a}	3.20^{a}	0.41^{b}	86.06^{b}
SOC	5.00^{a}	4.50^{c}	0.95^{a}	2.40^{a}	0.41^{ab}	86.74^{b}
SOD	5.20^{b}	4.50^{b}	1.16^{a}	3.00^{a}	0.43^{b}	85.71^{b}
OVC	5.00^{a}	3.00^{a}	1.19^{a}	3.60^{ab}	0.32^{a}	86.89^{b}
OVD	5.40^{b}	5.00^{c}	2.14^{a}	5.60^{b}	0.36^{a}	83.50^{a}

Values followed by the same letter in the same column are not significantly different at $P < 0.05$
SUC- Sun Drying Control; SUD- Sun Drying; SOC- Solar Drying Control; SOD-Solar Drying; OVC- Oven Drying Control; OVD- Oven Drying

3.3 Influence of drying methods on vitamin C and β-carotene contents of samples

The influence of drying methods on the vitamin C and β-carotene contents of the honey-treated banana samples was analysed and the results are shown in Table 2. It was observed that the sun drying method had the lowest value of both vitamin C (79.32mg/100g) and β-carotene (614.85µg/100g) contents among the three methods while the oven drying method recorded the highest values (81.70mg/100g; 1361.16µg/100g). This may be due to the exposure of the banana slices to the direct light of the sun in the sun and solar drying methods, as these vitamins are highly prone to oxidative degradation in the presence of heat, light, and oxygen (Goztepe *et al.*, 2022). The values of vitamin C obtained in this study are in the same range as 85.56mg/100g reported by Hussain *et al.*, (2020) for honey-treated dried banana slices but higher than 68.5 mg/100g and 65.3 mg/100g reported for oven-dried stinging nettle and spinach respectively (Shonte *et al.*, 2020). However, higher values of β-carotene (52504 (µg/100 g and 40847 (µg/100 g) were reported by the same authors. Drying conditions could have a great effect on heat and light labile β-carotene and ascorbic acid.

Table 2: Vitamin C And β-carotene Contents of Dried Honey-Treated Banana Samples

Samples	Vitamin C(mg/100g)	β-carotene (µg/100g)
SUC	66.00[a]	986.54[a]
SUD	79.32[a]	614.85[a]
SOC	70.95[a]	1396.95[b]
SOD	80.01[ab]	1227.25[b]
OVC	72.06[a]	1946.91[b]
OVD	81.70[b]	1361.16[b]

Values followed by the same letter in the same column are not significantly different at $P < 0.05$.
SUC- Sun Drying Control; SUD- Sun Drying; SOC- Solar Drying Control; SOD-Solar Drying; OVC- Oven Drying Control; OVD- Oven Drying

4. CONCLUSION

This study investigated the influence of drying methods on some qualities of dried honey-treated banana fruit slices. It can be concluded from the study that the oven-drying method is most suitable for drying honey-treated banana slices as it helped to retain the proximate properties of the dried banana and the moisture content was within the safe storage moisture contents for dried fruits. Also, higher vitamin C and β-carotene contents were observed in the oven-dried banana sample when compared with the other drying methods. Therefore, the oven-drying method can be used to preserve ripe banana fruit from spoilage. Further studies can be carried out by using more advanced drying methods with lower drying air temperature and/or resident time such as freeze and spray drying for the preservation of bananas.

5. REFERENCES

Adepoju, L. A., Osunde, Z. D., and Falua, K. J. (2021). Changes in Proximate Composition, Vitamin C and β-Carotene Contents of Oven Dried Pawpaw (Carica papaya) Fruit as Influenced by Pretreatment Methods. *FUOYE Journal of Engineering and Technology*, *6*(1), 10–14. https://doi.org/10.46792/fuoyejet.v6i1.566

AOAC. (2005). *Official method of Analysis.* (Method 935.14 and 992.24; 18th Editi). Association of Officiating Analytical Chemists.

Badr, M., El Bessoumy, R., and Eissa, A. (2022). Effect of microwave pretreatment on some operating conditions for drying banana slices using infrared/convection dryer. *Archives of Agriculture Sciences Journal*, *5*(1), 195–210. https://doi.org/10.21608/aasj.2022.249620

Bolarinwa, I. F., and Ajetunmobi, R. I. (2020). Influence of Osmotic Pre-treatment and Drying on Physicochemical, Microbial, and Storage Stability of African Star Apple. *FUOYE Journal of Engineering and Technology*, *5*(1), 11–16. https://doi.org/10.46792/fuoyejet.v5i1.466

Bozkir, H., Ergun, A. R., Tekgul, Y., and Baysal, T. (2019). Ultrasound as pretreatment for drying garlic slices in microwave and convective dryer. *Food Science and Biotechnology*, *28*(2), 347–354. https://doi.org/10.46792/fuoyejet.v5i1.466

Citra, F., Almira Aulia, G., Indiarto, R., Hodizah Asyifaa, A., Citra Angiputri Adiningsih, F., and Rahmalia Achmad, S. (2021). Conventional And Advanced Food-Drying Technology: A Current Review Article in. *International Journal of Scientific & Technology Research*, *10*(01), 99–107.

Cristina Pagliari Braga, R., Pereira Ruiz, S., and Silva de Aquino, D. (2021). Drying kinetics and the effect of blanching pretreatment in the physical characteristics of the dehydrated banana. *Revista Brasileira de Tecnologia Agroindustrial*, *15*(2), 3626–3647.

Dadhaneeya, H., Nayak, P. K., Saikia, D., Kondareddy, R., Ray, S., and Kesavan, R. krishnan. (2023). The impact of refractance window drying on the physicochemical properties and bioactive compounds of malbhog banana slice and pulp. *Applied Food Research*, *3*(1), 100279. https://doi.org/10.1016/j.afres.2023.100279

Dereje, B., & Abera, S. (2020). Effect of pretreatments and drying methods on the quality of dried mango (Mangifera Indica L.) slices. *Cogent Food and Agriculture*, *6*(1), 1–24. https://doi.org/10.1080/23311932.2020.1747961

Elangovan, E., & Natarajan, S. K. (2021). Experimental research of drying characteristic of red banana in a single slope direct solar dryer based on natural and forced convection. *Food Technology and Biotechnology*, *59*(2), 137–146. https://doi.org/10.17113/ftb.59.02.21.6876

Ferreira, T. H. B., & Freitas, M. L. F. (2019). Production, physical, chemical and sensory evaluation of dried banana (Musa Cavendish). *Emirates Journal of Food and Agriculture*, *31*(2), 102–108. https://doi.org/10.9755/ejfa.2019.v31.i2.1912

Ghasemi-Varnamkhasti, M., and Aghbashlo, M. (2014). Electronic nose and electronic mucosa as innovative instruments for real-time monitoring of food dryers. *Trends in Food Science & Technology*, *38*(2), 158–166.

Ghimire, R., Yadav, P. K., Khanal, S., Shrestha, A. K., Devkota, A. R., and Shrestha, J. (2021). Effect of different levels of gibberellic acid and kinetin on quality and self-life of banana (Musa spp.) fruits. *Heliyon*, *7*(9), e08019. https://doi.org/10.1016/j.heliyon.2021.e08019

Goztepe, B., Kayacan, S., Bozkurt, F., Tomas, M., Sagdic, O., and Karasu, S. (2022). Drying kinetics, total bioactive compounds, antioxidant activity, phenolic profile, lycopene and β-carotene content and color quality of Rosehip dehydrated by different methods. *LWT*, *153*. https://doi.org/10.1016/j.lwt.2021.112476

Guiné, R. P. F., Barroca, M. J., Gonçalves, F. J., Alves, M., Oliveira, S., and Mendes, M. (2015). Artificial neural network modelling of the antioxidant activity and phenolic compounds of bananas submitted to different drying treatments. *Food Chemistry*, *168*(October 2017), 454–459. https://doi.org/10.1016/j.foodchem.2014.07.094

Hamawand, I., Yusaf, T., & Bennett, J. (2014). Study and modelling drying of banana slices under superheated steam. *Asia-Pacific Journal of Chemical Engineering*, 1–13. https://doi.org/10.1002/apj

Hussain, A., Tahseen, S., Miano, F., Marri, A., and Kumar, D. (2020). Application of Pre-treatments on Banana Slices for Improving Drying Characteristics. *Food Science and Quality Management*, *103*, 35–41. https://doi.org/10.7176/fsqm/103-06

Jha, P., Meghwal, M., Prabhakar, P. K., and Singh, A. (2021). Exploring effects of different pre-treatments on drying kinetics, moisture diffusion, physico-functional, and flow properties of banana flower powder. *Journal of Food Processing and Preservation*, *45*(4), 1–15. https://doi.org/10.1111/jfpp.15356

Kumari, D., and Samsher. (2015). Effect of sample to sugar syrup solution ratio on osmotic drying behaviour of banana. *South Asian Journal of Food Technology and Environment*, *01*(01), 52–57. https://doi.org/10.46370/sajfte.2015.v01i01.07

Macedo, L. L., Vimercati, W. C., Araújo, S., and Quint, L. J. (2020). Effect of drying air temperature on drying kinetics and physicochemical characteristics of dried banana. *Food Process Engineering*, *e13451*, 1–10. https://doi.org/10.1111/jfpe.13451

Maseko, K. H., Regnier, T., Meiring, B., Wokadala, O. C., & Anyasi, T. A. (2024). Musa species variation, production, and the application of its processed flour: A review. In *Scientia Horticulturae* (Vol. 325). Elsevier B.V. https://doi.org/10.1016/j.scienta.2023.112688

Monteiro, R. L., and Carcio, B. A. M. (2016). *A microwave multi-flash drying process for producing crispy bananas*. *178*, 1–11. https://doi.org/10.1016/j.jfoodeng.2015.12.024

Mwende, R., Owino, W., and Imathiu, S. (2018). *Effects of pre-treatment during drying on the antioxidant properties and color of selected tomato varieties*. *December 2017*, 503–511. https://doi.org/10.1002/fsn3.581

Nguyen, V. P., Tran, H. X. N., and Phan, T. L. K. (2023). Effect of pre-treatments on qualities and storage life of banana dried by using solar dryer dome. *IOP Conference Series: Earth and Environmental Science*, *1155*, 1–15. https://doi.org/10.1088/1755-1315/1155/1/012020

Noordia, A., Mustar, Y. S., and Kusnanik, N. W. (2020). Foam mat drying of banana juice: varieties of ripe banana analysis and egg albumen foam. *Food Science and Technology (Brazil)*, *40*(2), 465–468. https://doi.org/10.1590/fst.24918

Puangsuwan, K., Punvichai, T., and Karrila, S. (2021). *Hybrid infrared with hot air drying of Pisang-Awak banana: Kinetics and shrinkage quality*. *July*. https://doi.org/10.1111/jfpe.13827

Radojčin, M., Pavkov, I., Kovačević, D. B., Putnik, P., Wiktor, A., Stamenković, Z., Kešelj, K., and Gere, A. (2021). Effect of selected drying methods and emerging drying intensification technologies on the quality of dried fruit: A review. *Processes*, *9*(1), 1–21. https://doi.org/10.3390/pr9010132

Seyedabadi, E., Khojastehpour, M., and Abbaspour-fard, M. H. (2018). Online measuring of quality changes of banana slabs during convective drying. *Engineering in Agriculture, Environment and Food*, *November 2016*, 0–1. https://doi.org/10.1016/j.eaef.2018.10.004

Shonte, T. T., Duodu, K. G., and de Kock, H. L. (2020). Effect of drying methods on chemical composition and antioxidant activity of underutilized stinging nettle leaves. *Heliyon*, *6*(5), 1–10. https://doi.org/10.1016/j.heliyon.2020.e03938

Techane, T. (2022). Effect of Ripening Stages and Drying Method on the Physico-chemical and Sensory Pro perties of Keitt Mango (Mangiferaindica L .) Sliced Chips. *Open Access Journal of Agricultural Research*, *7*(3), 1–10. https://doi.org/10.23880/oajar-16000295

Wong, C. W., Teoh, C. Y., and Putri, C. E. (2017). Effect of enzymatic processing, inlet temperature, and maltodextrin concentration on the rheological and physicochemical properties of spray-dried banana (Musa acuminata) powder. *Journal of Food Processing and Preservation*, 1–9. https://doi.org/10.26656/fr.2017.4(4).033

Zikri, A. H. B., Tien, B. Y., Hui, B. Y., and Han, W. K. (2022). Effects of processing parameters on the quality and properties of mango kenel flour: A mini review. *Malaysian Journal of Analytical Science*, *26*(4), 742–754. https://doi.org/10.1590/0100-29452018419

PAPER 49 - INVESTIGATING THE INFLUENCE OF LEAN CONSTRUCTION TECHNIQUES ON THE COST PERFORMANCE OF CONSTRUCTION PROJECTS IN SELECTED STATES OF NIGERIA

S. A. Yaro*, A.D. Adamu, I. Saidu, and M. O. Anifowose

Department of Quantity Surveying, Federal University of Technology Minna
*Email: sunny.yaro@yahoo.com

ABSTRACT
In recent discussions about the optimisation of construction processes, the concept of lean construction has emerged as a promising avenue for confronting the industry's numerous challenges and elevating project performance to new heights. Lean construction is based on the principle of maximising value while minimising waste, which resonates strongly with the modern ethos of sustainability and resource optimisation. Hence, the purpose of this study is to investigate the influence of lean construction techniques on the cost performance of construction projects in Nigeria. The study adopted a quantitative method to collect data from 294 participants. The study used a descriptive-analytical method, using the Mean Item Score (MIS) to analyse the collected data. The findings revealed that all the lean construction techniques have an influence on the cost performance of construction projects, with 5S (Sort, Straighten, Shine, Standardise, and Sustain) ranking topmost. The findings of this study help in the provision of empirical evidence of the effectiveness of lean construction techniques in the Nigerian construction industry context in terms of cost performance of construction projects and filling a significant gap in the existing body of knowledge in construction business management.

KEYWORDS: Construction, Cost, Lean, Performance, Project, Techniques

1.0 INTRODUCTION

The construction industry is a global economic driver, with a significant impact on Gross Domestic Product (GDP) growth and job opportunities (Anaman & Osei-Amponsah, 2007). According to recent World Bank data, the construction sector contributes significantly to the GDP of both developed and developing countries (Oladinrin *et al.,* 2012). Furthermore, the construction industry accounts for roughly 10% of global GDP, with variations seen across regions and economies (Krausmann *et al*., 2009).

However, while the construction industry is a key player in economic growth, it faces a slew of challenges that limit its potential impact and efficiency (Okanlawon *et al*., 2023). This is because the industry is plagued by inefficiencies, cost overruns, delays, and quality concerns, all of which present formidable challenges to project stakeholders and impede overall performance (Zahoor, 2023). One of the most significant challenges confronting the construction industry is inefficiency, which stems from outdated practices, fragmented workflows, and insufficient coordination among project participants (Hardin & McCool, 2015). The traditional construction approach frequently employs sequential processes and siloed decision-making, resulting in inefficient resource utilisation and productivity bottlenecks (Shimizu & Hitt, 2004). As a result, projects frequently experience delays and cost increases, eroding stakeholder confidence and jeopardising project success (Taye, 2016). Furthermore, cost overrun is also a common problem in the construction industry, where projects routinely exceed their budgetary allocations due to inaccurate estimates, unforeseen expenses, and scope changes (Bekr, 2015). According to research, cost overruns occur frequently in construction projects across the globe (Le-Hoai *et al*., 2008), with some studies estimating that more than 90% of projects exceed their original budgets. These overruns not only strain project finances but also erode trust among project stakeholders and damage the industry's reputation for dependability and accountability (Le-Hoai *et al*., 2008). Hence, various concepts and methodologies have emerged in recent years to curb the menace and reposition the construction industry. These methodologies include lean construction and Integrated Project Delivery (IPD). However, lean construction stands out as a particularly promising approach (Forbes & Ahmed, 2010).

Recently, the concept of lean construction has emerged as a promising approach to address these challenges and improve project performance. Lean Construction is a project management and production methodology based on lean manufacturing principles, which were first developed by the Toyota Production System (Koskela, 2020). It aims to

optimise the construction process by reducing waste, increasing value, and encouraging continuous improvement at all stages of a project's lifecycle (Barth & Formoso, 2021). Furthermore, lean Construction emphasises collaboration, efficiency, and the elimination of non-value-added activities to increase productivity, lower costs, and improve project outcomes (Demirkesen *et al*., 2022). Although lean construction has the potential to significantly improve the construction industry, there appears to be a lack of emphasis on its impact on cost performance in construction projects. Despite the promising benefits it provides, such as streamlined processes and reduced waste, there appears to be insufficient emphasis on understanding how lean principles impact the financial aspects of construction projects. This gap in attention is significant given the considerable potential for lean methodologies to optimise cost efficiency throughout project lifecycles. Hence, this study aims to investigate the influence of lean construction techniques on the cost performance of construction projects in Nigeria.

2.0 REVIEW OF RELATED LITERATURE

2.1 Construction Project Performance

According to Koelmans (2004) and Beleiu *et al*. (2015), project success is defined as meeting the objectives outlined in the project plan. Hence, a successful project can be identified by meeting its technical requirements, sticking to its schedule, and staying within the budget (Beleiu *et al*., 2015; Merrow, 2011). As a result, cost, quality, and timeliness are all important factors in project success, and they must always match client expectations (Alzahrani & Emsley, 2013). However, it is widely acknowledged that project completion delays frequently result in increased costs, which is a global phenomenon (Kaliba *et al*., 2009).

Various researchers have developed alternative frameworks to measure the success of a project. For instance, Simon-Eigbe *et al*. (2022) recommended measuring process implementation, project apparent value, and customer satisfaction at the end of the project. It also proposed a comprehensive framework for assessing the success of a project, they suggested that the success of the project should be evaluated against short-term and long-term goals. The framework includes efficiency (completion of the project within the planned time and cost); customer interests in the final product; business success and plans (market opportunities).

2.1.1 Cost Performance

Cost is a crucial factor that greatly affects project outcomes and plays a significant role in the entire project management process (Belassi & Tukel, 1996; Tam *et al*., 2020). It is considered a key factor in determining the success of a project (Tam *et al*., 2020). Cost performance analysis is a tool used to assess whether a project is staying within its budget or matching its actual spending (Pienkowski *et al*., 2021). This analysis is based on four important cost-related metrics: Total Budget Cost (TBC), Cumulative Budget Cost (CBC), Cumulative Actual Cost (CAC), and Cumulative Earned Value (CEV) (Osamudiamen *et al*., 2022).

Simon-Eigbe *et al*. (2022) stated that cost overruns occur when the ultimate expenditures of a project exceed the initially projected costs. Moreover, academics have emphasised that cost overrun is a major obstacle in the construction industry (Nuako *et al*., 2024). As a result, they have emphasised that errors in the initial cost estimation process are the main causes of these budget overruns (Amini *et al*., 2023). Furthermore, research has shown that inflation within projects leads to increasing costs, with differences observed in material, equipment, and labour costs in various geographical areas (Musarat *et al*., 2021). Hence, contracts with subcontractors may include provisions to reduce the impact of inflation risks, which are mutually agreed upon with clients. Furthermore, the presence of inadequacies in project planning and a lack of managerial expertise have been identified as contributing factors to errors in the utilisation of technical data (El Khatib *et al*., 2020). Hence, cost concerns are further intensified by market-related factors, such as the high expenses associated with machinery.

Mansfield *et al*. (1994) opine that exerting a substantial impact on both the financial and temporal aspects of construction projects. The factors include variations in prices, incorrect initial assessments, delays caused by working extra hours, extra tasks, fraudulent actions, illegal payments, and the use of faster construction methods. The presence of insufficient contract management practices, in addition to difficulties associated with subcontractors and designated suppliers, is emphasised by Kaliba *et al*. (2009). Moreover, intricacies within the financial procedures of client

organisations can result in delays in payments, which can create financial difficulties for contractors and disrupt project timelines (Ithana, 2020).

2.3 Application of Lean Construction Techniques in the Global Construction Industry

In recent years, there has been a significant focus on implementing lean construction techniques in the global construction industry (Ahmed *et al*, 2021). This approach aims to improve project efficiency, minimise waste, and enhance overall project outcomes. lean construction, based on the principles of lean production, provides a methodical approach to project management that emphasises maximising value and minimising waste during the construction process (Francis & Thomas, 2020). One of the most common applications of lean construction techniques is project planning and scheduling (Mohammadi *et al.*, 2022). Hence, construction teams can improve collaboration, communication, and project transparency by implementing principles such as the Last Planner System (LPS) (Venkatesh & Venkatesan, 2021). LPS emphasises continuous improvement, allowing teams to identify and mitigate potential delays, resulting in improved project timelines and overall efficiency (Schimanski *et al.*, 2020).

According to Braglia *et al*. (2022), another area of application is supplying chain management. Lean Construction principles encourage the use of just-in-time (JIT) delivery practices, which reduce inventory and storage costs (Si *et al*., 2020). Therefore, construction firms can improve project productivity and lower costs by coordinating closely with suppliers and subcontractors to streamline material flow, reduce lead times, and mitigate the risk of material shortages. Furthermore, lean construction techniques can also help improve construction site operations. 5S practices (sort, set in order, shine, standardise, sustain) help organise and optimise as workspaces, resulting in safer and more efficient work environments (Mohammadi *et al*., 2022). Additionally, visual management techniques like Kanban boards and daily huddles promote real-time communication and problem-solving, allowing teams to respond quickly to issues and maintain project momentum.

Research in Nigeria suggested that the utilisation of the lean approach in the Nigerian construction industry will impact positively on project performance in terms of cost, time, quality, and health and safety (Adamu and Abdulhamid, 2015; Nwaki & Eze, 2020). Despite the abundance of research on lean techniques and their obvious benefits such as streamlined processes and waste reduction, there appears to be a noticeable lack of focus on understanding how lean principles affect the overall performance of construction projects.

3.0 RESEARCH METHODOLOGY

This study utilised a quantitative methodology, specifically a questionnaire survey, to investigate the impact of lean construction techniques on the cost performance of construction projects in Nigeria. Quantitative methods are beneficial for collecting unbiased data and enabling precise communication through statistical analysis (Mohajan, 2020). In addition, a thorough examination of the current body of literature was undertaken to ascertain the impact of lean construction techniques on cost performance. Subsequently, these were organised into a survey that was disseminated to relevant stakeholders in the industry. The survey asked respondents, who were project managers, site managers, quality assurance managers, safety managers, and equipment managers with knowledge of lean construction, to evaluate their level of agreement or disagreement with the identified influences using a 5-point Likert scale.

To address the difficulties in precisely defining the research population, researchers have used a combination of non-probability sampling techniques, such as snowball sampling, quota sampling, and purposeful sampling, to select participants (Mweshi & Sakyi, 2020). Therefore, this study utilised the purposive sampling method, intentionally choosing participants who had specific characteristics or qualities that were in line with the research objectives. Purposeful sampling, also known as purposive sampling, is a method of sampling commonly used in qualitative research that does not rely on probability (Douglas, 2022). It involves deliberately choosing participants or cases that have specific characteristics or qualities that are relevant to the research goals (Cash *et al*., 2022). The selection of this method was based on its ability to specifically identify individuals who possess pertinent knowledge, expertise, or experiences on the research topic.

A total of 350 questionnaires were distributed electronically via Google Forms to the specified professionals in the position of project managers, quality assurance managers, safety managers, equipment managers, and site managers

of the 71 registered members of the Federation of Construction Industry (FOCI) in Abuja, Kaduna, and Lagos as at December 2023. However, only 294 responses were fully completed by the participants, validated, and deemed appropriate for subsequent statistical analysis. However, to determine the internal consistency and reliability of the questionnaire, the study employed the Cronbach Alpha Reliability Test (CART). The test returned a value of 0.976, which is more than the acceptable threshold of 0.70 as postulated by Oyewobi *et al*. (2023) and Okanlawon *et al*. (2023). The gathered data was analysed using the Mean Item Score (MIS) as a measure of descriptive statistics. The analysis was conducted using Statistical Package for Social Science (SPSS) version 26 and Microsoft Excel.

4.0 RESULTS AND DISCUSSION

4.1 Demographic Findings

The demographic data reveals that 43% of the participants are employed as project managers, while 27% work as site managers. 16% hold positions as quality assurance managers, 8% as equipment managers, and 6% as safety managers. The distribution of responses indicates that organisations tend to favour project managers who can effectively address inquiries, which implies that these project managers have a higher level of expertise in understanding lean concepts. Furthermore, the findings indicate that 58% of participants have obtained either an HND or BSc degree, while 33% have a Master's degree. This suggests that the respondents possess adequate academic qualifications to understand and answer the questions effectively. The data also indicates that 38% of the respondents are Quantity Surveyors, 26% are Engineers, 18% are Builders, and 14% are Architects. This suggests that the respondents' professional backgrounds provide relevant expertise for the research. In addition, the results indicate that 37% of the participants work in the construction industry, 14% in civil engineering projects, 3% in large-scale engineering projects, 30% are involved in both construction and civil works, and 16% are engaged in all sectors. The distribution of responses indicates that the respondents have a thorough grasp of the lean approach, thereby confirming the validity of their answers. Moreover, a significant 52% of participants indicate possessing a decade or more of professional experience and having knowledge of lean practices, which emphasises the trustworthiness and accuracy of the data presented in the study.

4.3 Descriptive Statistics for the Influence of Lean Construction Techniques on the Cost Performance of Construction Projects in Nigeria

Table 1 presents the results of the MIS used to rank the influence of lean construction techniques on the cost performance of construction projects in Nigeria. The table revealed that the topmost-ranked lean construction technique that influences the cost performance of construction projects in Nigeria is 5S (Sort, Straighten, Shine, Standardise, and Sustain) with an MIS score of 4.02. This suggests that implementing 5S principles results in significant improvements in cost management, resource utilisation, and overall project efficiency (Cash *et al*., 2022). Furthermore, the widespread adoption of 5S demonstrates its practicability and adaptability to a variety of construction contexts, cementing its position as a preferred lean technique among industry professionals. This finding is in line with the study of Al-Aomar (2011). It also highlights the importance of systematic organisation, cleanliness, and standardisation in improving cost performance and operational excellence in Nigerian construction projects. The finding also resonates with the conclusions of Enshassi *et al*. (2019) and Gómez-Cabrera *et al*. (2020). The table also revealed that Concurrent Engineering, Construction Process Analysis, Six Sigma and Pareto analysis with an MIS of 3.98, 3.95, and 3.85 are the mid-ranked lean construction technique that influences the cost performance of construction projects. The findings of this research stand with the study of Durdyev and Ismail (2012) which stated that on-site productivity issues during project implementation are primarily caused by the project's management, financing, and workforce characteristics. However, the study ranked Kanban (Pull System) with MIS 3.84, and Kaizen with MIS 3.80 as the least ranked lean construction technique that influences the cost performance of construction projects in Nigeria. The overall results showed a high average mean score above 3.50 according to the Likert scale ranking rule of 1 = strongly disagree; 2 = disagree; 3 = undecided; 4 = agree; and 5 = strongly agree, this high agreement in rating affirmed that all the lean construction techniques have a significant influence on cost performance of construction project in Nigeria and are effective in improving Nigeria's construction projects.

Table 1: Descriptive Statistics for the Influence of Lean Construction Techniques on the Cost Performance of Construction Projects in Nigeria

LCT	Lean Construction Techniques/Tools	Mean	Std. Deviation	Rank
LCT1	5S (Sort, Straighten, Shine, Standardise, and Sustain)	4.02	0.93	1
LCT20	Total Productive Maintenance (TPM)	3.99	0.93	2
LCT37	Team Preparation	3.99	0.95	2
LCT2	Concurrent Engineering	3.98	0.93	3
LCT5	Six Sigma	3.96	0.98	4
LCT40	Root Cause Analysis	3.96	1.02	4
LCT3	Construction Process Analysis	3.95	0.99	5
LCT6	Pareto Analysis	3.93	1.00	6
LCT33	Work Standardisation	3.93	0.96	6
LCT16	Poka-Yoke (Error Proofing)	3.92	1.04	7
LCT23	Work Structuring	3.92	1.01	7
LCT31	PDCA (Plan, Do, Check, Act)	3.91	0.99	8
LCT30	SMART Goals	3.9	1.04	9
LCT36	Just-in-Time (JIT)	3.9	1.01	9
LCT28	Preventive Maintenance	3.9	0.92	9
LCT38	Muda Walk	3.89	0.98	10
LCT8	Failure Mode and Effects Analysis (FMEA)	3.89	1.02	10
LCT34	Suggestion schemes	3.89	0.96	10
LCT22	Synchronize/Line Balancing	3.88	0.98	11
LCT39	Value Stream Mapping	3.88	0.99	11
LCT32	Setup Reduction	3.87	0.97	12
LCT35	Statistical Process Control	3.87	0.97	12
LCT19	Bottleneck Analysis	3.87	1.01	13
LCT10	FIFO line (First In, First Out)	3.86	0.99	14
LCT21	Visual Management	3.86	1.01	14
LCT9	Continuous Flow	3.85	1.01	15
LCT4	Check Sheet	3.85	1.01	15
LCT17	First Run Studies	3.85	1.01	15
LCT18	Time and Motion Study	3.85	0.96	15
LCT25	5 Whys (Why, what, where, who, when)	3.85	0.95	15
LCT11	Jidoka/Automation	3.84	1.02	16
LCT14	The Last Planner	3.84	1.04	16
LCT7	Check Points and Control Points	3.83	0.99	17
LCT29	Quality Function Development (QFD)	3.83	1.05	17
LCT27	Daily Huddle Meetings	3.82	1.01	18
LCT24	Multi-Process Handling	3.81	0.98	19
LCT12	Kanban (Pull System)	3.8	1.07	20
LCT13	Kaizen	3.8	1.04	20
LCT26	Fail-Safe for Quality	3.8	0.93	20
LCT15	Heijunka (Level Scheduling)	3.77	1.03	21

Source: Researcher's Analysis of Data (2024)

5.0 CONCLUSION

This study sought to assess the influence of lean construction techniques on the cost performance of construction projects in Nigeria. The findings revealed that all the lean construction techniques have an influence on the cost performance of construction projects, with 5S (Sort, Straighten, Shine, Standardise, and Sustain) ranking topmost. This finding emphasises the importance of incorporating lean principles into construction management practices, especially in a developing country like Nigeria, where cost optimisation is critical for long-term project outcomes. However, while the study provides useful insights into the impact of lean construction techniques on cost performance, it is critical to recognise the potential limitations and complexities of real-world implementation. As a result, additional research and practical experimentation are recommended to investigate the nuanced dynamics and contextual factors that may influence the efficacy of lean methodologies in the Nigerian construction industry. Also, further studies are required to provide more evidence of the impact of lean techniques on cost performance using project case studies.

References

Ahmed, S., Hossain, M. M., & Haq, I. (2021). Implementation of lean construction in the construction industry in Bangladesh: awareness, benefits and challenges. *International Journal of Building Pathology and Adaptation*, *39*(2), 368-406.

Al-Aomar, R. A. (2011). Applying 5S LEAN Technology: An infrastructure for continuous process improvement. *International Journal of Industrial and Manufacturing Engineering*, *5*(12), 2638-2643.

Alzahrani, J. I., & Emsley, M. W. (2013). The impact of contractors' attributes on construction project success: A post construction evaluation. *International journal of project Management*, *31*(2), 313-322.

Amini, S., Rezvani, A., Tabassi, M., & Malek Sadati, S. S. (2023). Causes of cost overruns in building construction projects in Asian countries; Iran as a case study. *Engineering, Construction and Architectural Management*, *30*(7), 2739-2766.

Anaman, K. A., & Osei-Amponsah, C. (2007). Analysis of the causality links between the growth of the construction industry and the growth of the macro-economy in Ghana. *Construction management and economics*, *25*(9), 951-961.

Barth, K. B., & Formoso, C. T. (2021). Requirements in performance measurement systems of construction projects from the lean production perspective. *Frontiers of Engineering Management*, *8*, 442-455.

Bekr, G. A. (2015). Identifying factors leading to cost overrun in construction projects in Jordan. *Journal of Construction Engineering, Technology and Management*, *5*(3), 25-33.

Belassi, W., & Tukel, O. I. (1996). A new framework for determining critical success/failure factors in projects. *International journal of project Management*, *14*(3), 141-151.

Beleiu, I., Crisan, E., & Nistor, R. (2015). Main factors influencing project success. *Interdisciplinary Management Research*, *11*(2), 59-72.

Braglia, M., Dallasega, P., & Marrazzini, L. (2022). Overall Construction Productivity: a new lean metric to identify construction losses and analyse their causes in Engineer-to-Order construction supply chains. *Production Planning & Control*, *33*(9-10), 925-942.

Cash, P., Isaksson, O., Maier, A., & Summers, J. (2022). Sampling in design research: Eight key considerations. *Design studies*, *78*, 101077.

Demirkesen, S., Sadikoglu, E., & Jayamanne, E. (2022). Investigating effectiveness of time studies in lean construction projects: case of Transbay Block 8. *Production Planning & Control*, *33*(13), 1283-1303.

Douglas, H. (2022). Sampling techniques for qualitative research. In *Principles of social research methodology* (pp. 415-426). Springer.

Durdyev, S., & Ismail, S. (2012). Pareto analysis of on-site productivity constraints and improvement techniques in construction industry. *Scientific Research and Essays*, *7*(7), 824-833.

El Khatib, M., Nakand, L., Almarzooqi, S., & Almarzooqi, A. (2020). E-Governance in Project Management: Impact and Risks of Implementation.

Enshassi, A., Saleh, N., & Mohamed, S. (2019). Application level of lean construction techniques in reducing accidents in construction projects. *Journal of Financial Management of Property and Construction*, *24*(3), 274-293.

Forbes, L. H., & Ahmed, S. M. (2010). *Modern construction: lean project delivery and integrated practices*. CRC press.

Francis, A., & Thomas, A. (2020). Exploring the relationship between lean construction and environmental sustainability: A review of existing literature to decipher broader dimensions. *Journal of cleaner production*, *252*, 119913.

Gómez-Cabrera, A., Salazar, L. A., Ponz-Tienda, J. L., & Alarcón, L. F. (2020). Lean tools proposal to mitigate delays and cost overruns in construction projects. Proceedings of the 28th Annual Conference of the International Group for Lean Construction (IGLC28), Berkeley, CA, USA,

Hardin, B., & McCool, D. (2015). *BIM and construction management: proven tools, methods, and workflows*. John Wiley & Sons.

Ithana, L. M. (2020). *Payment Processes as Factors Impede the Successful Implementation of Construction Projects at WT Business Group in Namibia* Botho University].

Kaliba, C., Muya, M., & Mumba, K. (2009). Cost escalation and schedule delays in road construction projects in Zambia. *International journal of project Management*, *27*(5), 522-531.

Koelmans, R. (2004). Project success and performance evaluation. *Information and Management Journal*, *41*, 229-236.

Koskela, L. (2020). Theory of lean construction. In *Lean construction* (pp. 2-13). Routledge.

Krausmann, F., Gingrich, S., Eisenmenger, N., Erb, K.-H., Haberl, H., & Fischer-Kowalski, M. (2009). Growth in global materials use, GDP and population during the 20th century. *Ecological economics*, *68*(10), 2696-2705.

Le-Hoai, L., Lee, Y. D., & Lee, J. Y. (2008). Delay and cost overruns in Vietnam large construction projects: A comparison with other selected countries. *KSCE journal of civil engineering*, *12*, 367-377.

Mansfield, N. R., Ugwu, O., & Doran, T. (1994). Causes of delay and cost overruns in Nigerian construction projects. *International journal of project Management*, *12*(4), 254-260.

Merrow, E. W. (2011). *Industrial megaprojects: concepts, strategies, and practices for success*. John Wiley & Sons.

Mohajan, H. K. (2020). Quantitative research: A successful investigation in natural and social sciences. *Journal of Economic Development, Environment and People*, *9*(4), 50-79.

Mohammadi, A., Igwe, C., Amador-Jimenez, L., & Nasiri, F. (2022). Applying lean construction principles in road maintenance planning and scheduling. *International journal of construction management*, *22*(12), 2364-2374.

Musarat, M. A., Alaloul, W. S., & Liew, M. (2021). Impact of inflation rate on construction projects budget: A review. *Ain Shams Engineering Journal*, *12*(1), 407-414.

Mweshi, G. K., & Sakyi, K. (2020). Application of sampling methods for the research design. *Archives of Business Review–Vol*, *8*(11).

Nuako, F., Ghansah, F. A., & Adusei, T. (2024). Critical success factors for cost overrun minimization in public construction projects in developing countries: the case of Ghana. *Construction Innovation*.

Okanlawon, T. T., Oyewobi, L. O., & Jimoh, R. A. (2023). Evaluation of the drivers to the implementation of blockchain technology in the construction supply chain management in Nigeria. *Journal of Financial Management of Property and Construction*(ahead-of-print).

Oladinrin, T., Ogunsemi, D., & Aje, I. (2012). Role of the construction sector in economic growth: Empirical evidence from Nigeria. *FUTY Journal of the Environment*, *7*(1), 50-60.

Osamudiamen, B., Ihensekhie, A., & Oghomwen, S.-E. (2022). Factors Affecting Project Performance of Building Construction Projects in Federal Capital Territory (FCT) Abuja, Nigeria. *Current Journal of Applied Science and Technology*, *41*(35), 44-53.

Oyewobi, L., Okanlawon, T. T., Ibrahim, K., & Jimoh, R. A. (2023). Influence of blockchain adoption barriers and drivers on potential application areas in the construction lifecycle: partial least squares structural equation modelling (PLS-SEM) approach. Engineering, Construction and Architectural Management.

Pienkowski, T., Cook, C., Verma, M., & Carrasco, L. R. (2021). Conservation cost-effectiveness: a review of the evidence base. *Conservation Science and Practice*, *3*(5), e357.

Schimanski, C. P., Marcher, C., Pasetti Monizza, G., & Matt, D. T. (2020). The Last Planner® system and building information modeling in construction execution: From an integrative review to a conceptual model for integration. *Applied Sciences*, *10*(3), 821.

Shimizu, K., & Hitt, M. A. (2004). Strategic flexibility: Organizational preparedness to reverse ineffective strategic decisions. *Academy of Management Perspectives*, *18*(4), 44-59.

Si, T., Li, H. X., Hosseini, M. R., Ji, Y., & Liu, C. (2020). A solution to Just-in-Time delivery for off-site construction: a conceptual model. Construction Research Congress 2020,

Simon-Eigbe, B., Aiminhiefe, M., & Bamidele, B. (2022). Factors Affecting Project Performance of Building Construction Projects in Federal Capital Territory (FCT) Abuja, Nigeria. *Current Journal of Applied Science and Technology*, 44-53. https://doi.org/10.9734/cjast/2022/v41i353960

Tam, C., da Costa Moura, E. J., Oliveira, T., & Varajão, J. (2020). The factors influencing the success of on-going agile software development projects. *International journal of project Management*, *38*(3), 165-176.

Taye, M. (2016). *Assessment of time and cost overruns in construction projects (case study at defense construction enterprise)* St. Mary's University].

Venkatesh, P. K., & Venkatesan, V. (2021). Experiences from the implementation of last planner system® in construction project. *Indian Journal of Engineering and Materials Sciences (IJEMS)*, *28*(2), 125-141.

Zahoor, M. H. (2023). *Evaluation of Critical Factors Leading to Cost Overrun in Building Projects using Structural Equation Modeling* CAPITAL UNIVERSITY].

PAPER 50 – ENHANCING EDUCATIONAL EFFICIENCY TOWARDS SUSTAINABLE EDUCATION USING AI AND ROBOTICS SOLUTIONS FOR ADMINISTRATIVE OPTIMIZATION: A REVIEW

David I. Agbemuko[1], Imhade P. Okokpujie[1,2], Momoh J. E. Salami[3]

[1]Department of Mechanical and Mechatronics Engineering, Afe Babalola University, Ado-Ekiti, Ekiti State, Nigeria
[2]Department of Mechanical and Industrial Engineering Technology University of Johannesburg Doornfontein Campus Johannesburg, South Africa
Email: davidagbemuko.ad@gmail.com; ip.okokpujie@abuad.edu.ng; mjesalami@gmail.com

ABSTRACT
This review paper explores integrating artificial intelligence (AI) and robotics technologies to enhance educational efficiency and contribute to sustainable education. The traditional manual recording and collation of graded examination scripts in educational institutions are time-consuming and prone to errors, diverting educators' resources from more impactful teaching and learning activities. This review aims to streamline administrative processes by leveraging AI and robotics, liberating educators' time for strategic planning and complex challenges. While delving into existing automated solutions for educational data management, robotics and automation in education, and image processing techniques for grade recording, it also discusses data extraction methods for student information retrieval, highlighting their strengths and shortcomings. Aligned with United Nations Sustainable Development Goal 4 (Quality Education), this paper underscores the potential for technology to revolutionize traditional processes in education. Moreover, it creates implications for other SDGs, particularly SDG 9 (sustainable industrialization and foster innovation) and SDG 17 (Partnerships for the Goals), emphasizing the transformative impact of AI and robotics in educational administration.

***KEYWORDS*:** Students grades recording, Artificial intelligence, Machine learning, Image processing, Computer vision, Robot awareness, Robot manipulator, Sustainable development goals

1. INTRODUCTION

In our educational institutions, the traditional manual recording and collation of graded examination scripts present a time-consuming and labor-intensive endeavor. The tendency of the process to be inefficient and error-prone adds even further complexity to the challenge. It has caused educators to invest substantial time and effort in such administrative tasks to meticulously record the students' scores (Sandnes, 2023). Even worse is that the arduous nature of manual data entry diverts the educators' valuable resources from more impactful teaching and learning activities, which would, in turn, hinder an overall educational experience or learning cycle in our institutions down the road (Kayode & Ayodele, 2015). Moreover, the reliance on manual data entry could also elevate the risk of data inaccuracies and delays, which could, in turn, compromise the integrity of student records, thus leading to miscommunications and discrepancies in assessment outcomes and consequently hindering the educators' ability to make well-informed decisions based on timely and accurate data (Tang, 2015).

Given the already outlined challenges faced with the traditional recording and collation of students' graded scripts and the importance of such tasks, blending efficiency in managing things and introducing new technologies like artificial intelligence and robotics becomes important (Selwyn et al., 2021). This is why educational institutions have increasingly emphasized the need for optimizing administrative processes by leveraging the advancements in artificial intelligence and robotics, thus changing things in a big way. The introduction of artificial intelligence (AI)and robotics brings significant benefits to any administrative domain, as its automation capabilities could help liberate valuable time by taking up routine tasks, enabling administrators in such a domain to focus on strategic planning and complex challenges (Ahmad et al., 2022). Moreover, it also reinforces the integrity of administrative processes in that domain by minimizing human errors through its capability for precision and accuracy, thus fostering reliability and trust in many data-driven decisions (Qeshmy et al., 2019).

Therefore, any educational institution looking to prioritize administrative efficiency and data-driven decision-making could use an intelligent and automated solution for handling most—if not all—of its administrative tasks.

An example of such a task, as already mentioned in the first paragraph, would require streamlining the script handling process with the employment of an integration of several concepts ranging from the field of artificial intelligence to that of robotics. The convergence of both fields would imply the utilization of sophisticated image processing algorithms to fulfil student information retrieval from the scripts and robotic manipulation and control algorithms to fulfil faster examination script handling. Harnessing these concepts not only addresses the challenges of manual data collation but also underscores the immense potential for technology to amplify educational endeavors, such that as the lines between innovation and education blur, an intelligent automated students' marks collation system would stand as a testament to the potential for technology to seamlessly integrate with educational objectives, ultimately shaping a more efficient and impactful learning environment.

This paper has embarked on a comprehensive review of key concepts for realizing an intelligent student's marks collation system, focusing on integrating artificial intelligence (AI) and robotics technologies. By examining the existing literature on automated solutions for educational data management, awareness, and manipulation in robotics and automation, and image capture, preprocessing, and data extraction techniques, this review has laid the groundwork for a transformative approach to administrative optimization in educational institutions. By emphasizing educational efficiency, the paper aligns with the United Nations Sustainable Development Goal 4 (SDG4) of ensuring quality education for all. However, its impact extends beyond this goal, with implications for other SDGs, particularly SDG 9 (Industry et al.) and SDG 17 (Partnerships for the Goals). Highlighting the use of Artificial Intelligence and robotics in educational administration, this paper emphasizes how these technologies can revolutionize traditional processes, freeing up time and resources for educators to concentrate on strategic planning and complex challenges. Moreover, the precision and accuracy offered by these technologies can enhance the integrity of administrative processes, fostering reliability and trust in data-driven decision-making. In essence, this review sets the stage for the development and implementation of intelligent solutions that can transform educational administration, ultimately contributing to the overarching goal of sustainable education.

2. AUTOMATED SOLUTIONS FOR EDUCATIONAL DATA MANAGEMENT

The increasing integration of technology into educational processes and the continual progress of computer systemshaveallowed for collecting and storing large volumes of data associated with educational systems. However, educational institutions face enormous problems digesting this data to draw relevant insights. In fact, according to Martins et al. (2018), the sheer volume of data emanating from multiple sources and in varied forms exceeds human capabilities for unassisted analysis and significant information extraction, and this is why automated analytical approaches are used to extract essentialknowledge from raw data, a process critical for making educated decisions. Educational Data Mining (EDM) was developedto extract relevant insights that might influence companies. It derives from three major fields: statistics, computer science, and education (as represented in Figure 1). The intersections of these domains give birth to similar subdomains that are closely connected to EDM. Computer-aided education, data mining, and analytical learning are examples of these.

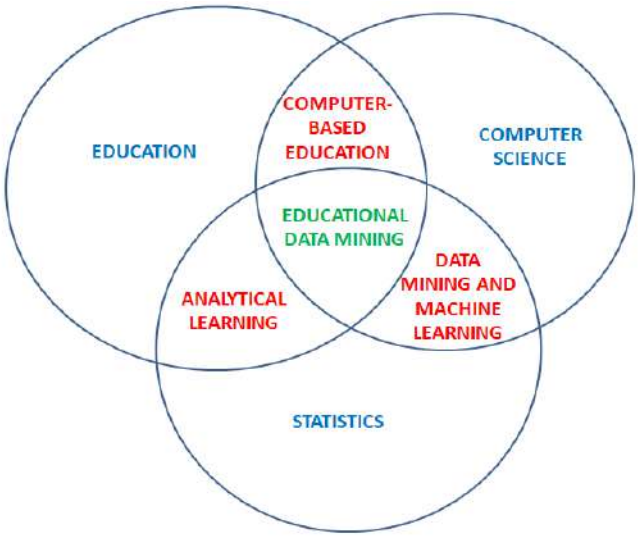

Figure 1: A Diagrammatic Representation Describing the Domains of EDM

Educational data mining is a new subject that focuses on developing strategies for analyzing specific data from educational environments to improve students' and their learning environments' understanding. The objective is to transform primary educational data into meaningful insights that can be used to make educated decisions and conduct research. Data mining and analytics in education have advanced despite their slower acceptance than other disciplines. However, dealing with online learning data is difficult owing to its unique characteristics. While all data types have sequential aspects, the temporal distribution of educational data is unusual. For example, a skill may be repeated throughout the school year but in different circumstances. Educational data mining has successfully modelled many student learning phenomena in intelligent online systems. The accuracy of these models increases year after year, and their usefulness expands. Several essential factors support the distinct growth of educational data, and these include recognizing that crucial information is not isolated to a single data stream, improving model quality through improved approaches, and admitting the presence of more documented detector instances than real intervention situations are among these (Silva & Fonseca, 2017).

Upadhyay and Katiyar (2014) state that educational data mining generally unfolds into four stages; the primary stage focuses on discovering relationships hidden within the data of the educational setting; these interactions are critical because they serve as the foundation for numerous data mining approaches such as classification, clustering (described in Figure 2), and regression. Once these links have been disclosed, the next phase entails a vital task: verifying them. This stage tries to confirm that the detected associations have true significance and is not purely accidental, thus reducing the danger of data overfitting. Following successful validation, the third stage begins, in which these authenticated associations are used to anticipate future events and trends in the learning environment. This predictive skill enables educators and institutions to change and improve their techniques. Finally, in the fourth step, these forecasts are used as instruments for informed decision-making to improve the results and experiences of the learning environment.

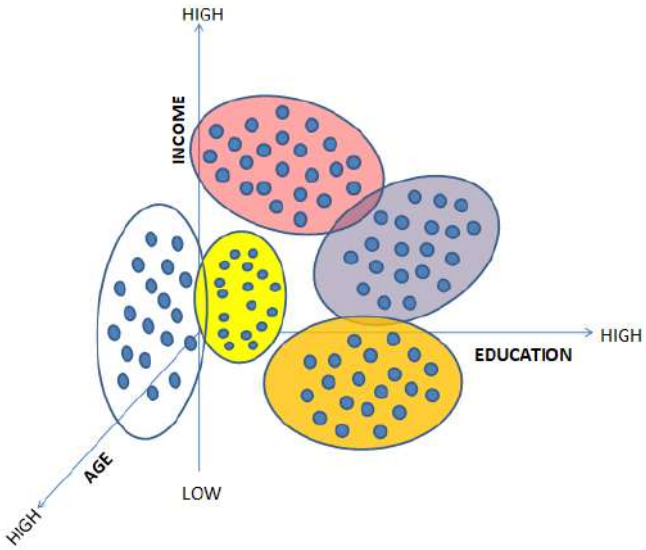

Figure 2: A Diagrammatic Description of a Clustering Algorithm (An Actual Cluster Analysis of the Incomes and Outcomes in Europe's Education presented by Silva 2014)

Predicting how well students will do in their studies is a big deal in educational data mining (EDM), so it is getting more attention. By making these predictions, we can determine which students might struggle academically. This helps educators step in early with guidance or help, keeps track of how students are doing to improve their learning path, and suggests suitable learning materials. According to Xiao et al. (2022), the CRISP-DM is a Cross-Industry Standard Process that some researchers utilize to develop a student-performance prediction model. They explain that six necessary steps form the CRISP-DM execution process, the first of which involves knowledge of the business's objectives, an imagination of its purpose, and an articulation of the function of the DM (Data Mining) project. This first phase requires project planning, constraint identification, and an emphasis on identifying the DM task needs. The second step would be to comprehend the data environment, find necessary data tables and fields, and examine

data features, which are all part of the process. The third step focuses on data preparation, which includes data integration, cleansing, and possible transformation. The next phase is model creation, which includes the design and construction of analytical models. The model is then evaluated through experimental testing. The predictive model is refined and pushed out in the last step, deployment, depending on its anticipated use.

Kaur et al. (2015) focused on identifying students with slower learning progress using a predictive data mining methodology and classification algorithms. He used a real-world dataset from a high school, with the open-source program WEKA assisting in identifying critical variables. The student academic records dataset is examined and applied using WEKA to numerous classification methods, including Multilayer Perception, Nave Bayes, SMO, J48, and REPTree. As a result, statistical results for each classification technique are generated, followed by a complete comparison of these five classifiers. This comparison aims to assess accuracy levels and identify the best-performing categorization method. Finally, the results show that Multilayer Perception is the best performer; with a 75% accuracy rate. Sivasakthi (2014) conducted a study to predict the success of first-year bachelor students in a Computer Application course based on their introductory programming ability. This was accomplished using classification-based algorithms in a predictive data mining strategy. Student population size, scores in college-level introductory computer programming, and grades on an exam consisting of 60 programming problems were all included in the dataset. Using the WEKA program, the obtained data was exposed to numerous categorization methods, including Multilayer Perception (MLP), Nave Bayes, SMO, J48, and REPTree. This method produced statistical analysis generated from all of the categorization algorithms. These statistics were used to thoroughly compare the five classifiers, with the primary goal of predicting accuracy and determining the most effective classification technique. According to the study's findings, the MLP algorithm performed best, with an accuracy rate of 93%. As a result, the MLP algorithm displayed significant promise and efficiency as a classifier, as evidenced by the study's findings.

The performance of classifiers during educational data mining can also be increased using Feature Selection (FS) algorithms to remove irrelevant data from the educational dataset. Zaffar et al. (2017) presented an analysis of the performance of feature selection algorithms on student data sets because selecting relevant features for student prediction models is a susceptible issue for educational stakeholders, as they have to make decisions based on the results of prediction models. This research study thoroughly evaluated six unique feature selection (FS) methods. Cfs-Subset-Eval is one of the algorithms tested, and it determines feature relevance by considering individual predictive prowess and feature redundancy. The second approach was Chi-SquaredAttributeEval, which computes attribute significance using chi-squared statistics relevant to class associations. The third technique, FilteredAttributeEval, works by ranking and choosing characteristics based on their significance to a target variable as defined by a specified evaluation measure. GainRatioAttributeEval, the fourth algorithm, provides a non-symmetrical measure to correct information gain biases. The sixth approach was the Principal Components algorithm, a dimensionality reduction strategy that involves converting original variables into new, independent components that embody critical information while keeping variation. Finally, ReliefAttributeEval evaluates attribute importance by incrementally selecting examples. This work aims to highlight the strengths and limits of each FS method, leading to a better understanding of their value across different datasets and problem areas. The study's findings demonstrated that the performance of feature selection algorithms inside the Weka tool did not change much. However, among the several feature selection approaches explored, it was shown that using principal components in combination with the Random Forest classifier produced the best results.

Figueira (2016) predicted students' future grades using principal component analysis to generate a decision tree based on three main features extracted from Moodle logs after discussing the statistical analysis of these features and demonstrating how they cannot be used independently to model our data. The three main features extracted and computed from the retrieved logs were the number of platform accesses by each student throughout the semester, the percentage of coverage of the entire course online activities and given lecture notes stored in the Moodle platform, and finally, the percentage of correct sequences of accesses to the pedagogical material made available. Although each of the selected attributes provides significant descriptions of student behavior, the analysis revealed that when they are accessible in isolation, various issues arise. However, using principal component analysis, he was able to choose the most influential traits after integrating all three key features. Table 1 presents a summary of approaches and outcomes in educational data mining. With these studies, it can be confirmed that the significance of effectively representing students' information, such as their grades, has been presented in the literature.

Table 1: Examination of Approaches and Outcomes in Educational Data Mining Studies

AUTHORS	PROBLEM/ OBJECTIVE	ALGORITHM/ TECHNIQUE USED	FINDINGS/GAPS
Duan et al. (2017)	In grouping categorical data, compare a novel algorithm to established clustering approaches.	Entropy-based K-modes clustering algorithm (ER-k-modes).	ER-k-modes performs better than traditional methods in terms of accuracy and convergence for purity, clustering accuracy, and F1-measure.
Singh et al. (2016)	Systematically examines students' academic performance and its influencing factors	Uses Multiple Regression Analysis in a post facto research design.	Research findings show that learning facilities, communication skills, and parental guidance significantly affect academic performance.
Rana & Garg (2016)	Assess students in third-semester Information Technology, focusing on Digital Electronics.	Apply Clustering and Classification Algorithms.	Hierarchical algorithm is less accurate than K-means but better than Naïve Bayes or Logistic Regression; all are fast algorithms
Batool et al. (2023)	Review of 260 studies over 20 years to identify top student performance prediction tools.	Clustering algorithms; Classification algorithms; WEKA tool	Key findings: ANN, Random Forest popular in data mining; WEKA used for predicting student progress. Educational history, demographics crucial for prediction.

3. AWARENESS AND MANIPULATION IN ROBOTICS AND AUTOMATION

Robotics and automation have experienced considerable advancements in recent decades, ushering in unparalleled technological progress. These fields, once relegated to fantasy and science fiction, have now risen to prominence and play key roles across a wide range of sectors (such as manufacturing, banking or education), consequently having a tangible influence on our everyday lives. This incredible revolution centred on the ongoing development of robotics and automated systems, particularly in the domains of perception and manipulation, as the remarkable ability of robots to actively see, analyse, and engage with their environment has now become a critical driver for innovation. The beginning of this age of innovation, as pointed out by Demir et al. (2019), is marked by a relentless march toward the achievement of Industry 4.0's goal – titled "Smart Manufacturing for the Future." and it is the expanding network of robotic and artificial intelligence (AI) capabilities, armed with the promise to reshape the core of our businesses, society, and daily lives, that underscores its vision. Meanwhile, despite the fruition of navigating an ever-changing terrain of the fourth industrial revolution, there is an alluring prospect of industry 5.0 on the horizon, characterised by the developing cooperation between humans and robots – also known as 'human-robot collaboration'.

The study by Gorbenko et al. (2012) defines a self-aware system as one that exhibits superior adaptability in handling unfamiliar situations compared to a system lacking self-awareness. Such a self-aware system can monitor and reflect upon its internal states, enabling introspection and self-adjustment. For genuine self-awareness in a robot, the robot needs to be capable of acknowledging its internal conditions. These internal states encompass emotions, beliefs, desires, intentions, expectations, and processes like sensation, perception, conceptualisation, simulation, action, planning, and cognition. Throughout any recognition process, the robot's awareness of its emotions, perceptions, beliefs, and objectives becomes indispensable. Without awareness, robot developers would be compelled to explicitly outline every action and behaviour, ensuring the robot functions according to its intended purpose and design objectives. This task becomes incredibly challenging when dealing with open, intricate, and constantly changing environments. In such scenarios, specifying precise actions and behaviours for all potential conditions and situations becomes an onerous endeavour. Conventional robot development approaches, tailored for well-defined problems, do not readily adapt to the complexity and dynamism of such environments. The sheer magnitude and potentially infinite variety of circumstances to account for makes it impractical to expect that robot developers can anticipate and design suitable responses for all conceivable scenarios.

This is why Rahmani & Rinner (2022) argue that self-awareness is a characteristic difficult to deploy on robots, as it is a broad term adapted from cognitive science and psychology that describes the characteristic of a system that

knows 'itself' based on its logical sense and internal representations (where this knowledge could take different forms founded on perceptions of both internal and external phenomena, and is crucial for being able to foresee and respond to unknown situations). The difficulty level is defined by specific fundamental challenges, which require autonomous robots to develop the capacity to learn inference models from sensor inputs, determine the current state and the present condition of their surroundings using these models, and detect any anomalies in observed behaviour compared to inferred behaviour. Therefore, extracting valuable information from sensory data is central to a robot's awareness, as it forms the foundation for perceiving and comprehending its internal and external environment. Increasing efforts regarding the design of the sensory perception and capabilities in robots would therefore result in increasing development of the robot's awareness capabilities, creating more impact in our sectors and lives.

For instance, Zabalza et al. (2019) presented a thorough case study that highlights the integration of advanced innovative sensing capabilities into a robotic arm manipulator, specifically the KUKA KR90 R3100, with the main goal of providing the robotic system with the ability to avoid collisions in real-time and plan its path dynamically, crucial for navigating through dynamically changing environments. This favours the manufacturing sector, with an increasing demand for more autonomous and flexible manufacturing in unstructured settings. To achieve this, a sophisticated machine vision module harnesses the power of cost-effective RGB cameras and a colour detection technique based on the hue, saturation, and value (HSV) colour space. With this approach, the robot's sensor perception capacity can detect and precisely localise randomly moving obstacles within its operational domain. The success of this project hinges on the smooth integration of three interconnected components: machine vision, path planning, and robot control (as described in Figure 3), which work in parallel while ensuring real-time operation and continuous communication among themselves. The machine vision module (while acting as a server) diligently tracks dynamic obstacles. On the other hand, the path planning module plays a crucial role as it determines the best paths for pick-and-place tasks by analyzing the data from the machine vision system. The resulting geometric paths, culminating in this complex interplay, are then communicated to the robot control module, which drives the robot along the designated routes. Ultimately, this integrated system stands as a remarkable testament to the potential of intelligentsensing and adaptive reasoning in robotics; by enabling quick responses to rapidly changing environments, this technological innovation brings us closer to a future where robots can autonomously navigate complex, ever-changing surroundings with agility and precision.

Another example can be taken in favour of the health sector, where suturing tasks are crucial to ensure the integrity of any surgical operation. Talasaz et al. (2016) delved into the vital realm of robotics-assisted minimally invasive surgery (RAMIS) with a focus on the impact of haptic feedback on suturing performance utilising an advanced haptics-enabled dual-arm master-slave tele-operation system, which is capable of measuring forces during tool-tissue interaction across all seven Degrees-of-Freedom (DOFs). His study evaluates sensory perception through two specific tasks: tissue puncturing and knot-tightening. A cohort of sixteen subjects participated in trials where their performance was evaluated from multiple dimensions, including force consistency, accidental tissue contact incidence, extent of tissue damage, suture knot quality, and task completion time. The findings underscore the nuanced nature of haptic feedback, such that for tissue puncturing, it was revealed that visual force feedback had limited utility, as different users required varying levels of force based on needle penetration. However, direct force feedback emerged as the hero, enabling users to apply gentler force and minimise tissue damage. The research emphasizes the essential role of combining visual and direct force feedback in achieving effective knot tightening. Direct force feedback minimizes accidental tissue contact and damage, while visual force feedback ensures secure knot tightening and maintains consistent force levels across various trials and users. In summary, Talasaz et al. (2016) underscore the importance of sensory perception in medical robotics, offering a nuanced perspective on the role of haptic and visual feedback in optimising surgical outcomes, thereby advancing the field of RAMI.

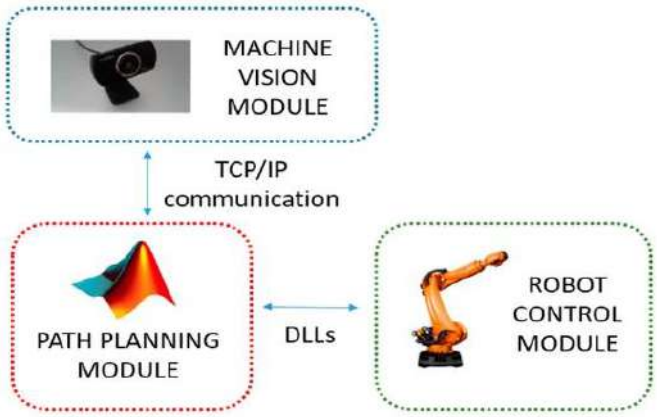

Figure 3: The proposed system's overview with three concurrent modules: (i) Machine Vision (incorporating intelligent sensing), (ii) Path Planning (involving reasoning and decision-making), and (iii) Robot Control (managing movement coordination).

Lee & Nicholls (1999) said, "The final frontier for robots is not space, but our living rooms". This is why the field of robots is expanding to include complex environments like our homes, hospitals, banks and even schools. For robots and humans to work side by side in such complex environments to achieve common goals, it, therefore, becomes imperative for robots to learn to grasp and manipulate objects with dexterity while being 'conscious' of the presence of humans. Kappassov et al. (2015) reviewed the significance of tactile sensing in dexterous robot hand manipulation, emphasising its role in providing information on interaction forces and surface properties at contact points. Tactile sensing, according to Kappassov et al. (2015), is critical for achieving autonomous and effective dexterous manipulation with robot hands; however, depending on the task, the sensor has different design specifications for humanoid robots, prosthetic hands, manufacturing, or large tactile system implementation; whereas in autonomous manipulation applications, tactile sensors need to satisfy requirements for object characterisation and identification (e.g., they estimate the compliance, thermistor temperature, etc.). He further explained that tactile sensor design parameters for manipulation include spatial resolution, sensitivity, and wiring issues. Higher spatial resolution is advantageous for in-hand object manipulation and tactile feedback control. However, it is limited in cases requiring high sensitivity or frequency response due to longer acquisition time and increased susceptibility to electromagnetic interference. Sensitivity, defined as the lowest observable pressure/force fluctuation, is essential for sensitive object handling yet also lowers dynamic range. Furthermore, limiting the amount of wiring on the workspace of the robot hand is critical, and it can be accomplished with integration issues handled by smart wiring, shielding, and protocols such as serial communication.

When George et al. (2019) looked into the use of a bidirectional neuro-myoelectric prosthetic hand that conveys biomimetic sensory feedback, they discovered that electro-myographic recordings from residual arm muscles could be decoded to provide independent and proportional control of a six-DOF prosthetic hand and wrist, specifically the DEKA LUKE arm. Additionally, it was found that by turning on the prosthesis' touch sensors, chronically implanted Utah Slanted Electrode Arrays allowed for the intraneural micro-stimulation of residual sensory nerve fibers, producing tactile perceptions in the phantom hand. The subjects showed improved grip force accuracy and dexterity when receiving sensory input. Through active research, it was also noted that the participant could distinguish between soft and hard materials and between minute and large objects. The participant could identify the objects significantly faster than standard encoding approaches that focused on the strength of the present stimulus when the sensory input was designed to mimic natural sensory signals. Accordingly, it was suggested that artificial touch may be altered by patterning sensory feedback, and it was demonstrated that patterns with biological inspiration produced more interpretable and practical perceptions. In the report, George et al. (2019)also assessed the impact of sensory feedback on object interactions by performing a task that required moving a fragile object that broke when the grip force was too strong. The task was performed with and without the sensory feedback functionality and with full and divided attention. The variable of split attention was relevant to evaluate since human actions frequently require dividing attention between numerous concurrent subtasks, like holding a container while turning off its lid. To mimic split attention, the individual was instructed to complete the same activity while counting backwards. The experiment revealed that when participants were given sensory feedback, they moved the object more frequently and

quickly. However, when participants' attention was divided, although the feedback-induced performance increase continued, the impact on duration remained statistically noteworthy (as described in Figure 4 and Figure 5).

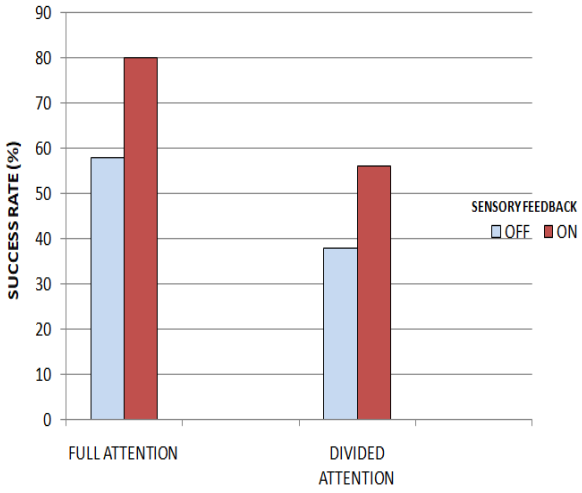

Figure 4: Evaluating The Success Rate of The Participant's Task Against Enabled or Disabled Sensory Feedback and A Full or Divided Attention

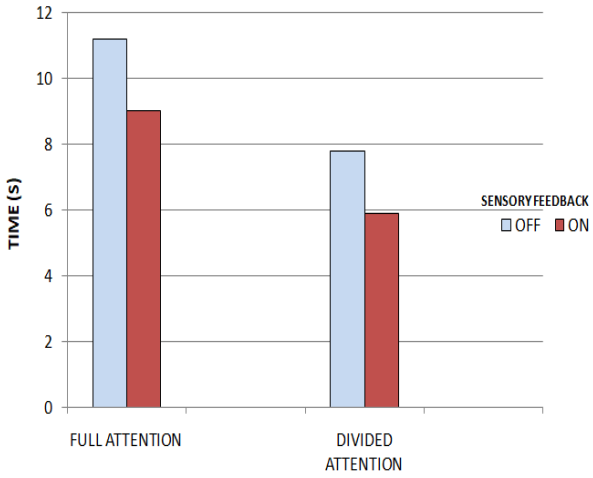

Figure 5: Evaluating The Speed of Task Completion Against Enabled or Disabled Sensory Feedback and a Full or Divided Attention

In a study by Valle et al. (2018) focused on enhancing the neural stimulation provided to trans-radial amputees with intra-neural electrodes, various encoding strategies were compared regarding their effectiveness and the naturalness of the tactile feedback they delivered. The findings of this research highlighted a critical balance between naturalness and efficacy in providing sensory feedback to these individuals. One key observation was that bio-mimetic frequency modulation was perceived as more natural, replicating a more lifelike sensory experience. On the other hand, amplitude modulation proved to be more advantageous for tasks demanding precise identification of applied force, enhancing overall performance. Remarkably, it was discovered that the ideal compromise between naturalness and sensitivity in tactile feedback could be achieved through "hybrid" encoding strategies, with these hybrid approaches combining bio-mimetic frequency and amplitude neuro-modulation simultaneously, resulting in a synergy that significantly improved the gross manual dexterity of the subjects during functional tasks. Furthermore, this simultaneous modulation approach maintained high levels of manual accuracy; the hybrid encoding strategies advanced manual capabilities and positively impacted prosthesis embodiment. These strategies reduced abnormal phantom limb sensations, often called the "telescoping effect." Consequently, the study recommended the preference for hybrid encoding strategies in delivering sensory feedback to trans-radial amputees with intra-neural electrodes, and these hybrid strategies excelled in providing both highly sensitive and natural percepts, effectively enhancing the overall quality of life and functionality for individuals with limb loss. Table 2 shows the summary analysis of awareness of the manipulation of the evaluation system.

Table 2: Further Examination of Awareness and Manipulation in Automation and Robotics

AUTHORS	OBJECTIVE/ PROBLEM	SOFTWARES/TOOLS USED	FINDINGS/GAPS
Sharma et al. (2020)	Hierarchical object-centric controllers for tasks.	Reinforcement learning method for controllers.	Technique improves efficiency, generalization, transfer.
Batista et al. (2020)	Identify cylindrical robot arm kinematics.	LS, RLS, RLSPO identification techniques	RLSPO improves complex identification accuracy.
Wong et al. (2023)	Develop a strategy for the robotic arm to pick and place objects.	CS-RRT (Changing Strategy RRT) and RRT (Rapidly-Exploring RRT) efficiency.	CS-RRT reduces computation time.

Van-Tuijl et al. (2018)	To develop a novel end-effector for trimming bushes	A morphological chart to make design decisions.	Cable weight caused end-effector issues.

4. IMAGE CAPTURE, PREPROCESSING AND DATA EXTRACTION TECHNIQUES

A class of techniques known as 'digital image processing' deals with applying computer algorithms to manipulate digital images, and the word 'manipulate' here refers to applying computer algorithms to alter, enhance, or transform digital images for various purposes, such as improving their quality, extracting information, or achieving specific visual effects. Image processing could, therefore, be described as a process of improving an already-existing image or extracting significant information from it. In research, Shahriar LI (2020) noted that an image's quality is always a critical factor in raising the likelihood that various image recognition applications would be successful. They claimed that since extracting features from unprocessed noisy pictures is more complex, high-quality images have a higher recognition or classification rate than unprocessed noisy images. Therefore, pre-processing is usually done before extracting characteristics from the picture to overcome application errors that must have happened due to low-quality images. Image processing techniques can be broadly classified into three categories (as described in Figure 6): image enhancement, image restoration, and image analysis. Qi et al. (2021) surveyed image enhancement algorithms, aiming to conduct a thorough and systematic analysis of various techniques in this Image enhancement. Image enhancement is essential in image processing and primarily focuses on improving image quality for specific applications. According to Qi et al., the two main categories of traditional methods are spatial domain processing, which directly modifies pixel information through techniques like modified histograms and improved unsharp masks, and frequency domain processing, involving transformations like Fourier, discrete cosine, and discrete wavelet transforms. He further stated that as image enhancement technology rapidly evolves, novel methods such as the retinex model, fuzzy theory, and neural networks have emerged. Specific methods highlighted in the survey include histogram equalisation, the Retinex model, visual cortex neural networks, and deep learning, each with advantages and disadvantages. Spatial domain methods are praised for their simplicity, low complexity, and real-time implementation. However, they face challenges like insufficient robustness and imperceptibility, as finding a universally effective method is hindered by factors such as algorithm non-universality, evaluation index choices, noise influence, and optimal parameter selection. The complexity of image enhancement technology necessitates a careful balance between method advantages and addressing inherent limitations. Figure 7 below describes the whole framework of image enhancement techniques in the space.

In a research, Ignatov et al. (2018) proposed an innovative deep-learning solution named Weakly Supervised Photo Enhancer (WESPE), and it was aimed at automatically translating images captured by cameras with limited capabilities into high-quality DSLR-like images. Unlike previous approaches requiring extensive annotated datasets for training, WESPE operates under weak supervision, thus eliminating the need for a large set of aligned original/enhanced photo pairs. The model is trained using two distinct datasets: one from the source camera and the other comprising high-quality images sourced from the internet (even if they are visually unrelated). The primary focus of the study lies in the comprehensive evaluation of the proposed solution's performance, as which they employed standard objective metrics, conducted a subjective user study, and introduced a virtual rater in the form of a separate Convolutional Neural Network (CNN) trained on Flickr data, to mimic human raters. This virtual rater is then used to provide reference scores for both original and enhanced images. The extensive evaluation, spanning many datasets such as DPED, KITTI, Cityscapes, and images from various smartphone generations, indicated that WESPE yields comparable or even superior qualitative outcomes compared to state-of-the-art, supervised methods. By sidestepping the need for a large annotated dataset of aligned pairs, WESPE introduces a practical and efficient approach to photo enhancement, showcasing its potential for real-world application. The emphasis on thorough evaluation, incorporating both objective and subjective assessments, strengthens the credibility of their findings, providing a valuable contribution to the field of image enhancement through deep learning.

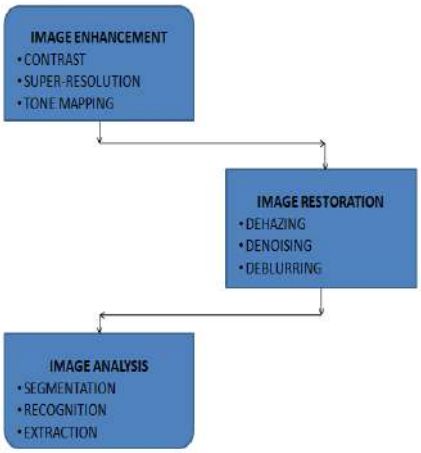

Figure 6: The Major Categories in the Field of Image Processing

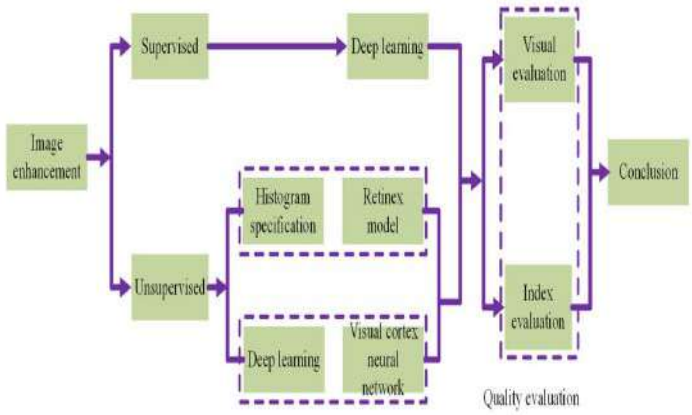

Figure 7: A Conceptual Framework of What Could Be Done During Image Enhancement

In an experiment, Asamoah et al. (2018) compared the efficacy of three image-enhancing techniques at different degrees of image defection. Three techniques were employed to improve picture contrast: contrast-limited adjusted histogram equalization (CLAHE), histogram equalization (HE), and image contrast adjustment (AHE). The Signal Noise Ratio (SNR), Image Quality Index (IQI), Similarity Index (SI), Pearson Correlation Coefficient (r), Mean Squared Error (MSE), Root Mean Squared Error (RMSE), Peak Signal Noise Ratio (PSNR), Mean Absolute Error (MAE), and Signal to Noise Ratio (SNR) are the eight enhancement parameters used in the study to evaluate the output of these three image contrast enhancement algorithms. However, special attention was paid to IQI and SI percentage values. Furthermore, after applying each image enhancement approach to the test photographs, the study visually compared the improved photos. In this experiment, the system's resilience was essentially tested using four test photos. An upgraded picture with better contrast and visualisation was the resultant output. The original test picture and its output image are then contrasted. When compared to image adjustment (AHE) and contrast limited adjustment (CLAHE) image contrast enhancement strategies, the findings demonstrated that the histogram equalisation (HE) methodology is the most effective method. The outcomes show that the histogram equalisation (HE) methodology is an excellent way to enhance images and may be applied effectively to minimise picture faults. Stated differently, it may be applied to increase the contrast and visibility of pictures. As a result, the study demonstrated that histogram equalisation is the optimal image processing technique for boosting contrast in visually weak photos. Given that the study found that the histogram equalisation technique is among the best methods for enhancing contrast in image processing, the suggested method is hence defined as one that enhances both the computer analysis and human viewers' ability to interpret and perceive information in images. It can also be inferred that effectively managing vagueness and ambiguity in a picture may be achieved by applying the histogram equalisation image-enhancing approach. Therefore, it may be advised that any system, like ultra-scan sound machines, that analyses pictures and outputs them to people for decision-making incorporate the suggested contrast enhancement approach.

Singh and Shree (2016) did a thorough comparative examination of methods for effectively eliminating noise from images, which is a difficulty made worse by changes in the surrounding environment or other variables. The main concern is noise problems that cause considerable degradation of images during capture or transmission by varying the pixel values, either by turning them on or off. The study clarifies the importance of image smoothing in image processing, where various filtering methods and algorithms are available, each with unique advantages and disadvantages based on a prior understanding of the noise. Recognising noise's critical impact on image deterioration, Singh and Shree broadened their scope by including a comparative comparison of noise reduction approaches. They stated that the image restoration process has two main stages: deterioration and restoration. The degradation model modifies the original image by adding blur and additive noise. In contrast, the restoration model uses filters to restore the degraded image (the entire process is shown in Figure 8). The goal of this second stage is to effectively eliminate blur and noise, giving an approximation of the original image. By applying previous knowledge of degradation phenomena, restoration filters aim for the best possible outcomes; specific methods work better in the frequency domain than others in the spatial domain, and the impact of restoration filters is usually

gauged by the closeness of the approximated picture to the original.Table3 depicts a summary of the different findings of this session.

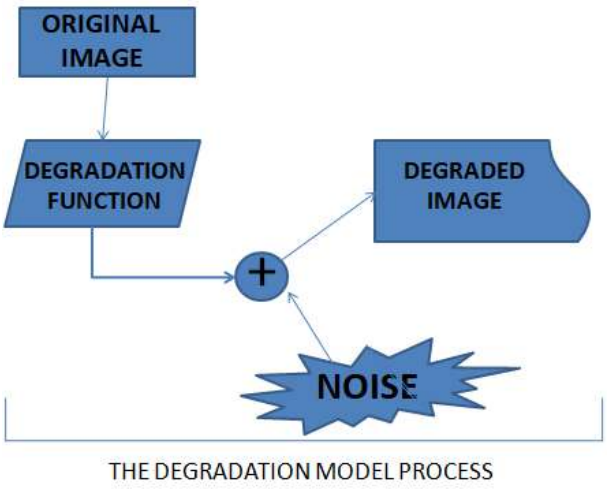

Figure 8a: The Degradation Model Process

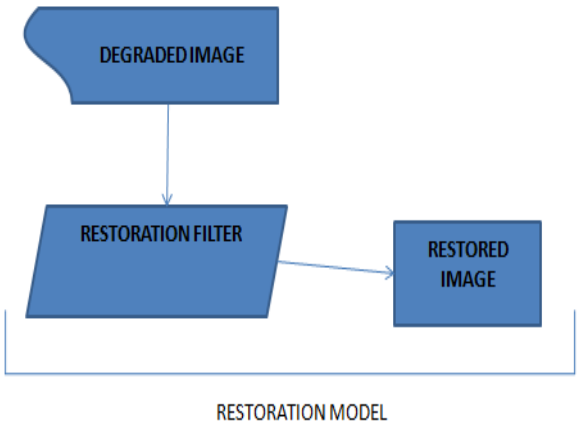

Figure 8b: The Restoration Model Process

Table 3: Further Examination of Image Capture, Preprocessing and Analysis

AUTHORS	OBJECTIVE/ PROBLEM	SOFTWARE OR TOOLS USED	FINDINGS/GAPS
Kabiraj et al., (2023)	Plate number recognition, super-resolution	SRGAN (Enhanced-Super Resolution with Generative Adversarial Network), ReLU (Rectified Linear Unit), OCR, super-resolution.	OCR accuracy drops, and ESRGAN improves.
Jin et al. (2020)	Diagnosing illnesses from facial images.	OpenCV (uses HOG features and linear SVM classifier); CNN (Deep et al.)	The results indicate that usingCNN is best for small datasets.
Zhao et al. (2021)	3D cell instance segmentation and tracking.	Voxel-Embed Algorithm; GPU with 12GB of memory; 3D datasets	Proposed approach excels with memory efficiency
Khan et al. (2022)	Improve object detection in diverse conditions.	Automatic White Balance (AWB), policy augmentations, and Image-to-Image-translation (I2IT) techniques. SSD-MobileNetV2 and the TensorFlow2 framework. Malaysia Traffic Sign Dataset (MTSD).	AWB is less effective; a combo of policy augmentation & I2IT is better.

5. CHALLENGES AND FUTURE TRENDS

Developing an automated marks collation system entails overcoming several formidable challenges. Firstly, the absence of standardised data formats in educational data management presents a significant obstacle(Fayomi et al., 2019; Okokpujie et al., 2019a; Fayomi et al., 2018a). Integrating data across systems without uniformity becomes cumbersome, potentially leading to inaccuracies and duplicates in the collation process (Khosravi et al., 2023). Secondly, the high costs of implementing advanced robotic systems pose a barrier. Beyond the financial investment, training educators to utilize these technologies effectively adds another layer of complexity, demanding resources and time (Schmidt & Tang, 2020).Moreover, image processing difficulties further complicate the development of an automated marks organization system. Defining "meaningful regions" within images and accurately representing objects remains intricate, especially in automated grade recording. These challenges highlight the need for sophisticated algorithms to accurately process and interpret visual data (Mackenzie et al., 2023).

On the brighter side, educational robotics and AI integration advancements offer promising solutions. As educational robotics revolutionizes learning experiences by equipping students with essential skills, integrating AI technologies can enhance the automation and efficiency of mark collation systems (George, 2023). Deep learning techniques, particularly entity relation extraction, demonstrate superior performance compared to traditional methods. Leveraging these advancements can streamline the collation process and improve accuracy by extracting intricate features from various data sources, including student comments. This process will enhance the educational sector for high-level performance of students evaluation process(Fayomi et al., 2018b; Okokpujie et al., 2018; Okokpujie et al., 2019b). Also, the effective collaborations of researchers in mechanical and mechatronics engineering will assist in bridging the gap of many difficulties to achieve the primary purpose of sustainable development goals in education.

6. CONCLUSION

In conclusion, this review paper has provided a comprehensive review of key concepts essential for developing a clever computerized system for compiling student marks, aligning with enhancing educational efficiency towards sustainable education. By exploring existing automated solutions for educational data management, robotics, and automation in education, image processing techniques for grade recording, and data extraction methods for student information retrieval, this review has laid a foundation for innovative advancements in educational administration.

i. By leveraging artificial intelligence (AI) and robotics solutions for administrative optimization, this review paper directly addresses the United Nations Sustainable Development Goal 4 (SDG4) of ensuring quality education. Furthermore, its implications extend to other SDGs, particularly SDG 9 (Industry, Innovation, and Infrastructure) and SDG 17 (Partnerships for the Goals), highlighting the potential for technology to revolutionise traditional processes and liberate educators' time for strategic planning and complex challenges.

ii. Synthesizing relevant research findings and identifying areas for innovation, this review paper lays a foundation for developing intelligent solutions that can transform educational administration. This review underscores the potential for technology to enhance administrative efficiency, ultimately contributing to a more sustainable and impactful educational experience.

REFERENCES

Ahmad, S. F., Alam, M. M., Rahmat, M. K., Mubarik, M. S., & Hyder, S. I. (2022). Academic and administrative role of artificial intelligence in education. *Sustainability*, *14*(3), 1101.https://doi.org/10.3390/su14031101

Alonso-Tapia, J., & Panadero, E. (2010). Effects of self-assessment scripts on self-regulation and learning. *Infancia y aprendizaje*, *33*(3), 385-397. https://doi.org/10.1174/021037010792215145

Añulika, E. A., Bala, E., &Nyap, C. D. (2014). Design and Implementation of result processing system for public secondary schools in Nigeria. *International Journal of Computer and Information Technology*, *3*(01).

Asamoah, D., Ofori, E., Opoku, S., & Danso, J. (2018). Measuring the performance of image contrast enhancement technique. *International Journal of Computer Applications*, *181*(22), 6-13.

Batista, J., Souza, D., Dos Reis, L., Barbosa, A., & Araújo, R. (2020). Dynamic model and inverse kinematic identification of a 3-DOF manipulator using RLSPSO. *Sensors*, *20*(2), 416. https://doi.org/10.3390/s20020416

Batool, S., Rashid, J., Nisar, M. W., Kim, J., Kwon, H. Y., & Hussain, A. (2023). Educational data mining to predict students' academic performance: A survey study. *Education and Information Technologies*, *28*(1), 905-971.https://doi.org/10.1007/s10639-022-11152-y

Bischoff, R., & Guhl, T. (2010). The strategic research agenda for robotics in europe [industrial activities]. *IEEE Robotics & Automation Magazine*, *17*(1), 15-16. https://doi.org/10.1109/MRA.2010.935802

Charalampous, K., Kostavelis, I., &Gasteratos, A. (2017). Recent trends in social aware robot navigation: A survey. *Robotics and Autonomous Systems*, *93*, 85-104. https://doi.org/10.1016/j.robot.2017.03.002

Chen, L., Chen, P., & Lin, Z. (2020). Artificial intelligence in education: A review. *Ieee Access*, *8*, 75264-75278. https://doi.org/10.1109/ACCESS.2020.2988510

Chitradevi, B., & Srimathi, P. (2014). An overview on image processing techniques. *International Journal of Innovative Research in Computer and Communication Engineering*, *2*(11), 6466-6472.

Demir, K. A., Döven, G., & Sezen, B. (2019). Industry 5.0 and human-robot coworking. *Procedia computer science*, *158*, 688-695.https://doi.org/10.1016/j.procs.2019.09.104

Duan, Q., Yang, Y. L., & Li, Y. (2017). Rough K-modes clustering algorithm based on entropy. *IAENG International Journal of Computer Science*, *44*(1), 13-18.

El Naqa, I., & Murphy, M. J. (2015). *What is machine learning?* (pp. 3-11). Springer International Publishing. https://doi.org/10.1007/978-3-319-18305-3_1

Fayomi, O. S. I., Okokpujie, I. P., &Fayomi, G. U. (2019). An innovation concept towards bridging the gaps between teaching and research. *Procedia Manufacturing*, *35*, 775-781.https://doi.org/10.1016/j.promfg.2019.06.022.

Fayomi, O. S. I., Okokpujie, I. P., &Kilanko, O. (2018, September). Challenges of research in contemporary Africa world. In *IOP Conference Series: Materials Science and Engineering* (Vol. 413, No. 1, p. 012078). IOP Publishing. **https://doi.org/**10.1088/1757-899X/413/1/012078

Fayomi, O. S. I., Okokpujie, I. P., & Udo, M. (2018, September). The role of research in attaining sustainable development goals. In *IOP Conference Series: Materials Science and Engineering* (Vol. 413, No. 1, p. 012002). IOP Publishing. https://doi.org/10.1088/1757-899X/413/1/012002.

Figueira, A. (2016, July). Predicting grades by principal component analysis: A data mining approach to learning analytics. In *2016 IEEE 16th International Conference on Advanced Learning Technologies (ICALT)* (pp. 465-467). IEEE.https://doi.org/10.1109/ICALT.2016.103

Forsyth, D. A., & Ponce, J. (2002). *Computer vision: a modern approach*. prentice hall professional technical reference. https://doi.org/10.1109/TIP.2023.3275535

George, A. S. (2023). Preparing Students for an AI-Driven World: Rethinking Curriculum and Pedagogy in the Age of Artificial Intelligence. *Partners Universal Innovative Research Publication*, *1*(2), 112-136.https://doi.org/10.5281/zenodo.10245675.

George, J. A., Kluger, D. T., Davis, T. S., Wendelken, S. M., Okorokova, E. V., He, Q., ... & Clark, G. A. (2019). Biomimetic sensory feedback through peripheral nerve stimulation improves dexterous use of a bionic hand. *Science Robotics*, *4*(32), eaax2352.https://doi.org/10.1126/scirobotics.aax2352

Ghazal, T. M., Hasan, M. K., Ahmad, M., Alzoubi, H. M., &Alshurideh, M. (2023). Machine Learning Approaches for Sustainable Cities Using Internet of Things. In *The Effect of Information Technology on Business and Marketing Intelligence Systems* (pp. 1969-1986). Cham: Springer International Publishing. https://doi.org/10.1007/978-3-031-12382-5_108

Gorbenko, A., Popov, V., & Sheka, A. (2012). Robot self-awareness: Exploration of internal states. *Applied Mathematical Sciences*, *6*(14), 675-688.

Hall, L. (2015). 2015 NASA Technology Roadmaps (Archive).

Hamet, P., & Tremblay, J. (2017). Artificial intelligence in medicine. *Metabolism*, *69*, S36-S40. https://doi.org/10.1016/j.metabol.2017.01.011

Hanif, R., Tariq, S., & Nadeem, M. (2011). Personal and job related predictors of teacher stress and job performance among school teachers. *Pakistan Journal of Commerce and Social Sciences (PJCSS)*, *5*(2), 319-329.

Hassel, S., & Ridout, N. (2018). An investigation of first-year students' and lecturers' expectations of university education. *Frontiers in psychology*, *8*, 2218.

Ignatov, A., Kobyshev, N., Timofte, R., Vanhoey, K., & Van Gool, L. (2018). Wespe: weakly supervised photo enhancer for digital cameras. In *Proceedings of the IEEE Conference on Computer Vision and Pattern Recognition Workshops* (pp. 691-700). https://doi.org/10.48550/arXiv.1709.01118

Jin, B., Cruz, L., & Gonçalves, N. (2020). Deep facial diagnosis: deep transfer learning from face recognition to facial diagnosis. *IEEE Access*, *8*, 123649-123661. https://doi.org/10.1109/ACCESS.2020.3005687

Kabiraj, A., Pal, D., Ganguly, D., Chatterjee, K., & Roy, S. (2023). Number plate recognition from enhanced super-resolution using generative adversarial network. *Multimedia Tools and Applications*, *82*(9), 13837-13853. https://doi.org/10.1007/s11042-022-14018-0

Kappassov, Z., Corrales, J. A., &Perdereau, V. (2015). Tactile sensing in dexterous robot hands. *Robotics and Autonomous Systems*, *74*, 195-220. http://dx.doi.org/10.1016/j.robot.2015.07.015

Kaur, P., Singh, M., & Josan, G. S. (2015). Classification and prediction based data mining algorithms to predict slow learners in education sector. *Procedia computer science*, *57*, 500-508.https://doi.org/10.1016/j.procs.2015.07.372

Kayode, G. M., & Ayodele, J. B. (2015). Impacts of teachers' time management on secondary school students' academic performance in Ekiti State, Nigeria. *International Journal of Secondary Education*, *3*(1), 1-7.http://dx.doi.org/10.11648/j.ijsedu.20150301.11

Khan, A., Shah, I. M., Khan, S., & Gul, S. (2012). Teachers' stress, performance & resources. *International Review of Social Sciences and Humanities*, *2*(2), 10-23.

Khan, M. J. K. M. B., Shah, N. M., & Mokhtar, N. (2022). Detection and classification of road signs in raining condition with limited dataset. https://doi.org/10.1007/s11760-022-02414-w

Khosravi, H., Sadiq, S., & Amer-Yahia, S. (2023). Data management of AI-powered education technologies: Challenges and opportunities. *Learning Letters*.https://doi.org/10.59453/XLUD7002

Kolbjørnsrud, V., Amico, R., & Thomas, R. J. (2016). How artificial intelligence will redefine management. *Harvard Business Review*, *2*(1), 3-10.

LeCun, Y., Bengio, Y., & Hinton, G. (2015). Deep learning. *nature*, *521*(7553), 436-444. https://doi.org/10.1038/nature14539

Lee, M. H., & Nicholls, H. R. (1999). Review Article Tactile sensing for mechatronics—a state of the art survey. *Mechatronics*, *9*(1), 1-31.https://doi.org/10.1016/S0957-4158(98)00045-2

Mackenzie, A., Lewis, E., & Loveland, J. (2023). Successes and challenges in extracting information from DICOM image databases for audit and research. *The British Journal of Radiology*, *96*(1151), 20230104.https://doi.org/10.1259/bjr.20230104.

Mahesh, B. (2020). Machine learning algorithms-a review. *International Journal of Science and Research (IJSR).[Internet]*, *9*(1), 381-386. http://dx.doi.org/10.21275/ART20203995

Martins, M. P., Miguéis, V., & Fonseca, D. (2018). Data mining educacional: umarevisão da literatura. In *13th Iberian Conference on Information Systems and Technologies (CISTI)*. Institute of Electrical and Electronics Engineers.http://dx.doi.org/10.23919/CISTI.2018.8399281

Mason, M. T. (2018). Toward robotic manipulation. *Annual Review of Control, Robotics, and Autonomous Systems*, *1*, 1-28.

Megalingam, R. K., Katta, N., Geesala, R., Yadav, P. K., & Rangaiah, R. C. (2018, December). Keyboard-based control and simulation of 6-DOF robotic arm using ROS. In *2018 4th International Conference on Computing Communication and Automation (ICCCA)* (pp. 1-5). IEEE.https://doi.org/10.1109/CCAA.2018.8777568

Okokpujie, I. P., Fayomi, O. S. I., & Leramo, R. O. (2018, September). The role of research in economic development. In *IOP Conference Series: Materials Science and Engineering* (Vol. 413, No. 1, p. 012060). IOP Publishing.https://doi.org/10.1088/1757-899X/413/1/012060.

Okokpujie, I. P., Fayomi, O. S. I., & Oyedepo, S. O. (2019b). The role of mechanical engineers in achieving sustainable development goals. *Procedia Manufacturing*, *35*, 782-788.https://doi.org/10.1016/j.promfg.2019.06.023.

Okokpujie, I. P., Fayomi, O. S. I., Ogbonnaya, S. K., &Fayomi, G. U. (2019a). The wide margin between the academic and researcher in a new age university for sustainable development. *Energy procedia*, *157*, 862-870.https://doi.org/10.1016/j.egypro.2018.11.252.

Ouyang, F., & Jiao, P. (2021). Artificial intelligence in education: The three paradigms. *Computers and Education: Artificial Intelligence*, *2*, 100020. https://doi.org/10.1016/j.caeai.2021.100020

Paneru, S., & Jeelani, I. (2021). Computer vision applications in construction: Current state, opportunities & challenges. *Automation in Construction*, *132*, 103940. https://doi.org/10.1016/j.autcon.2021.103940

Petrou, M. M., & Petrou, C. (2010). *Image processing: the fundamentals*. John Wiley & Sons.

Philipp, A., & Kunter, M. (2013). How do teachers spend their time? A study on teachers' strategies of selection, optimisation, and compensation selection, optimisation, and compensation strategies over their career cycle. *Teaching and teacher education*, *35*, 1-12. https://doi.org/10.1016/j.tate.2013.04.014

Prilop, C. N., Weber, K. E., & Kleinknecht, M. (2021). The role of expert feedback in the development of pre-service teachers' professional vision of classroom management in an online blended learning environment. *Teaching and Teacher Education*, *99*, 103276. https://doi.org/10.1016/j.tate.2020.103276

Qeshmy, D. E., Makdisi, J., da Silva, E. H. D. R., & Angelis, J. (2019). Managing human errors: Augmented reality systems as a tool in the quality journey. *Procedia Manufacturing*, *28*, 24-30.https://doi.org/10.1016/j.promfg.2018.12.005

Qi, Y., Yang, Z., Sun, W., Lou, M., Lian, J., Zhao, W., ... & Ma, Y. (2021). A comprehensive overview of image enhancement techniques. *Archives of Computational Methods in Engineering*, 1-25. https://doi.org/10.1007/s11831-021-09587-6

Rahmani, M., & Rinner, B. (2022). Towards Self-Awareness in Multi-Robot Systems. In *Proc. Austrian Robotics Workshop* (pp. 1-2).

Rana, S., & Garg, R. (2016, February). Application of hierarchical clustering algorithm to evaluate students performance of an institute. In *2016 second international conference on computational intelligence & communication technology (CICT)* (pp. 692-697). IEEE.

Saldaña, E., Siche, R., Luján, M., & Quevedo, R. (2013). Computer vision applied to the inspection and quality control of fruits and vegetables. *Brazilian journal of food technology*, *16*, 254-272. https://doi.org/10.1590/S1981-67232013005000031

Sandnes, F. E. (2023, August). FLINK: An Educator's Tool for Linking Inaccurate Student Records. In *International Conference on Innovative Technologies and Learning* (pp. 143-152). Cham: Springer Nature Switzerland.https://doi.org/10.1007/978-3-031-40113-8_14

Schipper, B. C. (2014). Awareness. *Available at SSRN 2401352*.

Schmidt, J. T., & Tang, M. (2020). Digitalization in education: challenges, trends and transformative potential. *Führen und Managen in der digitalen Transformation: Trends, Best Practices und Herausforderungen*, 287-312.

Selwyn, N., Hillman, T., BergvikenRensfeldt, A., & Perrotta, C. (2021). Digital technologies and the automation of education—key questions and concerns. *Postdigital Science and Education*, 1-10.https://doi.org/10.1007/s42438-021-00263-3

Shahriar, M. T., & Li, H. (2020). A study of image pre-processing for faster object recognition. *arXiv preprint arXiv:2011.06928*. https://doi.org/10.48550/arXiv.2011.06928

Sharma, M., Liang, J., Zhao, J., LaGrassa, A., & Kroemer, O. (2020). Learning to compose hierarchical object-centric controllers for robotic manipulation. *arXiv preprint arXiv:2011.04627*.https://doi.org/10.48550/arXiv.2011.04627

Silva, C. (2014). Does education matter. Vocational education and social mobility strategies in young people of Barcelona and Lisbon. A comparative study. ULHT, 94.

Silva, C., & Fonseca, J. (2017). Educational data mining: a literature review. *Europe and MENA Cooperation advances in information and communication technologies*, 87-94.https://doi.org/10.1007/978-3-319-46568-5_9

Singh, P., & Shree, R. (2016). A comparative study to noise models and image restoration techniques. *International Journal of Computer Applications*, *149*(1), 18-27.

Singh, S. P., Malik, S., & Singh, P. (2016). Research paper factors affecting academic performance of students. *Indian Journal of Research*, *5*(4), 176-178.

Sivasakthi, M. (2017, November). Classification and prediction based data mining algorithms to predict students' introductory programming performance. In *2017 International Conference on Inventive Computing and Informatics (ICICI)* (pp. 346-350). IEEE.https://doi.org/10.1109/ICICI.2017.8365371

Talasaz, A., Trejos, A. L., & Patel, R. V. (2016). The role of direct and visual force feedback in suturing using a 7-DOF dual-arm teleoperated system. *IEEE transactions on haptics*, *10*(2), 276-287.https://doi.org/10.1109/TOH.2016.2616874

Tang, F. (2015, October). Design on Registration and Query System for Sports Test Scores of Students. In *International Conference on Education, Management and Information Technology* (pp. 690-694). Atlantis Press.https://doi.org/10.2991/icemit-15.2015.142

Toennies, K. D., & Toennies, K. D. (2012). Image Storage and Transfer. *Guide to Medical Image Analysis: Methods and Algorithms*, 83-109. https://doi.org/10.1007/978-1-4471-2751-2_3

Touzet, C. F. (2000). Robot awareness in cooperative mobile robot learning. *Autonomous Robots*, *8*, 87-97. https://doi.org/10.1023/A:1008945119734

United Nations Department of Economic and Social Affairs. (2023). *The Sustainable Development Goals Report 2023: Special Edition*. UN.

Upadhyay, N., & Katiyar, V. (2014). A survey on the classification techniques in educational data mining. *International Journal of Computer Applications Technology and Research*, *3*(11), 725-728.

Valle, G., Mazzoni, A., Iberite, F., D'Anna, E., Strauss, I., Granata, G., ... &Micera, S. (2018). Biomimetic intraneural sensory feedback enhances sensation naturalness, tactile sensitivity, and manual dexterity in a bidirectional prosthesis. *Neuron*, *100*(1), 37-45. https://doi.org/10.1016/j.neuron.2018.08.033

Van Tuijl, B. A. J., Tielen, A. P. M., Mencarelli, A., & Hemming, J. (2018). Structured design of a novel end-effector for a bush trimming robot. In *Proceedings of the European Conference on Agricultural Engineering AgEng2018* (pp. 188-196). Wageningen University & Research.

Wiley, V., & Lucas, T. (2018). Computer vision and image processing: a paper review. *International Journal of Artificial Intelligence Research*, *2*(1), 29-36. https://doi.org/10.29099/ijair.v2i1.42

Wong, C. C., Chen, C. J., Wong, K. Y., & Feng, H. M. (2023). Implementation of a Real-Time Object Pick-and-Place System Based on a Changing Strategy for Rapidly-Exploring Random Tree. *Sensors*, *23*(10), 4814.https://doi.org/10.3390/s23104814

Xiao, W., Ji, P., & Hu, J. (2022). A survey on educational data mining methods used for predicting students' performance. *Engineering Reports*, *4*(5), e12482.https://doi.org/10.1002/eng2.12482

Zabalza, J., Fei, Z., Wong, C., Yan, Y., Mineo, C., Yang, E., ... & Ren, J. (2019). Smart sensing and adaptive reasoning for enabling industrial robots with interactive human-robot capabilities in dynamic environments—A case study. *Sensors*, *19*(6), 1354.https://doi.org/10.3390/s19061354

Zaffar, M., Hashmani, M. A., & Savita, K. S. (2017, November). Performance analysis of feature selection algorithm for educational data mining. In *2017 IEEE conference on big data and analytics (ICBDA)* (pp. 7-12). IEEE.https://doi.org/10.1109/ICBDAA.2017.8284099

Zhao, M., Liu, Q., Jha, A., Deng, R., Yao, T., Mahadevan-Jansen, A., ... & Huo, Y. (2021). VoxelEmbed: 3D instance segmentation and tracking with voxel embedding based deep learning. In *Machine Learning in Medical Imaging: 12th International Workshop, MLMI 2021, Held in Conjunction with MICCAI 2021, Strasbourg, France, September 27, 2021, Proceedings 12* (pp. 437-446). Springer International Publishing. https://doi.org/10.1007/978-3-030-87589-3_45

PAPER 53 - INTEGRATION OF AI ALGORITHM INTO EDGE DEVICES FOR PREDICTIVE MAINTENANCE OF INFRASTRUCTURE IN SMART CITIES

D. A. Opeyemi

Department of Civil Engineering, Olusegun Agagu University of Science & Technology, Okitipupa, Ondo State, Nigeria.
Email: da.opeyemi@oaustech.edu.ng

ABSTRACT
As AI continues to evolve, there are new/emerging areas of research for leveraging AI in smart cities and infrastructure to enhance United Nations Sustainable Development Goals to meet the needs of humanity and the society. One of the key research areas is edge computing and AI, it represents the ongoing evolution of AI in smart cities and infrastructure, focused on addressing complex challenges and maximizing the benefits of AI technology for infrastructure maintenance and sustainable development. This paper presents overview of integration of AI algorithms directly into edge devices to ensure efficient and effective deployment. The integration of AI algorithms into edge devices are discussed, which involves several steps and considerations ranging from understanding what edge computing is, choice of suitable edge devices, selection of AI models, AI model optimisation, model deployment, development of data processing and inference, integration of edge devices with appropriate connectivity solutions, implementation of robust security measures to protect AI models, data, and communications on edge devices, and finally to the setting up of monitoring and management systems to monitor the performance of AI models on edge devices. AI on edge devices enables real-time monitoring of infrastructure health, detecting anomalies promptly to prevent potential failures.

KEYWORDS: AI, edge devices, predictive maintenance, smart cities, infrastructure, algorithm

1. INTRODUCTION

The United States Community Analysis Bureau in the 1960s and 1970s used databases, aerial photography and cluster analysis to collect data. Also directed resources and issued reports in order to direct services, mitigate against disasters and reduce poverty, leading to a conception and creation of first smart cities. Furthermore, technology providers seeking to understand the implications of technology on daily life, came up with how smart technologies and other innovations could create joined-up municipal solutions, thereby becoming the second generation of smart city. Finally, the third generation of smart city took the control away from technology providers and city leaders, instead creating a model that involved the public and enabled social inclusion and community engagement.This third generation model was adopted by Vienna, who created a partnership with the local Wien Energy company, allowing citizens to invest in local solar plants as well as working with the public to resolve gender equality and affordable housing issues (ESC, 2016). Such adoption has continued around the world, including in Vancouver, where 30,000 citizens co-created the Vancouver Greenest City 2020 Action Plan.

In the last 50 years, according to WESS, 2013, the world population has grown exponentially at an average rate of 1.2% per year. In 2007, for the first time in the history of mankind, the number of people living in cities surpassed the number of people living in rural areas. It is estimated that the proportion will exceed 70% by 2050. As the UN World Economic and Social Survey 2013 suggested, Africa, Asia, and other developing regions will be housing an estimate of 80% of the world's urban population in the coming years. In the period from 1950 to 2010, small cities saw a net increase of 1.3 billion people, while medium cities (632 million) and large cities (570 million) saw about half as much growth.

Given the avenues of socio-economic development that urban areas have to offer, migration to urban cities has become synonymous to opportunities and prosperity for millions of people around the world. As a result, urban areas are getting more and more congested. Along with the associated natural population growth, local and national policies, and environmental changes, urban migration and congestion are expected to be continuous trends (WESS, 2013).
While urbanization brings advantages, it also brings challenges. Rapid urbanization adds pressure to the resource base, and increases demand for energy, water, and sanitation, as well as for public services, education, and health care. Consequently, social, economic, and environmental issues have become tightly interconnected. Cities greatly contribute to environmental degradation on local, regional, and global scales. Studies have demonstrated that they

are accountable for 70% of global greenhouse gas emissions as well as 60-80% (un.org) of global energy consumption (unhabitant.org).

To make the cities sustainable under such aforementioned conditions, cities become smarter by efficient management of resources and infrastructure, greener environment, and smart governance resulting in a better quality of living of its citizens. All of which can be enhanced by the effective use of AI to carry out predictive maintenance of infrastructure (Carvalho *et al.*, 2019). AI driven predictive maintenance can monitor the condition of infrastructure assets such as roads, bridges, utilities, etc. by analyzing data from edge devices and historical maintenance records. It can predict failures before they occur, saving time and money. Therefore, the integration of AI algorithms directly into edge devices to ensure efficient and effective deployment is pivotal in the maintenance of infrastructure (Cardoso and Ferreira, 2020). By strategically implementing AI in this area, smart cities can improve efficiency, sustainability, and quality of life for residents while optimizing resource utilization and reducing environmental impact (Adunadepo and Sunday, 2016).

AI code for infrastructure maintenance in smart cities typically involves predictive maintenance algorithms that analyze data from sensors and historical maintenance records to predict failures before they occur. Common physical and service infrastructures include: smart energy, smart buildings, smart transportation, smart water, smart waste, smart physical safety and security, smart health care and smart education (Kussl and Wald, 2023; Herath and Mittal, 2022; IBM, 2012; ITU-T, 2014).

2. MATERIALS AND METHODS

Edge computing plays a crucial role in enabling distributed, efficient, and responsive computing environments, particularly in scenarios where low latency, high availability, and real-time processing are essential.

By following the overview process, highlighted steps shown below, and considering the specific requirements of the edge environment, one can effectively integrate AI algorithms directly into edge devices for various applications such as real-time analytics, predictive maintenance, intelligent surveillance, and IoT automation.

Edge Computing

Edge computing refers to processing data closer to the source of generation, i.e., at the edge of the network rather than in a centralized cloud. This reduces latency, conserves bandwidth, and enhances privacy. Understanding edge computing concepts is fundamental to integrating AI at the edge.

Edge devices encompass a wide range of hardware and devices that are situated at the edge of a network and can perform computing tasks locally. These devices typically collect, process, and transmit data to centralized systems or other edge devices. A list of common edge devices are Internet of Things (IoT) devices (Park *et al.*, 2018), Edge Servers, Gateways, Edge Routers, Embedded Systems, Industrial Controllers, Smart Cameras, Edge Computing Devices, Mobile Devices, Unmanned Aerial Vehicles (UAVs) or drones, and Wearable Devices. These are just some examples of edge devices, and the list continues to expand as technology evolves and new devices are developed to support edge computing and AI applications.

Edge computing is a distributed computing paradigm that brings computation and data storage closer to the location where it is needed, rather than relying solely on centralized data centers or cloud services. In edge computing, data processing occurs near the edge of the network, often on devices such as IoT devices, edge servers, gateways, and other edge devices. This approach aims to reduce latency, conserve bandwidth, improve application performance, and enhance data privacy and security.

Choice of Suitable Edge Devices

The next task is to identify the edge devices suitable for hosting AI algorithms. These could include IoT devices, sensors, cameras, edge servers, or even smartphones with sufficient computational power and memory capacity to run AI models.

Choosing a suitable edge device for predictive maintenance of infrastructure in smart cities depends on various factors such as the complexity of the predictive models, the amount of data to be processed, the required computational power, and the specific infrastructure assets being monitored. Here are some suitable edge devices for predictive maintenance in smart cities: Edge Servers, Industrial IoT Gateways, Embedded Systems, Edge Computing Platforms, Edge AI Devices, and Cloud-Managed Edge Devices. Ultimately, the choice of a suitable edge device for predictive maintenance depends on the specific use case, budget considerations, scalability requirements, and integration with existing infrastructure and data systems within smart cities. It is essential to evaluate factors like processing power, connectivity options, data storage capacity, and security features when selecting an edge device for predictive maintenance applications.

Selection of AI Models

Choose AI models that are optimized for edge deployment. This typically involves selecting lightweight models with lower computational and memory requirements, such as MobileNets, TinyML models, or quantized versions of larger models like TensorFlow Lite or ONNX Runtime models (Ouadah *et al.*, 2022; Achouch, *et al.*, 2022).
The best AI model for predictive maintenance of infrastructure depends on various factors such as the type of infrastructure, the availability and quality of data, computational resources, and the specific goals of the predictive maintenance strategy. However, some commonly used AI models and techniques for predictive maintenance in infrastructure include Machine Learning Models, Deep Learning Models, Hybrid Models, Time Series Forecasting Models, and Anomaly Detection Techniques. It is important to note that the best AI model for predictive maintenance may vary depending on the specific infrastructure assets, data characteristics, maintenance requirements, and available resources. It is often beneficial to experiment with different models, conduct thorough validation and testing, and consider domain expertise when designing a predictive maintenance system for infrastructure in smart cities.

Model Optimization
Optimize the chosen AI models in the above further to reduce their size and computational complexity. Techniques such as model pruning, quantization, and knowledge distillation can help in creating smaller and faster models suitable for edge devices.
AI model optimization for predictive maintenance of infrastructure in smart cities involves improving the performance, efficiency, and scalability of AI models used for predicting equipment failures, identifying maintenance needs, and optimizing maintenance schedules (Ren, 2021). Here are key strategies and techniques for AI model optimization in predictive maintenance: feature engineering; data preprocessing; model selection; hyperparameter tuning; model training; model evaluation; feature selection; model compression; ensemble learning; and continuous monitoring and updating. By implementing these AI model optimization strategies, organizations can enhance the effectiveness of predictive maintenance solutions in smart cities, leading to improved asset reliability, reduced downtime, optimized resource allocation, and cost savings.

Edge Device Software Environment
Set up the software environment on edge devices to support AI model deployment. This may involve installing frameworks or specialized libraries designed for edge AI, along with any necessary dependencies (Jung *et al.*, 2020).
Setting up the edge device software environment for predictive maintenance of infrastructure in smart cities involves configuring the necessary software components, tools, libraries, and dependencies on the edge devices to enable AI-based predictive maintenance capabilities. Highlighted below are the key steps and components involved in the edge device software environment setup: Ensure that the edge device is running a suitable operating system that supports the required software and libraries for AI model deployment and execution. Install and configure AI frameworks and libraries for developing, training, and deploying predictive maintenance models on the edge device. If using a dedicated edge computing platform, follow the platform's installation and setup instructions to deploy AI models, manage resources, and monitor performance on the edge device. Use tools and frameworks for deploying AI models on edge devices efficiently. Set up data pipelines and preprocessing routines on the edge device to ingest, preprocess, and prepare data for AI model inference. Configure the edge device to perform AI model inference and prediction based on incoming data from sensors, IoT devices, or data streams. Ensure that the edge device is properly connected to the network and integrated with other edge devices, gateways, cloud services, or central servers as needed (Park *et al.*, 2018). Implement robust security measures on the edge device, including data encryption, secure boot processes, access controls, and authentication mechanisms. Set up monitoring and management tools to track the performance of AI models, monitor resource utilization, detect anomalies, and troubleshoot issues on the edge device. Lastly, establish procedures for continuous updates, maintenance, and version control of software components, AI models, and dependencies on the edge device.
By following these steps and configuring the edge device software environment accordingly, organizations can deploy and operate AI-driven predictive maintenance solutions effectively on edge devices within smart cities' infrastructure.

Model Deployment
Deploy the optimized AI models onto the edge devices. This can be done using deployment tools provided by AI frameworks or through custom scripts tailored to the target edge device platform.
Deploying an optimized AI model onto an edge device for predictive maintenance in smart cities involves several steps to ensure successful deployment and efficient operation. A general guide on how to deploy an optimized AI model onto an edge device is: prepare the optimized AI model, configure edge device, package, and deploy model, integrate with data sources, testing and validation, monitoring and maintenance, security and access controls, and scalability and flexibility. By following these steps and best practices, organizations can effectively deploy

optimized AI models onto edge devices for predictive maintenance in smart cities, enabling proactive asset management, reduced downtime, and optimized maintenance workflows (Cheng *et al.*, 2020).

Data Preprocessing and Inference

Develop data preprocessing pipelines on edge devices to prepare input data for AI models. Implement inference mechanisms that allow edge devices to run predictions based on incoming data from sensors, cameras, or other sources.

Developing data preprocessing and inference pipelines for predictive maintenance of infrastructure in smart cities involves several steps to prepare input data, perform feature engineering, run predictive models, and generate actionable insights. To develop data preprocessing and inference for predictive maintenance, a quick guide is outlined below: Gather relevant data sources for predictive maintenance, including sensor readings, maintenance logs, historical failure data, environmental factors, and operational parameters. Perform data cleaning to handle missing values, outliers, and inconsistencies in the data. Use techniques such as imputation, filtering, and data validation to ensure data quality. Identify and engineer relevant features from raw data that can serve as input variables for predictive maintenance models. Implement preprocessing steps such as scaling, normalization, encoding categorical variables, time-series aggregation, and feature extraction based on the specific predictive maintenance requirements. Evaluate model performance using appropriate metrics on validation datasets to assess predictive capabilities and generalization. Configure thresholds, rules, or decision logic to interpret model predictions and trigger maintenance actions, notifications, or alarms based on predicted outcomes, Optimize computational resources, memory usage, and processing speed to handle large volumes of data and ensure timely predictions for proactive maintenance actions. Monitor key metrics such as processing time, resource utilization, and prediction accuracy. Finally, enable seamless communication and collaboration between data scientists, maintenance teams, and stakeholders to facilitate proactive maintenance planning and execution, By following these steps and best practices, organizations can develop robust data preprocessing and inference pipelines for predictive maintenance of infrastructure in smart cities, enabling data-driven decision-making, optimized asset management, and reduced downtime.

Integration with Edge Connectivity:

Integrate edge devices with appropriate connectivity solutions to facilitate data exchange with other devices, cloud services, or central servers.

Integrating edge devices with appropriate connectivity solutions for predictive maintenance of infrastructure in smart cities involves selecting suitable communication protocols, networking technologies, and connectivity options to enable seamless data exchange, real-time monitoring, and remote management. Here is a guide on how to integrate edge devices with connectivity solutions: Identify the specific connectivity requirements for edge devices involved in predictive maintenance, including data transmission rates, latency constraints, reliability, scalability, and security considerations. Choose appropriate communication protocols based on the nature of data, communication patterns, and network environments. Evaluate networking technologies and connectivity options suitable for edge devices, such as Wi-Fi, Ethernet, cellular (4G/5G), etc. If using edge gateways or intermediate devices, configure and integrate them with edge devices to manage connectivity, protocol translation, data aggregation, and secure communication. Consider network segmentation, firewall rules, intrusion detection systems, and security best practices for securing edge device connectivity in smart city environments. Apply data compression techniques and optimization strategies to minimize data transmission overhead, reduce bandwidth usage, and improve communication efficiency. Configure quality of service parameters such as message priority, delivery guarantees, and network bandwidth allocation based on the importance and urgency of predictive maintenance data. Set up remote monitoring and management capabilities for edge devices to monitor connectivity status, network performance, data throughput, and device health. Implement load balancing, failover mechanisms, and redundant network paths to ensure high availability, fault tolerance, and continuous operation of predictive maintenance systems in smart cities. Furthermore, follow best practices and guidelines from industry organizations to ensure compliance and adherence to quality standards in connectivity implementations. By following these steps and considerations, organizations can effectively integrate edge devices with appropriate connectivity solutions for predictive maintenance of infrastructure in smart cities, enabling efficient data exchange, real-time monitoring, and proactive maintenance actions.

Security and Privacy

Implement robust security measures to protect AI models, data, and communications on edge devices is very crucial. The use of encryption, authentication mechanisms, secure boot processes, and access controls to prevent unauthorized access and data breaches are mandatory (Khan and Salah, 2018).

Implementing robust security measures is very crucial to protect AI models, data, and infrastructure in smart cities from potential cyber threats, unauthorized access, data breaches, and malicious attacks. The key strategies and best practices for implementing security measures in predictive maintenance systems are briefly described here: Implement encryption protocols for secure communication between edge devices, servers, and cloud platforms. Implement strict access controls and authentication mechanisms to ensure that only authorized users and devices can access AI models, data repositories, and maintenance systems. Use secure communication protocols for transmitting data between edge devices, gateways, and backend systems. Ensure that communication channels are encrypted and authenticated. Regularly update firmware and software components on edge devices to patch security vulnerabilities, improve performance, and ensure compliance with security standards. Practice data minimization by collecting and storing only necessary data for predictive maintenance purposes. Implement network segmentation to segregate critical infrastructure assets, AI models, and data repositories from less secure network segments. Deploy intrusion detection systems and intrusion prevention systems to monitor network traffic, detect suspicious activities, and block malicious attempts to access or exploit vulnerabilities. Store backup data securely in off-site locations or cloud storage with encryption and access controls. Conduct regular security audits, vulnerability assessments, and penetration testing to identify and remediate security weaknesses in AI models, infrastructure components, and data handling processes. Last but not the least, provide cybersecurity training and awareness programs for employees, contractors, and stakeholders involved in managing and operating predictive maintenance systems, By implementing these robust security measures and best practices, organizations can enhance the resilience, integrity, and confidentiality of AI models, data, and infrastructure in smart cities, mitigating cybersecurity risks and ensuring trusted operation of predictive maintenance systems.

Monitoring and Management

The concluding process of effectively integrating AI algorithms directly into edge devices for various applications such as real-time analytics, predictive maintenance, intelligent surveillance, etc. is monitoring and management. Set up monitoring and management systems to monitor the performance of AI models on edge devices, track resource utilization, detect anomalies, and remotely manage edge deployments as needed.

Setting up monitoring and management systems to monitor the performance of AI models on edge devices involves implementing tools, metrics, logging mechanisms, and alerting systems to track key performance indicators, resource utilization, and inference outcomes. Here is a step-by-step guide to set up effective monitoring and management for AI models on edge devices: Establish baseline performance metrics and thresholds to monitor deviations, anomalies, and performance degradation. Choose suitable monitoring tools, platforms, or frameworks for monitoring AI model performance on edge devices. Implement logging libraries, frameworks,etc. within AI model code to record timestamped logs and performance data during inference. Aggregate and centralize performance data from multiple edge devices using centralized monitoring servers, cloud platforms, or edge-to-cloud architectures. Customize dashboards with widgets, widgets, and alerts to track critical KPIs, detect anomalies, and identify performance bottlenecks on edge devices. Set up alerts for abnormal behavior, performance deviations, model failures, or system errors. Use analytics tools, machine learning algorithms, and anomaly detection techniques to analyze performance data, detect patterns, and predict future performance trends. Use predictive analytics, workload profiling, and performance modeling to forecast resource needs, plan upgrades, and optimize edge device infrastructure for efficient AI model execution. Incorporate user feedback, operational insights, and lessons learned from monitoring into ongoing performance improvement initiatives for edge devices and AI models. By following these steps and best practices, organizations can set up effective monitoring and management systems to monitor the performance of AI models on edge devices, optimize resource utilization, ensure reliable inference outcomes, and proactively address performance issues in smart city infrastructure.

3. PREDICTIVE MAINTENANCE AI ALGORITHM

Infrastructure maintenance in smart cities typically involves predictive maintenance algorithms that analyze data from sensors and historical maintenance records to predict failures before they occur. A simplified typical example of AI algorithms to be integrated directly into edge devices using Python and the scikit-learn library for machine learning can be written as follows:

AI Algorithm to be Integrated into Edge Devices

```
import pandas as pd
from sklearn.model_selection import train_test_split
from sklearn.ensemble import RandomForestClassifier
from sklearn.metrics import accuracy_score

# Load historical maintenance data
data = pd.read_csv('maintenance_data.csv')
```

```
# Preprocess data
X = data.drop('failure', axis=1) # Features (sensor readings, maintenance history, etc.)
y = data['failure'] # Target variable (1 for failure, 0 for no failure)

# Split data into training and testing sets
X_train, X_test, y_train, y_test = train_test_split(X, y, test_size=0.2, random_state=42)

# Train a Random Forest Classifier
clf = RandomForestClassifier(n_estimators=100, random_state=42)
clf.fit(X_train, y_train)

# Make predictions on the test set
predictions = clf.predict(X_test)

# Evaluate model performance
accuracy = accuracy_score(y_test, predictions)
print(f'Accuracy: {accuracy}')

# Use the trained model for predictive maintenance
new_data = pd.read_csv('new_sensor_data.csv') # New sensor data for prediction
new_predictions = clf.predict(new_data)

# Output the predictions for maintenance scheduling
print('Predicted maintenance schedule:')
for index, prediction in enumerate(new_predictions):
if prediction == 1:
print(f'Asset {index + 1}: Maintenance required')
else:
print(f'Asset {index + 1}: No maintenance needed')
```

The description that could be used to effectively convey the sequential steps involved in integrating AI into edge devices is shown in Fig. 1 below.

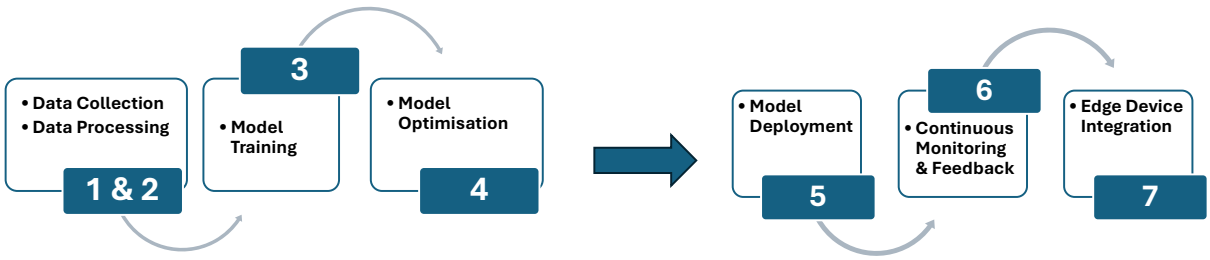

Figure 1: Steps involved in the AI integration into Edge Devices

4. CONCLUSION

Integrating AI algorithms into edge devices for predictive maintenance of infrastructure offers a transformative approach with several noteworthy conclusions such as: AI on edge devices enables real-time monitoring of infrastructure health, detecting anomalies promptly to prevent potential failures. By minimizing the need for constant human intervention and enabling predictive maintenance, AI-driven edge devices can significantly reduce operational costs. Predictive maintenance ensures higher reliability of critical infrastructure, minimizing downtime and enhancing overall performance. Ensuring robust data privacy and security measures is crucial when deploying AI on edge devices, safeguarding sensitive information, and preventing unauthorized access. AI algorithms on edge devices offer scalability and flexibility, adapting to diverse infrastructure types and evolving maintenance requirements. Enhanced data analytics and AI capabilities empower better decision-making processes, optimizing maintenance schedules and resource allocation. Efficient maintenance through AI-driven edge devices can contribute to reduced environmental impact by minimizing resource wastage and energy consumption.

In conclusion, the integration of AI algorithms in edge devices for predictive maintenance heralds a new era of proactive infrastructure management, offering unprecedented efficiency, reliability, and sustainability benefits.

REFERENCES

Achouch, M.; Dimitrova, M.; Ziane, K.; Sattarpanah Karganroudi, S.; Dhouib, R.; Ibrahim, H.; & Adda, M. (2022). On predictive maintenance in industry 4.0: Overview, models, and challenges. *Appl. Sci*. 2022, 12, 8081.

Adunadepo, A. M. D., & Sunday, O. (2016,. February). Artificial intelligence for sustainable development of intelligent buildings. In Proceedings of the 9th CIDB Postgraduate Conference, Cape Town, South Africa (pp. 1–4).

Cardoso, D. & Ferreira, L. (2020). Application of predictive maintenance concepts using artificial intelligence tools. *Appl. Sci*. 2020, 11, 18.

Carvalho, T.P.; Soares, F.A.; Vita, R.; Francisco, R.D.; Basto, J.P.; Alcalá, S.G. A systematic literature review of machine learning methods applied to predictive maintenance. Comput. Ind. Eng. 2019, 137, 106024.

Cheng, J.C.P.; Chen, W.; Chen, K.; & Wang, Q. (2020). Data-driven predictive maintenance planning framework for MEP components based on BIM and IoT using machine learning algorithms. Autom. Constr. 2020, 112, 103087.

Economic and Social Council (ECS), Commission on Science and Technology for Development Nineteenth session, Smart cities and infrastructure, Geneva, 9–13 May 2016

Herath, H.M.K.K.M.B. & Mamta Mittal (2022). Adoption of artificial intelligence in smart cities: A comprehensive review, International Journal of Information Management Data Insights, Volume 2, Issue 1, 2022, 100076, ISSN 2667-0968,

http://www.gartner.com/it-glossary/predictive-analytics/

http://www.unhabitat.org/downloads/docs/E_Hot_Cities.pdf

http://www.un.org/en/sustainablefuture/cities.shtml

IBM, Smart Education (2012). https://www.ibm.com/smarterplanet

ITU-T (2014). Focus Group on Smart Sustainable Cities: An overview of smart sustainable cities and the role of information and communication technologies

ITU-T (2015). Focus Group on Smart Sustainable Cities: Overview of smart sustainable cities infrastructure

Jung, D., Tran Tuan, V., Dai Tran, Q., Park, M. & Park, S. (2020). Conceptual framework of an intelligent decision support system for smart city disaster management, Applied Sciences, 10 (2) (2020), p. 666

Khan, M.A. & Salah, K. (2018). IoT security: Review, blockchain solutions, and open challenges, Future generation computer systems, 82 (2018), pp. 395-411

Kussl, S. & Wald, A. (2023). Smart Mobility and its Implications for Road Infrastructure Provision: A Systematic Literature Review. Sustainability 2023, 15, 210

Park, E., Del Pobil, A.P., & Kwon, S.J. (2018). The role of Internet of Things (IoT) in smart cities: Technology roadmap-oriented approaches, Sustainability, 10 (5) (2018), p. 1388

Ren, Y. (2021). Optimizing predictive maintenance with machine learning for reliability improvement. ASCE-ASME J. Risk Uncertain. Eng. Syst. Part B Mech. Eng. 2021, 7, 030801

Ouadah, A.; Zemmouchi-Ghomari, L.; & Salhi, N. (2022). Selecting an appropriate supervised machine learning algorithm for predictive maintenance. Int. J. Adv. Manuf. Technol. 2022, 119, 4277–4301

WESS. (2013). http://www.un.org/en/development/desa/policy/wess/wess_current/wess2013/WESS2013.pdf

PAPER 54 - SPECTROSCOPIC PROPERTIES AND PERFORMANCE EVALUATION OF A NOVEL BIO-BASED BRAKE FLUID PRODUCED FROM ROSELLE OIL WITH COPPER OXIDE NANO ADDITIVE

U. I. Ramalan[1], M. U. Kaisan[1*], H. A. Dandajeh[2], A. S. Mohammed[1]

[1]Department of Mechanical Engineering, Ahmadu Bello University, Zaria, Nigeria.
[2]Hydraulic Equipment Development Institute, NASENI, Kano, Nigeria.
[*]Email: usmanramalanibrahim@gmail.com

ABSTRACT
A bio-based brake fluid was produced from Roselle oil with Nano copper oxide as an additive. The spectroscopic, and Physicochemical properties of the blended brake fluid were evaluated and its performance was simulated using computational fluid dynamic (CFD) on the ANSYS workbench. From the kinematic viscosity analysis, it was observed that there was a linear increase in the viscosity with an increase in the nanoparticle with a 43.3% increase in viscosity due to the inclusion of 0.3 wt.% of CuO nanoparticle. The increment is attributed to physical barriers created by the nanoparticle that generate more internal friction to the flow of oil molecules. The performance evaluation of the bio-based brake fluid under various operating conditions, including temperature, pressure, and velocity flowrate, demonstrated its ability to maintain consistent and reliable performance across a range of challenging scenarios. This finding indicates the versatility and suitability of the developed brake fluid for automotive applications. The comparison of the bio-based brake fluid with conventional brake fluid offers a clear understanding of its advantages and competitiveness, which shows that the produced bio-based brake fluid is a viable alternative in automotive applications. The production of bio-based brakefluid offers novelty in this research area and this achievement represents a significant step towards developing eco-friendly and sustainable alternatives to conventional petroleum-based brake fluids.

KEYWORDS*:* Bio-Based Brake Fluid; Simulation; Physico-chemical properties; Roselle Oil; Copper Oxide; Nanoparticle

1.0 INTRODUCTION

1.1 Background to the study

Motor vehicle brake fluids are used to deliver energy to the actuation mechanism in the hydraulic drive of a car's brake assembly and remove heat from the brake discs (Garcia-Leon *et al.*, 2023). The key criteria for braking fluids are high operating temperatures, strong low-temperature and viscosity-temperature qualities, physical and chemical stability, metal corrosion protection, inactivity concerning mechanical rubber components, and lubricating action (Astakhov, 2022). Synthetic braking fluid consists of diethylene glycol, di-, tri-, and tetraethylene glycol monoalkyl ethers. They include inhibitors that prevent corrosion of metallic brake components and minimize oxidation at high temperatures. To raise the boiling point of braking fluids, tris (methyl glycol) borates are added (Chen*et al.*, 2023). The working fluid is an essential component of machine hydraulic systems. The primary function of the working fluid is to transmit energy between the driving and driven components of a machine's drivesystem. In contemporary hydraulic systems, the working fluid serves several vital roles (Olszak *et al.*, 2020). These duties include lubricating moving components, dissipating heat, removing solid pollutantsfrom the system, sealing the system, and limiting corrosion. Kinematic viscosity, density, boiling temperature, freezing point, and specific heat are the fundamental physical properties of working fluids(Ma *et al.*, 2020). Working fluids in hydraulic systems should be anti-wear, anti-corrosive, and resistantto oxidation and thermal deterioration. Kinematic viscosity is a fundamental physical property of the working fluid; the amount of flow losses inside the hydrodynamic working region is determined by thisproperty (Olszak *et al.*, 2020). To reduce flow losses, it is recommended that working fluids have a verylow viscosity. The viscosity coefficient value is temperature-dependent. A low boiling point promotes the development of cavitation events. A large increase in the hydrodynamic clutch's operating temperature might result in a loss in working fluid quality due to oxidation and thermal degradation. This is why the working fluid should have anti-oxidative qualities to provide the requisite durability (Wong *et al.*, 2022). The working fluid in hydrodynamic clutches should be anti-foaming and anti-corrosive, as well as non-decomposable. Foaming in the working environment increases the possibilityof hydraulic fluid leaks through the sealing. Hydraulic working fluids are manufactured from oils acquired from crude oil processing. Their makers undertake attempts to develop products based on rawmaterials with reduced negative consequences on the environment (Olszak *et al.*, 2020). For a variety of reasons, employing water in hydrokinetic systems outperforms oil. Water's viscosity is substantially lower than that of oils, it is unaffected by temperature, and its thermal conductivity is five times that ofoil. Water does not offer a fire or explosive risk. The primary drawbacks of restricting the use of waterin hydraulic systems are a restricted range of operating temperatures, corrosion of steel (which commonly makes up the elements of hydraulic systems), and low lubricity (Manring and Fales, 2019). However, the lower limits of the working temperature can be moved by employing additives that reduce thewater's freezing point. Corrosion can be prevented by utilizing stainless steel or anticorrosion coatingson normal steel. The most recent form of working fluid utilized in hydraulic devices, including hydrodynamic clutches, is the two-component fluid, primarily electrorheological fluids (Olszak *et al.*, 2020). The solid phase of electrorheological fluids is made up of organic or inorganic particles that may readily be polarized by an electric field. Mineral oils, plant oils, liquid paraffins, and kerosene are examples of nonconductive liquids in the liquid phase. The following additives are utilized to improve the electrorheological effect: water, acids, inorganic salts, alcohol, and esters. Natural goods such as starch,cellulose, resins, and rubber are used in the solid phase of electrorheological fluids to minimize non-ecological content. A two-component electrorheological fluid composed of starch and silicon oil is commonly utilized. Aside from culinary uses, oils, and vegetable fats, as well as their derivatives, are key raw materials in a variety of industries.

Cosmetics, medicines, biofuels, paints, adhesives, coatings,surfactants, solvents, and adjuvants are some of the applications for it (Srivastava *et al.*, 2022). Plant oil-based products are safe for the environment and human health, and they are often biodegradable (Salih and Salimon 2021). Plant oils have been used as braking fluid for centuries, extending back to the use of olive oil in antiquity. This work evaluated the potential of a Roselle oil-based brake fluid with Nano copper oxide additive, The Roselle oil was obtained from the market, and the base oil was characterized by its spectroscopic properties before the formulation. The base oil was blended with some varying weight percent of Nanocopper particles through ultra-sonication. The Nano-based fluid was then subjected to various characterization as well as simulation. The results obtained from the physicochemical properties of the bio-based brake fluid were compared with the conventional brake fluid (ASTM standards).

1.2 Aim and Objectives

This research aims to develop and characterize a bio-based brake fluid using roselle oil with Nano copper oxide additive and simulate its performance under different operating conditions.

The specific objectives are to:

i. Develop bio-based brake fluid from Roselle oil and synthesize, characterize the Nano copper oxide additive for the brake fluid.
ii. Determine the physio-chemical, spectrochemical, and tribological properties of the developed brake fluid
iii. Evaluate the performance of roselle oil-based bio-based brake fluid with Nano copper oxide additive under different operating conditions.
iv. Compare the performance of the developed roselle oil-based bio-based brake fluid with the conventional brake fluid.

2.0 THEORETICAL ANALYSIS

2.1 Hydraulic braking system

A hydraulic braking system in automobiles is the brake operating system that uses fluid for its operation. It is a highly efficient braking system. It is a self-lubrication system hence no external lubrication is required (Gatti *et al.*, 2023). In this system, with less effort, we can achieve high braking force. The hydraulic braking system works on the principle of Pascal's

The hydraulic braking system in automobiles is a highly efficient braking mechanism that relies on fluid for its operation. This system is designed to be self-lubricating, eliminating the need for external lubrication. As a result, it offers convenience and reduces maintenance requirements. One of the significant advantages of the hydraulic braking system is its ability to achieve high braking force with minimal effort (Saiteja *et al.*, 2022). The functionality of the hydraulic braking system is based on Pascal's Law, as described by (Kumar *et al.*, 2021). Pascal's Law states that in a confined fluid system, any pressure applied at one point is transmitted equally in all directions. In the context of the braking system, when the brake pedal is depressed, the force is transferred through the brake fluid to the brake calipers, leading to the application of braking force on the wheels. This principle ensures consistent and reliable braking performance. Overall, the hydraulic braking system stands as a reliable and effective solution for automobile braking, making driving safer and more manageable (Hua *et al.*, 2023).

PASCAL'S LAW: - The Pascal law states that "Pressure at any point in a static fluid is equal in all directions". Hence, Pascal's law is used in the hydraulic braking system to apply the brake (Ravikumar, 2022).

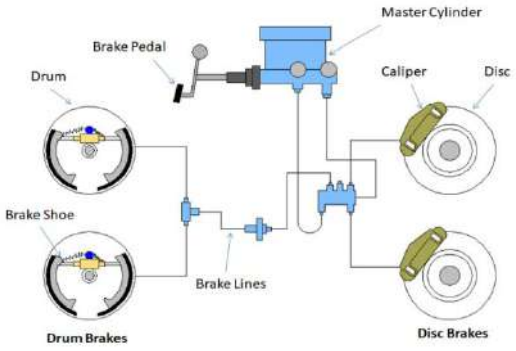

Figure 1: Hydraulic Braking System (Source: www.mechanicalboosters.com)

2.1.2 The principle of operation of the hydraulic braking system

When the driver presses the brake pedal, the piston presses the oil inside the master cylinder. Oil flows from the master cylinder to cylinder 2 through a pipeline. Now, Oil enters inside cylinder 2. Hence each piston expands due to oil pressure. Due to piston movement, brake shoes expand inside the brake drum. Therefore, due to friction between the shoes & brake drum, the wheel stops (Hilgers, 2023).

When the driver presses the brake pedal, it activates the master cylinder, causing the piston inside it to pressurize the brake fluid. This pressurized brake fluid then flows through a pipeline to cylinder 2. As the brake fluid enters cylinder 2, it exerts pressure on each piston, causing it to expand. The movement of the pistons, in turn, leads to the expansion of the brake shoes inside the brake drum.

With the brake shoes expanding against the inner surface of the brake drum, friction is generated, resulting in the wheels coming to a stop. This frictional force between the brake shoes and the brake drum is what enables the braking action and brings the vehicle to a halt (Hilgers, 2023)

When the driver presses the brake pedal, it activates the master cylinder, causing the piston inside it to pressurize the brake fluid. This pressurized brake fluid then flows through a pipeline to cylinder 2. As the brake fluid enters cylinder 2, it exerts pressure on each piston, causing it to expand. The movement of the pistons, in turn, leads to the expansion of the brake shoes inside the brake drum.

With the brake shoes expanding against the inner surface of the brake drum, friction is generated, resulting in the wheels coming to a stop. This frictional force between the brake shoes and the brake drum is what enables the braking action and brings the vehicle to a halt (Hilgers, 2023).

2.2 Brake Fluid Basics

Brake fluid is possibly the single most neglected component of the automobile. Most high-performance drivers check their tire pressures and change their engine oil at frequent intervals, but virtually no one ever changes the brake fluid in their street car. The function of brake fluid is to provide an incompressible medium to transmit the driver's foot pressure on the brake pedal through the master cylinder(s) to the calipers to clamp the friction material against the discs (Levy *et al.*, 2020). The foot pressure is multiplied by the mechanical pedal ratio and the hydraulic ratio of the master cylinders, booster (if used), and caliper piston(s). This is a simple concept when fresh, all brake fluids are virtually incompressible and the system works as well as its mechanical and hydraulic design allows. There can be, however, significant problems in the proper functioning of brake fluid (Kershaw, 2023). Overheated brake fluid can (and will) boil in the caliper. Boiling produces gas bubbles within any boiling fluid. Gas is compressible so boiling brake fluid leads to a "soft" brake pedal with long travel. In extreme cases, overheated brake fluid necessitates "pumping the brake pedal" to get a pedal at all (Hilgers, 2023). Brake fluids are classified by both "dry boiling point" and "wet boiling point". They are also classified by the US Department of Transportation (DOT) rating, DOT 3, DOT 4, DOT 5, and DOT 5.1. The U.S. Government specifications for brake fluid, FMVSS 116, do not dictate the chemical composition of a given classification, or "grade" of brake fluid. Instead, FMVSS116 defines the properties of the fluid, such as dry and wet boiling points (referred to as the equilibrium reflux boiling points, dry and wet), the viscosity of the brake fluid grade at certain temperatures, high-temperature stability, corrosion characteristics, and the effects of the fluid on seals, as well as other physical properties like the tendency to jell or separate (called stratification) or form sludge and/or crystalline deposits (Schroeder *et al.*, 2019). Boiling point and viscosity are the most relevant properties to most consumers, including high-performance customers. Viscosity is an important factor for proper operation of ABS and Active Handling Control systems on modern vehicles since in most cases the pressure and volume of fluid transferred is not measured. Instead, flow through a valve with a given orifice size over time is the control mechanism, so fluid maximum viscosity is a key characteristic (Yadav and Kale, 2020)

2.2.1 Dot 3 brake fluids

These Brake fluids are usually glycol ether-based, but as stated earlier, that is not because they are required to be (Mwanakasale *et al.*). The brake fluid industry has determined by consensus that glycol ether fluids are the most economical way to meet the requirements. By definition, DOT 3 fluids must have a minimum dry boiling point (measured with 0 percent water by volume) of 401°F and a minimum wet boiling point (measured with 3.7 percent water by volume) of 284°F. The specification says little more as far as the performance enthusiast is concerned (Pillay and Dhanale, 2019).

2.2.2 Dot 4 brake fluids

These brake fluids are also glycol ether-based, but have a measure of borate esters added for improved properties including increased dry and wet boiling points. A seldom talked about characteristic is that because of this chemistry, the DOT 4 fluid will have a more stable and higher boiling point during the early portion of its life, but ironically once the fluid does actually begin to absorb water its boiling point will typically fall off more rapidly than a typical DOT 3. By FMVSS116 standards, DOT 4 fluids must have a minimum dry boiling point of 446°F and a minimum wet boiling point of 311°F. DOT 4 is the grade applicable to the most race-engineered brake fluid in the world today, especially regarding viscosity limit. Note that although the DOT 4 designation has a minimum dry and wet boiling point, a DOT 4 racing brake fluid may have a dry boiling point over 600F. Its viscosity is challenged, however, to be under the viscosity limit of 1,800 mm^2/sec. Some claimed racing brake fluids exceed this important limit. Caution should be exercised if these fluids are used in race cars with ABS systems. This does not mean that DOT 4 fluids are necessarily better than DOT 3 fluids. Remember, the boiling points listed are minimums. There are certain DOT 3 fluids with higher boiling points than some DOT 4 fluids. The real differentiating factor is that DOT 4 fluid should be changed more often than a DOT 3 fluid, because of the effects and rates of water absorption (Verhagen and Kelarakis, 2020)

2.2.3 Dot 5 brake fluid

The original DOT 5 fluid specification was expected to be fulfilled by silicone-based (SSBF) composition. It was designed for use in applications where its resistance to water absorption (and therefore low corrosion) was desired - like in military equipment (Oladele *et al.*, 2020). It has also found use in antique cars because it does not dissolve paint finishes. With SSBF, unfortunately, these characteristics were only achieved by unacceptably high compressibility.

As such, the DOT 5 grade SSBF is of little value to any conventional automotive or high-performance application. Subsequently, there have been non-silicon-based fluids developed that meet DOT 5 wet and dry boiling point specifications and viscosity requirements. They are referred to as DOT 5.1 grade fluids, remember that the specifications are minimums and therefore the non-SSBF DOT 5 fluids do not offer the highest boiling points available. There are no DOT 5.1 brake fluids that exceed the dry and wet boiling points of the best currently available DOT 4 racing brake formulas (Campaoa *et al.*, 2023). They do meet the lower viscosity specifications, however. One last note on the DOT ratings: Systems designed for a particular type of fluid (especially before the wide distribution and use of DOT 4 fluids) should continue to be filled with that fluid. For example, in a car that was delivered with DOT 3 fluid, the internal components of the system (seals, brake hoses, and fittings for example) were specifically designed and tested for compatibility with the chemical composition of DOT 3 fluid. Because the DOT 4 grade fluid typically contains a different chemical composition, the compatibility of system components may be an issue (Guo *et al.*, 2021).

2.3 Roselle (Hibiscus sabdariffa L.)

Roselle (Hibiscus sabdariffa L.), a member of the Malvaceae family, is a significant annual crop cultivated successfully in tropical and sub-tropical climates (Arowosafe *et al.*, 2022). Globally, there are more than 300 species of hibiscus, and one of them is Roselle (Hibiscus sabdariffa Linn.). Roselle oil, derived from the seeds of the Roselle plant, is an essential oil highly valued for its medicinal, culinary, and industrial applications. The oil is extracted through a process called cold-pressing, ensuring that its natural properties remain preserved as no heat is involved in the extraction method. The Roselle plant, also known as Hibiscus or Sorrel, is a tropical shrub that serves various purposes. Two main types of Roselle are recognized: Hibiscus sabdariffa var altissma and Hibiscus sabdariffa var sabdariffa (Geja and Kassahun, 2020). The former, altissma, is a nearly branchless variety that can reach a height of 3-5 meters. Its flowers are yellow, and the calyces are red or green. Although it has a high fiber content, it is not typically used for food. The latter, sabdariffa, grows in a bushy manner with multiple branches. Its flowers are either axillaries or found in terminal racemes, characterized by white petals with a reddish center at the base of the stamina column. The calyx enlarges as the plant matures. Var. Altissima is economically significant for its jute-like fiber and is cultivated in India, the East Indies, Nigeria, and South America. Var. sabdariffa, on the other hand, is exploited for its calyces and fiber (Chin, 2022).

Figure 2: A. Roselle plant and B. Seed and Oil

3.0 MATERIALS AND METHODS/METHODOLOGY/EXPERIMENTAL PROCEDURE

This section should include apparatus and equipment setup, work materials, design, experimental methods, problem formulation, etc, as applicable.

3.1 Materials

The materials required to carry out this research include Roselle bio-based oil (sourced from a farm center in Kano State, Nigeria), Copper acetate, Sodium hydroxide, Oleic acid, Ethanol, Phosphoric acid, (purchased from local stores in Zaria, Nigeria) and Aluminium-Silica Alloy.

3.2 Determination of Free Fatty Acid

1g of oil sample was weighed in a conical flask. 2.5 ml of propane-2-ol was used to dissolve theoil in the sample. Then, two drops of phenolphthalein were added to the mixture. Two additional solutions were made in a conical flask using the same process as before, resulting inthree solutions. 0.1M of KOH was put into the burette and titrated against the biodiesel oil samples. After seeing a color charge from yellow to pink, the beginning and final measurements were recorded, followed by the total average titer value (Animasaun *et al.*, 2021). The acidvalue was estimated using Equations 1 and 2.

$$Acid\ value = \frac{molar\ mass\ of\ KOH \times titre\ value}{mass\ of\ oil} \quad (1)$$

$$FFA = \frac{Acid\ value}{2} \quad (2)$$

3.3 Esterification of Roselle oil

In one experiment, 900g of roselle oil was measured and weighed in a conical flask with a weighing balance. The conical flask containing the oil sample was heated to 60 ℃ using a magnetic stirrer. Afterstarting the agitation and heating, Equations 3 and 4 were used to compute 143.8g of methanol and 3.2g of sulfuric acid. Then, both solutions were added to the flask.

$$Amount\ of\ Methane = 2.25\ \times \%FFA\ \times mass\ of\ oil \quad (3)$$

$$\text{Amount of sulphuric acid } = 0.05 \times \%\text{FFA} \times \text{mass of oil} \quad (4)$$

Where: Mass of oil =1g; Molarity of KOH =0.1m; Mass of KOH =56.1g

After one hour of continuous agitation at 60 ℃, the mixture was transferred to a separating funnel andallowed to settle. Over time, methanol, water, and H_2SO_4 separated to the upper section of the separating funnel, leaving the denser oil at the bottom. This enabled simple separation and the oil was then carefully emptied into a clean, conical flask. The pretreatment esterification procedure was designed to lower the proportion of Free Fatty Acids (FFA) in the oil to less than or equal to 0.5%. This esterification method most likely comprised the interaction of roselle oil with methanol and sulfuric acid, resulting in the creation of esters and water-soluble components that could be extracted from the oil. This step is critical in preparing the oil for subsequent processing or usage because lower quantities of free fatty acids are often needed for varioususes (Edwin *et al.*, 2023).

3.4 Transesterification Process of the Esterified oil

Following a successful esterification process in which the proportion of Free Fatty Acids (FFA) was decreased to less than 0.5 percent, a transesterification phase was performed. The technique sought to turn the esterified oil into biodiesel (Hani *et al.*, 2021). 15% methanol and 1% catalyst (NaOH) were measured and weighed. The estimated quantity of NaOH was mixed with the measured methanol. Themethanol-NaOH solution was mixed with 900 g of esterified oil. The resultant mixture was placed ona magnetic stirrer set to 60°C for agitation and heating. This state was maintained for one hour, which aided the transesterification process. Following the reaction, the solution was transferred to a separator funnel. It was left to stand for a while, and the denserglycerol settled to the bottom due to its higher density than the biodiesel. The denser glycerol layer wasdrained via the separating funnel. After removing the glycerol, the lighter biodiesel layer was carefullydrained into a clean conical flask. This complete technique guaranteed that the esterified oil was successfully converted into biodiesel and that the various products were efficiently separated.

3.5 Synthesis of Copper Oxide Nanoparticles

A multi-step technique was used to synthesize CuO nanoparticles and then modify their surfaces. A round bottom flask was used to make an aqueous solution containing 0.03 mol of copper acetate. 1.2 mL of glacial acetic acid was added to the copper acetate solution. The mixture was heated to 100°C while continuously stirring. To the heated solution, add 0.5 g of NaOH until the pH reaches 7. This resulted in the development of a large volume of black precipitate. The black precipitate was separatedby centrifugation and rinsed four times with deionized water. The washed precipitate was dried in openair for 24 hours. The surface of the CuO nanoparticles was changed to facilitate mixing. To enhance the interfacial characteristics of the mixes, oleic acid was chemically adsorbed as a carboxylate onto the nanoparticle surface. Initially, 6g of nanoparticles were dispersed in 400 mL of warmed ethanol (60°C). Stirring was done for 15 minutes to ensure uniform dispersion. Following dispersion, 0.27 mL of oleic acid was added and the solution was agitated for 2 hours. The solution wasthen centrifuged to separate the ethanol and oleic acid combination. The obtained nanoparticle materialwas baked in an oven at 75 degrees Celsius to eliminate excess surfactant (Adekunle and Oparanti, 2023). This process, reported by (Patel *et al.*, 2022), included several precise stages to synthesize and alter the CuO nanoparticles for future blending and application as part of the Nano-brake fluid.

3.6 Nano Brake Fluid Formulation

The Nano-brake fluid was developed by synthesizing four separate samples, each of which had treated CuO nanoparticles (NP) distributed in bio-based oil. These nanoparticles were introduced at varying weight percentages, ranging from 0.1 to 0.3 wt. percent, with intervals of 0.1 wt. (Reddy *et al.*, 2023). The obtained samples are labeled as shown in Table 1. An ultrasonication procedure was used to disperse nanoparticles inside the base oil in these three samples. The ultrasonication technique lasted three hours, with 90-minute intervals throughout. The sonication was carried out at a frequency of 59 Hz, using 100% power and maintaining a temperature of 75°C (Putnik *et al.*, 2020). The major purpose of this stage was to ensure that nanoparticles were thoroughly mixed and evenly distributed inside the base oil. Following the sonication procedure, the resultant mixes were vacuum-dried for a predetermined time. This drying technique was intended to minimize the impacts of gas bubbles and moisture created during the sonication process (Kutlu *et al.*, 2022). The goal of this rigorous method was to generate homogeneous and stable formulations of the Nano-brake fluid samplesfor further testing and assessment (Patel *et al.*, 2022).

Table 1: Sample Description

Sample Code	Description
Base Oil	Roselle oil
NBF 1	Ester + 0.1% CuONP
NBF 2	Ester + 02%CuONP
NBF 3	Ester + 0.3%CuONP

3.7 TEM characterization

A TEM method was used to thoroughly investigate the morphology of copper oxide (CuO) nanoparticles after surface modification (Ansari *et al.*, 2022). These investigations were performed to have a better knowledge of the nanoparticles' properties.

3.8 Determination of Physicochemical Properties

3.8.1 Specific gravity

The specific gravity of both the base oil and Nano brake fluid samples was determined using an electronic weighing balance. The computation of specific gravity was performed according to the equation expressed as 6 (Dharmegowda, 2022). The ASTM D1298 standard was followed for thismeasurement, specifying that the specific gravity of a brake fluid should be determined under atmospheric conditions. important to note that specific gravity is a dimensionless quantity (WOMA,2021). Specific gravity is a key property that provides insights into the density and weight of a substancecompared to the density of a reference material, often water. This measurement is useful in understanding the relative heaviness or lightness of different substances, including brake fluid, and behave under various conditions (Ilie and Cristescu, 2023).

$$Specific\ gravity = \frac{W_2 - W_1}{W_3 - W_1} \quad 5$$

3.8.2 Kinematics viscosity

The viscosities of the Nano brake fluid samples were determined using a viscometer bath. Each samplewas immersed in a constant temperature bath set at 100 °C. The viscosity measurement was conductedby the ASTM D445 method and utilized a calibrated viscometer (Huang D, 2020). The calibrationconstants for the viscometer were specified as 0.08867 and 0.74020. Viscosity is a critical property of brake fluid that reflects their flow characteristics and resistance to shear forces under differentconditions (De, 2023). Measuring viscosity at distinct temperatures provides valuable insights into howa brake fluid's viscosity changes with temperature variations, which can be crucial for understanding its performance across different operational environments (Agrawal and Khairnar, 2022).

3.9 Spectroscopic Analysis

The spectroscopic analysis of both the base oil and the newly formulated Nano brake fluid was conducted using different techniques, which include Fourier Transform Infrared (FTIR) spectroscopy,and Gas Chromatography (GC). These techniques were adopted from the approach outlined by (Bonnar,2023) and were utilized to gain insights into the samples' chemical composition and structural characteristics. FTIR spectroscopy provides information about the functional groups present in the molecules by analyzing their vibrational modes. This technique is particularly useful for identifying various chemical bonds and groups within the samples. Gas Chromatography (GC) was used for separating and analyzing the individual components of a complex mixture. Bypassing the sample through a chromatographic column, different components are separated based on their interactions with the stationary phase, providing data about the sample's composition.

3.10 Thermal Analysis

The base oil's oxidative stability and the best sample's physicochemical and tribological properties wereassessed using a Perkin-Elmer differential scanning calorimeter DSC-7. The equipment underwent calibration using pure indium, and the baseline was established using an empty open aluminum pan (Fatahi *et al.*, 2023). Into open aluminum pans, oil samples weighing 5.0 ± 0.5 mg were placed and positioned within the equipment's sample chamber. The isothermal temperature was programmed across four distinct levels (110, 120, 130, and 140 °C), with purified oxygen (99.8%) being circulatedthrough the sample's enclosure at a rate of 50 ml/min (Skornia, 2020).

3.11Modelling and simulation

3.11.1 CAD modelling and simplification of a brake fluid

CAD (Computer-Aided Design) modelling and simplification of a brake fluid system involve creating a 3D representation of the system components and simplifying the geometry as needed foranalysis or simulation purposes. An overview of the process:

1. Begin by identifying the components that make up the brake fluid system, such as calipers, rotors, brake pads, fluid channels, reservoirs, and lines. Gather relevant dimensions and specifications for each component.
2. Select a suitable CAD software package that supports 3D modelling.Popular options include SolidWorks 2019 vision. Familiarize yourself with the software's features and tools.
3. Start a new project in the CAD software and set the appropriate units and scale for your design.
4. Begin modelling each component of the brake fluid system by creating 3D geometries based on the gathered dimensions and specifications. Use appropriate tools such as sketches, extrusions, sweeps, and fillets to accurately represent the geometry.
5. Assemble the individual components to create a complete representation of the brake fluid system as shown in Plate 1 (a and b). Ensure that the connections, alignments, and clearances between components are accurately modeled.
6. Depending on the complexity of the simulation or analysis you plan to perform; it may be necessary to simplify the geometry of the brake fluid system. This can involve removing small details, simplifying intricate features, or creating simplified versions of certain components while still preserving their essential functionality.
7. Validate the simplified model (see Plate 1c) by comparing itwith the original design and ensuring that it retains the critical features necessary for accurate analysis. Consult with domain experts or engineering standards to determine acceptable levelsof simplification for your specific simulation objectives.
8. Save your CAD model in the appropriate file format for the software (step)

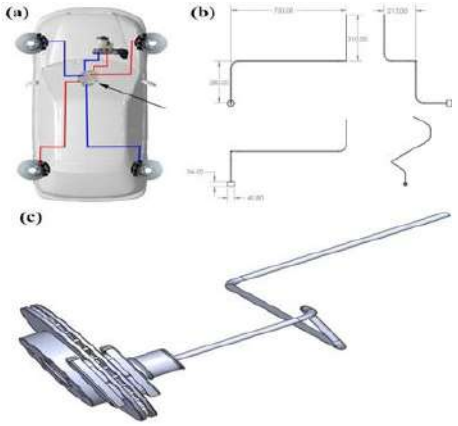

Plate 1: (a) Honda Civic, CR-X 1991 Model Brake System (b) Dimension for the brake fluid line system (c) 3D model of the brake fluid system, caliper, piston, and brake dis

3.11. 2 Numerical simulation

Numerical simulation of a brake fluid involves using computational fluid dynamics (CFD) techniques to simulate the flow, heat transfer, and other relevant phenomena occurring within a brake system. An overview of the steps involved in conducting a numerical simulation of a brake fluid:

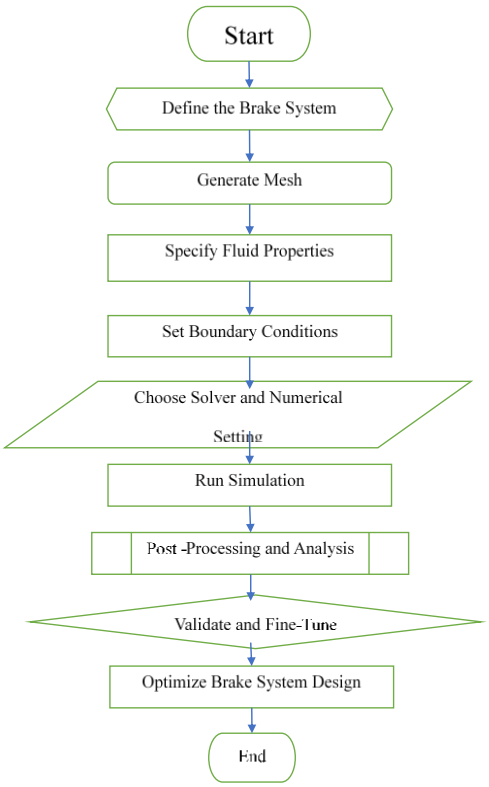

Figure 3: Simulation Experimental Flowchart

1. Clearly define the objectives of the simulation, such as analyzing the flow characteristics, temperature distribution, pressure drop, or other specific parameters within the brake system**.**
2. Create a 3D model of the brake system geometry as shown in Plate 2 using CAD software or import a pre-existing model. Next, generate a computational mesh that discretizes the geometry into small elements or cells, ensuring appropriate resolutionnear critical areas such as gaps, contact surfaces, and boundary layers. The nodes and elements for mesh information are 134243 and 584906

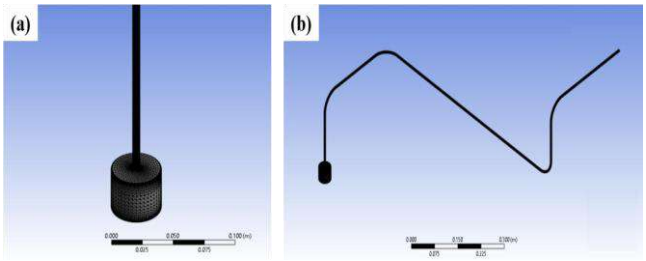

Plate 2: 3D model of the brake system geometry

3. Choose a suitable CFD solver, such as ANSYS Fluent based on the complexity and requirements of the simulation. Set numerical settings, such as theturbulence model, discretization schemes, time step (for transient simulations), and convergence criteria.
4. Define the properties of the brake fluid, including density, and viscosity. These properties can be obtained from the manufacturer's datasheet or through experimental measurements.
5. Define the boundary conditions for the simulation. This includes specifying the inlet velocity or pressure, outlet conditions (e.g., pressure or flow rate), as well as any additional conditions required for specific components or areas of interest within the brake system, and the inlet pressure for the brake fluid 3.447MP
6. Choose a suitable CFD solver, such as ANSYS Fluent based on the complexity and requirements of the simulation. Set numerical settings, such as theturbulence model, discretization schemes, time step (for transient simulations), andconvergence criteria.
7. Launch the simulation using the selected solver and numerical settings. Monitor the convergence of the solution by observing residuals or other convergence indicators.Adjust settings as necessary to ensure a converged and accurate solution.

8. Once the simulation is complete, analyze the results to extract the desired information. This may include visualizing velocity and pressure contours, temperature distribution, pressure drop, or other relevant parameters. Consider using post-processing tools within the CFD software or exporting data for further analysis in dedicated visualization software.
9. Validate the simulation results against experimental data or known benchmarks to assess the accuracy and reliability of the model. Make any necessary adjustments to the geometry, boundary conditions, or fluid properties based on the validation results. Additionally, use the simulation results to optimize the brake system design, such as improving flow efficiency or heat dissipation.
10. If required, iterate through the simulation process, making refinements to the model, mesh, or simulation settings to achieve more accurate and reliable results

4.0 RESULTS AND DISCUSSION

4.1 TEM Analysis

The TEM results revealed important information on the nanoscale characteristics and distribution of nanoparticles inside the oil matrix. The TEM images shown in Plate 3 (a and b) demonstrated the spatial organization and dispersion of the CuO nanoparticles. The photos show the nanoparticles as black patches against a lighter backdrop, indicating an electron density contrast similar to what Stewart *et al.* found (2021). Plate 3 shows that the nanoparticles are uniformly dispersed throughout the epoxidized Roselle oil matrix, indicating good integration and dispersion. In addition to dispersion, TEM enabled the investigation of nanoparticle size and form. The observation in Plate 3 (a and b) demonstrates the spherical nature of the nanoparticles. Furthermore, the shape and morphology of the nanoparticles were evaluated, revealing information about their structure as observed by Jhaveri et al (2021). Furthermore, even though the particles were more spherical, the size ranges demonstrate that the bulk of the particles were less than 20nm in diameter. CuO nanoparticles in epoxidized Roselle oil exhibit a predominant spherical form, suggesting effective production and integration. Furthermore, the lack of particle clustering or agglomeration when dispersed in oil demonstrates the successful preparation of the Nano particle-reinforced bio-based brake fluid, which is critical for obtaining desirable characteristics and performance gains, as reported by Kamarulzaman et al (2023). Controlled particle size and restricted size dispersion are critical for ensuring consistent material characteristics. Furthermore, the spherical form of the nanoparticles improves compatibility and interfacial interactions within the composite, which influences the material's properties.

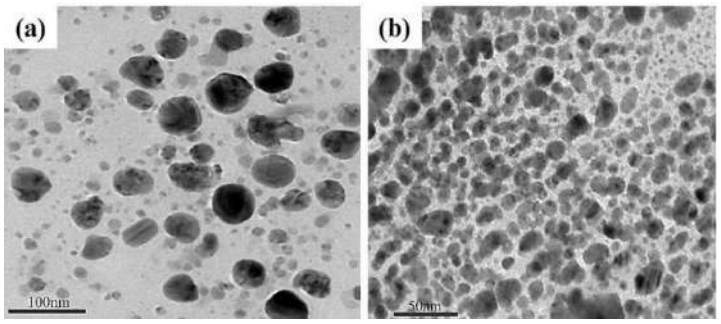

Plate 3: TEM of Nano Particles at (a) 100nm(b) 50nm

4.2 Specific Gravity

Figure 2 shows the effect of increasing copper oxide nanoparticles on the specific gravity of the Roselle oil. CuO nanoparticles have a higher density than the esterified Roselle oil, so adding the nanoparticles increases the overall density of the mixture, and therefore, increases the specific gravity as observed by Salgado *et al.* (2021). However, the magnitude of this effect would depend on the concentration of the nanoparticles. At lower concentrations, the effect on the specific gravity was relatively small, but at higher concentrations, the effect became more pronounced. It is also possible that the inclusion of CuO nanoparticles could affect the surface properties of the blended Roselle oil, which could affect its specific gravity as observed by Praveenkumar *et al.* (2023). For example, if the nanoparticles form clusters or aggregates at the surface of the oil, this increases its effective density and leads to a higher specific gravity. The highest specific gravity of 0.8586 was observed at 0.2 wt.% inclusion of the CuO nanoparticle as reported by Cruz (2019).

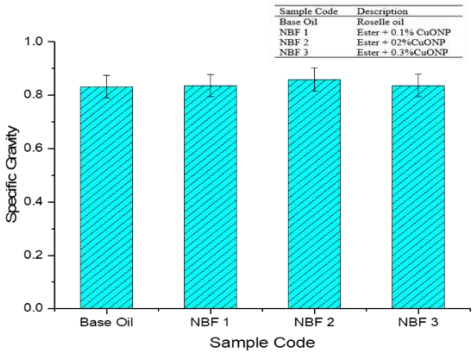

Figure 2: The specific gravity of Roselle oil containing CuO nanoparticles.

4.3 Kinematic Viscosity at 100℃

Figure 3 shows the kinematic viscosity of the blended brake fluid at 100 ℃ which presents the viscous behavior of the different blended oil. It was observed that there was a linear increase in the viscosity with an increase in the nanoparticle. Generally, there was a 43.3% increase in the viscosity of the blended roselle with the inclusion of CuO nanoparticles up to 0.3%. There was a 13.6% rise in the viscosity of the roselle oil with a 0.1% inclusion of CuO at 100 ℃. A further increase shows a linear rise in the kinematic viscosity as discussed by Santhosh *et al.* (2021). The inclusion of CuO nanoparticles in Roselle oil has different effects on the viscosity of the oil, depending on several factors, such as the concentration, size, and surface properties of the nanoparticles, as well as the temperature of the system as reported by Hasanin and Youssef (2022). In general, the addition of nanoparticles increases the viscosity of the oil due to the increase in particle-to-particle interactions and the hindered flow of the oil. This effect can be more pronounced at higher nanoparticle concentrations or smaller particle sizes, where the nanoparticles can form aggregates or clusters that further increase the viscosity as observed by Jadhav *et al.* (2022). However, in some cases, the nanoparticles can also decrease the viscosity of the oil due to their ability to act as lubricants or reduce the intermolecular forces between the oil molecules. This effect can be more noticeable at low concentrations or larger particle sizes, where the nanoparticles are more dispersed and have less impact on the overall viscosity of the oil. Sample NBF 3 gave the optimum values and it was then considered for other analysis.

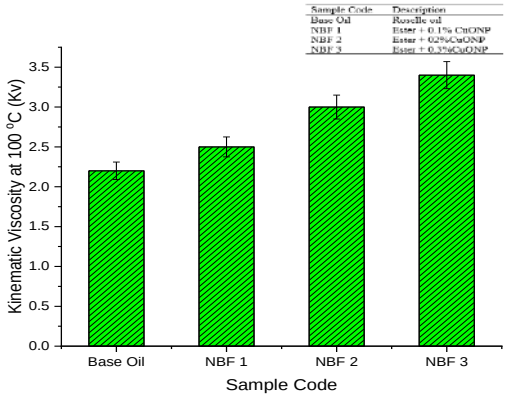

Figure 3: Kinematic Viscosity of the Developed Oil at 100℃

4.4 Thermal Analysis of Roselle Oil and its CuO Nano Particle Blends

The Differential Scanning Calorimetry (DSC) analysis was performed to evaluate the thermal propertiesof roselle oil to assess its suitability as a hydraulic oil. Hydraulic oils are essential for ensuring proper lubrication, cooling, and efficient operation of hydraulic systems. Understanding the thermal behavior of roselle oil is crucial in determining its stability and performance under high temperatures and operating conditions. The temperature range for the analysis was set from 50 °C to 500 °C. Figure 4 illustrates the obtained thermogram of roselle oil. The DSC thermogram of roselle oil exhibits several thermal transitions. The endothermic reaction observed in the temperature range of 100-200°C suggestsa phase transition or melting event within the oil. This indicates that the oil undergoes a transition froma solid or semi-solid state to a liquid state, absorbing heat from the surroundings in the process as observed by Chen *et al.* (2023). The slight exothermic reaction observed in the temperature range of 200-250°C indicates a heat-releasing process within the oil. This exothermic effect might be attributedto a minor chemical reaction or decomposition of certain components present in the oil as reported by Almoselhy (2021). However, the magnitude of this exothermic peak is relatively low (maximum of 0.15 mW/mg), indicating a relatively small amount of heat being released. As the temperature increases,a more significant endothermic reaction is observed in the temperature range of 250-300 °C. This suggests another phase transition or a change in the molecular structure of the oil, requiring the absorption of heat energy. At around 300°C, a reverse occurs with a large and significant exothermic reaction.

This exothermic effect indicates a substantial release of heat from the oil. It could be associated with a more significantchemical reaction, decomposition, or degradation of the oil's components as observed by Fakayode *et al.* (2023). The sustained exothermic behavior from 300 °C to 420 °C suggests a continuous heat-releasing process within this temperature range. Beyond 420 °C, the reaction shifts back to an endothermic character, indicating further phase transitions or changes in the oil's molecular structure that require the absorption of heat. The significant exothermic reaction observed in the temperature range of 300-420 °C indicates that roselle oil may undergo thermal degradation or decomposition at elevated temperatures. This could lead to a decrease in its stability, viscosity, and lubrication properties,which are crucial for effective brake performance as discussed by Raya *et al.* (2020). Moreover, the endothermic and exothermic reactions observed in the temperature range specific to the DSC analysis suggest complex thermal behavior and potential chemical reactions occurring within the oil. These reactions may impact the oil's stability, consistency, and reliability as a brake fluid but this is only at very y elevated temperatures which proves the suitability of the oil as a braking fluid as observed by Azarpour et al. (2022)

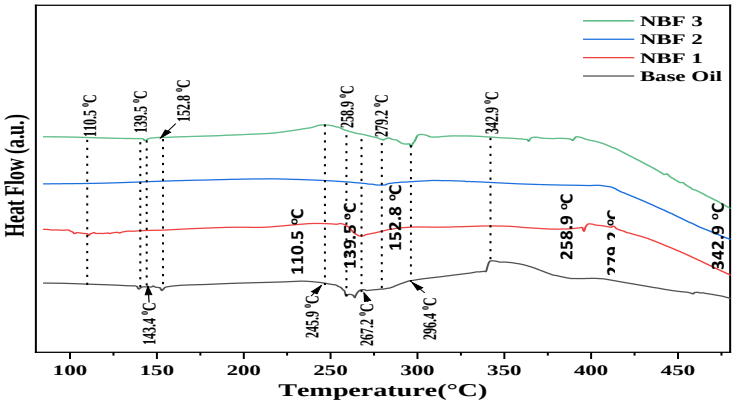

Figure 4: DSC thermogram of oil with Nano Particle Concentration

4.5 Spectroscopic Analysis

4.5.1 FTIR Analysis of the Roselle Oil and NBF3

The FTIR spectra for the Epoxidized Roselle oil and the Roselle oil with 0.3 wt.% of CuO nanoparticles are illustrated in Figure 5. The FTIR spectra observed for the two samples are similar with a distinct difference in the intensity of some bands as observed in NBF3. Within the single bond region (2500-4000 cm^{-1}), the hydroxyl group (O-H) stretching vibration was seen at 3613-3422 cm^{-1} attributed to thepresence of water content in oil. The presence of hydroxyl groups suggests that there might be residualmoisture or water content in the bio-lubricant as observed by Trejo-Coceres *et al.* (2023). The presence of peaks at 3422 cm^{-1} (indicating hydroxyl groups) in the bio-based brake fluid can potentially have several effects on its mechanical properties. The presence of these functional groups might increase theviscosity, making the fluid thicker. Higher viscosity can affect the flow and circulation of the fluid within the braking system, potentially leading to reduced brake performance and responsiveness. Brakefluids need to have high boiling points to withstand the high temperatures generated during braking asobserved by Mladenov *et al.* (2021). Also, in this region, the peak at 2925-2855 cm^{-1} corresponds to theC-H stretching vibration in methyl (-CH_3) or methylene (-CH2-) groups. It indicates the presence of aliphatic hydrocarbons in the brake fluid. Aliphatic hydrocarbons can contribute to increased viscosity,making the fluid thicker. This might affect the flow and circulation of the fluid, potentially leading to reduced brake performance and responsiveness. Aliphatic hydrocarbons can enhance the lubricating properties of the brake fluid, reducing friction and wear. Improved lubrication can positively influencethe mechanical performance and durability of the braking system. From the double bond region (1500-2000 cm^{-1}), the peak observed at 1740 cm^{-1} in the FTIR spectrum of the bio-based brake fluid suggests the presence of a carbonyl group (C=O) stretching vibration. Thepeak at 1740 cm^{-1} corresponds to the stretching vibration of the carbonyl (C=O) group. This suggests the presence of carbonyl-containing compounds, such as esters, ketones, or aldehydes, in the brake fluid. Carbonyl-containing compounds may affect the viscosity of the brake fluid as observed by Rani and Shanker (2021). The presence of certain esters or ketones can lower the viscosity, making the fluid less viscous. This can potentially improve the flow and circulation of the fluid within the braking system, leading to enhanced brake performance and responsiveness. The lubricating properties of the brake fluid can be influenced by the presence of carbonyl groups. Certain esters, for example, are knownto exhibit good lubricity, reducing friction and wear on brake components. This can positively impact the mechanical performance and durability of the braking system. The presence of carbonyl groups canalso affect the thermal properties of the brake fluid. Carbonyl-containing compounds, such as esters, tend to have relatively low boiling points compared to hydrocarbons. The presence of these compoundsin the brake fluid may contribute to a lower boiling point, potentially impacting the fluid's resistance tovaporization at high temperatures. The thermal stability of the brake fluid may be influenced by the presence of carbonyl groups (Rogulska, 2023). Some carbonyl-containing compounds, particularly aldehydes, may exhibit lower thermal stability and may be prone to degradation or chemical changes atelevated temperatures. This

can impact the overall thermal stability and performance of the brake fluidas imported by Campaoa *et al.* (2023). In the fingerprint region (600-1500 cm^{-1}), the peaks observed at 1438 cm-1 and 1461 cm^{-1} in the FTIRspectrum of the bio-based brake fluid indicate the presence of specific functional groups. Peaks at 1438cm^{-1} and 1461 cm^{-1} are typically associated with the bending vibrations of methyl (-CH3) groups. The presence of methyl groups might contribute to increased viscosity, making the fluid thicker. Higher viscosity can impact the flow and circulation of the fluid, potentially leading to reduced brake performance and responsiveness. Methyl groups can potentially enhance the lubricating properties of the brake fluid, reducing friction and wear. Improved lubrication can positively influence the mechanical performance and durability of the braking system. The presence of methyl groups might have a limited direct impact on the thermal properties of the brake fluid. However, they can indirectly influence thermal stability by contributing to the overall chemical composition and stability of the fluid.It's important to note that the concentration and nature of the methyl groups will determine the specificeffects on the mechanical and thermal properties of the brake fluid. With the fingerprint region, C-O functional group was observed at 1161 cm^{-1} which suggests a possible formation of aldehyde compoundand other secondary compounds while C-H symmetrical angular deformation was seen at 721 cm^{-1}.

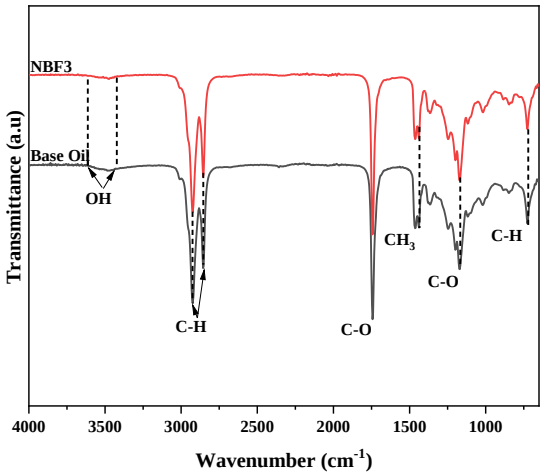

Figure 5: FTIR Spectrum of Epoxidized Roselle Oil and NBF3

4.5.2 GC-MS Analysis

From Figure 6, the dominant methyl ester is 9,12- octadecenoic acid, methyl ester, and 14- methyl pentadic-a-enoic acid methyl ester. The monounsaturated fatty acid has a low melting point which makes them suitable for usage in biofuel or biodiesel (Aslan, 2023). However, the unsaturatedcompound is prone to oxidative and rancidification (Ampofo *et al.*, 2022). The presence of saturated fatty acid helps to provide oxidative stability to the biodiesel or biofuel (Donoso *et al.*, 2020). The methyl ester present in this profile are Hexadecanoic acid, methyl ester occurring in peaks 5,6,7, and 8with a total area percentage of 7.15%, 9,12-octadecanoic acid methyl ester with an area percentage of 9.67%, 10,13-octadecadienoic acid methyl ester with 5.21%, 9,12 octadecadienoic acid methyl ester area % of 6.05%, 17-octadecanoic acid methyl ester occurring in peak 17, 27 with a total area of 3.91%,14-methyl pentadic-9-enoic acid methyl ester with area of 6.6%. In this profile, we have Saturated FattyAcid (SFA) which include (Hexadecanoic acid methyl ester, heptadecanoic acid, methyl ester, 9,12- octa-decanoic acid methyl ester) and Monounsaturated Fatty Acid (MUFA) which include (7- hexadecenoic acid, methyl ester, 17-octadecenoic acid methyl ester, 10-octadecenoic acid, methyl esterand 14- hexadecenoic -9-enoic acid methyl ester). Monounsaturated fatty acids have low melting pointswhich makes them suitable for usage in biodiesel or biofuel as observed by Arshad *et al.* (2022). However, the unsaturated compound is prone to oxidation and rancidification as reported by Jurid *et al.* (2020). The presence of saturated fatty acids helps to provide oxidation stability to the biodiesel or biofuel as observed by Adu-Mensah *et al.* (2019).

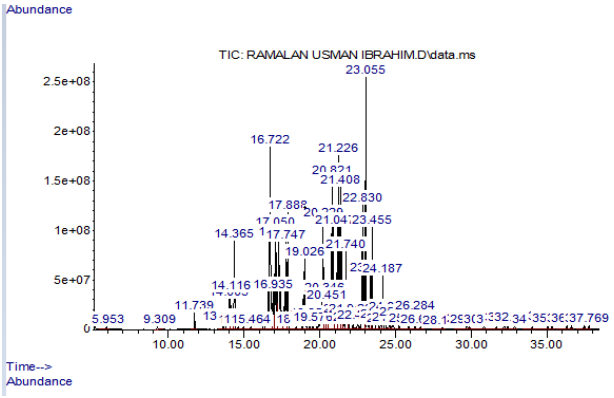

Figure 6: GC-MS spectrum of Roselle brake fluid

The GC-MS spectrum for the brake oil with the inclusion of 0.3 wt.% Cu nanoparticle is illustrated in Figure 7. The dominant methyl ester observed in the spectrum is 9-octadecenoicacid, methyl ester, (E), and Hexadecanoic acid, methyl ester. The main methyl ester compoundsseen in the profile are Hexadecanoic acid occurring in peaks 7 and 8 with a total area percentageof 28.96%, 9-Octadecenoic acid, methyl ester occurring in peaks with total area percentage of25.85%, Pentadecanoic acid, 14-methyl-, methyl ester with 7.9%, Oxiraneoctanoic acid, 3- octyl-, methyl ester with 3.53%. Similar to the profile presented in Figure 4, saturated fatty acids seen in the profile include Hexadecanoic acid methyl ester, and 9- octa-decanoic acid methyl ester. The methyl ester compound is the dominant compound in the profile as against the aldehyde compound. The addition of copper nanoparticles causes the reduction or the disappearance of some peaks. The presence of saturated fatty acids helps to provide oxidationstability to the biodiesel or biofuel as observed by Adu-Mensah *et al.* (2019)

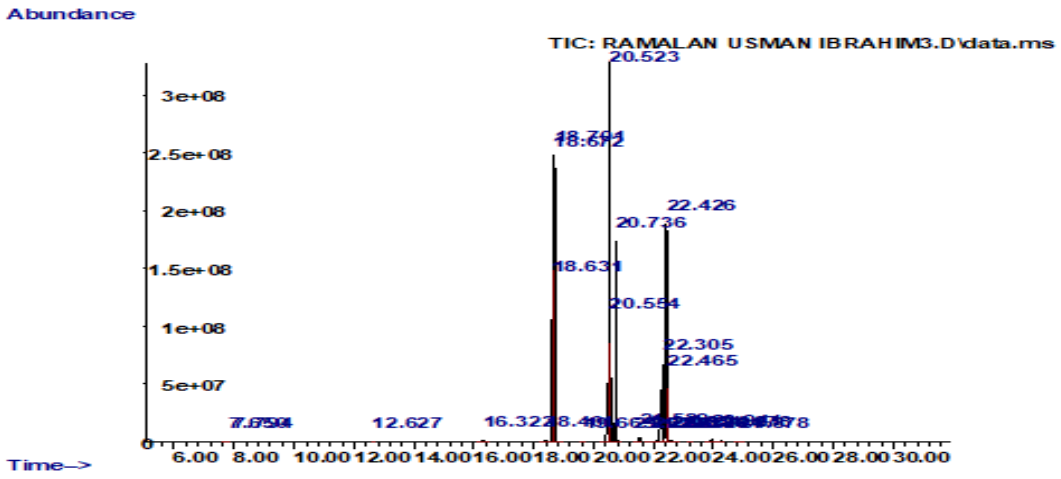

Figure 7: GC-MS spectrum of Roselle brake fluid with 0.3 wt.% Cu nanoparticles

4.6 CFD Simulation Study

4.6.1 Simulation Analysis

Contour plots illustrating the characteristics of brake line fluid for the based oil are depicted for (a) pressure, (b) temperature, and (c) velocity. Figure 8 displays the contour plots for pressure, temperature, and velocity corresponding to a pressure inlet of 3.447 MPa

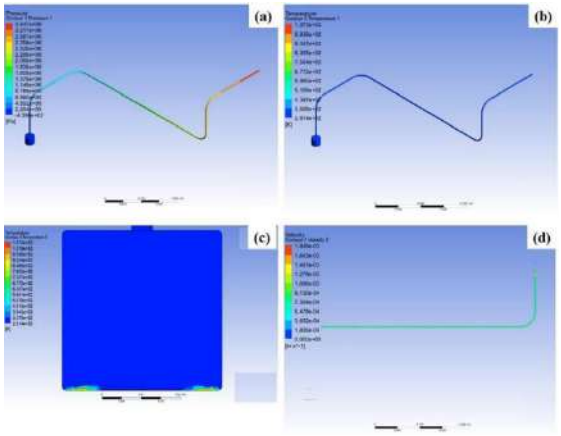

Figure 8: Roselle-based oil (a) at pressure inlet 3.447 MP (b) at temperature inlet 3.447 MPa

(c) at velocity inlet 3.447 MPa (d) complete simulation

Contour plots illustrating the characteristics of brake line fluid NBF3 at 0.3% weight concentration are depicted for (a) pressure, (b) temperature, and (c) velocity. Figure 9 displays the contour plots for pressure, temperature, and velocity corresponding to a pressure inlet of 3.447 MPa

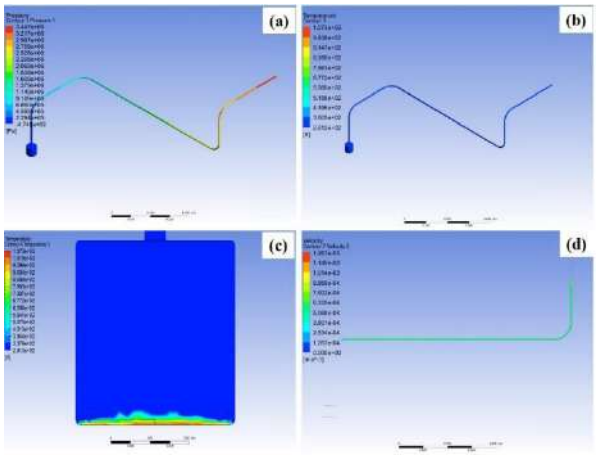

Figure 9: 0.3%wt Nano brake fluid (NBF3) (a) at pressure inlet 3.447 MPa (b) at temperatureinlet 3.447 MPa (c) at velocity inlet 3.447 MPa (d) complete simulation

4.6.2 Analysis, Validation, and Discussion

In this section, we delve into the analysis, validation, and discussion of the brake line flow model solution and the results it has yielded. The information obtained from these results holds significant importance as it offers valuable insights into the behavior of brake fluid flow within the brake line, consequently facilitating the process of designing brake fluid lines. According to Figure 8(a), the pressure inlet value was 3.447 MPa, while -4.61026 MPa was obtained as the outlet pressure. This indicates a substantial pressure reduction along the brake fluid line. The outlet pressure nearly reaches zero or even exhibits a minor negative value, which implies a significantpressure decrease along the course of the flow as observed by Tu *et al.* (2020). This suggests the presence of a reverse pressure along the brake fluid line. Two primary reasons account for this reversepressure phenomenon: **Outlet Sealing:** The absence of an opening for fluid egress at the outlet can unilaterally lead to a pressure decline. **High Inlet Flow Rate:** The heightened flow rate of the inlet pressure also induces a reverse pressure into the system as reported by Lee *et al.* (2020). A notable distinction among the four samples of the brake fluid oil is reflected in the outlet value, which demonstrates a negative measure of -4.61026 MPa. The implications of this research underscore that pressure drop in a brake fluid line is generally detrimentalto the overall performance and safety of the braking mechanism. Pressure drop can culminate in reducedbraking force, elongated stopping distances, and a less responsive brake pedal as observed by Gumiel*et al.* (2023). From Figure 8 (b), it can be observed that due to

the high flow rate of brake fluid, the primary area affected by temperature differences is the portion in contact with the brake caliper. The rest of the system experiences minimal temperature impact. The main region where temperature variance occurs is the cylinder area. The brake's intermittent application—stepping on and releasing the brake—limits the duration for consistent heat transfer. Consequently, the temperature throughout the system remainsrelatively constant until it reaches the cylinder. This is where a slight temperature difference triggers heat transfers and the contour pattern for the based oil shows a slight heat transfer movement at the bottom of the piston as observed by He *et al.* (2023). Temperature difference and heat transfer in a brake fluid system play a crucial role in the overall performance and safety of the braking system. Thetemperature difference refers to the variation in temperature between different points within the brake fluid line or system. The temperature difference drives the heat transfer process, where heat flows fromareas of higher temperature to areas of lower temperature as observed by Scarano *et al.* (2020). Heat transfer is the movement of thermal energy from one region to another due to a temperature difference.In the context of a brake fluid line or system: Heat Generation: During braking, friction between the brake pads and rotors generates heat. This heat is transferred to the brake fluid, increasing its temperature. Heat Dissipation: Brake systems are designed to dissipate heat efficiently to prevent overheating as reported by Leon *et al.* (2019). Heat is transferred from the brake fluid to the surroundingair through components like brake calipers, rotors, and brake lines. Adequate cooling mechanisms prevent the brake fluid from reaching critical temperatures that can lead to brake fade or fluid boiling. Thermal Expansion: As the brake fluid heats up, it expands. This expansion can lead to increased pressure within the brake lines, affecting the brake pedal feel. Brake systems are designed to accommodate this thermal expansion without compromising performance. Cooling: Adequate ventilation and airflow around brake components help cool down the brake fluid and prevent excessivetemperature build-up. Both too-high and too-low temperatures can negatively impact brake system performance. High temperatures can lead to brake fade, fluid boiling, and degradation of brake fluid, while low temperatures can affect fluid viscosity and brake responsiveness as reported by Dehhaghi *et al.* (2021). Brake fluid with a high boiling point is used to handle high temperatures generated during aggressive driving. Additionally, proper brake system design, quality components, and regular maintenance help manage temperature-related issues. In summary, temperature difference and heat transfer are essential considerations in brake systems to ensure safe and effective braking performance. Brake systems are designed to manage heat effectively, balancing the need for efficient heat dissipation and fluid performance under varying operating conditions. Figure 8 (c): It demonstrates that the velocity flow within the brake line predominantly exhibits a laminar pattern. Laminar flow refers to a fluid motion characterized by a Reynolds number (Re) of lessthan 2000 as observed by Li *et al.* (2022). The research aligns with this observation, affirming that theflow within a brake line largely maintains a laminar state. This is further supported by the contour patterns observed within the brake line pipe, which depict the characteristics of laminar flow. The primary emphasis lies in understanding the velocity alteration upon entering the cylinder area. Despitea consistent velocity flow, the noteworthy aspect pertains to the subtle variations in color transitions on the contour pattern as reported by Gildersleeve and Amitay (2020). These color transitions signifythe rate of change in velocity, and they are particularly pronounced when the velocity enters the cylinderarea. This transition zone signifies the point at which the velocity experiences a distinct alteration and a subsequent reduction. In essence, the research underscores the prevalence of laminar flow within the brake line, with a specific focus on the velocity shift as it enters the cylinder area. The variations in color and the associated changes in velocity distribution contribute to a comprehensive understandingof how the velocity diminishes in this critical region also observed by Rodriguez and Ajo (2021). The velocity of brake fluid in a brake fluid line can have several effects on the performance of the braking system. The velocity of the fluid is directly related to the flow rate, which is the amount of fluidpassing through the line per unit of time. Here are the effects of velocity in a brake fluid line: Brake Response and Pedal Feel: Higher fluid velocity can lead to quicker brake response and a more immediate pedal feel. This means the brakes engage more rapidly when the pedal is pressed, enhancingthe driver's control and confidence. Braking Force: The velocity of the brake fluid influences the forceapplied to the brake pads or shoes. Higher fluid velocity can result in increased braking force, potentiallyimproving the overall braking performance of the vehicle. Heat Dissipation: Higher fluid velocity can aid in dissipating heat generated during braking. This is particularly important in high-performance driving or heavy braking situations where excessive heat build-up can lead to brake fade as reported byRobitschek (2021). Pressure Drop: Excessive velocity or flow rate in the brake fluid line can cause pressure drop issues. Pressure drop can lead to reduced braking force and a spongy brake pedal feel. Cavitation: Extremely high velocity in localized areas may lead to cavitation, which is the formation and collapse of vapor bubbles due to low pressure. Cavitation can be damaging to the brake system andaffect braking performance. Fluid Boiling: Very high velocity can generate significant heat in the brakefluid, potentially leading to fluid boiling. Boiling brake fluid can create air bubbles, resulting in a spongy brake pedal and reduced braking effectiveness. In Figure 9 (a), the pressure inlet registers a value of 3.447 MPa, while the outlet pressure is noted as - 8.08623 MPa. This data indicates a substantial pressure reduction along the brake fluid line. The outletpressure nearly reaches zero or even exhibits a minor negative value, implying a significant pressure

decrease along the course of the flow as observed by Tu *et al.* (2020). This suggests the presence of a reverse pressure along the brake fluid line. Two primary reasons account for this reverse pressure phenomenon: Outlet Sealing: The absence of an opening for fluid egress at the outlet can unilaterally lead to a pressure decline. High Inlet Flow Rate: The heightened flow rate of the inlet pressure also induces a reverse pressure into the system as reported by Lee *et al.* (2020). A notable distinction amongthe four brake fluid oil samples is reflected in the outlet value, which demonstrates a negative measureof -8.08623 MPa. The implications of this research underscore that pressure drop in a brake fluid line is generally detrimental to the overall performance and safety of the braking mechanism. Pressure drop can culminate in reduced braking force, elongated stopping distances, and a less responsive brake pedalas observed by Gumiel *et al.* (2023). From Figure 9 (b): This can be observed that due to the high flow rate of brake fluid, the primary areaaffected by temperature differences is the portion in contact with the brake caliper. The rest of the system experiences minimal temperature impact. The main region where temperature variance occurs is the cylinder area. The brake's intermittent application—stepping on and releasing the brake—limits the duration for consistent heat transfer. Consequently, the temperature throughout the system remainsrelatively constant until it reaches the cylinder. This is where a slight temperature difference triggers heat transfer and the contour pattern for the NBF3 shows more change in heat transfer movement at thebottom of the piston than the based oil, NBF1, and NBF2 as observed by Tornatore *et al.* (2021). Temperature difference and heat transfer in a brake fluid line or system play a crucial role in the overallperformance and safety of the braking system. The temperature difference refers to the variation in temperature between different points within the brake fluid line or system. The temperature difference drives the heat transfer process, where heat flowsfrom areas of higher temperature to areas of lower temperature as observed by Scarano *et al.* (2020). Heat transfer is the movement of thermal energy from one region to another due to a temperature difference. In the context of a brake fluid line or system: Heat Generation: During braking, friction between the brake pads and rotors generates heat. This heat is transferred to the brake fluid, increasingits temperature. The heat dissipation in Brake systems is designed to dissipate heat efficiently to preventoverheating as reported by Tamilselvan *et al.* (2023). Heat is transferred from the brake fluid to the surrounding air through components like brake calipers, rotors, and brake lines. Adequate cooling mechanisms prevent the brake fluid from reaching critical temperatures that can lead to brake fade or fluid boiling. Thermal Expansion: As the brake fluid heats up, it expands. This expansion can lead to increased pressure within the brake lines, affecting the brake pedal feel. Brake systems are designed to accommodate this thermal expansion without compromising performance. Cooling needs adequate ventilation and airflow around brake components to help cool down the brake fluid and prevent excessivetemperature build-up. Both too-high and too-low temperatures can negatively impact brake system performance. High temperatures can lead to brake fade, fluid boiling, and degradation of brake fluid, while low temperatures can affect fluid viscosity and brake responsiveness. Brake fluid with a high boiling point is used to handle high temperatures generated during aggressive driving. Additionally, proper brake system design, quality components, and regular maintenance help manage temperature-related issues. Generally, temperature difference and heat transfer are essential considerations in brake systems to ensure safe and effective braking performance. Brake systems are designed to manage heat effectively,balancing the need for efficient heat dissipation and fluid performance under varying operating conditions. Low temperature in a brake fluid line can have several effects on the brake system and its performance: Increased Viscosity: At low temperatures, brake fluid becomes thicker and more viscous.This increased viscosity can lead to reduced brake system responsiveness, causing a delay in brake engagement and potentially resulting in longer stopping distances. Delayed Brake Response: The increased viscosity of the brake fluid at low temperatures may cause a delay in brake response, especially during the initial application of the brakes. This delay can affect the driver's ability to modulate the braking force effectively. Potential Brake Fade: In extremely low temperatures, the thickened brake fluid may struggle to maintain consistent braking force, especially during prolonged orheavy braking. This can lead to brake fade, where the braking effectiveness decreases over time due toincreased friction and heat generation. Reduced Performance in Emergency Situations: In emergency braking situations, the delayed brake response and reduced effectiveness due to low-temperature brakefluid can impact the vehicle's ability to come to a quick stop, potentially increasing the risk of accidents. Possible ABS Malfunction: In vehicles equipped with an Anti-Lock Braking System (ABS), low- temperature brake fluid may affect the system's performance, potentially causing it to function less efficiently or malfunction. To mitigate the negative effects of low temperature on the brake fluid line, it's essential to use brake fluid with a suitable low-temperature rating as reported by Schroeder *et al.* (2019). Brake fluids with a low viscosity at low temperatures, such as DOT 3 or DOT 4 brake fluids, are commonly used in most vehicles. Additionally, storing the vehicle in a sheltered area or garage canhelp prevent the brake fluid from reaching extremely low temperatures and improve its responsivenessduring cold weather conditions. Figure 9 (c): It demonstrates that the velocity flow within the brake line predominantly exhibits a laminarpattern. Laminar flow refers to a fluid motion characterized by a Reynolds number (Re) of less than 2000 as observed by Li *et al.* (2022). The research aligns with this observation, affirming that the flowwithin a brake line largely maintains a laminar state. This is further supported

by the contour patterns observed within the brake line pipe, which depict the characteristics of laminar flow. The primary emphasis lies in understanding the velocity alteration upon entering the cylinder area. Despite a consistent velocity flow, the noteworthy aspect pertains to the subtle variations in color transitions onthe contour pattern as reported by Gildersleeve and Amitay (2020). These color transitions signify therate of change in velocity, and they are particularly pronounced when the velocity enters the cylinder area. This transition zone signifies the point at which the velocity experiences a distinct alteration and a subsequent reduction. The velocity of brake fluid in a brake fluid line can have several effects on the performance of the braking system. The velocity of the fluid is directly related to the flow rate, which is the amount of fluidpassing through the line per unit of time. Here are the effects of velocity in a brake fluid line: Brake Response and Pedal Feel: Higher fluid velocity can lead to quicker brake response and a more immediate pedal feel. This means the brakes engage more rapidly when the pedal is pressed, enhancingthe driver's control and confidence. Braking Force: The velocity of the brake fluid influences the forceapplied to the brake pads or shoes. Higher fluid velocity can result in increased braking force, potentially improving the overall braking performance of the vehicle. Heat Dissipation: Higher fluid velocity can aid in dissipating heat generated during braking. This is particularly important in high-performance driving or heavy braking situations where excessive heat build-up can lead to brake fade as reported byRobitschek (2021). Pressure Drop: Excessive velocity or flow rate in the brake fluid line can cause pressure drop issues. Pressure drop can lead to reduced braking force and a spongy brake pedal feel. Cavitation: Extremely high velocity in localized areas may lead to cavitation, which is the formation and collapse of vapor bubbles due to low pressure. Cavitation can be damaging to the brake system andaffect braking performance. Fluid Boiling: Very high velocity can generate significant heat in the brakefluid, potentially leading to fluid boiling. Boiling brake fluid can create air bubbles, resulting in a spongy brake pedal and reduced braking effectiveness. It's essential to strike a balance in brake fluid velocity to ensure optimal brake system performance andsafety. Automotive engineers carefully design brake systems to control fluid velocity, selectingappropriate line diameters and lengths to achieve efficient and reliable braking as discussed by Eshgarf*et al.* (2022). Regular brake system maintenance, including brake fluid checks and replacements, is crucial to maintaining proper fluid velocity and ensuring the brakes perform effectively and safely. Table 2 presents the simulation condition of the based oil and the developed Nano brake fluid

Table 2: A Scale of the simulation condition of roselle-based oil and Nano brake fluid (NBF)

Scale & grade	Oil samples	Pressure	Temperature	Velocity	Remarks
1, Very low	Based oil	2	1	4	Low pressure, very low temperature, high velocity
4, High	NBF3	3	2	1	Medium (-) pressure, low temperature, very low velocity

4.7 Comparative analysis with conventional brake fluid and the developed bio-based brake fluid properties:

The comparison between the developed bio-based brake fluid and the conventional brake fluid provided valuable insights in Table 3. This shows that the developed bio-based brake fluid with Nano copper oxide additives shows promising potentials like lower kinematic viscosity, lower density, higherviscosity index, and higher flash point as observed by Bitire *et al.* (2022). However, its higher pour point and significantly lower boiling point could be potential drawbacks that need to be considered in specific application scenarios, especially under extreme conditions.

Table 3: Comparison between the properties of conventional brake fluid and developed bio-based brake fluid

Brake fluid properties	Properties of conventional brake fluid	Properties of the developed bio-based brake fluid with Nano copper oxide additives
Kinematic viscosity @100℃	1.5 to 1.8cst	1.2cst
Density	0.95 to 0.98 g/cm3	0.92 g/cm3
Viscosity index	Nil	3.4

Specific gravity	0.95 to 0.98	0.86
Pour point	-40 ℃ to -50 ℃	3 ℃
Flash point	140 ℃ to 260 ℃	210 ℃
Boiling point	205 to 230 ℃	145

4. CONCLUSION

This study aimed to evaluate the potential of bio-based brake fluid with a Nano copperoxide additive. The specific objectives were successfully achieved, and the key findings are summarized as follows: A bio-based brake fluid was formulated using Roselle oil and Nano copper oxide additive. The additive, with nanoparticles under 20nm in diameter, was synthesized and characterized by TEM, while XRD analysis revealed a CuO nanoparticle crystallite size of 9.22 nm to ensure effective dispersion and compatibility within the brake fluid. The brake fluid evaluation demonstrated stable physio-chemical properties, with a kinematic viscosity of 3.5cSt at 0.3wt%, suitable for prolonged use. The spectrochemical analysis identified the C-H stretching vibration peak at 2922 cm-1 in the FTIR spectrum. Additionally, tribological tests revealed reduced friction (0.057) and wear prevention (0.3592 mm3n-1m-1) at a 0.3wt% CuO nanoparticle concentration, confirming improved brake fluid efficiency and durability. The performance evaluation of the bio-based brake fluid under various conditions, including temperature, pressure, and velocity flow rate which has an inlet at 3.447MPa showed consistent and reliable performance in challenging scenarios. This suggests the brake fluid's adaptability and suitability for real-world automotive use. The bio-based brake fluid exhibited comparable properties in kinematic viscosity of blended Roselle oil at 1.2cSt compared to 1.5 to 1.8cSt of conventional brake fluid properties. Indicating its potential as a viable alternative to conventional brake fluids in the automotive industry. Based on the study's findings, the following recommendations are made for further research and practical implementation: To assess the long-term stability and durability of the bio-based brake fluid with the Nano copper oxide additive, extended testing and monitoring should be carried out. This will provide crucial insights into the fluid's performance and integrity over an extended service life. To ensure the practical applicability and effectiveness of the bio-based brake fluid in actual automotive systems, comprehensive real-world testing should be conducted on different vehicle models and under diverse driving conditions. This will validate the fluid's performance and contribute to its successful integration into the automotive market. Further research could focus on optimizing the concentration of Nano copper oxide additive in the brake fluid to achieve the best balance between enhanced performance and cost-effectiveness. Conducting a comprehensive life cycle assessment will enable a thorough evaluation of the environmental benefits of the bio-based brake fluid. This assessment should consider factors such as raw material sourcing, production processes, usage, and end-of-life disposal to provide a holistic understanding of its ecological impact. This research significantly contributes to the knowledge and understanding of bio-based brake fluids with Nano copper oxide additives in the following ways: The successful development and characterization of a bio-based brake fluid using Roselle oil and Nano copper oxide additive demonstrate the potential of sustainable alternatives in the automotive industry. The synthesis and characterization of the Nano copper oxide additive for the brake fluid highlight the importance of nanotechnology in enhancing the performance properties of lubricants and fluids. The study's detailed assessment of physico-chemical, spectrochemical, tribological properties, and performance under different operating conditions provide valuable insights into the suitability and reliability of the bio-based brake fluid.

5. ACKNOWLEDGEMENT

Every piece of work is accomplished with the input of one person to another, and this one is not an exception. The never-ending inputs, fine-tuning, and thorough supervision of Dr. M. U. Kaisan and Dr.H. A. Dandajeh can never be left unacknowledged and the amiable head of the department, Dr.M. O. Afolayan, the entire staff of the department of Mechanical Engineering who contributed towards making this project a success. I wish to also express my profound gratitude to my family especially my late son Abubakar Sadeeq Usman, my wife, Hadiza Danjuma Alkali, and my late father Mal. Ramalan Ibrahim II, my mother Khadija Ahmed, and my brothers and sisters, Engr Umar Sabo Mohammed for their patience, prayers, love, and encouragement which most of the time kept me pinned and geared to the task. The contributions of my classmates and my senior colleagues, for their intellectual debates and contribution to this research topic, I acknowledge them.

REFERENCES

Adekunle, A., and Oparanti, S. (2023). A Review on Physicochemical and Electrical Performance of Vegetable Oil-Based Nanofluids for High Voltage Equipment. Electric Power Systems Research, 214,108873.

Adu-Mensah, D., Mei, D., Zuo, L., Zhang, Q., and Wang, J. (2019). A Review on Partial Hydrogenationof Biodiesel and Its Influence on Fuel Properties. Fuel, 251, 660-668

Agrawal, V. K., and Khairnar, H. (2022). Experimental & Analytical Investigation for Optimization ofDisc Brake Heat Dissipation Using Cfd

Almoselhy, R. (2021). Comparative Study of Vegetable Oils Oxidative Stability Using DSC and Rancimat Methods. Egyptian Journal of Chemistry, 64(1), 299-312

Animasaun, D. A., Ameen, M. O., and Belewu, M. A. (2021). Protocol for Biodiesel Production by Base-Catalyzed Transesterification Transesterification Method. In Biofuels and Biodiesel (pp. 103-113). Springer.

Ansari, F., Sheibani, S., and Fernandez-Garcoa, M. (2022). Surface Modification of Cu2O-CuO Photocatalyst on Cu Wire through Decorating with TiO2 Nanoparticles for Enhanced Visible Light Photocatalytic Activity. Journal of Alloys and Compounds, 919, 165864.

Arshad, M., Mohanty, A. K., Van, A. R., Riddle, R., Todd, J., Khalil, H., and Misra, M. (2022). Valorization of Camelina Oil to Biobased Materials and Biofuels for New Industrial Uses: a Review. RSC advances, 12(42), 27230-27245.

Azarpour, A., Zendehboudi, S., Mohammadzadeh, O., Rajabzadeh, A. R., and Chatzis, I. (2022). A Review on Microalgal Biomass and Biodiesel Production through Co-cultivation Strategy. Energy Conversion and Management, 267, 115757.

Bitire, S. O., Nwanna, E. C., and Jen, T.-C. (2022). The Impact of CuO Nanoparticles as Fuel Additives in Biodiesel-blend Fuelled Diesel Engine: A Review. Energy & Environment, 0958305X221089217.

Bonnar, C. (2023). On the Integrated Analysis and Forensic Interpretation of Gunshot Residues. Flinders University, College of Science and Engineering.

Campaoa, G. G., Basantes, S. A., Garcoa, E. A., and Larco, D. J. (2023). Analysis of the Plastic Point of Brake Fluid in L3 Category Vehicles at Preset Times. Revista Tecnol'gica Ciencia y Educaci'n Edwards Deming, 6(2).

Chen, M., Yue, Z., Wu, Y., Wang, Y., Li, Y., and Chen, Z. (2023). Thermal Stable Polymer-based Solid Electrolytes: Design Strategies and Corresponding Stable Mechanisms for Solid-state Li Metal Batteries. Sustainable Materials and Technologies, e00587.

Cruz, F. A. (2019). Flow visualization of silica Nano fluid injection for enhanced oil recovery in a micromodel based on well-sorted grain-size porous media.

De Jesus Moura, G. (2023). Developing Tack Coat Specification for Long-Lasting Composite Pavement Performance (Doctoral dissertation).

Dehhaghi, M., Panahi, H. K., Aghbashlo, M., Lam, S. S., and Tabatabaei, M. (2021). The Effects of Nano Additives on the Performance and Emission Characteristics of Spark-ignition Gasoline Engines: ACritical Review with a Focus on Health Impacts. Energy, 225, 120259.

Dharmegowda, I. Y., Muniyappa, L. M., Siddalingaiah, P., Suresh, A. B., Gowdru, C. M., and Prakash, C. (2022). MgO Nano-catalyzed Biodiesel Production from Waste Coconut Oil and Fish Oil Using Response Surface Methodology and Grasshopper Optimization. Sustainability, 14(18), 11132.

Donoso, D., Bolonio, D., Lapuerta, M., and Canoira, L. (2020). Oxidation Stability: the Bottleneck forthe Development of a Fully Renewable Biofuel from Wine Industry Waste. ACS omega, 5(27), 16645-16653.

Edwin, M., Nila, J. N., & Nair, M. S. (2023). Biofuel production: An initiative of environmentally sound technologies (ESTs) or Green technologies. In Environmental Sustainability of Biofuels (pp. 99-136). Elsevier.

Eshgarf, H., Nadooshan, A. A., and Raisi, A. (2022). An Overview on Properties and Applications of Magnetorheological Fluids: Dampers, Batteries, Valves and Brakes. Journal of Energy Storage,

50, 104648.

Fakayode, O. A., Wahia, H., Zhang, L., Zhou, C., and Ma, H. (2023). State-of-the-art Co-pyrolysis of Lignocellulosic and Macroalgae Biomass Feedstocks for Improved Bio-oil Production-A Review. Fuel,332, 126071.

Fatahi, H., Claverie, J. P., & Poncet, S. (2023). Characterization by differential scanning calorimetry of thermal storage properties of organic PCMs with operating temperature of 150° C. The Journal of Chemical Thermodynamics, 186, 107136.

García-León, R. A., Páez-Gómez, D., & Guerrero-Gómez, G. (2023). Theoretical design of a brake discs tribological machine. International Journal of System Assurance Engineering and Management, 14(4), 1530-1542.

Gildersleeve, S., and Amitay, M. (2020). Vortex Dynamics of a Low Aspect Ratio Cantilevered Cylinder Immersed in a Boundary Layer. Journal of Fluid Mechanics, 901, A18.

Gumiel, A. J. Mabe, J. Burguera, F. Jimenez, J. and Barruetabena, J. (2023). Next-GenerationPedal: Integration of Sensors in a Braking Pedal for a Full Brake-by-Wire System. *Sensors*. 2023; 23(14):6345. https://doi.org/10.3390/s23146345

Hani, E. B., Marashli, A., Shalby, M., & Al-Rawashdeh, H. (2021). Experimental Investigation of Basic Properties Biodiesel Fuels (B100, B20, B5) Produced from Waste Cooking Oil (WCO) Using Trans-Esterification Process. International Journal of Renewable Energy Sources, 6.

Hasanin, M. S., and Youssef, A. M. (2022). Ecofriendly Bioactive Film Doped CuO Nanoparticles Based Biopolymers and Reinforced by Enzymatically Modified Nanocellulose Fibers for Active Packaging Applications. Food Packaging and Shelf Life, 34, 100979.

He, X., Xu, J., Yu, X., and Xie, J. (2023). Distinguishing Evaporation-like and Boiling-like Modes of Pseudo-boiling in Supercritical Pressures. International Journal of Heat and Mass Transfer, 214, 124417.

Huang, Y., Li, F., Bao, G., Wang, W., and Wang, H. (2020). Estimation of Kinematic Viscosity of Biodiesel Fuels from Fatty Acid Methyl Ester Composition and Temperature. Journal of Chemical & Engineering Data, 65(5), 2476-2485.

Ilie, F., and Cristescu, A.-C. (2023). Experimental Study of the Correlation between the Wear and the Braking System Efficiency of a Vehicle. Applied Sciences, 13(14), 8139.

Jadhav, R. M., Kumar, G., Balasubramanian, N., and Sangwai, J. S. (2022). Synergistic Effect of NickelNanoparticles with Tetralin on the Rheology and Upgradation of Extra Heavy Oil. Fuel, 308, 122035.

Jhaveri, J., Raichura, Z., Khan, T., Momin, M., and Omri, A. (2021). Chitosan Nanoparticles-insight into Properties, Functionalization and Applications in Drug Delivery and Theranostics. Molecules, 26(2), 272.

Jurid, L. S., Zubairi, S. I., Kasim, Z. M., and Ab, K. I. (2020). The Effect of Repetitive Frying on Physicochemical Properties of Refined, Bleached and Deodorized Malaysian Tenera Palm Olein duringDeep-fat Frying. Arabian Journal of Chemistry, 13(7), 6149-6160.

Kamarulzaman, M. K., Hisham, S., Kadirgama, K., Ramasamy, D., Samykano, M., Said, Z., and Pandey, A. (2023). Improvement in Stability and Thermophysical Properties of CNC-MXene Nanolubricant for Tribology Application. Journal of Molecular Liquids, 381, 121695.

Kutlu, N., Pandiselvam, R., Kamiloglu, A., Saka, I., Sruthi, N., Kothakota, A., . . . Maerescu, C. M. (2022). Impact of Ultrasonication Applications on Color Profile of Foods. Ultrasonics Sonochemistry,89, 106109.

Lee, C., Nguyen, T.-T., Adha, R. S., Shon, H. K., and Kim, I. S. (2020). Influence of Hydrodynamic Operating Conditions on Organic Fouling of Spiral-wound Forward Osmosis Membranes: Fouling-induced Performance Deterioration in FO-RO Hybrid System. Water Research, 185, 116154.

León, R. A. G., Solano, E. F., & Quiñones, Á. S. (2019). Brake discs: A technological review from its analysis and assessment. Informador técnico, 83(2), 217-234.

Li, P., Zhang, K., Wang, J., Meng, H., Nicosia, A., and Ferro, V. (2022). Overland Flow Hydrodynamic Characteristics in Rough Beds at Low Reynolds Numbers. Journal of Hydrology, 607, 127555.

Ma, J., Shahsavar, A., Al-Rashed, A. A., Karimipour, A., Yarmand, H., and Rostami, S. (2020). Viscosity, Cloud Point, Freezing Point, and Flash Point of Zinc Oxide/SAE50 Nanolubricant. Journal of Molecular Liquids, 298, 112045.

Manring, N. D., and Fales, R. C. (2019). Hydraulic Control Systems. John Wiley & Sons.

Mladenov, G., Damyanov, I., & Valkovski, T. (2021, June). Research and selection of parameters determining the efficiency of the braking system of cars to improve traffic safety and environmental performance. In 2021 56th International Scientific Conference on Information, Communication and Energy Systems and Technologies (ICEST) (pp. 153-156). IEEE.

Olszak, A., Osowski, K., Musialek. I., Rogo, E., Kesy, A., and Kesy, Z. (2020). Application of Plant Oils as Ecologically Friendly Hydraulic Fluids. Applied Sciences, 10(24), 9086.

Patel, J., Soni, A., Barai, D. P., & Bhanvase, B. A. (2023). A minireview on nanofluids for automotive applications: Current status and future perspectives. Applied Thermal Engineering, 219, 119428.

Praveenkumar, T., Rath, B., Devanesan, S. Alsahi, M. S., Jhanani, G., Gemede, H. F., . . . Daniel, F. (2023). Performance and Emission Characteristics for Karanja Biodiesel Blends Assisted with Green Hydrogen Fuel and Nanoparticles. Journal of Energy Resources Technology, 145(11).

Putnik, P., Pavlić, B., Šojić, B., Zavadlav, S., Žuntar, I., Kao, L., ... & Kovačević, D. B. (2020). Innovative hurdle technologies for the preservation of functional fruit juices. Foods, 9(6), 699.

Rani, M., and Shanker, U. (2021). Plastic Degradation and Its Environmental Implications. Degradationof Plastics, 99, 290-324.

Raya, S. A., Mohd, S. I., Abbas, A. A., and Abubakar, U. A. (2020). A Critical Review of Development and Demulsification Mechanisms of Crude Oil Emulsion in the Petroleum Industry. Journal of Petroleum Exploration and Production Technology, 10, 1711-1728.

Reddy, M. K., Muralidharan, K., Chandra, R. S., Varma, P. K., Venugopal, K., Vignesh, R. V., . . . Priyadharshini, G. S. (2023). Influence of Nanophase Particles on the Physical, Chemical and Tribological Characteristics of SAE15W40. Journal of Bio-and Tribo-Corrosion, 9(1), 20.

Robitschek, D. (2021). From Mechanical to Regenerative Braking-Implications of the Transition towards Electric Mobility on Aspects of Deceleration and Tribological Brake Additives. Wien.

Rodroguez, T. V., and Ajo, F. J. (2021). Aquifer Monitoring Using Ambient Seismic Noise Recorded with Distributed Acoustic Sensing (DAS) Deployed on Dark Fiber. Journal of Geophysical Research: Solid Earth, 126(4), e2020JB021004.

Rogulska, M. (2023). The Influence of Diisocyanate Structure on Thermal Stability of Thermoplastic Polyurethane Elastomers Based on Diphenylmethane-Derivative Chain Extender with Sulfur Atoms. Materials, 16(7), 2618.

Salih, N., and Salimon, J. (2021). A Review on Eco-friendly Green Biolubricants from Renewable andSustainable Plant Oil Sources. Biointerface Res. Appl. Chem, 11(5), 13303-13327

Santhosh, R., Nath, D., and Sarkar, P. (2021). Novel Food Packaging Materials including Plant-based Byproducts: A Review. Trends in Food Science & Technology, 118, 471-489.

Scarano, A., Inchingolo, F., and Lorusso, F. (2020). Facial Skin Temperature and Discomfort When Wearing Protective Face Masks: Thermal Infrared Imaging Evaluation and Hands Moving the Mask. International journal of environmental research and public health, 17(13), 4624

Schroeder, Z., Pruski, K., Sebastian, T., Muzzell, P., Dusenbury, J., and US, A. C. (2019). Brake FluidStandarization for Anti-Lock Braking Systems (BFABS) Benchtop Testing Report. Warren,

Michigan:US Army. Obtenido de https://apps. dtic. mil/sti/pdfs/AD1091780.pdf.

Skornia, K. M. (2020). Treatment of Winery Wastewater Using a Vertical Flow Constructed Wetland with Adsorption Media. Michigan State University.

Srivastava, R. K., Bothra, N., Singh, R., Sai, M. C., Nedungadi, S. V., and Sarangi, P. K. (2022). Microbial Originated Surfactants with Multiple Applications: A Comprehensive Review. Archives of Microbiology, 204(8), 452.

Stewart, S., Wei, Q., and Sun, Y. (2021). Surface Chemistry of Quantum-Sized Metal Nanoparticles under Light Illumination. Chemical Science, 12(4), 1227-1239.

Tamilselvan, A., Mohamed, N. N., Sudhan, V., Kesav, R. N., Deepakkumar, S., and Sankar, S. (2023). Fabrication of a Water Sprayer System for the Enhancement of Heat Dissipation in Disc Brake. AIP Conference Proceedings. 2492. AIP Publishing

Toe, C. Y., Tsounis, C., Zhang, J., Masood, H., Gunawan, D., Scott, J., and Amal, R. (2021). Advancing Photoreforming of Organics: Highlights on Photocatalyst and System Designs for Selective OxidationReactions. Energy & Environmental Science, 14(3), 1140-1175.

Tornatore, C., Marchitto, L., and Valentino, G. (2021). Technologies for Knock Mitigation in SI Engines'A Review. Engines and Fuels for Future Transport, 325-349.

Trejo-Coceres, M., Sonchez, M. C., and Marton-Alfonso, J. (2023). Impact of Acetylation Process of Kraft Lignin in Development of Environment-Friendly Semisolid Lubricants. International Journal of Biological Macromolecules, 227, 673-684.

Tu, Y., Xu, S., Xu, M., Liu, H., and Yang, W. (2020). Numerical Study of Methane Combustion under Moderate or Intense Low-oxygen Dilution Regime at Elevated Pressure Conditions up to 8 Atm. Energy, 197, 117158.

WOMA, T. Y. (2021). Tribological Evaluation of Lubricants Developed from Selected Vegetable Based Oils for Industrial Applications

Wong, J. F., Hong, H. J., Foo, S. C., Yap, M. K., and Tan, J. W. (2022). A Review on Current and Future Advancements for Commercialized Microalgae Species. Food Science and Human Wellness, 11(5), 1156-1170.

Zhang, M., Cheng, Q., Chen, T., Wei, X., and Meng, L. (2022). Development and Characterisation Research on SnO2 Al2O3 NiO/SO42- Catalysed Epoxidation of Soybean Oil under Hydraulic Cavitation. Applied Organometallic Chemistry, 36(4), e6617.

APPENDICES

Nano Brake Fluid Sample

PAPER 55 - EXPERIMENTAL STUDY ON THE EFFECTS OF PARTIAL REPLACEMENT OF CEMENT WITH EGGSHELL POWDER ON CONCRETE PROPERTIES

Ibrahim Tunde Yusuf[1], Yusuf Olawale Babatunde[1*], Farouq A. Ojo[1], Turki S. Alahmari[2]

[1]Department of Civil Engineering, Faculty of Engineering and Technology, University of Ilorin, Ilorin, Nigeria.
[2] Department of Civil Engineering, Faculty of Engineering, University of Tabuk, Tabuk, Saudi Arabia.

*** E-mail**: babatunde.oy@unilorin.edu.ng

ABSTRACT

Concrete, an essential construction material, accounts for a significant portion of global carbon emissions due to the high energy consumption and greenhouse gas emissions associated with cement production. This study investigated the potential of waste Eggshell Powder (ESP) as a sustainable alternative to partially replace cement in concrete production. The chemical characterization through X-ray Diffraction (XRD) and X-ray Fluorescence (XRF) of the waste ESP was analysed. Four different concrete mixes were cast with the inclusions of ESP at 0%, 5%, 10%, and 15% replacement of cement. The workability of the fresh concrete mixes, compressive strength, split tensile strength, and flexural strength of the hardened concrete mix samples at 28 days of curing were evaluated following the relevant standards. The XRF results showed the presence of CaO in waste ESP, which indicates its suitability as a supplementary cementitious material. The obtained results showed an increment in workability, compressive strength, flexural strength, and split tensile strength properties of the concrete as the content of the waste ESP increased up to 10%. Beyond that, a significant reduction in these properties was observed. The maximum compressive strength of 30.2 N/mm^2 was obtained at 10% inclusion of waste ESP in the concrete mix.

KEYWORDS: Eggshell powder (ESP), Ordinary Portland Cement (OPC), X-ray Diffraction (XRD), Split-Tensile strength, Compressive Strength, Flexural strength, Workability.

1.0 INTRODUCTION

Concrete, being one of the most widely used construction materials, bears a significant environmental footprint due to its energy-intensive production process and high consumption of raw materials, particularly cement (Alnahhal, 2018; Divya *et al.*, 2017; Jhatial *et al.*, 2020). Cement production is a major source of greenhouse gas emissions, primarily carbon dioxide (CO_2), thereby contributing significantly to global climate change (Ujin *et al.*, 2016). There is a pressing need to explore sustainable alternatives and innovative techniques to mitigate the environmental impact of concrete production while maintaining its structural integrity and durability. One of the innovative approaches involves the utilization of waste materials or by-products as partial replacements for traditional cement in concrete mixtures. This approach would not only reduce the demand for cement but also find a valuable use for waste materials that would otherwise end up in landfills. Waste eggshells are readily available in abundance from various food processing industries, making them an attractive option for sustainable construction (Kumar *et al.*, 2017; Nandhini and Karthikeyan, 2021). This research endeavours to investigate the effect of partial replacement of cement with waste eggshell powder in concrete production, an initiative that holds promise in promoting sustainable construction practices. The utilization of waste eggshells in concrete production aligns with the principles of the circular economy, waste reduction, and sustainable development (Masta *et al.*, 2015; Mohammed *et al.*, 2016).

Research studies have been carried out on the behaviour of concrete containing waste eggshell powder. The presence of waste eggshell powder in concrete affects its workability. There was a reduction in workability with increasing eggshell powder content (Sutcu *et al.*, 2019; Islam *et al.*, 2020). This can be mitigated through adjustments in the water-cement ratio or superplasticizers. Yerramala (2014) used different Eggshell Powder (ESP) contents in concrete

by substituting 5 – 15% of cement with ESP. The results showed that ESP could positively be utilized as a partial replacement of cement in concrete. The strengths were higher than control concrete at 5% ESP replacement, indicating that 5% ESP is the optimum content for maximal strength. They suggested that the ESP with other cementitious materials such as fly ash could improve the performance of concrete. Gowsika *et al.* (2014) experimentally investigated the influence of eggshell powder as a replacement for cement in concrete mortar. The waste eggshell powder was added at dosages of 5%, 10%, 15%, 20%, 25%, and 30% by weight of cement in concrete mortar. They reported an increase in compressive strength for concrete mortar containing 5% of waste eggshell powder. Beyond that, the compressive strength decreased. It was proposed that the use of admixtures such as Saw Dust ash, Fly Ash and micro-silica could enhance the strength of the concrete mortar.

This research work is relatively distinct from the previous studies because the targeted strength is relatively higher (25MPa) which extends its application in various structural works and forms, also in order to increase the specific surface area alongside the reactivity,75μm fineness of the eggshell powder was used to ultimately allow for substantial strength development.

2.0 MATERIALS AND METHODS

2.1 Source and Preparation of Materials

The materials used in the study were Ordinary Portland Cement (OPC), waste eggshell, fine aggregate and coarse aggregate. The OPC of grade 43, which conforms with British Standard BS 12:1996 was locally sourced. The waste eggshell was locally sourced from food vendors at Tanke, Ilorin, Kwara State, Nigeria. It was thoroughly washed under running water to remove impurities and sun-dried as shown in Figure 1. Afterwards, it was crushed and milled into powder. The chemical characterization of the waste eggshell powder and cement samples was carried out through X-ray Fluorescence (XRF) and X-ray Diffraction (XRD) analysis at the Nigerian Mining Research, Kaduna, Nigeria. The fine and coarse aggregates used were natural river sand and natural crushed stone. The maximum sizes of the fine and coarse aggregates were 5 mm and 20 mm respectively. The physical properties of the materials were determined and the result is presented in Table 1.

Figure 1: Sun drying of Washed Eggshell

Table 1: Basic Properties of Materials

Material	Bulk Density (gm/cc)	Specific gravity	Standard consistency(%)	Initial setting time(min)	Final setting time(min)	Fineness(%)	Water Absorption (%)
Cement	-	3.1	3	38	480	5.3	-
Waste Eggshell Powder	0.81	0.86	-	-	-	-	-
Fine Aggregate	-	2.62	-	-	-	-	1.45
Coarse Aggregate	-	2.65	-	-	-	-	0.39

2.2 Production of Concrete Samples

The UK BRE mix Design method, formerly the Department of Environment (DOE) method was used to obtain the proportion of the materials for a concrete with target compressive strength at 28 days of 25 MPa. The mix-proportion of the control concrete is provided in Table 2. The waste eggshell powder was incorporated as a replacement for cement in the concrete mix. The content of the waste eggshell powder was 5%, 10% and 15% of the cement in four different concrete mixes. The water/cement ratio of 0.5 was fixed for all the mixes. The mixes are conveniently designated as M_1, M_2, M_3 and M_4. After batching the derived proportion of the materials, they were thoroughly mixed in a concrete mixer to give a homogenous entity. The workability of the freshly mixed concrete was determined for each mix. Afterwards, the fresh concrete was cast in 100 x 100 x 100 mm cube-size moulds, 100 x 100 x 300 mm beam-size moulds and 100 x 200 mm cylinder moulds as shown in Figure 2. A table vibrator was used to compact the concrete in the mould. The cast concrete samples were cured in water for 28 days. At the elapse of the curing period, the compressive strength, split-tensile strength, and flexural strength of the hardened concrete were determined in accordance with BS EN 206 (1), BS 1881: 117-83 (2) and BS EN 12390 – 5: 2009 standards respectively.

Table 2: Mix Proportions of Concrete Materials

Mix	Mix ID	W/C	Water (L/m^3)	Cement (kg/m^3)	ESP Weight (kg/m^3)	Fine Agg. (kg/m^3)	Coarse Agg. (kg/m^3)
M_1	Normal concrete	0.50	60.71	117.86	0.00	195.50	229.50
M_2	5% ESP concrete	0.50	60.71	94.29	5.89	195.50	229.50
M_3	10% ESP concrete	0.50	60.71	70.72	11.79	195.50	229.50
M_4	15% ESP concrete	0.50	60.71	46.43	17.68	195.50	229.50

Figure 2: Concrete Samples

3.0 RESULTS AND DISCUSSION

3.1 Chemical Characterization

Table 1 shows the chemical composition of the waste eggshell powder and cement determined through XRF analysis. The XRF characterization made it possible to identify elements present in materials. The chemical composition shows that calcium oxide (CaO) is the most abundant component in the waste eggshell powder, which is comparable with that obtained for cement. Since waste eggshell powder is rich in CaO as cement, therefore, it would be a suitable replacement binder for cement in concrete. However, the value of the LOI is high, which means there is a high amount of carbon in the waste eggshell powder. The XRD analysis result of the waste ESP sample is represented in Figure 3.

Table 2: XRF Characterization of Waste Eggshell Powder and Cement

Chemical Properties	Cement (%)	Eggshell powder(%)
SiO_2	22.350	0.387
AL_2O_3	10.880	0.194
Fe_2O_3	5.870	413.2 ppm
CaO	55.710	53.039
TiO_2	0.490	30.7 ppm
Ag_2O	0.543	0.340
MgO	1.150	780.5 ppm
SO_3	1.590	0.291
K_2O	0.170	0.106
Others	–	0.104
Loss on ignition (L.O.I)	1.230	40

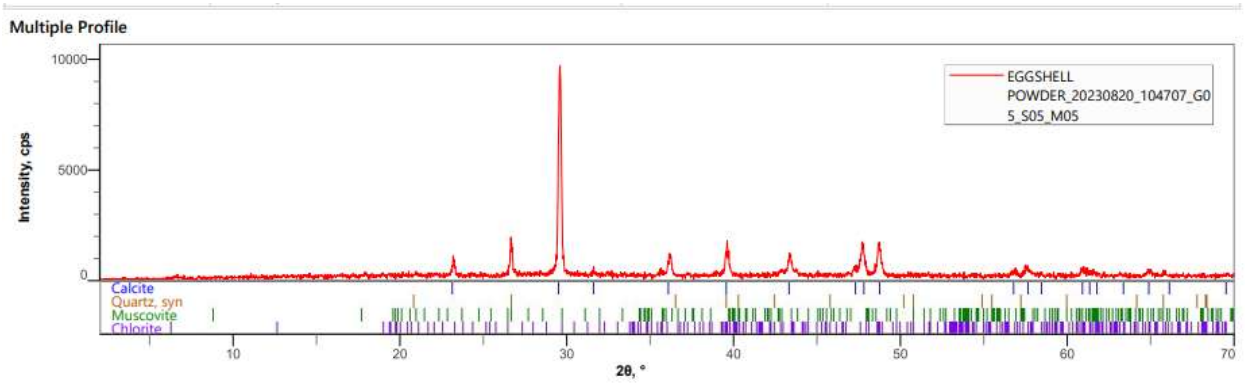

Figure 3: XRD Result of Eggshell Powder

3.2 Workability of the Concrete Mix with Eggshell

Figure 4 depicts the obtained workability values for all concrete mixes. It can be observed that the concrete workability increased as the content of waste eggshell powder increased up to 10%. The increment could be due to the water absorption property of the waste eggshell powder. Beyond the 10% addition of waste eggshell powder, there was a reduction in the workability of the concrete due to the resulting high stiffness.

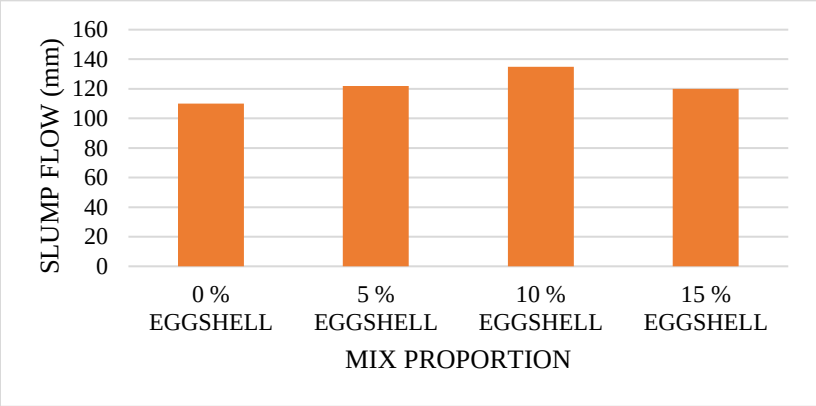

Figure 4: Workability of Concrete mix with varying percentages of Eggshell

3.3 Strength Properties of the Concrete

Table 3: Average Compressive, Split-tensile and Flexural Strengths of the Concrete Samples

ESP	Average Compressive Strengths (N/mm^2)	Standard Deviation	Average Split-Tensile Strengths (N/mm^2)	Standard Deviation	Average Flexural Strengths (N/mm^2)	Standard Deviation
0% ESP	26.6	1	0.84	1	3.05	1
5% ESP	28.9	0.1	1.14	0.1	3.39	0.205
10% ESP	30.2	0.8	1.64	0.04	3.52	0.1
15% ESP	21.2	1.8	1.00	0.04	2.97	0.03

Table 3 presents the obtained average compressive, split tensile and flexural strengths results of concrete containing waste ESP at different dosages. At 28 days, the obtained compressive strength of the control mix was 26.60 N/mm^2. There was an increased trend of compressive strength of the concrete as the waste eggshell powder increased up to 10%. The inclusion of eggshell powder paved an active path in covering up the voids present in the control concrete mix. The eggshell is majorly constituted of calcium contents that when added to the cementitious system, highly reacts to cement by generating a larger network of calcium silicate hydrate (CSH) minerals. This rise in CSH gels converted the microstructure of the cement mortar to be denser at 28 days. At a higher content of 15%, there was a significant reduction in compressive strength. Compared with normal concrete, the compressive strength increased by 8.7%, 13.5% at 5% and 10% replacement and decreased by 20.3% at 15% replacement of cement in concrete mix.

Similarly, the results showed that the split tensile strength and flexural strength of concrete increased as the replacement of cement with waste eggshell powder increased. The increment continued till the 10% replacement. Further increase in the percentage of waste eggshell powder resulted in a significant reduction in split tensile strength and flexural strength of the concrete. In comparison with normal concrete, the split-tensile strength increased by 35.7%, 95.2% and 19.1% at 5%, 10% and 15% replacement of cement in the concrete mix. In the same vein, the flexural strength increased by 11.2%, 15.4% at 5% and 10% replacement and decreased by 2.6% at 15% replacement of cement in the concrete mix. This, in conformity with previous studies, indicated that 10% of conventional cement

can be substituted with waste eggshell powder without affecting the strength properties but rather enhancing these properties.

4.0 CONCLUSIONS

The XRF results showed that waste eggshell powder is rich in CaO components, hence, it is suitable as a replacement for conventional OPC.

The compressive strengths of the concrete obtained were 26.6 N/mm^2, 28.90 N/mm^2, 30.20 N/mm^2, and 21.20 N/mm^2 for different mix combinations containing 0%, 5%, 10% and 15% of waste ESP at 28 curing days. The flexural strengths of the concrete were gotten to be 3.05 N/mm^2, 3.39 N/mm^2, 3.52 N/, and 2.97 N/mm^2 for concrete mixes with 0%, 5%, 10% and 15% of waste ESP. The split tensile strengths of the concrete were gotten to be 0.84 N/mm^2, 1.14 N/mm^2, 1.64 N/mm^2, and 1.0 N/mm^2 for concrete mixes with 0%, 5%, 10% and 15% of waste ESP.

The results show that 10% inclusion of eggshell powder resulted in a much more packed microstructure while simultaneously attaining the greatest strength. This was related to the existence of calcium carbonate in eggshell powder, which efficiently interacts with the cement and produces the CSH gel network, reducing voids in the cementitious system. This contributes to the strength and longevity of the material. Greater replacement of eggshell powder above the optimum content of 10% resulted in a decline in the strength values.

Based on this study, it is recommended that further research on the durability characteristic of concrete containing ESP should be carried out. Additionally, the potential of ESP in geo-polymer concrete should also be investigated. Finally, relevant authorities should also collaborate in the management and disposal of eggshell wastes to save the environment from pollution and encourage more research in this area of study.

ACKNOWLEDGEMENT

We would like to thank all of those who have supported this research. The pick-up vendors at Tanke, Ilorin and especially the Departments of Civil Engineering at the University of Ilorin and the University of Tabuk, among others, that have supported and facilitated the research activities.

REFERENCES

B. Divya, K. Vasanthavalli, R. Ambalavanam. (2017). 'Investigation on Cement Concrete at Mixed with Egg Shell Powder. *Int. J. Innovative Res. Sci., vol,-6,*.

Dhanalakshmi, N.J. Sowmya, A. Chandrasheka. (2015). A Comparative Study on EggShell Concrete with Partial Replacement of Cement by Fly Ash, *Int. J. Res. Appl. Sci. & Eng. Technol. (IJRASET), Vol.-3, Special Issue-1*.

S.A. Raji, A.T. Samual. (2015). Eggshell as a fine aggregate in concrete for sustainable construction. *Int. J. Sci. & Technol. Res., vol.-4, issue 09,*.

Bysani Mythili, Chennupati Sobha Rani, Naralasetti Srinivasarao. (2017). A study on limited substitution of eggshell powder with cement in concrete. *International Journal of Scientific Engineering and Technology Research, Vol. 06, Issue. 04, pp. 0763-0766*.

D. Gowsika, S. Sarankokila, K. Sargunan, . (2014). Experimental investigation of eggshell powder as a partial replacement with cement in concrete, *International Journal of Engineering Trends and Technology, Vol. 14, Issue. 2, pp. 65-6*.

Dinesh. N, Rameshkumar. R, Arunachalam, Chandraseka, Gautam. P. (2001). Partial replacement of fine aggregate by rice husk ash and eggshell powder, *International Journal of Innovative Science and Research, Vol. 3, Issue.1, pp.1-17*.

Doh Shu Ing, Chin Siew Choo. (2014). Eggshell powder: potential filler in concrete, *Malaysian Technical Universities Conference on Engineering and Technology.*

G. Sree Lakshmi Devi, P. Srinivasa Rao, C. Venkata Siva Rama Prasad,. (2021). Experimental investigation on compressive strength of quaternary blended concrete using different mineral admixtures. *Mater. Today: Proc. 46*.

M. Mohamad Ansari, M. Dinesh Kumar, J. Milan Charles, G. Dr. Vani,. (2016). Replacement of Cement using Eggshell Powder. *SSRG Int. J. Civil Eng., vol.-3,*.

Mohadi R., Anggraini K., Riyanti F., Lesbani A. (2016). Preparation of calcium oxide from chicken eggshells, Sriwijaya. *Journal of Environment, 1, 32–35*.

Mohamed Ansari M, Dinesh Kumar M, Milan Charles J. (2016). Replacement of Cement using Eggshell Powder. *International Journal of Civil Engineering, Vol. 3, Issue no. 3, pp.1-2*.

Prosper Pliya, Duncan Cree. (2015). Limestone-derived eggshell powder as a replacement in Portland cement mortar. *Construction and Building Materials, 95, 1-9*.

R. Jayasankar, N. Mahindran, R. Ilangovan. (2010). Studies on concrete using fly ash, rice husk ash and eggshell. *International Journal of Civil and Structural Engineering, Vol. 1, Issue. 3, pp. 362-37*.

PAPER 56 - PROCESS OPTIMIZATION OF TREATMENT METHODS AND EXTRUSION TEMPERATURE FOR NUTRITIONAL COMPOSITION OF RICE PASTA ENRICHED WITH *CIRINA BUTYROSPERMI*

M.S Sanusi[1*], O. L. Oke[1], A.B. Bello[1], M. O. Idowu[2], I.B. Adedeji[3], S.A. Olaleye[1], H. T. Iyiola-Adeyemo[4], A. A. Tajudeen[1], S.O. Alasi[1]
[1]Department of Food Engineering, University of Ilorin, Ilorin, Nigeria.
[2]Department of Food Technology, University of Ibadan, Nigeria.
[3]Department of Food and Nutritional Science, University of Reading, United Kingdom.
[4]Memorial Hermann Greater Heights Hospital, Texas, United States.
[*]Email: sanusi.ms@unilorin.edu.ng

ABSTRACT
Food security remains a critical global challenge, necessitating the exploration of sustainable and nutrient-rich food alternatives such as edible insects and non-thermal technologies. This study investigated the effect of different treatment methods (boiling, ultrasound treatment, and a combination of partial boiling and ultrasound treatment) and extrusion temperature (70, 80 and 90°C) on the nutritional composition (crude protein, in-vitro protein digestibility, calcium, zinc and iron contents) of rice pasta enriched with Cirina butyrospermi. The effect of treatment methods and extrusion temperature on crude protein ranged from 15.85 to 18.27%, in-vitro protein digestibility (80.42-88.55%), calcium (48.53-56.25 mg/100g), zinc (2.42-3.56 mg/100g) and iron (3.34-5.13 mg/100g), respectively. Pasta subjected to combined partial ultrasound and partial boiling treatments at high extrusion temperatures exhibited the highest crude protein, calcium, zinc, and iron content. In contrast, lower extrusion temperatures enhanced the in-vitro protein digestibility of the pasta, irrespective of the treatment method. The optimum conditions for desirable rice pasta enriched with Cirina butyrospermi were achieved at an extrusion temperature of 80°C, combined with a partial ultrasound and partial boiling treatment method. Conclusively, exploring edible insects like Cirina butyrospermi and efficient processing methods could aid in developing an improved nutrient-rich rice pasta.

KEYWORDS: *Cirina butyrospermi*, Ultrasound, Nutritional composition, Gluten-free, Extrusion, Rice Pasta

1.0 INTRODUCTION

Pasta is a cereal-based food product that has gained wide popularity due to its convenience, nutritional benefits, and enticing tastes. It comes in a variety of unusual sizes and shapes. During pasta manufacturing, durum wheat semolina is the most preferred raw material due to the unique characteristics of its protein and gluten as well as its high concentration of yellow pigment (Meena *et al.*, 2019). However, there is an increasing consumer demand for gluten-free products, especially pasta, which has resulted from the rise in gluten intolerances and consumer awareness of celiac disease. Among gluten-free pasta, rice pasta accounts for a higher share of the gluten free pasta market due to its bland flavor, high digestibility, and hypoallergenic properties (Taddei *et al.*, 2021). Rice pasta is a popular gluten-free alternative to traditional wheat-based pasta. However, compared to wheat, rice flour has a low protein content and a relatively poor ability to develop a cohesive network, which impairs its technological performance (Marengo *et al.,* 2018). Several studies have recently emphasized the need to improve the nutritional quality of cereal-based GF (gluten free) products, highlighting the low content of essential micronutrients in these products when compared with their wheat-based counterparts (Marengo *et al.,* 2018). One possible solution to this problem is to incorporate edible insects into the pasta, as they are a sustainable and nutrient-dense source of protein.

Edible insects have gained great relevance as a food source due to their high nutritional value and the creation of alternative protein sources that align with sustainability goals for food production. Nevertheless, insects have low consumer acceptability due to social influences, disgust, cultural taboos, and habits (Sun-Waterhouse *et al.,* 2016). Thus, incorporating them into common foods, such as pasta, is a way to facilitate consumer acceptance by eliminating any insect-revealing features, like appearance or smell. *Cirina butyrospermi*, commonly known as the shea caterpillar, is a species of edible caterpillar found in West Africa. It is known for its association with the shea tree (*Vitellaria paradoxa*), from which it feeds. The shea caterpillar has garnered significant attention due to its nutritional value, culinary applications, and potential economic benefits. The shea caterpillar has been traditionally consumed by various ethnic groups in West Africa, where it is considered a delicacy. It is highly regarded for its high protein content, essential fatty acids, and mineral composition (Mbayahaga and Kouebou, 2018). Within the realm of food processing, two distinct but complementary technologies have gained prominence: ultrasound treatment and extrusion. Ultrasound treatment is a non-thermal processing method that utilizes high-frequency sound waves to induce structural and functional changes in food ingredients (Bermúdez-Aguirre *et al.,* 2011). In the context of edible insects, ultrasound treatment could have the potential to improve texture, reduce potential

allergenicity, and enhance the bioavailability of essential nutrients found in edible insects (Kim *et al.*, 2019). Extrusion, on the other hand, is a well-established technique in pasta production and is ideally suited for incorporating edible insects. From the literature, Azzollini *et al.* (2018) and Wójtowicz *et al.* (2023) examined the effects of formulation and extrusion conditions on the properties of yellow mealworm larvae and house crickets, respectively. Despite several studies on the application of edible insects and extrusion conditions on the properties of enriched extruded products, the literature is sparse on the utilization of *Cirina butyrospermi* as a novel protein source in rice pasta production and its impact on the crude protein, in-vitro protein digestibility and mineral contents (iron, zinc, and calcium) under the influence of various treatment methods. Therefore, this study aimed to investigate the effects of treatment methods ((boiling, ultrasound treatment, and a combination of partial boiling and ultrasound treatment) and extrusion temperature on the nutritional composition of rice pasta enriched with *Cirina butyrospermi*.

2.0 MATERIALS AND METHODS

2.1 Materials

Broken white rice (25kg) of FARO 44 was purchased from 3Q rice processing centre in Ilorin, Kwara State, Nigeria. The rice was milled into rice flour with a particle size of 0.30 mm mesh size using a developed hammer mill. Dried *Cirina butyrospermi* were obtained from Yeetiny Agro Foodies Ltd in Ilorin, Nigeria. Other ingredients such as bicarbonate, carboxymethyl cellulose (CMC) and salt were bought from a grocery shop in Ilorin, Kwara State, Nigeria.

2.2 *Cirina butyrospermi* Powder Preparation

The dried *Cirina butyrospermi* (6 kg) were soaked in 12 l of water for 2 h, then strained and divided into three equal portions. One portion was boiled at 100°C for 30 min, the second portion underwent 30 min of ultrasound treatment using an ultrasonic cleaner (Model CJ:008 China) set at 40 kHz and 50 W, and the third portion underwent a combined treatment (15 min each). After treatment, the *Cirina butyrospermi* were wet milled using an electric food processor (Mr. Steel Model: SUS 304, China), dried at 50°C for 30 min, sieved through a plastic strainer with a mesh size of 20 mm to remove the exoskeleton, and then packed in a resealable nylon storage pouch for later use.

2.2 Experimental design

To develop rice pasta enriched with *Cirina butyrospermi*, a Face Centre Composite Design of response surface methodology was used with Design Expert (Version 13) to analyze the interaction between treatment methods (ultrasound, boiling, and combined ultrasound and boiling) for *Cirina butyrospermi* powder and extrusion temperature (70, 80, and 90°C) on pasta nutritional composition. The significance of extrusion temperature and treatment method on the nutritional composition of the pasta were determined at 95%, 99% and 99.9% confidence level using Analysis of Variance (ANOVA).

2.3 Production of rice pasta enriched with *Cirina butyrospermi*

Figure 1 depicts the production flowchart for rice pasta enriched with *Cirina butyrospermi*. The dry mix formula comprised 1000 g of rice flour, 30 g of *Cirina butyrospermi* powder, 5 g of carboxymethyl cellulose, 5 g of sodium bicarbonate, and 5 g of salt per batch. The quantity of *Cirina butyrospermi* powder varied based on the treatment method. The mixture was blended with potable water, constituting 60% of the total mass, using a Sokany Stand Mixer (Model: Cx-6612, China). Extrusion cooking was performed utilizing a co-rotating twin-screw extruder (Model: HN-65, Zhuoheng Product, Jinan City, Shandong Province, China), which was outfitted with three electric band heaters, a hopper, a cutter, and a 3 mm die. The extruder temperatures were configured to 60°C and 70°C, controlled by the first and second heating bands, respectively. The temperature of the final heating band, governing the exit barrel, was adjusted within the range of 70°C to 90°C. Samples were fed into the hopper and conveyed into the barrel screw at a constant speed of 300 rpm, where cooking occurred. After extrusion through the 3 mm die, the pasta was collected, cooled, and dried in a fabricated oscillatory dryer at 50°C for 20 mins. Subsequently, the pasta was packed in a resealable nylon storage pouch for further quality analysis.

Fig. 1: Flow chart of the production of rice pasta enriched with *Cirina butyrospermi*

2.4 Nutritional composition

The crude protein content of the rice pasta was determined using the method established by the Association of Official Analytical Chemists, AOAC (2012). The degree of in-vitro protein digestibility (IVPD) determination of the extruded rice pasta was analyzed using the method described by Hsu *et al.* (1977) while the Ca, Zn, and Fe contents were determined using a flame atomic absorption spectrophotometer (VARIAN model AA240FS, US).

2.5 Optimization

The numerical optimization of the nutritional composition and validation of the optimization were done using the technique described by Sanusi *et al.* (2022).

2.6 Statistical Analysis

Samples were measured in triplicate and the results are presented as means ± standard deviations. Statistical analyses were done using SPSS version 20.0 to determine significant differences between means by the Duncan multiple's test of one-way ANOVA.

3.0 RESULTS AND DISCUSSION

3.1 Effect of extrusion temperature and treatment methods on the nutritional composition of rice pasta enriched with *Cirina butyrospermi*

3.1.1 Crude protein content

The crude protein content of rice pasta enriched with *Cirina butyrospermi*, influenced by extrusion temperature and treatment methods, varied between 15.85 and 18.27% (Table 1). The lowest and highest crude protein contents were observed at extrusion temperatures of 70°C and 80°C with partial ultrasound and partial boiling treatments, respectively. Partial ultrasound and partial boiling treatment were observed to favour the crude protein content of the pasta, which had the highest crude protein content. However, it was observed that there was no significant difference at p>0.05 between the rice pasta produced at 80ºC when boiling treatment and partial ultrasound and partial boiling treatment were used. Lower extrusion temperatures reduce the crude protein content, while high extrusion temperatures generally favours high crude protein content. Table 2 revealed that extrusion temperature, treatment method, quadratic interaction of extrusion temperature and treatment method have a significant influence on the protein content of the rice pasta. The quadratic model presented in Table 2 exhibited high coefficients of determination ($R^2 = 0.86$, $R^2_{adj} = 0.82$), indicating its adequacy in describing the effects of extrusion temperature and treatment methods. The polynomial model's F-value (18.69) and P-value (0.0001) further supported its significance. Figure 2 depicts that the optimal crude protein content was achieved at 80°C with partial ultrasound and partial boiling treatment. The increase in crude protein content with higher extrusion temperatures and partial ultrasound and partial boiling treatment could be attributed to protein denaturation which enhances its availability and digestibility. This finding aligns with previous research by Rafiq *et al.* (2018) on pasta. Compared to other protein-fortified pastas, rice pasta enriched with *Cirina butyrospermi* exhibited a higher crude protein content reported by Carcea (2020) and Bolarinwa and Oyesiji (2021). Thus, it a potential nutritious alternative for individuals with dietary restrictions such as celiac disease.

3.1.2 In-vitro protein digestibility (IVPD)

The in-vitro protein digestibility (IVPD) content of rice paste enriched with *Cirina butyrospermi* was significantly influenced by extrusion temperature and treatment methods at $p < 0.05$ and ranged from 80.42 to 88.55% (Table 1). The highest and lowest IVPD occurred in pasta treated with partial ultrasound and partial boiling methods at 70 and 80°C, respectively. Table 2 indicates that extrusion temperature, quadratic interaction of extrusion temperature and treatment method have a significant influence on the IVPD of the rice pasta. Generally, lower

extrusion temperatures favour the IVPD of pasta regardless of the treatment method as illustrated in Figure 2. This could be attributed to lower extrusion temperatures which could result in less denaturation of proteins. Protein denaturation can lead to the unfolding of protein structures, making them less accessible to digestive enzymes. By preserving the native structure of proteins, they are more readily digested in vitro. This corroborates with the study of Adeleye *et al.* (2020), who reported higher protein digestibility at lower extrusion temperature for pigeon pea compared to higher extrusion temperature. Ultrasound treatment showed a profound influence on the increased IVPD in this study while partial ultrasound and partial boiling treatments as well increased the protein digestibility of the enriched rice pasta. This is due to the mechanism by which the cavitation effect is produced during sonication treatment which enhances the flexibility of protein molecules by changing the interaction between protein molecules (such as hydrophobic interaction, hydrogen bonding, and disulfide bonds). The quadratic model for IVPD exhibited high coefficients of determination (R^2 = 0.76, R^2_{adj} = 0.68), indicating its adequacy in predicting the rice pasta IVPD.

3.1.3 Mineral contents

Mineral content serves as an essential quality indicator for pasta, contributing significantly to human body development and function. The influence of extrusion temperature and treatment methods on the mineral content of rice enriched with *Cirina butyrospermi* is presented in Table 1. Calcium, zinc, and iron contents of the rice pasta ranged from 48.53 to 56.25 mg/100g, 2.42 to 3.56 mg/100g, and 3.34 to 5.13 mg/100g, respectively.

Table 1: Effect of treatment methods and extrusion temperature on the nutritional composition of rice pasta enriched with *Cirina butyrospermi*

TM	ET	Crude Protein (%)	IVPD (%)	Calcium (mg/100g)	Zinc (mg/100g)	Iron (mg/100g)
1	70	16.05±0.01^{g}	88.13±0.00^{b}	48.60±0.00^{h}	2.42±0.00^{i}	3.34±0.00^{i}
1	90	17.19±0.03^{c}	87.15±0.00^{f}	53.90±0.00^{d}	3.14±0.00^{c}	4.89±0.00^{d}
3	70	16.43±0.00^{f}	87.85±0.00^{d}	52.04±0.00^{g}	2.85±0.00^{g}	3.76±0.00^{g}
3	90	17.03±0.00^{d}	85.61±0.00^{g}	55.27±0.00^{c}	3.13±0.00^{d}	5.10±0.00^{c}
2	70	15.85±0.02^{h}	88.55±0.00^{a}	48.53±0.00^{i}	2.70±0.00^{h}	3.58±0.00^{h}
2	90	17.86±0.00^{b}	82.52±0.00^{h}	56.06±0.01^{b}	3.32±0.00^{b}	5.12±0.00^{b}
1	80	16.87±0.02^{e}	87.25±0.00^{e}	52.43±0.00^{f}	2.90±0.00^{f}	4.82±0.00^{e}
3	80	18.25±0.02^{a}	88.01±0.00^{c}	53.53±0.00^{e}	3.10±0.00^{e}	4.53±0.00^{f}
2	80	18.27±0.00^{a}	80.42±0.00^{i}	56.25±0.00^{a}	3.56±0.00^{a}	5.13±0.00^{a}

TM – Treatment method, ET – Extrusion temperature, IVPD – In-vitro protein digestibility, 1 – Ultrasound treatment, 2 – Partial ultrasound and partial boiling treatment and 3 – Boiling treatment. Values within columns with dissimilar superscript letters are significantly ($p \leq 0.05$) different from each other.

Table 2: Polynomial regression coefficients of treatment methods and extrusion temperature on the nutritional composition of rice pasta enriched with *Cirina butyrospermi*

Intercept	Crude Protein	In vitro protein digestibility	Calcium	Zinc	Iron
A_0	18.14	81.760	55.42	3.45	5.04
A	0.6261***	-1.540**	2.67***	0.2747***	0.7318***
B	0.2700*	-0.176	0.9929**	0.1023**	0.0577*
AB	-0.1330	-0.315	-0.5075	-0.1088*	-0.0520
A^2	-1.13***	2.080*	-2.09**	-0.3151***	-0.5760***
B^2	-0.4200*	4.190***	-1.40*	-0.3186***	-0.2535**
R^2	0.8617	0.7561	0.8601	0.8993	0.9543
R^2 adj	0.8156	0.6748	0.8135	0.8658	0.9391
F-value	18.69	9.30	18.44	26.80	62.69
P-value	0.0001	0.0003	0.0001	0.0001	0.0001

∗Significant at 95% confidence level. ∗∗Significant at 99% confidence level. ∗∗∗Significant at 99.9% confidence level, A_0 – Intercept, A – Extrusion temperature, B – Treatment method, AB - Interaction of extrusion temperature and treatment method, A^2 and B^2 are the quadratic interaction of extrusion temperature and treatment methods and R^2 is the coefficient of determination.

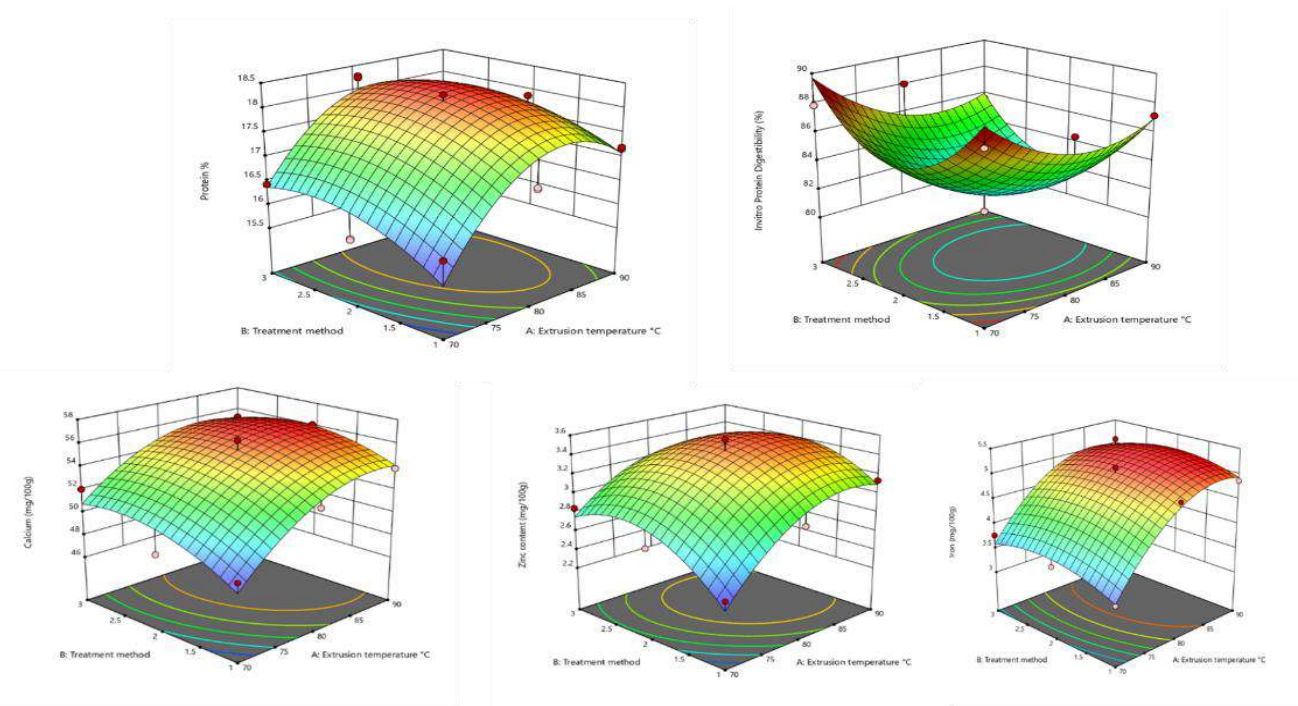

Fig. 2: Effect of treatment method and extrusion temperature on the protein content, in-vitro protein digestibility, calcium, zinc and iron of rice pasta enriched *with Cirina butyrospermi*

The partial ultrasound and partial boiling treatment methods with an extrusion temperature of 80°C yielded the highest calcium, zinc, and iron contents. Extrusion temperature, treatment methods, and their quadratic interaction significantly impacted mineral contents, while the interaction of extrusion temperature and treatment method had a significant effect on the zinc content (Table 2). Increasing extrusion temperatures favoured mineral contents across all treatment methods, which could be due to starch structure changes in rice dough at higher extrusion temperatures. These alterations induce transformations and interactions leading to molecular changes in starch molecule size and distribution, thereby enhancing mineral content. These findings align with those of da Silver *et al.* (2016), who reported similar outcomes in pasta quality assessment using a brown rice and corn meal blend. The quadratic model for mineral contents demonstrated high coefficients of determination (R^2 = 0.86, 0.90, and 0.95 for calcium, zinc, and iron, respectively) and adequacy for prediction. The high F-value and low P-value of the quadratic model further supported its significance.

3.2 Optimization of extrusion temperature and treatment method

To optimize the process, protein, in-vitro protein digestibility, calcium, zinc, and iron were considered as key nutritional composition. Numerical optimization of treatment methods and extrusion temperature was conducted to develop rice pasta enriched with *Cirina butyrospermi* with maximum nutritional content. The optimization analysis revealed that treatment method 2 (partial ultrasound and partial boiling) combined with an extrusion temperature of 80°C yielded an optimized rice pasta with predicted protein content of 18.24%, in-vitro protein digestibility of 81.57%, calcium content of 56.25 mg/100g, zinc content of 3.51 mg/100g, and iron content of 5.24 mg/100g. Experimental values under the optimum conditions were 18.26% for protein, 82.90% for in-vitro protein digestibility, 57.12 mg/100g for calcium, 3.71 mg/100g for zinc, and 5.60 mg/100g for iron. The percentage variation between experimental and predicted values ranged from 0.11% to 6.87%. An optimal desirability of 0.98 was achieved, indicating the adequacy of the optimization. Sanusi *et al.* (2023) stated in their study, desirability closer to unity signifies higher accuracy in the optimum conditions. Therefore, the optimal variable range obtained can be utilized to produce desirable rice pasta enriched with *Cirina butyrospermi* (Figure 4).

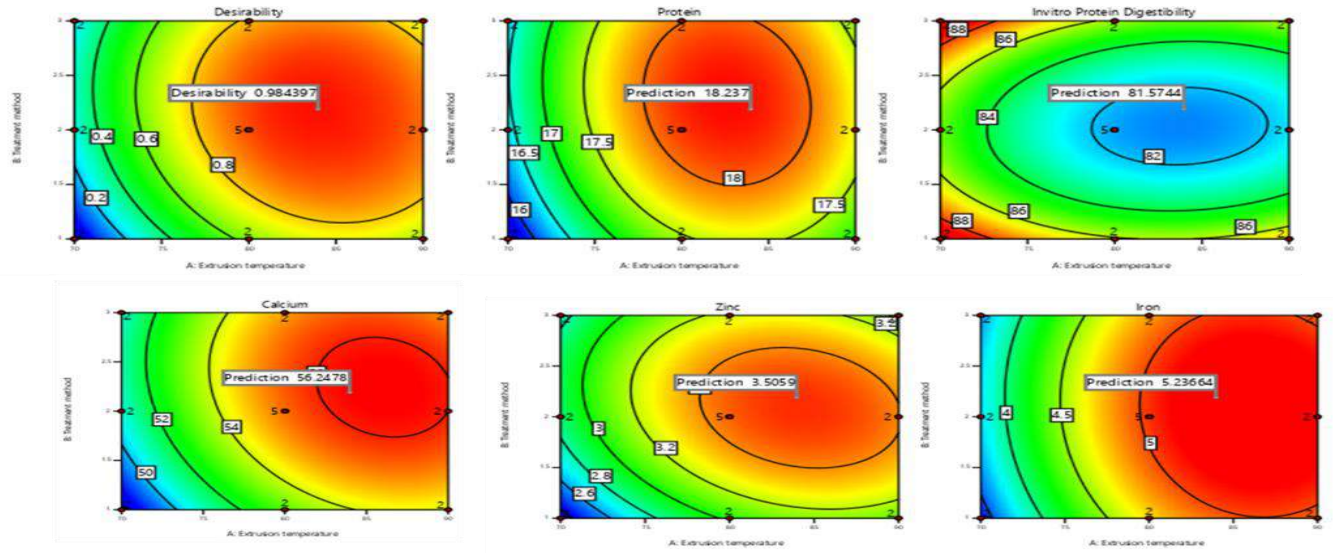

Fig. 4: Numerical optimization of treatment methods and extrusion temperature of nutritional composition of rice pasta enriched with *Cirina butyrospermi*

4.0 CONCLUSION

This study examined how different treatment methods (ultrasound, partial ultrasound and partial boiling, and boiling) and extrusion temperature affect rice pasta enriched with *Cirina butyrospermi*. Both the extrusion temperature and treatment methods significantly influenced the crude protein, calcium, zinc, and iron contents of the rice pasta. The linear effect of extrusion temperature significantly affected the in-vitro protein digestibility. Lower extrusion temperature (70°C) combined with partial ultrasound and partial boiling increased the in-vitro protein digestibility of the enriched rice pasta. Optimal levels of crude protein, calcium, zinc, and iron were achieved at an extrusion temperature of 80°C with a combination of partial ultrasound and partial boiling treatment. Generally, increasing extrusion temperature elevates mineral content, irrespective of the treatment method applied. The second-order polynomial models developed for the nutritional composition were statistically adequate. These results offer valuable insights into how treatment methods and the inclusion of the edible insect *Cirina butyrospermi* can boost the nutritional quality of rice pasta. This could pave the way for developing nutritious and sustainable food products in the future.

REFERENCES

Adeleye, O. O., Awodiran, S. T., Ajayi, A. O. and Ogunmoyela, T. F. (2020). Effect of high-temperature, short-time cooking conditions on in vitro protein digestibility, enzyme inhibitor activity and amino acid profile of selected legume grains. *Heliyon*, 6(11).

Association of Official Analytical Chemists AOAC (2012) Official methods of analysis of the Association of Analytical Chemists International, 19th edition. AOAC, Gaithersburg, Maryland.

Azzollini, D., Derossi, A., Fogliano, V., Lakemond, C. M. M. and Severini, C. (2018). Effects of formulation and process conditions on microstructure, texture and digestibility of extruded insect-riched snacks. *Innovative Food Science and Emerging Technologies*, *45*, 344-353.

Bolarinwa, I.F. and Oyesiji, O.O. (2021) Gluten-free rice-soy pasta: proximate composition, textural properties and sensory attributes. *Heliyon*, 7(1):1-7 https://doi.org/10.1016/j.heliyon.2021.e06052

Bermúdez-Aguirre, D., Mobbs, T. and Barbosa-Cánovas, G.V. (2011) Ultrasound applications in food processing. *Ultrasound Technologies for Food and Bioprocessing*, 1: 65-105

Carcea, M. (2020). Quality and nutritional/textural properties of durum wheat pasta enriched with cricket powder. *Foods*, 9(9): 1298

da Silva E.M.M., Ascheri, J.L.R., Ascheri, D.P.R. (2016) Quality assessment of gluten-free pasta prepared with a brown rice and corn meal blend via thermoplastic extrusion. *LWT-Food Science and Technology*, 68:698-706

Hsu, H. W., Vavak, D. L., Satterlee, L. and Miller, G. A. (1977). A multienzyme technique for estimating protein digestibility. *Journal of Food Science*, *42*(5), 1269-1273.

Kim, T.K., Yong, H.I., Kim, Y.B., Kim, H.W., and Choi, Y.S. (2019) Edible insects as a protein source: A review of public perception, processing technology, and research trends. *Food Science of Animal Resources*, 39(4): 521

Marengo, M., Amoah, I., Carpen, A., Benedetti, S., Zanoletti, M., Buratti, S. and Iametti, S. (2018). Enriching gluten-free rice pasta with soybean and sweet potato flours. *Journal of Food Science and Technology*, 55, 2641-2648.

Mbayahaga, J. and Kouebou, C.P. (2018) Edible caterpillars of the Shea tree caterpillar (*Cirina butyrospermi*): Traditional knowledge, nutritional value and potential for sustainable development in Burkina Faso. *International Journal of Agriculture and Biological Science*, 14(4):101-109

Meena, G.S., Dewan, A., Upadhyay, N., Barapatre, R., Kumar, N. and Singh, A.K. (2019). Fuzzy analysis of sensory attributes of gluten free pasta prepared from brown rice, amaranth, flaxseed flours and whey protein concentrates. *Journal of Food Science and Nutrition Research*, 2(1):22-37

Rafiq, A., Sharma, S. and Singh, B. (2018) Effect of pregelatination on rheology, cooking and antioxidant activity of pasta. *Journal of Food Science and Technology*, 55:1756-1766

Sanusi M.S., Sunmonu, M.O., Abdulkareem, A., Alaka, A. (2022) Modelling and optimization of the quality indices for the production of ingredient-mix based dried chicken product (chicken kilishi). *Scientific Journal of Meat Technology*, 63(1): 33-50. https://doi.org/10.18485/meattech.2022.63.1.4

Sanusi, M. S., Sunmonu, M. O., Alasi, S. O., Adebiyi, A. A., & Tajudeen, A. A. (2023). Composition, bioactive constituents and glycemic index of brown rice-watermelon seeds extruded snacks as stimulated by extrusion conditions. *Applied Food Research*, 3(1), 100287.

Sun-Waterhouse, D., Waterhouse, G. I., You, L., Zhang, J., Liu, Y., Ma, L. and Dong, Y. (2016) Transforming insect biomass into consumer wellness foods: A review. *Food Research International*, 89:129-151.

Taddei, F., Galassi, E., Nocente, F. and Gazza, L. (2021) Innovative milling processes to Improve the technological and nutritional quality of parboiled brown rice pasta from contrasting amylose content cultivars. *Foods*, 10(6): 1316

Wójtowicz, A., Combrzyński, M., Biernacka, B., Oniszczuk, T., Mitrus, M., Różyło, R. and Oniszczuk, A. (2023). Application of Edible Insect Flour as a Novel Ingredient in Fortified Snack Pellets: Processing Aspects and Physical Characteristics. *Processes*, *11*(9), 2561.

PAPER 57-OPTIMAL ALLOCATION OF STATCOM ON POWER TRANSMISSION NETWORK USING DRAGONFLY ALGORITHM

J. Abubakar[1*], S. Salisu[2], B. Jimoh[2], A. A. Umar[2], A. Yusuf[3]

[1*] Department of Consult. and Production, National Research Institute for Chemical Technology, Zaria, Nigeria.
[2] Department of Electrical Engineering, Ahmadu Bello University, Zaria, Nigeria.
[3] Department of Outstation, National Research Institute for Chemical Technology, Zaria, Nigeria.
[*]Email: tsannigida@yahoo.com

ABSTRACT

Power transmission networks operate closer to their voltage stability limits, due to daily escalating demand of electrical energy. Such issue leads to voltage instability, which may pilot system collapse. Emerging Flexible Alternating Current Transmission Systems (FACTS) devices are engaged to attain appropriate utilization of the existing transmission networks. This work proposed a novel Artificial Intelligence (AI) approach explicitly, Dragonfly Algorithm (DA,) in determining the optimal allocation of Static Compensator (STATCOM) for voltage stability enhancement in the network. The simulation was conducted using Newton Raphson Load Flow (NRLF) method on IEEE 30-bus test system. The DA results were compared to those of the Genetic Algorithm (GA).With GA approach, two STATCOMs were optimally located at buses 19 and 20. The Voltage Profile Enhancement Index (VPEI) achieved was 1.0334, with optimal size of 36.74 MVar each, after 8 iterations. In the case of DA, the devices were located at buses 19 and 24 with optimal size of 36.80 MVar each after 5 iterations, with a VPEI of 1.0505. The results have generally signified the efficacy of DA over GA algorithm.

KEYWORDS: DA algorithm, NRLF, Power quality, Static compensator, VPEI.

1. INTRODUCTION

At present, power demand is escalating in an enormous rate owing to the advanced revolution of electrical load. As such, transmission lines are likely to experience congestion (Dasa *et al.* 2020). This congestion may lead to electrical load malfunction, poor power quality, which results in objectionable effects such as voltage instabilities and so forth (Nikum *et al.* 2020). To find out the instability in a network, numerous techniques of power flow analysis are involved. Newton Raphson (NR) method, among others, is employed in this work, due to its robust convergence characteristics as compared to other methods. Transmission networks are bounded by voltage instabilities. Consequently, voltage stability control has become necessary. FACTS compensators explicitly; Static Compensator (STATCOM), and the likes are needed for such effective voltage control (Afolabi *et al*. 2020). The STATCOM device optimal allocation can be achieved using either of the AI emerging techniques and hence DA in this study. DA is an AI swarm-based optimization method second-handed in solving single and multi-objective optimization problems (Meraihi *et al*., 2020). It has static and dynamic natural swarming behaviours (Baiche *et al*., 2019).

Some researchers have worked on STATCOM for effective voltage control on power transmission systems among which are: (Vandana and Verma 2014) worked on voltage stability enhancement through the optimal location of STATCOM, where Genetic Algorithm (GA) was employed for the optimal location of STATCOM. The algorithm used the natural method for selection of certain parameters; mutation, crossover and fitness function. The optimal positioning of this device improved the voltage profile of some buses on IEEE 14 30 bus power systems, reduced the losses, and the system performance.

Shaswat, *et al*. (2018) presented work on the optimal siting of STATCOM voltage stability enhancement and loss minimization on a 9-Bus IEEE power system. Valeriya *et al*. (2018) worked on STATCOM using a Particle Swarm Optimization (PSO) algorithm on two distinct networks (IEEE 14 and 30 bus networks) which provided stability and reliability of the grids with minimized power losses. Ganggang *et al*. (2019) presented work on optimal positioning of STATCOM with and without Battery Energy Storage (BES) and two benchmark power systems. The results depicted a considerable improvement in voltage profiles of the network. In the year (2020), Sreedharana, *et al*. presented a study on power system loading margin enhancement by optimal STATCOM incorporation on IEEE 14-bus test system. The STATCOM integration enhanced the voltage profiles of the network.

Afolabi *et al*. (2020) offered a study on 132 kV Bida power transmission network. The results revealed a significant voltage profile improvement as compared those of the base case. Zobaa and Al-Majali (2024) proposed a Mixed Integer Distributed Ant Colony Optimization (MIDECO) in allocating STATCOM devices optimally for voltage stability improvement while minimizing device cost of installation.

The aforementioned research works reviewed yielded promising results but characterized by intuition-based manual device placement, converging at local minima solution and high computational time. This research work shows that application of DA in the optimal sizing and siting of STATCOM improved the power quality and bus voltage profiles of the entire system, in an efficient and competent mode.

1.1 Overview of IEEE 30-Bus Test System

The standard IEEE 30-bus test system consists of 41 transmission lines and 6 generating stations. The single line diagram of the network is shown in Figure 1. The voltages have been constrained within the limits of 0.95 p.u to 1.1 p.u. The line data, buses data, the minimum and maximum limits of the test system are in per unit taking into consideration a base power of 100 MVA (Bagha and Kumar 2019).

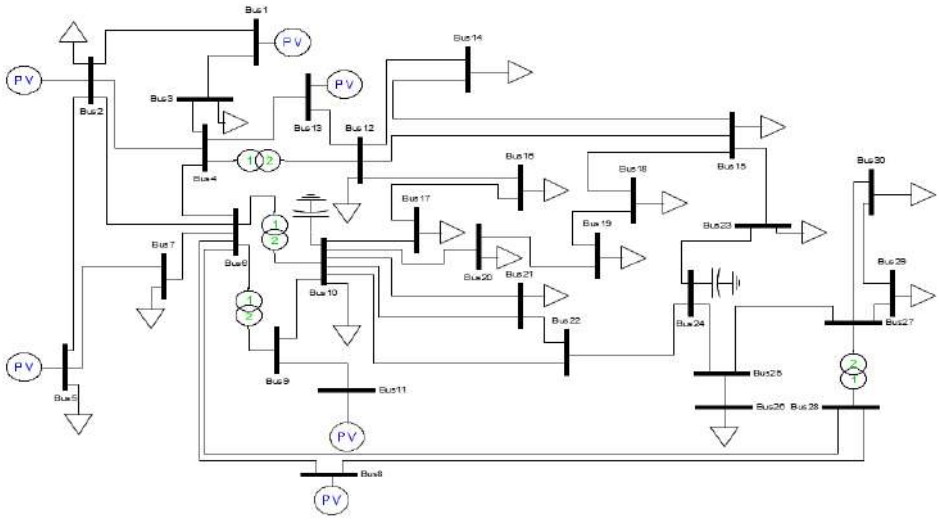

Figure 1: Single Line Diagram of IEEE 30-Bus Test System (Bagha and Kumar 2019)

1.2 Static Compensator (STATCOM)

STATCOM provides mutually capacitive and inductive control and leads to controlling its output current above the rated highest limit independently despite the amount of system voltage, even as near to the ground typically 0.15 p.u. as shown in Figure 2 (Mathur and Varma, 2002).

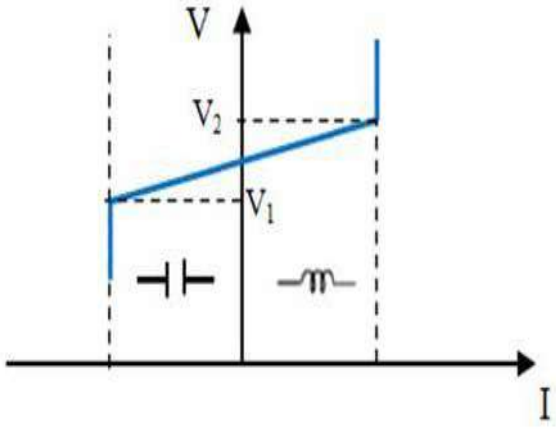

Figure 2: Voltage- Current Characteristics of STATCOM (Mathur and Varma, 2002).

2. THEORETICAL ANALYSIS

The mathematical theories involved in achieving the results are presented in this section.
The path representation of STATCOM integrated to bus *i* of an *N*-bus power network is presented in Figure 3.

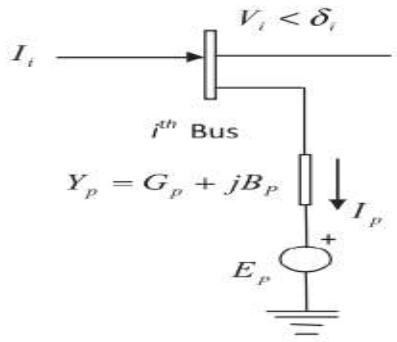

Figure 3: STATCOM Steady State Representation (Dutta *et al*., 2016)

From the equivalent circuit of Figure 3, (Musa and Mustapha, 2015):

$$E_p = \quad E_p \angle \theta_p \tag{1}$$

$$V_i = \quad V_i \angle \theta_i \tag{2}$$

*E*p stands for voltage source in series connection with impedance, *Vi* depicts voltage at bus *i*, θ_P is the admittance angle between the ith and kth buses and θ_i signifies admittance angle at bus *i*.

Now, the STATCOM voltage source and the complex power are given by Equations (3) and (4).

$$V_p = E_p(\cos \delta_P + j \sin \delta_P) \tag{3}$$

δ_P = Angle of STATCOM voltage source

The complex power of STATCOM is certain by Equation (4):

$$\mathrm{S_p} = \mathrm{E_p I_P}^* = \mathrm{E_p Y_P}^* \left(\mathrm{E_P}^* - \mathrm{V_p}^*\right) \tag{4}$$

$\mathrm{Y_p}$ describes an admittance of STATCOM shunt coupling transformer.

The power flow equations of the candidate are given by Equations (5) and (6) (Dutta *et al*., 2016).

$$P_m = P_p + \sum_{k=1}^{n} |V_i||V_k||Y_{ik}| \cos(\theta_{ik} - \delta_i + \delta_k) \tag{5}$$

The subscript i and k stand for sending end and receiving end buses. Whereas, m denotes bus to which a device is connected.

$$Q_m = Q_p + \sum_{k=1}^{n} |V_k||Y_{ik}| \sin(\theta_{ik} - \delta_i +) \tag{6}$$

The power equation required to evaluate the load flow problem is specified by Equation (7).

$$P_{Ep} = -G_p \left|E_p\right|^2 + \left|V_{ip}\right| |E_P| |Y_P| \tag{7}$$

P_{Ep} represents source of STATCOM power consumed, V_{ip} depicts voltage at the i_p^{th} bus, $\mathrm{G_p}$ and $\mathrm{B_p}$ are conductance and susceptances of the device.

Step vector (DX) and position vector (X) were applied to improve the location of swarms (Mirjalili, 2015) and are given by Equations (8) and (9) (Baiche *et al*., 2019):

$$\Delta X_{t+1} = (sS_1 + aAiX_i + cC_{il} + fF_i + eE_i) + w\Delta X_i \tag{8}$$

S and S_1 stands for weight leverage and i-th individual separations, *a and* A_i weight and i-th individual alignment, *c* and C_i denote weight and i-th individual cohesions, *f* an F_i represent factor of food source and food source of the i-th individual, *e* and E_i describes enemy distraction weight factor and i-th individual enemy position, *w* depicts Weight of inertia and *t* is the counter of iteration.

$$X_{t+1} = X_t \ + \Delta X_{i+1} \tag{9}$$

t stands for the current iteration.

Le´vy flight factor in Equation (10) is used to restructure the random manners of the flies (Mirjalili, 2015):

$$X_{t+1} = X_t \ + Le´vy(d) \times X_t \tag{10}$$

d Stands for position vectors dimension.

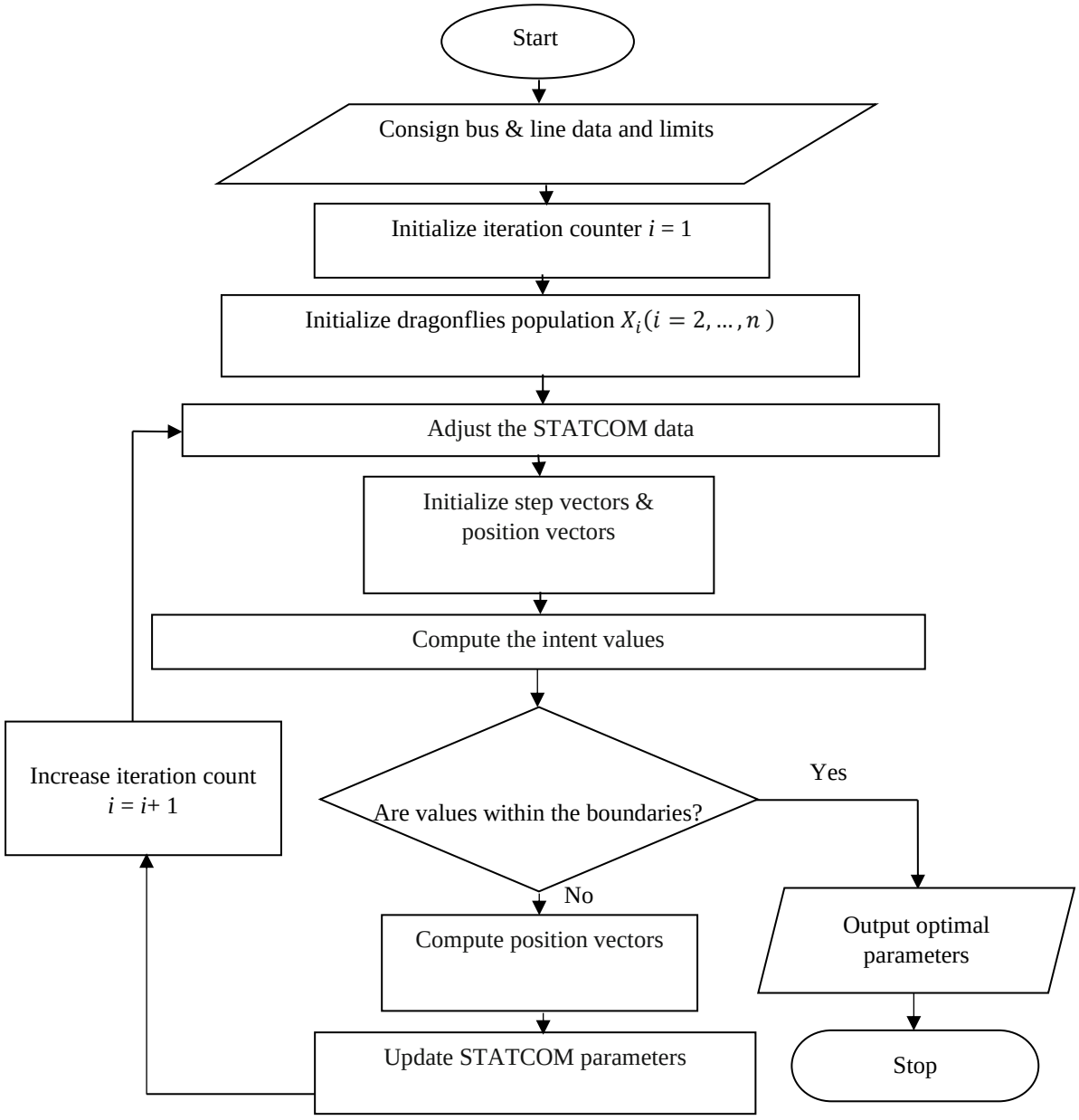

Figure 4: Flow chart of DA (Abubakar *et al*., 2021)

The $VPEI$ was employed in comparing the performance analysis between the approaches and is given by Equation (11) (Abubakar *et al*., 2021).

$$VPEI = (VPI_{WSSC})/(VPI_{WOSSC}) \quad (11)$$

Where VPI_{WSSC} and VPI_{WOSSC} stand for voltage profile index with and without static compensator.

$$VPI = \frac{1}{N_B}\sum_{k=1}^{N_B} VP_k \quad (12)$$

VP_k is the voltage profile at k^{th} bus and N_B describes total number of load nodes in the network.

3. METHODOLOGY

The methodologies adopted in achieving the set objectives are discussed in this section.

3.1 Conditions for sizing and siting of STATCOM

Three assumptions were made in finding the optimal size and location of the STATCOM device as follows:
a. STATCOM working at unity power factor.
b. Only single device can be placed at a bus.
c. For a multiple device, the STATCOMs should be of common capacity and stochastically chosen.

3.2 Parameter assortment

The parameters of DA adopted in this research work are obtainable in Table 1.

Table 1: DA parameter assortments

Definition	Factor	Values
Inertia weight	*w*	0.4 – 0.9
Weight of Separation	*s*	2
Weight of alignment	*a*	2
Food source weight	*f*	2
Enemy distraction weight	*e*	2
Cohesion weight	*c*	0.1
Bus voltage limit (pu)	VP	0.95-1.05

3.3 Formulation of Objective Function

The fitness function and constraints (equality and non-equality) formulated to achieve the set objectives for this work are given by Equations (13) to (21),

$$f = Max \sum_{i=1}^{i=N_B} F(V_B), \{SSC(C_{SSC}, N_{SSC})\} \quad i = 1,2,3 \ldots N \quad (13)$$

$$F(V_B) = 0 \ \ if \ 0.95 \leq Vi \leq 1.05 \quad (14)$$

f stands for fitness function to be optimized, $F(V_B)$ is the violation function of bus voltage, N_B signifies the number of buses within the network and Vi represents the voltage at *ith* bus, C_{SSC} denotes capacity of STATCOM device and N_{SSC} represents bus location of STATCOM device.
Otherwise, $F(V_B)$ will be given by Equation (15) (Abubakar *et al*., 2021),

$$F(V_B) = log\varphi(\ F(V_B) * abs\left[\frac{V_{i(nominal)} - V_i}{V_{i(nominal)}}\right]\left[\frac{1}{lin}\right] \quad (15)$$

$\varphi($ $F(V_B)$ is the index value for percentage of bus voltage against acceptable limit, $V_{i(nominal)}$ stands for nominal voltage magnitude at bus *i and Lin* denotes integer coefficient to regulate voltage variations.

Subject to:

$$P_L = P_G - P_D(V, \delta) \quad (16)$$

$$Q_L = Q_G - Q_D(V, \delta) \quad (17)$$

$$P_{Gi}^{Min} \leq P_{Gi} \leq P_{Gi}^{Max} \; i = 1,2,3 \ldots N \quad (18)$$

$$Q_{Gi}^{Min} \leq Q_{Gi} \leq Q_{Gi}^{Max} \; i = 1,2,3 \ldots N \quad (19)$$

$$V_i^{Min} \leq V_i \leq V_i^{Max} \quad (20)$$

$$V_{sh}^{Min} \leq V_{sh} \leq V_{sh}^{Max} \quad (21)$$

P_L and Q_L stand for active and reactive power losses, P_G and Q_G are the generated active and reactive powers, and $P_D(V, \delta)$ and Q_D depict active and reactive power demands Q_{Gi}^{Min} and Q_{Gi}^{Max} are lower and upper limits of reactive generated powers, V_i^{Min} and V_i^{Max} denote lower and upper limits of bus voltage, V_{sh}^{Min} and V_{sh}^{Max} are the lower and upper limits of STATCOM shunt voltage.

4. RESULTS AND DISCUSSION

The simulation results obtained without and with STATCOM device incorporated have been presented in this section. The voltage magnitudes of the network buses without STATCOM devices are presented in Figure 5.

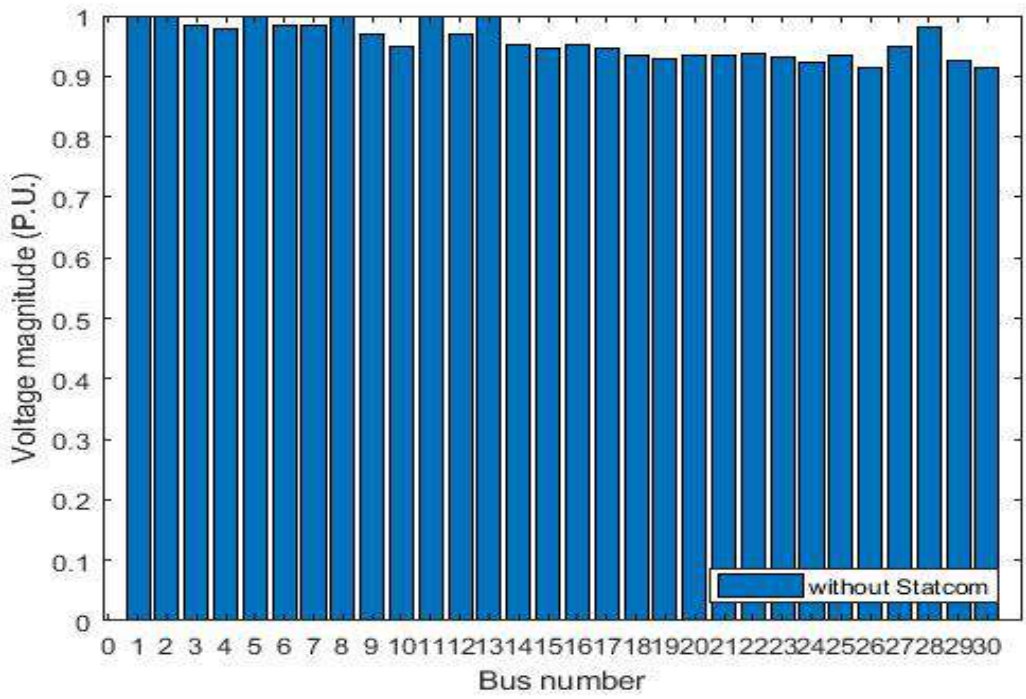

Figure 5: Voltage Profile of the network without STATCOM

It is identified that fifteen buses are outside the steady acceptable bus voltage limit (0.95 - 1.1 p.u) and therefore considered weak.

Following the optimal placement of STATCOM using GA at buses 19 and 20 as shown in the work of (Vandana and Verma, 2014), these weak bus voltage profiles were improved significantly, except for six buses that are still outside the range as shown in Figure 6.

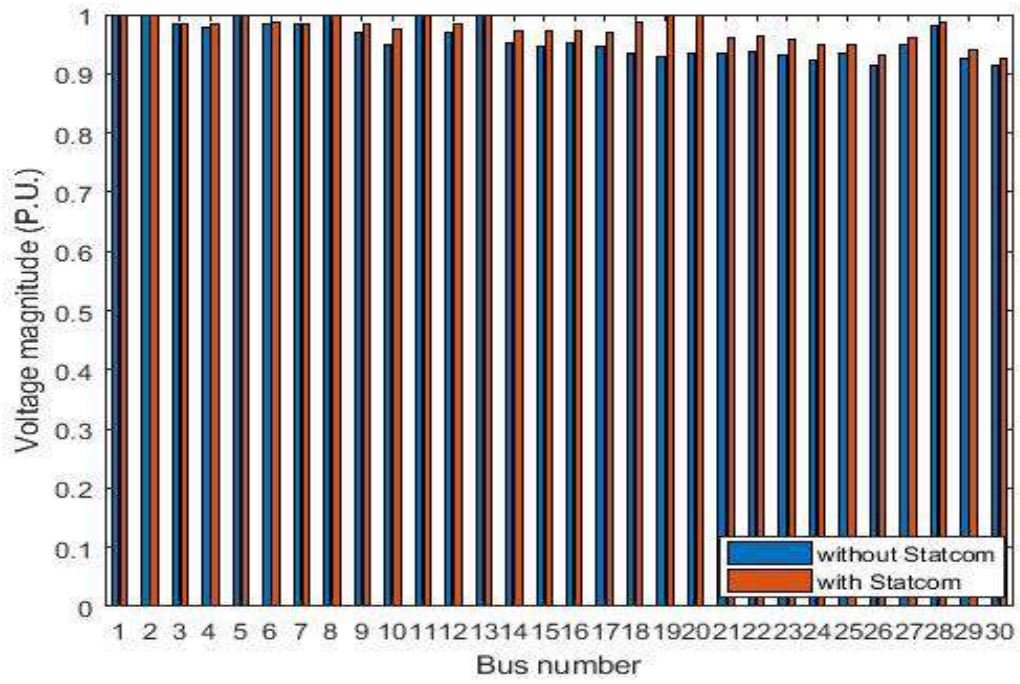

Figure 6: Voltage Profile of the network using GA

Subsequently, DA was employed in the optimal allocation of STATCOMs at buses 19 and 24. It is observed that the voltage profiles of the entire network's buses were within an acceptable voltage limit, as shown in Figure 7.

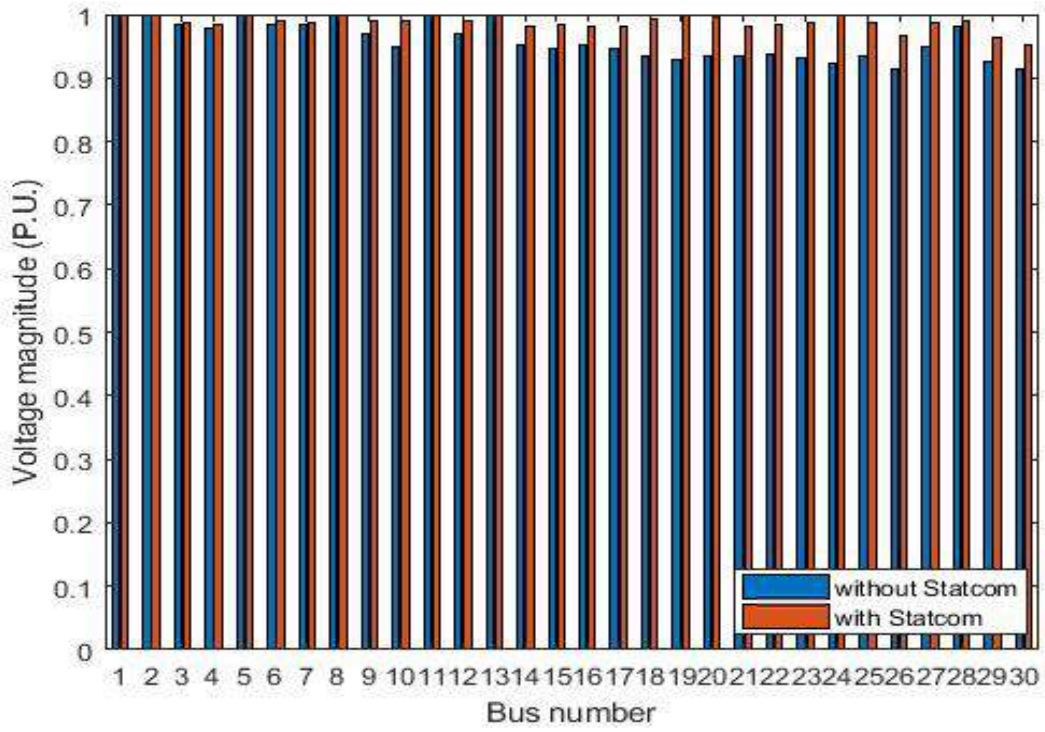

Figure 7: Voltage Profile of the network using DA

Figure 8 shows that the VPEI was found to be 1.0334 using GA and subsequently 1.0505 when DA was optimally applied.

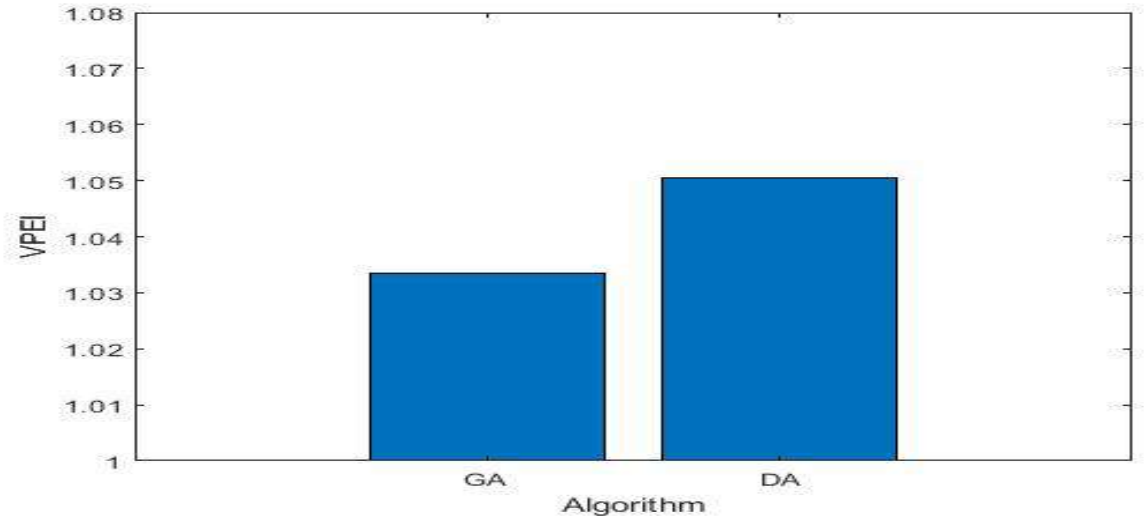

Figure 8: Comparison of VPEI between GA and DA algorithm

The executive summary of the entire simulation results attained at the base and optimal scenarios are presented in Table 2.

Table 2: Summary of the simulation results

Case	No. of Iteration	Bus Location	STATCOM Size (MVar)	VPI	VPEI
Base Case	-	-	-	3.785	-
GA	8	19, 20	36.74	3.912	1.0334
DA	5	19, 24	36.80	3.977	1.0505

5. CONCLUSION

In this research work, AI technique has been employed for the optimal allocation of STATCOM devices on IEEE 30-bus test system, to address the issue of voltage instability across the network. In comparison of results obtained, the proposed DA technique shows more effective and robust simulation results than GA algorithm. The simulation results established the following findings and contributions:

i. That the overall system voltage profile was found weak at the base case due to voltage limit violations of some buses.
ii. That the introduction of AI in the optimal allocation of STATCOM devices enhanced the voltage stability of the entire system.
iii. Better understanding of artificial intelligence techniques explicitly DA's optimization behaviour and its application in real-world power system.

Recommendation for Further Work

For advanced computational efficiency, only the weak buses of the network could be considered as the searching space in the exploration as well as exploitation phases and the use of hybridized AI techniques for the optimal allocation of FACTS devices with high penetration renewable energy sources should also be employed.

REFERENCES

Abubakar J., Yusuf J. & Jimoh B. (2021). Voltage Stability Enhancement by Optimal Sizing and Siting of Static Synchronous Compensator using Dragonfly Algorithm. *Zaria Journal of Electrical Engineering Technology.* Vol. 10 No. 2. ISSN: 0261 – 1570.

Afolabi O. A., Nkeleme V. O., Alimi T. A. & Shallum T., A. (2020). Impact of Facts Devices (STATCOM) on Voltage Improvement and Transmission Losses Reduction on 132 KV Bida Power Transmission Systems Network. *IJIRETSS.* P-ISSN: 2465-7298 | e-ISSN: 2467-8163 Volume 7, Number 1 February, 2020.

Archita Vijayvargia (2016). Comparison between Different Load Flow Methodologies by Analysing Various Bus Systems. *IJEE.* ISSN 0974-2158 Volume 9, Number 2 pp. 127-138. International Research Publication House.

Bagha G. and Kumar A. (2019). Load Flow Analysis of IEEE-30 Bus System Using FACTS Devices. *Proceedings of ICAEEC-, IIIT* Allahabad India, 31st May - 1st June,2019.

Baiche K, Meraihi Y, Hina MD, Ramdane-Cherif A, Mahseur M (2019). Solving graph colouring problem using an enhanced binary dragonfly algorithm. *Int J Swarm Intell Res (IJSIR).* 10(3):23–45.

Dasa A., Dawnb S. & Gope S. (2018). A Review on Optimal Placement of FACTS Devices. *Proceedings of ICCIIoT.* Elsevier-SSRN (ISSN: 1556-5068).

Dutta S. A., Provas K. R. & Debashis N. (2016). "Optimal location of STATCOM using chemical reaction optimization for reactive power dispatch problem". *ASEJ*, pp: 233–247.

Ganggang T.U, Yanjun Li & Xiang J. (2019). "Analysis, Control and Optimal Placement of Static Synchronous Compensator with/without Battery Energy Storage". *Energies*, *12*,4715; oi:10.3390/en12244715.

Guha K., Laskar N.M., Gogoi H.J. (2017). Novel analytical model for optimizing the pull-in voltage in a flexure MEMS switch incorporating beam perforation effect. *National Institute of Technology*, Silchar, Assam 788010, India., 2017.

Mathur, R.M., & Varma, R.K. (2002). Thyristor-Based Facts Controllers for Electrical Transmission Systems. *IEE Series PRESS on Power Engineering.* ISBN 0-471-20643-1, p417-418, 2002.

Meraihi, Y., Ramdane-Cherif, A. & Acheli D. (2020). Dragonfly algorithm: A Comprehensive Review and Applications. *Neural Comput & Applic* 32, 16625–16646 (2020).

Mirjalili S. (2015). Dragonfly algorithm: a new meta-heuristic optimization technique for solving single-objective, discrete, and multi-objective problems". *The Natural Computing Applications Forum.* DOI 0.1007/s00521-015-1920-1, 2015.

Musa B. U. & Mustapha M. (2015). Modelling and Simulation of STATCOM for Reactive Power and Voltage Control. *JMEST*. ISSN: 3159-0040 Vol. 2 Issue 2, February - 2015

Nikum, K., Saxena, R. & Wagh, A. (2020). Power Quality Issues in Commercial Load - Impact and Mitigation Difficulties in Present Scenario. In: Kumar, *ICCCE*. Lecture Notes in Electrical Engineering, vol 698. Springer, Singapore. https://doi.org/10.1007/978-981-15-7961-7, 2021.

Shaswat C., Ramakanta J., Sanhita M., Swain S.& Panda P. (2018). "Optimal Allocation of STATCOM FACTS Controller for Loss Reduction and Voltage Stability Enhancement in a Nine Bus Power System". *JCI*; 8(3): 12–16p, 2018.

Sreedharana S., Joseph T., Veni C., Vishnu J., & Vipin D. (2020). Power System Loading Margin Enhancement by Optimal STATCOM Integration. *CEESD*. https://doi.org/10.1016/j.compeleceng.2019.106521.

Vandana T. & Verma, S.N. (2014). Voltage stability enhancement through optimal location of STATCOM. *Proceedings of 3rd IRF International Conference*, Hyderabad, India.

Valeriya T., Josef T. & Zdenek M. "A Novel (2018). Power Losses Reduction Method Based on a Particle Swarm Optimization Algorithm Using STATCOM". *IJAER* ISSN 0973-4562 Volume 11, Number 23 pp. 11494-11500.

Zobaa A., F. and Al-Majali, B., H. (2024). A Novel Optimal Allocation of STATCOM to Enhance Voltage Stability in Power Network. *Ain Shams Engineering Journal.* https://doi.org/10.1016/j.asej.2024.102658.

PAPER 59-DEVELOPMENT OF EXPERIMENTAL DATA CENTRE FOR IMPROVEMENT OF PEDAGOGY IN UNIVERSITY OF ILORIN, NIGERIA

J. A. Adesina*, J. F. Opadiji, A. T. Ajiboye,
Department of Computer Engineering, Faculty of Engineering, University of Ilorin, Kwara State, Nigeria
*Email: adesina.ja@unilorin.edu.ng

ABSTRACT

In a bid to enhance teaching and assessment in the Department of Computer Engineering at the University of Ilorin, Nigeria, an Experimental Data Centre (EDC) was created. This platform aims to improve lecturer-student interaction by offering various services such as access to course materials, audio-visual classes, group projects, real-time assessments, and research support. The EDC development encompasses data center architecture design, system implementation, service deployment, and performance evaluation. It connects to the university's internet with a 2.4 Gbps bandwidth and has a 5 KVA online inverter backup. Currently, it hosts two servers with a total storage of 40 TB, running both Windows and Linux OS. Services include Moodle LMS, BigBlueButton for virtual classrooms, Rocket Chat for messaging, live streaming, Document Management System, and an e-book repository. Testing and debugging are ongoing, and managed by departmental staff with stringent data security measures. Future plans involve expanding the EDC to other faculties within the university in phased upgrades.

Keywords: Courseware, Data Centre, Learning Management System, Pedagogy, virtualization

INTRODUCTION

The development of an experimental data centre was hinged on the demand for institutional deployment and improvement of pedagogy at the Department of Computer Engineering of the University of Ilorin. The commitment to facilitate lecturer-student engagement in pedagogic processes, provide a ubiquitous platform for access to courseware, audio-visual class interactions, group project development, real-time assessment of students, and leverage web infrastructure for staff and student researches, among other services was the cardinal focus of the implementation. The deployment leveraged research study on implementation framework using virtualization technology (Bie, 2019; Md. Faizul et al., 2012). Fung et al., (2016) decimating the need to procure servers per services to be deployed (Bie, 2019; Paweł et al., 2023), harnessing the power of computing for improved availability of resources, effective resource utilization, and increased service capacity (Zhen-heng et al., 2010). The optimal utilization of resources targeted equitable distribution of storage, RAM and compute power. We reviewed the power demands premised on the architectural design of the EDC, and deployed 5 KVA online inverter system, which was efficiently distributed for the equipment. This ensured optimal use of energy devoid of wastage with several services seamlessly deployed across the servers.

The experimental data centre (EDC) has overarching facilities for storage, networking (switches, firewalls, routers), power distribution systems, cooling systems (Md. Faizul et al., 2012). Virtualization, a prominent foundational infrastructure technology for cloud computing was deployed across the installed servers. The basic principles of cloud computing involve providing on-demand access to shared computing resources, which can be rapidly provisioned and released with minimal management effort or service-provider interaction. Cloud computing is known for its flexible and scalable IT architecture, which eliminates the fixed corresponding relationship between application services and hardware resources. This flexibility allows for more efficient resource utilization, reduced energy consumption, and improved overall system security and high availability capabilities (Zhen-heng et al., 2010). Hence, virtualization ensures the optimization of resource allocation. It is also referred to as the simulation of specific computational resources leveraging dedicated physical/ hardware resources using hypervisors such as Xen Orchestra, Proxmox, vSphere, VMware (Bie, 2019; Paweł, et al., 2023).

Our implementation reviewed the inherent potential impact of services deployed at the data centre such as Massive Open Online Courses (MOOCs), Electronic Document Management Systems (EDMS), eBook repository as services with attendant impact on democratisation of learning and their role as a tool for the provision of ubiquitous access to higher education (Abdellah, et al., 2020; Mpho-Entle, 2022). The research on deployment of

Massive Open Online Courses MOOCs in Africa (Abdellah, et al., 2020; Mpho-Entle, 2022) opened up the challenges of ICT infrastructure availability and the demand for prioritizing MOOC project delivery as a prominent discussion.

LITERATURE REVIEW

The review of researches on data centre implementation in universities, Higher Education Institution (HEI) were examined for a contextual review of the challenges and decision on the implementation strategy to be adopted.

In the context of the research, virtualization refers to the process of creating a virtual version of something, such as a server, operating system, storage device, or network resource (Zhen-heng, et al., 2010). The discussions were hinged on server virtualization technology, which allows computing resources to be virtualized on physical servers and built into a virtual resource pool. By subdividing the computing resources of a physical server into virtual computing resources, resource allocation grain-size can be reduced to a CPU and 1G bytes of memory, and even less. This approach simplifies the entire system resources and creates a unified "resource pool," which opens up the physical limitation of resources and allows for more flexible and efficient resource allocation. Hence, it is a departure from the traditional data centre implementation. Traditional university data centres suffer from low utilization rates, inability to share resources, difficulty in adapting to changes, and heavy maintenance workload (Bie, 2019).

Virtualization technology addresses these issues by creating a virtual computing environment that abstracts and transforms entity resources, shields hardware platform heterogeneity, and provides users with independent, isolated, and secure computing or running environments on demand. This allows for efficient resource reuse and transparent sharing, ubiquitous access, and centralized management of hardware and software resources. The research highlighted the challenges of data centre implementation in the University as high-availability issues, resource utilization problems, and manageable issues. These challenges can be considered as limitations in the current approach to data center construction in digital campuses. Hence, it emphasizes the need for more flexible, efficient, and high-availability solutions to address these challenges without delving into the services deployed and its impact on pedagogy, leveraging Moodle, and eBook repository among a host of other services.

With the H3C Cloud deployment in a digital campus, explored the construction of a university data centre (Bie, 2019). H3C CAS is a cloud computing management software that automates and manages cloud computing resources, including servers, storage, and network devices. As a proprietary solution, it provides a unified management platform for cloud computing resources, supports virtualization technology, and enables administrators to manage and monitor the entire cloud infrastructure from a single console. H3C CAS is used in university data centres to integrate and redistribute server resources, providing basic architecture resources to all teachers and students. This process enables the loading of network and storage hardware into a resource pool, providing basic architecture resources to all teachers and students. The virtualization technology ensures the creation of independent, isolated, and secure computing environments on demand, leading to improved resource utilization and flexible allocation for the university data centre. Bie, (2019) supports the advantages outlined in Zhen-heng et al. (2010) on virtualization technology such as resource pooling, on-demand allocation, flexibility and their need for deployment at data centres in a University as against the traditional deployment methods. Meanwhile, the researches on data centre deployment by Bie, (2019) and Zhen-heng et al., (2010) did not explore the impact of teacher-learner centric services in a University community but highlighted enhanced access to resources, flexibility, cost effectiveness, and scalability as vital impacts of its deployment.

METHODOLOGY

This study aims to document the findings of the deployment of an Experimental Data Centre in an academic setting of the department of Computer Engineering, University of Ilorin. This is focused on accessing staff-student interaction for courseware delivery, audio-visual class interactions, group project development, and real-time assessment of students. The computer Engineering department has student enrolment of three hundred and fifty-eight (358) within the (2019-2023) session. The increasing need to effectively cater for student learning improve pedagogical experiences, provide ubiquitous access, and eliminate the loss of access to proprietary projects hosted in the cloud due to subscription challenges, formed the core of the deployment and functional assessment of the EDC. Hence, MOOC leveraging Moodle, one of the services deployed on the EDC and used as a supplementary

element for learning (Mpho-Entle, 2022), eBook repository, EDMS are used for the assessment of the effectiveness of the EDC deployment.

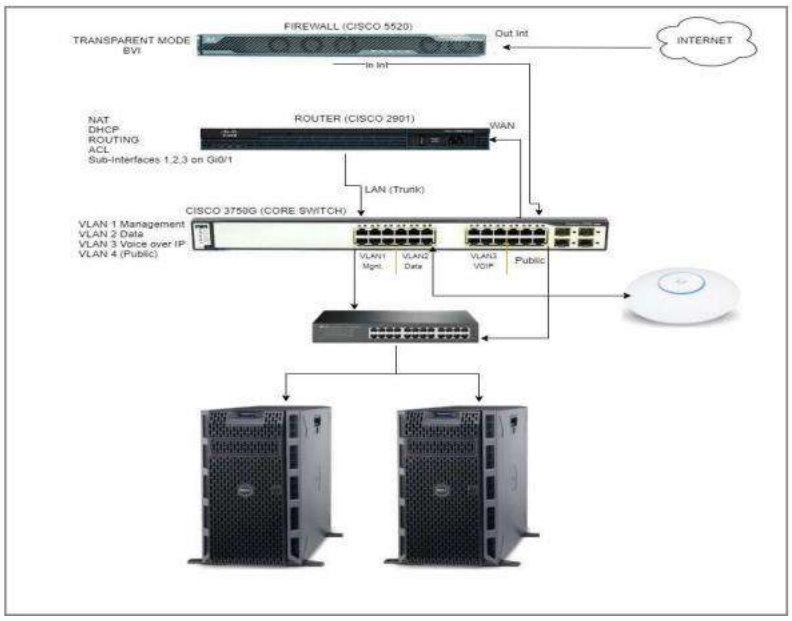

Figure 1: Experimental Data Centre design implementation.

ARCHITECTURE OF THE EDC

The point –to-point (PTP) internet infrastructure with capacity for 300 mbps full duplex throughput was deployed at the edge. This ensured seamless multiple traffic type transfer spanning data, storage, video and voice unto a single converged point. The schematic diagram of the experimental data centre as shown in Figure 1, depicts PTP as internet access through the firewall (CISCO 5520). A Cisco firewall was configured at the edge of the network for the protection of all services deployed and distributed on the router and core switch. The firewall in the setup is for the implementation of security of traffic based on defined rules of the EDC. This is linked to the core switch where the various VLANs were defined. As shown on the core switch (CISCO 3750 G) in Figure 1, VLAN 1 was configured for Management, VLAN 2 for Data, VLAN 3 for Voice Over Internet Protocol (VOIP), and VLAN 4 for public connections. The router was configured to allow both intranet and internet communications for the services deployed on the DELL T630 servers having two (2) Ethernet ports configured for both communications. The configuration allowed the assigned IP addresses (public and private) for the deployed services to be accessible over the network. The services on local deployment include eBook repository and EDMS. This was implemented as a layer of security measure, ensuring access to the services only within the University network. The servers have two (2) power supply units (PSUs) with power ratings of 500W. The PSUs were distributed with each port connected to the 5 KVA inverter system and 3.5 KVA Uninterruptible Power System (UPS). The power design and its distribution was targeted at ensuring optimal availability, thus, reducing to the barest minimum, downtime.

The two DELL T630 servers installed for the EDC deployment has 20 TB HDD, 32 core CPU each and were both virtualized using Proxmox (proxmox virtual environment) and Xen Orchestra as hypervisor for the deployment of base Operating System (OS) for the defined services to be used for improved pedagogical experience at the Department of Computer Engineering of the University of Ilorin as shown in table 1. The services deployed premised on the OS for the base virtualization determines the disk, memory and CPU utilization. The deployment usage status for Xen Orchestra memory is high as 72.77% and CPU utilization as 52% due to the concurrent services deployed for auto start after boot. This is lower to the deployment on Proxmox with memory and CPU usage stats of 6.4% and 0.2% respectively as captured in Table 1. Detailed breakdown of the resource allocation per service is captured in Table 2. The graphical depiction of the services deployed on Xen Orchestra is displayed on the interface in Figure 2 with the graph of visualization of the vCPU for the services in Figure 3.

Proxmox was configured on a public IP while the Xen Orchestra was configured for local access within the University network. Meanwhile, shared storage pool was created on both deployment as OS repository for various

providers' variant such as Ubuntu 22.04, 20.04, 18, 16, Windows server 2019, 2022, thereby ensuring their seamless use for the various services deployed.

Table 1: Experimental Data Centre Server Configuration

S/N	Server Name	Host name	Resource available	Base Virtualization	Deployment Usage status	OS deployed	Services Deployed
1	DELL T630	CPE01	Storage: 20TB RAM: 64GB CPU: 32	Proxmox	Disk: 36.9% Memory: 6.4% CPU: 0.2% of 32 CPUs	Ubuntu 20.04	Web server
						Windows Server 2019	Web server
						Linux	XOACE
2	DELL T630	CPE02	Storage: 20TB RAM: 64GB CPU: 32	Xen Orchestra	Disk: 3.9% Memory: 46.57GB (72.77%) CPU: 52% of 32 CPUs (at startup) Load average: 0.95 at peak (0.262 on average)	Ubuntu 22.04	eBook Repository
						Ubuntu 20.04	Moodle LMS
						Ubuntu 20.04	Bigbluebutton
						Ubuntu 20.04	XOACE- Xen Orchestra Community
						Ubuntu 18.04.6	Videostreaming
						Ubuntu 18.04.6	UniFi-Controller (Software Defined Solution)
						Ubuntu 20.04	Electronic Document Management System (EDMS)

Table 2: Experimental Data Centre Services architecture

S/N	Host Name	Service deployed	Resources allocated per service
1	**CPE01**		Storage 0.0%, RAM 24.2%
		Webserver	vCPU 1.7% of 2 CPUs Host Memory Usage 1.6%
			Storage 0.0%, RAM 86.8%
		WinServer	vCPU 0.2% of 16 CPUs Host Memory Usage 22.0%
			Storage 0.0%, RAM 20.0%
		Xen Orchestra	vCPU 0.8% of 4 CPUs Host Memory Usage 1.3%
2	**CPE02**		Storage 20GiB, RAM 3.93GiB
		Moodle	vCPU 8, startup 4% Topology 2 sockets with 4 cores per socket
			Storage 50GiB, RAM 5GiB
		BigBlueButton	vCPU 8, startup 20% Topology: 2 sockets with 4 cores per socket

	Storage 309GiB, RAM 8GiB
Video Livestream	vCPU 4, startup 0.2%
eBook Repository	Storage 1.5TiB, RAM 10 GiB vCPU 4, startup 66 % Topology: 2 sockets with 4 cores per socket
Electronic Document Management System (EDMS)	Storage 30GiB, RAM 10GiB vCPU 3, startup 65 %
XOACE	Storage 20GiB, RAM 3GiB vCPU 2, startup 0.1%
Wireless Controller	Storage 50GiB, RAM 4GiB vCPU 2, startup 1%

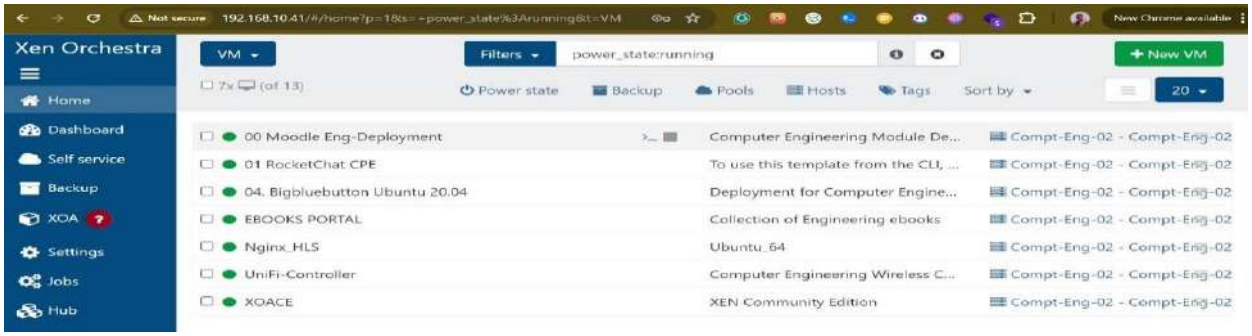

Figure 2: Xen orchestra Service deployment

The visual analysis of vCPU utilization in Xen Orchestra dashboard as captured in Figure 3, provides valuable insight into infrastructure management of the various services as it impacts service level performance and resource allocation. The line chart shows the trends in vCPU usage for the seven services premised on allocated vCPU number, RAM quantity, and total space utilized by the service. The line chart provides a snapshot of service deployment, thereby ensuring proactive monitoring, early detection of performance issues, timely mitigation of issues, and enabling resource optimization decisions.

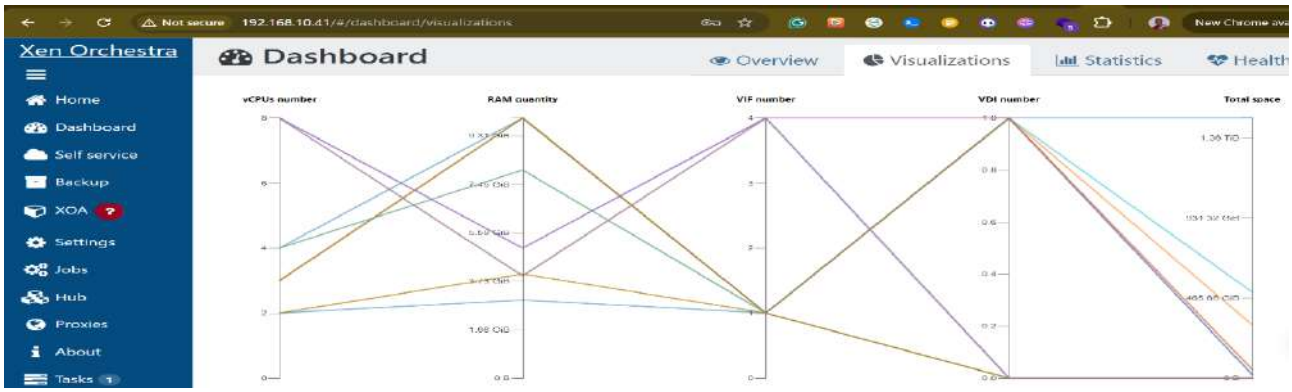

Figure 3: Xen Orchestra Dashboard showing visualizations of vCPUs for services.

RESULTS AND DISCUSSION

The services deployed were tested viz a viz connectivity, system administration, security protocol, and performance evaluation. The network architecture deployed ensured a seamless bandwidth for the access of the services hosted on the EDC. At the peak of network demand for public access, the EDC network had 40mbps full duplex connectivity. This was occasioned by the interference experienced on the frequency channel, thus impacting the full utilization of the 300mbps bandwidth capacity of the connected point-to-point radios.

The services deployed are set on auto start, hence accounting for the spike in the initial CPU usage as shown in the graphs in Figure 4 (2 hours) at 0.52 before maintaining a level below 0.45 on average. The cumulative memory utilization of the services deployed is 46.57 GB. The CPU usage which is crucial for assessing the workload on the system shows that the configuration deployed is efficient and the system is not under load which could result in performance degradation. The memory usage which peaked at 72.57% (46.57) as shown in Table 1, deployment usage statistics, and implementation graph in Figure 4 evidenced that the memory is efficiently allocated and not impacting the performance of infrastructure. The graph aids in identifying memory-intensive processes thereby ensuring optimization of memory allocation and preventing resource contention issues.

Meanwhile, the EDC was not hampered by the network clog at the central pool due to the dedicated point-to-point radio and public IP assigned.

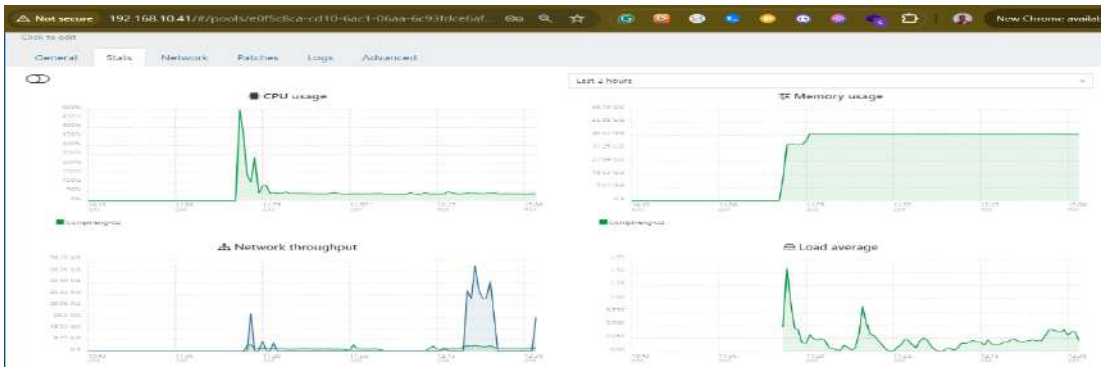

Figure 4: Xen Orchestra Statistics of CPU usage, Network throughput, Memory usage and Load average (Last 2hours)

The administration of the EDC was focused on only the defined users of the department of Computer Engineering which include Staff and students. The current student population of the Department of Computer Engineering considered for the deployment of the services made it scale easily for the deployment of courseware. The services on CPE01 were not always accessed by the faculty except on needs basis for project deployment on the webservers. The concurrent demand on the services on CPE02 were accessed based on the overall demand for the available infrastructure.

The performance metrics adopted for the research was focused on system uptime, response time, resources utilization, and data throughput. At the peak of use, the graph of utilization is at 75percent, with some warnings on the XOACE, with notifications that only one core of the vCPU is available as the 31 out of the 32 cores have been allocated to various services deployed. The warning affirmed the scalability advantage of virtualization as services not in use could be temporarily halted, allowing for the judicious scaling of services premised on resources available. Based on the fact that most of the services were deployed on the intranet, the rate of data transfer uploading and downloading resources was fast, within the bandwidth capacity of the switches.

The configuration encapsulating bandwidth, computer power, and storage requirements ensured the utilization demand which does not peak above the defined threshold. The accessibility and active utilization of the deployments affirm the impactful role of massification of education delivery leveraging MOOCs.

CONCLUSION

The development and implementation of the Experimental Data Centre at the University of Ilorin exemplify the transformative and disruptive potential of cloud computing and virtualization technologies in educational settings. By leveraging these technologies, institutions can enhance pedagogical processes, improve resource utilization, and expand access to education. This affirmed the need for continued investment in infrastructure development. This is crucial in maximizing the benefits of such computing initiatives spanning cloud services provisioning, virtualization technologies, and security of educational resources, thereby fostering a culture of innovation in higher education.

REFERENCES

Abdellah Idrissi Jouicha, Khalid Berrada, Rachid Bendaoud, Said Machwate, Abdellatif Miraoui, & Daniel Burgos. (2020). *Starting MOOCs in African University: The Experience of Cadi Ayyad University, Process, Review, Recommendations, and Prospects. 8*. https://doi.org/10.1109/access.2020.2966762

Bie Wang. (2019). *Construction Research of University Data Centre of Cloud Computing Based on Virtualization Technology*. 569. https://doi.org/10.1088/1757-899X/569/5/052022

Fung Po Tso, Simon Jouet, & Dimitrios P. Pezaros. (2016). Network and server resource management strategies for data centre infrastructures: A survey. *Computer Networks*, *106*, 209–225. http://dx.doi.org/10.1016/j.comnet.2016.07.002

Md. Faizul Bari, Raouf Boutaba, Rafael Esteves, Lisandro Zambenedetti Granville, Maxim Podlesny, Md Golam Rabbani, Qi Zhang, & Mohammed Faten Zhani. (2012). Data Center Network Virtualization: A Survey. *IEEE communication surveys & tutorials*.

Mpho-Entle Puleng Modise. (2022). *The Potentiality of MOOCs as a Tool for Widening Access to Higher Education in the African Context: A Systematic Review*. *21*(5), 84–103. https://doi.org/10.26803/ijlter.21.5.5

Paweł Poczekajłoa, Robert Suszyńskia, & Andrzej Antosza. (2023). The use of modern methods of virtualization and shared network functions to optimize the resources used. *Procedia Computer Science*, *225*, 2773–2780.

Zhen-heng Liu, Hong Shen, Tian-gong Li, & Lian-ying Sun. (2010). *Application Research of Data Center Constructing in Digital Campus*.

PAPER 62 – SOCIO-ECONOMIC IMPACT ASSESSMENT OF IDOFIAN DAM, IFELODUN LOCAL GOVERNMENT AREA, KWARA STATE, NIGERIA.

O.O. Olla[1], K.A. Adeniran[2], A.G. Adeogun[3], K.C. Achime[4], A.T. Baker[5]
[1,5]Department of Land and Water Engineering, National Centre for Agricultural Mechanization (NCAM), Ilorin, Nigeria.
[2]Department of Agric and Biosystems Engineering, University of Ilorin, Nigeria
[3]Department of Civil Engineering, Kwara State University, Malete, Kwara State
[4]Department of Research Outreach, Nigerian Stored Products Research Institute, Ilorin, Nigeria
[*] Email: femiolla2014@gmail.com

ABSTRACT
A dam is a barrier/structure that impounds water and retains it for later use. This study was conducted to assess the socio-economic impact of Idofian dam on its catchment local communities; ten communities were selected for this assessment. Research methods include key informant interviews and a structured questionnaire survey. Key informant interviews were held with community heads while 300 questionnaires were randomly administered among respondents within the communities. The impact was analyzed based on descriptive statistics using SPSS software. The results showed that 85.3% respondents admitted awareness of environmental hazards with 0.7 % of it admitted occurrence of societal conflict, 23.6% occurrence of drought, 0.8% occurrence of flood, 4.5% for herdsmen invasion, 4.5% for sickness, while 65.4% were undecided. On the other hand, only 10% admitted getting any benefit from the dam while 90% claimed not to derive any benefit from the dam. Monthly income of majority (54.7%) of respondents falls between ₦31,000-50,000. The study shows that 75% of the respondents are farmers, while other occupations as traders, civil servants, private sector and the unemployed were 11.3%, 9.9%, 2.2% and 2.2%, respectively. The study also showed that the dam could be a more useful resource for catchment communities.

KEYWORDS: water resource, dam, catchment communities, socio-economic impact,

1. INTRODUCTION

The impacts of large dam constructions on host communities varies and is numerous. These include direct and indirect impacts on the socio-economic, chemical, and bio-physical environments. Dam constructions are normally large-scale investments meant to fulfill numerous socio-economic benefits. While there are benefits associated with dam construction, such projects often pose serious problems with far reaching implications. Numerous scholars (Canter, 1985; Mudzengi, 2012; Bond and Manyanya, 2002) concur that dam construction can cause severe socio-economic negative impacts. The construction of Kariba Dam situated in Zambezi River basin between Zambia and Zimbabwe caused devastating disease and loss of livelihoods among the Tonga people (Bond and Manyanya, 2002). With growing worldwide environmental awareness, there is increasing attention on the impacts of dams on communities. The socio-economic survey is one of the most important tools and plays a very important role in research work; it is often used to design methods for collecting information about the executed project and resources as a means of improving understanding of local resource management systems, resource use, and their impact (Malekhoseini & Mirakzedeh, 2014). It therefore implies that there is need for a better understanding of the socio-economic impacts of dam construction. Since construction of the dam in 1981, the socio-economic impacts of Idofian dam have not been studied by any researcher, hence the significance of the current study in filling an important research gap. The assessment of such impacts can help to promote sustainable development strategies in the settlements for future [Huiyi, 2013, Tilt et. al. 2009] The objectives of this study were to evaluate the positive socio-economic impacts of Idofian dam to surrounding communities, evaluate the negative socio-economic impacts of Idofian dam to host communities and to recommend possible measures to mitigate the negative socio-economic impacts and enhance the positive impacts.

1.1. DESCRIPTION OF STUDY AREA

Idofian dam is located about twenty-three (23) kilometres away from Ilorin town, and along Ilorin-Lokoja highway and about 5 km off the main road at GaaGata junction (figure 1). The Dam is built on the path of River Odunrun, a tributary of Oyun river on a longitude N08.363^0 and Latitude E04.69^0 The catchment area is 61km^2(Fig 2). A concrete dam was constructed on River Odurun between Idofian and Elerinjare communities, by the National Centre for Agricultural Mechanization (NCAM) and Kwara State Water Corporation.

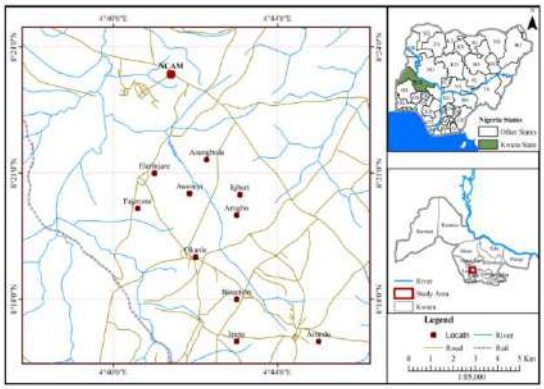

Fig 1: Map of Kwara State showing catchment communities

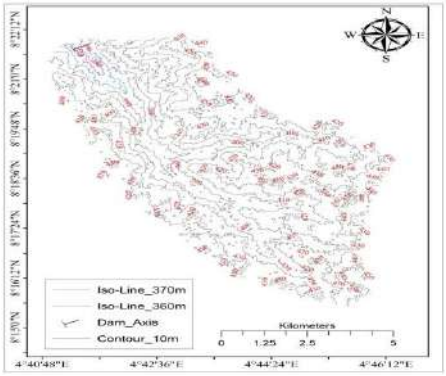

Fig. 2: Topographical map of catchment

Table 1: Coordinates Of Sampling Points (Communities)

Location:	Latitude (degrees)	Longitude (degrees)
Elerinjare	8.349	4.676
Asungbolu	8.355	4.705
Fajeromi	8.336	4.677
Igberi	8.341	4.718
Awoniyi	8.342	4.698
Irapa	8.283	4.717
Amodu	8.283	4.75
Basanyin	8.3	4.717
Okanle	8.31	4.7
NCAM	8.48	4.58

2. THEORETICAL ANALYSIS

Research tools for this study included key informant interviews and a structured questionnaire survey. Sample survey interviews were carried out with the community heads and a staff of the National Population Commission, Ilorin, Nigeria. Krathwohl (1993) states that a sample survey selects a small number of units from a population to enable researchers to make reliable inferences about the nature of that population. Households were used as sampling units. The sampling frame consisted of 300 households from the study area. This sampling frame was obtained from the Kwara State office of the National Population Commission situated in Ilorin, Kwara State, Nigeria

Sample Size Determination: The number of households selected to take part in the research was determined using the Pagoso Formula (Lauraya and Sala, 1995). The method estimates sample size (n) from, population size (N) and sampling error (E) using the following formula:

$$n = \frac{N}{1+N(E)^2} \quad (1)$$

where n = sample size, N=Total population of all communities, and E = Allowable Error

Therefore, using an estimated Total Population of 13, 399 for the 10 communities in the catchment of the dam gives a value of 277.75. Therefore, a sample size of 300 was taken randomly for all the communities. A total of 300 questionnaires were administered in the host communities for the dam to obtain data on how their livelihoods are being impacted upon by the construction of Idofian dam (Peter et.al. 2019). The survey questionnaires were targeted at household heads. The stratified random sampling method was used to select households to take part in the questionnaire survey. The households were first stratified according to village boundaries in the study area. Random sampling was then used in each stratum.

3. METHODOLOGY

According to Nabi et. al. 2019, descriptive statistics are very important and useful for describing the basic features of demographic data such as age, education, employment status etc., and also show or summarize the data in a meaningful way. The stratified systematic sampling method was used to select households to take part in the questionnaire survey. The households were first stratified according to village boundaries in the study area. The impact was analyzed based on descriptive statistics using SPSS software.

4. RESULTS AND DISCUSSION

4.1. Catchment community information

Fig. 1-4 reveals information about the social status of the catchment communities. Fig 1 shows the gender of the the community with majority (75%) being farmers, 11% being traders, 10% were civil servants while 2% were in the private sector and unemployed, respectively

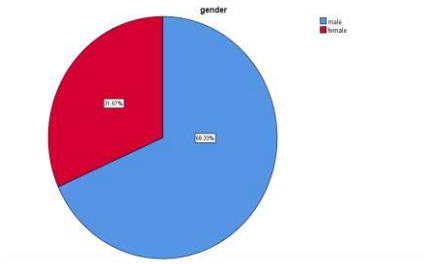

Fig 1: Gender distribution of the respondents from the ten catchment communities

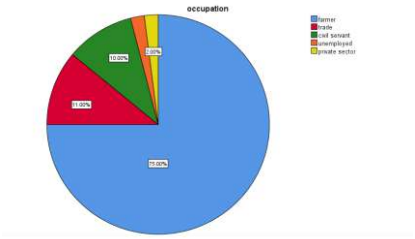

Fig 2: Gender distribution of the respondents from the ten catchment communities

Fig 3 revealed that majority of the people were married (75%), 9.33% were divorced, 13% were single while 2.67% were widows while fig 4 shows that 87.09% were aware of the existence of the Idofian dam in their environment; 12.91% were unaware.

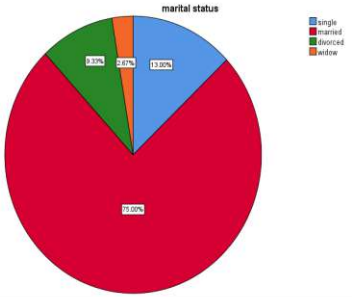

Fig 3: Marital status of respondents

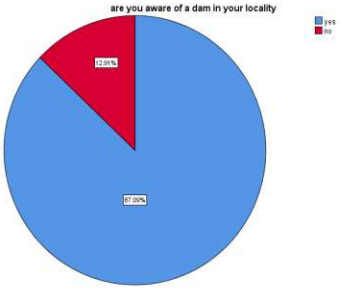

Fig 4: Level of awareness of dam

4.2 Positive Impacts: Figures 5 to 9 reveal some of the positive impacts of the Idofian dam on the neighboring communities. Fig 5 reveals that 54.67% of the people earn a monthly income less than the present minimum wage in Nigeria, i.e. below thirty thousand naira, 19.67% earns between thirty-one thousand and fifty thousand naira, while the remaining 3.3% earn between fifty-one thousand naira and one hundred thousand naira monthly. Fig 6 above shows that 7.69% of the people were using available water within the catchment for fishing while 92.31% were not. Majority of the people involved in fishing most likely carry out their fishing activities within the dam.

Fig 7 shows that 95.45% of the people use water for raising livestock, part of these includes the livestock rearers making use of the water from the dam and some using other water sources available within the community. Other water sources available within the community include boreholes, well and stream. However, 4.55% responded that they don't use water for livestock purposes. Fig 8 above shows that 41.37% of using water for irrigation within the communities, while 58.63 were not using the available water for irrigation; this includes irrigation using underground water sources such as boreholes and wells in some of the communities present within the catchment and research institute such as NCAM with standard irrigation structures making use of underground water sources. However, there are few farmers around the dam area using the dam water for surface irrigation purposes.

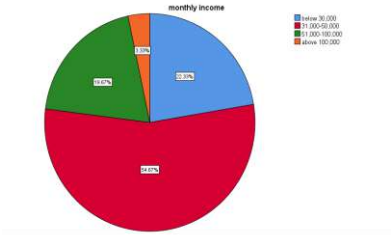

Fig 5: Monthly income of the community

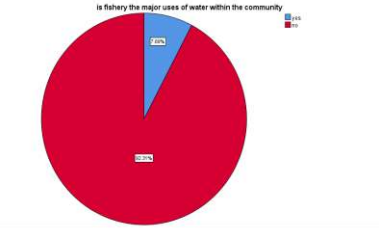

Fig 6: Fishery as a major water use

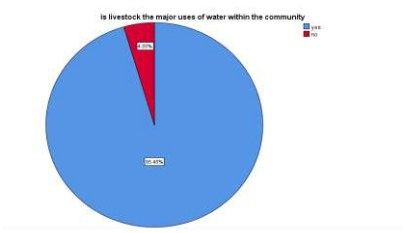

Fig 7: Livestock as a major water use

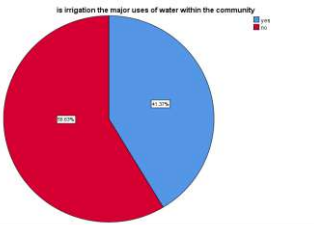

Fig 8: Irrigation as a major water use

4.3 Negative impacts

Figures 9 to 11 reveal some of the positive impacts of the Idofian dam on the neighboring communities. Fig 9 shows that 89.19% of the people claimed not to derive any benefit from the dam while 9.80% admitted that they derive some benefits from it. 1.01% of the people were undecided. The implication of this large percentage claiming not to benefit from the dam is that some of the water use within the community might be from other water sources available within the communities, such as borehole, well and stream. Fig 11 below shows that Water borne diseases such as cholera, dysentery, Escherichia Coli, etc. were admitted as a water related diseases in the catchment communities; this may not be unconnected with the presence of the dam within the catchment. 59.80% admitted it as. a water related challenge while 40.20% did not see it as a water related challenge.

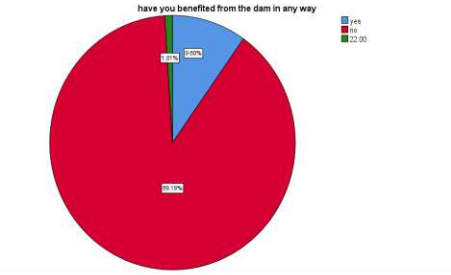

Fig 9: Benefit of dam to the catchment communities

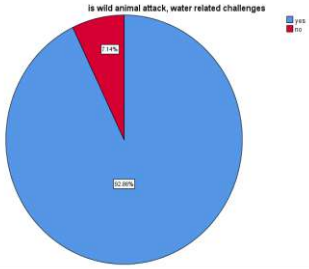

Fig 10: Wild animal attack as a water related challenge

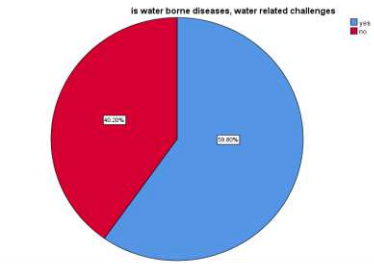

Fig 11: Water borne diseases as a water-related challenge

4. RECOMMENDATION

The study has revealed some positive impacts of the Idofian dam as well as some negative impacts. It is however important that actual capacity of the dam be determined to see how best the resources can be better put to use and alleviate some of its negative impacts.

Acknowledgement

The contribution of the Management of the National Centre for Agricultural Mechanization (NCAM) in part sponsorship of this project at inception is highly appreciated; the support of the staff of the National population Commission and that of the Ministry of Water Resources in data supply for this work is also immensely appreciated. Cooperation enjoyed by the community heads of all the communities involved in the study goes a long way to

seeing the eventual success of the work. The tremendous efforts of my supervisor to get this work done successfully cannot be over-emphasized.

REFERENCES

Bond, P. and Manyanya, M. (2002). Zimbabwe's Plunge: Exhausted Nationalism, Neoliberalism, and the search for Social Justice, Weaver Press Limited, Harare.

Canter, L. (1985). Environmental Impact of Water Resources Projects. Michigan: Lewis Publishers.

Huiyi C. 2013. Sustainable Development in China's Decision Making on Large Dams: A case study of the Nu River Basin, Sweden, Uppsala University press,.

Krathwohl, D.R. (1993). Methods of Educational and Social Science Research: An Integrated Approach. New York: Longman.

Lauraya, F.M. & Sala, A.L.R. (1995). Performance Determinants of Irrigation Associations in National Irrigation Systems in Bicol, The Philippines: An Analysis. Manila: IIMI.

Mudzengi, B.K. (2012). An Assessment of the Socio-Economic Impacts of the Construction of Tokwe-Mukosi Dam in the Mazungunye Area: Bikita District of Zimbabwe, Journal of Sustainable Development in Africa, Vol. 14, No. 4, pp. 1-17.

Malekhoseini A., and Mirakzedeh A.A. 2014. Assessment of social impacts of Sonqure's Soleimanshah dam on the regions that are under influence of irrigation and drainage network of dam. Journal of Rural Research. 5 (3), 589,

Nabi B,B, Altaf A.S , Abdul Latif Q. , Imtiaz A.B. 2019. Socio-economic impact assessment of small dams based on T-Paired Sample Test using SPSS Software. Civil Engineering Journal Vol. 5, No. 1, pp. 158.

Peter, B.O., Kwadwo, O, Edmond A. A, Albert A and Angel N.M. 2016 The impacts of dams on local livelihoods: a study of the BuiHydroelectric Project in Ghana. International Journal of Water Resources Development. 32 (2), 286. doi: 10.1080/07900627.2015.1022892.

Tilt B., Braun Y. and He D. 2009.Social impacts of large dam projects: A comparison of international case studies and implications for best practice. Journal of Environmental Management, 90 (3), 249.

PAPER 63-EFFECTS OF RICE HUSK ASH ADDITION ON THE REFRACTORY PROPERTIES OF OWO CLAY

T. M. Onyia[1*], N. E. Idenyi[2]
[1]Department of Metallurgical and Materials Engineering, Enugu State University of Science and Technology, Agbani, Nigeria.
[4]Department of Mechanical Engineering, Ebonyi State University, Abakaliki, Nigeria.
*Email: tobias.onyia@esut.edu.ng

ABSTRACT
This research investigates the impact of rice husk ash (RHA) addition on the refractory properties of Owo clay. The clay is blended with RHA in increments of 5% for each experimental run. The blended material undergoes exposure to temperatures ranging from normal crucible liner conditions to 1200 °C, followed by characterization for shrinkage, porosity, density, water absorption, and modulus of rupture. Results indicate that total shrinkage increases with RHA content until stability is reached at 10%. Porosity decreases with increasing RHA content, with the 10% RHA blend showing the most consistent decrease. RHA enhances compressive strength, reaching a peak of 24 N/MM² at 5% RHA and 1200 °C, and a minimum of 10 N/MM² at 5% RHA and 900 °C, with moderately significant values for 10% RHA. Bulk density increases with decreasing porosity as temperature rises. Overall, the 10% RHA-Owo Clay blend demonstrates the most suitable properties for industrial applications.

KEYWORDS: Owo clay, Physical properties, Chemical composition, Rice Husk Ash (RHA), Refractoriness.

1. INTRODUCTION

The inherent or tailored properties of any engineering material, including clay, are crucial to its intended purpose. Humanity has utilized natural clay minerals since the dawn of civilization. Despite the shared basic structural and chemical characteristics among all clay minerals, each possesses a unique set of properties dictating its interactions with other chemical species. Due to variations in chemistry and structure, clays find applications across diverse industries. Clay samples contribute to the manufacturing of bricks, floor tiles, and paper, their usage is dependent on the presence of mineral oxides such as Fe_2O_3, MgO, CaO, and Na_2O.

According to Galindo *et al.*, (2007), Compositional, technical, and safety specification of clay to be used as pharmaceutical and cosmetic product, 2007 the family of clay minerals, phyllosilicates, consists of hydrated Alumina-Silicates with significant proportions of Mg, K, Ca, Na, Fe, and occasionally Ti, Mn, or Li elements. Kefas *et al.*, 2007, Clays are favoured in ceramic production due to their refractory potential and the presence of Akali metal oxides Na_2, K_2, and CaO. While kaolin, smectites, palygorskite, and sepiolite all feature octahedral and tetrahedral sheets as fundamental building blocks, their structures and chemical compositions differ significantly. The diverse industrial applications of clay in ceramics and refractory materials have led to an increasing demand for enhanced efficiency in clay usage across industries. Various studies have been conducted to modify or tailor clay properties. Quesada *et al.*, (2017) successfully demonstrated that incorporating 10% rice husk ash and 30% wood ash in bricks met standard requirements for clay masonry units, employing comprehensive analytical techniques including particle size distribution analysis, X-ray diffraction (XRD), X-ray fluorescence (XRF), thermal analysis, elemental analysis, and scanning electron microscopy (SEM). These findings contributed to the development of sustainable and compatible construction methods by showcasing the potential use of these ash materials in brick manufacturing.

Temitope *et al.*, (2021) found that calcined clay partial cement substitution outperforms in terms of skid resistance and comparable abrasion value, while sawdust ash can effectively substitute for cement in non-pavement concrete applications like flooring and bricks due to its lower water absorption and slightly higher compressive strength. Crystalline-based admixture (CBA) emerges as a preferable alternative when substantial chemical admixture is required to enhance qualities such as mechanical strength, skid resistance, and abrasion resistance in pavement concrete. Rahman (1987) through analysis of Atterberg limits, linear shrinkage, density, compressive strength, and water absorption of bricks, demonstrated that the addition of Rice Husk Ash (RHA) improves consistency and workability, reduces brick density and linear shrinkage, increases compressive strength and water absorption (within acceptable limits), and shortens firing time required for well-burned bricks. Clay-sand-RHA mixtures enable the production of lightweight bricks with enhanced characteristics suitable for load-bearing walls. Kazim, Abbas *et al.*, (2016) investigated the mechanical and durability characteristics of clay bricks made from waste materials like rice husk ash and sugarcane bagasse ash, highlighting the potential for recycling and environmental

preservation. Incorporating 5% RHA and SBA in brick manufacture not only meets compressive strength requirements but also enhances resistance to sulphate attack and efflorescence, reduces weight, provides moderate weather resistance, high insulation, and acceptable freeze-thaw performance, promoting economical and sustainable building methods. Sultana *et al.*, (2014) produced rice husk ash specimens by burning at 750 °C for 2 hours, subjecting them to varying temperatures from 800 °C to 1100 °C in electric furnaces for mechanical strength testing. Increasing RHA proportion showed no effect on compressive strength, possibly due to the black colour and high unburnt carbon content in the rice husk ash utilized (SiO2: 74.2%). Mohan, Sathyanarayana, & Roa, (2012) found no strength improvement upon including waste RHA in bricks. Sarker & Basak, (2011) obtained RHA by burning rice husk in an unregulated atmosphere for clay replacement in brick production. Water absorption increased and crushing strength decreased in two phases with RHA addition, indicating a significant decline in strength beyond 20% RHA addition. Agbede & Joel, (2011) investigated RHA's impact on burnt clay bricks' characteristics, utilizing RHA from burnt rice husk at a rice mill for test specimen preparation. They observed a 6% increase in compressive strength with 2% RHA (49.8% SiO2). Inconsistencies in strength gains across previous studies likely stem from variations in chemical characteristics of waste RHA. Safeer *et al.*, (2017) found that clay bricks containing coal and wheat husk additives exhibited larger voids/pores, reduced thermal conductivity, low thermal diffusivity, high water absorption, and decreased compressive strength while meeting international standards for quality bricks, making them suitable as thermal insulators.

GHMJ & BVA, 2018 discovered that waste RHA from brick firing processes can enhance fired clay bricks' durability as an additive. This study investigates the engineering properties of cement and fly ash stabilized soil for roadway construction, including tests for compressive strength, tensile strength, stiffness, SEM, and XRD techniques, revealing that cement and fly ash improve the mechanical properties of stabilized soils, and the specimen with 8% cement and 2% fly ash at 14-day curing meets the splitting tensile strength requirement for the base layer of road construction according to Viet Nam. Onyia *et al.* (2023) in his study of clay samples from Owo and Eha-Ndiagu towns were processed and blended in different ratios, and firing tests at varying temperatures revealed that the 60:40 blend exhibited the best properties, including the lowest water absorption coefficients, highest total shrinkage, highest bulk density, highest apparent density, and lowest apparent porosity. Agbede & Joel, (2011) research looked at the effect of rice husk ash (RHA) on the qualities of clay brick, using blends of 2 to 10% RHA and testing for Atterberg limits, specific gravity, compressive strength, and water absorption, as well as X-ray diffraction and geochemical analyses on the soil and RHA. He continued by saying that the addition of 2% RHA improved the water absorption and compressive strength characteristics, with a maximum compressive strength of 18.64 MN/m^2 and a lowest water absorption value of 14.8%, indicating that Ibaji clay can be used for brick production with or without additives, but the inclusion of 2% RHA is recommended to improve the properties of the burned clay bricks. According to literature, RHA and groundnut shell improve the refractory properties of bricks, whereas clay is used in a variety of industries including cement production, fertilizer manufacturing, insecticide production, advanced chemical processing due to its reactivity and catalytic activity, as well as the pharmaceutical and food processing sectors. Some of these applications require processing or blending with other materials, such as rice husk ash, to increase certain preferred characteristics of the finished product. A number of investigations have been conducted to investigate the usage of RHA as a concrete addition to improve its strength and durability. Danupon *et al.*, (2008) study demonstrated the viability of using incinerated Rice husk ash (RHA) as a clay substitute for high-quality bricks, with RHA's organic properties providing additional heat input to the furnace, allowing for up to 50% RHA additives in lightweight brick production, an optimal firing temperature of 1050 °C, improved physical and mechanical properties of the bricks, and the potential of RHA as an alternative, cost-effective, and environmentally friendly material. Rice husk ash (RHA), a secondary derivative produced by roasting (burning) rice husk in boilers, is a potential source of amorphous reactive silica (90-96%) with numerous uses in material science. As a basic element of sand, silica is combined with clay to make refractory materials and with cement to make concrete. Kishore *et al.*, (2011) research examined the mechanical properties of high strength concrete by substituting different levels of Rice Husk ash for ordinary Portland cement, casting and testing 144 specimens, and obtaining encouraging results that indicated an optimal replacement of 10% rice husk ash in both M40 and M50 grade concrete. Tashima *et al.*, (2004) investigated the feasibility of incorporating RHA in concrete and concluded that the outcome was favourable for the use of concrete with RHA in the building industry while Nair *et al.*, (2006) investigated RHA as an alternative to cement for rural housing, highlighting that approximately 90-95% of reactive silica in RHA contributes to its pozzolanic behaviour.

Onyia *et al.,* (2023) discovered that samples with higher percentages of rice husk and lower percentages of groundnut shell exhibited the best modulus of rupture performance, indicating that strength increases with higher rice husk content and indicating their potential use as refractory linings due to higher percentage of silica and low percentage of lignin. Rice husk cellulose and lignin are removed during the burning process, leaving behind silica, with RHA production accounting for around 20% of the dried rice husk. Many countries face difficulties in disposing of rice husk due to its low nutritional value and delayed decomposition, making it unsuitable for agricultural usage as manure. When rice husk is burned under regulated conditions, the resulting RHA residue has an average particle size of 5 to 10 micrometres and a particularly high specific surface area surpassing 250 m-2 g.

Despite the huge research success attained in Clay characterization with additives such as rice husk ash (RHA) to improve the chemical, physical, mechanical, and thermal properties, its knowledge has not been applied to investigate and improve the refractory potentials of Owo clay using RHA as an additive. The important properties of RHA such as excellent inert inhibitor, fine texture, reinforcement material, and thermal resistance/shock. There is a potential that Owo clay and RHA admixture will produce a great refractory material following all characteristics shown in Tables 1 and 2.

Table 1: Physical Properties of Rice Husk Ash

S/N	PARTICULARS	PROPERTIES
1	Colour	Grey
2	Shape Texture	Irregular
3	Mineralogy	Non-Crystalline
4	Particle Size	<45 microns
5	Odour	Odour
6	Specific gravity	2.3
7	Appearance	Very fine

Source: Kulkarni et al, (Kulkarni, GovindMiegal, Bodhale, & Tande, 2014)

Table 2: Chemical Properties of Rice Husk Ash (%)

S/N	PARTICULARS	PROPORTIONS
1	Silicon dioxide	86.94
2	Aluminium oxide	0.2
3	Iron oxide	0.1
4	Calcium oxide	0.3-2.2
5	Magnesium oxide	0.2-0.6
6	Sodium oxide	0.1-0.8
7	Potassium oxide	2.15-2.30
8	Ignition oxide	3.15-4.4

Source: Kulkarni et al (Kulkarni, GovindMirgal, Bodhale, & Tande, 2014)

2. MATERIALS AND METHODS/METHODOLOGY/EXPERIMENTAL PROCEDURE

2.1 SAMPLE PREPARATION

The rice husk and clay for this piece were both sourced from Nkanu East, Enugu State, specifically Owo town for the clay and Ugboka for the rice husk. The samples were hand-picked and collected along a pit dug into the clay deposit to reduce the possibility of contamination. The clay sample was collected and placed in polythene bags for later drying, pulverizing, and sieving before analysis. The rice husk was also obtained from the Ugboka rice mill. The rice husk was heated to 7000 degrees Celsius in a closed system before being allowed to cool. Following that, each clay sample was manually crushed, graded into fine aggregates, batched, and sieved. The ground rice husk ash was sieved through a 710-micron mesh and rated. The raw materials for production were weighed using a Metra TI.300 Model electronic weighing balance. The clays were precisely fired at various temperatures after shaping, according to the composition Table 3.

Table 3: Experimental Procedure

Samples	Owo Clay		Rice Husk Ash		Water	Firing Temp.
	Wt. %	Wt.(g)	Wt. %	Wt.(g)	Vol (cm)	°C
A	95	2850	5	150	400	900,1000,1100,1200
B	90	2700	10	300	400	900,1000,1100,1200
C	85	2550	15	450	400	900,1000,1100,1200
D	80	2400	20	600	400	900,1000,1100,1200
E	75	2250	25	750	400	900,1000,1100,1200

This technique manually combined raw materials, varying ratios of clay and rice husk ash were used to create compositions A, B, C, D, and E. After thorough mixing and weighing, water was added to each sample, followed by settling for 24 hours. The procedure was repeated for consistency. Material was forced into wooden molds (7.00 cm long, 5.00 cm wide, 1.00 cm high) using gravitational force. Samples air-dried for a week, turned regularly, then oven-dried at 100°C for 6 hours. They were loaded into a gas kiln and gradually fired to burn off carbon. Finally, samples were fired at 900, 1000, 1100, and 1200 °C.

2.3 PHYSICAL TEST ANALYSIS

The physical properties were analysed using the American Society for Testing and Materials International standard for linear shrinkage, bulk density, porosity, water absorption, refractoriness test, spalling count test, and compressive strength test.

The green test sample was marked with a sharp object measuring 7 cm in length at the centre point. After drying and firing, the changes in length of the marks were measured to calculate linear drying shrinkage, firing shrinkage, and total shrinkage of the samples according to Equations 1 to 3.

$$\%\ \text{Drying shrinkage} = \frac{Wet\ length - Dry\ length}{Dry\ length} \times \frac{100}{1} \quad (1)$$

$$\%\ \text{Firing shrinkage} = \frac{Dry\ length - Fired\ length}{Dry\ length} \times \frac{100}{1} \quad (2)$$

$$\%\text{Total shrinkage} = \frac{Wet\ length - Fired\ length}{Wet\ length} \times \frac{100}{1} \quad (3)$$

The samples' length, breadth, and height were measured and recorded. In preparation for the test, the samples were fired to the required temperatures. An electronic weighing balance was used to determine the dry weight (W) in air. The obtained results were used to calculate the sample's bulk volume using Equation 4 and, as a result, the bulk density, according to Equation 5, expressed in g/cm3.

$$\text{Bulk Volume of Brick} = (L \times B \times H)cm^3 = LBHcm^3 \quad (4)$$

$$\text{Therefore, Bilk Density} = \frac{W}{LBH(cm^3)} \quad (5)$$

In preparation for the test, the samples were fired to the required temperatures. The dry weight (Dw) in air was measured with an electronic weighing balance and immersed in a boiling water vessel for 2 hours. When the water level did not cover the bricks again during the boiling process, more water was added to keep it there. For 4 hours, the samples were allowed to cool to room temperature in the water vessel. The samples were taken out of the water and weighed; the weight difference between the boiled and unboiled bricks was recorded as water porosity. This will be calculated as a percentage of the original weight. The porosity was calculates according to Equation 6.

$$\%\ \text{porosity} = \frac{Wet\ weight - Dry\ weight}{LBH(cm^3) \times Dry\ weight\ of\ the\ sample} \times \frac{100}{1} \quad (6)$$

Water absorption is a measure of the clay body's maturity. For this study, rectangular bars test pieces with dimensions of 7.00cm x 5.00cm x 1.00cm were used. The test samples were weighed to the nearest gram after being fired at various temperatures. The fired samples were then boiled for two hours before cooling. The samples' surfaces were dried with a dry towel before being weighed again. The following equation was used to calculate the percentage of water absorption.

$$percentage\ water\ absorption = \frac{saturated\ weight - dry\ weight}{dry\ weight} \times \frac{100}{1} \quad (7)$$

The Shuen's formula (Equation 8) was used for estimation of refractoriness.

$$\frac{360 + Al_2O_3 - RO}{0.228} = K \quad (8)$$

where K = Refractoriness (°C); $A1_2O_3$ = Alumina content in the clay (or materials); RO = Sum of all other oxides beside SiO_2 in the clay (or materials) 360, and 0.228 is a constant.

The number of thermal cycles (heating and cooling) was used to calculate spalling resistance. Our insulating bricks should be able to withstand many cycles of heating and cooling without cracking, in addition to being refractory. The refractory brick test pieces were thoroughly dried before being placed in the cold furnace and heated at a rate of 5°C/minute until the furnace temperature reached 1000°C. The samples were then removed one after the other using a pair of tongs, cooled in air for 10 minutes, and then observed for cracks. In the absence of cracks, the bricks were put back into the furnace and reheated for a further period of 10 minutes and cooled for another 10 minutes. This process of heating, cooling and observing for cracks was repeated until cracks were observed.

A Schmidt hammer, also known as a rebound hammer, is a device that measures the elastic properties or strength of concrete or rock, mainly surface hardness and penetration resistance. The hammer measures the rebound of a spring-load mass impacting against the surface of the sample. The test hammer will hit the bricks at a defined energy. Its rebound is dependent on the hardness of the concrete and is measured by the test equipment. By reference to the conversion chart, the rebound value can be used to determine the compressive strength.

2.4 CHEMICAL TEST ANALYSIS

Table 4: Physical properties of fire clay.

Constituent	Fire Clay
Linear Shrinkage (%)	7-10%
Apparent Porosity	20-30 %
Bulk Density	1.71-2.1g/cm^3
Cold Crushing Strength	1500kg/cm^3 (22.9-59N/mm^2)
Thermal Shock Resistance Cycle	25-30 Cycles
Refractoriness	1500-1700°C

(Chima , Nwoye, & Nnuka , Enhancement of refractory properties of blended clay with groundnut shell and rice husk additives, 2017)

Table 5: Chemical Composition/Properties of Clay according to International Standard.

Constituent Material	Fired Clay (%)	Refractory Brick (%)
$Si0_2$	55 - 75	51-70
AuO_3	25 -45	25-40
K_2O	< 2.0	—
Fe_2O_3	0.5-2.0	0.5-2.4
MgO	< 2.0	—

(Chima , Nwoye, & Nnuka , Enhancement of refractory properties of blended clay with groundnut shell and rice husk additives, 2017)

Chemical analysis of the clay sample revealed the percentage composition of the oxides required for the clay. The clay's chemical composition is SiO_2, AUO_3, K_2O, Fe_2O_3, and MgO. Chemical analysis of clay samples was performed using the X-Ray Fluorescence (XRD) method, and the results were recorded. The chemical composition of the clay used in this study revealed that it contains 51-70% silica and 0.5-2.4% iron oxide Fe_2O_3.

3. RESULTS AND DISCUSSION

3.1 Linear Shrinkage

The total shrinkage presented in Figure 1 shows that at a firing temperature of 900 ^{0}C, the total shrinkage decreased as the rice husk ash increased, which can be attributed to the RHA's inability to burn-off at that temperature. It is also worth noting that as the firing temperature increased, so did the total shrinkage. Furthermore, at firing

temperatures of 1000, 1100, and 1200 °C, total shrinkage increased with increase in rice husk ash. The higher the temperature at which the mixture is fired, the more it loses the rice husk ash and constitutional water, causing shrinkage and reducing porosity; additionally, the more a clay body shrinks, the less porous it becomes and thus the denser.

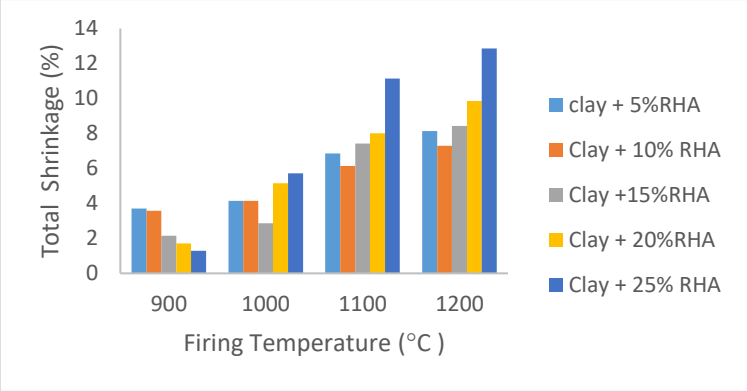

Figure 1: Graph of Total shrinkage against Firing Temperature

3.2 Bulk Density

From Figure 2, the result of bulk density of the mixture, it was observed that the bulk densities of the clay mixtures at different temperatures decreased with increase in the rice husk ash content. At all temperatures, the value obtained for clay + 25 wt% RHA falls within the range of 1.62g/cm^3 – 2.05 g/cm^3 which is within the standard range of 1.71-2.1 g/cm^3 as shown in Table 4 and accepted that blend clay satisfied the condition for fire bricks. According to, some of the factors known to affect these properties include treatment during manufacturing, the nature of the materials in the clay sample, and the proportion of the clay mixture with their size affecting the bulk density. This increase in bulk density at 1200 °C can be attributed to a slight reduction in porosity at 1100 °C and 1200 °C, as well as an increase in linear shrinkage.

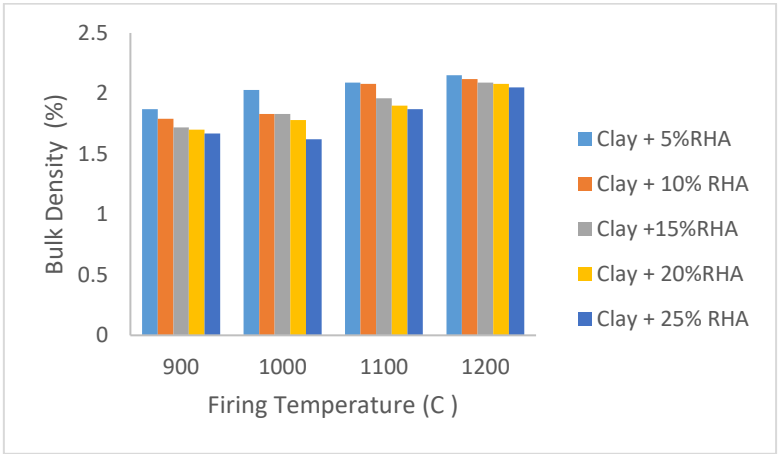

Figure 2: Graph of Bulk density against Firing Temperature

3.3 Porosity

According to the Porosity graph shown in Figure 3, the percentage porosity at 900 °C and 1000 °C increased relatively with increasing rice husk ash content. With respect to the increase in rice husk ash content, the differential increase in percentage porosity at 1100 ^{0}C and 1200 ^{0}C was found to be greater than that at 900 ^{0}C and 1000 ^{0}C. The porosity of the mixture decreased at 1100 °C and 1200 °C; the decrease in porosity at 1100 °C and 1200 °C was caused by an increase in firing temperature from 1100 °C to 1200 °C. At temperatures ranging from 1100 °C to 1200 °C, the mixtures have lost their absorbed moisture and constitutional water, resulting in increased shrinkage and decreased/reduced porosity; additionally, the more a clay body shrinks, the less porous it becomes.

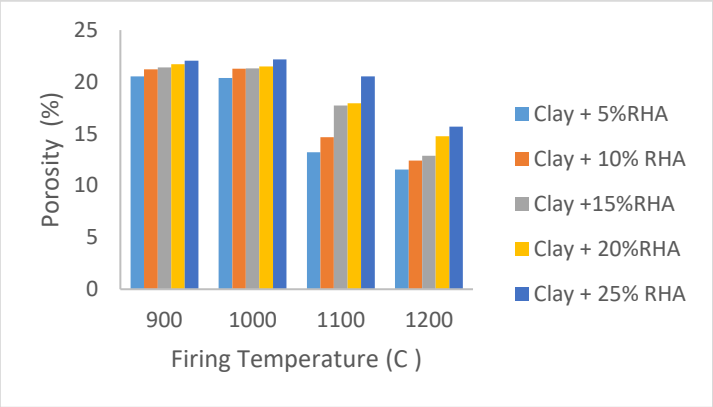

Figure 3: Graph of Porosity against Firing Temperature

3.4 Water Absorption

The results of water absorption (%) of the clay mixture at firing temperatures of 900 ^{0}C, 1000 ^{0}C, 1100 ^{0}C, and 1200 ^{0}C are shown in Figure 4. Water absorption capacities decreased with increasing rice husk ash content at different firing temperatures. It was also discovered that as the firing temperature increased, the clay mixture's water absorption capacity decreased.

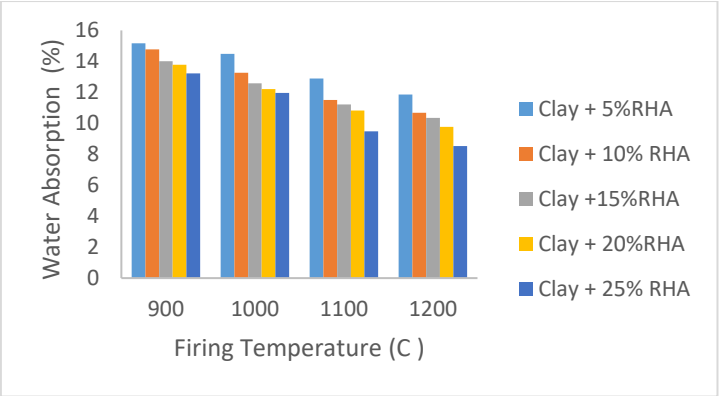

Figure 4: Graph of Water absorption against Firing temperature

3.5 Refractoriness Test

The estimated refractoriness was found to be 1710 °C.

From the chemical composition. $A1_2O_3$ = 36.0% and RO = 6.009%

$$\frac{360 + 36.0 - 6.009}{0.228} = \frac{389.991}{0.2281}$$

Therefore K= 1710^{o}C

3.6 Spalling Count Test

Figure 5 shows the thermal shock resistance results. It showed that the material's thermal shock resistance increased slightly from 26 cycles to 30 cycles. The values, however, are still within the acceptable range of 20 - 30 cycles, as recommended by some researchers (Chester, 1873).

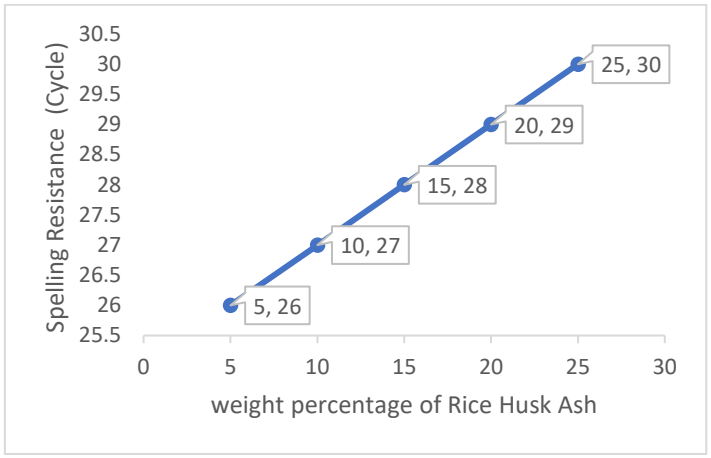

Figure 5: Line Graph of Spalling Resistance against Weight percentage of Rice Husk Ash

3.7 Compressive Strength

From the Compressive Strength shown in Figure 6, the maximum values obtained at 900 ^{0C}, 1000 ^{0C}, 1100 ^{0C} were progressively approaching the International Standard value of 22.9-59 N/mm^2. At 1200 ^{0C}, the value obtained were increasing and became matured at sample D with 24 N/mm^2 that met the standard range of 22.9-59 N/mm^2.

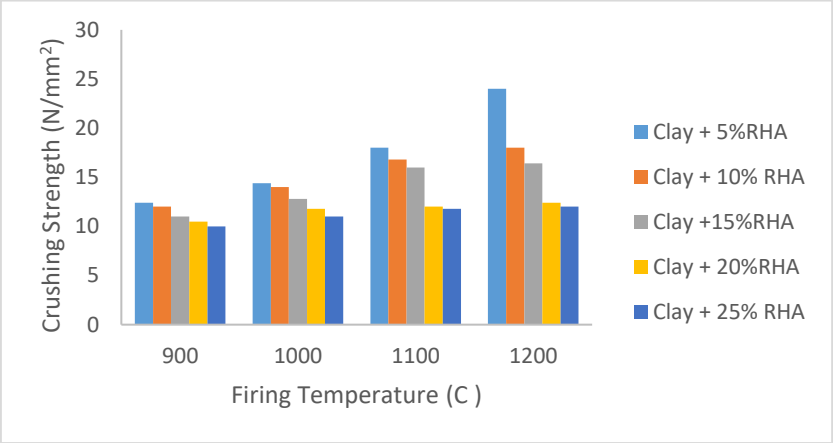

Figure 6: Graph of Crushing strength against Firing temperature

4. CONCLUSION

In conclusion, our research investigated the refractory potentials of Owo clay when enhanced with rice husk ash (RHA) as an additive. Through a systematic analysis of various properties, we observed distinct trends influenced by both RHA content and firing temperature. Specifically, our findings reveal that firing shrinkage decreases with increasing RHA content, while total shrinkage increases. Moreover, the percentage porosity decreases with rising firing temperature but increases with higher RHA content. Additionally, bulk density decreases with increased RHA content but rises with higher firing temperatures. These trends in property evolution suggest a complex interplay between RHA composition, firing conditions, and resultant material characteristics.

Our results further indicate that the 90:10 blend of Owo clay-RHA emerges as the most suitable for industrial applications, demonstrating optimal performance across multiple properties. This finding underscores the potential of Owo clay-RHA admixtures as high-quality refractory materials with favourable mechanical and thermal attributes.

Looking ahead, our study sets the stage for future research endeavours aimed at refining the synthesis and performance optimization of Owo clay-RHA refractory materials. By delving deeper into the underlying mechanisms governing material behaviour and exploring additional parameters, such as particle size distribution

and sintering conditions, researchers can further enhance the utility and applicability of these innovative materials in various industrial settings. Ultimately, the insights gleaned from our study contribute to the broader body of knowledge on clay characterization and additive-based material enhancement, paving the way for the development of advanced refractory solutions with enhanced performance and sustainability

4.1 RECOMMENDATION

The following recommendations were made;

- Rice rush ash is suitable for use as clay reinforcement for the production of refractory bricks.

Eha-Ndiagu clay + 10 weight percentage of rice husk ash is suitable for production of refractory bricks

REFERENCES

A., L. G., C. , V., & P. Cerezo. (2007). Compositonal, technical and safety specifications of clay to be used as pharmaceuticals and cosmetic products. *Applied clay science, 36*(1-3), 51-65.

Agbede , I. O., & Joel, M. (2011). Effects of Rice husk ash on the properties of Ibaji burnt clay bricks. *American Journal of Scientific and Industrial Research , 4*(2), 674-677.

Agbede I. O., & Joel M. (2011). Effects of Rice Husk Ash on the Properties if Ibaji burnt clay bricks. *American journal od scientific and Industrial Research*.

Chester, J. (1873). Refractories, production and properties. *The iron and steel institute, 3*(13), 295-314.

Chima , O. M., Nwoye, C. I., & Nnuka , E. E. (2017). Enhancement of refractory properties of blended clay with groundnut shell and rice husk additives. *American journal of engineering research , 6*(6), 218-226.

Chima , O. M., Nwoye, C. I., & Nnuka , E. E. (2017). Enhancement of refractory properties of blended clay with groundnut shell and rice husk additives. *American journal of engineering research, 6*(6), 218-226.

D., E. Q., M., A. F.-s., J., A. L.-P., & A., I. M. (2017). Characterization and evaluation of Rice husk ash and wood ash in sustainable clay matrix brick. *Ceramics international, Elsevier, 43*(1), 436-475.

Danupon , T., Perapong , T., & Sarawut , J. (2008). Effects of rice husk ask on characteristics of lightweight clay brick. *Technology and Innovation for sustainable Development conferencce, Khon Kaen univ*, 28-29.

Galindo, L. A., Viseras, C., & Cerezo , P. (April 2007). Compositional, technical and safety specifications of clay to be used as pharmaceutical and cosmetic productd. *Applied Clay Science, 36*(3), 51-63.

Galindo, L. A., Viseras, C., & Cerezo, P. (2007). Compositional, technical and safety specification of clay to be used as pharmaceutical and cosmetic product. *Applied Science Science , 36*(3), 51-63.

GHMJ , S., & BVA, P. (2018). Effect of waste rice husk ash (RHA) on structural, thermal and acoustic properties of fired clay bricks. *Journal of Building Engineering , 18*, 252-259.

H. M. Kefas, D., O. P., & T., M. C. (2007). Characterization of Mayo-Belwa Clay,. *Leonardo Electronic Journal Practices and Technology , II*(2), 123-130.

I.O. Agbede, & M. Joel. (2011). Effects of Rice husk ash (RHA) on the properties of clay bricks. *Am. Journal science industrial research , 4*(2), 674-677.

J. Subashi De Silva, & B.V.A. Ferera. (2018). Effects of waste Rice husk ash on structural, therma and acoustic properties of fired clay bricks. *Journal of building engineering, 3*(18), 252-259.

Kazim, S. M., Abbas, S., Muhammed, A. S., Munir, J. M., & Khitab, A. (2016). Manufacturing of sustainable clay bricks: Utilization of waste sugarcane bagasse and rice husk ash. *Construction and Building Materials , 20*, 29-41.

Kefas, H. M., Patrick, O. D., & Chriroma, M. T. (2007). Characterization of Mayo-Belwa Clay. *Leonardo Electronic Journal of Practices and Technology*(2), 123-130.

Kishore, R., Prakash, J. P., & Bhikshma, V. (2011). Study on Strength characteristicss of high strength rice husk ash concrete. *Procedia Engineering, 14*, 2666-2672.

Kulkarni, S. M., GovindMiegal, P., Bodhale, P. P., & Tande, N. S. (2014). Effect of rice husk ash on properties of concrete. *Journal of civil engineering and environment technology, 1*(1), 26-29.

Kulkarni, S. M., GovindMirgal, P., Bodhale, P. P., & Tande, N. S. (2014). Effect of rice husk ash on properties of concrete. *Journal of civil engineering and environmental technology , 1*(1), 26-29.

M., A. R. (1987). Properties of clay-sand-rice husk ash mixed bricks. *The int'l journal of cement composites and lightweight concrete , 9*(3).

M., S. K., Safeer , A., Muhammed , A. S., Muhammad, J. M., & Anwar, K. (2016). Manufacturing of sustainable clay bricks: Utilization of waste sugarcane bagasse and Rice husk ash. *Construction and Building materials, 2*(120), 29-41.

M., S. S., M., I. H., M., A. R., & M., H. K. (2011). Influence of Rice husk ash and Fly ash on properties of red clay. *J. Sciecne Industrial Res., 2*(4), 906-910.

Mohan, V. M., Sathyanarayana, V. P., & Roa, S. K. (2012). Influence of rice husk ash on the properties of red clay. *Internationational Journal of Engineering Research Application , 2*(5), 906-910.

Nair, G. D., Jagadish, S. K., & Fraaiy , A. (2006). Reactive Pozolanas from RHA: An alternative to cement for rural housing. *Cement and Concrete Research, 36*, 1062-1071.

Nguyen, D. T., & Phan , V. T. (2021). Engineering properties of soil stabilized with cement and fly ash sustainable road construction. *international journal of engineering, 34*(12), 2665-2671.

Onyia , T. M., Onyia , P. E., Ugwuoke , N. F., Romanus, F. O., Iyida, L. O., & Idenyi, N. E. (2023). Exploring the benefits of incorporating rice husk and groundnut shell in refractory bricks. *International journal of innovative scientific and engineering technologies research, 11*(2), 31-38.

Onyia, T. M., Onyia , P. E., Romanus, F. O., Iyida, L. O., Ugwuoke, N. F., & Idenyi, N. E. (2023). Investigaing the Physio-chemical properties of blended Owo clay and Eha ndiagu clay. *International Journal of Innovative Scientific and Engineering Technologies Research, 11*(2), 39-45.

Quesada, E. D., Felipe-Sese, A. M., Lopez-Perez, A. J., & Molina, I. A. (2017). Characterizaztion and evaluation of Rice husk ash and wood ash in sustainable clay matrix brick. *Ceramics International, Elsevier, 43*(1), 463-475.

Rahman , M. A. (1987). Properties of Clay-sand-rice husk ash mixed bricks . *The International journal of cement composites and lightweight concrete , 9*(2).

Safeer , A., Yaseen Igbal, & Raz , M. (2017). Effects of coal and wheat husk additive on the physical, thermal and mechanical properties of clay bricks. *Elsevier*.

Safeer Ahmad, Yaseen Igbal, & Raz Muhammad. (2017). Effects of coal and wheat husk addictives on the physical, thermal and mechanical properties of clay brick. *Elsevier*.

Sultana , M. S., Hossain, I. M., Rahman, A. M., & Khan, H. M. (2014). Influence of Rice husk ash and fly ash on the properties of red clay. *Journal of Scientific research, 6*(3), 412-430.

T., H., Sarker, S., & Basak, B. (2011). Utilization potential of Rice husk ash as a construction materials in rural areas. *Civil Engineering, 39*(2), 175-188.

Tashima, M. M., CAR, S., Jorge , L. A., & Barbosa, M. B. (2004). The possibility of adding the rice husk ash (RHA) to the concrete. *International RILEM conference on the use of recycled materials in building and structures* , 8-11.

Temitope , F. A., Adebayo , O. S., Daniel , O. O., Olunfunke, O. A., & B., O. O. (2021). zEffects of calcined clay, sawdust ash and chemical admixture on strenght and properties of concrete for pavement and flooring application using Taguchi approach. *Case study in Construction Materials, Elsevier, 15*.

PAPER 64 – LEVERAGING MACHINE LEARNING TO IDENTIFY SUCCESS FACTORS IN COMPUTING FINAL YEAR PROJECTS

A.Z. Umar[1*], H.S. Tuge[2], Y.G. Ibrahim[1]

[1] Department of Software Engineering and Cybersecurity, Al-Qalam University Katsina
[2]Department of Software Engineering, Cosmopolitan University Abuja
*Email: azumar@auk.edu.ng

ABSTRACT
Two of the Sustainable Development Goals (SDGs), Quality Education and Reduced Inequalities, can be pursued concurrently by adapting to individual learners' differences, facilitated by predictive machine learning models, to complement the inclusive access to education. This paper aims to identify factors contributing to the successful final year and software development-based projects in the computing discipline using machine learning techniques. Identifying these factors will play a crucial role in providing tailored support to future students. Scores from relevant courses, Cumulative Grade Point Average, the project aggregate score, and a questionnaire on the potential application of related subjects were collected from computer science students of Al-Qalam University Katsina, Nigeria. The study utilized multiclass supervised learning. The dataset was small and unbalanced, thus data augmentation and balancing techniques were applied to evaluate their effects. Data discretization was applied to continuous features. The experiment followed a 2 X 2 X 3 design. A Random Forest model was trained and evaluated based on accuracy and F1 metrics. The results showed that augmentation had slightly reduced overfitting. Similarly, data balancing was found to have better F1 across all cases. These findings highlight the importance of consciously sourcing and storing local datasets for future analysis.

KEYWORDS: predictive machine learning, undergraduate capstone project, Sustainable Development Goals.

1. INTRODUCTION

Two of the Sustainable Development Goals (SDGs) are Quality Education (Goal No. 4) and Reduced Inequalities (Goal No. 10). These two goals can be pursued concurrently through not only inclusive access but also by adapting to individual learners' differences, also known as personalized learning. Artificial Intelligence (AI) refers to the replication of human intelligence in machines, enabling them to undertake tasks that typically require human intelligence(Chowdhary, 2020; Kaul et al., 2020). Machine Learning (ML) is a subset of AI that focuses on developing algorithms that enable computers to learn patterns and insights derived from data and make predictions or decisions based on data without being explicitly programmed to do so(Janiesch et al., 2021).

Machine Learning has been massively deployed in higher education and more especially in the computing discipline(Ng et al., 2023). Nonetheless, some of the emerging evidence of AI in education is predictive modelling (Bates et al., 2020). For instance, (Akçapınar et al., 2019) conducted a study with 76 second-year university students registered in a computing course at two Peruvian universities from 2020-2022. They concluded that 74% of the students who were unsuccessful at the end of term could be accurately predicted through the use of a specific algorithm in as short as 3 weeks from the beginning of the course. Similarly, (Tsai et al., 2020)investigated the use of big data and artificial intelligence to understand student backgrounds and predict dropout probabilities. Using data from 3,552 students at a Taiwanese university, statistical and deep learning methods were employed to predict dropout probabilities. The results showed accuracies of 68% and 77% for the statistical and deep learning methods, respectively. These findings suggest that interventions based on predictive analytics could improve inclusiveness and adaptation to individual learners' differences thereby contributing to achieving SDGs Goal No.4 and Goal No. 10.

There are many other studies in the literature (see (Souai et al., 2022)for a comprehensive summary). However, these studies either address other generic aspects of students' performance different from final year software development projects or use datasets of a specific context(Akçapınar et al., 2019; Vives et al., 2024). Thus, this research is motivated by the lack of home-grown datasets and models that are crucial for evidence-based and data-driven decision making. There has been over reliance on datasets from internet sources to train machine learning models that are supposedly meant to be impactful to the immediate community.

In this context, this paper aims to identify factors contributing to the successful completion of final year projects in the computing discipline using machine learning techniques. This is crucial as students today often encounter challenges in initiating and completing innovative projects that align with current trends. The final year project serves as a capstone experience that integrates and applies the knowledge and skills acquired throughout a student's academic journey. It is one of the high-impact educational practices that promote student engagement and deep learning. Therefore, it plays a pivotal role in a well-rounded education in which the degree or the certificate matches the expected skills, as the former and latter are not mutually exclusive (D. Ku, 2008).

Thus, the following are the specific objectives of the paper:

i. To identify the most important features contributing to the success of software development-based projects among undergraduate students in the computing discipline in Nigeria.
ii. To assess the impact of equal-width discretization on the performance of an already tuned machine learning model
iii. To assess the impact of synthetic data augmentation on the performance of a machine learning model trained on a limited and unbalanced dataset.
iv. To evaluate the effect of data balancing on the performance of machine learning models trained on a limited and unbalanced dataset.

The structure of the remainder of the paper is as follows: The next section provides the theoretical foundation for the components utilized in the Methodology section. Section 3 (Methodology) elaborates on the methods employed in the study. Section 4 presents the results, followed by discussions. Finally, Section 5 concludes the paper

2. THEORETICAL ANALYSIS

This section presents the theoretical basis of the components utilized in the Methodology section and the metrics used in evaluating the machine learning model.

2.1 Hyperparameter tuning using Grid Search cross-validation:

Grid Search Cross-Validation aims to find the optimal hyperparameters $\emptyset^*$ that minimize the loss function L. More specifically, given the parameter grid:

$$\text{p: p} = \{(\emptyset_{1,1}, \emptyset_{1,2,} \dots, \emptyset_{1,n}), (\emptyset_{2,1}, \emptyset_{2,2,} \dots, \emptyset_{2,n}), \dots, (\emptyset_{m,1}, \emptyset_{m,2,} \dots, \emptyset_{m,n})\} \quad (1)$$

Where m, in (1) above is the number of combinations in the grid. Then for each $pi\ \epsilon$p: the model, M, is trained with hyperparameters $\emptyset_i$ on k fold cross validation using the dataset, D, and the average loss Li is calculated across all folds. The combination of p^* that minimizes loss:$p^* = argmin_{p \in P}\ L_i$ are then selected. The optimal hyperparameters $\emptyset^*$ are the hyperparameters corresponding to:

$$p^* : \emptyset = (\emptyset_{p,1}, \emptyset_{p,2,} \dots, \emptyset_{p,n}) \quad (2)$$

2.2 Equal-width feature discretization

For equal-width discretization, the range of values for each feature is divided into equal-width intervals. The width of each bin or interval given by Equation (3)

$$\Delta x = \frac{x_{max} - x_{min}}{n_{bins}} \quad (3)$$

Where x_{max} is the maximum value of a feature is, x_{min} is the minimum value of a feature, n_{bins} is the number of bins (intervals)

2.3 Gini index for determining feature importance

Gini Index $G(F) = 1 - \sum_{i=1}^{K} p^i$ (4)

Where: p^i is the proportion of samples in a feature set F that belong to class $i\ and\ K$ is the total number of classes. Gini index is a measure of impurity or entropy and the feature importance is on how much it reduces the impurity across all the nodes of the trees, in the forest, in which it appears because it contributes more to the overall predictive power of the model.

2.4 Metrics

$$Accuracy = \frac{Number\ of\ correct\ predictions}{Total\ nymbe\ of\ predictions} \text{ X } 100 \quad (5)$$

$$F1 = 2\text{X}\frac{Precision\ X\ Recall}{Precicion + Recall} \quad (6)$$

The Precision and the Recall are given in Equations (7) and (8) respectively

$$\text{Precision} = \frac{True\ Positive\ Predictions}{True\ Positive\ Predictions + False\ Positive\ Predictions} \quad (7)$$

$$Recall = \frac{True\ Positive\ Predictions}{True\ Positive\ Predictions + False\ Negative\ Predictions} \quad (8)$$

3. METHODOLOGY

3.1 Data collection and pre-processing

The data was collected from the final year computing students of Al-Qalam University Katsina, Nigeria after getting clearance from Research Ethic Committee of the University and as part other research(Umar & Ado, 2021, 2022) to understand students' pain points. Relevant protocols of the Nigerian Data Protection Regulations were also strictly observed(Abubakar et al., 2022). Data points such as students' scores in Data Structure (DS) and Object-Oriented Programming (OOP) courses were extracted from students' second and third-year examination results, influenced by a previous study (Khan et al., 2021), as these courses are considered relevant, if not prerequisite, for software development projects. Additionally, current Cumulative Grade Point Average (Current CGPA) and final aggregate scores on projects primarily focused on software development were included as data points. Furthermore, a questionnaire was used to collect data on the potential application of System Analysis and Design (SAD) and Software Engineering (SE) in the students' project execution. Table 1 presents the measurement items for the SAD and SE.

Table 1: Questions on students' **s**elf-assessment of SAD and SE techniques

Construct	**Question**	**Measurement Item**	
System Analysis and Design (SAD)	Please indicate your level of agreement with each of the following statements	SAD1	I used fact finding techniques from System Analysis and Design (SAD) in my project.
		SAD2	I used System Analysis techniques from System Analysis and Design (SAD) in my project.
		SAD3	I used System design techniques from System Analysis and Design (SAD) in my project.
Software Engineering (SE)	Please indicate your level of agreement with each of the following statements	SE1	I used the knowledge of system architecture from Software Engineering course in my project.
		SE2	I generally applied the principle of Software Engineering in my project.
		SE3	I generally applied the principle of Software Engineering in my project.

Random Forest model was chosen because it allows for the creation of an ensemble of decision trees to model the relationship between independent and dependent variables. It is known for its robustness and ability to handle high-dimensional data(Majeed & Hwang, 2023).

Figure 1 presents the summary of the methods used. The data was pre-processed to remove null values, especially in DS and OOP as some students were found to have dropped one course or the other.

As the sample drawn was only for the students who undertook software development projects, the size was found to be small, 96 records to be precise, which may be prone to over fitting the machine learning model. In addition, the dataset was imbalanced as the grades were mostly As, followed by Bs and the small number of Cs.

Firstly, the hyperparameters of the Random Forest were chosen with the implementation of Grid Search cross-validation library (GridSearchCV[1]) and parameterized with 5 cross validation (see HP tuning in Figure 1). hyperparameter tuning is the process of finding the optimal settings of how the model learns from data. Table 2 presents the best hyperparameters returned from the tuning process. The values in Table 2 correspond to Equation (2) in section 2.1 above.

[1] https://scikit-learn.org/stable/modules/generated/sklearn.mod el_selection.GridSearchCV.html

Table 2: Hyperparameters used in training Random Forest model

Hyper Parameter	Value
max_depth	10
max_features	Sqrt
min_samples_leaf	4
min_samples_split	10
n_estimators	10

Secondly, optional equal with discretization was implemented (see Equation (3) in section 2.3 above and Discretization in Figure 1) in such a way that it could be toggled on/off.

Thirdly, we utilized Recursive Feature Elimination (RFE)(Ramírez-Hernández & Fernandez, 2007) to determine the most important features(Feature Selection in Figure 1). RFE considers feature interactions and dependencies [7] and is also a flexible technique compatible with various machine learning algorithms and metrics. Therefore, we integrated Decision Tree into RFE to leverage the Gini Index (see Equation (4) in section 2.3 above) for determining feature importance, as employed in Decision Tree(Myles et al., 2004).

Fourthly, Conditional Tabular Generative Adversarial Network (CTGAN)(Xu et al., 2019), which extends the conventional Generative Adversarial Network (GAN) framework(Goodfellow et al., 2020; Gui et al., 2023) was used for the data augmentation. CTGAN was used to ensure that the synthetic samples not only resemble the marginal distribution of the original data but also maintain conditional dependencies between attributes.

Lastly, Synthetic Minority Over-sampling Technique (SMOTE) (Elreedy & Atiya, 2019) was used to balance the dataset. SMOTE is a popular data balancing technique which works by creating synthetic data points for the minority class, effectively increasing its size and reducing the imbalance between the classes.

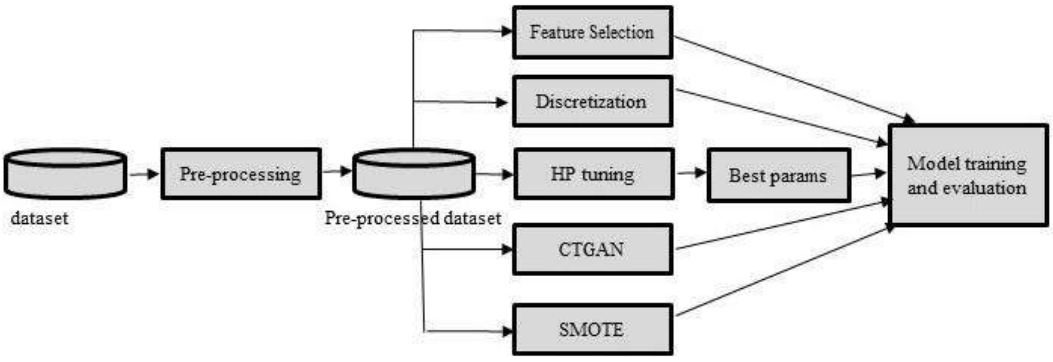

Figure 1: Summary of the methods used

Consequent to the above, the experimental design was treated as 2 X 2 X 3 with three levels as follows:

i. With and without feature selection (2)
ii. With and without discretization (2)
iii. With no augmentation, with augmentation using GAN, and with SMOTE balancing (balancing is also a form of augmentation)

Therefore, the number of conducted experiments was 2 X 2 X 3 =12 (See Table 3).

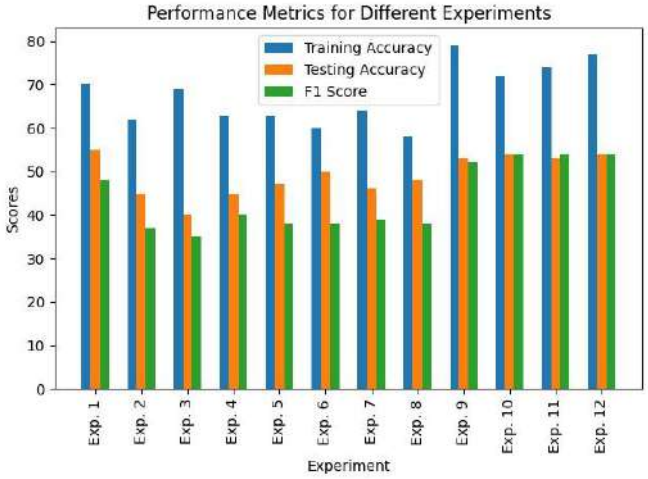

Figure 2: Summary of the results

4. RESULTS AND DISCUSSION

As a result of feature selection using RFE and Gini index, Current CGPA, OOP, DS, SAD1, and SE3 were returned as the most important features that predict a successful final year software development-based project (O1).

Looking at Figure 2 and Table 3, several observations can be inferred. For the feature selection, experiments 3, 7, 11, and 12 show some improvements in training accuracy, but do not consistently lead to improvements in testing accuracy and F1 score. This suggests that feature selection might help in reducing the complexity of the model by focusing on relevant features during training. However, it does not necessarily improve the model's generalization performance on unseen data. This could be because some of the removed features may still contain valuable information for classification (still on O1).

Table 3: Experiments and the recorded results

Exp.	Dataset Condition	Training Accuracy (%)	Testing Accuracy (%)	F1(%)
1	Raw dataset	70	55	48
2	Raw dataset with continuous features discretized	62	45	37
3	Raw dataset with feature selection	69	40	35
4	Raw dataset with feature selection continuous features discretized	63	45	40
	Augmented dataset with CTGAN			
5	Augmented dataset	63	47	38
6	Augmented dataset with continuous features discretized	60	50	38
7	Augmented dataset with feature selection	64	46	39
8	Augmented dataset with feature selection and continuous features discretized	58	48	38
	Balanced Dataset with SMOTE			
9	Balanced dataset	79	53	52
10	Balanced dataset with continuous features discretized	72	54	54
11	Balanced dataset with feature selection	74	53	54
12	Balanced dataset with feature selection and with continuous features discretized	77	54	54

On the Effect of Discretization of continuous features, experiments 2, 4, 6, 8, 10, and 12 also show mixed results across different experiments. The feature selection discretization, as a pre-processing step, might have no impact because the model has already been tuned, which implies that it has been optimized for performance (O2). The model may have already captured the relevant patterns in the data, making further pre-processing less necessary.

In the experiments where the dataset is augmented with CTGAN (Experiments 5 to 8), we observe reduced overfitting (lower values in the difference between training and testing accuracies) as the algorithm was modest its accuracies (O3). On the Effect of data balancing using SMOTE: In the experiments where the dataset is balanced (Experiments 9 to 12), we observe generally higher F1 scores. Therefore, the model is better in terms of balance between precision and recall (O4).

5. CONCLUSION

In conclusion, this paper explores the utilization of machine learning techniques to identify success factors in computing final year projects, aiming to contribute to Quality Education and Reduced Inequalities as outlined in the Sustainable Development Goals. Feature selection, discretization, data augmentation, and data balancing were evaluated for their impact on model performance. The results indicate that while feature selection may reduce model complexity, it does not consistently improve generalization performance, suggesting the potential value of retained features. Discretization of continuous features showed mixed results, highlighting the need for careful consideration of its application. Data augmentation exhibited an impact in reducing overfitting. Notably, data balancing consistently led to higher F1 metric across all experiments, emphasizing its importance in mitigating class imbalance issues. Overall, this study underscores the significance of locally sourced datasets and tailored machine learning models for evidence-based decision-making in educational settings. By identifying key success factors in computing final year projects, educators can better support students, ultimately contributing to the advancement of Quality Education and Reduced Inequalities –two(2) of the Sustainable Development Goals.

REFERENCES

Abubakar, M. M., Armaya'u, Z. U., & Abubakar, M. (2022). Personal Data and Privacy Protection Regulations: State of compliance with Nigeria Data Protection Regulations (NDPR) in Ministries, Departments, and Agencies (MDAs). *2022 5th Information Technology for Education and Development (ITED)*, 1–6.

Akçapınar, G., Altun, A., & Aşkar, P. (2019). Using learning analytics to develop early-warning system for at-risk students. *International Journal of Educational Technology in Higher Education*, *16*(1). https://doi.org/10.1186/s41239-019-0172-z

Bates, T., Cobo, C., Mariño, O., & Wheeler, S. (2020). Can artificial intelligence transform higher education? In *International Journal of Educational Technology in Higher Education* (Vol. 17, Issue 1). https://doi.org/10.1186/s41239-020-00218-x

Chowdhary, K. R. (2020). Fundamentals of artificial intelligence. In *Fundamentals of Artificial Intelligence*. https://doi.org/10.1007/978-81-322-3972-7

Elreedy, D., & Atiya, A. F. (2019). A Comprehensive Analysis of Synthetic Minority Oversampling Technique (SMOTE) for handling class imbalance. *Information Sciences*, *505*, 32–64. https://doi.org/10.1016/j.ins.2019.07.070

Goodfellow, I., Pouget-Abadie, J., Mirza, M., Xu, B., Warde-Farley, D., Ozair, S., Courville, A., & Bengio, Y. (2020). Generative adversarial networks. *Communications of the ACM*, *63*(11), 139–144. https://doi.org/10.1145/3422622

Gui, J., Sun, Z., Wen, Y., Tao, D., & Ye, J. (2023). A Review on Generative Adversarial Networks: Algorithms, Theory, and Applications. *IEEE Transactions on Knowledge and Data Engineering*, *35*(4), 3313–3332. https://doi.org/10.1109/TKDE.2021.3130191

Janiesch, C., Zschech, P., & Heinrich, K. (2021). Machine learning and deep learning. *Electronic Markets*, *31*(3), 685–695. https://doi.org/10.1007/s12525-021-00475-2

Kaul, V., Enslin, S., & Gross, S. A. (2020). History of artificial intelligence in medicine. In *Gastrointestinal Endoscopy* (Vol. 92, Issue 4, pp. 807–812). https://doi.org/10.1016/j.gie.2020.06.040

Majeed, A., & Hwang, S. O. (2023). Quantifying the Vulnerability of Attributes for Effective Privacy Preservation Using Machine Learning. *IEEE Access*, *11*, 4400–4411. https://doi.org/10.1109/ACCESS.2023.3235016

Myles, A. J., Feudale, R. N., Liu, Y., Woody, N. A., & Brown, S. D. (2004). An introduction to decision tree modeling. In *Journal of Chemometrics* (Vol. 18, Issue 6, pp. 275–285). https://doi.org/10.1002/cem.873

Ng, D. T. K., Lee, M., Tan, R. J. Y., Hu, X., Downie, J. S., & Chu, S. K. W. (2023). A review of AI teaching and learning from 2000 to 2020. *Education and Information Technologies*, *28*(7), 8445–8501. https://doi.org/10.1007/s10639-022-11491-w

Ramírez-Hernández, J. A., & Fernandez, E. (2007). Control of a re-entrant line manufacturing model with a reinforcement learning approach. *Proceedings - 6th International Conference on Machine Learning and Applications, ICMLA 2007*, 330–335. https://doi.org/10.1109/ICMLA.2007.35

Souai, W., Mihoub, A., Tarhouni, M., Zidi, S., Krichen, M., & Mahfoudhi, S. (2022). Predicting At-Risk Students Using the Deep Learning BLSTM Approach. *Proceedings - 2022 2nd International Conference of Smart Systems and Emerging Technologies, SMARTTECH 2022*, 32–37. https://doi.org/10.1109/SMARTTECH54121.2022.00022

Tsai, S. C., Chen, C. H., Shiao, Y. T., Ciou, J. S., & Wu, T. N. (2020). Precision education with statistical learning and deep learning: a case study in Taiwan. *International Journal of Educational Technology in Higher Education*, *17*(1). https://doi.org/10.1186/s41239-020-00186-2

Umar, A. Z., & Ado, S. G. (2021). Emergency Remote Learning During COVID-19 Lockdown: Al-Qalam University Katsina Students' Experience. In Prof. Afolayan A. Obiniyi, Prof. Rasheed Gbenga Jimoh, Dr. Uyinomen O. Ekong, Prof. Steve Adesina, & Prof. Folorunsho Olaiya (Eds.), *International Conference on Information Technology in Education and Development (ITED)* (pp. 167–174).

Umar, A. Z., & Ado, S. G. (2022). Emergency remote teaching during COVID-19 lockdown: Al-Qalam University Katsina lecturers' experience. *Bayero Journal of Pure and Applied Sciences*, *13*(1), 393–399.

Vives, L., Cabezas, I., Vives, J. C., Reyes, N. G., Aquino, J., Condor, J. B., & Altamirano, S. F. S. (2024). Prediction of Students' Academic Performance in the Programming Fundamentals Course Using Long Short-Term Memory Neural Networks. *IEEE Access*, *12*, 5882–5898. https://doi.org/10.1109/ACCESS.2024.3350169

Xu, L., Skoularidou, M., Cuesta-Infante, A., & Veeramachaneni, K. (2019). Modeling tabular data using conditional GAN. *Advances in Neural Information Processing Systems*, *32*.

PAPER 65 – A STUDY OF KINETICS AND ENERGY USAGE IN KETTLE BOILING OF WATER

A. G. Adeniyi[1*], J. O. Ighalo[2], K. O. Iwuozor [3], M. A. Ajala[1], E. C. Emenike[3], M. A. Amoloye[1], F. M. Oladipo-Emmanuel[1], C. A. Amure[1]

[1]Department of Chemical Engineering, Faculty of Engineering and Technology, University of Ilorin, Ilorin, P. M. B. 1515, Nigeria
[2] Department of Chemical Engineering, Nnamdi Azikiwe University, P. M. B. 5025, Awka, Nigeria
[3] Department of Pure and Industrial Chemistry, Nnamdi Azikiwe University, P. M. B. 5025, Awka, *Nigeria.*
*Email: adeniyi.ag@unilorin.edu.ng

ABSTRACT
This study was geared towards examining the kinetics and energy consumption during the use of different types of household kettles to boil water for domestic use. The effect of the power rating and the water volume as it affects different aspects of the process was also keenly examined. The metal kettles were of ratings 1500W and 2500W with sizes of 2.2L and 1.7L respectively while the plastic kettles were both of 1850W with the new and old being 2.2L and 1.7L respectively. These were the commercially available grades. It was also observed from the kinetic studies that for kettles of higher power ratings, the rate of boiling will always be faster than for lower power ratings. For plastic kettles of the same rating, the kinetics are similar for both the old and the new kettles. From the consideration of the energy usage, it was observed that for most of the kettles, there was energy loss during the process. The energy wastage was between 10-50% for most non-efficient kettle experiments. It was noted that the use of plastic kettles instead of metallic did not in any way improve the energy conservation of the boiling process.

***KEYWORDS*:** Kettle, Boiling, Energy, Kinetics, Heating, Water

1. INTRODUCTION

The domestic conservation of energy is gradually coming to the fore as energy optimisation is becoming more paramount bearing in mind the impending global energy crisis. In a bid for domestic energy conservation and cost mitigation, the energy usage of household appliances needs to be properly understood and regulated. Household kettles are frequently examined as they are a frequently and widely used appliance and characterised by considerable electricity utilisation (Adeniyi et al., 2023; Hassan et al., 2011). In general, energy transfer (in the form of heat) can be modelled for a variety of processes to gain a better understanding of the mechanisms and factors affecting the process (Adeniyi & Ighalo, 2018) and help determine better ways of conserving energy. In this respect, the domestic kettle can be examined in a variety of ways.

Some studies have considered different aspects of the use of domestic kettles. Murray et al. (2015) studied the ways of improving energy efficiency of kettle use based on usage patterns. It was observed that total consumption was less dependent on kettle type and more on usage pattern. An energy efficient usage pattern was also presented as a case study in the work. In another similar study, Murray et al. (2016) considered the energy saving potential of domestic kettle usage. Their study presented scalable tools for predicting and quantifying energy consumption of the domestic kettle and inefficient use due to over-boiling by employing only widely available smart metre data. It was facilitated by a proposed mathematical model that estimates water fill levels of the kettle from the consumed power measurements. The proposed methods were based on regression analysis and ANFIS-based demand prediction. Gallego-Schmid et al. (2018) conducted a life cycle analysis of domestic plastic and metallic kettles and compared with eco-kettles. From their study, it was observed that the use stage contributes 80% of the environmental impacts. It was also put forward that the environmental impact of the eco-kettles was over 30% lower.

Marcinkowski and Zych (2017) in their study pin-pointed that the environmental impact was majorly due to electricity consumption. Appelhof (2008) considered the redesigning of the domestic kettle for energy conservation, cost management and increase is sales. Hassan et al. (2011) redesigned the heating coil of the electric kettle and studied the heat transfer in a CFD environment to improve the over performance of the domestic device. Telenko et

al. (2009) utilised the electric kettles as a case study in reviewing the design for environment guidelines. Besides the studies on domestic kettles reviewed above, several other studies have considered different aspects of the application of industrial kettles (DeGiorgio, 2017; Manrique et al., 2014). In general, only a few studies have been done to specifically consider the energy analysis and boiling kinetics as it applies to the use of domestic kettles. The aim of this study is to examine the kinetics and energy consumption during the use of different types household kettles to boil water for domestic use. The effect of the power rating and the water volume as it affects different aspects of the process is also keenly examined.

2. MATERIALS AND METHODS

2.1 Materials

The household kettles used for this study were obtained from Ilorin city, Nigeria. The metal kettles were of ratings 1500W and 2500W with sizes of 2.2L and 1.7L respectively. These are the popular grades of metal kettles that is commercially available. The plastic kettles were both of 1850W with the new and old being 2.2L and 1.7L respectively. All kettles utilised have an auto-off mechanism. The power supply utilised was 220V, 50Hz which is the commercial power supply rating in Nigeria. The water utilised in the experiments is the conventional treated and packaged water available to municipal households.

2.2 Procedure of experiments

The experimental set-up for this work is a simple one. The configuration is presented in figure 1. The thermocouple is used to measure and log the temperature after a specific time interval as heating progresses.

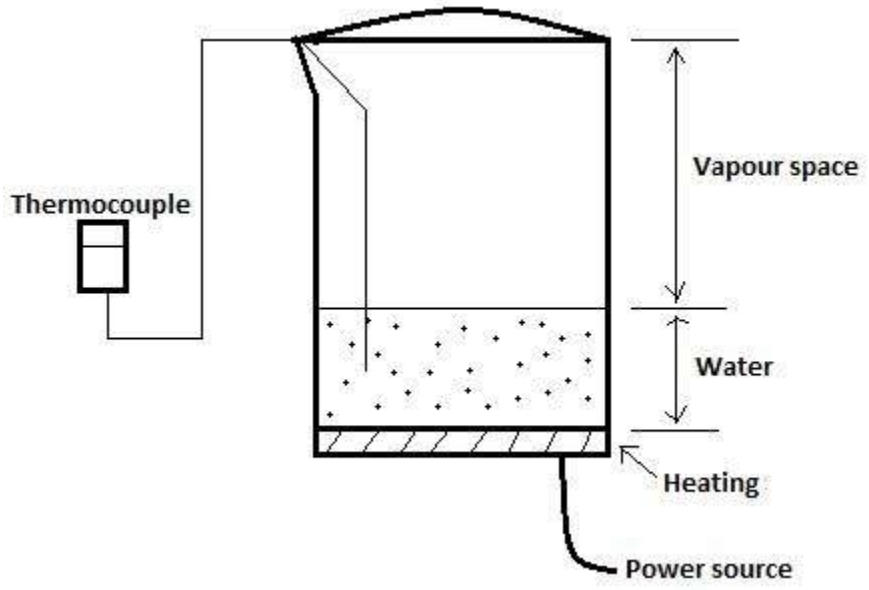

Figure 1. Experimental setup

The required volume of water in litres is measured into the kettle. The required volume is measured based on the target water level and kettle capacity. Three target water levels were utilised in this study; one-third (1/3), two-third (2/3) and full (1).

$$Required\ volume\ (L) = \frac{Kettle\ capacity\ (L)}{Target\ water\ level} \qquad (1)$$

After pouring in the required volume of water into the kettle, the Constantine wire of the thermocouple was introduced to get to midway of the water level. The kettle was closed and plugged to a power source. Temperature reading commenced the same second the power button was switched on the temperature was logged every two seconds until boiling began. Logging continued until the auto-off mechanism responded to the water temperature

and switched off automatically thereby signalling the end of an experimental run. Fresh quantity of water (at room temperature) was used for subsequent runs with care taken to ensure the kettle heating element has cooled back to room temperature before the next experiment with the same kettle.

2.3 Energy consumption

The energy consumption for each experiment was computed using the simple expression in equation 2;

$$E = P.t \quad (2)$$

Where E is energy consumption in Joules (J), P is the power rating (lower limit) of the kettle in watts (W) and t is the total time for the process in seconds (s). The total time t is obtained from the summation of the heating time (t_1) and the boiling time (t_2).

$$t = t_1 + t_2 \quad (3)$$

Heating time (t_1) is the time it takes from the commencement of heating till vigorous boiling begins. **Boiling time (t_2)** is the time it takes for the kettle auto-off mechanism of the kettle to be triggered after the commencement of boiling. The energy consumption can also be expressed in kilowatt hours (kWh). This can be achieved by the following expression since 1 kWh is 3600 kJ.

$$E\ (kWh) = \frac{E\ (kJ)}{3600} \quad (4)$$

The kilowatt hour (kWh) is more suitable for representing energy consumption in electrical appliances. To be able to determine the energy conservation potential of the different kettles, we will need to know the theoretical energy (E_0) required to raise the temperature of water from the starting temperature to the point where the kettle automatically switched off. It can be determined using equation 5.

$$E_0 = mc\Delta T \quad (5)$$

Where m is the mass of water in kg, c is the specific heat capacity of water (4.21 kJ/kg.k) and ΔT is the change in temperature. The conversion of water volume to mass was done using the density of water (1 kg/L).

$$\%\ Energy\ wastage = \frac{E-E_0}{E} \times 100 \quad (6)$$

2.4 Kinetic studies

The kinetic constant of kettle boiling in $^oC/s$ can be obtained by the slope of a temperature progression plot. The temperature progression plot is the plot of temperature against time.

$$y = mx + c \quad (7)$$

$$T_{(i)} = Kt_{(i)} + T_{(0)} \quad (8)$$

Where $T_{(i)}$ is the temperature of the water at time i ($t_{(i)}$). K is the kinetic constant in $^oC/s$ obtained from the slope of the temperature progression plot while $T_{(0)}$ is the temperature at time zero ($t_{(0)}$). The temperature at time zero is the temperature before the heating of the water which is the same as the room temperature and found to be 27^0C for all experiments.

2.5 Parametric studies

The parameters affecting the behaviour and performance of kettle boiling of water was studied using response surface methodology on Design expert 10.0.1. Only the results of the metal kettle were considered using RSM. This is due to the constraint of a minimum of 2 factors for any RSM models. The factors/parameters varied in the evaluation of the metal kettles were power rating and liquid volume (expressed as a function of liquid level). For the plastic kettles however, only power rating was considered. The plastic kettle experiments were however compared with metal kettles to examine the effect of heat loss via metal conduction on the performance of the system. The experimental design was chosen as 'historical data' and the results/findings of the experiment were inputted directly into the software for computation and development of 3D response surface plots based on the already obtained experimental results. The plots will show the relationship and effect of process parameters on the performance of the

metal kettles in the boiling of water. The effect of liquid volume in plastic kettle boiling performance was evaluated using simple plots.

3. RESULTS AND DISCUSSION

Using the method described in the previous section, the experiments were run for each kettle from room temperature to boiling point and timed. In this section, the results are presented and analysed.

3.1 Results of experiments

Figure 2 shows the temperature progression for the 1500W metal kettle of 2.2L capacity. The process was completed in 138, 338 and 412 seconds for the 1/3rd, 2/3rd and full kettles respectively. It can be observed that the temperature climbed faster with time at lower volumes than at higher volumes. The energy required to raise the water from room to boiling temperature is higher for a larger mass of water hence this observation. From equation 5, we see that theoretical energy (E_0) required is directly proportional to the mass of the water (m). The temperature progression is also far less rapid for the 2/3rd and full kettles than for the 1/3rd level.

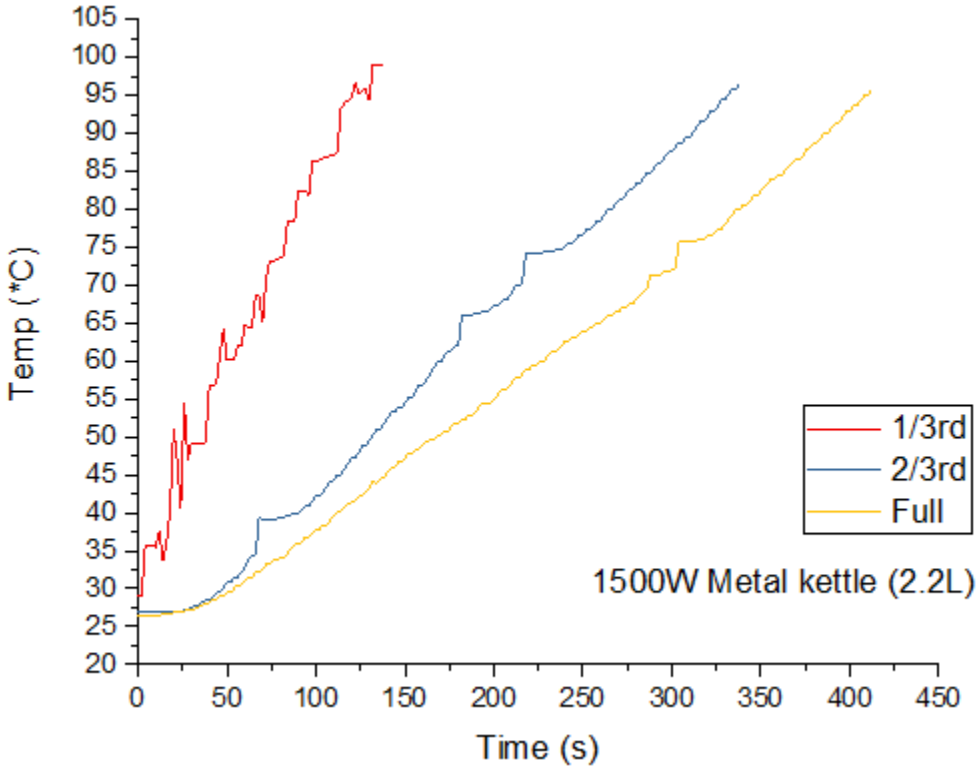

Figure 2: Temperature progression for 1500W metal kettle (2.2L)

Figure 3 shows the temperature progression for the 2500W metal kettle of 1.7L capacity. The process was completed in 102, 144 and 256 seconds for the 1/3rd, 2/3rd and full kettles respectively. As similarly observed from the 1500W kettle, the time required for boiling is lesser for lesser volumes of water. This has already been explained. An interesting observation is the 2/3rd water level for both experiments. For the 1500W kettle, the 2/3rd level is almost as slow as the full while for the 2500W kettle the 2/3rd level is almost as fast as the 1/3rd level. This informs that the relationship between the water volume and power rating as a function of boiling time and/or is most probably non-linear. This was subsequently confirmed in later sections of this work as the non-linearity is observed in the convolutions of Figures 7a and 8b.

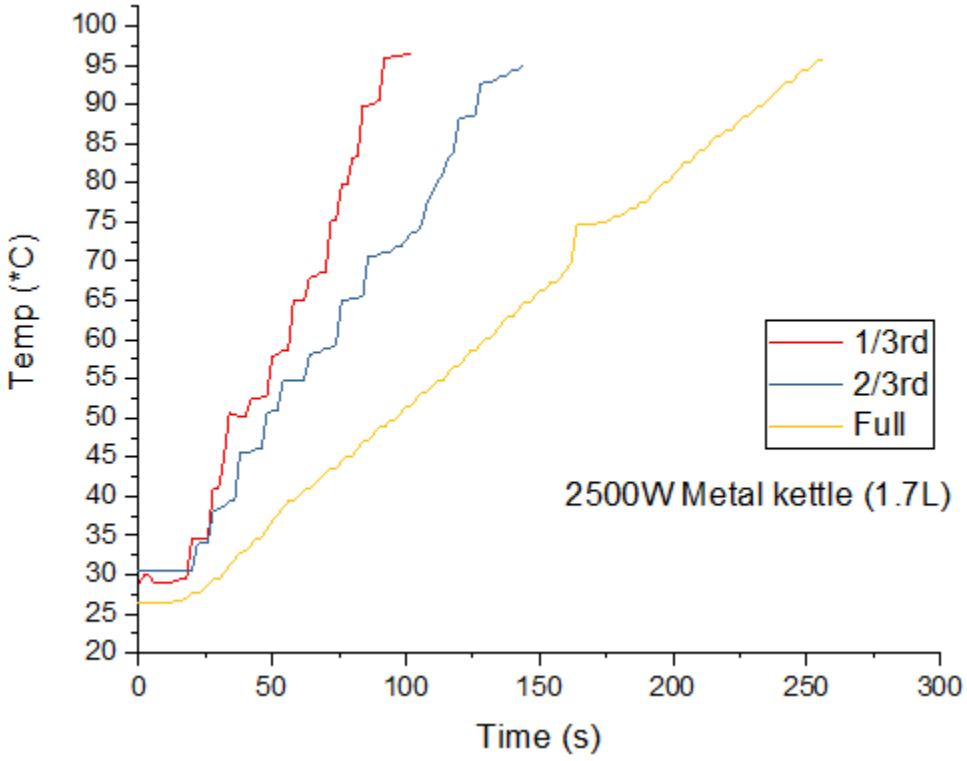

Figure 3: Temperature progression for 2500W metal kettle (1.7L)

Figure 4 shows the temperature progression for the 1850W old and new plastic kettles of 1.7L and 2.2L capacity respectively. For both the old and the new kettles it is observed that the temperature climbed faster with time at lower volumes than at higher volumes. The energy required to raise the water from room to boiling temperature is higher for a larger mass of water. Studying the plot carefully (2/3rd and 1/3rd for old vs new), it can be observed that the older already used kettle does not have a lower performance. Interestingly, the temperature progression is even marginally higher (for most of the time range) than for the new kettle. We can infer that the newness of household kettles does not offer any advantage over older already in use kettles in this regard.

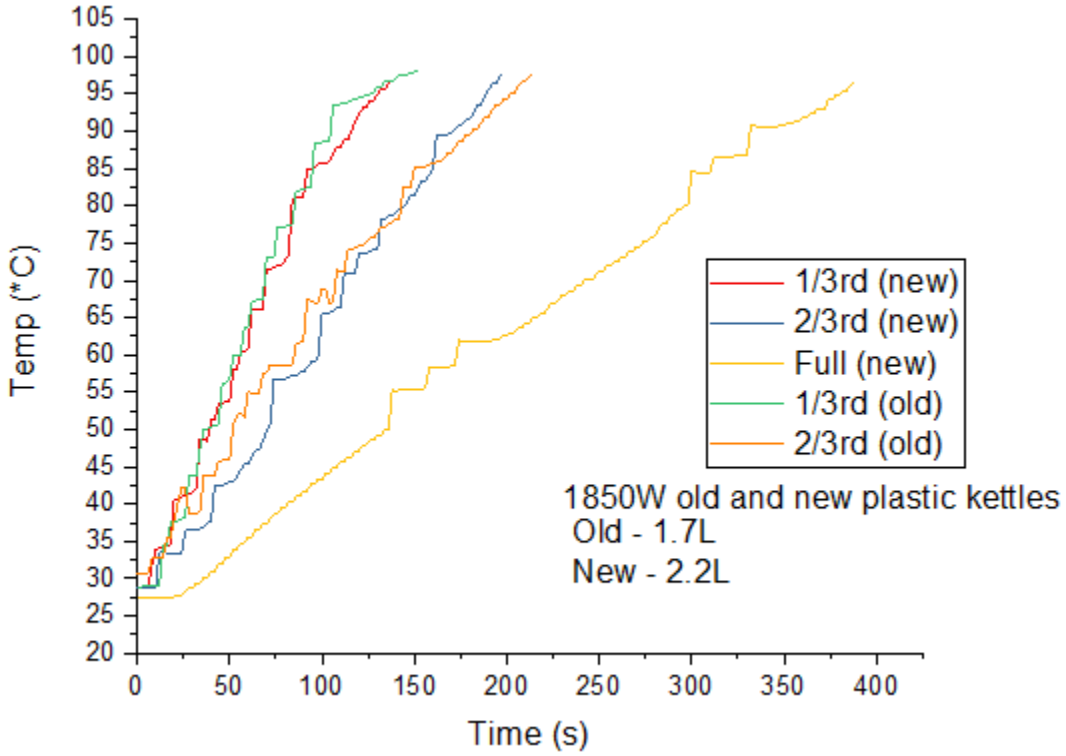

Figure 4: Temperature progression for 1850W old and new plastic kettle

The results for all experiments are presented in Table 1. The heating time is the time it takes from the commencement of heating till vigorous boiling begins. Boiling time is the time it takes for the kettle auto-off mechanism of the kettle to be triggered after the commencement of boiling. The total time is the time for the entire process which is a summation of both the heating and boiling time. The energy consumption was computed in kilojoules and kilowatt-hours using equations 2 and 4 respectively. These results form the basis of the kinetic, parametric and energy studies presented in the forgoing subsections.

Table 1: Summary of results for the kettle experiments

Kettle Type and Volume	Water level	Power Rating (W)	Heating time (s)	Boiling time (s)	Total time (s)	Energy consumption (kJ)	Energy consumption (kWh)
Metal (2.2 L)	1/3rd	1500	128	10	138	207.0	0.0575
Metal (2.2 L)	2/3rd	1500	314	24	338	507.0	0.1408
Metal (2.2 L)	Full	1500	402	10	412	618.0	0.1717
Metal (1.7 L)	1/3rd	2500	88	14	102	255.0	0.0708
Metal (1.7 L)	2/3rd	2500	128	16	144	360.0	0.1000
Metal (1.7 L)	Full	2500	242	14	256	640.0	0.1778
Plastic (2.2 L) New	1/3rd	1850	128	10	138	255.3	0.0709
Plastic (2.2 L) New	2/3rd	1850	180	18	198	366.3	0.1018
Plastic (2.2 L) New	Full	1850	372	16	388	717.8	0.1994
Plastic (1.7 L) Old	1/3rd	1850	128	24	152	281.2	0.0781
Plastic (1.7 L) Old	2/3rd	1850	190	24	214	395.9	0.1099

3.2 Kinetic studies

Studying the kinetics of the process, the logged data was plotted on Microsoft excel 2016 and the equation obtained shown (see Figures 5a-k). The kinetic constant in $^{o}C/s$ is the slope of the plot. The intercept is the temperature at time zero before the heating of the water and it is the same as the room temperature ($27^{0}C$ for all experiments). The summary of the results is presented in Table 2.

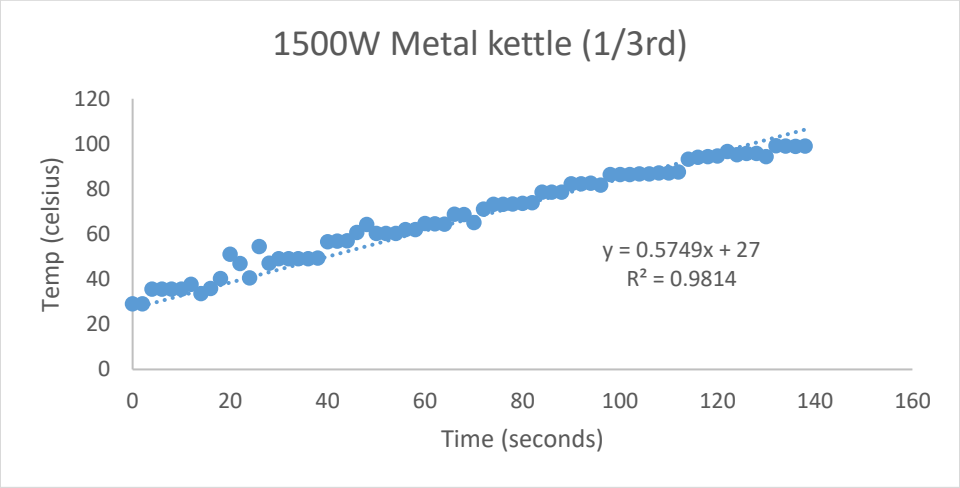

(a)

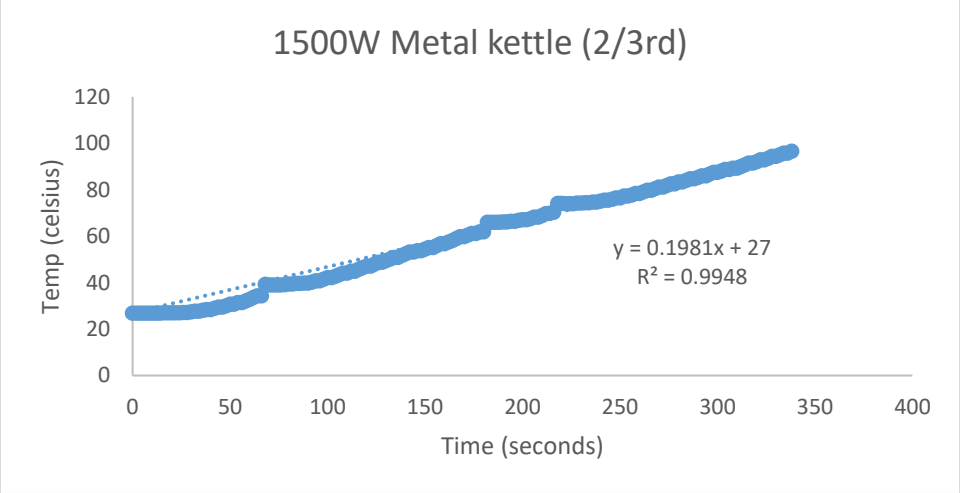

(b)

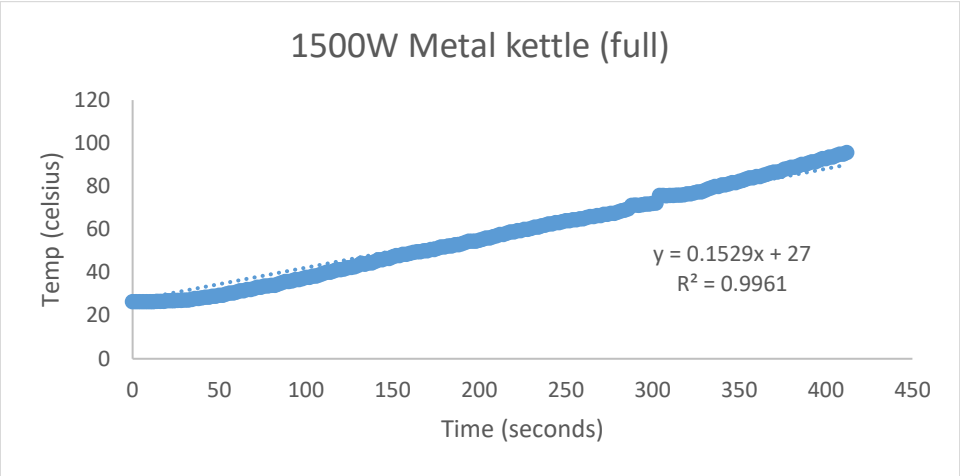
1500W Metal kettle (full)
Temp (celsius)
Time (seconds)
y = 0.1529x + 27
R² = 0.9961
0
20
40
60
80
100
120
0
50
100
150
200
250
300
350
400
450

(c)

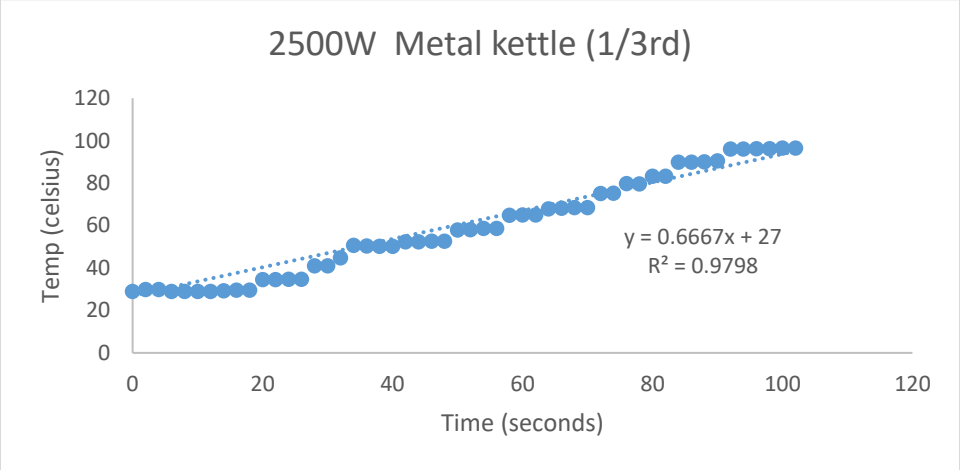
2500W Metal kettle (1/3rd)
Temp (celsius)
Time (seconds)
y = 0.6667x + 27
R² = 0.9798
0
20
40
60
80
100
120

(d)

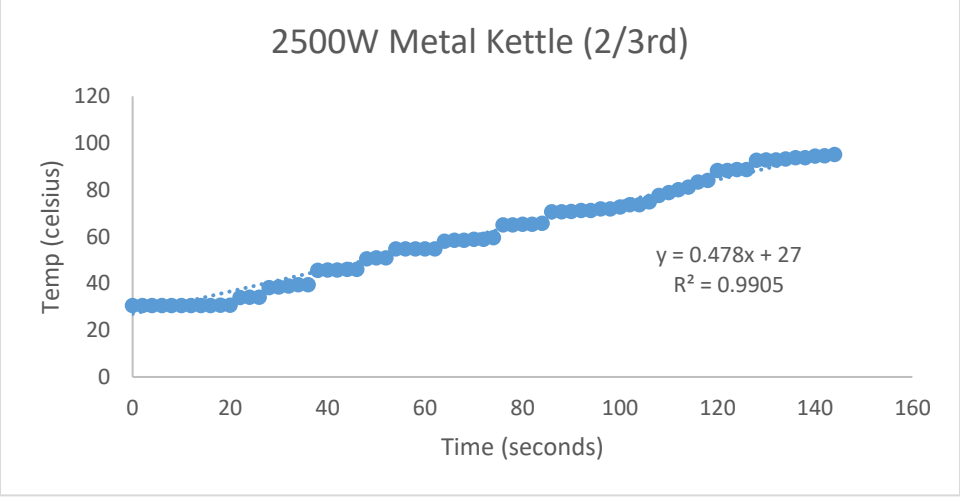
2500W Metal Kettle (2/3rd)
Temp (celsius)
Time (seconds)
y = 0.478x + 27
R² = 0.9905
0
20
40
60
80
100
120
140
160

(e)

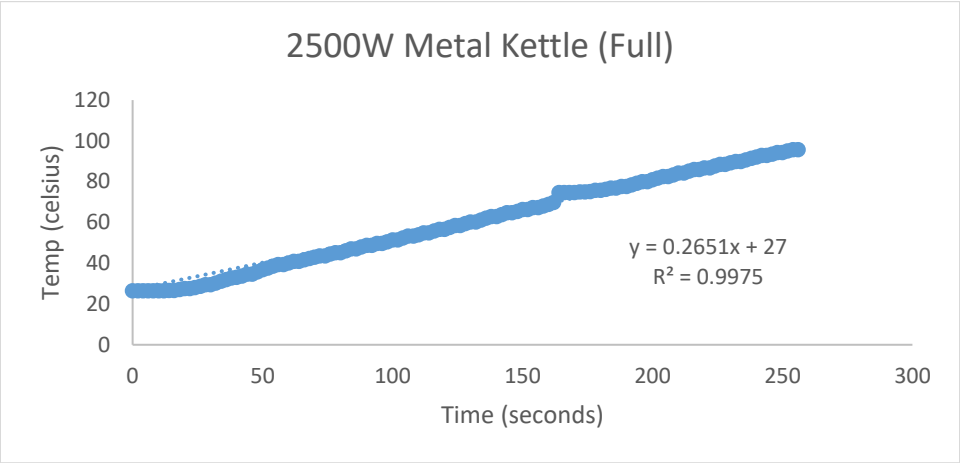
2500W Metal Kettle (Full)
Temp (celsius)
Time (seconds)
y = 0.2651x + 27
R² = 0.9975
0
20
40
60
80
100
120
0
50
100
150
200
250
300

(f)

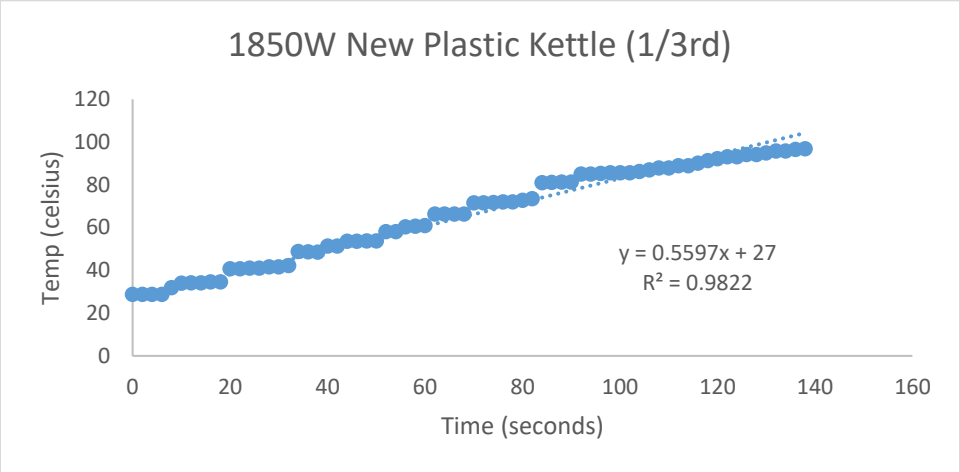
1850W New Plastic Kettle (1/3rd)
Temp (celsius)
Time (seconds)
y = 0.5597x + 27
R² = 0.9822
0
20
40
60
80
100
120
140
160

(g)

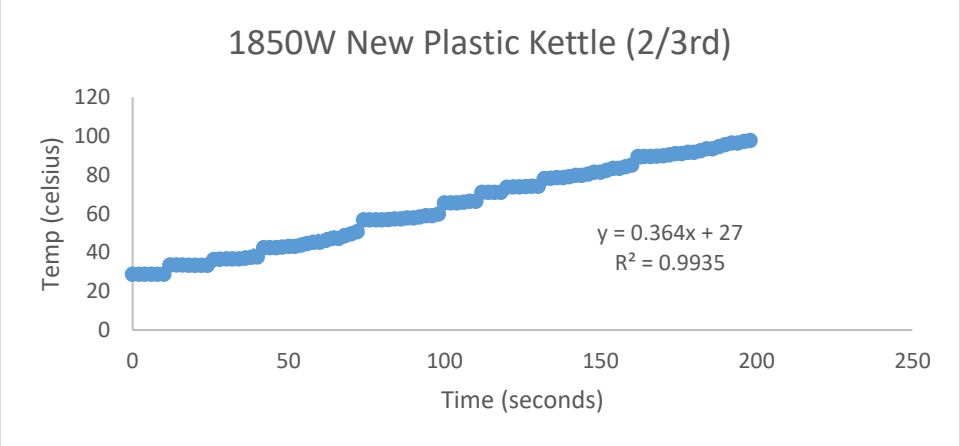
1850W New Plastic Kettle (2/3rd)
Temp (celsius)
Time (seconds)
y = 0.364x + 27
R² = 0.9935
0
20
40
60
80
100
120
0
50
100
150
200
250

(h)

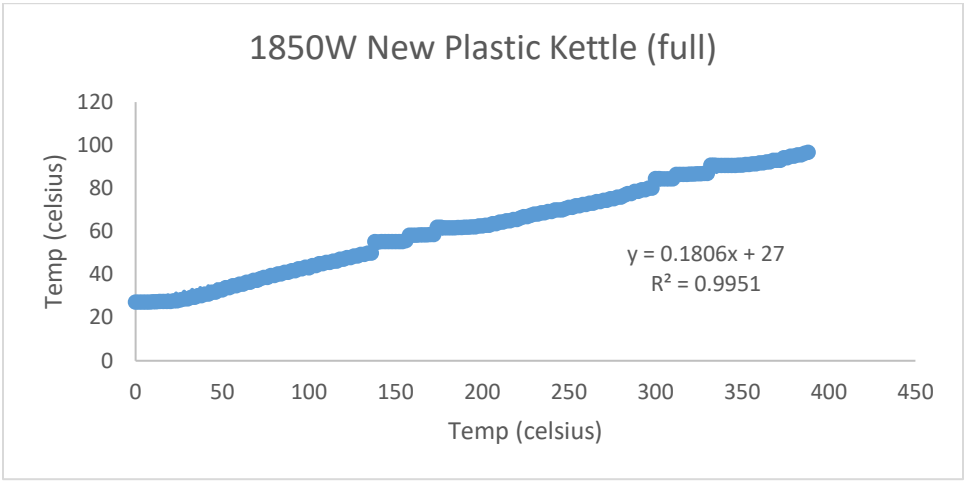

(i)

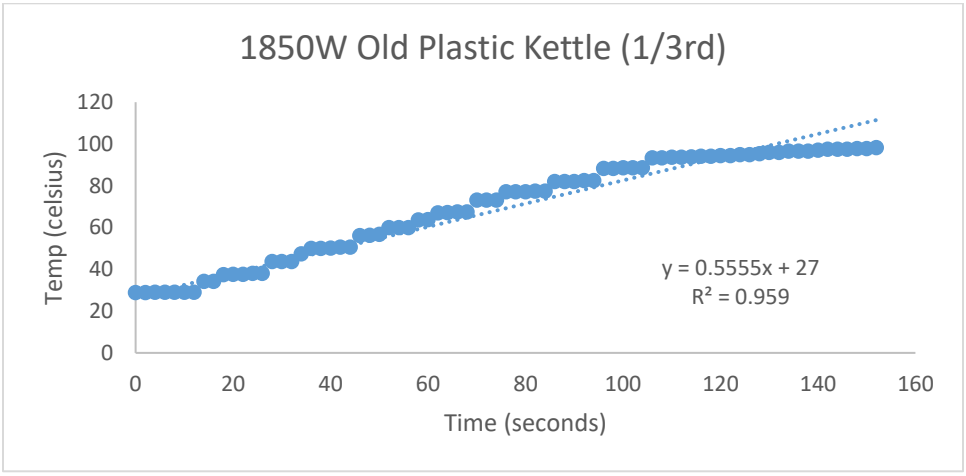

(j)

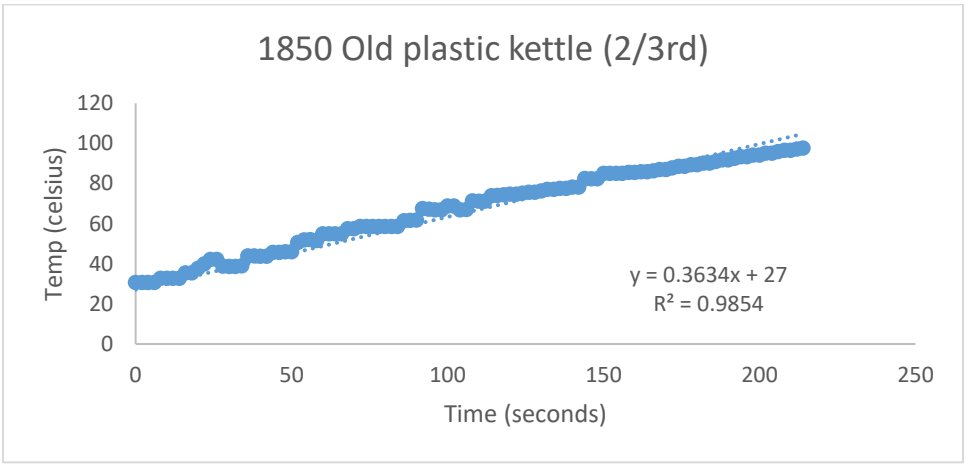

(k)

Figures 5 (a-k): Kinetic plots for kettle boiling

Table 2: Summary of kinetic constants in kettle boiling

Kettle Type and Volume	Water level	Rating (kW)	Kinetic constant (ºC/min)	R^2
Metal (2.2 L)	1/3rd	1500	0.5749	0.9596
Metal (2.2 L)	2/3rd	1500	0.1981	0.9798
Metal (2.2 L)	Full	1500	0.1592	0.9762
Metal (1.7 L)	1/3rd	2500	0.6667	0.9594
Metal (1.7 L)	2/3rd	2500	0.4780	0.9874
Metal (1.7 L)	Full	2500	0.2651	0.9866
Plastic (2.2 L) New	1/3rd	1850	0.5597	0.9804
Plastic (2.2 L) New	2/3rd	1850	0.3640	0.9927
Plastic (2.2 L) New	Full	1850	0.1806	0.9928
Plastic (1.7 L) Old	1/3rd	1850	0.5555	0.9544
Plastic (1.7 L) Old	2/3rd	1850	0.3634	0.9667

From Table 2, we observe that for higher power ratings, the rate of boiling will always be faster than for lower power ratings. Also, the rate of boiling for larger volumes of water is also lower than for smaller volumes of water. For plastic kettles of the same rating, the kinetics are similar for both the old and the new kettles. The reliability of the results presented in table 2 is portrayed by the coefficient of determination (R^2 value). Most of the plots contained between 50 and 200 data points. To obtain such high values of coefficient of determination for plots of such large data points buttresses the accuracy of the results well.

3.3 Energy conservation

The energy consumed by the kettles have already being computed and presented in table 2. However, to get a better understanding of the energy conservation, the theoretical energy requirement to boil the input mass of water was computed. The theoretical energy requirement and the energy wastage were computed using equations 5 and 6 respectively and the results presented in Table 3.

Table 3: Summary of energy wastage by the different kettles

Kettle Type and Volume	Power Rating (W)	Water level	m (kg)	Kettle energy consumption E, (kJ)	Theoretical energy requirement E_0, (kJ)	Energy wastage (kJ)	% Energy wastage
Metal (2.2 L)	1500	1/3rd	0.73	207.0	206.0	1.0	0.48
Metal (2.2 L)	1500	2/3rd	1.47	507.0	431.4	75.6	14.91
Metal (2.2 L)	1500	Full	2.2	618.0	640.0	None	-
Metal (1.7 L)	2500	1/3rd	0.57	255.0	162.2	92.8	36.39
Metal (1.7 L)	2500	2/3rd	1.13	360.0	307.2	52.8	14.67
Metal (1.7 L)	2500	Full	1.7	640.0	495.3	144.7	22.61
Plastic (2.2 L) New	1850	1/3rd	0.73	255.3	208.9	46.4	18.17
Plastic (2.2 L) New	1850	2/3rd	1.47	366.3	426.4	None	-
Plastic (2.2 L) New	1850	Full	2.2	717.8	642.8	75.0	10.45
Plastic (1.7 L) Old	1850	1/3rd	0.57	281.2	166.5	114.7	51.46
Plastic (1.7 L) Old	1850	2/3rd	1.13	395.9	319.2	76.7	19.37

For most of the kettles energy was lost during the process. This is because the energy spent was higher than that required to raise the water to boiling temperature. The energy wastage was between 10-50% for most non-efficient kettle experiments. There do not seem to be any relationship and/or between water volume, power rating and kettle type with the energy conservation of household kettles during the boiling of water. In terms of magnitude (in kJ) this energy loss may be comparatively small but it goes a long way to portray the efficiencies of these device. Energy loss can be attributed to the conduction of heat unto the metallic and/or plastic components of the kettles as the heating was in progress. It is interesting to note that the use of plastic kettles instead of metallic ones does not in any way improve the energy conservation of the boiling process.

3.4 Parametric studies

The two key parameters in this study are the volume of water in the kettle and the power rating of the kettles. These parameters will be exhaustively examined as a function of boiling time, total time, boiling kinetics and energy consumption.

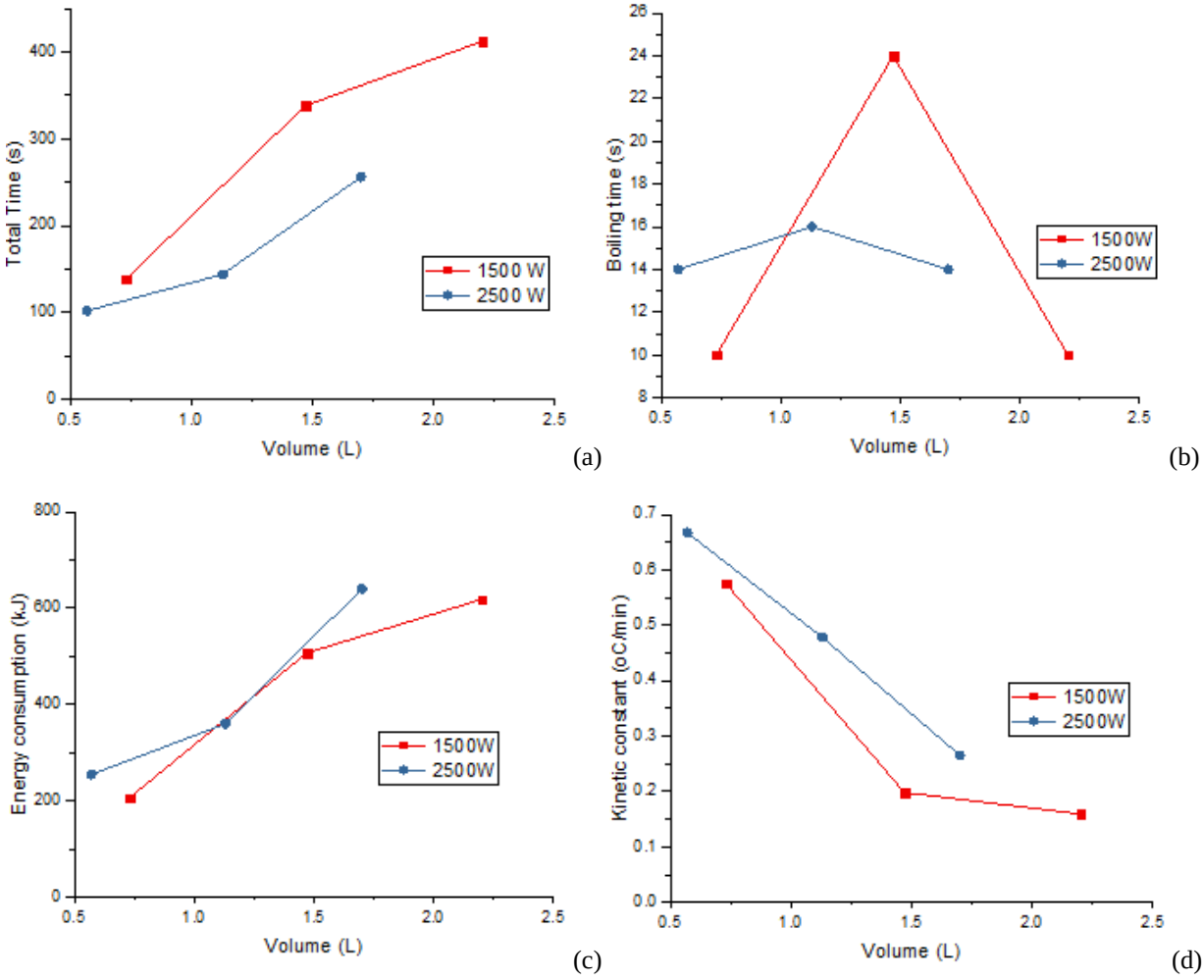

Figures 6 (a-d): Performance of the metal kettles

Figures 6a to 6d show the performance of the metal kettles. From Figure 6a, we observe that for kettles of all ratings, the time for boiling increases for higher volumes of water. Also, boiling time is lower for the kettle with 2500W power than that of 1500W power. This is because, for a device of higher power rating, more energy is transferred per time to the liquid hence less time is required to achieve boiling temperature. Figure 6b shows optimum boiling time at intermediate water levels for both ratings of kettles. Figure 6c reveals that the energy consumption of the kettles increases with larger volumes of water. This relationship is independent of the power rating of the kettle. Figure 6d reveals that boiling is faster for smaller volumes of water than for larger volumes. Kettles with a higher power rating will boil water faster than those with a lower power rating. Response surface plots were developed to elucidate the possible interactions between these two parameters as they affect boiling time, total time, boiling kinetics and energy consumption.

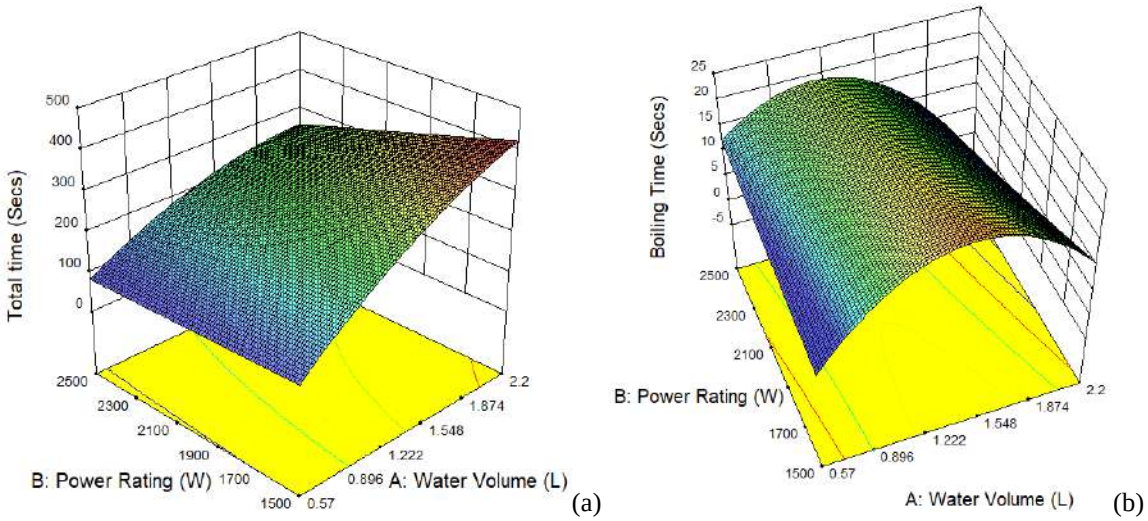

Figures 7 (a-b): Effect of power rating and water volume on total process time and boiling time

From Figure 7a, we observe that the total time for boiling increases with water volume in the kettle and this is the same for all levels of power rating. Total time for boiling is less for higher power ratings and this is more pronounced when the volume of water is much. For little volumes of water, the boiling time will not be too different between a lower rated and a higher rated kettle. Figure 7b shows that the response of the auto-off mechanism of the kettle at the point of boiling is highest at intermediate water volume and this is sustained for all levels of power rating.

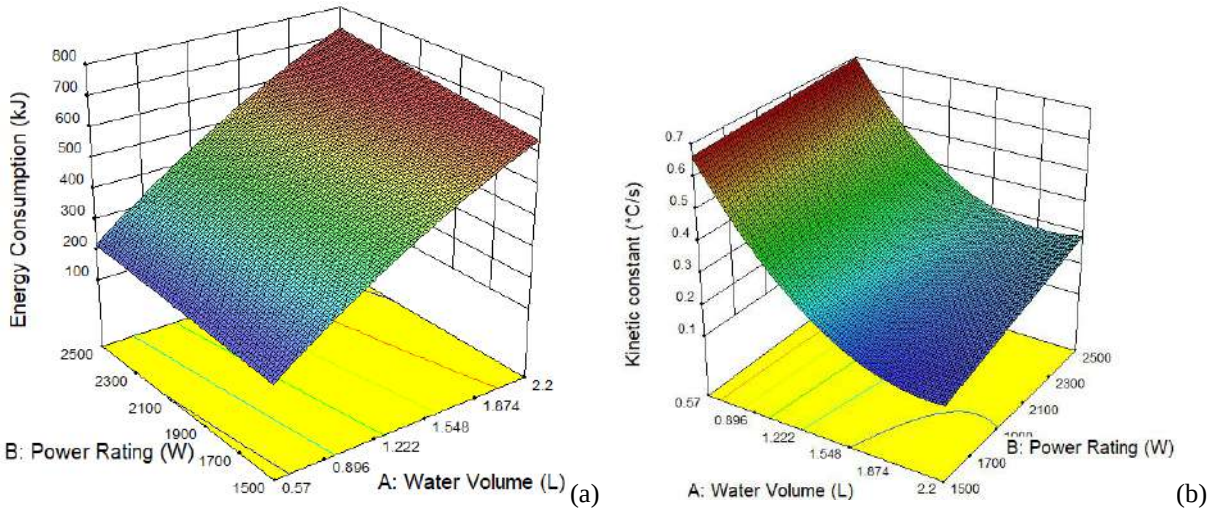

Figures 8 (a-b): Effect of power rating and water volume on energy consumption and boiling kinetics

From Figure 8a, we see that the energy consumption increases linearly with increasing water volume and this is independent of the power rating of the kettle. It is also observed that energy consumption is marginally higher for higher rated kettles. This can be due to an increased energy loss in the process. When the energy transfer per time into the system is vigorous, the increased entropy will facilitate higher convection losses alongside the fairly constant conduction losses to the sides of the vessel. Figure 8b elucidates an exponential increase in boiling kinetics for lower volumes of water. This has already been previously explained. Having examined the study of parameters for the metal kettles, we will take a look at the plastic kettles. The approach for these will be quite different as all the kettles have the same power rating. We will then be considering the effect of the usage extent (brand new vs already in use) on the performance of the kettles.

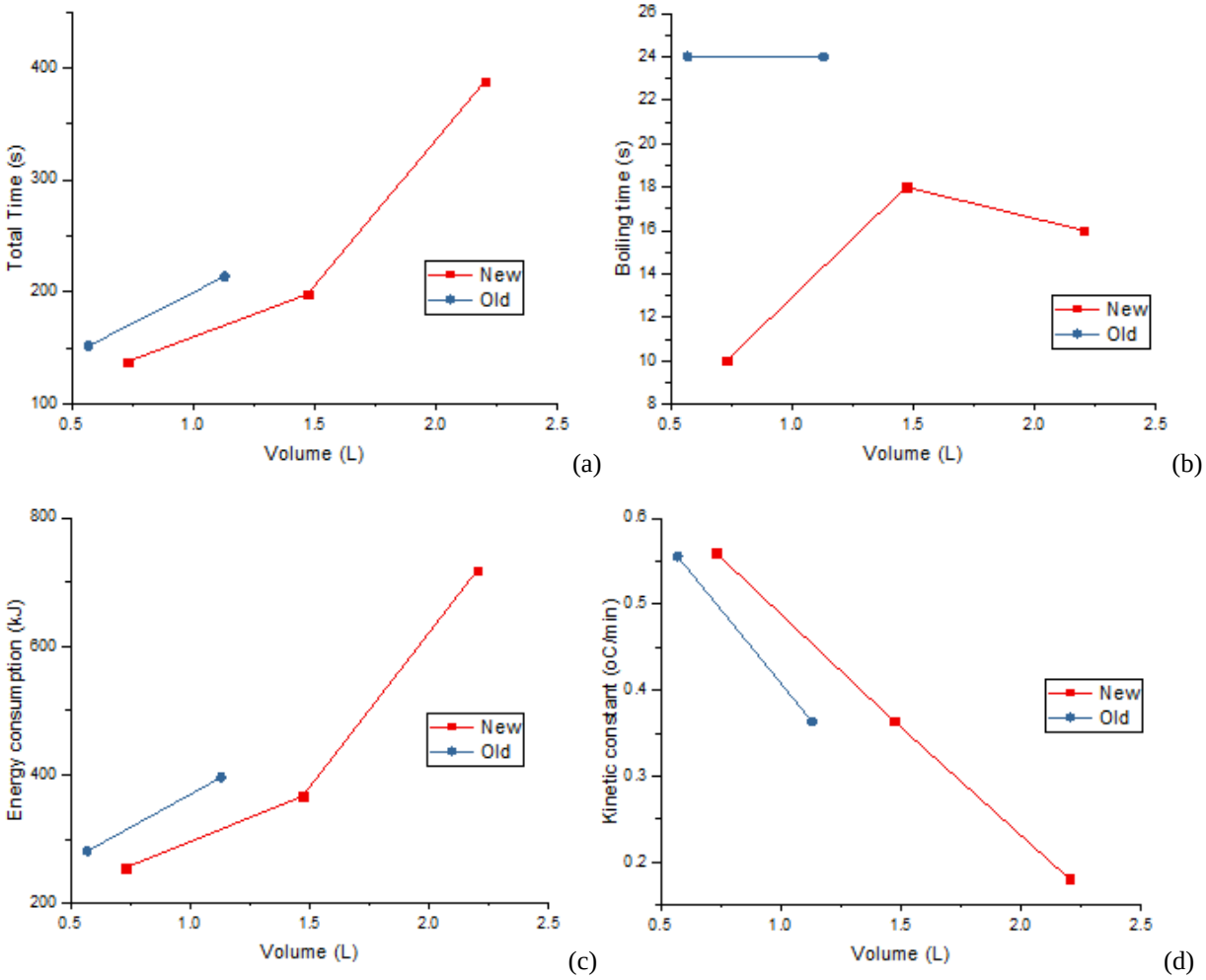

Figures 9 (a-d): Performance of the plastic kettles

From Figure 9a, the relationship between water volume and total boiling time for plastic kettles is same as observed for metal kettles. However, the brand new kettles utilised a shorter total time than for the corresponding old kettle. This is expected as the performance of the new kettles is supposed to be higher in than for the older kettles. This finding should not be misconstrued with the findings of the kinetics and temperature progression. These latter parameters are not based on time alone but on temperature rise also. Figure 9b showed that the behaviour of the time of boiling for the brand new plastic kettles is similar to those of the metal kettles though this was not observed for the plastic kettles. Figure 9c reveals that the energy consumption of the new kettles is higher than for old kettles. This simply reveals that newer kettles are more energy efficient and this begins to get poorer with extended use. The relationship of boiling kinetics and water volume is the same for oil and new kettles (see Figure 9d) as well as for metal kettles (see Figures 6d).

4. CONCLUSION

From the study, several findings were made. Temperature progression profiles revealed the rapidity of temperature rise with time and showed that larger volumes of water in the kettles will lead to a less rapid temperature climb. It was also observed from the kinetic studies that for kettles of higher power ratings, the rate of boiling will always be faster than for lower power ratings. Also, the rate of boiling for larger volumes of water is also lower than for smaller volumes of water. For plastic kettles of the same rating, the kinetics are similar for both the old and the new kettles. From the consideration of the energy usage, it was observed that for most of the kettles, there was energy

loss during the process. The energy wastage was between 10-50% for most non-efficient kettle experiments. There did not seem to be any relationship between water volume, power rating and kettle type on the energy conservation of the process. Energy loss can be attributed to the conduction of heat unto the metallic and/or plastic components of the kettles as the heating was in progress. It is interesting to note that the use of plastic kettles instead of metallic did not in any way improve the energy conservation of the boiling process. Parametric studies revealed the relationship between the different input parameters and the observed results for both metal and plastic kettles.

REFERENCES

Adeniyi, A., Odimayomi, K., Emenike, E. C., Iwuozor, K., & Ndagi, M. (2023). Preparation of activated carbon monolith from waste biomass using solvated polystyrene-based binder. *Advances in Materials and Processing Technologies*, 1-13. https://doi.org/10.1080/2374068X.2023.2189679

Adeniyi, A. G., & Ighalo, J. O. (2018). Heat Transfer Modelling of the Open Sun drying of ogbono (Irvingia gabonensis) seeds. 29th Colloquium and Congress of the Nigerian Association of Mathematical Physics, Omu-aran, Nigeria.

Appelhof, H. (2008). Redesign of an Electric Kettle as part of a Horizontal Product Line. *GPD*.

DeGiorgio, N. (2017). *Kettle cooling and sustainability project* California Polytechnic State University]. San Luis Obispo.

Gallego-Schmid, A., Jeswani, H. K., Mendoza, J. M. F., & Azapagic, A. (2018). Life cycle environmental evaluation of kettles: Recommendations for the development of eco-design regulations in the European Union. *Science of the Total Environment, 625*, 135–146.

Hassan, M. A., Daud, R., & Jamaludin, S. N. S. (2011). Design and Analysis for the Improvement of Electric Kettle Performance.

Manrique, V., García, L., & Alfonso, J. (2014). Experimental evaluation of energy efficiency in a gasheated self-contained steam jacketed kettle. *IOP Conf. Series: Materials Science and Engineering*, *59*.

Marcinkowski, A., & Zych, K. (2017). Environmental performance of kettle production: Product life cycle assessment. *Management systems in production engineering*, *25*(4), 255-261.

Murray, D., Liao, J., Stankovic, L., & Stankovic, V. (2015). How to make efficient use of kettles: Understanding usage patterns. *Conference on Energy Efficiency in Domestic Appliances and Lighting*, 1-13.

Murray, D. M., Liao, J., Stankovic, L., & Stankovic, V. (2016). Understanding usage patterns of electric kettle and energy saving potential. *Applied Energy*, *171*, 231–242.

Telenko, C., Seepersad, C. C., & Webber, M. E. (2009). *A method for developing design for environment guidelines for future product design* Proceedings of the ASME 2009 International Design Engineering Technical Conferences & Computers and Information in Engineering Conference,

PAPER 66 -PRODUCTION AND CHARACTERIZATION OF CASSAVA PERIDERM EPOXY COMPOSITES

J. A. Adebisi[1], A. D. Abdulraheem[1*], M. A. Abdulhakeem[1], M. Ndagi[2], R. J. Owolabi[1], I. I. Ahmed[1]

[1]Department of Materials and Metallurgical Engineering, University of Ilorin, Ilorin, Nigeria.
[2]Department of Mechanical Engineering, University of Ilorin, Ilorin, Nigeria.
[*]Email: abdulraheem.ad@unilorin.edu.ng

ABSTRACT
This study focuses on the investigation of the physical and mechanical properties of cassava periderm epoxy composites. The locally sourced cassava periderm was sun-dried, pulverized, and sieved to obtain a size <100 µm. Various proportions of cassava periderm powder ranging from 0 to 20 wt% were mixed thoroughly with epoxy resin and cast into composites using fabricated silicone moulds. Cassava periderm particulate reinforcements were produced. The developed composites were examined for their hardness, density, water absorption, tensile, and flexural strengths. The addition of reinforcement lowers the tensile properties and improves the bending modulus of the composites. The produced cassava periderm-reinforced composite has a lower density and can be used for lightweight materials. These materials are used in the automobile industries to produce parts like car dashboards, steering wheels, door panels, and center consoles, among others.

KEYWORDS: Composite, Epoxy, Cassava periderm, Agricultural waste, Mechanical properties.

1. INTRODUCTION

Composite materials offer unique benefits over traditional materials like metal, polymer, or concrete, such as low weight, thermal and chemical resistance, and electrical insulation (American Composite Manufacturing Association, 2023). Composites consist of two phases: matrix and reinforcement, with reinforcement fibres being either natural fibres or synthetic manmade fibres. Agricultural wastes have been used to produce numerous useful materials to mitigate the challenges associated with their disposal. They have been used to produce solid fuel briquettes, cellulose, adsorbents, activated carbon, refectory and ceramic products, silica, silicon, livestock feed, inhibitors, biofuels, construction materials, lignin, and composite reinforcement (Agunsoye *et al*., 2017, Agbenyeku and Aneke, 2014 , Heuzé *et al*., 2014, Aigbodion *et al*., 2010, Kalderis *et al*., 2008, Kurniawan *et al*., 2011, Ki *et al*., 2013, Liu *et al*., 2014, Odusote *et al*., 2016, Achinivu *et al*., 2014, Adepoju *et al*., 2016, Venkateswaran *et al*., 2012, Le Normand *et al*., 2014). Agricultural wastes are generally burnt or disposed indiscriminately, this results in environmental pollution with adverse effects on climate (IEA, 2016), Adebisi *et al*., 2017a, stated that Nigeria is the largest producer of cassava, and thus generate cassava periderm as a complete waste with no specifically known value. Wastes such as cassava periderm is a significant source of natural fibre and can be used as a reinforcement for epoxy composites. This research aims to investigate the properties of cassava periderm epoxy composites by preparing particulate reinforcements, examining the effect of cassava periderm addition on the physical and mechanical properties of epoxy composites. These properties include, the material's hardness, density, and water absorption, tensile and flexural strength. Natural fibres are cheap, environmentally friendly, and easily accessible, making composites from cassava waste not only environmentally friendly but also encouraging the creation of wealth from waste. Previous research has produced silica from cassava periderm (Adepoju *et al*., 2016), while coconut shell particle-reinforced composites were produced by reinforcing shell particles into the epoxy matrix (Bhaskar & Singh, 2013).

2. MATERIALS AND METHODS

2.1 Materials:

Cassava periderm from cassava (*Manihot esculenta*) obtained from Sasa market, Osogbo, Osun State. Epoxy resin (Bisphenol A, density 1.15-1.2 g/cm^3) and hardener (Diethylenetriamine, density 1-1.05 g/cm^3), silicone (Visa High Quality 6000), HDF board, nails, artist knife, polyethylene film sheets, mixing bowls, stirring rod, sieve shaker, and wax were also used. The facilities/equipment used for this study include a digital weighing balance, Universal Testing Machine, Scanning Electron Microscopy (SEM) with Energy Dispersive X-ray analysis (EDX), Vicker Hardness Tester (eVlck-30T), electric milling machine, metallurgical microscope (Amscope) and oven.

2.2 Method:

Figure 1: Preparation of cassava periderm powder from (a) cassava periderm, (b) washing of the periderm, (c) sun drying, and, pulverised to obtain (d) cassava periderm powder.

Cassava periderm (CP) was separated from cassava tuber, washed, sun-dried, and pulverized. The resulting CP was sieved to obtain particle sizes <100 μm. Tensile and flexural silicone moulds were fabricated using ASTM Standards D638 (Type 1) and D790, respectively. The mould boxes were then completely laminated internally using film sheet. The film sheet was then waxed to ease releasing.

Table 1 presents composites formulation. The neat epoxy was produced using 186 g of epoxy and 93 g of hardener in ratio 2 to 1. The mixture was mixed thoroughly for 10 minutes before pouring into the silicone moulds, and left to cure. Composites were produced using same mixture ratio of epoxy and hardener but with addition of cassava periderm powder as filler. Stirring of the epoxy and hardener was done for 5 minutes prior to addition of cassava periderm with additional 5 minutes stirring. For a 5 wt.% addition, 14.68 g of cassava periderm was measured and poured into the mixture. The mixture were then poured into the moulds, and allowed to cure at room temperature for 15 hours. This process was repeated for 10, 15, and 20 wt.% additions. With 20 wt.%, compaction was needed to prevent blow holes. Thereafter, all the samples were cured in the oven for 2 hours at 121°C and allowed to cool down in the oven.

Table 1: Composites formulation

Run	Resin (E+H)	Reinforcement	Resin (E+H)	Reinforcement
	%	**%**	**g**	**G**
1	100	0	279	0.00
2	95	5	279	14.68
3	90	10	279	31.00
4	85	15	250	44.12
5	80	20	250	62.50

Density test was carried out and the values were calculated using the Equation 1:

$$Density = \frac{Mass\ (g)}{\text{Volume} cm^3} \quad (1)$$

Water absorption: water absorption test was carried out according to ASTM standard D5339 tests. The percentage of water absorbed was then calculated using Equation (2).

$$W.A.(\%) = \frac{W_2 - W_1}{W_1} \times 100 \quad (2)$$

Where;
W_1 = Oven dry weight of the specimen in grams (g),
W_2 = Specimen weight after soaking in water for the specified duration (g),
W.A. = percentage of water absorbed by the specimens (%).

Tensile Test

The composite's tensile strength was tested using a Universal Instron Testing Machine. The composite samples were prepared according to ASTM D638. The thickness of the samples was measured at three different positions along the length of the specimen and the average thickness use for calibration. The test speed used was 2mm/min with the gauge length fixed at 10.00 mm.

Flexural Test

The same proportion used for the tensile was used for the flexural test. Flexural test measures a polymer composite beam's bending force and resistance to bending, revealing a material's rigidity and its ability to curve before deformation. The flexural test measures the force required to bend a beam under three-point loading situations. The three-point bending test was performed in accordance with ASTM-D790 standards.

Hardness Test

The hardness of the samples was examined using Vickers hardness tester (eVlck-30T) in the Research lab, Materials and Metallurgial Engieering, University of Ilorin. In each case, three samples were examined for each wt% and the average value was obtained.

3. RESULTS AND DISCUSSION

Density

The density of neat epoxy is 1.22±0.03 g/cm3 as presented in Figure 7. The theoretical density used range from 1.1- 1.15 g/cm3. The observed and theoretical densities are in close proximity of about 3.5% error margin. The addition of reinforcement lowers the densities of the composites. This may be due to light weight of the biomass used. The rate of decrease in density decreased after 10 wt.% addition of cassava periderm. Decrease in the density of epoxy composites reinforced with sugarcane bagasse was reported by Tewari et al. (2012).

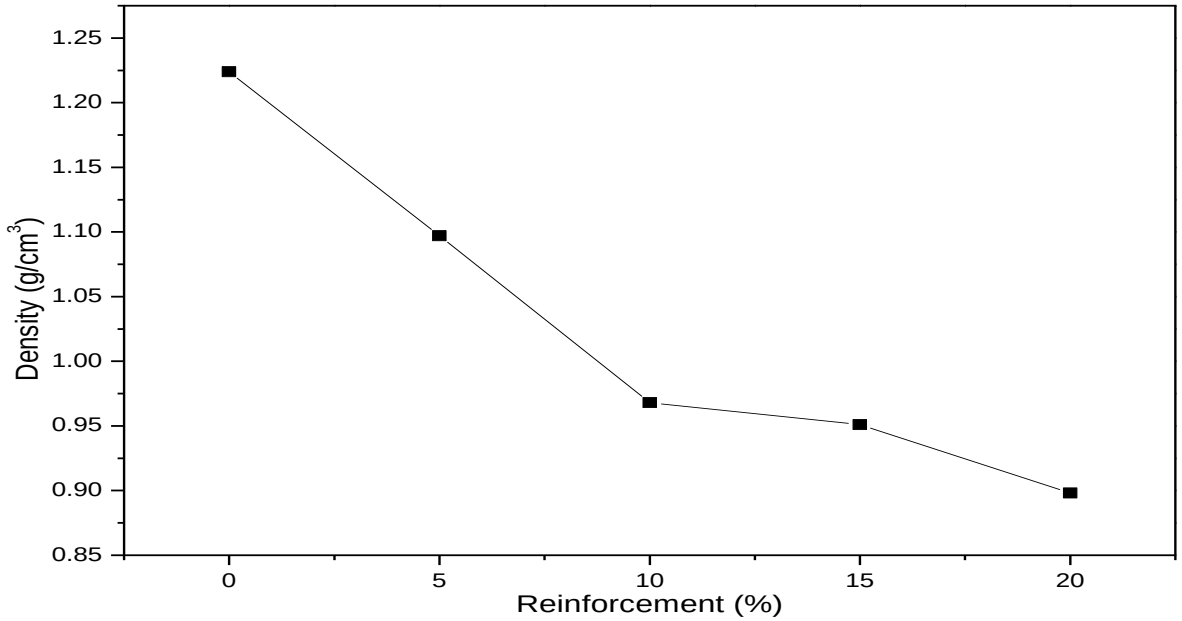

Figure 2: Density graph for cassava periderm epoxy composites.

Water Absorption Test

Figure 3 shows the water absorption for the neat and reinforced epoxies. The neat epoxy reveals a very low absorption rate compared to all the reinforced epoxies. The water absorbed for about 10 days is 0.0024% compared to 0.018, 0.016, 0.026 and 0.018% for 5, 10, 15 and 20 wt.% reinforcement loading, respectively. The addition of reinforcement increases the water absorption rate of the composites. The rate of water absorption for 20 wt.% cassava periderm was initially very high until after 100 hours where 10 wt.% loading shows a rapid absorption level. The composite has the maximum water absorption rate at 15 wt.%. The water absorption capacity was reported to be proportional to the reinforcement loading (Bhaskar & Singh, 2013). The rate of water absorption is not uniform for all the composites. This may be due to presence of voids or low interfacial bonding of the reinforcement to the matrix.

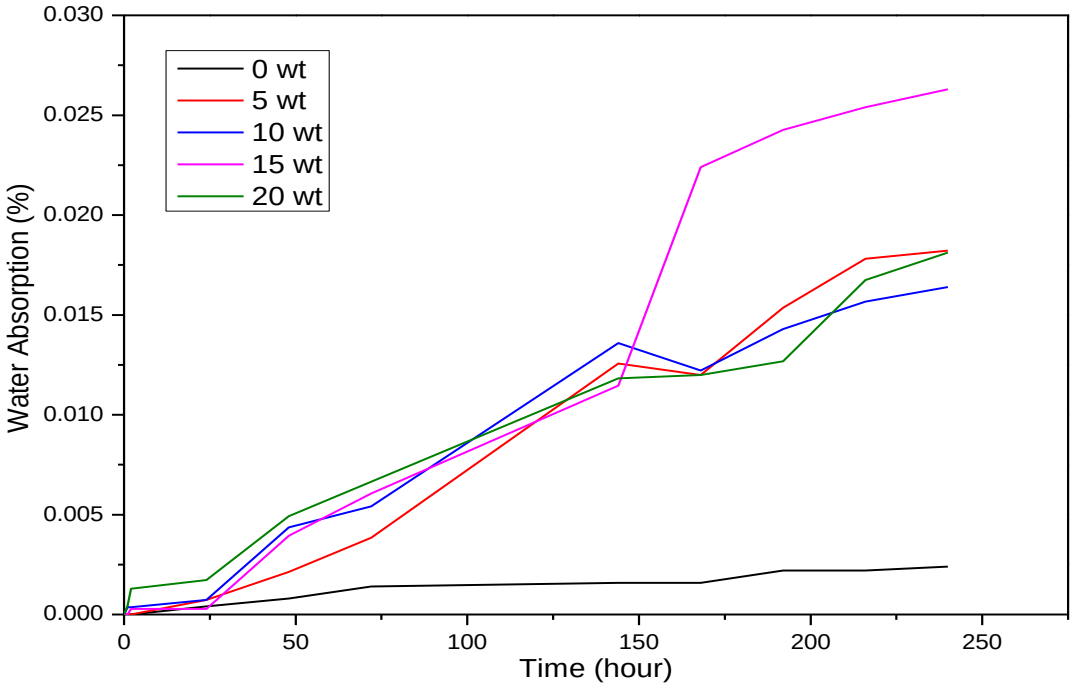

Figure 3: Water absorption cassava periderm epoxy composite.

Mechanical Properties

Tensile Test

The young modulus of neat epoxy is 944.93 N/mm^2. As the reinforcement increases, there is gradual decrese in young modulus. The strength of the composite is dependent on the reinforcement. The lowest young modulus was achieved by 20% PALF which procured 2.17 GPa (Mathivanan *et al.*, 2014).

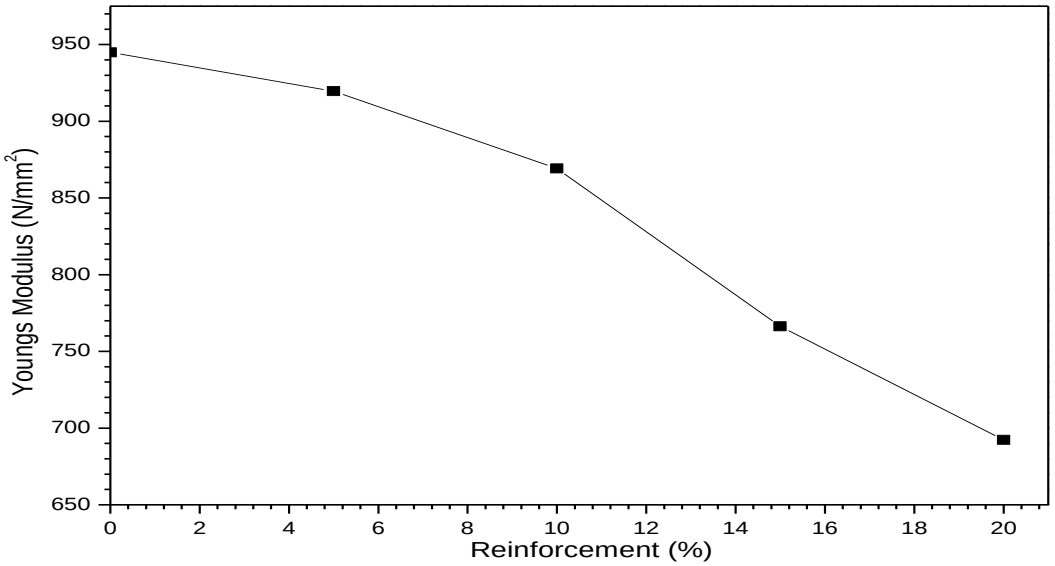

Figure 4: Young's Modulus for cassava periderm epoxy composite.

Flexural Test

The Bending modulus of 0-10 wt% increases which improves the properties, while that of 15-20 wt% decreases. The result showed decrease in flexural modulus at higher weight fractions (20%) of fibre loading (Mathivanan *et al.*, 2014)

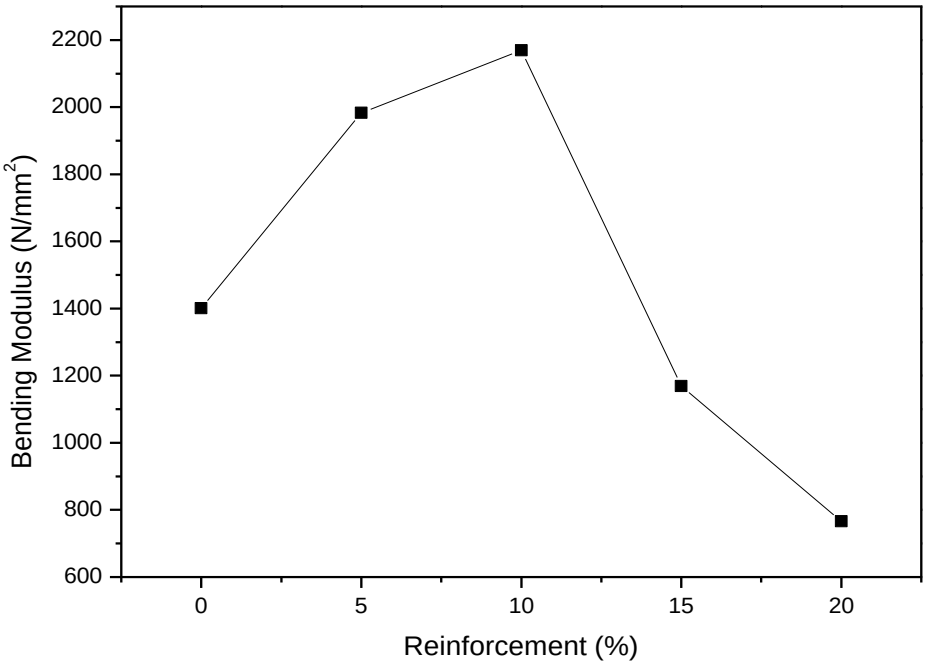

Figure 5: Bending Modulus for cassava periderm epoxy composite.

Hardness Test

The hardness of 0 wt% increases which improves the properties, while that of 5 and 15 wt% decreases. Hardness increased with addition of epoxy compare to addition of cassava periderm powder.

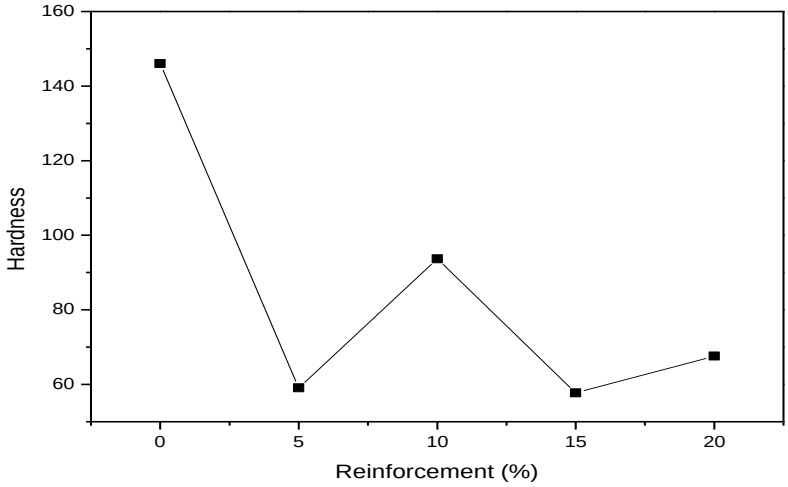

Figure 6: Hardness for cassava periderm epoxy composite.

4. CONCLUSION

Cassava periderm particulate reinforcements were successfully produced. The composite has a lower density and can be used to produce lightweight materials. Reinforcing the material increases the water absorption hence making it more hygroscopic. The addition of reinforcement lowers the tensile properties and improves the bending modulus of the composites.

It is therefore recommended that, more mechanical tests such as impact tests and thermal conductivity should be carried out on the composites to establish optimum formulation and explore areas of application.

REFERENCES

Adepoju, A., Adebisi, J. A., Odusote, J. K., Ahmed, I. I., & Hassan, S. B. (2016). Preparation of silica from cassava periderm. The Journal of Solid Waste Technology and Management, 42(3), 216-221.
Bhaskar, J., & Singh, V. K. (2013). Water Absorption and Compressive Properties of Coconut Shell Particle Reinforced-Epoxy Composite. *J. Mater. Environ. Sci.*, *4*(1), 113-118.
Tewari, M., Singh, V., Gope, P., & Chaudhary, A. K. J. J. M. E. S. (2012). Evaluation of mechanical properties of bagasse-glass fiber reinforced composite. *3*(1), 171-184.
https://3dfortify.com/composites-replace-traditional-materials/
Mathivanan, D., Siregar, J., Bachtiar, D., Rejab, R., & Cionita, T. (2014). Effect of Fibre Loading on The Flexural Properties of Natural Fibre Reinforced Polymer Composites. *Applied Mechanics and Materials, 695*, 85-88. doi:10.4028/www.scientific.net/AMM.695.85.

PAPER 67-DESIGN AND FABRICATION OF AN ADAPTABLE MIXER FOR POLYMER MATRIX COMPOSITE PRODUCTION

J. A. Adebisi[1], O. Q. Ajao[1], M.O. Bello[1], O. J. Akinola[1,*], S. I. Talabi[2], I. I. Ahmed[1]

[1]Department of Materials and Metallurgical Engineering, University of Ilorin, Ilorin, Nigeria.
[2]Oak Ridge National Laboratory, Oak Ridge, Tennessee.
[*]Email: 18-30gn019@student.unilorin.edu.ng

ABSTRACT
Production of polymer matrix composites requires a homogeneous mixture of at least two substances, usually matrix and reinforcement(s). Mixing of the substances manually results in an inhomogeneous mixture marred with inconsistencies of mixing parameters which affects the properties of the composites. In a bid to proffer a solution, this work focuses on the design, fabrication, and evaluation of an adaptable mixer. SolidWorks was used for the design of the mixer and the machine was locally fabricated using mild steel. The machine was evaluated using varied mixing speeds compared with manual mixing of an epoxy composite. The composites were assessed with flexural samples using ASTM D790 and visual observation. It was observed that the speed of mixing has a great impact on the flexural strength and quantity of bubbles. The mixer produces a homogeneous mixture at a sufficiently short time at low speeds. The machine will be useful for batch production of composites between 200 and 2000 cm^3 in laboratories and small-scale industries.

KEYWORDS: Polymer matrix, Composite, Reinforcement, Adaptable Mixer.

1. INTRODUCTION

Mixing is crucial in polymer matrix composite production, ensuring even distribution of reinforcement materials and minimizing defects. Various techniques like hand layup and injection moulding require effective mixing. Different mixing machines, such as the Banbury mixer and extruder, have been developed to enhance efficiency. At the University of Ilorin's Department of Material and Metallurgical Engineering, manual mixing for polymer matrix composite production leads to inconsistent mixtures with bubbles and uneven material distribution, therefore compromising research reliability. This study aims to design and fabricate an adaptable mixer for polymer matrix composite production.

Polymers are large molecules made of repeating units called monomers, connected by covalent bonds. They can be natural or synthetic, with synthetic ones categorized as either thermoplastics (which can be reshaped upon heating) or thermosetting (which cannot be reshaped after forming) (Ravve, 2013). Composites are essential materials comprised of a strong reinforcement and a softer matrix, such as wood with cellulose fibres as reinforcement and lignin as the matrix. They're classified into metal, ceramics, and polymer matrix composites. Polymer matrix composites (PMCs) use polymers as the matrix, reinforced with materials like glass or carbon fibres. PMCs are classified as thermosets or thermoplastics for production.

Polymer matrix composite production involves material preparation, mixing, moulding, curing, and sometimes surface finishing. Various techniques have been used for this process over time. Some of these techniques are: Autoclave-Based Method, Resin Transfer Moulding (RTM), Pultrusion, Filament Winding, Hand Layup and Spray Techniques. Moreover, Insufficient knowledge and neglect in mixing affect production costs in both industrial and small-scale setups for polymer matrix composites (PMCs). PMCs involve solid-liquid mixing, like reinforcing carbon black in rubber. The components of the PMC mixer are: AC Motor, Mixer tube, Motor shaft, Mixer frame and the Impeller. The machine ensures homogeneity in mixing polymer and fibre for polymer matrix composites (PMCs). Methods like static mixers, ribbon mixers, and stirrers achieve this by creating flow and direct contact with materials (Hidayat et al., 2022).

2. THEORETICAL ANALYSIS

The mixer is a laboratory-scale equipment designed for a one-time mixture of constituents that provide specimens for tensile tests, flexural tests, impact tests, thermal conductivity tests, and water absorption tests. The mixer is designed based on volume and consists of impellers, reaction vessels, a motor, and a speed controller. The ASTM standard was followed to calculate the volume of the reaction vessels, and the obtained results from the design calculations are presented in the table below.

Table 1: Design calculation values

Parameters	Denotations	Values	units
The density of polymer matrix composite	ρ	1400	Kg/m^3
The volume of the vessel (Experimental)	V_S	1,270,774.2	mm^3
The volume of the vessel (mass mixing)	V_S	3459682.8	mm^3
Diameter of the vessel (Experimental)	D	100	mm
Height of the vessel (Experimental)	H	161.8	mm
Diameter of the vessel (mass mixing)	D	165	mm
Height of the vessel (mass mixing)	H	260	mm
The diameter of the open and pitched blade impeller (Experimental)	d	85	mm
The diameter of the open and pitched blade impeller (mass mixing)	d	140	mm
The diameter of the modified impeller	d_a	152	mm
Height of the open and pitched blade impellers	h	18	mm
Height of the modified impeller	h_a		mm
Clearance in open & and pitch blade impeller	C	25	mm
Clearance in modified impeller	C_a	12	mm
The viscosity of the polymer	μ_0	1,000	cp
The viscosity of the polymer matrix composite	μ	2,750	cp
Standard power number	$N_{p_{standard}}$	1.2	-
Reynolds number	N_{RE}	101.8	-
Viscosity power factor	F_{μ}	1.7	-
Power number	N_p	2.04	
Power of motor	P_{motor}	0.25	hp
Torque of the open and pitch blade impeller shaft	T	1.78	Nm
Diameter for the open and pitch blade impeller shaft	d_o	6	mm

3. MATERIALS AND METHODS/METHODOLOGY/EXPERIMENTAL PROCEDURE

3.1 **Materials**

The equipment is made of mild steel with thicknesses between 2 and 4 mm for the frame and external components, while stainless steel with thicknesses ranging from 2 to 12 mm is used for the reaction vessel and impellers, including blades. Additionally, the electric motor has specifications that include 0.28 hp, rotation of 1350 - 1660 rpm, current of 2 A, and voltage of 220 - 240 volts, and the speed controller is achieved using a variable digital voltage adjustable regulator transformer for single-phase power supply.

Design of mixer

SolidWorks software was utilized to create detailed images, including projections and 3-D drawings, of the mixer. The cylindrical mixer frame measures 390 mm in height and 272 mm in diameter, with a hollow top for the motor shaft to pass through. A vertical plate holds the motor in place. The reaction vessel, also cylindrical,

has dimensions of 161.8 mm in height and 100 mm in diameter. An opening on the mixer frame allows for easy removal of the reaction vessel, while a plate beside the frame holds the speed regulator.

Design of impellers

SolidWorks was utilized to design the impellers, which are screwed onto the motor shaft for easy removal. The blades are designed to avoid contact with the vessel walls. Three impellers were designed: an open impeller with four vanes, an angled pitch-blade impeller, and a modified impeller.

3.2 **Fabrication of the Mixer**

Fabrication of the framework

The framework fabrication began with a rectangular mild steel plate (300 mm by 200 mm) bent into a cylindrical shape. At the top, a 4 mm thick mild steel was welded into a hollow circle for the motor shaft. Another circle at the bottom holds the reaction vessel. An opening at the center back allows light into the mixing chamber. Additionally, a vertical steel plate holds the motor in place on top of the frame.

Fabrication of the reaction vessels

For the experimental reaction vessel, a 3mm steel plate was rolled into a diameter of 100 mm and a height of 161.8 mm. A circle plate of the same diameter was welded to one end. The second vessel measured 165 mm in diameter and 260 mm in height. Steel bars were used to create handles on the vessel sides.

Fabrication of the impellers

The impellers were fabricated using a stainless steel shaft with threading at both ends. For the open and pitch-blade impellers, two sets of blades were made: one set measuring 85 mm by length and the other 140 mm. The modified impeller, with a height of 290 mm, has fixed blades positioned at 60° angles on the shaft.

Assembly of the mixer

The motor is securely positioned and screwed in place, with an impeller blade attached to one end of the shaft. The reaction vessel is placed inside the frame with the materials to be mixed, and then the other end of the shaft is screwed onto the motor inside the frame.

Optimization

To fix wobbling and vibration, the shaft height was reduced, and dead load was added to the bottom chamber. A steel sheet covered the bottom opening, filled with a sand-cement mixture, and covered with a circular plate for the vessels to sit on

3.3 **Testing**

Visual inspection

In testing the mixer, epoxy was mixed with glitters in a reaction vessel and poured into a mold for solidification. The mold, shaped like a disposable cup, consisted of two nested cups. Three molds were produced. Epoxy-glitter mixing was done using the mixer at two speeds (10 V and 25 V), while one sample was manually mixed. All samples were poured into the molds and allowed to cure.

Flexural test

The flexural properties of resin polymer samples were evaluated according to ASTM D790 standard in a three-point bending test. Eight specimens were produced: two each at voltages of 10 V, 15 V, and 20 V using the mixer, and two produced manually. A comparison was illustrated graphically.

4. **RESULTS AND DISCUSSION**

The mixing process involves several components working together. The motor provides power for the mixing operation, while the framework supports the motor and holds the reaction vessels in place. The reaction vessel is where the mixing occurs, and the impeller transmits rotational energy from the motor to the constituents being mixed. Finally, the speed controller regulates the rotation of the impeller, ensuring that the mixing process is performed at the desired speed. Altogether, these components form a cohesive system for mixing various substances efficiently and effectively.

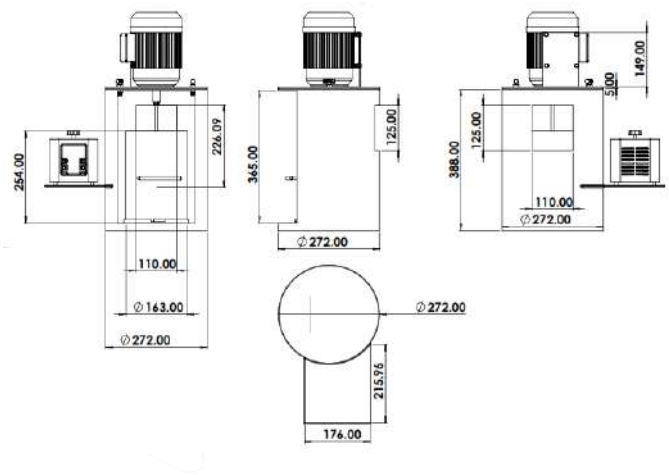

Figure 1: projection drawing of the mixer

Design of adaptable impellers
The impeller consists of:

- Various impeller blades in direct contact with the constituents.
- The shaft, holding the impeller blades on one end and connected to the motor on the other.

Figure 2: The designed impeller blades, (a) pitch-blade (b) open blade

4.1 **Fabrication of the mixer**
In optimizing the mixer, stainless steel was used for components in direct contact with constituents to prevent contamination. Mild steel was used for the framework, while impeller height was reduced and a sand-cement dead load added to resist vibration.

Figure 3: (a) fabricated mixer (b) fabricated impellers

Optimization of designed mixer
To optimize the mixer, a design drawing addresses the effects of shaft vibration and wobbling, with dimensions in millimeters (mm). It includes the height and position of the dead load, as well as the new height of the impellers.

4.2 **Evaluation**

After solidification, a physical evaluation was conducted to determine the effectiveness of different mixing methods. The results showed that mixer mixing was faster than manual mixing, and mixer-mixed samples cured faster than manually mixed ones. Low-speed mixer samples had minimal bubbles, indicating that this method is ideal for applications where bubble formation is undesirable. On the other hand, high-speed mixer samples were evenly distributed but had bubbles, which may be acceptable for certain applications. Manual mixing resulted in fewer bubbles than high-speed mixing but more than low-speed mixing. These findings suggest that the choice of mixing method should depend on the specific requirements of the application in question.

Figure 4: Samples produced. (a) Manual mixing (b) Mixing with mixer at 10V (c) Mixing with mixer at 25V

Flexural Test

The flexural specimens used for bending tests are labelled as follows:

- Specimen "1": Mixed at 10 V, no bubble presence observed.
- Specimen "2": Mixed at 15 V, little bubbles on edges.
- Specimen "3": Mixed at 20 V, surface filled with bubbles.
- Specimen "4": Mixed manually, small cluster of bubbles on surface.

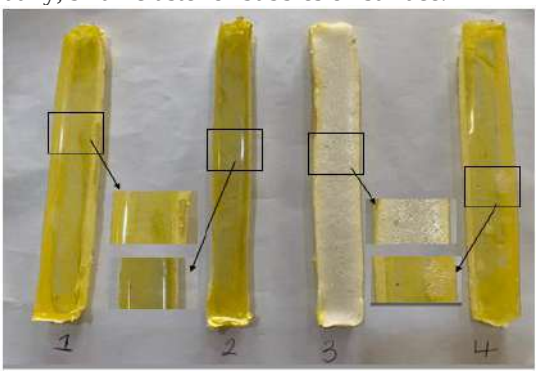

Figure 5: Flexural samples (1) mixed at 10 V (2) mixed at 15 V (3) mixed at 20 V (4) mixed manually

Upon plotting the graph of force/load against deflection during the bending test:

- The manually mixed specimen exhibited the highest peak at 739.100 N, indicating the highest resistance.
- Next on the curve, the specimen mixed at a low speed (10 V) showed a peak of 651.200 N.
- The two curves below, representing samples mixed at a faster speed (20 V), had peak values of 164.100 N and 103.100 N, indicating lower resistance to the applied bending force.

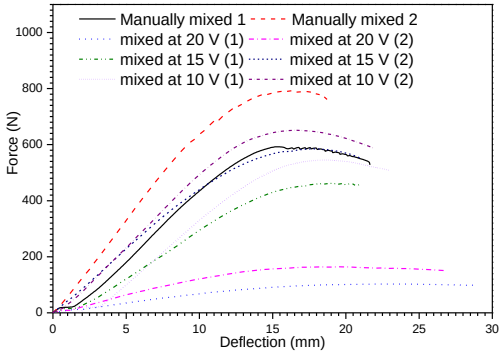

Figure 6: Plot of bending force against deflection

Additionally, a comparison of the stress experienced by the samples at peak load, measured in newtons per square millimeter (N/mm²), is presented below. This value indicates the maximum load the samples can withstand before failure, and is depicted with error bars.

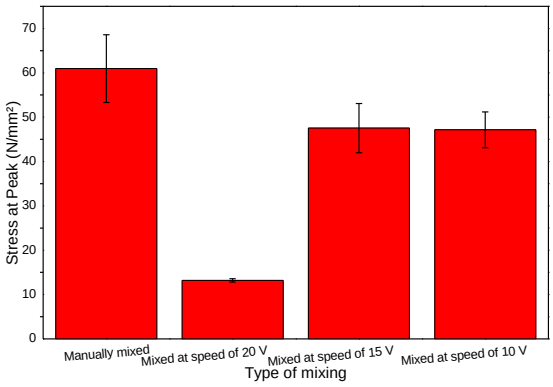

Figure 7: Plot of stress at peak

The stress at break represents the level of stress experienced by the samples at the point of failure, measured in N/mm². Below is a comparison illustrated with error bars.

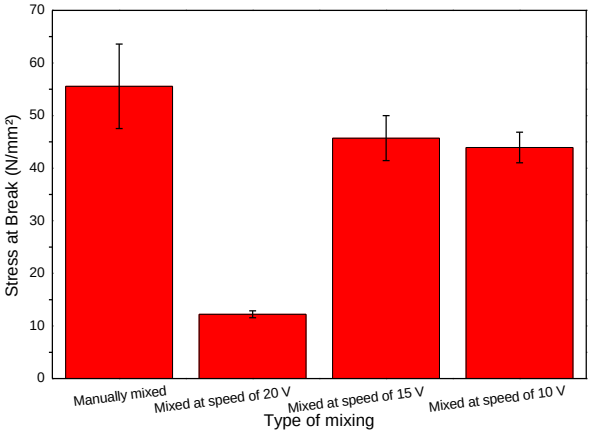

Figure 8: Plot of stress at break

Finally, a plot of the bending modulus, accompanied by error bars for each sample, is provided. This parameter, also known as the flexural modulus or modulus of elasticity in bending, quantifies the stiffness of the samples and represents their resistance to bending deformation.

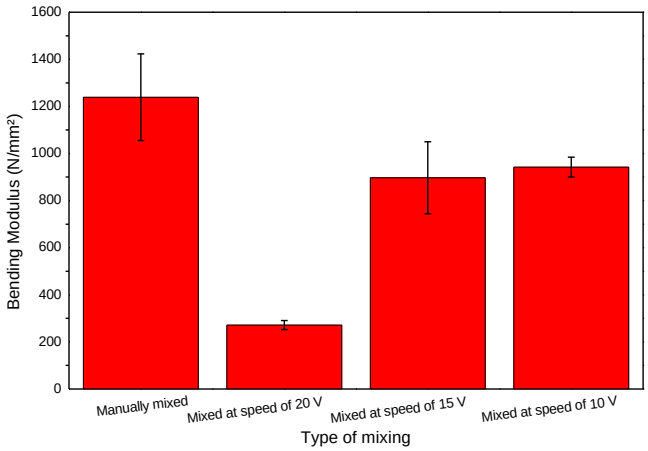

Figure 9: Plot of the bending modulus

5. CONCLUSION

The mixer, designed using SolidWorks, handles composite volumes from 200 to 2,000 cm3 with speed control. Impellers, including pitch-blade and open types, were fabricated using arc welding with stainless steel containers. The mixer affects flexural strength, with higher speeds reducing strength and increasing bubbles. This work provides insights for similar mixing system designs in materials science, suitable for laboratory and small-scale industry polymer composite production. It is therefore recommended that further testing should be done to validate the mixer's performance with various polymer matrix composites and additives, exploring lower mixing speeds. Likewise, scaling up the mixer design for larger production volumes, adapting principles for industrial-scale mixing systems.

REFERENCES

Chawla, K. K. (2012). *Composite materials: science and engineering*: Springer Science & Business Media.

Chopey, N. P. (1993). *Handbook of chemical engineering calculations*.

Clyne, T. W., & Hull, D. (2019). *An introduction to composite materials*: Cambridge University Press.

Dickey, D., & Fasano, J. (2003). Handbook of Industrial Mixing: Mechanical design of mixing equipment. 1247-1332.

Divya, H., Naik, L. L., & Yogesha, B. (2016). Processing techniques of polymer matrix composites–A review. *International Journal of Engineering Research General Science, 4*(3), 357-362.

Green, D. W., & Southard, M. Z. (2019). *Perry's chemical engineers' handbook*: McGraw-Hill Education.

Hidayat, R., Irawan, E., Prasetiyo, E. E., & Setiawan, F. (2022). Mixer Design Equipped With Heating Control Elements For Manufacturing Composite Materials. *Journal of Applied Mechanical Engineering Renewable Energy, 2*(2), 52-61.

Hughes, A., & Drury, B. (2019). *Electric motors and drives: fundamentals, types and applications*: Newnes.

Ji, S. (2004). A generalized mixture rule for estimating the viscosity of solid‐liquid suspensions and mechanical properties of polyphase rocks and composite materials. *Journal of Geophysical Research: Solid Earth, 109*(B10).

Kessler, M. R. (2012). Polymer Matrix Composites: A Perspective for a Special Issue of Polymer Reviews. *Polymer Reviews, 52*(3), 229-233. doi:10.1080/15583724.2012.708004

Khurmi, R., & Gupta, J. (2005). *A textbook of machine design*: S. Chand publishing.

Nienow, A. W., Edwards, M. F., & Harnby, N. (1997). *Mixing in the process industries*: Butterworth-Heinemann.

Okwabi, R. (2016). Design and construction of a hand-operated mixer machine for food fortification. *International Research Journal of Engineering Technology, 3*(9), 6-15.

Patel, M. R. (2012). *Introduction to electrical power and power electronics*: CRC Press.

Prabhu, P., Karthikeyan, B., Vannan, R. R. R. M., & Balaji, A. (2022). Mechanical, thermal, and morphological analysis of hybrid natural and glass fiber-reinforced hybrid resin nanocomposites. *Biomass Conversion Biorefinery*, 1-15.

Ravve, A. (2013). *Principles of polymer chemistry*: Springer Science & Business Media.

Saba, N., Jawaid, M., Sultan, M. J. M., physical testing of biocomposites, f.-r. c., & composites, h. (2019). An overview of mechanical and physical testing of composite materials. 1-12.

Simanjorang, M. R., Susanto, H., & Bukhori, M. L. (2022). Design And Construction Of Mixer With Variable Speed For Manufacturing Nanoparticle Composite Materials. *Teknika STTKD: Jurnal Teknik, Elektronik, Engine, 8*(2), 257-266.

Tong, W. (2014). *Mechanical design of electric motors*: CRC press.

U.S. Department of Energy Washington, D. C. (1992). *DOE Fundamentals Handbook: Electrical Science, Volume 4*: United States. Department of Energy. Technical Information Center.

Wang, W., & Manas‐Zloczower, I. (2001). Temporal distributions: The basis for the development of mixing indexes for scale‐up of polymer processing equipment. *Polymer Engineering Science, 41*(6), 1068-1077.

Yang, B., Sato, M., Kuriyama, T., & Inoue, T. (2006). Improvement of a gram‐scale mixer for polymer blending. *Journal of Applied Polymer Science, 99*(1), 1-5.

PAPER 69 - THE EFFECTS OF POOR WASTE MANAGEMENT: AN OVERVIEW OF THE ENVIRONMENTAL CHALLENGES IN NIGERIA

[1]Ayobamidele, S.J., [2]Oke, A.M., [2]Aremu, T.E., [2]Taiwo, T.B. and [2]Atoyebi, K.O.

[1]Department of Vocation and Technical Education, University of Ilesa, Ilesa, Osun State
[2]Department of Agricultural Engineering, Adeleke University, Ede, Osun State

ABSTRACT
Solid waste management is a major environmental challenge in most Nigerian cities. Waste generation rate in Nigeria is estimated at 0.65-0.95 kg/capita/day which gives an average of 42 million tonnes of wastes generated annually. This is more than half of 62 million tonnes of waste generated in sub-Sahara Africa annually and where and how to channel these wastes becomes a huge problem for the nation. This study examines the problems and prospects of solid waste management in some selected Nigerian cities using the mixed method of data collection. The findings revealed that waste management in Nigerian cities is largely monopolized by the agencies of state governments (sub-national governments) which have limited capacity to tackle the problems of solid waste management in their cities. In addition, 52 % of wastes generated are organic wastes which create additional disposal problems. Although the problems of solid waste management in Nigeria range from poor collection and disposal methods; lack or poor waste management database; insufficient financial resources; non-compliance to laws and lack of awareness on dangers of poor sanitary habits, this paper argues that a robust waste data base, strict policies and regulation are important for effective solid waste management in Nigeria

KEYWORDS: Solid waste, environmental challenge, mixed method, poor collection and disposal methods

1. INTRODUCTION

Management of municipal solid waste in Nigeria has suffered neglect from the government, environmental agencies and the general public. This negligence leads to several health issues such as direct injuries from contaminated sharp objects, water borne diseases from contamination by excreta and heavy metal components of municipal solid waste as well as floods resulting from drain obstructions. All these culminate in the possibilities for the transmission of food and water borne zoonoses, vector-borne diseases and the emergence and re-emergence of new zoonoses (Akinyemi et al., 2012; Oresanya, 2011). To ensure environmental protection and public health, more efforts are required by the government, environmental agencies and the general public. These efforts should be geared towards public enlightenment, enactment and enforcement of policies and legislations on sanitation, improvement of funding, monitoring and supervision, recycling waste and development of landfills to improve the standard of solid waste management in Nigeria (Giusti, 2009). Municipal solid waste commonly known as garbage or refuse is a waste type consisting of everyday items that are discarded by the public with variation from country to country. Municipal solid waste changes significantly with time and may include durable goods, non-durable goods, containers and packaging, food wastes and yard trimmings, and miscellaneous inorganic wastes (Yoshizawa et al., 2002). They are classified based on their composition as biodegradable (food and kitchen waste, green waste), recyclable (glass, bottles, plastics, metals), electrical (electrical appliances, televisions, computers), hazardous (paints, chemicals, light bulbs), and toxic (pesticides, herbicides) wastes (Oresanya, 2011). Four hierarchy ranking strategies have been developed by the United States of America for municipal solid waste management based on environmental friendliness from the most to the least preferred methods. These include; source reduction and reuse, recycling or composting, energy recovery as well as treatment and disposal ((Akinyemi et al., 2012). The management of this waste is gradually becoming a major challenge in developing countries like ours as a result of industrialization, urbanization and the increasing human and animal populations (NPC, 2006). The increasing demand for food and other life essentials arising from the increasing global population results in increased amount of waste which are not adequately managed in Nigeria resulting in the contamination of air, water and soil. These environmental contaminations pose serious public health threats (Hoornweg, and Bhada-Tata, 2012).

2. SOLID WASTE MANAGEMENT

Solid waste may be defined as all discarded solid materials resulting from households, industrial, healthcare, constructional, agricultural, commercial, and institutional sources. Solid waste generated in a city is often referred to as municipal solid waste (Akinyemi et al., 2012; Oresanya, 2011). In other literature and jurisdictions this category may exclude sewage, dissolved solids in water, and industrial waste. For this paper, no exclusions were

made for the reason that in most developing countries, most of the solid waste is not sorted at source, collection, transportation and disposal points. Thus, municipal waste in the context of developing countries may include waste that would not ordinarily be considered municipal waste. Solid or municipal solid waste management refers to the planning, financing and implementation of programs for solid waste collection, transportation, treatment and final disposal in an environmentally and socially acceptable manner (Karshima and Bobbo, 2016). Failure to adhere to set standards at any of the various stages constitutes "poor solid waste management". Solid waste management practices greatly vary across regions, countries and even within country. Modern waste management approaches encourage reduced waste generation, re-use, recycling, composting, and safe disposal through landfills, however, these are often not practiced. In developing countries, a large proportion of waste is not re-used (Yoshizawa et al., 2002). Waste sorting is also rare and therefore this makes it difficult to re-cycle or compost. As a result, a large proportion of solid waste in developing countries is disposed of on open dump sites and many times burnt (Karshima and Bobbo, 2016). The variations in waste management practices are often a reflection of existence of laws and policies governing waste management and extent of their enforcement, available funding, composition and quantity of waste generated. In many developing countries, solid waste management is the responsibility of both the municipal authorities and private providers (Ogu, 2000; Ogbonnaet al., 2012). Collection is often from source or temporary dumping ground, and final disposal is often at an open dumping site on the outskirts of the city. Dumping sites are often sprawling open grounds where truckloads deposit the waste. Dumped waste is often scavenged for usable articles, recyclable materials and many times burnt to reduce the bulk. Due to limited solid waste sorting at any stage, solid waste composition is complex and may contain industrial, medical, electronic, and human waste dumped on the same open grounds where all the other municipal waste is dumped.

2.1 WASTE CLASSIFICATION

Municipal solid waste is often categorized into two major groups: organic and inorganic. The organic municipal solid waste can further be divided into three categories: putrescible, fermentable, and non-fermentable. Putrescible wastes include products such as foodstuff that decompose fast. Fermentable wastes decompose rapidly, but without the unpleasant accompaniments of putrefaction while non-fermentable wastes tend to resist decomposition and, therefore, break down very slowly (Yoshizawa et al., 2002). Inorganic solid waste includes articles like metals, plastics, and other non-biodegradable materials. In terms of toxicity, some solid wastes are classified as hazardous including pesticides, medical waste, electrical waste, herbicides, fertilizers and paints and are recommended to be disposed of in special ways and not to be mixed with general municipal waste. Solid waste in developing countries characteristically has a high content of organic matter compared to that in developed countries (Yoshizawa et al., 2002). For example, studies conducted in the region estimated that in Juba South Sudan, organic waste constituted about 31% of all waste by weight, 61% in Ghana and 54% by weight in an Ethiopian town Jimma. The high organic content has implications for waste management including recycling, but also a potential source of ill-health if mismanaged (Karija et al., 2013)

2.2 EFFECTS OF POOR WASTE MANAGEMENT

2.2.1. Contamination of underground water

Water is vital to life and the existence and quality of life of the people living in a region depends on access to good clean water. Ground water is a crucial link in the hydrologic cycle because it is the source of most of the water in rivers, lakes and wells which are usually municipal sources of water. Contamination of ground water often results from poor municipal waste management. A study by Karija et al., (2013) showed that drinking water contaminated by municipal solid waste contained faecal coliform counts ranging between 15.25 MPN/100ml of water against the recommended 0 MPN/100ml of water. This may be a confirmation that human and animal excreta are components of municipal solid waste in developing countries as was earlier reported. Heavy metals including lead, cadmium, mercury and arsenic from municipal solid waste are also washed into surface and ground water posing serious public health threats. Common sources of these heavy metals in waste may include paint containers and other lead coated containers for lead, cadmium batteries and cigarette stumps for cadmium, broken mercury thermometers and barometers for mercury and containers of arsenic pesticides and wood preservatives for arsenics (Karija *et al*., 2013). These substances are not recycled in Nigeria and are frequently dumped together with household waste ending in the contamination of drinking water sources for humans and animals. Generally, the health effects of heavy metals can be life threatening and may range from headache, irritability, memory deterioration, diminished intellectual capacity, kidney damage, liver disease and bioaccumulation that leads to cancer (Jones*et al*., 2008: Karija *et al.*, 2013).

2.2.2. Possible emergence, re-emergence and maintenance of diseases

The disposal of dead animals of unknown causes on waste sites especially those within human settlements may pose serious public health threats considering the fact that 61% of infectious disease of humans are of animal origin. These dead animals can pose health risk to children, adult scavengers and waste workers visiting these sites. There are possibilities of dead animals disposed at waste sites initiating outbreaks of anthrax in humans and other animals if death is due to this disease especially with the fact that anthrax spores can remain viable in the environment for more than a decade. Human outbreaks arising from human contact with animals that died as a result of anthrax have been documented. According to the Independent Monitoring Board of the Global Polio Eradication Initiative report of April, 2014, Nigeria was still considered among the four countries still endemic for poliomyelitis virus; however, the country recorded its last case of poliomyelitis in July 2014 (Jones *et al*., 2008: Karija *et al*., 2013). Considering the fact that this disease is associated with poor sanitation, maintaining this polio free status requires in addition to strategic vaccination adequate sanitation. Other diseases associated with poor sanitation are cholera, geohelminth infections, typhoid, cysticercosis among others. Adequate MSW management will reduce the incidence of these diseases in Nigeria (Jones *et al*., 2008: Karija *et al*., 2013).

2.2.3. Breeding sites for disease vectors and rodents

Poor municipal solid waste management can lead to the breeding of insect vectors and rodents that are capable of transmitting various diseases. The public health risk becomes higher if these sites are located within human settlements. For instance, municipal solid waste sites either holds water or block drainages resulting in water stagnancy and breeding of mosquitoes which are capable of transmitting malaria. It is estimated that approximately one million people in Africa die from malaria alone each year and most of these are children under five years (Raji *et al*., 2007). Other diseases transmitted by mosquitoes are the dengue virus and yellow fever. Rodents from municipal solid waste sites can also enter neighboring houses posing residents of such houses to potential risks of diseases like Lassa hemorrhagic fever. House flies from waste sites can find their ways into neighboring houses and in the process transmit several diseases including cholera mechanically from excreta of infected persons when they come into contact with human food (Karshima and Bobbo, 2016)

2.2.4. Transmission of food and water borne endemic diseases

One of the public health implications of dumping waste within human settlements is the risk of transmission of food and water borne endemic zoonoses. These endemic zoonotic pathogens which are usually associated with human and animal excreta on waste dumping sites are usually washed by rains into surface or ground water, contaminating these sources of water for humans and animals, resulting in illness. In addition, food animals serving as vertebrate intermediate hosts can feed on human excreta, acquiring infections which are later transmitted to humans causing serious health problems. Common sanitary food and water borne endemic zoonoses documented in Nigeria include taeniasis/ cysticercosis, hydatidosis/ echinococcosis, campylobacteriosis (Karshima and Bobbo, 2016: Yoshizawa *et al.,* 2002).
Sharp objects such as syringes, scalpels and razor blades disposed at waste dumping sites can cause serious injuries to children visiting these sites either to defecate or play as it is very common in Nigeria. Municipal waste management workers and waste scavengers are also at risk of injuries caused by these sharp objects. These objects can also pose serious health risks to these groups of people if contaminated with infectious pathogens. For instance, in the year 2000 alone the World Health Organization estimated that contaminated syringes caused 21 million hepatitis B virus, 2 million hepatitis C virus and 260,000 human immune-deficiency virus infections worldwide (Yoshizawa *et al.,* 2002). These risks are particularly higher in developing countries where scavenging at waste disposal sites and manual sorting of hazardous waste from health-care establishments is common. Another direct effect may include environmental pollution associated with the decaying of the long-standing waste (Yoshizawa *et al.,* 2002).

2.3. POSSIBLE INTERVENTION STRATEGIES

Enactment and enforcement of policies and legislations will serve as useful strategies in improving solid waste management in Nigeria as poor solid waste management was associated with weakness of policy enforcement and implementation. The legislative arms of Government at the local, state and federal levels are encouraged to take up their responsibilities by enacting new laws and policies that will govern the management of municipal solid waste in Nigeria to ensure the protection of the general public from the hazards associated with this menace. With legislations in place, the general public will have the understanding of what is required of them by the law and will abide by them (Raji *et al*. 2007). This can be achieved through the formulation of sanitary committees at the local, state and national legislatures who would sponsor and support all sanitation bills. There is also need for enforcing the existing legislations such as the harmful waste act of 1988, the national environmental standards

and regulations enforcement agency act of 2007, the environmental impact assessment act of 1992 as well as the national environmental sanitation and waste control regulations of 2007 among others (Anijiofor *et al*., 2013). Nigerian laws should also enforce areas such as monitoring and supervision of agencies regulating environmental sanitation and solid waste management, waste recycling and landfill development outside human settlement. The absence of these landfills leads to indiscriminate disposal of waste in Nigeria as seen in Figures 1 and 2. Public education on the principles and effect of waste minimization and recycling is also a critical part of the waste management process. The Nigerian public should be enlightened on the risk of allowing children to scavenge and defecate on refuse dumping sites and the disposal of dead animals on these sites. Waste scavengers and waste management workers should also be encouraged to use protective wears when working to protect themselves against direct injuries from used sharp objects. The public should also be educated on the consequences of indiscriminate defecation and waste disposal within human settlements. Indiscriminate defecation can also be controlled through the provision of toilet facilities at strategic areas for the Nigerian populace especially those living without toilets. All this can be achieved through the use of schools, environmental extension workers and the media (Karija *et al*., 2013).

Another major challenge associated with poor waste management in Nigeria is the poor funding of agencies coordinating sanitation. For instance, the average fund allocations for sewerage, drainage and refuse services by all the states in Nigeria dropped from 163 million USD between 1981 and 1985 to 17.4 million USD between 1990 and 1992 while local government allocations during the same period dropped from 45 million USD to 5 million USD. The resultant effect of this drastic drop in fund allocations will be of course poor waste management (Raji *et al*., 2007). And so, ensuring a healthy environment in Nigeria requires proper funding of Environmental agencies to be able to carry out this responsibility effectively. Funding may be done by government at the local, state and national levels as well as non-governmental organizations. Private sector involvement in environmental sanitation and municipal solid waste management was encouraged. This can be achieved through the complete utilization of fund allocations for sanitation and MSW management without diversion by government representatives. With this, there will be willingness to donate towards this noble purpose knowing that their donations will be used judiciously. Other ways to encourage their involvement may be through reasonable taxation and favorable economic policies that will enable businesses to strive positively. Attitudinal change in the area of self-control towards misappropriating public funds allocated for sanitation and waste management will also go a long way in helping in the management of municipal solid waste, thus creating a health environment that will impact positively on public health (Raji *et al*., 2007).

3. CONCLUSION

Health hazards associated with poor municipal solid waste management are real and pose serious public health threads ranging from the transmission of endemic zoonoses to the emergence and re-emergence of new zoonoses arising either from direct or indirect effects of poor waste management. These health hazards can be reduced to minimal levels through public education, enactment and re-enforcement of policies and legislations, improvement of funding, monitoring and supervision, recycling waste and development of landfills among others. It is pertinent that all human settlements regardless of their sizes and locations to develop landfill for proper waste management which will preserve the environment and promote the wellbeing of the Nigerian public.

REFERENCES

Akinyemi, K. O., Oshundare, Y. O., Oyeyinka, O. G., & Coker, A. O. (2012). A retrospective study of community-acquired Salmonella infections in patients attending public hospitals in Lagos, Nigeria. *The Journal of Infection in Developing Countries*, *6*(05), 387-395.

Anijiofor, S. C., Jimoh, O. D., &Ogwueleka, T. C. (2013). Cost Optimization Model for Effective Solid Waste Management in Minna, Niger State, Nigeria. *Nigerian Journal of Hydrological Sciences*, *2*, 16-26.

Giusti, L. (2009). A review of waste management practices and their impact on human health. *Waste management*, *29*(8), 2227-2239.

Hoornweg, D., andBhada-Tata, P. (2012). What a waste: a global review of solid waste management.

Jones, K. E., Patel, N. G., Levy, M. A., Storeygard, A., Balk, D., Gittleman, J. L., &Daszak, P. (2008). Global trends in emerging infectious diseases. *Nature*, *451*(7181), 990-993.

Karija, M. K., Shihua, Q. I., andLukaw, Y. S. (2013). The impact of poor municipal solid waste management practices and sanitation status on water quality and public health in cities of the least developed countries: The case of Juba, South Sudan. *International Journal of Applied Science and Technology*, *3*(4), 87-99.

Karshima, S. N., &Bobbo, A. A. (2016). Isolation and PCR characterisation of thermophilic Campylobacter species in dogs presented to selected veterinary clinics in Jos, Nigeria.

National Population Commission of Nigeria. Population figures (2006) Retrieved from http://www.national populationcommission.ng

Ogbonna, D. N., Chindah, A., andUbani, N. (2012). Waste management options for health care wastes in Nigeria: A case study of Port Harcourt hospitals. *Journal of public health and Epidemiology*, *4*(6), 156-169.

Ogu, V. I. (2000).Private sector participation and municipal waste management in Benin City, Nigeria. *Environment and Urbanization*, *12*(2), 103-117.

Oresanya, O. (2011). Sustainable solid waste management in developing countries-Lagos as a case study (Lagos emerging mega city).presented at the meeting of the The 1st Oyo State environment summit.

Raji, M., Adekeye, J., Kwaga, J., Bale, J., &Henton, M. (2007). Serovars and biochemical characterization of Escherichia coli isolated from colibacillosis cases and dead-in-shell embryos in poultry in Zaria-Nigeria. *Veterinarskiarhiv*, *77*(6), 495.

Yoshizawa, K., Rimm, E. B., Morris, J. S., Spate, V. L., Hsieh, C. C., Spiegelman, D., ... & Willett, W. C. (2002). Mercury and the risk of coronary heart disease in men. *New England Journal of Medicine*, *347*(22), 1755-1760.

Zurbrugg, C. (2002). Urban solid waste management in low-income countries of Asia how to cope with the garbage crisis. *Presented for: Scientific Committee on Problems of the Environment (SCOPE) Urban Solid Waste Management Review Session, Durban, South Africa*, *6*, 1-13.

PAPER 72 - ENERGY-EFFICIENT TECHNIQUES IN MASSIVE MIMO: A REVIEW

A. O. Adebayo[1], R. Salihu[2], A. Musa[1,3] O. Ogunbiyi[1]

[1]Department of Electrical and Computer Engineering, Kwara State University, Malete, Nigeria.
[2]Department of Civil and Environmental Engineering, Kwara State University, Malete, Nigeria
[3]Institute for Intelligent Systems, University of Johannesburg, South Africa
*E-mail: abdullateef.adebayo19@kwasu.edu.ng

ABSTRACT
Massive multiple-input multiple-output (MIMO) technology promises significant capacity and spectral efficiency gains for fifth generation (5G) and beyond 5G (B5G) networks. However, the deployment of large-scale antenna arrays poses challenges in terms of energy consumption and operational costs. This paper provides a comprehensive review and analysis of various energy efficiency techniques proposed for massive MIMO systems. We classify these techniques into four categories: hardware-based, signal processing-based, resource allocation-based, and network-level techniques. For each technique, we discuss the principles of operation, advantages, limitations, and existing research findings. We also present a comparative analysis highlighting the trade-offs between energy efficiency, performance, complexity, and cost. Furthermore, we identify open challenges and potential future research directions in the field of energy-efficient massive MIMO. The insights provided in this paper can assist researchers, engineers, and practitioners in designing and deploying energy-efficient massive MIMO systems for next-generation wireless networks.

KEYWORDS: Massive MIMO, energy efficiency, hardware optimization, signal processing, resource allocation, network-level techniques.

1. INTRODUCTION

This Massive MIMO technology, a key enabler for fifth-generation (5G) and beyond 5G (B5G) networks, promises substantial capacity and spectral efficiency gains by employing a large number of antennas at the base station (BS) to serve multiple users simultaneously (Bhatti, 2019; Chataut & Akl, 2020). However, the deployment of such a large-scale antenna array system poses significant challenges in terms of energy consumption and operational costs (Senger & Malik, 2022).

The energy consumption of massive MIMO systems is substantially higher compared to traditional MIMO systems due to the increased number of radio frequency (RF) chains, digital signal processing (DSP) units, and power amplifiers required to support the numerous antenna elements (Ou et al., 2022). Consequently, energy efficiency has emerged as a critical design objective in massive MIMO systems, not only from an economic perspective but also from an environmental standpoint, as the information and communication technology (ICT) sector accounts for a significant portion of global energy consumption and carbon emissions (L. Liu et al., 2020).

To address these challenges, researchers and engineers have proposed numerous energy efficiency techniques spanning hardware design, signal processing algorithms, resource allocation strategies, and network-level optimization. This paper provides a comprehensive review and analysis of these techniques, along with a comparative analysis of their relative merits, drawbacks, and trade-offs.

2. ENERGY CONSUMPTION IN MASSIVE MIMO SYSTEMS

Massive MIMO systems, characterized by the deployment of many antennas at the base station, offer significant performance improvements in terms of capacity, spectral efficiency, and link reliability. However, these benefits come at the cost of increased energy consumption, which is a critical concern from both economic and environmental perspectives.

The major sources of energy consumption in massive MIMO systems can be categorized as follows:

A. **RF Chains:** Each antenna element in a massive MIMO system requires a dedicated RF chain, consisting of components such as power amplifiers, low-noise amplifiers, mixers, and analog-to-digital converters (ADCs). These RF components are responsible for a significant portion of the overall energy consumption, particularly the

power amplifiers, which are known to be highly power-hungry components (Murakami et al., 2022). As the number of antenna elements increases in massive MIMO systems, the energy consumption associated with the RF chains scales up linearly.

B. **Digital Signal Processing (DSP):** The large-scale antenna arrays in massive MIMO systems necessitate advanced signal processing techniques, including channel estimation, precoding, and data detection algorithms. These computationally intensive operations are typically performed by dedicated DSP units, such as field-programmable gate arrays (FPGAs) or application-specific integrated circuits (ASICs). The energy consumption of these DSP units can be significant, particularly for complex algorithms and high data rates (Morsali et al., 2020).

C. **Cooling Systems:** The increased number of RF chains and DSP units in massive MIMO systems generate substantial heat, which necessitates the deployment of efficient cooling systems. These cooling systems, including fans, air conditioning units, and liquid cooling solutions, consume additional energy to maintain the desired operating temperatures and prevent overheating (Sermeno et al., 2014).

D. **Baseband Processing and Control:** The baseband processing unit, responsible for tasks such as data encoding/decoding, modulation/demodulation, and control signaling, contributes to the overall energy consumption in massive MIMO systems. As the number of users and data streams increases, the computational load on the baseband processor also increases, leading to higher energy consumption (Li et al., 2019).

E. **Backhaul and Fronthaul:** In massive MIMO systems, the large amount of data generated by the numerous antenna elements needs to be transported between the baseband unit and the remote radio heads (RRHs) over fronthaul links. Similarly, the aggregated user data must be transferred to the core network over backhaul links (Gonzalez-Diaz et al., 2021). The energy consumption associated with these high-capacity front-haul and back-haul links can be significant, especially in distributed or cloud-based massive MIMO architectures.

The need for energy-efficient techniques in massive MIMO systems arises from several factors, including operational costs, environmental impact, battery life and mobility, network densification, and the requirements of emerging applications.

3. ENERGY EFFICIENCY TECHNIQUES FOR MASSIVE MIMO

The energy efficiency techniques for massive MIMO systems can be classified into four main categories: hardware-based, signal processing-based, resource allocation-based, and network-level techniques. Table I provides a summary of these techniques, their key principles, advantages, and limitations.

Table I: Summary of Energy Efficiency Techniques for Massive MIMO

Category	Technique	Key Principles	Advantages	Limitations	REF.
Hardware-based Techniques					
	Antenna Selection	Activate a subset of antennas based on channel conditions	Reduced power consumption, lower hardware complexity	Performance degradation, potential for increased interference	(Cai et al., 2019; Du et al., 2022; Yang et al., 2019, 2019)
	Power Amplifier Efficiency	Improve power amplifier efficiency using techniques like Doherty PAs, envelope tracking, digital predistortion	Significant energy savings potential	Increased hardware complexity and cost	(Du et al., 2022; Ou et al., 2022)
	Low-Resolution ADCs	Employ low-resolution ADCs to reduce power consumption	Reduced power consumption and hardware complexity	Performance degradation, increased computational complexity	(Musa & Adebayo, 2023; Y. Sun and Y. Zhang, 2020; Z. Wang, Y. Sun, and Y. Zhang, 2020)
	Hardware Sharing/Multiplexing	Share hardware resources like RF chains and baseband processing units	Reduced hardware complexity and cost, lower power consumption	Potential performance degradation, increased complexity in signal processing and synchronization	(Belaoura et al., 2020; Händel & Rönnow, 2020; Mokhtari et al., 2019; J. Zhang et al., 2017)
Signal Processing-based Techniques					
	Low-Complexity Precoding	Employ approximation techniques to reduce computational complexity of precoding	Reduced computational complexity and energy consumption	Potential performance trade-offs compared to optimal precoding	(Al-Kamali & D'Amours, 2022; Gaspar et al., 2023; Ku et al., 2021; Ribeiro et al., 2020)
	Energy-Efficient Channel Estimation	Leverage channel sparsity and spatial correlation to reduce pilot overhead and estimation complexity	Reduced computational complexity and energy consumption	Potential performance degradation, increased algorithm complexity	(Gao et al., 2019; Mo et al., 2018; Mutlu & Kabalci, 2023; Nguyen et al., 2021)

Resource Allocation-based Techniques					
	Sleep Mode and Discontinuous Transmission	Deactivate or turn off hardware components during periods of low traffic or inactivity	Significant energy savings during low traffic periods	Potential performance degradation during high traffic, increased complexity in resource management	(García-Morales et al., 2020; D. Liu et al., 2022; Riera-Palou et al., 2023)
	Energy-Aware Resource Allocation	Optimize time, frequency, and spatial resource allocation to achieve energy efficiency	Improved energy efficiency while maintaining performance	Increased complexity in resource allocation algorithms	(Bartsiokas et al., 2022; Kenney et al., 2022; Su et al., 2022)
Network-level Techniques					
	Coordinated Multi-Point (CoMP) Transmission	Leverage cooperation among multiple base stations to mitigate interference and reduce transmit power	Improved energy efficiency through interference mitigation and load balancing	Increased complexity in coordination and signaling, potential for increased backhaul/fronthaul requirements	(Naser et al., 2022; Shahsavari et al., 2021; Sheu & Huang, 2021)
	Cloud/Centralized Radio Access Network (C-RAN)	Centralize baseband processing to enable resource sharing and cooperative signal processing	Improved energy efficiency through resource sharing and load balancing	High bandwidth requirements for fronthaul links, increased complexity in centralized processing and control	(He et al., 2016; Norouzi & Champagne, 2021; D. Zhang et al., 2016)

Building upon the insights from Table I, Table II presents a comparative analysis of the energy efficiency techniques. This table examines the trade-offs between performance, energy efficiency, hardware complexity, cost, scalability, flexibility, combination potential, and application-specific considerations. This comparative analysis enables researchers and practitioners to better understand the strengths, weaknesses, and suitability of each technique for different massive MIMO deployment scenarios and requirements.

Table II: Comparative Analysis of Energy Efficiency Techniques for Massive MIMO

Techniques	Performance	Energy Efficiency	Hardware Complexity	Cost	Scalability	Flexibility	Combination Potential	Application Specific Considerations
Antenna Selection	✓	✓✓✓	✓	✓✓	✓✓✓	✓✓	Combines well with advanced signal processing techniques	Well-suited for dynamic user environments; less effective in static conditions
Power Amplifier Efficiency	✓✓	✓✓✓	✓✓✓	✓✓✓	✓	✓	Effective with digital predistortion for enhanced performance	High cost but essential for high-demand areas
Low-Resolution ADCs	✓	✓✓✓	✓✓	✓✓	✓✓✓	✓✓✓	Often paired with error correction techniques to manage increased noise	Optimal for cost-sensitive deployments; compromises signal quality
Hardware Sharing and Multiplexing	✓	✓✓✓	✓✓	✓✓✓	✓✓✓	✓✓✓	Synergizes with CoMP and C-RAN to optimize resource usage	Best for densely populated networks with variable demand
Low-Complexity Precoding	✓✓	✓✓	✓	✓✓	✓	✓	Can be integrated with channel estimation techniques to reduce overall computational demands	Suitable for real-time processing limitations
Energy-Efficient Channel Estimation	✓✓	✓✓✓	✓✓	✓✓	✓✓	✓✓	Works well with low-resolution ADCs to enhance system efficiency while managing noise	Effective in predictable environments with stable channel characteristics
Sleep Mode and Discontinuous Transmission	✓✓	✓✓✓	✓	✓✓✓	✓✓	✓✓	Complementary to dynamic resource allocation strategies for optimal energy management	Critical for IoT applications to extend device battery life
Energy-Aware Resource Allocation	✓✓	✓✓✓	✓✓	✓✓	✓✓✓	✓✓✓	Integrates seamlessly with sleep modes and discontinuous transmission to maximize efficiency	Varies with user density and traffic patterns; complex algorithms required
CoMP Transmission	✓✓✓	✓✓✓	✓✓✓	✓✓	✓✓	✓	Enhances potential when used with hardware sharing and multiplexing strategies	Best for urban areas with high user density and network traffic
C-RAN	✓✓	✓✓✓	✓✓✓	✓✓✓	✓✓	✓✓✓	Beneficial in combination with CoMP to leverage centralized resources and processing	Suited for centralized network architectures; high fronthaul bandwidth requirements

Legend

- ✓: Basic support or low impact
- ✓✓: Moderate support or medium impact
- ✓✓✓: High support or significant impact

4. OPEN CHALLENGES AND FUTURE RESEARCH DIRECTIONS

Results Despite the significant advancements in energy-efficient massive MIMO techniques, there are several open challenges and promising future research directions to explore:

A. **Emerging Technologies Integration**: Researchers should focus on incorporating energy efficiency considerations into emerging communication technologies, such as millimeter-wave, terahertz communications, integrated access and backhaul (IAB), and joint communication and sensing (JCAS). Developing energy-efficient solutions that leverage the unique capabilities of these cutting-edge systems will be crucial for realizing their full potential.

B. **AI/ML-driven Optimization:** Exploring the application of artificial intelligence (AI) and machine learning (ML) techniques holds great promise for further improving energy efficiency in massive MIMO systems. AI/ML-based approaches can enable adaptive resource allocation, intelligent signal processing, and autonomous optimization, leading to significant gains in energy savings without compromising performance.

C. **Renewable Energy Integration:** Integrating renewable energy sources, like solar or wind power, into massive MIMO base stations can provide a more sustainable and environmentally friendly solution. Designing efficient energy management systems that seamlessly combine renewable energy generation, storage, and consumption will be a key focus area to enhance the overall energy efficiency of massive MIMO deployments.

D. **Green IoT**: Addressing the specific energy efficiency requirements of Internet of Things (IoT) applications within the massive MIMO framework is crucial. Developing energy-efficient massive MIMO solutions tailored for IoT, considering factors like low power consumption, extended battery life, and scalability, will be essential for enabling the widespread adoption of energy-efficient IoT systems.

E. **Experimental Validation and Testbeds:** Conducting extensive experimental validation and field trials is necessary to bridge the gap between theoretical studies and practical implementation. Establishing robust testbeds and experimentation platforms will allow researchers and engineers to evaluate the real-world performance, identify practical challenges, and refine the proposed energy efficiency techniques for massive MIMO systems.

F. **Cross-layer Optimization:** Exploring holistic, cross-layer optimization approaches that consider the interplay between hardware, signal processing, resource allocation, and network-level techniques can lead to further improvements in energy efficiency. Developing comprehensive frameworks that seamlessly integrate these various aspects can unlock synergistic benefits and unlock the full potential of energy-efficient massive MIMO systems.

G. **Standardization and Industry Collaboration**: Fostering collaboration between academia, industry, and standardization bodies will be crucial for driving the widespread adoption of energy-efficient massive MIMO solutions. Actively contributing to the development of industry standards and promoting the integration of energy efficiency as a key design objective can accelerate the deployment of energy-efficient massive MIMO systems in next-generation wireless networks.

By addressing these open challenges and exploring these future research directions, the research community can continue to make significant strides in enhancing the energy efficiency of massive MIMO technology, paving the way for more sustainable and eco-friendly wireless networks.

5. CONCLUSION

This paper has provided a review and analysis of energy efficiency techniques for massive MIMO systems, categorizing them into hardware-based, signal processing-based, resource allocation-based, and network-level approaches. The comparative analysis highlights the trade-offs between energy efficiency, performance, complexity, and cost. While significant progress has been made, open challenges remain, including integrating emerging technologies, leveraging AI/ML, incorporating renewable energy, addressing IoT needs, and conducting experimental validation. By addressing these areas, the research community can drive the development of truly energy-efficient and high-performance massive MIMO systems for sustainable 5G and beyond wireless networks.

REFERENCES

Al-Kamali, F. S., & D'Amours, C. (2022). Low-Complexity Hybrid Precoding for Subarray Architecture mmWave MIMO Systems. *IEEE Access*, *10*. https://doi.org/10.1109/access.2022.3190511

Bartsiokas, I., Gkonis, P. K., Kaklamani, D. I., & Venieris, I. S. (2022). ML-Based Radio Resource Management in 5G and Beyond Networks: A Survey. *IEEE Access*, *10*. https://doi.org/10.1109/access.2022.3196657

Belaoura, W., Shakir, M. Z., & Qaraqe, K. A. (2020). Impact of Hardware Impairments on the Performance of Millimeter-Wave Massive MU-MIMO Systems with Distributed Antennas. *2020 IEEE Eighth International Conference on Communications and Networking (ComNet)*. https://doi.org/10.1109/comnet47917.2020.9306107

Bhatti, S. (2019). Massive MIMO, mm Wave and 5G Technology Insights and Challenges. *3C Tecnología_Glosas De Innovación Aplicadas a La Pyme*. https://doi.org/10.17993/3ctecno.2019.specialissue2.498-517

Cai, J., Zhong, R., & Li, Y. (2019). Antenna selection for multiple-input multiple-output systems based on deep convolutional neural networks. *PLOS ONE*, *14*(5), e0215672. https://doi.org/10.1371/journal.pone.0215672

Chataut, R., & Akl, R. (2020). Massive MIMO Systems for 5G and beyond Networks—Overview, Recent Trends, Challenges, and Future Research Direction. *Sensors*, *20*(10). https://doi.org/10.3390/s20102753

Du, L., Tan, Y., Li, Y., & Chen, Y. (2022). On the Energy Efficiency of Multicell Massive MIMO with Antenna Selection and Power Allocation. *Wireless Communications and Mobile Computing*, *2022*, 1–11. https://doi.org/10.1155/2022/7224731

Gao, S., Dong, P., Pan, Z., & Li, G. Y. (2019). *Deep Learning based Channel Estimation for Massive MIMO with Mixed-Resolution ADCs* (arXiv:1908.06245). arXiv. http://arxiv.org/abs/1908.06245

García-Morales, J., Femenias, G., & Riera-Palou, F. (2020). Energy-Efficient Access-Point Sleep-Mode Techniques for Cell-Free mmWave Massive MIMO Networks With Non-Uniform Spatial Traffic Density. *IEEE Access*, *8*. https://doi.org/10.1109/access.2020.3012199

Gaspar, D., Mendes, L. L., & Pimenta, T. C. (2023). A review on principles, performance and complexity of linear estimation and detection techniques for MIMO systems. *Frontiers in Communications and Networks*, *4*. https://doi.org/10.3389/frcmn.2023.968370

Gonzalez-Diaz, S., García-Saavedra, A., Oliva, A. de la, Costa-Pérez, X., Gazda, R., Mourad, A., Deiß, T., Mangues-Bafalluy, J., Iovanna, P., Stracca, S., & Leithead, P. (2021). Integrating Fronthaul and Backhaul Networks: Transport Challenges and Feasibility Results. *IEEE Transactions on Mobile Computing*, *20*(2). https://doi.org/10.1109/tmc.2019.2948641

Händel, P., & Rönnow, D. (2020). MIMO and Massive MIMO Transmitter Crosstalk. *IEEE Transactions on Wireless Communications*, *19*(3). https://doi.org/10.1109/twc.2019.2959534

He, A., Wang, L., Chen, Y., Wong, K.-K., & Elkashlan, M. (2016). Throughput and Energy Efficiency for S-FFR in Massive MIMO Enabled Heterogeneous C-RAN. *2016 IEEE Global Communications Conference (GLOBECOM)*. https://doi.org/10.1109/glocom.2016.7842326

Kenney, B., Majid, A. J., Moradi, H., & Farhang-Boroujeny, B. (2022). *Single Carrier Modulation Resource Allocation for Massive MIMO with Virtual Antennas*. Scite.Ai. https://doi.org/10.36227/techrxiv.19325666.v2

Ku, H.-W., Fang, W.-H., Tso, H.-L., Tsai, P.-Y., & Huang, Y.-H. (2021). Low-Complexity Wideband Hybrid Precoding for mmWave MIMO-OFDM. *2021 IEEE International Symposium on Circuits and Systems (ISCAS)*. https://doi.org/10.1109/iscas51556.2021.9401397

Li, K., McNaney, J., Tarver, C., Castañeda, O., Jeon, C., Cavallaro, J. R., & Studer, C. (2019). Design Trade-offs for Decentralized Baseband Processing in Massive MU-MIMO Systems. *2019 53rd Asilomar Conference on Signals, Systems, and Computers*. https://doi.org/10.1109/ieeeconf44664.2019.9048727

Liu, D., Domenico, A. D., Piovesan, N., Geng, X., Bao, H., Song, Q., & Debbah, M. (2022). A Survey on 5G Radio Access Network Energy Efficiency: Massive MIMO, Lean Carrier Design, Sleep Modes, and Machine Learning. *IEEE Communications Surveys &Amp; Tutorials*, *24*(1). https://doi.org/10.1109/comst.2022.3142532

Liu, L., Wang, Z., & Cui, S. (2020). Intelligent Reflecting Surface Assisted Massive MIMO Communications. *2020 IEEE 21st International Workshop on Signal Processing Advances in Wireless Communications (SPAWC)*. https://doi.org/10.1109/spawc48557.2020.9154291

Mo, J., Schniter, P., & Heath, R. W. (2018). Channel Estimation in Broadband Millimeter Wave MIMO Systems With Few-Bit ADCs. *IEEE Transactions on Signal Processing*, *66*(5), 1141–1154. https://doi.org/10.1109/TSP.2017.2781644

Mokhtari, Z., Sabbaghian, M., & Dinis, R. (2019). A Survey on Massive MIMO Systems in Presence of Channel and Hardware Impairments. *Sensors*, *19*(1). https://doi.org/10.3390/s19010164

Morsali, A., Haghighat, A., & Champagne, B. (2020). Generalized Framework for Hybrid Analog/Digital Signal Processing in Massive and Ultra-Massive-MIMO Systems. *IEEE Access*, *8*. https://doi.org/10.1109/access.2020.2998064

Murakami, T., Taniguchi, R., Ogawa, T., & Takatori, Y. (2022). Performance Evaluation of Uplink Multiuser MIMO-OFDM System With Single RF Chain Receiver. *IEEE Access*, *10*. https://doi.org/10.1109/access.2022.3216008

Musa, A., & Adebayo, A. O. (2023). Energy Efficiency Optimization in Massive MIMO Systems with Low-Resolution ADCs. *2023 2nd International Conference on Multidisciplinary Engineering and Applied Science (ICMEAS)*, 1–6. https://doi.org/10.1109/ICMEAS58693.2023.10379348

Mutlu, U., & Kabalci, Y. (2023). Deep Learning Aided Channel Estimation in Intelligent Reflecting Surfaces. *2023 5th Global Power, Energy and Communication Conference (GPECOM)*, 513–518. https://doi.org/10.1109/GPECOM58364.2023.10175750

Naser, S., Bariah, L., Jaafar, W., Muhaidat, S., Al-Qutayri, M., Uysal, M., & Sofotasios, P. C. (2022). Coordinated Beamforming Design for Multi-User Multi-Cell MIMO VLC Networks. *IEEE Photonics Journal*, *14*(3). https://doi.org/10.1109/jphot.2022.3169233

Nguyen, L. V., Swindlehurst, A. L., & Nguyen, D. H. N. (2021). SVM-based Channel Estimation and Data Detection for One-Bit Massive MIMO Systems. *IEEE Transactions on Signal Processing*, *69*, 2086–2099. https://doi.org/10.1109/TSP.2021.3068629

Norouzi, S., & Champagne, B. (2021). Energy-Efficient User Clustering and Downlink Beamforming for MIMO-SCMA in C-RAN. *IEEE Access*, *9*. https://doi.org/10.1109/access.2021.3104259

Ou, Q., Wang, Y., Bao, L., Wang, Y., She, R., Zhang, N., & Ma, W. (2022). Power Allocation in Smart Grid Aided Cell Free Massive MIMO Systems for URLLC Applications. *Journal of Physics: Conference Series*, *2310*(1). https://doi.org/10.1088/1742-6596/2310/1/012069

Ribeiro, L. N., Schwarz, Š., Almeida, A. L. F. de, & Haardt, M. (2020). *Low-Complexity Massive MIMO Tensor Precoding*. Scite.Ai. https://doi.org/10.48550/arxiv.2009.09729

Riera-Palou, F., Femenias, G., Lopez-Perez, D., Piovesan, N., & De Domenico, A. (2023). Sleep Mode Strategies for Energy Efficient Cell-Free Massive MIMO in 5G Deployments. *2023 IEEE International Conference on Communications Workshops (ICC Workshops)*. https://doi.org/10.1109/iccworkshops57953.2023.10283562

Senger, S., & Malik, P. K. (2022). A comprehensive survey of massive-based on antennas. *International Journal of RF and Microwave Computer-Aided Engineering*, *32*(12). https://doi.org/10.1002/mmce.23496

Sermeno, S., Bideaux, É., Brun, X., & Ameur, O. (2014). Heavy Duty Vehicle Cooling System Auxiliary Load Management Control: An Application of Linear Control Strategy (MIMO and SISO). *Volume 8A: Heat Transfer and Thermal Engineering*. https://doi.org/10.1115/imece2014-39534

Shahsavari, S., Nosrati, M., Hassanzadeh, P., Ashikhmin, A., Marzetta, T. L., & Erkip, E. (2021). *Multi-point Coordination in Massive MIMO Systems with Sectorized Antennas*. Scite.Ai. https://doi.org/10.48550/arxiv.2104.10805

Sheu, J.-S., & Huang, K.-M. (2021). Performance Comparison for Single-User and Multi-User Network MIMO Cellular Systems with Power Management. *Applied Sciences*, *11*(21). https://doi.org/10.3390/app112110298

Su, Y., Gao, H., & Zhang, S. (2022). Energy-efficient resource management for CCFD massive MIMO systems in 6G networks. *Journal of Systems Engineering and Electronics*, *33*(4). https://doi.org/10.23919/jsee.2022.000085

Y. Sun and Y. Zhang. (2020). Energy-efficient massive MIMO systems with low-resolution ADCs: A deep reinforcement learning approach. *IEEE Transactions on Wireless Communications*, *vol.19*(2), 726–740.

Yang, P., Zhu, J., Xiao, Y., & Chen, Z. (2019). Antenna selection for MIMO system based on pattern recognition. *Digital Communications and Networks*, *5*(1), 34–39. https://doi.org/10.1016/j.dcan.2018.10.001

Z. Wang, Y. Sun, and Y. Zhang. (2020). Deep learning-based pilot design for energy-efficient massive MIMO systems with low-resolution ADCs. *IEEE Transactions on Wireless Communications, vol.19*(no.6), 4185–4200.

Zhang, D., Tariq, M., Mumtaz, S., Rodríguez, J., & Sato, T. (2016). Integrating energy efficiency analysis of massive MIMO-based C-RAN. *EURASIP Journal on Wireless Communications and Networking*, *2016*(1). https://doi.org/10.1186/s13638-016-0778-y

Zhang, J., Wei, Y., Björnson, E., Han, Y., & Li, X. (2017). Spectral and energy efficiency of cell-free massive MIMO systems with hardware impairments. *2017 9th International Conference on Wireless Communications and Signal Processing (WCSP)*. https://doi.org/10.1109/wcsp.2017.8171057

PAPER 73-DEVELOPMENT OF A SMART BALLOT BOX SYSTEM FOR ENHANCED ELECTION SECURITY IN NIGERIA

A. O. Adedokun[1] S. A. Olayanju[2]

[1]Department of Computer Engineering, Federal University of Technology PMB 704, Akure, Ondo State, Nigeria
[2]Department of Electrical Electronics Engineering, University of Ilorin, Kwara State

ABSTRACT

Electing competent leaders through a trusted and transparent electoral process is essential for the critical development of any nation. However, politicians most especially in Nigeria employed various tactics such as vote buying, bribing electoral officials, manipulating votes, and ballot box snatching to undermine the integrity of elections. All these tactics most especially ballot box snatching undermine democracy, denying citizens their voting rights and eroding trust in the electoral system. This hinders national growth, perpetuates instability, reduces political accountability, and stifles the voice of the people. This research proposes the development of a smart ballot box system equipped with a location tracking feature, designed to restrict access to authorized electoral officers. Only authorized personnel can open the ballot box using fingerprint recognition after the voting process is completed. The system sends a notification to the electoral authority for appropriate action once the ballot box is accessed. In the event of ballot box snatching, the integrated device within the ballot system will transmit its location for tracking purposes, enabling the relevant authorities to take immediate action. The system comprises a microcontroller, a fingerprint sensor for authentication, a GPS sensor for real-time location tracking, and a GSM module for instant alerting and monitoring.

KEYWORDS: Ballot Box, Fingerprint, GPS, Tracking, Electoral Process

1. INTRODUCTION

The current voting system in Nigeria faces significant challenges, including ballot box snatching, election rigging, and multiple voting, which undermine the transparency of our elections. Voting serves as a formal expression of choice between multiple candidates or courses of action, typically through hand-counted paper ballots or a show of hands (Yasha, 2016). In democratic societies, voting is crucial for collecting and reflecting the opinions of the people. Traditionally, voting takes place at centralized locations known as polling stations, where voters cast their votes under the supervision of authorized officials. After the voting process concludes, votes are manually counted, and the results are declared. Like other democratic processes, voting demands transparency, participation, and accountability (Mohamed, 2016). To enhance the efficiency and accuracy of voting, computerized voting systems like Lever Voting Machines (LVM), Punched Cards for Voting (PCV), Optical Mark-Sense Scanners, and Direct Recording Electronic (DRE) systems have been developed (Mohamed, 2016). However, many voting systems in institutional bodies have been plagued by irregularities, compromising the integrity of the democratic process. There is an urgent need to improve the voting system by developing a robust voting system capable of minimizing these irregularities and ensuring an effective electioneering process. In Nigeria, since the return to democratic rule in 1999, elections have been conducted manually, with voters using ballot papers and ballot boxes to cast their votes. This manual voting process has been associated with numerous challenges and often leads to post-election violence (Davis, 2007).

Various methods have been employed to safeguard the integrity of elections, ranging from traditional physical counting to innovative technologies like Internet voting. In Nigeria, the Independent National Electoral Commission (INEC) introduced the Permanent Voters Card (PVC) card reader to electronically authenticate voters, aiming to combat electoral malpractices. The card reader debuted during the presidential election on March 28, 2015. However, despite its introduction, the full potential of PVC functionality remains untapped due to the absence of a comprehensive central database for voter authentication, hindering efforts to mitigate malpractices. Failure to ensure the integrity of ballot boxes during elections opens the door to fraudulent activities such as ballot stuffing, undermining the credibility of the electoral process (Kuboye and Akinwomi, 2022). The introduction of the Biometric Voter Authentication System (BVAS) in the 2019 and 2023 electoral process in Nigeria has significantly reduced instances of rigging and vote manipulation. However, some politicians have resorted to tactics such as snatching ballot boxes to discredit the voting process. This research aims to enhance the ballot boxes security by providing tools to track and identify any hoodlums or corrupt electoral officers attempting to manipulate the election. By leveraging advanced technology and real-time monitoring capabilities, this initiative seeks to safeguard the integrity of the electoral process and ensure fair and

transparent elections.

2. Theoretical Analysis

In this research, the theoretical analysis of a fingerprint sensor involves understanding the underlying principles of biometric authentication, which relies on unique patterns in an individual's fingerprints. This analysis typically encompasses concepts from signal processing, pattern recognition, and biometrics to interpret and match fingerprint images accurately.

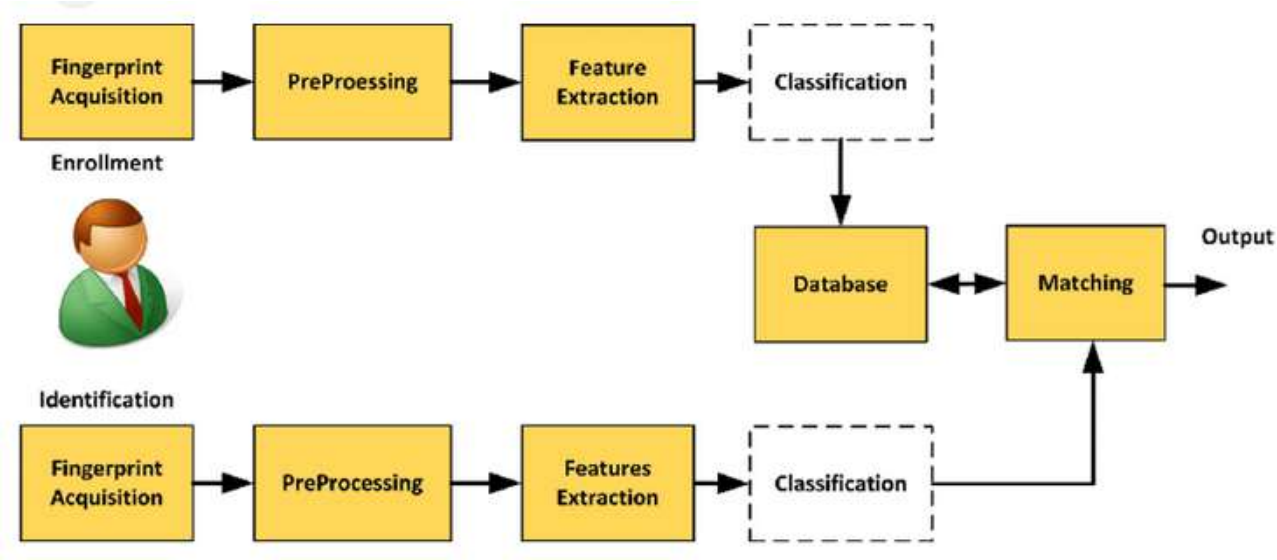

Figure 1: Fingerprint enrollment and detection flow diagram.

3. MATERIALS AND METHODS

Figure 2 shows the block diagram of the proposed system. The system's hardware consists of five primary components: Arduino Uno, power supply unit, Fingerprint sensor, Ultrasonic sensor, GSM and GPS module

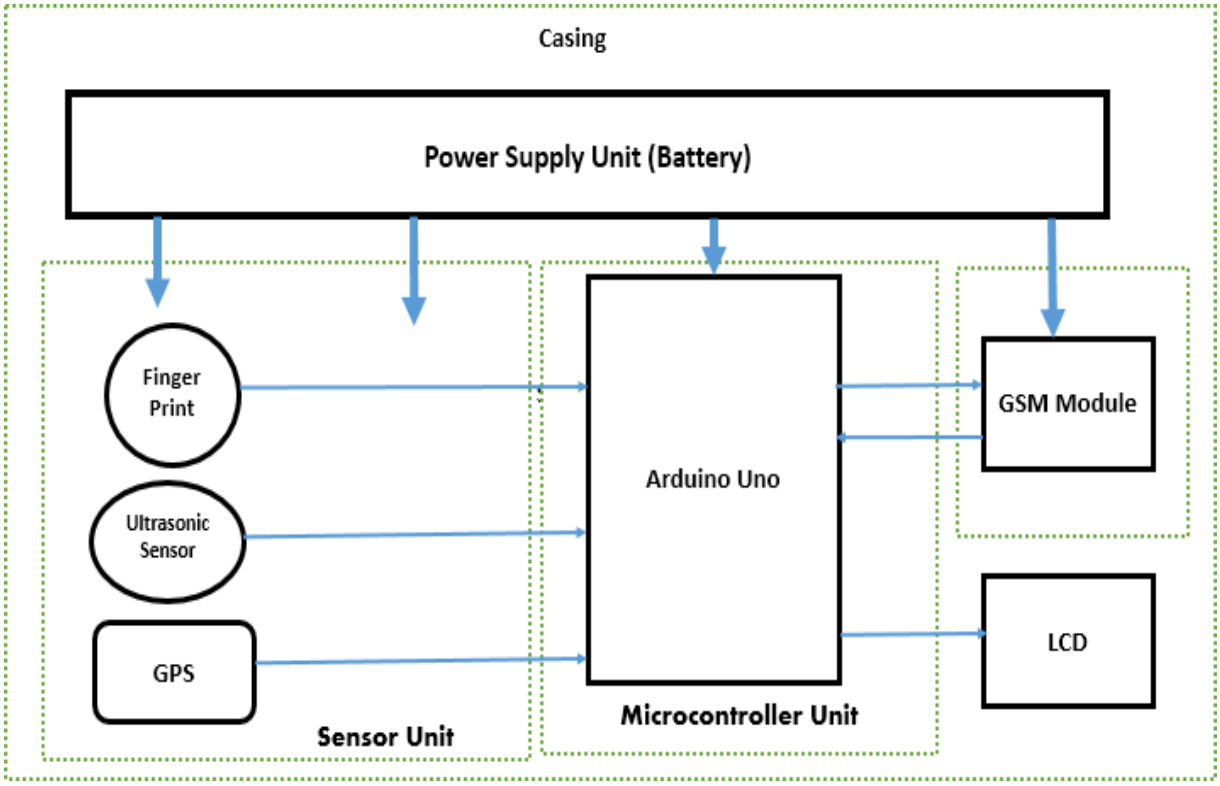

Figure 2: Block Diagram

3.1 The Hardware Components

The Arduino Uno serves as the central processing unit, coordinating the functions of the various components to ensure seamless operation. The fingerprint sensor provides secure authentication, allowing only authorized personnel to access the ballot box. The ultrasonic sensor enhances security by detecting any unauthorized attempts to tamper with the ballot box. Lastly, the GSM and GPS modules enable real-time communication and location tracking, facilitating immediate response to any irregularities or attempts at election manipulation. Together, these hardware components contribute to achieving the research aim of enhancing election security and transparency.

3.1.1 Arduino Uno

The Arduino Uno is a microcontroller board built around the ATmega328P microcontroller (datasheet). It features 14 digital input/output pins, of which 6 can function as PWM outputs, along with 6 analog inputs. Additionally, it is equipped with a 16 MHz quartz crystal, a USB connection, a power jack, an ICSP header, and a reset button. The board is self-contained, requiring only a USB connection to a computer or an AC-to-DC adapter or battery for power.

This user-friendly design allows for experimentation without the fear of irreparable mistakes; in the worst-case scenario, the microcontroller chip can be easily replaced at a minimal cost.

Figure 3: ATMEGA 328 Circuit Connection

The name "Uno," meaning "one" in Italian, was chosen to commemorate the release of Arduino Software (IDE) version 1.0. The Arduino Uno, along with the 1.0 version of the Arduino Software (IDE), served as the standard reference for the Arduino platform, which has since evolved with newer releases. As the inaugural model in a series of USB-based Arduino boards, the Uno has become the benchmark for the Arduino ecosystem (Flecter et al., 2012). The microcontroller includes three timers/counters that facilitate tasks such as generating accurate time delays, producing PWM signals, and counting events. Programming can be conducted using different development environments, with the user-friendly Arduino IDE being a popular choice. The ATMEGA328 features power-saving modes and low energy consumption, making it well-suited for applications that require battery power or energy efficiency.

3.1.2 Fingerprint Sensor Module

Fingerprint sensor modules, such as the one depicted in the accompanying figure, have simplified the integration of fingerprint recognition into this project. This facilitates effortless fingerprint collection, registration, comparison, and search processes. Equipped with FLASH memory, these modules can store fingerprints and are compatible with any microcontroller or system featuring TTL serial communication. Their versatility makes them suitable for a wide range of applications, including security systems, door locks, time attendance systems, and more (Yasha, 2016).

Figure 4: Fingerprint Sensor Module

3.1.3 GSM Module (SIM 800)

the SIM800 module operates on the AT command set, a standardized set of commands designed for managing and configuring modem-like devices. These commands facilitate functionalities such as transmitting text messages, initiating phone calls, and accessing the internet. By issuing specific AT commands to the module, users can encode and transmit data or messages over the GSM network to their intended recipients. Additionally, the module can be programmed to send messages to the appropriate authorities in case of irregularities or security breaches during the electoral process.

3.1.4 GPS Module

The GPS (Global Positioning System) module receives signals from satellites to accurately determine its location on Earth. It calculates its position by measuring the time it takes for signals from multiple satellites to reach the module, each containing information about the satellite's position and the precise time of signal transmission. By triangulating this data, the GPS module can ascertain its latitude, longitude, and altitude coordinates. In this research, the GPS module plays a pivotal role in pinpointing the exact location where the microcontroller-based smart device is installed. Should the device detect any irregularities or security breaches during the electoral process, such as unauthorized access or tampering, the GPS module captures and records the geographical coordinates of that specific location. This capability enables real-time tracking and

monitoring of the device's movement and ensures timely intervention by the relevant authorities to safeguard the integrity of the electoral process.

3.1.5 Ultrasonic Sensor

The ultrasonic sensor serves as a proximity detection tool, capable of measuring distance by emitting high-frequency sound waves and calculating the time taken for the waves to reflect back. This sensor plays a crucial role in detecting any unauthorized attempts to tamper with the ballot box or interfere with the electoral process. When triggered by suspicious activity, the ultrasonic sensor sends signals to the microcontroller, initiating immediate alerts and activating the GPS module for location tracking, facilitating swift response by the relevant electoral authorities. (Baballe et. al, 2023).

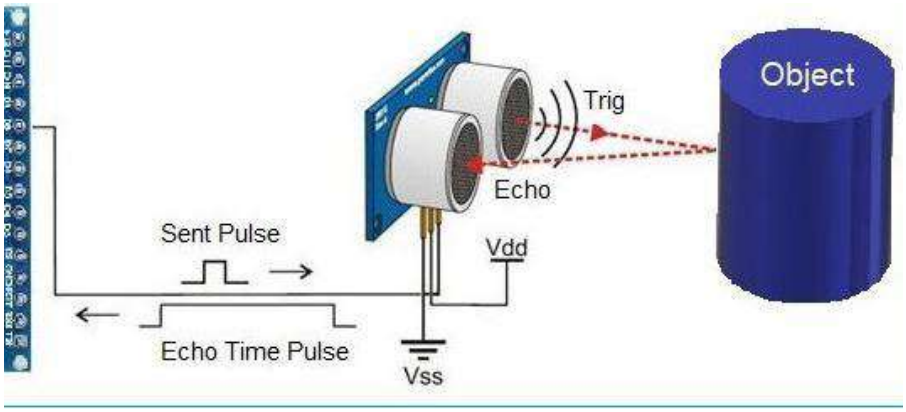

Figure 5: Ultrasonic Sensor (Baballe et. al, 2023).

3.2 Proposed Device Circuit Design and Simulation

As shown in Figure 6, In this research project, the Arduino board serves as the central processing unit, orchestrating the functionalities of the connected hardware components. The ultrasonic sensor detects proximity and measures distances by emitting and receiving high-frequency sound waves, providing a safeguard against unauthorized access or tampering with the ballot box. The fingerprint sensor enables secure authentication, ensuring that only authorized personnel can access the ballot box for legitimate purposes. The GPS module captures precise geographical coordinates, facilitating real-time tracking and monitoring of the device's location during the electoral process.

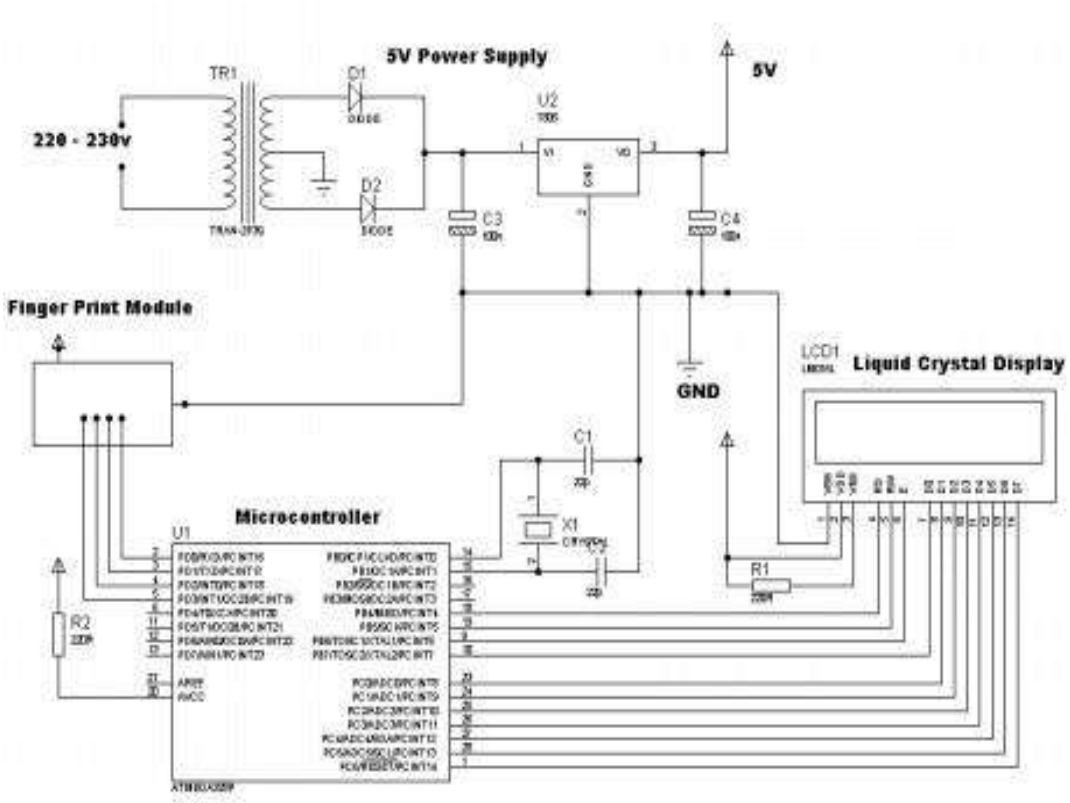

Figure 6: Proposed Device Circuit Diagram

This proposed device, the GSM module enables communication over the cellular network, allowing the device to send alerts and notifications to the relevant authorities in case of irregularities or security breaches. The hardware circuit is interconnected in a manner that allows seamless communication between these components. Specifically, the Arduino board interfaces with each hardware component, receiving input data from the ultrasonic sensor and fingerprint sensor, processing this information, and triggering appropriate actions, such as sending alerts via the GSM module or activating the GPS module for location tracking. This integrated approach ensures the security, transparency, and integrity of the electoral process.

4. RESULTS AND DISCUSSION

As shown in Figure 7, the complete design and construction of the device. The integration of Arduino board, ultrasonic sensor, fingerprint sensor, GPS, and GSM module in this research project has demonstrated promising capabilities in enhancing the security and transparency of the electoral process. Preliminary testing has confirmed the reliable functionality of each component, with the Arduino board effectively coordinating the interactions between the various hardware modules. The ultrasonic sensor successfully detected proximity and potential tampering attempts, while the fingerprint sensor provided secure authentication measures. Additionally, the GPS and GSM modules enabled real-time tracking and communication, ensuring timely alerts and responses to any irregularities during the electoral process. These findings suggest that the proposed system holds significant potential for improving election security and integrity.

Figure 7: Device Fabrication

5. CONCLUSION

The developed system integrating Arduino board, ultrasonic sensor, fingerprint sensor, GPS, and GSM module presents a promising solution for enhancing the security and transparency of electoral processes. The successful integration and testing of these components demonstrate the feasibility of utilizing advanced technology to mitigate election-related challenges such as tampering and unauthorized access. Moving forward, further refinement and implementation of the system in electoral contexts could significantly contribute to ensuring fair and credible elections.

REFERENCES

Baballe, M. A., Mukhtar, I. B., Ayagi, S. H., & Umar, F. M. (2023). Obstacle Avoidance Robot using an ultrasonic Sensor with Arduino Uno. Global Journal of Research in Engineering & Computer Sciences, 3(5), 14–25. https://doi.org/10.5281/zenodo.10015177

Davis, R.(2007). Developing a methodology for observing electronic voting, Program associate in the Carter Center's Democracy program.

Flescher, P., Benjamin, N., Astoyao, N., and Robert, A. (2012). Design and Development of GSM/GPS Based Vehicle Tracking and Alert System for Commercial Inter-City Buses. In IEEE 4th International Conference on Adaptive Science & Technology (ICAST).

Kuboye, B. M., & Akinwomi, A. E. (2022). Real-Time Ballot Box Monitoring System. *Communications on Applied Electronics (CAE)*, 7(38). ISSN: 2394-4714. New York, USA: Foundation of Computer Science (FCS).

Mohamed, S. (2016), Design of E-voting using fingerprint recognition system for secured voting. Middle East Journal of Scientific Research 24 (techniques and algorithms in emerging technologies):385-390, 2016.

Yasha Dorzeelepcha, Design of electronic voting machine using microcontroller. International Journal of Engineering Trends and Technology (IJETT)- 32(5).

PAPER 74 – Sizing Distributed Energy Resources for Robiyan Village in Ogun State, Nigeria

R.A. Zubair[1], P.O. Olabisi[2]

[1]Department of Electrical/Electronic and Telecommunication Engineering, Bells University of Technology, Ota, Ogun State, Nigeria.
[2]Department of Computer Engineering, Bells University of Technology, Ota, Ogun State, Nigeria.

ABSTRACT

The current grid infrastructure of today continues to struggle to meet growing energy demand, climate and environmental concerns, as well as the growing need for resiliency against natural disasters and cyber-attacks. Distributed Energy Resources (DER) provide a viable and sustainable energy source for transforming the present grid network into a smart future-ready grid. The deployment of a DER in a microgrid requires careful consideration of several factors. This study aims to size a DER system comprising of the grid, solar PV, battery energy storage system (BESS) as well and diesel generating set into a micro-grid. The study objectives include the modelling of an optimally sized DER into the smart grid to efficiently meet user energy demand and the analysis of the impact of the smart grid on the coverage area. Using the Homer Pro, optimal DER sizes are determined by considering key metrics such as energy cost, reliability, and environmental impact. The final system size comprises 1MVA of DG, 1.7MWp of solar and 6MWh of BESS, for the ideal grid, solar PV, battery and diesel generator scenario. The emission level was reduced by more than 45% when the renewable energy-based DER and storage were introduced.

KEYWORDS: DER, Smart Grid, Microgrid, Solar PV, BESS,

1. INTRODUCTION

The substantial surge in the demand for electricity, climate, and environmental concerns as well as the extensive implementation of variable renewables such as wind and solar power, subsequently imposes higher demands on power grids (Akkara & Selvakumar, 2023). The traditional electricity grid system faces several challenges, including higher integration of renewable energy sources, power losses during electricity transmission, and imperatives related to grid modernization (Hossain *et al*, 2018). The Nigerian Electricity Regulatory Commission's (NERC) quarterly for the third quarter of 2023 on the grid performance highlights key challenges with the Nigerian national grid. Average availability dropped to 4211 MW from 4387 MW in Q2, with hourly generation decreasing from 4059 MWh to 3924 MWh (NERC, 2023). Integrating DERs into the existing distribution network and turning it into a smart grid with multiple microgrids present capable of grid-connected and islanded operation would help solve the energy demand gap challenge from the bottom up, one location at a time. Smart grids are advanced electrical networks that leverage digital technologies, sensors, and software to optimize the synchronization efficiently and effectively between the supply and demand of electricity in real-time (IEA, 2023). Furthermore, these smart grids are designed to ensure that costs associated with electricity generation, transmission, and distribution are minimized, while simultaneously guaranteeing the stability and reliability of the grid (Muhammad, 2024). This study aims to size Distributed Energy Resources (DERs) for a smart grid network.

Specifically, this research objectives are to: [i] model an optimally sized DER system in a smart grid to efficiently meet users' energy load and energy demand. [ii] analyse the impact of the smart grid on the coverage area.

2. THEORETICAL ANALYSIS

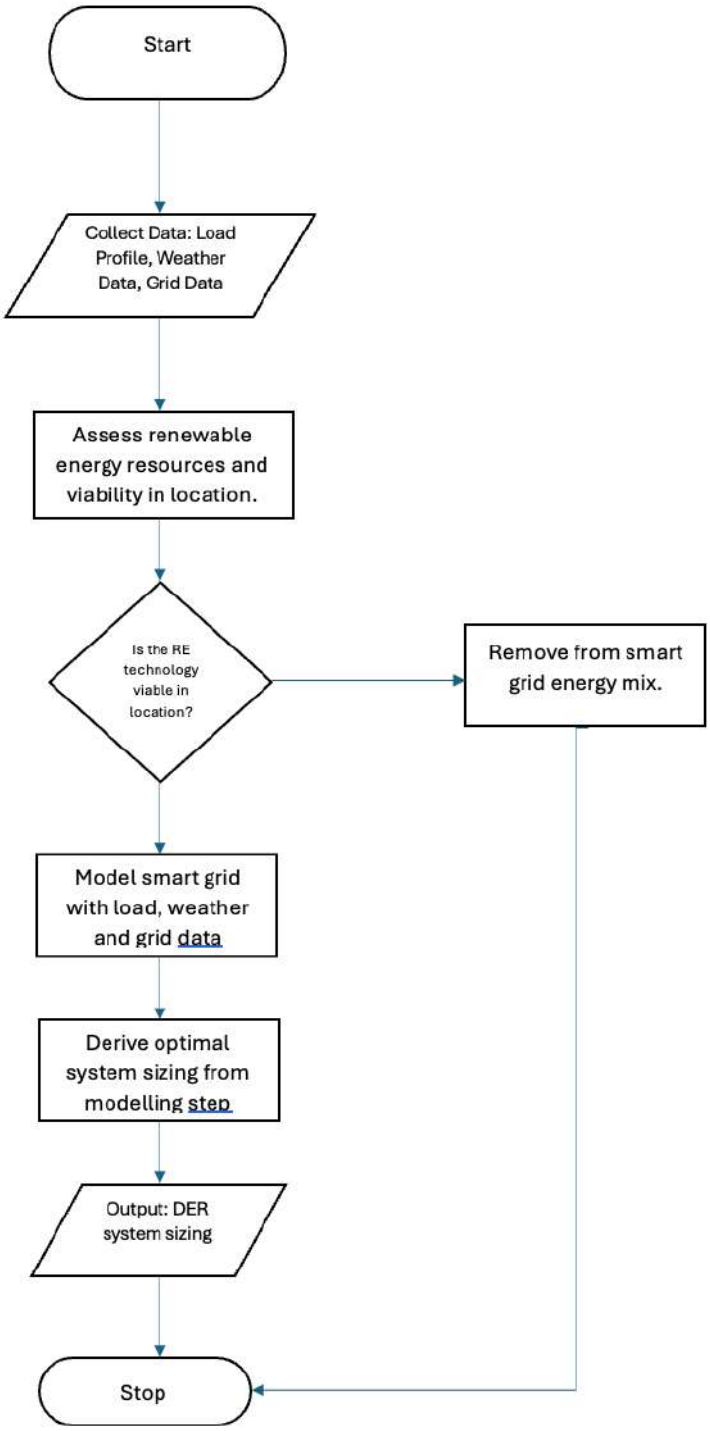

Figure 1: DER Sizing Framework for Grid-Interactive Microgrid

The methodology for optimally sizing a DER for a micro-grid with grid interaction is shown in Figure 1, here, available meteorological data, load demand, distribution network data and grid availability data are collected. The viability of various renewable energies is considered, and the micro-grid is then modelled with the collected data.

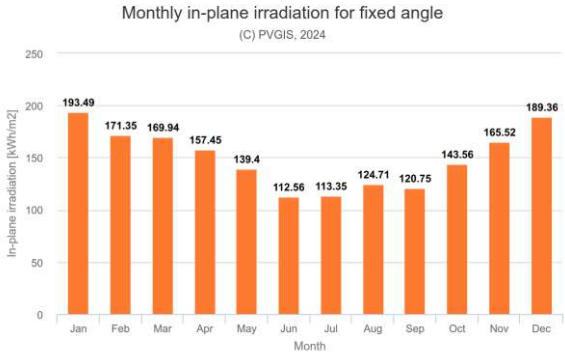

Figure 2: Solar Irradiance plot against time for a year

Photovoltaic (PV) System Model

The output power of the Solar Photovoltaic System (SPVS) denoted as (Pout SPVS) is calculated using Equation (1), which accounts for temperature effects on photovoltaic performance. Solar radiation data for the study site were obtained from the PVGIS meteorological database (European Commission, 2022), depicted in Figure 2, showing solar irradiance data for a typical meteorological year (TMY)

$$PV_{out\ SPVS} = \left(1 + \alpha_p(T_c - T_{c\ STC})\right) Y_{SPVS} f_{SPVS} \left(\frac{G_T}{G_{T,STC}}\right) \quad (1)$$

α_p is the temperature coefficient of power $(\%/°C)$; T_c is the cell temperature of the PV panels (◦C); $T_{c\ STC}$ is the temperature of the PV panels under standard test conditions (STC), Y_{SPVS} is the nominal capacity of the SPVS that is, power output under STC; f_{SPVS} is the derating factor of the SPVS; GT is the incident radiation in the current time step (kW/m^2), and $G_{T,STC}$ is the irradiation under STC (1 kW/m^2).

Battery Energy Storage System (BESS) Model

The battery energy storage system provides the system with several capabilities including backup power, black start and autonomy during nighttime with no solar irradiation and grid supply. It is modelled using the state of charge (SOC), charging and discharging efficiency as well as the maximum allowable power the battery storage can safely deliver over a given period – an hour in this case.

$$SOC\ (t) = SOC(0) + \eta_c \sum_{k=0}^{t} P_{CB}(k) + \eta_d \sum_{k=o}^{t} P_{DB}\ (k) \quad (2)$$

$$\begin{pmatrix} B_{min} \leq SOC \leq Bmax \\ B_{min} = (1 - DOD)B_{max} \end{pmatrix} \quad (3)$$

$$0 \leq P_{DB}(k) \leq P_{max} \quad (4)$$

where $SOC(0)$ is the state of charge of the battery at $t = 0$; η_c is the charging efficiency; $\sum P_{CB}$is the electrical power supplied to the BESS at a time t; $\sum P_{DB}$ is the discharge power from BESS at a time t; η_d is the discharge efficiency; B_{min} and $Bmax$ are the minimum and the maximum allowable battery bank capacities (kWh) of the BESS, respectively; DOD is the depth of discharge of the BESS, and Pmax is the maximum hourly discharging power.

Diesel Generator

The diesel generator provides backup power during periods of grid outages and low or no solar insolation, for continuity of service, it is better to include the DG as part of the generation assets of the smart grid. The generator's operating restriction is given by the following equation:

$$0 \leq P_{DB}(k) \leq P_{max}$$

where the power supply from PG can at no time exceed its maximum power PG, max during its operation in the power system. The electricity production of the generator is proportional to its fuel consumption which is given by the following equation:

$$F_G = B_G P_{G,N} + A_G P_G \tag{5}$$

where F_G is the fuel consumption of the diesel generator (L/h); $P_{G,N}$ is the nominal power of the diesel generator (kW); P_G is the output power of the diesel generator (kW); B_G is the generator fuel intercept coefficient (L/h/kWnominal), and A_G is the generator fuel slope (L/h/kWout). Both coefficients for the fuel consumption curve are defined according to the operation parameters of the diesel generator

Net Present Cost (NPC)

Homer Pro minimizes the Net Present Cost (NPC) of the target power system with the following expression:

$$min(C_{NPC,i}) = \sum_{all\ element}[\ [-R_{0,i} + \sum_{t=0}^{T}\left[\frac{R_{t,i}}{(1+x)^t}\right] \tag{6}$$

The total annualized cost of the entire system $C_{ann,tot}$ is given by Equation:

$$C_{ann,tot} = C_{NPC}\frac{i(1+i)^N}{(1+i)^N-1} \tag{7}$$

where $C_{ann,tot}$ is in units of USD/year, i is the annual real discount rate (%) and N is the planning horizon (years). The levelized cost of energy (LCOE) is calculated by dividing the total annual cost of the target power system over one year by the total energy generated in the same period. It is represented by the following equation:

$$LCOE = \frac{C_{ann,tot}}{P_{prim}} \tag{8}$$

where $LCOE$ is given in USD/kWh a metric for understanding the unit cost of energy delivered over the asset's lifetime period, and P_{prim} is the primary served load (kWh/year).

Renewable Fraction (*RF*)

The renewable fraction (fren) is the fraction of the energy delivered to the load produced from the proposed renewable components in the power system. It is given by the following equation:

$$f_{ren} = 1 - \frac{E_{fossil\ gen}}{E_{load}} \tag{9}$$

where $E_{fossil\ gen}$ (kWh/year) is the electricity generation from non-renewable sources, and E_{load} (kWh/year) is the total electricity consumed by the electrical load. The renewable fraction is vital in determining both the Net Present Cost (NPC) and CO_2 emissions of a system. Increasing renewable energy penetration usually results in higher capital costs but lower CO_2 emissions, as shown in the equation. Conversely, systems relying more on fossil fuels often have lower capital costs but higher CO_2 emissions. Thus, optimizing indicators such as the renewable fraction is crucial for designing efficient hybrid power systems.

3. MATERIALS AND METHODS/METHODOLOGY/EXPERIMENTAL PROCEDURE

The area of this study is in the Robiyan/Ibaragun community of Ogun state. For this study, the five distribution transformers (DTs) at the tail end of the feeder were selected. This is to help in understanding how much impact appropriate citing and sizing of DER can have on the customer/communities with the worst voltage drop experience and quality of service.

Load Data

The five DTs selected were each installed with an energy data logger for 2-3 weeks to capture key electrical parameters like the terminal voltage at the point of common connection (PCC), frequency, real and apparent power as well as the energy consumption for the logging period.

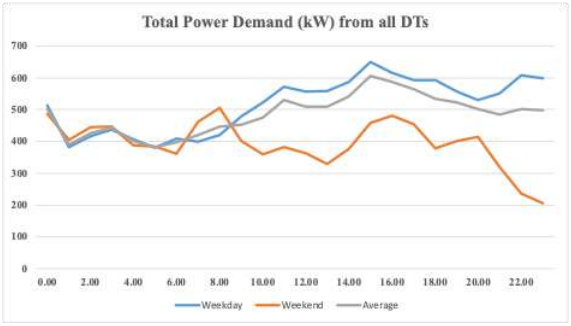

Figure 3: Cumulative load profile of community

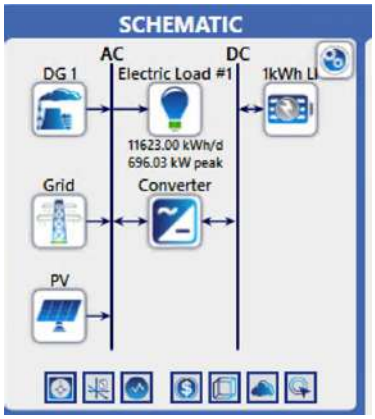

Figure 4: Schematic of Smart Grid Set Up

Micro-Grid System Architecture

The smart grid system architecture comprises the grid, the medium voltage (MV) network, part of which hosts the smart grid's coverage area, distribution transformers (DTs) and the DER power plant which includes the PV arrays and battery energy storage system (BESS). Recloser(s) are inserted at the point of common connection (PCC) between the smart grid and the rest of the utility grid. This serves the purposes of linking the rest of the smart grid to the main grid, isolation in cases of fault or grid outages (anti-islanding) and synchronization to the rest of the grid when the service is good for reconnection. The DER generates energy at low voltage (400 V) which is then fed to a step-up transformer for integration with the rest of the medium-voltage lines. This is illustrated in Figure 4 below with the names and capacity of the five (5) distribution transformers within the smart grid network.

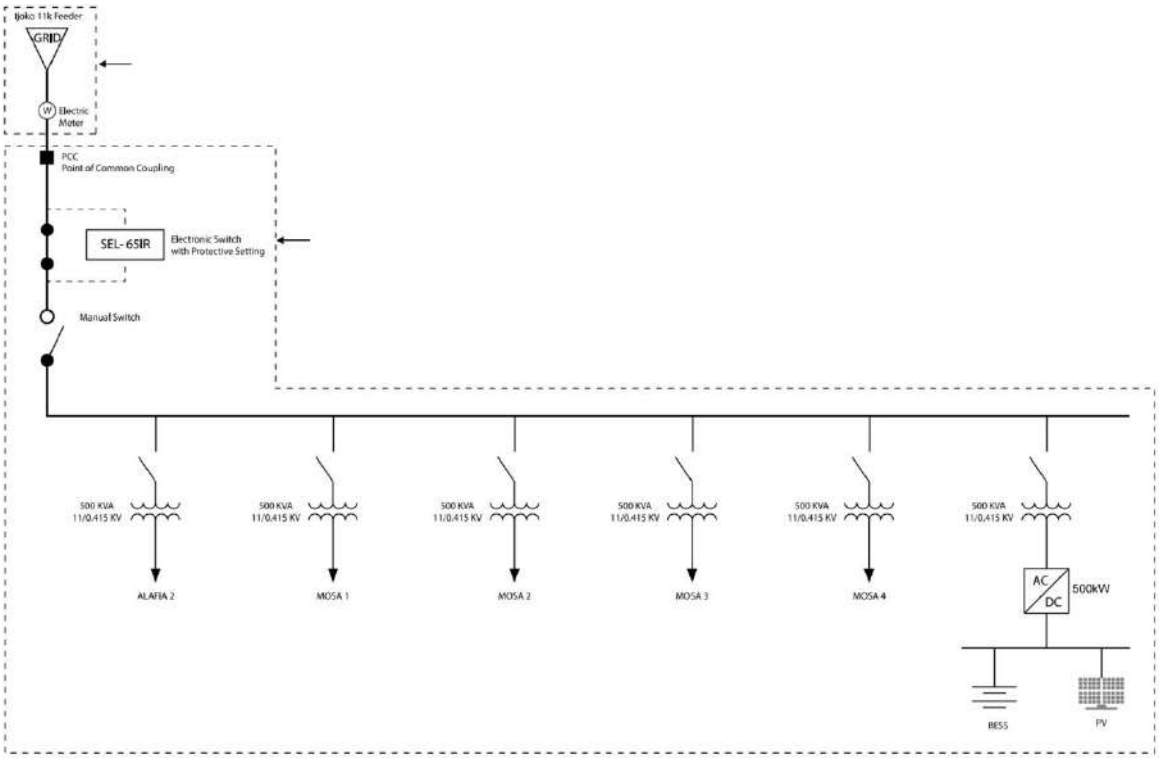

Figure 5: Network Architecture of the Microgrid

Homer Inputs/Asssumptions		
	Units	
HOMER financial inputs		
Discount rate	%	15.0%
Inflation rate	%	12.0%
Real discount rate	%	2.6%
Project lifetime	yr	20
Exchange rate	NGN/USD	1500
Solar		
Solar type	N/A	Generic flat
CAPEX	$/kW	300
Replacement cost	$/kW	300
Fixed O&M	$/kW-yr	10
Lifetime	Yr	25
Solar panel derating factor	%	80%
Diesel		
Generator type	N/A	Autosize
CAPEX	$/kW	280
Replacement cost	$/kW	280
Fixed O&M	$/kW/hr	0.01
Lifetime	hr	15000
Fuel cost	$/L	1.06
Minimum loading	%	25%
Lithium ion battery		
CAPEX	$/kW	350
Replacement cost	$/kW	250
Fixed O&M	$/kW-yr	3
Lifetime	Yr	7
Battery lifetime throughput	kWh	6000
Grid		
Average tariff	NGN/MWh	52000
Average tariff	$/kWh	0.0347

Figure 6: Homer Input and Assumptions

Microgrid Sizing Methodology

Optimally sizing a DER in a smart grid involves dimensioning the PV array size, battery energy storage size, backup diesel generator size, as well as the control algorithm, using the resilience, reliability, emission reduction and cost-effectiveness as the objective function is carried out in the hybrid optimization of modern energy resources HOMER Pro software (Homer Energy, 2024). The load profile data and meteorological data – temperature and solar irradiance are used to drive the Homer model as well as the economic data like unit costs of the various subsystem components, inflation, and estimated project life. Grid hours of availability and reliability, tariff structure as well and the generator dispatch strategy all have crucial impacts on the overall system recommendation.
Various simulation scenarios were set up, results from each simulation run were recorded and the results were compared based on the constraints itemized above:

1. **Grid Mode:** This represents the base case, a basis of comparison for other scenarios developed in the sizing process. The AC power grid is connected through the AC bus, while the community aggregated load is also connected through the same bus.
2. **DG + Grid Mode:** The diesel plus grid scenario is modelled with an aggregated generator size that can support the entire load of the community. Here, both the power sources i.e. grid, and DG are connected through the AC bus which also connects the community load.
3. **Grid + DG + Solar PV:** A third scenario adds solar PV in addition to the grid and the DG. The PV system has a PV inverter with maximum power point tracking capabilities integrated within it.
4. **Grid + DG + Solar PV + BESS:** The last scenario adds storage to the combination of the grid, DG, and solar PV grid configuration. Here, a battery energy storage system made of the lithium-ion battery stores the excess energy from all sources and provides the energy during periods of energy deficit.

4. RESULTS AND DISCUSSION

The results of the grid-only scenario provide an accurate picture of the current service level from the utility to the study area. The provision of less than 12 hours of power impacts businesses and livelihoods within the service area. This has resulted in all homes and businesses providing their backup power using cheap, inefficient, noisy and polluting petrol and diesel generating sets usually referred to locally as “I better pass my neighbour”, a development that has, made Nigeria the highest importer of generators in Africa according to (IRENA, 2023). The grid plus diesel generator scenario aggregates the energy gap resulting from the inability of the utility grid to provide 24-hour power by augmenting the grid supply with a centralized backup diesel generator. Here, there is no unmet energy demand, however, the energy cost has more than increased by five

times. Also, there is now a significant amount of emission from the diesel plant deployed as support for the main utility network supply. The addition of solar PV resulted in a renewable energy fraction of 25% into the total energy mix, a 23% reduction in diesel fuel consumption, avoided CO_2 emission of 760 metric tons annually and a more affordable energy tariff to the community. Adding battery energy storage further improves the performance of the intermittent renewable energy source as it provides firm capacity for the system. The grid and the combination of solar PV plus storage contribute over 80% of the total energy production of the smart grid. This in essence has significantly reduced the impact of diesel price escalations and scarcity.

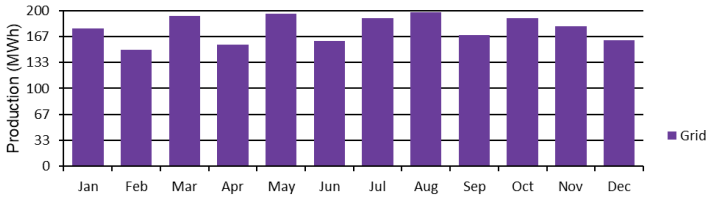

Figure 6: Grid Only scenario energy mix

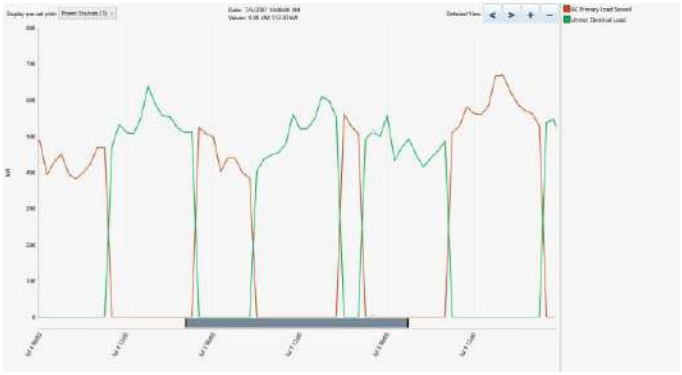

Figure 7: Graph of energy supplied and unmet load showing the energy gap with grid-only mode

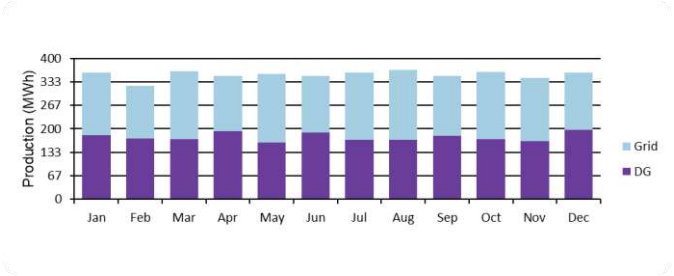

Figure 8: Percentage of energy contribution between grid and diesel generator (DG)

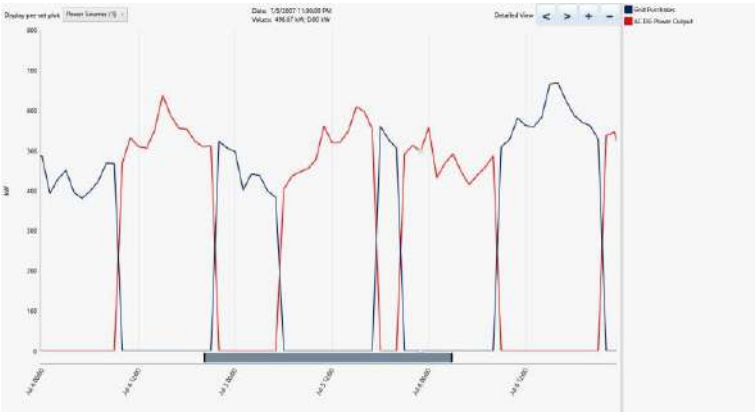

Figure 9: Grid of power supplied by using the blend of grid and DG

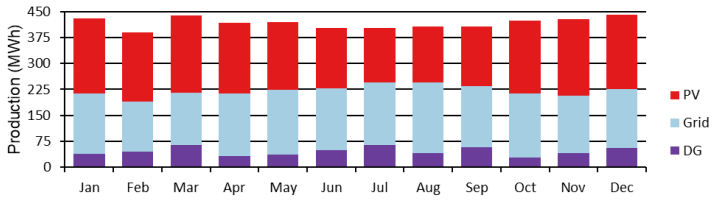

Figure 10: Energy contribution between grid, Solar PV and DG

Table 1: Summary of Homer Simulation Result for all four scenarios.

	SCENARIO	1	2	3	4
OUTPUT	PV (MWp)	-	-	1.04	1.77
	DG (MVA)	-	1	1	1
	BESS	-	-	-	6.00
	NPC (M$)	1.13	13.11	11.7	9.03
	LCOE ($/kWh)	0.04	0.2	0.18	0.14
	Renewable fraction (%)	-	-	25	37.7
	CO2 Emission (MT/year)	-	3,001.00	2,560.00	1,750.00
	Grid Production (GWh/year)	2.12	2.12	1.49	2.10
	PV Production (GWh/year)	-	-	1.38	2.35
	Diesel Production (GWh/year)	-	2.12	1.66	0.55
	Total Production (GWh/year)	2.12	4.24	4.54	5.01

5. CONCLUSION

This study emphasizes the efficacy of well-designed distributed energy resources (DERs) in fulfilling energy demands within designated service areas, presenting a promising alignment with the objectives outlined in the Electricity Act of 2023, which allows state governments to set up electricity markets within their states (Ekpo, 2023) . However, it is important to acknowledge a limitation stemming from the reliance on limited historical data, particularly at the feeder and distribution transformer levels. This necessitates future research endeavours to explore approaches focused on the injection substation levels, which would facilitate broader coverage and potentially lead to further reductions in the levelized cost of energy and end-user tariffs.

REFERENCES

1. IEA. (2023). *Smart Grids.* Paris: IEA. Retrieved February 12, 2024, from https://www.iea.org/energy-system/electricity/smart-grids
2. Muhammad, K. (2024). Smart grids and renewable energy systems: Perspectives and grid integration. *Energy Strategy Review, 51*. doi:https://doi.org/10.1016/j.esr.2024.101299
3. Akkara, S., & Selvakumar, I. A. (2023). Review on Optimization Techniques Used for Smart Grids. *Measurements: Sensors, 30*(100918). doi:https://doi.org/10.1016/j.measen.2023.100918
4. IRENA. (2023). *Renewable Energy Roadmap: Nigeria.* International Renewable Energy Agency, Abu Dhabi.
5. European Commission. (2022, March 01). *Photovoltaic performance*. Retrieved March 2024, from PHOTOVOLTAIC GEOGRAPHICAL INFORMATION SYSTEM: https://re.jrc.ec.europa.eu/pvg_tools/en/tools.html
6. Hossain, E., Hossain, J., & Un-Noor, F. (2018). Utility Grid: Present challenges and their Potential solutions. *IEEE Access*(6), 60294–60317.
7. Homer Energy. (2024). *Homer Energy*. Retrieved February 2024, from Homer Pro: https://homerenergy.com/products/pro/
8. NERC (Nigerian Electricity Regulatory Commission). (2023). *NERC Quarterly Report: Third Quarter Report.* Abuja: NERC.
9. Ekpo, E. O. (2023, November 3). *The Electricity Act, 2023: Imperatives and Opportunities for the States.* Retrieved January 2024, from http://ngfrepository.org.ng:8080/jspui/handle/123456789/5579

PAPER 75- ENHANCING COST-EFFICIENCY IN MICRO-GRID SYSTEMS: A HYBRID OPTIMIZATION APPROACH FOR UNIT COMMITMENT PLANNING

B.I Gwaivangmin[1], G.A Bakare[2], Y.S Haruna[3] and A.L Amoo[4]

Department of Electrical and Electronics Engineering
Abubakar Tafawa Balewa University, Bauchi
Email: bgwaivangmin@gmail.com

ABSTRACT
In the face of escalating power supply expenses, efficient unit commitment planning within micro-grid systems becomes imperative. This study delves into optimizing a diverse blend of micro-pumped hydro storage, solar PV, diesel generators, and public power supply to determine the University of Jos's most cost-effective hourly load demand over the next 24 hours. Employing a robust optimization methodology, the research dynamically manages each power source's activation, departing from fixed operational hours. Through a comparative examination involving Particle Swarm Optimization (PSO), which yielded a total generation cost of ₦127,216.00, Genetic Algorithm Particle Swarm Optimization (PSO-GA), which achieved a total generation cost of ₦104,120.00, and Hybrid Particle Swarm Optimization with a local search algorithm (Hybrid-PSO), resulting in a total generation cost of ₦54,264.00, the study underscores Hybrid-PSO's superiority in power generation cost by 57% compared to PSO and 48% compared to PSO-GA. Thus, favoring it as the optimal technique. This envisaged unit commitment strategy ensures a dependable and sustainable power supply, effectively tackling the rising expenses. Adoption of this approach augments micro-grid systems' cost-efficiency while fulfilling load demand prerequisites, offering pivotal insights for optimal optimization methods' selection in micro-grid systems to enhance operational efficiency and economic viability amid mounting power supply costs.

KEYWORDS*:* Efficiency, Escalating, Hybrid, Load Demand, Optimization, unit Commitment

1. INTRODUCTION

1.1 Background of the Study

Electricity is vital for societal progress, as underscored by IEA (2019), IRENA (2019), and NERC (2020), yet nations like Nigeria face persistent power disruptions, impeding economic growth and societal development. Institutions like the University of Jos rely heavily on stable electricity provision, but irregular supply from the grid and alternate sources disrupts operations. Micro-grid systems offer a solution, delivering efficient power to remote areas, as noted by Lu et al. (2018) and Palizban and Huang (2018), utilizing a mix of renewables and non-renewables. However, integrating these sources efficiently poses a challenge, as discussed by Wang and Zhang (2019), Morales-España et al. (2019), and Shi et al. (2018). They emphasize unit commitment planning's significance, optimizing power source activation to meet demand while minimizing costs, recognizing the economic impracticality of continuous operation.

To overcome the challenge of unreliable power supply, energy storage solutions like pumped hydro energy storage (PHES) are utilized to store surplus energy during low-demand periods and release it during peak-demand times. Additionally, integrating diverse power sources such as solar photovoltaic (PV), diesel generators, and public power supply is pursued to strengthen energy reliability and efficiency. A hybrid system comprising solar PV, pumped hydro energy storage, diesel generator, and public power supply. To optimize the scheduling of these power sources for enhanced efficiency, cost-effectiveness, and reliability, various optimization techniques like Particle Swarm Optimization (PSO)Genetic Algorithm Particle Swarm Optimization (PSO-GA), and Hybrid Particle Swarm Optimization with a local search algorithm (Hybrid-PSO) are explored.

The power supply within the 11 kV dedicated feeder network of the University of Jos, spanning an 8.7 km network as illustrated in Figure 1, typically provides an average of 22-23 hours of availability with a voltage range of 215-240V single phase. While this availability is beneficial for education and learning, it poses a considerable financial burden to the institution due to high electricity costs. Efforts have been made to alleviate this financial strain, including attempts to reduce electricity expenses by limiting the hours of electricity use in student hostels and prohibiting the use of heavy electrical equipment. However, these measures have not resulted in significant savings. This study aims to optimize power generation scheduling at the University of Jos to minimize costs over 24 hours. Objectives include developing a hybrid micro-grid model and comparing

optimization methods (PSO, PSO-GA, Hybrid-PSO) for cost-effective unit commitment. Research indicates soaring electricity expenses, emphasizing unit commitment's importance in minimizing generation costs.

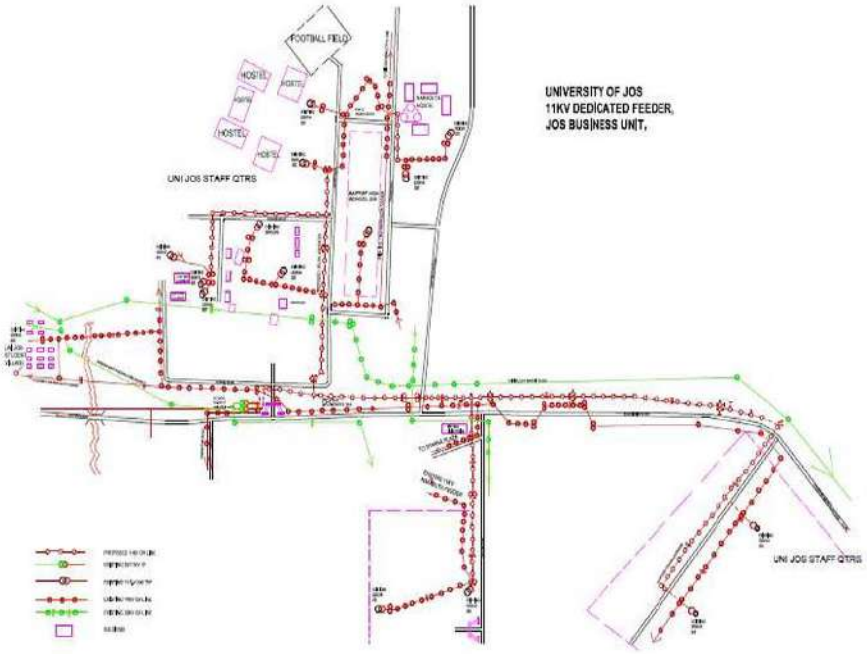

Figure 1. A sketch of the 11 Kv dedicated Feeder of the University of Jos.

1.2 Literature Review

The literature on unit commitment optimization in hybrid energy systems encompasses a variety of methodologies aiming to integrate renewable energy sources while ensuring grid reliability and cost-effectiveness. Alawieh et al. (2019), Chen et al. (2019), Huang et al. (2019), and Omojola et al. (2019) explore different optimization approaches, revealing gaps in addressing uncertainties associated with renewables and demand response. Soliman et al. (2019), Wang and Shi (2019), Zhang et al. (2019), and Zhou et al. (2019) contribute novel methodologies but emphasize the need for further validation and comparative analysis. Additional studies by Liu et al. (2021), Li et al. (2021), Zhang and Wang (2021), Wang et al. (2021), and Zhang et al. (2021) indicate a growing interest in this research domain. Further contributions from Kumar et al. (2022), Lai et al. (2022), Liu et al. (2022), Niu et al. (2022), Pan et al. (2022), Shang and Liu (2022), Sahebi and Bozorg (2022), Sun et al. (2022), Wang et al. (2022), Wei et al. (2022), Zhao et al. (2022), Zuniga et al. (2022), Patel et al. (2023), Yang et al. (2023), Zhang et al. (2023), and Zhong et al. (2023) contribute to this exploration, with Kumar et al. (2022) focusing on a hybrid wind-solar-battery energy system, Lai et al. (2022) introducing a multi-objective short-term unit commitment model, and Liu et al. (2022) addressing uncertainty in hybrid power systems with demand response. However, limitations across these studies underscore the need for comprehensive validation, comparative analysis, and robust consideration of uncertainties to ensure practical effectiveness in unit commitment optimization methodologies for hybrid energy systems.

2. THEORITICAL ANALYSIS

Unit commitment in power systems is influenced by numerous factors, such as demand forecasts, generator availability, fuel prices, renewable energy variability, transmission constraints, environmental regulations, and market conditions. Balancing economic efficiency, grid stability, and environmental sustainability is crucial in optimizing unit commitment decisions. This requires careful consideration of the interactions among these factors to ensure cost-effectiveness, reliability, and compliance with environmental standards during power system operations.

2.1 Fundamental Concept of Unit commitment

According to research by Abdou and Tkiouat (2018), Morales-España et al. (2019), Zhang and Bose (2020), Unit Commitment (UC) in power systems involves strategizing power plant operations to accommodate fluctuating demand while accounting for costs and reserves. Additionally, Salman and Kusaf (2021) delineate the formulation of the UC optimization problem as follows:

Objective function:

$$Min \sum_{i=1}^{NG} \sum_{t=1}^{NT} [F_{ci}(P_{it}) * I_{it} + SU_{it} + SD_{it}] \quad (1)$$

Where "*i*" represents the generating unit index, "*t*" denotes the time index, "$F_{ci}(P_{it})$" signifies the function describing the production cost of unit "*i*", "P_{it}" indicates the power generation of unit "*i*" at time "*t*", "I_{it}" reflects the commitment state of unit "*i*" at time "*t*", "SU_{it}" represents the start-up cost of unit "*i*" at time "*t*", and "SD_{it}" represents the shut-down cost of unit "*i*" at time "t".
The function $F_i(P_i)$ can be formulated as:

$$F_i(P_i) = a_i + \beta_i P_i + \gamma_i P_i^2 \quad (2)$$

Here, a_i, β_i, and γ_i represent coefficients associated with the production cost of unit *i*, and P_i denotes the power generation of unit *i*. Other constraints may include power balance, ramping limit, minimum ON and OFF time, operating reserves, spinning reserves etc as the case may be.

2.2 The Particle Swarm Optimization (PSO) Model:
According to recent studies by Wang et al. (2021), Li et al. (2021), Zhang et al. (2021), Jiang et al. (2021), Guo et al. (2021), Chen et al. (2021), Wang et al. (2021), and Yang et al. (2021), the Particle Swarm Optimization (PSO) model can be formulated as follows: Let $X_i(t)$ denote the position of the i-th particle in the search space at time t, and each particle possesses a velocity $V_i(t)$ determining its movement within the search space. This iterative update process is governed by the following equations:
Update particle velocity:

$$V_i(t+1) = w \cdot V_i(t) + c_1 \cdot rand_1 \cdot (P_{i,best} - X_i(t)) + c_2 \cdot rand_2 \cdot (P_{g,best} - X_i(t)) \quad (3)$$

where:*w* is the inertia weight, c_1 and c_2 are acceleration coefficients, $rand_1$ and $rand_2$ are random values between 0 and 1, $P_{i,best}$is the best position found by particle *I*, $P_{g,best}$ is the best position found by any particle in the swarm.

i. Update particle position:

$$X_i(t+1) = X_i(t) + V_i(t+1) \quad (4)$$

These equations are applied to each particle in the swarm iteratively until a termination condition is met, such as reaching a maximum number of iterations or achieving a satisfactory solution.

2.3 The Hybrid PSO
Let X_i be the position of particle *i* in the search space, and V_i be its velocity. In Hybrid PSO, the velocity and position updates are performed as follows:

Velocity update:

$$V_i(t+1) = w \cdot V_i(t) + c_1 \cdot r_1 \cdot (P_{best} - X_i) + c_2 \cdot r_2 \cdot (G_{best} - X_i) + c_3 \cdot r_3 \cdot (X_{best}t - X_i) \quad (5)$$

Position update:

$$X_i(t+1) = X_i t) + V_i(t+1) \quad (6)$$

Where: *w* is the inertia weight, c_1, c_2, and c_3 are the acceleration coefficients, r_1, r_2, and r_3 are random values in the range [0, 1], P_{best} is the best position found by particle *i* so far, G_{best} is the best position found by any particle in the swarm, $X_{best}t$ is the best position found by any particle in the previous iterations.
This model combines the standard PSO algorithm with a local search algorithm, where X_{best} represents the best solution found by the local search. By incorporating this hybrid approach, Hybrid PSO aims to strike a balance between exploration and exploitation, allowing for efficient search in the solution space.

2.4 The Hybrid PSO-GA
As per recent studies by Zhang et al. (2020), Guan et al. (2020), Shi et al. (2021), Jiang et al. (2021), Wang et al. (2021), Li et al. (2021), Zhang et al. (2021), and Gao et al. (2021), the mathematical formulation for Hybrid PSO-GA (Particle Swarm Optimization with Genetic Algorithm) can be outlined as follows: Let Xi represent the position of particle i within the search space, and vi denote its velocity. In the Hybrid PSO-GA approach, updates to the velocity and position are conducted using the following equations:
Velocity update:

$Vi(t+1) = w \cdot Vi(t) + c_1 \cdot r_1 \cdot (Pbest - X_i) + c_2 \cdot r_2 \cdot (Gbest - X_i)$ (7)

Position update:

$X_i(t+1) = X_i(t) + V_i(t+1)$ (8)

After updating the positions, a selection mechanism is applied to determine which particles will undergo crossover and mutation. This selection process is based on their fitness values. Then, the genetic operators, including crossover and mutation, are applied to the selected particles to create offspring.
Crossover: Two parent particles are selected based on their fitness values. A random crossover point is chosen, and the particles exchange information beyond this point to create two offspring particles.
Mutation: Randomly selected particles undergo mutation, where a small random change is applied to their positions.
The offspring particles generated through crossover and mutation are then evaluated for their fitness, and the best ones replace the worst particles in the swarm.
This hybrid approach combines the exploration capability of PSO with the exploitation ability of GA, aiming to strike a balance between exploration and exploitation to efficiently explore the search space and find optimal solutions.

3. MATERIALS AND METHOD

The study optimizes power supply at the University of Jos using demand prediction, validated with real data, incorporating demand response and meteorological data for solar power modeling.Meteorological data, solar irradiance, temperature, and cloudiness index, were used as inputs in unit commitment of a hybrid power system. These data help predict the availability and variability of solar energy. By incorporating meteorological data into the unit commitment algorithm, the system optimized the scheduling of power generation units based on expected renewable energy generation levels. It employs three optimization algorithms (PSO, PSO-GA, HPSO) in Python to enhance micro-grid efficiency and reliability.

3.1 The mathematical formulation of the Unit Commitment Problem can be expressed as:

Parma and Doshi (2018) Viewed UC as optimizing power generation for 24 hours at minimal cost, considering various sources and operational constraints.
The objective function of the Unit Commitment problem aims to minimize the total cost of electricity generation, expressed as:

$$Minimize\ Fc = \sum_{i=1}^{T}\sum_{i=1}^{N}\left[F_i\left(P_i(t)\right) + SC_i(t) + SD_i(t)\right] \quad (9)$$

The fuel cost F_i (P_ii(t)) associated with unit$i$ in any given time interval t is a function of the generator power output. The production cost of unit i can be approximated as a quadratic function of real power outputs from the generating units, and it is defined as follows:

$$(P_i(t)) = a_i + b_i P_i(t) + c_i P_i^2(t) \quad (10)$$

The start-up cost of the generator depends on the duration the unit has been offline prior to start-up. In this study, the time-dependent start-up cost is defined as shown in Equation (11):

$$SC_i = hcosti:\ T_i^{off} \le X_i^{off} \le T_i^{off} + cshour \quad (11)$$

In this study, the shut-down (SD) cost for each unit is typically assigned a constant value. However, for the purposes of this work, the shut-down cost has been set equal to zero for each unit.

a) System Constraint

The combined power output from the hybrid system, comprising diesel generators, solar photovoltaic (PV) panels, pumped hydro energy storage systems, and public power supply generating units, must satisfy the hourly load demand $P_d(t)$:

$$P_d(t) = \sum_{j=1}^{N} P_i(t) + P_v(t) + P_{pumped}(t) + P_{pbu}(t) \quad (12)$$

b) **Generation Limits**

The real power generation of each generator is bounded by lower and upper limits, ensuring that generation remains within this range. This constraint is defined as:

$$P_{imin} \le P_i(t) \le P_{imax} \quad (13)$$

$$P_{wmin} \le P_w(t) \le P_{wmax} \quad (14)$$

c) Unit Minimum up and down time constraints

The inequality constraints specifying the minimum up and down time limits of generating units are expressed as:

$$T_j^{on} \le X_j^{on} \quad (15)$$

$$T_i^{off} \leq X_i^{off} \quad (16)$$

The Objective function Fc in equation (9) can be expanded as below:

Let:

g be the status of the diesel generator (0 for off, 1 for on) for each hour. p be the status of the public power supply (0 for off, 1 for on) for each hour. s be the status of the solar PV (0 for off, 1 for on) for each hour. h be the status of the pumped hydro energy storage (0 for off, 1 for on) for each hour. N be the number of intervals in horizon of planning. *pv* be the solar PV power generation (kW). *pumped* be the pumped hydro power generation (kW).*pub* be the public power supply (kW).l_{pv}be the solar losses coefficient for each hour.l_{pumped} be the pumped hydro losses coefficient for each hour.$demand_t$ be the electricity demand (kW) for each hour.

$$Minimize\ Fc = \sum_{j=1}^{T}\sum_{j=1}^{N}\{g_{cost} * g_t + p_{cost} * p_t + gstart_{cost} * xt + gshutdown_{cost} * (1 - xt) + s_{cost} * s_t(1 - l_{pv}, t) + h_{cost} * h_t(1 - l_{pumped}, t) + demand_t.pub_t\} \quad (17)$$

Subject to:

i. Power balance constraint:

$$g_t + p_t + s_t(1 - l_{pv}, t) + h_t(1 - l_{pumped}, t) + pubt = demandt + p_{vt} + pumpedt$$

Diesel generator start-up and shutdown constraints:

x_t=$g_t - 1 - g_t$; Diesel generator status constraint: $g_t \in \{0,1\}$; Public power supply status constraint: $p_t \in \{0,1$;Solar PV status constraint: $s_t \in \{0,1\}$;Pumped hydro energy storage status constraint: $h_t \in \{0,1\}$;Solar losses coefficient constraint: $l_{pv}, t \in \{0,1\}$;Pumped hydro losses coefficient constraint: $l_{pumped}, t \in \{0,1\}$;Electricity demand constraint: $demand_t \geq 0$

Where,

Fc is the total operating cost. g_{cost} is the cost of operating the diesel generator per unit power (kW). p_{cost} is the cost of using the public power supply per unit power (kW). $gstart_{cost}$ is the start-up cost of the diesel generator (constant). $gshutdown_{cost}$ is the shutdown cost of the diesel generator (constant). s_{cost} is the cost of using the solar PV per unit power (kW). h_{cost} is the cost of using the pumped hydro energy storage per unit power (kW). $g_t$is the status of the diesel generator at time *t* (0 or 1). $p_t$is the status of the public power supply at time *t* (0 or 1). At time *t*, x_t represents the start-up status of the diesel generator (0 or 1), and s_t denotes the status of the solar photovoltaic (PV) system (0 or 1). is the start-up status of the diesel generator at time *t* (0 or 1). s_t is the status of the solar PV at time *t* (0 or 1). h_t is the status of the pumped hydro energy storage at time *t* (0 or 1).

The parameters used for this work were:

Particle Swarm Optimization (PSO):

1. Swarm size: 100 particles.
2. Inertia weight (w): 0.8.
3. Cognitive parameter (c1):1.5.
4. Social parameter (c2): 2.0
5. Maximum number of iterations: 100 iterations.

Genetic Algorithm (GA):

1. Population size:100

3.2 Demand Response

In this study, the 24-hour electricity demand forecast is and meteorological data are detailed in Table 1. Additionally, weather data impacting solar power generation was sourced from NASA's website.

Table 1: the 24 hours Data used for the Unit Commitment

Time (Hours)	Load Demand(kW)	Cloudiness Index	Temperature (°C)	Solar Irradiance(W/m^2)
1:00-2:00	340.330	1	18	0
2:00-3:00	311.010	1	18	0
3:00-4:00	332.010	1	18	0
4:00-5:00	548.710	0.98	17	0
5:00-6:00	655.410	1	17	109
6:00-7:00	945.010	0.95	18	385
7:00-8:00	1204.120	1	20	543
8:00-9:00	1280.330	0.41	23	708
9:00-10:00	1139.920	0.38	26	773
10:00-11:00	1041.220	0.68	27	745
11:00-12:00	890.040	0.52	28	742
12:00-13:00	780.820	0.67	29	662
13:00-14:00	765.100	0.55	29	635

14:00-15:00	868.800	0.13	29	449
15:00-16:00	890.400	0.42	28	223
16:00-17:00	932.770	0.05	27	0
17:00-18:00	917.520	0	24	0
18:00-19:00	908.500	0.02	22	0
19:00-20:00	938.770	0.16	20	0
20:00-21:00	848.310	0.71	20	0
21:00-22:00	629.920	0.88	20	0
22:00-23:00	563.960	1	19	0
23:00-24:00	413.250	0.8	19	0
24:00-1:00	341.25	1	19	0

4. RESULTS AND DISCUSSION

4.1Simulation Results of the PSO Model

The data collected were simulated using, PSO toolbox for anaconda (Spyder) on the Python platform. The load demand data of the demand response was used to write a code in Python with the unit commitment model and the result is shown in Figure 3:

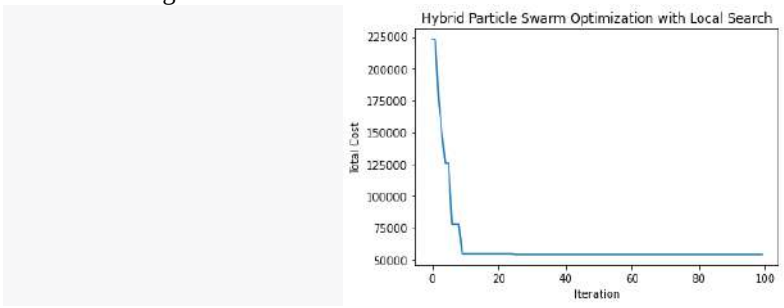

Figure 3: The Total cost and Number of Generations for Hybrid Particle Swarm Optimization

Figure 3 demonstrates the effectiveness of the Hybrid particle Swarm Optimization (HPSO) in optimizing unit commitment costs for the microgrid. The graph shows a clear downward trend in total cost**,** starting at roughly ₦225,000.00 for the first generation and rapidly decreasing to about ₦54,000.00 from the 10th to the 100th generation. This significant **cost reduction** over generations strongly suggests that HPSO converges towards an optimal solution, successfully minimizing costs for the unit commitment problem.

4.2 Simulation Results of the PSO-GA Model

The data collected were simulated using, PSO-GA for PYTHON

The 24-hour data collected was used to write a Python SA code with the unit commitment model and the results is shown in Figure 4.

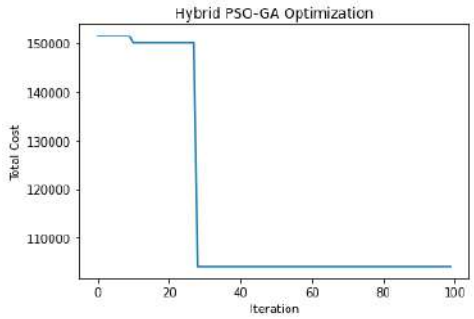

Figure 4: The Total cost and Number of iterations for PSO-GA

Figure 4, shows the total cost of the unit commitment using PSO-GA. From the graph it can be seen that the total convergence cost decreased from about ₦160, 000.00, at about 1 generation to about ₦150, 000.00 at 25th generation. Then convergence to about ₦104, 000 at the 26th generation.

4.3 Simulation Results of the PSO Model

The data collected were simulated using PSO for PYTHON. The load demand data of the demand response was used to write a PSO code in python with the unit commitment model and the result is shown in Figure 5.

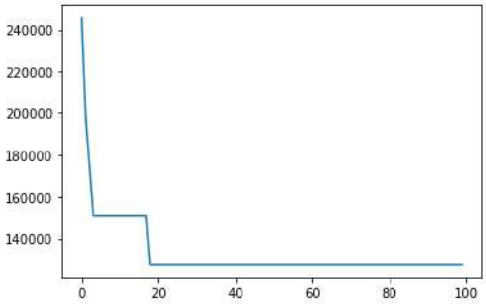

Figure 5: The Total cost and Number of Generations for PSO

Figure 5 demonstrates the effectiveness of the Particle Swarm Optimization (PSO) in optimizing unit commitment costs for the micro-grid. The graph shows a clear downward trend in total cost**,** starting at roughly ₦240,000.00 for the first generation and rapidly decreasing to about ₦150,000.00 by the 18th generation, then converging to about ₦120,000.00at the 19th generation. This significant cost reduction over generations strongly suggests that the PSO algorithm converges towards an optimal solution**,** successfully minimizing costs for the unit commitment problem.

Table 2: Minimized Cost of Power

Power Source Generation Method	Total cost of Generation (₦)
HPSO	54,264.00
PSO-GA	104,120.00
PSO	127,216.00

Table 2 demonstrates that the HPSO outperforms other optimization methods in cost-effectiveness for the micro-grid system: HPSO achieves the lowest total generation cost of ₦54.264.00, showcasing its proficiency in minimizing costs. PSO results in a higher cost of ₦127,216.00, suggesting its method may be less efficient for this specific micro-grid setup. PSO-GA falls between HPSO and PSO with a cost of ₦104,120.00. Although it doesn't surpass HPSO, it outperforms PSO, highlighting its competitiveness.

5. CONCLUSION

This study addresses the need for efficient unit commitment planning in micro-grid systems amidst rising power supply expenses. By optimizing various energy sources such as micro-pumped hydro storage, solar PV, diesel generators, and public power supply, the research aims to determine the University of Jos's most cost-effective hourly load demand over 24 hours. Using a robust optimization methodology, which dynamically manages each power source's activation, the study departs from traditional fixed operational hours, enhancing flexibility. Comparative analysis involving Particle Swarm Optimization (PSO), Genetic Algorithm Particle Swarm Optimization (PSO-GA), and Hybrid Particle Swarm Optimization with a local search algorithm (Hybrid-PSO) identifies Hybrid-PSO as the optimal technique due to its superior power generation cost.

REFERENCES

Abdou, I and Tkiouat,M (2018) Unit Commitment Problem in Electrical Power System: A Literature Review. International Journal of Electrical and Computer Engineering (IJECE) 8 (3)pp. 1357- 1372.

Alawieh, M., Zeineldin, H. H., and Sun, Y. (2019). A multi-objective enhanced electromagnetism-lie algorithm for short-term unit commitment of hybrid renewable energy systems. Applied Energy, 242, 800-816. https://doi.org/10.1016/j.apenergy.2019.03.128.

Chen, C., Kang, C., and Li, X. (2019). Optimal Unit Commitment for Integrated Renewable Energy Systems Based on Improved Particle Swarm Optimization. Energies, 12(3), 554.

Chen, Z., Li, Y., Li, Z., & Li, S. (2019). Optimal unit commitment for integrated renewable energy systems with enhanced particle swarm optimization. Applied Energy, 255, 113779.

Gao, Y., Zhang, Y., & Xu, Z. (2021). Hybrid Particle Swarm Optimization with Improved Inertia Weight for Solving Constrained Optimization Problems. Applied Soft Computing, 108, 107580.

Guan, J., Sun, Y., & Zhang, H. (2020). A hybrid genetic algorithm and particle swarm optimization for engineering optimization problems. Engineering Optimization, 52(8), 1419-1434.

Huang, W., He, R., Wang, Z., Yao, L., and Xu, Z. (2019). Multi-objective dynamic unit commitment of microgrid considering renewable generation and demand response. Energies, 12(5), 826. doi: 10.3390/en12050826

International Energy Agency (IEA). (2019). *World Energy Outlook 2019.* Paris: IEA.

International Renewable Energy Agency (IRENA). (2019). *Africa 2030: Roadmap for a Renewable Energy Future.* Abu Dhabi: IRENA.

Jiang, Y., Wang, J., & Zhang, S. (2021). A Hybrid Particle Swarm Optimization and Genetic Algorithm for Multimodal Optimization Problems. IEEE Access, 9, 81731-81741.

Kumar, S., Kumar, R., and Kumar, R. (2022). Optimal unit commitment of hybrid wind-solar-battery energy system using whale optimization algorithm. Journal of Ambient Intelligence and Humanized Computing, 13(2), 2285-2301.

Lai, C. T., Hsu, S. Y., and Hong, C. M. (2022). Multi-Objective Short-Term Unit Commitment with Renewable Energy Considering Demand Response and Vehicle-to-Grid Systems. Energies, 15(3), 549. doi: 10.3390/en15030549"in three lines and point out its limitations.

Li, J., Huang, H., & Gu, C. (2021). A hybrid optimization algorithm based on particle swarm optimization and genetic algorithm. Complexity, 2021, 6633920.

Li, J., Xiang, W., & Ding, Y. (2023). Research on the development status and prospects of pumped hydro energy storage technology in China. Energy Reports, 9(2), 3326-3334.

Liu, X., Zhang, Q., and Wu, Y. (2022). Optimal unit commitment for a hybrid power system considering demand response and uncertainty. IEEE Transactions on Sustainable Energy, 13(1), 408-417
Lu, L., Yang, H., & Burnett, J. (2018). *Recent advances in optimization of microgrid: A review.Renewable and Sustainable Energy Reviews, 71*, 836-854.

Morales-España, G., et al. (2019). *Optimization of Unit Commitment in Energy Systems.* New York: Springer.

NASA. (2023)Meteorological Data from NASA's Earth Observing System. Retrieved October 16, 2023, from https://earthdata.nasa.gov/

Nigerian Electricity Regulatory Commission (NERC). (2020). *2019 Fourth Quarter Report.* Abuja: NERC.

Niu, D., Xue, Y., Cao, Y., Yuan, X., and Qiu, M. (2022). Multi-objective unit commitment for integrated energy systems considering demand response and renewables. Energies, 15(4), 1647. doi: 10.3390/en15041647

Omojola, O., Li, F., Rong, H., and Huang, S. (2019). Multi-objective unit commitment for renewable-integrated power systems considering wind power ramping constraints. Applied Energy, 240, 876-888. https://doi.org/10.1016/j.apenergy.2019.02.039

Palizban, O., & Huang, A. Q. (2018). *Optimal Energy Management of Hybrid Renewable Energy Systems: A Review.IEEE Transactions on Sustainable Energy, 9*(4), 1672-1685.

Pan, L., Li, B., Li, J., Li, S., and Li, J. (2022). Coordinated unit commitment and economic dispatch of a wind-PV-battery hybrid power system considering uncertainties. Applied Energy, 310, 117893.

Parmar,A and Doshi,D (2018) Solution of Unit Commitment Problem by using Artificial Intelligence Method. International Journal for Innovative Research in Science &Technology (5)6. ISSN (online): 2349-6010

Patel, H. K., Yadav, S., and Pandit, M. (2023). Optimal unit commitment for a renewable energy-integrated microgrid using modified whale optimization algorithm. Electric Power Systems Research, 200, 107335. doi: 10.1016/j.epsr.2022.107335

Sahebi, H., and Bozorg, M. (2022). Multi-Objective Dynamic Unit Commitment for Hybrid Energy Systems Considering Uncertainty and Demand Response. Applied Energy, 308, 117785. doi: 10.1016/j.apenergy.2022.117785

Salman,D and Kusaf,M (2021) Short-Term Unit Commitment by Using Machine Learning to Cover the Uncertainty of Wind Power Forecasting.Sustainability.13,13609. https://doi.org/10.3390/ su132413609.

Shang, X., and Liu, C. (2022). Unit commitment optimization of wind-power integrated energy storage system based on an improved particle swarm optimization algorithm. Energy Sources, Part A: Recovery, Utilization, and Environmental Effects, 44(1), 121-138.

Shi, H., & Wang, Z. (2021). A hybrid optimization algorithm based on particle swarm optimization and genetic algorithm for job-shop scheduling problem. Mathematics, 9(17), 2143.

Shi, Y., Zhang, W., & Liu, C. (2021). A Hybrid Particle Swarm Optimization Algorithm for Large Scale Optimization. Complexity, 2021, 6645069.

Soliman, M. H., Zobaa, A. F., and Abdelaziz, A. Y. (2019). Day-ahead scheduling of a renewable-based microgrid considering unit commitment and network constraints. Energies, 12(8), 1483. https://doi.org/10.3390/en12081483

Sun, Y., Gao, Z., Chen, X., Zhang, J., and Gao, W. (2022). Multi-objective Unit Commitment Considering Hybrid Energy Systems and Demand Response. IEEE Transactions on Sustainable Energy, 13(1), 659-669. doi: 10.1109/TSTE.2021.3075861

Wang, W., Liu, W., and Sun, Y. (2022). A combined rule-based and heuristic algorithm for unit commitment optimization of wind-hydrogen energy systems. Applied Energy, 318, 117928.

Wang, Y., and Shi, Y. (2019). Day-ahead unit commitment for hybrid renewable energy systems considering flexible demand response. Energies, 12(9), 1782. doi: 10.3390/en12091782.

Wang, Q., and Cui, Z. (2020). Simulated annealing for global optimization: Recent advances and applications. *Engineering Optimization*, 52(6), 974-996.https://doi.org/10.1080/0305215X.2019.1608771

Wang, L., Chen, G., & Li, H. (2021). A Hybrid Particle Swarm Optimization Algorithm with Improved Mutation Strategy. Journal of Computational Science, 54, 101319.

Wang, Y., Wang, S., & Zhang, D. (2021). A novel hybrid optimization algorithm based on particle swarm optimization and genetic algorithm. IEEE Access, 9, 93687-93695.

Wei, X., Gao, S., and Chen, H. (2022). A new unit commitment method of wind-solar energy storage hybrid system based on differential evolution algorithm. Journal of Energy Storage, 54, 103177.

Yang, Z., Xu, Z., Zhang, Y., Ma, F., and Cao, G. (2023). Joint Operation of Multi-Microgrids in Distribution Networks Considering Renewable Energy and Electric Vehicles. IEEE Transactions on Power Systems, 38(1), 280-291. doi: 10.1109/TPWRS.2022.3044204

Zhou, Y., Oo, A. M. T., and Wong, K. P. (2019). Optimal unit commitment with renewable energy integration using improved multi-objective moth-flame optimizer. Energies, 12(9), 1802. https://doi.org/10.3390/en12091802

Zhang, R., Ma, L., Zhang, L., and Fang, Z. (2019). Enhanced deterministic unit commitment with hybrid power system and demand response. IEEE Transactions on Sustainable Energy, 10(1), 396-405. https://doi.org/10.1109/TSTE.2018.2822921

Zhang, Y., & Bose, S. (2020). *Unit Commitment under Uncertainty: Robust, Stochastic and Chance-Constrained Approaches.* New York: Springer.

Zhang, H., Shi, Z., & Wang, Z. (2020). A novel hybrid optimization algorithm based on particle swarm optimization and genetic algorithm. In 2020 IEEE 11th

Zhang, F., Song, Y., Zhao, J., Wei, W., and Zhang, X. (2020). Optimal operation of a hybrid wind-pumped hydro storage system considering energy balance and economic benefits. Applied Energy, 266, 114951. https://doi.org/10.1016/j.apenergy.2020.11495

Zhang, Y., Wang, L., & Chen, X. (2021). A hybrid particle swarm optimization-genetic algorithm approach for multi-objective optimization problems. Applied Soft Computing, 98, 106898.

Zhang, H., Wang, X., & Zhao, Y. (2021). A Hybrid Particle Swarm Optimization Algorithm for Large-Scale Global Optimization. Soft Computing, 25(13), 9501-9518.

Zhang, Y., Wang, H., Liu, X., & Chen, Y. (2021). Hybrid Particle Swarm Optimization for Solving Constrained Optimization Problems. IEEE Transactions on Evolutionary Computation, 25(5), 853-866.

Zhang, X., Zhang, Y., Ji, X., Ye, P., and Li, J. (2023). Unit commitment of integrated energy systemconsidering conditional value-at-risk and P2G. Electric Power Systems Research, 221, 109398. https://doi.org/10.1016/j.epsr.2023.109398

Zhao, Y., Liu, H., and Wei, W. (2022). A hybrid moth-flame optimization algorithm for unit commitment of a wind-photovoltaic-battery hybrid power system. Applied Energy, 314, 117790

Zhong, W., Zhong, M., Zhang, C., and Li, J. (2023). A Hybrid Model for Unit Commitment in Hybrid Energy System. IET Generation, Transmission & Distribution, 17(1), 1-9. doi: 10.1049/gtd2.11978

Zuniga Vazquez, D. A., Ruiz Duarte, J. L., Fan, N., and Qiu, F. (2022). N-1-1 contingency-constrained unit commitment with renewable integration and corrective actions. Annals of Operations Research, 316(1), 493-511. https://doi.org/10.1007/s10479-021-04204-y

PAPER 77- UTILIZING MACHINE LEARNING ALGORITHMS FOR FOOD SAFETY MANAGEMENT: APPLICATIONS IN MONITORING AND ENSURING THE SAFETY OF FOOD LIPIDS

P.A. Obasa [1*], B.A. Adejumo [1], J. Agajo [2], S Olorunsogo [1].

[1] Department of Agricultural and Bioresources Engineering, Federal University of Technology, Minna.
[2] Department of Computer Engineering, Federal University of Technology, Minna.
[*] peter.obasa@futminna.edu.ng

ABSTRACT

This research examines how food safety management and machine learning are used to monitor and ensure palm oil safety. Triacylglycerides (TAGs) make up more than 95% of dietary lipid (palm oil), which is high in saturated fat, particularly palmitic acid. Conventionally, monitoring lipid content and safety are frequently characterized by a high level of manual work, a high cost of test sample/ equipment maintenance, and a lengthy time required even with the use of sophisticated machines like uHPLC, and GCMS. Considering Free fatty acids test on palm oil A, B, C, D, E, F, G, and H samples with values of 11.5 mgKOH/g, 10 mgKOH/g, 12 mgKOH/g, 7 mgKOH/g, 11 mgKOH/g, 8 mgKOH/g, 11 mgKOH/g and 14 mgKOH/g respectively. Comparing the imaging processing (black box models) of the samples in system training, a more unique approach will be needed. Machine learning can swiftly and cheaply assess lipid data for safety risks. Machine learning swiftly evaluates lipid data and discovers safety concerns, a viable solution. This paper examines current literature, impartial machine learning merits and cons, and food lipid research.

KEYWORDS: Analysis, Food, Intelligence, Lipid, Monitoring**.**

1. INTRODUCTION

Ensuring the safety of food is a matter of utmost importance for consumers, food producers, and regulatory organizations (Youngik, 2023). To ensure the safety and quality of food products, it is necessary to closely monitor several factors, such as the lipid content, and structural attributes (Figure 1). Kunlun and Huiyan (2023) reported that lipids have crucial functions in food since contribute to taste, consistency, and nutritional content. Nevertheless, it can also function as a substrate for lipid oxidation and the creation of detrimental chemicals, which cause hazards to the health of consumers (Youngik, 2023).

Fats, oils, and cholesterol are food lipids that are necessary for human nutrition and taste (Zheng et al.,2022). If not adequately managed, lipid-containing foods might deteriorate and contaminate, putting consumer health at risk (Delia *et al.,* 2021). Thus, effective food lipid safety techniques and technologies are needed throughout the production, processing, and distribution chain (Hasok, 2023).

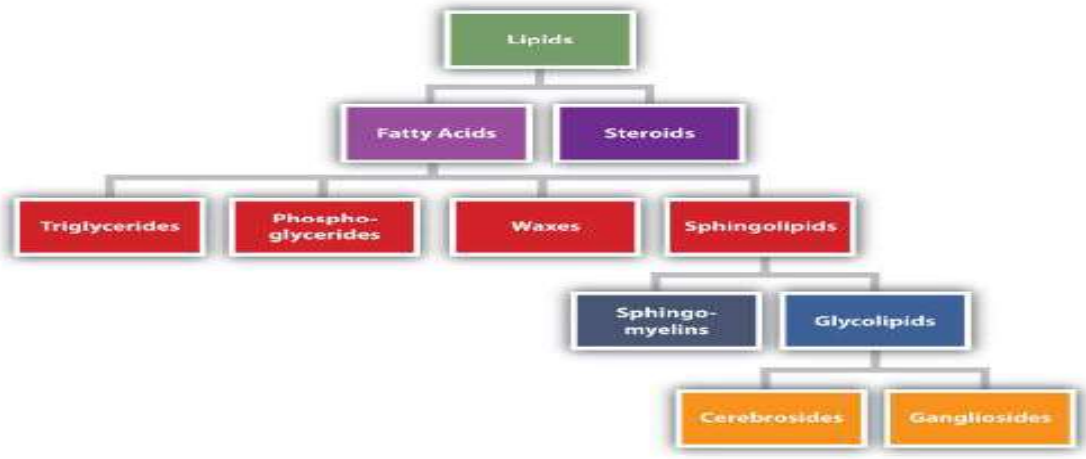

Figure 1: Structural Relationships of lipid (Source: Saylordotorg, 2023).

Machine learning (ML) algorithms may be a better way to monitor food lipid content than traditional approaches (Fayas *et al.,* 2023; Tatiana, 2023). These methods allow rapid analysis of massive datasets to identify trends that may signal lipid or chemical safety problems. Convolutional neural networks and supervised learning can improve food safety by characterizing lipids in real time, non-destructively, and cheaply (Magarelli *et al.,* 2023). This is possible using these algorithms. The combination of machine learning and electrochemical biosensors improves the detection and differentiation of lipids in complex food compositions. To assure food industry lipid sample quality and safety, machine learning and advanced sensing technologies work well.

An overview of the use of machine learning in food lipid safety

Machine learning is essential for improving food safety, specifically lipid safety. It facilitates the prediction of optimal solutions for optimizing food processing (Vinay *et al.,* 2023). It helps in identifying foodborne pathogens and outbreaks (Pujahari *et al.,* 2022) and automates the categorization of important literature in systematic reviews on food safety (Vandenbulk *et al.,*2022). Moreover, machine learning technologies have a role in enhancing the quality, safety, and traceability of food, while also minimizing waste (Zhe *et al.,* 2023). Machine learning approaches are employed in nondestructive technologies to check food quality, specifically lipid safety. These algorithms effectively handle complex data and construct calibration models (YuanJun *et al.,* 2022). In general, the research emphasizes the substantial influence of machine learning in guaranteeing food safety, specifically lipid safety, through diverse applications throughout the food business.

Multiple research projects have examined the application of machine learning algorithms in the field of food safety management, specifically emphasizing the monitoring of lipids. constructed a neural network model to forecast the process of lipid oxidation in edible oils by using spectroscopic data. This technique is consistent with other research endeavors that employ artificial intelligence to evaluate the quality of oil (Tatiana *et al* 2023). The model is expected to incorporate many spectral data preprocessing techniques to improve the accuracy of predictions, as observed in similar studies (JaeHwan *et al.,* 2022). The model can accurately identify antioxidants in oils by utilizing deep learning architectures such as CNN and RNN, resulting in a high classification accuracy (Sara *et al.,* 2023). Additionally, the study underscores the relevance of monitoring the degrees of oxidation in oils to guarantee the safety and quality of the product, emphasizing the importance of precise prediction methods (Yifan and Marc, 2023; Lu *et al*.,2020).

Integrating machine learning algorithms into food safety management systems provides several benefits, such as improved efficiency, precision, and scalability (Figure 2). Through the automation of lipid data analysis, these algorithms can expedite decision-making and intervention, consequently minimizing the likelihood of foodborne infections and guaranteeing consumer trust.

Figure 2: Machine Learning Algorithms (Source: Gao *et al.,* 2020)

Nevertheless, there are still obstacles that need to be addressed, specifically with the accessibility and accuracy of data used to train machine learning models. Moreover, the comprehensibility of these models and the incorporation of results into current food safety regulations necessitate thoughtful deliberation.

2. Food Lipids Significance in Nutrition and Safety Concerns

A. Comprehending the composition and importance of dietary lipids in nutrition:

Fats, or lipids, are vital to human nutrition and physiology. Wulff et al. (2023) and Domínguez et al. (2022) found that it provides twice the calories per gram compared to carbs and proteins. Cellular structure, energy storage, metabolite regulation, and gene expression depend on lipids (Martin-Perez *et al.,* 2022). Due to their hydrocarbon chain topologies, these compounds are hydrophobic. It is crucial to signaling pathways, membrane formation, and energy storage (Arellano et al.,2023). Fatty acids, fats, phospholipids, glycolipids, and lipoproteins are all lipids with different properties and activities (Tanyitiku *et al.,* 2023). Lipid categories and roles affect health and disease prevention, making balanced lipid consumption essential for overall health. Food lipids help fat-soluble vitamins (A, D, E, and K) and phytochemicals absorb. Omega-3 and omega-6 fatty acids are important lipids since the body cannot produce them and relies on nutrition for fatty acids (Figure 3).

Figure 3: Types of Cooking Oil (Source: Cookist, 2023).

1: Sesame oil, 2: Avocado oil, 3: Hemp oil, 4: Grape Seed oil 5: Flaxseed oil, 6: Peanut oil 7: Extra Virgin Olive Oil.

B. Primary safety considerations related to lipid-containing foods:

Rancidity is the oxidative deterioration of lipids, leading to the generation of unpleasant aromas and odors, a reduction in nutritional quality, and the possible creation of harmful compounds (Adejumo *et al.,* 2019).

- Contamination: Lipid-rich foods have the potential to be contaminated with pathogens such as Salmonella, Listeria, and E. coli, particularly when appropriate handling and storage procedures are not adhered to.

- Trans fats: The consumption of trans fats, which are produced through the process of hydrogenation, has been associated with an elevated risk of developing heart disease.

C. The necessity for efficient surveillance and control methods for lipid safety:

Unsafe lipid-based products are harmful and must be regulated (Xu *et al.,* 2020). For lipid maintenance, ischemic heart disease and diabetes necessitate monthly lipid profile monitoring (Carsten *et al.,* 2022). Propensity scores eliminate pharmacy surveillance bias and adjust for confounding variables in comparative safety studies. The Quality-by-Design strategy emphasizes total control for lipid product quality and patient safety. Lipid levels must be examined once a medicine is licensed to detect side effects and address public concerns. Effective clinical lipid safety surveillance requires a thorough understanding of processes and statistical analytics (Brown, 2021). Maintenance of high quality: Lipid-containing foods must be checked for freshness, stability, and microbiological contamination to ensure safety.

3. Challenges and Future Directions

Machine learning (ML) encounters obstacles in food safety management, including the intricacy of data processing, the requirement for proficient operators, and the inconsistency in testing settings (Hassan *et al.,* 2023) in samples like lipids can have the same physical appearance but physicochemical properties different, example of an ongoing machine learning biosensor system for lipid quality assessment (Figure 4) using methodology by (Siyanbola *et al.,* 2020). The examples of sample Free fatty acids for palm oil (A, B, C, D, E, F, G, H) were 11.5 mgKOH/g, 10 mgKOH/g, 12 mgKOH/g, 7 mgKOH/g, 11 mgKOH/g, 8 mgKOH/g, 11 mgKOH/g, and 14 mgKOH/g respectively. This makes the issue of using imaging (black box model) machine learning much more biased for food qualities, as also stated by Kevin *et al.,* 2020. Currently, there is no known method that enables the identification of different types of oil solely based on this specific property. Daimiwal *et al.,* 2023 reported the use of an Image Processing algorithm and smart sensor measurement and Instrumentation on oil samples but not qualities.

Machine learning models without explainability and bias can harm products with internal parameters. Decision-making systems that ignore prejudice may discriminate against certain demographic groups (Zhao et al.,2023; Anna *et al.,* 2023). Overlooking explainability can also impair bias detection and mitigation in computer vision models, affecting model reliability and fairness (Yuying et al.,2022). In distributed machine learning environments, where openness is key, inconsistent explanations due to limited training data might erode model trust, hampering ethical applications across food manufacturing. Thus, machine learning models must be explainable and fair to reduce biases, increase transparency, and promote ethical behaviour in society and industry.

There need to develop machine learning for food lipids to overcome the use of conventional techniques is slow, stressful, and takes a lot of manual work, that depends on the skills of experts, which makes it difficult to efficiently discover quality issues as fast as possible (Max, 2023). Furthermore, guaranteeing the quality of food entails addressing concerns such as contamination, spoilage, and mismanagement at every stage of the supply chain, which poses challenges in terms of monitoring and preventing problems (Yuan-Jun *et al.,* 2022).

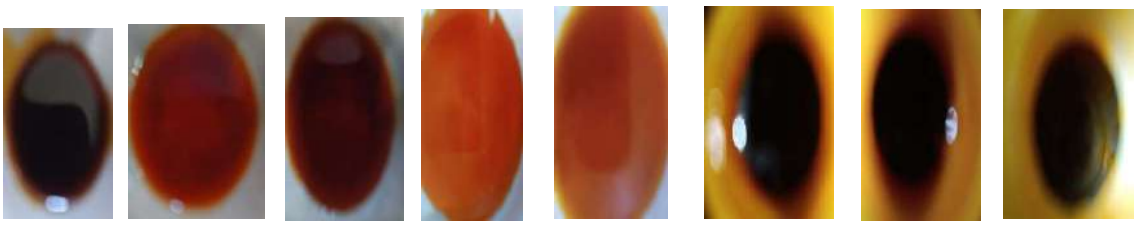

Figure 4: Palm oil Samples for image processing Machine Learning.

Artificial intelligence technologies speed up and improve quality monitoring control. Increased food distribution efficiency and cheaper pricing assistance will solve food production problems (Jun *et al.,* 2022). Combining machine learning algorithms with nondestructive technology like electronic noses allows for fast and affordable food quality assessment in numerous areas. This method avoids subjectivity and lengthy analysis (Alberto *et al.,* 2023). Effective lipid safety surveillance and control systems face data quality, user involvement, and process comprehension issues. Poor data quality, integration, and visualization are data issues (Kreimeyer *et al.,* 2022). User expectations and involvement in automated solution development are challenges (Carsten *et al.,* 2022). Mean particle diameter and particle distribution tailing for lipid safety must be regulated to ensure patient safety (Kellsey *et al.,* 2021). These data-related concerns require advanced methods like natural language processing and proven mathematical models. Additionally, user participation in system development is essential. Maintaining product quality and patient safety requires a detailed understanding of process parameters and control strategies.

B. Future research directions and potential applications

Progress in non-destructive technologies including machine vision, electronic nose, and spectrum imaging will drive food lipid safety machine learning algorithm development. Deep learning is also examined (Sravya *et al.,* 2023). These technologies effectively analyze complicated data and generate calibration models to evaluate lipid quality and safety. For biosensing systems devices, white box models with internal test settings are recommended. These systems detect and monitor biomolecules, toxins, and chemicals using biological molecules or living cells (Obasa *et al.,* 2023). CNNs can detect fruit freshness, showing that machine learning algorithms can inexpensively and non-destructively evaluate lipid quality by the use of external feature tests (Yuan-Jun *et al.,* 2022). AI and IoT improve food safety inspection data training, showing that deep learning can address food industry lipid safety issues (Habib *et al.,* 2023). Deep Learning (DL) outperforms manual feature extractors and standard food science methods. Non-invasive analytical methods and machine learning algorithms can be used to monitor food quality and safety, especially Extra Virgin Olive Oil. Food safety has improved due to machine learning's ability to predict antibiotic resistance, outbreaks, and risks. These findings suggest that machine learning research could improve food lipid safety and quality by looking into the gray box model a type of model that combines aspects of both black box and white box models.

4. Ethical and regulatory considerations in the use of machine learning for food safety

Several strategies could ensure precision and fairness in food lipid safety machine learning algorithms. In developing equitable machine learning algorithms, proactive conduct is crucial since it can greatly affect results (Vinay*et al.,* 2023; Revathi, 2023). Machine learning algorithms can automatically categorise relevant papers, saving effort and ensuring a thorough food safety literature review (Yufeng *et al.,* 2023). A supervised end-to-end learning strategy can also help identify oil-specific fatty acid patterns. This can help identify oil adulteration and mislabeling (Shaina, 2023). Pathogen genomes and other data streams can be analyzed using machine learning to predict antibiotic resistance, illness origins, and foodborne outbreaks (Tarini, and Ilias. 2023). These steps enhance machine learning algorithms' food lipid safety accuracy and fairness. This study covers several significant aspects.

A. Ethical Considerations

As machine learning revolutionizes food lipid analysis, ethical issues arise. Food industry lipid (palm oil) analysis utilizing machine learning: ethical considerations. To promote appropriate and equitable use of these technologies, ethical frameworks and guiding principles must be examined to address data privacy, bias mitigation, and transparency to encourage informed debate and ethical decision-making in this rapidly evolving sector.

Machine learning algorithms are trained on biased data, which can lead to skewed models. This may overemphasize some food producers or ignore food category concerns.

Transparency and Explainability: ML models are black boxes since their decision-making process is opaque. Lack of transparency may damage system trust (Revathi, 2023). Protection and secrecy of food safety data. Machine learning models may require large amounts of sensitive data. Data security and privacy must be maintained throughout the process.

B. Regulatory Affairs

To ensure food safety with machine learning technologies, regulatory issues must be included. The intersection of food lipid analysis with machine learning reveals the challenges, opportunities, and regulations that affect this emerging field. Regulatory Alignment: Machine learning may conflict with food safety regulations. Emerging technologies may demand regulatory changes (Yufeng *et al.,* 2023).

Considering Model Collection and Reliability:

The model presents a collection of principles that ensure the reliable application of machine learning in the context of food safety. These principles include security, accountability, fairness, explainability, and transparency, with privacy serving as an overarching concept.

Facilitating open and transparent communication among all stakeholders (developers, regulators, industry, consumers) is crucial for establishing trust and resolving concerns. Through meticulous examination of these ethical and regulatory factors, can guarantee that machine learning (ML) is employed responsibly and efficiently to enhance the safety of our food supply.

5. CONCLUSION

In conclusion, machine learning algorithms can check food lipid safety to improve quality and reliability. Machine learning algorithms can identify contaminants, adulterants, and lipid degradation using spectroscopy, chromatography, and image analysis, but oil types and quality must be identified. Machine learning reduces consumer health risks and enhances regulations. Scalable and adaptable machine learning algorithms can improve lipid for food safety and regulatory compliance. With robust data analysis, predictive modeling, and quality assurance solutions, machine learning improves food safety risk assessment and mitigation to preserve public health and food product confidence.
Researchers must innovate, invest in technical infrastructure, and collaborate to improve food safety and reliability via machine learning using the grey box model to strike balances. Food safety management must be proactive, data-driven, and resilient to new dangers using cutting-edge technology that studies the internal structure of food lipids as judgment bias for machine learning.

REFERENCES

Adejumo, B. A., Agboola, J. B., Orhevba, B. A., Obasa, P. A., & Simeon, M. I. (2019). Optimisation of the productionparameters of Delonix Regia Methylester using Box-Behnkendesign.http://repository.futminna.edu.ng:8080 /jspui/handle/12345678/4864.

Alberto, T., Christian, R., & Rallou, T. (2023). An Intercontinental Machine Learning Analysis of Factors Explaining Consumer Awareness of Food Risk. Future foods, doi: 10.1016/j.fufo.2023.100233.

Anna, Arias-Duart., Victor, Gimenez-Abalos., Ulises, Cortés., Dario, Garcia-Gasulla. (2023). Assessing Biases through Visual Contexts. Electronics,doi: 10.3390/electronics12143066.

Arellano, H., Nardello-Rataj, V., Szunerits, S., Boukherroub, R., & Fameau, A. L. (2023). Saturated long chain fatty acids as possible natural alternative antibacterial agents: Opportunities and challenges. *Advances in Colloid and Interface Science*, 102952. doi: 10.1016/b978-0-323-91599-1.00003-1.

Brown, R. E. (2021). *A precision medicine approach to lipid monitoring in the secondary prevention of cardiovascular disease* (Doctoral dissertation, University of Glasgow). https://scholar.google.com/scholar?hl=en&as_sdt=0%2C5&q=Rosemary%2C+Elisabeth%2C+Brown.+%282021%29.

Carsten, G., Volker, K., Peter, C. (2022). A New Control Strategy for High-Pressure Homogenization to Improve the Safety of Injectable Lipid Emulsions. Pharmaceutics, doi: 10.3390/pharmaceutics14081603.

Cookist (2023). 10 Yummy Types of Cooking Oil and How to Use Them: https://www.cookist.com/10-yummy-types-of-cooking-oil-and-how-to-use-them/ extracted on 12th April 2024.

Daimiwal, N., Shriram, R., Shinde, H., Kulkarni, R., & Galewad, A. (2023). Oil Quality Analysis Using Image Processing. In *Smart Sensors Measurement and Instrumentation: Select Proceedings of CISCON 2021* (pp. 129-137). Singapore: Springer Nature Singapore.

Delia, B., Rodriguez-Amaya., Fereidoon, S. (2021). Oxidation of lipids. doi: 10.1016/B978-0-12-817380-0.00004-X.

Dominguez, R., Pateiro, M., Purriños, L., Munekata, P. E. S., Echegaray, N., & Lorenzo, J. M. (2022). Introduction and classification of lipids. In *Food Lipids* (pp. 1-16). Academic Press. doi: 10.1016/b978-0-12-823371-9.00018-6.

Fayas, A., O., Nibouche., James, U., Jun, J., Liu., Jordan, Beth, Vincent., Hui, W. (2023). Miniature spectrometer data analytics for food fraud. Journal fur Verbraucherschutz und Lebensmittelsicherheit-Journal of Consumer, doi: 10.1007/s00003-023-01439-8.

Habib, S., Harish, K., Ali, A. (2023). Artificial Intelligence and Deep Learning-Based System for Agri-Food Quality and Safety Detection. Wasit journal of computer and mathematics science, doi: 10.31185/wjcms.l45.

Hasok, C. (2023). Advancements in Food Processing Technologies: Enhancing Safety, Quality, and Sustainability. Indian Scientific Journal Of Research In Engineering And Management, doi: 10.55041/ijsrem23682.

Hassan, A., Talha, A., Shamas, M. (2023). Review on food quality assessment using machine learning and electronic nose system. Biosensors And Bioelectronics: X, doi: 10.1016/j.biosx.2023.100365.

JaeHwan, L., Won, Young, O. (2022). Methods determining the degree of oxidation in edible oils and prediction for the oxidative stability. Food Science and Industry, doi: 10.23093/fsi.2022.55.4.432.

Jun, K, Han., T, Li., Yun, He., Quan, G. (2022). Using Machine Learning Approaches for Food Quality Detection. Mathematical Problems in Engineering, doi: 10.1155/2022/6852022.

Kellsey, A., Peterson., Gurleen, K., Eugenia, G., Sulagna, Mookherjee., Kim, A., Poli., Mandeep, S., Sidhu., Radmila, L. (2021). Challenges in Optimizing Lipid Management in Women.. Cardiovascular Drugs and Therapy, doi: 10.1007/S10557-021-07273-0.

Kevin, L., Kun, P., Zhe, Yu., Rong, Hui, X. (2020). Pattern recognition based on machine learning identifies oil adulteration and edible oil mixtures.. Nature Communications, doi: 10.1038/S41467-020-19137-6.

Kreimeyer, K., Spiker, J., & Botsis, T. (2022). Overcoming Major Barriers to Build Efficient Decision Support Systems in Pharmacovigilance. In *ICIMTH* (pp. 398-401). doi: 10.3233/shti220749.

Kunlun, L.,& Huiyan, Z. (2023). Lipid oxidation in foods and its implications on proteins. Frontiers in Nutrition, doi: 10.3389/fnut.2023.1192199.

Lu, C. H., Li, B. Q., Jing, Q., Pei, D., & Huang, X. Y. (2023). A classification and identification model of extra virgin olive oil adulterated with other edible oils based on pigment compositions and support vector machine. *Food Chemistry*, *420*, 136161.

Magarelli, G., Freire, A. M., & Silva, L. P. (2023). Electrochemical sensors coupled with machine learning for food safety and quality inspection. In *Food Quality Analysis* (pp. 171-200). Academic Press.

Martin-Perez, M., Urdiroz-Urricelqui, U., Bigas, C., & Benitah, S. A. (2022). The role of lipids in cancer progression and metastasis. *Cell metabolism*, *34*(11), 1675-1699. https://www.cell.com/cell-metabolism/pdf/S1550-4131(22)00447-8.pdf.

Max, S. (2023). AI Tools in Food Quality Monitoring. doi: 10.59646/csebookc12/004.

Obasa P.A, Adejumo B.A, Agajo J, Olorunsogo S (2023). Development of Adaptive Biosensor system approach for food products in storage (A Review*) Iconic Research And Engineering Journals* Volume 6 Issue 10 ISSN: 2456-8880.

Pujahari, R. M., & Khan, R. (2022). Applications of machine learning in food safety. In Artificial Intelligence Applications in Agriculture and Food Quality Improvement (pp. 216-240). doi: 10.4018/978-1-6684-5141-0.ch012.

Revathi, K. (2023). Machine Learning Algorithm Based Meat Spoilage Detection: To Avoid Foodborne Infection. International Research Journal on Advanced Science Hub, doi: 10.47392/irjash.2023.s042.

Sara, S., Maja, B., Davor, V., Jasenka, G, K., Ana, J, T., Tamara, J. (2023). Development of ANN Models for Prediction of Physical and Chemical Characteristics of Oil-in-Aqueous Plant Extract Emulsions Using Near-Infrared Spectroscopy. Chemosensors doi10.3390/chemosensors11050278.

Saylordotorg (2023). Lipids, https://saylordotorg.github.io/text_the-basics-of-general-organic-and-biological-chemistry/s20-lipids.html.

Shaina, R. (2023). Connecting Fairness in Machine Learning with Public Health Equity. arXiv.org, doi: 10.48550/arXiv.2304.0476.Sravya *et al.,* 2023.

Tanyitiku, M., & Mohajer, M. (2023). Luca Serventi, Kaichao Yang, Congyi Liu. *Sustainable Food Innovation*, 59. doi: 10.1007/978-3-031-12358-0_5.

Tarini, N., & Ilias, T. (2023). Machine learning models to predict micronutrient profile in food after processing. Current research in food science, doi: 10.1016/j.crfs.2023.100500.

Tatiana, O., Salvatore, Campisi, Pinto., C., Randieri., Andrea, P., Charles, L., Zeev, W. (2023). Semi-Autonomic AI LF-NMR Sensor for Industrial Prediction of Edible Oil Oxidation Status. Sensors, doi: 10.3390/s23042125.

VandenBulk, L. M., Bouzembrak, Y., Gavai, A., Liu, N., van den Heuvel, L. J., & Marvin, H. J. (2022). Automatic classification of literature in systematic reviews on food safety using machine learning. Current Research in Food Science, 5, 84-95. doi: 10.1016/j.crfs.2021.12.010.

Vinay, P., Shivangi, S., Kshirod, K., Dash., Rahul, Singh., Shaikh, Ayaz, Mukarram., Bela, Kovacs., E.G., H. (2023). Machine Learning Algorithms and Fundamentals as Emerging Safety Tools in Preservation of Fruits and Vegetables: A Review. Processes, doi: 10.3390/pr11061720.

Wulff, A. B., & Nordestgaard, B. G. (2023). Lipids and lipoproteins. *Danish Medical Journal*, *70*(7).https://content.ugeskriftet.dk/sites/default/files/2023-06/A03230185_WEB.pdf.

Xu, S., Robert, D., Wellman., Patrick, J., Heagerty., Jennifer, C., Nelson., Jennifer, C., Nelson., Andrea, J., Cook., Andrea, J., Cook. (2020). Safety surveillance and the estimation of risk in select populations: Flexible methods to control for confounding while targeting marginal comparisons via standardization. Statistics in Medicine, doi: 10.1002/SIM.8410.

Yifan, B., & Marc, P. (2023). Mechanisms of lipid oxidation in water-in-oil emulsions and oxidomics-guided discovery of targeted protective approaches.. Comprehensive Reviews in Food Science and Food Safety, doi: 10.1111/1541-4337.13158.

Youngik, Y. (2023). Food Safety Assurance Systems: Food Safety and Quality Management Systems. doi: 10.1016/b978-0-12-822521-9.00243-4.

YuanJun, Lin., Ji, M., Qi-Jun, Wang., Da-Wen, S. (2022). Applications of machine learning techniques for enhancing nondestructive food quality and safety detection. Critical Reviews in Food Science and Nutrition, doi: 10.1080/10408398.2022.2131725.

Yufeng, J., Tseng., Pei-Jiun, Chuang., Michael, A. (2023). When Machine Learning and Deep Learning Come to the Big Data in Food Chemistry. ACS omega, doi: 10.1021/acsomega.2c07722.

Yuying, Zhao., Yu, Wang., Tyler, Derr. (2022). Fairness and Explainability: Bridging the Gap Towards Fair Model Explanations. doi: 10.48550/arXiv.2212.03840

Zhao, Y., Wang, Y., & Derr, T. (2023). Fairness and explainability: Bridging the gap towards fair model explanations. In Proceedings of the AAAI Conference on Artificial Intelligence (Vol. 37, No. 9, pp. 11363-11371). doi: 10.1609/aaai.v37i9.26344.

Zhe, L., Shuzhe, W., Yudong, Zhang., Yichen, Feng., Jiajia, L., Hengde, Z. (2023). Artificial Intelligence in Food Safety: A Decade Review and Bibliometric Analysis. Foods, doi: 10.3390/foods12061242.

Zheng, Z., Yu-Lian, L., Feng, Z., Ran, Xin., Xu-Hui, Huang., Yuying, Zhang., Dong, Zhou., Lei, Qin. (2022). Unraveling the Thermal Oxidation Products and Peroxidation Mechanisms of Different Chemical Structures of Lipids: An Example of Molecules Containing Oleic Acid.. Journal of Agricultural and Food Chemistry, doi: 10.1021/acs.jafc.2c06221.

PAPER 78- QUALITY MANAGEMENT AS A TOOL TO MINIMIZE CONSTRUCTION WASTE TOWARDS A SUSTAINABLE BUILT ENVIRONMENT: THE CONSULTANTS' PERSPECTIVE

Buhari Saulawa Shehu[1], Ifeyinwa Ijeoma Obianyo[1*], Abdulhameed Danjuma Mambo[1], Abubakar Dayyabu[1], Akeem Amuda[1]

[a]Department of Civil Engineering, Nile University of Nigeria, Abuja, Nigeria
* Email: ifeyinwa.obianyo@nileuniversity.edu.ng

ABSTRACT

Construction industry generates significant amount of solid waste which could be attributed to poor quality management of resources in construction projects. This research paper examines the management of construction waste in Nigeria's Federal Capital Territory, focusing on consultants' perspectives. Using a 1 to 5 Likert scale, responses were qualitatively analyzed using SPSS software. The Relative Importance Index (RII) was calculated using Excel to determine the rank of factors. Initial research identified seventeen potential waste causative factors, however, RII analysis identified top 10 most significant waste causative factors with "Poor Materials Handling and Storage" being the most influential factor with a mean of 4.57. Pearson product correlation analysis showed a low correlation between "Inexperience designer" and "complicated design", which was statistically significant in the technical factor section. There were no correlating factors in the Management Factor Section, Workers Factor Section, and External Factor Section, indicating their independence. Consultants, according to the Chi-square test, acknowledged the crucial role of quality management in waste reduction within construction projects, emphasizing the importance of early identification and proper handling to reduce and mitigate waste. The findings highlight the need for quality waste management practices in F.C.T, Nigeria, in order to promote sustainability in construction activities.

KEYWORDS: Construction Waste, Quality Management, Waste Causative Factors, Waste Management

1. INTRODUCTION

Waste has emerged as a significant concern for both advanced and developing nations [1]. The amount of waste produced is consistently rising due to factors such as population expansion, individual lifestyle preferences, consumption habits, and advancements in technology. While waste creation might be unavoidable, minimizing it is achievable and can be done across all construction phases, starting from planning to demolition, an effective way to handle waste is by reducing it through thoughtful design, which lessens the burden on subsequent waste management phases [2]. Typically, waste arises from multiple factors working together rather than just one. It encompasses both material losses and unnecessary tasks, adding expenses without enhancing the product. In construction, waste diminishes efficiency, effectiveness, value, and profitability. Therefore, pinpointing its causes is crucial to reduce waste. Materials and resources play a crucial role in bolstering the construction sector. Nevertheless, many materials utilized in the industry aren't renewable, prompting a crucial need for the industry to transition towards employing recycled materials and embracing sustainable waste reuse in construction and demolition endeavors (Yang, 2020).

Despite the increasing global emphasis on sustainable construction practices, there exists a critical gap in understanding the efficacy of quality management strategies in mitigating construction waste from the viewpoint of consultants. Within the context of the built environment, there lacks comprehensive research examining how consultants perceive, implement, and harness quality management tools to curtail construction waste, hindering the attainment of a truly sustainable built environment. This gap necessitates a focused investigation into the consultants'

perspective on utilizing quality management as a pivotal tool to minimize construction waste, thereby unveiling essential insights crucial for advancing sustainable construction practices in F.C.T. Nigeria.

This research underscores the pivotal role of minimizing waste generation in ensuring the success and efficiency of waste management. Despite the increasing global emphasis on sustainable construction practices, there exists a critical gap in understanding the efficacy of quality management strategies in mitigating construction waste from the viewpoint of consultants. Within the context of the built environment, there lacks comprehensive research examining how consultants perceive, implement, and harness quality management tools to curtail construction waste, hindering the attainment of a truly sustainable built environment. This gap necessitates a focused investigation into the consultants' perspective on utilizing quality management as a pivotal tool to minimize construction waste, thereby unveiling essential insights crucial for advancing sustainable construction practices in F.C.T. Nigeria.

2. THEORETICAL ANALYSIS

2.1 Waste management in construction

Adewuyi maintained the fact that the construction sector holds significant importance in fulfilling societal requirements and improving overall life standards [3]. According to Salah and Din 2020, Construction holds a vital position in advancing a nation's infrastructure, yet the industry grapples with a significant challenge: construction waste [4]. Unlike many other sectors, construction tends to produce a substantial amount of waste. Throughout various stages of construction, such as excessive cement mixing, leftover concrete materials due to design alterations, rework, demolitions, and instances of subpar workmanship, waste is consistently generated. Construction materials are squandered during building, driving up project expenses, cutting into profits, and harming the environment. Recycling this waste is challenging, leaving cities with inadequate disposal space.

Efficient waste disposal is an urgent concern for numerous developing nations like Nigeria. Reports indicate that Nigeria experiences a high rate of construction waste generation, with less sustainable disposal methods in use. 13.6% material wastage, and there are more materials being wasted than what was initially estimated. This excessive material waste persists despite the high levels already accounted for. There is a lack of focus on managing construction waste in Nigeria and suggested that insufficient disposal methods and a lack of awareness might be the culprits [5]. Kareem and Asa 2020 provided evidence to back up their findings, it was elaborated that the large amount of waste produced is because of the easy access to cheap ways to dispose of it. This indicates the necessity for both government regulations and organizational guidelines.

2.2 Causative Factors of Generation of Waste

Construction waste is produced at every stage of a project, starting from pre-construction, continuing through construction, and extending to the finishing phase [6]. Identifying and comprehending the root causes of this waste right from its origin and the amount of construction waste isn't solely determined by the type of construction or the company involved. It's also influenced by the project site and the individuals participating in the project. The success of waste minimization in construction relies on how much the behavior of those involved in the process shifts concerning waste concerns.

Wastes from construction comes from various origins which encompass the pre-production stages, like material creation, design, material acquisition, and scheduling. Various methods exist to evaluate the primary roots, origins, and reasons behind construction waste [7]. Around 33 percent of on-site material waste is believed to stem from architects not implementing waste-reduction strategies effectively during a project's design phase. Furthermore, customers play a role, whether directly or indirectly, in generating waste on the premises. At the project level, the disposal of construction waste affects stakeholders' financial gains, reputation, project efficiency, and output. On a

larger scale, this waste contributes to environmental issues at both national and global levels. Governments also face financial burdens due to the costs associated with managing construction waste and its associated challenges.

2.3 Construction Waste Management and Minimization

During the project phases, a significant amount of waste is generated, particularly during planning and execution, it's crucial to prioritize material considerations. Efficient utilization and reuse of materials play a pivotal role in minimizing construction and demolition waste throughout each stage. Effectively managing construction waste has challenges, hindering the successful implementation of certain methods. Consequently, there's a genuine necessity for a thorough examination of prevalent strategies used in reducing waste in construction such as waste management practices, such as collecting, sorting, and reusing waste after it's produced, and source reduction measures [8]. The latter, when effectively applied, improve construction processes, leading to minimized waste generation.

3. MATERIALS AND METHODS

The methodology employed in this study aimed to delve into the perspectives and insights of consultants within the construction industry regarding the pivotal role of quality management in mitigating construction waste, ultimately contributing to the realization of a sustainable built environment. A purposive sampling technique was employed to select participants, targeting consultants with extensive experience and expertise in construction quality management. The sample encompassed a diverse range of consultants from different specialties and roles within the construction domain to ensure varied perspectives and comprehensive data collection. This method involves systematically identifying, organizing, and interpreting recurring themes and patterns in the data, enabling the extraction of meaningful insights and emerging trends concerning the role of quality management in waste reduction from the consultants' viewpoint.

The 1st procedure is the identification of various construction waste causative factors was done by a survey of questionnaires to consultants, (Project managers, Engineers Contractors and Quantity surveyors involved in construction projects. The Relative Importance Index (RII) was calculated using SPSS software. By Likert Scale, data analysis was done using the RII values of the identified risk factors for both the 'probability' and 'impact' of the risk. For this purpose, Likert scale ranging from 1-5 was used. The Likert scale ranged as 1= "strongly disagree" to 5= "strongly agree".

Further explanation of how the Relative Importance Index is calculated:

1. Collecting Data: Gather data on multiple variables that might influence a specific outcome or dependent variable.
2. Normalizing Data: Normalize the data to guarantee that all variables exist on a comparable scale. This step is crucial for preventing bias in the results.
3. Assigning Weights: Participants or experts frequently assign weights to each variable based on their perceived importance. Typically, one assigns these weights on a scale, such as 1 to 5, with a higher number indicating greater importance.
4. Calculating: Calculate the Relative Importance Index for each variable by multiplying the normalized score by the assigned weight. The formula often expresses this as follows:

$$RII = \left(\frac{\text{Normalized Score} \times \text{Weight}}{\text{Sum of (Normalized Scores} \times \text{Weights)}}\right)$$

SPSS software was also used to compute response frequency, percentages and mean. Qualitative analysis (Pearson's correlation and Chi-square analysis) was also done on the questionnaire survey responses.

The Pearson correlation coefficient (r) is one of the most common methods of measuring a linear correlation. It is a number between –1 and 1 that measures the strength and direction of the relationship between two variables. When one variable changes, the other variable changes in the same direction while the Chi-square analysis is a method used to interpret a two-way table and describe the problem of multiple comparisons. All these analysis methods are used to determine the most significant factors in the research.

4. RESULTS AND DISCUSSION

Causative factors identification of construction wastes in F.C.T, Abuja, Nigeria, was obtained from project managers, engineers, and contractors and quantity surveyors' perspective. 129 responses were gathered during the study out of the 132 targeted persons.

Relative Importance Index was calculated using Excel to determine the Rank. The RII results indicated that the top 10 most significant Waste causative factors in construction projects faced by Project Managers, Engineers and Contractors and Quantity surveyors in F.C.T, Abuja. Nigeria is; (1) Poor Materials Handling and Storage, (2) Lack of waste management, (3) Reworks Due to Errors, (4) Poor supervision/ Poor site management, (5) Waste resulting from packaging and leftover from cutting and shaping, (6) Poor site condition, (7) Accidents, (8) Effect of weather, (9) Non-availability of equipment, (10) Damage caused by workers and Workers' mistakes during construction.

Further analysis on SPSS computed the mean of the data as shown in Table 1 below deduced that Poor Materials Handling and Storage with a mean of 4.57 is the most causative factor. Other causative factors include Lack of waste management, Poor supervision/ Poor site management and Reworks Due to Errors amongst others.

Table 1: Descriptive Statistical Mean

Waste Causative Factors	**Mean**
Technical Factors	
Frequent design changes	2.65
Complicated design	2.02
Inexperience designer	2.53
Poor design quality	2.03
Management Factors	
Poor site condition	3.70
Non-availability of equipment	3.36
Lack of waste management	4.39
Poor supervision/ Poor site management	4.03
Reworks Due to Errors	4.02
Workers Factors	
Waste resulting from packaging and leftover from cutting and shaping	3.88

Poor Materials Handling and Storage	4.57
Damage caused by workers and Workers' mistakes during construction	2.64
Insufficient training for workers	1.85
Shortage of skilled workers and Lack of experience	2.08
External Factors	
Accidents	3.67
Effect of weather	3.31
High level of Vandalism	2.09

4.1 Pearson's Correlation Analysis

Using the 2-tailed Pearson correlation analysis, which is a valuable tool in waste management for construction projects that can help identify, quantify, and prioritize wastes, ultimately leading to more effective waste mitigation strategies and informed decision-making, below are the results from the Pearson Correlation of the listed causative factors.

Table 2: Pearson correlation (2-tailed) among the Technical Factor

		Frequent design changes	Complicated design	Inexperience designer	Poor design quality
Frequent design changes	Pearson Correlation	1	.181*	0.04	0.099
	Sig. (2-tailed)		0.041	0.655	0.265
Complicated design	Pearson Correlation	.181*	1	-.254**	-0.084
	Sig. (2-tailed)	0.041		0.004	0.344
Inexperience designer	Pearson Correlation	0.04	-.254**	1	.190*
	Sig. (2-tailed)	0.655	0.004		0.031
Poor design quality	Pearson Correlation	0.099	-0.084	.190*	1
	Sig. (2-tailed)	0.265	0.344	0.031	
	N	129	129	129N 129	129

From Table 2, as the data suggests, Inexperience designer with -0.254 is the only correlated factor in the technical factor section. Pearson product correlation of Inexperience designer correlating with Complicated design was found to have a low correlation and statistically significant ($r=-.254$, $p<0.004$). The negative correlation indicates the inverse proportionality of both variables to each other.

As the data suggests, there is no correlating factors in the Management Factor Section, Workers Factor Section and External Factor Section as each factor is independent of each other.

4.2 Chi-Square Analysis

After Pearson's correlation was conducted on Waste causative factors and only 2 of the causative factors had a negative low correlation in the technical section as the only correlating factor, further Chi-square analysis was done on the quality management practices responses gotten from the respondents.

Table 3: Quality management practices responses

Question	No	Yes	Total
Do you think consultants play a crucial role in promoting sustainable construction through Quality Management?	0	5	5
Do you believe that implementing Quality Management can significantly reduce construction waste?	13	111	124
Total	13	116	129

Table 3 show that most respondents (116 out of 129) think consultants play a crucial role in promoting sustainable construction through Quality Management and believe that implementing Quality Management can significantly reduce construction waste.

Table 4: Impact of quality management practices on construction waste generation responses

Question	No	Yes	Total
Would you like to integrate Quality Management for waste reduction in your construction projects?	0	5	5
Do you believe that implementing Quality Management can significantly reduce construction waste?	11	113	124
Total	11	118	129

Table 4 shows that most respondents (113 out of 129) would like to integrate Quality Management for waste reduction in your construction projects and believe that implementing Quality Management can significantly reduce construction waste.

Table 5: Role of consultants in promoting sustainable construction through quality management

Question	No	Yes	Total
Would you like to integrate Quality Management for waste reduction in your construction projects?	10	3	13
Do you think consultants play a crucial role in promoting sustainable construction through Quality Management?	1	115	116
Total	11	118	129

Table 5 shows that most respondents (115 out of 129) think consultants play a crucial role in promoting sustainable construction through Quality Management and would you like to integrate Quality Management for waste reduction in your construction projects.

4.3 Hypotheses Testing results analysis

H1: Poor Materials Handling and Storage contribute significantly to construction waste within the consultant's scope in F.C.T, Nigeria.

True: From the data collected and analysis done by the Relative Importance Index, Poor Materials Handling and Storage stands as the most significant waste causative factors in construction projects and contribute significantly to construction waste within the consultant's scope in F.C.T, Nigeria.

H2: Consultants perceive quality management as a pivotal aspect in waste reduction, emphasizing the need for standardized processes and continual improvement.

True: Conducting surveys and interviews with consultants proved that where robust quality management practices were implemented there is a direct link between these practices and the achievement of sustainability goals. Projects that integrated quality management principles such as resource optimization, efficient material usage, and adherence to sustainable construction standards showed notable improvements in environmental performance indicators. This suggests that effective quality management plays a significant role in advancing sustainability objectives within the built environment of F.C.T in Nigeria. Also, the Chi-square analysis from responses in Table 4.6 shows that consultants play a crucial role in promoting sustainable construction through Quality Management. This suggests that consultants' perception of effective quality management indeed contributes to waste minimization.

H3: The current waste management strategies employed in construction projects in F.C.T, Nigeria, are effective, sufficient and effectively mitigate, reduce waste in construction projects

False: This hypothesis assumes that the existing waste management strategies in projects within the Federal Capital Territory are adequate and effective. However, evidence and analysis revealed deficiencies in these strategies, indicating the potential for improvement. The existing strategies, though in place, often lack comprehensiveness or adherence in addressing the entirety of waste generated, leading to inefficiencies in waste reduction. Despite efforts, there are notable gaps in mitigating all potential adverse effects of construction waste, including environmental pollution and resource depletion.

4.4 Waste Handling Actions/Management Strategies

The research commenced by examining seventeen potential waste causative factors. Through RII analysis, it became evident that factors risks were less significant or relevant to the specific cases being studied. This observation stemmed from the recognition that construction work is heavily influenced by diverse environments and locations, thereby exposing projects to various waste generation throughout and after the construction process. Therefore, early identification of waste causative factors and their proper handling will help reduce these wastes and also mitigate them when encountered in the future thereby promoting quality waste management practices in F.C.T, Nigeria.

5. CONCLUSION

The findings from this study underscore the significant impact of quality management practices on addressing construction waste within the built environment, as perceived by consultants involved in construction projects in DADA Construction services limited, GILMOR Construction Company and Federal Road Maintenance Agency FERMA alongside other construction firms in F.C.T, Abuja, Nigeria. Consultants unanimously recognize the pivotal role of quality management in waste reduction. They perceive it not only as a tool for ensuring compliance but also as a proactive approach towards minimizing errors, optimizing resources, and fostering a culture of efficiency within construction projects. Their insights serve as a foundational framework for stakeholders to develop and implement strategies that effectively leverage quality management practices in minimizing construction waste, thus contributing to a more sustainable and resilient built environment for future generations. The findings of the study emphasize the integration of sustainability principles within quality management frameworks. An environmentally conscious approach, coupled with stringent quality controls, is fundamental in achieving a sustainable built environment by curbing wasteful practices. The findings of the study emphasize the integration of sustainability principles within quality management frameworks. An environmentally conscious approach, coupled with stringent quality controls, is fundamental in achieving a sustainable built environment by curbing wasteful practices. Lastly, the research echoes the fundamental principles outlined in ISO 9001 and ISO 14001, emphasizing the integration of quality and environmental management systems where consultants recognize the significance of these standards in guiding their practices towards waste reduction and sustainable development goals.

ACKNOWLEDGMENT

Special thanks and gratitude go to Nile university in Nigeria for the utmost support during the extensive research throughout the research. Furthermore, sincere gratitude to the civil engineering lecturers and entire staff at nile university for the constant support and guidance and the prestigious university of Ilorin for providing a supportive medium.

REFERENCES

Abioye, A. O. (2015). Sustainable Approach to Managing Construction and Demolition Waste: An Opportunity or a New Challenge? *International Journal of Innovative Research in Science, Engineering and Technology*, Vol. 4, Issue11, November.

Adewuyi, T. (2012). Construction Material Waste Planning and Control Techniques on Building Sites in South-South of Nigeria. Ph.D. Thesis, Department of Building, Faculty of Environmental Studies, University of Uyo, Uyo, Nigeria

Ahmed, A., Othman, E., & Ibrahim, A. N. (2014). "The Impact of Lean Construction Techniques on Waste Reduction." Procedia Engineering. [DOI: 10.1016/j.proeng.2018.07.063]

Ajani, O. (2007). Determinants of an effective solid waste management in Ibadan Metropolis Oyo State, Nigeria. J. Food Agric. Environ., 6, 152–157.

Alhawamdeh, M. (2023). *Environmental Sustainability*. *January 2021*. https://doi.org/10.18848/2325-1077/CGP/v18i01/1-33

Asase, M., & Yanful, E. M. (2009). Comparison of municipal solid waste management systems in Canada and Ghana: A case study of the cities of London, Ontario, and Kumasi,Ghana. Waste Management. 29, 2779–2786.

Nagapan, S., Rahman, I. A., Asmi, A., Memon, A. H., & Latif, I. (2012). *Issues on Construction Waste : The Need for Sustainable Waste Management*. *December*. https://doi.org/10.1109/CHUSER.2012.6504333

Osmani, M. (2013). "Design Waste Mapping: A Project Life Cycle Approach." In Proceedings of the Institution of Civil Engineers - Waste and Resource Management 166 (3): 114–127. https://doi.org/10.1680/warm.13.00013.

Salah, E., & Din, U. (2020). International Journal of Advance Engineering and Research. *International Journal of Advance Engineering and Research Development*, *6*(December 2019), 270–276. https://doi.org/10.21090/IJAERD.28000.

Yang, Y. (2020). Sustainable construction waste management in China: Challenges, strategies, and opportunities.

PAPER 79 -THE POTENTIAL OF JATROPHA CURCAS EXTRACT (JATROPHA CURCAS OIL) IN MODIFICATION OF BITUMEN

O. I. Jimoh[1], A. Dayyabu[1], I. I. Obianyo[1], D. Akinmade[2,3]

[1]Department of Civil Engineering, Nile University of Nigeria, Abuja, Nigeria.
[2]Faculty of Civil Engineering & Geoscience, Delft University of Technology, The Netherlands.
[3]Nigerian Building and Road Research Institute, Abuja, Nigeria.
[*]Email: issajimoh2@gmail.com

ABSTRACT
This research objective is to determine the feasibility of Jatropha Curcas Extract as a novel bio modifier by evaluating the interactions between Jatropha Curcas Oil (JCO) and bitumen, incorporating JCO into bitumen, and comparing the index, chemical, and performance properties of the modified samples with 60/70 Penetration Grade (PG) neat bitumen. JCO was chosen because it is a cheap, non-edible, renewable, environmentally friendly crop with high unsaturated fatty acids which makes it suitable as a biolubricant with good binding properties. Besides, this is also a way to reduce the environmental impacts of bitumen, improve sustainability by promoting the use of renewable resources, save cost, and enhance the rheological properties of bitumen. JCO was extracted from the Jatropha seeds by mechanical means and used to modify neat 60/70 PG bitumen. The unmodified and modified bitumen samples were tested for their index (penetration, softening, flash, and fire point tests), chemical (Fourier transform infrared spectroscopy) and rheological (dynamic shear rheometer-frequency sweet test) properties. The results achieved for a base and modified bitumen were analyzed and compared. These results showed that the use of JCO as a bio modifier in bitumen shows benefits in health, environmental, economic, and rheological perspectives.

KEYWORDS: Jatropha curcas oil, bio-modifier, penetration grade, bitumen, unmodified bitumen, penetration, softening test, flash, and fire point test, chemical properties, Fourier infrared transform spectroscopy, rheological properties, dynamic shear rheometer.

1. INTRODUCTION

It is impossible to disregard the significant role that liquid asphalt binders play in the development, upkeep, and repair of bituminous pavements. In addition, it is thought that bituminous surfaces cover more than 98% of Nigeria's 40.000 km of paved roads (Idusuyi, 2018). A variety of asphalt binder modifiers have been evaluated, developed, and used recently as a result of efforts to get improved binder properties. These modifiers aim to improve the performance of the basic binder and, in turn, the performance of the pavement (Zhang et al., 2020). Additionally, to improve the price and effectiveness of traditional binders due to rising expenses associated with them, several low-cost asphalt modification and extension approaches have been developed (Idusuyi, 2018). To maintain the high-temperature qualities of asphalt binder while enhancing its performance, particularly at the lower end of the service temperature range, a variety of oil-based modifications have recently been introduced (Zhang et al., 2020).

While a great deal of research has been done on how various polymer modifiers affect the properties of asphalt binders and how they work, little is known about the basic principles behind oil modification and how to best utilize its qualities. Furthermore, there is a lack of research on the effects of these novel bio binders and extenders on both short- and long-term performance(Idusuyi, 2018). In the highway sector, binder modification is becoming more and more significant. To improve binder qualities, a chosen additive must either interact chemically or molecularly with the binder to form a new balance system or secondary network inside asphalt binders (Zhang et al., 2019). To address these challenges and enhance the properties of bitumen, researchers are exploring eco-friendly additives for enhancing bitumen properties. Jatropha curcas, is a promising candidate due to its unique chemical composition and potential benefits in bitumen modification. Jatropha curcas oil, extracted from seeds, has been used in biodiesel production and medicinal uses. However, the potential of Jatropha curcas extract as a bitumen modifier remains relatively unexplored, highlighting the need for further exploration in the field of bio-modification.

The tables below show the physio-chemical properties of JCO. Table 1 shows the physical properties of JCO. From Table 2, the chemical tests show that JCO is majorly comprised of linoleic acid, palmitic acid, stearic acid, and oleic acid which are unsaturated fatty acids useful for their good adhesive properties.

Table 1. Physical Properties of JCO

Property	Value
Colour	golden yellow
Boiling Point	12 ^{o}C
pH	5.2
Specific Gravity	0.919
Density	0.73g/cm^3
Viscosity	8.0

Table 2. Fatty Acid Composition of JCO

Fatty Acid Composition	%
Oleic acid	14.3
Linoleic acid	49.1
Palmitic acid	14.3
Stearic acid	15.8
Linolenic acid	1.0
Myristic acid	2.98
Arachidic	1.83

Hence this study aims to evaluate the potential of Jatropha curcas oil in the realm of bitumen modification which would help to reduce the quantity of bitumen used (saving cost), increase sustainability, reduce environmental and health impacts by reducing carbon footprints in line with sustainable development goals and improve the performance properties of bitumen.

2. THEORETICAL REVIEW

Since the high cost of crude oil has been affecting bitumen production for a number of years, many academics are very interested in bio-waste materials and bio-oils as a way to reduce reliance on products generated from petroleum (Sun et al., 2019). This method has long been known to work, and it has been demonstrated that biomass or bio-waste products can be excellent sources of bio-binder (Rasman et al., 2018).

In a study, Asli H et al., (2018) investigated the effects of Waste Cooking Oil (WCO) as a rejuvenator for old bitumen on its index parameters. Several groups of aged bitumen were blended with 1, 2, 3, 4, and 5% of WCO at a constant speed of 200 rpm and temperature of 130°C. The findings revealed that the viscosity test and softening point results showed no discernible difference between the original and revitalized bitumen. Rasman et al., (2018) conducted a comparative experimental study to evaluate the physical and rheological properties of base bitumen and Waste Cooking Oil (WCO) modified bitumen. WCO was added to bitumen 80/100 pen at different bitumen weight concentrations, namely 1%, 2%, and 3%. The results showed that adding WCO to virgin bitumen caused it to become softer and more temperature sensitive. In terms of resistance to rutting, modified bitumen with a performance grade of PG 64—which is equivalent to the original bitumen—was produced by adding WCO up to 2%.Lin et al., 2022investigated bitumen modified by bio-oil from the manufacturing of bamboo charcoal in terms of its rheological characteristics and aging performance. The outcome showed that bitumen with bio-oil added softened it compared to basic bitumen. Additionally, bio-bitumen showed better resistance to fatigue fracture at shorter crack lengths and less Glover-Rowe characteristics when it came to brittleness. Abayomi et al., (2019) evaluated the performance of crumb rubber – bio-oil modified hot asphalt for sustainable highway pavements with varying percentages by volume (5%, 10%, 15%, and 20%) of bio-oil used for modification of bitumen. From this study, experimental results showed an increase in the base bitumen's flash point, fire point, and softening point.

Al-Omari et. al., (2018) examined the feasibility of bitumen modification with Waste Vegetable Oil (WVO). By bitumen volume, five percentages of WVO (by weight) were used; 1%, 2%, 4%, 6%, and 8%. The result of the study showed an increase in ductility, flash and fire points, resistance to rutting, penetration, and temperature susceptibility. Conversely, higher bitumen bio-oil modification levels (10%) led to increased fatigue resistance and low-temperature performance as demonstrated in the research conducted (Ullah et.al, 2021).

From the above studies, it can be seen that improved bitumen properties are majorly obtained at lower modification levels (1% to 10%). Hence this research will adopt similar levels by weight of bitumen (2%, 4%, 6%, and 8%).

3. EXPERIMENTAL PROCEDURE

This research aims to evaluate the potential of JCO as a novel bio-modifier in the modification of 60/70 Penetration Grade bitumen and this achieved through the following objectives:

i. Extract bio-oil from the Jatropha seeds and test its chemical composition

ii. Bitumen modification using the extracted bio-oil at various percentages (2%, 4%, 6% and 8%).
iii. Determine the physical, chemical and rheological properties of bitumen modified with Jatropha seeds bio-oil at various percentages.

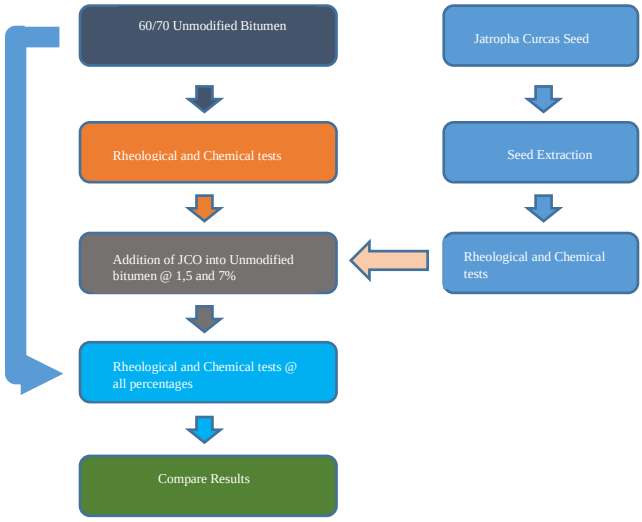

Figure 1. Experimental Flow Chart for the Study

3.1 Materials and Sample Preparation

3.1.1 Materials

The materials used in this study were conventional 60/70 PG bitumen and Jatropha curcas oil (JCO) as a modifier. The Jatropha Curcas seeds were obtained and extracted at the National Research Institute for Chemical Technology (NARICT) plantation in Zaria, Kaduna State, Nigeria. 60/70 PG bitumen was obtained from Ringardas Nigeria Limited (ASCA) in Abuja, Nigeria. The bio-oil was extracted from the Jatropha Curcas seed using a Cold Press Mechanical Grinding Machine and then passed through a Filtration Machine to ensure a bio-oil that is clean, pure, and free of contaminants.

Figure 2. Cold Press Machine

Figure 3. Filtration Machine

3.1.2 Sample Preparation

In compliance with AASHTO T-316, the bitumen was heated to a temperature of about 135-170 ^{o}C then blended with various percentages of JCO (2%,4%,6%, and 8%) by weight while continuously stirring at a rate of 300 rpm for 20 minutes and a constant temperature of 150 ^{o}C to ensure good homogeneity.

3.2 Laboratory Tests

3.2.1 Penetration

The penetration test was conducted to evaluate the JCO-modified bitumen's applicability, hardness, and consistency. Under AASHTO T 49, the typical test procedure for bituminous material penetration is explained. A standard needle was used to measure the penetration, which was measured in tenths of millimeters, through the bitumen sample under a 100g load and for five seconds at a temperature of 25°C. It is crucial to remember that bitumen with a lower penetration value has a firmer consistency, whereas greater penetration values indicate softer consistency.

3.2.2 Softening

The softening point test was used to evaluate the JCO-modified bitumen's temperature susceptibility. AASHTO T 53 specifies the standard technique of testing for softening points (Ring and Ball Apparatus). Two discs of specimens were formed using shouldered brass rings to conduct the test. Subsequently, the rings, or samples, were assembled and submerged in a beaker of water. Each ring, or sample, was loaded with a 3.5g steel ball. The water was heated from its starting temperature of 5ºC to a controlled rate, typically 5 ºC per minute. The mean temperature measured when the two balls covered in soft bitumen touched the bottom plate, which is located 25 mm below the rings, is the softening point. Bitumen's softening point is used to classify it, verify its homogeneity, and indicate its propensity to flow at high temperatures. In warm climates, a higher softening point is desired as it implies reduced vulnerability to temperature changes.

3.2.3 Flash and Fire Points

To ensure the safety and quality control of JCO-modified bitumen, it is important to assess its flammability and safety characteristics. This was done with the help of the Flash and Fire point test. According to (ASTM D92) which determines the temperature at which asphalt materials can safely be heated. About 70 ml of the samples were filled into the test cup and the thermometer was fixed and dipped into the sample (it shouldn't touch the bottom of the test cup). Heat was then applied to the sample gradually and continuously and a test flame was passed across the cup at specific intervals, the temperature at which the sample ignited for about a second was recorded (flash). Heating continued till the sample attained sustained combustion for at least 5 seconds (fire), this temperature was recorded. The temperature at which bitumen will flash for one second in a specific situation is known as the flash point. The lowest temperature at which bitumen will sustain combustion for five seconds in a specific situation is known as the "fire point."

3.2.4 Fourier Transform Infrared Spectroscopy (FTIR)

In a bid to identify molecular compounds and functional groups present in the samples, we employed the FTIR test which is a valuable analytical tool for understanding the relationship between bitumen and JCO. By using a scanning microscope, samples are scanned and their chemical properties are observed. The fingerprint of a sample is shown by the Fourier Transform Infrared Spectroscopy (FTIR), where the absorption peaks correlate to the vibration frequencies between the chemical bonds. The FTIR equipment exposed the material to infrared light with a wavelength range of 10,000 to 100 cm^{-1}, of which some were absorbed and some went through. The absorbed radiation was converted into vibrational and/or rotational energy by the sample molecules. The resulting signal is the molecular fingerprint of the sample and normally runs from 4000 cm^{-1} to 400 cm^{-1}. It emerged as a spectrum at the detector. FTIR analysis is an excellent method for chemical identification in materials since every molecule or chemical structure will produce a unique spectral fingerprint (Geçkil, 2019).

3.2.5 Dynamic Shear Rheometer (DSR)

In this study to ensure quality, there is a need to predict the rheological properties and performance of JCO-modified bitumen under various environmental and loading conditions, this was done with the aid of the DSR test. The Standard test method for determining the rheological properties of asphalt binder using the Frequency Sweep Tests with the aid of the dynamic shear rheometer is described in AASHTO T315-19. Following the standard procedure for testing (AASHTO T 315-19), complex shear modulus (G*) and phase angle (δ) were determined over a temperature ranging from 0ºC to 70ºC at an interval of 10ºC for low, intermediate, and high temperature, the frequency range of 10 Hz to 0.1 Hz and a strain load of 0.1%. This test involved subjecting all the bitumen samples to temperature and mechanical circumstances in a bid to assess the viscoelastic properties of the bitumen samples. This was done with the aid of the Kinexus + dynamic shear rheometer. This investigation was done in compliance with (EN,2012) specifications for determining complex shear modulus (G*) and phase angle (δ).

Figure 4. Loading Specimen onto the DSR machine

4. RESULTS AND DISCUSSION

4.1 Penetration

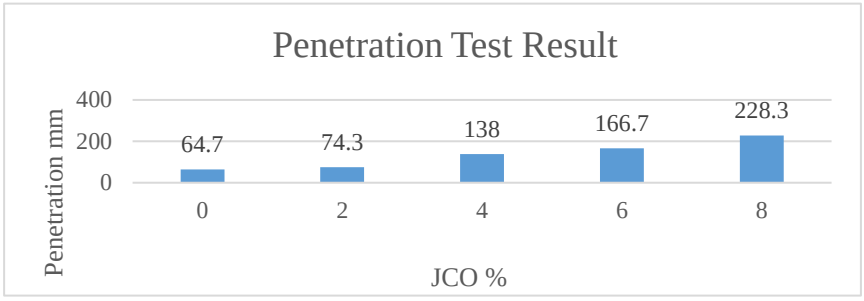

Figure 5. Penetration Test Results

The penetration test results reveal a distinct increase in the penetration values as the percentage of Jatropha curcas oil (JCO) increases. Compared to the control, the addition of 2% JCO shows a slight increase in penetration, suggesting a marginal softening effect. However, as the JCO content rises to 4%, 6%, and 8%, a significant increase in penetration is observed. This trend indicates a notable reduction in the stiffness of the modified bitumen. The initial softening effect at 2% JCO may offer benefits in specific applications requiring increased flexibility. However, the substantial increase in penetration at higher JCO concentrations raises considerations regarding the potential impact on rutting resistance and long-term durability.

4.2 Softening

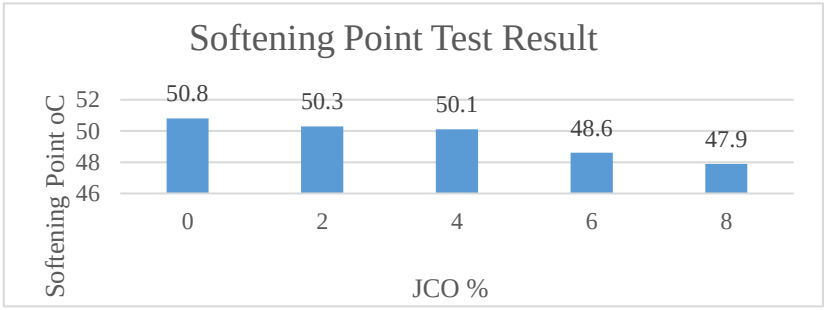

Figure 6. Softening Point Test Results

The softening point test results reveal subtle variations in the temperature at which bitumen samples transition from a solid to a semi-solid state. As observed in Figure 6, the incorporation of Jatropha curcas oil (JCO) at different percentages exhibits a subtle downtrend in softening point values. The marginal fluctuations within the range of 47.9°C to 50.8°C suggest that the presence of Jatropha curcas oil has a limited impact on the softening point of the JCO-modified bitumen.

The minor variations in softening point values among the control and JCO-modified bitumen samples indicate that, within the tested concentration range, Jatropha curcas oil does not significantly alter the temperature at which the bitumen softens. The relatively consistent softening points suggest that the addition of JCO at the investigated percentages does not induce a notable change in the overall stiffness or deformability of the bitumen matrix. This finding is crucial, particularly in applications where maintaining a specific softening point is essential for ensuring the stability and performance of bituminous materials. The observed stability in softening point values may contribute to the predictability and reliability of the JCO-modified bitumen in various climatic conditions.

4.3 Flash and Fire Points

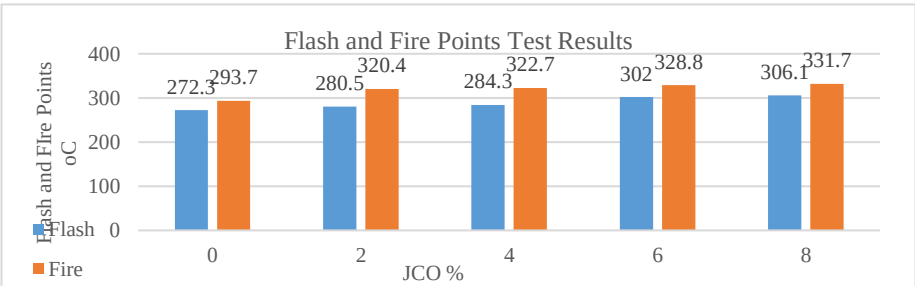

Figure 7. Flash and Fire Test Results

The flash and fire point test results reveal intriguing insights into the flammability characteristics of the modified bitumen samples. The flash point exhibits a gradual increase with the addition of Jatropha curcas oil, indicating an improved resistance to low-temperature ignition. This enhancement aligns with the expectation that bio-based additives, contribute to a higher flash point, thereby reducing the risk of ignition under lower temperature conditions. Simultaneously, the fire point values also exhibit a noteworthy rise as the percentage of Jatropha curcas oil increases. The fire point represents the temperature at which sustained combustion occurs. The observed increase in fire point values implies an augmented resistance to sustained combustion for the modified bitumen samples. This is particularly evident with the samples containing 6% and 8% JCO, showcasing a substantial elevation in fire point compared to the control. The combined analysis of flash and fire point results underscores the multifaceted impact of Jatropha curcas oil on the flammability characteristics of bitumen. The elevated flash point and, more prominently, the increased fire point of the modified samples suggest a potential improvement in the safety profile of bituminous materials. This is particularly relevant in applications where fire resistance is a critical factor.

The Penetration, Softening point and Flash and Fire results show a strong correlation with a study by Al-Omari et.al. (2018); an increase in the amount of bio-oil (WVO) in bitumen resulted in an increase in the penetration, improved resistance to ignition and combustion, improved flowability and workability of bitumen and a reduction in the softening point values i.e temperature susceptibility.

4.4 Fourier Transform Infrared Spectroscopy

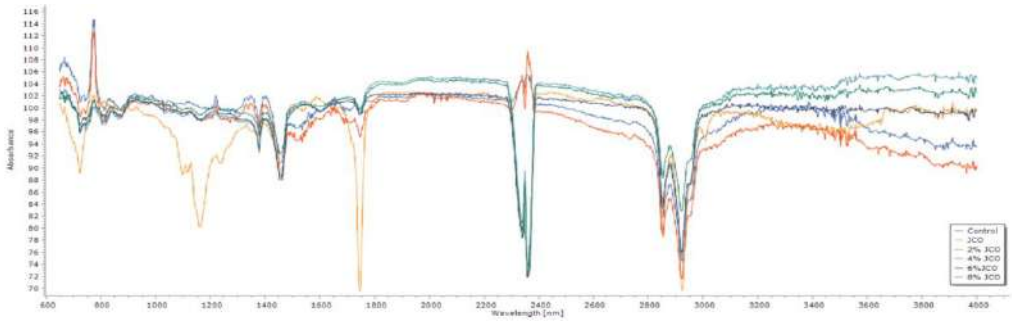

Figure 8. Superimposed FTIR Spectra

The chemicals, functional groups, and chemical structure of the materials were identified using FTIR. From Figure 8, the JCO spectrum reveals that the alkene peak was at 2924.18 cm-1. Two additional strong alkene peaks were at 2360.95 cm-1 and 1743.71 cm-1. Methyl, Ester carbonyl, and alkene compounds formed relatively weak peaks at 1458.23 cm-1, 1161.19 cm-1, and 721.40 cm-1 (aromatic ring), respectively. According to these analyses, the JCO was primarily composed of alkenes, which are aromatic rings, with traces of methyl and Ester carbonyl groups, primarily C, H, and O. Similar findings using Biochar were also obtained by Feng et.al., (2022) and Sheng et. al., (2014). On the other hand, the chemical structure of 60/70 neat bitumen used in this study has its alkene peak formed at 2920.32 cm-1 and two other weak peaks at 1456.30 cm-1 (methyl) and 732.97 cm-1 (alkene). These findings indicate the control bitumen comprises mainly aromatic alkene groups and traces of methyl group. This high content of aromatic carbon alongside a corresponding high content of aromatic carbon in JCO will help in achieving homogeneity and stability in the JCO-modified bitumen. FTIR spectra of the JCO-modified bitumen samples at various percentage modifications (2,4,6 and 8%) revealed similar absorption frequency peaks (2920.32 cm-1, 2360.95 cm-1, and 1456.30 cm-1), functional groups (C-H stretching and bending) and compounds (alkene and methyl groups). Comparing the spectra and analysis of the JCO-modified bitumen samples with that of neat bitumen, they all share peaks at 2920.32 cm-1 and 2360.95 cm-1 corresponding to alkene -CH2- (methylene) and that at 1456.30 cm-1 corresponds to methyl -CH3-. It is however worthy of note that the JCO-modified bitumen showed a similar position as the characteristic peaks, chemical structure, functional groups, and compounds as the neat bitumen. The main components of all bitumen samples are aromatic, and hydrocarbon compounds. This result shows that the stable homogeneous mixture of JCO and bitumen is purely physical, and no chemical alterations were formed or made due to this modification, as the internal chemical structure showed no distinctive difference or formation of new compounds.

4.5 Dynamic Shear Rheometer

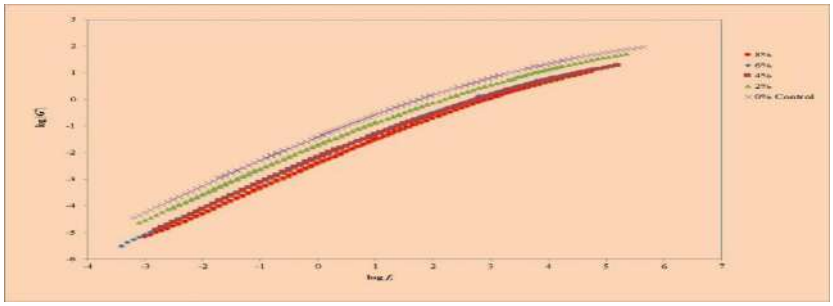

Figure 9. A master curve showing complex shear modulus - reduced frequency relationship on a log scale

Feng et. al, (2022) in their study (Biochar for asphalt modification), explained that a lower complex modulus of binders reduces the resistance to rutting in pavements and vice versa. From Figure 9 above, it can be seen that the complex modulus reduced with an increase in frequency (i.e when log *f*T was -1Hz, the corresponding moduli for the bitumen samples were -2.3, -2.7, -3.2,-3.3, and -3.6 kPa). A significantly lower complex modulus of binder translates to lower resistance to rutting in pavements. However, it can be seen that comparing the base bitumen's modulus at -1Hz (-2.3kPa) and that of 2% modification (-2.7kPa), the complex modulus of 2% JCO modified bitumen reduced by 17.39%. This shows that the resistance to deformation of the binder is reduced by the addition of JCO. Also, it can be seen that compared to the control bitumen, an increase in the percentage of JCO reduced the upward tendency of complex shear modulus (i.e the reduction in the effect of complex shear modulus on binder) thus reflecting better lower temperature properties which invariably implies improved resistance to shrinkage and this translates to better anti-cracking performance of the binder.

5. CONCLUSION

In the realm of bio modification of asphalt binder, this study explored bitumen modification with various percentages of Jatropha Curcas Oil (2,4,6 and 8%). After modification, the index and rheological properties of the base and modified bitumen were investigated. The following primary conclusions were drawn based on the experimental test results;

i. The marginal reduction in softening point and a distinct uptrend in penetration values indicate that JCO reduces the binder's viscosity and resistance to deformation.
ii. The continuous increase in flash and fire points with a corresponding increase in the percentage of JCO in bitumen directly translates to enhanced quality control and safety characteristics as the incorporation of JCO makes it less prone to ignition and combustion.
iii. The FTIR analysis of the base and modified bitumen samples revealed similar functional groups, compounds, and frequency peaks. The FTIR analysis for JCO showed that it comprises aromatic rings mainly alkenes and traces of methyl and ester carbonyl groups. This high content of aromatic carbon with a corresponding high content of aromatic carbon in bitumen contributed majorly to achieving a stable suspension in the JCO-modified bitumen samples. In addition, no chemical reaction was detected in the binder modification process.
iv. The incorporation of JCO lowered the complex shear modulus of the binder which indicates a reduced resistance to deformation but reflects improved low-temperature performance of the binder with better resistance to shrinkage and cracking.

Thus, the use of JCO as a bitumen modifier is feasible. Owing to better low-temperature performance, better resistance to ignition and combustion, improved shrinkage and anti-cracking performance, and its stability with bitumen. A more in-depth analysis of the Life Cycle Assessment, Cost Savings Assessment, Environmental Implications, Long Term Durability, and the Limitations of widespread adoption will be carried out in future research.

Based on the aforementioned conclusions, the following recommendations are advised or suggested:

i. Having obtained notably high penetration values in the JCO-modified bitumen samples, it is recommended to employ a modification process for lower penetration grade bitumen to elevate it to a higher PG that meets the predominant 60/70 PG standard used in Nigeria.
ii. It is recommended that JCO be explored as a rejuvenator in bitumen from Reclaimed Asphalt Pavements.
iii. In conclusion, this thesis recommends exploring Scanning Electron Microscope (SEM) analysis techniques to have a deeper and more refined understanding of JCO-modified bitumen at a microscopic level.

ACKNOWLEDGEMENT

This research appears in its current form due to the assistance and guidance of several people. For this reason, I would want to sincerely thank every one of them, including the ones who aren't mentioned below. I express my gratitude to the National Building and Roads Research Institute (NBRRI) and the National Research Institute for Chemical Technology (NARICT) for their significant contributions to my academic pursuits and for their unwavering support. Finally, from the deepest of my heart, I would like to thank my family and friends for their care, support, and encouragement.

REFERENCES

Abayomi, M. E., J, G. A., John L, R. A., D, R. O., & Dc, R. O. (2019). Article ID: IJMET_10_02_029. International Journal of Mechanical Engineering and Technology (IJMET), 10(2), 273–287. http://www.iaeme.com/ijmet/issues.asp?JType=IJMET&VType=10&IType=02http://www.iaeme.com/IJMET/index.asp274http://www.iaeme.com/IJMET/issues.asp?JType=IJMET&VType=10&IType=02

Al-Omari A. A, Khedaywi T. S, & Khasawneh M. A. (2018). Laboratory characterization of asphalt binders modified with waste vegetable oil using Superpave specifications. International Journal of Pavement Research and Technology In Press.

Asli H, Ahmadinia E, Zargar M, & Karim M R. (2012). Investigation on physical properties of waste cooking oil – rejuvenated bitumen binder. Construction and Building Materials, 37, 398–405.

Feng Ma, Jiasheng Dai, Zhen Fu, Chen Li, Yalu Wen, Meng Jia, Yujie Wang, Ke Shi (2022). Biochar for asphalt modification: A case of high-temperature properties improvement. Journal of Science of the Total Environment 804 (2022) 150194

Geçkil, T. (2019). Physical, Chemical, Microstructural, and Rheological Properties of Reactive Terpolymer-Modified Bitumen. Materials, 12(6). https://doi.org/10.3390/MA12060921

Idusuyi D.U. (2018). THE MODIFICATION OF ASPHALT BINDERS USING BIO-OIL IN FLEXIBLE PAVEMENTS.

Lin, H., Chen, Q., Luo, X., Zhang, Y., Miao, K., Li, T., & Wang, K. (2022). Characterization of rheological properties and aging performance of bitumen modified by bio-oil from bamboo charcoal production. Journal of Cleaner Production, 338, 130678. https://doi.org/10.1016/J.JCLEPRO.2022.130678

Rasman, M., Hassan, N. A., Hainin, M. R., Putra Jaya, R., Haryati, Y., Shukry, N. A. M., Abdullah, M. E., & Kamaruddin, N. H. M. (2018). Engineering properties of bitumen modified with bio-oil. MATEC Web of Conferences, 250. https://doi.org/10.1051/matecconf/201825002003

Sheng, Z., Huang, B., Ye, X.P., Xiang, S., Jia, X., 2014. Utilizing bio-char as a bio-modifier for asphalt cement: a sustainable application of bio-fuel by-product. Fuel 133, 52–62.

Sun, Z., Yi, J., Chen, Z., Xie, S., Xu, M., & Feng, D. (2019). Chemical and rheological properties of polymer-modified bitumen incorporating bio-oil derived from waste cooking oil. Materials and Structures/Materia et Constructions, 52(5), 1–11.

Ullah, S., Bilal, S., Zaidi, A., & Aman, A. (2021). Evaluating the Properties of Bio-oil Modified Bitumen Derived from Cotton Stalk Waste.

Zhang, B., Chen, H., Zhang, H., Kuang, D., Wu, J., & Zhang, X. (2019). A Study on Physical and Rheological Properties of Rubberized Bitumen Modified by Different Methods. Materials 2019, Vol. 12, Page 3538, 12(21), 3538. https://doi.org/10.3390/MA12213538

Zhang, X., Zhang, K., Wu, C., Liu, K., & Jiang, K. (2020). Preparation of bio-oil and its application in asphalt modification and rejuvenation: A review of the properties, practical application, and life cycle assessment. Construction and Building Materials, 262, 120528.

PAPER 80 – DEPLOYING 3-STAGE SWITCH MODE TECHNIQUE AT BASE STATIONS TO OPTIMIZE ENERGY CONSUMPTION IN WIRELESS COMMUNICATION NETWORKS

C. C. Nwaogu[1], C. K. Okoro[2], O. A. Amadi[3]

[1,2]Department of Electrical Electronic Engineering, Abia State Polytechnic Aba, Nigeria
[1,2]Department of Computer Engineering, Abia State Polytechnic Aba, Nigeria
[3]AkanuIbiam Fed. Poly Unwana
[*]Email: cxtopher20091@gmail.com

ABSTRACT
This work focused on the deployment of a 3-stage mode technique at a base station to optimize energy consumption in a wireless communication network. The projected rise in wireless communication traffic has necessitated the advancement of Energy Efficient (EE) techniques for the design of wireless communication systems, thereby providing high operating costs of conventional wireless cellular networks and scarcity of energy resources in low-power applications. Considering the current energy concerns, the base station is the hub of bulk energy consumption with the interest in improving energy efficiency at the base station level for future generation networks. This work examined different ways of deploying energy efficient techniques at the base stations in order to make the base station more energy efficient and to examine the paradigm shifts by using switch mode approaches to enhance energy efficiency at the base station level. The research adopted three switch modes techniques. Three switching stages were considered namely, Sleep mode, Safe mode, and ON modes. With the three switch mode technique, the energy efficiency was improved significantly when compared with the two switch mode technique.

KEYWORDS: Energy efficiency, switch modes, Base station, sleep mode, safe mode, Network

1. INTRODUCTION

Energy consumption has become a key concern in the design and operation of wireless communication systems. Indeed, communication networks have been created for over a century with the goal of improving performance metrics like data rate, throughput, and latency. However, in the previous decade, energy efficiency has risen as a new significant figure of merit due to economic, operational, and environmental issues (Hammi, 2015).

Rising energy consumption is one of the key concerns linked with global warming, and decreasing mobile communication network energy consumption has gained a lot of attention since it accounts for a substantial amount of overall information and communication technology energy consumption. In a wireless network, the base station uses the majority of the energy (Wu, et al., 2015). Energy efficiency has a slew of advantages, including lower expenses at home and in the economy, fewer greenhouse gas emissions, and less reliance on imported energy. As a result, one of the most significant supports in the design of future generations of wireless networks will be energy efficiency. Future generation systems will serve an unprecedented number of devices, providing ever-present connectivity as well as innovative and rate-demanding services. It is forecasted, that by 2030 there will be more than 50 billion connected devices (Ericsson white paper, 2011), i.e. more than 6 connected devices per person, including not only human-type communications, but also machine-type communications.

2. THEORETICAL ANALYSIS

Increased energy consumption is one of the key challenges linked with global warming, and decreasing the energy consumption of mobile communication networks has gotten a lot of attention since it accounts for a considerable amount of overall information and communication technology energy consumption. Energy is expensive to both operators and users, its production has negative environmental impacts such as global warming. Reducing the energy consumption of mobile communication networks has gained significant attention since it takes a major part of global energy consumption (Lee et al., 2013).

In order to reduce energy waste and preserve our environment, new approaches to wireless network design and operation are needed. Energy efficiency is maximized to obtain better average performance. 5G wireless

networks constitute a major communication infrastructure for ever-present connectivity in the future, with the increasing expansion of mobile access to the Internet and its services. Mobile communication networks use a large portion of the overall energy consumed by information and communication technology, hence reducing the energy usage has gotten a lot of attention.

In order to avert the energy crunch, new approaches to wireless network design and operation are needed. The key point, on which there is general consensus in the wireless academic and industry communities, is that the 1000× capacity increase must be achieved at a similar or lower power consumption as today's networks (NGMN alliance, 2015). This implies that the efficiency with which each Joule of energy is used to transmit data must grow by a factor of 1000 or more. The GreenTouch consortium ("The GreenTouch Project," 2016) was created in 2010 as an open global pre-competitive research cooperative with the purpose of increasing network energy efficiency.

Increased energy consumption is one of the key challenges linked with global warming, and decreasing the energy consumption of mobile communication networks has gotten a lot of attention since it accounts for a considerable amount of overall information and communication technology energy consumption. Since future generation networks are predicted to have higher traffic loads, the impact of mobile communication network energy consumption will grow more serious.

The principal energy consumer in mobile communication networks is the base station (BS), and its energy consumption is determined by traffic load, which varies depending on geographic location. There has been a lot of effort put into the energy savings of a BS in order to lower the energy consumption of mobile communication networks, but there is still a lot more work to be done. The main premise of reducing a BS's energy usage is to turn off as many of its components as feasible when they are no longer needed or in use. The base station can be put to sleep by simply turning off the energy to most of its components when they are not in use. If there is minimal traffic on a BS and the traffic can be handled by neighboring BSs, the BS can be shut down to conserve energy more dramatically (Jahid et al., 2016). However, because the user equipment (UEs) covered by the central BS can also be serviced by neighboring BSs with overlapping coverage, the central BS can be switched off to conserve energy while the UEs are served by neighboring BSs.

There are various reasons why future generations of wireless networks should be more energy efficient, which include: design issues, green technology policies, cost savings for businesses, end user happiness as well as national development. Most of the energy utilized by wireless devices is converted to heat, which poses problems to equipment utilization, governments, and end users. With this work, wireless devices in base stations will produce less heat as energy efficiency protocols will be deployed. Also, less energy would be required to operate the base stations and maintain the temperature of their surroundings because the gadgets will produce less heat. Hence, eliminating or reducing this problem of loss of energy through heat. Secondly, in terms of green technology policy: today, practically most governments in the world are dealing with an energy crisis. Environmental issues, such as the problem of greenhouse gas emissions, are also of concern to society. The utilization of more energy leads to the production of more greenhouse gases. This work would offer an energy enhanced 5G-base stations to the world which would in turn reduce the entire global energy consumption.

Future generation wireless networking vendors must have their products certified for mandatory requirements of low energy consumption in order to enter Nigerian markets. Implementing energy-efficient wireless network equipment could minimize energy consumption, making it easier for them to achieve energy-efficiency certifications. It would bring about a reduction in operational costs for the operators as they make payments according to the amount of energy used. Base stations consume a lot of energy when transmitting or receiving wireless signals. It is possible that the service provider will save money on electricity. There are seven prominent areas that must be improved to achieve good energy efficiency in future generation networks. Two of the most notable areas are the introduction of a newer Radio Resource Control (NRRC) state for setting signaling and the reduction of unnecessary state changes. The second goal is to improve base station energy efficiency. The third goal is to achieve energy efficiency while remaining aware of potential interference.

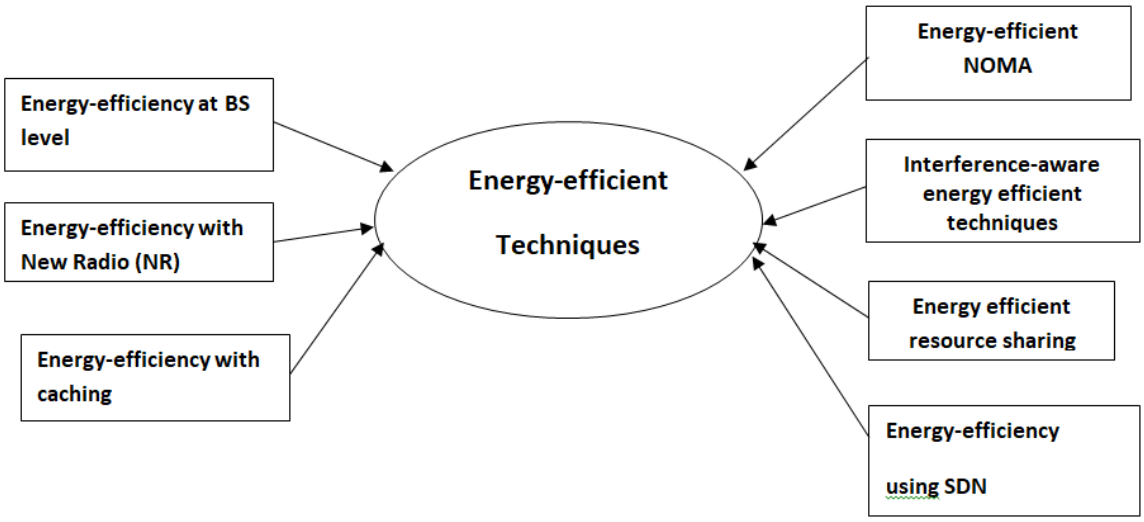

Figure 1: Outline of the energy-efficiency schemes (Nwaogu., 2023).

To understand the power consumption problems in cellular BSs, one must explore the components of a network base station system and the power consumption of its parts. The target system for the base station efficiency analysis is the 5G network system with support for multiple transmit antennas, but this work will restrict the study to four (4) transmit antennas per sector. This system can exploit the space domain to achieve high data throughputs. The research considered a macro cell base station with three (3) sectors with four (4) parabolic reflect transmit antennas per sector. Each of the parabolic transmit antennas is designed to have an Effective Radiated Power (ERP) of 67dBW. The four (4) transmit chains deployed for the four (4) antennas therefore require twelve (12) Power Amplifiers (PA) and antennas per macro cell base station. At the micro cells level, each micro cell base station consists of an isotropic antenna which radiate energy within the cell of coverage.

3. MATERIALS AND METHODS

The materials used for the work include: (i) Baseband signaling unit/ Baseband (BB) interface: ii) Antenna/Antenna interface (AI): (iii) Mains Power supply unit (iv) RF chains (v) Power amplifier (vi) Cooling unit (vii) Network analyzer (viii) User equipment modules, (ix) Software tools used (Mathlab/ Simulink 2023a)

3.1 System Setup for Base Station Switching States

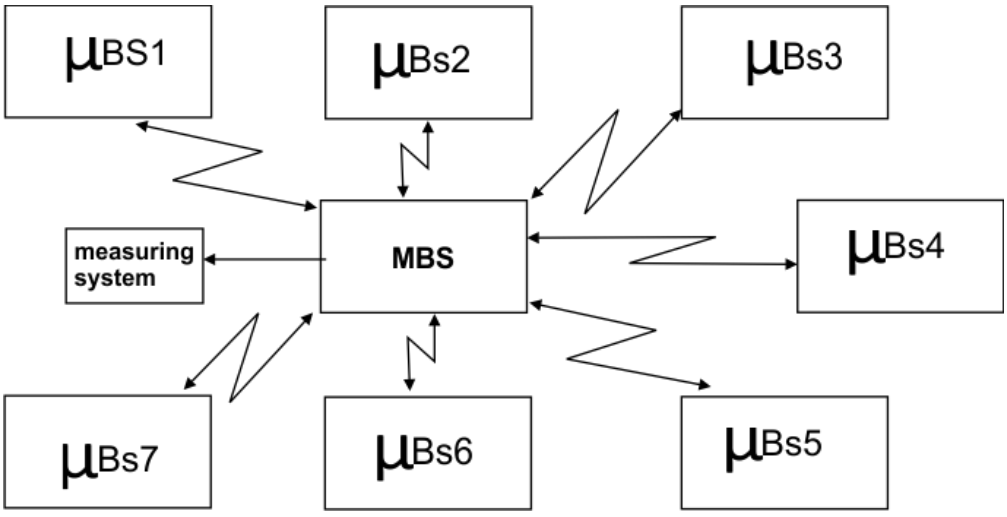

Figure 2. Block diagram showing system setup of base station switching

Figure 2 represents a system set up of a heterogeneous network cluster is made up of seven micro cells. There is a control and data plane. In the cluster the macro cell base station (MBS) serves as the control plane and is designed to be ON permanently in the network, while the micro cell base stations (µBS) is in charge of the data transmission in each cell and around its neighbourhood. The micro cell base stations are design to switch modes between ON, SAFEMODE and SLEEP modes depending on the traffic. The MBS controls the µBS on when to switch ON, SAFEMODE or SLEEP modes through the Radio Access Technology (RAT) located on the MBS.

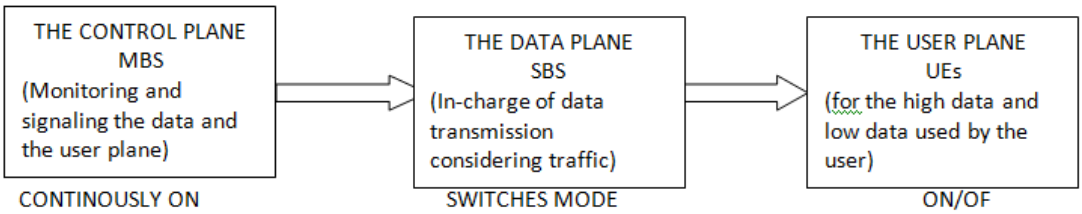

Figure 3: Block Diagram showing the stages in Proposed Energy saving scheme

The switch mode system as used in the study consists of three stages as shown in figure 3, which are the control plane, the data plane and the user plane. The control plane consists of the macro cell base station (MBS). This stage is meant to be always ON for twenty four hours. It is the control plane that monitors the data plane to signal the **µBS** to come ON, go on SAFE mode or SLEEP modes. The data plane consists of the small cell base stations. It is in charge of data transmission. Hence considering the traffic/ the number of connectivity of user equipment, it could be ON, SAFE mode or SLEEP mode. At this stage saving of power could be achieved. The User plane is the stage where all the high data consuming and low data consuming devices are located. They could be ON or on SLEEP (dormant) mode, they could be mobile or statically located. They are also monitored by the control plane as well, while the data plane handles the data.

Using the equation (1) the total energy consumed by base stations per day in a cluster can be obtained and hence energy efficiency for the system could be computed, considering the peak and the off peak period

$$E_{cons}^{day} = \sum\left(K_{BS}^{active} * U_{op}^{BS}\right) * hour \quad (1)$$

Where E_{cons}^{day}= energy consumed per day K_{BS}^{active}= number of active base stations U_{op}^{BS}= Power consumed by the base station when it is on, "hour"= The number of hours in the day it operated.

$$E_{cons}^{day} = P_{tot} * time \quad (2)$$

$$P_{tot} = P_a + n(P\mu on + P\mu_{sleep} + P\mu sfm) + P_{transition} \quad (3)$$

Where P_{tot} is the total power consumed in the network per cluster.$P_a$is the power consumed by the macro cell base station, $P_{\mu ON}$is the total power consumed by the small cell base station when it is in ON mode, $P_{\mu sleep}$ is the total power consumed by the micro cell base station when in sleep mode. $P_{\mu sfm}$, is the total power consumed by the small cell base station when it is in safe mode while n is the number of the micro cell base station that is active at a period. $P_{transition}$is the total power consumed by the base station when transiting from one state to another. We assume that all user equipment within the cluster covered by a macro Base station receives a control signal from the macro base station. Secondly, it is assumed that the maximum power ratings of all micro base stations within a cluster are equal. The links between a user equipment and a micro base station (M_i) is represented with βij. This is represented in equation 3.

$$\beta_{ii} \begin{cases} 1 & \text{If } V_j \text{ is connected with mi } (0 \leq i < k+1,\ 0 \leq j < n) \\ 0 & \text{otherwise} \end{cases} \quad (4)$$

$$t_r = \begin{cases} 1, \text{ If Vj request for service, } (0 \leq i < n) \\ 0, \quad \text{otherwise} \end{cases} \tag{5}$$

In equation (5) above, t_r represents the data service request of user equipment V_j. The data rate as a result of traffic is denoted as $r_i$and it is shown in equation (6).

$$r_i = \begin{cases} 1, \ V_j \text{ requires high data rate} \\ 0, \ V_j \text{ requires low data rate} \end{cases} \tag{6}$$

In equation (7) A_j is related with whether M_i is in ON state or not while in equation (8), E_j is related with whether the M_i is in safe mode (sfm) or not. Equation (9) F_j is related with whether M_i is in sleep state or not

$$A_j = \begin{cases} 1 & \text{if } M_i \text{ is in on state} \\ 0 & otherwise \end{cases}, (0 \leq j < g + 1) \tag{7}$$

$$E_j = \begin{cases} 1 & \text{if } M_i \text{ is in sfm state} \\ 0 & otherwise \end{cases}, (0 \leq j < g + 0.5) \tag{8}$$

$$F_j = \begin{cases} 1 & \text{if } M_i \text{ is in sleep state} \\ 0 & otherwise \end{cases}, (0 \leq j < g) \tag{9}$$

The state transitions of a micro cell base station are expressed using X_j for transition between on and off,, $D_j$for transition between safe mode and on modes and $Q_i$for transition between sleep mode and safe mode. Their values are as shown in equations (10); (11) and (12);

$$Xj = \begin{cases} 1, & \text{if Mi switches between on state and off state} \\ 0, & otherwise \end{cases}, (0 \leq j < g + 1) \tag{10}$$

$$Dj = \begin{cases} 1, & \text{if Mi switches between Sfmd and on state tate} \\ 0, & otherwise \end{cases} (0 \leq j < g + 0.5) \tag{11}$$

$$Qj = \begin{cases} 1, & \text{if Bi switches between sleep mode and safe mode} \\ 0, & otherwise \end{cases}, (0 \leq j < g) \tag{12}$$

Using the above equations the power consumption of an M_i, $P_{(mj)}$ is obtained as in equation (13):

$$P_{(m_j)} = Zj * (1 - F_j) * \left(P_{\mu o}^{\square} + g_s * P_{\mu o}^{tx}(j)\right) + F_j x(1 - E_j) * P_S^e + Ej * \frac{(1-Fj)}{2} * \left(P_{\mu o}^{\square} + g_s * P_{\mu o}^{tx}(j)\right) \tag{13}$$

Where if a micro cell base station is in an ON state, the power consumption is calculated as a steady sum of the consumed power and load dependent power consumption, if a micro cell base station is in safe mode, then the power consumption in that mode is used for the calculation. The power amplifier consumption is in the intermediate and if a micro cell base station is in sleep mode, then the power consumption in that mode is used for the calculation. Regarding load dependent power consumption, $P_{\mu o}^{tx}(j)$is shown in equation (14).

$$P_{\mu o}^{tx}(j) = P_{\mu o}^{tx,max} * \sum_0^{k-1} \left(tr * \beta_{ij} * \frac{(r_i * c_{max} + (1 - r_i) * c_{min})}{c_{\mu}^{max}}\right) \tag{14}$$

The power consumption of the macro base station (P_a) could be calculated using equation 15. Where P_{amax}^f is the maximum fixed power of the macro cell base station, g_m is the power gradient of the macro cell base station and P_a^{tx} is the transmit of the macro cell base station

$$P_a = P_{amax}^f + g_m + P_a^{tx} \tag{15}$$

Where the value of P_{amax}^{f} is as shown in equation (16)

$$P_{amax}^{f} = P_{a}^{tx,max} * \sum_{0}^{k-1} \left(tr * \beta_{ij} * \frac{(r_i * c_{max} + (1 - r_i) * c_{min})}{c_{\mu}^{max}} \right) \quad (16)$$

During modes/states transition of the micro cell base station µBS, $P_{transition}$, is calculated using equation 16

$$P_{transition} = \sum_{0}^{k-1} \left(X_j * (1 - D_j) * P_{on-off} + D_j * (1 - Q_j) * P_{sfm-on} + Q_j * (1 - X_j) * P_{sleep-sfm} \right) \quad (17)$$

$$P_{amax} = P_a + \text{Ptransition} \quad (18)$$

The maximum energy consumption of an MBS is P_{amax} and thus the power consumption of a Macro cell base station during off peak P_a should be less than P_{amax},

4. RESULTS AND DISCUSSION

The results of the simulations are discussed in this section.

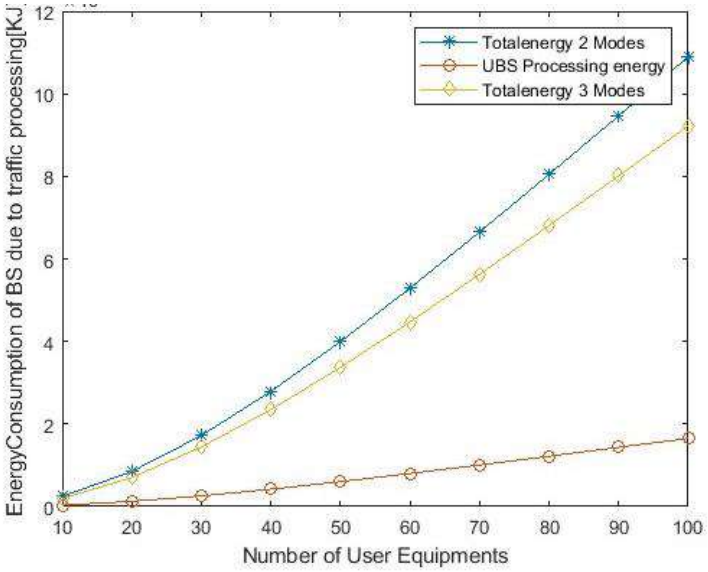

Figure 4: Energy consumption of user equipment due to traffic processing

Figure 4 shows the total energy consumption of µBSs due to traffic processing using the 2-mode and 3-mode switching systems as well as the total energy of µBSs corresponding with an increase in the number of user equipment connected to the network. As could be observed the two modes system, consumes higher energy when compared with the proposed three switch modes scheme in this work. Secondly, the total energy consumption of the cluster µBSs is proportional to the number of user Equipment connected to the network. The effect of traffic on the base station energy consumption indicates a better performance when a three modes scheme is deployed compared with the two modes scheme hence bringing about an improvement in the energy efficiency in the system.

Figure 5 shows the energy consumption during traffic processing in joules (J) for the two modes and three modes schemes respectively with change in the number of micro cell base stations (µBSs). It could be observed that during the off peak traffic period less number of base stations are connected and the energy consumption of the two schemes are almost equal. As the traffic increases the number of µBSs increases and the total energy consumption increases.

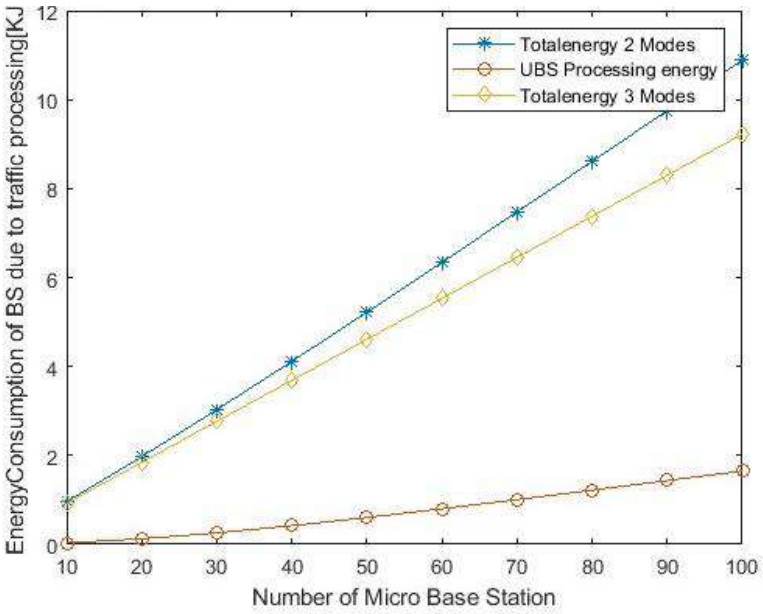

Figure 5: Total energy consumption of BS due to traffic processing(M-file Appendix V)

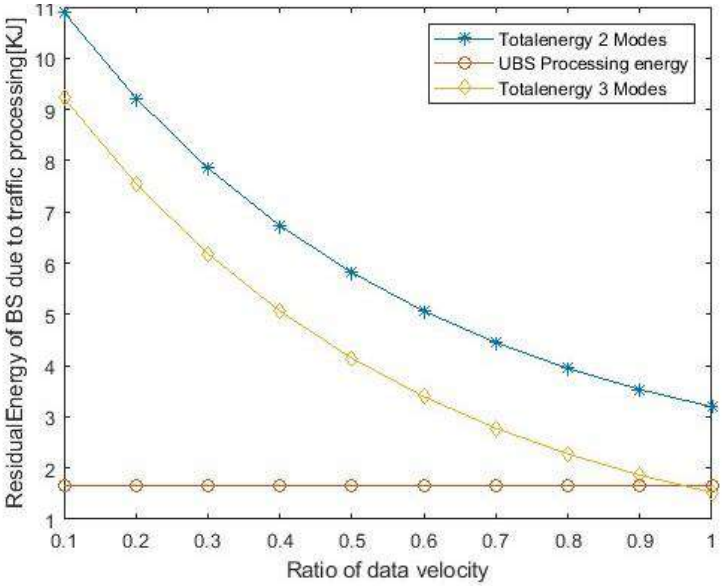

Figure 6: Residual Energy due to traffic processing (M-file Appendix V)

Figure 6 shows the average residual energy versus the rate of transmit data measured at continuous (regular) intervals of a network using the three modes and the two modes scheme. From figure 6 the residual energy for the three modes scheme is less than that of the two modes scheme. To extend wireless network lifespan, there is a need for efficient energy control mechanisms to reduce energy intake at the base station level. At the same time, energy efficient methods should be deployed at all layers of the network which should be proportional to changes in traffic.

5. CONCLUSION

A heterogeneous setting of seven cellular cluster was designed. Each cluster was designed with a modified small cell and a three stage switch modes: ON/SAFE MODE/SLEEP mode scheme. This three stage switch modes was proposed for a heterogeneous network with the introduction of a separate control and data planes. This energy saving scheme has a threshold when the small cells (µBS) switch to SLEEP or SAFE mode or ON using a switch mode hence reducing power in low or normal traffic hours. This scheme provided 21.47% increase in energy efficiency. The scheme resulted in beneficial simulated outcomes and can be applied to improve the energy consumption issue.

REFERENCES

Auer, G., Giannini, V., Desset, C., Godor, I., Skillermark, P., & Olsson, M. (2011). How much energy is needed to run a wireless network? IEEE Wirel. Commun. 2011, 18, 40–49.

Ericsson White Paper, (2011.)."More than 50 billion connected devices," Ericsson, Tech. Rep. 284 23-3149 Uen,

Fehske, A., Fettweis, G., Malmodin, J., & Biczok, G. (2011) The global footprint of mobile communications: The ecological and economic perspective. IEEE Commun. Mag. 49, 55–62.

Hammi, O. (2015). Efficient Linear Amplification for LTE Base Stations using Digitally Predistorted Overdriven Power Amplifiers. IEEE Trans. Broadcast. 2015, 61, 398–406.

Isabona J.,& Srivastava V. M. (2017). Downlink Massive MIMO Systems: Achievable Sum Rates and Energy Efficiency Perspective for Future 5G Systems. Wirel. Pers. Commun: 96:2779–2796. doi: 10.1007/s11277-017-4324-y.

Jahid, A., Shams A. B., & Hossain, M. F., (2016)."Energy cooperation among BS with hybrid power supply for DPS CoMP based cellular networks," in 2016 2nd International Conference on Electrical, Computer & Telecommunication Engineering(ICECTE), pp. 1–4, Rajshahi, Bangladesh.

Nwaogu, C. C. (2023) Modeling Energy efficiency for 5G network with separated data and control planes. A Ph.D dissertation, Michael Okpara University of Agriculture Umudike, Nigeria.

Kumar, W., & Kalaiselvi, Y.W. (2014).A novel power saving scheme for base stations in 5G network. Int. J. Mob. Device Eng. 2014, 1, 29–36.

Lee, K.S., Kim, H. S., Kim, Y. T., & Kim, B.H. (2013). DANCE: Small AP on/off algorithms in ultra dense wireless network. J. Korean Inst. Commun. Inf. Sci. 38, 1135–1144.

"The 1000x data challenge," Qualcomm, Tech. Rep. [Online]. Available: http://www.qualcomm.com/1000x

PAPER 81 – INVESTIGATION OF EFFECTIVE EARTH RADIUS FACTOR (k-FACTOR) AND ITS APPLICATION TO RADIO COMMUNICATIONS OVER NORTH WESTERN NIGERIA

[1]*A. Akinbolati**,** A. Y. Sabiru [2], F. N. Ikechiamaka[1], A. F. Akpaneno[3] and K. R. Ekundayo[4]

[1]Department of Physics, Federal University Dutsin-Ma, Nigeria
[2]Department of Physics, Umaru Musa Yaradua University, Nigeria
[3]Department of Geophysics, Federal University Dutsin-Ma, Nigeria
[4]Department of Mechatronics Engineering, Federal University Dutsin-Ma, Nigeria
*Email: aakinbolati@fudutsinma.edu.ng

ABSTRACT
This study investigated the long-term variations in *k*-factor over North West, Nigeria. Data (1980-2020) of temperature, pressure and humidity at the surface, 100 m and 250 m above ground level from the European Centre for Medium-Range Weather Forecasts (ECMRWF) ERA-5 were deployed. Computations were made using the latest ITU-R, Rec. P.453, 2019. The Study reveals that *k*-factor exhibits seasonal and location dependence. The obtained *k*- factor for the study areas are higher than the ITU-R standard value of, $\frac{4}{3}$ (1.33). The range of the mean values for twelve months across the seven locations of the study is 1.597- 5.362 where the first and second highest values are 5.362 and 5.243 in September and October in Gusau respectively. The lowest value is 1.597 in February obtained in Sokoto. The overall mean values for the dry season in Katsina, Kaduna, Dutse, Sokoto, Gusau, Birnin Kebbi and Kano are 1.805, 1.851, 1.978, 1.776, 1.532, 1.901 and 2.014 and for the wet season we have 3.273, 3.738, 3.212, 2.590, 3.849, 2.469 and 3.598 respectively. The findings from all locations indicate that radio signal propagation would be affected by super-refractive conditions, thus the need to compensate for this to enhance quality of service.

KEYWORDS: Effective earth radius factor (*k*-factor), radio signal propagation, super refraction, North West Nigeria

1. INTRODUCTION

Radio wave propagation is affected by the characteristics of the atmosphere (Akinbolati et al., 2016). The atmospheric variable has the ability to reflect, diffract, scatter and absorb the radio wave propagation (Akinbolati and Agunbiade, 2020). The troposphere which rises from the surface of the earth to about 20 km at the equator, 17 km at the mid latitude and 7 km at the poles; is the atmosphere`s component where most weather phenomena take place (Akinbolati and Ajewole, 2020). Disaster predictions, wireless communications, environmental monitoring, aerospace, etc. all benefit from the effect of tropospheric variation. For instance, worse conditions of radio signal propagation can cause higher fading on wireless communication links and subsequently lower receiver power levels. The k-factor is useful in the prediction of local radio waves propagation conditions. Typically, a design value of *k*=1.33 is often assigned in locations where the values are not known (Ojo et al., 2017). Studies have also shown that its value is location based and should not be assumed constant for all environments. Since k-factor is weather and climate dependent, it is therefore imperative for regular studies to be carried out using up to date data in order to capture the effects of climate change. It also represents a spatial average, which can only otherwise be obtained from simultaneous meteorological surroundings along the propagation path. The k-factor is the radius of a hypothetical spherical Earth, without an atmosphere, for which propagation paths follow straight lines (Ojo et al., 2017).

2. THEORETICAL ANALYSIS AND METHODOLOGY

Radio refractivity N is a measure of changes in refractive index n of air from unity, N is a dimensionless quantity defined in (1) and measured in N-units.

$$N = (n-1)\times 10^6 \tag{1}$$

The radio refractivity N can be expressed in terms of meteorological variables as:

$$N=\frac{77.6}{T}\left(P+4810\frac{e}{T}\right)(N\text{-}units) \quad (2)$$

Where, *N* depends on pressure P (hPa), temperature T (K) and water vapour pressure *e* (hPa) (Ayantunji et al., 2011; Akinbolati and Ajewole, 2020). Meteorological activity in the atmosphere is dynamic in nature (Akinbolati et al., 2020), which often leads to the variation of its refractive index. The refractivity gradient, on the other hand, is a measure of how the refractive index varies with increasing height (Adelakun et al., 2020). This is given as:

$$\frac{dN}{dh} = 77.6\frac{1}{T}\frac{dP}{dh}\left(\frac{77.6}{T^2}+\frac{746512e}{T^3}\right)\frac{dT}{dh}+\frac{373256}{T^2}\frac{de}{dh} \quad (3)$$

where h is the height (m).

But the water vapour pressure *e* cannot be acquired directly, hence using its relationship with relative humidity H (%), we can have:

$$e=\frac{H}{100}e_s \quad (4)$$

where $e_s$is the saturated vapor pressure at a particular temperature t (°C), and it is defined as:

$$e_s = 6.1121\exp\left(\frac{17.502t}{(t+240.97)}\right) \quad (5)$$

The latest ITU-R Rec. P. 453 (2019) has made amendments to (5) as presented in (6):

$$e_s = \mathrm{EF}\times 6.1121\times\exp\left(\frac{\left(18.678-\frac{t}{234.5}\right)\times t}{(t+257.14)}\right) \quad (6)$$

(valid between −40 °C and + 50 °C), and:

$$EF_{water} = 1 + 10^{-4}[7.2 + P\times(0.0320 + 5.9\times10^{-6}\times t^2)] \quad (7)$$

Equations (6) was used to calculate the saturated vapour pressure e_s, with the substitution of (7). Equations (4) and (2) were used to calculate the water vapour pressure and the radio refractivity values respectively.

The k-factor can be derived from the vertical refractivity gradient, ΔN, in the first kilometres above the ground, Δ*N* is obtained from two refractivity values as given in (Ojo et al., 2017):

$$\frac{dN}{dh}=\frac{N_2-N_1}{h_2-h_1} \quad (6)$$

where N_1 and $N_2$are the refractivity values at heights h_1 and h_2, respectively. In this study $h_1$and $h_2$are at the surface and 100 m Above Ground Level respectively.

The k-factor can be expressed as indicated in (7) (Abu-Almal and Al-Ansari, 2010; Ojo et al., 2017). Where, $\frac{dN}{dh}$ is the rate of change of refractivity indices with height. This was used for k-factor computations in this work.

$$k = \frac{1}{1+\frac{\left(\frac{dN}{dh}\right)}{157}} \quad (7)$$

Table 1, presents the ITU-R standard values for k-factor and the associated anomalous propagation. Results were compared to these values in order to project the anomalous propagation over the study area.

Table 1: ITU-R standards on k-factor and the associated anomalous propagation

(Sabiru *et al*., 2024)

k = 1.33	**1.33 > k >0**	**∞ > k >1.33**	**- ∞< k< 1.33**
Normal refraction or standard atmosphere	Sub-refraction	Super-refraction	Ducting

3. RESULTS AND DISCUSSION

The *k*-factor was computed for the period of forty-one years. For all the study locations the *k*-factor starts with steady values in the first three months i.e., from January to March, then it increases steadily from March up to September or October where it reaches its peaks level, some few trends reach its peak at November. The *k*-factor then rapidly decreases and by December it returns to values that are approximately similar to the initial values of the first three months of the year. The variation of the *k*-factor of all study locations follows nearly the same trend in all the years under study except Kaduna. *k*-factor of Kaduna starts with steady values in the first three months i.e., from January to March, then its sky rockets from March to May then its stays steady for five months in October it falls to values that are near to the initial values of the first three months of the year at November and the values stay around there for the remaining month of the year.

The monthly mean of the effective earth radius factor (*k*-factor) values are depicted in Figure 1. Figure 1(a) demonstrates that the *k*-factor of Kebbi remains approximately constant for the first three months of the year, after which it steadily increases until October. From that point onward, it gradually decreases until the end of the year. At Kano the *k*-factor remains constant for the first two months of the year, after which it steadily increases until October. From that point onward, it gradually decreases until the end of the year as shown in Figure 1(b). The *k*-factor for Sokoto exhibits similar behaviour to that of Kano, as illustrated in Figure 1(f). On the other hand, for Katsina, Dutse, and Gusau, the k-factor remains constant during the first two months of the year followed by continuous increases until September. Subsequently, it starts to decrease for the remaining months, as shown in Figures 1(c), 1(e), and 1(g). In the case of Kaduna, it remains constant for two months, then steadily increases until May, and remains constant until September. Finally, it decreases for the rest of the months in the year as shown in Figure 1(d).

The range of the mean values of the k-factor of the twelve months across the seven locations of the study is 1.597 - 5.362 whereas the first and second highest values are 5.362 and 5.243 for the months of September and October and are all from Gusau, then followed by 5.108 of October which is obtained from Kano respectively. The lowest mean value is 1.597 in February and it is acquired at Sokoto.

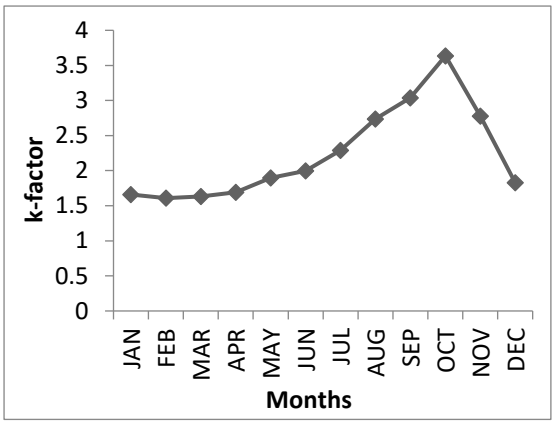

(a)

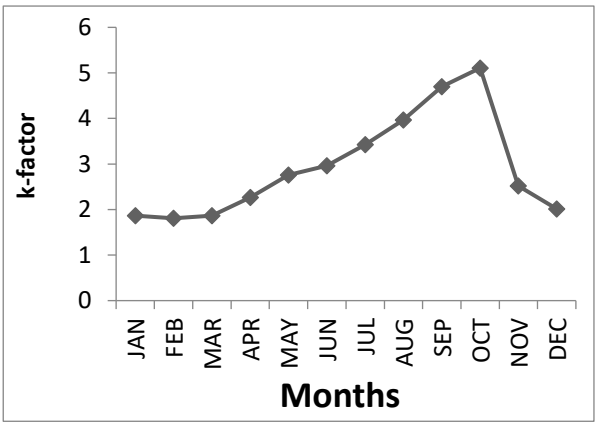

(b)

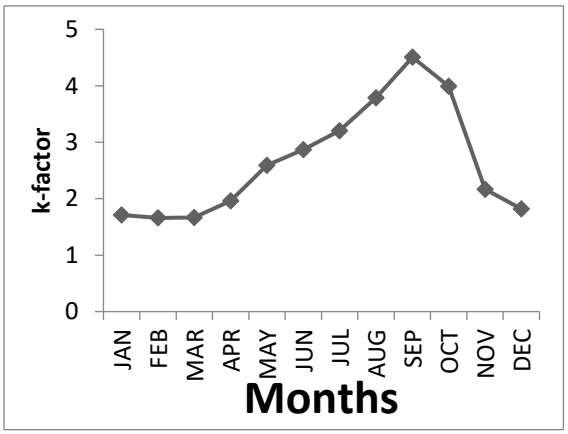

(c)

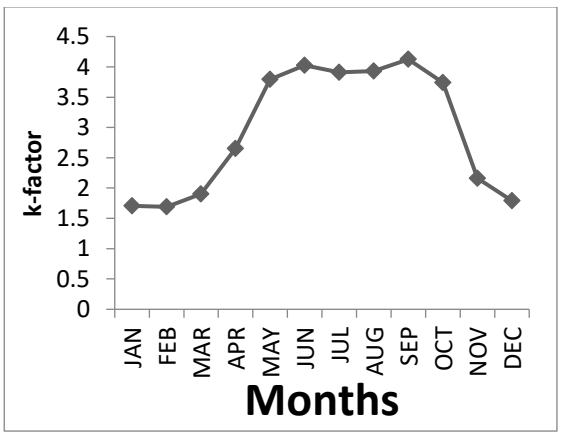

(d)

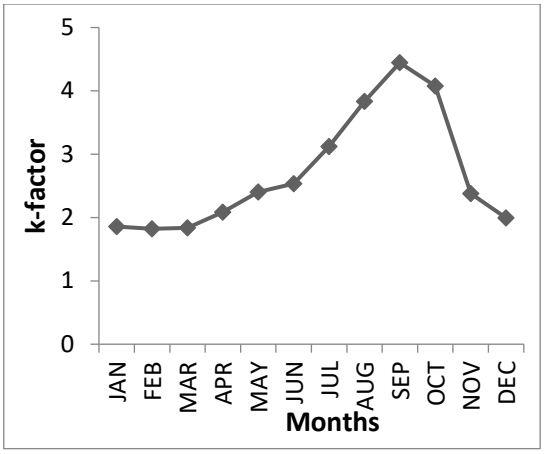

(e)

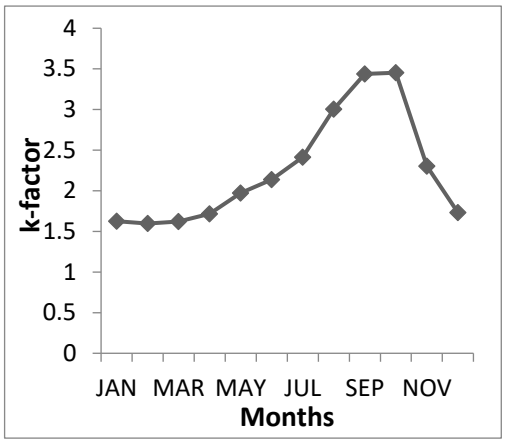

(f)

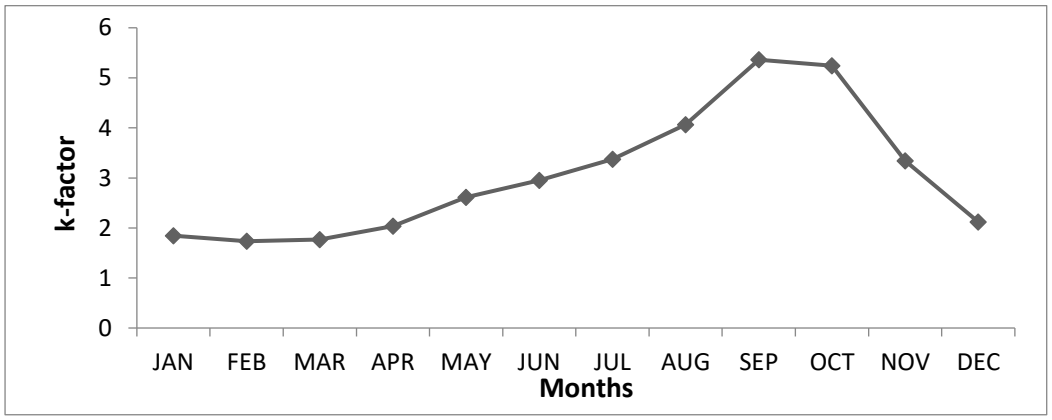

(g)

Figure 1: Mean *k*-factor at (a) Birnin Kebbi (b) Kano (c) Katsina (d) Kaduna (e) Dutse (f)Sokoto and (g)Gusau.

Figure 2(a) shows the variation of the *k*-factor during the dry season of the study area. The *k*-factor values in the research areas exhibit distinct variations. In Kebbi, the *k*-factor ranges from 1.608 to 2.778, with the highest value occurring in November and the lowest in February. Over a forty-one-year period, the average dry season *k*-factor is 1.901. In Kano, the *k*-factor values range from 1.808 to 2.520, peaking in November and reaching a minimum in February. The average dry season *k*-factor for the forty-one-year period is **2.014.** Similarly, for Katsina, the *k*-factor ranges from 1.659 to 2.164, with maximum values in November and minimum values in February.

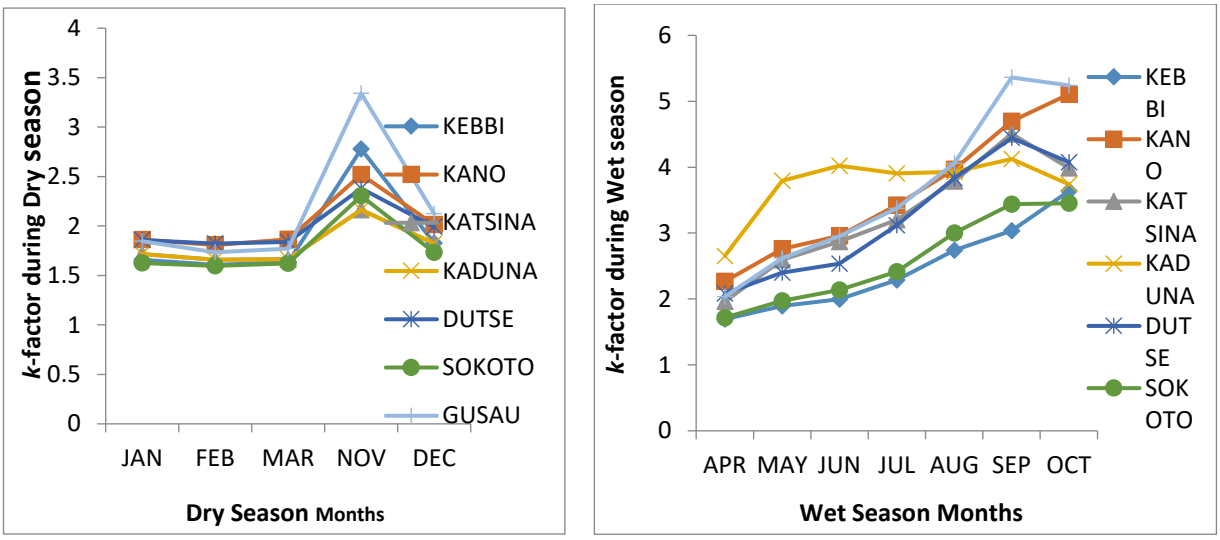

(a) (b)

Figure 2: The mean values of the *k*-factor during (a) the dry season months and (b) the wet season months over each of the study Areas

The average dry season *k*-factor over forty-one years is **1.805**. In Kaduna, the k-factor ranges from 2.160 to 1.690, with the highest value in November and the lowest in February. The average dry season *k*-factor value is **1.850**. For Dutse, the *k*-factor varies from 1.822 to 2.380, with maximum and minimum values in November and February, respectively. The average value for the dry season is **1.978**. In Sokoto, the *k*-factor ranges from 1.597 to 2.304, with maximum and minimum values occurring in November and February. The average dry season *k*-factor for the forty-one-year period is **1.776**. Finally, in Gusau, the *k*-factor ranges from 1.734 to 3.340, with the highest value in November and the lowest in February. The average dry season *k*-factor for the forty-one-year research period is **1.533**. These *k*-factor variations across different locations and months are essential in understanding the dynamics of the region's atmosphere and their radio signal communication implications. Figure 2(b) shows the results of the *k*-factor mean values for wet season months over the study areas. The *k*-factor values during the wet season display distinct variations. In Kebbi, the *k*-factor ranges from 1.694 to 3.636 with an average wet season value of **2.470** while in Kano, it ranges from 2.267 to 5.107, reaching its maximum in October and minimum in April. The average wet season value is **3.598**. Similarly, in Katsina, the *k*-factor ranges from 1.961 to 4.505. The average wet season value is **3.272**. In Kaduna, the *k*-factor ranges from 2.655 to 4.124 with an average wet season value of **3.738**. For Dutse, the *k*-factor varies from 2.083 to 4.444, with an average of 3.213. In Sokoto, it ranges from 1.717 to 3.453 with an average of **2.591**. Lastly, in Gusau, the *k*-factor ranges from 2.035 to 5.362 with an average of **3.849**. Notably, higher *k*-factor values were observed during the wet season compared to the dry season months, indicating significant variations in the regions' moisture conditions.

4. CONCLUSION

The k-factor for the seven capital cities in north western Nigeria, has been investigated. The overall findings show super refractive anomalous propagation (∞ **> k >1.33**) in the North Western States of Nigeria under the period of study (1980-2020) and most likely for the years ahead by climatic projections. The implication of this; is the attenuation effect of radio waves propagated in the region through super refraction. Radio engineers and scientists should take these findings into consideration for effective reanalysis of wireless communications and links design over the study areas so as to enhance quality of service and promote the socio-economic activities of the citizens.

ACKNOWLEDGEMENT

Authors acknowledge the European Centre for Medium-Range Weather Forecasts (ECMWF) ERA-5, as the source for the secondary data used for analysis.

REFERENCES

Abu-Almal, A, and K. Al-Ansari, "Calculation of effective earth radius and point refractivity gradient in UAE". *International Journal of Antennas and Propagation*. Vol.2010, Article ID 245070, 2010.

Adelakun. A.O., Ojo, J.S., and Edward, V.O, Quantitative analysis of Complexity and non- linear trend of radio refractivity gradient in the troposphere. Advances in Space Research, 59 (12), 2611-2515, 2020

Akinbolati, M. O. Ajewole, A. T. Adediji and J. S.Ojo " Propagation curves and coverage areas of digital terrestrial television base stations in the tropical zone" *Elsevier Heliyon, e03599, 2020,* https://doi.org/10.1016/j.heliyon.2020.e03599

A. Akinbolati and O. J. Agunbiade, "Assessment of Error Bounds for Path Loss Prediction Models for TV White Space Usage in Ekiti State, Nigeria," *I.J. Information Engineering and Electronic Business,* vol.3, pp.28-39, 2020. DOI: 10.5815/ijieeb.2020.03.04

A. Akinbolati and M. O. Ajewole, "Investigation of Path Loss and Modeling for Digital Terrestrial Television over Nigeria," *Elsevier Heliyon, e04101,* 2020, https://doi.org/10.1016/j.heliyon.2020.e04101

A. Akinbolati, O. Akinsanmi and K. R. Ekundayo, "Signal Strength Variation and Propagation Profiles of UHF Radio Wave Channel in Ondo State, Nigeria," *I.J. Wireless and Microwave Technologies,* vol.4, pp.12-28, 2016. DOI: 10.5815/ijwmt.2016.04.02

B.G. Ayantunji, P. N. Okeke and J. O. Urama (2011)," Diurnal and Seasonal Variation of Surface Refractivity over Nigeria", *Progress in electromagnetic research B,* vol 30, pp.201-222, 2011.

International Telecommunications Union, Radio Study Group (ITU-R), *Recommendation on Radio refractivity,* ITU-Rec. P. 453(2019).

O. L. Ojo, J. S. Ojo and P. Akinyemi, "Characterization of Secondary radioclimatic variables for microwave and millimeter wave link design in Nigeria", *Indian Journal of Radio and Space Physics,* vol.46, pp.83-90,2017

S. A. Yaradua, A. Akinbolati, F. N. Ikechiamaka and B. T. Abe, "Characterization of some Secondary Radio-Climatic Factors for Reliable Radio Wave Propagation and Link's Design over North Western Nigeria" *Advances in Space Research (Elsevier),*2024,

PAPER 82- EVALUATING THE ENGINEERING SOLUTION TO CHOLERA PREVALENCE IN OFFA LOCAL GOVERNMENT AREA OF KWARA STATE

O.A. Mokuolu[1*], F.A. Ahmed[1]
[1]Department of Water Resources and Environmental Engineering, Faculty of Engineering and Technology, University of Ilorin, Ilorin, Nigeria

*Email: Mokuolu.oa@unilorin.edu.ng

ABSTRACT
Cholera is a global threat to public health associated with high mortality and morbidity. The disease has become a source of great concern in Offa Local Government Area (LGA) of Kwara State due to its prevalence therein. Hence, this study assessed the risk of a cholera outbreak in Offa by identifying its causative factors, examining its most vulnerable areas, evaluating the community awareness level, and assessing the nature of health risks related to cholera. 110 questionnaires were administered with a total of 100 (90.9%) returned. A simple random sampling technique was used and thereafter analyzed using Microsoft Excel and descriptive statistics such as charts, histograms, and frequency tables. This study identified inadequate access to clean water and sanitation, low levels of community awareness, poor hygienic practices, poor public health systems, and inadequate waste management in the community as the major causative factors to the cholera epidemic. It also shows that only 32% of respondents were aware of the epidemic whilst a majority (68%) of respondents were unaware. Four hazards (dumpsites, open toilets, stagnant waters, and shallow wells) were found to be dominant in the vulnerable areas. It was recommended that raising awareness through community sensitization, and education, as well as providing access to adequate public health services, especially to high-risk areas was the panacea.

KEYWORDS: Public health, cholera epidemic, awareness, clean water, sanitation

1. INTRODUCTION

In the last four decades, the World Health Organization (WHO) Global Health Observatory (GHO) reported that over 3.5 million cases of cholera were recorded in Africa (Mokuolu *et al.,*2017). The main factors responsible for the above epidemic include unsafe water supply, increased person-to-person transmission, unclean food safety, high population density, and poor environmental factors that promote the breeding of inadequate hygiene. These factors are commonly associated with the long-standing civil unrest in many countries of the region that leads to poverty and overcrowding in addition to poor public health systems (Guerin *et al.,* 2003).
According to Tomori (2002) and the United Nations Development Programme (UNDP) report, the main risk factors for the continued occurrence of cholera include lack of access to adequate safe water and sanitation. Sub-Saharan Africa has an estimated 55% access to clean water and only 18% have access to improved sanitation.
Cholera outbreaks occurred during the dry season in some rural parts of Nigeria, this pattern is precisely observed in Calabar, the southern part of Nigeria (Udoh *et al.,* 1992), where cholera outbreaks mostly occurred during the dry season. This could be attributed to the scarcity of potable water during the dry season and therefore the tendency of people to obtain drinking and cooking water from alternative sources with a higher risk of contamination which includes stagnant water bodies (Adagbada *et al.,* 2012). In most Nigerian towns and cities water supply and sanitation are grossly inadequate for domestic and personal hygiene, despite the gains of the International Drinking Water and Sanitation Decade campaign of the 1980s. In many informal settlements, water-borne and filth-related diseases especially diarrhea and cholera are common. Less than half of urban households in most Nigerian cities have piped water and flush toilets. The rest depend on crowded and sometimes distant communal water taps or draw water from wells, streams or itinerant water vendors. Pit latrines and buckets are still in use, often shared by many families. People commonly defecate and urinate in the open or in nearby bushes, so that food and water can be easily contaminated from exposure to human waste (Nwaka, 2005).
The indiscriminate dumping of waste is increasing and is compounded by a cycle of poverty, population explosion, decreasing standards of living, poor governance, and low level of environmental awareness. Hence, these wastes are illegally disposed of in any available space, known as open dumps (Izugbara and Umoh, 2004). Solid waste from the

different collection systems in the various districts in Minna is transported to various dump sites at the outskirts of the city. Piles of solid wastes are also found along roads, underneath bridges, in culverts and drainage channels, and other open spaces (Adeoye, *et al.,* 2011). Such uncontrolled waste disposal not only creates serious environmental problems and affects human and animal health, but also causes financial and socio-economic losses (Kalu *et al*., 2009). Improper management of solid waste has serious environmental and health consequences (Ayo *et al.,* 2010). The hazard associated with improper solid waste disposal and the associated environmental health impact should therefore be of utmost concern to waste management experts. It may lead to unprecedented health consequences (Chen *et al.*, 2010).
Between February and June 1, 2018, Cholera outbreaks occurred in nine States in Nigeria with five (5) Northern States recording death cases. A cumulative total of 3,039 suspected cases were recorded in Adamawa, Yobe 5, Borno, and Bauchi States 6, and 50 cholera-related deaths 7. The figures of death could be higher, as States continue to record isolated cases. States with recorded fatalities include; Borno State, 3 deaths; Yobe State, 15 deaths; Kano State, 4 deaths; Adamawa State, 16 deaths; Bauchi State, 12 deaths. Other States with suspected cases include; Ekiti, Ebonyi Kaduna, and Zamfara States. The World Health Organization (WHO), however, linked the outbreak in Borno State to areas where vaccination was not conducted while the practices of open defecation increased susceptibility to contracting Cholera. Other affected States reportedly traced the outbreak of the disease to water contamination. In the case of Adamawa State, 90% of residents in the affected Mubi LGAs- the second most populous town in the State rely on water supply from vendors who source water from boreholes meant for irrigation along River Yedzaram.
Cholera is more common where there is poor sanitation. Fabamise *et al*., (2017) opined that cholera bacteria enter the body through the mouth, often in food or water that has been contaminated with human waste, due to poor sanitation and hygiene. They can also enter by eating seafood that is raw or not completely cooked shellfish native to estuary environments, such as oysters or crabs. Poorly cleaned vegetables irrigated by contaminated water sources are another common source of infection. Non-improved sanitation for urban areas is recorded at 6.6% whilst some facilities though improved are shared amongst households (48.5%) hence both non-improved and shared facilities are classified as unhygienic as they do not effectively separate human waste from human contact (Fabamise *et al.,* 2017). The rural situation is worse as only 30.8% constitute toilets. A combination of factors therefore led to the cholera disease outbreak as the urban areas were affected most compared to rural settings, yet urban areas have high coverage. Flush toilets require the availability of water which is often cut therefore leading to unhygienic conditions or resorting to open defecation.
This study assessed the breakout of a cholera epidemic in parts of the Offa local Government area (LGA) of Kwara State, Nigeria by examining the contributing factors, assessing the level of individual awareness, and recommending appropriate control measures.

2. METHODOLOGY

Research Population
According to the National Population Commission (2006) was estimated at 120,100. The study area, Offa LGA, with a total land area of 36,825 square meters (14,218 square miles), is bounded by longitudes 4^0 42.8’ and 4^0 46.2’E and latitudes 8^0 09.0’ and 8^0 12.5’N.

Sampling techniques

Sampling Size
To estimate the population of an area, the method described by Tunde (2007) was adopted. This method stated that several households x average size of households = population of the area.
Using this method, the following population was arrived at the settlement in the study area.
Number of households = 159
The average size of household = 7
Hence, the population of the area = 7 X 159 = 1113
The population of the study area was estimated at 1113 inhabitants.
Based on a 10% sampling survey, 110 copies of the questionnaire were randomly administered to the residents prone to epidemics in the study area.

Sampling Procedure
A two-stage random sampling procedure was employed to select the respondents. The first stage was the selection of all three identified dump sites and the random selection of five collection points. The second stage was the random

selection of 70 residents living very close to each identified collection point area and residents around each dumpsite. A total of 110 questionnaires were administered but 100 that gave consistent responses were used for analysis.

Data Analysis

The data collected from the field was subjected to statistical analysis. This was possible after the questionnaire had been coded. The data were analysed using descriptive surveys such as bar charts, pie charts; histograms, and Microsoft Excel. The following methods of data presentation were used in analysing collected data, namely; tables, percentages, maps, and photographs.

3. RESULTS AND DISCUSSION

Distribution of the questionnaire

Out of the One Hundred and Ten (110) questionnaires that were administered to the target audience, only One Hundred (100) respondents returned their questionnaire for analysis. This made the return rate 90.9% which is statistically significant at 5% and useful in eliciting the required information for the exercise.

Socio-demographic Analysis of Respondents

The responses showed that 64% of the respondents were male while 36% were female. The majority of the respondents were males, accounting for 64% while females only carried 36%

Table 1: Educational level of the respondents

Educational level	Frequency	Percentage (%)
Primary	37	37.0
Secondary	43	43.0
Tertiary	20	20.0
Total	**100**	**100**

Identification of Cholera Hazard in Offa LGA

A reconnaissance survey carried out confirmed the level of vulnerability that people were exposed to in Offa. The main challenge that contributed to the frequent occurrence of cholera outbreaks in the area was poor environmental conditions favouring disease transmission. The locations of the vulnerable areas to living places were accurately mapped out through the Global Positioning System (GPS) and the results are shown in Table 2.

The distance of hazard points to living places and the descriptions of the places exposed to cholera risk. The distance of the dump site was measured at 5 meters to residential buildings and the source of their drinking water. The severity of the hazard in the area was very high as a result of the closest distance source of drinking water to the dump site and poor personal hygiene. Toilets in some parts of the study area were located close to the source of their drinking water (well water, tap water, and borehole). There was a high possibility of linkage between toilet and well water which serves as a source of drinking water for the community.

Table 2: Field Data for the Location of the Vulnerable Areas Epidemics in Parts of the study area.

Hazard Location	Distance (meters)		Description
Dumpsite	N08° 9' 53.2" E004° 31' 27.3"	5	Dumpsite very close to residential building leading to environmental pollution of the area. A food seller was also close to the dump site
Open Toilet	N08° 10' 54.4" E004° 34' 26.5"	4	Toilet located near the kitchen and well water which can pollute the source of their drinking water.

Stagnant water	N08° 12' 56.2" E004° 35' 25.4"	6	Stagnant water very close to living areas which was poor environmental condition favouring disease transmission.
Shallow water	N08° 14' 57.6" E004° 36' 24.2"	3	Shallow water and dumpsite near houses that can promote breeding of disease transmitting vectors.
Toilet	N08° 36' 58.0" 58.0"	4	Well water near toilet and dumpsite. The E004° 36' community is likely vulnerable to cholera and dysentery due to contamination of the source of their drinking water

Level of Awareness on Cholera Epidemics in Offa LGA

The level of awareness of cholera risk in the study area was identified through a series of questions that the respondents were asked. The result of the analyses of the responses showed the majority of the respondents (68%) claimed to be unaware of epidemics while 32% did. There was a great difference in the level of awareness of respondents indicating that many residents do not take cognizance of the factors contributing to the frequent occurrence of risk outbreaks.
The research also examined the effective measures put in place to prepare for, protect against, and respond to the risks of cholera outbreaks in the area. The results indicated that 9% of the respondents went for good personal hygiene as a means of minimizing risks of an outbreak, 24% suggested that good public health systems are the effective way of preventing the risks, 16% of the respondents revealed spelling community awareness as a measure to prevent the outbreak. Public education was also suggested by 14% of the respondents. Table 4 shows the factors contributing to the risk of cholera epidemic in the study area.

Table 4: Factors contributing to the risks of Cholera epidemics in the study area

Factors	Frequency	Percentage (%)
Poor personal hygiene	19	19.0
Poor Public Health Systems	36	36.0
Inadequate safe water & food	25	25.0
Poor waste management	12	12.0
Lack of proper awareness	8	8.0

4. CONCLUSION

Cholera outbreaks remain a major public health challenge in Offa LGA of Kwara State, causing a significant burden of illness, disability, and mortality. The main problems with the frequent occurrence of cholera outbreaks are driven by multiple factors, including weak public health systems, poor personal hygiene, inadequate safe water and food, overcrowding, inadequate living spacing, and poor environmental conditions favouring disease transmission.
Most people living around the waste deposition areas complain of ill health conditions resulting from pollution and attacks from disease vectors. This study also assessed the level of awareness of the risks of outbreaks in the study area. The report showed that close to two-thirds of respondents (59%) were unaware of the risk of an outbreak while only (31%) claimed awareness.

REFERENCES

Adagbada A.O, Adesida S.A, Nwaokorie F.O, Niemogha M.T, Coker A.O (2012). Cholera epidemiology in Nigeria: An overview. *Pan African Medical Journal*. Vol. 12:1.

Adeoye, B. and Dung-Gwom, J.Y (2007). "The Environmental Health Problems Associated with Solid Waste Management in Gwagwalada-Abuja" Abuja *Journal of Geography and Development* Vol. 1, No. 1

Ayo B., Hassan T.I., Ibrahim B., Rafee M.M. (2010). The practice and challenges of solid waste management in Damaturu, Yobe State, Nigeria. *Journal of Environmental Protection*. Vol.1:4. Pp 384-388.

Chen X., Geng Y., Fujita T. (2010). An overview of municipal solid waste management in China. *waste management*. Vol.30 Pp716-724.

Fabamise O.M., Iluku-Ayoola O., Olowoyeye E.A. (2020). Prevalence and causes of malaria Among children in Ekiti- -State, Nigeria. Journal of Health, Medicine, and Nursing, Vol. 76 Pp56-62.

Guerin P. J, Brasher C, Baron E, MicD, Grimont F, Ryan M, AavitslP, Legros O. (2003): *Shigelladysenterriae*serotype I in West Africa: intervention strategy for an outbreak in SierraLeone. *Lancet*, 362: 705-06.

Izugbara, S. and UmohN. (2004). "Waste Management Within the Context of Sustainable Development". Environment in Nigeria. Vol. 2. Pp 80-90

Mokuolu O.A, Adu D.A, Aremu A.S. (2017). Clean water as a source reduction for cholera: A review of the African experience. SMU medical journal.Vol.4:2. 8-29.

Nwaka,A. (2005). Urban Environmental Pollution: A Critical Analysis. A Synopsis. Presented at the University of Calabar .

Tomori O. (2002). Yellow fever in Africa: public health impact and prospects for control in the *21st*century. *Biomedica*22{2):178-210.

PAPER 83: PERFORMANCE EVALUATION OF ECO-FRIENDLY AGRO-ANIMAL RESIDUES COMPOSITE BRAKE PAD: A REVIEW

M. Okunlola[1], K. O. Abdulrahman[1], A. S. Adekunle[1]
[1]Department of Mechanical Engineering, University of Ilorin, Ilorin 240003, Nigeria.

Email: okunlolanrewajumojeed@gmail.com

ABSTRACT
The importance of braking in automobiles cannot be overemphasized as it is the crucial part that regulates/controls motion during operation. However, the brake pad is majorly made of asbestos composite and has been severally reported to cause health hazards to manufacturers, users and maintenance personnel in the industry. This has made researchers carry out an intensive investigation on substitutes for asbestos in brake pad production and Nigeria's locally sourced agro-animal residue composites have displayed a huge potential for brake pad application. This review paper presents the properties of brake friction material made from agro-animal residue composite. It is found that the properties of agro-animal residue brake friction material are closely related to that of asbestos brake pads and therefore can replace the cancerous asbestos product available in the market and provide a safe environment in the automobile industry.

KEYWORDS**:** Agro-animal residues, Automobile, Compositions, Brake Pads, Braking system, Properties

1. INTRODUCTION

A brake is a mechanical device in an automobile which controls motion by absorbing energy from a moving system (Adekunle *et al*., 2023). It is used for slowing or stopping a moving vehicle, wheel, or axle, or to prevent motion, most often accomplished through friction (Mathew & Muruga Lal Jeyan 2018). Production and development of brake pad materials can be dated back as far as 1897 (Kumar *et al*., 2021; Adeyemi *et al*., 2016). The arrangement of the component part of automobile braking systems is presented in Figure 1.

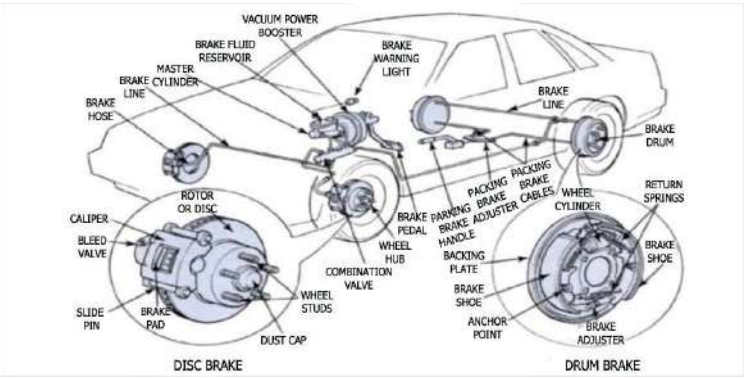

Figure 1: Arrangement of the component part of the automobile braking system (Srikanth, 2013)

Automobile brakes can be divided into two categories namely; drum brakes and disc brakes (Kumar *et al*., 2021). In drum brake, brake shoes are situated inside the drum and the brake shoe is forced outward (expand) with the help of a piston connected to the shoes and pressed against the drum when the brake is applied. The most significant difference between drum brakes and disc brakes is that the brake shoes in drum brakes are usually enclosed while the brake pads in disc brakes are usually exposed to the environment, which makes brake pads dissipate the absorbed heat faster than the drum brakes (Adeyemi *et al*., 2016; Aigbodion & Agunsoye 2010; Bono & Dekyrger 1990). Brake pad materials are usually classified as belonging to one of the four principal categories such as: Non-metallic, semi-metallic, metallic and ceramic materials. Metallic and ceramic friction materials show better thermal stability and wear characteristics as compared to non-metallic but they generate more noise and increase the wear rate of the disc material thereby reducing the span of the brake disc. Ceramic materials can withstand extremely high temperatures and generate less noise during usage but are costly which makes them suitable for high-speed vehicles where cost is not an issue such as racing cars (Adekunle *et al.*, 2023). Non-metallic brake pads of which asbestos is used as a major composite are the cheapest.

Owing to the effectiveness of asbestos in braking, chrysotile asbestos was used as a composite in brake linings. However, studies conducted in 1989 by the National Institutes of Health reported that a rarely high proportion of brake mechanics were afflicted with pleural and peritoneal mesothelioma, both of which were linked to chrysotile

and asbestos exposure. Public health authorities made a widespread recommendation against inhaling brake dust. Since then, chrysotile has been prohibited in many advanced countries, like Australia in late 2003 by the National Occupational Health and Safety Commission of the Commonwealth (Chan & Stachowiak, 2004). It has been progressively substituted in most brake linings and pads by fibres like synthetic aramids (Adeyemi *et al*., 2016). The paper published by Blau 2001 reported the additive effects of different kinds of non-asbestos materials on friction material for brake pads. As a result of these efforts, asbestos-free organic, semi-metallic and metallic friction lining materials are now increasingly being utilized.

It is now generally known that during application, asbestos releases hazardous gases which cause damage to human health and this is not desirable, thus; leading to searches for substitute materials that are easy to come by and human-friendly. Asbestos is pronounced carcinogenic with associated diseases that include asbestosis, mesothelioma, lung cancer and other cancers (Anon, 2004). Because of this adverse effect, asbestos is no longer acceptable for brake lining production, therefore; new asbestos-free friction materials are encouraged to be developed. Brake pads are tested to ascertain properties that make them suitable for the application. Properties to be determined include abrasion resistance, friction coefficient, hardness, tensile strength, specific gravity, compressive strength, oil absorption, water absorption, thermal conductivity, disc temperature and stopping time (Dagwa & Ibhadode 2006).

Non-asbestos organic (NAO) based friction materials are multi-ingredient systems that contain more than 10 ingredients to achieve performance properties expected of good friction material as a single material cannot give the properties (Adekunle *et al*., 2023). The ingredients used for the formulation of brake pads are classified into four major categories, namely; binder, fibres, friction modifiers and fillers based on the major function they perform apart from controlling friction and wear resistance. The central part of a system which binds the ingredients firmly to maintain their structure for it to perform the desired function in the friction materials is known as a binder. Friction modifiers help to control the desired range of friction and the fibres incorporated give rise to the strength of the structure. Good friction material should possess a relatively high coefficient of friction, good thermal conductivity, minimum wear rate and good wear resistance when subjected to heavy loads and high speeds (Chan & Stachowiak, 2004).

2.0 Agro-animal residues in brake friction material development

There is an evolution of new materials and constituents currently used in automobile brake friction material after the phasing-out of asbestos, which had gained widespread acknowledgements as a carcinogen, although the introduction of the asbestos restriction in some countries only came about in 1989. Bashar *et al*. (2012) developed brake friction material from coconut shells (filler), epoxy resin (binder), iron chips (reinforcement), methyl ethyl ketone peroxide (catalyst), cobalt nephthanate (accelerator), iron and silica (abrasives), and brass (friction modifier) using particle size of 710µm. The research concluded that the higher the percentage of coconut powder in the specimen, the lower the breaking strength, hardness, compressive strength, and impact, thus high percentage of ground coconut powder induces brittleness, which is in line with the conclusion that the tensile and impact strength of treated and untreated palm kernel nut shells polymer composite decreases with increase in its filler content (Ishidi *et al*., 2011).

Yawas *et al*. (2013) researched the Morphology and properties of periwinkle shell asbestos-free brake pads. This work used the periwinkle shell as an alternative for asbestos using five (5) different particle sizes (710, 500, 355, 250, and 125µm). It was concluded that the finer the particle size, the better the properties and the sample with a particle size of 125 µm gave the best results in terms of specific gravity, coefficient of friction, water absorption, oil absorption, hardness and compressive strength of 1.01g/cm^3, 0.35-0.42, 0.39%, 0.37%,116.7 HRB and 147 N/mm^2 respectively

A research study carried out by Idris *et al*., 2013 titled 'Eco-friendly asbestos free brake-pad: Using banana peels' investigated and produced brake pads from banana peels to replace asbestos with phenolic resin (phenol-formaldehyde) as binder. With variation of phenolic resin percentage from 5 to 30 in an interval of 5%wt. The composition was varied. The results of the compressive strength, hardness and specific gravity of the samples increased with the increased percentage of phenolic resin. The oil absorption, water absorption, wear rate and percentage of charred decreased as the percentage of phenolic resin increased. The samples with 25 per cent of un-carbonized banana peels and 30 per cent of carbonized banana peels gave better performance.

Also, in 2015; maize husks (MH) based composite friction material for brake pads was investigated by Ademoh & Adeyemi. In the work, pulverized maize husk was sieved to 300µm with epoxy resin as the binder. The deduction from the laboratory tests such as: hardness, wear rate, tensile strength, compressive strength and thermal conductivity decreases with an increase in content therefore the higher the binder, the higher the value of the properties while the case is reversed for the properties like density, coefficient of friction water absorption and oil

absorption. It was concluded that maize husk particles could be effectively used as a replacement for asbestos and many bio-mass friction materials in automobile brake pad production. In addition, the developed composite brake friction material is eco-friendly without any known health implications, unlike asbestos-lined friction material that releases poisonous substances to the environment.

In conjunction with the ongoing studies of the development of eco-friendly (asbestos-free) brake pads, an alternative production of composite brake friction material was conducted by Adeyemi *et al*., (2016) where agro-waste cocoa bean shells (CBS) particles were used as filler in composite brake friction material formulation. The developed brake friction materials were investigated by subjected to physical, mechanical and tribological tests. The results obtained for the agro-waste based friction material properties like density, water absorption, oil absorption, abrasion resistance, coefficient of friction, thermal conductivity, hardness, tensile strength, and compressive strength were compared favourably with that of commercial friction materials and other existing ones. Sample labelled 'comp. 3' gave superior performance over others with density, water absorption, oil absorption, abrasion resistance, coefficient of friction, thermal conductivity, hardness, tensile strength, and compressive strength of 1.010g/cm^3, 1.188%, 0.275%, 3.934×10E^{-6}, 0.32, 0.2387W/mk, 120.33MPa, 16.882MPa, and 23.150MPa, respectively. It was concluded that cocoa bean shells (CBS) which is an agro-waste material can be effectively used as a replacement for asbestos in friction material for brake pads.

Abhulimen & Orumense (2017) studied the Characterization and development of asbestos-free brake pads, using snail shells and rubber seed husks. The investigation was carried out with a view of replacing the use of asbestos using sieve grades of 125, 250, 350, 500 and 710µm and was characterised by being subjected to X-ray Fluorescence Spectroscopy (XRF), X-ray diffraction (XRD), thermogravimetric analysis (TGA) and differential thermal analysis (DTA). The composite brake friction material was produced in the ratio of 65% snail shell, 10 % rubber seed husk and 25% resin using compression moulding and the particle size of 125 µm gave the best properties in terms of hardness, compressive strength, abrasion resistance, density, coefficient of friction and porosity.

A blend of sawdust, steel dust, silicon carbide, graphite, and epoxy resin has also been used to develop eco-friendly friction material for brake pads by Lawal *et al.* (2017). The study reported a wear rate of 3.23mg/m for the best sample produced. The composite brake friction material's higher wear resistance was attributed to the sample's higher compressive strength, which indicates that there is proper bonding between the composite's particle arrangement and the intermolecular relation are firmly bonded with little pour spaces, which gives rise to low moisture absorption during the percolation test. Adekunle *et al*., (2019) studied the Development of Asbestos-free brake pads using Bamboo leaves. In this study, 100, 200 and 350µm particle sizes were used to produce friction materials samples with composite formulations of 15% steel dust, 10% graphite, 20% resin, and silica carbide varies five (5) times between 35-55% and 0-20% for each particle sizes. The produced samples were subjected to physico-mechanical and tribological testing (hardness, compressive strength, density, porosity, wear rate and flame resistance) and the best performance was recorded for Sample 'A' of a particle size of 100µm.
Lawal *et al.,* (2019) examined the production of automobile friction material for brake pads and the potential of agro-based composites of cashew nut shells and Nigerian gum Arabic binder. The composites were formulated alongside steel dust, silicon carbide, and graphite as additives. The produced friction material showed some favourable properties, such as improved hardness, compressive strength, frictional coefficient, wear rate, and good thermal stability. Popoola *et al*., (2021) investigated the use of palm kernel shells, coconut shells, seashell and cow bone as base materials to develop automobile brake pads. The aforementioned agricultural wastes were mixed in a ratio of 45% base material, 30% binder, 10% filler, 10% lubricant, and 5% abrasive. The samples were produced using sieve grades of 150 µm particle size and were compressed in a mould at a pressure of 15MN/m2 and a temperature of 195^{o}C. The results were compared with both commercial asbestos-based brake pads and laboratory formulated palm kernel shell-based brake pads. Sample 'S3' is a combination of palm kernel shell, coconut shell and seashell; The results of this research work have shown that a combination of agricultural waste materials; coconut shell, seashell, palm kernel shell and cow bone could be very useful in producing brake pad samples using compressive moulding techniques. Sample S3 and S5 gave a better performance in terms of compressive strength and hardness with values of (83.192N/mm^2, 76.74BHN) and (81.126 N/mm^2, 70.05BHN) respectively. Okyere & Amedorme (2023) conducted a study on the utilisation of palm kernel shells, rice straw, rice husk and rice panicles as base material with epoxy resin as a binder for Automobile brake pads. Other additives in the composites include aluminium silicon as abrasive and graphite as lubricant using moulding techniques to produce brake pads. The performance of the produced brake pad was conducted and compared with the existing commercial (asbestos-lined) brake pad which was used as a control sample. The results obtained from the produced samples showed that the particle size had a significant influence on the performance of the brake pad and the sample with 125µm particle size was found to have less hardness, density, water absorption, oil absorption and thermal conductivity while tensile strength and wear resistance of the composite were better than those of particle size of 355 µm and 500 µm. The work concluded that the composite of 125µm gave the best

performance with specific gravity, density, water absorption, oil absorption, wear rate, hardness, compressive strength, tensile strength and thermal conductivity A typical example of agro-residue and asbestos-lined brake pad is shown in Figure 2.

Figure 2: Brake pad (a) Agro composite brake pad (b) Asbestos lined brake pad

Adekunle *et al.* (2023) carried out research which demonstrated that the non-metallic friction material constituent can be replaced by eco-friendly composites of seashells (base material), sawdust (fillers), and other additives such as Palm kernel shell (abrasive), charcoal (lubricant), metal chips (reinforcement) and epoxy resin (binder). The work conducted the physico-mechanical and tribological properties of the developed friction material and was found to be more effective in performance than the reference sample purchased in the market

The performance of brake friction material developed from agro and animal residues is presented in Table 1.

Table 1: Summary of properties of Agro-animal residues brake friction material.

Author(s)	Material	Physical Properties			Mechanical Properties			Tribological Properties		
		Density	H_2O	Oil	HDN	Tens	Com	COF	Th C	WR
Adekunle *et al*., 2023	Seashell	1.015	20.247	13.326	57.4	---	17.741	0.315	2.799	0.0614 mm^3 /Nm
Okyere & Amedorne 2023	PKS, RS, RH, and RP	2.47	1.3	1.01	125	15.03	25.4	---	0.689	0.35mg/m
Popoola *et al*., 2021	PKS, CS, SS & CB	3.705	5.905	1.295	76.74	---	83.192	0.44	---	---
Adekunle *et al*., 2019	Bamboo leaves	1.746	7.37	----	258	---	111	---	---	12.21g/km (10^{-2})
Uzochukwu *et al*., 2019	CH and PS	1.79	1.01	0.71	93	---	86.94	0.31	---	3.56×10^{-4}
Ishola *et al*., 2017	Palm kernel shell	1.51	0.11	----	269	---	131	---	---	1.684mg/m
Lawal *et al*., 2017	Sawdust	1.91	3.23	----	258	---	113	---	---	3.23
Adeyemi *et al*., 2016	Cocoa beans	1.01	1.19	0.28	120.3	16.88	23.2+	0.35	0.338	3.934
	PKS+CBS+ MH	0.852	0.91	0.58	127.8	20.22	10.3+	0.40	0.372	2.146
Afolabi *et al*., 2015	Palm kernel shell	---	5.05	2.23	55.7	23	----	0.735	---	$9.57E^{-7}$
	cow bone	---	5.53	4.16	46.0	21	----	0.677	---	$1.44E^{-6}$
Ademoh & Adeyemi, 2015	Maize Husk	0.852	0.725	0.660	99.34	14.41	6.779	0.37	0.330	4.470 E^{-6} g/m
Egeonu *et al*., 2015	PKS and CS	---	0.0470	---	63.0	---	----	0.362	---	0.00334g/sec
Katsina *et al*., 2015	cow hooves	---	1.54	0.83	72.67	---	84.23	0.42	---	2.08×10^{-4}
Edokpia *et al*., 2014	Egg Shell	1.650	3.21	1.15	99.1	---	103.0	0.30	---	4.000
Deepika *et al*., 2013	Palm kernel shell)	----	5.03	0.44	92	6.8	103.5	0.44	1.46	4.4 mg/m
Idris *et al*., 2013	Carbonized BP	1.20	3.0	---	71.6	---	61.20	0.35	---	4.67mg/m
	Uncarbonized BP	1.26	3.21	---	98.8	---	95.6	0.40	---	4.15 mg/m
Yawas *et al*., 2013	Periwinkle	1.01	0.39	0.37	116.7	---	147	0.41	---	---
Bashir *et al*., 2012	Coconut Shell	1.20	3.0	---	71.6	---	61.2	---	---	4.67 mg/m
Aigbodion *et al*., 2010	Bagasse	1.430	3.48	1.11	100.5	---	105.6	0.42	---	4.200

Key note: Water absorption (H_2O); oil absorption (Oil); Hardness (HDN); Tensile strength (Tens); Compressive strength (Com); Coefficient of friction (COF); Thermal conductivity (ThC); Wear rate (WR); Palm kernel shell (PKS); Coconut Shell (CS), Seashell (SS); Cow bone (CB), Cow hooves (CH), Periwinkle shell (PS); Cocoa beans shell (CBS); Maize husk (MH); Banana peel (BP), Rice Husk (RH), Rice Straw (RS), Rice Panicle (RP).

3.0 CONCLUSION

Agro-animal residues have displayed a huge potential for asbestos-free brake friction material and with this promising outlook of the properties obtained with over 80% recommendation from the literature of agro-animal residues and confine performance with health hazardous asbestos lined brake pad, The commercialisation of agro-animal friction material for brake pad production should be encouraged to beat the toxic substances release to the environment by the automobile to make a safe environment for the road users, maintenance personnel and manufacturers during automobile operation as well as converting agro-animal residues materials to an engineering product which serves as an addition to the country's gross domestic products.

REFERENCES

Abhulimen E. A. & Orumense F. F. O. (2017). Characterization and development of asbestos-free brake pad, using snail shell and rubber seed husk. *African Journal of Engineering Research*, *5*(2), pp (24-34), ISSN: 2354-2144.

Adekunle A., Okunlola M., Omoniyi P., Adeleke A., Ikubanni P., Popoola T., & Ibrahim H. (2023). Development and analysis of friction material for eco-friendly brake pad using seashell composite. *Scientia Iranica, 30*(5), 1562-1571. dio:10.24200/SCI2022.59835.6464

Adekunle N. O., Oladejo K. A., Kuye S. I & Aikulola A. D. (2019). Development of asbestos-free Brake pads using bamboo leaves. *Nigerian Journal of Environmental Sciences and Technology (NIJEST), 3*(2). ISSN (print): 2616-051X; ISSN (electronic): 2616-0501.

Adeyemi I. O., Ademoh N. A. & Okwu M. O. (2016). "Development and assessment of composite brake pad using pulverized cocoa beans shells filler". *International Journal of Materials Science and Applications, 5*(2), pp. 66-78. doi: 10.11648/j.ijmsa.20160502.16. ISSN: 2327-2635 (Print); ISSN: 2327-2643 (Online)

Adeyemi, I. O., Ademoh A. N & Thankgod E. Boye (2016). Development of Asbestos-Free Automotive Brake Pad Using Ternary Agro-Waste Fillers. *Journal of Multidisciplinary Engineering Science and Technology (JMEST), 3*(7), 2458-9403.

Ademoh A. Nuhu & Adeyemi I. Olabisi. (2015). Development and Evaluation of Maize Husks (Asbestos-Free) Based Brake Pad. *International Institute for Science, Technology and Education (IISTE): Industrial Engineering Letters -IEL*, *5*(2), pp. 67–80.

Afolabi Mayowa, Abubakre O.K., Lawal S.A. & Raji Abdulkabir (2015). Experimental investigation of palm kernel shell and cow bone reinforced polymer composites for brake pad production. *International Journal of Chemistry and Materials Research, 3*(2), 27-40. DOI: 10.18488/journal.64/2015.3.2/64.2.27.40

Aigbodion, V. S., Akadike, U., Hassan, S. B., Asuke, F. & Agunsoye, J. O. (2010). Development of Asbestos – free Brake Pad Using Bagasse. *Tribology in industry*, *32*(1), 45–50.

Anon (2004). Automotive Brake Repairs Trends and Safety Issues. Retrieved from http//www.sirim.my/amtee/pm/brake.hltm

Bashar Dan-Asabe Peter, Madakson B., & Manji Joseph (2012). Material Selection and Production of a Cold-worked Composite Brake Pad. *World Journal of Engineering and Pure and Applied Science (WJEPAS), 2*(3), pp. 96.

Blau, J. P. (2001). Compositions, Functions and Testing of Friction Brake Materials and their Additives. Being a report by Oak Ridge National Laboratory for U.S. Dept. of Energy. Retrieved from http://www.Ornl.- gov/-webworks/cppr/y2001/rpt/112956.pdf, 78–80.

Bono S. G. & Dekyrger, W. J. (1990). Auto Technology, Theory and Service (2nd ed.). *DELMAR Publishers*, New York, 45–48.

Chan D. & Stachowiak G.W (2004). Review of Automotive brake friction materials. School of Mechanical Engineering, University of Western Australia, Crawley, Australia. *J. Automobile Engineering. Proc. Instn Mech. Engr,s, 2*(18).

Dagwa, I. M. & Ibhadode, A. O. A. (2006). Determination of Optimum Manufacturing Conditions for Asbestos-free Brake Pad Using Taguchi Method. *Nigerian Journal of Engineering Research and Development,* Basade Publishing Press Ondo, Nigeria, *5*(4), pp. 1–8.

Dagwa, I. M. & Ibhadode, A. O. A. (2005). Design and Manufacture of Automobile Disk Brake Pad Test Rig. *Nigerian Journal of Engineering Research and Development*, *4*(3), pp. 15-24.

Deepika K., Bhaskar Reddy C. & Ramana Reddy D. (2013). Fabrication and Performance Evaluation of a Composite Material for Wear Resistance Application. *International Journal of Engineering Science and Innovative Technology (IJESIT), 2*(6), pp. 1-6.

Edokpia, R. O., Aigbodion, V. S., Obiorah, O. B. & Atuanya, C. U. (2014). Evaluation of the Properties of Ecofriendly Brake Pad Using Egg Shell Particles–Gum Arabic. ScienceDirect, *Elsevier,* DOI: 10.1016/j.rinp.2014.06.003

Elakhame Z. U., Omowunmi O.J., Komolafe A. O., Olotu O.O., Kaffo P.O., Alausa N. A., Obe Y.J.& Ojuolape A.A (2017). Manufacture of Automotive brake pads from sawdust Composites. *International Journal of Scientific & Enginnering Research, 8*(8), Pg 1228-1234

Egeonu Darlington & Okolo Chukwumaobi Oluah Patrick (2015). Production of Eco-Friendly Brake Pad Using Raw Materials Sourced Locally in Nsukka. *Journal of Energy Technologies and Policy*, *5*(11), (2224-3232), www.iiste.org

Idris, U. D., Aigbodion, V. S., Abubakar, I. J. & Nwoye, C. I. (2013). Eco-friendly asbestos free brake-pad: Using banana peels. *Journal of King Saud University – Engineering Sciences*

Ishidi, E. Y., Kolawole, E. G. & Sunmonu, K. O. (2011). Morphology and thermal property of alkaline treated palm kernel nut shell HDPE composite. *Journal of Emerging Trends in Engineering and Applied Sciences (JETEAS)*, *2*(2), pp.346-350.

Ishola Mohammed Tiamiyu, Ojo Olatunji Oladimeji & Kaffo Omoniyi Paul (2017). Development of Eco-friendly Automobile Brake Pad Using Different grade sizes of Palm Kernel Shell Powder. *Current Journal of Applied Science and Technology, 23*(2):1-4. ISSN:2231-0843.

Katsina C. B., Mark Okoli & Mathew S. A. (2015). Development of automobile brake lining using pulverised cow hooves, *Leonardo Journal of science*, *2*(2), p. 98-108.

Kumar Naveen, Ajaya Bharti, Goyal H.S. & Kunvar Kant Patel (2021). The Evolution of Brake Friction Materials: A Review, *Materials Physics and Mechanics,* 47, 796-815

Kumar P. Manoj, Harish Bachina, Gowthaman S. and Rajesh K. 2017. Development and study of tribological properties of Biocomposite for brake pad application. International journal of mechanical and production Engineering Research and Development (IJMPERD), *7*(6), pg 263-270, ISSN (P) :2249-6890, (E): 2249-8001.

LAWAL S. S, BALA K. C. & ALEGBEDE A. T. (2017). Development and production of brake pad from sawdust composite. *Leonardo Journal of Sciences*, pp. 47-56.

Mathew B. C. & Muruga Lal Jeyan J. V. (2018). Experimental wear analysis of silicon carbide disc brake pad assembly*, Journal of Emerging Technologies and Innovative Research (JETIR)*, *5*(11), ISSN:2349-5162.

Olele, P.C., Nkwocha, A.C., Ekeke, I.C., Ileagu, M.O. & Okeke, E. O. (2016). Assessment of Palm Kernel Shell as Friction Material for Brake Pad Production. *International Journal of Engineering and Management Research*. 6(1), ISSN (ONLINE): 2250-0758, ISSN (PRINT): 2394-6962, ISSN (ONLINE): 2250-0758, ISSN (PRINT): 2394-6962

Popoola O.T., Rabiu A.B., Ibrahim H.K., Omoniyi P.O., Babatunde M.A., Muhammed N. & Isiaq F.O. (2021). Production of Automobile Brake Pads from Palm Kernel Shell, Coconut Shell, Seashell and Cow Bone. *Adeleke University Journal of Engineering and Technology*, *4*(2), 92 – 101, ISSN: 2714 – 2450.

Publication of the International Ban Asbestos Secretariat (2013). Australia. Retrieved fromhttp://www.commerce.wa.gov.au/worksafe/content/safety_topics/Asbestos/Ban_on_chrysotile_asbestos.html

Srikanth Sivaramakrishnan (2013). Discrete Tire Modelling for Anti-lock Braking System Simulations, Goodyear Tire and Rubber Company, *ResearchGate*, https://www.researchgate.net/publication/275889946

Uzochukwu M.I, Aiyejagbara M.O, & Ugbaja M.I (2019). Property Investigation of Cow horn /Periwinkle Shell Epoxy Composite for Automobile Brake Pad Linings. *Journal of Emerging Trends in Engineering and Applied Sciences (JETEAS)*, *10*(2), pp 48-53, (2141-7016).

Yawas, D. S., Aku, S. Y. & Amaren, S. G. (2013). Morphology and properties of periwinkle shell asbestos-free brake pad. *Journal of King Saud University – Engineering Sciences*.

PAPER 84 - INVESTIGATING THE MECHANICAL BEHAVIOR OF GEOPOLYMER CONCRETE AFTER EXPOSURE TO ELEVATED TEMPERATURES

M. A. M. Rihan [1,2 *], R. O. Onchiri [3], N. Gathimba [4], B. Sabuni [5]

[1] Pan African University Institute for Basic Sciences, Technology, and Innovation, hosted at the Jomo Kenyatta University of Agriculture and Technology, P. O. Box 62000-00200, Nairobi, Kenya.
[2] Civil Engineering Department, Faculty of Engineering, University of Kordofan, El Obeid 51111, Sudan.
[3] Department of Building and Civil Engineering, Technical University of Mombasa (TUM), P.O.BOX 90420-80100, Mombasa, Kenya.
[4] Department of Civil, Construction and Environmental Engineering, Jomo Kenyatta University of Agriculture and Technology, Kenya.
[5] Department of Civil and Structural Engineering, Masinde Muliro University of Science and Technology, P.O. Box 190 50100, Kakamega Kenya.
[*]Corresponding author: moharihan20@gmail.com , rihan.mohammed@students.jkuat.ac.ke

ABSTRACT

Geopolymer or alkali-activated binders are being recognized as an eco-friendly and sustainable substitute for ordinary Portland cement (OPC). Geopolymers offer environmental advantages and possess notable mechanical properties, such as exceptional high-temperature endurance. While numerous studies have examined the thermal properties of geopolymer concrete, there is limited research on the behavior of fly ash and sugarcane bagasse ash-based geopolymer concrete at high temperatures. Therefore, the current work examines the mechanical characteristics of geopolymer concrete (GPC) made up of fly ash and sugarcane bagasse ash after exposure to high temperatures. The mechanical properties of the GPC and OPC concrete specimens were evaluated after they were heated to elevated temperatures of 200 °C, 400 °C, 600 °C, and 800 °C. This study results revealed that heated GPC specimens have an 18% loss in compressive strength compared to unheated GPC specimens when exposed to 200 °C. However, when heating GPC specimens to 400 °C, 600 °C, and 800 °C, their compressive strength (C_{str}) decreases by approximately 27%, 66%, and 74%, respectively.

KEYWORDS: Geopolymer concrete, Sugarcane bagasse ash, Elevated temperature, Mechanical properties

1 INTRODUCTION

Factory production of ordinary Portland cement (OPC) uses a substantial amount of fuel and also leads to the release of carbon dioxide (CO_2) into the ecosystem (Alahmari et al., 2023; Rihan & Abdalla Abdalla, 2024). Roughly 10% of the worldwide CO_2 releases are attributed to the production of OPC (H.M & Unnikrishnan, 2023). The increasing focus on utilizing construction materials with minimal carbon emissions as a substitute for cement is driven by the abundant availability of naturally occurring resources (Manjunath *et al.,* 2019). Besides the worries about climate change, the durability and sustainability of concrete have significant consequences (Kanagaraj et al., 2022). Certain alumino-silicate materials can result in the formation of geopolymer concrete (GPC) when activated with an alkaline solution.

Geopolymer, which uses industrial byproducts as a source material activated by alkaline solutions, has been shown to be the most appropriate substitute for cement. In 1978, Davidovits introduced Geopolymers, a revolutionary family of inorganic polymer binders (Moradikhou *et al.,* 2023). Geopolymers, which are inorganic aluminosilicate compounds, consist of an alkaline solution and a raw material rich in SiO_2 and Al_2O_3 (Aslani & Asif, 2019). GPC production reduces the usage of cement and employs eco-friendly binder resources such as Fly Ash (FA) (Ahmad *et al.,* 2022), slag (Sedaghatdoost et al., 2019), Rice Husk Ash (RHA) (Saloni et al., 2021), Metakaolin (MK) (Amin *et al.,* 2022), Palm Oil Fuel Ash (POFA) (Bashar *et al.,* 2022), Sugarcane Bagasse Ash (SCBA) (M. A. M. Rihan *et al.,* 2024), etc. In addition to the binder material, another significant factor in the manufacturing of GPC is the Alkaline Solution (AS), which consists of a blend of silicate and hydroxide based on sodium (Na) or potassium (K) (Islam *et al.,* 2015). According to recent literature, GPC reduces CO_2 by 70% based on raw material consumption for concrete production (Turner & Collins, 2013). Furthermore, the GPC created with alkaline activators can demonstrate excellent fire resistance as well as strong resistance to chemical attack. Recent research indicates that geopolymer cement shows promise as a superior substitute for producing concrete under elevated temperatures (Hussin *et al.,* 2015).

Previous research has indicated that GPC exhibits superior durability properties compared to traditional OPC concrete (Singh et al., 2024). For example, prior research has evaluated the resistance of slag and FA-based GPC against attacks by acid, sulphate, and chloride, with generally favorable findings (Manjunath et al., 2019). Hassan et al (Hassan et al., 2020) found that GPC samples treated in ambient and elevated temperatures exhibited resistance to temperatures up to 600 °C. Conversely, the OPC concrete experiences a notable decrease in strength when heated to 400 °C. Amin et al (Amin et al., 2022) inspected the influence of high temperatures on GPC, exposing it to temperatures differing from 100 to 700 °C. They found that the GPC mixes began to weaken at 200 °C as a result of internal cracks and debonding. In an evaluation involving GPC samples exposed to 200, 400, and 600 °C temperatures, Albidah et al. (Albidah et al., 2022) discovered that the rate of reduction in (C_{str}) rose when the temperature was elevated from ambient conditions to 200 °C, but it decreased less when the temperature grew up from 200 to 400 °C. Additionally, the residual strength varied between 56% and 34%. According to Ozbayarak et al. (Özbayrak *et al.,* 2023), strength reduced as exposure temperature increased for GPC specimens.

Researchers have focused more on employing agricultural and industrial waste such as FA, MK, RHA, corncob ash, and GGBS as binder materials for the creation of GPC, and their studies have demonstrated positive outcomes. The durability performance of GPC at higher temperatures based on FA-SCBA has not been thoroughly researched. Therefore, the goal of this investigation is to assess the behaviour of FA-SCBA-based GPC when it is exposed to higher temperatures of 200°C, 400°C, 600°C, and 800° C.

2 EXPERIMENTAL PROGRAM

2.1 Materials Used

2.1.1 FA and SCBA

FA was brought in from India, and SCBA was collected from Sukari Industries Ltd in Western Kenya. A chemical analysis was performed on FA and SCBA using X-ray fluorescence (XRF) and the outcomes are displayed in Table 1. Figure 1 depicts the X-ray diffraction (XRD) patterns for FA and SCBA. The predominant mineralogical phases in FA were quartz, chlorite, and muscovite, whereas SCBA had more quartz phases. Figure 2 depicts the scanning electron microscopy (SEM) images of the FA and SCBA, offering a more detailed representation of the particle's structure. The SCBA particles are shaped like fibrous and uneven flakes, with spherical surface capillary pores.

2.1.2 Aggregates

The coarse aggregate, made from crushed stone, had a 2.66 specific gravity, and up to 12.5 mm in maximum size. The fine aggregate comprised 30% quarry dust and 70% river sand, which were filtered through an ASTM 0.18 mm sieve and then dried in an oven at 105°C for 24 h

2.1.3 Alkaline activators

In this experiment, Na_2SiO_3 and NaOH were used as activators. They were bought from Euro Industrial Chemicals in Nairobi, Kenya. The Na_2SO_3 had a specific gravity of 1.530 at a temperature of 20 ° C. It had a Na_2O: SiO_2 ratio of 1:2.10, with Na_2O accounting for 13.76% and SiO_2 accounting for 28.9%. The NaOH pearls utilized in the investigation have a minimum purity of 99%.

Table 1 Oxide Content of SCBA and FA.

Contents	SiO_2	Al_2O_3	Fe_2O_3	CaO	K_2O	MgO	P_2O_5	TiO_2	MnO	LOI
SCBA	76	9	4.2	3.1	3.83	2.7	0.69	0.46	0.2	0.97
FA	54	19.6	6.9	7.9	2.2	6.9	0.34	0.88	0.1	1.87

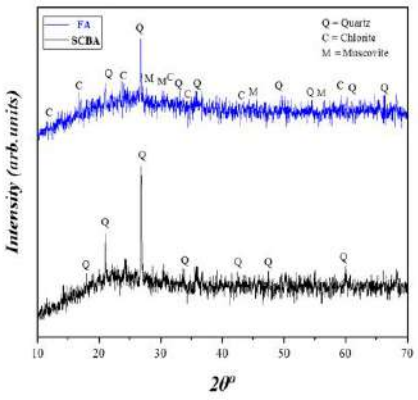

Figure 1. XRD analysis of FA and SCBA.

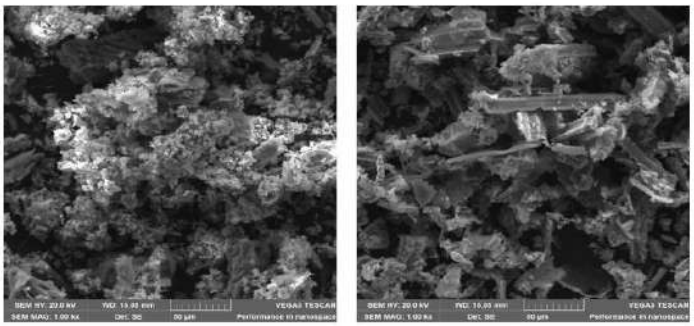

(a) FA (b) SCBA

Figure 2. Scanning electron microscope of FA and SCBA

2.2 Mix proportions

This study uses geopolymer mixture proportion as presented in Table 2 (M. Rihan *et al.,* 2024). The GPC mixture contained 72% aggregates, with fine aggregate making up around 41% of the total aggregates. The activator/FA proportion was 0.35, The ratio between Na_2SiO_3 and NaOH was 1.5., and the molarity of NaOH was 14. Table 2 provides the percentage of components needed for 1 m^3 of GPC mixture based on the previously mentioned proportions.

Table 2 GPC and OPC concrete mix (kg/m3)

Mix No	FA	SCBA	OPC	Coarse aggregate	Fine aggregate	Na_2SiO_3	NaOH	S. P	Curing regime
1	500	-	-	1000	700	105	70	12.5	80 ° C
2	475	25	-	1000	700	105	70	12.5	80 ° C
3	-	-	500	1000	700	105	70	12.5	Water

2.3 Casting and specimen curing

The aggregates, both fine and coarse, were well mixed for 3-4 minutes. Following this, FA and SCBA were added and blend dry for an additional 4 to 5 minutes before the alkaline solution was introduced. The Na_2SiO_3 and NaOH were added and mixed for 4 minutes to create geopolymer concrete. After the mixing was finished, the prepared GPC was placed into a mould and cured in an oven at 80°C for 24 h.

2.4 High -Temperature furnace

In the present experiment, the high-temperature furnace is utilized to expose GPC specimens to extremely high temperatures of up to 800 °C. Figure 3 shows the detailed processes of generating heat and cooling at high temperatures. GPC samples were subjected to different temperatures of 200, 400, 600, and 800 °C to analyze their mechanical characteristics. After being taken out of the furnace, the samples were let to cool for 24 hours at room temperature before undergoing testing.

2.5 Testing method

2.5.1 Weight loss

By comparing the weight of the OPC and GPC samples before and after they were exposed to high temperatures, the weight loss of the specimens was evaluated. Equation 1 is used to assess the weight loss of the GPC specimens following their exposure to elevated temperatures. The following formula is utilized to calculate the weight reduction as a percentage.

$$Weight\ loss\ (\%) = \frac{W_1 - W_2}{W_1} \times 100 \quad (1)$$

W_1 refers to the weight of the specimen before being subjected to temperature, W_2 refers to the weight of the specimen after subjected to temperature.

2.5.2 Compressive strength loss

The elevated temperature test was conducted in accordance with ASTM E119 – 20. A total of 18 cubes of 100 mm size were cast. After a period of 28 days, the samples were placed inside an electric furnace and exposed to temperatures of 200, 400, 600, and 800 °C for a duration of two hours. After being removed from the furnace, the specimens were left to cool and the residual compressive strength was assessed.

3 RESULTS AND DISCUSSION

3.1 Visual appearance

Figure 4 displays photos of the specimens from different mixtures both before and after being exposed to temperatures up to 800 °C. A change in color was observed in the specimen when it was subjected to greater temperatures. In the initial stages of the heating procedure, the GPC specimen did not exhibit any cracks. The moisture content evaporates from the GPC specimens as a result of rising temperatures, changing their color and causing cracks. When the temperature rose to 600 °C and 800 °C, hairline cracks began to emerge on the surface of the GPC samples; however, cracking was not visible when the temperature was between 200 and 400 °C. The GPC specimen's color changed from dark brown to light brown after it was exposed to temperatures of 600 °C and 800 °C.

3.2 Loss in mass

Figure 5 displays the experimental findings on the reduction in weight of OPC concrete and GPC when subjected to various temperatures. As Figure 5 illustrates, the OPC experienced a weight loss of around 8.31% when subjected to a temperature of 800° C, whereas the GPC only saw a weight reduction of 6.9%. Previous research (Albidah *et al.,* 2020) showed that weight loss at temperatures up to 200 ◦C was caused because of

the lack of free water in pores and partly by chemically bound water from the dehydration of geopolymer gel. At temperatures above 200 ◦C, the dehydration and de-hydroxylation of the hydroxyl groups in the geopolymer gel were responsible for the weight loss (Chan & Zhang, 2022).

3.3 Loss in compressive strength

Figure 6 shows the residual C_{str}, for each tested mixture as a function of exposure temperatures: 200, 400, 600, and 800 °C. All mixtures, the figure shows, typically lost compressive strength as the temperature rose from room temperature to 800 °C; However, the rate of decline decreased when the temperature rose from ambient temperature to 200 °C. The main reasons for strength loss during exposure to high temperatures are mass loss and thermal deformation brought on by moisture evaporation. The water in the specimen migrates to the outside surface where it evaporates, consisting of both free and chemically bound water. This process damages the interior microstructure of the specimen, leading to a reduction in C_{str}.

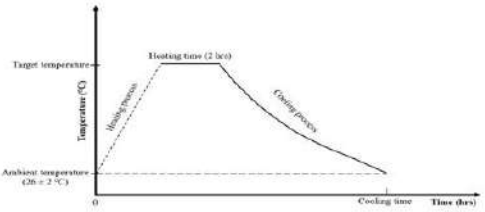

Figure 3. Heating–cooling process of elevated temperature used.

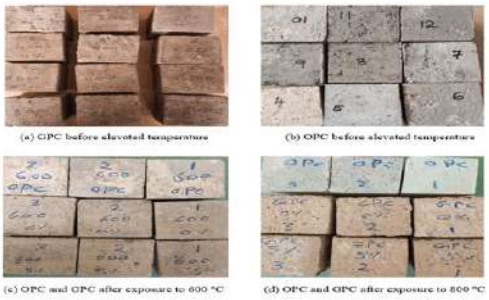

Figure 4. Photograph of samples before and after exposure to extreme temperatures.

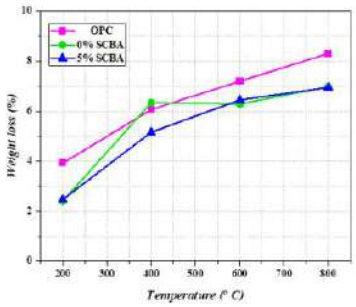

Figure 5. Impact of the temperature on FA-SCBA geopolymer concrete.

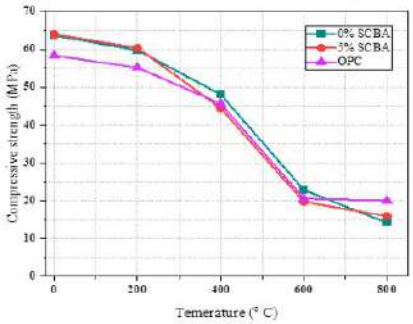

Figure 6. Temperature's effects on compressive strength

4 CONCLUSION

This investigation looked at the impact of exposing fly ash-sugarcane bagasse ash-based GPC to temperatures of 200 °C, 400 °C, 600 °C, and 800 °C. The results were assessed based on visual observations and tests conducted, including Cstr development and weight loss % resulting from exposure to high temperatures. The following conclusions are drawn in considering the findings of the aforementioned study:

- Heated GPC specimens have an 18% loss in compressive strength compared to unheated GPC specimens when exposed to 200 °C. Higher temperatures lead to additional decreases in compressive strength. When heating GPC specimens to 400 °C, 600 °C, and 800 °C, their C_{str} decreases by approximately 27%, 66%, and 74%, respectively.
- The weight loss for the GPC specimens increases slightly as the temperature rises. Weight reduction at 800 °C for GPC containing 0% SCBA is 6.98%, while for GPC containing 5% SCBA, it is 6.95%. Nevertheless, the weight loss of the OPC samples is found to be 8.31% at a temperature of 800 °C.

5 FUTURE RECOMMENDATIONS

To better understand the effect of elevated temperature on fly ash-sugarcane bagasse ash based geopolymer concrete, the microstructure/nanostructure and chemistry of geopolymer after exposure to elevated temperature must be thoroughly explored.

REFERENCES

Ahmad, A., Ahmad, W., Aslam, F., & Joyklad, P. (2022). Compressive strength prediction of fly ash-based geopolymer concrete via advanced machine learning techniques. *Case Studies in Construction Materials*, *16*, e00840. https://doi.org/https://doi.org/10.1016/j.cscm.2021.e00840

Alahmari, T. S., Abdalla, T. A., & Rihan, M. A. M. (2023). Review of Recent Developments Regarding the Durability Performance of Eco-Friendly Geopolymer Concrete. *Buildings*. https://doi.org/10.3390/buildings13123033

Albidah, A., Abadel, A., Alrshoudi, F., Altheeb, A., Abbas, H., & Al-Salloum, Y. (2020). Bond strength between concrete substrate and metakaolin geopolymer repair mortars at ambient and elevated temperatures. *Journal*

of Materials Research and Technology, *9*(5), 10732-10745. https://doi.org/https://doi.org/10.1016/j.jmrt.2020.07.092

Albidah, A., Alqarni, A. S., Abbas, H., Almusallam, T., & Al-Salloum, Y. (2022). Behavior of Metakaolin-Based geopolymer concrete at ambient and elevated temperatures. *Construction and Building Materials*, *317*, 125910. https://doi.org/https://doi.org/10.1016/j.conbuildmat.2021.125910

Amin, M., Elsakhawy, Y., Abu el-hassan, K., & Abdelsalam, B. A. (2022). Behavior evaluation of sustainable high strength geopolymer concrete based on fly ash, metakaolin, and slag. *Case Studies in Construction Materials*, *16*. https://doi.org/10.1016/j.cscm.2022.e00976

Aslani, F., & Asif, Z. (2019). Properties of Ambient-Cured Normal and Heavyweight Geopolymer Concrete Exposed to High Temperatures. *Materials (Basel)*, *12*(5). https://doi.org/10.3390/ma12050740

Bashar, I. I., Alengaram, U. J., & Jumaat, M. Z. (2022). Enunciation of embryonic palm oil clinker based geopolymer concrete and its engineering properties. *Construction and Building Materials*, *318*, 125975. https://doi.org/https://doi.org/10.1016/j.conbuildmat.2021.125975

Chan, C. L., & Zhang, M. (2022). Behaviour of strain hardening geopolymer composites at elevated temperatures. *Cement and Concrete Composites*, *132*, 104634. https://doi.org/https://doi.org/10.1016/j.cemconcomp.2022.104634

H.M, T., & Unnikrishnan, S. (2023). Durability and elevated temperature behaviour of geopolymer concrete developed with ground granulated blast furnace slag and sugarcane bagasse ash. *Journal of Building Pathology and Rehabilitation*, *8*(2), 106. https://doi.org/10.1007/s41024-023-00354-7

Hassan, A., Arif, M., & Shariq, M. (2020). Mechanical Behaviour and Microstructural Investigation of Geopolymer Concrete After Exposure to Elevated Temperatures. *Arabian Journal for Science and Engineering*, *45*(5), 3843-3861. https://doi.org/10.1007/s13369-019-04269-9

Hussin, M. W., Bhutta, M. A. R., Azreen, M., Ramadhansyah, P. J., & Mirza, J. (2015). Performance of blended ash geopolymer concrete at elevated temperatures. *Materials and Structures*, *48*(3), 709-720. https://doi.org/10.1617/s11527-014-0251-5

Islam, A., Alengaram, U. J., Jumaat, M. Z., Bashar, I. I., & Kabir, S. M. A. (2015). Engineering properties and carbon footprint of ground granulated blast-furnace slag-palm oil fuel ash-based structural geopolymer concrete. *Construction and Building Materials*, *101*, 503-521. https://doi.org/https://doi.org/10.1016/j.conbuildmat.2015.10.026

Kanagaraj, B., Anand, N., Andrushia, A. D., & Lubloy, E. (2022). Investigation on engineering properties and micro-structure characteristics of low strength and high strength geopolymer composites subjected to standard temperature exposure. *Case Studies in Construction Materials*, *17*, e01608. https://doi.org/https://doi.org/10.1016/j.cscm.2022.e01608

Manjunath, R., Narasimhan, M. C., & Umesha, K. M. (2019). Studies on high performance alkali activated slag concrete mixes subjected to aggressive environments and sustained elevated temperatures. *Construction and Building Materials*, *229*, 116887. https://doi.org/https://doi.org/10.1016/j.conbuildmat.2019.116887

Moradikhou, A. B., Safehian, M., & Golafshani, E. M. (2023). High-strength geopolymer concrete based on coal washing waste. *Construction and Building Materials*, *362*, 129675. https://doi.org/https://doi.org/10.1016/j.conbuildmat.2022.129675

Özbayrak, A., Kucukgoncu, H., Aslanbay, H. H., Aslanbay, Y. G., & Atas, O. (2023). Comprehensive experimental analysis of the effects of elevated temperatures in geopolymer concretes with variable alkali activator ratios. *Journal of Building Engineering*, *68*, 106108. https://doi.org/https://doi.org/10.1016/j.jobe.2023.106108

Rihan, M., Onchiri, R. O., Gathimba, N., & Sabuni, B. (2024). Mechanical and Microstructural Properties of Geopolymer Concrete Containing Fly Ash and Sugarcane Bagasse Ash. *Civil Engineering Journal*, *10*(4). https://doi.org/10.28991/CEJ-2024-010-04-018

Rihan, M. A. M., & Abdalla Abdalla, T. (2024). Factors Influencing Compressive Strength in Fly Ash-Based Geopolymer Concrete: A Comprehensive Review. *Iranian Journal of Science and Technology, Transactions of Civil Engineering*. https://doi.org/10.1007/s40996-024-01413-w

Rihan, M. A. M., Alahmari, T. S., Onchiri, R. O., Gathimba, N., & Sabuni, B. (2024). Impact of Alkaline Concentration on the Mechanical Properties of Geopolymer Concrete Made up of Fly Ash and Sugarcane Bagasse Ash. *Sustainability*, *16*(7). https://doi.org/10.3390/su16072841

Saloni, Parveen, Pham, T. M., Lim, Y. Y., Pradhan, S. S., Jatin, & Kumar, J. (2021). Performance of rice husk Ash-Based sustainable geopolymer concrete with Ultra-Fine slag and Corn cob ash. *Construction and Building Materials*, *279*, 122526. https://doi.org/https://doi.org/10.1016/j.conbuildmat.2021.122526

Sedaghatdoost, A., Behfarnia, K., Bayati, M., & Vaezi, M. s. (2019). Influence of recycled concrete aggregates on alkali-activated slag mortar exposed to elevated temperatures. *Journal of Building Engineering*, *26*, 100871. https://doi.org/https://doi.org/10.1016/j.jobe.2019.100871

Singh, R. P., Vanapalli, K. R., Jadda, K., & Mohanty, B. (2024). Durability assessment of fly ash, GGBS, and silica fume based geopolymer concrete with recycled aggregates against acid and sulfate attack. *Journal of Building Engineering*, *82*, 108354. https://doi.org/https://doi.org/10.1016/j.jobe.2023.108354

Turner, L. K., & Collins, F. G. (2013). Carbon dioxide equivalent (CO2-e) emissions: A comparison between geopolymer and OPC cement concrete. *Construction and Building Materials*, *43*, 125-130. https://doi.org/https://doi.org/10.1016/j.conbuildmat.2013.01.023

PAPER 87 - FLEXURAL PERFORMANCE OF RICE HUSK ASH-CEMENT CONCRETE REINFORCED WITH OIL PALM *(Elaeis guineensis)* BROOM FIBRE

T. O. Mohammed[1*], A. A. Jimoh[1], Y. O. Babatunde[1], R. O. Sanni[2], A. Sanni[2]

[1]Department of Civil Engineering, University of Ilorin, Ilorin, Nigeria.
[2]Department of Civil Engineering, Kwara State Polytechnic, Kwara State, Nigeria.
[*]Email: taobanj1@gmail.com.

ABSTRACT

Concrete is the most widely used building material worldwide. It is usually made of cement, water, and aggregates. However, because cement prices have been rising steadily, rice husk ash (RHA), an agricultural waste gotten from rice husk, has been utilized in place of certain cements. Although it is known to be weak under tension, concrete is strong in compression. Over the years, concrete has been reinforced using a variety of techniques and materials to address this weakness. Therefore, in this study, oil palm broom fiber (OPBF) was added at volume fractions of 0.5%-5% by weight of RHA-cement at 0.5 interval and compared with the control sample. M25-grade concrete was used with RHA as a 10% partial replacement of cement. The effect of fibre inclusion on the workability and flexural strengths of concrete were determined. Based on the results, the addition of OPBF led to decrease in workability. On the other hand, a significant improvement was observed in the flexural strengths of concrete with the addition of OPBF, achieving a higher flexural strength than the control sample. The highest flexural strength was achieved with the addition of 3% of OPBF; a further addition of fibers beyond 3% decreased the strength.

KEYWORDS: Oil Palm Broom Fiber, Rice Husk Ash, Cement, Concrete, Flexural Strength and Eco-friendly.

1. INTRODUCTION

According to Sohu *et al.* (2017), the construction sector is seen as the backbone of every nation and is essential to both social and economic development. Concrete is one of the most widely utilized building materials in the construction sector (Lakhiar *et al*., 2018), and as a result, demand has increased. Concrete's availability and durability contributed to its rising popularity (Lakhiar *et al*., 2018). It has found applications in wide range of constructions such as residential houses, skyscrapers, bridges, pavements, and dams. However, by the early 1800s, it was understood that concrete lacked tensile strength, ductility, and the capacity to withstand potential breaking since it was weak in tension and extremely strong in compression (Agarwal *et al.*, 2014; Behbahani *et al*., 2011). Once a breakdown occurs, almost all loading capacity may be lost, which eventually restricts its use and application (Agarwal *et al.*, 2014).
Because concrete is a mixture of cement, sand, coarse particles, and water, the coarse aggregates give the structure self-weight. However, this already substantial self-weight grows significantly with the reinforcing of steel bars, increasing the dead-load stress on the structures. In addition, steel bars raise the cost of building and make steel non-renewable (Agarwal *et al*., 2014). In an effort to lessen concrete's brittleness, experts have looked for alternatives. Concrete can overcome this drawback by adding short, sporadically distributed fibers.

Fibers can be used to strengthen concrete's resistance to shrinkage cracking, increase its tensile strength, and improve the concrete's deformation characteristics. In recent times, fiber-reinforced concrete (FRC), has gained popularity. When mixed, hundreds of tiny fibers are randomly distributed throughout the concrete to create fiber-reinforced concrete (FRC), which enhances the qualities of concrete in every direction (Rana, 2013). Although a variety of natural and synthetic fibers have been used in FRC, over the past 20 years, the usage of steel fibers has dramatically increased in the construction of roads, parking lots, industrial pavements, and airports due to its ability to improve structural behavior (Sorelli *et al.*, 2006).

However, the ongoing rise in infrastructure costs, energy requirements, and environmental effects has made substitutes for traditional structural reinforcements like steel necessary. While using steel in concrete has many benefits, it is costly and unsustainable for the environment. With fibers derived from plants, this is not the case.

Fibrous plants are easily regenerated and restocked in developing countries in the tropics, are substantially more affordable to process, and are environmentally friendly. In contrast, steel is imported following the process of

extracting iron ore and subsequent refinement. The process of extracting these fibers involves low-energy methods, like chopping the required plant portions or just collecting the leftover plant material and retting it.
Because of their remarkable mechanical qualities, the ribs of the oil palm tree's leaflets—also referred to as oil palm broom fiber (OPBF)—have recently drawn the attention of researchers (Momoh and Dahunsi, 2017; Momoh and Osofero, 2019; Momoh et al., 2020). According to reports, OPBF has an average tensile strength of 389 MPa, a density of 450–840 kg/m^3, and a water absorption rate of 44.7% in 24 hours. Unlike other vegetable fibers, OPBF has a low affinity for water, does not decay readily, and has a tensile strength-to-weight ratio that is around five times that of steel (Momoh *et al*., 2020). In the review by Momoh and Osofero (2020), an example of various fiber kinds from the oil palm tree is provided.

As of 2017, Nigeria's annual rice output had reached over 15 million metric tonnes. Currently, rice is produced in about 34 states, with the majority of them producing it three times a year (Ahmad, 2017). Silica is found in rice husk ash (RHA), a byproduct of rice husk. Because rice husk is a pozzolanic material, it can be burned to produce Rice Husk Ash (RHA), an agricultural waste that can be a close substitute for cement. About 20 % of the 690 million metric tonnes of rice paddy generated annually worldwide was made up of rice husk (Rice market monitor, 2009). RHA, the residue left over after rice husk is completely burned under regulated conditions, comprises 90–96 percent silicon dioxide in an amorphous form. RHA particles have a very high specific surface area—more than 250 m^3/g—and range in size from 5 to 10 µm (Bui, 2001).

Tariq *et al.* (2021) revealed that the change in compressive, splitting and flexural strength of samples with replacement percentage of RHA up to 18% and that of control specimen is minimal and when RHA is added to concrete as a supplemental cementitious material, the mix becomes more affordable and eco-friendlier. In a similar study, Muleya *et al.* (2021) also revealed that partial replacement of cement with up to 30 % of RHA offer cost-benefit analyses with a focus on enhancing the standard of living for rural populations in rice-growing areas, in addition to producing high-quality and practical concrete.

According to Zaid *et al.* (2021), Concrete was not significantly affected by the 10% replacement of cement with RHA, and the addition of steel fibers and admixtures like superplasticizer can increase the material's economic viability for the building sector. Jhatial *et al.* (2018) also investigated the effect of steel fibers on the compressive and flexural strength of concrete and revealed that adding steel fibers to concrete to reinforce it causes the material to become more ductile and resistant to cracking, improving the mechanical qualities of the concrete (Compressive and Flexural strength) but leads to decrease in workability as the steel fibers addition percentage increases. In similar study by Ghaffar *et al.* (2014), it was also revealed that the improvement in various strengths is obtained with the addition of steel fibres in the plain concrete and the optimum gain in strength of concrete depends on the amount of fibre content. Yaswanth and Premkumar (2017) studied the behaviour of concrete reinforced with bristle coir fibers and revealed that adding Bristle Coir Fibers to concrete leads to improvement in compressive, split tensile and flexural strength of the concrete and the maximum strength is achieved at 1.5% of fibers by total volume of concrete. In similar study by Sohu *et al.* (2018), it was revealed that the workability of concrete reduces when plastic fibres were added and the flexural strength improved up to 16.5% compared to the control sample. Momoh and Dahunsi (2017) also revealed the inclusion of Oil Palm Broom Fibres (OPBF) in reinforcing laterite-based roof tiles and cement mortar improves flexural strength by more than 120 % and the 10 mm mesh size with a calculated fibre volume of 5% of the volume of a roofing tile was chosen as optimum. Previous researches made use of Steel fibres and other natural fibres to reinforce concrete, OPBF have also been used in reinforcing laterite-based roof tiles and cement mortar but this research used oil palm broom fibers with RHA as percentage replacement of cement and their effect on the workability, and flexural strengths of concrete were studied. Therefore, this experimental work was carried out to study the flexural performance of concrete produced with rice husk ash as a partial replacement of cement when it is reinforced with oil palm broom fibers (OPBF) at different volume fractions.

2. MATERIALS AND METHODS

2.1 Materials

The materials used for this research work are mainly Oil Palm Broom Fiber (OPBF), rice husk ash, cement, water, fine aggregate (sharp sand), coarse aggregate (granite) and superplasticizer.

Table 1:Proportion of Concrete Mixes

MIX	CEMENT (Kg/m^3)	RHA (Kg/m^3)	SAND (Kg/m^3)	GRANITE (Kg/m^3)	WATER (Kg/m^3)	SP (Kg/m^3)	OPBF (Kg/m^3)	REMARKS
MIX 1	378.0	42.0	698.0	1162.0	210.0	4.20	0.00	Control - 10% RHA + 0% OPBF
MIX 2	378.0	42.0	698.0	1162.0	210.0	4.20	2.10	10 % RHA + 0.5% OPBF
MIX 3	378.0	42.0	698.0	1162.0	210.0	4.20	4.20	10 % RHA + 1.0% OPBF
MIX 4	378.0	42.0	698.0	1162.0	210.0	4.20	6.30	10 % RHA + 1.5% OPBF
MIX 5	378.0	42.0	698.0	1162.0	210.0	4.20	8.40	10 % RHA + 2.0% OPBF
MIX 6	378.0	42.0	698.0	1162.0	210.0	4.20	10.50	10 % RHA + 2.5% OPBF
MIX 7	378.0	42.0	698.0	1162.0	210.0	4.20	12.60	10 % RHA + 3.0% OPBF
MIX 8	378.0	42.0	698.0	1162.0	210.0	4.20	14.70	10 % RHA + 3.5% OPBF
MIX 9	378.0	42.0	698.0	1162.0	210.0	4.20	16.80	10 % RHA + 4.0% OPBF
MIX 10	378.0	42.0	698.0	1162.0	210.0	4.20	18.90	10 % RHA + 4.5% OPBF
MIX 11	378.0	42.0	698.0	1162.0	210.0	4.20	21.00	10 % RHA + 5.0% OPBF

The OPBF was gotten from Ipata market in Ilorin, Nigeria. The diameter of the OPBFs were measured with vernier calliper and it ranged from 1.8mm to 2.2mm. Then, it was cut with scissors to 45mm length, which gave an average aspect ratio of 22.5. The moisture content, water absorption and tensile strength of the OPBF were determined. The Rice husk was collected from rice milling company situated at Ojagboro area of Ilorin, Nigeria. A controlled incineration chamber at the Fabrication Workshop, Department of Mechanical Engineering, Institute of Technology, Kwara State Polytechnic, Ilorin, Nigeria was used to calcine the rice husk. The Rice Husk Ash (RHA) was obtained by allowing rice husk to undergo a controlled combustion at 700℃ for 4 hours. After 4 hours, the grey coloured rice husk ash was produced and the ash produced was ground for some minutes and passed through sieve 0.6mm. The chemical composition of the RHA was determined using X-ray fluorescence (XRF). Fine aggregate used for this experiment was sand. The sand was obtained from a construction site in the University of Ilorin, Ilorin, Nigeria. Coarse aggregate used for this experiment was granite. Granite of sizes ranging between 5 mm to 20 mm was procured from a construction site in the University of Ilorin, Ilorin, Nigeria. The Specific gravity (SG), Water absorption capacity (WAC), Particle Size Analysis (Sieve Analysis) and Moisture content (MC) of the aggregates were determined in accordance with BS EN 12620 (2013). An Ordinary Portland cement of grade 42.5R and manufactured by Dangote cement company was obtained from a local cement distribution store along Tanke road, Ilorin, Kwara State, Nigeria. Tap water obtained from the Soil Laboratory at the Department of Civil Engineering, University of Ilorin, Ilorin, Nigeria, was used for this research conforms to the requirements of the British Standard (BS) code; BS EN 1008(2002) (Mixing water for concrete). AXION TUFFCRETE liquid polymer in accordance with manufacturer's specification were used as superplasticizer to enhance the flow of the concrete mix when OPBF were added.

Figure 1: Oil palm broom fibres

2.2 Preparation of concrete mix with RHA and OPBF

2.2.1 Mix design of the concrete

The concrete mix design was done in accordance with the Department of Environment (DOE) method with a characteristic strength of 25 N/mm^2 at 28 days.

The proportion of the materials in each of the concrete mixes were presented in Table 1. The RHA was incorporated in the mixes at fixed 10 % replacement of cement, while the OPBF was added in the mix from 0 – 5 % of the cementitious material (RHA and cement) at 0.5 % interval. The superplasticizer used was 1% by weight of the cementitious material. The materials were batched by weight and mixed thoroughly to achieve homogenous concrete paste. The workability of the fresh concrete for each mix was determined in accordance with BS 1881-102 (1983). The apparatus used include mould, scoop, sampling tray, tamping rod, and rule. Concrete beam moulds of $100\text{mm} \times 100\text{mm} \times 500$ mm sizes were cast as samples for each concrete mix. The samples were cured in water at room temperature for 7 and 28 days. At expiration of the curing days, the flexural strength of the hardened concrete beams was tested in accordance with BS 1881-118 (1983). The apparatus used include universal testing machine (UTM), pressure bar, supports, dial indicator with holder, and beam moulds.

3. RESULTS AND DISCUSSION

3.1 Physical and Chemical Properties of Materials

3.1.1 Result of tests on Oil palm broom fiber (OPBF)

The result of tests done on OPBF are given in table below. The average moisture content of the OPBFs after a 24 hours period of oven-drying at 103^{0}C was found to be 12.44% and the average Water Absorption capacity of OPBFs for a 24 hours period of available moisture was 29.54% of its original weight. The result shows an average tensile strength of 105.38 N/mm^2, average modulus of elasticity of 15774.04 N/mm^2 and average maximum strain of 1.36%.

Table 2: Physical and Mechanical properties of OPBF

Parameters	Moisture Content (%)	Water Absorption (%)	Mean Diameter, D (mm)	Mean Length, L (mm)	Aspect Ratio, (L/D)	Youngs Modulus (N/mm^2)	Tensile Strength (N/mm^2)	Strain @peak (%)
OPBF	12.44	29.54	2.0	45	22.5	15774.04	105.38	1.36

3.1.2 Result of chemical analysis of Rice Husk Ash

The result of chemical analysis of the RHA are presented below. The combined percentages of Silicon Oxide, Iron Oxide and Aluminum Oxide was gotten to be 80.86% which is more than 70% and this shows that RHA is a good pozzolanic material according to BS EN 450-1 (2012).

Table 3: Chemical Compositions of RHA

Chemicals	SiO_2	Fe_2O_3	Al_2O_3	Na_2O	CaO	MgO	K_2O	SO_3	LOI
Cement (%)	18.64	3.21	4.89	0.38	58.9	1.81	0.14	1.35	-
RHA (%)	63.80	6.32	10.74	1.62	9.78	3.81	3.26	0.06	5.48

3.1.3 Result of tests on fine and coarse aggregate

The results of physical test done on the aggregates are shown in the table below. The Coefficient of uniformity (Cu) of sand is 3.0 which is less than 4 and its Coefficient of curvature (Cc) is 1.33 which lies between 1 and 3, hence it is regarded as a Well Graded Sand (SW). The average specific gravity of sand is 2.66 and falls within the specified range of 2.63 and 2.67. The water absorption capacity and moisture content are 1.21% and 1.63% respectively.

Table 4: Physical properties of Aggregates

Properties	Cu	Cc	SG	WAC (%)	MC (%)
Sand	3.0	1.33	2.66	1.21	1.63
Granite	2.43	1.42	2.77	0.91	0.4

The Coefficient of uniformity (Cu) of granite is 2.43 which is less than 4 and its Coefficient of curvature (Cc) is 1.42 which lies between 1 and 3, hence, this indicate that it is well graded. The average specific gravity, water absorption capacity and moisture content of the granite are 2.77, 0.91% and 0.4% respectively. This indicates that it is in a basic state of saturated and surfaced dried condition.

3.2 Tests on Fresh and Hardened concrete

3.2.1 Workability of fresh concrete (slump test)

The average slump values of the concrete mixes are shown in Figure 2. It can be seen that 54.50 mm slump was recorded when no fiber was added to the concrete, but when OPBF were added into concrete, the slump value started to decrease. With the inclusion of 0.5 % of OPBF in the concrete, the slump value decreased from 54.50 to 51.60 mm which is 5.32% reduction in workability. The decrease in workability continues gradually till 5% addition of OPBF. Thus, it can be said that the addition of OPBF has negative impact on the workability of concrete. This may be due to the fact that the number of fibers increases with the increase in percentage of OPBF, thus causing difficulty in movement for other ingredients of concrete, thus reducing its workability.

Figure 2: Effect of OPBF on the workability of fresh RHA-cement concrete

3.2.2 Flexural strength of the hardened concrete beams

The summary of average flexural strength of the concretes after the two ages of curing and comparison between samples containing oil palm broom fibres and control sample are shown in Table 5. From Table 5, the variation in strength of samples with respect to control sample were gotten using $V = \frac{S-C}{C} \times 100(\%)$, where V is the % variation in flexural strength, S is the average flexural strength of samples containing OPBF, and C is the average flexural strength of control sample. This shows the percentage increase in the flexural strength of samples containing OPBF when compared to the control sample.

From Figure 3, It can be observed that the flexural strength of the RHA-cement concrete increased as the curing ages increased. Also, there was increment in flexural strength of RHA-cement concrete as the percentage of OPBF in the concrete increased up to 3 %. Beyond that there was a gradual decline in flexural strength. The increment can be attribute to the ability of OPBF to effectively limit the formation, propagation and widening of cracks in the concrete. This, however, leads to increase in flexural strength. However, there is an upper limit of OPBF (3%) which can be used to reinforce concrete and improve the ductility of concrete. Beyond this limit, a continuous increase in fiber content results in the balling effect and an inappropriate bond with the concrete, which reduces flexural strength.

Table 5: Flexural strength comparison of samples containing OPBF to control sample

S/N	Vf (%)	Average flexural strength (N/mm^2)		Variation in strength w.r.t control concrete sample (%)	
		7 days	28 days	7 days	28 days
1	0	3.24	4.05	-	-
2	0.5	3.69	4.29	13.89	5.93
3	1	3.78	4.74	16.67	17.04
4	1.5	4.14	5.04	27.78	24.44
5	2	4.23	5.28	30.56	30.37
6	2.5	4.47	5.46	37.96	34.81
7	3	4.68	5.76	44.44	42.22
8	3.5	4.38	5.43	35.19	34.07
9	4	4.17	5.10	28.70	25.93
10	4.5	4.02	4.83	24.07	19.26

11	5	3.90	4.53	20.37	11.85

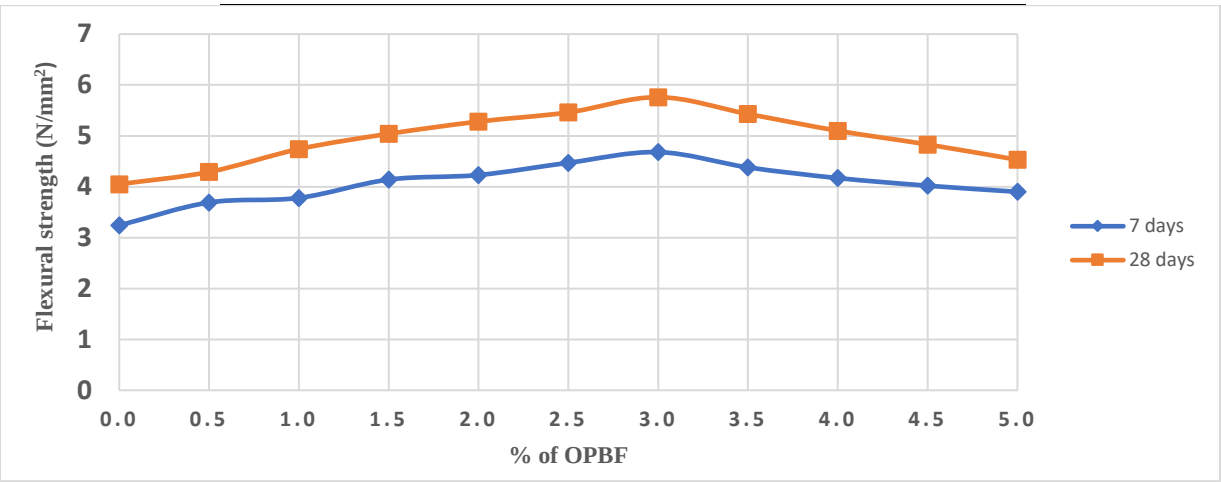

Figure 4: Effect of OPBF on the flexural strength of RHA-cement concrete

4. CONCLUSION

The following are the conclusions made from the outcome of the experimental investigation:

i. OPBF when used as reinforcement in RHA-cement concrete leads to reduction in workability. The slump value decreased from 54.5 mm in control sample to 20.4 mm in 5% OPBF volume fraction. As the OPBF volume fraction increases, the workability decreases.
ii. The addition of OPBF to RHA-cement concrete increased the flexural strength, which led to an improvement in the ductility property of the concrete. The concrete reinforced with 3% OPBF by volume fraction achieved the highest flexural strength of 5.76 N/mm^3 after 28 days of curing, which was 42.22% higher than the control sample.
iii. The addition of OPBF to RHA-cement concrete had a significant impact on the flexural strength due to the improvement in the ductility behavior of the concrete. The increase in flexural strength ranged from 5.93% to 42.22% after 28 days of curing.

Based on the conclusions from this research, it is therefore recommended that:

i. The optimum dosages of oil palm broom fibre in RHA-cement concrete is 3% volume fraction for flexural strength which achieved minimal reduction in workability and a further increase in dosage will result in a reduction in flexural strength.

ii. Oil palm broom fibre is good as reinforcement to improve the brittleness in concrete and lead to the ductility behaviour of concrete.

REFERENCES

Agarwal, A., Nanda, B., & Maity, D. (2014). Experimental investigation on chemically treated bamboo reinforced concrete beams and columns. *Construction and Building Materials*, 71, 610-617.

Ahmad, M. (2017). Rice production in Nigeria hits 15 million tonnes. *Premium Times*. https://www.premiumtimesng.com/agriculture/agric-news/240287-rice-production-nigeria-hits-15-million-tonnes-official.html

Behbahani, H., Nematollahi, B. & Farasatpour, M. (2011). Steel fiber reinforced concrete: A review. *In the International Conference on Structural Engineering Construction and Management (ICSECM2011), Kandy, Sri-Lanka.*

BS EN 197-1. (2000). *Cement Composition, Specification and Conformity Criteria for Common Cements*. British Standards Institute, London, United Kingdom.

BS EN 450-1. (2012). *Fly ash for concrete. Part 1. Definition, Specification and Conformity Criteria*. British Standards Institute, London, United Kingdom.

BS EN 1008. (2002). *Mixing Water for Concrete*. British Standards Institution, London, United Kingdom.

BS EN 12620. (2013). *Aggregates for Concrete*. British Standards Institution, London, United Kingdom.

BS 1881-102. (1983). *Method for determination of slump*. British Standards Institution, London, United Kingdom.

BS 1881-111. (1983). *Method of normal curing of test specimens.* British Standards Institution, London, United Kingdom.

BS 1881-118. (1983). *Method for Determination of flexural strength*. British Standards Institution, London, United Kingdom.

BS 1881-125. (1986). *Methods for mixing and sampling of fresh concrete*. British Standards Institution, London, United Kingdom.

Bui, D. D. (2001*). Rice husk ash as a mineral admixture for high performance concrete*. Doctoral dissertation, Delft University of Technology, Delft, 122.

Ghaffar, A., Chavhan, A. S. & Tatwawadi, R. S. (2014). Steel Fibre Reinforced Concrete. *International Journal of Engineering Trends and Technology (IJETT)*, 9(15), 791-797.

Jhatia, A. A., Sohu, S., Bhatti, N., Lakhiar, M. T. & Oad, R. (2018). Effect of Steel Fibres on the Compressive and Flexural Strength of Concrete. *International Journal of Advanced and Applied Sciences*, 5(10), 16-21.

Lakhiar, M. T., Sohu, S., Bhatti, I. A., Bhatti, N., Abbasi, S. A., & Tarique, M. (2018). Flexural performance of concrete reinforced by plastic fibers. *Engineering, Technology and Applied Science Research,* 8(3), 3041-3043.

Momoh, E. O. & Dahunsi, B. I. O. (2017). Suitability of oil-palm-broom-fibres as reinforcement for laterite-based roof tiles. *International Journal of Software & Hardware Research in Engineering*, 5 (4), 27–35.

Momoh, E. O. & Osofero, A. I. (2019). Behaviour of oil palm broom fibres (OPBF) reinforced concrete. *Construction and Building Materials,* 221, 745–761.

Momoh, E. O. & Osofero, A. I. (2020). Recent developments in the application of oil palm fibres in cement composites. *Frontiers of Structural and Civil Engineering*, 14 (1), 94–108, https://doi.org/10.1007/s11709-019-0576-9.

Momoh, E. O., Osofero, A. I., Martinez-felipe, A. & Hamza, F. (2020). Physico-mechanical behaviour of oil palm broom fibres (OPBF) as ecofriendly building material. *Journal of Building Engineering* 30, 101208.

Muleya, F., Muwila, N., Tembo, C. K., & Lungu, A. (2021). Partial replacement of cement with rice husk ash in concrete production: an exploratory cost–benefit analysis for low-income communities. *Engineering Management in Production and Services*, 13(3), 127-141. http://doi.org/10.2478/emj-2021-0026.

Onuaguluchi, O. & Banthia, N. (2016). Plant-based natural fibre reinforced concrete composites: a review. *Cement & Concrete Composites*, 68, 96–108.

Rana, A. (2013). Some studies on steel fiber reinforced concrete. *International Journal of Emerging Technology and Advanced Engineering*, 3(1), 120-127.

Sohu, S., Halid, A., Nagapan, S., Fattah, A., Latif, I., & Ullah, K. (2017). Causative factors of cost overrun in highway projects of Sindh province of Pakistan. In the *IOP Conference Series: Materials Science and Engineering, IOP Publishing*, Bandung, Indonesia, 271(1), 012036.

Sohu, S., Lakhiar, M. T., Bhatti, I. A., Bhatti, N., Abbasi, S. A. & Tarique, M. (2018). Flexural Performance of Concrete Reinforced by Plastic Fibers. *Engineering, Technology & Applied Science Research*, 8(3), 3041-3043.

Sorelli, L. G., Meda, A., & Plizzari, G. A. (2006). Steel fiber concrete slabs on ground: A structural matter. *ACI Structural Journal*, 103(4): 551-558.

Tariq, K. A., Sohaib, M. & Baig, M. A. (2021). Effect of Partial Replacement of Cement with Rice Husk Ash on Concrete Properties. *An International Journal for Engineering and Information Sciences*, 16(3), 83–87. http://doi.org/10.1556/606.2021.00409.

Yaswanth, K. K. & Premkumar, G. (2017). An Experimental Study on Behaviour of Concrete Reinforced with Bristle Coir Fibers. *International Journal of Civil Engineering and Technology*, 8(3), 982–990.

Zaid, O., Ahmad, J., Siddique, M. S. & Aslam, F. (2021). Effect of Incorporation of Rice Husk Ash Instead of Cement on the Performance of Steel Fibers Reinforced Concrete. *Frontiers in Materials*, 8, 665625. https://doi.org/10.3389/fmats.2021.665625.

PAPER 88 - A REVIEW ON EXTENDING NETWORK LIFETIME OF WIRELESS RECHARGEABLE SENSOR NETWORKS: CURRENT TRENDS AND FUTURE PERSPECTIVES

[1*]S.A. Mikail, [2]A. D. Usman, [3]A. M. S. Tekanyi, [4]K. A. Abubilal, [5]A. M. Abba, [6]I. Yau, [7]M. J. Musa, [8]U. Abubakar

[1,2,3,4,5,6,7]Department of Electronics and Telecommunications Engineering, Ahmadu Bello University, Nigeria
[8]Department of Computer Engineering, Ahmadu Bello University, Zaria, Nigeria
[*]Email: samikail@abu.edu.ng

ABSTRACT
Advancement in Wireless Energy Transfer (WET) has led to a significant development in Wireless Rechargeable Sensor Networks (WRSN), whose sensors are replenished via WET using a Wireless Charging Vehicle (WCV). One of the challenges in WRSN is how to ensure nodes remain alive using minimal energy by the WCV. Some schemes extend the lifetime of WRSN by using a mobile WCV that collects data from the network and replenishes the nodes based on the assumption the nodes are capable of simultaneous target monitoring and energy reception. Others only allow replenishing the energy of the nodes when they are not in the state of sensing and transmission. This paper reviewed about 40 recent research papers from high impact factor journals and reputable conferences to determine the extent of development in extending the lifetime of WRSN. The analysis of the review shows that 25% of them allowed simultaneous energy replenishment with data gathering, consisting of 10% that employed a mobile sink. 7.5% prevents upsetting the low-cost requirement of the nodes by executing the two tasks at different time instances. 10% proposed partial recharging of nodes by the WCV as the best way to reduce the energy consumption of mobile data.

KEYWORDS: Algorithms, Clustering, Energy Recharging, Mobile charger, review, and sensor nodes

1. INTRODUCTION

Wireless sensor networks (WSNs) convert data from the physical world to the cyber world. WSNs comprise sensor nodes that collect data and forward it toward a sink or a base station for further processing (Amin et al., 2020). The sensor nodes have low storage memory, are of low processing power, and embedded with batteries of limited capacity. When nodes are dead, the exhausted batteries are replaced or a new set of nodes are deployed. Either of the operations lead to a temporal disruption of the network operation. In addressing the problem of low network lifetime of WSN, researchers had focused on minimizing the energy consumption of nodes during target monitoring (Abidi & Ezzedine, 2017; Abuarqoub et al., 2017; Bagci, 2016; Darabkh, Al-Maaitah, Jafar, & Khalifeh, 2018), which is a temporary solution. The WRSN paradigm provided a better means of enhancing the residual energy of nodes, thanks to the advancement in WET technologies. Nodes in WRSN have batteries that are replenish-able via wireless energy transfer. Most of the available solutions for energy replenishment in WRSNS considered energy replenishment operations independent of data gathering. Some other schemes assumed that the nodes perform the two functions simultaneously, which could increase the processing power requirements of nodes, that translates to an increase in the cost of sensor nodes.

This paper, therefore, reviews recent literature from high impact factor journals and reputable conferences and examines the development of schemes for lifetime extension in WRSN.

2. METHODOLOGY

Only journal and conference papers of high reputation were reviewed. Academic publications on lifetime extension for WRSN are broadly divided into three groups: (1) Those that considered energy recharging independent of data forwarding. This approach assumes a fixed or variable energy consumption rate for the nodes and focuses on minimizing the number of dead nodes and the energy usage of the WCV. (2) those that considered simultaneous energy replenishment and data forwarding by sensor nodes. In this approach, the assumption is that the nodes can simultaneously receive energy via WET and perform data sensing and forwarding within the network. (3) This category argues that the simultaneous execution of the two tasks offset the low-cost requirement of the sensor node. Therefore, schemes that execute the two tasks at different time intervals to preserve the low-cost requirement of sensor nodes are proposed.

A taxonomy for reviewed papers in terms of the energy replenishment approach, Level of energy replenishment (full or partial), and other network performers matrices are presented in Table 1

Table 1: Taxonomy of Reviewed Literature

S/No	References	Partial recharge	Energy recharging only	Concurrent energy recharging and data gathering	Data gathering and energy recharging at separate time instances	Network lifetime	Network Operating expenditure (OPEX)	WCV energy consumption	Packet latency	Network throughput	Mobile sink
1	Guo *et al.*, (2014)			✓		✓		✓			
2	L. He *et al.*, (2015)		✓					✓			
3	Han *et al.*, (2018)			✓		✓					
4	Xu *et al.*, (2018)		✓					✓			
5	C. Lin *et al*., (2018)		✓								
6	Kaswan *et al.*, (2018)		✓			✓					
7	Purkar & Deshpande, (2018)		✓			✓					
8	khadim *et al.*, (2018)		✓			✓					
9	F. Zhang *et al.*, (2018)		✓			✓					
10	Mukherjee *et al.*, (2018)			✓		✓					
11	Han, Yang, *et al.*, (2019)		✓								
12	Yang *et al.*, (2019)			✓							
13	Y. Liu *et al.*, (2019)			✓						✓	
14	Y. Liu *et al.*, (2019)			✓							✓
15	F. Liu *et al*., (2019)		✓			✓					

16	(Z. Chen & Shen, 2019)			✓							
17	(Priyadarshani et al., (2021)	✓				✓					
18	Zhong *et al.*, (2021)		✓				✓				
19	Lu, (2021)										
20	Tian *et al.*, (2021)						✓				
21	R. Kumar & Mukherjee, (2021)		✓				✓				
22	Li *et al.*, (2021)				✓	✓					
23	H. Guo *et al.*, (2021)		✓					✓			
24	Angurala *et al.*, (2021)					✓					✓
25	Boukerche *et al.*, (2021)			✓					✓		
26	Tomar & Jana, (2021)		✓				✓				
27	J. Li et al., (2022)		✓				✓				
28	Susan & Balasubramanian, (2022)		✓			✓			✓		
29	Hong *et al.*, (2022)		✓					✓			
30	Nguyen *et al.*, (2022)		✓				✓				
31	Jiao *et al.*, (2022)			✓			✓				✓
32	Huong *et al.*, (2022)		✓			✓					
33	Kumar *et al.*, (2022)		✓			✓					
34	(Rahaman & Azharuddin, 2022)		✓					✓			

35	Chen *et al.*, (2022)		✓				✓	✓			
36	M. Zhang, (2022)			✓							✓
37	Srinivas *et al.*, (2022)		✓				✓			✓	
38	Mikail *et al.*, (2022a)	✓				✓		✓	✓		
39	Mikail *et al.*, (2020)	✓			✓	✓	✓	✓	✓		
40	Mikail *et al.*, (2022b)	✓			✓	✓	✓	✓			

3. RESULTS AND DISCUSSION

Results of the review showed that there is significant devotion of attention to the development of simultaneous energy replenishment and data forwarding schemes. The schemes have low-complex recharging algorithms since the WCV recharges nodes from sojourning points, rather than visiting them individually. The simultaneous execution of the two tasks could require two separate circuits: one for receiving energy via WET and the other for sensing and forwarding data within the network. The two circuits, as against one in sensor nodes, mean an increase in size, processing power, and memory requirements of the nodes, which translates to offsetting the low-cost requirement of the nodes. It is a requirement that the sensor node should be of low cost for ease of affordability. The schemes could not provide solutions on how to avoid an increase in the low-cost requirement of the sensor nodes and on whether simultaneous execution of the two tasks is realistically possible without a new sensor design. 25% of the 40 papers reviewed considered energy replenishment concurrently with data gathering but failed to address how the low-cost requirement of sensor nodes will be maintained. 10% of such schemes used the mobile sink that travels to collect data from nodes within the network, with a separate WCV for energy recharging. Mobile data gathering led to frequent changes in data forwarding path that result in non-uniform distribution of energy in the network.

One of the possible ways to prevent offsetting the low-cost requirement of sensor nodes is to allow data gathering at different time instances from energy recharging. Schemes that replenish the energy of sensor nodes at instances when the nodes are not in the state of sensing and transmission have been proposed. Thus, it involves sharing the single circuity between the task of data sensing or transmission and energy replenishment via WET. The networks in the schemes operate based on the Time Division Multiple Access (TDMA) such that a node uses its allocated time slot to sense and transmit data and then goes into a sleeping mode for the rest of the time slots. When a node needs energy replenishment, it receives it while in the sleeping mode, before it is due to use its next allocated time slot. The schemes led to a high reduction in the energy usage of WCV and significantly increase the average lifetime of the network, but increases the complexity of recharging algorithms. Hence these schemes provide a significant stepping stone for realistic deployment of WRSN provided the complexity can be handled. About 7.5% of the reviewed papers operate based on this approach.

There is generally little attention devoted to WRSN schemes based on data gathering and energy recharging at different time instances probably due to the high complexity of the energy recharging algorithms. Thus, future research direction could be schemes that perform the two functions at different time instances with low energy recharging complexity which will pave the way for realistic deployment of WRSN with low-cost hardware (high complexity of recharging algorithm could translate to more complex node design which increases the overall cost of the sensor nodes and the network).

4. CONCLUSION

Wireless Rechargeable Sensor Network (WRSN) paradigm has solved the energy bottleneck of the Wireless Sensor Network (WSN) by enabling wireless energy transfer to nodes. However, the problem of ensuring a high network lifetime with low energy of Wireless Charging Vehicle (WCV) still exists. Lots of research work attempted to solve the problem using different approaches: some allowed recharging of sensor nodes when they are performing data sensing and transmission, while others allow energy replenishment of nodes only when they are not in the state of sensing and transmitting. Of the 40 papers reviewed, 25% considered energy replenishment concurrently with data gathering but failed to address how to avoid offsetting the low-cost requirement of sensor nodes. 10% of such schemes used a mobile sink for data gathering and separate wireless charger that recharges the energy of nodes. The use of a mobile sink and a separate charger led to frequent changes in the data forwarding path, which result in non-uniform distribution of energy in the network. 7.5% preserved the low-cost requirement of sensor nodes and improved the network lifetime using low energy by the WCV. In addition, 10% of these schemes argued that partial energy recharging leads to more savings in the energy consumption of the WCV, though with increased frequency of sending energy recharging requests. The review established that future research will focus on development of energy algorithms with low complexity so that the low-cost requirement of sensor nodes is preserved. Similarly, there is the need for novel routing protocols for mobile sink schemes that would balance the energy consumption of sensors to achieve uniform energy distribution in the network.

ACKNOWLEDGEMENT

We appreciate the contribution of our colleagues from the Faculty of Engineering, Ahmadu Bello University, who provided insight and expertise that greatly enhanced the research.

REFERENCES

Abidi, W., and Ezzedine, T. (2017) "New Approach for Selecting Cluster Head based on LEACH Protocol for Wireless Sensor Networks," Proceedings of the 12th International Conference on Evaluation of Novel Approaches to Software Engineering, ENASE, 114–120.

Abuarqoub, A., Hammoudeh, M., Adebisi, B., Jabbar, S., Bounceur, A., and Al-Bashar, H. (2017) "Dynamic clustering and management of mobile wireless sensor networks," Computer Networks, 117, 62-75.

Amin, A., Liu, X. H., Saleem, M. A., Henna, S., Islam, T. U., Khan, I., … Forsat, M. (2020) "Collaborative Wireless Power Transfer in Wireless Rechargeable Sensor Networks," Wireless Communications and Mobile Computing, 2020.

Angurala, M., Bala, M., and Bamber, S. S. (2021) "A novel technique for energy replenishment and load balancing in wireless sensor networks," Optik, 248, 168136.

Bagci, F. (2016) "Energy-efficient communication protocol for wireless sensor networks," Ad-Hoc and Sensor Wireless Networks, 30

Boukerche, A., Wu, Q., and Sun, P. (2021) "A novel joint optimization method based on mobile data collection for wireless rechargeable sensor networks," IEEE Transactions on Green Communications and Networking, 5(3), 1610–1622.

Chen, J., Yu, C. W., and Cheng, R. H. (2022) "Collaborative Hybrid Charging Scheduling in Wireless Rechargeable Sensor Networks," IEEE Transactions on Vehicular Technology, 71(8), 8994–9010.

Chen, Z., and Shen, H. (2019) "Joint mobile data collection and energy supply scheme for rechargeable wireless sensor networks," Proceedings - 2019 20th International Conference on Parallel and Distributed Computing, Applications and Technologies, PDCAT 2019, 496–500.

Dai, H., Liu, Y., Yu, N., Wu, C., Chen, G., He, T., and Liu, A. X. (2021) "Radiation Constrained Wireless Charger Placement," IEEE/ACM Transactions on Networking, 29 (1), 48–64.

Dande, B., Chen, S. Y., Keh, H. C., Yang, S. J., and Roy, D. S. (2021) "Coverage-Aware Recharging Scheduling Using Mobile Charger in Wireless Sensor Networks," IEEE Access, 9, 87318–87331.

Darabkh, K. A., Al-Maaitah, N. J., Jafar, I. F., and Khalifeh, A. F. (2018) "Energy efficient clustering algorithm for wireless sensor networks," Proceedings of the 2017 International Conference on Wireless Communications, Signal Processing and Networking, WiSPNET 2017, 590-594.

Farzinvash, L., Najjar-ghabel, S., and Javadzadeh, T. (2019) "International Journal of Electronics and Communications (AEÜ) Regular paper A distributed and energy-efficient approach for collecting emergency data in wireless sensor networks with mobile sinks," AEUE - International Journal of Electronics and Communications, 108, 79–86.

Guo, H., Wu, R., Qi, B., and Liu, Z. (2021) "Lifespan-Balance-Based Energy-Efficient" IEEE Sensor Journal, 21(24), 28131–28142.

Guo, S., Wang, C., and Yang, Y. (2014) "Joint mobile data gathering and energy provisioning in wireless rechargeable sensor networks," IEEE Transactions on Mobile Computing, 13(12), 2836–2852.

Han, G., Yang, X., Liu, L., Chan, S., and Zhang, W. (2019) "A Coverage-Aware Hierarchical Charging Algorithm in Wireless Rechargeable Sensor Networks," IEEE Network, 33(4), 201–207.

Han, G., Yang, X., Liu, L., and Zhang, W. (2018) "A joint energy replenishment and data collection algorithm in wireless rechargeable sensor networks," IEEE Internet of Things Journal, 5(4), 2596–2604.

He, L., Kong, L., Gu, Y., Pan, J., and Zhu, T. (2015) "Evaluating the On-Demand Mobile Charging in Wireless Sensor Networks," IEEE Transactions on Mobile Computing, 14(9), 1861–1875.

Heinzelman, W. B., Chandrakasan, A. P., and Balakrishnan, H. (2002) "An application-specific protocol architecture for wireless microsensor networks," IEEE Transactions on Wireless Communications, 1(4), 660–670.

Hong, Y., Luo, C., Li, D., Chen, Z., Wang, X., and Li, X. (2022) "Energy efficiency optimization for multiple chargers in Wireless Rechargeable Sensor Networks," Theoretical Computer Science, 922, 93–205.

Huong, T. T., Van Cuong, L., Hai, N. M., Le, N. P., Vinh, L. T., and Binh, H. T. T. (2022) "A bi-level optimized charging algorithm for energy depletion avoidance in wireless rechargeable sensor networks," Applied Intelligence, 52 (6), 6812–6834.

Jiao, W., Tian, M., and Xu, Y. (2022) "A Combining Strategy of Energy Replenishment and Data Collection in Wireless Sensor Networks," IEEE Sensors Journal, 22 (7), 7411–7426.

Kan, Y., Chang, C. Y., Kuo, C. H., and Roy, D. S. (2022) "Coverage and Connectivity Aware Energy Charging Mechanism Using Mobile Charger for WRSNs," IEEE Systems Journal, 16(3), 3993–4004.

Kaswan, A., Tomar, A., and Jana, P. K. (2018) "An efficient scheduling scheme for mobile charger in on-demand wireless rechargeable sensor networks," Journal of Network and Computer Applications, 114, 123–134.

Khadim, R., Maaden, A., Ennaciri, A., and Erritali, M. (2018) "An Energy-Efficient Clustering Algorithm for WSN Based on Cluster Head Selection Optimization to Prolong Network Lifetime," International Journal of Future Computer and Communication, 7(3), 51–57.
Kumar, N., Swain, G., and Routray, S. (2022) "On-demand charging planning for WRSNs based on weighted heuristic method," International Journal of Information Technology (Singapore), 14 (2), 667–674.
Kumar, R., and Mukherjee, J. C. (2021) "On-demand vehicle-assisted charging in wireless rechargeable sensor networks," Ad Hoc Networks, 112, 102389.
Li, J., Sun, G., Wang, A., Lei, M., Liang, S., Kang, H., and Liu, Y. (2022) "A many-objective optimization charging scheme for wireless rechargeable sensor networks via mobile charging vehicles," Computer Networks, 215, 109196.
Li, S., Fu, L., He, S., and Sun, Y. (2017) "Near-optimal co-deployment of chargers and sink stations in rechargeable sensor networks," ACM Transactions on Embedded Computing Systems, 17(1), 1-19.
Li, S., He, S., Hu, K., Fu, L., Chen, S., and Chen, J. (2021) "Operation State Scheduling towards Optimal Network Utility in RF-Powered Internet of Things," IEEE Transactions on Mobile Computing, 20 (11), 3117–3130.
Lin, C., Zhou, J., Guo, C., Song, H., Wu, G., and Obaidat, M. S. (2018) "TSCA: A temporal-spatial real-time charging scheduling algorithm for on-demand architecture in wireless rechargeable sensor networks," IEEE Transactions on Mobile Computing, 17 (1), 211–224.
Liu, F., Lu, H., Yu, C., and Liu, Y. (2019) "An Energy-balanced Data Collection Framework with Wireless Charging for Rechargeable Sensor Networks," IEEE Wireless Communications and Networking Conference, WCNC, 1-6.
Liu, Y., Lam, K. Y., Han, S., and Chen, Q. (2019) "Mobile data gathering and energy harvesting in rechargeable wireless sensor networks," Information Sciences, 482, 189–209.
Mikail, S. A., Danjuma, U. A., Tekanyi, A. M. S., Ahmad, K. A., and Abba, A. M. (2022a) "A Spatio-Temporal Non-Concurrent Data Gathering and Energy Replenishment in Wireless Rechargeable Sensor Networks (ST-NCDR)," Proceedings of the 2022 IEEE Nigeria 4th International Conference on Disruptive Technologies for Sustainable Development, NIGERCON 2022, 1-5.
Mikail, S. A., Usman, A. D., Abubilal, K. A., and Momodou, A. (2022b) 1st International Conference on Innovative Academic Distributed Energy Replenishment and Data Gathering for Wireless Rechargeable Sensor Networks, 384–388.
Mikail, S. A., Wang, J., and Zhang, S. (2020) "Distributed clustering and operational state scheduling in wireless rechargeable sensor networks," In International Journal of Sensor Networks, 34(1), 26-37.
Mukherjee, M., Lu, Y. R., Matam, R., and Choudhury, N. (2018) "Energy trading in sleep scheduling for wireless rechargeable WSNs," 2018 10th International Conference on Communication Systems and Networks, COMSNETS 2018, 429–431.
Nguyen, T. D., Nguyen, T., Nguyen, T. H., Nguyen, K., and Le Nguyen, P. (2022) "Joint Optimization of Charging Location and Time for Network Lifetime Extension in WRSNs," IEEE Transactions on Green Communications and Networking, 6(2), 1186–1197.
Priyadarshani, S., Tomar, A., and Jana, P. K. (2021) "An efficient partial charging scheme using multiple mobile chargers in wireless rechargeable sensor networks," Ad Hoc Networks, 113, 102407.
Purkar, S. V., and Deshpande, R. S. (2018) "Energy Efficient Clustering Protocol to Enhance Performance of Heterogeneous Wireless Sensor Network: EECPEP-HWSN," Journal of Computer Networks and Communications.
Rahaman, S. M. A., and Azharuddin, M. (2022) "A cluster based charging schedule for wireless rechargeable sensor networks using gravitational search algorithm," Wireless Networks, 28 (7), 3323–3336.
Srinivas, M., Donta, P. K., and Amgoth, T. (2022) Mobile Charger Utility Maximization through Preemptive Scheduling for Rechargeable WSNs, 126–131.
Susan, T. S. A., and Balasubramanian, N. (2022) "Scheduling on-demand charging request in wireless rechargeable sensor network with fruit fly optimization-based path selection," International Journal of Information Technology (Singapore), 14(5), 2377–2388.
Tian, M., Jiao, W., and Chen, Y. (2021) "A joint energy replenishment and data collection strategy in heterogeneous wireless rechargeable sensor networks," Sensors, 21(9), 2930.
Tomar, A., and Jana, P. K. (2021) "A multi-attribute decision making approach for on-demand charging scheduling in wireless rechargeable sensor networks," Computing, 103(8), 1677–1701.
Wang, R., Xu, X., Ran, X., Liu, Y., and Xue, L. (2021) "Minimum Nodes Deployment for Mixed Energy Replenishment in Rechargeable WSNs," IEEE Sensors Journal, 21(14), 16282–16290.

Wang, Y., Wang, F., Zhu, Y., Liu, Y., and Zhao, C. (2021) "Optimization strategy of wireless charger node deployment based on improved cuckoo search algorithm," Eurasip Journal on Wireless Communications and Networking, (1), 1–18.

Xu, W., Liang, W., Jia, X., Xu, Z., Li, Z., and Liu, Y. (2018) "Maximizing Sensor Lifetime with the Minimal Service Cost of a Mobile Charger in Wireless Sensor Networks," IEEE Transactions on Mobile Computing, 17(11), 2564–2577.

Yang, X., Han, G., Liu, L., Qian, A., and Zhang, W. (2019) "IGRC: An improved grid-based joint routing and charging algorithm for wireless rechargeable sensor networks," Future Generation Computer Systems, 92, 837–845.

Zhang, F., Zhang, J., and Qian, Y. (2018) "A Multi-Node Rechargeable Algorithm via Wireless Charging Vehicle with Optimal Traveling Path in Wireless Rechargeable Sensor Networks," International Conference on Ubiquitous and Future Networks, ICUFN, 2018-July, 531–536

Zhang, M., and Cai, W. (2022) "Data Collecting and Energy Charging Oriented Mobile Path Design for Rechargeable Wireless Sensor Networks," Journal of Sensors.

Zhong, P., Xu, A., Zhang, S., Zhang, Y., and Chen, Y. (2021) "EMPC: Energy-Minimization Path Construction for data collection and wireless charging in WRSN," Pervasive and Mobile Computing, 73, 101401.

Zhu, X., Shi, S., Lu, Y., and Li, X. (2021) "Charging Route Planning for Wireless Rechargeable Sensor Networks," 2021 IEEE 4th International Conference on Electronics Technology, ICET 2021, 1089–1094.

PAPER 89 - DETERMINATION OF HEALTH AND SAFETY COST IN BUILDING CONSTRUCTION FOR SUSTAINABLE PROJECTS DELIVERY

J. E. Mamman [1]*, I. Mohammed[2], & A. A. Oke[2]
[1]Department of Quantity Surveying, The Federal Polytechnic, Bida, Nigeria
[2]Department of Quantity Surveying, Federal University of Technology, Minna, Nigeria
ekemenajuliet@mail.com*

ABSTRACT

The poor health and safety (H&S) record in the construction industry suggests that the sector is far from being sustainable. This situation manifests as the poor handling of occupational health and safety management, and is due to contractor not allocating sufficient financial resources to the management of H&S compliance. The study determined the H&S cost in building construction projects. The study's population were building construction projects that had been completed within the last three years in Abuja. The study employed project bills of quantities (BOQ) as the source of data, and percentiles as the method of data analysis. Study's results revealed that scaffold, plant and equipment were the H&S cost items that were most often provided for in the BOQ. It was concluded that on the average, 1.02% of the total project cost value would be required for providing workplace safety through Collective Protective Measure (CPM). The highest amount that could be spent on CPM /M^2 of construction area in Nigeria was (₦27,155.20). The research has recommended that a separate section be created for H&S in the BOQ to aid in the detailed estimation of H&S cost items. Apart from encouraging uniformity in the pricing of H&S items in the BOQ, it will help main contractors during the bidding phase, because the cost of H&S, especially CPM can be estimated in detail.

***KEYWORDS*:** Building, Construction, Health and Safety, Safety Cost, Sustainable, Projects

1. INTRODUCTION

Construction work is considered one of the most dangerous occupations due to the high rate of occupational accidents (Yang *et al*., 2021). The poor health and safety (H&S) record in the construction industry suggests that the construction sector is far from being sustainable (Chigara & Smallwood, 2019). Disregarding safety can create adverse effects on sustainable development (Nawaz *et al*., 2019), since injuries of construction workers do not only affect the H&S and quality of life, they also incur direct and indirect costs of construction accidents (Hinze *et al*., 2013; Nawaz *et al*., 2019). The high rate of injuries on construction sites is recognised to have significant financial effects on the construction sector as a whole (Okoye, 2018). Yoon *et al*. (2013) revealed that corporate losses from occupational accidents stood between 5–10% of the profits across all industries, and 8.5% of the tender price in the construction industry in the UK. According to ILO (2018), poor occupational and health practices cost the economy 3.94% of global GDP annually, which translates to 3,447.68 billion US$ in monetary terms (Stasista, 2018).

One of the factors impacting negatively on the health and safety performance of the construction industry in most developing countries Nigeria inclusive, is that health and safety is not prioritised, and the implementation of construction safety measures is presumed as a burden (Windapo, 2013; Okoye & Okolie, 2014; Udo *et al*., 2016). This presumption is reinforced by the poor funding of occupational health and safety management by contractors; amounts sufficient for the management of health and safety compliance are not allocated in the BOQs for proposed projects (Hamid *et al*., 2014). Furthermore, Lopez- Alonso *et al*. (2016) noted that occupational health and safety (OHS) cost are not recorded individually in the accounting system of construction firms; as a result the items that constitute these expenditures are non-identifiable. This situation arises because most firms lack information on the costs of measures for preventing accidents. Contractors are thus, unaware of how much would be adequate for OHS provision.

The costs connected to construction H&S costs on site includes: price for materials, supplies as well as labour used to enhance working conditions and lower the accident rate as well as the costs associated with the incidents and accidents themselves (Lopez-Alonso *et al*., 2016). A number of authors have identified several health and safety costs items as well as health and safety costs to construction projects. According to estimates from Tang *et al*. (2004); Smallwood

(2011); Gurcanli *et al*. (2015); Latib *et al*. (2016); Otaru *et al*. (2018); Yilmaz and Kanit (2018); Ghousi *et al*. (2018);Yilmaz and Ugur (2019); Adekunle *et al*. (2020); Mamman and Oke (2022) and Fitriani *et al*. (2022), the cost of implementing H&S management system within a construction projects ranges between 0.21% to 10% of the contract sum. On estimating the cost of health and safety using Collective Protective Measures (CPM), a tool for estimating OHS costs for small and medium scale building projects was developed by Yilmaz and Kanit (2018). Findings revealed that OHS cost percentage to total cost of construction was 5.15% and 8.47 USD/ m^2 was the OHS cost per unit area and CPM 7.11% to project cost and H&S cost items consist of the costs for safety staff, costs for safety education and training, costs of PPE, costs of CPM, laboratory examinations fee.

Ghousi *et al*. (2018) determined the effect of costs of safety on safety risk in commercial building. Result revealed that the cost for health and safety was estimated to be 1.5% of construction budget on safety programme and CPM 1.11% to project cost and health and safety cost items includes safety training, PPE, side guards, fences, safety net, caution signs and safety tapes, abutment, radio, safety switch. A health and safety cost model was developed by Ahn *et al*. (2021) in order to sustainably manage residential high-rise building in Korea. They established the percentage values of PPE and CPM to be 9.8% and 49.5% of the project cost respectively; H&S cost items were identified as cost of labour and salary of H&S managers, the cost of facilities for safety, cost of PPE purchase along with equipment for safety on sites, worker training events cost, the cost of worker health care, and the fee for technical advice for head office overhead. Research have shown that little has been done in the aspect of estimating the cost of health and safety using Collective Protective Measures (CPM) as the major cost items. This is the gap in knowledge this study intends to fill by determining the cost of CPM H&S items in the BOQ. This study intends to proffer solution to this problem by achieving the following objectives, which are to:

(i) Identify the health and safety cost items in the BOQ, and,
(ii) Estimate the health and safety cost for CPM in building construction projects.

2. RESEARCH METHOD

The study's population was comprised of building construction projects managed by quantity surveying firms registered in Abuja by the Quantity Surveyors Registration Board of Nigeria (QSRBN) as at July 2021 (QSRBN, 2021). Purposive sampling, which is a non-probability sampling technique, was adopted for the selection of the study's participants. A lack of information on the actual number of projects that met the study's criteria informed the decision to adopt a purposive sampling approach. These criteria were three, outlined as follows: (i) building projects that were either ongoing or had been completed within the last three years, (ii) building projects that had their BOQs' preliminary section broken-down cost wise, as well as (iii) the possession of detailed knowledge about CPMs by the construction professional in charge of the project site. This last criterion, according to Patton (2001) is a key factor in the choice of the purposive sampling technique.

The quantitative data employed by this study was the costs of CPM on building projects in Abuja, which was obtained from the projects' BOQs. Collective Protective Measures (CPM) is the type of protection that is not tied to persons or particular work activities. The information employed in the derivation of CPM costs was extracted from two main sources: (i) the preliminary section of the bill of quantities of the projects sampled and (ii) Literature reviewed such as Smallwood (2011); Gurcanli *et al*., (2015); Malan and Smallwood (2015); Yilmaz and Kanit (2018); Yilmaz and Ugur (2019). The number of items considered as CPM varied from project to project; however a maximum of six items were included, these six items were (i) first aid, (ii) temporary fencing, (iii) scaffolding, plant and equipment, (iv) hoardings and barriers, (v) protection against damage and (vi) other safety measures (such as 'access for workmen').

A total of 76 BOQs were collected from the archival records of QS firms, but only 40 projects were found to meet the criteria for this study after thorough filtering for relevance and fitness for purpose. The 36 BOQs were discarded because the Standard Methods of Measurement used in the preparation of the BOQs were not in accordance with BESMM4; in addition the preliminaries sections of some of the BOQs were not broken down (in other words, did not provide details of items that had been included). The BESMM4 specifies twenty-one subheadings under which the requirements of main contractors could be priced, and which involve H&S to varying levels. This was presented in Table 1. Only six (6) of these subheadings were identified from both H&S literature and general practice by contractors as pertaining specifically to CPM on construction projects; these six subheads were indicated by a tick mark (√) in Table 1, and it was on these items that cost data was collected.

Table 1: Main Contractors Requirements in the BOQ

S/Nr	Code	MAIN CONTRACTORS REQUIREMENTS (Description from BESMM4)	Identified as CPM from literature and contractors' practice
1	1.2.2.1.5	Temporary hut, store, material storage	
2	1.2.2.1.5	Temporary lab, workshop & shed	
3	1.2.2.1.5	Welfare and Safety (Toilet/Latrines/drying room)	
4	1.2.2.5.6	First Aid	√
5	1.2.2.7.3	Fire point	
6	1.2.3.2.4	Temporary Electricity supply	
7	1.2.3.1.3	Temporary Water	
8	1.2.4.1.2	Watching and lighting (Security staff)	
9	1.2.4.3.1	Temporary Fencing	√
10	1.2.5.1.7	(PPE)	
11	1.2.5.2.1	Hoardings and Barriers	√
12	1.2.5.3.1	Control of pollution (prevention of nuisance)	
13	1.2.5.2.10	Other safety measures (access for Workmen)use of proper, sufficient, and if required, special scaffolding, hoists etc.	√
14	1.2.6.1	Protection of works	
15	1.2.6.6	Protection of works (Existing Installation)	
16	1.2.8.1	Scaffolding, Plant and Equipment	√
17	1.2.8.2.1	Temporary Works	
18	1.2.11.1.3	Clearing rubbish	
19	1.2.11.1.4	Pest control (Exterminate and Prevent pests)	
20	1.2.11.3.1	Cleaning on Completion	
21	1.2.14.1.1	Insurance Declaration (Contractor's All-Risk)	
22	1.2.2.3.5	Temporary Storm water Drainage	
23	1.2.6.1	Factory inspection	
24	1.2.5.2.	Protection against damage (fans, gantries, guardrails, the likes)	√

A major challenge encountered in this study was the lack of uniformity in the format of BOQs; this would not have been the case if a standard format of reporting H&S cost items had been available and adopted. This feature limited the number of BOQs that were found suitable for use in the study. Descriptive statistics was used in analyzing the data through the use of Microsoft Excel spreadsheets and was presented in the form of simple percentiles.

3. RESULT AND DISCUSSION

3.1 Analysis of Respondent's Demographics

Descriptive analysis was performed on the data and the results were presented in Table 2. In terms of the educational qualification of the respondents, the results in Table 2 revealed that more than half of the respondents 62.5% possessed either Higher National Diplomas (HND) or Bachelor of Science/Bachelor of Technology (B.Sc/B.Tech) degrees in various construction disciplines. A further 20% respondents had obtained Master of Science/Master of Technology (MSc/MTech) degrees; 7.5% respondents did not specify the types of qualifications held by them. While a further 5% of the respondents had obtained National Diploma (ND) and Doctor of Philosophy (PhD) degrees respectively. These results show that all of the respondents have undergone courses of instruction in various disciplines related to the construction industry, implying they are knowledgeable about construction management as well as health and safety.

The data relating to the profession of the respondents showed evidence of skewness towards the Quantity Surveying profession. This was because 72.5% of the respondents were Quantity Surveyors, 12.5% of the respondents were Engineers, and 7.5% of the respondents were Architects and Builder respectively. The large number of Quantity Surveyors was necessary, because of the technical nature of the financial information required by the study. However, this result also showed that experiential knowledge from other professionals in the construction industry was tapped and used in this study, thus adding to the reliability of the findings of the study.

With respect to working experience, it was revealed that 32.5% of the respondents had worked for 5-9 years, while there were 27.5% respondents who had worked for 10-14 years. 15% of the respondents had acquired working experience of more than 20 years, while those with less than 5 years' experience comprised 12.5% of the sample. This implied that responses from the respondents could be considered as based on experience of health and safety on construction projects. The analysis of the respondent demographics were intended to satisfy the criterion of Patton (2001) that respondents under purposive sampling must possess relevant knowledge of the subject under study; the findings obtained from the analysis have shown that this criterion has been satisfied.

Table 2: Respondents' Demographics

Parameter	Frequency	Percent (%)
Qualification		
ND	2	5.0
HND/BSC/BTech	25	62.5
MSc/MTech	8	20.0
PhD	2	5.0
Others	3	7.5
Total	***40***	***100.0***
Profession		
Quantity surveyor	29	72.5
Builder	3	7.5
Engineer	5	12.5
Architect	3	7.5
Total	***40***	***100.0***
Working Experience		
<5 years	5	12.5
5-9 years	13	32.5
10-14 years	11	27.5
15-19 years	5	12.5
20 years and above	6	15.0
Total	***40***	***100.0***

3.2 Identification of Health and safety Cost items in the Bill of Quantities (BOQ)

This section identified the health and safety cost items in the BOQ. The cost of health and safety for the study was derived from the cost of Collective Protective Measures (CPM). The information employed in the derivation of CPM costs items were gotten from the review of literature, such as Smallwood (2011); Gurcanli *et al*., (2015); Malan and Smallwood (2015); Yilmaz and Kanit (2018); Yilmaz and Ugur (2019). Safety protection goes beyond personal protection only; the entire workplace also needs to be protected from unauthorized incursions and unsafe working practices. Table 3 identified the health and safety cost items in the BOQ, result revealed that the costs of providing scaffolding, plant and equipment were provided for in all of the 40 projects that were surveyed. The findings is in line with Otaru *et al*. (2018); Malan and Smallwood (2018) who identified scaffolding as one of the top important H&S cost items. In 90% of the projects, provision was made for the costs of temporary fencing and first aid. This is in agreement with Tang *et al*. (2004); Gurcanli *et al*. (2015); Ghousi *et al*. (2018) who identified fencing and first aid as the most important H&S cost items on construction site. The rest three items of CPM costs (i) hoarding and barriers, (ii) protection against damage and (iii) other safety measures (such as 'access for workmen') were only priced by about half of the sample of 40 projects that were surveyed.

Table 3: Identification of Health and safety Cost items in the BOQ

S/N	Health and Safety Cost items in BOQ	Frequency	Percentage	Ranking
1	Scaffolding, Plant and Equipment	40	100	1
2	Temporary Fencing	36	90.00	2
3	First aid	36	90.00	2
4	Hoardings and Barriers	21	52.50	4
5	Protection Against Damage	21	52.50	4
6	Other safety measures (Access for workmen)	11	27.50	6

3.3 Estimating health and safety cost in the bill of quantities for building construction projects

This section presents the costs of the CPM components priced in the 40 projects. The information employed in the derivation of CPM costs was extracted from the preliminary section of the bill of quantities of the 40 projects sampled The number of items considered as CPM varied from project to project; however a maximum of six items were included, these six items were (i) first aid, (ii) temporary fencing, (iii) scaffolding, plant and equipment, (iv) hoarding and barriers, (v) protection against damage and (vi) other safety measures (such as 'access for workmen'). The total CPM cost was related to the (i) Total Project Cost (TPC) and (ii) Gross Floor Area (GFA), as presented in Table 4 and Table 5. Result on the computation of CPM cost as a proportion of the total cost of projects was presented in Table 4; providing H&S would require between 0.15% and 9.79% of the total cost of projects, although the average value of CPM cost as a proportion of total project cost was 1.02%. This percentage value is lower than what is in previous researches such as the 1.11%, 7.11% and 49.5% established (Ghousi *et al*., 2018; Yilmaz and Kanit, 2018; Ahn *et al.*, 2021). This disparity could be due to variations in size, complexity and type of projects. Furthermore, none of the values employed for comparison were derived from construction industries at a similar level of development as that of Nigeria. Level of advancement of the construction industry in the countries where these studies were sited could also be a reason why the observed disparity exists. Lastly, it will take further research to unravel the impact of using only 6 out of 24 items on the comparability of the CPM cost as a proportion of total project cost.

Table 4: Computation of Cost of Collective Protective Measures to Total Project Cost

Project	Total CPM Cost	Total Project Cost	CPM Cost As % of Total Project Cost
1	3,000,000.00	179,168,916.18	1.67
2	462,418.32	115,425,377.94	0.40
3	15,016,825.85	153,390,480.00	9.79
4	700,000.00	269,092,892.75	0.26
5	404,646.75	269,092,892.75	0.15
6	945,000.00	263,619,794.82	0.36
7	1,319,000.00	647,361,909.45	0.20
8	4,400,000.00	186,704,270.84	2.36
9	1,850,000.00	261,065,710.75	0.71
10	378,105.60	122,232,133.81	0.31
11	25,711,786.65	2,625,326,180.02	0.98
12	896,000.00	195,950,245.40	0.46
13	6,527,248.45	666,623,420.10	0.98
14	388,939.20	125,734,353.21	0.31
15	14,487,000.00	688,126,228.94	2.11
16	398,438.40	128,804,911.11	0.31
17	952,000.00	228,305,474.78	0.42
18	8,065,083.05	823,679,438.38	0.98
19	2,038,545.00	506,056,330.96	0.40
20	6,750,000.00	243,283,404.79	2.77
21	459,062.40	142,043,382.73	0.32
22	789,666.40	181,880,725.74	0.43
23	9,623,646.40	982,856,744.36	0.98

24	512,942.40	165,821,449.11	0.31
25	9,250,000.00	697,688,335.24	1.33
26	3,400,000.00	255,002,560.40	1.33
27	15,896,698.18	1,253,308,886.37	1.27
28	6,705,040.14	741,404,557.05	0.90
29	6,975,097.20	767,011,860.89	0.91
30	6,397,157.90	631,980,919.67	1.01
31	6,128,136.04	804,083,695.02	0.76
32	6,386,197.38	630,898,120.05	1.01
33	6,135,160.42	805,005,376.95	0.76
34	5,894,821.67	759,955,377.51	0.78
35	5,456,915.00	1,158,850,565.88	0.47
36	3,105,000.00	969,766,039.70	0.32
37	5,262,267.44	1,115,910,245.02	0.47
38	5,313,917.46	1,179,859,664.31	0.45
39	16,267,541.31	2,883,968,720.00	0.56
40	5,251,203.37	896,130,605.85	0.59
Average			**1.02**

The CPM cost per square metre of the construction area of the projects was presented in Table 5. The findings revealed that CPM cost per square metre of construction area (CPM/M^2) varied between ₦298.22 and ₦27,155.20; the average cost of CPM per square metre of construction area was ₦4,142.80. In Turkey, Yilmaz and Kanit (2018) and Yilmaz *et al*. (2019) had established $1,198 and $65 as the cost of CPM/$M^2$; at an exchange rate of ₦400 to $1, this gives a comparable value of ₦479,200 and ₦26,000. It was observed that the highest value of CPM cost/M^2 in Nigeria was only comparable to the lowest value obtained by Yilmaz *et al*. (2019) in Turkey. While this disparity could be due to variations in size, complexity and type of project, it is most likely that differences in the level of advancement of the construction industry in Nigeria and Turkey is a much stronger reason. Another aspect of the comparability of the CPM cost/M^2 is the fact that the impact of using only 6 out of 24 items specified by the BESMM4 in Nigeria is at present unknown. This will require further research efforts.

Table 5: Computation of Cost of Collective Protective Measures to Gross Floor Area

Project	Gross Floor Area (M^2)	Total CPM Cost	CPM Cost/ M^2
1	333	3,000,000.00	9,009.01
2	440	462,418.32	1,050.95
3	553	15,016,825.85	27,155.20
4	593	700,000.00	1,180.44
5	593	404,646.75	682.37
6	673	945,000.00	1,404.16
7	678	1,319,000.00	1,945.43
8	700	4,400,000.00	6,285.71
9	884	1,850,000.00	2,092.76
10	980	378,105.60	385.82
11	990	25,711,786.65	25,971.50
12	1020	896,000.00	878.43
13	1030	6,527,248.45	6,337.13
14	1033	388,939.20	376.51
15	1187	14,487,000.00	12,204.72
16	1253	398,438.40	317.99
17	1287	952,000.00	739.70
18	1293	8,065,083.05	6,237.50
19	1293	2,038,545.00	1,576.60
20	1400	6,750,000.00	4,821.43
21	1413	459,062.40	324.88
22	1607	789,666.40	491.39

23	1640	9,623,646.40	5,868.08
24	1720	512,942.40	298.22
25	1860	9,250,000.00	4,973.12
26	1973	3,400,000.00	1,723.26
27	2027	15,896,698.18	7,842.48
28	2047	6,705,040.14	3,275.54
29	2047	6,975,097.20	3,407.47
30	2047	6,397,157.90	3,125.14
31	2047	6,128,136.04	2,993.72
32	2047	6,386,197.38	3,119.78
33	2047	6,135,160.42	2,997.15
34	2453	5,894,821.67	2,403.11
35	2593	5,456,915.00	2,104.48
36	2627	3,105,000.00	1,181.96
37	3300	5,262,267.44	1,594.63
38	3827	5,313,917.46	1,388.53
39	4900	16,267,541.31	3,319.91
40	2000	5,251,203.37	2,625.60
Average			**4,142.80**

4. CONCLUSION

In determining health and safety cost of building projects, it was concluded that on the average, 1.02% of the total project cost value would be required for providing workplace safety through CPM. Whether owing to the dynamics of foreign exchange rates or level of advancement of the construction industry in different countries, the highest amount that could be spent on CPM per square meter of construction area in Nigeria (₦27,155.20) was only comparable to the lowest value obtained by other researchers in Turkey (₦26,000). The research has recommended that a separate section be created for health and safety in the BOQ to ensure the detailed estimation of H&S cost items, which will aid proper utilization of the amount earmarked for the cost of health and safety.

This study has several limitations. One of the limitations was the use of only 6 out of 24 items specified by the BESMM4 for building up the cost of CPM in Nigeria. This was occasioned by the general practice of contractors, where a significant number of these 24 CPM items are routinely left unpriced in BOQs. A further limitation is that there is an observed tendency by contractors to provide a breakdown of the Preliminaries section of BOQs only for relatively large projects. The size/value of projects is thus a factor in the level of detail provided for CPM projects in BOQs. Resolving these limitations will require that a regulatory body such as the QSRBN in conjunction with the trade association of quantity surveying in Nigeria (the NIQS) produce a schedule of items included in CPM of projects; for flexibility, the items included in such a list could vary based on the size/value of the project. For example, larger projects could have more items while smaller projects have fewer items on their CPM schedule. Contractors should then be mandated to include a cost against each CPM item for a project. Such a move will help main contractors during the projects bidding stage, because the cost of H&S, especially CPM can be estimated in detail. In addition, comparability of tenders will improve, since all contractors price CPM based on a uniform schedule of items. A further study should determine the cost of other health and safety costs components such as Personal Protective Equipment (PPE) and safety training.

REFERENCES

Ahn, H., Son, S., Park, K. & Kim, S. (2021). Cost assessment model for sustainable health and safety management of high-rise residential buildings in Korea, *Journal of Asian Architecture and Building Engineering*, 21(3), 1-13.

Adekunle, E.O., Shittu, A. A. & Ibrahim, S. (2020). Impact of Health and Safety Prevention Cost on Construction Cost in Kwara state. Proceedings of the 5th Research Conference of the NIQS (RECON 5) 9 – 10 November 2020, 23- 34.

Chigara, B. & Smallwood, J. (2019). Sustainability Principles for Construction Health and Safety (H&S) Management. *Journal of Construction,* 12 (3) 5-19.

Fitriani, R. Latief, Y. & Marhayudi, P. (2022). The Security Cost as Part of Construction Safety Cost: Case Study of Flats Construction. *International Journal of Safety and Security Engineering*. 12 (1), 47-53.

Ghousi, R., Khanzadi, M., & Mohammadi, A.K. (2018). A Flexible Method of Building Construction Safety Risk Assessment and Investigating Financial Aspects of Safety Program. *International Journal of Optimization in Civil Engineering, 8(3),433-452.*

Gurcanli, G. E., Bilir, S. M. & Sevim, M. (2015). Activity based risk assessment and safety cost estimation for residential building construction projects, *Safety Science,* Elsevier, 80: 1-12.

Hamid, A.R.A., Singh, B. & Salleh, A.S.M. (2014). Cost of Compliance with Health and Safety Management System among Contractor in Construction Industry. National Seminar on Civil Engineering Research (SEPKA2014), Training Center, UTM Skudai. FKA-PGSS FKA-UTM. 14-15 April (2014) 1-10.

Hinze, J., Godfrey, R., & Sullivan, J. (2013). Integration of construction worker safety and health in assessment of sustainable construction. *Journal of.* Construction Engineering and Management, 139, 594–600.

ILO (International Labour Organization). (2018). Safety and health at work. International Labour Organization, Geneva, Switzerland. See: https://www.ilo.org/global/topics/safety-and-health-at-work/lang--en/index.htm.

Latib, F.A., Zahari, H.Z.A., Hamid, A.R.A. &Yee, K.C.W.H. (2016). Implementing occupational safety and health requirements in construction project. *Journal of Advanced Research in Applied Sciences and Engineering Technology*, 5 (1) 53-63.

Lopez-Alonso, M., Ibarrondo-Davila, M. P. & Rubioa, M. C. (2016). Safety cost management in construction companies: A proposal classification IOS Press Work 54 (2016) 617–630 DOI:10.3233/WOR-162319

Malan, R. & Smallwood, J. (2018). Financial Provision for Construction Health and Safety, in Streamlining Information Transfer between Construction and Structural Engineering. Edited by Shiau, J., Vimonsatit, V., Yazdani, S., and Singh, A. Copyright © 2018 ISEC Press ISBN: 978-0-9960437-7-9

Mamman, E. J & Oke, A. A. (2022). Estimating the Costs of Health and Safety for Building Construction Projects in Abuja. International Journal of Built Environment and Earth science. 8 (4) 175-192.

Misnan, M. S., Yusof, Z. M., Mohamed, S. F., & Othman, N. (2012). Safety Cost in Construction Projects. The 3rd International Conference on Construction Industry Padang-Indonesia, April 10-11th 2012

Nawaz, W., Linke, P. & Koc, M. (2019). Safety and sustainability nexus: A review and appraisal. *Journal of Cleaner Production*, 216 (10) 74–87.

NIQS (2015). Building and Engineering Standard Method of Measurement 4th Edition. The Nigerian Institute of Quantity Surveyors (NIQS), Emirati Innovative Services, Abuja. www.nigs.org.ng

Okoye, P. & Okolie, K. (2014). Exploratory Study of the Cost of Health and Safety Performance of Building Contractors in South-East Nigeria. British Journal of Environmental Sciences, 2(1), 21–33.

Okoye, P.U. (2018). Occupational Health and Safety Risk Levels Building Construction Trades in Nigeria. *Construction Economics and Building*, 18(2), 92-109. https://dx.doi.org/10.5130/AJCEB.v18i2.5882.

Otaru, S. Ibrahim, S., Mohammed, Y. D. & Olaku, P. A. (2018). Assessment of the Cost Impacts of Health and Safety Practices on Construction Projects in Abuja, Nigeria. Environmental Technology & Science Journal, 9 (1) 45-55.

Patton, M. Q. (2001). Evaluation, knowledge management, best practices, and high quality lessons learned. *American Journal of Evaluation*, 22(3), 329-336.

QSRBN. (2021). Quantity Surveyors Registration Board of Nigeria List of Registered Quantity Surveyors and Registered Quantity Surveying firms with current practice licence and list of Institutions offering Quantity Surveying with valid professional accreditation. Daily Trust Monday, July 19, 2021. Page 36 – 39.

Smallwood, J. J. (2011). Financial Provision for Health and Safety (H&S) in Construction, in Proceedings of the CIB W099 Conference Prevention: Means to the End of Safety and Health Injuries, Illness and Fatalities, Washington D.C., USA, August 24-26, 2011.

Statista, 2018. Global GDP (gross domestic product) at current prices. Statista, Inc. New York, USA. See: https://www.statista.com/statistics/268750/global-gross-domesticproduct-gdp/. (accessed 19/11/2019).

Tang, S.L., Ying, K.C., Chan, W.Y. & Chan, Y.L. (2004). "Impact of social safety investments on social costs of construction accidents". *Construction Management and Economics*, 22(9), 937-946.

Udo, E. U., Usip, E. E. & Asuquo, F. C. (2016). Effect of Lack of Adequate Attention to Safety Measures on Construction Sites in Akwa Ibom State, Nigeria. *Journal of Earth Sciences and Geotechnical Engineering*, 6(1), 113-121.

Windapo, A. O. (2013). Relationship between degree of risk, cost and level of compliance to occupational health and safety regulations in construction. *Construction Economics and Building*, *13*(2), 67-82.

Yang, K., Kim, K., & Go, S. (2021). Towards Effective Safety Cost Budgeting for Apartment Construction: A Case Study of Occupational Safety and Health Expenses in South Korea. *Sustainability*, 13 (1335) 1-13.

Yilmaz, M., & Kanit, R. (2018). A practical tool for estimating compulsory OHS costs of residential building construction projects in Turkey. *Safety Science*, 101(2018), *326–331*

Yilmaz, M. & Ugur, L.O. (2019). Comparison of Estimated OHS Costs with Actual Costs in Maintenance and Repair Projects of Public Buildings. *International Journal of Occupational Safety and Ergonomics*, 25(3), 331-347.

Yoon, S.J., Lin, H.K., Chen, G., Yi, S., Choi, J., & Rui, Z. (2013) Effect of Occupational Health and Safety Management System on Work-Related Accident Rate and Differences of Occupational Health and Safety Management System Awareness between Managers in South Korea's Construction Industry. *Safety Health Work* 4(20), 1-9.

PAPER 91 - ACHIEVING QUALITY EDUCATION THROUGH AI: PREDICTING ENGINEERING STUDENT RETENTION AT THE UNIVERSITY OF ILORIN

I. O. Muniru[1*], S. A. Yahaya[1] , S. Saminu[1]

[1]Department of Biomedical Engineering, University of Ilorin, Ilorin, Nigeria.
[*]Email: muniru.oi@unilorin.edu.ng

ABSTRACT
Nigerian universities collect a wealth of student data on entrance exams, grades, and demographics. This data presents a valuable opportunity to improve educational outcomes, particularly by predicting and preventing student dropout. However, technical limitations often impede its effective utilisation. This study introduces an approach using KNIME's no-code Automated Machine Learning to analyze entrance exam scores such as UTME, Post UTME, and O' Level data for predicting first-year engineering student dropout risk. Two experiments were conducted two experiments and with a 5-fold cross-validation technique, AUC >0.75% was achieved in all models in both experiments. These results suggest that AI-powered dropout prediction can empower educators to identify at-risk students early and implement targeted interventions, such as academic advising or support groups, to improve student's performance. Furthermore, this study underscores the use of no-code platforms for developing AI solutions, as its adoption among educators and administrators would foster educational innovations that could contribute towards achieving Sustainable Development Goal 4 (i.e Quality Education).

KEYWORDS: Dropout Pprediction, Student Rretention, AutoML, Predictive Aanalytics, Education Advancement

1. INTRODUCTION

Every year, Nigerian universities collect vast amounts of student data, encompassing exam scores, attendance records, and engagement metrics. However, leveraging this data effectively for administrative and academic outcomes is often limited by the technical challenges of implementing advanced data analytics (Oyelade, Ezugwu & Alese, 2020; Ade-Ibijola & Iyamu, 2019), like predictive analytics through Machine Learning (ML); an approach in AI that involves building intelligent models that learn from historical data without explicit instructions (Kotsiantis, 2013). Automated Machine Learning (AutoML) has emerged as a viable solution to enable people (e.g. administrators and educators) with no or minimal coding skills to apply advanced analytics in decision-making (He *et al*., 2021). AutoML streamlines the development of ML applications, handling tasks such as data preprocessing, feature selection, model training, and hyperparameter tuning autonomously (He *et al*., 2021; Zöller & Huber, 2021; Almohammadi *et al*., 2021). Platforms like KNIME provide a user-friendly and no-code environment for complex data analysis and ML experimentation (KNIME AG., 2021).

In engineering programs, the transition from the first to the second year is critical; the challenges of rigorous coursework and adjustment to university life can lead to increased dropout rates (Hirschy & McClendon, 2004). This period is crucial for academic success, necessitating early identification and support for at-risk students. A recent study by Nguyen et al. (2020) has highlighted the potential of ML to analyse academic data effectively to predict student success and identify those at risk of dropping out. Another study by Almohammadi *et al*. (2021) specifically demonstrates the application of AutoML in educational settings.

This study aims to use data obtained from entrance exam scores including the UTME, Post UTME, and O' Level scores of engineering students at the University of Ilorin from 2014 – 2019 to predict the dropout risks of first-year students using AutoML. In addition, the research aims to broaden the discussion on AI and ML's role in education, advocating for the adoption of no-code analytics platforms like KNIME to democratise access to AI skills (Berthold et al., 2020), thereby supporting educational innovation that could promote the global goal of quality education for all (i.e SDG 4) (United Nations, 2015).

2. THEORETICAL ANALYSIS

The theoretical underpinning of using AutoML in this study integrates statistical learning theory (Vapnik, 1999) and optimization theory (Boyd & Vandenberghe, 2004). Statistical learning theory ensures that models generalise effectively to new data, aiming to minimise the expected loss, which is represented as:

$$E\left[L\left(Y,\hat{f}(X)\right)\right] = \int L\left(y,\hat{f}(x)\right) P(x,y)\ dx\,dy \quad \ldots\ldots\ldots\ldots\ldots\ldots\ (1)$$

where L is the loss function, Y is the true outcome, $\hat{f}(x)$ is the predictive model's output for input x and $P(x, y)$ is the joint probability distribution of X and Y. Concurrently, optimization theory is employed to efficiently navigate the algorithm space and find the optimal parameters θ that minimises the cost function $J(\theta)$, which represents the prediction error (see equation 2).

$$\min_{\theta} J(\theta) = \min_{\theta} \sum_{i=1}^{n} L\left(y_i, f(x_i; \theta)\right) \ldots\ldots\ldots\ldots\ldots\ldots \quad (2)$$

where n is the number of data points, x_i and y_i are the features and target of the i-th data point respectively and $f(x_i; \theta)$ represents the model parameterised by θ.

These two theories encapsulate the core theoretical aspects of AutoML, emphasizing the balance between model accuracy and complexity, and the search for the most effective model parameters.

3. METHODOLOGY

3.1 Problem Formulation

This study formulates the prediction of students dropping out in the first year as a binary classification task, where the outcome variable is whether a student will "cross" or "drop out". This predictive insight is intended to enable timely interventions such as academic advising or support programs, to improve student retention rates.

3.2 Dataset

The dataset for this study was obtained from the entrance records of engineering students at the University of Ilorin, spanning the academic years 2014 to 2019. It includes information for 1899 students, of which 366 (approximately 19%) are those of the dropped out. The features encompass various academic indicators, including O'Level subjects (Agricultural Science, Biology, Chemistry, Civic Education, Economics, English, Further Mathematics, Mathematics, and Physics), UTME subjects (Mathematics, Physics, Chemistry, and English), and the students' Post UTME score. Additionally, the Mode of Entry (Remedial or UTME), Gender, State of Origin, and Age were included.

3.3 Experimental Method

Figure 1 summarises the AutoML experimental methods in this study. Two experiments were conducted: one with the original dataset and another using the synthetic minority over sampling (SMOTE) algorithm to address data imbalances. Both were assessed using Receiver Operating Curve - Area Under Curve (ROC-AUC) analysis of a 5-fold cross-validation technique (see appendix for the implementation of this flow in the KNIME platform).

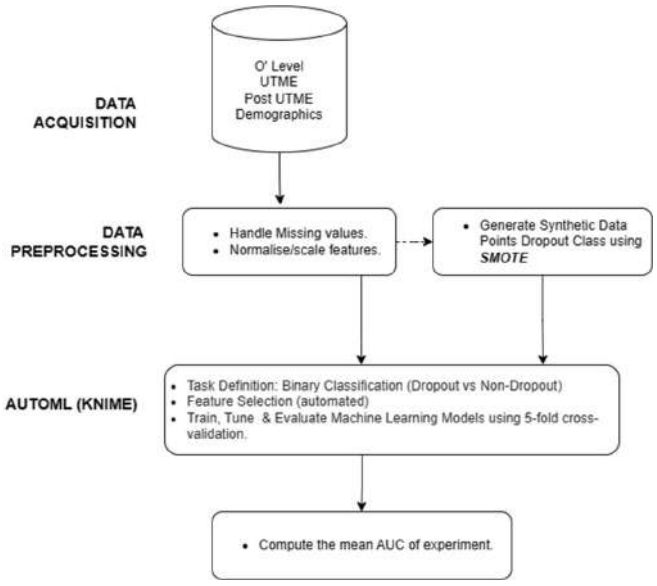

Figure 1. Schematic of the flow of AutoML Experiment.

4. RESULTS AND DISCUSSION

The results of the experiments are presented as ROC-AUC shown in Figure 2 and Figure 3. The findings from the ROC curve analysis are indicative of a strong predictive capability for identifying dropout risk among first-year engineering students. Both experiments yielded AUC values > 75%, suggesting that the predictive models have substantial discriminatory power. These findings align with established research indicating that AUC values above 0.7 are generally considered acceptable for predictive models (Hosmer, Lemeshow, & Sturdivant, 2013). The application of the SMOTE algorithm in the second experiment is a standout factor, which led to an increase in AUC values (> 0.95) across the board. This underscores the influence of data quality and preprocessing in predictive modelling - a sentiment echoed by Chawla *et al*. (2002).

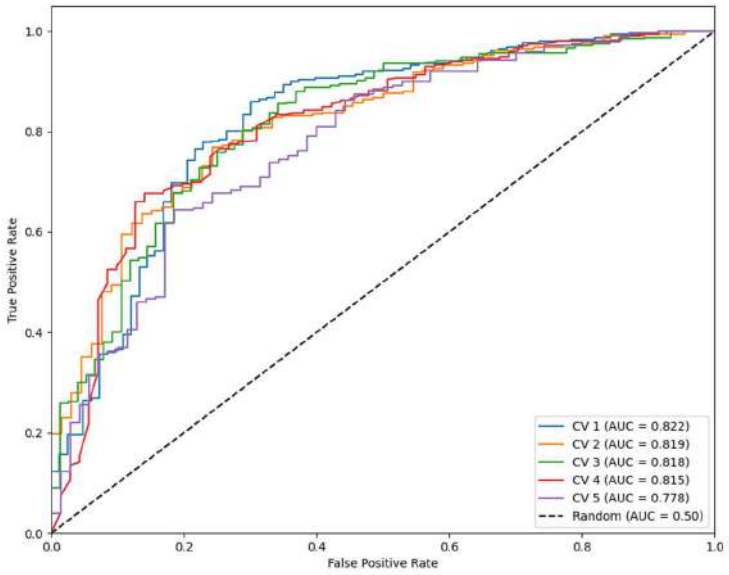

Figure 2. ROC Curves with normal data

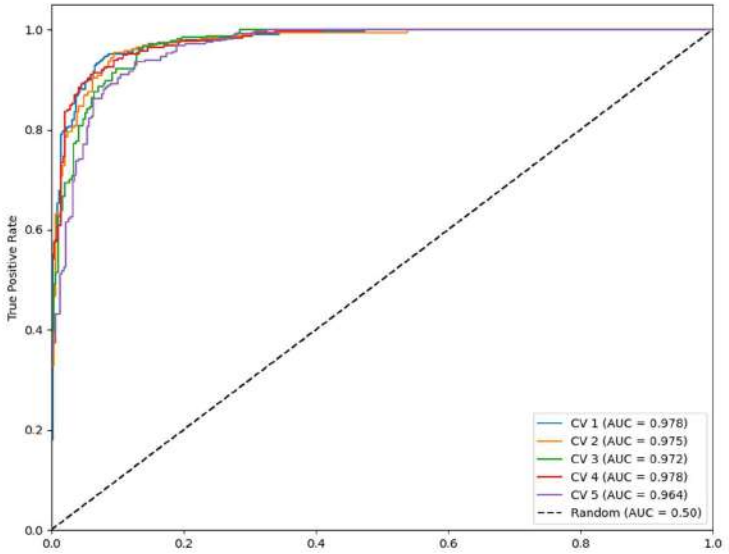

Figure 3. ROC Curves with SMOTE-Resampled Data

5. CONCLUSION

In conclusion, this study highlights the potential of AI-powered tools, such as AutoML, to predict first-year dropout risks among engineering students effectively, with AUC values of the predictive models significantly exceeding the 75% benchmark. These tools can enable educators to pinpoint at-risk students early, allowing for the deployment of targeted interventions such as academic advising or support groups, which are crucial in enhancing student retention and success (Xing, 2019).

Moreover, the findings advocate for the adoption of no-code platforms like KNIME in developing AI solutions, making it accessible for educators and administrators with limited coding expertise. This accessibility is likely to spur educational innovations and could significantly contribute to achieving SDG 4, which focuses on ensuring inclusive and equitable quality education. The study thus underscores the transformative potential of integrating sophisticated analytics into educational practices, recommending broader use of AI technologies to foster a proactive educational environment.

REFERENCES

Ade-Ibijola, A., & Iyamu, I. (2019). Implementing Machine Learning in Developing Countries: Challenges and Prospects. African Journal of Computing & ICT, 12(2), 1-10.

Almohammadi, K., Hagras, H., Alghazzawi, D., & Aldabbagh, G. (2021). A survey on the use of Artificial Intelligence in Higher Education. *International Journal of Artificial Intelligence in Education*, 31(1), 1-39. https://doi.org/10.1007/s40593-020-00211-7

Berthold, M. R., Cebron, N., Dill, F., Gabriel, T. R., Kötter, T., Meinl, T., Ohl, P., Thiel, K., & Wiswedel, B. (2020). KNIME - the Konstanz Information Miner: Version 2.0 and Beyond. ACM SIGKDD Explorations Newsletter, 11(1), 26-31. https://doi.org/10.1145/1656274.1656280

Boyd, S., & Vandenberghe, L. (2004). Convex Optimization. Cambridge University Press.

Hirschy, A. S., & McClendon, S. A. (2004). Understanding and reducing college student departure. *ASHE-ERIC Higher Education Report*, 30(3).

Chawla, N. V., Bowyer, K. W., Hall, L. O., & Kegelmeyer, W. P. (2002). SMOTE: Synthetic Minority Over-sampling Technique. *Journal of Artificial Intelligence Research*, 16, 321-357.

He, X., Zhao, K., & Chu, X. (2021). AutoML: A survey of the state-of-the-art. Knowledge-Based Systems, 212, 106622.

Hosmer, D. W., Lemeshow, S., & Sturdivant, R. X. (2013). *Applied Logistic Regression* (3rd ed.). John Wiley & Sons.

KNIME AG. (2021). KNIME Analytics Platform for Teaching. KNIME Whitepaper.

Kotsiantis, S. B. (2013). Supervised Machine Learning: A Review of Classification Techniques. *Informatica*, 31(3), 249-268.

Nguyen, T., Zhang, G., & Johnston, L. (2020). Predicting student success using machine learning algorithms in an undergraduate engineering program. *IEEE Transactions on Education*, 63(4), 273-279.

Oyelade, O. N., Ezugwu, A. E., & Alese, B. K. (2020). Application of Data Mining Techniques in Higher Education: A Review. *Procedia Computer Science*, 163, 202-211.

United Nations. (2015). Sustainable Development Goals - 17 Goals to Transform our World. United Nations. Retrieved from https://www.un.org/sustainabledevelopment/education/

Vapnik, V. (1999). An overview of statistical learning theory. *IEEE Transactions on Neural Networks*, 10(5), 988-999.

Xing, W. (2019). Big Data and Educational Analytics. *Frontiers of Education* in China, 14(4), 481-504

Zöller, M.-A., & Huber, M. F. (2021). Benchmark and Survey of Automated Machine Learning Frameworks. *Journal of Artificial Intelligence Research*, 70, 409-472.

APPENDIX

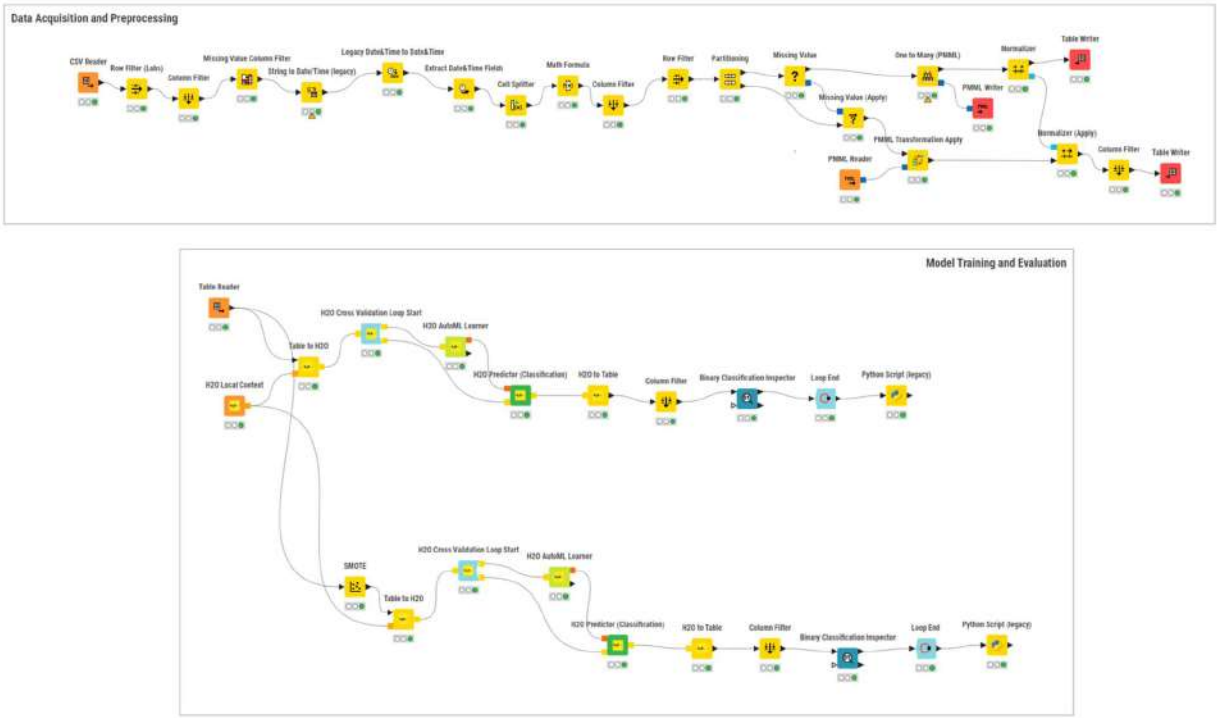

Appendix 1. Drag and Drop Implementation of AutoML in KNIME

PAPER 93 - DEVELOPMENT AND CHARACTERIZATION OF SUGARCANE BAGASSE – PLANTAIN PEEL - POLYESTER COMPOSITES

J. A. Adebisi[1], R. J. Owolabi[1*], J. O. Adegbola[1], A. D. Abdulraheem[1], I. I. Ahmed[1], M. O. Bello[1]

[1]Department of Materials and Metallurgical Engineering, University of Ilorin, Ilorin, Nigeria.
[*]Email: ramatowolabi05@gmail.com

ABSTRACT
The research study encompasses the production of composites using polyester resin, plantain peel wastes, and sugarcane bagasse fibre. It is aimed at reducing the effects of these agricultural wastes on the environment. This is done by developing materials that can have a wide range of applications. In this research study, two kinds of agricultural wastes (sugarcane bagasse fibre and plantain peel powder) of varying percentages were used to reinforce polyester. The materials used for the production of the composite were constrained to – polyester (75% - 100%), sugarcane bagasse fibre (0% - 7.23%), and plantain peel powder (0% - 25%). Afterward, the developed composites were subjected to physical, mechanical, and morphological characterization. Test results investigated are shown in the work.

KEYWORDS: Composite materials, Polyester composite, Sugarcane bagasse, Plantain peel, Agricultural waste, Reinforcement fibres, Mechanical properties.

1. INTRODUCTION

Composites are materials formed by blending a matrix and reinforcement, creating a non-homogeneous material. They are used in various engineering areas due to their versatility and properties, such as stiffness, high strength, toughness, and corrosion resistance. Composites can be classified into five main groups based on the type of matrix used, such as metal matrix composites (MMC), polymer matrix composites (PMC), ceramic matrix composites (CMC), carbon-carbon composites (CCC), and intermetallic matrix composites. Fillers in composites include fibers, carbon or aramid fibers, and glass.

According to (Dholakiya, 2012), polyesters are produced globally in large quantities, resulting in a surplus. This surplus is further exacerbated by the large amount of bagasse generated, which is often burned as a secondary source of power or used as fertilizer. In Nigeria, a significant portion of this waste is disposed of as waste, contributing to climate change and contributing to the low feed value of plantain peel waste. The research study was prompted by the urgent need to minimize environmental pollution and utilize surplus materials for sustainable product development. Hence, the study aims at characterizing a composite material that is a blend of polyester resin, plantain peel particles, and sugar cane bagasse fibre. There are a series of researches that had precede this study.

(Hemnath, Anbuchezhiyan, NanthaKumar, & Senthilkumar, 2021) evaluated the tensile and flexural properties of composites made from sugarcane bagasse fiber and Rice husk powder in polyester according to ASTM standards. (Abd El-Baky, Megahed, El-Saqqa, & Alshorbagy, 2021) evaluated the effects of essential parameters like relative fibres content and stacking sequence, on hybrid composites. It was found that bagasse fibre increases elasticity, impact strength, and water absorption capacity, but reduces ultimate tensile and bending strength.

2. MATERIALS AND METHODS

a. Materials:

Sugarcane bagasse (SB) and plantain peel (PP) were collected from sugar factory and restaurants in Ilorin metropolis Kwara state, respectively. Sodium hydroxide, polyester resin, methyl-ethyl-ketone peroxide (MEKP) as catalyst, and cobalt naphthenate as accelerator, were purchased from Omega Super Global Trading Services Ltd., Tanke, Ilorin. Distilled water was obtained from Chemistry Laboratory, University of Ilorin. Other materials used in this study include syringe, beaker, glass stirrer rod, digital weighing balance, measuring cylinder, wooden tensile mould, acrylic flexural mould.

2.2 Methods:

In order to prepare pure polyester (control sample), 167.16 g of polyester was measured into a glass beaker. 2.89 g of methyl-ethyl-ketone peroxide (MEKP) was added using a 3 ml syringe and mixed thoroughly for 2 minutes. Then, 1.54 g of cobalt naphthanate was added to the mixture using another 3 ml syringe. The mixture was then stirred thoroughly for additional 2 minutes. The ratio of polyester, methyl-ethyl-ketone peroxide, and cobalt

naphthenate used in this research is 100:2:1 by volume, respectively according to (Adediran et al., 2021). The moulds used were prepared according to ASTM-D638 for tensile specimen and ASTM D-790 for flexural specimen (Omiwale, Odusote, & Alabi, 2017). They were then lined with masking tape and lightly rubbed with resin releasing agent for easy removal of sample from the moulds. The mixture was then poured in the already prepared moulds and left for about 1 hour for curing. Similarly, the processes were repeated for development of single-phase composites using the composite formulation in Table 1. To prepare the single-phase composite S5-P0, 171.58 g of polyester resin, methyl-ethyl-ketone peroxide, and cobalt naphthenate was prepared as indicated above for the control sample, then 8.84 g of sugarcane bagasse was added and mixed uniformly with a glass rod for 3 minutes. The slurry composite was then poured in the already prepared moulds.

Table 1: Formulation of the composites produced

Sample ID	**Polyester**	**Sugarcane Fibre**	**Plantain Peel Powder**
	%	%	%
S4-P12	84.62	3.58	11.80
S6-P19	75.00	5.98	19.02
S0.6-P24	75.00	0.63	24.38
S5-P0	95.10	4.90	0.00
S0.2-P0	99.80	0.20	0.00
S7-P14	78.92	7.23	13.85
S7-P7	85.62	7.23	7.15
S0-P12	87.21	0.00	12.80
S5-P0	95.10	4.90	0.00
S4-P12	84.62	3.58	11.80
S6-P19	75.00	5.98	19.02
S0-P5	95.50	0.00	4.50
S4-P12	84.62	3.58	11.80
S4-P12	84.62	3.58	11.80
S0-P19	81.20	0.00	18.80
S2-P8	90.31	2.22	7.47
S7-P3	90.04	7.23	2.73
S0-P25	75.00	0.00	25.00
S7-P0	92.77	7.23	0.00
S0-P0	100.00	0.00	0.00

3. RESULTS AND DISCUSSION

Figure 1 shows the density of single-phase reinforced polyester- sugarcane bagasse and plantain peel composites. The composites showed decrease in density compared to the neat polyester as the proportion of either sugarcane bagasse or plantain peel increases. This is in concord with work reported by (Tewari et al., 2012). For polyester-sugarcane bagasse composites, the densities decreased from 1.256 g/cm^3 to 1.117, 1.061 and 0.994 g/cm^3 for neat polyester to 0.2 wt.%, 5 wt.%,, and 7 wt.%, filler additions, respectively. This shows a decrease rate of 0.0169 with coefficient of determination of 92.1% ($Density = -0.0169 \times sugarcane\ baggase + 1.126$, $R^2 = 0.921$). Similarly, plantain peel reveals a lower rate of decrease in density from 1.256 to 1.225, 1.199, 1.165, and 1.124 for unreinforced polyester to 5 wt.%, 12 wt.%, 19 wt.%, and 25 wt.%, respectively. The slope is 0.005 with a coefficient of determination of 98.24% ($Density = -0.005 + 1.2546 \times plantain\ peel$, $R^2 = 0.9824$). Hence, sugarcane bagasse decreases the density of polyester than plantain peel and consequently enhances production of less dense sugarcane bagasse polyester composites.

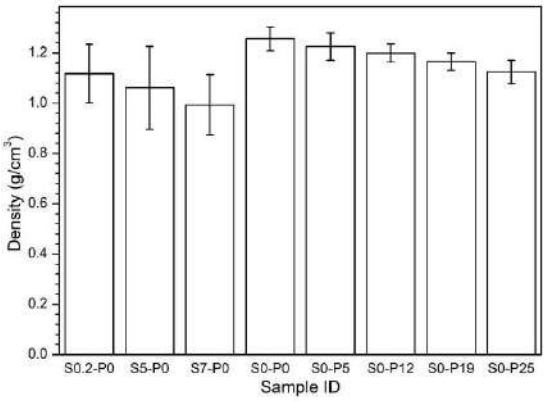

Figure 1: Density Graph for single-phase reinforcement of polyester/sugarcane bagasse/plantain peel composite

Figure 2 shows the water absorption graph of single-phase reinforced polyester- sugarcane bagasse and plantain peel composites. The composites showed increase in water absorption compared to the neat polyester as the proportion of either sugarcane bagasse or plantain peel increases. This is in concord with work reported by (Tewari et al., 2012). For polyester- sugarcane bagasse composites, the water absorption increased from 0.48% to 0.92, 2.07 and 2.82% for neat polyester to 0.2 wt.%, 5 wt.%, and 7 wt.%, filler additions, respectively. This shows an increase rate of 0.2721 with coefficient of determination of 98.7% ($Water\ Absorption = 0.2721 \times sugarcane\ baggase + 0.301$, $R^2 = 0.9874$). Similarly, plantain peel reveals an increase rate in water absorption from 0.48% to 1.45, 1.79, 2.61, 3.74% for unreinforced polyester to 5 wt.%, 12 wt.%, 19 wt.%, and 25 wt.%, respectively. The slope is 0.1138 with a coefficient of determination of 93.43% ($Water\ Absorption = 0.1138 \times plantain\ peel + 0.6623$, $R^2 = 0.9343$). Comparing 5 wt.% of both sugarcane bagasse and plantain peel which is 2.07% and 1.45% respectively to neat sample which is 0.48%, both filler additions retain water as an increase in water absorption is observed. However, sugarcane bagasse is observed to have higher increase of 0.62 and a coefficient of determination of 100% ($Water\ Absorption = 0.62 \times plantain\ peel \times sugarcane\ baggase + 0.83$, $R^2 = 1.0$).

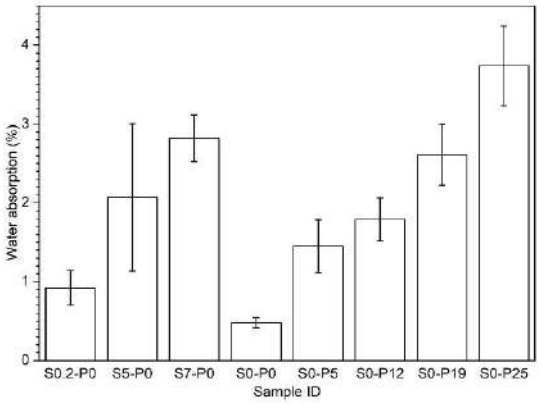

Figure 2: Water Absorption Graph for single-phase reinforcement of polyester/sugarcane bagasse/plantain peel composite

Figure 3 shows the morphological analysis of the composites using the Scanning Electron Microscope (SEM).

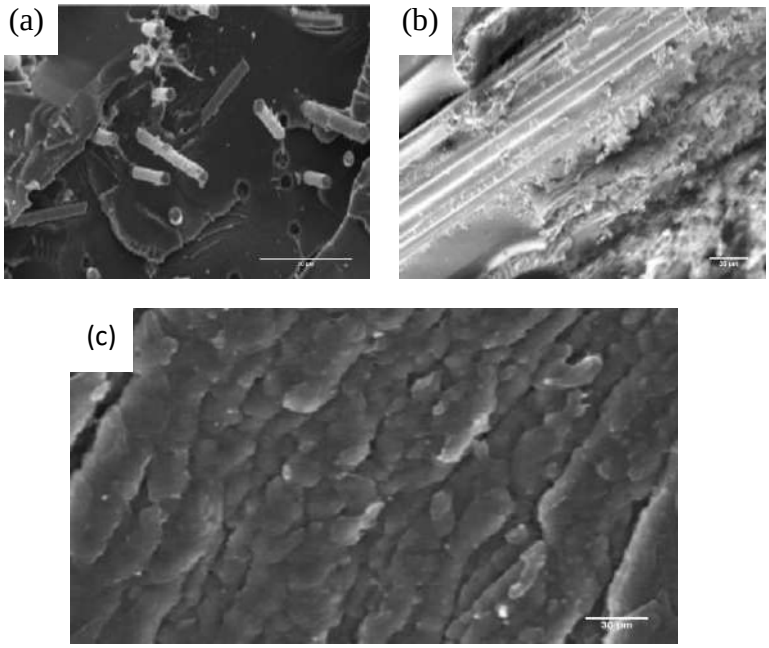

Figure 3: Micrograph of (a) S5-P0 (b) S0-P5, and (c) S0-P0

Figure 4 shows the Youngs Modulus Graph for single-phase reinforcement of polyester / sugarcane bagasse / plantain peel composite. It is observed that addition of filler increases the Youngs Modulus as the neat sample (S0-P0) has the lowest value. The 5 wt.% of sugarcane bagasse appears lower than expected and this maybe due to the presence of defects. Comparing 7 wt.% of sugarcane bagasse and 12 wt.% of plantain peel, sugarcane bagasse is observed to have a higher increase in Youngs Modulus than plantain peel. From the graph, the encapsulation of particles seems not to be even, and hence Youngs Modulus decreases as filler increases in S0-P12, S0-P19, and S0-P25 respectively. This is also in agreement with (Abd El-Baky et al., 2021) works. Figure 5 shows the stress-strain curve for single-phase reinforcement of polyester/sugarcane bagasse/ plantain peel composite which shows that all the composites are ductile and have a definite yield point.

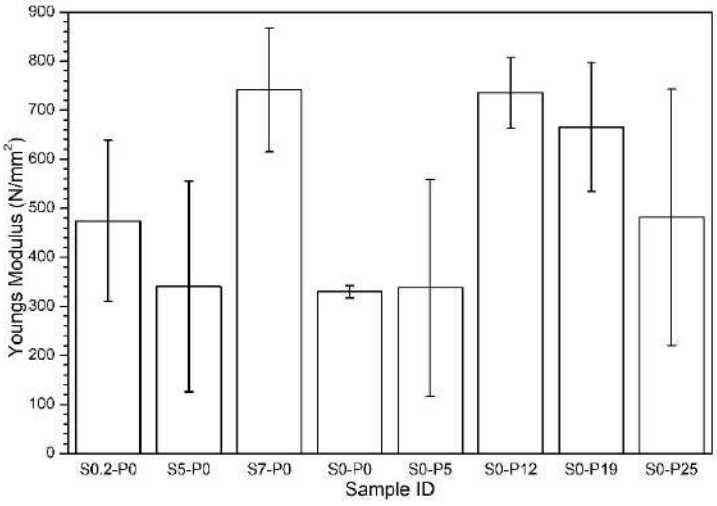

Figure 4: Youngs Modulus Graph for single-phase reinforcement of polyester/sugarcane bagasse/plantain peel composite

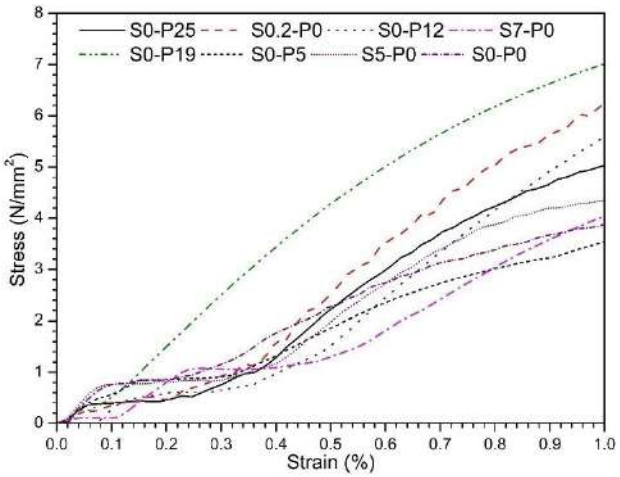

Figure 5: Stress-strain curve for single-phase reinforcement of polyester/sugarcane bagasse/ plantain peel composite

Figure 6 shows the Bending Modulus Graph for single-phase reinforcement of polyester/sugarcane bagasse/plantain peel composite. And according to (Hemnath et al., 2021), addition of filler improves the composite and it can be observed that encapsulation of particles is not even, hence there is a decrease around S0-P19 as weight percentage of plantain peel increases. Figure 7 shows Force-Deflection curve for the single-phase reinforcement composite and it depicts low resistance to elongation.

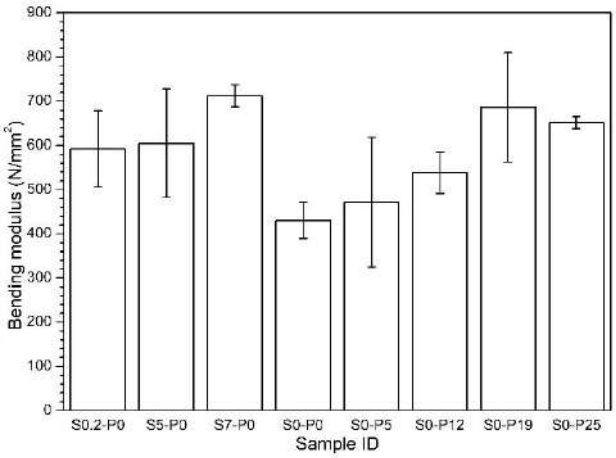

Figure 6: Bending Modulus Graph for single-phase reinforcement of polyester/sugarcane bagasse/plantain peel composite

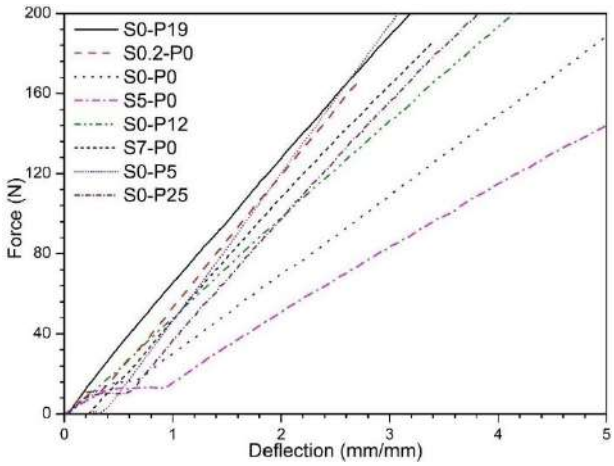

Figure 7: Force-Deflection curve for single-phase reinforcement of polyester/sugarcane bagasse/ plantain peel composite

4. CONCLUSION

Composites of sugarcane bagasse and plantain peel particulate reinforcements was successfully produced. The composite is seen to have a lower density and an increased water absorption rate compared to the neat sample. This implies that it can be used to produce lightweight materials and also hygroscopic. The addition of filler also increases both tensile and flexural properties.

It is recommended that more mechanical tests such as impact tests and thermal conductivity should be carried out on the composites to establish optimum formulation and explore areas of application.

ACKNOWLEDGEMENT

Special regards to my Academic mentor, Dr. J. A. Adebisi, the Head of Department, Materials and Metallurgical Engineering, University of Ilorin for his guidance in putting up this paper. Also, my undergraduate supervisor, Engr. James Adegbola and my colleague, Ahmad Abdulraheem.

REFERENCES

Abd El-Baky, M. A., Megahed, M., El-Saqqa, H. H., & Alshorbagy, A. E. (2021). Mechanical properties evaluation of sugarcane bagasse-glass/polyester composites. *Journal of Natural Fibers, 18*(8), 1163-1180.

Adediran, A. A., Edoziuno, F. O., Nwaeju, C. C., Odoni, B. U., Adesina, O. S., & Olayanju, A. (2021). Functional and morphological characterization of hybrid particulate reinforced polyester composites. *Materials Today: Proceedings, 44*, 2813-2819.

Dholakiya, B. (2012). Unsaturated polyester resin for specialty applications. *Polyester, 7*(Sep), 167-202.

Hemnath, A., Anbuchezhiyan, G., NanthaKumar, P., & Senthilkumar, N. (2021). Tensile and flexural behaviour of rice husk and sugarcane bagasse reinforced polyester composites. *Materials Today: Proceedings, 46*, 3451-3454. doi: https://doi.org/10.1016/j.matpr.2020.11.786

Omiwale, T., Odusote, J., & Alabi, A. (2017). Tensile Properties and Hardness of Coconut Fibre and Wood Dust Filler Reinforced Polyester Hybrid Composites. *USEP: Journal of Research Information in Civil Engineering, 14*, 1134-1145.

Tewari, M., Singh, V., Gope, P., & Chaudhary, A. K. (2012). Evaluation of mechanical properties of bagasse-glass fiber reinforced composite. *J. Mater. Environ. Sci, 3*(1), 171-184.

PAPER 94 - SYNTHESIS AND ELECTRODEPOSITION OF ZINC-CALCIUM NANOPARTICLES FOR IMPROVED SURFACE PERFORMANCE

Sani Mohammed Adams [1], Ismaila Idowu Ahmed[2], and Victor Sunday Aigbodion [1, 3]

[1]Department of Metallurgical and Materials Engineering, University of Nigeria, Nsukka 410001, Nigeria.
[2]Department of Materials and Metallurgical Engineering, University of Ilorin, Ilorin 240003, Nigeria
[3]Faculty of Engineering and the Built Environment, University of Johannesburg, Auckland Park 534, South Africa.

ABSTRACT
This study investigates the impact of electrodeposition parameters on the creation of novel nanocomposite coatings comprising zinc with calcium oxide nanoparticles (CaOnp) derived from oyster shells. The key electrodeposition parameters were studied including the concentration of CaOnp in grams per liter, current density, deposition temperature, and deposition time. The experimental findings showed: optimal conditions for electrodeposition occurred at 10g/l of CaOnp, a deposition temperature of 80°C, a current density of 1.5A/cm², and a deposition time of 15 minutes. The research demonstrates that discarded oyster shells can effectively be utilized for the electrodeposition process on mild steel to improve both corrosion resistance and hardness values.

KEYWORDS: Synthesis, Electrodeposition, Nanoparticles, Coating, Calcium oxide.

1. INTRODUCTION

Electroplated zinc coatings have recently garnered attention from researchers due to their extensive use in safeguarding ferrous metals for various industrial purposes like strips, sheets, steel wires, fabricated metal parts, and tubes (Aigbodion, 2020). These coatings are known for acting as sacrificial layers that shield steel against corrosion. However, they can deteriorate quickly in harsh conditions, impacting their longevity and effectiveness (Aigbodion *et al.*, 2019). To enhance the corrosion resistance of zinc coatings in challenging environments, additional metallic elements like Ni, Co, and metallic oxides are commonly incorporated to address these shortcomings (Winand, 2010). Previous research has shown that composite coatings with metallic oxide improve mechanical properties, wear, oxidation, and corrosion when compared to traditional metallic coatings (Muresan, 2016; Popoola, Malatji, & Fayomi, 2016). Additionally, incorporating environmentally friendly nanoparticles from agro-wastes onto zinc metallic coatings helps to minimize hazardous chemical agents (organic chelating and complexing) and high-cost metallic elements, and, overall, reduces coating cost and environmental impact (Praveen & Venkatesha, 2009).

Kumar *et al.* (2015) and Rekha and Srivastava (2019) studied the corrosion behavior of Zn composites using nano-sized carbon particles. A 3.5 wt.% NaCl electrolyte solution was used as the corrosive medium. They observed that the composites had higher anodic potentials. Malatji *et al*. (2016) showed that the use of Al_2O_3, SiO_2 beyond 5g/l in the Zn metal matrix led to the formation of segregation and agglomerates and reduced corrosion performance. Vathsala and Venkatesha (2011) reported on the corrosion behavior of Zn/ZrO_2 nanoparticles wherein they observed that the addition of ZrO_2 nano-particles improved corrosion protection, formed stable passivation, and affected the electrode reaction kinetics. Again, Fayomi et al. (2011) investigated the influence of process parameters on the zinc coating properties of mild steel. They identified that the optimal properties were obtained at an 8V coating voltage for a duration of 15 minutes. Additionally, Kul *et al.* (2020) explored the impact of $ZnCl_2$ concentration, electrodeposition time, and current density on the surface roughness, brightness, and current efficiency of zinc coating on mild steel. They employed a central composite design for optimization and determined that the ideal coating time was 4 minutes.

In this study, zinc co-deposition on mild steel was conducted using CaO nanoparticles derived from oyster shell waste. The use of CaOnp derived from Oyester was an attempted substitution aims to replace the currently utilized expensive, hazardous, and carcinogenic metallic oxide nanoparticles in electrodeposition processes. Oyster shells were selected for the production of CaO nanoparticles due to their high calcium carbonate ($CaCO_3$) content, which can be calcinated to calcium oxide (CaO) when heated above 700 °C. The key parameters considered in this research are g/l CaOnp, current density, temperature, and deposition time, which will be optimized for the best composite coating's performance.

2. MATERIALS AND METHODS

2.1 Materials

The oyster shells utilized in this study were gathered from the seaside in Rivers State, Nigeria. Mild steel, comprising 98% Fe, 0.25% C, 1.03% Mn, 0.20% Si, 0.28% S, and 0.04% P, was employed. The HCl and NaOH utilized in this research were procured from Joel Chem, University of Nigeria, Nsukka.

2.2 Method

2.2.1 Production of CaO nanoparticle

The CaO nanoparticles were produced following the method outlined in work of Adams *et al*., (2022). Initially, oyster shells were cleaned by washing off any remaining debris with deionized water and subsequently dried at 80°C. These cleaned shells were then ground into a fine powder using a ball milling machine. The resulting oyster shell powder was calcined and dissolved in 500 ml of 1M HCl. The mixture was stirred for 5 hours and then filtered to yield a $CaCl_2$ solution. Next, 250 ml of 1M NaOH solution was added to the $CaCl_2$ solution and stirred for 3 hours. The resulting mixture underwent centrifugation and washing with deionized water until reaching a pH of 7. The gel $Ca(OH)_2$ was aged for 24 hours at 100°C, filtered, and the filtrate was subsequently heated for 24 hours in a muffle furnace at 900°C to produce calcium oxide nanoparticles. The reaction mechanism is described by Equations 1–3 in reference (Adams *et al.*, 2022).

$$\text{(Oystershell) } CaCO_3(s) + 2HCl(aq) \rightarrow CaCl_2(aq) + H_2O(l) + CO_2(g) \quad (1)$$

$$CaCl_2(aq) + 2NaOH(aq) \rightarrow Ca(OH)_2(s) + 2NaCl(aq) \quad (2)$$

$$Ca(OH)_2(s) + \text{Heat} \rightarrow CaO(s) + H_2O \quad (3)$$

2.2.2 Composite coating production

The Taguchi-grey method (GRA) was utilized for multi-objective optimization in experimental design to assess the correlation effect between hardness values, corrosion rate, and electrical conductivity, using the following chemical reactions: the processing parameters considered were CaO nanoparticles (CaOnp), current density, deposition temperature, and time. These parameters were chosen based on their relevance to coating integrity optimization (Hussain et al., 2020). The specific factors and levels used in the study are detailed in Table 1, which was established following preliminary experiments.

Table 1: Factors and levels used in the work

Process parameter	Level 1(1)	Level 2 (2)	Level 3(3)
CaOnp (g/l)	10	20	30
Current density (A/cm^2)	1	1.5	2.0
Deposition temperature (^oC)	40	60	80
Deposition time (min.)	15	10	5

Before electrodeposition (Figure 1), the mild steel substrates underwent mechanical cleaning using 400–1200 grit emery papers and degreasing with acetone. An alkaline electrocleaning treatment was then applied to degrease the substrate with 20 g/L Na_2CO_3 and 35 g/L NaOH for 2 hours. Subsequently, the samples were activated in a 30% HCl solution for 60 seconds, rinsed with distilled water, and dried. The novel composites were developed using the electrodeposition method, with a bath composition of 100 g/L $ZnCl_2$, 5 g/L thiourea, 15 g/L boric acid, and 100 g/L KCl. Table 2 was utilized for formulating the composite coating production. The bath mixture was stirred for 24 hours using an aquarium pump and a magnetic stirrer. The substrate served as the cathode, zinc metal as the anode, positioned vertically 12 mm inside the bath, while direct current from the rectifier was connected to the electrodes. The data obtained from hardness testing, corrosion rate analysis, and electrical conductivity experiments was analyzed. Subsequently, the results were transformed into S/N ratio values.

Figure 1: Photograph of the electrodeposition process showing (a) equipment and (b) coated samples

2.2.3 Characterization of the deposited samples

Determination of the CaOnp particle size was done using the Joel JEM-2100F model transmission electron microscopy (TEM). First, the CaOnp powder was dissolved in ethanol and then placed on a carbonized copper mesh sheet. After drying, the sample was analyzed using TEM.

3. RESULTS AND DISCUSSION

3.1 TEM image of CaOnp

The morphologies of CaOnp were observed to have a particle size of 48.5 nm in diameter, appearing round and spherical in random distribution. Figure 2 did not show any sign of segregation or agglomeration among the particles. In the EDS analysis of the CaOnp, the presence of Ca, Si, O, and C elements were detected. The prominent Ca peak confirmed that the CaOnp derived from oyster shells and this is consistent with Tongwanichniyom *et al.*, (2021) report stating that oyster shells typically contain 96% calcium carbonate ($CaCO_3$).

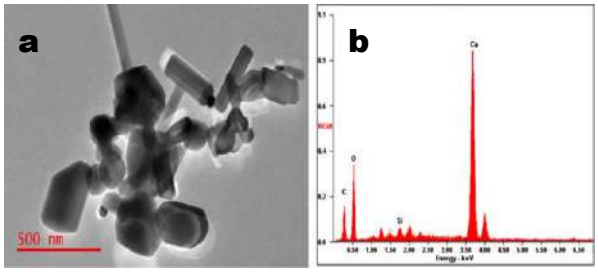

Figure 2: TEM (a) and EDS (b) of the CaOnp

3.3 Microstructure of the deposited samples

The microstructure is commonly utilized to assess the integrity of coated samples. Figure 3 displayed the SEM image and the EDS of the samples showing visible evidence of CaOnp on the surface of the samples (see Figure 3b). A comparison between Figures 3a and 3b and 3c and 3d reveals differences between the uncoated and coated samples. The uncoated sample (Figure 3a) exhibits a clear surface with no deposited material. In contrast, the sample coated at 1.5 A/cm^2 (Figure 3b) shows the presence of small nanocrystalline nodules of CaOnp uniformly covering the entire surface and this is consistent with the presence of Zn and Ca revealed by EDS in Figure 3d against the substrate EDS in Figure 3c containing neither Zn nor Ca. The higher CaOnp content achieved at a current density of 1.5 A/cm^2 was attributed to the proper dissolution of CaOnp, leading to the formation of Zn-CaOnp globules. The microstructure exhibited Zn-CaOnp and revealed a second-phase bonding strength of CaOnp due to increased dissolution. The SEM image (Figure 3b) obviously showed the presence of particles on the substrate which is an indication of effective coating. Again, it was also observed that increasing the current density from 1.5 A/cm^2 to 2.0 A/cm^2 leads to a partially coated sample. The non-uniform coating at this current density is due to reduced nucleation density, cathodic current efficiency, and grain refinement. This observation aligns with Roventi's findings (Roventi *et al.*, 2017), which noted that introducing Al_2O_3 into the Zn–Ni matrix results in a more even distribution of Al_2O_3 in the zinc matrix, smaller crystallites, fewer surface defects, and a denser deposit.

An Energy Dispersive Spectrometer (EDS) was utilized to analyze the SEM images, with the EDS spectrum shown in Figure 3c. The EDS analysis revealed a prominent Fe peak and the absence of Zn and Ca in the substrate, as illustrated in Figure 3a. There was a notable increase in Zn and Ca levels in the EDS analysis of the coated samples, as depicted in Fig. 3c. The sample coated at 1.5A/cm^2 exhibited a higher Ca content of 2.8% compared to the coating at a current density of 2.0A/cm^2, which showed a Ca content of 1.8%. This finding is in line with the research conducted by Tongwanichniyom *et al.* (2021).

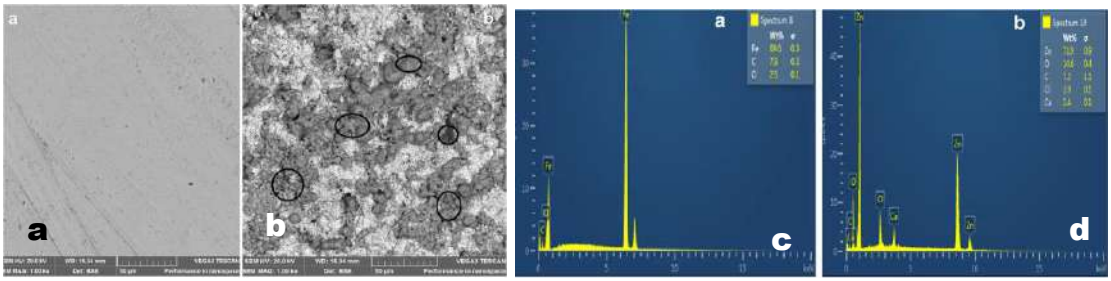

Figure 3: SEM surface images of (a) substrate, (b) coated sample at 1.5A/cm^2 current density, and corresponding EDS spectrum of (c) substrate and (d) coated sample at 1.5A/cm^2 current density

3.4 Atomic Force Microscopy

The surface roughness of the samples were analyzed using an atomic force microscope (AFM). Figure 4 depicts the AFM spectra of the samples coated at current densities of 1.5 and 2.0 A/cm^2. It was observed that the sample coated at 1.5 A/cm^2 exhibited lower surface roughness compared to the one coated at 2.0 A/cm^2. Specifically, the surface roughness increased from 0.7 to 2.4 nm at 1.5 and 2.0 A/cm^2, respectively, indicating a 70.83% rise in surface roughness. The presence of CaOnp sticking and segregation on the Ca-rich Zn matrix led to increased surface roughness at the higher current density of 2.0 A/cm^2. Additionally, both samples displayed numerous peaks of varying heights.

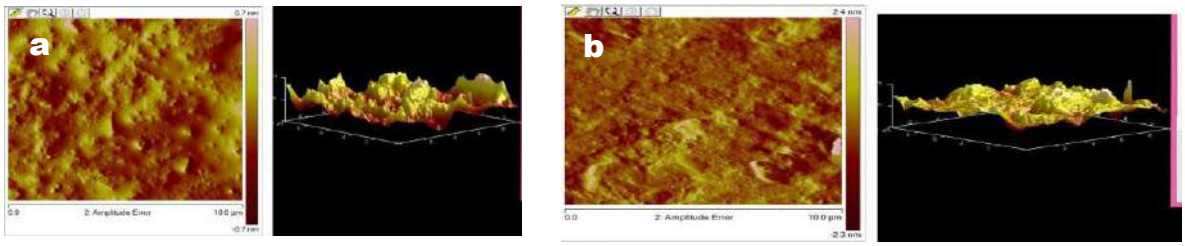

Figure 4: AFM surface images of coated sample at (a) 1.5A/cm^2 and (b) 2A/cm^2 current density

3.5 X-Ray Diffraction

Figure 5 Shows the XRD spectra of the coatings developed on mild steel. The Zn-CaOnp coating exhibited a stable phase and micro-crystalline structure with various peaks. In contrast, the substrate only displayed two primary phases on the crystallographic plane of (111) and (101), corresponding to Fe (cubic) and C (hexagonal) respectively. The coated samples showed the presence of (104) and (102) phases of CaO (rhombohedral) and ZnO (cubic) structures, along with the Fe (cubic) and C (hexagonal) phases. Additionally, more diffraction peaks were sporadically observed in the coated sample at 1.5A/cm^2, supporting the earlier conclusion that more CaOnp transferred to the cathode during electrodeposition.

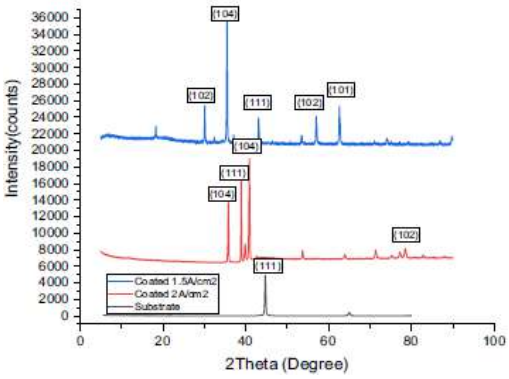

Figure 5: XRD Spectrum of the samples

These results align with a previous study by Aigbodion and Akinlabi (2019), which used eggshell as a deposition material for the electrodeposition of mild steel. Additionally, as the average crystalline size decreased, both microstrain and average dislocation density increased. This can be attributed to the fact that when the crystallite size of the deposited CaOnp at a current density of 1.5A/cm^2 decreases, more grains and grain boundary interfaces are generated, resulting in higher average dislocation density and microstrain (Liu *et al*. 2020). Therefore, in this study, the electrodeposition of mild steel with Zn-CaOnp exhibited higher dislocation density and microstrain due to smaller crystal grains. The reduced crystallite size of the deposited sample is the primary reason for the lower corrosion resistance and higher hardness values observed. These findings are consistent with the work of (Premkumar, Elayaperumal, Arulvel, & Jagatheeshwaran, 2019).

4. Conclusions

New insights have been gained in the study of electrodeposition parameters for a newly discovered reinforcement (oyster) in coatings of mild steel. It can be concluded that the presence of CaOnp in the Zn matrix significantly affects the structure of nodules and grain boundaries in the Zn-CaOnp coatings due to dissolution. The conditions for optimal electrodeposition of CaOnp on mild steel substrate were achieved at the concentration of 10g/l CaOnp, a deposition temperature of 80°C, a current density of 1.5A/cm^2, and a deposition time of 15 minutes. The research concludes that waste oysters can be used to improve the surface characteristic of the mild steel through electrodeposition.

REFERENCES

Adams, S. M., Atikpo, E., Aigbodion, V. S., & Odo, L. I. (2022). CaCO 3 derived from eggshell waste for improving the hardness values and wear behavior of composite coating on mild steel via co-deposition. *The International Journal of Advanced Manufacturing Technology*, 1-14.

Aigbodion, V. (2020). Explicit simultaneous enhancement of adhesion strength and wear resistance of functional value-added epoxy-functionalized rice husk ash nanoparticle composite coating. *The International Journal of Advanced Manufacturing Technology, 109*(7), 2205-2214.

Aigbodion, V., & Akinlabi, E. (2019). Explicit microstructural evolution and electrochemical performance of zinc-eggshell particles composite coating on mild steel. *Surfaces and Interfaces, 17*, 100387.

Aigbodion, V., Neife, S., & Suleiman, I. (2019). Surface modification of mild steel by co-deposition using Zn-ZnO-Ant hill particulate composite coating in simulated sea water. *Proceedings of the Institution of Mechanical Engineers, Part M: Journal of Engineering for the Maritime Environment, 233*(3), 857-867.

Fayomi, O., Tau, V., Popoola, A., Durodola, B., Ajayi, O., Loto, C., & Inegbenebor, A. (2011). Influence of plating parameter and surface morphology on mild steel.

Hussain, M. M., Ma, H., Huang, M., Gao, Z., Cao, J., Wang, C., . . . Kunwar, A. (2020). Fabrication of cerium myristate coating for a mechanochemically robust modifier-free superwettability system to enhance the corrosion resistance on 316L steel by one-step electrodeposition. *Surface and Coatings Technology, 398*, 125970.

Kul, M., Oskay, K. O., Erden, F., Akça, E., Katırcı, R., Köksaı, E., & Akıncı, E. (2020). Effect of process parameters on the electrodeposition of zinc on 1010 steel: central composite design optimization. *International Journal of Electrochemical Science, 15*(10), 9779-9795.

Kumar, M. P., Singh, M. P., & Srivastava, C. (2015). Electrochemical behavior of Zn–graphene composite coatings. *RSC Advances, 5*(32), 25603-25608.

Liu, J., Yan, J., Pei, Z., Gong, J., & Sun, C. (2020). Effects of Mo content on the grain size, hardness and anti–wear performance of electrodeposited nanocrystalline and amorphous Ni–Mo alloys. *Surface and Coatings Technology, 404*, 126476.

Malatji, N., Popoola, A., Fayomi, O., & Loto, C. (2016). Multifaceted incorporation of Zn-Al 2 O 3/Cr 2 O 3/SiO 2 nanocomposite coatings: anti-corrosion, tribological, and thermal stability. *The International Journal of Advanced Manufacturing Technology, 82*, 1335-1341.

Muresan, L. M. (2016). Electrodeposited Zn-nanoparticles composite coatings for corrosion protection of steel *Handbook of nanoelectrochemistry* (pp. 333-353): Springer.

Popoola, P. A., Malatji, N., & Fayomi, O. S. (2016). *Fabrication and properties of zinc composite coatings for mitigation of corrosion in coastal and marine zone* (Vol. 32): InTech London, UK.

Praveen, B., & Venkatesha, T. (2009). Generation and corrosion behavior of Zn-nano sized carbon black composite coating. *International Journal of Electrochemical Science*, *4*(2), 258-266.

Premkumar, A., Elayaperumal, A., Arulvel, S., & Jagatheeshwaran, M. (2019). Partial dissolution of precipitated-calcium carbonate (P-CaCO3) in electroless nickel-phosphorus (Ni-P) coating and its surface characterization. *Materials Research Express*, *6*(6), 066409.

Rekha, M., & Srivastava, C. (2019). Microstructure and corrosion properties of zinc-graphene oxide composite coatings. *Corrosion Science*, *152*, 234-248.

Roventi, G., Giuliani, G., Pisani, M., & Bellezze, T. (2017). Electrodeposition of Zn-Ni-ZrO2, Zn-Ni-Al2O3 and Zn-Ni-SiC Nanocomposite Coatings from an Alkaline Bath. *International Journal of Electrochemical Science*, *12*(1), 663-678.

Tongwanichniyom, S., Pattamapitoon, T., Sangvichien, N., & Phornphisutthimas, S. (2021). Production of calcium oxide from waste oyster shells for a value-added application of antibacteria. *Ecol. Enviroment Conserv*, *27*, 539-549.

Vathsala, K., & Venkatesha, T. V. (2011). Zn–ZrO2 nanocomposite coatings: Elecrodeposition and evaluation of corrosion resistance. *Applied Surface Science*, *257*(21), 8929-8936.

Winand, R. (2010). Electrodeposition of zinc and zinc alloys. *Modern electroplating*, 285-307.

PAPER 95 - ANALYSIS AND SIMULATION OF A GRID-TIED INVERTER USING SIMULINK

G. A. Olarinoye[1*] and I. O. A. Omeiza[2]

[1]Department of Electrical Engineering, Ahmadu Bello University Zaria, Nigeria.
[2]Department of Electrical & Electronics Engineering, University of Ilorin, Ilorin, Nigeria.
[*]Email: baolarinoye@abu.edu.ng

ABSTRACT
The grid-tied inverter is one way to interface renewable power sources such as solar PV, batteries, fuel cells, and wind power to the utility grid and ensure efficient conversion, control, and exchange of electric power from these sources to the utility grid and vice-versa. The grid-tied inverter also alleviates the challenges of satisfying grid code standards which power system operators demand for renewable energy integration to the grid. In this paper, the model of the grid-tied inverter and associated controllers is developed, analysed, and simulated for active power flow control. A reference current of -114 A is demonstrated to provide an active power flow of 100 kW to a three-phase power grid via current control using two PI controllers in the synchronous reference frame. The three-phase inverter is powered from a DC voltage of 800 V. Simulation results of active power, inverter, and grid voltages and currents prove the effectiveness of the phase-locked loop and current control method applied for stable and reliable power supply from the DC source to the grid.

KEYWORDS: grid-tied inverter, synchronous reference frame, phase-locked loop, active power, grid.

1. INTRODUCTION

In recent times, the Nigerian government has taken the initiative to promote renewable power generation sources such as hydro and solar plants. This is part of efforts to meet the ever-increasing demand for electrical energy in the country. It is also an effort to mitigate greenhouse gas emissions, global warming, and climate change phenomena associated with the production of electrical energy from fossil fuels (Energy Commission of Nigeria, 2005; Masum and Mamun, 2024). It is estimated that by 2025 the share of renewable energy generation will account for 10% of Nigeria's total energy consumption (Nigeria Renewable Energy Master Plan, 2014). This plan coupled with the recent revelation by the Federal Government of Nigeria to increase power generation from a paltry 4000 to 6000 MW by the end of 2024, through the deployment of hydro and solar power plants will very likely see the emergence of grid-tied inverter solutions in the national grid. Renewable energy sources are intermittent in nature and cannot be connected directly to the utility grid (Qureshi and Potdar, 2021; Vendoti *et al*., 2024). Besides, DC power from sources such as solar panels needs to be converted to AC power before it can be injected into the utility grid (Blaabjerg *et al.*, 2006). Moreover, power system operators require that certain standards be met in order to ensure the adequate connection of renewable energy sources such as photovoltaic panels and wind energy conversion systems to the utility grid (Evju, 2007). These standards include control of active and reactive power, low Total Harmonic Distortion (THD) of grid current, grid synchronization, excellent transient response, and maximum power extraction among other requirements (Patel, Gupta and Babu, 2019). One way to achieve these standards is through the use of the grid-tied inverter and its control strategy (Marangalu *et al.*, 2024). The inverter converts variable or constant DC power to controllable ac power at high efficiency and its control strategy is a key consideration to meeting the grid code requirements of power system operators and therefore to ensuring proper integration between the renewable energy source and the grid (Fatima, Siddiqui and Sinha, 2024). The grid-tied inverter is designed to transfer controllable power at the given voltage and to facilitate synchronization between its output and the utility grid (Kumar *et al*., 2024). The grid-tied inverter structure is illustrated in Figure 1. Grid connected inverters are operated in the direct power, voltage, PQ or current control mode for transfer of power to the utility grid (Kumar *et al*., 2024). The control can become complex depending on whether the control mode is grid supporting or grid forming. A study of a three-phase two-stage solar PV Inverter for grid connection was conducted by Fatima, Siddiqui and Sinha (2022). The system was implemented in MATLAB/Simulink. Although active power flow to the grid was demonstrated, the analysis of the grid-tied inverter and its control algorithm was not evident in the work, which makes it difficult for a reader to understand the system model and the interaction between the inverter and the grid.

In this paper, the model of the grid-tied inverter and its associated current controllers is developed, analysed, simulated and discussed. A simple control strategy is demonstrated in which the real and reactive components of the grid current are controlled for real and reactive power flow to the grid. The grid voltages and currents are transformed to a reference frame rotating at the same frequency as the grid voltages. This reference frame is also

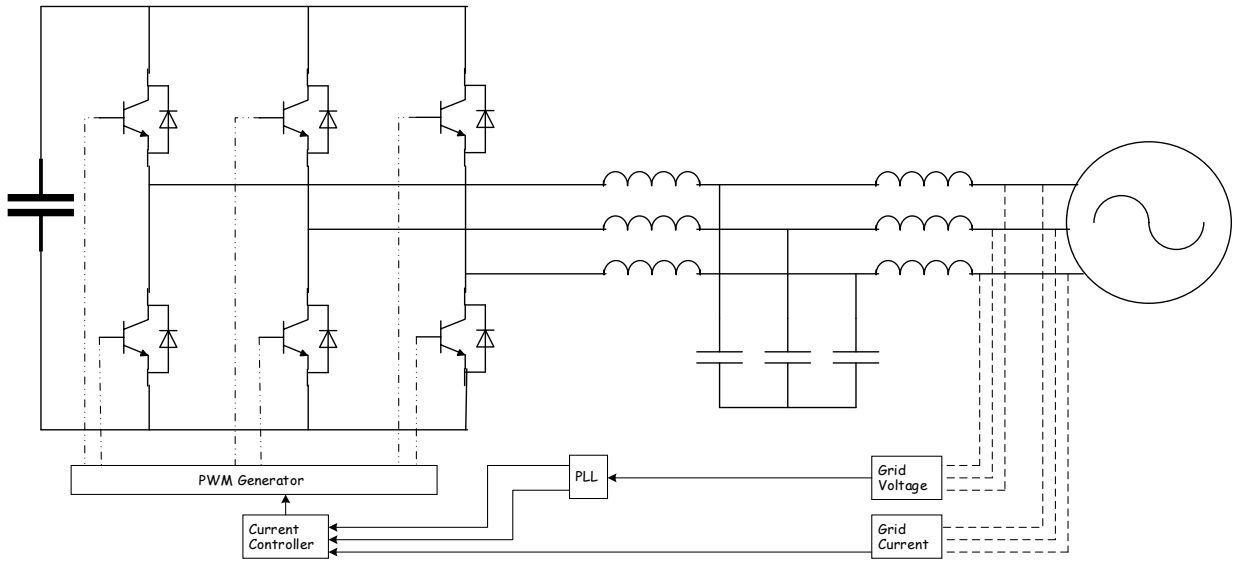

Figure 1: Grid-tied Inverter structure

known as the synchronous reference frame and it makes it easy to achieve control through linear PI controllers. The paper is organized as follows; section two provides the development of the models of the three-phase inverter, grid-tied inverter, inverter control, controller design, and the phase locked loop (PLL) for grid synchronization. Section three presents the simulation results and discussion while section 4 concludes the paper.

2.1 Three-phase Inverter Model

The three-phase inverter topology is shown in Figure 2. The output voltages referred to the negative point of the DC bus v_{ao}, v_{bo} and v_{co} can be obtained from the Figure as follows;

$$v_{ao} = V_{dc}s_{ag} \quad (1)$$
$$v_{bo} = V_{dc}s_{bg} \quad (2)$$
$$v_{co} = V_{dc}s_{cg} \quad (3)$$

$s_{ig} \in \{0,1\}$ and $i = a, b, c$

Inverter output voltages are synthesized by commanding the appropriate switching pulses of the Insulated Gate Bipolar Transistors (IGBTs) of the inverter i.e. s_{ag}, s_{ag} and s_{ag}. By different combinations of these pulses, it is possible to create AC output voltages with fundamental components of different amplitude and frequency. Phase voltages v_{an}, v_{bn} and v_{cn} are derived from Figure 2 as follows;

$$v_{an} = v_{ao} - V_{no} \quad (4)$$
$$v_{bn} = v_{bo} - V_{no} \quad (5)$$
$$v_{cn} = v_{co} - V_{no} \quad (6)$$

where V_{no} is the voltage between the negative rail of the inverter and the neutral point of the load.

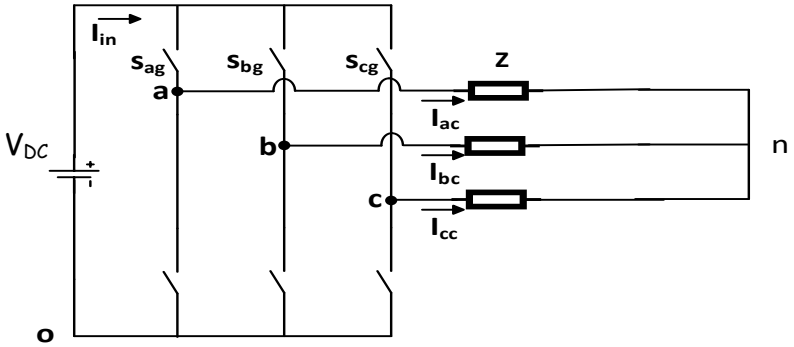

Figure 2: The three-phase inverter topology

Phase voltages with respect to the switching functions/commands are derived from (1) – (6) and provided as follows;

$$v_{an} = \frac{V_{dc}}{3}\left(2s_{ag} - s_{bg} - s_{cg}\right) \quad (7)$$

$$v_{bn} = \frac{V_{dc}}{3}\left(2s_{bg} - s_{ag} - s_{cg}\right) \quad (8)$$

$$v_{cn} = \frac{V_{dc}}{3}\left(2s_{cg} - s_{ag} - s_{bg}\right) \quad (9)$$

The three-phase inverter is controlled using the technique of sine pulse width modulation (SPWM) among many other options which include the third harmonic injection, space vector modulation, etc. A triangular carrier signal, V_{tri} is compared with the reference or modulating signal and for a Unipolar SPWM, the inverter output voltages are created with commands s_{ag}, s_{bg} and s_{cg} taking values of logic '1' whenever the modulating signals v_{ab}^{*}, v_{bc}^{*}, $v_{ca}^{*} > V_{tri}$.

v_{ab}^{*}, v_{bc}^{*}, v_{ca}^{*} are also referred to as the reference voltages for lines *a*, *b*, and *c* respectively. These reference or modulating signals are the direct result of the current control algorithm. When compared with the triangular signal, switching functions or pulses are generated for the control of the inverter switches.

2.2 Grid-tied Inverter Model

The *d-q* model equations of the grid inverter with LCL filter are now developed from the space vector model of the grid-tied inverter. The equivalent circuit is provided in Figure 3.

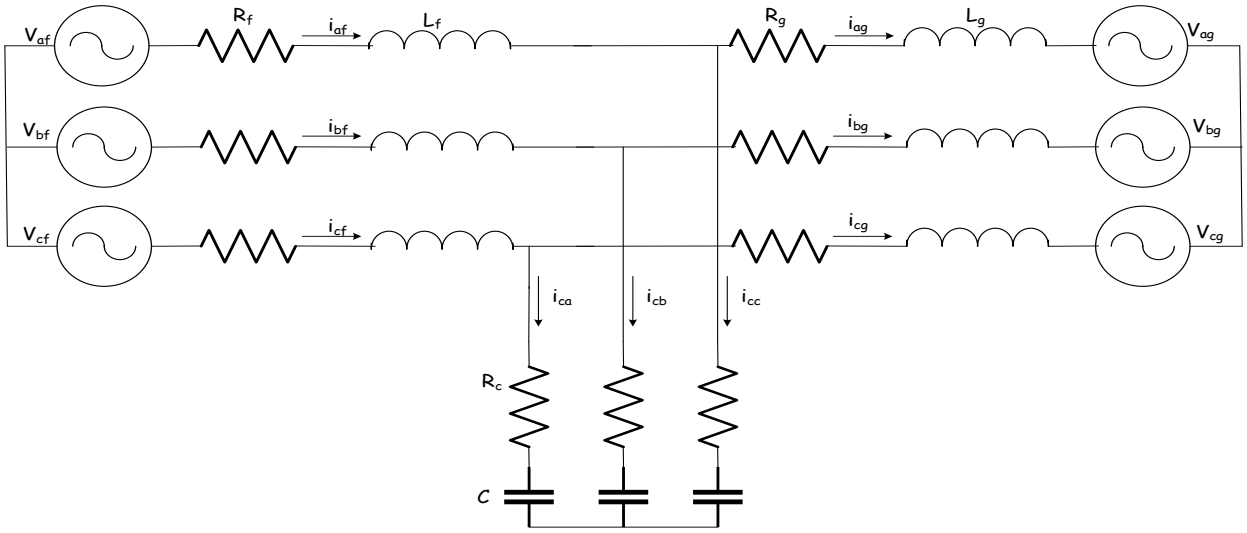

Figure 3: Equivalent circuit of the grid-tied inverter

Using linear circuit theory, the equations describing the grid-tied inverter system of Figure 3 are derived as;

$$v_{af} = R_f i_{af} + L_f p i_{af} + v_{ca} \quad (13)$$

$$v_{bf} = R_f i_{bf} + L_f p i_{bf} + v_{cb} \quad (14)$$

$$v_{cf} = R_f i_{cf} + L_f p i_{cf} + v_{cc} \quad (15)$$

$$v_{ca} = R_g i_{ag} + L_g p i_{ag} + v_{ag} \quad (16)$$

$$v_{cb} = R_g i_{bg} + L_g p i_{bg} + v_{bg} \quad (17)$$

$$v_{cc} = R_g i_{cg} + L_g p i_{cg} + v_{cg} \quad (18)$$

L_f is the inductance of the inverter side of the filter. R_f is the parasitic resistance of the inverter-side filter. L_g and R_g are the inductance and parasitic resistance of the grid side of the filter respectively. v_{af}, v_{bf} and v_{cf} are the phase voltages of the inverter. i_{af}, i_{bf} and i_{cf} are the output currents of the inverter. v_{ag}, v_{bg} and v_{cg} are the grid voltages while i_{ag}, i_{bg} and i_{cg} are the grid currents. The space vector model of equations (13)-(18) in the synchronous reference frame is given as follows (Abad, 2017);

$$\overrightarrow{\boldsymbol{v}_f^e} = R_f\overrightarrow{\boldsymbol{i}_f^e} + L_f p\overrightarrow{\boldsymbol{i}_f^e} + R_g\overrightarrow{\boldsymbol{i}_f^e} + L_g p\overrightarrow{\boldsymbol{i}_g^e} + \overrightarrow{\boldsymbol{v}_g^e} + j\omega_e L_f\overrightarrow{\boldsymbol{i}_f^e} + j\omega_e L_g\overrightarrow{\boldsymbol{i}_g^e} \quad (19)$$

where ω_e is the angular frequency of the grid voltage. $\boldsymbol{v}_f^e$, $\boldsymbol{v}_g^e$ $\boldsymbol{i}_g^e$and $\boldsymbol{i}_f^e$ are space vectors in the synchronous reference frame and are defined as;

$$\boldsymbol{v}_f^e = v_{df} + jv_{qf} \quad (20)$$
$$\boldsymbol{v}_g^e = v_{dg} + jv_{qg} \quad (21)$$
$$\boldsymbol{i}_f^e = i_{df} + ji_{qf} \quad (22)$$
$$\boldsymbol{i}_g^e = i_{dg} + ji_{qg} \quad (23)$$

Equations (19)-(23) can be used to obtain the *d-q* model of the grid-tied inverter and is given as;

$$v_{df} = R_f i_{df} + L_f p i_{df} + R_g i_{dg} + L_g p i_{dg} + v_{dg} - \omega_e L_f i_{qf} - \omega_e L_g i_{qg} \quad (24)$$
$$v_{qf} = R_f i_{qf} + L_f p i_{qf} + R_g i_{qg} + L_g p i_{qg} + v_{qg} + \omega_e L_f i_{df} + \omega_e L_g i_{dg} \quad (25)$$

If we assume that $i_{df} \approx i_{dg} = i_d$ and $i_{qf} \approx i_{qg} = i_q$ then equations (24)-(25) become

$$v_{df} = (R_f + R_g) i_d + (L_f + L_g) p i_d + v_{dg} - \omega_e (L_f + L_g) i_q \quad (26)$$
$$v_{qf} = (R_f + R_g) i_q + (L_f + L_g) p i_q + v_{qg} + \omega_e (L_f + L_g) i_d \quad (27)$$

Equations (26) and (27) are first order non-linear systems for which v_{df} and v_{qf} are inputs and i_d and i_q are outputs. The voltage commands needed to give the desired currents, i_d and i_q, are obtained with a feedback-based solution using current controllers. The formulation for the controller gains will be performed using equations (26) and (27). Expressions $\omega_e(L_f + L_g) i_q$ and $\omega_e(L_f + L_g) i_d$ in the equations are cross-coupling terms (Gupta *et al*., 2022; Abad, 2017) which will be cancelled in the control structure in order to provide for linear control of current.

Three phases active and reactive power are expressed in the *d-q* reference frame as follows (Abad, 2017);

$$P = \frac{3}{2}(v_q i_q + v_d i_d) \quad (28)$$
$$Q = \frac{3}{2}(v_q i_d - v_d i_q) \quad (29)$$

Where P and Q are the active and reactive power respectively. Either of the quantities can be controlled by controlling the *d-q* currents.

2.3 Inverter Control

The inverter control is based on the synchronous reference frame theory. The grid voltages are sensed and transformed first to their equivalent synchronous reference frame or *d-q* voltages where they become DC quantities and are then used for inverter control (Abad, 2017). Inverter three-phase currents are sensed and transformed as well to their *d-q* equivalents. Control is performed in the synchronous reference frame in which the active component of the inverter current i_d is regulated to provide active power control. The reactive component of the inverter current i_q is regulated as well to provide reactive power control. PI controllers are employed for the current control. Despite their drawbacks of poor compensation capability of low order harmonics, PI controllers still give a very satisfactory response when controlling DC variables. The reference currents i_d^* and i_q^* and the actual currents are used to generate error signals which are passed to their corresponding PI controllers.

2.4 Controller Design

From equations (26) and (27), after the cancellation of the coupling terms, the model equations at open loop for the LCL filter yield the following;

$$V_{df} = (R_f + R_g) i_d + (L_f + L_g) p i_d \quad (30)$$
$$V_{qf} = (R_f + R_g) i_q + (L_f + L_g) p i_q \quad (31)$$

The cancellation of the cross-coupling terms is carried out at the output of the PI controllers. v_{dg} and v_{qg} are added to the output of the PI controllers as feed-forward terms.

The current closed loops can be represented ideally according to the following transfer functions;

$$\frac{i_d(s)}{i_d^*(s)} = \frac{sk_p + k_i}{[(L_f + L_g)s^2 + s(R_f + R_g + k_p) + k_i]} \quad (34)$$

$$\frac{i_q(s)}{i_q^*(s)} = \frac{sk_p+k_i}{\left[(L_f+L_g)s^2+s(R_f+R_g+k_p)+k_i\right]} \quad (35)$$

The expressions for the PI controller gain, k_p and k_i were obtained by comparing the normalized denominator of equation (34) with the standard second-order denominator, as follows;

$$s^2 + s\left(\frac{R_f+R_g+k_p}{L_f+L_g}\right) + \frac{k_i}{L_f+L_g} \equiv s^2 + 2\zeta\omega_n s + \omega_n^2 = 0 \quad (36)$$

where upon k_p and k_i were obtained as;

$$k_p = \left(L_f + L_g\right)2\zeta\omega_n - (R_f + R_g) \quad (37)$$

$$k_i = \left(L_f + L_g\right)\zeta\omega_n^2 \quad (38)$$

ζ is the damping ratio. ω_n is the natural frequency.

The PI controller gains are calculated as 0.38 and 40 for k_p and k_i respectively, assuming double real poles for simplicity, using the following parameters;

Rated power = 10 kVA, V_{grid} = 415 V, V_{DC} = 800 V, switching frequency = 10 kHz, $R_f = R_g$ = 0.01 Ω, $L_f = L_g$ = 0.5 mH, C = 100 µF, ζ = 1 and ω_n = 200 rad/s.

For the SPWM, the relationship between modulation index and inverter voltages are given as;

$$v_{df} = m_d \frac{V_{dc}}{2} \quad (39)$$

$$v_{qf} = m_q \frac{V_{dc}}{2} \quad (40)$$

v_{df} and v_{qf} are therefore multiplied by $\frac{2}{V_{dc}}$ to obtain m_d and m_q which are transformed to the *abc* reference frame in order to produce the voltage references for the three-phase inverter control. It is these references that are applied to the SPWM block to generate the commands for the inverter switches.

2.5 Phase Locked Loop

For the three-phase voltage and current transformations, the phase angle θ of the grid voltage is needed. This angle is estimated by the PLL. Its closed loop nature provides stability and perturbation rejections to the angle estimation. It is a simple but effective synchronization method. It synchronizes the inverter frequency to the grid voltage frequency. The PLL is synchronized by using the *d-q* coordinates of the grid voltages. It extracts the phase angle from the grid voltages to keep the controlled current in phase with the grid voltage. The Simulink implementation of the PLL is provided in Figure 3.

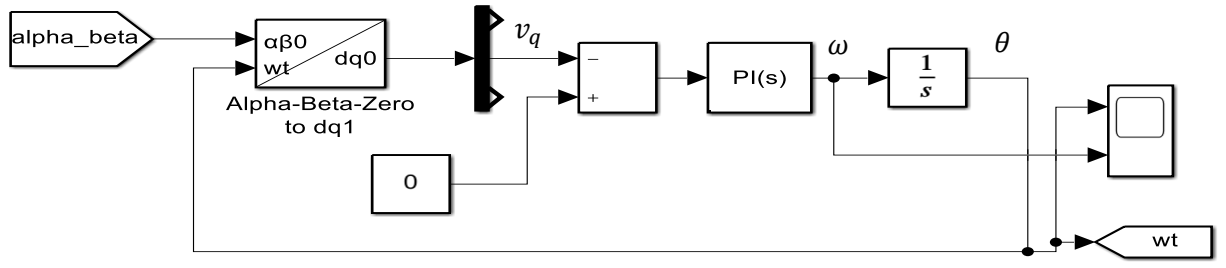

Figure 3: Simulink implementation of the PLL

2.6 Simulink Implementation

The Simulink implementation of the grid-tied inverter and its control are presented in Figure 4 and Figure 5 respectively.

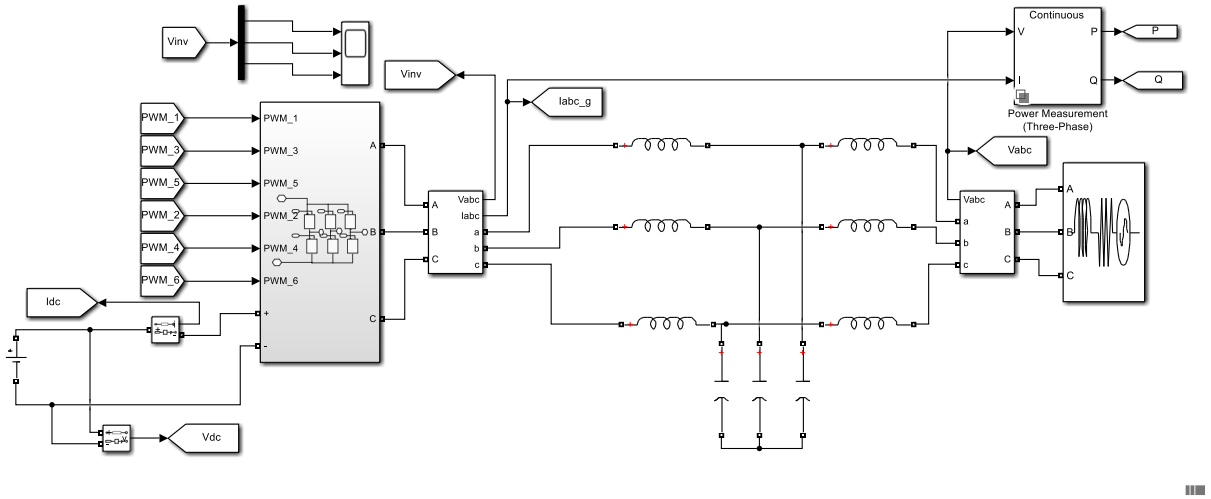

Figure 4: Grid inverter implementation in Simulink

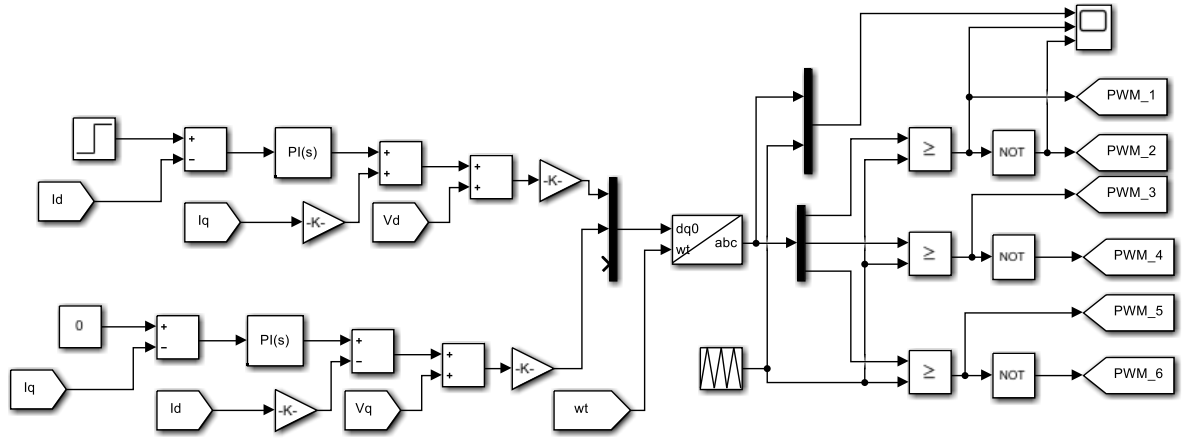

Figure 5: Inverter control implementation in Simulink

3. RESULTS AND DISCUSSION

The inverter output voltage is shown in Figure 6 and the grid voltages are shown in Figure 7(a). Whereas, the inverter out voltages are square waveforms containing harmonics of the switching frequency, the grid voltages are sinusoidal waveforms. The LCL filter is clearly very effective in filtering out the high-frequency harmonics of the inverter voltage. The grid currents are shown in Figure 7(b). They can be observed to be sinusoidal three-phase currents that are 120^0 out of phase with one another. Active power flow control is performed by setting the reactive component of the current i_q equal to zero and setting a non-zero reference for the active current component of power. With the active current component set to -114A (which corresponds to a rated power of 100kW) initially, only active power flows to the grid. There is no reactive power flow. This is demonstrated in the result of Figure 7(c) by the fact that the grid current is in phase with the grid voltage, indicating that the power factor is unity. The reference current was reduced, by half, to -56A at a time of 0.5s of simulation time while still maintaining the reactive component at a value of zero. This is the reason why the grid current is seen to reduce by half in Figures 7(b) and (c). The peak value of the current can be seen to be equal to the reference value of the active component of the current.

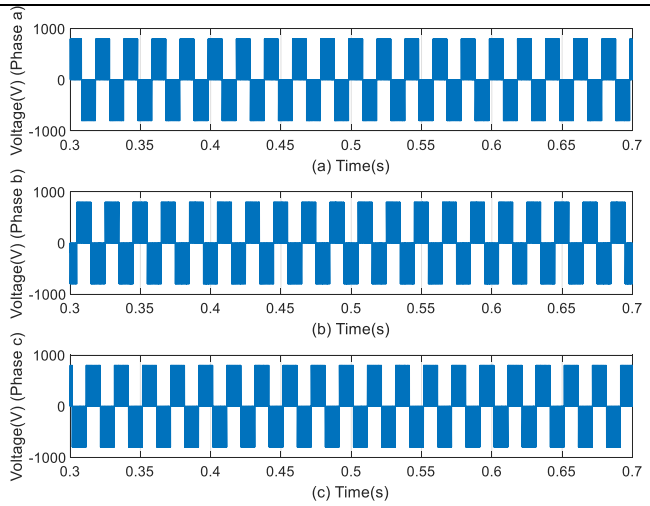

Figure 6: Inverter output voltages

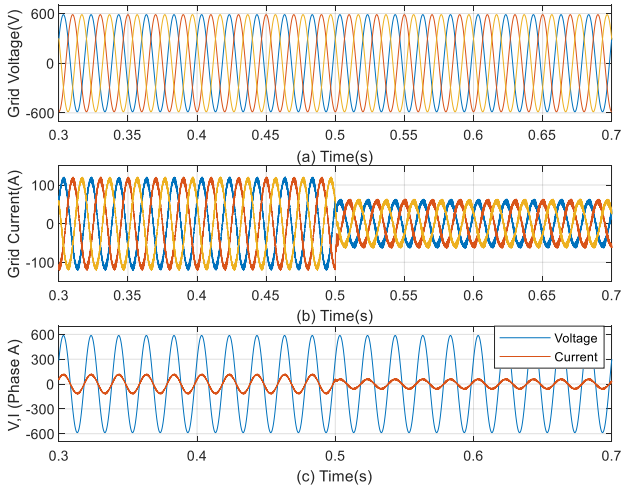

Figure 7: (a) Grid voltages (b) Grid currents (c) Voltage and current of Phase '*a*'

The plot of active and reactive power can be seen in Figure 8. Clearly reactive power under this condition is zero. The active power is observed to be equal to 100kW initially and then this value is reduced by half from the time of 0.5s in accordance to the reference value set for the active current component. It is clear that simulation results verify the analysis set forth in section 2. The modulating signals passed to the PWM generator and the triangular carrier signal of 10kHz are presented in Figure 9(a). It can be seen that the process is not over modulated or under modulated. Modulation signals have a magnitude slightly less than 1 which is appropriate.

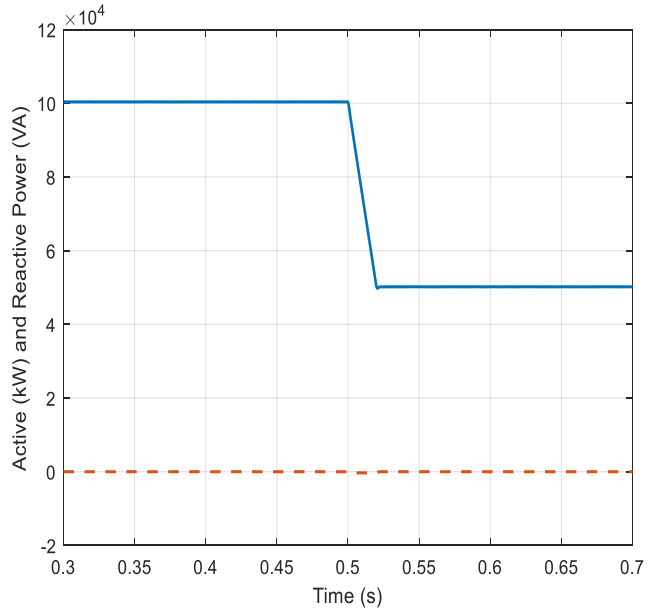

Figure 8: Active and reactive power

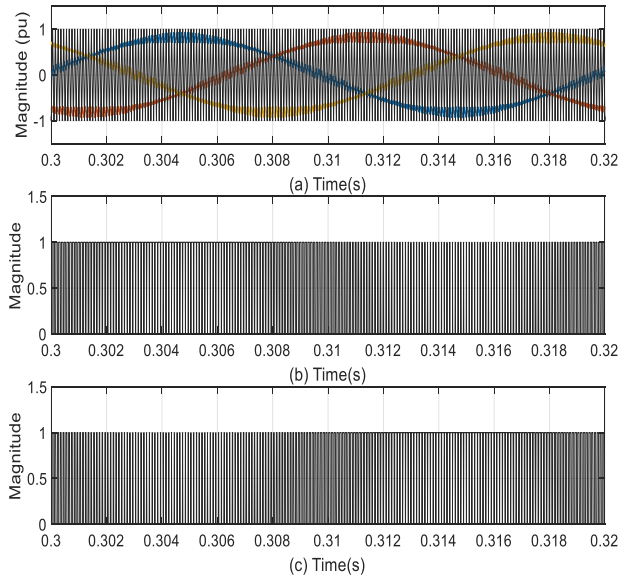

Figure 9: (a) modulating and carrier signals (b) switching pulse for top switch of phase '*a*'

The switching pulses for the top and bottom switches of phase '*a*' of the inverter are shown in Figures 10(a) and (b). The phase angle of the grid voltage, θ, is illustrated in Figure 10(a). It is the output of the PLL and it can be seen that it changes from 0 to 314 radians between 0 and 1s giving a constant angular frequency of 314 rad/s for the grid voltage and current as seen in Figure 10(b).

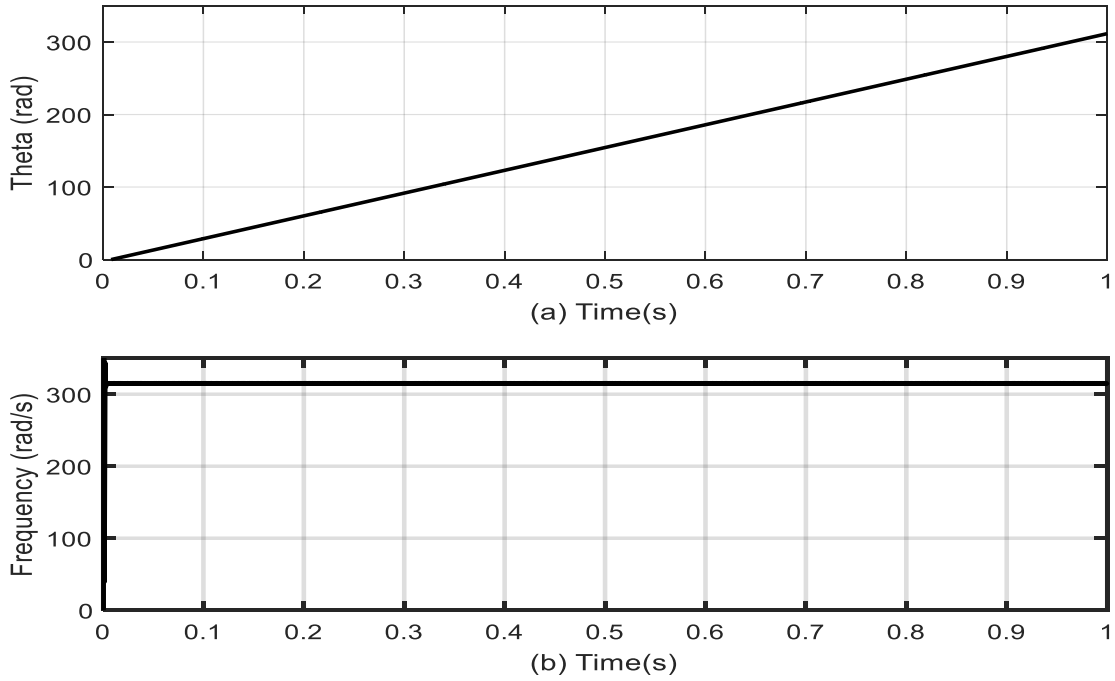

Figure 10: (a) Phase angle of grid voltage and current (b) frequency of grid voltage and current

4. CONCLUSION

The operation of the grid-tied inverter in the synchronous reference frame has been demonstrated in this paper. The model of the three-phase inverter, grid-tied inverter, and control structure was developed, analysed, and simulated in the Simulink environment. Active power flow control in the synchronous reference frame was effectively demonstrated. A reference value of -114 A was set for the active component of current while a value of zero was set for the reactive component of current thereby producing active power of 100kW at the three-phase power grid. Grid voltages and currents were observed to be in phase under this condition. A *dq* current controller with PI control was developed and designed and a simple PLL was adopted to realize the control in the synchronous reference frame. Simulation results of active power, reactive power, inverter, and grid voltages and currents prove the effectiveness of the PLL and current control method applied in this work. Although this control approach is fairly straightforward and easy to understand, the implementation of the control with PI controllers is discouraging because of the cancellation terms and the voltage feed-forward approach. Other controllers such as proportional resonance and dead-beat current controllers are often preferred to the PI current controllers and are recommended because of their fast dynamics and ease of implementation.

REFERENCES

1. Abad G. (2017). Power electronics and electric drives for traction applications. John Wiley and Sons. United Kingdom.
2. Blaabjerg, F., Teodorescu, R., Liserre, M. and Timbus, A. V. (2006). Overview of Control and Grid Synchronization for Distributed Power Generation Systems. IEEE Transactions on Industrial Electronics. 53(5): 1398-1409. doi: 10.1109/TIE.2006.881997.
3. Energy Commission of Nigeria (2005). Renewable energy master plan, Final report. Section 1.5 – 1.7 - Nigeria's renewable energy vision, p35 – 38. https://www.iceednigeria.org/resources/nov.-2005.pdf
4. Fatima, M., Siddiqui, A. S. and Sinha, S. K. (2024). Utilizing Feedforward Compensation, Active and Reactive Power Control of a Grid-Tied Three-Phase Inverter. IEEE International Conference on Computing, Power and Communication Technologies (IC2PCT), Greater Noida, India, pp. 802-806, doi: 10.1109/IC2PCT60090.2024.10486684.
5. Fatima, M., Siddiqui, A. S. and Sinha, S. K. (2022). Implementation of Three-Phase two Stage Solar PV Inverter for Grid Connection. 8th International Conference on Advanced Computing and Communication Systems (ICACCS), Coimbatore, India, pp. 1325-1329, doi: 10.1109/ICACCS54159.2022.9785351.

6. Gupta, A. K., Pragallapati, N., Joshi, M. S. and Agarwal, V. (2022). A Novel Per Unit (P.U.) Integer Format Applied to the Control of a Grid-Tied Solar PV Inverter. IEEE Transactions on Industrial Informatics, vol. 18, no. 2, pp. 735-743, doi: 10.1109/TII.2021.3067922
7. Kumar, R., Chaudhari M. A. and Chaturvedi, P. (2024). Analysis of Synchronverter and PLL-Less Control for Three-Phase VSI in AC Microgrids. Third International Conference on Power, Control and Computing Technologies (ICPC2T), Raipur, India, pp. 810-816, doi: 10.1109/ICPC2T60072.2024.10474759.
8. Marangalu, M. G., Kurdkandi, N. V., Monfared, K. K., Talebian, I., Neyshabouri, Y. and Vahedi, H. (2024). A New High Step-Up SC-Based Grid-Tied Inverter with Limited Charging Spike for RES Applications. IEEE Open Journal of Power Electronics, 5, pp. 295-310. doi: 10.1109/OJPEL.2024.3366165.
9. Masum, S. M. and Al Mamun E. (2024). Comparative Study of Grid-Tied PV Systems in Bangladesh's Coastal Gems. International Conference on Green Energy, Computing and Sustainable Technology (GECOST), Miri Sarawak, Malaysia, pp. 420-424, doi: 10.1109/GECOST60902.2024.10474676.
10. Nigeria Renewable Energy Master Plan (2014). International Energy Agency. Retrieved 2nd August 2014.
11. Patel, N., Gupta, N., and Babu, B. C. (2019). Design, development and implementation of grid-connected solar photovoltaic power conversion system. Energy Sources, Part A: Recovery, Utilization and Environmental Effects. 43(22): 2915-2934. https://doi.org/10.1080/15567036.2019.1668506
12. Qureshi, S. A and Potdar, M. S. (2021). A Comparative Analysis & Simulation of Phase Locked Loop for a Grid synchronized Photovoltaic System. IEEE International Conference on Mobile Networks and Wireless Communications (ICMNWC), Tumkur, Karnataka, India, pp. 1-7, doi: 10.1109/ICMNWC52512.2021.9688442.
13. Evju, S. E. (2007). Fundamentals of Grid Connected Photo-Voltaic Power Electronic Converter Design. Unpublished MSc thesis in Energy and Environment. Department of Electrical Power Engineering, Norwegian University of Science and Technology.
14. Vendoti, S., Inayathullaah, M. A., Chiranjivi, M., Fabbina, C., Kavin, K. S. and Malathi, P. (2024). A WECS fed Grid Tied DC-DC LUO Converter for Energy Management in Electric Vehicle System, 2nd International Conference on Computer, Communication and Control (IC4), Indore, India, pp. 1-7, doi: 10.1109/IC457434.2024.10486647.

PAPER 96 - CONCRETE COMPRESSIVE STRENGTH ASSESSMENT USING ARTIFICIAL NEURAL NETWORK

O. A. Ibrahim[1*], D. E. Osegbowa[2], J. Sule[3], A. O. Shofolahan[4], S. O. Ibrahim[5], and J. Wasiu[6]

[1,2,3,6]Department of Civil Engineering, Edo State University Uzairue, Edo State, Nigeria
[4,5]Department of Civil Engineering, University of Ilorin, Ilorin, Nigeria.
[*]Email: Ibrahim.abdulrazaq@edouniversity.edu.ng

ABSTRACT
Artificial intelligence (AI) has the potential to transform the way civil engineers design, build, and manage infrastructure. Despite the potential benefits of integrating artificial intelligence into Civil Engineering, there is a lack of study on the effective implementation and optimization of AI systems in the industry, as well as concerns about job displacement and ethical considerations. In this study, concrete compressive strength predictive model was used for Artificial Neural Network (ANN), with data from construction sites. A Python library called TensorFlow was used for Neural networks in deep learning for the prediction. A comparative analysis was conducted by determining the average compressive strength of six (6) 100x100mm concrete cubes through laboratory testing. The graphs obtained followed a straight line pattern. In the model's training data, the average value of cement was about 281kg. When compared to the value of cement for sample 3 (181.4 Kg). The mean absolute error for the test data is approximately 6 and 7 meaning, if we have a prediction **X**, the correct value would be X ± 6 MPa and X ± 7 MPa respectively. This shows the model's evaluation is very good with a limited error value.

KEYWORDS: Artificial Intelligence, Artificial Neural Network, Compressive strength, Tensor Flow, Python Library

1. INTRODUCTION

Artificial intelligence (AI) is a rapidly growing field that has gained significant attention in recent years due to its potential to revolutionize various industries, including Civil Engineering. Civil Engineering is a broad field that encompasses the design, construction, and maintenance of infrastructure, such as buildings, roads, bridges, and water supply systems. The application of AI in Civil Engineering has the potential to improve efficiency, accuracy, and safety in various aspects of the industry. One of the most promising applications of AI in Civil Engineering is in the field of structural engineering. AI algorithms can be trained to analyse large amounts of data and identify patterns that may not be immediately apparent to human engineers. This can lead to more accurate predictions of structural behaviour, allowing engineers to design structures that are more resilient to extreme weather conditions, earthquakes, and other hazards.

Another area where AI can be applied is in the design and optimization of transportation systems. AI algorithms can be used to analyse traffic patterns and optimize traffic flow, reducing congestion and improving safety on the roads (Einbeck and Dwyer, 2011). Additionally, AI can be used to optimize the routing and scheduling of public transportation systems, such as buses and trains. AI can also be applied in the field of water resources engineering. By analysing large datasets, AI algorithms can be used to model and predict water availability and quality, as well as to optimize the design and operation of water supply and treatment systems (Park, 2022). This can help ensure that communities have access to clean and reliable sources of water. However, the use of AI in Civil Engineering also raises concerns about the potential for job displacement and the need for ethical considerations in the development and deployment of AI systems. Therefore, it is important for civil engineers and policymakers to carefully consider the potential benefits and drawbacks of AI applications in Civil Engineering. Several studies have already been conducted on the application of AI in Civil Engineering. For example, a study by (Kim et al, 2021) explored the use of deep learning algorithms to predict the compressive strength of concrete. Another study by (Chen et al., 2020) investigated the use of machine learning algorithms to predict soil erosion in river basins. These studies demonstrate the potential for AI to improve various aspects of Civil Engineering.

ANNs can be regarded as an engineering counterpart of a biological neuron. The interconnected processing units are called artificial neurons and replicate the functioning of biological neurons.
Individually, the neurons perform trivial functions, but collectively, in the form of a network, they are capable of solving complicated problems (Flood and Kartam, 2010). ANNs rely on past knowledge and when presented with input-output data pairs they construct a functional relationship through a process of learning. The learning ability of neural networks is attributed to the adjustment in the intensity of the inter-neuron connection or the synaptic weight value. Adaptability to changing input-output data, non-linear function mapping, and the ability to capture unknown relationships, make ANNs a versatile tool for modelling real-world problems. The sub-sections elaborate the neural network applications in the field of Civil Engineering.

Vanluchene and Sun (2015) presented an introduction to the neural network by using a back-propagation algorithm to solve three different structural engineering problems related to pattern recognition, decision-making, and problems that have numerically complex solutions. Hajela and Berke (2008) examined the role of neural computing in structural engineering by obtaining the optimum weight of a truss. Rogers (2005) applied neural networks to structures having a large degree of freedom and showed that neural networks present computationally less expensive options compared to conventional structural analysis programs. Mukherjee & Deshpande (2018) developed a neural network for the initial design of reinforced-concrete rectangular single-span beams. The network predicts a good initial design (i.e. tensile reinforcement required, depth of the beam, width, cost perimeter, and the moment capacity) for a given set of input parameters (i.e. span, dead load, live load, concrete grade, and steel type). Adeli and Park (2020) developed a neural dynamics model for the optimum design of structures. Elazouni et al. (2018) showed how neural networks can be used for estimating resource requirements at the conceptual stage of design.

2. THEORETICAL ANALYSIS

The specimens are loaded till failure in a compression testing machine conforming to the standard (EN 12390-4, 2000). The maximum load reached is recorded and the compressive strength is obtained by the following equation:

$$\partial = \frac{P}{A} \quad (1)$$

Where, P stands for maximum load,
A stands for the area of Specimen = 10000mm^2 and
∂ stands for the compressive strength in N/mm^2

3. MATERIALS AND METHODS

This section goes through the detailed step-by-step process used to achieve a concrete compressive strength predictive model with the use of Artificial Neural Network (ANN), given data from any construction site. A Python library called Tensor Flow which is used for Neural networks in deep learning has been used in this study to achieve prediction of the concrete compressive strength. The block diagram of these step-by-step processes used to achieve concrete compressive strength prediction is shown in Figure 1.

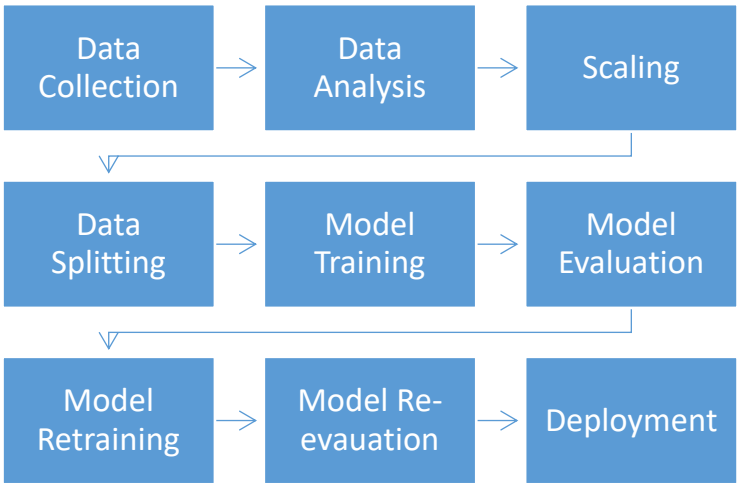

Figure 1: Block diagrams of processes involved in this study

3.1 *Data Collection*

Ideally, the data could be collected across different platforms on the construction site but in this study, the dataset was collected from Kaggle (an online machine-learning community). The data used are shown in Table 1.

Table 1: An example of Dataset

	cement	slag	ash	water	superplastic	coarseagg	fineagg	age	strength
0	141.3	212.0	0.0	203.5	0.0	971.8	748.5	28	29.89
1	168.9	42.2	124.3	158.3	10.8	1080.8	796.2	14	23.51
2	250.0	0.0	95.7	187.4	5.5	956.9	861.2	28	29.22
3	266.0	114.0	0.0	228.0	0.0	932.0	670.0	28	45.85
4	154.8	183.4	0.0	193.3	9.1	1047.4	696.7	28	18.29
5	255.0	0.0	0.0	192.0	0.0	889.8	945.0	90	21.86
6	166.8	250.2	0.0	203.5	0.0	975.6	692.6	7	15.75
7	251.4	0.0	118.3	188.5	6.4	1028.4	757.7	56	36.64
8	296.0	0.0	0.0	192.0	0.0	1085.0	765.0	28	21.65
9	155.0	184.0	143.0	194.0	9.0	880.0	699.0	28	28.99

3.2 **Exploratory Data Analysis (EDA)**

After the image data has been collected, the data analysis is done to extract meaningful insight from the data collected. The whole dataset is visualized with plots, graphs, and diagrams. This is immediately followed by feature extraction to remove unwanted fields and add some wanted fields. For the dataset obtained for this example (concrete compressive strength), no feature engineering was done because all the fields are useful.

3.3 **Data Splitting**

The data is divided into a Training set and a Test set. The AI model is taught (trained) on the Training set which is 85% of the data and the model is tested on the remaining 15% (test set). Data split is done so that the model's performance can be properly evaluated.

3.4 **Scaling**

When using Artificial Neural Networks (ANN), all the data has to be scaled in a way that is presentable to the network. A neural network was modelled mathematically after the human brain so the data inputs have to be numerical data. The data also have to be scaled so the model doesn't attach importance to the "Big" numbers and disregards the small ones. There are different columns in the dataset so applying a scaler called MinMaxScaler helps to scale all the columns.

3.5 **Model Training**

After the data has been collected, scaled, and pre-processed i.e., the data has been made useful for the Artificial Intelligence (AI) model, the data is passed into the model for training. The Strength column is the target column while the remaining fields are like the input columns. A number of materials like cement, slag, ash, water, superplastic, coarse aggregate, fine aggregate, and age are provided in the input column and it will make a mathematical equation that maps to the target column. An example of how the model is trained is shown in Table 2. The model Improves as the loss (error) keeps decreasing with time.

Table 2: Image of a model training

```
Epoch 1/400
7/7 [==============================] - 21s 2s/step - loss: 1574.8621 - val_loss: 1527.4272
Epoch 2/400
7/7 [==============================] - 8s 1s/step - loss: 1569.4303 - val_loss: 1523.5089
Epoch 3/400
7/7 [==============================] - 3s 478ms/step - loss: 1565.3453 - val_loss: 1519.8348
Epoch 4/400
7/7 [==============================] - 3s 481ms/step - loss: 1561.4303 - val_loss: 1515.5925
Epoch 5/400
7/7 [==============================] - 3s 486ms/step - loss: 1556.5781 - val_loss: 1509.8098
Epoch 6/400
7/7 [==============================] - 3s 523ms/step - loss: 1549.6456 - val_loss: 1501.4088
Epoch 7/400
7/7 [==============================] - 3s 485ms/step - loss: 1540.2104 - val_loss: 1489.2513
Epoch 8/400
7/7 [==============================] - 3s 480ms/step - loss: 1525.7208 - val_loss: 1471.5735
Epoch 9/400
7/7 [==============================] - 3s 478ms/step - loss: 1504.9470 - val_loss: 1446.1705
```

3.6 Model Evaluation

The AI model (Figure 2) was then tested to see if it has really learnt anything. Model Evaluation is also done to know just how much the AI knows. This helps in checking if the AI needs more improvement or not. Performance metrics such as mean squared error, mean absolute error and explained variance score are used to evaluate the model's performance. the metrics to be used depend on the project type. for classification tasks, metrics such as accuracy, f1-score, precision and recall would be used but for regression tasks, metrics used are mean squared error, mean absolute error and explained variance.

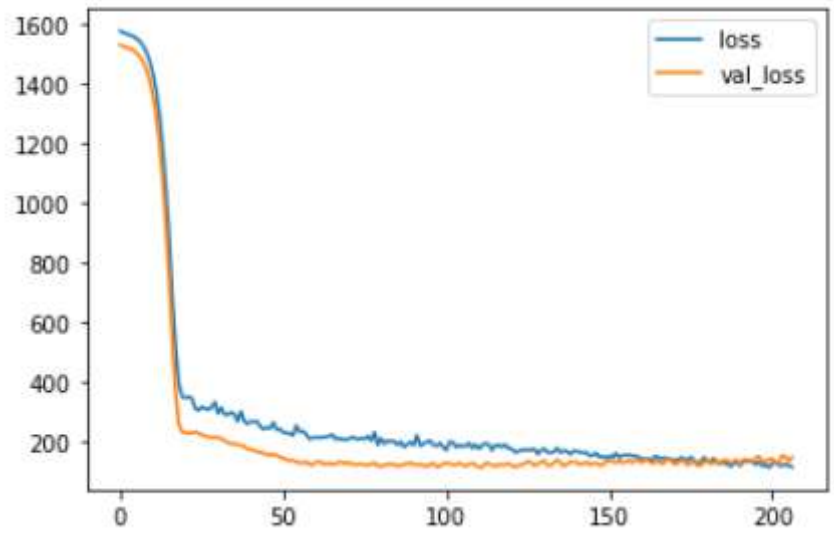

Figure 2*:* A Graph of the model training and loss reducing

3.7 Model Re-Evaluation and Training

After the model has been trained and evaluated, if the performance is okay then a different model is trained on all the datasets using the parameters of the previous one.

3.8 Deployment

After all the processes have been achieved, the model is then deployed to a web platform or a mobile app platform where any user can input cement, slag, ash, water, superplastic, coarse aggregate, fine aggregate, age values and get the concrete strength. Keep in mind the accuracy of the model would be put in place even after this. So, if the model predicts 24 for a set of inputs, the final output would be 24±2. If the model has a mean squared error of 2.

4 RESULTS AND DISCUSSION

A comparative analysis was conducted by determining the average compressive strength of six (6) 100x100mm concrete cubes through laboratory testing. Subsequently, the same dataset was utilized within an Artificial Neural Network (ANN) AI model to predict the compressive strength of concrete. Here are the outcomes of this analysis.

4.1 **Laboratory test**

After the failure load has been recorded, the compressive strength for each concrete cube is determined and reported in Table 3 and Table 4 respectively.

Table 3: Concrete Compressive Strength (7 days)

Weight (kg)	**Load (kN)**	**Strength (MPa)**
2.55	248	24.8
2.62	212	21.2
2.47	160	16.0
	Average	**20.67**

Table 4: Concrete Compressive Strength (28 days)

Weight(kg)	**Load(kN)**	**Strength (MPa)**
2.52	252	25.2
2.54	272	27.2
2.56	236	23.6
	Average	**25.33**

Table 5: Model Architecture Model: "sequential"

Layer (type)	output shape	param #
Dense (dense)	(none, 19)	171
Dropout (dropout)	(none, 19)	0
Dense_1 (dense)	(none, 19)	380
Dense_2 (dense)	(none, 19)	380
Dropout_1 (dropout)	(none, 19)	0
Dense_3 (dense)	(none, 19)	380
Dense_4 (dense)	(none, 1)	20

Total params:1,331; Trainable params:1,331; Non-trainable params:0

The model was trained for 42 training cycles called Epochs. An Early stop function was also put in place so that the model doesn't over fit which would give us a very bad performance. As seen in Figure 3 the training loss and evaluation losses are almost the same which shows that there was no overfitting.

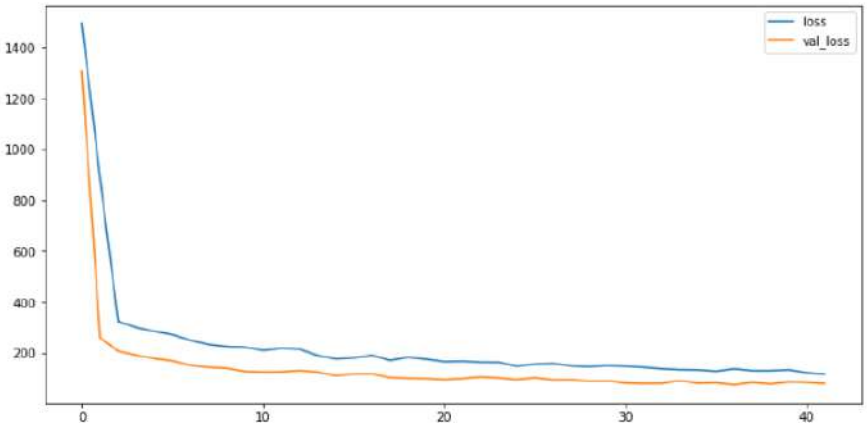

Figure 3: Model Training

Figures 4 and 5 present the results for the evaluation of the training and testing data respectively. The blue line across the scatter plot is the best line of best fit, this is what our graph would look like if we had 0 errors. The graphs are good because the graphs tend to follow the pattern of a straight line.

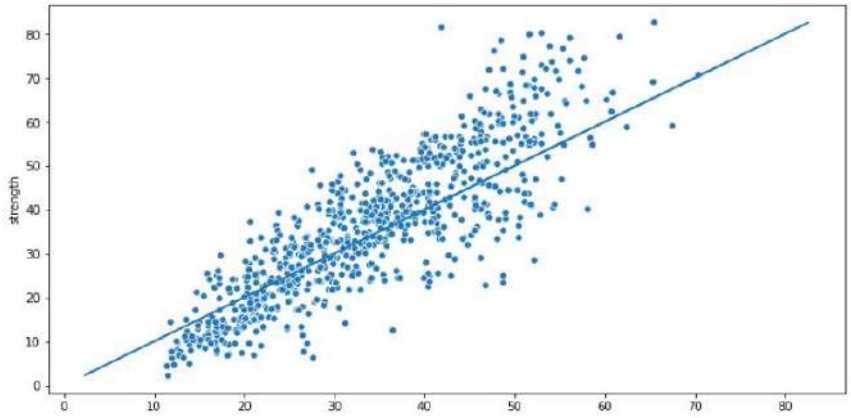

Figure 4: Result on Training Data

The evaluations on the training data are as follows:

MAE (Mean Absolute Error)
Train data (875 samples): 7.148730394374303
MSE (Mean Squared Error)
Train data (875 samples): 83.72776811995872
RMSE (ROOT means Squared Error)
Train data (875 samples): 9.150287870879184
Explanation: The mean absolute error was used in this study for the model evaluation. The mean absolute error for the training data is approximately 7 meaning, if we have a prediction **X**, the correct value would be X ± 7 MPa

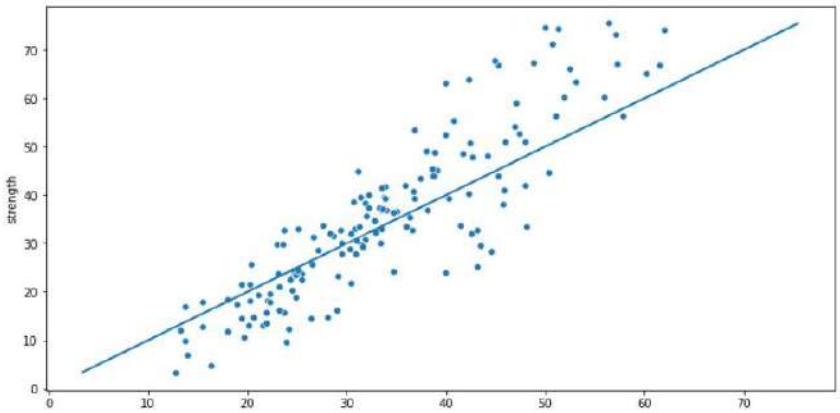

Figure 5: Result on Test Data

The mean absolute error was used in this study for the model evaluation. The mean absolute error for the test data is approximately 6 meaning, if we have a prediction **X**, the correct value would be X ± 6 MPa.

Table 6: Model's result

	Sample 1	Sample 2	Sample 3
Cement (Kg)	3.99	3.99	181.4
Water (Kg)	1.79	1.79	169.6
Slag	0.0	0.0	0.0
Ash	0.0	0.0	167
Fine Aggregate (Kg)	4.83	4.83	777.8
Coarse Aggregate	8.27	8.27	1055.6
Superplasticizer	0.0	0.0	7.6
Age (days)	7	28	14
Strength (Mpa)	20.67	25.3	21.60
Model's prediction	38.7	40.8	17.45
Error	18.0	15.5	4.15

In the model's training data, the average value of cement is about 281kg. When compared to the value of cement for sample 1 (3.99 Kg), the values are very much far apart. So, a limitation of this model is that the data it was trained on is limited. The model would only perform well on a dataset with high values of cement.

For sample 3, the model's evaluation is very good with a limited error value. The data inputted into the model was well suited for the model's prediction. The data from sample 3 is very much in range with the model's training data. Therefore, this model would perform very well when given cement values ranging from 120 to 500 kg.

5 CONCLUSION

From the study, the conclusions are;

1. The Artificial Neural Network (ANN) is largely dependent on the volume of data fed into it. The ANN would be able to sift through different data points and get a suitable outcome. A dataset containing just 1030 data points is insufficient if the power of the ANN is to be fully utilized, it would be better if there were more data points.
2. The Concrete Manufacturing dataset only contains a large, mixture of cement quantities ranging from 120 to 500 kg in a m^3 mixture. Therefore, the model cannot be used to evaluate the result of smaller cement mixtures (they would be considered outliers and their error values would be great)
3. The model's performance would change for better or worse depending on the hyper parameter used. If the hyper parameters (number of layers, number of neurons, optimizer, epochs, and loss) were to be

changed, the model's output would be different. Therefore, a very skilled Machine Learning Engineer is very much needed for a good AI task.

ACKNOWLEDGEMENT

I thank Almighty God for the success of this work, the Civil Engineering Staff of Edo University Uzairue, and all authors cited.

REFERENCES

Adeli, H. and Park, H.S. (2020). A neural dynamics model for structural optimization-Theory, Computers and Structures, 57(3), 383-390.

Chen, J., Yan, J., Zhai, L., Yang, X., Chen, X., and Chen, Y. (2020). Prediction of soil erosion in river basins using machine learning techniques. Journal of Hydrology, 586, 124818.

Einbeck, J., & Dwyer, J. (2011). Using principal curves to analyse traffic patterns on freeways. Transportmetrica, 7(3), 229–246.

Flood, I. & Kartam, N. (2010). Neural Networks in Civil Engineering. I: Principles and Understanding, Journal of Computing in Civil Engineering, 8(2), 131-148.

Hajela, P. and Berke, L. (2008). Neurobiological Computational Models in Structural Analysis and Design, Computers and Structures, 41(4), 657-667.

Kim, H., Kim, H., Hong, Y. W., & Byun, H. (2018). Detecting Construction Equipment Using a Region-Based Fully Convolutional Network and Transfer Learning. Journal of Computing in Civil Engineering, *32*(2).

Kim, Y., Cho, K., Cho, H., & Lee, Y. (2021). Prediction of compressive strength of concrete using deep learning models. Automation in Construction, 124, 103669.

Mukherjee, A. and Despande, J.M. (2018). Modelling Initial design process using Artificial Neural Networks, Journal of Computing in Civil Engineering, 9(3), 194-200.

Park, J. (2022). Development of a model to predict water quality using an automated machine learning algorithm. Journal of the Korean Society of Water and Wastewater, 36(6), 329–337.

Rogers, J.L. (2005). Simulating Structural Analysis with Neural Network, Journal of Computing in Civil Engineering, 8(2), 252-265.

Vanluchene, R.D. & Sun, R. (2015). Neural Networks in Structural Engineering, Computer-Aided Civil and Infrastructure Engineering, 5(3), 207-215.

PAPER 97 - PHYSICOCHEMICAL PROPERTIES OF FUEL GAS PRODUCED FROM GROUNDNUT SHELL WASTES USING DOWNDRAFT GASIFIER

E. O. Babatunde[1*]., S. O Ebhodaghe[2]., C. L. Eke[3]., O. A. Mokuolu[4], M. A. Olutoye[3].

[1]Department of Chemical Engineering, University of Ilorin, Ilorin, Nigeria.
[2]Chemical Engineering Department,University of Benin, Benin City, Nigeria.
[3]Chemical Engineering Department, Federal University of Technology, Minna, Nigeria.
[4]Department of Water Resources and Environmental Engineering, University of Ilorin, Ilorin, Nigeria.
[*]Email: babatunde.eo@unilorin.edu.ng

ABSTRACT
The use of groundnut shell wastes for fuel gas production have not been adequately addressed. This is important for more energy recovery from wastes. In this study, fuel gas is produced and analyzed from groundnut shell wastes, a common biomass. Fuel gas was produced through a downdraft gasification process. Two steel alloy barrels and galvanized iron pipes of various lengths and diameters were used in the manufacture. More details were provided on the waste's gasification process, and test performance of the gasifier. Operating parameters of the process include duration of experiment, flowrate and pressure of air supply, feed rate, producer gas, char generation, and char flowrate. Further gas cleaning and treatment were recommended.

KEYWORDS: Fuel gas, groundnut shells, downdraft gasification, production parameters.

1. INTRODUCTION

Nigerian farmers frequently discard groundnut shells, which are produced in the globe in about 40.18 million tons (Mamman, 2023). About 45 weight percent of cellulose, 33 weight percent of lignin, and other chemicals are among the main chemical elements found in the shells (Queirós et al, 2020). Groundnut shell wastes have various valuable applications. They can be utilized as a substitute for cement, fine aggregate, and coarse aggregate in construction materials, such as concrete and mortar (Mahmoud et al, 2012, Premalatha et al, 2022, Sathiparan et al, 2023). Additionally, groundnut shells can serve as effective biosorbents for removing heavy metals and pollutants from wastewater, contributing to environmental protection (Sathiparan et al, 2023). Furthermore, waste groundnut shells can be transformed into useful materials through physical, chemical, and thermal treatments, resulting in products suitable for water treatment, gas sensing, and energy storage applications (Zhan et al, 2021).

In energy applications, groundnut shell wastes can specifically be used for fuel production (Pawar and Panwar, 2020). Current research on fuel production from groundnut shell wastes includes various innovative approaches (Suraj et al, 2020; Razi and Sasmal, 2022). Studies have explored anaerobic digestion (AD) of peanut shells (PS) with organosolv and ultrasound pretreatments, showing potential for biofuel production. Studies on downdraft gasification of groundnut shell wastes involve assessing its feasibility and efficiency for energy production. These have shown that groundnut shells can be effectively utilized in gasification processes, leading to the production of concentrated fuel gas (Faraji, and Saidi, 2022; Faraji and Saidi, 2023).

There is limited information in the literature on the production of groundnut shell fuel gas using the downdraft gasification technique. The need for more research is imperative because groundnut shell waste is a raw material with a high heating value that may be used in the gasification process. Thus, this study aims to produce and analyse fuel gas from groundnut shell wastes using a downdraft gasification technique.

2. MATERIALS AND METHODS

All the materials were sourced locally in Nigeria. The feedstock (groundnut shell) was obtained from farmers in some agricultural waste dump sites in Benue State, Nigeria.

2.1 Feedstock Analysis

The groundnut shell was used in its natural loose form for the determination of its physical properties. The equivalent diameter of pore space, surface area and the permeability coefficient were obtained by calculations using the parameters measured in experiments. Also, the particle and bulk densities, bed voidage and specific surface area of the groundnut shell were obtained. For bed voidage, it is the volume of water which occupied the voids in a known volume of biomass bed. This is performed three times, and the mean was calculated for each parameter. For bulk density, the weight of the biomass packaged loosely was gotten with a weighing scale while the volume of the biomass is also calculated using $V=\prod r^2h$, since the gasifier tube is cylindrical. The sum of the fractional volume of the bed contained by the void spaces is often gotten by water substitution method in chemical engineering. According to this method gives a direct indication of the mean overall bed voidage.

2.2 Experimental Analysis on gasification of loose groundnut shell

In about 5 experiments, the gasification system was fed with loose groundnut shell and in each experiment various parameters such as biomass feed rate, biomass bed height in the gasifier, air flow rate, pressures at four points along the gasifier height, bed temperatures at eight points along the gasifier height, pressures and temperatures at salient points in the gasification system, PG flow rate, condensate collection rate, tar and particulates concentration, PG composition, mass balance, and energy balance, were measured and analysed.

3. RESULTS AND DISCUSSION

3.1 Test Performance of the gasifier:

All experiment were carried in a fixed bed downdraft gasifier reactor. The Oxidant that enabled the firing of the gasifier is the atmospheric air which was drawn into the system through the pores of the packed groundnut shell bed from the top of the burning tube. The process is a self-nourishing auto thermal system because there is no external source of heat energy added. Therefore, the biomass as a fuel burns itself to release the desired gas. The initiation of the experiment was done by feeding in some amount of pure carbon at the reduction zone such that it filled up the stainless-steel shaker bowl beneath the burn tube. The blower was started and allowed to blow for 10 min. Some water molecules trapped in the system during that time was enabled to escape. A rolled-up newspaper was inserted through the ignition pipe and lit at its outer end. As the blower sucked in air into the system, the flame was drawn into the system and entered straight to the burn tube in the gasifier through the ignition pipe. Also, as flame entered the system, it came in contact with the charcoal or carbon in the shaker bowl and it lit it up so that after some time the charcoal heated up to a hot red flame. Then the groundnut shell was immediately fed from the top of the gasifier. At steady state condition, the biomass continued to burn while the ignition pipe was capped, and the top of the burn tube left open. During this period, the only entrance of oxygen into the system was through the top of the burn tube as air from the environment percolated into the system through the groundnut shells.

The quantity of air drawn into the system was regulated with a rheostat connected to the blower. After 2 min, a white non-combustible smoke was released at the outlet, then after some 10 min, the resultant gas became combustible as the gas was flared to establish its combustibility. The blower pulled out the gas from the gasifier, through the cyclones, the heat exchanger, the filter bed, through itself, then the outlet pipe. These movements of the gas reduced the temperature before it reached the outlet. Also, the drop in temperature was mostly influenced by the high temperature silicone gel sealant used to lag the interiors of the pipes and the unit operations.

In the cyclone, the produced gas entered spirally and in that circular motion passed through the first cyclone filter, dropping the heavier particulates (tars and water) into the jar coupled below the cyclone. The gas being lighter then moves upward to the second cyclone where the same technique was also applied. In the heat exchanger, the gas initially entered the 2 inches diameter pipe at the top and then dispersed through the six (6) one inch diameter

pipes of lengths, 15 inches each, then moved collectively through the 2 in diameter pipe at the base of the heat exchanger. From the base of the heat exchanger, the gas approached the filter bed vessel. The 2 inches diameter pipe that introduced the gas into the filter bed had some perforations made below it. The perforations enabled the gas to lick through and make an upward movement through the filter materials to the lid of the filter, through the blower and then out to the outlet pipe.

The reduction and pyrolysis zone temperatures were taken with the infrared thermometer to monitor and measure temperature data. The produced gas samples were collected at an interval with an improvised gas collector which was a urine bag and motorcycle tyre tube. This was due to the unavailability of a Teflon gas sample bag. The collected gas samples were analysed in National Research Institute for Chemical Technology (NARICT) using the non-dispersive infrared sensor (NDIR). The residual char and ash present were also weighed at the end of the experiment. To turn off the gasifier the inlet and outlet ports were capped. The different gasification reaction is regulated by the physical properties of a biomass. The way it reacts when heated depends on the particle size. It may lump the throat of the burner if the size is too enormous and will lead to reduced gas generation.

Before the choice of feed stock was made, the behaviours of groundnut shell, rice husk, maize hub and wood chips were observed in the gasifier. After the groundnut shell exhibited a good performance, Rice husks was used as a second feedstock and due to the local milling method of rice around this part of the country, the husk particles were really disintegrated to fine particles thereby causing clogging and clinkering. The percolation of oxygen into the system was not done with easy thereby creating a puffing combustion.

The second feedstock that was compared with groundnut shell was corn-cob. The performance was checked after it was experimented on the designed gasifier. Some amount of the corn-cob was gotten from a local farmer in Lugbe, Abuja. The dried corn-cob was broken into smaller sizes. During the experiment, it was observed that the cobs were not flaring easily and probably the surface area needed to be increase in other to increase the rate of combustion. With this discovery, the use of groundnut shell was ruled out as hammer mills and flakers might be needed to crush the cobs. This might involve more cost especially for the target rural farmers which would need to have this technology. Wood chips were used as a third feedstock to compare to groundnut shell. The wood chips had a smoother process than rice husk and corn-cob. The physical property of the groundnut shell was compared to that of wood chips. The percentages of volatile matter, fixed carbon, Ash, Carbon, Hydrogen, Nitrogen and Oxygen as shown in Table 1.

Table 1: Physical/chemical properties of groundnut shells and fuel wood

Properties	**Unit**	**Groundnut shells**	**Fuel wood (Tippayawong et al. 2009)**
Volatile matter	(%wt./wt.)	65.11	79.0
Fixed carbon	(%wt./wt.)	22.28	14.8
Ash	(%wt./wt.)	3.19	5.9
C	(%wt./wt.)	47.97	45.7
H	(%wt./wt.)	5.79	3.7
N	(%wt./wt.)	0.93	0.2
O	(%wt./wt.)	39.70	44.6
HHV	MJ/Kg	17.69	

In Table 1, it is obvious that the proximate and ultimate analysis of groundnut shell were commensurate with wood fuel. This implies that the ash content of the groundnut shell was lesser than the wood fuel, thereby reducing the existence of clinkering and slagging in the system. The volatile content is not too high for the producer gas to be fed directly into an IC (Internal Combustion) engine. This enables a tranquil direct burning of the gas produced. The voidage of loose groundnut shell bed was as elevated as 0.8, which means that a large volume of oxidation zone during gasification obtained the voidage of a bed of long cylinders (h/d=5.29) to be 0.35-0.4. The voidage data will be useful for flow modelling purposes. The value of the permeability coefficient is frequently used to give an indication of the ease with which a fluid can flow through a bed of particles. The loose groundnut shell has low permeability coefficient and suffered higher pressure drop as presented in Table 2. The shape and size of the groundnut shells were uniform and despite the low density (<<200kg/m3).

Table 2: Physical and packed bed properties of loose Groundnut shell

Parameters			Groundnut Shell
Particle density	ρ_p	kg/m^3	440
Bulk density	ρ_b	kg/m^3	0.75
Bed Voidage	E		0.8
Quantity of bed biomass in the gasifier	m= ρ_bV	Kg	0.027
Specific surface area of particle	$S = \frac{Surface, area}{Particle\ \ volume}$	m^2/m^3	2390
Specific surface area of bed	S_B=S(1-e)	m^2/m^3	478
Equivalent diameter of pore space.	$d'm = \frac{e}{S_B}$	Mm	2
Pressure drops for air flow of 0.0022 m^3/s	ΔP/Δh	mm of WC/m	6

Table 3: The proximate and ultimate analyses of groundnut shell

Parameters			Groundnut Shell
Proximate analysis (db)			
Volatile Matter Fixed Carbon Ash	VM FC ASH	% % %	72.2 22.4 5.4
Ultimate analysis (dafb)			
Carbon Hydrogen Nitrogen Oxygen	C H N O	% % % %	47.9 4.8 1.5 45.8
Higher Heating Value	HHV	MJ/kg	19.13

Determination of operating Parameters of Groundnut shell Gasification

The basic operating parameters of the gasification system were obtained in the experiments lasting for 40 mins. The experimental results relating to the operating parameters were discussed in the following sections. These operating parameters are given in Table 4.

Table 4: Major operating parameters of groundnut shell gasification system

Parameter	Value
Duration of experiment	40 mins
Gasification air flow rate	8.07 kg/h
Pressure of air supply	20- 105 mmWC
Groundnut feed rate	0.77 kg/h
Producer Gas flow rate	9.43 kg/h
Char generation rate	0.3 kg/h
Condensate collection rate	0.246 kg/h

By analysing these parameters in Table 4, operators can optimize the groundnut shell gasification system's performance, identify operational inefficiencies, and make informed decisions to enhance productivity and sustainability. The 40 mins duration of experiment provides insight into the stability and consistency of the system over a specified period. Longer durations may reveal trends or variations in performance. The air flow rate of 8.07 kg/h is crucial for maintaining the gasification process. Optimal air flow ensures efficient combustion and gas production. Deviations from the desired rate may indicate inefficiencies or operational issues.

The pressure of air supply of 20-105 mmWC affects the gasification process's temperature and residence time. Maintaining the pressure within the specified range is important for stable and efficient operation. Fluctuations outside this range may impact gas quality and production rate.

On the groundnut feed rate (0.77 kg/h), the feed rate determines the amount of biomass (groundnut shells) supplied to the gasifier. Monitoring this parameter helps maintain a steady gas production rate and prevents overloading or underutilization of the system. The producer gas flowrate indicates the system's output, which is essential for assessing its capacity and efficiency. Higher flowrates suggest higher gas production, while lower rates may indicate issues such as incomplete combustion or restricted gas flow. Char generation is an inevitable byproduct of gasification. Monitoring the char generation rate helps understand the system's carbon conversion efficiency and assess the potential for char utilization or disposal. The condensate collection rate of 0.246 kg/h reflects the presence of volatile components in the producer gas that condense into liquid form.

4. CONCLUSIONS

In this study, a common biomass, groundnut shell wastes were used to investigate the production and analysis of fuel gas. The groundnut shell feedstock was used to produce fuel gas through a downdraft gasification process. Analysing the parameters and optimize the groundnut shell gasification system's performance, identify operational inefficiencies, to enhance productivity and sustainability. Monitoring this parameter helps evaluate the gas quality and assess the need for further gas cleaning or treatment.

REFERENCES

Faraji, M. and Saidi, M., (2022). Process simulation and optimization of groundnut shell biomass air gasification for hydrogen-enriched syngas production. International Journal of Hydrogen Energy, 47(28), pp.13579-13591.

Faraji, M. and Saidi, M., (2023). Experimental and simulation study of peanut shell-derived activated carbon and syngas production via integrated pyrolysis-gasification technique. Process Safety and Environmental Protection, 171, pp.874-887.

Mahmoud, H., Belel, Z.A. and Nwakaire, C., (2012). Groundnut shell ash as a partial replacement of cement in sandcrete blocks production. International Journal of Development and sustainability, 1(3), pp.1026-1032.

Mamman, P. (2023). Anaerobic Digestion of Groundnut Shell with Cow Dung for Biogas Production (Doctoral Dissertation).

Pawar, A. and Panwar, N.L., (2020). Experimental investigation on biochar from groundnut shell in a continuous production system. Biomass Conversion and Biorefinery, pp.1-11.

Premalatha, P.V., Kumar, S.S., Murali, C.S. and Aadithiya, K.V., (2022). Profound probing of Groundnut Shell Ash (GSA) as pozzolanic material in making innovative sustainable construction material. Materials Today: Proceedings, 49, pp.1275-1280.

Queirós, C.S., Cardoso, S., Lourenço, A., Ferreira, J., Miranda, I., Lourenço, M.J.V. and Pereira, H. (2020). Characterization of walnut, almond, and pine nut shells regarding chemical composition and extract composition.

Razi, M.O. and Sasmal, S., (2022). Organosolv pre-treatment of groundnut (Arachis hypogaea) shell and its upshot. Biomass Conversion and Biorefinery, 12(11), pp.5221-5228.

Sathiparan, N., Anburuvel, A. and Selvam, V.V., (2023). Utilization of agro-waste groundnut shell and its derivatives in sustainable construction and building materials–A review. Journal of Building Engineering, 66, p.105866.

Sathiparan, N., Anburuvel, A., Selvam, V.V. and Vithurshan, P.A., (2023). Potential use of groundnut shell ash in sustainable stabilized earth blocks.

Suraj, P., George, J., Arun, P. and Muraleedharan, C., (2020). Theoretical and experimental feasibility study of groundnut shell gasification in a fluidized bed gasifier. Biomass Conversio and Biorefinery, 10, pp.735-742.

Zhan, Y., Zhou, H., Guo, F., Tian, B., Du, S., Dong, Y. and Qian, L., (2021). Preparation of highly porous activated carbons from peanut shells as low-cost electrode materials for supercapacitors. Journal of Energy Storage, 34, p.102180.

PAPER 98 - ADVANCEMENTS IN AUTOMATED COOLING AND EXHAUST SYSTEMS: TOWARDS SUSTAINABLE THERMAL MANAGEMENT

T.E. Akinshola[1]*, A.I. Olanrewaju[1], H.A. Bello[1], A.O. Dele[1], I. Adedeji[1], A. Onijala[1], A.O. Otuoze[1].

[1]Department of Electrical and Electronics Engineering, Faculty of Engineering and Technology, University of Ilorin, Ilorin, Kwara State, Nigeria.
*Email: akinsholatemidayo@gmail.com

ABSTRACT

As industries strive for sustainability, major advancements in cooling/exhaust systems become more vital and play a pivotal role in achieving near-maximum efficiency with regard to thermal management. To this effect, this paper seeks to provide a comprehensive overview of one key strategy for improving temperature control systems in industrial settings. With a strategic focus on modifying existing ventilation technology, attention is directed towards qqa breakthrough automation system that hybridizes the crucial components of both cooling and exhaust systems. This discussion shall be centered around the design, construction, and testing/analysis of a novel automated cooling exhaust system with multiple modes of control. Additional features include temperature regulation, real time speed monitoring for cooling fans, and toxic fumes detection system. The experiments performed in this article expound on the functionality of this prototype, its sensitivity to different sources of toxic fumes, as well as the stark contrast between present day commercially available systems and the model put forward by this report. As this paper navigates through these complex discussions, a greener future is envisioned, where advancements in automated cooling/exhaust systems propel humanity towards adopting more sustainable and more eco-friendly industrial practices.

KEYWORDS: Sustainability, Cooling/Exhaust, Microcontroller, Speed Control, Fumes Detector, Automated Temperature Regulation

1. INTRODUCTION

In the contemporary landscape of industrial innovation, one primary component is common to every industrial or manufacturing establishment; a cooling/ventilation system. Ironically, not much has changed in terms of improvements to these systems since the start of the industrial age. Modern research by Amanowicz *et al.* (2023) buttresses the significance of advancements in industrial ventilation systems for improved temperature control and energy efficiency. In this new era of sustainable technological practices, it has become pertinent to seek new and better means of achieving the desired objectives. By building upon the work of Cioc *et al*. (2004) on automated temperature regulation systems, this paper presents a solution to optimizing thermal management by merging two crucial elements of industrialization—cooling and exhaust systems—thus, aggregating their advantages as well as eradicating the need for two separate structures.

Additionally, this research addresses the critical issue of toxic fumes detection especially in large-scale industrial environments, aligning with the findings of Parri *et al*. (2023) on advancements in emissions monitoring technologies. An integrated toxic fumes detection system creates an all-encompassing approach to environmental sustainability in industrial operations. Central to this theme, is the design and implementation of an intelligent automated cooling system prototype as suggested by Prince *et al.* (2021), to test and analyze the veracity of the previously outlined claims. As this paper navigates through the intricacies of the system's developmental process and explores the system's potential applications, a greater understanding of the need for a future where sustainability is not just an aspiration, but a tangible reality, is acquired.

2. THEORETICAL ANALYSIS

Per the aforementioned objectives, the aim of this paper borders on designing a cooling system with multiple modes of control and exhaust Functionality. An Atmega328p microcontroller is selected as this system's primary control unit. For the proposed prototype, an array of EM relays will be used to achieve the different levels of speed control and reverse polarity for exhaust mode. A DHT11 temperature sensor and an MQ-2 fumes detector will serve as both temperature feedback and fumes level inputs into the system. To implement the different modes of user control, an IR

remote control module is used to incorporate a wireless remote control, a Bluetooth HC-06 module for receiving remote voice activation commands, and manual push buttons for manual control.

Figure 1 depicts a graphical representation of the interconnectivity of the system's constituting parts. The Atmega328p acts as the central control unit as expected, branching out unto each designated control mode. The Bluetooth voice activation, manual push buttons, and IR remote control all act as the external control modes, while the temperature control mode incorporates automated temperature control into the system. Based on specific preset temperature values, the system toggles between the different speed levels, keeping the temperature within the stipulated range.

Another noteworthy feature is the system's exhaust mode functionality. The microcontroller repeatedly reads the MQ-2 fumes sensor until a HIGH signal is detected. As preconditioned by the microcontroller's programming, a polarity reversal process is initiated, causing the air vent's fan blades to rotate in the opposite direction and extract toxic fumes and air, fueling during a fire outbreak. For the prototype, 12V electromagnetic relays achieve polarity reversal functionality for AC-powered air vent fans. Other additional features include the display, alarm buzzers, and LED indicators, which give the system audio and visual feedback capabilities.

Figure 2 on the other hand, depicts the process flow logic in the system's decision-making process. As a system override, top priority is given to the exhaust mode functionality per precautionary safety directives. In the absence of fumes/flammable gas, control of the vent fans is passed unto the 3 external control modes, with wireless Bluetooth activation taking priority, before remote control and manual push buttons are considered successively in that order. All three external control modes can switch between three-speed levels for the fans and shut the vent fans off. Automated Temperature control is given the least priority in the system, and it is set as the default mode in the absence of external "stimuli".

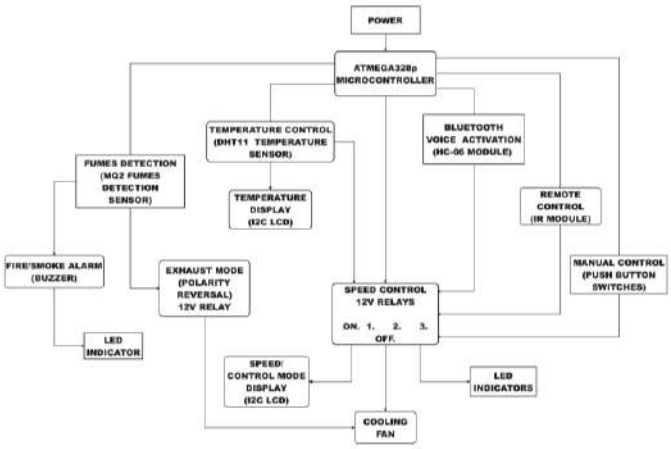

Figure 1. Block Diagram of the system.

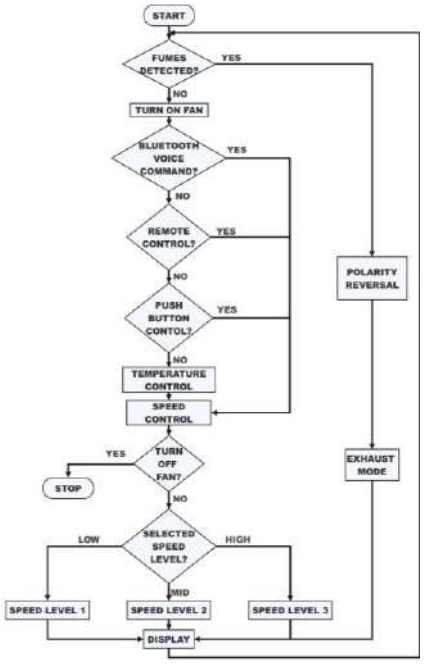

Figure 2. Process Flowchart for the Cooling/Exhaust System

3. METHODOLOGY

The circuit schematic diagram illustrated in Figure 3 describes the bare wire connections between the constituting components within the system. Once more, the Atmega328p microcontroller—represented by the Arduino board—takes its place as the system's central control unit. As can be seen in the circuit schematic, five 12V relays for achieving varying speed levels and polarity reversal are connected to the microcontroller unit via C1815 transistors in common-base mode. The transistors offer the 5V Atmega328p the ability to control higher voltage components such as the 12V electromagnetic relay. The EM relays control over the AC supply to the AC fans. Successively decreasing AC

voltage—220V, 180V and 150V—provides the three different speed levels through REL3, REL2 and REL1, respectively, while REL4 and REL5 reverse the supply terminals to the fans.

For the temperature sensing component, a DHT11 is connected via pin A0 of the microcontroller, and the fumes detector is connected through pin A1 as an analogue sensor. Push Buttons B1-B5 are connected to digital set pins similar to LEDs 1-5 and the alarm buzzer. The push buttons and the LEDS control indicate the 3 levels of speed, automated Temperature control and Exhaust mode, respectively. An I2C LCD serves as the display terminal for the system where the nominal operating conditions of the system can be monitored. It finds its connection to the Microcontroller's I2C pins A4 and A5.

An HC-06 Bluetooth module and an IR remote control sensor are the system's two wireless means of control. An IR LED receiver connects to the digital pin 2 of the Atmega328p and passes the received signals from the remote control module through that line. On the other hand, the HC-06 is connected via serial communication pins 0(Rx) and 1(Tx) through which Data is transmitted and simultaneously received.

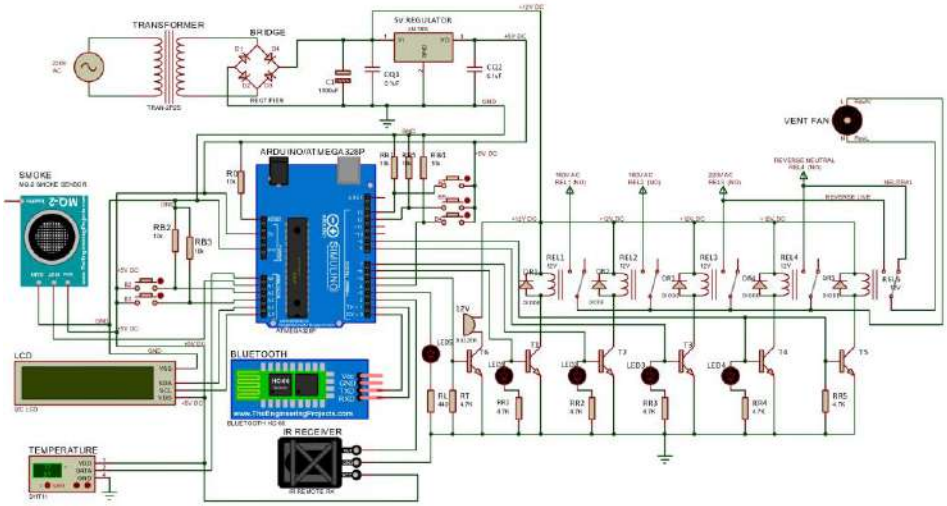

Figure 3. Schematic Circuit Diagram for the Cooling/Automation System

4. FABRICATION PROCESS

To test the veracity of the aforementioned claims and for experimentation purposes, a prototype of this Automated cooling/Exhaust System has been constructed in accordance with the schematic circuit designs discussed in Figure 3. The heart of this circuit consists of a Printed Circuit Board on which all major components are embedded. Copper traces within the PCB act as wires interconnecting all the constituting parts as given by the design. A suitable acrylic enclosure has been provided to protect the PCB and other sensitive circuit components from the external environment. Hence, necessary provisions were made for components and modules, such as temperature sensors, fumes detectors, etc., that monitor parameters within the outer environment by means of flex cable connectors from the components into the circuit Board within the enclosed packaging.

4.1. *Printed Circuit Board (PCB) Design And Fabrication*

With the Proteus v8 Design Suit software—and a bit of skill—the circuit schematic was transformed into a Printed Circuit Board layout design, accounting for all constituting components and their wire connections. A plain copper-clad board carrying an imprint of this PCB layout was etched in a copper solvent chemical mixture, leaving behind the wire traces that serve as the PCB's conductors.

Figure 4 shows a drilled and soldered PCB carrying all its necessary components. Having performed the required continuity and short-circuit tests, the circuit board received power via a 12V transformer, and all preliminary voltage tests were carried out to ensure proper circuit operation.

Figure 4. Printed Circuit Board for the Automated Cooling/Exhaust System

4.2. Programming and Packaging

Portrayed in Figure 5 is a section of the C++ algorithm written to the memory of the Atmega328p microcontroller to perform its specified tasks. The algorithm includes pin/port declarations, digital i/o functions, analog reading and filtering functions, serial com block for the HC-06 module, etc. The Bluetooth HC-06 module interfaces with the user's mobile device through the use of the blue application, as shown in Figure 7. The major control functions, such as speed control, automated control, exhaust control, fumes alert, temperature range settings, etc. can be accessed by the system's user.

On the outer shell of the inner PCB system and serving as the enclosure is a white acrylic box, as depicted in Figure 6 custom-shaped slots were made on the box's surface to accommodate the 20x4 LCD, the five buttons, and LEDs, the DHT11 temperature sensor and the MQ-2 fumes sensor. In addition to functionality, the enclosure performs its role in terms of aesthetics and user-friendliness, giving the prototype a finished outlook.

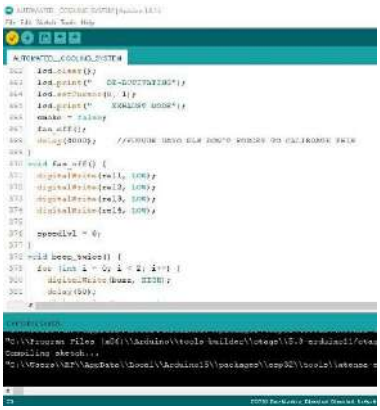

Figure 5. C++ Code for the Automated Cooling/Exhaust System

Figure 6. Packaging Box for the Automated Cooling/Exhaust System

Figure 7. Bluetooth Application for Interfacing with HC-06 module

5. TECHNICAL EVALUATION, EXPERIMENTATION AND DISCUSSION

The following experiments were carried out in a metallic 2 cubic meter (2m x 2mx 2m) enclosed space using 18in, 230W air vent fan blades. A custom-made slot on one side of the 2m³ enclosure is cut out to the exact dimensions of the vent, creating a semi-closed system where the fan blades alone are responsible for feeding in or feeding out air from within the system. A gas burner is used to introduce heat into the system, and frozen ice cubes take heat out of the system.

5.1 Heat/Temperature Auto-regulation Test

This experiment aims to test the temperature-regulating capacity of the cooling system at a nominal room Temperature of 27.6°C. Using the Bluetooth application, the desired operating temperature is set to 26°C and an operating range of ± 2°C.

5.1.1 High-Temperature Regulation

The enclosed space is preheated to specific temperature levels. The cooling/exhaust system is then activated, and the time taken for the system to recover back to the preset 26°C is recorded. This process is repeated for 12 different temperature levels from 29°C to 40°C.

Table 1 represents the data acquired from temperature regulation experiments conducted on the cooling system. It can be observed that there is a steady exponential incline in the amount of time it takes the system to recover to its preset operating temperature, and the difference in the time taken between each successive temperature level increases rapidly as the temperature approaches 40°C. It should be noted, however, that this experiment makes no provision for the heat lost naturally through convection from the enclosure's heated surface to the atmosphere.

Table 1. Recorded Data Table for High-Temperature Auto-regulation

Temperature (°C)	29	30	31	32	33	34	35	36	37	38	39	40
Time (s)	124.71	131.30	140.66	158.58	177.33	196.47	211.01	232.09	267.25	305.09	351.70	408.99

5.1.2 Low Temperature Regulation

On the other hand, a similar experiment for temperature levels lower than the desired preset operating temperature of 26°C and an operating range of ±2°C is performed using frozen ice cubes to lower the temperature to the desired level. The cooling system is then activated, the ice cubes are removed, and the amount of time taken by the system to regulate the temperature back up to its preset value is recorded. A room temperature of 29.1°C is recorded at the commencement of this experiment, and this process shall be repeated for 5 different low-temperature values from 23°C to 19°C.

Observed during the experiment, the cooling fans were shut down by the designed electronic system as expected, allowing the transference of heat from the external atmosphere to increase the inner temperature of the system through natural heat convection. Thus, the values obtained in Table 2 from this experiment are largely dependent on the nominal room temperature of the surrounding atmosphere. This, in part, explains the exponential increment in time difference between successive experiments as the room temperature is dropped to a lower level by each test.

Table 2. Recorded Data Table for Low-Temperature Auto-regulation

Temperature (°C)	23	22	21	20	19
Time (s)	227.02	279.33	341.60	398.85	492.00

5.2 Exhaust Functionality Test

The tests on the functionality of the automated cooling/exhaust system will not be complete until experiments are carried out on the exhaust system as well. The MQ-2 fumes detector contained within the system will be the major focus as its sensitivity largely determines the reactiveness of the exhaust system to fumes and other flammable fluids. The following experiments will be based on the amount of time taken from the introduction of fumes into the enclosure to the activation of the polarity reversal process. Up until the activation of exhaust mode, the system shall remain in the default cooling mode. Hence, It should be taken into consideration that there is a slight delay from the deactivation of the cooling system to the activation of the polarity reversal exhaust system. This is done so as not to damage the windings of the vent fan's motor.

5.2.1 Response Time against Distance

This experiment aims to test the reactive response of the exhaust system as a function of the proximity from the source of the fumes to the location of the sensor. For this test, a simple ignited paper shall serve as the fume source, and the

experiment is repeated for every 500cm directly from under the sensor's position to the opposite end of the enclosure. This limits the sample values to just five experiments.

As can be inferred from Table 3, there is an incremental change in the amount of time taken from the introduction of the fume source to the activation of the exhaust mode. It should be noted once again that these recorded values include the artificial delay from deactivation of the cooling system to activation of the exhaust system, intentionally designed to prevent the fan's motor from damage by reversing its polarity while still in its residual spin from the previous cooling mode.

Table 3. Recorded Data Table for Exhaust Mode Response with Distance

Distance (cm)	0	500	1000	20	19
Time (s)	5.33	8.01	9.79	10.60	13.42

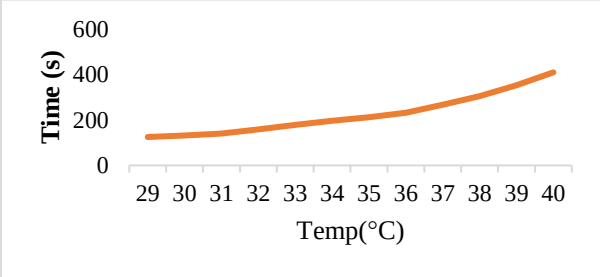

Figure 8. Graph of High-Temperature Auto-regulation Data against Time

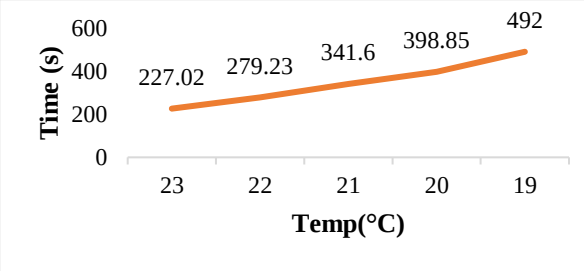

Figure 9. Graph of Low-Temperature Auto-regulation Data against Time

Table 4. Recorded Data Table for Exhaust Mode Response with Distance

Material	**Time (s)**
Paper	12.99
Cotton Cloth	14.83
Wood	21.09
Plastic	25.33
Soldering Lead	(No response)
Acid(Sulphuric)	15.03
Liquefied Petroleum Gas (LPG)	4.70

5.2.2 Response Time against Material

The next phase of the Exhaust mode experiments involves testing the reactive response time from various fume sources. This experiment gives an insight into the limits of the cooling/exhaust system's application. A list of sources of flammable materials and toxic fumes cutting across several fields of application, such as data server farms, agriculture, industrial kitchens, poultry, manufacturing plants, etc., has been curated to form the basis for this experiment. Each material will be ignited (where necessary) and placed at the maximum obtainable distance—2m—within the testing enclosure, while the amount of time taken for the activation of the exhaust mode will be recorded.

Table 4 represents the varied results from seven selected fume sources, with Liquefied Petroleum Gas (LPG) being the most reactive material and plastic being the least. Fumes from the lead gave no reaction, thus solidifying the possibility for the system's application in Electronics manufacturing workspaces, as there would be no false positives.

5.2.3 Comparative Analysis

This additional sub-chapter discusses the effects of introducing an exhaust mode functionality into the system as opposed to the single cooling systems that are currently commercially available. As a means of highlighting the advantages and differences between both systems, this test was carried out using ignited sheets of paper as the source of the fumes under three conditions: Deactivated System, Activated Cooling System, and Activated Exhaust System.

It was observed that the experiment with the activated cooling system in the presence of the ignited sheets of paper burned so much more than the experiment with the total deactivated system. A reason for this would be the fact that air mixture acts as a source of fuel for ignition; hence, the larger the amount of air, the much more dangerous the ignition would become. On the other hand, the experiment with the activated exhaust system had a suction effect on the closed system, thereby extracting both air—fuel source—and fumes into the outer environment.

6. CONCLUSION

This study presents a comprehensive exploration of a prototype for an automated cooling/exhaust system, emphasizing sustainable thermal management. Through meticulous experimentation, the system's proficiency in regulating temperature across varying conditions is demonstrated, showcasing its adaptability and autonomous nature. Additionally, investigation into the system's exhaust functionality revealed its direct responsiveness to diverse fume sources and varying distances, highlighting its potential for hazard mitigation. The inclusion of an exhaust mode proved instrumental in enhancing safety measures, as evidenced by the comparative analyses. Overall, the findings underscore the vital role of automated cooling/exhaust systems in industrial settings for promoting sustainability, safety, and efficiency across industries, paving the way for a greener and more resilient future.

ACKNOWLEDGMENT

Special thanks to Engr. Dr. A.O. Otuoze under whose guidance, mentorship and support this project was made possible.

REFERENCES

Amanowicz, Ł., Ratajczak, K., & Dudkiewicz, E. (2023). Recent Advancements in Ventilation Systems Used to Decrease Energy Consumption in Buildings—Literature Review. Energies, 16(4), 1–39. https://doi.org/10.3390/en16041853

Cioc, I. B, Lita, I., Teodorescu, M., DA Visan, D. A. 2004. Meeting the Challenges of Electronics Technology Progress. *27th International Spring Seminar on Electronics Technology. 3, 429-433.*

Parri, L., Tani, M., Baldo, D., Parrino, S., Landi, E., Mugnaini, M., & Fort, A. (2023). A Distributed IoT Air Quality Measurement System for High-Risk Workplace Safety Enhancement. Sensors, 23(11), 1–13. https://doi.org/10.3390/s23115060

Prince, & Hati, A. S. (2021). A comprehensive review of energy-efficiency of ventilation system using Artificial Intelligence. Renewable and Sustainable Energy Reviews, 146, 111153. https://doi.org/10.1016/j.rser.2021.111153

PAPER 99 - ASSESSING AGRICULTURAL CROP WASTE AS SUSTAINABLE CEMENTITIOUS BINDERS IN CONSTRUCTION: A CRITICAL REVIEW

L.Z. Tuleun[1*] and A.A. Adedeji[1]

[1]Department of Civil Engineering, University of Ilorin, Ilorin, Nigeria
*Email: tuleun@gmail.com

ABSTRACT

With a view to addressing environmental challenges associated with various agricultural crop waste disposal techniques and the greenhouse gas effect linked to the cement production process, various research works have been conducted on the possibility of converting these agro-waste products into cementitious binders for use as construction material. This study seeks to examine the various studies conducted on the physical and chemical characteristics of rice husk ash (RHA) and corncob ash (CCA) and their viability for partial substitution for cement in the production of mortar and concrete. The review scope encompassed the chemical analysis, microstructural analysis of the RHA and CCA in concrete, and the effects of partially replacing cement with these ash materials on the properties of fresh and hardened concrete. The chemical analysis test results indicated that the ash derived from agricultural waste primarily comprised alumino-siliceous material, thereby satisfying the criteria for pozzolanic materials. The consistent addition of RHA and CCA resulted in a reduction in workability. However, the mechanical properties outcomes demonstrate promising potential, as the integration of RHA and CCA resulted in concrete with enhanced strength compared to plain concrete, with optimal outcomes achieved at a 10% replacement level. In conclusion, the review revealed that agricultural crop residues meet the properties of pozzolanic materials and hold significant potential to substitute cement by up to 10% without compromising the performance of concrete.

***KEYWORDS*:** Rice Husk Ash, Corncob Ash, Cementitious binders, Pozzolans, Concrete

1.0 INTRODUCTION

The global focus on sustainable waste management, environmental degradation, and greenhouse gas emissions underscores the importance of research in discovering sustainable alternatives to certain products, notably Portland cement (OPC). Concrete is the largest volume of material globally used, mostly in infrastructural works, with cement constituting the major binding component in the mix. However, the usage of this particular material tends to have a negative effect on the environment. One issue worthy of mentioning is its impact on global warming. Currently, approximately 3 billion tons of Portland cement are utilized globally, with roughly 400 kg of carbon dioxide gas being emitted for every 600 kg of cement produced, constituting around 5–8% of all anthropogenic CO_2 emissions (Steinberger *et al*., 2010; Madhu *et al*., 2019). In 2019, statistics also showed that China was the largest producer of cement, estimated at 2.2 billion metric tons, followed by India with an estimated value of 320 million metric tons. Andrew. (2019) projected an increase from 3.27 billion metric tons in 2010 to 4.83 billion metric tons by 2030. Another notable aspect to address is how agricultural crop waste is disposed of globally. Conventional methods involve discarding waste onto unproductive land and burning agricultural residues in open fields, a practice by farmers and industrialists that results in substantial land and air pollution. In Asia alone, burning crop residues in fields constitutes 34% of the total biomass burned annually (Streets *et al*., 2003). Especially in agriculture-dependent economies such as China and India, this open-field burning notably adds to greenhouse gas emissions (Streets *et al*., 2003). Hence, it is crucial to explore more sustainable and environmentally friendly methods for agricultural waste disposal. These challenges have prompted researchers to delve into the possibility of utilizing more sustainable materials for construction purposes. It has also been discovered that certain agro-waste ash materials contain pozzolans that enhance the mechanical properties and durability of cementitious materials through both chemical and physical mechanisms (Moraes *et al*., 2019).

Pozzolans, being the main stimulating factor as defined by Arthanari *et al*. (1981), are siliceous materials that, in their natural state, possess no inherent cementitious properties. However, when processed, they react in the presence of water with lime to form calcium silicate compounds of low solubility that exhibit cementitious and binding properties. These materials are categorized into natural and artificial sources, with examples such as clay and shale, which are calcined to become active, and naturally occurring pozzolanas like volcanic tuff and pumicite, while good blast furnace slag and fly ash represent artificial varieties. In developed nations, Arthanari *et al.* (1981) suggest utilizing fly ash, a residue generated from burning pulverized coal, to replace a portion of cement in

construction. This replacement typically falls within the 10-30% range in terms of the weight of cement used. Additionally, studies conducted by Aprianti *et al*. (2015); Ujin *et al*. (2017); Jhatial et al. (2019); Taye *et al*. (2021); and Farid *et al*. (2021) have demonstrated that select agricultural waste products can also serve as partial replacement materials for both cement and aggregates in concrete and mortar. Mixtures of Portland cement and pozzolanic material are referred to as pozzolanic cement, offering several advantages such as good resistance to chemical attack, low heat of hydration evolution, cost-effectiveness, improved workability, reduced bleeding, and enhanced impermeability (Manasseh, 2010). However, these cements also come with disadvantages, including a slower rate of strength development and increased shrinkage.

Based on recent literature, the chemical characteristics, morphological analysis, rheological, and mechanical properties of rice husk ash (RHA) and Corn cob ash were evaluated.

2. LITERATURE REVIEW

2.1 *Chemical Characterization of Rice Husk Ash (RHA) and Corncob Ash (CCA)*

The preparation process plays a crucial role in the production of pozzolanic cementitious binders. One significant test conducted by researchers to assess the reactive potential of agricultural waste in concrete is the chemical composition test. Before conducting this test, the materials are first treated by grinding to achieve a fine particle size and then calcined at controlled temperatures. From recent works, the type of test varies from one researcher to the other. In the case of rice husk ash, an investigation conducted by various researchers showed that silica oxide, aluminium oxide, and Iron Oxide are the main elements contained in the RHA. Table 1 presents the results of the chemical composition test of RHA conducted by various researchers from various countries. They all adopted the use of an X-ray fluorescence spectrometer (XRF) in testing. From their results, the summation of SiO_2, AlO_3, and FeO_3 was greater than 70, thus fulfilling the criteria for the materials to be regarded as pozzolanic. However, results obtained by Salas *et al*. (2009) exhibited the highest percentage of 91.10 followed by that of Khan *et al*. (2012) which had a percentage of 90.08. Antiohos *et al*. (2013), Raheem and Karem (2017), Zareei *et al*. (2017) had percentages within the range of 84-90%. Results by Faried *et al*. (2021), Abiodun and Jimoh (2018), and Krishna *et al*. (2016) had values in the range of 70-80%. However, for the class of pozzolans, research by Antiohos *et al*. (2013) examined a Greek RHA, and they discovered that even though the summation oxides was 87.98 greater than the benchmark of 70, the result of LOI was 6.3% above 4% requirement, and 1.3% for MgO was less than 5%. The LOI was 6.3, hence falling within the class N, in accordance with the ASTM C 618—19 standard requirements. Zareer *et al*. (2017) attempted to investigate the RHA in high-strength concrete, they ground their RH and calcined it at a temperature of 600^0c for 5 hours. Their result of chemical analysis showed a minimal LOI of 0.54 while meeting the other criteria. This meant the RHA fell within the class F classification. The results of the remaining researchers also fell within the class F category.

Table 1: Chemical Composition of Rice Husk Ash (RHA)

Authors	Chemical compositions (oxides %)									$SiO_2 + Al_2O_3 + Fe_2O_3$
	SiO_2	Al_2O_3	Fe_2O_3	CaO	MgO	SO_3	K_2O	Na_2O	LOI	
Khan *et al*. (2012)	86.80	0.895	2.435	0.45	0.55	—	—	—	2.5	90.08
Antiohos *et al*. (2013)	86.50	0.92	0.56	1.12	1.30	0.05	1.58	0.43	6.3	87.98
Raheem and Kareem (2017)	82.14	1.34	1.27	1.21	1.37	0.17	2.09	0.14	—	84.75
Zareei *et al*. (2017)	86.70	0.04	0.61	0.39	1.32	9.8	0.01	—	—	87.38
Krishna *et al*. (2016)	76.8	0.41	1.045	0.93	0.27	—	2.64	0.1	—	78.22
Abiodun and Jimoh (2018)	61.33	2.20	8.43	6.53	2.33	—	11.90	2.53	—	71.97
Salas *et al*. (2009)	90.00	0.68	0.42	8.14	0.35	—	—	0.32	—	91.10
Faried *et al*. (2021)	70.36	1.54	0.68	4.51	1.35	3.23	8.73	1.09		72.58

In 2020, the global maize production was estimated to reach 1.03 million thousand tons. In the preceding year of 2019, maize cultivators worldwide expanded their cultivation to cover 192 million hectares, marking an increase of 3 million hectares from 2018 (Latifundist.com, 2019; World Data Atlas, 2020). Notably, the United States, China, Brazil, Argentina, and Ukraine stood out as the top maize-producing nations, collectively contributing to about 75.18% of the total production. Corncob ashes (CCA) have emerged as a promising agricultural by-product, possessing pozzolanic characteristics that render them potentially valuable as a partial alternative to cement (Adesanya and Raheem, 2009, 2010; Owolabi *et al*., 2015; Singh *et al*., 2018; Memon *et al*., 2019; Desai, 2018; Bheel and Adesina, 2021). Researchers undertook analyses utilizing X-ray fluorescence (XRF) and energy-dispersive X-ray spectroscopy (EDS) to ascertain the chemical compositions, with the outcomes delineated in

Table 2. These results reveal that the combined levels of SiO_2, Al_2O_3, and Fe_2O_3 surpassed 70%, with the maximum sulfur trioxide (SO_3) content falling below 4%. Consequently, they satisfy the criteria for classification as class N pozzolanic material, as per ASTM C 618–19.

Table 2: Chemical Composition of Corn Cob Ash (CCA)

Chemical compositions (Oxides %)	Authors					
	Adesanya and Raheem (2009, 2010)	Owolabi *et al.* (2015)	Singh *et al.* (2018)	Memon *et al.* (2019)	Desai (2018)	Bheel and Adesina (2021)
Country	Nigeria	Nigeria	India	Pakistan	Gujarat	Pakistan
SiO_2	66.38	64.90	64.56	63.73	62.30	67.23
Al_2O_3	7.48	10.79	9.42	15.08	6.25	6.34
Fe_2O_3	4.44	4.75	5.12	5.32	4.40	5.33
CaO	11.57	10.24	12.00	6.56	10.57	10.75
MgO	2.06	2.08	3.01	4.56	1.86	ND
SO_3	1.07	2.53	ND	ND	1.02	1.04
K_2O	4.92	4.30	ND	2.05	3.89	5.42
Na_2O	0.41	0.43	ND	0.10	0.36	0.37
Others	1.67	—	5.89	2.60	9.35	3.52
$SiO_2 + Al_2O_3 + Fe_2O_3$	**78.30**	**80.44**	**79.10**	**84.13**	**72.95**	**78.90**

2.2 Morphology Analysis

Memon *et al*. (2019) conducted a material characterization of corn cob ashes (CCA) using SEM techniques. They observed that CCA displayed finer portions and a porous morphology, attributed to the presence of micropores, perforations, and tubules. Figures 1 depict the macro- and micromorphology of corncob ash, respectively. These figures highlight that corncob is structured into three layers: chaff, woody ring, and pith. It was noted that the three portions of the corncob exhibit high absorbency, with the pith and chaff being more absorbent than the woody ring portion (Memon *et al*., 2019). Additionally, they identified that the CCA particles contain long, extremely porous, and perforated tubules. Further analysis indicated that CCA possessed micropores with a size of 0.5 µm and perforations of 10 µm. Scanning electron microscopy (SEM) results revealed particle agglomeration with an approximate size of up to 10 µm, resembling the shape of bacteria. The XRD crystallographic pattern unveiled that CCA consisted of quartz and stishovite at 2θ values of 28.240 (d = 3.157 Å) and 30.730 (d = 2.907 Å), respectively.

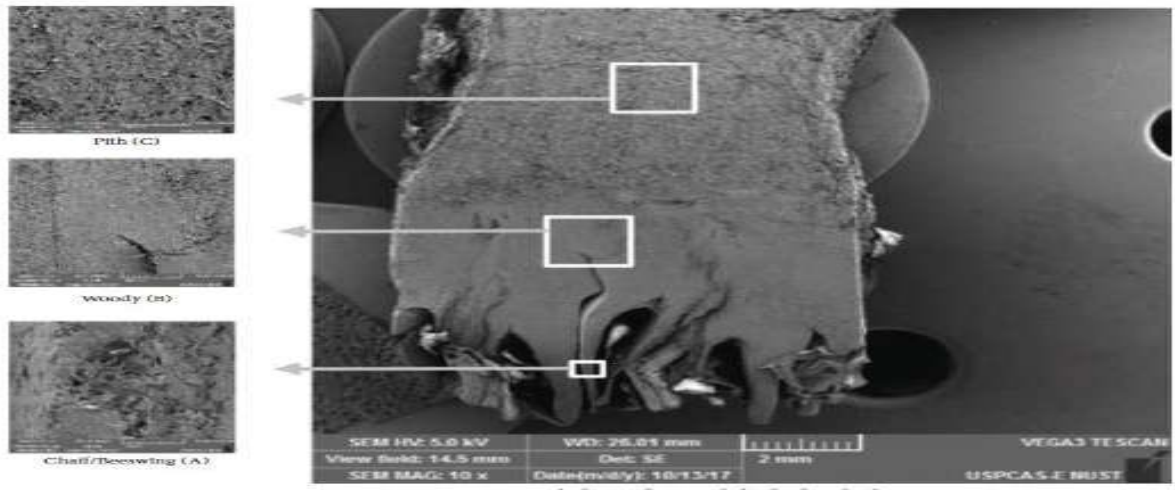

Figure 1: Scanning Electron Microscopy analysis of Corn Cob Ash (CCA)

Regarding Rice Husk Ash (RHA), The presence of diverse metal ions within rice husks and unburned carbon affects both the purity and hue of the husk. Analyses using X-ray diffraction (XRD) and scanning electron microscopy (SEM), carried out by researchers such as Salas *et al*. (2009), Abiodun and Jimoh (2018), Raheem and Kareem (2017), Antiohos *et al*. (2013), and Khan *et al*. (2012), revealed that the husk exhibits an amorphous nature and is primarily composed of silica, cristobalite, and to a lesser extent, tridymite. The X-ray diffraction (XRD) pattern of rapidly cooled RHA, depicted in Figure 10, illustrates a distinctive hump observed in the X-ray diffraction (XRD) pattern which indicates the amorphous nature of rice husk ash (RHA), while the peaks

corresponding to SiO_2 demonstrate its crystalline property. This implies that RHA contains both amorphous and crystalline components. The significant peak revealing the crystalline nature of SiO_2 in RHA is detected at a 2-theta angle of 26.64. Reports by Agwa *et al*. (2020), and Tayeh *et al*. (2021) suggested that burning rice husks leads to ash with a high silica content. When the burning process is conducted under controlled conditions, the silica present in rice husk ash (RHA) tends to be in the amorphous state, rendering it suitable as a cement replacement material due to its high pozzolanic activity. The scanning electron microscopy (SEM) images of) rice husk ash is depicted in Figure 2.

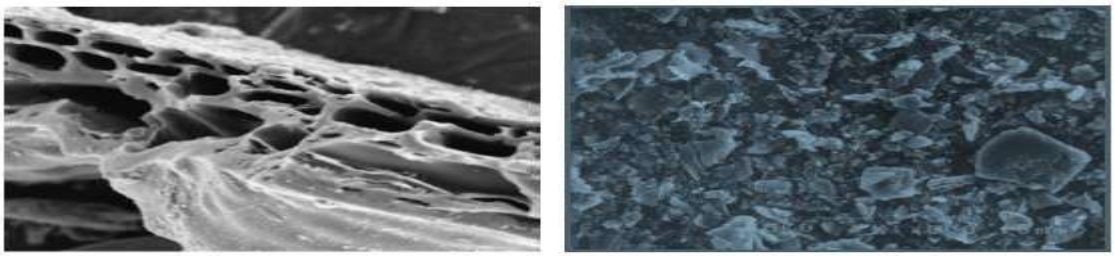

Figure 2: Scanning Electron Microscopy analysis of Greek and Pakistan Rice Husk Ash (RHA)

Similarly, the RHA samples exhibit a morphology resembling rolling hills, with areas showing heterogeneous morphology also identified. This structure is likely formed during the burning process of the original husk, where the initial coverings maintain their shape, resulting in a teeth-like outer surface (Ramezanianpour *et al*., 2009). The figure also demonstrates that the RHA powder comprises irregularly shaped particles with micropores, which could substantially influence the properties of concrete. The porous morphology may originate from the combustion of the organic components within the RHA (Ahmadi *et al*., 2007).

2.3 Effect on the Fresh Properties of Mortars and Concrete

Numerous studies have indicated that the incorporation of corncob ashes (CCA) tends to reduce the workability of concrete. Adesanya and Raheem (2010) as well as Owolabi *et al*. (2015) evaluated the workability of CCA-based concrete through slump tests, varying the percentage replacement, mix ratio, and water-cement ratio. According to the combined slump test results presented in Figure 3, the workability significantly decreased with the addition of CCA content in concrete. This suggests that additional water is required to maintain workability during the cement hydration process (Syagga *et al*., 2001; Shihembetsa *et al*., 2002; Bui *et al*., 2005), possibly due to the larger surface area of CCA when compared to cement.

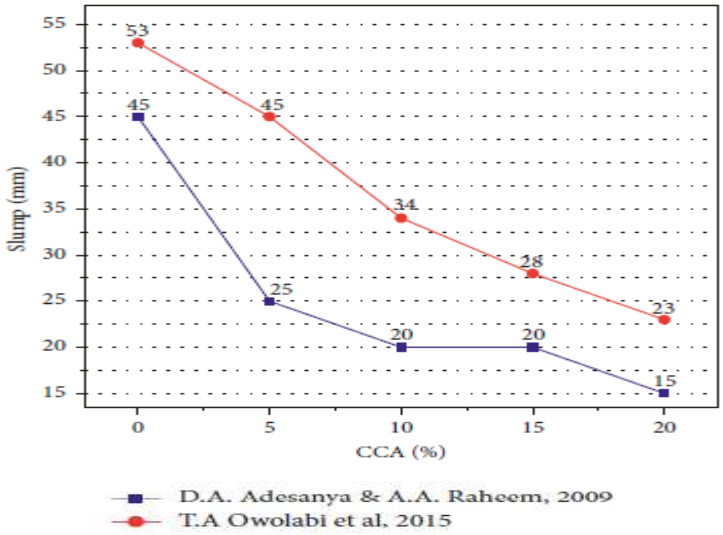

Figure 3: Slump test values of Corn Cob Ash (CCA)

Rice husk ash (RHA) blended cement finds practical use in scenarios where a low rate of heat development is desired, such as in mass concrete applications. Raheem and Kareem (2009) conducted a study where RHA replaced ordinary Portland cement by various percentages: 5%, 7%, 11.25%, 15%, 20.25%, and 25%. Their findings indicated that compared to the control mix, both the initial and final setting times increased with the

addition of RHA up to 15%, while the flowability of the mix decreased with the ash addition. Furthermore, they observed improvements in soundness and consistency with increasing percentages of RHA. In the case of 15% RHA content compared to the normal mix, Raheem and Kareem (2009) reported significant increases in initial setting time (151%), final setting time (190%), and consistency (21%). However, Krishna *et al*. (2016) presented contradictory findings. They utilized RHA content ranging from 5% to 20% to partially replace cement and observed a decrease in both initial and final setting times with increasing RHA percentages, while consistency showed a slight increase. Specifically, for 15% RHA content, there was a reduction of 47% in initial setting time, 11% in final setting time, and an increase of 14% in consistency. This variance in results could be attributed to the high porosity of RHA.

2.4 Effect on the Hardened properties of Mortar and Concrete

Singh *et al*. (2018) conducted various tests indicating that the compressive strength of concrete mixtures incorporating corncob ashes (CCA) as a pozzolanic cementitious material decreased as the temperature exceeded the standard room temperature (20°C). They performed laboratory tests on compressive strength for concrete exposed to different elevated temperatures (150°C, 300°C, 450°C, and 600°C), with CCA content ranging from 5% to 20% as partial cement replacement at a water-binder ratio of 0.45. The strength of CCA concrete exhibited a decrease for temperatures exceeding 300°C. It was observed that the maximum compressive strength was attained at a temperature of 300°C for all mixes, with the optimal CCA content being 10%. Despite reductions in strength observed with increasing CCA percentages, they suggested that this reduction is primarily attributed to the disintegration and evaporation of chemically bound water at this stage.

Relative to the control mix, the compressive strength of concrete blended with corncob ashes (CCA) initially decreases at early ages but shows significant improvement over time. Owolabi *et al*. (2015) and Desai (2018) examined the potential of partially replacing cement in concrete with CCA at varying percentages (5%, 10%, 15%, and 20%), and (10%, 20%, and 30%) at different curing periods, with water-to-cement ratios of 0.65 and 0.55, respectively. Compared to the control mix, the compressive strength of concrete specimens with 20% CCA content decreased by a maximum of 40.43% and 45.80% (Owolabi *et al*., 2015) and 20.10% and 9.11% (Desai, 2018) at curing ages of 7 days and 28 days, respectively. These findings are consistent with those of Adesanya and Raheem (2010) and Bheel and Adesina (2021).

According to various researchers' findings, the split tensile and flexural strength of corncob-based concrete increased with curing age. Desai (2018) noted that the addition of corncob ashes (CCA) to concrete led to a reduction in tensile strength. Specifically, at 7 days and 28 days of concrete age with 20% CCA content, the split tensile strength decreased by 20% and 9%, respectively, compared to the control mix. Similarly, for the same CCA content, a slight decrease in flexural strength relative to the control mix was observed, dropping from 6.59 to 6.44 N/mm² (2.28%) at 90 days of age, while better strength was achieved with 10% CCA. They concluded that the inclusion of 10% CCA in concrete produces concrete with peak tensile and flexural strength. In a similar research conducted by Adesanya and Raheem, they observed an increase in tensile strength with curing age. They however attributed the increase in strength to the continuous hydration of the OPC due to the pozzolanic reaction between the silica oxides in the CCA and hydroxides in the OP, resulting in further densification of the concrete matrix.

Jamil *et al*. (2013) investigated the effect of the blend of RHA on the compressive strength of mortar and concrete. They varied the RHA in mortar at an interval of 5% from 0% to 35% and within a curing period of 28 days. Based on their finding, it was observed that mortar incorporated from 5 to 25% had strength values that were higher than that of the reference; that of 35% equalled the strength value of the reference mix. Their outcome tallied with the findings recorded by (Zareei *et al*., 2017). Similar research was carried out by Khan *et al*. (2012). They examined the behaviour of RHA concrete with and without the use of superplasticizers. They noticed higher strength values for RHA concrete with SP than RHA concrete without SP. Regarding both mixes, a decrease in strength was documented with the addition of the RHA, and an increase in strength was noticed with an increase in curing age. In contrast, Zareei *et al*. (2017) recommend the 20% RHA content to achieve a maximum compressive strength of 93.28 MPa, 12% greater than that of the control, provided the concrete is cured for a period of 28 days. The presence of RHA at 20% may have resulted in a microstructural improvement at the interfacial zone (ITF), thus leading to a more dense concrete (Gastaldini *et al*., 2009 ;). Figure 4 compares the results compressive strength of RHA concrete of various researchers at the curing age of 7 and 28 days.

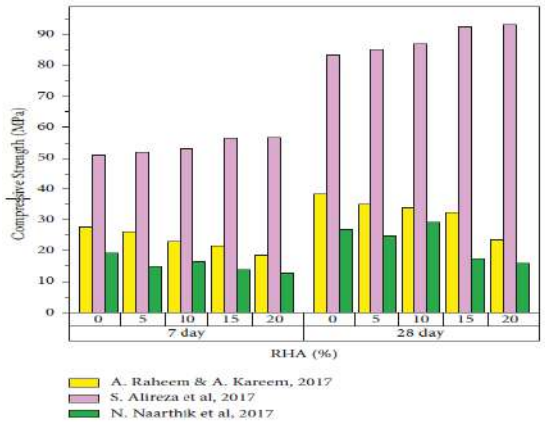

Figure 4: Compressive strength of RHA Concrete.

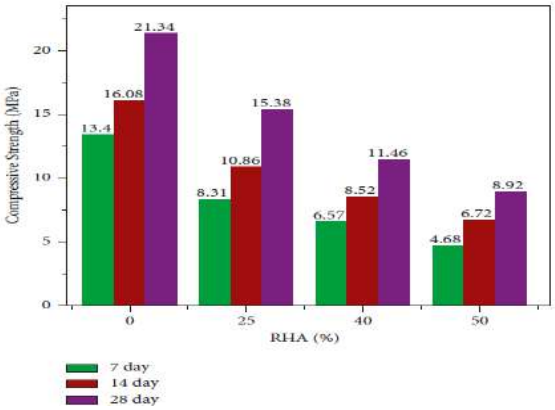

Figure 5: Compressive strength of Concrete with and without SP

Krishna *et al*. (2016) explored the effects of incorporating different percentages of rice husk ash (RHA) on the flexural strength and split tensile strength of concrete. They found that adding 10% RHA increased the flexural strength by 19.9%, from 2.11N/mm^2 to 2.53N/mm^2, compared to 0% RHA. However, with 15% RHA, there was a slight decrease of 0.17N/mm^2 (8.06%) in flexural strength. The study also noted that split tensile strength generally increased with higher RHA content, reaching its peak at 10% RHA. This enhancement in strength was attributed to the reinforcement of the interfacial transition zone (ITZ) by the silica content in RHA, leading to stronger bonding between cement mortar and aggregates. However, beyond 10% RHA, there were diminishing returns, resulting in reductions in split tensile strength.

Khan *et al*. (2015) conducted a series of tests to evaluate the flexural strength of concrete beams using pure Ordinary Portland Cement (OPC) and blends containing 0%, 25%, 30%, and 40% of rice husk ash (RHA) as a replacement for OPC. Based on their findings, the load-bearing capacity of normal concrete beams exceeded that of RHA concrete beams both at the onset of initial cracking and at failure. They observed that the deflection of concrete beams at the midpoint decreased as the RHA content increased. Notably, for beams containing 25% RHA, there was a notable performance in flexure, with a failure load of 32mm compared to the 38mm recorded for the control mix.

3. CONCLUSION

Based on the extensive reviews of the aforementioned studies focusing on the pozzolanic properties, workability, and mechanical aspects associated with utilizing agricultural waste products as substitutes for cement, the following conclusions can be drawn:

1. X-ray diffraction investigations have shown that CCA and RHA possess alumino-siliceous properties in accordance with ASTM C618 standards for pozzolanic materials. They contain amorphous silica, which is capable of undergoing a secondary reaction when used as substitutes for cement.
2. The workability of fresh concrete exhibited a declining pattern as the proportion of CCA and RHA increased. This phenomenon can be attributed to their elevated surface area and porous characteristics, which absorbed the mixing water in the concrete. Conversely, the mechanical strength of concrete, when partially substituting cement with CCA and RHA, demonstrated enhancement. This improvement is attributed to the involvement of amorphous silica in a secondary reaction, resulting in the formation of densified tetrahedral gels.
3. The enhanced mechanical strength observed in concrete mixes containing RHA, and CCA led to improvements in the morphology of the concrete.

ACKNOWLEDGEMENT

We wish to specifically acknowledge the soil mechanics laboratory technicians of the Federal University of Agriculture, Makurdi for their guidance during the material testing process.

REFERENCE

Abiodun, Y.O., and Jimoh, A.A. (2018). Microstructural charac- terisation, physical and chemical properties of rice husk ash as viable Pozzolan in building material: a case study of some Nigerian grown rice varieties," Nigerian Journal of Tech- nology, 37(1), 71–77.

Adesanya D.A. and. Raheem, A.A. (2010). A study of the permeability and acid attack of corn cob ash blended cements, Construction and Building Materials, 24(3), 403–409.

Adesanya, D.A. and Raheem, A.A. (2009). A study of the work- ability and compressive strength characteristics of corn cob ash blended cement concrete, Construction and Building Materials, 23(1), 311–317.

Agwa, I.S., Omar, O.M., Tayeh, B.A. and Abdelsalam, B.A.(2020). Effects of using rice straw and cotton stalk ashes on the properties of lightweight self-compacting concrete, Construction and Building Materials, 235, Article ID 117541, 2020.

Ahmadi, M.A., Alidoust, O., Sadrinejad, I and Nayeri, M. (2007). Development of mechanical properties of self - compacting concrete contain rice husk ash, International Journal of Computer, Information, and Systems Science, and Engi- neering, 1(4), 259–262.

Andrew R.A., "Global CO2 emissions from cement pro- duction," Earth System Science Data, 10(1), 195–217.

Aprianti E., Shafigh P., Bahri S. and Farahani J.N. (2015). Sup- plementary cementitious materials origin from agricultural wastes-A review, Construction and Building Materials, 47, 176–187.

Arthanari, S. Augustine, A.G., Dayanithi, P., Ramaswamy, S., Sethurathnam. A., and Thanikachalam, V. (1981). Building Technology and Valuation. Tata Mc.Graw-hill, New Delhi.

ASTM C 618 – 19, (2019) Standard Specifications for Coal Fly Ash and Raw or Calcined Natural Pozzolan for Use in Concrete, ASTM, West Conshohocken, PA, USA.

Bheel, N. and Adesina, A. (2021). Influence of binary blend of corn cob ash and glass powder as partial replacement of cement in concrete, Silicon, 13(5), 1647–1654.

Bui, B.B., Hu, J. and Stroeven, P. (2005). "Particle size effect on the strength of rice husk ash blended gap-graded Portland cement concrete, Cement and Concrete Composites, 27(3)357–366.

Desai, H, (2018). Experimental study on corn cob ash powder as partial replacement of cement in concrete, International Research Journal of Engineering and Technology (IRJET), 5(6), 724–728.

Faried, A.S., Mostafa, S.A., Tayeh, B.A. and Tawfik, T.A. (2021)Mechanical and durability properties of ultra-high per- formance concrete incorporated with various nano waste materials under different curing conditions, Journal of Building Engineering, 43, Article ID 102569.

Faried, A.S., Mostafa, S.A., Tayeh, B.A. and Tawfik, T.A. (2021). The effect of using nano rice husk ash of different burning degrees on ultra-high-performance concrete properties, Construction and Building Materials, 290, Article ID 123279, 2021.

Gastaldini, A.L.G, Isaia, G.C., Hoppe, T.F., Missau, F. and Saciloto, A.P. (2009). Influence of the use of rice husk ash on the electrical resistivity of concrete: a technical and economic feasibility study, Construction and Building Materials, 23(11), 3411–3419.

Jamil, M., Kaish, A.B.M.A, Raman, S.N., and Zain, M.F.M. (2013). Pozzolanic contribution of rice husk ash in cementitious system, Construction and Building Materials,47,588–593.

Jhatial, A.A., Sohu,S., Memon, M.J., Bhatti, N. U. K., and Memon, D. (2019). Eggshell powder as partial cement replacement and its effect on the workability and compressive strength of concrete, International Journal of Advances in Applied Sciences, 6(9), 71–75.

Khan, R., Jabbar, A., Ahmad, I., Khan, W., Khan, A.N., and Mirza, J. (2012). Reduction in environmental problems using rice- husk ash in concrete, Construction and Building Materials, 30, 360–365.

Krishna, N.K., Sandeep, S. and Mini, K.M. Study on concrete with partial replacement of cement by rice husk ash, IOP Conference Series: Materials Science and Engineering, 149(10, Article ID 012109, 2016.

Latifundist.com, "Top 10 Corn producing countries," 2019, https://latifundsist.com/en/rating/top-10-stran-po-vyrashivaniyu-kukuruzy-v-2019-godu.

Madhu K., Prasad and Eswanth P. (2019). Mechanical and dura- bility properties of concrete by partial replacement of cement with banana leaves ash, Journal of Antimicrobial Chemo- therapy: A Journal of Composition Theory, 7, 0731–6755.

Memon, S.A., Javed, U and Khushnood, R.A. (2019). Eco-friendly utilization of corncob ash as partial replacement of sand in concrete, Construction and Building Materials, 195, 165–177.

Moraes, M.J.B., Moraes, J.C.B., Tashima, M.M., Akasaki, J.L., Soriano, L., Borrachero, M. V. and Pay J. (2019). Production of bamboo leaf ash by auto-combustion for pozzolanic and sustainable use in cementitious matrices, Construction and Building Materials, 208, 369–380. https://doi.org/10.1016/j.conbuildmat.2019.03.007.

Raheem, A.A. and Kareem, M.A. (2017). Chemical composition and physical characteristics of rice husk ash blended cement, International Journal of Engineering Research in Africa, 32, 25–35, Trans Tech Publications Ltd.

Ramezanianpour, A.A., Mahdikhani, M. and Ahmadibeni, G.H. (2009) The Effect of rice Husk Ash on Mechanical Properties and Durability of Sustainable Concretes.

Salas, A., Delvasto, S., de Gutierrez, S.R.M and Lange, D. (2009). Comparison of two processes for treating rice husk ash for use in high performance concrete, Cement and Concrete Research, 39(9), 773–778.

SAntiohos, S.K., Tapali, J.G., Zervaki, M., Sousa-Coutinho, J., Tsimas, S. and Papadakis, V.G. (2013). Low embodied energy cement containing untreated RHA: a strength development and durability study, Construction and Building Materials, 49, 455–463.

Shihembetsa, L.A. and Waswa-Sabuni, B. (2002). Burnt clay waste as a pozzolanic material in Kenya, Journal of Civil Engineering, JKUAT, 7(1), 21–28.

Singh, K., Singh, J. and Kumar, S. A (2018) sustainable environ- mental study on corn cob ash subjected to elevated temperature, Current World Environment, 13(1), 144–150.

Steinberger J.K, Krausmann F. and Eisenmenger N. (2010). Global patterns of materials use: a socioeconomic and geophysical analysis, Ecological Economics, 69(5), 1148–1158.

Streets, D.G., Yarber, K.F., Woo, J.H. and Carmichael, G.R. (2003). Biomass burning in Asia: annual and seasonal estimates and atmospheric emissions. Global Biogeochem. Cycles 17. https://doi.org/10.1029/2003gb002040.

Syagga, P.M., Kamau, G.N., Waswa-Sabuni, B and Dulo, S.O. (2001). Letters and viewpoints potentials of using waste burnt clay as a pozzolanic material in Kenya, Discovery and Innovation, 13(3), 114–118.

Tayeh, B.A., Alyousef, R., Alabduljabbar, H., and Alaskar, A. (2021a). Recycling of rice husk waste for a sustainable concrete: a critical review, Journal of Cleaner Production, 312, Article ID 127734.

Tayeh, B.A., Hadzima-Nyarko, M., Zeyad, A.M. and Al- Harazin, S.Z. (2021). Properties and durability of concrete with olive waste ash as a partial cement replacement, Advances in concrete construction, 11(1), 59–71.

Ujin F., Ali K.S. and Hanur Harith Z.Y. (2017). The effect of eggshells ash on the compressive strength of concrete, Key Engineering Materials, 728,402–407, Trans Tech Publications Ltd, 2017.

World Data Atlas, "Maize production quantity. Maize production by Country," 2020, http://www.knoema.com.

Zareei, S.A., Ameri, F., Dorostkar, F., and Ahmadi, M. (2017). Rice husk ash as a partial replacement of cement in high strength concrete containing micro silica: evaluating durability and mechanical properties, Case Studies in Construction Ma- terials, 7, 73–81.

PAPER 101 - MERCERIZATION OF COCONUT COIR: CONCENTRATION-DEPENDENT EFFECTS OF SYNTHETIC AND NATURAL TREATMENTS AT UNIFORM DURATION

M. Sanusi[1*], J.K Odusote[2], T.I Olanrewaju[2], A.O Salaudeen[2]

[1]Department of Mechanical Engineering, University of Ilorin, Ilorin, Nigeria.
[2]Department of Materials and Metallurgical Engineering, University of Ilorin, Ilorin, Nigeria.
[*]Email: sanusi.m@unilorin.edu.ng

ABSTRACT
Despite the widespread use of mercerization in treating cellulosic materials, there is a lack of understanding about the effects of different alkaline sources and concentrations. This study investigated the structural, compositional, and morphological changes induced by mercerization on coconut coir samples using FTIR and SEM analyses. FTIR analysis revealed a 92.3% increase in the O-H stretching vibration peak intensity at 3690.1 cm-1 in Sample I, indicating significant changes in the hydrogen-bonding environment and crystalline structure, potentially converting cellulose I to cellulose II. SEM analysis showed an increase in carbon content, ranging from 89.46 atomic concentration (Sample G, 20% synthetic alkaline) to 94.16 atomic concentration (Sample F, 10% synthetic alkaline). A reduction in nitrogen content, indicating fewer proteinaceous compounds/organic impurities, was observed, with the lowest level of 4.73 atomic concentration in Sample E (5% synthetic alkaline). Sample C (20% natural alkaline) exhibited the highest purity, with 93.70 atomic concentrations of carbon and 4.98 atomic concentrations of nitrogen. Mercerization effectively reduced inorganic impurities, with Sample C showing the lowest levels of calcium (0.32 atomic concentration) and aluminum (0.31 atomic concentration), particularly with natural alkaline treatments. The findings provide quantitative insights for optimizing treatment conditions and tailoring cellulosic material properties. Notably, a 20% natural alkaline concentration resulted in the highest purity and most effective impurity removal, making it a promising treatment condition for further exploration.

KEYWORDS: Synthetic alkali, Natural alkali, SEM, FT-IR, Hydrogen Bonding, Functional group.

1. INTRODUCTION

The volume of waste generated in today's world poses a threat to the earth's sustainability (Abubakar et al., 2022) From overflowing landfills choked with construction debris to vast gyres of swirling plastic choking our oceans, the silent assault of our insatiable consumption habits is etched across every landscape. This environmental albatross weighs heavily, disrupting ecosystems, contaminating air and water with insidious toxins, and ultimately jeopardizing the very foundations of our existence (Abd El-Salam & G, 2015)

The challenges of improper disposition of waste extend beyond overflowing landfills and polluted waterways but a complex, cascading environmental disruption and degradation. Improper waste disposal leaches harmful chemicals into the waterbodies poisoning the lifeblood of our communities (Vaverková, 2019). Plastic waste fragments infiltrate the ecosystem and wreak havoc on marine life, burning of these wastes also releases potent greenhouse gases, which accelerate the relentless march of climate change and its associated peril (Blair & Mataraarachchi, 2021). To face these challenges, a beacon of hope emerges in the form of recyclability of waste which resonates a clarion call across all sectors to embrace responsible resource utilization and prioritize environmental well-being (Tiwari, 2023).

With the urgent need for the choice of materials in building our world, the traditional reliance on petroleum-based composites, and resource-intensive materials is giving way to a demand for sustainable alternatives (Nasr et al., 2023). Excellent material for sustainability must not only be lightweight and high-performing but must also possess an unquestionable environmental footprint and must be highly efficient and embrace recyclability and leverage available renewable resources (Cebon & Ashby, 2006). Fiber composite stands out as a beacon of hope, the innovative blends integrating fibers such as jute, hemp, and

flax into polymer matrices offer numerous advantages over their traditional counterparts (Shaghaleh et al., 2018), the lightness of these materials improves the mechanical properties of composite materials which makes them light and translate to weight reduction and in turn improves fuel efficiency in most applications, especially automobile industries. These materials boast superb thermal and acoustic insulation properties enhancing comfort and contributing to energy savings in buildings and vehicles (Verma & Senal, 2019). Perhaps the most profound advantage of fibers lies in their very essence, natural fibers like coconut coir are readily available and biodegradable which makes them suitable for composite materials (Paul et al., 2022).

Coconut coir emerges as excellent sustainability extracted from the husk of coconuts, a ubiquitous and abundantly replenishable resource, The coir of coconut has qualities that align perfectly with interfacial reactions with composite materials, and its natural abundance minimizes reliance on cultivated resources reducing the environmental footprints associated with its production (Ellis-Suriani et al., 2021) Its low density makes it a featherweight champion, promoting fuel efficiency and minimizing energy consumption (Prasad & Rao, 2011), coconut coir has thermal and acoustic properties contributing to energy efficiency (Mahmud et al., 2023).

2.0 MATERIALS & METHODS

2.1 Study area

Coconut husk fiber was sourced from Odo Oba located between Ilorin and Ibadan, Odo Oba is located at latitudes of 8.0743° N, and longitudes4.1872° E, odo oba has a tropical savanna climate and an average annual temperature of Odo Oba is 62° degrees and 224″ of rain in a year with an average humidity of 71% and a UV-Index of 7.

2.2 Experimental setup

The coconut husk, initially fibrous, underwent a pounding process to transform it into a powdered coir, resulting in a smoother texture. Figures 1 and 2 illustrate the coconut husk in its fibrous state and post-pounding. A 4.75mm sieve was employed to separate shafts from the blended coconut husk during the coir production process.

Figure 1: Coconut husk.

Figure 2: Pulverised coir

Sodium hydroxide (NaOH) and potassium carbonate (K_2CO_3) are employed as pretreatment agents in the mercerization process of coconut husk coir, representing synthetic and natural sources for the pretreatment of the coir fibers.

The mercerization process began with carefully preparing two distinct alkaline solutions: one using sodium hydroxide (NaOH) and the other potassium hydroxide (K_2CO_3). The concentrations of these solutions were carefully determined through pretesting. In our experiment, 25g of NaOH and K_2CO_3 were separately dissolved in 500 ml of water for precise concentrations.The treatment was optimized by finding that a 500 ml concentrate with 20g of coconut coir yielded optimal results. After mercerization, thorough rinsing removed residual alkali, crucial for fiber integrity. The neutralization process with acetic acid counterbalanced the alkaline treatment, essential for stable fiber performance.

Samples A-D were treated with potassium carbonate (K_2CO_3) solutions at concentrations of 25, 50, 100, and 150 mol/m³ for 4 hours. Similarly, samples E-H were treated with sodium hydroxide (NaOH) solutions at the same concentrations and duration. This setup allows for the investigation of alkaline treatment effects on coconut coir. Sample I, untreated coconut coir, serves as the control. Comparing treated samples (A-H) with the control (I) enables the assessment of structural, compositional, and morphological changes induced by the treatments and differences between K_2CO_3 and NaOH effects.

Experiment Conditions for Mercerization Process with Varying NaOH and Potash Concentrations

Table 1: Natural Alkali Treatment Parameters

Experiment	K_2CO_3 (%)	K_2CO_3 conc.(mol/m3)	Time (Hours)
A	5	25	4
B	10	50	4
C	20	100	4
D	30	150	4

Table 2: Synthetic Alkali Treatment parameters

Experiment	NaOH (%)	NaOH conc. (mol/m3)	Time (Hours)
E	5	25	4
F	10	50	4
G	20	100	4
H	30	150	4

The table presents experiments on two sets of samples, investigating the effects of potassium carbonate (K_2CO_3) and sodium hydroxide (NaOH) alkaline sources at concentrations of 25, 50, 100, and 150 mol/m³, with a 4-hour treatment time. For K_2CO_3, the samples are labeled A-D, while for NaOH, the samples are E-H. Expressing concentrations in mol/m³ allows accurate comparison between the two alkaline species and correlation of observed effects with molar concentrations. This systematic approach to different samples provides insights into optimal alkaline conditions and potential differences between the sources.

3. RESULTS

The morphology for both synthetic and natural treated coir was checked at SEM- R&D laboratory, National Steel Raw Material Exploration Agency Kaduna State Nigeria, using a Scanning Electron Microscope (SEM) (Model: Phenom-ProX desktop SEM) with the following specifications: 2.5 nm resolution, 5-20 kV accelerating voltage, secondary/backscatter electron detectors, piezo stage for up to 100 mm samples. Also, Fourier Transform InfraRed (FTIR) was carried out to study the functional groups. The FTIR analysis was done at Ahmadu Bello University Zaria Central Research Laboratories using an Agilent Cary 630 FTIR spectrometer with a diamond ATR crystal, mid-IR range of 4000-400 cm^{-1}, sensitivity of 7 $x10^{-6}$. Figures *3-12* show the morphology and Energy-Dispersive Xray-Spectroscopy **(EDS)**.

Table 3: EDS for Natural Alkali mercerized coir samples (Samples A-D) and Control/un-mercerized coir sample (Sample I).

Element Name	**A**		**B**		**C**		**D**		**I**	
	Atomic conc.	Weight conc.	Atomic conc.	Weight conc.	Atomic conc.	Weight conc.	Atomic conc.	Weight conc.	Atomic conc.	Weight conc.
Carbon (C)	92.28	89.91	89.19	85.04	93.70	90.95	90.50	86.45	88.24	81.13
Nitrogen (N)	6.60	7.50	9.20	10.23	4.98	5.64	7.16	7.97	8.19	8.78
Calcium (Ca)	0.14	0.46	0.69	2.18	0.32	1.05	0.23	0.74	0.38	1.16
Aluminium (Al)	0.14	0.32	0.08	0.18	0.31	0.69	0.68	1.47	0.09	0.19
Silicon (Si)	0.28	0.64	0.19	0.43	0.20	0.45	0.71	1.58	0.18	0.38
Iron (Fe)	0.00	0.00	0.15	0.68	0.08	0.34	0.11	0.50	0.00	0.00
Sodium (Na)	0.18	0.33	0.08	0.15	0.06	0.11	0.19	0.34	0.18	0.31
Magnesium (Mg)	0.23	0.46	0.10	0.20	0.21	0.42	0.22	0.43	0.10	0.18
Chlorine (Cl)	0.06	0.16	0.12	0.34	0.07	0.21	0.11	0.32	0.69	1.87
Phosphorus (P)	0.03	0.09	0.04	0.10	0.06	0.14	0.03	0.07	0.00	0.00
Sulfur (S)	0.05	0.12	0.04	0.10	0.00	0.00	0.05	0.13	0.00	0.00
Titanium (Ti)	0.00	0.00	0.03	0.13	0.00	0.00	0.00	0.00	0.17	0.63
Potassium (K)	0.00	0.00	0.08	0.25	0.00	0.00	0.00	0.00	1.79	5.37

Table 4: EDS for Synthetic Alkali mercerized coir samples (Samples E-H) and control/un-mercerized coir sample (Sample I).

Element Name	**E**		**F**		**G**		**H**		**I**	
	Atomic conc.	Weight conc.	Atomic conc.	Weight conc.	Atomic conc.	Weight conc.	Atomic conc.	Weight conc.	Atomic conc.	Weight conc.
Carbon (C)	93.23	89.29	94.16	91.78	89.46	83.09	92.80	89.10	88.24	81.13
Nitrogen (N)	4.73	5.28	4.91	5.58	6.05	6.55	5.06	5.66	8.19	8.78
Calcium (Ca)	0.62	1.99	0.52	1.68	0.50	1.54	0.54	1.72	0.38	1.16
Aluminum (Al)	0.45	0.96	0.12	0.27	0.65	1.36	0.31	0.67	0.09	0.19
Silicon (Si)	0.35	0.78	0.00	0.00	0.20	0.45	0.50	1.12	0.18	0.38
Iron (Fe)	0.16	0.70	0.00	0.00	0.08	0.33	0.00	0.00	0.00	0.00
Sodium (Na)	0.19	0.34	0.00	0.00	0.21	0.37	0.36	0.66	0.18	0.31
Magnesium (Mg)	0.13	0.26	0.13	0.26	0.75	1.41	0.15	0.29	0.10	0.18
Chlorine (Cl)	0.08	0.22	0.07	0.20	0.09	0.26	0.09	0.25	0.69	1.87
Phosphorus (P)	0.07	0.18	0.00	0.00	0.00	0.00	0.08	0.19	0.00	0.00
Sulfur (S)	0.000	0.00	0.09	0.23	0.03	0.07	0.09	0.23	0.00	0.00
Titanium (Ti)	0.00	0.00	0.00	0.00	0.08	0.29	0.00	0.00	0.17	0.63
Potassium (K)	0.00	0.00	0.00	0.00	0.17	0.52	0.04	0.11	1.79	5.37

Figures 3-12: SEM Images for coir samples A-I.


Figure 3. Sample A.

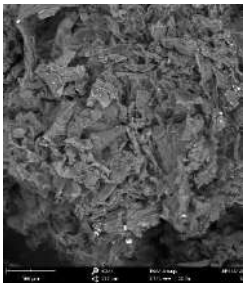
Figure 4. Sample B.

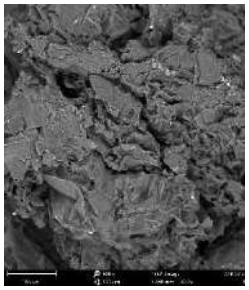
Figure 5. Sample C.

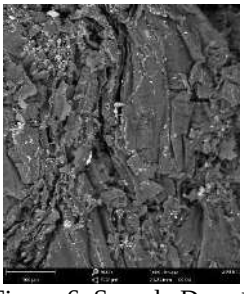
Figure 6. Sample D.

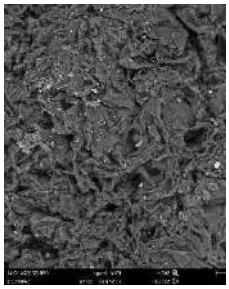
Figure 7. Sample E.

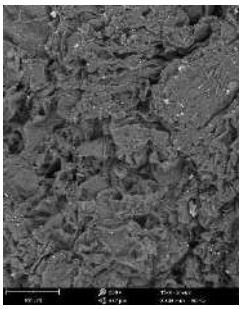
Figure 8. Sample F.

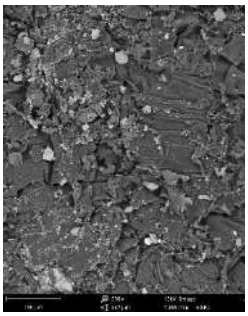
Figure 9. Sample G.

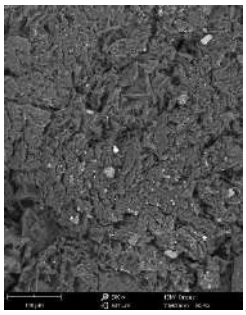
Figure 10. Sample H.

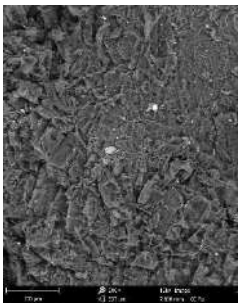
Figure 11. Sample I.

Figures 13-14: FTIR for natural and synthetic alkali treated coir.

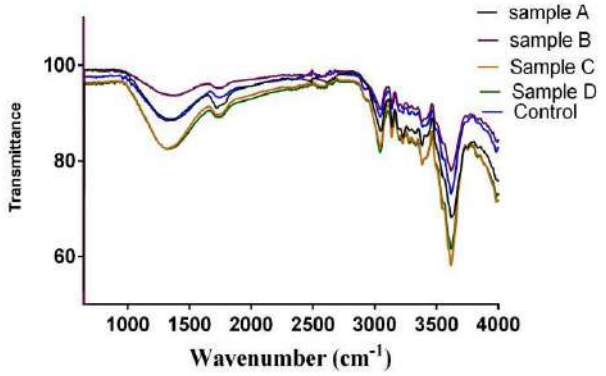

Figure 13: FTIR for natural pretreatment.

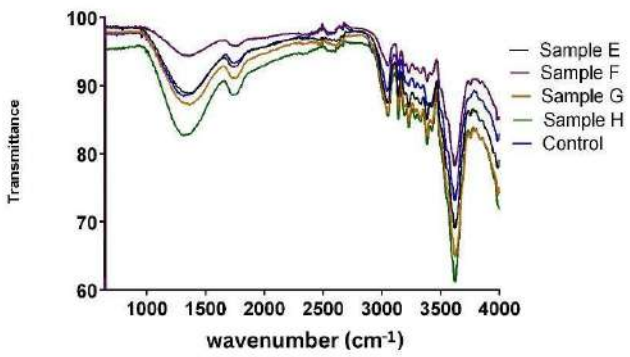

Figure14: FTIR for synthetic pretreatment.

4. DISCUSSION

The progressive increase in alkaline treatment concentrations using potassium carbonate (K_2CO_3) for Samples A to D and sodium hydroxide (NaOH) for Samples E to H resulted in increasingly severe morphological modifications and structural disruptions to coconut coir fibers, corroborating previous research findings(Bahrami et al., 2022; Jayamani et al., 2014a; Verma & Goh, 2021). Mild treatments (Samples A and E) exhibit surface etching, roughening, and swelling, attributed to the removal of non-cellulosic constituents and disruption of intermolecular hydrogen bonding (Jayamani et al., 2014b). Moderate treatment concentrations (Samples B and F) led to significant structural distortions, fragmentation, and disintegration due to the extensive removal of hemicellulose and lignin components, exposing and degrading the cellulose microfibrils (Bahrami et al., 2022).

Severe treatments (Samples C, D, G, and H) resulted in extensive fiber degradation, dissolution, and collapse, indicating severe depolymerization and disintegration of the cellulose chains under harsh alkaline conditions (Xu & Sun, 2016). Notably, sodium hydroxide (NaOH) induced more severe fiber degradation and disintegration compared to potassium carbonate (K_2CO_3) at comparable molar concentrations, owing to its stronger alkaline nature. The observed changes in fiber morphology and surface topography can significantly influence the mechanical, thermal, and interfacial properties of the resulting biocomposites (Amiandamhen et al., 2020; Latif et al., 2019).

The FTIR data shows that mercerization causes some serious structural changes to the cellulose, converting it from the cellulose I form to the cellulose II allomorph. Evidence of this is in how the O-H stretching peaks between 3700-3900 cm^-1 shift around, indicating changes in the hydrogen bonding and overall crystalline structure.

The higher alkaline concentrations, especially at 10%, did a better job driving that conversion to cellulose II. But at 20-30% concentration.

Mercerization also got rid of or modified some oxidized and esterified groups. The peaks at 1733.2 cm^{-1} would indicate those groups are just straight-up absent after treatment. There may even be some new structural differences introduced, at least with the 30% sample that had a new peak at 663.5 cm^{-1}.

Looking at the O-H stretch around 3300 cm^{-1}, the peaks decrease as the mercerization level increases. Suggests there are fewer hydroxyl groups left over. The C-H stretch at 2900 cm^{-1} and the C=C stretch at 1600 cm^{-1} show the aliphatic and aromatic structures present.

That C-O/C-O-C peak around 1030 cm^{-1} decreases too, implying some changes to the cellulose and hemicellulose components. Interestingly, a few of the mercerized samples had new peaks in the 2035-2050 cm^{-1} range, which could mean new functional groups were formed during the process.

The big picture is that mercerization seriously restructures the cellulose, helps remove lignin and impurities, and messes with the functional groups in the coconut coir fibers. All tied back to the effects of that alkaline treatment.

CONCLUSION

In conclusion, the FTIR and SEM analysis gave a critical look at how different alkaline sources and concentrations fundamentally alter the structure, composition, and even physical form of cellulosic materials during mercerization. Alkaline concentrations around samples A and E seemed to be the most effective in converting cellulose I to cellulose II crystalline form and stripping out lignin impurities.

These findings correlating treatment conditions and the resulting material characteristics are a game-changer. Now researchers and engineers can make informed decisions on alkaline solutions and design treatment conditions to predictably achieve targeted properties in cellulosic products - whether for textiles, biomedicals, or other composite applications.

REFERENCES

Abd El-Salam, M. M., & G, I. A.-Z. (2015). Impact of landfill leachate on the groundwater quality: A case study in Egypt. *J Adv Res*, *6*(4), 579-586. https://doi.org/10.1016/j.jare.2014.02.003

Abubakar, I. R., Maniruzzaman, K. M., Dano, U. L., AlShihri, F. S., AlShammari, M. S., Ahmed, S. M. S., Al-Gehlani, W. A. G., & Alrawaf, T. I. (2022). Environmental Sustainability Impacts of Solid Waste Management Practices in the Global South. *Int J Environ Res Public Health*, *19*(19). https://doi.org/10.3390/ijerph191912717

Amiandamhen, S. O., Meincken, M., & Tyhoda, L. (2020). Natural Fibre Modification and Its Influence on Fibre-matrix Interfacial Properties in Biocomposite Materials. *Fibers and Polymers*, *21*(4), 677-689. https://doi.org/10.1007/s12221-020-9362-5

Bahrami, R., Bagheri, R., & Dai, C. (2022). Influence of Fine Structure on the Variations of Thermal and Mechanical Properties in Flax Fibers Modified with Different Alkaline Treatment Conditions. *Journal of Natural Fibers*, *19*(13), 5239-5257. https://doi.org/10.1080/15440478.2021.1875367

Blair, J., & Mataraarachchi, S. (2021). A Review of Landfills, Waste and the Nearly Forgotten Nexus with Climate Change. *Environments*, *8*(8), 73. https://www.mdpi.com/2076-3298/8/8/73

Cebon, D., & Ashby, M. F. (2006). Engineering Materials Informatics. *MRS Bulletin*, *31*(12), 1004-1012. https://doi.org/10.1557/mrs2006.229

Ellis-Suriani, Z., Norsa'adah, B., Othman, A., & Siti-Azrin, A. H. (2021). Association between secondhand smoke exposure at home and cognitive performance among rural primary school children in Malaysia. *Tob Induc Dis*, *19*, 27. https://doi.org/10.18332/tid/133638

Jayamani, E., Hamdan, S., Rahman, M. R., & Bakri, M. K. B. (2014a). Investigation of Fiber Surface Treatment on Mechanical, Acoustical and Thermal Properties of Betelnut Fiber Polyester Composites. *Procedia Engineering*, *97*, 545-554. https://doi.org/https://doi.org/10.1016/j.proeng.2014.12.282

Jayamani, E., Hamdan, S. B., Rahman, R., & Bakri, M. K. B. (2014b). Investigation of Fiber Surface Treatment on Mechanical, Acoustical and Thermal Properties of Betelnut Fiber Polyester Composites. *Procedia Engineering*, *97*, 545-554.

Latif, R., Wakeel, S., Zaman Khan, N., Noor Siddiquee, A., Lal Verma, S., & Akhtar Khan, Z. (2019). Surface treatments of plant fibers and their effects on mechanical properties of fiber-reinforced composites: A review. *Journal of Reinforced Plastics and Composites*, *38*(1), 15-30. https://doi.org/10.1177/0731684418802022

Mahmud, M. A., Abir, N., Anannya, F. R., Nabi Khan, A., Rahman, A. N. M. M., & Jamine, N. (2023). Coir fiber as thermal insulator and its performance as reinforcing material in biocomposite production. *Heliyon*, *9*(5), e15597. https://doi.org/https://doi.org/10.1016/j.heliyon.2023.e15597

Nasr, Y., El Zakhem, H., Hamami, A. E. A., El Bachawati, M., & Belarbi, R. (2023). Comprehensive Review of Innovative Materials for Sustainable Buildings' Energy Performance. *Energies*, *16*(21), 7440. https://www.mdpi.com/1996-1073/16/21/7440

Paul, S., Islam, M. S., & Elahi, T. E. (2022). Comparative effectiveness of fibers in enhancing engineering properties of Earth as a building Material: A review. *Construction and Building Materials*, *332*, 127366. https://doi.org/https://doi.org/10.1016/j.conbuildmat.2022.127366

Prasad, A. V. R., & Rao, K. M. (2011). Mechanical properties of natural fibre reinforced polyester composites: Jowar, sisal and bamboo. *Materials & Design*, *32*(8-9), 4658-4663. https://doi.org/10.1016/j.matdes.2011.03.015

Shaghaleh, H., Xu, X., & Wang, S. (2018). Current progress in production of biopolymeric materials based on cellulose, cellulose nanofibers, and cellulose derivatives [10.1039/C7RA11157F]. *RSC Advances*, *8*(2), 825-842. https://doi.org/10.1039/C7RA11157F

Tiwari, A. (2023). Advancement of Materials to Sustainable & Green World. *Advanced Materials Letters*, *14*(3), 2303-1724. https://doi.org/10.5185/amlett.2023.031724

Vaverková, M. D. (2019). Landfill Impacts on the Environment—Review. *Geosciences*, *9*(10), 431. https://www.mdpi.com/2076-3263/9/10/431

Verma, D., & Goh, K. L. (2021). Effect of Mercerization/Alkali Surface Treatment of Natural Fibres and Their Utilization in Polymer Composites: Mechanical and Morphological Studies. *Journal of Composites Science*, *5*(7), 175. https://www.mdpi.com/2504-477X/5/7/175

Verma, D., & Senal, I. (2019). 6 - Natural fiber-reinforced polymer composites: Feasibiliy study for sustainable automotive industries. In D. Verma, E. Fortunati, S. Jain, & X. Zhang (Eds.), *Biomass, Biopolymer-Based Materials, and Bioenergy* (pp. 103-122). Woodhead Publishing. https://doi.org/https://doi.org/10.1016/B978-0-08-102426-3.00006-0

Xu, J. K., & Sun, R. C. (2016). Chapter 19 - Recent Advances in Alkaline Pretreatment of Lignocellulosic Biomass. In S. I. Mussatto (Ed.), *Biomass Fractionation Technologies for a Lignocellulosic Feedstock Based Biorefinery* (pp. 431-459). Elsevier. https://doi.org/https://doi.org/10.1016/B978-0-12-802323-5.00019-0

PAPER 102 - INFLUENCE OF MULTI-CROSS SECTIONAL TUBE CONFIGURATIONS ON THERMO-HYDRAULIC PERFORMANCE OF SHELL AND TUBE HEAT EXCHANGERS

I. O. Alabi[1*], A. A. Dare[2], M. O. Petinrin[2]

[1]Department of Mechanical Engineering, Elizade University Ilara-Mokin, Ondo State, Nigeria
[2]Department of Mechanical Engineering, University of Ibadan, Nigeria
[*]Email: ismaila.alabi@elizadeuniversity.edu.ng

ABSTRACT
In effective energy management, Shell-and-Tube-Heat-Exchangers (STHEs) combined with Straight-Tube-Geometries (STG) is linked to low heat duty and high-pressure drop, which raise the energy demand of a plant in process industries. These have not been sufficiently addressed by recently produced STHEs with modified tube designs. Multi-cross-Sectional-Tube-Geometrical (MSTG) configurations have the potential to improve fluid pressure along flow lines, but their applications in STHEs are sparsely reported. Therefore, this study was designed to investigate the influence of MSTG configurations on the STHEs' performances. STHE with Convergent-Divergent-Tube-Geometry (CDTG) and Divergent-Convergent-Tube-Geometry (DCTG) configurations of Penetration Angles (PA), 45 and 90° were evaluated numerically using the finite volume method for Flow Rate (FR) ranging from 0.6 - 2.6 kg/s. Global-Thermo-Hydraulic-Performance (GTHP) indices; Weighted-Shell-Gain-Performance-Factor (WSGPF), Weighted-Performance-Evaluation-Index (WPEI), and Weighted-Thermal-Performance-Factor (WTPF) were assessed. The GTHP values obtained for STHE-MSTG (i.e. CDTG &DCTG) were 60 - 93% higher than those obtained in STHE-STG for all FR and at 45 and 90° PAs, with the maximum at 45° PA and the lowest at 90° PA. Tube-side pressure drops in STHE-MSTG configurations were reduced by 72– 73% in comparison with that obtained in STHE-STG. Incorporating MSTG into the design of shell and tube heat exchangers led to improved performance.

KEYWORDS: Shell-and-tube heat exchanger, Tube-Geometry, Penetration angles, Performance indices

1. INTRODUCTION

Heat exchangers (HEXs) are the main energy consumers in the manufacturing, air conditioning, refrigeration, space applications, petrochemical, food and beverage, chemical and petrochemical plants, petroleum refineries, natural gas processing, and sewage treatment industries. They are also required in power generation, waste heat recovery, and power production facilities (to cool down hot exhaust gases or to preheat the incoming air stream (Ismail *et al.*, 2017)).

The shell-and-tube heat exchanger (STHE) falls within the class of tubular heat exchangers (Feng *et al*., 2019), which have the ability to transport two fluids in opposing directions and in two phases (Milani Shirvan *et al.*, 2018). With the goal to transfer heat between the two fluids, which can be liquids or gases on either the shell or tube side (Dubey *et al.*, 2014b), either from the tube side to the shell side through the tube walls or vice versa, thereby balancing the temperature (Qian *et al.*, 2021), the STHE system primarily consists of a bundle of tubes mounted in a large cylindrical shell with the tube axis parallel to the shell. There are several different processes and occurrences in STHE (Adesina *et al*., 2018; Sandeep and Alkesh, 2012). It has been reported that about 60% of the total heat exchangers used in several industrial processes and areas are STHEs (Chen *et al*., 2013; Kansal and Fateh, 2014; Mohammadi *et al*., 2020; Roy *et al.*, 2019; Sharma *et al.*, 2021; Youcef and Saim, 2019; Youcef and Saim, 2020) due to their simple manufacture and suitability under various working conditions (Guo *et al.*, 2021) as well as superior advantages (Chen *et al.*, 2013; Dubey *et al.*, 2014b; Milani Shirvan *et al.*, 2018; Qian *et al.*, 2021) and applications (Dubey *et al.*, 2014a; Igwe and Agu, 2016).

In many industrial processes, the total performance of the plants depends on the thermo-hydraulic efficiency of STHEs. As a function of pressure drop (PD), the efficiency of STHEs in thermal energy transfer at low pumping power results in a significant decrease in energy consumption, which raises the plants' financial gain. Therefore, in plants with a network of STHEs, the functions of these interconnected HEXs become increasingly important for meeting the plants' energy needs.

The tube-side cross-sectional structure of the STHEs, which is infrequently documented in the literature, has drawn more attention (Chambon *et al.*, 2020). A combined shell and tube heat exchanger model featuring circular tubes and

elliptical tubes with a 90° attack angle was presented by (Saffarian *et al.*, 2019). In comparison to shell and tube heat exchangers with circular tubes and elliptical tubes with an attack angle of 90° and 0°, a heat exchanger with ellipsoidal tubes near the shell and circular tubes in the middle of the shell demonstrated the maximum heat transfer. A shell-and-tube heat exchanger with a rectangular shape was numerically modeled by (Slimene *et al.*, 2021). The investigators found that the rectangular cross-section shell, which performs better than its cylindrical equivalent in comparison with data from the literature, was responsible for the overall high effectiveness of their design. A comparative analysis of helical coil and straight tube heat exchangers was conducted by (Shirgire *et al.*, 2014). The outcome demonstrated that the heat exchanger's geometry has an impact on the heat transfer coefficient. The heat transfer and flow properties on the shell side of a helically coiled trilobal tube (HCTT) heat exchanger were investigated experimentally and numerically by (Wang *et al*., 2019). Geometrical characteristics including helix pitch, coil diameter, and helix height were taken into consideration by (Zaboli *et al.*, 2019). The findings demonstrated that the shell and coil heat exchanger's heat transfer coefficients were positively impacted by the geometric parameters of the coil. Ji *et al.*'s study (Ji *et al.*, 2021) examined the heat transmission and vibration caused by fluid in helical elastic tube bundles. The study made a greater positive impact on energy use and industrial production.

However, corrugated tubes as one of the coarsening surface methods have also been investigated (Ajaykumar *et al.*, 2016; Gondane and Jibhakate, 2018; Harish *et al*., 2018; Sadighi Dizaji *et al.*, 2015; Shahril *et al*., 2017). Shahril *et al.* (2017) examined the thermo-hydraulic performance of a shell-and-double concentric tube heat exchanger (SDCTHEX). The SDCTHEX was shown to perform better at heat transfer while preserving a smaller pressure drop. Ajaykumar *et al.'s* (2016) study used computation and experimentation to examine how well shell and tube heat exchangers with finned tubes performed at different flow rates. It was discovered that the use of finned tubes affected the fluid-to-fluid heat transfer. The impact of low-fin and plain tubes on shell and tube heat exchanger performance was created and compared by Harish *et al.* (2018). The tube side pressure drop of the low fin tube heat exchanger was found to be 1.2 to 1.5 times better than that of the plain tube heat exchanger when the water flow rate was varied. Gondane and Jibhakate (2018) also determined that the STHE with a corrugated tube gave the maximum value of the convective heat transfer coefficient. For a specific heat exchanger, (Prabakaran *et al*., 2016) tested three distinct tube bundles: smooth, micro-finned, and corrugated tubes with heat transfer rate and pressure drop. From a performance perspective, corrugated tubing was found to be superior to other materials.

To provide an overview of the main strategies and designs that are now available, the most important relevant research papers (Ajaykumar *et al*., 2016; Gondane and Jibhakate, 2018; Harish *et al*., 2018; Sadighi Dizaji *et al.*, 2015; Shahril *et al.*, 2017) have been examined. The majority of studies focused on STHEs with Straight-Tube Geometries (STG), which are linked to high-pressure drops and low heat duty, both of which increase a plant's energy requirements. These constraints have not been sufficiently addressed by recently produced STHEs with modified tube designs, which have made the ongoing quest for tubes with better performance necessary.

A perfect scenario for pipe flow obstructions is for the flow to increase in pressure while decreasing in speed. Because fluid flow pressure and flow speed are inversely correlated, there should not be much of a pressure drop. The concept of loss in flow served as the inspiration for this idea. Anytime there is a flow obstruction caused by the addition of divergent or convergent pipes, the fluid flow pressure rises and the flow velocity is significantly reduced, leading to a low-pressure drop. Therefore, this study was designed to investigate the influence of multi-cross-sectional tube geometrical configurations such as convergent-divergent and divergent-convergent tube configurations on the STHEs' performances.

2. METHODOLOGY

In this study, finite volume-based ANSYS FLUENT 19.2 software was used to numerically simulate shell and tube heat exchangers with three different tube configurations: divergent-convergent tube geometries (DCTG), convergent-divergent tube geometries (STG), and straight tube geometries (STG) created from CREO-Parametric CAD software. The computer system used for this simulation had an Intel® CoreTM i7 2.50GHz CPU and 16 GB of RAM. The working fluid flow arrangements at the shell and tube inlets were counter-flow directions in all heat exchanger analyses. In order to ascertain the impact of the tube's construction on the performance of heat exchangers, the fluid pressure drop on the tube side was also taken into account.

2.1 Geometry Parameters and Configurations of Selected STHEs

Due to their high heat transmission properties, the new tube designs that were explored included the convergent-divergent (CD) and divergent-convergent (DC) with 45 and 90° penetrating angles, 30° triangular tube layout, and 25% horizontal cut single-segmental baffles (see Fig. 1). Because of their prevalence in the STHE industries, single-

segmental baffled straight tube geometrical configurations have been widely utilized as standards for comparison (Mukherjee, 1998). It served as a foundation for comparison in this study as well. Table 1 displays the geometrical parameters of the chosen shell and tube heat exchangers (STHEs) used in this study:

From Table 1, the shell inside diameter was determined from the tube bundle diameter, *Db* using the relationship in equations 1 and 2 obtained from (Sinnott, 2013).

$$D_b = d_0 \left(\frac{N_t}{K_0}\right)^{\frac{1}{n_0}} \quad (1)$$

$$D_s = D_b + c_{sb} \quad (2)$$

where N_t stands for the number of tubes, *do* is the tube outside diameter, n_0 and K_0 are constants; hence for a triangular pitch of 1.25*do* and one-tube pass STHE, K = 0.319 and n = 2.142. Also, c_{sb} is the shell-bundle clearance, and for outside packed head STHE, the value of c_{sb} was obtained from shell bundle clearance chart

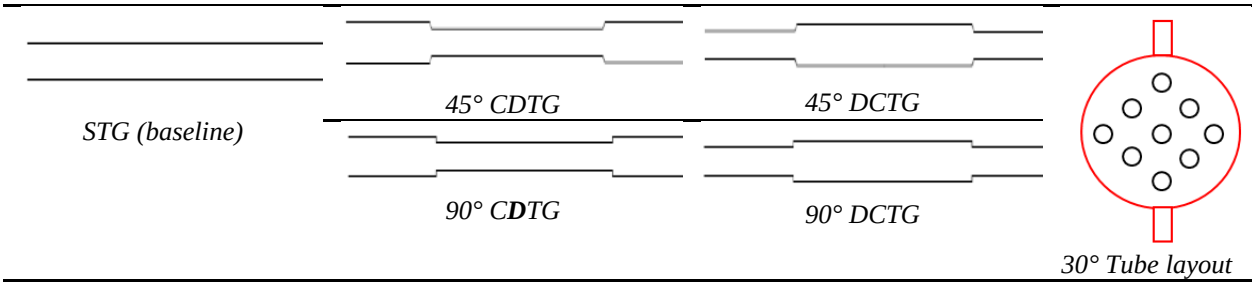

Fig. 1: Geometrical configuration of the tubes

2.2 The Thermo-physical Properties of Fluids and Shell-and-Tube Heat Exchanger Materials

Water is the only working fluid that is taken into account in this research work on both the shell and tube sides. Tables A and B (Appendix B) present, respectively, the fluid materials used in this work and the thermo-physical parameters of the shell and tube.

Table 1: Geometry Parameters of Selected STHE

Component	Description	Value
Baffle	Number of baffles	1-4
	Baffle spacing	90 - 225 mm
	Diameter of baffle plate	105 mm
	Baffle hole (diameter), Baffle cut	15 mm, 25%
Tube-side	Tube diameter (divergent part), d_{dt}	ϕ 15 mm
	Tube diameter (convergent part), d_{ct}	ϕ 10 mm
	Inlet & outlet diameter (control)	ϕ 15, 13 mm
	Tube length (Total), L_T	450 mm
	Layout pattern	Triangular (30^0)
	Pitch	$1.25d_{dt}$
Shell-side	Shell inside diameter, D_s	105 mm
	Shell outside diameter, D_E	107 mm
	Length of shell	450 mm

2.3 Computational Modelling

The governing equations for the shell-and-tube heat exchanger's fluid flow and heat transfer were derived from the conservation of mass, momentum, and energy. Since there is a lot of turbulent fluid flow, turbulence terms are added to the equations.

2.3.1 Assumptions

The following assumptions guided the formulation of the models:

a. It was assumed that the flow was turbulent and incompressible.

b. A single-phase Newtonian fluid was supposed to be the fluid.
c. The physical characteristics of the fluid were assumed to be constant.
d. There was little evidence of the gravity effect, volume force, heat source, or thermal radiation.
e. There were barely any leaks between the baffle and the tubes.
f. Although it was not taken into account in the energy formulation, the STHE was thought to have a small shell-side fouling resistance.

2.3.2 Governing Equations

ANSYS was used to build a hydrodynamic model based on the unstructured-grid finite volume method. The model was based on the solution of continuity, momentum, and energy (Naqvi and Wang, 2019):

A. Continuity equation:

$$\rho \nabla . u = 0 \quad (3)$$

B. Momentum equation:

$$\rho u . \nabla u = -\nabla P + \nabla . (\mu + \mu_T)[\nabla u + (\nabla u)^T] - \frac{2}{3}\rho k I \quad (4)$$

C. Energy equation:

$$\nabla\left(\rho c_p u T - k . \nabla T\right) = 0 \quad (5)$$

D. Turbulent model:

The tortuous flow pattern created by the tube bundle and baffles in shell-and-tube heat exchangers makes it easy for turbulence to begin on the shell side (Kuppan, 2013). Thus, the Two-Equation Reynolds-Averaged Navier-Stokes (RANS) turbulent (k-ε) model was integrated in addition to these equations and is given below (Alfarawi, 2020; Ikpotokin *et al.*, 2019; Piyush *et al.*, 2019):

i. **Turbulent kinetic energy equation (k):**

$$\rho \frac{\partial k}{\partial t} + \rho u . \nabla k = \nabla . \left(\left[\mu + \frac{\mu_T}{\sigma_k}\right] \nabla \mathrm{k}\right) + P_k - \rho \varepsilon \quad (6)$$

$$P_k = Productionterm = \mu_T [\nabla u : (\nabla u + (\nabla u)^T)] \quad (7)$$

Where, $\nabla . \left(\left[\mu + \frac{\mu_T}{\sigma_k}\right] \nabla \mathrm{k}\right)$ is the diffusion term;

ii. **Turbulent energy dissipation rate equation (ε):**

$$\rho \frac{\partial \varepsilon}{\partial t} + \rho u . \nabla \varepsilon = \nabla . \left(\left[\mu + \frac{\mu_T}{\sigma_\varepsilon}\right] \nabla \varepsilon\right) + C_{\varepsilon 1} \frac{\varepsilon}{k} P_k - C_{\varepsilon 2} \rho \frac{\varepsilon^2}{k} \quad (8)$$

$$\mu_T = Turbulent\ viscosity = \rho C_\mu \frac{k^2}{\varepsilon} \quad (9)$$

The model closure constants are: $C_{\varepsilon 1} = 1.44;\ C_{\varepsilon 2} = 1.92; C_\mu = 0.09; \sigma_k = 1.0; \sigma_\varepsilon = 1.3$ (Ikpotokin *et al.*, 2019; Saffarian *et al.*, 2019)

2.3.3 Boundary Conditions, Solvers Selection, and Mesh Description

The physical condition of the computational domain's boundaries greatly influences the solutions to the governing equations (Bergman *et al.*, 2019). Table 2 shows the mass flow, temperature, and pressure boundary conditions utilised for the tube-side and shell-sides, respectively. The chosen values agreed with the findings of the study conducted by (Petinrin, 2016). At the outlets of the tubes and shell, the Dirichlet boundary conditions were applied, using the gauge pressure as the outlet pressure. The segregated method was selected as the approach for solving the computational problems in this study due to its resilience, adaptability, and memory efficiency in addressing nonlinear multi-physics problems such as conjugate heat transfer, multiphase, and combustion problems (Kelecy, 2008). To improve the precision and quality of the results, fine mesh was made around the shell, tube, and baffles in each of the chosen designs. Based on the accuracy of the results in a short amount of time, the range of grids formed from the series of independence tests that were run falls between 1343231 and 2138820 elements, from the meshing nodes between 369549 and 612956. A minimum of nine hours were needed for each simulation, contingent on the intricacy of the structures and additional input factors. Figure 2 displays a mesh created for one of the models.

2.4 Performance criteria

Heat duty and pumping power are two critical factors that must be evaluated for the rating and thermo-hydraulic performance study of any heat exchanger. While the pumping power is a function of pressure drop (or drag coefficient and friction coefficient for shell and tube, respectively), the heat duty is a function of the heat transfer coefficient (or Nusselt number). The newly developed shell and tube heat exchangers were analyzed numerically to evaluate their performance. The results are discussed here in terms of three Global Thermo-Hydraulic Performance (GTHP) criteria. These include (see Appendix B): Thermal Performance Factor (TPF), Shell Gain Performance Factor (SGPF), and Performance Evaluation Index (PEI). Figure 2 illustrates a mesh generation unit.

Table 2: Boundary conditions

Boundary	Boundary type	values
Inlet shell	Mass flow inlet	0.6 - 2.1 kg/s & 300.15 K
Outlet shell	Pressure outlet	0 Pa (Gauge pressure)
Inlet tube	Mass flow inlet	0.05 kg/s & 373.15 K
Outlet tube	Pressure outlet	0 Pa (Gauge pressure)
Shell wall	Wall, stationary, no slip, adiabatic	adiabatic
Baffle	wall	conducting

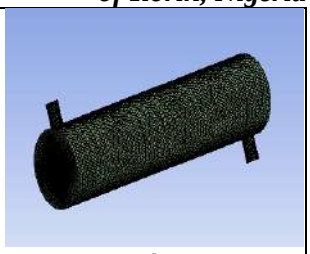

Fig. 2: Mesh Generation

3. RESULTS AND DISCUSSION

3.1 Mean Flow and Thermal Fields

The velocity, temperature, and pressure nephograms, as well as the impact of the multi-stage cross-sectional tube geometrical structure on heat transfer and flow characteristics in a shell and tube heat exchanger at the same operating conditions, are among the results of mean flow and thermal fields presented in this subsection.

3.1.1 Velocity Nephogram

The streamlined patterns coloured by the velocity magnitude presented in Fig. 3 of the velocity map make it easier to discern that the flow velocity increases in the area between the bottom of the shell and the edge of the first baffle. In contrast to STHE-STG, which exhibits a high frequency of recirculation, the figure clearly demonstrates that recirculation disappears in the STHE-CDTG and STHE-DCTG when the flow moves from right to left in the shell-side. This is an indication of high turbulence and also high heat duty (Prasad and Venkatesh, 2023; Sadikin *et al*., 2018). In addition, the flow pattern displayed by STHE-STG is fully perpendicular to the tube bundle (Wu and Qian, 2022; Zahid *et al.*, 2023). This is an indication that vibration is induced in the tube bundle assembly of those STHEs as a result of direct impulsive force on the tube bundles which occurs when the fluid flow is perpendicular. Thus, the overall performance of those STHEs is affected. According to (Zahid *et al.*, 2023) and also (Wu and Qian, 2022), the vibrations induced can be minimised if the shell-side fluid flow strikes the tube bundle longitudinally. However, the flow pattern displayed by STHE-CDTG and STHE-DCTG is approximately homogenous and also non-perpendicular. This is an indication that the vibrations induced in those STHEs (STHE-CDTG and STHE-DCTG) are less compared to the STHE-STG. Vibration significantly impacts the efficacy and efficiency of STHEs. It also reduces the overall efficiency and results in the STHEs assembly failure (Zahid *et al.*, 2023).

The heat duty also known as the heat transfer coefficients for the shell-side of STHE-CDTG, STHE-DCTG, with no repetition, and STHE-STG are plotted against the mass flow rate at 45 and 90 degrees, respectively, in Figures 6. The heat duty for the STHE-CDTG @ 90° s is significantly higher than that of the STHE-DCTG and STHE-STG, respectively. However, the result of shell-side heat duty (0 – 25 kW/m^2.K) obtained in this study improves by 60%, 89.2%, and 28 % in comparison to those (0 – 10 kW/m^2.K) obtained by (Petinrin and Dare, 2020) and (0 – 2.7 kW/m^2.K) obtained by (Ben Slimene *et al.*, 2022), (0 – 18 kW/m^2.K) obtained by (Gaikwad and Parmar, 2021), respectively, but the pattern of this result conforms to that obtained by Petinrin and Dare (2020), where the values of heat duty increase as the flow rate increases.

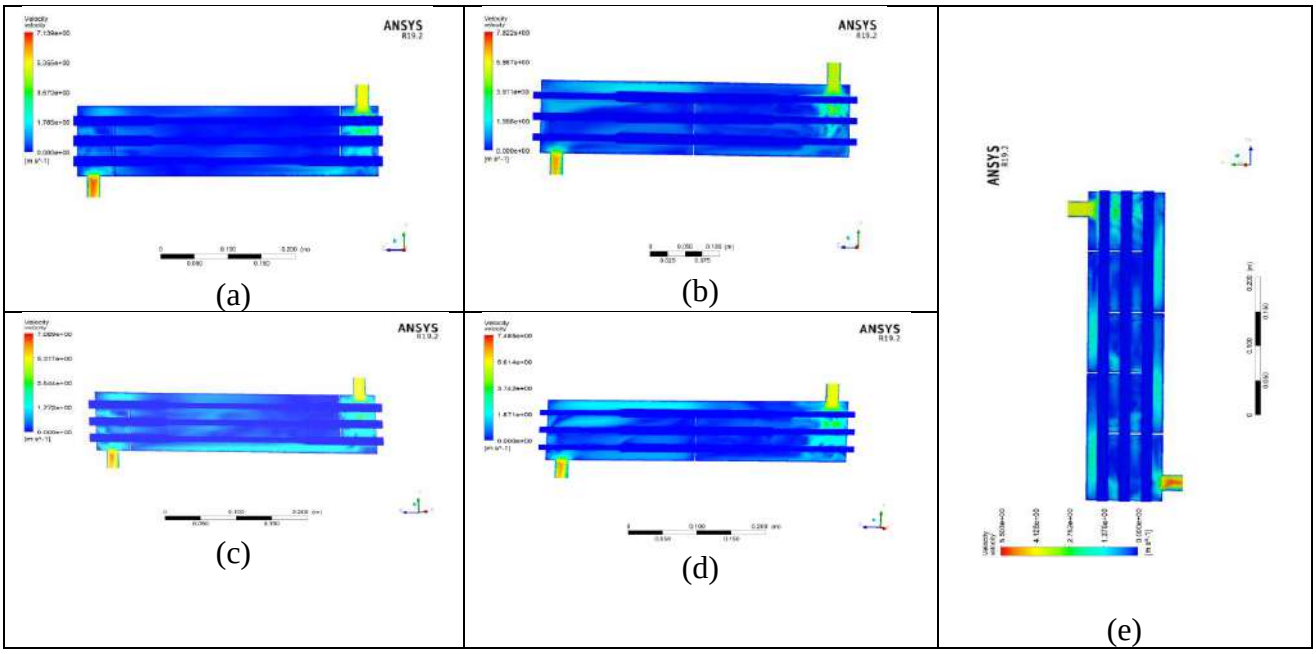

Fig. 3: Velocity nephogram for (a) CDTG @ 45° (b) DCTG @ 45° (c) CDTG @ 90° (d) DCTG @ 90° (e) STG

The pressure drop of the shell-side of 45 and 90 degrees' STHE-CDTG and STHE-DCTG, with no repetition, and STHE-STG alters the mass flow rate from 0.6 to 2.6 kg/s, respectively, are plotted in Figure 7. Plot trends (ΔP increases as mass flow rate increases) are consistent with Kuppan's (2013) findings and Petinrin's (2016) study analysis. The pressure drop values from the shell-side of the STHE-CDTG and STHE-DCTG with no repeat are a bit higher than that of the STHE-STG. The results of pressure drop obtained in this study ($0.200 \leq \Delta P \leq 30.0$ kPa) conform to those reported in the literature ($\Delta P \geq 0$) by Petinrin (2016), Petinrin and Dare (2020), (Shinde and Chavan, 2018) and Wang *et al.* (2018), respectively. In addition, the results of ΔP obtained in this study reduced by 44.06% - 99.56 % in comparison to results ($0 \leq \Delta P \leq 407.266$ kPa) reported by Youcef and Saim (2019), ($1.5 \leq \Delta P \leq 71.5$ kPa) reported by (Mohanty and Arora, 2020), ($0 \leq \Delta P \leq 100.0$ kPa) reported by (Musilim *et al*., 2017) and ($0 \leq \Delta P \leq 9000.0$ kPa) reported by Shahril *et al.* (2017), respectively. Shell-side heat duty in the selected STHEs is illustrated in Fig. 4 while Shell-side pressure drop in the selected STHEs is illustrated in Fig. 5.

The average values of WSGPF for STHEs with multi-cross-sectional tube configurations as displayed in Figure 8 are 81–86.79% and 79–80.19% more than the value of WSGPF obtained in the baseline (STHE-STG) at 45° and 90°, respectively. The results ($1.0 \leq$ WSGPF ≤ 2.20) obtained appreciate well in comparison to that (WSGPF ≥ 1.0) observed by Petinrin (2016), ($0.3 \leq$ WSGPF ≤ 0.7) reported by (Li *et al*., 2020) and ($0.5 \leq$ WSGPF ≤ 1.20) reported by Naqvi and Wang (2019). Figure 9 shows the comparison of the Weighted Performance Evaluation Index (WPEI) of the STHE-CDTG and STHE-DCTG to the STHE-STG at different mass flow rates. Since the average values of WPEI for STHEs with multi-cross sectional tube configurations are 77–83% and 76–82.3% better than the value obtained in the baseline (STHE-STG) at 45° and 90°, respectively. The results ($1.0 \leq$ WPEI ≤ 1.90) obtained appreciate by 27.9% in comparison to that ($1.27 \leq$ WPEI ≤ 1.37) observed by (Luo *et al.*, 2021).

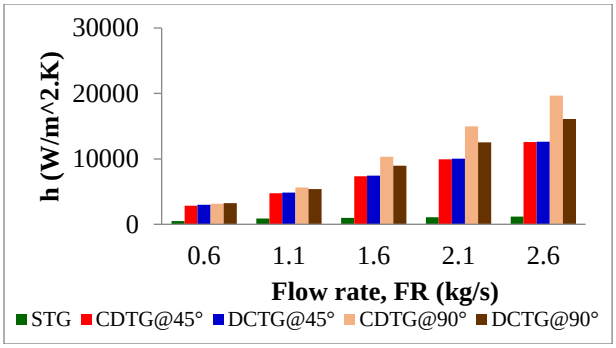

Fig. 4: Shell-side heat duty in the selected STHEs

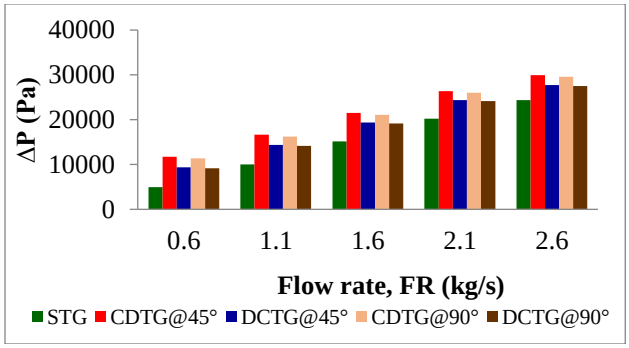

Fig. 5: Shell-side pressure drop in the selected STHEs

WSGPF for the selected STHEs is illustrated in Fig. 6 while WPEI for the selected STHEs is illustrated in Fig. 7.

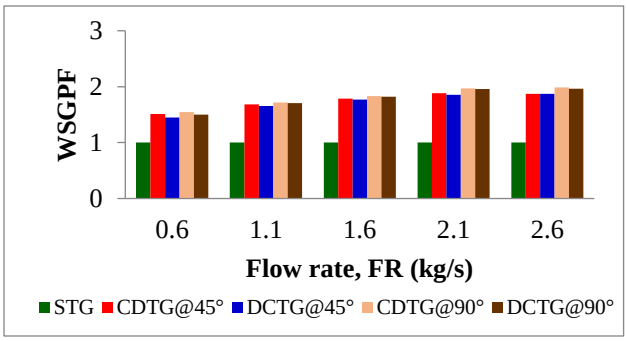

Fig. 6: WSGPF for the selected STHEs

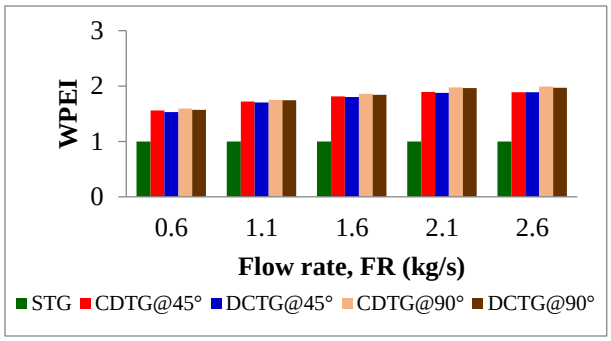

Fig. 7: WPEI for the selected STHEs

WTPF for the selected STHEs is illustrated in Fig. 8 while Tube-side pressure drop for the selected STHEs is illustrated in Fig. 9. The values of WTPF for STHEs with multi-cross sectional tube configurations are 77.66 – 83.71% and 76.19 – 82.88% better than the value obtained in the baseline (STHE-STG) at 45° and 90°, respectively, as displayed in figure 10. The results obtained conforms to $1.75 \leq WTPF \leq 2.15$ observed by Alfarawi (2020). It was also discovered that the value of WTPF increases as the shell-side fluid's flow rate (cold water) increases as observed also by Shirvan *et al.* (2018) where the WTPF is larger than unity ($WTPF \geq 1$). Then, from the perception of energy savings STHE-MSTGs are better. Plots comparing the numerical findings of the pressure drops in the heat exchanger's tube side at 45 and 90 degrees angles of penetration are displayed in Figure 11. It can be observed that the pressure drops from the STHEs with multi-cross sectional tube geometrical (CDTG and DCTG) configurations reduced by 72–73% when compared with that obtained in the baseline. Thus, the tube-side pressure drop obtained in this study compared to 13 kPa obtained by Shahril *et al.* (2017), 3 kPa reported by Wang *et al.* (2018).

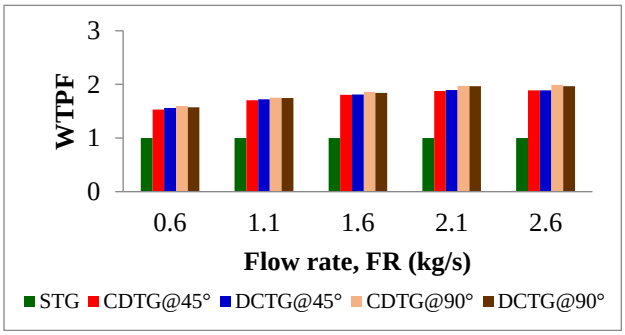

Fig. 8: WTPF for the selected STHEs

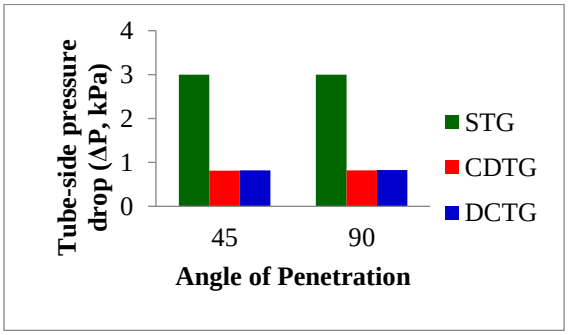

Fig. 9: Tube-side pressure drop for the selected STHEs

4. CONCLUSION

This study attempts to investigate the influence of multi-cross sectional tube geometrical (MSTG) configuration utilizing CDTG and DCTG configurations with 45 and 90 degrees angles of penetrations thermo-hydraulic performance characteristics in shell-and-tube heat exchangers for the same mass flow was made. The numerical simulations are conducted with ANSYS Fluent 19.2 software. Through simulation, pressure drop, heat transfer coefficient, and global thermo-hydraulic performance indices for the heat exchanger geometry were determined. Comparing multi-cross sectional tube geometries to conventional straight and plain tube geometries, the numerical results showed a significant improvement in the thermo-hydraulic performance of shell-and-tube heat exchangers with a significant increase in heat transfer rate, a reduction in tube-side pressure drop, and a slight increase in shell-side pressure drops. This is due to a notable drop in the recirculation flow magnitude when compared to a typical STHE with STG. When compared to STHE with standard STG integrated with segmental baffles, the incorporation of multi-cross sectional tube designs greatly enhanced the shell-side heat duty, reduced tube-side pressure drop, but somewhat increased shell-side pressure drops. To have a processing facility that is dependable, enhanced, efficient, and economical, multi-cross sectional shell-and-tube heat exchangers can be utilized as an alternative to the baseline.

ACKNOWLEDGEMENT

The authors are very grateful to anonymous referees for their careful and diligent reading of the paper and helpful suggestions. This research has not received any sponsorship.

REFERENCES

Adesina, O. K., Olanrewaju, A. I., Peter, O. A., & Iyiola, A. O. (2018). Parametric and Quantitative Analysis on the Development of Shell and Tube Heat Exchanger. *International Journal of Advanced Engineering, Management and Science*, *4*(6), 451–459. https://doi.org/10.22161/ijaems.4.6.4

Ajaykumar, V., Titus, R., & Sudhakar, T. (2016). *Computational and Experimental Investigation of Shell and Tube Heat Exchanger with Finned Tubes under Various Flow Rates*. *3*(1), 191–196.

Alfarawi, S. (2020). *Evaluation of Hydro-Thermal Shell-Side Performance in a Shell-and-Tube Heat Exchanger: CFD Approach*. *66*(1), 104–119.

Ben Slimene, M., Poncet, S., Bessrour, J., & Kallel, F. (2022). Numerical investigation of the flow dynamics and heat transfer in a rectangular shell-and-tube heat exchanger. *Case Studies in Thermal Engineering*, *32*, 101873. https://doi.org/10.1016/j.csite.2022.101873

Bergman, T. L., Lavine, A., & Incropera, F. P. (2019). *Fundamentals of heat and mass transfer* (Eighth edition. Wiley abridged print companion). John Wiley & Sons, Inc.

Chambon, A., Anxionnaz-Minvielle, Z., Cwicklinski, G., Guintrand, N., Buffet, A., & Vinet, B. (2020). Shell-and-Tube Heat Exchanger Geometry Modification: An Efficient Way to Mitigate Fouling. *Heat Transfer Engineering*, *41*(2), 170–177. https://doi.org/10.1080/01457632.2018.1522093

Chen, G. D., Zeng, M., Chen, Q. Y., Peng, B. T., & Wang, Q. W. (2013). Shell-and-Tube Heat Exchangers with Helical Baffles. In Q. Wang, Y. Chen, & B. Sundén (Eds.), *WIT Transactions on State of the Art in Science and Engineering* (1st ed., Vol. 1, pp. 89–130). WIT Press. https://doi.org/10.2495/978-1-84564-818-3/004

Dubey, V. V. P., Verma, R. R., Verma, P. S., & Srivastava, A. K. (2014a). *Performance Analysis of Shell & Tube Type Heat Exchanger under the Effect of Varied Operating Conditions*. *11*(3), 08–17.

Dubey, V. V. P., Verma, R. R., Verma, P. S., & Srivastava, A. K. (2014b). *Steady State Thermal Analysis of Shell and Tube Type Heat Exchanger to Demonstrate the Heat Transfer Capabilities of Various Thermal Materials using Ansys*. *14*(4), 25–30.

Feng, H., Chen, L., Wu, Z., & Xie, Z. (2019). Constructal design of a shell-and-tube heat exchanger for organic fluid evaporation process. *International Journal of Heat and Mass Transfer*, *131*, 750–756. https://doi.org/10.1016/j.ijheatmasstransfer.2018.11.105

Gaikwad, S., & Parmar, A. (2021). Numerical simulation of the effect of baffle cut and baffle spacing on shell side heat exchanger performance using CFD. *Chemical Product and Process Modeling*, *16*(2), 145–154. https://doi.org/10.1515/cppm-2020-0033

Gondane, R., & Jibhakate, Y. M. (2018). *Design and CFD Analysis of Shell and Tube Heat Exchanger using Plain Tube and Corrugated Tube*. *4*(3), 2192–2199.

Guo, Z., Shan, J., Li, J., & Levtsev. (2021). Numerical Simulation of The Effect of Baffle on Heat Transfer Performance of Shell-and-Tube Heat Exchanger. *Bulletin of Science and Practice*, *7*(1), 248–253. https://doi.org/10.33619/2414-2948/62/24

Harish, R., Santosh, G., Rudragouda, R. P., & Santoshkumar, V. (2018). Design, Manufacturing And Testing Of Shell And Tube Heat Exchanger And To Compare The Performance Using Plain Tubes And Lowfin Tubes. *International Journal of Research in Engineering and Technology*, *07*(09), 47–51. https://doi.org/10.15623/ijret.2018.0709006

Igwe, J. E., & Agu, C. S. (2016). *Comparative Analysis of Different Fluids in One Shell Pass And Two Tube Heat Exchanger*. *5*(8), 81–87.

Ikpotokin, I., Uguru-Okorie, D., Osueke, C. O., Dare, A. A., & Petinrin, M. O. (2019). *Numerical Investigation of Shell and Tube Heat Exchanger with Parabolic Segmental Baffle Cut*. *10*(1), 1221–1234.

Ismail, F. B., Ali, M., Simic, M., & TEOa, S. S. (2017). Numerical Analysis and Improvement of the Heat Exchanger Designed For Co-Generating Units. *Procedia Computer Science*, *112*, 2240–2248. https://doi.org/10.1016/j.procs.2017.08.132

Ji, J., Gao, R., Chen, Q., Chen, W., & Zhang, J. (2021). Analysis on Fluid-Induced Vibration and Heat Transfer of Helical Elastic Tube Bundles. *Journal of Thermophysics and Heat Transfer*, *35*(1), 171–178. https://doi.org/10.2514/1.T6033

Kansal, S., & Fateh, M. S. (2014). *Design and Performance Evaluation of Shell and Tube Heat Exchanger using CFD Simulation*. *3*(7), 1663–1666.

Kelecy, F. J. (2008). *Coupling momentum and continuity increases CFD robustness*. *2*(2), 49–51.

Kuppan, T. (2013). *Heat exchanger design handbook* (2nd ed.). Boca Raton: Taylor and Francis.

Li, N., Chen, J., Cheng, T., Klemeš, J. J., Varbanov, P. S., Wang, Q., Yang, W., Liu, X., & Zeng, M. (2020). Analysing thermal-hydraulic performance and energy efficiency of shell-and-tube heat exchangers with longitudinal flow based on experiment and numerical simulation. *Energy*, *202*, 117757. https://doi.org/10.1016/j.energy.2020.117757

Luo, X., Chen, B., Min, M., Jin, M., & Liu, H. (2021). Numerical Simulation of Shell and Tube Heat Exchanger Based on Fluent. *IOP Conference Series: Earth and Environmental Science*, *791*(1), 012084. https://doi.org/10.1088/1755-1315/791/1/012084

Milani Shirvan, K., Mamourian, M., & Abolfazli Esfahani, J. (2018). Experimental investigation on thermal performance and economic analysis of cosine wave tube structure in a shell and tube heat exchanger. *Energy Conversion and Management*, *175*, 86–98. https://doi.org/10.1016/j.enconman.2018.08.103

Mohammadi, M. H., Abbasi, H. R., Yavarinasab, A., & Pourrahmani, H. (2020). Thermal optimization of shell and tube heat exchanger using porous baffles. *Applied Thermal Engineering*, *170*, 115005. https://doi.org/10.1016/j.applthermaleng.2020.115005

Mohanty, S., & Arora, R. (2020). CFD Analysis of a Shell and Tube Heat Exchanger with Single Segmental Baffles. *International Journal of Automotive and Mechanical Engineering*, *17*(2), 7890–7901. https://doi.org/10.15282/ijame.17.2.2020.08.0589

Mukherjee, R. (1998). *Effectively design shell-and-tube heat exchangers*.

Musilim, A. A., Nwagwo, A., & Uche, O. K. (2017). *Effect of Baffle Cut Sizes on Temperature and Pressure Drop at various Mass Flow Rate in A Shell and Tube Heat Exchanger*. *6*(1), 1–10.

Naqvi, S. M. A., & Wang, Q. (2019). Numerical Comparison of Thermohydraulic Performance and Fluid-Induced Vibrations for STHXs with Segmental, Helical, and Novel Clamping Antivibration Baffles. *Energies*, *12*(3), 540. https://doi.org/10.3390/en12030540

Petinrin, M. O. (2016). *Performance Characteristics of Shell-and-Tube Heat Exchangers with Selected Baffle Configurations* [Ph.D]. Department of Mechanical Engineering, University of Ibadan.

Petinrin, M. O., & Dare, A. A. (2020). Numerical and Experimental Investigation on Performance of Convex-Cut Baffles in Shell-and-Tube Heat Exchanger. *Journal of Engineering Research and Reports*, 8–26. https://doi.org/10.9734/jerr/2020/v13i317101

Piyush, G., Avdhesh, Kr. S., & Raj, K. (2019). Shell Side CFD Analysis of a Small Shell-and-Tube Heat Exchanger with Elliptical Tubes. *International Journal of Performability Engineering*, *15*(9), 2294. https://doi.org/10.23940/ijpe.19.09.p2.22942304

Prabakaran, S., Manojprabhakaran, G., & Gopi, P. (2016). *CFD Integrated Optimum Design and Prototyping of Shell and Tube Heat Exchanger*. *1*(4), 38–48.

Prasad, Y. V., & Venkatesh, J. D. (2023). *Analysis of Shell-and-Tube Heat Exchanger Performance using Segmental Baffles through Computational Fluid Dynamics*. *10*(6), 126–133.

Qian, X., Lee, S. W., & Yang, Y. (2021). Heat Transfer Coefficient Estimation and Performance Evaluation of Shell and Tube Heat Exchanger Using Flue Gas. *Processes*, *9*(6), 939. https://doi.org/10.3390/pr9060939

Roy, U., Pant, H. K., & Majumder, M. (2019). Detection of significant parameters for shell and tube heat exchanger using polynomial neural network approach. *Vacuum*, *166*, 399–404. https://doi.org/10.1016/j.vacuum.2018.11.047

Sadighi Dizaji, H., Jafarmadar, S., & Mobadersani, F. (2015). Experimental studies on heat transfer and pressure drop characteristics for new arrangements of corrugated tubes in a double pipe heat exchanger. *International Journal of Thermal Sciences*, *96*, 211–220. https://doi.org/10.1016/j.ijthermalsci.2015.05.009

Sadikin, A., Khian, N. Y., Hwey, Y. P., Al-Mahdi, H. Y., Taib, I., Sadikin, A. N., Md-Salleh, S., & Ayop, S. S. (2018). *Effect of Number of Baffles on Flow and Pressure Drop in a Shell Side of a Shell and Tube Heat Exchangers*. *28*(2), 156–164.

Saffarian, M. R., Fazelpour, F., & Sham, M. (2019). Numerical study of shell and tube heat exchanger with different cross-section tubes and combined tubes. *International Journal of Energy and Environmental Engineering*, *10*(1), 33–46. https://doi.org/10.1007/s40095-019-0297-9

Sandeep, K. P., & Alkesh, M. M. (2012). *Shell and Tube Heat Exchanger Thermal Design with Optimization of Mass flow rate and Baffle Spacing*. *2*, 130–135.

Shahril, S. M., Quadir, G. A., Amin, N. A. M., & Badruddin, I. A. (2017). Thermo hydraulic performance analysis of a shell-and-double concentric tube heat exchanger using CFD. *International Journal of Heat and Mass Transfer*, *105*, 781–798. https://doi.org/10.1016/j.ijheatmasstransfer.2016.10.021

Sharma, S., Sharma, S., Singh, M., Singh, P., Singh, R., Maharana, S., Khalilpoor, N., & Issakhov, A. (2021). Computational Fluid Dynamics Analysis of Flow Patterns, Pressure Drop, and Heat Transfer Coefficient in Staggered and Inline Shell-Tube Heat Exchangers. *Mathematical Problems in Engineering*, *2021*, 1–10. https://doi.org/10.1155/2021/6645128

Shinde, S., & Chavan, U. (2018). *Numerical and experimental analysis on shell side thermo-hydraulic performance of shell and tube heat exchanger with continuous helical FRP baffles*. *5*, 158–171.

Shirgire, N. D., Thakur, A., & Singh, S. (2014). *Comparative Study and Analysis between Helical Coil and Straight Tube Heat Exchanger*. *4*(8), 130–133.

Sinnott, R. K. (2013). *Chemical Engineering Design* (4th ed., Vol. 6). Elsevier. https://doi.org/10.1016/C2009-0-61216-2

Slimene, M. B., Poncet, S., Bessrour, J., & Kallel, F. (2021, June). *Numerical ModellingOf a Rectangular Shell-And-Tube Heat Exchanger*. The 6th World Congress on Momentum, Heat and Mass Transfer. https://doi.org/10.11159/enfht21.lx.306

Wang, G., Wang, D., Peng, X., Han, L., Xiang, S., & Ma, F. (2019). Experimental and numerical study on heat transfer and flow characteristics in the shell side of helically coiled trilobal tube heat exchanger. *Applied Thermal Engineering*, *149*, 772–787. https://doi.org/10.1016/j.applthermaleng.2018.11.055

Wu, Z., & Qian, C. (2022). Study on Behavior of the Heat Exchanger with Conically-Corrugated Tubes and HDD Baffles. *ChemEngineering*, *6*(1), 1. https://doi.org/10.3390/chemengineering6010001

Youcef, A., & Saim, R. (2019). Computational Analysis of Turbulent Flow and Thermal Transfer in a Shell and Tube Heat Exchanger. *International Journal of Heat and Technology*, *37*(4), 1043–1051. https://doi.org/10.18280/ijht.370413

Youcef, A., & Saim, R. (2020). Numerical Analysis of the Baffles Inclination on Fluid Behavior in a Shell and Tube Heat Exchanger. *Journal of Applied and Computational Mechanics*, *Online First*. https://doi.org/10.22055/jacm.2020.32925.2103

Zaboli, M., Ajarostaghi, S. S. M., Noorbakhsh, M., & Delavar, M. A. (2019). Effects of geometrical and operational parameters on heat transfer and fluid flow of three various water based nanofluids in a shell and coil tube heat exchanger. *SN Applied Sciences*, *1*(11), 1387. https://doi.org/10.1007/s42452-019-1431-2

Zahid, H., Mubashar, A., Waqas, M., Siddiqi, M., Munir, U., & Naqvi, S. (2023). Experimental and CFD simulation study of shell and tube heat exchangers with different baffle segment configurations. *Thermal Science*, *27*(1 Part B), 843–853. https://doi.org/10.2298/TSCI220124075Z

Appendix A

Nomenclature

CAD	-	Computer Aided Design
CD	-	Convergent-Divergent
CDTG	-	Convergent-Divergent Tube Geometry
c_p	-	Specific heat capacity (W/m.K)
DC	-	Divergent-Convergent
DCTG	-	Divergent-Convergent Tube Geometry
HEX	-	Heat Exchanger
k	-	Thermal Conductivity (W/mK)
MSTG	-	Multi-cross Sectional Tube Geometry
NTU	-	Number of Transfer Units
Nu	-	Nusselt number
p	-	Pressure (Pa)
Pr	-	Prandtl number
Re	-	Reynolds number
STG	-	Straight Tube Geometry
STHE	-	Shell-and-Tube Heat Exchanger
T	-	Temperature (K)
T	-	Time (second)

Greek symbols

ρ	Density (kg/m^3)
μ	Dynamic Viscosity (kg/m.s)
μ_T	Turbulent Eddy Viscosity (Pas)
ε	Effectiveness
Δp	Pressure drop, Pa
ΔT	Temperature difference, C

Subscripts

0	Initial values
in	Inlet
out	Outlet
t	tube
s	shell
i	Inside
o	Outside
w	Wall
av	Average
c	cold fluid

TEMA	-	Tubular Exchanger Manufacturers Association	h	hot fluid	
u	-	Velocity component (m/s)			
WFSN	-	Weighted Field Synergy Number			
WPEC	-	Weighted Performance Evaluation Criterion			
WPEI	-	Weighted Performance Evaluation Index			
WSGPF	-	Weighted Shell Gain Performance Factor			
WSHTC	-	Weighted Shell Heat Transfer Coefficient			
WTPF	-	Weighted Thermal Performance Factor			

Appendix B

Table A: Thermo-physical Properties of Shell and Tube Materials

	Shell (Galvanized steel)			**Baffle (Galvanized steel)**			**Tube (copper)**		
Material Properties	ρ (kg/m^3)	K (J/kg.K)	C_p (W/m.K)	ρ (kg/m^3)	K (J/kg.K)	C_p (W/m.K)	ρ (kg/m^3)	K (J/kg.K)	C_p (W/m.K)
	8933	401	385	8933	401	385	8055	15.1	480

Table B: Thermo-physical Properties of Fluid Materials

	Tube (Hot Water)				Shell (Cold Water)			
Material Properties	ρ (kg/m^3)	K (J/kg.K)	C_p (W/m.K)	μ (kg/m.s)	ρ (kg/m^3)	K (J/kg.K)	C_p (W/m.K)	M (kg/m.s)
	998.2	0.6	4182	0.001003	998.2	0.6	4182	0.001003

Appendix C

Performance criteria	Weighted form
$TPF = \frac{Nu_{new}/Nu_{control}}{\left(f_{new}/f_{control}\right)^{1/3}}$	$WTPF = \frac{TPF_{new} - TPF_{control}}{(TPF_{new} + TPF_{control})/2}$
$\mathrm{SGPF}, \Gamma = \frac{\left(\frac{h}{\Delta P}\right)_{new}}{\left(\frac{h}{\Delta P}\right)_{straighttube}}$	$WSGPF = \frac{SGPF_{new} - SGPF_{control}}{(SGPF_{new} + SGPF_{control})/2}$
$PEI, \eta = \frac{h}{\Delta P^{1/3}}$	$WPEI = \frac{PEI_{new} - PEI_{control}}{(PEI_{new} + PEI_{control})/2}$

PAPER 103 - PARAMETRIC STUDY ON NATURAL VENTILATION: A CASE STUDY OF ENGINEERING CENTRAL WORKSHOP, FEDERAL UNIVERSITY OF TECHNOLOGY MINNA

E. F. Olorundare[1*], I. Bori[2],

[1]Department of Mechanical Engineering, Federal University of Technology, Minna, Nigeria.
[2]Department of Mechanical Engineering, Federal University of Technology, Minna, Nigeria.
[*]Email:efolorundare365@gmail.com

ABSTRACT
This study provides a literature review on natural ventilation principles, factors affecting airflow, thermal comfort, and the use of Computational Fluid Dynamics (CFD) in building design. The researchers created a detailed 3D model of a workshop and conducted simulations using the DesignBuilder-EnergyPlus software suite. The simulations focused on thermal comfort and were performed on a baseline model with a window-to-wall ratio (WWR) of 30%. The results showed that occupants experienced thermal discomfort for 30.74% of the year, with the remaining 69.26% being comfortable, ranging from "hot" to "slightly warm" sensations. The study then explored the impact of different interventions. Implementing lighting control improved thermal comfort, resulting in a 1.37% increase in the number of hours occupants experienced comfort. The introduction of mechanical ventilation without cooling had a minimal impact on thermal comfort (1.17% improvement). However, when mechanical ventilation and scheduled cooling were combined, there was a significant improvement. The predicted thermal sensation ranged from "slightly warm" to "slightly cool," with most occupants experiencing "neutral" conditions. This strategy increased comfort hours by 14.62% compared to the baseline. While lighting control and mechanical ventilation with fans offered minimal benefits, the combination of mechanical ventilation and scheduled cooling significantly enhanced occupant comfort.

KEYWORDS: natural ventilation, Computational Fluid Dynamics (CFD), thermal comfort, sensational vote, simulation

1. INTRODUCTION

Indoor natural ventilation has gained significant attention in recent years as an energy-efficient and sustainable approach to providing fresh air and maintaining optimal indoor air quality.

This article by (Santamouris *et al*., 2020) provides a comprehensive review of passive cooling technologies in urban buildings, with a focus on the feasibility of using natural wind for maintaining indoor thermal comfort. The review discusses various strategies and techniques, such as natural ventilation, wind catchers, and wind-driven ventilation systems. It explores the advantages, challenges, and potential applications of these technologies in densely populated areas. The article also examines case studies and simulation studies to evaluate the effectiveness and energy efficiency of using natural wind for indoor cooling. These studies found that the popularity of natural ventilation depends on the climate.

Numerous studies conducted in the last five years have demonstrated the benefits of natural ventilation in various building types, including offices (Zemei *et al*., 2019), educational facilities (Montazeri and Azizkhani, 2018), and residential buildings (Saadatian *et al*., 2019). However, (Yang *et al.,* 2019) provide a comprehensive review of thermal comfort in indoor environments with non-uniform air temperature and air velocity distributions. It specifically focuses on the impact of uneven distribution on occupants' perception of thermal conditions. The review incorporates findings from both computational fluid dynamics (CFD) simulations and field measurements. Several studies have explored the application of CFD modelling in the context of indoor natural ventilation. For example, Liu *et al.* (2018) conducted a CFD simulation to investigate the natural ventilation performance of a multi-storey office building. The study examined the influence of window configurations, wind directions, and wind speeds on airflow patterns and thermal comfort. The findings indicated that specific combinations of window openings and wind directions could significantly improve indoor air quality and thermal conditions.

The research is focused on developing a comprehensive understanding of the airflow patterns and thermal comfort conditions and using this information to identify and evaluate design strategies that can improve indoor air quality and energy efficiency. The ultimate goal is to provide architects, engineers, and building owners with practical

guidelines for designing effective and sustainable natural ventilation systems. However, the application and performance of natural ventilation strategies in workshop environments, such as the Engineering Central Workshop at the Federal University of Technology, Minna, have received limited attention. Workshops often present unique challenges due to their specific operational requirements, high heat loads from machinery and equipment, and variable occupancy patterns (Holman, 2020). These factors can significantly impact the effectiveness of natural ventilation strategies, necessitating a comprehensive understanding of the parametric factors influencing their performance.

The aim of this research is to carry out a parametric study on natural ventilation for the case of the engineering central workshop, Federal University of Technology, Minna. This will be achieved via the following objectives: to establish the pattern of the natural ventilation of the workshop, re-design a better ventilation pattern for the workshop and evaluate and compare the results of the redesign to that of the original workshop design.

This study is justified by the challenges posed by excessive heat within the workshop, which can adversely affect the working environment, productivity, and occupant comfort, prompting for lot of questions which this research intends to address.

2. THEORETICAL ANALYSIS

Thermal comfort models and indices

To assess and quantify thermal comfort, numerous models and indices have been developed. One widely used model is the Predicted Mean Vote (PMV) index, proposed by Fanger (1970), which calculates the average thermal sensation vote based on the predicted thermal sensation of occupants. The PMV index considers six primary factors that affect thermal comfort which are air temperature, mean radiant temperature, relative humidity, air velocity, clothing insulation, and metabolic rate. The resulting thermal sensation is classified on a seven-point scale from "cold" to "hot." Other indices, such as the Adaptive Thermal Comfort (ATC) model (ASHRAE, 2017), take into account the adaptive behaviours of occupants in response to changing environmental conditions.
Based on the state of an ambient environment, Carrilho da Graça (2017), provides a comprehensive review of thermal comfort models. It discusses the different approaches and categorizes thermal comfort models into static and dynamic types. These cover the underlying principles, parameters, and methodologies used in each type of model. It also discusses the advantages, limitations, and applications of static and dynamic thermal comfort models. Cheung and Rao (2018), discuss various models commonly used to assess thermal comfort, including the PMV model and the Adaptive Thermal Comfort model. The authors examine the Predicted Mean Vote (PMV) model, which is widely used for predicting thermal comfort based on factors such as air temperature, humidity, clothing insulation, metabolic rate, and air speed. The PMV model can then be applied to these simulations to predict the thermal sensation of occupants and identify potential areas of discomfort. This integration allows for iterative design optimization to achieve better thermal comfort conditions (Li *et al.*, 2021; Yao *et al*., 2019).
The PMV index has a seven-point scale (Table 1) for participants to express thermal sensations under given thermal environments.

Table 1: Seven-point thermal sensation scale (Fanger 1970)

Cold	Cool	Slightly cool	Neutral	Slightly warm	Warm	Hot
– 3	– 2	– 1	0	1	2	3

The relationship of the PMV index to the imbalance between actual heat from the body and the heat required for thermal comfort at a specified activity in a given thermal environment can be described by the following equation.

$$PMV = (0.303e - 0.036M + 0.028) \quad (1)$$

Where M is the metabolic rate and L is the thermal load defined as the difference between the internal production of heat and heat loss to the actual environment.
However, there are discrepancies between the PMV prediction and the actual mean vote (AMV) of occupants in buildings (Kim *et al.* 2015).
To overcome these limitations, an adaptive predicted mean vote (aPMV) model, as shown in Eq. (2), was proposed by Chen *et al*. (2020) to introduce an adaptive coefficient into the PMV model based on the black box theory:

$$= PMV/((PMV\ 1 + \lambda \times PM)) \quad (2)$$

where λ is an adaptive coefficient which considers culture, climate, social, psychological and behavioural adaptations.
Since the metabolic rate is difficult to measure or estimate, it is normally assumed to be constant for some specified activities in the PMV model Gilani *et al*. (2016)
The activity level can be modified to improve the accuracy of the PMV model.

$$M = 0.1092 \times (MPA \times 0.0296) \quad (3)$$

where MPA is the mean arterial blood pressure.

Li and Zhang (2018) provide a comprehensive review of the evaluation of thermal comfort in naturally ventilated buildings, specifically addressing the limitations of using PMV. The review critically examines the challenges and discrepancies associated with using PMV to predict the mean comfort votes of a group of people in everyday building conditions, so PMV model was improved with the following equation.

$$PMVnew = 0.8 \times (PMV - DPMV) \quad 4$$

Where $DPMV$ is the deviation correction function associated with indoor and outdoor climates and 0.8 is the regression coefficient.

3. METHODOLOGY

The study on natural ventilation design involves the use of computational fluid dynamics (CFD) modelling to determine the best design parameters for achieving better ventilation in an indoor environment (Engineering Central Workshop, Federal University of Technology, Minna). To achieve this, the following are the materials and methods that will be employed for this process:

Materials

i. Computer with Designbuilder incorporated with Computational Fluid Dynamics (CFD) Software (EnergyPlus)
ii. Building Information/Geometry: (Federal University of Technology, Mechanical Workshop)
iv. Climate Data
vi. Ventilation System Specifications parameters such as window dimensions, opening types, ventilation rates, and control strategies.
v. Tape rule

Methods

i. **Assessment of the case study components and external environment**.
This involves conducting a thorough assessment of the case study components, which includes the Engineering Central Workshop building itself and its surrounding environment. This assessment involves evaluating the building's construction materials, architectural design, existing ventilation systems, and outdoor conditions such as wind patterns and solar exposure. Understanding these factors is crucial for identifying potential areas of improvement and determining the baseline conditions for the subsequent analysis.

ii. **Modelling of Central Engineering workshop building baseline model**
A baseline model of the Central Engineering Workshop building was created. This model serves as a representation of the building's geometry and characteristics, including its layout, dimensions, windows, openings, and other relevant features. The model was developed using DesignBuilder software tools.

iii. **Thermal comfort analysis of the baseline model**
Thermal comfort analysis was conducted with the aid of EnergyPlus software. This analysis aims to evaluate and quantify the thermal comfort conditions within the building. Various parameters such as indoor air temperature, humidity, air velocity, and radiant temperature are assessed against established comfort metrics. The analysis helps identify any potential thermal discomfort issues within the building under the existing conditions.

iv. **Simulation of the different improvements in thermal comfort strategies.**
Simulations were performed to assess the impact of different natural ventilation efficiency improvement strategies and building thermal comfort strategies. These simulations involve altering parameters such as Lighting control, Mechanical ventilation without cooling, and Mechanical ventilation with cooling, as well as incorporating airflow control mechanisms. The simulations help evaluate how these strategies affect the ventilation performance and thermal comfort conditions within the building. The strategies to improve natural ventilation efficiency and corresponding thermal comfort were then simulated.

4. RESULTS AND DISCUSSION

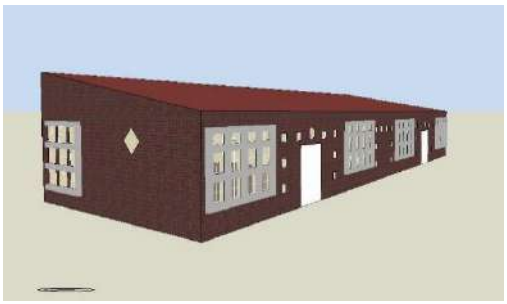

Figure 1: South orientation of the building 3D model

Figure 2: Building main facade and surroundings

Figure 1, presents the 3D model geometry and layout of the engineering central workshop FUTMinna, with a total floor area of 1230m^3 while Figure 2, contains the main building workshop façade and its environment.

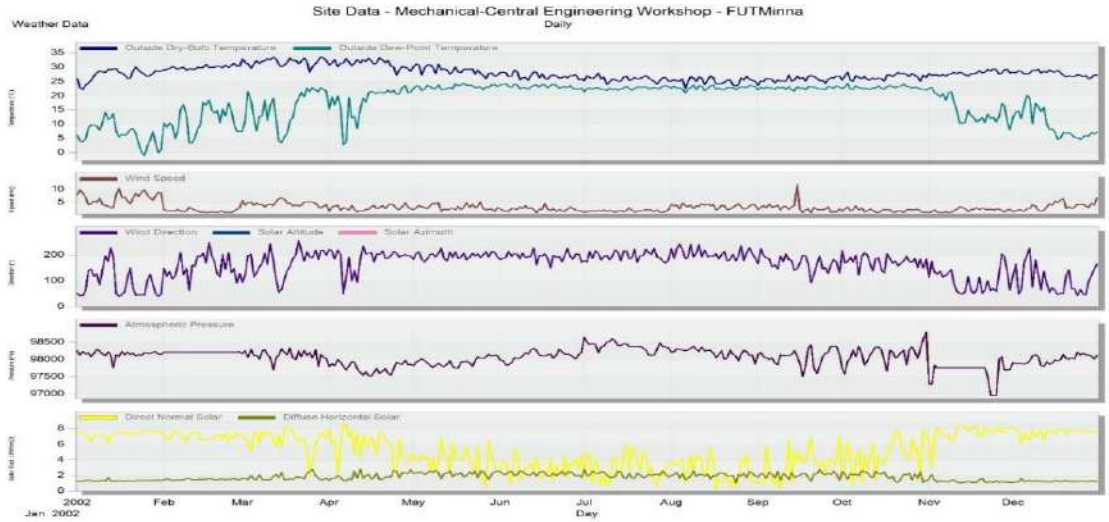

Figure 3: Site data (1 Jan – 31 Dec) for zone conditions reported for an occupied period

Figure 3: shows site data (outside dry-bulb temperature, outside dew-point temperature, wind speed, wind direction, solar altitude, solar azimuth, atmospheric, direct normal solar and diffuse horizontal solar energy) reported for occupied periods only with a maximum outside dry-bulb temperature of 31.88 ^{o}c in the month of March and a minimum of 25.21 ^{o}c in August. The maximum outside dew-point temperature is 23.46 ^{o}c in the month of April and the minimum is 8.88 ^{o}c in January. Wind speed reaches a maximum of 11.98m/s during the month of September and a minimum of 2.25 m/s in May, while the maximum atmospheric pressure is 98386.23 Pa during the month of July and the minimum of 97656.21Pa experienced in November. Direct normal solar energy amounting to a maximum of 232.26 kWh is experienced in December and a minimum of 82.95 kWh in August, while the maximum diffuse horizontal solar energy is 69.7 kWh in May and a minimum of 37.8 kWh in November.

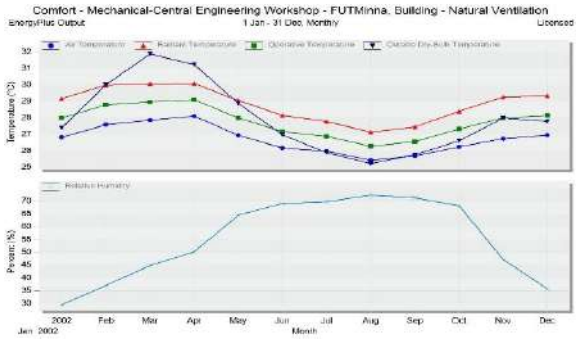

Figure 4: Comfort data - (Baseline model)

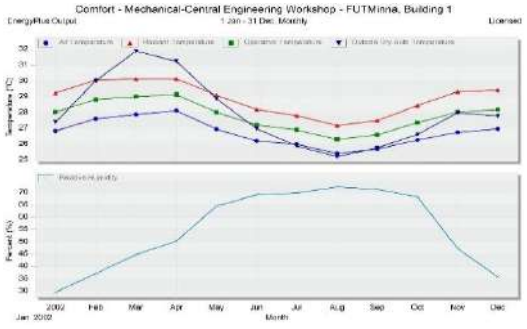

Figure 5: Comfort Data - (Lighting Control)

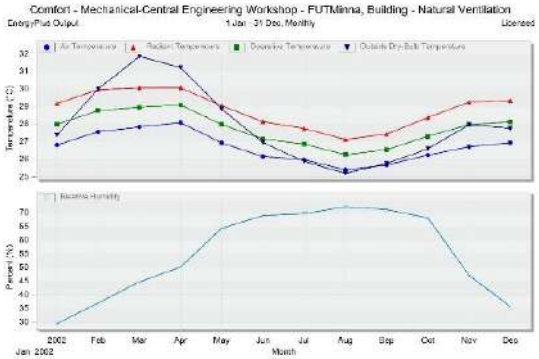

Figure 6: Comfort Data - Mechanical ventilation (Fans)

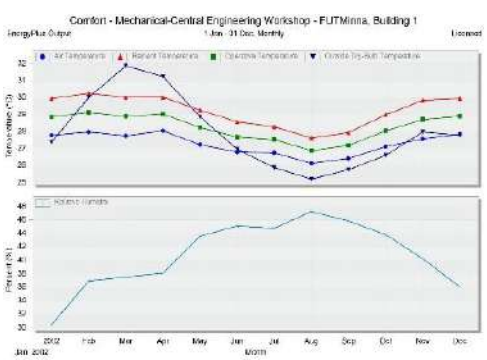

Figure 7: Comfort Data – (Fan + cooling)

Figure 4-7 presents baseline and various strategies for environmental comfort data simulated such as air temperature registered, radiant temperature reached, operative temperature and relative humidity throughout the year. It is generally observed that maximum temperatures are relatively between the month of March and April.

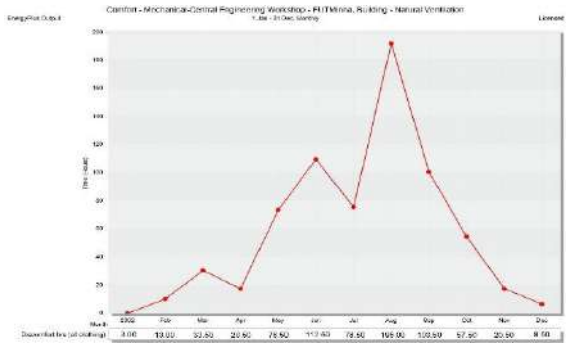

Figure 8: Discomfort hours (Baseline model)

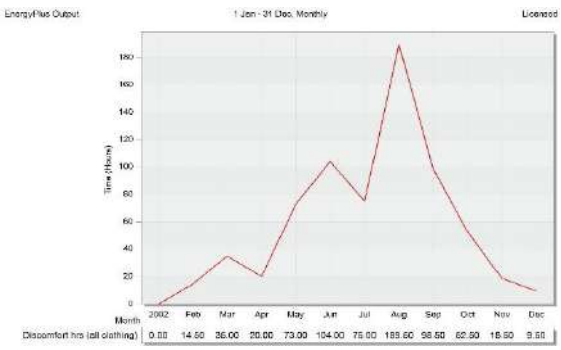

Figure 9: Discomfort hours (Lighting control)

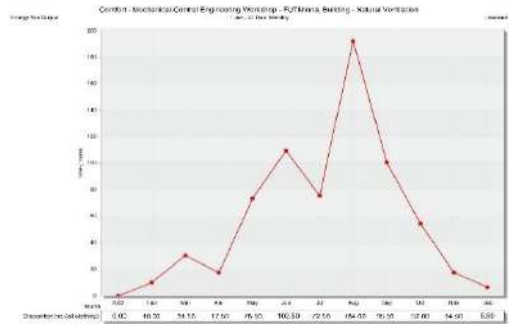

Figure 10: Discomfort hours Mechanical ventilation (Fans)

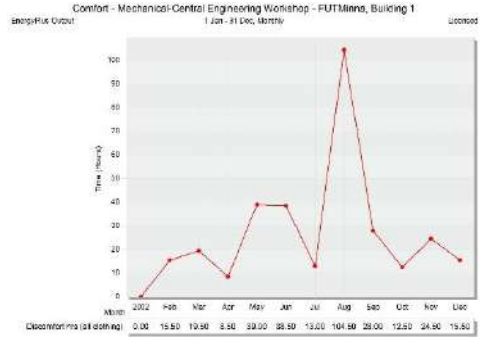

Figure 11: Discomfort hours (Fan + Cooling)

Figure 8, shows that occupants experienced discomfort for 722 hours throughout the year for the baseline model. This is 30.74% discomfort against 69.26% comfort hours out of the total simulation period.

In Figure 9, it can be seen that occupants experienced a total of 690 hours of discomfort throughout the year. This is 29.37% discomfort against 70.63.40% comfort hours out of the total simulation period and hence reductions in the baseline model discomfort by 1.37%. This reduction is attributed to reduced internal gains due to when lighting control is used in the building.

Figure 10, displays that occupants experienced discomfort for 662.5 hours throughout the year. This is 28.20% discomfort against 71.8% comfort hours out of the total simulation period, there is a reduction in the baseline model discomfort by 1.17%.

Figure 11, presents discomfort hours, occupants experienced discomfort for 319 hours throughout the year. This is 13.58% discomfort against 86.42% comfort hours out of the total simulation period, which represents a significant reduction in the baseline model discomfort by 14.62%. This reduction is totally attributed to the scheduled introduction of cooled air into the building.

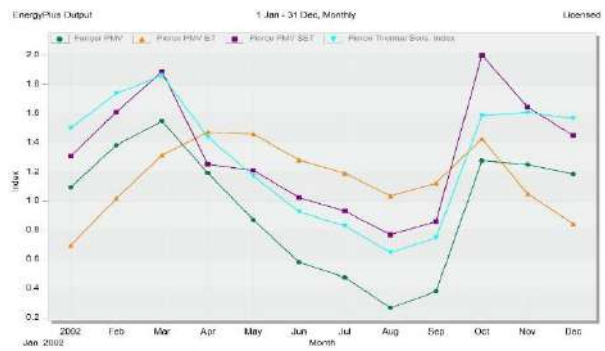

Figure 12: Predicted thermal comfort sensation votes (Baseline model)

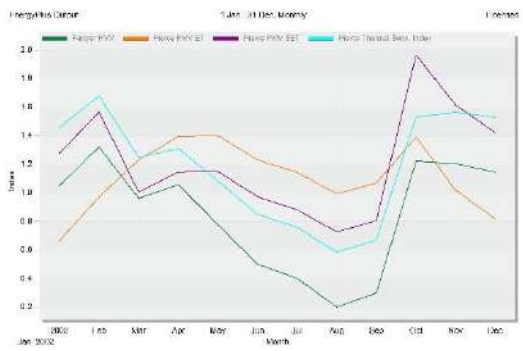

Figure 13: Predicted thermal comfort sensation votes (Lighting control)

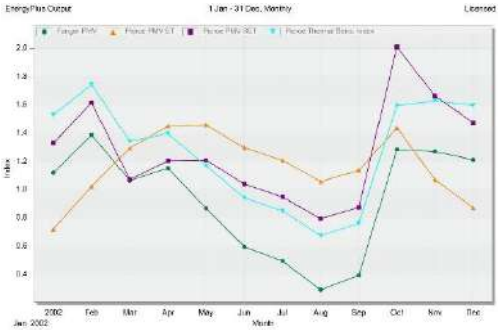

Figure 14: Predicted thermal comfort sensation votes Mechanical ventilation (Fan)

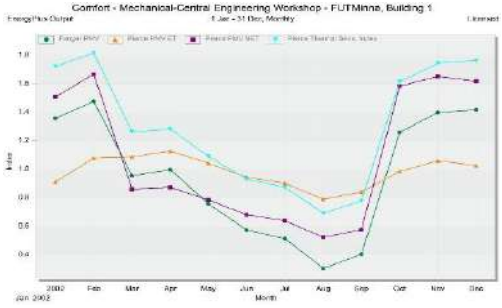

Figure 15: Predicted thermal comfort sensation votes (Mechanical ventilation & Cooling)

Figure 12, presents the predicted thermal comfort sensation index based on Fanger PMV, Pierce PMV ET, Pierce PMV SET and Pierce Thermal Sensation thermal comfort predictive models. The Fanger PMV model predicts thermal comfort close to neutral while the Pierce PMV SET model predicts the worst scenario of all models. It's observed that predicted thermal comfort sensation is slightly improved on application of lighting control, Figure 13, presents predicted thermal comfort sensation votes based on Fanger PMV, Pierce PMV ET, Pierce PMV SET and Pierce thermal sensation predictive model. Figure 14 shows that predicted thermal comfort sensation is majorly from hot to slightly warm on the application of mechanical ventilation. While Figure 15, presents predicted thermal comfort sensation results. It is observed that occupancy thermal sensation votes significantly reduced on application of mechanical ventilation with cooling. Based on the seven points thermal comfort scale, it's observed that the predicted votes placed the comfort sensation majorly between slightly warm and slightly cool for the entire year.

5. CONCLUSION

This study on natural ventilation: applied to engineering central workshop, Federal University of Technology Minna, Niger State, successfully achieved its objectives:

(i) The pattern of natural ventilation in the workshop, through the assessment of various components and external environment, a comprehensive understanding of the workshop's existing conditions and its surroundings was obtained. This provided valuable insights into the baseline ventilation patterns and identified areas for potential improvement. DesignBuilder and EnergyPlus software were used to model the building and perform simulations based on the ASHRAE 55-2004 method. The baseline model predicted thermal comfort votes between "hot" and "slightly warm," with occupants experiencing 30.74% discomfort hours and 69.26% comfort hours throughout the year.

(ii) Better redesigned ventilation pattern were obtained through implementing a lighting control strategy resulted in a slight improvement, shifting the predicted thermal sensation to between "hot" and "neutral." However, the improvement in comfort hours was (1.37%). Similarly, mechanical ventilation with fans showed minimal improvement (1.17%), leaving the predicted thermal sensation between "hot" and "slightly warm." Significant improvement was achieved with mechanical ventilation and scheduled cooling, which placed the predicted thermal sensation between "slightly warm" and "slightly cool," with the majority of occupants experiencing "neutral" conditions. This strategy increased comfort hours by 14.62% compared to the baseline.

(iii) By evaluating and comparing the results with the original workshop design. The study assessed the efficiency and effectiveness of the existing ventilation system. This analysis served as a reference point for evaluating the performance of the redesigned ventilation pattern. These findings highlight the potential of mechanical ventilation and scheduled cooling to improve thermal comfort in naturally ventilated buildings in hot and humid climates like Minna, Niger State. While lighting control and mechanical ventilation with fans offered minimal benefits, the combination of mechanical ventilation and scheduled cooling significantly enhanced occupant comfort.

The following recommendations were proposed:

i. Implement the redesigned ventilation pattern: The study highlights the benefits of the redesigned ventilation pattern in terms of improved airflow, thermal comfort, and energy efficiency. It is recommended to implement the proposed design changes in the Engineering Central Workshop to enhance the indoor environment and reduce energy consumption.

ii. Regular maintenance and monitoring: To ensure the continued effectiveness of the natural ventilation system, regular maintenance and monitoring are essential. This includes cleaning and maintaining

ventilation openings, inspecting airflow paths, and periodically evaluating indoor air quality and thermal comfort.

iii. Further research and validation: While this study provides valuable insights, further research and validation are recommended for conducting on-site measurements and comparing them with simulation results can help validate the accuracy of the models and provide more robust conclusions.

Overall, this parametric study on natural ventilation in the Engineering Central Workshop contributes to knowledge by providing a detailed understanding of the existing ventilation patterns, proposing a better ventilation design, evaluating its performance, and offering practical recommendations for enhancing natural ventilation in workshop environments.

ACKNOWLEDGEMENT

I would like to acknowledge the significant contribution of my supervisor, Engr. Dr Bori Ige, for exceptional support, which were instrumental to the successful completion of this research work. I also extend my appreciation to Engr. Prof. K.C Bala, the Head of the Department of Mechanical Engineering, FUTMinna for his valuable support in bringing this work to fruition. I am also thankful to other member of the department including Prof. 'Femi Olugboji, Prof James Okegbile, Engr. Dr Oyewole Adedipe for their support to the completion of this work.

REFERENCES

ASHRAE. (2017). ASHRAE Handbook - Fundamentals. American Society of Heating, Refrigerating and Air-Conditioning Engineers.

ASHRAE. (2017). ASHRAE Standard 55: Thermal Environmental Conditions for Human Occupancy. American Society of Heating, Refrigerating and Air-Conditioning Engineers.

Carrilho da Graça, G. (2017). Thermal comfort models: A review. Energy and Buildings, 140, 110-124.

Chen, J., Li, B., & Zhang, H. (2020). Development of an adaptive predicted mean vote model for thermal comfort prediction in buildings. Building and Environment, 181, 107057.

Cheung, S. S., & Rao, J. (2018). A review of thermal comfort models and indicators for indoor environments. Building and Environment, 132, 96-105.

Fanger, P. O. (1970). Thermal Comfort: Analysis and Applications in Environmental Engineering. Danish Technical Press.

Gilani SI-u-H, Khan MH, Ali M. (2016) Revisiting Fanger's thermal comfort model using mean blood pressure as a bio-marker: An experimental investigation. Applied Thermal Engineering. 109, Part A:35-43.

Holman, J. P. (2020). Heat transfer (11th edition). McGraw-Hill.

Kim JT, Lim JH, Cho SH, Yun GY. (2015) Development of the adaptive PMV model for improving prediction performances. Energy and Buildings.98:100-105

Li, B., & Zhang, H. (2018). Evaluation of thermal comfort in naturally ventilated buildings: A critical review. Building and Environment, 128, 50-61.

Li, R., Wang, H., Li, X., & Wang, Z. (2021). Numerical Study of the Thermal Comfort of a Naturally Ventilated Classroom in a Hot-Arid Climate. Sustainability, 13(2), 615.

Liu S, Liu J, Yang Q, Pei J, Lai D, Cao X, Chao J, Zhou C. (2018) Coupled simulation of natural ventilation and daylighting for a residential community design. Energy and Buildings. 68, Part B:686-695

Montazeri, H., & Azizkhani, M. (2018). The influence of window configuration on the natural ventilation performance of a school building. Building and Environment, 145, 426-438. https://doi.org/10.1016/j.buildenv.2018.09.031

Saadatian, O., Lim, C. H., Sopian, K., & Salleh, E. (2019). Review of windcatcher technologies. Renewable and Sustainable Energy Reviews, 13(4), 1823-1836. https://doi.org/10.1016/j.rser.2009.01.024

Santamouris, M., Ding, L., Fiorito, F., Oldfield, P., & Osmond, P. (2020). Review of passive cooling technologies in buildings in urban areas. Renewable and Sustainable Energy Reviews, 130, 109964.

Yang, L., Li, B., & Zhang, H. (2019). Thermal comfort in indoor environments with non-uniform air temperature and air velocity distributions: A literature review. Building and Environment, 155, 56-68.

Yao, R., Li, B., & Liu, J. (2019). Review of Natural Ventilation Design Methods for Residential Buildings. Energy and Buildings, 201, 109426.

Zemei, W., Yongfeng, L., Zheng, H., & Lin, W. (2019). Optimal design of natural ventilation in office buildings. Renewable Energy, 143, 1516-1536. https://doi.org/10.1016/j.renene.2019.05.099

PAPER 105 - BENEFICIATION OF NIGERIAN LITHIUM ORE BY FROTH FLOTATION TECHNIQUE USING FORMULATIONS FROM LOCAL REAGENTS: A REVIEW

A.A. Owoade[#1], J.A. Adebisi[1], S. I. Talabi[1,3], T. Yahya[1], R.M. Mahamood[1], S. Abdulkareem[2], I.I. Ahmed[1]

[1]Department of Materials and Metallurgical Engineering, University of Ilorin, Ilorin, Nigeria.
[2]Department of Mechanical Engineering, University of Ilorin, Ilorin.
[3]Manufacturing Science Division,2350 Cherahala Blvd, Oak Ridge National Laboratory, Knoxville, USA.

[#]Email: abdurrauf334@gmail.com

ABSTRACT

The use of lithium compounds in lithium-ion battery technology, portable electronic devices, and power storage systems has resulted in a significant growth in demand for lithium minerals in recent years. Froth flotation is the most widely used beneficiation method for lithium minerals. Froth floatation reagents namely; collectors, frothers, and depressants play key roles in lithium mineral flotation. However, the exorbitant costs and non-availability of conventional reagents used in the beneficiation of lithium ores make the production of lithium concentrates locally difficult. This review provided detailed, comprehensive, and valuable reference sources on the beneficiation of lithium ore by froth flotation technique using formulations from different conventional reagents. Various analyses including the mineralogical characterization of the lithium ore and the chemical characterization of the reagents were also reviewed. These analyses are going to provide information about the ore and the chemical composition of the convectional and the local reagents respectively. The chemical analyses of the reagents will also help to understand whether these reagents can be utilized in lieu of each other. This paper also discusses briefly the use of the Design of experiments (DOE) to choose optimal conditions that could apply to all the reagents considered.

KEYWORDS: beneficiation, design of experiments, froth floatation, lithium, reagents.

1. INTRODUCTION

Lithium is the third element of the periodic table. It is the lightest of all solid elements (d = 0.53 $g \cdot cm^{-3}$ at 20 °C), has the highest specific heat capacity, the smallest ionic radius of all the alkali metals, and a high electrochemical potential. Its two stable isotopes are ^{6}Li and ^{7}Li, with ^{7}Li being the most abundant (92.5%) (Coplen et al., 2002, Tomascak, 2004). Several radioisotopes have been observed, such as ^{3}Li, ^{4}Li, ^{5}Li, ^{8}Li, ^{9}Li, ^{10}Li, ^{11}Li, ^{12}Li, ^{13}Li (Audi et al., 2012), with ^{8}Li and ^{9}Li being the most stable, with a half-life of, respectively, 838 ms and 178 ms (Audi et al., 2003). Batteries, glass, ceramics, lubricants, refrigeration, nuclear, and optoelectronic industries are among the many industries that use lithium. As computers, digital cameras, mobile phones, and other electronic gadgets have advanced, the battery industry has emerged as the primary lithium consumer.

There are substantial economic reserves of lithium ore in several states in Nigeria. This is the primary raw material source utilized to produce lithium-ion batteries for electric car batteries and household appliance batteries. These states are Plateau, Oyo, Cross River, Nasarawa, Ekiti, Kwara, Kogi, and a few more. According to preliminary findings, lithium grades in lithium-producing mines worldwide are equivalent to those of ores found in Nigeria that contain lithium. (Onyenwe and Orah, 2022).

Hard rock minerals containing lithium that are frequently mined include eucryptite, lepidolite, petalite, and spodumene. Spodumene, an aluminosilicate of lithium, is the most prevalent and researched of the various varieties of lithium minerals. Compared to most other raw minerals, which often have 1-3% Li_2O, naturally occurring spodumene ($LiAlSi_2O_6$) has a stoichiometric chemical composition of 8.03 wt % Li_2O (Sardisco et al., 2022). Due to the similarity of the physical-chemical properties of lithium minerals (including spodumene) and their associated gangue minerals (e.g., quartz, feldspar, mica), it is often challenging to separate lithium minerals (Bulatovic, 2014). The typical beneficiation methods consist of flotation, hand sorting, heavy media separation, thermal treatment and magnetic separation.

For lithium minerals, including spodumene, flotation is the most used beneficiation technique (Filippov et al., 2019). Froth flotation was patented in 1905 for the concentration of ore (Mesa and Brito-Parada, 2019). Its cost-effectiveness and technical adaptability have made it the most significant mineral processing technique in the mining sector (Wills and Finch, 2015). Surface chemistry is the basis for froth flotation, which separates tiny mineral particles based on how hydrophobic they are. Little bubbles of gas, usually air, are dispersed during this

separation process inside a flotation tank, also known as a flotation cell. The pulp, an aqueous medium containing a mineral suspension, is kept in the tank. To increase the hydrophobicity of the important minerals in the pulp in a targeted manner, chemical reagents known as collectors are added. Figure 1 shows a typical diagram of a flotation process.

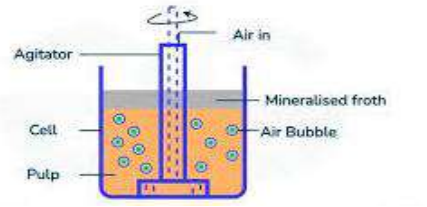

Figure 1: Froth floatation process

These hydrophobic particles have the ability to cling to the gas bubbles and rise, creating a froth layer that overflows when the concentrate rich in minerals does (Mesa and Brito-Parada, 2019). Flotation is the method most commonly used in industry to separate spodumene from related silicate minerals using fatty acid collectors like oxidized paraffin soap, sodium oleate, and naphthenic soap (Moon and Fuerstenau, 2003), while all these reagents mentioned are conventional, the aim of the research work will be focused on the use of alternative formulations from locally available materials namely; collectors (Palm kernel oil, sesame oil), frothers (Palm wine, dry gin) and depressants (Maize starch, cassava starch) as reagents for the beneficiation of Nigerian lithium ore by froth flotation technique.

2. LITHIUM

In today's business, lithium is one of the most important metals. Its applications span the pharmaceutical and aerospace industries, which rely on aluminium/lithium light alloys for their lithium-based bipolar disorder therapy medications. Producing Lithium-ion Batteries (LiBs) for electric cars and portable electronics is now the most significant use. Because salt-lake brines have lower production costs, they have dominated lithium production until recently. Following an increase in lithium prices, there was a renewed interest in alternative sources due to the constantly increasing demand for lithium compounds. 50% of the lithium produced worldwide currently comes from this other source, which is minerals rich in lithium (Schulz, 2017). Lithium minerals are numerous and include spodumene, eucryptite, petalite, bikitaite, etc (Labbé and Daw, 2012). Among those minerals, spodumene $LiAlSi_2O_6$ is the most common and the most studied. It gives a theoretical Li_2O content of 8 wt %. On the other hand, raw minerals in nature typically offer 1 to 2 wt % Li_2O with some notable exceptions such as Greenbushes, Australia which offers a high rate of 1.44 wt % Li (3.10 wt % Li_2O) (Kesler et al., 2012).

2.1 Availability

Almost 70% of the world's lithium reserves are found in the ABC region in South America, which includes Argentina, Bolivia, and Chile. In the Salars (Salt Flat or brine) of Bolivia, Argentina, and Chile, the concentrations of lithium range from 0.04 to 0.16 wt % (Meshram et al., 2014). According to (Yaksic and Tilton, 2009) the resource of lithium is estimated to be 64 Mt. Chile has the world's largest resource of brine (7.5 Mt, 1500– 2700 mg/L Li) containing lithium, followed by Bolivia (resource: 9.0 Mt with 532 mg/L Li) and Argentina (resource: 2.6 Mt, 400–700 mg/L Li) and these three countries account for almost 80% of the world's brine reserves (Mohr et al., 2012). Lithium resource estimates are widely reported (Clarke and Harben, 2009, Gruber et al., 2011, Evans, 2010b, Evans, 2010a). Lithium rock production began with lithium minerals (1899) in the USA (Garrett, 2004). Brine extraction has primarily taken place in South America and China since the first lithium was extracted from brines in Searles Lake, USA, in 1936. Atacama Salt Flat in Chile, where lithium is produced from Salar brine, is the world's greatest producer of lithium. In addition to Nevada in the United States, salt lakes in Tibet and Qinghai, China, are used for the manufacture of lithium from brines (Meshram et al., 2014).

2.1.1 Lithium Ore in Nigeria

A Ministry of Solid Mineral Development report states that over 44 distinct types of minerals have been found in 500 places throughout Nigeria (Onochoja, 2020). Due to their promising international markets, the government is concentrating its efforts on 35 industrial minerals that are widely available. Ore of lithium is one of these minerals. In Nigeria, lepidolite, petalite, and spodumene are the most frequent forms of lithium ores. Additionally, Nigeria exports these ores with little to no value addition to foreign purchasers. Lithium ore deposits can be found in several Nigerian states, including Kogi, Nasarawa, Ekiti, Kwara, Cross River, Oyo, and Plateau (Onochoja, 2020) . The nation is a big market for lithium-ion batteries due to the strong consumption of large quantities of lithium

final products, such as deep cycle and mobile phone batteries. It is anticipated that advantageous laws, such as tax breaks and subsidies, will encourage investment in regional mining, beneficiation, and use (Onochoja, 2020).

2.2 Types of Lithium ore

2.2.1 Petalite

Petalite is a monoclinic mineral with a framework silicate structure that is frequently found in pegmatites, including lepidolite, spodumene, and eucrypite. Petalite's theoretical lithium concentration is 2.27% (4.88% Li_2O), yet several deposits have varying amounts of Li between 1.4 and 2.2% (3.0–4.7% Li_2O) (Tadesse et al., 2019). Petalite is found in large concentrations in Australia, Brazil, Canada, and Zimbabwe. Additionally, reports of large amounts of petalite have come from Namibia, China, and Russia (Garrett, 2004, Wietelmann and Bauer, 2000) Eucryptite, a less frequent lithium mineral, is primarily found in conjunction with petalite. At high temperatures, natural petalite is transformed into β-spodumene, which makes it suitable for leaching (Garrett, 2004).

2.2.2 Lepidolite

Lepidolite is a mica that is used to make ceramics and glasses. Its composition is complicated and varies. Its Li content varies greatly, ranging from 3.0% Li_2O (1.39%) to 7.7% Li_2O (3.58%). In comparison to spodumene, lepidolite is less common in pegmatites. Zimbabwe, Canada, Namibia, Brazil, Portugal, and Argentina are countries with commercial lepidolite deposits (Garrett, 2004). Calcite, muscovite, feldspar, and quartz are the primary gangue minerals associated with lepidolite that must be separated to enrich lepidolite (Tadesse et al., 2019).

2.2.3 Spodumene

Spodumene is a tabular hard rock (monoclinic pyroxene) that is insoluble in dilute acids and has a single-chain structure made of lithium aluminium silicate (Bulatovic, 2014). A noticeable longitudinal cleavage is present. Because of its large Li concentration and the presence of widespread deposits, spodumene is the primary lithium-bearing silicate mineral that is currently being investigated and treated (Garrett, 2004). Pegmatite deposits contain spodumene along with other silicate minerals such as feldspar, micas, and quartz. (Bulatovic, 2014). While pure spodumene comprises 8.0% Li_2O, 27.4% Al_2O_3, and 64.6% SiO_2, a typical pegmatite Li ore from Kings Mountain, North Carolina, is composed of 20 wt % spodumene, 7% muscovite, 43% feldspar, and 30% quartz. (Moon and Fuerstenau, 2003).

2.2.3.1 Beneficiation of spodumene

1) Gravity and dense media separation

Before grinding, gangue minerals can be rejected using a preconcentration technology called dense media separation (DMS) or heavy media separation. DMS is frequently used to separate spodumene from other gangue silicates by taking advantage of the difference in specific gravity between the target and gangue minerals. Spodumene has a specific gravity of 3.1 to 3.2, which puts it somewhat heavier than the majority of gangue minerals, including muscovite (2.8), quartz (2.65), and albite (2.60). As a result, the gangue minerals separate from the spodumene by floating in a dense media with the proper specific gravity (Tadesse et al., 2019).

2) Magnetic separation

Lithium pegmatite ores are associated with gangue such as iron-bearing minerals that are difficult to separate from lithium minerals by DMS and/or flotation. Large amounts of iron-bearing gangue minerals can be removed by magnetic separation either before or after flotation to prepare the concentrate for use in the production of ceramics and glass. For instance, before spodumene flotation, iron-bearing minerals like tourmaline are removed from Greenbushes' pegmatite using a wet high-intensity magnetic separator. After screening the non-magnetic product at 400 µm, a spodumene concentrate with an assay of 7.5–7.7% Li_2O and less than 0.1% Fe_2O_3 is obtained (Tadesse et al., 2019).

3) Sensor-based sorting

Sorting is a method for dividing items according to their color, density, or electromagnetic characteristics, among other attributes. Both automated mechanical sorting and manual hand sorting are methods for sorting ore. The hand-sorting technique uses an ore's weight (density) and color to its advantage. Individuals with experience and understanding of these features use their hands to separate valuable ore from gangue (Fenby, 2014).The use of hand sorting in mineral processing has decreased due to the necessity of processing high volumes of low-grade ore and the requirement for fine milling to promote mineral liberation. (Wills and Finch, 2016).

4) Flotation

The method most frequently employed for the beneficiation of minerals containing lithium, including spodumene, is froth flotation. It is a method for concentrating lithium minerals from pegmatite ores that is based on the surface properties of minerals. When treating complicated or low-grade ores, it is especially used when the target minerals'

and gangue's average particle sizes are too close in specific gravity to allow for effective gravity separation. Lithium minerals from pegmatite ores have been concentrated using both reverse and direct flotation methods. Whereas spodumene is floated with anionic collectors in direct flotation to reject gangue minerals to the tailings, gangue minerals are floated with cationic collectors in reverse flotation to create spodumene concentrate (as tailings) (Tadesse et al., 2019). Several variables, such as the surface chemistry of the minerals, the kind and concentration of the collector, the pH of the pulp, the pre-treatment techniques used, and the existence of slimes, are known to affect the selective recovery of lithium minerals by flotation (Tadesse et al., 2019).

2.3 Flotation of spodumene

The flotation of spodumene from pegmatite ores commonly uses anionic collectors such as oleic acid, sodium oleate, sulphonated, and phosphorated fatty acids. Oleic acid can produce spodumene recoveries of more than 90% and a concentrate grade of 6.52% Li_2O. It was discovered that a combination of fatty acids in fuel oil, including rosin acid, linoleic acid, oleic acid, erucic acid, and arachidonic acid, was useful in the flotation of spodumene (Tadesse et al., 2019). When removing quartz, feldspar, and mica from spodumene using reverse flotation (gangue flotation), cationic collectors like amine acetate are commonly employed. More selective anionic collectors have taken the place of cationic collectors due to their poor flotation performance. It was said that employing a combination of anionic and cationic collectors can lead to increased selectivity in the flotation of spodumene from other gangue minerals including feldspar and mica (Xu et al., 2016a).

It was discovered that as the concentration of oleate ions increased, so did the adsorption density of sodium oleate and oleic acid onto spodumene (Moon and Fuerstenau, 2003, Yu et al., 2015). Research on the surface interaction of spodumene with these collectors showed that at pH 8–9, when spodumene flotation was at its highest, oleic acid and sodium oleate adsorption onto the spodumene surface was best (Moon and Fuerstenau, 2003, Yu et al., 2015). The pH level at which the zeta potential of the spodumene-oleate system changed significantly was also where maximum adsorption was seen (Moon and Fuerstenau, 2003). Additionally, research on the surface tension of oleic acid solutions showed that it was lowest at a pH of 8 to 9, which is also the pH at which spodumene floats the most. Strong hydrophobicity of the oleic acid collector was identified as the cause of the low surface tension of oleic acid at these pHs (Yu et al., 2015).

In contrast to single surfactants, mixed cationic/anionic collectors may have a synergistic impact, which has piqued researchers' interest recently (Vidyadhar and Rao, 2007). According to some research, a combination of collectors could increase the effectiveness of mineral flotation separation because their synergistic effects improve selectivity, the adsorption behaviour of the collector on the target mineral surface, and mineral recovery (Xu et al., 2013).

High recoveries are typically achieved with cationic collectors, such as dodecylamine, however, selectivity is often compromised (Wang et al., 2018). For example, recent research (Xu et al., 2016a, Xu et al., 2016b) demonstrated that excellent selectivity was achieved for the flotation of spodumene from feldspar when sodium oleate (NaOL) and dodecyl trimethyl ammonium chloride (DTAC) interacted at a molar ratio of 9:1. Additionally, spodumene recovery rose from 50% in the mixed scenario to 82.15% when NaOL was utilized alone as a collector. This observation's mechanism was partially explained by the fact that the combined NaOL/DTAC case had a denser molecular arrangement and higher surface activity than the single NaOL or DTAC cases (Tian et al., 2018).

According to investigations using the Fourier transform infrared, in the mixed NaOL/DTAC system, NaOL first interacts with Al sites on the spodumene surface, and then DTAC and NaOL complex and co-adsorb on the Stern layer (Tian et al., 2018).

Lithium pegmatite ores are floated using several conditioning reagents in addition to collectors. To increase mineral selectivity during flotation, gangue minerals or spodumene depressants are used. To depress spodumene in the reverse flotation of gangue minerals, the pulp is conditioned with starch and dextrin(Tadesse et al., 2019). When calcium ion-activated spodumene is floated with a combination of anionic and cationic collectors, it has been found that sodium carbonate will depress the flotation of feldspar (Xu et al., 2016a). The feldspar flotation recovery decreased from 95% to 20% with little impact on the spodumene recovery upon the addition of up to 6×10^{-3} mol/L Na_2CO_3 (Xu et al., 2016a). It was also found that sodium carbonate had a depressant impact on spodumene flotation (Tadesse et al., 2019). During the flotation of spodumene with oleate, quebracho extract has been utilized to depress quartz (Tadesse et al., 2019). The application of depressants in spodumene flotation has not been extensively studied.

Numerous studies have been conducted on the application of polyvalent metal cations, such as calcium and ferric ions, as activators in spodumene flotation (Wang and Yu, 2007, Jie et al., 2014, Yu et al., 2014). When calcium-

activated spodumene was floated with 75% oleic acid and 25% dodecyl trimethyl ammonium chloride, the highest recovery was achieved at pH of 11.6 (Wang and Yu, 2007). Liu et al. (2015) examined how calcium and magnesium ions affected the spodumene's ability to float. According to their findings, the concentration of calcium and magnesium ions increases as spodumene's flotation recovery increases. At pH 12.5 and 10.0, with Ca^{2+} and Mg^{2+} activation respectively, the maximum recoveries of spodumene were reported (Liu et al., 2015).

According to research on mineral surfaces, there may be more sodium oleate adsorption due to the existence of precipitated metal complexes like $Ca(OH)_2$ and $Mg(OH)_2$ as well as hydroxy complexes like CaOH(I) and MgOH(I) (Liu et al., 2015). Nevertheless, some reports suggest that calcium ions could also cause other gangue minerals, including feldspar, to float (Xu et al., 2016a). Similar to this, it is discovered that ferric ions improve spodumene flotation by surface adsorption, increasing interaction with sodium oleate (Moon and Fuerstenau, 2003, Jie et al., 2014). Ferric ions were shown to be more effective activators for spodumene flotation than calcium ions (Wang and Yu, 2007).

2.4 Extraction of lithium

2.4.1 Acid process

To process spodumene, roasting it at 1070–1100 °C is desired to convert α-spodumene to β-phase (Chen et al., 2011, Clarke, 2013, Tahil, 2010). Tahil (2010) reported the roasting of spodumene in a kiln at about 1100 °C. Lithium sulphate was produced by roasting the calcine and sulfuric acid mixture at 250 °C and then leaching the mixture in water. The reaction of β-spodumene with H_2SO_4 is shown Equation 1:

$$Li_2O{\cdot}Al_2O_3{\cdot}4SiO_{2(S)} + H_2SO_{4(CONC)} \rightarrow Li_2SO_{4(S)} + Al_2O_3 \cdot 4SiO_{2(S)} + H_2O_{(G)} \quad (1)$$

After adjusting the pH, purifying, and evaporating the solution, sodium carbonate can be added to recover lithium carbonate as shown in Equation 2.

$$Li_2SO4_{(AQ)} + Na_2CO_{3(AQ)} \rightarrow Li_2CO_{3(S)} + Na_2SO_{4(AQ)} \quad (2)$$

In 2012, Galaxy Resources in China put into service the world's first continuous facility that uses calcination—roasting calcine with H_2SO_4 and water leaching to convert spodumene concentrate to lithium carbonate (Clarke, 2013).

2.4.2 Alkaline process

Spodumene or lepidolite ore concentrations are crushed and calcined with limestone at 825–1050 °C in the alkaline process. After the calcine is produced, it is ground, pulverized, and treated with water to produce lithium hydroxide, which reacts with hydrochloric acid to form chloride. With this procedure, the recovery is roughly 85–90% (Meshram et al., 2014). The reaction during the calcination of spodumene with limestone can be represented as shown in Equation 3:

$$Li_2O{\cdot}Al_2O_3 \cdot 4SiO_{2(S)} + CaCO_3 \rightarrow Li_2O_{(S)} + CaO{\cdot}Al_2O_3 \cdot 4SiO_{2(S)} + CO_{2(G)} \quad (3)$$

2.4.3 Chlorination process

Depending on the type of mineral treated, a less popular technique is the chlorination process, which involves roasting the ore between 880 and 1100 °C in the presence of either Cl_2 or HCl. At higher temperatures (1100 °C), lithium in spodumene can be almost quantitatively converted to LiCl in 2.5 hours using Cl_2 (Barbosa et al., 2014); At the lower temperature (1000 °C), the recovery is shown to be rather poor (58%) (Meshram et al., 2014). During the chlorination process, around 98% of the lithium present in spodumene is transformed into its chloride, which may be leached using water, when the ore is sintered with NH_4Cl and $CaCl_2$ in a furnace at 750 °C (Meshram et al., 2014).

2.5 Characterization techniques

2.5.1 X-ray Fluorescence (XRF)

X-ray Fluorescence (XRF) is a technique used to quantify the concentration of various metal oxides in the ore. When the ore is exposed to X-rays, some components in the sample emit recognizable fluorescence light at particular wavelengths. The concentration of the elements in the sample is then correlated with the fluorescence intensity at a specific wavelength (Beckhoff et al., 2007). XRF has a limitation with regards to lithium and small atoms. It gives the information about the entire ore composition and also to determine the optimal liberation size in which the valuable mineral can be extracted.

2.5.2 ICP-OES (Inductively Coupled Plasma-Optical Emission Spectroscopy)

ICP-OES (Inductively Coupled Plasma-Optical Emission Spectrometry) is a technique that uses a spectrometer and plasma to detect the elemental composition of the lithium ore, most of which is dissolved in water. ICP-OES is more suitable for light weight element like lithium, hydrogen etc. (Khan et al., 2022). This technique will also show the amount of lithium content that will be obtained after comminution of the ore.

2.5.3 Fourier-Transform Infrared Spectroscopy (FTIR)

Fourier-Transform Infrared Spectroscopy (FTIR), is a technique used to determine the functional groups of the floatation reagents (Berna, 2017). This technique will be used to characterize the local reagent functional group in comparison to the conventional reagents. This chemical analyses of the will also help to understand whether the conventional and local reagents can be used in lieu of each other.

2.5.4 Gas Chromatography–Mass Spectrometry (GC–MS)

Gas Chromatography–Mass Spectrometry (GC–MS) will be used to analyze the chemical composition of convectional and local reagents. With the use of a gas chromatograph, determination of the composition of the reagents by separating its constituent parts, that is the quantity of each component that is there is possible (Mastovska, 2005). The analyses also aid in determining whether the reagents can be substituted for one another.

2.6 Design of experiments

Due to several samples investigated and the possible complex nature of this study, design of experiment (DOE) will be utilized to choose the optimal conditions that could apply to all the reagents considered. This will enable optimal experiment design to be used simultaneously for varying all the analyzed factors (Lazić and Velašević, 2004).

This is not the same as the classical (conventional) experimental design, which involves changing one independent variable (factor) while holding the remaining components constant. For every floatation test, 3^5 (243) experimental trials will be produced if this approach is used in the study. The three reagents (collectors, froth, and depressant) will be varied for five distinct values (level of variations). This will be too laborious and lead to numerous, hard-to-control experimental errors. It will take a lot of time and there may be no end to the difficulties in understanding the data. The interaction effects of associative factors are another significant condition that is not taken into account by the standard method (one factor at a time, or OFAT) (Lazić and Velašević, 2004). Most of these problems could be avoided by employing DOE which simultaneously varies all factors along with OFAT experimental trials. This will simultaneously increase the efficiency of empirical research.

3. CONCLUSIONS

The various techniques used in the beneficiation of lithium minerals from hard rock pegmatite ores containing spodumene, petalite and lepidolite have been reviewed. According to these reviews, flotation is the main beneficiation method used in many plants around the world due to the fact that its more economical and has better effect compared to other beneficiation methods. The success in separating lithium minerals from ores using the method depends significantly on the use of reagents, However, the high costs and non-availability of conventional reagents used in the beneficiation of lithium ores make the production of lithium concentrates locally difficult.

ACKNOWLEDGEMENT

The study was funded by Tertiary Education Trust Fund (TETFUND) under the auspices of National Research Fund (NRF) with Grant Reference: TETF/DR&D-CE/NRF/2020/SETI/31/ Vol .1. The financial support is duly acknowledged.

REFERENCE

AUDI, G., BERSILLON, O., BLACHOT, J. & WAPSTRA, A. H. 2003. The Nubase evaluation of nuclear and decay properties. *Nuclear Physics A,* 729**,** 3-128.

AUDI, G., KONDEV, F., WANG, M., PFEIFFER, B., SUN, X., BLACHOT, J. & MACCORMICK, M. 2012. The NUBASE2012 evaluation of nuclear properties. *Chinese Physics C,* 36**,** 1157.

BARBOSA, L. I., VALENTE, G., OROSCO, R. P. & GONZALEZ, J. A. 2014. Lithium extraction from β-spodumene through chlorination with chlorine gas. *Minerals Engineering,* 56**,** 29-34.

BECKHOFF, B., KANNGIEßER, B., LANGHOFF, N., WEDELL, R. & WOLFF, H. 2007. *Handbook of practical X-ray fluorescence analysis*, Springer Science & Business Media.

BERNA, F. 2017. Fourier transform infrared spectroscopy (FTIR). *Encyclopedia of Earth Sciences Series; Gilbert, AS, Ed.; Springer: Dordrecht, The Netherlands***,** 285-286.

BULATOVIC, S. M. 2014. Beneficiation of lithium ores. *Handbook of Flotation Reagents: Chemistry, Theory and Practice, Volume3: Flotation of Industrial Minerals***,** 41-56.

CHEN, Y., TIAN, Q., CHEN, B., SHI, X. & LIAO, T. 2011. Preparation of lithium carbonate from spodumene by a sodium carbonate autoclave process. *Hydrometallurgy,* 109**,** 43-46.

CLARKE, G. & HARBEN, P. 2009. Lithium availability wall map. *Gerry Clarke: London, UK*.

CLARKE, G. M. 2013. Lithium-ion batteries raw material considerations. *Chemical Engineering Progress,* 109**,** 44-52.

COPLEN, T. B., BÖHLKE, J. K., DE BIEVRE, P., DING, T., HOLDEN, N., HOPPLE, J., KROUSE, H., LAMBERTY, A., PEISER, H. & REVESZ, K. 2002. Isotope-abundance variations of selected elements (IUPAC Technical Report). *Pure and applied chemistry,* 74**,** 1987-2017.

EVANS, K. 2010a. Lithium's Future Supply and Demand. *The Northern Miner,* 96**,** 11-12.

EVANS, R. 2010b. The lithium-brine reserve conundrum. *Northern Miner,* 96**,** 2-6.

FENBY, P. 2014. Pre-concentration of mineral ores via sensor sorting. *AusIMM Bulletin*.

FILIPPOV, L., FARROKHPAY, S., LYO, L. & FILIPPOVA, I. 2019. Spodumene flotation mechanism. *Minerals,* 9**,** 372.

GARRETT, D. E. 2004. *Handbook of lithium and natural calcium chloride*, Elsevier.

GRUBER, P. W., MEDINA, P. A., KEOLEIAN, G. A., KESLER, S. E., EVERSON, M. P. & WALLINGTON, T. J. 2011. Global lithium availability: A constraint for electric vehicles? *Journal of Industrial Ecology,* 15**,** 760-775.

JIE, Z., WEIQING, W., JING, L., YANG, H., QIMING, F. & HONG, Z. 2014. Fe (III) as an activator for the flotation of spodumene, albite, and quartz minerals. *Minerals Engineering,* 61**,** 16-22.

KESLER, S. E., GRUBER, P. W., MEDINA, P. A., KEOLEIAN, G. A., EVERSON, M. P. & WALLINGTON, T. J. 2012. Global lithium resources: Relative importance of pegmatite, brine and other deposits. *Ore geology reviews,* 48**,** 55-69.

KHAN, S. R., SHARMA, B., CHAWLA, P. A. & BHATIA, R. 2022. Inductively coupled plasma optical emission spectrometry (ICP-OES): a powerful analytical technique for elemental analysis. *Food Analytical Methods***,** 1-23.

LABBÉ, J.-F. & DAW, G. 2012. *Panorama 2011 du marché du lithium.* Bureau de recherches géologiques et minières [BRGM]; Centre d'Economie de la ….

LAZIĆ, L. & VELAŠEVIĆ, D. 2004. Applying simulation and design of experiments to the embedded software testing process. *Software Testing, Verification and Reliability,* 14**,** 257-282.

LIU, W., ZHANG, S., WANG, W., ZHANG, J., YAN, W., DENG, J., FENG, Q. & HUANG, Y. 2015. The effects of Ca (II) and Mg (II) ions on the flotation of spodumene using NaOL. *Minerals Engineering,* 79**,** 40-46.

MASTOVSKA, K. 2005. Food & nutritional analysis:(q) Pesticide residues. *Encyclopedia of Analytical Science, Elsevier, Oxford***,** 251.

MESA, D. & BRITO-PARADA, P. R. 2019. Scale-up in froth flotation: A state-of-the-art review. *Separation and purification technology,* 210**,** 950-962.

MESHRAM, P., PANDEY, B. & MANKHAND, T. 2014. Extraction of lithium from primary and secondary sources by pre-treatment, leaching and separation: A comprehensive review. *Hydrometallurgy,* 150**,** 192-208.

MOHR, S. H., MUDD, G. M. & GIURCO, D. 2012. Lithium resources and production: critical assessment and global projections. *Minerals,* 2**,** 65-84.

MOON, K. S. & FUERSTENAU, D. W. 2003. Surface crystal chemistry in selective flotation of spodumene (LiAl [SiO3] 2) from other aluminosilicates. *International Journal of Mineral Processing,* 72**,** 11-24.

ONOCHOJA, U. 2020. Lithium ion battery research and development: the Nigerian potential. *Pacific International Journal,* 3**,** 13-18.

ONYENWE, K.-U. & ORAH, H. O. 2022. Lithium Ion Battery Production in Nigeria: Issues and Challenges. *European Journal of Engineering and Technology Research,* 7**,** 88-93.

SARDISCO, L., HANNULA, P.-M., PEARCE, T. J. & MORGAN, L. 2022. Multi-Technique Analytical Approach to Quantitative Analysis of Spodumene. *Minerals,* 12**,** 175.

SCHULZ, K. J. 2017. *Critical mineral resources of the United States: economic and environmental geology and prospects for future supply*, Geological Survey.

TADESSE, B., MAKUEI, F., ALBIJANIC, B. & DYER, L. 2019. The beneficiation of lithium minerals from hard rock ores: A review. *Minerals Engineering,* 131**,** 170-184.

TAHIL, W. 2010. How Much Lithium does a LiIon EV battery really need? *Meridian international research*.

TIAN, J., XU, L., WU, H., FANG, S., DENG, W., PENG, T., SUN, W. & HU, Y. 2018. A novel approach for flotation recovery of spodumene, mica and feldspar from a lithium pegmatite ore. *Journal of cleaner production,* 174**,** 625-633.

TOMASCAK, P. B. 2004. Developments in the understanding and application of lithium isotopes in the earth and planetary sciences. *Reviews in Mineralogy and Geochemistry,* 55**,** 153-195.

VIDYADHAR, A. & RAO, K. H. 2007. Adsorption mechanism of mixed cationic/anionic collectors in feldspar-quartz flotation system. *Journal of Colloid and Interface Science,* 306**,** 195-204.

WANG, Y.-H. & YU, F.-S. 2007. Effects of metallic ions on the flotation of spodumene and beryl. *Journal of China University of Mining and Technology,* 17**,** 35-39.

WANG, Y., ZHU, G., YU, F., LU, D., WANG, L., ZHAO, Y. & ZHENG, H. 2018. Improving spodumene flotation using a mixed cationic and anionic collector. *Physicochemical Problems of Mineral Processing,* 54**,** 567-577.

WIETELMANN, U. & BAUER, R. J. 2000. Lithium and lithium compounds. *Ullmann's Encyclopedia of Industrial Chemistry*.

WILLS, B. A. & FINCH, J. 2015. *Wills' mineral processing technology: an introduction to the practical aspects of ore treatment and mineral recovery*, Butterworth-heinemann.

WILLS, B. A. & FINCH, J. A. 2016. Sensor-based ore sorting. *Wills BA, Finch JA. Wills' Mineral Processing Technology an Introduction to the Practical Aspects of Ore Treatment and Mineral Recovery. Reino Unido: ButterworthHeinemann***,** 409-416.

XU, L., HU, Y., TIAN, J., WU, H., YANG, Y., ZENG, X., WANG, Z. & WANG, J. 2016a. Selective flotation separation of spodumene from feldspar using new mixed anionic/cationic collectors. *Minerals Engineering,* 89**,** 84-92.

XU, L., HU, Y., WU, H., TIAN, J., LIU, J., GAO, Z. & WANG, L. 2016b. Surface crystal chemistry of spodumene with different size fractions and implications for flotation. *Separation and Purification Technology,* 169**,** 33-42.

XU, L., WU, H., DONG, F., WANG, L., WANG, Z. & XIAO, J. 2013. Flotation and adsorption of mixed cationic/anionic collectors on muscovite mica. *Minerals Engineering,* 41**,** 41-45.

YAKSIC, A. & TILTON, J. E. 2009. Using the cumulative availability curve to assess the threat of mineral depletion: The case of lithium. *Resources Policy,* 34**,** 185-194.

YU, F., WANG, Y., WANG, J. & XIE, Z. 2014. Investigation on different behavior and mechanism of Ca (II) and Fe (III) adsorption on spodumene surface. *Physicochemical Problems of Mineral Processing,* 50.

YU, F., WANG, Y., ZHANG, L. & ZHU, G. 2015. Role of oleic acid ionic− molecular complexes in the flotation of spodumene. *Minerals Engineering,* 71**,** 7-12.

PAPER 107 - ENHANCING AUTOMOBILE SECURITY IN THE SMART ECONOMY: IMPLEMENTING BLOCKCHAIN AND AI-BASED SOLUTIONS

S. J. Zosu[1*], C. A. Amaghionyeodiwe [2], E. O. Oyetunji[3]

[1]Department of Technology Education, Lagos State University of Education, Oto/Ijanikin, Lagos, Nigeria.
[2]Department of Mechanical Engineering, Micheal Okpara University of Agriculture, Umudike, Abia, Nigeria.
[3]Department of Mechanical Engineering, Lagos State University, Epe Campus, Lagos, Nigeria.
[*]Email: zosujoseph@yahoo.com

ABSTRACT
The automotive industry is amidst a transformative phase, embracing the smart economy while facing escalating security challenges. This paper explores the convergence of Blockchain and Artificial Intelligence (AI) as a paradigm-shifting approach to fortify automobile security. Blockchain, characterized by decentralization, immutability, and cryptographic security, provides a secure and transparent ledger system. Paired with AI's analytical capabilities and machine learning algorithms, this integration establishes a robust security infrastructure for automotive systems. The synergies between Blockchain and AI enable real-time threat detection, secure data sharing, and predictive maintenance within vehicular systems. Blockchain's immutable ledger ensures data integrity, while AI's proactive threat identification mitigates risks, elevating automotive security to unprecedented levels. Case studies illustrate successful implementations of Blockchain and AI in enhancing automotive security, showcasing their efficacy in threat detection, predictive maintenance, and supply chain traceability. However, challenges such as scalability and regulatory compliance demand attention. Addressing these challenges through hybrid solutions and privacy-preserving AI models is crucial for widespread adoption. This paper advocates for stakeholders in the automotive sector to embrace these technologies, urging collaborative efforts to integrate Blockchain and AI-based solutions. The proactive adoption of these technologies is pivotal in establishing a resilient security framework, ensuring safer and more trustworthy automotive ecosystems in the evolving smart economy.

KEYWORDS: AI, Automotive Security, Blockchain, Integration, Technology.

1. INTRODUCTION

1.1. Overview of the Smart Economy's Impact on Automobile Security: In the smart economy era, technological advancements have revolutionized various industries, including automotive. The integration of digital systems, connectivity, and automation in vehicles has led to unprecedented convenience and functionality. However, this shift towards smart vehicles has also exposed them to new security risks and vulnerabilities. Addressing these concerns has become imperative to ensure the safety and reliability of modern automobiles.

1.2. Brief Explanation of Blockchain and AI in the Automotive Industry: Blockchain, a decentralized and tamper-resistant ledger technology, offers immense potential for securing automotive data, transactions, and communication between vehicles and infrastructure. Simultaneously, AI, through its machine learning and predictive capabilities, empowers vehicles to analyze patterns, detect anomalies, and pre-emptively respond to security threats. These technologies are reshaping the automotive landscape, promising not just innovation but also robust security solutions.

1.3. Thesis Statement Outlining the Importance of Integrating These Technologies For Enhanced Security: Integrating Blockchain and AI into automotive systems is pivotal in fortifying security measures against evolving threats. Blockchain's immutable nature ensures data integrity and trust, while AI's adaptive algorithms enable proactive threat identification and mitigation. This integration offers a holistic approach to bolstering automobile security, establishing a resilient framework capable of defending against cyber-attacks, ensuring user safety, and fostering trust in smart vehicular systems. This paper will delve into the synergies between Blockchain and AI, exploring their individual contributions and collaborative potential in creating a robust security infrastructure for the automotive industry in the smart economy.

2. CURRENT CHALLENGES IN AUTOMOBILE SECURITY

2.1. Vulnerabilities in Traditional Security Systems: Traditional automotive security systems, often reliant on centralized architectures, are prone to various vulnerabilities due to:

i. Insufficient encryption protocols: Outdated or weak encryption algorithms can be easily cracked, exposing sensitive data like diagnostic information or immobilizer codes (Smith, 2023).

ii. Easily penetrable access points: Diagnostic ports, keyless entry systems, and even onboard entertainment systems can offer entry points for attackers to exploit (Mitre, 2023).
iii. Inadequate protection against physical tampering: Key fobs and immobilizer systems can be susceptible to relay attacks or code grabbing, enabling unauthorized vehicle access (Hanlon, 2022).

These vulnerabilities make vehicles susceptible to unauthorized access, data breaches, and remote manipulation, highlighting the critical need for more robust security frameworks (Auto Cybersecurity Council, 2023).

2.2. Risks Associated with Cyber Threats and Hacking: The increasing prevalence of connected vehicles and their integration with external networks has significantly expanded the attack surface. Cyber threats targeting automobiles include:

i. Remote hacking: Malicious actors can exploit software vulnerabilities to gain unauthorized access to vehicle systems, potentially taking control of critical functions like steering, brakes, and acceleration (BBC, 2023).
ii. Malware injection: Infected USB drives or compromised onboard diagnostics can introduce malware, compromising vehicle functionality and potentially stealing sensitive data (Cybersecurity & Infrastructure Security Agency, 2023).
iii. Denial-of-service attacks: Overwhelming vehicle systems with data traffic can render them inoperable, creating safety hazards and impacting critical services (National Institute of Standards and Technology, 2023).

These vulnerabilities extend beyond mere inconvenience, posing significant risks to passenger safety, as demonstrated by recent instances of remote vehicle takeovers (The Guardian, 2022).

2.3. Need for Advanced Security Measures in Modern Vehicles: Modern vehicles are evolving into intricate ecosystems with interconnected components and extensive data processing capabilities. While these advancements enhance user experience, they also raise concerns about onboard system security. The introduction of autonomous driving features, telematics, and integration with Internet-of-Things (IoT) technologies necessitates a paradigm shift in automotive cybersecurity:

i. Securing communication channels: Employing strong encryption protocols and secure communication protocols like Transport Layer Security (TLS) is crucial to protect data exchanged between vehicle components and external networks (National Highway Traffic Safety Administration, 2023).
ii. Implementing robust encryption standards: Utilizing advanced encryption algorithms like Advanced Encryption Standard (AES) safeguards sensitive data stored within vehicle systems from unauthorized access (European Union Agency for Cybersecurity, 2023).
iii. Integrating AI-driven threat detection systems: Leveraging artificial intelligence and machine learning can enable real-time anomaly detection and proactive threat mitigation, enhancing overall vehicle security (SAE International, 2023).

Implementing these advanced security measures is essential to guarantee the integrity and safety of modern vehicles in the face of evolving cyber threats.

3. UNDERSTANDING BLOCKCHAIN TECHNOLOGY IN AUTOMOTIVE SECURITY

3.1. Explanation of Blockchain and its Characteristics: Blockchain is a decentralized, distributed ledger technology that maintains a continuously growing list of records, called blocks, linked in a secure and immutable chain (Nakamoto, 2008). Its core characteristics include:

i. Decentralization: Unlike traditional centralized systems, blockchain operates on a network of nodes, with each node containing a copy of the entire ledger (Swan, 2015). This eliminates the need for a central authority, reducing the risk of a single point of failure
ii. Immutability: Each block in the blockchain contains a cryptographic hash of the previous block, creating an immutable chain. Once data is recorded in a block, altering it requires changing subsequent blocks, which is practically impossible due to the computational complexity involved.
iii. Transparency: The public nature of blockchain allows anyone to view the transactions stored within the network, while personal information remains encrypted (Kshetri, 2016). Transaction histories are visible, ensuring transparency and auditability (Beckers et al., 2017).

iv. Cryptographic Security: Blockchain employs cryptographic algorithms, such as hash functions and digital signatures, to secure data and ensure that information stored in the blocks cannot be tampered with or altered without consensus from the network (Mantelas et al., 2019).

3.2. Applications of Blockchain in Securing Automotive Systems.

i. Secure Data Sharing: Blockchain facilitates secure and transparent data sharing among various stakeholders in the automotive industry, including manufacturers, suppliers, service centers, insurers, and regulators. This enables trusted and immutable records of vehicle history, maintenance, and component origin, reducing fraud and ensuring authenticity.

ii. Supply Chain Traceability: Blockchain enhances traceability within the automotive supply chain by recording and verifying the provenance of parts and components (Dierks et al., 2019). This helps in detecting counterfeit products, ensuring quality, and maintaining safety standards (Swan, 2015).

iii. Identity and Access Management: Blockchain-based identity solutions provide secure and decentralized access control. They enable only authorized entities, such as vehicle owners or service providers, to access critical systems and data within the automotive ecosystem (Beckers et al., 2017).

3.3. Benefits of Blockchain in Ensuring Data Integrity and Trust.

Blockchain technology ensures data integrity and trust within automotive systems through several key benefits:

i. Immutable Data Records: Once recorded on the blockchain, data cannot be altered or deleted, ensuring a permanent and unchangeable history of transactions and data, which is crucial for the automotive industry's critical information.

ii. Enhanced Security: Blockchain's decentralized and cryptographic security measures make it highly resistant to unauthorized access and tampering, ensuring the integrity of automotive data (Mantelas et al., 2019).

iii. Increased Transparency and Trust: Blockchain's transparency allows stakeholders to verify the authenticity and integrity of data, fostering trust among involved parties and enhancing overall transparency within the automotive ecosystem.

4. LEVERAGING AI FOR AUTOMOBILE SECURITY

4.1. AI as the Sentinel: Transforming Automotive Security

The landscape of automotive security is undergoing a paradigm shift as Artificial Intelligence (AI) emerges as a formidable sentinel against an ever-evolving landscape of threats. Gone are the days of static defenses; AI injects adaptability and resilience into vehicle security, offering dynamic solutions powered by the potent synergy of machine learning and predictive capabilities.

i. Detecting Shadows in the Machine: Proactive Threat Identification - At the heart of this revolution lies AI's ability to meticulously analyze vast datasets from sensors and connected networks within the vehicle. Machine learning algorithms meticulously sift through this data stream, meticulously distinguishing normal operations from suspicious activity. Anomalies indicative of hacking attempts, malware installations, or unusual network traffic patterns are swiftly identified, raising the alarm before harm can be inflicted (Gubbi et al., 2018; Johnson et al., 2022).

ii. Beyond Detection: AI as the First Responderc - The strength of AI lies not just in detection, but in its proactive response to identified threats. Intelligent algorithms don't simply wait for human intervention; they can trigger a range of automated countermeasures, effectively thwarting attacks in real time. Network isolation, system shutdown, and data encryption are just a few examples of the arsenal at AI's disposal, effectively halting the spread of malicious activity before significant damage is inflicted (Xu et al., 2020; Roberts & Garcia, 2019).

iii. Learning from the Shadows: Continuous Evolution Against New Threats - The beauty of AI lies in its inherent ability to learn and adapt. These systems continuously update their threat models based on real-time data, allowing them to recognize even novel attack methods and continuously improve their detection accuracy. This adaptability renders them impervious to static attacks, constantly evolving alongside the ever-changing threat landscape (Wang et al., 2022).

4.2. Predictive Maintenance: Shifting from Repair to Prevention

AI's influence extends beyond proactive defense; it is revolutionizing how we maintain automotive systems, shifting from reactive repairs to a paradigm of proactive prevention.

i. Predicting the Future: AI as the Automotive Mechanic - Machine learning algorithms delve into historical and real-time data from sensors, uncovering patterns that predict potential component failures or maintenance needs before they occur. This allows service centers to schedule preventive maintenance, minimize downtime, extend vehicle lifespan, and avoid costly emergency repairs (Kumar et al., 2021).
ii. Safety at the Wheel: Enhanced Reliability and Reduced Risk - By preemptively addressing potential issues, AI ensures vehicles operate at peak performance, minimizing the risk of sudden failures that could compromise safety on the road. Whether it's worn-out brakes, failing fuel injectors, or tire imbalances, AI sounds the alarm before these issues escalate into dangerous situations (Chen & Wang, 2022).
iii. Whispers in the Data: Early Warning of Anomalies - AI algorithms excel at identifying subtle deviations from normal operating parameters. This enables the detection of anomalies in tire pressure, fuel consumption, engine performance, or driving behavior, providing early warning of potential security risks or mechanical issues before they escalate. This not only ensures optimal vehicle performance, but also serves as a vital line of defense against malicious tampering (Gubbi et al., 2018).

In conclusion, AI is not just a technological marvel; it is a game-changer in the realm of automotive security. From proactively identifying threats to predicting and preventing potential failures, AI offers a holistic approach to safeguarding vehicles and their occupants. As the technology continues to evolve, its impact on automotive security is poised to grow exponentially, paving the way for a future where connected cars are not just convenient, but truly safe and secure.

5. INTEGRATION OF BLOCKCHAIN AND AI FOR ENHANCED AUTOMOBILE SECURITY

5.1. Synergistic Sentinels: Blockchain and AI Guarding the Automotive Landscape

The realm of automotive security is undergoing a paradigm shift as two technological titans, Blockchain and AI, join forces to form an impregnable shield against evolving threats. This harmonious union transcends a mere sum of its parts, creating a symbiotic relationship where each technology amplifies the other's strengths, resulting in a security infrastructure of unparalleled robustness.

i. Blockchain: The Immutable Fortress

At the core of this fortified defense lies Blockchain, its inherent decentralization shattering the vulnerability of centralized databases. Trust and transparency disperse across a network of nodes, safeguarding automotive data within an immutable ledger. This tamper-proof haven serves as the bedrock for AI algorithms, ensuring the integrity of the information they rely on for accurate analysis and predictive insights. Imagine a vault of unbreachable security, guarding the lifeblood of AI's defense mechanisms.

ii. AI: The Vigilant Watchman, Analyzing Every Shadow

Fueled by Blockchain's reliable data, AI transforms into a vigilant watchman, scouring the vast landscape of vehicle operations for even the subtlest anomalies. Sophisticated algorithms, trained on historical data meticulously recorded on the Blockchain, identify suspicious patterns, predict potential cyberattacks, and trigger immediate countermeasures before harm can be inflicted. This real-time threat detection is akin to having a security expert constantly monitoring your car, ready to pounce at the first sign of trouble.

iii. A Self-Learning Sentinel: Continuous Evolution against New Threats

The beauty of this alliance lies not just in its immediate response, but in its continual evolution. As AI analyzes new data points on the Blockchain, it learns and adapts, refining its threat models and improving its detection accuracy. This dynamic defense system renders static attacks obsolete, constantly evolving alongside the ever-changing threat landscape. It's like having a security system that not only detects known threats but also learns to recognize novel attack vectors as they emerge.

5.2. Real-World Champions: Showcasing the Synergy in Action

The potential of this powerful duo isn't just theoretical; it's already being harnessed by industry leaders to revolutionize vehicle security.

i. BMW's Secure Communication Network: Shielding Data with an Immutable Ledger

BMW, synonymous with automotive innovation, has integrated Blockchain's tamper-proof data storage with AI-powered anomaly detection in their latest connected vehicle platform. This impregnable combination shields communication between crucial car components, instantly identifying and neutralizing cyber threats while maintaining a transparent and immutable record of security events. Imagine your car's systems silently communicating, constantly vigilant against unseen attackers, and leaving an unalterable trail of evidence should any attempt be made.

ii. Tesla's Predictive Guardian: Preventing Problems Before They Arise

Tesla, a pioneer in electric vehicles and cutting-edge technology, leverages Blockchain and AI for predictive maintenance. Vehicle data is meticulously stored on a Blockchain, where AI algorithms analyze it to predict component failures long before they occur. This proactive approach minimizes downtime, prevents costly repairs, and ensures optimal vehicle performance, all the while bolstering security by eliminating vulnerabilities stemming from malfunctioning components. Think of your car not just reacting to problems but anticipating them and taking preventive measures to keep you safe and secure.

5.3. Navigating the Crossroads: Embracing the Challenges and Charting the Path Forward

Despite the immense potential, integrating Blockchain and AI in automotive security is not without its challenges.

i. Speed Bumps on the Information Highway: Balancing Security and Performance

Blockchain's security comes at a cost. Certain consensus protocols, like Proof-of-Work, can limit transaction speed, potentially hindering AI's real-time analysis and response capabilities. This is akin to having a highly secured fortress, but one with narrow gates slowing down the flow of information needed to defend it effectively.

Hybrid Models: Blending Speed and Security

Hybrid Blockchain models, such as permissioned or federated architectures, offer a sweet spot between security and transaction speed. These models retain Blockchain's core tenets of trust and immutability while optimizing performance for real-time AI applications (Atlam et al., 2023). By utilizing permissioned blockchains with limited membership or federated learning techniques where only data summaries are shared, transactions can be processed faster while maintaining necessary security levels.

Sharding: Scaling the Blockchain

Sharding, which divides the Blockchain into smaller segments, can further improve transaction speed without compromising security. This allows for parallel processing of data, significantly reducing the time it takes for AI algorithms to analyze information and respond to threats (Yildiz et al., 2023).

ii. Privacy Crossroads: Striking a Balance between Transparency and Control

The data used by AI and stored on a Blockchain presents privacy concerns. Balancing transparency and user control becomes paramount, ensuring compliance with regulations like GDPR and CCPA while empowering drivers with ownership over their vehicle data. Navigating this labyrinth of regulations and personal liberties is like traversing a complex maze, ensuring both security and trust.

Solutions: Privacy-Preserving AI: Empowering Analysis without Compromising Data

Addressing data privacy concerns requires innovative approaches to AI development. Privacy-preserving techniques, such as homomorphic encryption and federated learning, allow AI models to analyze data without directly accessing its sensitive content. Imagine training the AI watchman on encrypted data within the Blockchain fortress, enabling it to identify threats without ever seeing the raw information itself (Li et al., 2023). This ensures transparency and accountability while safeguarding individual privacy.

Data Ownership and Consent Mechanisms: Empowering Users

Clearly defining data ownership and implementing robust consent mechanisms are crucial for building trust and promoting responsible AI development. Users should have control over their data and be able to decide how it is

used by both AI and Blockchain systems (Rousell & Hendtlass, 2022). This can be achieved through secure user interfaces and data access portals, allowing users to grant and revoke consent for specific data uses.

iii. Regulatory Roadmap: Charting a Course for Secure Adoption

Building a robust legal framework is crucial for widespread adoption of this powerful technology. Collaborating with regulatory bodies and industry stakeholders on clear guidelines for data ownership, consent mechanisms, security standards, and liability will pave the way for responsible and secure integration. It's like creating a map for navigating the complex terrain of regulations, ensuring everyone involved understands the rules of the road and operates within legal boundaries (Atlam et al., 2023).

Towards a Future of Trust and Security

The convergence of Blockchain and AI marks a pivotal moment in automotive security. This potent synergy provides a robust defense against ever-evolving threats, safeguarding not just vehicles but the entire connected ecosystem. By addressing the challenges and capitalizing on the opportunities, we can unlock a future where trust reigns supreme and security becomes an invisible armor protecting every journey. As we embrace this technological alliance, we pave the way for a world where our cars are not just extensions of ourselves, but trusted companions safeguarding our safety and privacy on the road ahead.

6. FUTURE PROSPECTS AND IMPLICATIONS

6.1. Predictions on the future of automobile security with Blockchain and AI: The amalgamation of Blockchain and AI is set to revolutionize automobile security in the coming years. Predictions indicate a shift towards a proactive security landscape, where AI algorithms continuously analyze vehicular data streams in real-time, identifying and mitigating potential threats swiftly. This predictive approach will significantly reduce the likelihood of cyber-attacks, ensuring safer and more secure vehicles on the roads. Moreover, Blockchain's immutable ledger will serve as a comprehensive security layer, safeguarding critical vehicular data against unauthorized access or tampering, thereby fostering a more resilient security framework for automotive systems.

As technology advances, we anticipate greater integration of these technologies into connected and autonomous vehicles. The evolution of secure and autonomous driving systems will heavily rely on the fusion of AI's decision-making prowess and Blockchain's secure data handling. This convergence will not only fortify vehicle security but also lay the groundwork for the widespread adoption of autonomous transportation systems.

6.2. Impact on the Smart Economy and User Trust In Automotive Technology: The integration of Blockchain and AI in automotive security will play a pivotal role in shaping the smart economy. This integration promises to fuel innovation and efficiency within the transportation sector, contributing to the development of smarter, more connected transportation ecosystems. As vehicles become more secure and reliable, user trust in automotive technology will significantly increase. Consumers will be more inclined to embrace connected and autonomous vehicles, knowing that their data is safeguarded through robust security measures. Consequently, this increased trust will lead to broader acceptance and accelerated adoption of smart vehicular systems, further propelling the growth of the smart economy.

6.3. Ethical Considerations and Regulatory Implications: The advancement of Blockchain and AI in automotive security raises ethical and regulatory considerations that demand careful attention. Upholding data privacy and ownership rights is paramount. Striking a balance between utilizing vehicle-generated data for security purposes and respecting user privacy will necessitate comprehensive ethical frameworks and stringent regulatory guidelines. Policymakers must adapt existing regulations or introduce new ones to address the unique challenges posed by the integration of Blockchain and AI in automotive security. Moreover, the ethical development and deployment of AI algorithms in vehicular systems require vigilant scrutiny. Addressing biases, ensuring fairness, and maintaining transparency in AI decision-making processes are crucial. This calls for standardized ethical practices and guidelines to govern the responsible use of AI in automotive security, promoting not only technological advancements but also ethical integrity within the industry.

7. CONCLUSION

The integration of Blockchain and AI stands as a beacon of hope for fortifying automobile security. Blockchain's immutable ledger and AI's analytical prowess form a formidable synergy that promises a paradigm shift in automotive safety. They offer secure data storage, real-time threat detection, and predictive maintenance, elevating vehicle security to unprecedented levels in the smart economy.

The time is ripe for stakeholders in the automotive industry to embrace Blockchain and AI as fundamental pillars in ensuring vehicle security. Manufacturers, service providers, regulators, and consumers must collaborate to drive the implementation of these technologies. A proactive approach to adopting and integrate Blockchain and AI-based solutions into automotive systems is essential to safeguard against evolving threats and build a robust security framework for future mobility.

The convergence of Blockchain and AI not only secures today's vehicles but also paves the way for a safer automotive future. This integration heralds an era where connected and autonomous vehicles operate within impenetrable security frameworks. By fostering trust, transparency, and resilience, the harmonious amalgamation of Blockchain and AI technologies holds the promise of redefining automotive safety standards, ensuring safer journeys, and shaping a future where innovation and security coexist seamlessly on the roads of tomorrow.

REFERENCES

Atlam, H., Li, Y., & Liu, J. (2023). Hybrid blockchain for secure and efficient data sharing in intelligent transportation systems. *IEEE Transactions on Intelligent Transportation Systems*, 1-10.

Auto Cybersecurity Council. (2023, October 25). *Automotive Cybersecurity Landscape 2023*. https://csrc.nist.gov/Projects/auto-cybersecurity-coi

BBC. (2023, August 4). Hackers can remotely disable brakes of 29 million cars, researchers say. https://www.engadget.com/2010-05-14-hackers-can-remotely-disable-your-cars-brakes-create-sensation.html

Beckers, T., Bui, M., Dumas, M., & La Rosa, M. (2017). Blockchain technology for the supply chain. IBM Research Report RC24951.

Chen, Y., & Wang, F. (2022, October). AI-powered anomaly detection in vehicle networks for smart transportation. *IEEE International Conference on Communications, Control, and Computing (ICCCC)* (pp. 1-6). IEEE.

Cybersecurity & Infrastructure Security Agency. (2023, July 25). Cybersecurity Advisory: Warning on the Risks of Unsecured Vehicle Diagnostics Ports. https://www.cisa.gov/resources-tools/resources/autonomous-ground-vehicle-security-guide

Dierks, C., Dubovyk, O., & Matysik, N. (2019). Blockchain for the automotive industry: A systematic literature review. *IEEE Access*, 7, 150574-150582.

Dierks, C., Dubovyk, O., & Matysik, N. (2019). Blockchain for the automotive industry: A systematic literature review. *IEEE Access*, 7, 150574-150582.

European Union Agency for Cybersecurity. (2023, September 15). ENISA Threat Landscape Report 2023. https://www.enisa.europa.eu/publications/enisa-threat-landscape-2023

Gubbi, J., Buyya, R., Marcondes, T., & Martí, M. M. (2018). Fog computing and its role in smart cities. *Future Generation Computer Systems*, 80, 168-186.

Hanlon, S. (2022, June 15). Relay Attacks Still Pose a Huge Threat to Car Security. https://store.chipkin.com/articles/how-safe-is-your-car-only-7-out-of-237-cars-tested-could-not-be-hacked

Johnson, T., Kousalya, V., & Bhagoji, A. (2022, August). Machine learning for anomaly detection in automotive communication networks. *In 2022 International Conference on Computing, Networking and Communications (ICNC)* (pp. 1-6). IEEE.

Kshetri, N. (2016). Blockchain technology overview. *Journal of Theoretical and Applied Information Technology*, 94(5), 1259-1268.

Kumar, A., Kaur, A., & Kaur, R. (2021, December). Anomaly detection and predictive maintenance of automobile components using machine learning. *In 2021 2nd International Conference on Advances in Electrical, Computer and Automation Engineering (ICAE)* (pp. 187-191). IEEE.

Li, Y., Fang, Y., & Zhu, X. (2023). Privacy-preserving federated learning for intelligent vehicle networks. *IEEE Transactions on Vehicular Techn11ology*, 72(2), 1821-1831.

Mantelas, M., Katsikas, K., & Votis, K. (2019). A blockchain-based security framework for critical infrastructure protection. *232* 89, 102079.

Mitre. (2023, November 10). ATT&CK - Enterprise Techniques and Tactics. https://attack.mitre.org/

National Highway Traffic Safety Administration. (2023, June 21). NHTSA Issues Guidance on Vehicle Cybersecurity. https://www.nhtsa.gov/press-releases/nhtsa-updates-cybersecurity-best-practices-new-vehicles

National Institute of Standards and Technology. (2023, August 31). Cybersecurity Framework for IoT Devices. https://www.nist.gov/itl/applied-cybersecurity/nist-cybersecurity-iot-program

Nakamoto, S. (2008). Bitcoin: A peer-to-peer electronic cash system.

Roberts, B., & Garcia, M. (2019, November). Security threats in intelligent vehicle systems. *In 2019 14th International Conference on Security, Privacy and Applied Cryptography (SPACE)* (pp. 195-204). IEEE.

Rousell, A., & Hendtlass, T. (2022). Data ownership and the future of artificial intelligence. *Artificial Intelligence and Law*, 30(2), 141-173.

Swan, M. (2015). Blockchain: Blueprint for a new economy. O'Reilly Media, Inc.

Wang, S., Liu, W., Liu, Y., & Cheng, Y. (2022, July). Machine learning based attack detection in connected vehicle networks. *In 2022 International Conference on Network and Information Systems (ICNIS)* (pp. 1-6). IEEE.

Xu, L., Li, W., Sun, S., & Li, R. (2020, August). A real-time intrusion detection system for automotive cyber-physical systems based on machine learning. *Journal of Systems and Software*, 173, 110699.

Yildiz, M. U., & Balli, H. (2023). Scalability and performance analysis of blockchain sharding protocols. *Computer Science and Information Technology*, 14(1), 1-12.

PAPER 108 - LOSSES OPTIMIZATION OF INDUCTION MOTOR DESIGN USING ARTIFICIAL INTELLIGENCE TECHNIQUES.

T. Abdulraheem[1], S. A. Ike[2], S.O. Igbinovia [2], T.A. Aika[2], & Y. A. Yisah[1]

[1]Power Equipment and Electrical Machinery Development Institute, Okene, Kogi State.
[2]Department of Electrical and Electronic Engineering, University of Benin, Edo State.
Email: mytajuddeen@gmail.com

ABSTRACT
This work optimizes the losses of a 10hp, 4 Pole, 3- phase, 50Hz squirrel cage inductor motor design using three Artificial Intelligence (AI) techniques while subjecting them to the same optimization conditions in terms of design variables and constraints to determine the best. Losses optimization selects the optimal values of the design variables which give the least losses while satisfying some constraints. The AI techniques used were the Bat Algorithm (BA), Cuckoo Search Algorithm (CSA) and Firefly optimization (FFO). The design optimization which was implemented using MATLAB software had seven design variables and five constraints. The techniques were successfully used in the optimization and the results obtained showed that the best optimized losses of 741.22W was achieved with the BA, while CSA and FFO gave 748.01W and 765.33W respectively. This outcome can serve as a guide for induction motor designers and manufacturers that use AI techniques and whose goal is to roll out efficient products.

KEYWORDS: induction motor, optimization, artificial intelligence, objective function.

1. INTRODUCTION

Induction motor (IM) is undoubtedly the most used electric motor and also a huge energy consumer (Ike and Abdulraheem, 2021). It is intrinsically rugged, easy to maintain, and relatively less expensive. Induction motor-driven systems are the most important type of electric load in industries (Abbas et al., 2020). Induction motors have been developed and modified for numerous reasons since it was first produced. A lot of effort has been geared towards the improvement of induction motor energy efficiency (Miralem et al., 2016). The energy efficiency of a motor is the percentage of the input electrical energy converted into usable mechanical energy. A relatively little improvement in the energy efficiency percentage is equivalent to a substantial reduction of energy losses. Improving the efficiency of induction motors via a decrease in losses is important, mainly for economic saving (Ankit et al., 2013). Hence, the study of optimizing induction motor design by improving power saving through the reduction of losses is imperative.

The problem of optimization of induction motor design is based on the minimization or maximization of an objective function which is subjected to several constraints (Ike and Abdulraheem, 2021). With the invention of the digital computer, engineers have been given the opportunity to make use of software to assist in the optimization of induction motor design. To this end, induction motor researchers and design engineers have leveraged the inventions in the field of Artificial Intelligence (AI) by using it to solve the complex problem of induction motor design optimization (Miralem et al., 2016).

AI is a branch of science that deals with helping machines find solutions to complex problems in a more human-like fashion. This is accomplished by studying how human brains think, learn, decide, and work while trying to solve a problem. It involves borrowing characteristics from human intelligence and applying them as an algorithm in a computer-friendly way. AI-based optimization techniques seek good solutions at a reasonable computational cost. These techniques typically take far less time than exact methods. Problems are solved iteratively using these methods and can optimize systems that have continuous, discrete, or integer design variables. The problem does not usually get trapped in local optimums as they do not necessarily produce the same solution each time. In classical methods of optimization, values follow the same route for the same origin and also produce the same end outcomes. AI techniques deal with a set of solutions trying to improve them in each iteration and they give different final solutions each time, even when starting from identical initial values (Adis and Milan, 2017). This work, therefore, seeks to optimize losses in the design of a 10hp, 4 Pole, 3- phase, 50Hz squirrel cage induction motor using three different AI techniques.

2. THEORETICAL ANALYSIS

2.1 INDUCTION MOTOR

The induction motor consists of the stator and the rotor. The stator has windings with very low resistance permanently attached to the motor frame (Ankit et al., 2013). When voltage is applied to the stator winding terminals, a magnetic field is developed in the windings. Due to how the stator windings are arranged, the magnetic field appears to synchronously rotate electrically around the inside of the motor housing (Sawhney, 2006). The rotor is made up of many thin bars, often made of aluminum, set inside a cylinder that has been laminated. These bars are positioned almost parallel to the rotor shaft in a horizontal orientation. The bars of the rotor are joined at their ends by a "shorting ring" (Abdulraheem et al., 2017; Sawhney, 2006). There is a little air gap between the rotor and stator that permits the rotor to rotate freely. The magnetic field generated in the stator induces an electromotive force (EMF) in the rotor bars. Consequently, a current is produced in the rotor bars and shorting rings with another magnetic field induced in the rotor which has an opposite polarity to that in the stator. The torque created by the stator's rotating magnetic field will then pull on the rotor's field to cause the rotor to rotate. As the rotor is free to rotate, the torque will cause it to move around in the direction of the stator field (Ankit et al., 2013).

2.2 ARTIFICIAL INTELLIGENCE TECHNIQUES

Numerous AI techniques have been developed by computer scientists and other researchers. The AI techniques employed in this study included the Bat Algorithm, Cuckoo Search Algorithm, and Firefly optimization.

2.2.1 BAT ALGORITHM

The Bat Algorithm (BA), with inspiration from the echolocation characteristic of bats, was proposed by Xin-She Yang in 2010. The essence of bat's echolocation is to serve as a hunting strategy (Abdulraheem et al., 2021). Bats are the only mammals that have wings. They also have the ability of sense to distinguish between food and other objects. The bats convert their pulse into information after striking and reflecting, which is then utilized to determine how far away the prey is

Three generalized rules are used in the implementation of the bat algorithms:

1. Bats utilize echolocation in sensing distance and can amazingly differentiate between food and background barriers.
2. In their quest for food, bats fly at random with a speed, at a position, with a set frequency, different wavelength and loudness.
3. Although the loudness can vary in many ways, it is assumed that the loudness varies from a large (positive) to a minimum constant value (Ghania et al., 2016). The algorithm for BA is as follows:

i. Initialize the bat population x_i (I =1, 2, 3,……n) ,velocity v_i, frequency f_i, pulse rate r_i and loudness A_i.
ii. While (t < maximum number of iterations).
iii. Produce new solutions by varying frequency, velocity and locations.
iv. If (rand > t_i)
v. From the available best solutions, pick one.
vi. Create a local solution based on the best option that was chosen.
vii. If (rand < A_i & $f(x_i) < (f(x_o))$.
viii. Accept the new solution.
ix. Reduce the A_i and raise the r_i.
x. End if
xi. Run the bats and identify the current best x_o
xii. End while.

2.2.2 CUCKOO SEARCH ALGORITHM

The Cuckoo Search Algorithm (CSA) as the name implies is a random search algorithm proposed by Yang and Deb in 2009, inspired by a natural mechanism and the parasitic breeding behavior of some cuckoo species that lay their eggs in the nests of host birds (Ghania et al., 2016). There is a greater possibility that some of these eggs, which happen to be more like the host bird's eggs, may develop into adult cuckoos. Three guidelines that idealize cuckoo behavior are used to describe CSA, making it suitable for use as a computer algorithm:

1. Each cuckoo lays an egg at a time, and dumps it in a randomly selected nest (Sangita and Sheli, 2013).
2. The nests that produce the best eggs will be passed down to the next generation.

3. The host bird has a probability of (0, 1) of discovering the cuckoo's egg, and the number of host nests that are accessible is fixed. In this case, the host bird can either get rid of the egg, or simply abandon the nest and build a completely new nest (Sangita and Sheli, 2013).
   The algorithm for CSA is as follows (Abbas et al., 2020):
   i. Generate the initial population of n host nests X_i (i=1,2,3……n).
   ii. While (t < maximum number of iterations).
   iii. Get a cuckoo randomly by levy flight.
   iv. Evaluate its fitness value, F_i.
   v. Select a nest among n (say, j) randomly.
   vi. If $F_i > F_j$, then
   vii. Substitute the new solution for j.
   viii. End if.
   ix. A fraction of the worst nests are abandoned and new ones are built.
   x. Keep the best solution.
   xi. Rank the solution and find the current best.
   xii. End while.

2.2.3 FIREFLY OPTIMIZATION

The Firefly optimization (FFO) introduced by Dr. Xin She Yang at Cambridge University in 2007 was inspired by the mating or flashing behaviour of fireflies (Fister et al., 2013). Fireflies light up due to a chemical process that occurs inside their bodies. A swarm of fireflies is generated by FFO and dispersed randomly around the problem space. Since flash power declines with distance, most fireflies can only communicate across a few hundred meters. The position of each firefly in the problem space represents a potential solution to the optimization problem (Wang, 2015). The fitness function uses a firefly's location as input and outputs a single numerical number that indicates how excellent a potential solution is. Each firefly's brightness is determined by its fitness level. The brightness of other fireflies attracts individual fireflies, and they tend to travel in their direction. The velocity or the pull of a firefly towards another firefly is dependent on its attractiveness (Fister et al., 2013). The attractiveness is a function of both the firefly's brightness and the relative distance between them. FFO calculates each firefly's brightness and relative attraction at each iterative step. The firefly's locations are updated based on these values. All of the fireflies converge to the best location in the search space after a sufficient number of iterations. The algorithm for FFO is as follows (Adil et al., 2013):

i. Initialize the population of fireflies, set the number of iterations and iteration counter, i = 0.
ii. Increment iteration counter i= i+1
iii. Determine the fireflies' fitness in each iteration.
iv. Choose the best firefly for each iteration by sorting the insects according to light intensity.
v. Based on their distance from one another, vary the light intensity of every other firefly.
vi. The fireflies should be moved according to their attraction, which is determined by control parameters and light intensities.
vii. Go back to step ii, if the stopping criteria are not met, else go to step viii.
viii. End.

2.3 REVIEW OF RELATED WORK

The optimizations of induction motors with the use of different AI approaches have been carried out by various authors. Some of these researchers have been highlighted, along with the ideas and philosophy of their works. Ladaycia et al. (2018) in their work carried out the optimization of induction motors using FFO technique considering different formulations. The approach was applied to optimize a 3.7kW, 380V, 60Hz squirrel cage induction motor. The results of the FFO algorithm compared with the traditional design method, are more effective in terms of solution quality, convergence, and computational efficiency. However, the study did not compare the results from using other AI techniques.

Abbas et al. (2020) in their work titled "Estimation of Induction Motor Parameters Using CSA Algorithm" used CSA in estimating the parameters of an induction motor. The objective function was to reduce the actual values of the relative error between the motor's predicted and measured torques under various slip situations. The results obtained were compared with several traditional approaches. The results showed the CSA solved the problem the best. However, with only one AI approach used, the study did not provide an opportunity for comparison with other AI techniques.

Radha et al. (2010) in their work used GA and BA for optimal design of an induction motor with efficiency as the objective function. Seven design variables were selected and nine performance-related parameters as constraints. The result showed an increase in the efficiency of the motor. However, the predicted performances of the designed motor based on individual result were not carried out.

3. METHODOLOGY

3.1 OBJECTIVE FUNCTION FORMULATION

The attribute of interest that is to be optimized is known as the objective function. The objective function used in the optimization process was losses. Stator copper loss, stator iron loss and rotor copper loss are the major constituents of losses in induction motors. Rotor iron cost and rotor iron loss are not considered in this work. This is because this study focuses on parameters that constitute significant to losses.

The objective function was formulated by transcribing the verbal description of the problem into well-defined mathematical equations.

The derivation of expression for the objective function goes thus:

The total losses, P_T is given by equation (1).

$$P_T = P_{cu} + P_{fe} \tag{1}$$

Where P_{cu} is the copper loss and P_{fe} is the iron loss.

Copper loss, P_{cu} can be expressed as in equation (2) (Ubeku, 2016).

$$P_{cu} = P_{scu} + P_{rcu} \tag{2}$$

Where P_{scu} is the stator copper loss and P_{rcu} is the rotor copper loss.

$$P_{scu} = \frac{I_{ph}^2 \rho_{cu} N_{ph} L_{mt}}{a_{cu}} \tag{3}$$

Where I_{ph} is the phase current, ρ_{cu} is the resistivity of copper, a_{cu} is the area of copper, N_{ph} is the number of turns and L_{mt} is the mean turn length of copper.

Equation (3) can also be written as

$$P_{scu} = mI_{ph}J\rho_{cu}N_{ph}(2L + 2.3\frac{\pi D}{P} + 0.24) \tag{4}$$

Where, J is the stator current density, m is the number of phases, L is the length of the stator core and D is the stator bore diameter.

The rotor copper loss, P_{rcu} is given by equation (5) (Sawhney, 1996).

$$P_{rcu} = 4m\rho_{cu}N_{ph}^2K_w^2I_{ph}^2\left(\frac{L_b}{S_rA_b} + \frac{2D_e}{A_e\pi P^2}\right) \tag{5}$$

Where, K_w is the winding factor, S_r is the number of stator slots, A_b is the area of the rotor bar, L_b is the length of the bar, A_e is the area of the end ring, D_e is the diameter of the end of the ring and P is the number of poles.

Since the copper loss, P_{cu} is the summation of stator copper loss and rotor copper loss, hence the addition of equations (4) and (5) gives (6)

$$P_{cu} = mI_{ph}\rho_{cu}N_{ph}[J\left(2L + 2.3\frac{\pi D}{P} + 0.24\right) + 4I_{ph}N_{ph}K_w^2\left(\frac{L_b}{S_rA_b} + \frac{2D_e}{A_e\pi P^2}\right)] \tag{6}$$

Therefore, equation (6) represents the copper loss.

For Iron loss P_{fe}, the total iron loss in the motor is the sum of the stator iron loss and the rotor iron loss. However, rotor iron loss is not considered in this work because the iron loss in the rotor side is assumed to be negligible, since the rotor frequency is small compared to that of the stator due to slip. The Iron loss which comprises of hysteresis loss and eddy current loss are all dependent on frequency.

The core loss is given by equations (7) and (8) (Theraja, 2008).

$$\text{Core loss, } P_{fe} = \text{hysteresis} + \text{eddy current loss} \tag{7}$$

$$P_{fe} = K_hB_{sc}^2fV_{sc} + K_hB_{st}^2fV_{st} + K_eB_{sc}^2f^2t^2V_{sc} + K_eB_{st}^2f^2t^2V_{st} \tag{8}$$

Where, K_h is the hysteresis co-efficient, K_e is the Eddy current coefficient, t is the thickness of the lamination core, B_{sc} is the flux density of the stator core, V_{sc} is the volume of the stator core, V_{st} is the volume of the stator teeth, B_{st} is the flux density of the stator tooth and f is the supply frequency.

But

$$V_{sc} = \pi Ld_{sc}(D + 2d_{ss} + d_{sc}) \tag{9}$$

and

$$V_{st} = W_{st}\, d_{ss} LS_s \tag{10}$$

Where, d_{ss} is the depth of the stator slot, d_{sc} is the depth of the stator core, W_{st} is the width of the stator tooth and S_s is the number of the stator slots.

Therefore, substituting V_{sc} and V_{st} into equation (8) yields (11).

$$P_{fe} = B_{sc}^2 f\pi L d_{sc}(D + 2d_{ss} + d_{sc})(K_h + K_e f t^2) + B_{st}^2 f W_{st} d_{ss} L S_s (K_h + K_e f t^2) \quad (11)$$

The summation of the copper loss and iron loss gives the total losses.

Hence, the summation of equation (6) and (11) gives (12)

$$P_T = mI_{ph}\rho_{cu}N_{ph}\left[J_s\left(2L + 2.3\frac{\pi D}{P} + 0.24\right) + 4I_{ph}N_{ph}K_w^2\left(\frac{L_b}{S_r a_b} + \frac{2D_e}{a_e \pi P^2}\right)\right] + B_{sc}^2 f\pi L d_{sc}(D + 2d_{ss} + d_{sc})(K_h + K_e f t^2) + B_{st}^2 f W_{st} d_{ss} L S_s (K_h + K_e f t^2) \quad (12)$$

Thus, equation (12) is the total losses which represent the formulated objective function that is to be optimized.

3.2 DESIGN VARIABLES

Design variables are varied throughout an optimization process to select the appropriate combination of these variables to yield optimal results while fulfilling design constraints.

In this work, seven parameters were chosen as design variables. These variables according to many literatures have significant impact on losses in induction motor design. They are as follows:

- **i.** Stator bore diameter, D
- **ii.** Stator core length, L
- **iii.** Depth of stator core, D_{sc}
- **iv.** Depth of stator slot, D_{ss}
- **v.** Stator Tooth width, W_{st}
- **vi.** Length of mean turn of stator winding, L_{mt}
- **vii.** Length of air gap L_g

3.3 CONSTRAINTS

During the course of optimization when variables undergo decrement or increment, they should also be constrained to be within practical ranges. These constraints could be equality and inequality constraints. The following were the constraints imposed during the design optimization of the induction motor.

i. Peripheral linear speed, $V_s \leq 30$m/s
ii. Slot pitch, S_p ; $13.5 \leq S_p \leq 25$mm
iii. Specific electric loading, $Q \geq 18{,}000$AC/m
iv. Stator temperature rise, $\Theta \leq 70^0$C
v. Full load slip, $S \leq 0.05$ (5%)

The design variables were restricted to certain limits by specifying the lower limit and upper limit. The bound limits set for the design variables are shown in Table 1.

Table1: Bound limits for the design variables

Design variables	Description	Lower limit	Upper limit
D	Stator bore diameter	0.1600	0.1750
L	Axial length	0.1300	0.1450
D_{ss}	Depth of stator slot	0.0255	0.0265
D_{sc}	Depth of Stator core	0.0254	0.0264
L_{mt}	Mean turn length	0.8000	0.8300
W_{st}	Stator tooth width	0.0045	0.0055
L_g	Length of air gap	0.0004	0.0006

3.4 DESIGN SPECIFICATIONS

Table 2 presents the specifications used for the 10hp induction motor design optimization.

Table1. : Design specification for the 10hp inductor motor

Description	Value
Full load output power	10hp
Supply voltage	380 V
Number of poles	4
Synchronous speed	1500 r.p.m
Supply frequency	50Hz
Stator winding design connection	Delta
Number of phase	3
Full load p.f	0.87
Full load current per phase	8.85A
Stator winding factor, Kw	0.955
Ratio of core length to pole pitch	1
Stacking factor	0.9
Number of slots per pole per phase	3
Number of rotor slots	44
Flux density of the stator tooth	1.7Wb/m^2
Flux density of the stator core	1.4Wb/m^2
Specific Electric Loading	22,000Ac/m
Specific magnetic loading	0.45Wb/m^2
Coil span	9
Stator current density	5A/mm^2
Current density of rotor bar	6A/mm^2
Current density of end ring	8A/mm^2
Thickness of iron lamination	0.5mm

4. RESULTS AND DISCUSSION

Losses optimization of a 10hp induction motor was carried out using three (3) different AI techniques, subjecting them to identical conditions by using the same design variables and constraints. The codes for each technique were written, run, and results obtained. Because the AI techniques are stochastic in nature, they give different results almost each time they are run. Therefore, in order to get the best result from the techniques, each code was run at least twenty (20) times. The best result obtained from using BA, CSA, and FFO is presented in Tables 3, 4, and 5 respectively.

Table 3: Best result from the optimization of losses using BA at the 12th run

Optimized variables	Value
D	0.1600m
L	0.1303m
D_{ss}	0.0255m
D_{sc}	0.0254m
L_{mt}	0.8000m
W_{st}	0.0045m
L_g	0.0006m
Losses	**741.22W**

Table 4: Best result from the optimization of losses using CSA at the 13th run

Optimized variables	Value
D	0.1615m
L	0.1303m
D_{ss}	0.0257m
D_{sc}	0.0254m
L_{mt}	0.8080m
W_{st}	0.0047m
L_g	0.0006m
Losses	**748.01W**

Table 5: Best result in the optimization of losses using FFO at the 6th run

Optimized variables	Value
D	0.1605m
L	0.1428m
D_{ss}	0.0261m
D_{sc}	0.0264m
L_{mt}	0.8300m
W_{st}	0.0054m
L_g	0.0004m
Losses	**765.33W**

4.1 PREDICTED PERFORMANCES

Based on the result obtained from the AI techniques used for losses optimization of a 10hp induction motor design, the predicted performances such as its full load efficiency, full load torque, magnetizing current, and full load slip are presented in this section.

4.1.1 Full Load Efficiency

The full load efficiency is given by equation (13)

$$\text{Efficiency} = \frac{\text{output power}}{\text{input power}} \text{ X } 100 \quad (13)$$

Output power = 7460W
Input power = output power + losses
Losses = Iron losses + copper losses + friction and windage losses + stray loss
Assuming friction and windage losses = 2% of output power (Sawhney, 1996).
Friction and windage losses = 0.02 x 7460 = 149.2W
Also assuming stray losses = 1.5% of output power (Kim et al, 2014).
Stray losses = 0.015 x 7460 = 111.9 W
Table 6 gives the full load efficiency based on each technique.

Table 6: Full load efficiency

AI technique	Efficiency (%)
BA	88.16
CSA	88.08
FFO	87.91

4.1.2 Full load slip

The full load slip is given by equation (14) (Sahwney, 2006)

$$\text{Slip} = \frac{P_{rcu}}{P_{rcu}+P_{out}+P_{fw}} \quad (14)$$

Where P_{rcu} is the rotor copper loss given by equation (5); P_{out} is the output power and P_{fw} is the friction and windage losses.

Table 7 gives the full load slip based on each technique

Table 7: Full load slip

AI technique	Slip (%)
BA	1.95
CSA	1.96
FFO	1.89

4.1.3 Full load Torque

The full load torque is given by equation (15) (Sahwney, 2006)

$$\text{Full load torque} = \frac{9.55 \text{ X power output}}{n_s\ (1-S)} \quad (15)$$

n_s = 1500r.p.m; S = full load slip

Table 8 gives the full load torque based on each technique

Table 8: Full Load Torque

AI technique	Full load torque (N-m)
BA	46.61
CSA	48.45
FFO	48.42

4.1.4 Magnetizing Current

The magnetizing current is given by equation (16) Ubeku (2016).

$$\text{Magnetizing current per phase, } I_m = \frac{0.427 F_m P}{K_w N_{ph}} \quad (16)$$

Where F_m = Total mmf required for all the magnetic paths.

$F_m = F_g + F_i$

F_g = Mmf required for air gap

F_i = Mmf required for iron magnetic path (assuming it is 35% of the air gap mmf).

Mmf required for the air gap, $F_g = 800{,}000\ B_g K_g L_g$

K_g = Gap contraction factor for slots.

B_g = Gap flux density at 30^0 from pole axis.

L_g = Length of air gap.

Table 9 gives the magnetizing current based on each technique

Table 9: Magnetizing Current

AI technique	Magnetizing current per phase (A)
BA	3.15
CSA	3.50
FFO	2.56

5. CONCLUSION

A 10hp, 380V, 3-phase squirrel cage induction motor has been optimized successfully using three different AI techniques with seven geometric parameters as the design variables and losses as the objective function. The optimal values of these design variables and losses were obtained for each AI technique, with BA taking the lead ahead of CSA and FFO. Minimizing losses during the operation of an induction motor as a result of optimal design, helps to increase the efficiency of the motor thereby reducing running cost.

REFERENCES

Abbas J., Ali Asghar S. and Hossein L. (2020) "Estimation of Induction Motor Parameters Using COA Algorithm" Journal of Advances in Computer Research, Vol. 11, No. 4, pp. 117-130.

Adil H., Nishant G., Shruti G. and Divya G. (2013) "Firefly Algorithm for Unconstrained Optimization" IOSR Journal of Computer Engineering, Vol. 11, Issue 1, pp. 2745-2751.

Ankit C., Sharad S., and Vivek, S. (2013) "Efficiency Optimization of Three Phase Induction Motor by Slip Compensation: A Review" International Journal of Electronics and Electrical Engineering Vol. 1, No. 4, pp.45-58.

Fister I. J., Dušan F. & Iztok F.(2013) "A comprehensive Review of Cuckoo Search: Variants and Hybrids" Int. J. Mathematical Modelling and Numerical Optimisation, Vol. 4, No. 4, pp 56-64.

Ghania K., Belhadri M., Abdellah C. and Bernard M. (2016) "Comparison Of Cuckoo Search, Tabu Search And Ts-Simplex Algorithms For Unconstrained Global Optimization" Computer Modelling and New Technologies, Vol. 20, Issue 4, pp. 45-54.

Ike S.A. and Abdulraheem T. (2021) "An overview of Induction Motor Design Optimization using Artificial Intelligence Techniques'' An overview of Induction Motor Design Optimization using Artificial Intelligence Techniques, Vol. 1, Issue 9, pp. 2147-2156.

Kim D., Choi J., Chun Y., Koo D. and Han P. (2014) "The Study of the Stray Load and Mechanical Loss of Three Phase Induction Motor Considering Experimental Results" Journal of Electrical Engineering and Technology Vol., 9 Issue 1, pp. 32-38.

Ladaycia H., Boukadoum A. (2018) "Energy Optimal Consumption in Squirrel Cage Induction Motor Using Firefly Algo-rithm Optimization" Proceedings of Engineering and Technology- PET, pp14-19.

Miralem H., Tine M., Bojan Š. and Ivan Z. (2016) "Winding type influence on efficiency of an induction motor" Journal of Electrical Engineering, Vol. 3, Issue 5, pp. 45-52.

Radha T., Thanga R. C., Pascal B., Millie P. and Ajith A.(2010) "Optimal Design of Induction Motor for a Spinning Machine Using Population Based Metaheuristics" 2010 International Conference on Computer Information Systems and Industrial Management Applications (CISIM), pp. 341-346.

Sangita R. and Sheli S. C. (2013) "Cuckoo Search Algorithm using Lèvy Flight: A Review" International Journal of Modern Education and Computer Science, Vol. 5, Issue 10, pp. 1-9

Sawhney A.K (2006) "A course in Electrical Machine Design" Dhanpat Rai & Company, Sixth Edition, 2006, pp. 10-237

Ubeku U.E. (2016) "Lecture Note on Machine Design for Masters Student" Electrical and Electronics Engineering Department, University of Benin, Benin City.

PAPER 109 - A STUDY ON THE AWARENESS OF WIRE ARC ADDITIVE MANUFACTURING FOR ADVANCED MANUFACTURING TECHNOLOGIES IN NIGERIA

O. O., Gbadeyan[1,3*], T. E. Abioye[2,3], R. I. Tamuno[1]

[1]Power Equipment and Electrical Machinery Development Institute, (PEEMADI) Okene, Kogi State, Nigeria
[2]Department of Industrial and Production Engineering, Federal University of Technology, (FUTA) Akure, Ondo State, Nigeria
[3]Department of Mechanical Engineering, Federal University of Technology, (FUTA) Akure, Ondo State, Nigeria
[*]Email: yemitebox@yahoo.com

ABSTRACT

Additive Manufacturing (AM) technologies commonly referred to as '3D Printing' have shown a significant impact on manufacturing industries over the past decade. AM is now one of the fastest growing areas of research in the manufacturing and engineering world due to its ability to create three-dimensional complex and near-net shape parts in a layer-by-layer deposition process which is a key powerful force for breakthrough. Wire arc additive manufacturing (WAAM) is an AM technique that can be considered a modification of the classical gas metal arc welding (GMAW) process due to its high deposition rate, high material utilization, and short production lead time. This paper examines the awareness of WAAM for advanced manufacturing technology among respondents in Nigeria.

KEYWORDS*:* Wire Arc Additive Manufacturing; 3D Printing; Surface Enhancement; Defects; Post Processing.

1. INTRODUCTION

The creation of old and new products which entails some production activities such as information, computation, automation, software, and networking has been attributed to advanced manufacturing technologies over the years. Wire arc additive manufacturing (WAAM) as one of the additive manufacturing techniques is increasingly gaining attention globally in recent years in manufacturing sectors due to its advantages and environment friendliness. WAAM has been found among other wire-fed techniques to have a higher material deposition rate, less expensive, low production cost, simplicity in the facility set-up, and ability to fabricate large and intricate parts [1]. The additive materials for this AM technique include; nickel alloys, aluminum, titanium alloys, and stainless steel which can be used to produce parts in different shapes [2]. The usage of this technique has increased continuously in various industries such as aerospace, automotive, oil and gas, as well as in nuclear power technology [3]. The origin of the WAAM method can be traced back to the 1925s when it was proposed to use an electric arc as the heat source with filler wires as feedstock materials for the deposition of metal ornaments. Since then, there has been consistent progress in the development of this technology, particularly in the last 10 years. Today, it has become a promising fabrication process for various engineering materials. Compared to traditional subtractive manufacturing, the WAAM system can reduce fabrication time by 40–60% and post-machining time by 15–20% depending on the component size [4]. For instance, recent breakthroughs in WAAM technology have made it possible to fabricate aircraft landing gear ribs with a saving of approximately 78% in raw material when compared with the traditional subtractive machining process [4].

Over the years, wire arc additive manufacturing techniques have been developed in different countries of the world which include: France, the United Kingdom, the USA, Japan, and China. Thus, it may be suggested that the awareness level of this technology is strong in Asia, Europe, and America when compared with other continents. However, the presence of the technology is limited in Africa [5]. This shows that the level of awareness is generally low in Africa, particularly in Nigeria and more sensitization about the technology is needed in African countries, as there is a large consumer goods market for it, and embracing this additive technology technique can help to boost the gross domestic product [5]. The level of awareness of AM/WAAM technology has not been investigated in Nigeria which is the most populous black nation in the world with a population of over 200 million [6]. In Nigeria, there are more than 160 universities, 150 polytechnics, 145 colleges of education, 40 monotechnic and about 69 research institutions [7] that are not aware of this technology which means its awareness and usage in this country is still low. Thus, this paper set out to carry out review on the level of awareness of WAAM technology in Nigeria. Knowing the level of awareness can help technically to predict the acceptability and growth of this technology in Nigeria. Furthermore, through this

study, the defects associated with WAAM and post processing techniques for enhancement of parts fabricated by WAAM would also be addressed to limit the defects associated with WAAM produced parts.

2. WAAM Set-up

The combination of an electric arc as a heat source and wire as feedstock is referred to as WAAM and has been investigated for AM purposes since the 1990s [8]. Wire arc additive manufacturing (WAAM) is an AM technique that can be considered a modification of the classical gas metal arc welding (GMAW) process. Due to its high deposition rate, high material utilization, and short production lead time compared to powder-based direct energy deposition (DED) techniques, WAAM has been considered for applications in the aerospace, automotive, and marine sectors. In addition, several kinds of traditional arc welding techniques, such as gas metal arc welding (GMAW), gas tungsten arc welding (GTAW), and plasma arc welding (PAW), have also been applied to WAAM. All of these have different deposition features, and thus application fields. Other than these, some variants of GMAW, such as cold metal transfer (CMT) and tandem GMAW have also been created and used to improve the quality and efficiency of deposition in GMAW-based WAAM. However, from these existing methods, the faster deposition rate of GMAW (up to 160 g/min) makes it the ideal candidate for the large-scale parts production in short time spans and has become the most popular process in WAAM [9]. Plate 1 shows a typical WAAM setup.

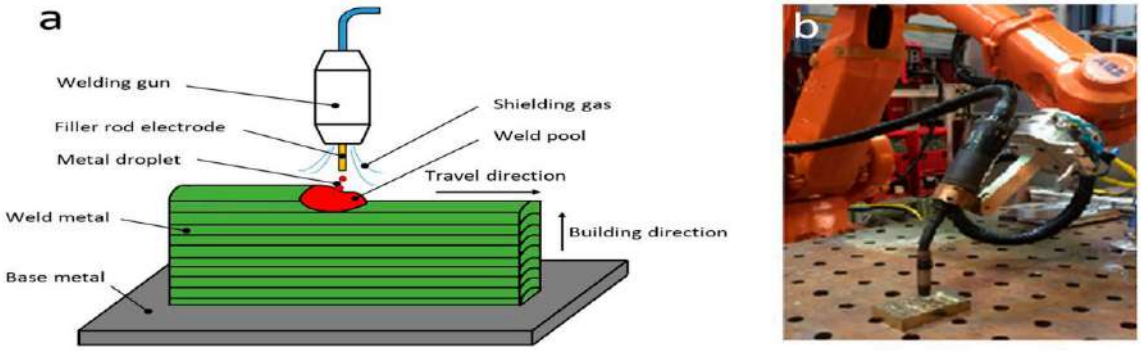

Plate 1: Schematic diagram of layer-by-layer deposition using GMAW process; and (b) the setup of the robotic GMAW process (source: [10]).

2.1 Variant of WAAM

WAAM uses alternative heat sources including gas metal arc welding (GMAW), gas tungsten arc welding (GTAW), plasma arc welding and cold metal transfer.

2.1.1 WAAM Gas Metal Arc Welding (GMAW)

GMAW is a welding process in which the source of heat is an arc format between the consumable metal electrode and the workpiece as illustrated in plate 2. The arc and the molten pool are protected from atmospheric contamination (i.e. oxygen and nitrogen) through the supply of inert gases including argon, helium, or an argon-helium mixture. Other shielding gases that have been effectively utilized for this purpose are carbon dioxide, argon-carbon dioxide mixture, and hydrogen-argon mixture [11]. GMAW is a semi-automatic process in which the arc lengths of the electrode and the feeding of the wire are automatically controlled [12]. It has a higher deposition rate compared to other WAAM

heat sources with a continuous flow of wire through the torch [13].

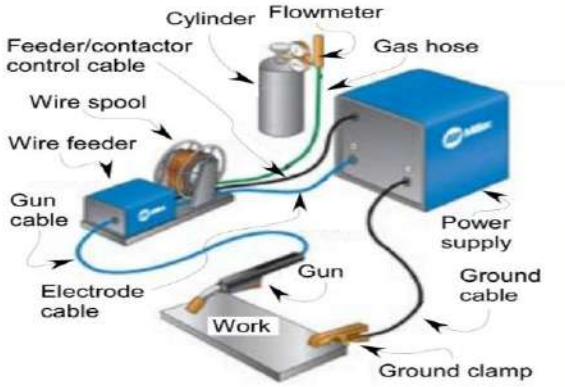

Plate 2: Gas metal arc welding (GMAW) process (source: [12]).

2.1.2 WAAM Gas Tungsten Arc Welding (GTAW)

Gas tungsten arc welding as indicated in plate 3 uses a non-consumable tungsten electrode and an inert gas for arc shielding. In this process, an electric arc is formed between a tungsten electrode and the base metal. The arc region is protected by an inert gas or mixture of gases. Although this type of welding is usually done with a single electrode, it may be sometimes done with several electrodes. In GTAW, shielding gas plays an important role. The composition of a shielding mixture in arc welding depends mostly on the kind of material to be welded. The selection of the shielding gas should, by all means, take into account chemical–metallurgical processes between the gases and the molten pool that occur during welding [12]. Its advantage over other arc welding techniques is that the wire feed orientation influences material transfer and the quality of the deposit during the deposition process is high [14].

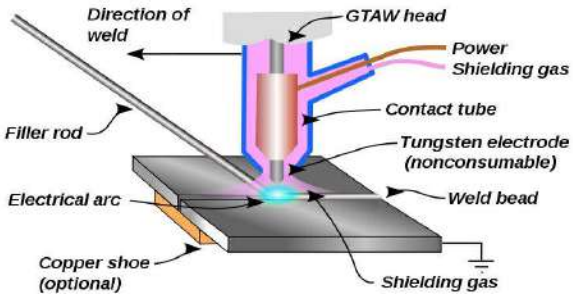

Plate 3: Gas tungsten arc welding process (Source: [12])

2.1.3 WAAM Plasma Arc Welding (PAW)

This is an advanced form of the gas tungsten arc welding process as shown in figure 3. It uses a constricted nozzle and two separate gas flows, which give rise to a concentrated plasma arc with a narrow columnar shape [15]. This technique is unique as it can perform both accurate cutting and welding of thin and thick metals. Presently, PAW has distinctive benefits and it is used across industries because of its accuracy (www.elprocus.com/plasma-arc-welding-working-types-applications/). It is advantageous over other heat sources because of the high-density arc which offers high quality weld with little distortion [14]. Other advantages of PAW include high penetration rate and the production of a steady arc. However, the process is expensive and noisy.

2.1.4 WAAM Cold Metal Transfer (CMT)

CMT is a modified process of gas metal arc welding that relies on a controlled dip transfer mode mechanism which was introduced in 2004 by Fronius of Austria [16]. In the CMT arc welding process, the wire feed rate is proportional to the current and voltage. This means that there will be an increase in heat input whenever there is an increase in wire feed rate [13]. It delivers beads with excellent quality, lower thermal heat input, and no spatter [8]. There are some

benefits associated with this process. The retraction of the wire during the short-circuiting phase is critical because spatter formation is reduced and the aesthetics of the weld bead is improved.

2.1 Challenges associated with WAAM

Due to the large heat energy involved, cracking, porosity, distortion, and dilution are major defects peculiar to WAAM processes. These defects are more prominent in severe environments and can eventually result in catastrophic failures. The occurrence of these defects can be related to thermal distortion and residual stress build-up often caused by the large heat accumulation, unsteady weld pools due to inappropriate selection of parameters, bad strategy of programming, environmental impact (such as gas pollution), and breakdowns of machines [17].

2.2.1 Crack and delamination

Cracking is caused in wire arc additive manufacturing due to incomplete melting of the underlying solid between layers. It cannot be corrected by post-process treatment, so it is advisable to pre-heat the substrate to avoid the defect. Delamination, which can also be referred to as the separation of adjacent layers takes place due to incomplete melting or insufficient re-melting of the underlying solid between layers. It is difficult to repair this defect by post-process treatment but can be prevented by pre-process treatment such as pre-heating the substrate [4].

2.1.2 Porosity

This defect as shown in plate 4 is often caused by the presence of surface contamination such as moisture, grease, sand, etc. on the workpiece. It can also be caused by an unstable deposition process due to inappropriate process condition selection, especially for the fabrication of complex-designed structures. Entrapment of gas during the deposition process can also result in pore formation in the built structure. Porosity is generally grouped into two which are raw material-induced or process induced. The WAAM raw material, including as-received wire and substrate, often has a degree of surface contamination, such as moisture, grease, and other hydrocarbon compounds that may be difficult to completely remove. These contaminants can be easily absorbed into the molten pool and subsequently generate porosity after solidification. Process-induced porosity is mainly caused by poor path planning or an unstable deposition process. When the deposition path is complex or the manufacturing process is changeable, insufficient fusion or spatter ejection is easily produced, creating gaps or voids in these influenced regions [1].

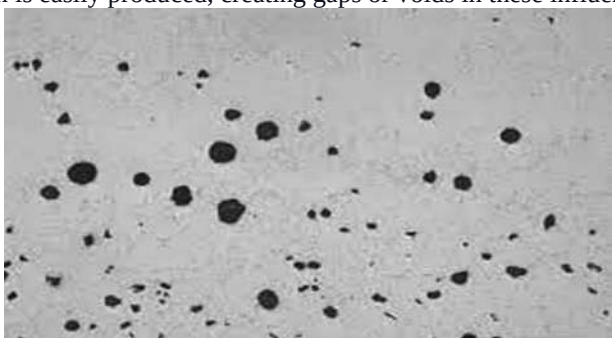

Plate 4: Porosity during deposition. (source: [1])

2.1.3 Residual Stress and Deformation

3 Deformation and residual stress are inherent to the WAAM process and it cannot be completely avoided. The residual stress can lead to distortion of the part, delamination of layers during deposition, as well as deterioration of fatigue performance and fracture resistance of the additively manufactured components. Therefore, there is a need for control and minimization of deformation and residual stress. Residual stress is caused as a result of the stress that remains in the material when all external loading forces are removed. Fortunately, several post-process treatments have been proven to effectively mitigate residual stress such as interpass cooling, interpass cold rolling, etc [4].

4 **2.1 Recent Post-Process Treatment in WAAM Process**

5 There is a need for post-process treatment in the WAAM process to improve material properties, reduce porosity and surface roughness, and also remove residual stress and distortion. Through this process, the majority of issues that affect the quality of deposition can be eliminated. Presently, there are several post-process treatment technologies to improve part quality in the WAAM process and these are enumerated below.

6 **2.3.1 Post-process Heat Treatment**

Post-process heat treatment is broadly used in wire arc additive manufacturing for residual stress reduction to enhance material strength and also as a way of controlling hardness. The selection of a proper heat treatment process depends on the target material, additive manufacturing methods, working temperature, and heat treatment conditions. If the heat treatment state is set incorrectly, the probability of cracking will increase under mechanical loading, as the combination of existing residual stress with load stress exceeds the material's design limitation. In addition, post-process heat treatment plays an important role in grain refinement. The decision to use post-process heat treatment depends on the material alloying system and also the pre-heat treatment state. Generally, high carbon content materials must be heat treated, while a few materials can be damaged by this technique. Therefore, in applying this treatment process to the WAAM component, the specific material and its application should be considered [4].

2.3.2 Interpass Cold Rolling

The rolling of each deposited layer of weld bead shows a reduction in residual stresses and distortion. This post-process treatment not only reduces the residual stress but also brings more homogeneous material properties. The cold rolling technique considerably lowers microstructural anisotropy by plastically deforming the deposition. A slotted roller is used to refine the microstructure and enhance tensile strength in the longitudinal direction by supporting external force. Interpass cold rolling also can play a critical role in the healing of hydrogen porosity in WAAM-fabricated aluminum parts [18].

2.3.2 Peening and Ultrasonic Impact Treatment

These types of post-process heat treatment are widely used in welding applications to reduce residual stress and improve the mechanical properties of the weld. Both techniques are cold mechanical treatments as illustrated in plate 5 [4]. The mechanical peening process produces compressive stresses at a limited depth below the component surface while ultrasonic impact treatment produces grain refinement, thus contributing to the improvement of mechanical strength. After ultrasonic impact treatment, the surface residual stress is reduced and the micro-hardness is increased compared to the as-fabricated sample [18].

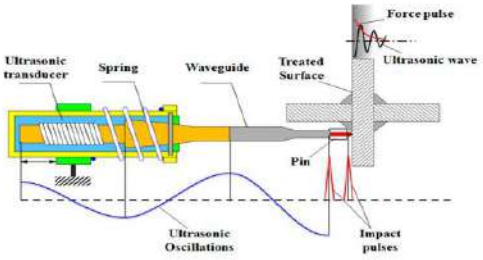

Plate 5: Ultrasonic impact treatment. (source: [1])

11.1 Future prospects and challenges.

In manufacturing processes, reduction and controlling of deformation, distortion, and residual stress are common challenges in the manufactured parts and WAAM's major current task is to develop proper inspection techniques. The growth in the production of intricate parts also resulted in the inspection of those parts. Since WAAM is known to be extremely sensitive to changes in process parameters, incorporating an in-process monitoring device into a closed-loop control system becomes critical because it allows for component rectification while they are still being manufactured. Internal flaws and high residual stresses might be avoided if this method is adopted [1]. Monitoring fusion welding has traditionally been done by measuring current, voltage, shielding gas flow rate, travel speed, and WFR. Sensors can also be used to monitor temperature in various regions, measure the size and shape of beads, evaluate weld pool characteristics, monitor the acoustic signal of deposition, detect electrical conductivity fluctuations, and measure oxygen levels during WAAM. Unlike in fusion-based welding where established process parameters are held constant for producing quality welds, building components via WAAM often requires careful modification of process parameters because of the variances in heat behavior throughout component manufacturing [1].

2.1 WAAM Awareness in Nigeria

To know the level of awareness of this wire arc additive manufacturing technique in Nigeria, data collection and analysis were carried out.

1. **Methodology**

An online questionnaire was designed and structured to collect data for this study. The questionnaire was principally designed to assess the level of awareness of WAAM technology in engineering research institutes, tertiary institutions, and industries in Nigeria. The questionnaire was administered to the engineering personnel working in these

institutions and industries. The questionnaire comprises two parts. The first section ascertained the level of education and other information about the respondents, while the second section surveyed their awareness of WAAM technology and the availability of WAAM equipment for research/teaching and manufacturing purposes. Scale '1–5' was used to rank the response as a guide for the respondent. The strongest response was rated '5' and the weakest '1', where '1' means very low, '2' means low, '3' means average, '4' means high and '5' means very high. Respondents were drawn from all fields of engineering, both in research institutions and academic institutions, making a total number of sixty-two (62) respondents involved in the survey. Data to determine the level of awareness of WAAM were extracted from the questionnaires received and data analysis was done.

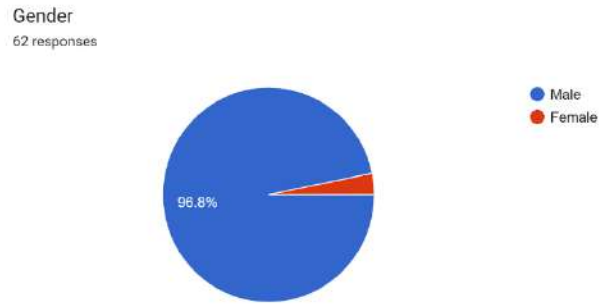

Figure 1: Gender percentage of the respondents

The gender consist of a male and female. As shown in figure 1, the percentage of male that attended to the questionnaire is 96.8% while the remaining percentage of 3.2% is for female which indicated that less female attended to the online form.

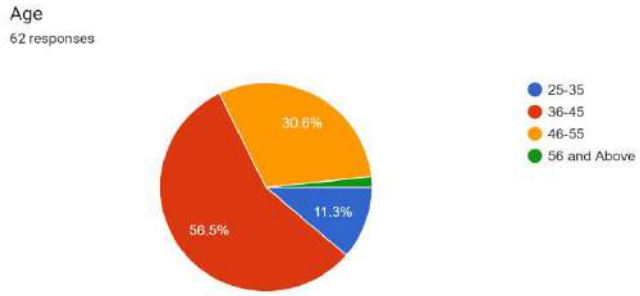

Figure 2: Age percentage of the respondents

The age considered for the survey is between 25 years and above and it was revealed in figure 2 that between 25-35 years which represent 11.3% of the 62 responses fill the form, 36-45 age bracket with the highest percentage of 56.5% completed the survey, 46-55 years represents 30.6% and 50 years and above which represent 1.6% completed the google form.

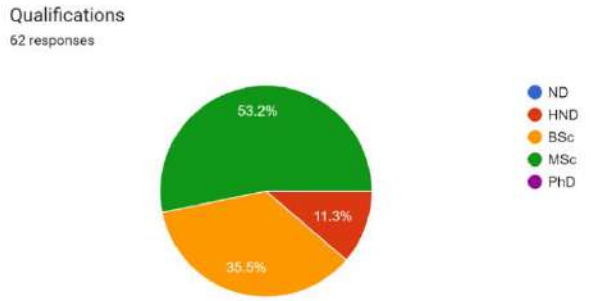

Figure 3: Percentage of respondents qualification.

Qualifications considered are national diploma, high national diploma, bachelor of science, master of science, and doctor of philosophy. From the chart in figure 3, nobody in the categories of national diploma and doctor of philosophy attended to the survey form. Responses in the category of master of science is 53.2% which signify the highest, 35.5% from bachelor of science, and 11.3% from higher national diploma.

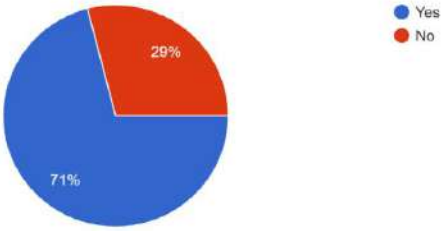

Figure 4: Percentage of respondents with AM awareness in Nigeria

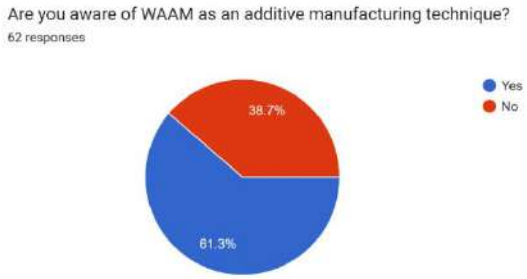

Figure 5: Percentage of respondents with WAAM awareness as AM technique

From the respondents, 61.3% of the 65 responses are aware of the WAAM as an additive manufacturing technique while 38.7% are not aware as shown in figure 4.

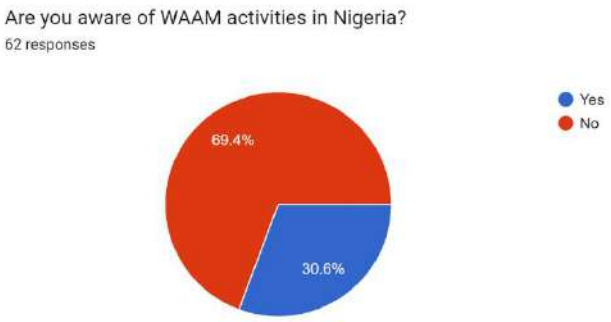

Figure 6: Respondents WAAM activities awareness in Nigeria

If yes, rate the level of awareness

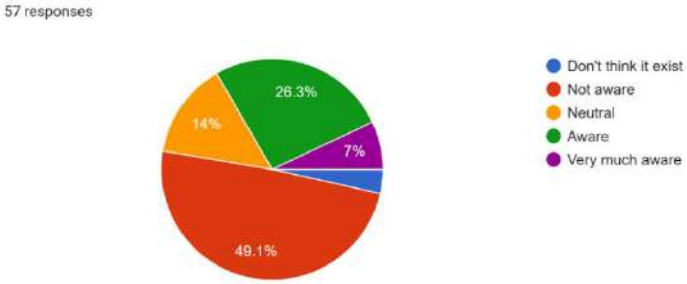

Figure 7: Respondents level of WAAM activities awareness in Nigeria

3. RESULTS AND DISCUSSION

Having collected the questionnaires from the respondents and analyzed them, it was found that out of the sixty-two (62) responses, forty-four (44) respondents indicated that they were aware of the existence of additive manufacturing technology and this amounts to 71% of the total responses analyzed, while the remaining eighteen (18) respondents, which is 21% of the total respondents, had not heard about this manufacturing technology before, as shown in Figure 4. Coming down to WAAM technology, the number of respondents who were aware of the technology was a bit high, thirty-eight (38) respondents which signify 61.3% as shown in Figure 5 but its awareness in the country, which could unlock the opportunities of the technology is very low (69.4%) as indicated in Figure 6, 7% of the respondents are very much aware of the activities in Nigeria while 26.3% are aware as shown in Figure 7. Other factors that contributed to a low level of awareness included a lack of exposure to the technology and a lack of skilled manpower. The availability of capable manpower to operate and train others on how to apply WAAM technology effectively, together with the availability of equipment in the Nigerian market, is expected to raise the level of awareness of this technology in Nigeria [5]. There can be widespread awareness and deployment of this technology across Nigeria, provided that affordable WAAM manufacturing equipment is made available in markets nationwide.

1. CONCLUSION

The investigation into the awareness of AM/WAAM technology in Nigeria was successful, with a 30.6% awareness level observed which is far less than what was expected. Despite the numerous opportunities that AM/WAAM technology affords, ranging from research to the production of goods for the market, the major challenge that the deployment of AM/WAAM technology faces is the unavailability of equipment and consumables at affordable prices in the Nigerian market. With intensive efforts towards procurement of AM/WAAM systems from abroad, local development of AM/WAAM systems, public exhibitions, and their products locally, and increasing research outputs in the area of AM/WAAM technology, the level of awareness and use of this technology will keep increasing, to exploit the opportunities offered by the technology for the development of Nigeria.

Link to Google Form Questionnaire: https://docs.google.com/forms/d/1LK6AuDa5Jh80qlFbw29Hjd3jMLQeBv9GFKD63YVC9pk/edit

REFERENCE

[1.] Bankong, B. D., Abioye, T. E., Olugbade, T. O., Zuhailawati, H., Gbadeyan, O. O., Ogedengbe T. I. (2022). Review of post-processing methods for high-quality wire arc additive manufacturing. Journal of Materials Science and Technology. Pp: 1-18.

[2.] Li, J.L.Z., Alkahari, M.R., Rosli, N.A.B., Hasan, R., Sudin, M.N., Ramli, F.R (2019). Review of wire arc additive manufacturing for 3D metal printing. International Journal of Automation Technology. Vol.13 (3); Pp: 1-8.

[3.] Wachter, M., Leicher, M., Hupka, M., Leistner, C., Masendorf, L., Treutler, K., Kamper, S., Esderts, A., Wesling, V., Hartmann, S. (2020). Monotonic and fatigue properties of steel material manufactured by wire arc additive manufacturing. Journal of Applied Science. Pp: 1-22.

[4.] Wu, B., Pan, Z., Ding, D., Cuiuri, D., Li, H., Xu, J., Norrish, J. (2018). A review of the wire arc additive manufacturing of metals: properties, defects and quality improvement. Journal of Manufacturing Processes. Vol.35; Pp: 127-139.

[5.] Farayibi, P.K., Abioye, T.E. (2017). A study on the awareness level of additive manufacturing technology in south-western Nigeria. African Journal of Science, Technology, Innovation and Development. Pp: 1-7.

[6.] World Fact, Book. 2023. Nigeria People 2023. USA: Central Intelligence Agency. Accessed July 21, 2023. http://www.theodora.com/wfbcurrent/nigeria/nigeria_people.html.

[7.] Nigerian Directory/Research Institutions. 2023. Accessed July 21, 2023. http://www.platgroupng.com/nigeria_directory/ research_institutions.php.

[8.] Williams, S.W., Martina, F., Addison, A.C., Ding, J., Parda, G., Colegrove, P. (2015). Wire + arc additive manufacturing. Journal of Materials Science and Technology. Pp: 1-8.

[9.] Lin, Z., Goulas, C., Ya, W., Hermans, M.J.M. (2019). Microstructure and mechanical properties of medium carbon steel deposits obtained via wire and arc additive manufacturing using metal-core wire. Metals Journal. Vol.9; Pp: 1-14.

[10.] Donghong, D., Zengxi, P., Duin, S.V., Huijun, L., Chen, S. (2016). Fabricating superior NiAl bronze components through wire arc additive manufacturing. Materials Journal. Vol.9; Pp: 1-12.

[11.] Ekpemogu, A.I., Ariwoola, O.E., Rasheed, A.A., Ogundele, O.A., Abioye, T.E., Ogedengbe, T.I. (2021). Mechanical properties of gas metal arc weldments of AISI 304 stainless steel using different shielding gas compositions. International Journal of Engineering Research in African. Vol.54; Pp: 1-11.

[12.] Gbadeyan, O.O. (2018). Analysis of mechanical properties and penetration depth of metal inert gas welding of AISI 304 austenitic stainless steel. A Thesis in the Department of Mechanical Engineering, Submitted to the School of Post Graduate Studies. Pp: 1-45.

[13.] Rosli, N.A., Alkahari, M.R., Abdollah, M.F.B., Maidin, S., Ramli, F.R., Herawan, S.G. (2021). Review on effect of heat input for wire arc additive manufacturing process. Journal of Materials Research and Technology. Vol.5; Pp: 2127-2145.

[14.] Dhinakaran, V., Ajith, J., Fahmidha, A.F.Y., Jagadeesha, T., Sathish, T., Stalin, B. (2019). Wire arc additive manufacturing (WAAM) process of nickel based superalloys- A review. Materials Today: Proceedings. Pp: 1-6.

[15.] Liu, Z.M., Wu, C.S., Liu, Y.K., Luo, Z. (2015). Keyhole behaviors influence weld defects in plasma arc welding process. Welding Journal. Vol.94; Pp: 281-290.

[16.] Lervag, M., Sorensen, C., Robertstad, A., Bronstad., B.M., Nyhus, B., Eriksson, M., Aune, R., Ren, X., Akselsen, O.M., Bunaziv, I. (2020). Additive manufacturing with superduplex stainless steel wire by CMT process. Metals Journal. Vol.10; Pp: 1-17.

[17.] Tawfik, M.M., Nemat-Alla, M.M., Dewidar, M.M. (2021). Enhancing the properties of aluminum alloys fabricated using wire + arc additive manufacturing technique- A review. Journal of Materials Research and Technology. Vol.13; Pp: 754-768.

[18.] Wu, B., Pan, Z., Ding, D., Cuiuri, D., Li, H., Xu, J., Norrish, J. (2018). A review of the wire arc additive manufacturing of metals: properties, defects and quality improvement. Journal of Manufacturing Processes. Vol.35; Pp: 127-139.

PAPER 110 - CHALLENGES RESPONSIBLE FOR THE DECLINE OF THE MANUFACTURING SECTOR IN NIGERIA

P.S Abam[1*], R.I Tamuno[1], T. Abdulraheem[1], S.A. Lawani[1], S.A, Subiy[1]

[1]Power Equipment Electrical Machinery Development Institute, Okene.

* Email: paulsotoye@gmail.com

ABSTRACT

The paper examined the challenges responsible for the decline of the manufacturing sector in Nigeria and the solution to these problems. The manufacturing sector is the hub of a vibrant national economy, the sector can harness the various available raw materials, process and transform them into marketable finished or partly finished goods through the use of human capital and other agents of production. The finished goods and services thus generated contribute meaningfully to the national gross domestic product GDP and generate income and employment opportunities for the citizenry of that nation. Secondary sources of information in this research are a communique from the annual general meeting of the Manufacturing Association of Nigeria, an Article and publication from the Central Bank of Nigeria, and reports from the National Bureau of Statistics in collecting the data. However, the Nigerian manufacturing sector is faced with many challenges, ranging from an unfriendly business environment, poor regulatory environment, poor infrastructures, multiple taxation, rising cost of capital interest rate, and a dearth of local skill and technology. The findings indicate that these challenges can be overcome by massive investment in the power and energy sector, the need to invest in human development of indigenous technology and local sourcing of raw materials, provision of land for manufacturing companies, and setting aside a tax-free period for these companies. The implementation of this solution will have a favorable impact on the manufacturing sector which will stimulate national economic growth.

***KEYWORDS*:** Manufacturing sector, National economy, Challenges, production, resources

1. INTRODUCTION

Converting raw resources into final consumer items, intermediates, or semi-finished commodities is the process of manufacturing. Manufacturing, like other industrial pursuits, boosts agriculture, diversifies the economy, and increases the country's gains from foreign exchange. It also makes it possible for local labor to learn new skills. Therefore, the economic state of a Nation is largely determined by her manufacturing capabilities, The United Kingdom's economy is very strong because of her high manufacturing capabilities (6^{th} in the world) compared to Nigeria with a gross domestic product (GDP) of $262.616 billion, United Kingdom (UK) annual GDP is $2.44 trillion in 2022. (Banjoko, 2009). Despite the government's efforts to increase industrial production and capacity utilization in the sector, there has been growing worry about the challenges in the manufacturing industry's output in Nigeria in recent years. Massive imports of finished goods and insufficient financial support for the manufacturing sector are the main causes of the sector's underwhelming performance in Nigeria, which has finally led to a decline in the capacity utilization of the industry in the nation. Because of the manufacturers' increased difficulty evaluating raw materials as a result of fierce rivalry from overseas companies, the level of Nigerian manufacturing organizations' performance would continue to drop (Owan *et al*., 2020). The manufacturing industry in Nigeria is now dealing with a number of difficulties. The lack of investment in research and development R&D and innovation is one of the main causes of the technological base's weakness. Due to restrictions on foreign exchange, manufacturers are heavily dependent on imported machinery, equipment, and spare parts, which is unsustainable. The sector's contribution to the gross domestic product, which has averaged 4% during the last five years, makes the deterioration clear (Joshua *et al.*, 2016). In light of the foregoing, the study aims to investigate the challenges responsible for the decline of the manufacturing sector in Nigeria.

Sustaining Nigeria's Manufacturing Sector in the Face of the Current Global Economic Recession as saying that the closure of production by many industries had become worrisome to manufacturers even as some companies in the country were relocating to Ghana, in the face of an unfavorable economic climate.

Continuing his commentary, Malaifa, *et al* (2018) reported that it is no longer news that many companies have divested from the Nigerian economy. It was gathered that in 2010, for example, the manufacturing sector accounted for nothing less than seven percent of the Gross Domestic Product (GDP). This, however, shrunk to 4.9 percent in 2012. As a result of inadequate infrastructure and high cost of production, the manufacturing capacity utilization has remained on a downward spiral. It is a known fact that about some years ago, Dunlop Nigeria Plc., the only surviving tire manufacturing company in Nigeria then, shut down its plants, laid off hundreds of its workers, and put some on half-pay. Dunlop Nigeria Plc and Michelin have since relocated to Ghana. Patterson Zochonis (PZ) has also relocated to Ghana, even as Cadbury Nigeria Plc, Unilever, and the International Institute of Tropical Agriculture (IITA) sacked a sizeable number of their workers over reported high cost of production and decaying infrastructure.

Reports from Ghana have it that a major investment drive to lure companies from Nigeria involves a 'mouth-watering' package, which company operators have found to be irresistibly attractive, It includes the donation of free piece of land to companies willing to migrate to any part of Ghana, a 10 -year tax holiday as well as other policy incentives that are not readily available in Nigeria. (Owan *et al*., 2020).

2. JUSTIFICATION OF THE STUDY

The Nigerian manufacturing sector has declined over a period of time and it has been observed that the sector was not performing. However, the unemployment rate, frequent decreases in the contribution of the manufacturing sector to GDP, and widespread poverty made us critically examine the challenges of the manufacturing sector and proffer solutions. The negative effects of the oil price collapse in the international oil market can be clearly seen in the sector's performance. Due to the global oil crisis, the revenues of the Nigerian government sharply declined which resulted in a reduction in foreign exchange earnings (Adenijinju *et al*, 2002). This in turn forced the government to take several initiatives with the intention of strictly controlling its trade. There were several import duties enacted in the form of import licenses and tariffs, and some quantitative restrictions were also imposed on the importation of certain items. As a result, the manufacturing sector was badly affected because the manufacturers faced multiple problems when obtaining raw materials and spare parts for their products and processes.

As a result of massive cutbacks in raw materials and spare parts, many of the country's industries were shut down and the capacity utilization in the manufacturing sector declined. This disturbing trend was also observed in most of the other manufacturing sub-sectors in the country.

The share of the manufacturing sector in the total GDP of the country also clearly declined during this era. In 2017 there was a 4% increase recorded in the manufacturing sector's share of GDP and this reached the level of 7% in 2019, but after that, it increased to less than 10% in just a few years. Table 1 illustrates the trends of GDP and the manufacturing output in Nigeria from 2016 -2022.

Table 1: Trends of GDP and manufacturing output in Nigeria from 2016 -2022

S/N	Year	GDP(₦ GDP Billion)
1	2016	67, 931.24
2	2017	68,490.98
3	2018	66, 799.94
4	2019	71,387.83
5	2020	70,422.74
6	2021	71,542.89
7	2022	69, 842.89

Source: National Bureau of Statistics

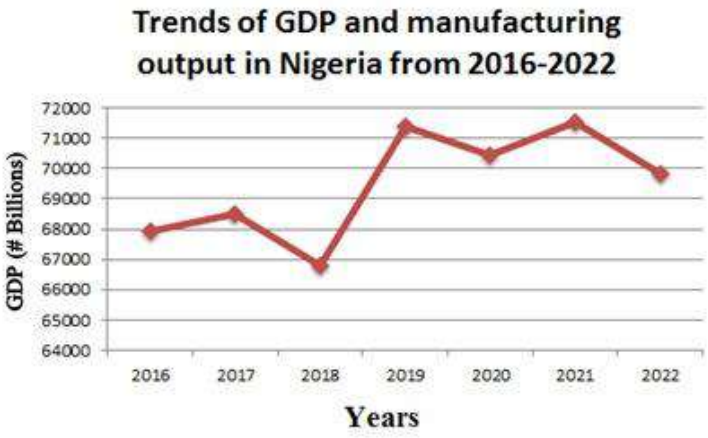

Fig. 1 Variation of Years with GDP (₦ Billion)
Source: National Bureau of Statistics

Table 1 and Figure 1 above show the trends of manufacturing output in Nigeria from 2016 – 2022. The value of manufacturing output in 2016 was ₦67.9 billion. The value in 2017 rose to ₦68.7 billion. The trend of manufacturing output declined to ₦66.7 billion in 2018, the value rose again in 2019 to ₦71.3 billion. There was a decrease in manufacturing output in 2020 at ₦70.1 billion, finally, there was a decrease in 2022 at ₦69.8 billion. The trends of manufacturing output in Nigeria show that there have been upward and downward trends in manufacturing in Nigeria between the periods examined in the study. Figure 2 shows the composition of the manufacturing sector in Nigeria in 2022

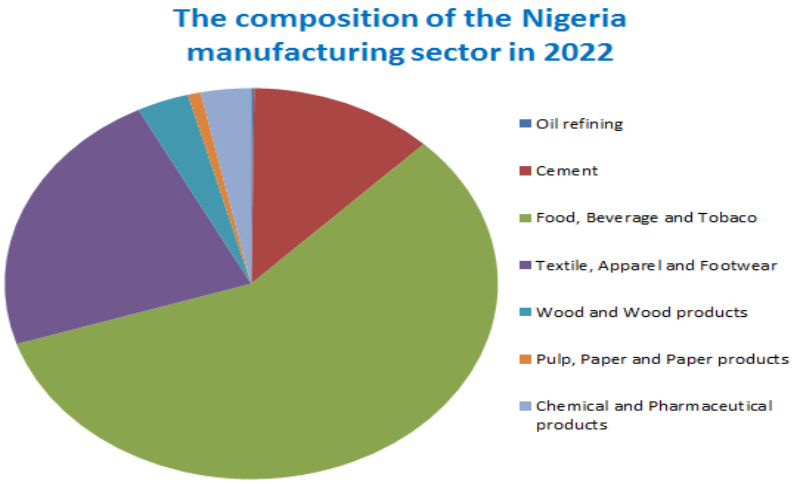

Fig. 2 Composition of the manufacturing sector in Nigeria in 2022
Source: National Bureau of Statistics

3. FACTORS RESPONSIBLE FOR THE DECLINE OF THE MANUFACTURING SECTOR IN NIGERIA

Despite the surge in economic activities and investment growth between 2016 to date resulting from a series of economic reforms embarked upon by the government and several industrialization initiatives, the manufacturing sector has not impacted very positively on the national economy. Not much employment has been generated by the sector and with the recent wave of relocation to neighboring countries by many companies like Dunlop (Nigeria) Plc, Michelin (Nigeria) Plc, and Nestle (Nigeria) Plc; the employment situation is getting worse. There is still widespread poverty. Economic indices show that the living standards of the average Nigerian have fallen and there are strong indications that Nigerians were better off in the 1980s than they are today (UNDP, 2017). The major factors responsible for the decline of the Nigerian manufacturing sector can be traced to the following challenges.

(1) **Unfriendly business environment** The Nigerian business environment is far from being friendly and congenial for manufacturing activities to thrive. The availability of critical infrastructures necessary to support the sector is far from being adequate, imports of essential raw materials are problematic and government bureaucracy is very cumbersome (MAN, 2017). The security concern has assumed more frightening dimensions, especially with the recent bandit attacks, armed robberies, and kidnapping episodes. As a result, the inflow of foreign investments has been held up while many companies have relocated to safer and more business-friendly environments outside the country.

(2) **Poor regulatory environment** Nigeria is characterized by a poor regulating environment. Laws are made and broken at will and enforcement machineries and agencies are seriously deficient and corrupt. Paradoxically, law enforcement agents like the police, Vehicles Inspection Officers, and tax officials who are supposed to uphold the law are the worst offenders. Corruption is at its highest level, particularly among public officials. Custom officers connive with smugglers to bring in cheap and fake imports across the borders. It is reported that every year regardless of the ban placed on the importation of textile materials, "Nigerian importers … bring in over N19 billion worth of fabrics and textiles from Dubai (Malaifa, 2018).

(3) **Infrastructural challenges** Nigeria's infrastructural challenges are so daunting to the extent that they have caused incalculable damage to the growth of the economy in general and the manufacturing sector in particular. The truth is that successive governments in Nigeria have not made adequate investments in public infrastructure to the level required to guarantee the sustainable growth of our economy. The nation's power supply is erratic and grossly inadequate. The Nigerian power sector has witnessed serious neglect over the years. For example, for a period of twenty years between 1979 and 1999, no new investment in the power sector took place despite the fact that our population and economy grew remarkably during this period. It is sad that the power sector cannot generate 4000 megawatts of electricity for an economy that requires between 40,000 and 50,000 megawatts for sustainable national growth and development. According to the Nigerian Bureau of Public Enterprises (BPE), "Nigeria requires $15-$20 billion of investment over the next three years to buy and develop electricity assets" Meanwhile, power outages have continued to stifle economic growth as most companies rely on generators. Many businesses particularly the SMEs, and artisans like welders, panel beaters, paint sprayers, and hairdressers are groaning heavily under the yoke of inadequate power supply. Our road networks all over the country are bad and have become death traps. Our railway networks are inadequate and our port infrastructures are not sufficient. Importers suffer endless delays in clearing their goods. Businesses all over the country are suffering from these infrastructural inadequacies.

(4) **Multiple taxation.** Another serious challenge facing the operators of our manufacturing sector is the problem of multiplicity of taxes, levies, and other spurious charges that have imposed a heavy cost burden on the companies thereby escalating the cost of doing business. Taxes and spurious charges imposed on manufacturing businesses in Nigeria are Education Tax Development Levy NSTF (National Science and Technology Fund) National Advertisement Fee NASENI (National Science and Engineering Infrastructure) Tax Tenement Rate Charge Value Added Tax Haulage and Permit Fee, others are Environmental Sanitation Tax Big Vehicle Emblem Fee Neighborhood Improvement charges Fire Service Charge Generating Plant Charge Environmental Pollution charge Commercial premises charges, Advert on Vehicle, Kiosk, shop and Business premises tax

(5) **Rising cost of capital** rising interest rates on borrowed loans have in the past risen to as high as 25% thereby constituting another crippling factor on the growth of the Nigerian manufacturing sector. In recent times, the lending rates have crashed but not sufficient enough to give the needed reprieve. The recent CBN banking reforms and recapitalization have made access to banking facilities more difficult as banks have become more cautious in granting credits to the operators of the real sector. With restricted access to bank facilities, the woes of the manufacturing sector have become even more compounded.

(6) **Dearth of local skills and technology** Dearth of local skills and indigenous technology has been another serious problem to the growth and development of the Nigerian economy and the manufacturing sector in particular. Sixty years after independence, there is still heavy reliance on imported technology and raw materials as not much attention has been given to the development of local-based technology without which no sustainable growth and development can be achieved.

Solution for Sustainable Growth of the Manufacturing Sector

The recommended solutions for achieving sustainable growth in the manufacturing sector must include the following:

(1) **A massive investment in the critical power and energy sector** that would ensure a complete and radical overhaul of our power sector has become imperative if we are to achieve a sustainable economy and a virile manufacturing sector. The present erratic electricity supply of less than 4000 megawatts is grossly inadequate when compared with South Africa's electricity supply of 40,000 megawatts even with her entire population of less than one-third of Nigeria's population. According to Adenikinju *et al*. (2002), about 35% of the setup investment of most manufacturing companies is spent on providing private electricity via the installation of heavy-duty generators. In a recent study, the Bureau of Public Enterprise (BPE) in the Nations Newspaper reported the nation needs to acquire and rehabilitate the 6 generation and 11 distribution successor companies, make provision for the 10 NIPP generation plants and related NIPP transmission and gas distribution network equipment. It is hoped that with the recent launching of the Power sector improvement roadmap by the past administration, the manufacturing sector would enjoy a new lease of life as many foreign and local investors who have abandoned our shore would find it convenient to return.

(2) **There is a need to invest massively in human capacity development** of indigenous technology and local sourcing of raw materials. Companies must be encouraged to invest in Research and Development of new modes and modern technology of production.

(3) **The government must deliberately provide a conducive environment for business to thrive.** This must include putting in place adequate security to protect investors' lives and investments, a good regulatory system, eliminating inconsistency in government policies, eliminating multiple taxations and extortion as well as the payment of additional and unofficial fees for public services that are supposed to be free. It is observed that foreign investors are often the easy targets of extortion and bribery by fraudulent public officials both at the local, state, and federal levels. Consequently, there is an urgent need for the harmonization and streamlining of our tax administration system as well as our investment laws in a manner that would facilitate expatriate quota processing and enhance the unhindered flow of foreign investments.

(4) **The government must often check and control the charging of high interest rates by overzealous banks** as such high rates often stifle the survival and profitability of many small and medium business organizations.

(5) **There is a need for improvement in our physical infrastructure.** Our road networks are bad, there is a lack of adequate water supply to many industrial estates, our rail system is not sufficient and there are poor facilities at our ports.

(6) **Our manufacturing sector must be recognized not only as a catalyst for creating wealth,** generating employment, and alleviating poverty but also as a major sector for enhancing national growth and development. As such, it must be accorded its due regard and priority in the scheme of things.

(7) **There is a need for a deep appreciation of the critical role of small and medium enterprises (SMEs) in the growth and development of our industrial sector.** Nigeria has not developed her SME's potential for rapid industrialization because the country has failed to realize that SMEs not only provide a breeding ground for developing and testing new entrepreneur skills and talents but also promote an indigenous-based economy.

Thus, an increased emphasis and attention to the development of our SMEs would be a viable solution for a sustainable manufacturing sector.

(8) **Enforcement of a virile fiscal discipline and moral orientation that would shift the focus of our legislators, politicians, and decision-makers from "sharing the cake to baking and enlarging the cake"**

(9) Reducing unwarranted bureaucracy that would, among others, facilitate and enhance easy and quick business registration and prompt clearance of goods at the ports.

(10) **Reinvigorating the fight against corruption in all facets of our public and private life has become imperative.**

(11) **Putting in place measures to deal with the emerging threats to national security from militia and religious fanatics** in the form of terrorism, killing, and kidnapping that have become the order of the day in Nigeria and a potential threat to foreign investors

Above all, there is a need for all stakeholders in the Nigerian economy, and the manufacturing sector in particular, to be more committed to saving the economy and the manufacturing sector in particular from the looming danger.

4. CONCLUSION

Looking at the state of the economy, the performance of the manufacturing sector, and the rising level of unemployment, poverty, and insecurity, Nigeria is already falling short of her Millennium Development Goals of halving the poverty level and creating a conducive environment for growth by the year 2025. However, as we embark on the journey of overcoming the challenges in the manufacturing sector, there is hope for a better future for this country if our policymakers borrow a leaf from the experiences of the fast-developing Asian countries of Malaysia, Singapore, India, and China. This hope must rest on the government developing the will, capacity, and determination to initiate policies and programmes that would turn around the fortunes of the Nigerian manufacturing sector and thereby enable it to perform its unique role of wealth creation, employment generation, and poverty alleviation.

5. Recommendation

Based on the findings, the following recommendations are made:

1 The government must work to revive the sector and also collaborate with private individuals and investors, it is crucial to remember that the government's efforts to boost manufacturing sector output by boosting capital spending must be properly handled, especially with regard to electricity supply, which is one of the main priorities of the current civilian.

2. The government should, through its agencies, lower the interest rate to entice private investors and business people to make investments that will boost Nigeria's economic growth.

3. To encourage additional investments in the Nigerian economy and ensure stability in the country's economic growth, the government, through the Central Bank of Nigeria (CBN), should lower the rate at which foreign currencies are converted to the Naira.

6. References

Adedipe, B. (2007). Manufacturing: way of out of Precipice. Zenith Economic Quarterly, Lagos, 2(12): 33-41

Adejugbe, A. (2004). Industrialization, Urbanization and Development in Nigeria, Lagos. Concepts Publications

Adenikinju, A. Soderling, L., Soludo, C. and Varoudakis, A. (2002). Manufacturing Competitiveness in Africa: Evidence from Cameroun, Cote d'Ivoire, Nigeria and Senegal. Journal of Economic Development and Cultural Change, 50(3): 649-664

Akinlo, E. A. (1996). Improving the Performance of the Nigerian Manufacturing Subsectors after Adjustment: Selected Issues and Proposals. Nigerian Journal of Economics and Social Studies, 38(2): 91-110.

Bamidele, R. O. (2005). Globalization and the Nigerian Manufacturing Sector. Nigerian Journal of Economics and Social Studies, 47(2): 281-332.

Banjoko, S. A. (2009). The Nigerian Manufacturing Sector: Bumpy Past and Shaky Future what Options for survival? University of Lagos Inaugural Lecture series.

Banjoko, S. A. (2002). Maximizing the Value of the Production System in the Nigerian Manufacturing Industries. Journal of Management Studies, 9 (January): Edition, 50-64.

Egwaikhide, F. O., Ekpo, A. H., Oyeranti O. and Ayodele O. (2001). Four Decades of Industrialisation in Nigeria: A Critical Analysis. Nigerian Journal of Economics and Social Studies, 42(2): 365-391.

Hall, A. (1992). Technological Capabilities and Industrialization. World Development, 20(2): 165-186

Joshua, S. R., Happy, D. G. and Dankumo, A. M. (2016). Growth of non-oil sectors: A key to diversification and economic performance in Nigeria. Public Policy and Administration Research, 6(3), 64-75

Owan, P., Garbini, J., and Devasia, S. (2020). Faster confined space manufacturing teleoperation through dynamic autonomy with task dynamics imitation learning. IEEE Robotics and Automation Letters, 5(2), 2357-2364.

PAPER 112 - CONCENTRATION LEVELS AND HEALTH IMPLICATIONS OF POLYCYCLIC AROMATIC HYDROCARBONS (PAHs) IN MAINSTREAM SMOKES FROM CIGARETTE AND MARIJUANA

J.A. Adeniran[1*], A.K. Oyeneye[1], K.A. Abdulraheem[2], E. T. Odediran[1], S. A. Atanda[1], B. T. Ogunlade[1]

[1]Department of Chemical Engineering, University of Ilorin, Ilorin, Nigeria.
[2]Department of Water Resources and Environment, Ahmadu Bello University, Zaria, Nigeria
[*]Email: adeniran.ja@unilorin.edu.ng

ABSTRACT
This study examined the concentration levels and health implications of particulate-bound PAHs in the mainstream smoke of selected cigarette and marijuana samples. The ring profile revealed that 3 ring congeners constituted the major constituents of the marijuana samples with a 73% percentage contribution. The carcinogenic and non-carcinogenic distribution showed that about 95% of the analysed marijuana samples (with a mean value of 11.324 µg) were found to be non-carcinogenic while only 5% of the samples were carcinogens and the analysed cigarette samples showed that about 89% (with a mean value of 10.29 µg) were found to be non-carcinogenic while only 11% of the samples were carcinogens. Health risk assessment associated with PAH revealed that for the marijuana samples, the WHO ILCR value was 75 folds higher than the acceptable level of 10^{-5}. The USEPA ILCR value was 5 folds higher than the acceptable level of10^{-6} . The approximated mean value of 8 indicated that the HQ value exceeded the acceptable level by 8 folds. The WHO ILCR value was 40 folds higher than the acceptable level of 10^{-5} while that of USEPA was 2.78 folds higher than the acceptable level of 10^{-6}.

KEYWORDS: Incremental lifetime cancer risk, carcinogenic PAHs, Hazard quotients, Mainstream smoke, Marijuana

1. INTRODUCTION

Tobacco smoke is the leading cause of lung cancer death, accounting for more than 85% of all lung cancer deaths (Bray *et al*., 2018). They are not only a causal agent for lung cancer but are also classified as one of the most dangerous cancer-causing agents in humans, a Group A carcinogen. There are various tobacco products that people of different ethnicities, and age groups take either through sniffing, smoking, or injecting into the bloodstream. One of the most popular products is cigarettes with a downward trend in its global consumption. However, alternative tobacco products such as cigars, cigarillos, and water pipes (shisha) have significantly grown in their usage *(Weitzman et al., 2016).* There has been a general misconception that water pipe (shisha) is a safer alternative to cigarettes owing to the fact that the smoke is filtered through water (Rankin, 2011), but in truth, the water does not effectively remove highly toxic pollutants such as heavy metals polycyclic aromatic hydrocarbons (PAHs), carbon monoxide and carcinogens which are constituents of smoke that are being produced by tobacco smoke (Pourgholam-Amiji and Khoshravesh, 2022). *Cannabis sativa*, often known as Indian hemp, hemp, ganja, hashish, hemp, grass, and marijuana, is a plant species belonging to the Cannabinaceae family. It contains the chemical compound THC (trans-Δ^9-tetrahydrocannabinol), with chemical formula $C_{19}H_{26}O_2$ believed to be accountable for the characteristic psychoactive effects of cannabis that results in the "high sensation" observed when marijuana is consumed (Boonyayothin *et al*., 2022). The dried leaves and flowers commonly referred to as marijuana can be hand-rolled or consumed in edibles such as cookies, rice, beans, and gummies. Some of the health effects of marijuana include; increased pulse and heart rate; distorted perceptions of time and space (toxic psychosis); an altered state of consciousness; hallucinations and feelings of unreality. Carcinogens in marijuana can cause respiratory issues.

The United States Environmental Protection Agency (USEPA) classified only sixteen out of the numerous PAHs present in the environment as priority pollutants. This priority PAHs include benzo[ghi]perylene (BghiP), fluoranthen (Flan), anthracene (Anth), benzo[a]anthracene (BaA), indeno[1,2,3-cd]pyrene (IcP), naphthalene (Naph), acenaphthalene (Acy), acenaphthene (Ace), phenanthrene (Phen), fluorene (Fln), pyrene (Pyr), chrysene (Chr), Benzo[b]fluoranthene (BbF), Benzo[k]fluoranthene (BkF), benzo[a]pyrene (BaP), dibenz[a,h]anthracene (DahA) (Kumar *et al*., 2014). Out of the 16 priority PAHs, benzo(a)pyrene is considered as the benchmark as it is the most toxic of the priority PAHs (AIRC, 2010). Seven of the 16 PAHs in this priority group (Chr, BaA, BbF, BkF, BaP, DahA, and IcP) have been identified as likely human carcinogens (Aslam *et al*., 2022; Han *et al*., 2019; Zhang *et al*., 2022). This study aimed to examine the concentration levels of Polycyclic Aromatic Hydrocarbons (PAHs) present in selected cigarette and marijuana smoke samples available in Nigeria as well as to estimate the health risks accompanying marijuana and cigarette smoking using some health indexes.

2 MATERIALS AND METHOD

2.1 Sample Collection and Chemical Analysis

Five brands of filtered cigarettes and raw marijuana carefully selected based on their consumption rate in Nigeria were investigated to quantify their related human health risk. Table 1 shows the sample code for the different brands of cigarettes and marijuana adopted for this research. Marijuana being contraband necessitated the application for ethical approval from the University of Ilorin's ethical review committee. The protocol (with identification number UERC/ENG/074) was fully approved by the University of Ilorin committee on ethical review with approval number UERC/ASN/2023/2459. Cigarette and marijuana samples were locally sourced and stored at room temperature, but carefully placed in a zipper-lock to avoid airborne contaminants.

Table 1: Sample codes for cigarette and marijuana

S/N	Sample	Sample Code	Brand Name	Brand Description
1	Cigarette	C1	Bohem	Imported/Filtered
2		C2	Gum	Imported/Filtered
3		C3	Oris	Imported/Filtered
4		C4	Rothmans	Imported/Filtered
5		C5	Royals	Imported/Filtered
1	Marijuana	M1	Arizona	Local/Unfiltered
2		M2	Colorado	Local/Unfiltered
3		M3	Jedi	Local/Unfiltered
4		M4	Local Igbo	Local/Unfiltered
5		M5	Loud	Local/Unfiltered

2.2 Description of Experimental Set-up

This study was conducted using a syringe-lung model (Figure 1) in the Environmental Engineering research laboratory of the Department of Chemical Engineering, University of Ilorin. The mainstream smoke of cigarettes and marijuana was collected using the syringe lung model (an improvised smoking machine specifically designed for this research). The syringe model comprised a 60 ml syringe and a pair of one-way air valves which prevents the inflow of smoke particles into the respiratory tract during puffing as well as outflow of the particle during sucking. A connecting hose was used to connect all the units and serve as an air passage for smoke particles. The cotton wool (representative lung) was used as a medium to collect the mainstream smoke samples. Adopting the ISO standards, the smoking machine drew puffs of cigarette smoke into the cotton wool, lasting 2 seconds at 60 seconds puff intervals (ISO 1986). Similarly, the procedure was repeated for the marijuana samples. Each experimental run lasted about 5 minutes. PAHs ladened wool was properly labelled and stored for further analysis.

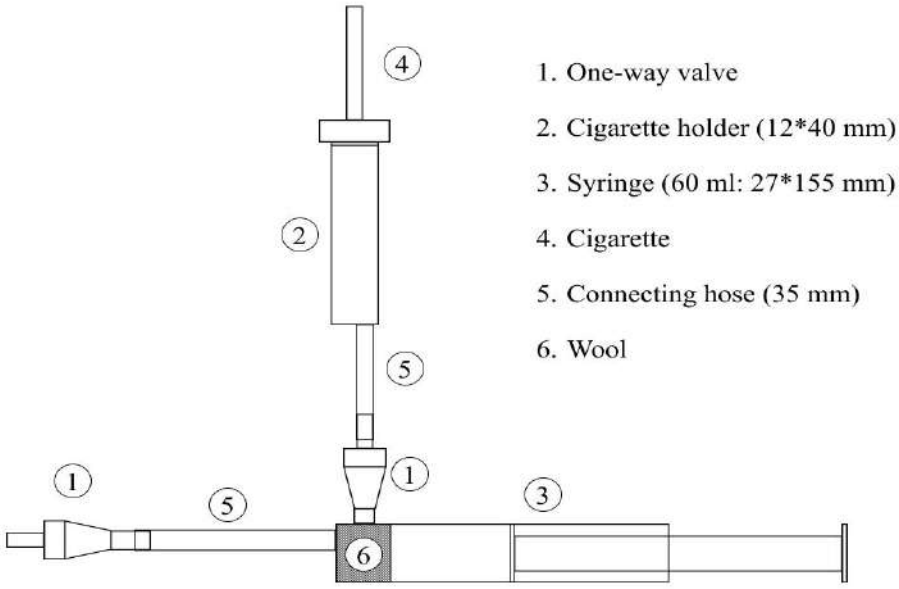

Figure 1: Smoking machine

2.3 Sample Digestion and Analysis

The smoke particles deposited on the cotton wool were extracted by solid-liquid extraction using Soxhlet apparatus by passing a solution of dichloromethane (DCM) over the cotton wool thereby washing out the residual pollutants from the wool. The smoke extract-DCM solution was then concentrated to obtain a pure extract of the smoke particles. Clean-up procedure was carried out using 5 g of silica gel column, eluted with 40 mL 1:1, DCM: Hexane (Olusola A Adesina, 2021). 20 ml of the extract was concentrated using a rotary evaporator under a gentle stream of nitrogen. The PAH analysis was carried out by injecting the sample into the Gas chromatography-mass spectrometry (GC-MS). Factors such as internal standard calibration, retention folds, and target qualifier ions were used for the identification and quantification of PAHs present in the analysed samples

2.2 Health risk analysis

The major health risk indexes measured in this study were; Toxicity equivalence (TEQ), Incremental life cancer risk (ILCR), and Hazard quotient (HQ). Calculations for TEQ, ILCR, and HQ for PAHs are given by Equations 1 to 4;

Toxicity equivalent quotient

$$TEQ = C \times TEF \quad (1)$$

Where; C is the individual concentration of PAHs, TEF is the toxic equivalent factor.

Incremental life cancer risk (ILCR)

$$ILCR = EC \times UR \quad (2)$$

Where EC is the exposure concentration, UR is the cancer unit risk. The values for cancer unit risk adopted in this research are 8.7×10^{-2} and 6×10^{-4} min^{-1} for WHO and USEPA, respectively. The exposure concentration can be calculated using Equation 3

$$EC = \frac{C \times ED \times EF}{AT} \quad (3)$$

Where; ED is the exposure duration in years (26 years), and EF is exposure frequency. Assuming a daily smoking habit of 365 days/year, AT is the mean exposure time in days equivalent to 25550.

Estimation for Hazard Quotient

$$HQ = \frac{C \times IR \times ED \times EF}{AT \times BW \times RfD} \quad (4)$$

RfD is the reference dose of PAHs (2×10^{-3})

3. RESULTS AND DISCUSSION

3.1 Concentration of PAHs in Cigarette and Marijuana Samples

The concentration of PAHs (µg/m^3) in the analysed marijuana samples is shown in Table 1. Only twelve out of the 16 priority PAHs were present in the analysed samples. Hence Benzo[k]fluoranthene (BkF), dibenz[a,h]anthracene (DhA), benzo[a]pyrene (BaP), indeno[1,2,3-cd]pyrene (IcP) were not detected in the samples. The most prevailing PAH in the analyzed marijuana sample was Fluorene which made up about 24.7%

of the total amount of PAH in all the samples. Phenanthrene, naphthalene, acenaphthalene, acenaphthene, and anthracene all made up a significant percentage of the PAH in the marijuana samples with 19.9, 17.5, 9.0, 9.5, and 9.0% respectively. A similar trend was reported in an early study by (Olusola Adedayo Adesina *et al*., 2022) Wei, *et al*., (2016). Similarly, for the cigarette sample, the most prevailing PAH was acenaphthalene which made up about 20% of the total PAHs in the samples. Anthracene, pyrene, acenaphthene, and chrysene all made up a significant percentage of the PAH in the cigarette samples with 17.5, 13, 11.97, and 11.31% respectively. This is attributable to the low molecular weight of these compounds. 3 out of the 7 carcinogenic PAHs (chrysene, benzo[a]anthracene, and Benzo[b]fluoranthene having mean concentration values of 0.416, 0.186, and 0.024 µg were observed in the marijuana. Conversely, the same carcinogenic PAHs were observed in cigarette samples with mean values of 1.312, 0.002, and 0.002 µg respectively. Figure 2 shows the concentration of PAHs in smoke samples of Cigarette and marijuana

The mean concentration of PAHs in the cigarette smoke samples showed the following trends: ACY> ANTH >PRY>ACE>CHRY>FLU>FLAN>NAPH> PHEN >B(ghi)P >B[a]A =BbFand FLU > PHEN > NAPH > ACE > ACY > ANTH > CHRY > FLAN >BaA> PRY > B(ghi)P >BbF in the marijuana samples.

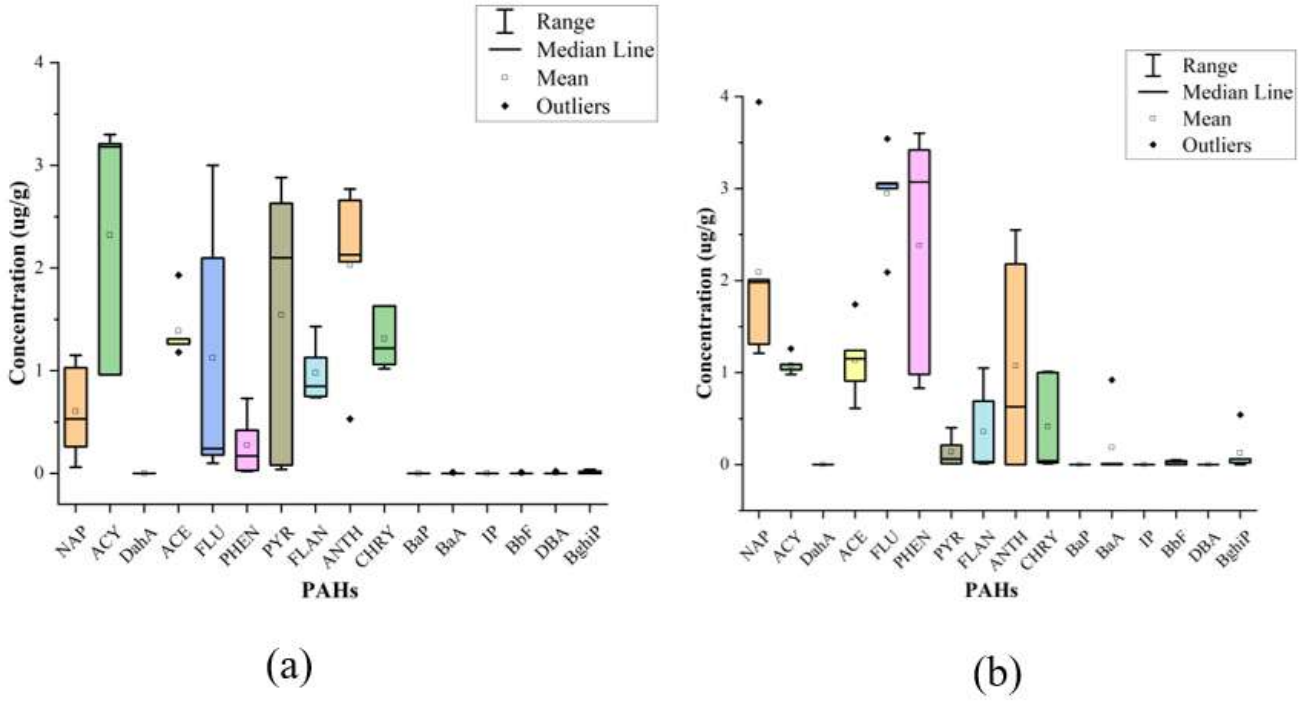

Figure 2: Concentration of PAHs in smoke samples of (a) Cigarette (b) marijuana

Table 1: Mean concentration of PAHs in the mainstream smoke of Cigarette and Marijuana

PAHs	Cigarette					Marijuana				
	Mean	SD	Min	Max	PAH %	Mean	SD	Min	Max	PAH %
NAPH	0.606	0.474	0.06	1.15	5.224	2.09	1.098	1.21	3.94	17.49
ACY	2.322	1.244	0.96	3.3	20.017	1.078	0.109	0.98	1.26	9.021
ACE	1.388	0.307	1.18	1.93	11.966	1.13	0.419	0.61	1.74	9.456
FLU	1.124	1.341	0.1	3	9.686	2.948	0.527	2.09	3.54	24.669
PHEN	0.274	0.302	0.02	0.73	2.362	2.38	1.361	0.83	3.6	19.916
PRY	1.546	1.386	0.04	2.88	13.328	0.138	0.168	0.01	0.4	1.155
FLAN	0.98	0.297	0.74	1.43	8.448	0.36	0.483	0.01	1.05	3.013
ANTH	2.03	0.895	0.53	2.77	17.5	1.072	1.215	0	2.55	8.971
BghiP	0.016	0.017	0	0.04	0.138	0.128	0.231	0	0.54	1.071
CHRY	1.312	0.3	1.02	1.63	11.31	0.416	0.538	0.01	1.01	3.481
BaA	0.002	0.004	0	0.01	0.017	0.186	0.41	0	0.92	1.556
BbF	0.002	0.004	0	0.01	0.017	0.024	0.023	0	0.05	0.201

3.2 *Classifications of PAHs*

3.2.1 Ring profile

PAHs are classified based on their ring profile, carcinogenic and non-carcinogenic distribution as well as molecular weight. Figures 3a and b show the ring profile and carcinogenic and non-carcinogenic distribution of PAHs present in the analysed samples of marijuana. About 73% of the PAHs detected in the marijuana samples were made up of 3 rings while Naphthalene (2 ring PAH) made up about 18%. About 9% of the total PAHs in the marijuana samples were observed to contain 4 rings. B[b]F was the only high molecular weight (5 benzene rings) slightly present in the samples having a percentage of 0.2%. Similarly, in the analysed cigarette samples about 62% of the PAHs detected were made up of 3 rings while Naphthalene (2 ring PAH) made up only 5%. About 33% of the total PAHs in the cigarette samples were observed to contain 4 rings. B[b]F was the only high molecular weight (5 benzene rings) slightly present in the samples having a percentage of 0.02%.

Another index used to classify PAHs is the molecular weight. Low molecular weight LMW is comprised of 2 and 3 rings, medium molecular weight MMW is made up of 4 ring PAHs while 5 and 6 ring PAHs are classified as high molecular weight HMW. For the marijuana samples, about 90.6% accounted for LMW, 9.2% MMW and 0.2% HMW. Similarly, for the cigarette samples about 66.89% accounted for LMW, 33.10% MMW, and 0.02% HMW.

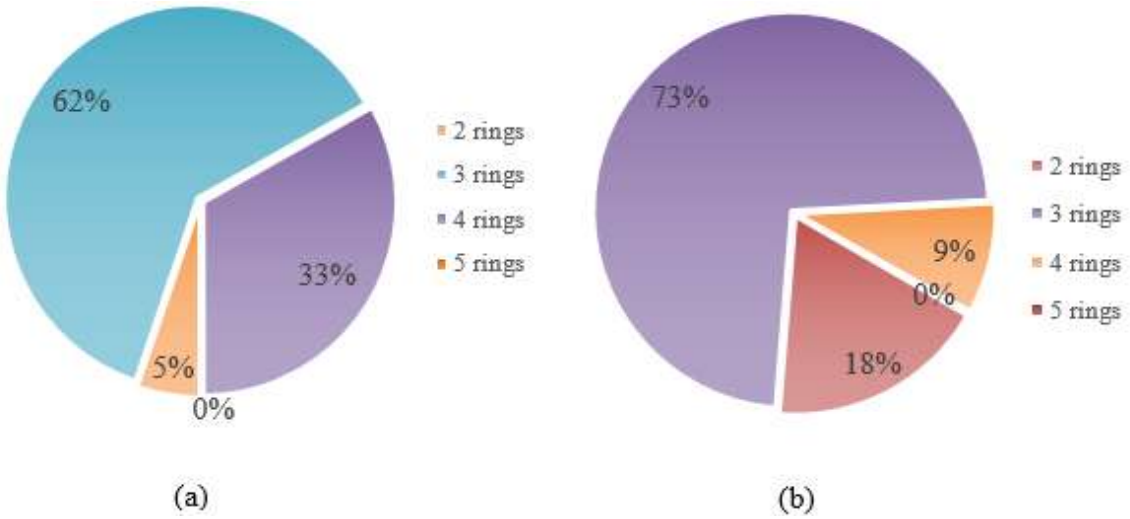

Figure 3: Ring profile classification of PAHs in (a) Cigarette (b) Marijuana

3.2.2 Carcinogenic and Noncarcinogenic Distribution

The carcinogenic and non-carcinogenic distribution showed that about 95% of the analysed marijuana samples (mean value of 11.324 µg) were found to be non-carcinogenic while only 5% of the samples were carcinogens. Similarly, the carcinogenic and non-carcinogenic distribution showed that about 89% of the analysed cigarette samples (mean value of 10.29 µg) were found to be non-carcinogenic while only 11% of the congeners present in the smoked samples were carcinogens.

B[a]P usually a marker for carcinogenic activity and stability of PAHs was not observed in the analysed sample. Similar trends have earlier been reported by (Olusola Adedayo Adesina *et al*., 2022).

3.3 Health Risk Analysis of PAHs

3.3.1 The Toxicity Equivalence

The toxicity equivalence (TEQ) of individual PAHs present in the samples of marijuana analysed was calculated by multiplying the individual PAH concentration with their respective toxicity equivalence factor. Table 2 shows the toxicity equivalence of all the individual PAH present in the smoked samples of cigarettes and marijuana. BghiP has the highest contributing factor of TEQ in all the marijuana samples analysed with a mean value of 0.128 µg/m3. Other congeners with high TEQ are BaA, ANTH, CHRY, and FLU, with mean TEQ values of 0.019, 0.011, 0.004, and 0.003 µg/m3, respectively. The total toxicity equivalence for various marijuana samples was found to be in the order; M2 (0.556) > M1 (0.135) > M4 (0.105) > M5 (0.061) > M3 (0.014), with a percentage

contribution of 64, 15, 12, 7 and 2%, respectively. Figure 4 illustrates cancer and non-cancer distribution of PAHs in Cigarette and Marijuana.

Similarly, for the cigarette samples, baring C1 where BghiP has the highest factor contribution, ANTH was found to be predominant in all other samples. Thus, ANTH has the highest TEQ contribution with a mean value of 0.02 µg/m3. Total toxicity equivalence for the various cigarette samples is in the order of C5 (0.072) > C1 (0.065) > C4 (0.062) > C3 (0.052) > C2 (0.039), with a percentage contribution of 26, 22, 21, 18 and 13%, respectively

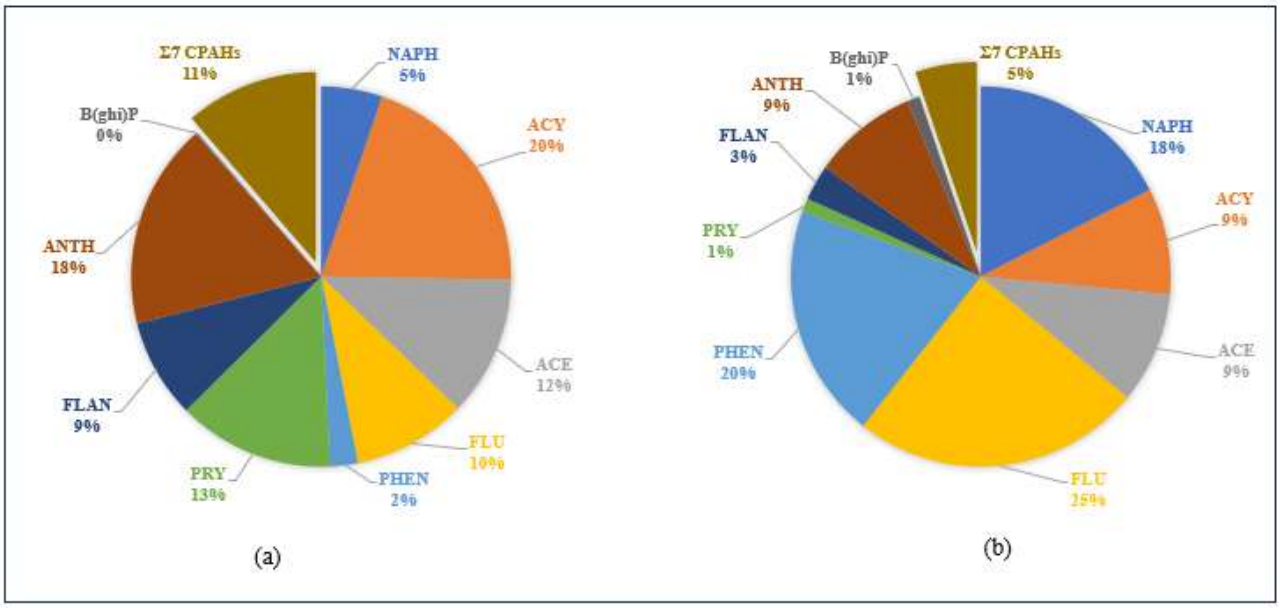

Figure 4: Cancer and Non-cancer distribution of PAHs in (a) Cigarette (b) Marijuana

3.3.2 Incremental Life Cancer Risk and Hazard Quotient

The mean value of the incremental life cancer risk of the marijuana samples based on WHO and USEPA risk factors were found to be 0.00075 and 5.176 ×10^(-6) respectively. This showed that the ILCR obtained using WHO risk factor was 75 folds higher than the acceptable level of 10^(-5). Similarly, the ILCR obtained using the USEPA risk factor was 5 folds higher than the acceptable level of 10^(-6). Sample M1 had the highest contributing factor for the WHO and USEPA ILCR. These values are subject to change with an increase in exposure frequency and duration of marijuana smoke. On the other hand, the mean value of the ILCR of the cigarette samples based on WHO and USEPA risk factors were found to be 0.00040 and 2.781 ×10^(-6) respectively. This indicated that the ILCR value exceeded the WHO limit by 40 folds. Similarly, the USEPA ILCR value was 2.78 folds higher than the acceptable level of 〖10〗^(-6). Thus, it can be inferred from the results that the cancer risk associated with marijuana was higher compared to that of cigarette. Continuous environmental exposure to PAHs may result in leukemia, skin cancer, and lung cancer (Li *et al*., 2017).

Hazard quotient values of the marijuana samples ranged between 0.63 and 25.43. The approximated mean value of 8 indicated that the HQ value exceeded the acceptable level by 8 folds. Similarly, the hazard quotients relating to cigarette ranged from 1.78 to 3.29 with an approximated mean value of 2.7. This indicated that the hazard quotient exceeded the acceptable level by 2.7 folds. Cancer Risk and Hazard Quotient of PAH Samples is illustrated in Table 3.

Table 2: PAHs Toxicity Equivalence in Samples of Cigarette and Marijuana

S/N	PAHs	TEQs									
		C1	**C2**	**C3**	**C4**	**C5**	**M1**	**M2**	**M3**	**M4**	**M5**
1	NAPH	0.0010	0.0012	0.0005	0.0003	0.0001	0.0039	0.0020	0.0020	0.0012	0.0013
2	ACY	0.0010	0.0010	0.0032	0.0033	0.0032	0.0013	0.0010	0.0010	0.0010	0.0011
3	ACE	0.0013	0.0013	0.0012	0.0013	0.0019	0.0006	0.0012	0.0009	0.0017	0.0012
4	FLU	0.0030	0.0021	0.0002	0.0001	0.0002	0.0031	0.0030	0.0021	0.0035	0.0031
5	PHEN	0.0007	0.0002	0.0004	0.0000	0.0000	0.0036	0.0034	0.0031	0.0008	0.0010
6	PRY	0.0001	0.0000	0.0021	0.0026	0.0029	0.0000	0.0002	0.0004	0.0000	0.0001
7	FLAN	0.0014	0.0011	0.0007	0.0009	0.0008	0.0007	0.0000	0.0000	0.0000	0.0011
8	ANTH	0.0053	0.0206	0.0277	0.0213	0.0266	0.0063	0.0000	0.0000	0.0255	0.0218
9	BghiP	0.0400	0.0000	0.0000	0.0200	0.0200	0.0200	0.5400	0.0000	0.0600	0.0200
10	CHRY	0.0102	0.0106	0.0163	0.0122	0.0163	0.0001	0.0004	0.0002	0.0101	0.0100
11	BaA	0.0010	0.0000	0.0000	0.0000	0.0000	0.0920	0.0000	0.0000	0.0010	0.0000
12	BbF	0.0000	0.0010	0.0000	0.0000	0.0000	0.0030	0.0050	0.0040	0.0000	0.0000
	TTEQs	**0.0650**	**0.0390**	**0.0524**	**0.0620**	**0.0719**	**0.1346**	**0.5562**	**0.0137**	**0.1049**	**0.0606**

Table 3: Cancer Risk and Hazard Quotient of PAH Samples

	CR		**HQ**
Sample	**WHO $\times 10^{-4}$**	**USEPA$\times 10^{-6}$**	
C1	3.34	2.3	2.97
C2	3.46	2.4	1.78
C3	4.86	3.4	2.41
C4	3.64	2.5	2.83
C5	4.86	3.4	3.29

Mean	4.03	2.8	2.66
M1	28.4	20.0	6.15
M2	1.61	1.1	25.43
M3	1.25	0.86	0.63
M4	3.31	2.3	4.40
M5	2.98	2.1	2.77
Mean	7.50	5.2	7.95

Acknowledgement
The author acknowledges the support of the Ethical review committee of the University who provided the ethical backing to carry out this research work and the Petroleum Technology Development Fund (PTDF) for the funding provided which played a crucial part to achieving this successful feat

Declaration of Competing Interest
The authors declare that they have no known financial interests or interpersonal relationships that might have influenced the research presented in this study.

REFERENCES

Adeniran, J. A., Abdulraheem, M. O., Ameen, H. A., Odediran, E. T., & Yusuf, M.-N. O. (2021). Source identification and health risk assessments of polycyclic aromatic hydrocarbons in settled dusts from different population density areas of Ilorin, Nigeria. *Environmental monitoring and assessment, 193*, 1-16.

Adeniran, J. A., Jimoh, B. F., Atanda, A. S., Adewoye, L. T., Yusuf, M.-N. O., Abdulraheem, K. A., Odediran, E. T., & Adesina, O. A. (2023). Health Risk Assessment of Polycyclic Aromatic Hydrocarbons from Cooking Fuels burning in Nigeria. *Polycyclic Aromatic Compounds*, 1-16.

Adesina, O. A., Tosin, O., Lala, M., Adeyemo, A. T., & Sonibare, J. (2022). Levels of Polycyclic Aromatic Hydrocarbon and Polychlorinated Biphenyl in the Mainstream Smoke of Cannabis Sativa and Health Implications. *Journal of Drug and Alcohol Research, 11*(10), 1-7.

Adesina, O. A., Adesina, A. O., & Adeniran, J. A. (2020). Level of polycyclic aromatic hydrocarbon emission in the ambient air and residual ash from a typical municipal solid waste open burning site in Nigeria. *Waste Disposal & Sustainable Energy, 2*, 105-111.

Ahmadipour, F., Sari, A. E., & Bahramifar, N. (2020). Characterization and health risk assessment of particulate-bound polycyclic aromatic hydrocarbons in Tehran, Iran. *Air Quality, Atmosphere & Health*, *13*, 1431-1438.

Aslam, R., Sharif, F., Baqar, M., & Shahzad, L. (2022). Source identification and risk assessment of polycyclic aromatic hydrocarbons (PAHs) in air and dust samples of Lahore City. *Scientific Reports*, *12*(1), 2459.

Benevenuto, S. G., Domenico, M. D., Yariwake, V. Y., Dias, C. T., Mendes-da-Silva, C., Alves, N. d. O., . . . Cardoso, M. S. (2022). Prenatal exposure to Cannabis smoke induces early and lasting damage to the brain. *Neurochemistry International, 160*, 105406.

Boonyayothin, W., Kobtrakul, K., Khositanon, P., Vimolmangkang, S., & Phoolcharoen, W. (2022). Development of a plant-produced recombinant monoclonal antibody against Δ-9-tetrahydrocannabinol (Δ9-THC) for immunoassay application. *Biotechnology Reports, 34*, e00725.

Bray, F., Ferlay, J., Soerjomataram, I., Siegel, R. L., Torre, L. A., & Jemal, A. (2018). Global cancer statistics 2018: GLOBOCAN estimates of incidence and mortality worldwide for 36 cancers in 185 countries. *CA Cancer J Clin, 68*(6), 394-424. doi:10.3322/caac.21492

Han, J., Liang, Y., Zhao, B., Wang, Y., Xing, F., & Qin, L. (2019). Polycyclic aromatic hydrocarbon (PAHs) geographical distribution in China and their source, risk assessment analysis. *Environmental Pollution, 251*, 312-327.

Kermani, M., Jafari, A. J., Gholami, M., Farzadkia, M., Shahsavani, A., & Norzaee, S. (2021). Polycyclic aromatic hydrocarbons in PM 2.5 atmospheric particles in Shiraz, a city in southwest Iran: Sources and risk assessment. *Arabian Journal of Geosciences, 14*, 1-10.

Li, Y., Song, N., Yu, Y., Yang, Z., & Shen, Z. (2017). Characteristics of PAHs in street dust of Beijing and the annual wash-off load using an improved load calculation method. *Science of the Total Environment, 581*, 328-336.

Mosallaei, S., Hashemi, H., Hoseini, M., Dehghani, M., & Naz, A. (2023). Polycyclic aromatic hydrocarbons (PAHs) in household dust: the association between PAHs, cancer risk and sick building syndrome. *Building and Environment*, *229*, 109966.

Mueller, A., Ulrich, N., Hollmann, J., Sanchez, C. E. Z., Rolle-Kampczyk, U. E., & von Bergen, M. (2019). Characterization of a multianalyte GC-MS/MS procedure for detecting and quantifying polycyclic aromatic hydrocarbons (PAHs) and PAH derivatives from air particulate matter for an improved risk assessment. *Environmental pollution*, *255*, 112967.

Nazmara, S., Sorooshian, A., Delikhoon, M., Baghani, A. N., Ashournejad, Q., Barkhordari, A., Basmehchi, N., & Kasraee, M. (2020). Characteristics and health risk assessment of polycyclic aromatic hydrocarbons associated with dust in household evaporative coolers. *Environmental pollution*, *256*, 113379.

Nowakowski, M., Rykowska, I., Wolski, R., & Andrzejewski, P. (2022). Polycyclic aromatic hydrocarbons (PAHs) and their derivatives (O-PAHs, N-PAHs, OH-PAHs): Determination in suspended particulate matter (SPM)–A review. *Environmental Processes*, *9*(1), 2.

Odediran, E. T., Adeniran, J. A., Yusuf, R. O., Abdulraheem, K. A., Adesina, O. A., Sonibare, J. A., & Du, M. (2021). Contamination levels, health risks and source apportionment of potentially toxic elements in road dusts of a densely populated African City. *Environmental Nanotechnology, Monitoring & Management*, *15*, 100445.

Olise, F. S., Ogundele, L. T., Olajire, M. A., Owoade, O. K., Oloyede, F. A., Fawole, O. G., & Ezeh, G. C. (2019). Biomonitoring of environmental pollution in the vicinity of iron and steel smelters in southwestern Nigeria using transplanted lichens and mosses. *Environmental monitoring and assessment*, *191*, 1-13.

Pourgholam-Amiji, M., & Khoshravesh, M. (2022). The Effect of Irrigation with Magnetically Treated Effluent on Uptake of Some Heavy Metals in Maize Cultivation. *Iranian Journal of Soil and Water Research ISNN*, *2423*, 7833.

Purkayastha, K. (2021). Benzene and Polycyclic Aromatic Hydrocarbons. *Environmental Scientist*, 58-61.

Sun, K., Song, Y., He, F., Jing, M., Tang, J., & Liu, R. (2021). A review of human and animals exposure to polycyclic aromatic hydrocarbons: Health risk and adverse effects, photo-induced toxicity and regulating effect of microplastics. *Science of the total environment*, *773*, 145403.

Wang, Y., Guo, G., Zhang, D., & Lei, M. (2021). An integrated method for source apportionment of heavy metal (loid) s in agricultural soils and model uncertainty analysis. *Environmental Pollution*, *276*, 116666.

Weitzman, M., Yusufali, A. H., Bali, F., Vilcassim, M. J. R., Gandhi, S., Peltier, R., . . . Gordon, T. (2016). Effects of hookah smoking on indoor air quality in homes. *Tob Control*, *26*(5), 586-591. doi:10.1136/tobaccocontrol-2016-053165

Yang, L., Zhang, H., Zhang, X., Xing, W., Wang, Y., Bai, P., Zhang, L., Hayakawa, K., Toriba, A., & Tang, N. (2021). Exposure to atmospheric particulate matter-bound polycyclic aromatic hydrocarbons and their health effects: a review. *International journal of environmental research and public health*, *18*(4), 2177.

Yu, Y., Li, Q., Wang, H., Wang, B., Wang, X., Ren, A., & Tao, S. (2015). Risk of human exposure to polycyclic aromatic hydrocarbons: A case study in Beijing, China. *Environmental Pollution*, *205*, 70-77.

Yusuf, R. O., Odediran, E. T., Adeniran, J. A., & Adesina, O. A. (2022). Polycyclic aromatic hydrocarbons in road dusts of a densely populated African city: Spatial and seasonal distribution, source, and risk assessment. *Environmental Science and Pollution Research*, *29*(29), 44970-44985.

Zhang, J., Liu, W., Xu, Y., Cai, C., Liu, Y., Tao, S., & Liu, W. (2019). Distribution characteristics of and personal exposure with polycyclic aromatic hydrocarbons and particulate matter in indoor and outdoor air of rural households in Northern China. *Environmental pollution*, *255*, 113176.

Zhang, X., Wang, X., Zhao, X., Tang, Z., Zhao, T., Teng, M., Liang, W., Wang, J., & Niu, L. (2022). Using deterministic and probabilistic approaches to assess the human health risk assessment of 7 polycyclic aromatic hydrocarbons. *Journal of Cleaner Production*, *331*, 129811.

PAPER 113 - EXIGENCY FOR SURFACE MODIFIED COIR AND ITS APPLICATIONS -A REVIEW

M. Ndagi[1*], I. A. Tijani[2], S. O. Yakubu[3], A. D. Abdulraheem[4], S. Abdulkareem[1]

[1]Department of Mechanical Engineering, University of Ilorin, Ilorin, Nigeria.
[2]Department of Chemical Engineering, University of Ilorin, Ilorin, Nigeria.
[3]Department of Mechanical Engineering, Nigeria Defence Academy, Kaduna, Nigeria.
[4]Department of Materials and Metallurgical Engineering, University of Ilorin, Nigeria.
[*]Email: ndagi.m@unilorin.edu.ng

ABSTRACT
Natural insulating materials like rock wool and coir offer numerous benefits and uses, but their hydrophilic nature is a serious problem. Recent studies have revealed that a minor increase of 13.9% in moisture content can result in a 312% gain in thermal conductivity values of biomass materials such as rock wool. This review paper delves into the work of researchers in the biocomposite field as they explore the root causes of hydrophilicity in coir and other biomass materials, propose methods to reduce hydrophilicity, and suggest strategies to enhance the hydrophobicity of coir and other biomass materials for industrial application purposes.

KEYWORDS: Coir, Hydrophilicity, Hydrophobicity, Water contact angle

1. INTRODUCTION

Efficient heat insulation is essential for preserving energy and mitigating global warming. With the depletion of fossil fuels, contemporary technologies are relying more and more on cost-effective and renewable energy sources. This change necessitates reassessing worldwide energy strategies, as we aim to discover creative and ethical solutions to fulfil our energy requirements (Kumar *et al*., 2020; Tayfun *et al*., 2023). To extend their lifespan, insulating materials must resist environmental conditions, such as high humidity and condensation (Dong *et al*., 2023; Zhang and Wang, 2013). moisture ingress in insulation materials has been found to contribute immensely towards the rapid degradation of insulation materials. By implication, the rapid degradation of insulating materials affects synthetic and non-synthetic insulating materials. This is evident in several researches (Gusyachkin *et al*., 2019; Hoseini and Bahrami, 2017; Lakatos and Kalmár, 2013; Li *et al*., 2020; Ndagi *et al*., 2021; Torres-Rivas *et al*., 2018; Zhu *et al*., 2015). It is known that temperature, moisture, and density are the most significant factors that affect the thermal conductivity coefficient of materials (Pásztory, 2021; Wang *et al*., 2023).

Biomass insulation materials such as coir have been found to possess properties that rival synthetic insulation properties such as polyurethane and polystyrene. Coir is a lignocellulosic material which has a thermal conductivity range from 0.014-0.2797 W/mK (Cai *et al*., 2022; Hoseini and Bahrami, 2017; Ndagi *et al*., 2021; Thakur *et al*., 2016). However, the water absorption capacity of coir has also been found to be as high as 412%, this is due to the presence of lignocellulosic compounds which make the fibre hydrophilic (Li *et al*., 2023; Marakana *et al*., 2021). The thermal conductivity of biomass samples compared with polyurethane is shown in Table 1.

Table 1. Thermal conductivity of biomass samples compared with polyurethane (Ndagi *et al*., 2021).

Sample	Ratio	Sieve Size	Thermal conductivity (W/m/K)	Density (g/cm^3)
Control			0.01832	0.1670
Coir +bagasse	50:50	0.5 mm	0.01472	0.2474
	60:40		0.01472	0.2765
	70:30		0.01472	0.2599
Coir + bagasse	50:50		0.01467	0.2453
	60:40	1.0 mm	0.01467	0.2515
	70:30		0.01467	0.2494

Muthuraj *et al.* (2019) compared thermal conductivities from several works of literature with their physical experiment as shown in Figure 1 and concluded that biomass materials can compare favorably with synthetic insulation materials.

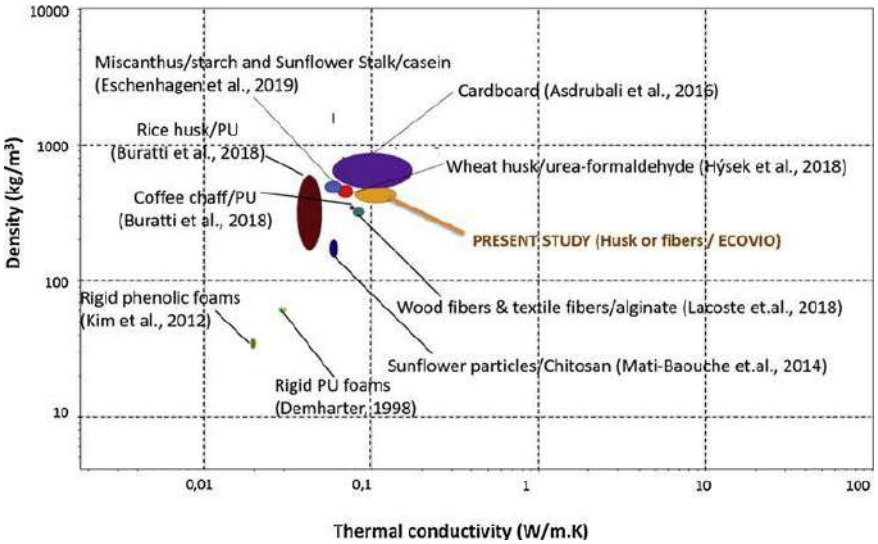

Figure 1 Thermal conductivity vs density of the different materials (Muthuraj *et al*., 2019)

In their research, Ndagi *et al*. (2021) summarized that Coconut coir and Sugarcane bagasse have lower thermal conductivity and lower thermal diffusivity compared to polyurethane, but, performed poorly in the water absorption test as compared to the control polyurethane sample. Sieve size and density played important roles in the thermo-physical and mechanical performance of the Bio-composite materials with a particle size of 1.0 mm having a higher density as coir percentage increased and performing better than 0.5 mm particle size in Mechanical and Thermal tests,1.0 mm particle size sample containing 70 % coir and 30 % bagasse is the most favourable for use as low temperature thermal insulating material to replace the synthetic ones presently used in low-temperature insulation application. Density has been found to have a significant impact on the thermal properties of insulation materials (Kumar *et al*., 2020; Owoeye *et al*., 2020; Pásztory, 2021)

K. F. Hasan *et al*. (2021), developed Novel insulation panels from multilayered coir short and long fibre reinforced phenol formaldehyde polymeric biocomposites. four composite panels of 360, 680, 800, and 1000 kg/m3 densities were formed through hot pressing technology. The thermal conductivity, microstructural, mechanical, and physical properties of the composite panels were investigated. Perceived thermal conductivity values ranged from 0.046280 (0.000494) to 0.062400 (0.001146) Wm–1 k–1 of the composites demonstrating superior insulation properties.

Coir fibre-reinforced composites have superior mechanical qualities compared to synthetic fibre-reinforced composites. However, the mechanical performance of coconut fibre-reinforced composites can be further increased by pretreating the surfaces of coir fibres. It has been reported that the tensile strength of coir-reinforced composites varies depending on fibre content and surface treatment factors. Studies have demonstrated that the tensile strength of coir fibre-reinforced epoxy composites can be greatly enhanced. For instance, a 40 wt% coir fibre-reinforced epoxy composite achieved tensile strengths of 77.99 MPa, which is 44% stronger than pure epoxy (Ahmed *et al*., 2017; Okpala *et al*., 2021; Singh *et al*., 2021).

2. COIR

Coconut coir, a waste product found in tropical countries, is a cost-effective filler for composites and insulation applications. Its high cellulose and lignin content makes it strong, durable, and resilient. The mesocarp, located in the centre of the fruit, is inedible and is a fibrous material (Mishra and Basu, 2020). Figure 2 is a photo illustration of a germinated coconut.

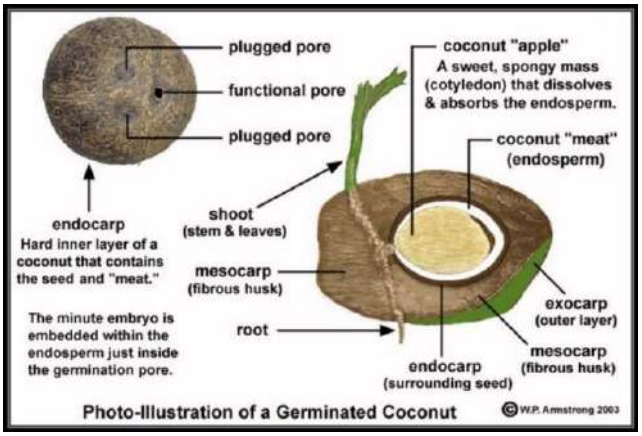

Figure 2: photo illustration of a germinated coconut (Mangat *et al*., 2023)

2.1 *Composition of Coir*

The main content of coconut fibre is cellulose, hemicellulose, and lignin. The lignin content in coconut fibres is very high.(Abraham *et al*., 2013; Arsyad *et al*., 2015). Coconut fibre has a green profile with 36.52% lignin, 33.61% cellulose, 29.27% pentosan, and 0.61% ash. In its dry state, it has 29.23% lignin, 26.00% total water-soluble, 23.81% cellulose, and 8.50% hemicelluloses(Azam, 2019; Mishra and Basu, 2020) Figure 3. Shows Structural representations of (A) cellulose, (B) hemicellulose, and (C) lignin in coconut fibre. The presence of these lignocellulosic compounds increases the hydrophilicity of coir which affects its thermophysical and mechanical strength.

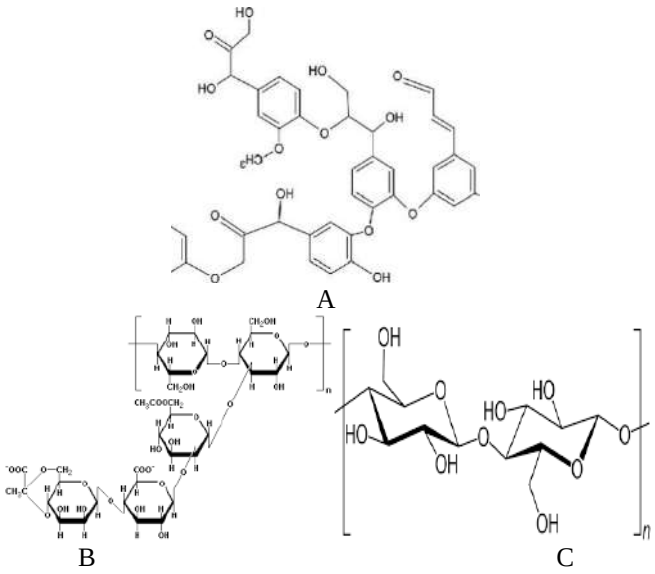

Figure 3. Structural representations of (A) cellulose, (B) hemicellulose, and (C) lignin. (Azam, 2019)

2.2 *Hydrophilicity of Coir*

Coir's hydrophilicity is influenced by its surface hydroxyl groups, cellulose, and porous structure. These factors allow it to easily interact with water molecules, and enhance its hydrophilicity. The porous structure also allows water to be absorbed, further enhancing its hydrophilic nature (Arsyad *et al*., 2015).

3. SURFACE MODIFICATION OF COIR

Coir surfaces can be modified through several methods including Mercerization, Acetylation aminopropyltriethoxy silane method, microwave method, and a combination of two or more methods stated above (Aravind *et al*., 2022; Hasan *et al*., 2021). however, most researchers modify the coir surface to improve its hydrophobicity and enhance its surface adhesion properties to the polymer matrix to improve the mechanical and physical properties of composites (Ali *et al*., 2018; Arsyad *et al*., 2015; Bakri *et al*., 2018; 2021; Bui *et al*., 2020; Cai *et al*., 2022; Ekpenyong *et al*., 2022; K. Hasan *et al*., 2021; Mir *et al*., 2013; Ng *et al*., 2018; Rahman and Khan, 2007; Sahu *et al*., 2020; Saw *et al*., 2011; Simimol *et al*., 2020; Singh *et al*., 2020; Sumi *et al*., 2018; Thakur *et al*., 2016) In their study, Mir *et al*. (2013) observed that, processing raw coir with chemicals results in the transformation of hydrophilic -OH groups into hydrophobic -OH Cr groups. As a result, the adhesion properties between the fibre surface and polymer matrix are enhanced. The treated surface underwent microstructural and

chemical examinations, which corroborated these findings. Figure 3 shows the relation between the tensile strength of raw coir, 3-hour treated coir, and 5-hour treated coir. The strength of the coir improved as hydrophobicity was substituted for hydrophilicity through chemical treatment. The level of success in cellulose removal is affected by the particle size of the coir and the period of immersion in the alkaline solution *(Rahayu et al*., 2022)**.**

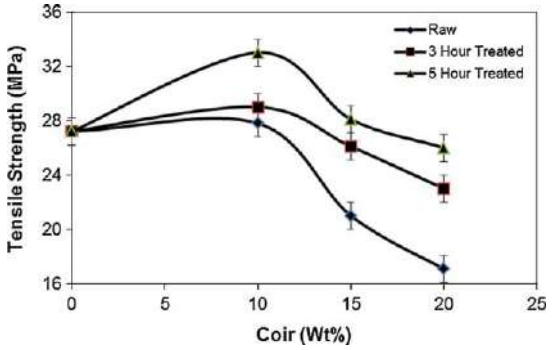

Figure 3 Variation of tensile strength of PP biocomposites reinforced with raw, 3h treated, and 5h treated coir (Mir *et al*., 2013).

3.1 *Mercerization*

The process of mercerization is an Alkaline treatment of fibres often employed in textile industries by applying NAOH to the surface of the fibre which causes the OH group present in the fibre to react with NAOH as shown in Equation 1 (Simimol *et al*., 2020).

$$Fiber - OH + NaOH \rightarrow Fiber\text{-}O\text{-}Na{+}{+}H2O \quad (1)$$

Fibres are immersed in sodium hydroxide solution of varying percentages of 5, 10, 15 and 20 kept overnight with occasional stirring. For neutralizing the acid,' they are then dipped into a 10% solution of HCl for half an hour, washed with running water, and air dried. The water/liquor ratio was maintained at 1: 24 at room temperature (Nurazzi *et al*., 2021).

Bakri *et al*. (2018) characterized coir fibres after treatment in various solutions of NAOH and inside a microwave oven at different intervals, Coir fibres were soaked in sodium hydroxide (NaOH) solution 5 wt.% for 24 hours. After soaking, fibres were rinsed and dried at room temperature for 48 hours. They sought to improve the mechanical strength of treated coir fibres. Figure 4 shows that the tensile strength of treated coir fibres improved significantly after Alkali treatment and 10-minute heating inside the microwave.

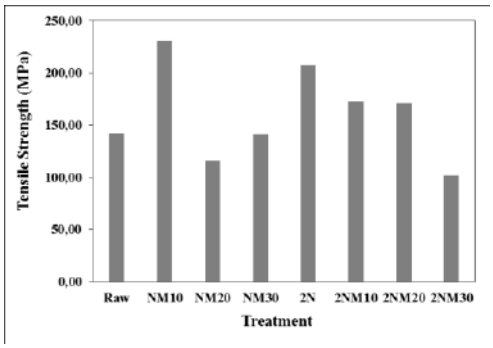

Figure 4 Tensile strength of raw and treated coir fibres.(Bakri *et al*., 2018)

Studies have shown that untreated natural fibres tend to be coated with substances like lignin, hemicellulose, wax, and oils. However, treating these fibres with alkali can result in a coarser and cleaner texture as some of the impurities are removed. Figure 5 illustrates this phenomenon. The alkali treatment also causes the fibre surfaces to become more uneven, reducing their diameter and increasing their aspect ratio. This increase in aspect ratio ultimately strengthens the interfacial bonding (Arsyad, 2019).

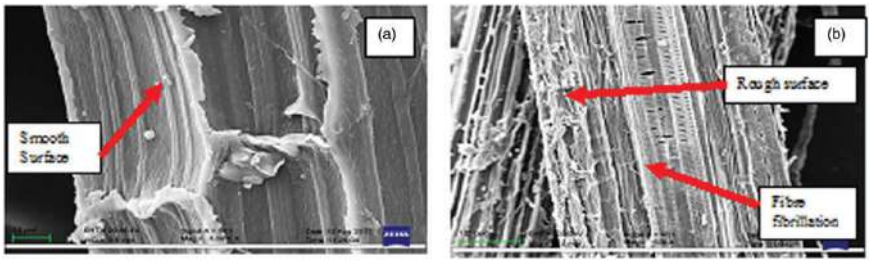

Figure 5. SEM images of sisal fibre: (a) untreated and (b) alkali-treated (Sahu *et al*., 2020)

3.2 *Acetylation*

Acetylation involves the grafting of acetyl groups onto cellulose fibres using the esterification method to plasticize the surface of the cellulose fiber as shown in equation 2. The durability of treated natural fibre samples in Alkaline and Acidic environments over some time was discussed by Sumi *et al*. (2018). They conducted tests on multiple treated coir specimens, exposing them to both alkaline and acidic environments for 12 months. The findings indicated that the degradation rates were slightly elevated in alkaline conditions when compared to acidic ones. Samples that were subjected to saline conditions or alternate wetting and drying conditions experienced a minor loss of tensile strength, which was less than 7%. The surface morphology of samples treated using the two chemical processes is shown in Figure 6(a and b) (Simimol *et al*., 2020).

$$Fibre\text{-}OH + CH3CO\text{-}OH \rightarrow Fibre\text{-}O\text{-}COCH3 + H2O \quad (2)$$

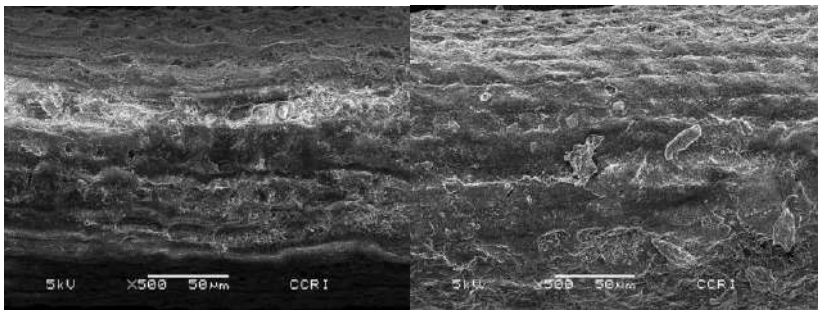

A B

Fig 6 (a) mercerisation (B) acetylation (Simimol et al., 2020)

3.3 *Aminopropyltriethoxysilane*

Aminopropyltriethoxysilane (APTES) is a crucial silicon compound in chemistry, used in the synthesis of materials. Metal oxide nanoparticles (MONP) are used for silanization, with amine incorporation improving dispersibility and antibacterial properties. APTES-MONPs are used in electrochemical sensors, catalysts, and Pickering emulsions (Zhang and Lai, 2022). Aminopropyltriethoxysilane (APTES) is a silane compound with the chemical formula C9H23NO3Si, used in the silanization process to functionalize surfaces with alkoxysilane molecules. It plays a significant role in the covalent bonding of organic films to metal oxides, particularly silica, and titania, which is crucial in biological and materials science (Piccinno *et al*., 2012) applications. The synthesis of APTES must be carried out with caution due to its toxicity and reactivity.

3.4 *Microwave Oven Method*

The microwave oven method of surface modification is a technology that can be used to modify the surface qualities of materials such as coir. This method involves the use of a microwave oven to produce plasma, which is then used for surface modification (Barnes *et al*., 2021).
In the context of coir, one study indicated that alkali-treated coir fibres may be changed by a silane coupling agent in a microwave oven. The application of microwave-assisted chemical treatments efficiently accelerated the esterification reaction, which improved the interfacial adhesion between the coir fibres and a PLA (polylactic acid) matrix.

4. EFFECT OF SURFACE MODIFICATION ON PROPERTIES OF COIR

Surface modification can significantly affect the properties of coir, particularly when it is used as a reinforcement in composite materials A study by Adediran *et al*. (2021) found that treating coir fibres with 1.5M NaOH improved the mechanical properties, thermal conductivity, and wear resistance of polypropylene composites reinforced with coir fibre and yam peel particulate. Coir Fiber Surface Treatment on Interfacial Properties of Reinforced Epoxy

Resin Composite. In their research, Ru, *et al*. (2022) showed that the combination of alkali treatment and aminopropyltriethoxysilane surface modification enhanced the interfacial bonding ability between coir fibres and epoxy resin, resulting in an interfacial shear strength and pullout energy of 6.728 MPa and 40.237 Nmm, respectively. Natural Fibre Reinforced Polyester: Surface modification of coir fibres with sodium hydroxide increased wettability and prevented the flotation and segregation of coir fibres.

4.1 *Mechanical Effects*

The influence of fibre surface modifications on the mechanical, thermal and morphological properties of coir/carbon fibre-reinforced epoxy-based hybrid composite was investigated by Singh *et al*. (2020). They found that treating fibres with NaOH resulted in superior mechanical properties compared to untreated samples. However, the tensile properties varied as the percentage of weight fibre loading decreased. The removal of lignin from the surface structure of coir fibres has been found to hurt the tensile strength of the fibre, in their research Bui *et al*. (2020) subjected different samples of coir fibres to alkali treatment and compared the results to raw untreated samples. Interestingly, samples were also subjected to boiling and results indicated that the Water absorption capacities of alkali-treated and raw fibre were found to be almost the same, but there was a remarkable reduction in the water absorption capacity of boiled fibre. The thermal conductivity decreased from 0.052 to 0.024W/M. K with the increase in density of the fibre bundles from 30 to 120 kg/m3. They also concluded that reduction in lignin. Pectin, fatty acid, and cellulose led to the reduced tensile strength of the treated fibres. Ru, Zhao, and Yang (2022) optimized coir at different NaOH concentrations and treatment temperatures and found that at a concentration of 4.12%, for 15.08 h and 34.21 ℃, the coir exhibited optimum mechanical values of tensile strength of 97.14 MPa, elastic modulus of 2.98 GPa and elongation of 29.35%, which were 38.28%, 39.91% and 25.59% higher than that of untreated coir fibre. Water absorbability was reduced by coating with a hydrophobic substance, their results showed that samples exhibited contact angle values in the range of 84° to 146°, thermal conductivity values in the range of 0.0511 to 0.0861 W/mK, and densities in the range of 0.678 to 0.99 g/cm^3. As a result of the compressive and flexural strength tests, it was found that the compressive strength of the specimens was very high, the highest compressive strength was found as 32.8093 N/mm^2.

4.2 *Thermal Effects*

Surface modification can significantly affect the thermal properties of coir fibre (Bensalah et al., 2021). In their research, Effect of Surface Modification on the Properties of Polypropylene Matrix Reinforced with Coir Fibre and Yam Peel Particulate, Adediran *et al*. (2021) used treated coir fibre and yam peel particulate to reinforce polypropylene composites. The coir fibres were treated with 1.5M NaOH. The results showed that the sample reinforced with treated 4 wt.% coir fibre and yam peel particulate had optimum mechanical properties. In a study by (Siakeng *et al*., 2018) titled Effects of Surface Treatments on Tensile, Thermal and Fibre-matrix Bond Strength of Coir and Pineapple Leaf Fibres with Poly Lactic Acid, They investigated the effects of alkali, silane, and calcium hydroxide on the tensile, morphological, thermal, and structural properties of Coir Fibres (CF) and Pineapple Leaf Fibres (PALF) to improve their interfacial bonding with Polylactic Acid (PLA) matrix. Scanning electron microscopy and Fourier transform infrared spectroscopy were used to observe the effectiveness of the chemical treatments in removing impurities. Alkali-treated fibres yielded the lowest fibre diameter and highest Interfacial Stress Strength (IFSS). Thermogravimetric Analysis (TGA) shows improved thermal stability in silane-treated CF and alkali-treated PALF. The study suggests that these treatments can help develop biodegradable CF and PALF-reinforced PLA biocomposites for industrial applications.

4.3 *Physical Effects*

Coir has limitations like hydrophilicity, wettability, and poor adhesion to the polymer matrix. These drawbacks can be overcome by using surface modification techniques such as physical (plasma, ultrasound, ultraviolet) and chemical (silane, alkali, acetylation, benzoylation, sodium chloride) treatments.).(Karim *et al*., 2017; Manalo *et al*., 2015; Ravi *et al*., 2018).Water on natural fibres can cause the growth of fungi and bacteria, which can lead to biocorrosion. Water uptake can also cause the fibre volume to change, resulting in cracks in composite materials(Türk *et al*., 2015).

Shams-Ghahfarokhi *et al*. (2019) developed a new technique to prepare a polyester woven fabric that was both hydrophobic and thermal insulating. They achieved this by using electro-spraying of nano-porous silica powder. The study involved electro-spraying a polyester woven fabric with silica aerogel particles using a fluorocarbon finishing method. The prepared fabrics were characterized using various techniques such as FTIR, SEM, and EDS and were compared with untreated samples in terms of physical properties such as heat transfer, water repellency, water contact angle, air permeability, and abrasion fastness. The results showed that the heat transfer decreased from 71.65% for the untreated fabric to 38.35% and 30.99% for the electro-sprayed fabrics after 16 and 24 hours respectively.

In their research,(Sahu *et al*., 2020) worked on A review of the properties of natural fibres and their bio-composites: Effect of alkali treatment. It was found that alkali treatment is the most cost-effective and efficient way to improve the bonding between fibres and polymers considering the concentration level of NaOH, the percentage of fibre loading, and the duration of immersion are the key factors that impact the improvement or decline of the mechanical, physical, and thermal properties of the alkali-treated biocomposite.

4.4 *Hydrophobicity Measurement*

The water-repellent properties of solid materials are typically characterized by contact angle measurements (Movasat *et al*., 2021). Contact angles are the standard way to find out how hydrophobic coir fibre is. This approach looks at the angle that a water droplet makes on the surface of the coir. Wider contact angles are signs of higher hydrophobicity or more efficient water resistance (Krainer *et al*., 2021). The rough nature of coir fibres makes standard contact angle measurements possibly impossible in the textile industry, where coir is widely used. As such, the water-repelling qualities of textiles are evaluated in environments that resemble real use, using various methods including wicking, water absorption, and spray testing (Azam, 2019). The demands of testing textiles or leather, in particular, are reported compared to simpler measurements performed on glass or metal plates (Borlandelli and Mahltig, 2022; Hilenberg *et al*., 2018; Kick *et al*., 2017). Contact angle measurements are a common method to determine the ability of a solid substrate to repel a liquid. To test the hydrophobicity or water-repellent property of a substrate, a drop of water is placed on its surface, and the contact angle is measured. The higher the contact angle, the better the substrate's ability to repel the liquid. If a substrate has a contact angle of more than 90_ with water, it is considered hydrophobic(Liang *et al*., 2013).

In their research, Hydrophobic treatment of wood fibrous thermal insulator by octadecyltrichlorosilane and its influence on hydric properties and resistance against molds; Kumar *et al*. (2016) treated wood fibres with Octadecyl trichlorosilane to enhance their hydrophobicity. The study also looked at how this treatment impacted the hygroscopic properties of the wood fibres. The results showed that the OTS treatment successfully increased the hydrophobicity of the fibres, as confirmed by FTIR, XPS, and SEM analyses. The treatment formed monolayers on the surfaces of the fibres, which changed their surface roughness and made them more hydrophobic, as demonstrated by the sessile drop water contact angle measurement results (Figure 7)

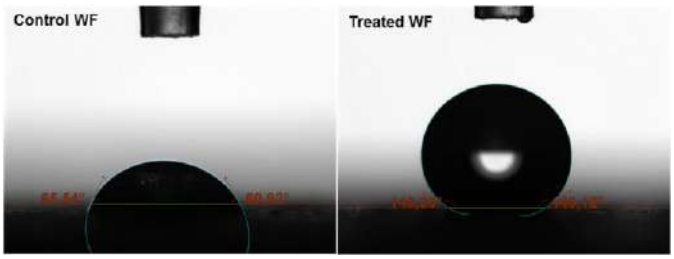

Fig. 7. Sessile drop water contact angle of control and treated wood fibres.(Kumar *et al*., 2016)

Erkmen and Sari (2023) used Waste papers, hazelnut shells, pinecones, and sheep wool to produce samples with filling rates of the materials optimized using the RSM method. This method is suitable for evaluating solid substrates with a plain geometry, such as metal or glass plates. However, for textile or leather substrates, it becomes more complicated due to the roughness of the substrate and its ability to absorb liquid. For instance, capillary effects cause even hydrophobic materials like polyester fabrics to absorb water (Bahners *et al*., 2020). The principle of drop tests is to have a set of different testing liquids with increasing wettability(Antonov *et al*., 2023). With increasing wettability, the repellent grade according to this liquid is also increased. To test against polar liquids, a set of testing liquids from water and isopropanol is used. The testing procedure involves placing a drop of the liquid on the textile fabric. If the drop does not sink into the textile substrate after a defined period, the textile passes the test and gets the rating. The test is repeated with liquids of higher ratings until the wettability of the used liquid is high enough and the drop sinks into the textile fabric(Antonov *et al*., 2023).One of the spray test methods used to determine the hydrophobicity of coir is known as the Bundesmann rain shower test, which combines the influence of spraying water with the mechanical treatment of the fabric. The Bundesmann rain test is a method used in textile engineering to evaluate the water-repellency of materials, particularly those that come into contact with the wearer, such as raincoats. Rubbing device: The back of the fabric is rubbed by a device to replicate the bending action when the cloth is worn. Measurement of Water Penetration: The water collected in the cups is measured to estimate penetration through the cloth. Measurement of Water Absorption: The fabric's increase in mass owing to water absorption is assessed after shaking off surplus water.

5. CONCLUSION

Several research have studied the use of coconut husks as a thermal insulation material, as mentioned in this review study. The topic of early deterioration of insulating materials, as well as its consequences for energy usage and economic repercussions, has also been explored. The hydrophilicity of biomass insulating materials, such as coir fibres, has been explored in various investigations, as indicated in this review study. However, the focus of these investigations has mostly been on boosting the mechanical strength of the fibres by changing the surface of the biomass fibres with a physical and chemical treatment to promote the adherence of the polymer matrix to the fibres. Despite these efforts, there is a need to investigate the impact of these surface modifications on the thermophysical and mechanical properties of the coir fibres, with an emphasis on their thermal conductivity, diffusivity, water-repellant properties, and their effect on coir. In addition, there is a need to develop strategies to increase the hydrophobicity of coir fibres by surface coating with hydrophobic substrates in Industrial applications.

REFERENCES

Abraham, E., Deepa, B., Pothen, L., Cintil, J., Thomas, S., John, M. J., . . . Narine, S. J. C. p. (2013). Environmental friendly method for the extraction of coir fibre and isolation of nanofibre. *92*(2), 1477-1483.

Adediran, A. A., Balogun, O. A., Akinwande, A. A., Mwema, F. M., Adesina, O. S., & Olayanju, A. (2021). Effect of surface modification on the properties of polypropylene matrix reinforced with coir fibre and yam peel particulate. *The Scientific World Journal*, *2021*, 1-12.

Ahmed, S., Ahsan, A., & Hasan, M. (2017). Physico-mechanical properties of coir and jute fibre reinforced hybrid polyethylene composites. *International Journal of Automotive and Mechanical Engineering*, *14*(4).

Ali, A., Shaker, K., Nawab, Y., Jabbar, M., Hussain, T., Militky, J., & Baheti, V. J. J. o. I. T. (2018). Hydrophobic treatment of natural fibers and their composites—A review. *47*(8), 2153-2183.

Antonov, D. V., Islamova, A. G., & Strizhak, P. A. J. M. (2023). Hydrophilic and hydrophobic surfaces: Features of interaction with liquid drops. *16*(17), 5932.

Aravind, D., Senthilkumar, K., Diwahar, P., Chandrasekar, M., Kumar, T. S. M., Parameswaranpillai, J., . . . Composites, i. (2022). Review on coir fiber surface modification by various techniques. 55-78.

Arsyad, M. (2019). Sodium Hydroxide and Potassium Permanganate Treatment on Mechanical Properties of Coconut Fibers. IOP Conference Series: Materials Science and Engineering,

Arsyad, M., Wardana, I., & Irawan, Y. S. (2015). The morphology of coconut fiber surface under chemical treatment. *Matéria (Rio de Janeiro)*, *20*, 169-177.

Azam, A. (2019). Hydrophobic treatment of natural fibers and their composites—A review.". *47*, 2153-2183.

Bahners, T., Gutmann, J. S. J. P. i. A., & Adhesives. (2020). Procedures for the Characterization of Wettability and Surface Free Energy of Textiles-Use, Abuse, Misuse and Proper Use: A Critical Review. *5*, 259-293.

Bakri, B., Naharuddin, A., Renreng, I., & Arsyad, H. (2018). Characterization of Coir Fibers after alkali and microwave treatments. *ARPN Journal of Engineering and Applied Sciences*, *13*(4), 1335-1339.

Banea, M. D., Neto, J. S., & Cavalcanti, D. K. J. G. c. (2021). Recent trends in surface modification of natural fibres for their use in green composites. 329-350.

Barnes, B. K., Ouro-Koura, H., Derickson, J., Lebarty, S., Omidokun, J., Bane, N., . . . Ogunmolasuyi, A. J. A. J. o. P. (2021). Plasma generation by household microwave oven for surface modification and other emerging applications. *89*(4), 372-382.

Bensalah, H., Raji, M., Abdellaoui, H., Essabir, H., Bouhfid, R., & Qaiss, A. e. k. J. T. I. J. o. A. M. T. (2021). Thermo-mechanical properties of low-cost “green” phenolic resin composites reinforced with surface modified coir fiber. *112*, 1917-1930.

Borlandelli, C. M., & Mahltig, B. J. A. T. E. F. T. (2022). Leather Types and Fiber-Based Leather Alternatives-An Overview on Selected Materials, Properties, Microscopy, Electron Dispersive Spectroscopy EDS and Infrared Spectroscopy. *1*(1), 1001.

Bui, H., Sebaibi, N., Boutouil, M., & Levacher, D. J. F. (2020). Determination and review of physical and mechanical properties of raw and treated coconut fibers for their recycling in construction materials. *8*(6), 37.

Cai, J., Li, Q., & Wu, C. J. M. R. E. (2022). Surface modification of recycled coir fibers with hybrid coating and its effect on the properties of ABS composites. *9*(2), 025307.

Dong, Y., Kong, J., Mousavi, S., Rismanchi, B., & Yap, P.-S. J. T. (2023). Wall insulation materials in different climate zones: A review on challenges and opportunities of available alternatives. *3*(1), 38-65.

Ekpenyong, N. E., Umoren, G. P., Udo, I. E., & Yawo, O. J. J. J. o. B. E. (2022). Assessment of Thermophysical and Mechanical Properties of Composite Panels Fabricated from Untreated and Treated Coconut Husk Particles for Structural Application. *2*, 4547.

Erkmen, J., & Sari, M. (2023). Hydrophobic thermal insulation material designed from hazelnut shells, pinecone, paper and sheep wool. *Construction and Building Materials*, *365*, 130131.

Gusyachkin, A., Sabitov, L., Khakimova, A., & Hayrullin, A. (2019). Effects of moisture content on thermal conductivity of thermal insulation materials. IOP Conference Series: Materials Science and Engineering,

Hasan, K., Horváth, P. G., Kóczán, Z., & Alpár, T. (2021). Thermo-mechanical properties of pretreated coir fiber and fibrous chips reinforced multilayered composites. *Scientific Reports*, *11*(1), 1-13.

Hasan, K. F., Horváth, P. G., Bak, M., & Alpár, T. J. R. A. (2021). A state-of-the-art review on coir fiber-reinforced biocomposites. *11*(18), 10548-10571.

Hasan, K. F., Horváth, P. G., Kóczán, Z., Le, D. H. A., Bak, M., Bejó, L., & Alpár, T. J. J. o. P. R. (2021). Novel insulation panels development from multilayered coir short and long fiber reinforced phenol formaldehyde polymeric biocomposites. *28*, 1-16.

Hilenberg, E., Taskin, E., Ehrmann, A. J. I. J. o. C. S., & Technology. (2018). Increased acid-resistance of lab-coats by hydrophobic finishing. *30*(6), 784-789.

Hoseini, A., & Bahrami, M. (2017). Effects of humidity on thermal performance of aerogel insulation blankets. *Journal of building engineering*, *13*, 107-115.

Karim, M., Zaman, I., Rozlan, S., Berhanuddin, N., Manshoor, B., Mustapha, M., . . . Chan, S. (2017). Structural characterization and mechanical properties of polypropylene reinforced natural fibers. Journal of Physics: Conference Series,

Kick, T., Grethe, T., & Mahltig, B. J. A. C. S. (2017). A natural based method for hydrophobic treatment of natural fiber material. *64*(2), 373-380.

Krainer, S., Hirn, U. J. C., Physicochemical, S. A., & Aspects, E. (2021). Contact angle measurement on porous substrates: Effect of liquid absorption and drop size. *619*, 126503.

Kumar, A., Staněk, K., Ryparová, P., Hajek, P., & Tywoniak, J. J. C. P. B. E. (2016). Hydrophobic treatment of wood fibrous thermal insulator by octadecyltrichlorosilane and its influence on hygric properties and resistance against moulds. *106*, 285-293.

Kumar, D., Alam, M., Zou, P. X., Sanjayan, J. G., Memon, R. A. J. R., & Reviews, S. E. (2020). Comparative analysis of building insulation material properties and performance. *131*, 110038.

Lakatos, Á., & Kalmár, F. (2013). Analysis of water sorption and thermal conductivity of expanded polystyrene insulation materials. *Building Services Engineering Research and Technology*, *34*(4), 407-416.

Li, X., Jin, X., Wu, Y., Zhang, D., Sun, F., Ma, H., . . . Xia, C. J. S. o. T. T. E. (2023). A comprehensive review of lignocellulosic biomass derived materials for water/oil separation. *876*, 162549.

Li, Y., Wang, H., Yang, L., & Su, S. (2020). Study on water absorption and thermal conductivity of tunnel insulation materials in a cold region under freeze-thaw conditions. *Advances in Materials Science and Engineering*, *2020*, 1-11.

Liang, J., Zhou, Y., Jiang, G., Wang, R., Wang, X., Hu, R., & Xi, X. J. J. o. t. T. I. (2013). Transformation of hydrophilic cotton fabrics into superhydrophobic surfaces for oil/water separation. *104*(3), 305-311.

Manalo, A. C., Wani, E., Zukarnain, N. A., Karunasena, W., & Lau, K.-t. J. C. P. B. E. (2015). Effects of alkali treatment and elevated temperature on the mechanical properties of bamboo fibre–polyester composites. *80*, 73-83.

Mangat, A., Sureshkumar, P., & Niyas, P. (2023). Structural analysis of coconut palm prior to the design of a coconut palm climber and derivation of allometric relationships-a study at KAU campus.

Marakana, P. G., Dey, A., & Saini, B. J. J. o. E. C. E. (2021). Isolation of nanocellulose from lignocellulosic biomass: Synthesis, characterization, modification, and potential applications. *9*(6), 106606.

Mir, S. S., Nafsin, N., Hasan, M., Hasan, N., Hassan, A. J. M., & Design. (2013). Improvement of physico-mechanical properties of coir-polypropylene biocomposites by fiber chemical treatment. *52*, 251-257.

Mishra, L., & Basu, G. (2020). Coconut fibre: its structure, properties and applications. In *Handbook of natural fibres* (pp. 231-255). Elsevier.

Movasat, M., Tomac, I. J. J. o. G., & Engineering, G. (2021). Assessment of physical properties of water-repellent soils. *147*(9), 06021010.

Muthuraj, R., Lacoste, C., Lacroix, P., & Bergeret, A. (2019). Sustainable thermal insulation biocomposites from rice husk, wheat husk, wood fibers and textile waste fibers: Elaboration and performances evaluation. *Industrial Crops and Products*, *135*, 238-245.

Ndagi, M., Kolawole, A. T., Olawale, F. M., & Sulaiman, A. (2021). Investigation of the thermo-physical and mechanical properties of coir and sugarcane bagasse for low temperature insulation. *International Journal of Engineering Materials and Manufacture*, *6*(4), 340-356.

Ng, Y., Shahid, S., & Nordin, N. (2018). The effect of alkali treatment on tensile properties of coir/polypropylene biocomposite. IOP Conference Series: Materials Science and Engineering,

Nurazzi, N., Harussani, M., Aisyah, H., Ilyas, R., Norrrahim, M., Khalina, A., . . . Structures. (2021). Treatments of natural fiber as reinforcement in polymer composites—a short review. *3*(2), 024002.

Okpala, C., Chinwuko, E., Ezeliora, C. J. I. R. J. o. E., & Technology. (2021). Mechanical Properties and Applications of Coir Fiber Reinforced Composites. *8*(7).

Owoeye, S. S., Matthew, G. O., Ovienmhanda, F. O., & Tunmilayo, S. O. J. C. I. (2020). Preparation and characterization of foam glass from waste container glasses and water glass for application in thermal insulations. *46*(8), 11770-11775.

Pásztory, Z. (2021). An overview of factors influencing thermal conductivity of building insulation materials. *Journal of building engineering*, *44*, 102604.

Piccinno, F., Gottschalk, F., Seeger, S., & Nowack, B. (2012). Industrial production quantities and uses of ten engineered nanomaterials in Europe and the world. *Journal of Nanoparticle Research*, *14*(9), 1109. https://doi.org/10.1007/s11051-012-1109-9

Rahayu, A., Hanum, F. F., Amrillah, N. A. Z., Lim, L. W., Salamah, S. J. J. o. F., & Composites, P. (2022). Cellulose Extraction from Coconut Coir with Alkaline Delignification Process. *1*(2), 106-116.

Rahman, M. M., & Khan, M. A. (2007). Surface treatment of coir (Cocos nucifera) fibers and its influence on the fibers' physico-mechanical properties. *Composites science and technology*, *67*(11-12), 2369-2376.

Ravi, M., Dubey, R. R., Shome, A., Guha, S., & Kumar, C. A. (2018). Effect of surface treatment on Natural fibers composite. IOP Conference Series: Materials Science and Engineering,

Ru, S., Zhao, C., Yang, S., & Liang, D. J. P. (2022). Effect of coir fiber surface treatment on interfacial properties of reinforced epoxy resin composites. *14*(17), 3488.

Ru, S., Zhao, C., & Yang, S. J. F. (2022). Multi-Objective Optimization and Analysis of Mechanical Properties of Coir Fiber from Coconut Forest Waste. *13*(12), 2033.

Sahu, P., Gupta, M. J. P. o. t. I. o. M. E., Part L: Journal of Materials: Design, & Applications. (2020). A review on the properties of natural fibres and its bio-composites: Effect of alkali treatment. *234*(1), 198-217.

Saw, S. K., Sarkhel, G., & Choudhury, A. (2011). Surface modification of coir fibre involving oxidation of lignins followed by reaction with furfuryl alcohol: Characterization and stability. *Applied Surface Science*, *257*(8), 3763-3769.

Shams-Ghahfarokhi, F., Khoddami, A., Mazrouei-Sebdani, Z., Rahmatinejad, J., & Mohammadi, H. (2019). A new technique to prepare a hydrophobic and thermal insulating polyester woven fabric using electro-spraying of nano-porous silica powder. *Surface and Coatings Technology*, *366*, 97-105.

Siakeng, R., Jawaid, M., Ariffin, H., & Salit, M. S. (2018). Effects of Surface Treatments on Tensile, Thermal and Fibre-matrix Bond Strength of Coir and Pineapple Leaf Fibres with Poly Lactic Acid. *Journal of Bionic Engineering*, *15*(6), 1035-1046. https://doi.org/10.1007/s42235-018-0091-z

Simimol, A., Sebastian, S., Ravindranath, D. A., & Jacob, A. (2020). Enhancement of Physical, Mechanicaland Morphological Properties of Coir by Mercerization and Acetylation. *Composites*, *8*, 9.

Singh, C. P., Patel, R. V., Hasan, M. F., Yadav, A., Kumar, V., & Kumar, A. J. M. T. P. (2021). Fabrication and evaluation of physical and mechanical properties of jute and coconut coir reinforced polymer matrix composite. *38*, 2572-2577.

Singh, Y., Singh, J., Sharma, S., Lam, T.-D., & Nguyen, D.-N. (2020). Fabrication and characterization of coir/carbon-fiber reinforced epoxy based hybrid composite for helmet shells and sports-good applications: Influence of fiber surface modifications on the mechanical, thermal and morphological properties. *Journal of Materials Research and Technology*, *9*(6), 15593-15603.

Sumi, S., Unnikrishnan, N., & Mathew, L. (2018). Durability studies of surface-modified coir geotextiles. *Geotextiles and Geomembranes*, *46*(6), 699-706.

Tayfun, Ü., Akar, A. Ö., rat, H. 횔. o. 횔., & Doğan, M. J. G. M. (2023). Performance enhancement of coir fiber-reinforced elastomeric polyurethane eco-composites via the enrichment of fiber surface using sustainable modifications. 1-12.

Thakur, K., Kalia, S., Kaith, B., Pathania, D., Kumar, A., Thakur, P., . . . Totaro, G. J. J. o. e. c. e. (2016). The development of antibacterial and hydrophobic functionalities in natural fibers for fiber-reinforced composite materials. *4*(2), 1743-1752.

Torres-Rivas, A., Palumbo, M., Haddad, A., Cabeza, L. F., Jiménez, L., & Boer, D. J. A. E. (2018). Multi-objective optimisation of bio-based thermal insulation materials in building envelopes considering condensation risk. *224*, 602-614.

Türk, M., Ehrmann, A., & Mahltig, B. J. T. J. o. T. T. I. (2015). Water-, oil-, and soil-repellent treatment of textiles, artificial leather, and leather. *106*(6), 611-620.

Wang, Y., Zhang, S., Wang, D., Liu, Y. J. E., & Environment, B. (2023). Experimental study on the influence of temperature and humidity on the thermal conductivity of building insulation materials. *4*(4), 386-398.

Zhang, M., & Wang, C. J. C. P. (2013). Fabrication of cotton fabric with superhydrophobicity and flame retardancy. *96*(2), 396-402.

Zhang, W., & Lai, E. P. J. S. (2022). Chemical functionalities of 3-aminopropyltriethoxy-silane for surface modification of metal oxide nanoparticles. *14*(12), 6535-6545.

Zhu, W., Cai, S., & Cremaschi, L. (2015). Thermal performance and moisture accumulation of fibrous mechanical pipe insulation systems operating at below-ambient temperature in wet conditions with moisture ingress. *Science and Technology for the Built Environment*, *21*(6), 862-875.

PAPER 114 - A REVIEW OF THE ROLE OF ARTIFICIAL INTELLIGENCE IN INFRASTRUCTURAL DEVELOPMENT OF SMART CITIES IN NIGERIA

T. O. Adekeye [1*], O. O. Adeleke[1]

[1]Department of Civil Engineering, University of Ilorin, Ilorin, Nigeria.
[*]Email: adekeyetimothy@gmail.com

ABSTRACT
Nigeria's rapid urbanization strains its aging infrastructure. This paper explores how Artificial Intelligence (AI) can revolutionize civil engineering, specifically addressing Nigeria's urban challenges and sustainability goals. AI offers unprecedented opportunities to improve efficiency, resilience, and sustainability in infrastructure projects. We examine AI's potential for structural health monitoring and risk assessment to prioritize maintenance and ensure infrastructure longevity. Furthermore, AI's potential was examined for smart infrastructure systems for optimized transportation, energy management, and sustainable practices. By implementing these AI-powered solutions and fostering collaboration among stakeholders, Nigeria can build more resilient, efficient, and sustainable cities for the future.

KEYWORDS: Artificial Intelligence, Smart Cities, Civil Engineering, Infrastructure, Nigeria

1. INTRODUCTION

In recent decades, Nigeria has undergone rapid urbanization, with its urban population expected to double by 2050, making it one of the fastest-growing urban regions globally (United Nations, 2018; Oluwatobi, 2019). This urban expansion presents both immense opportunities for economic growth and development, as well as significant challenges in terms of managing resources, infrastructure, and services to meet the needs of its burgeoning urban population (Onibokun and Kumuyi, 2007). As Nigeria strives to achieve sustainable development amidst this urban transition, leveraging artificial intelligence (AI) in the development of smart cities and infrastructure emerges as a promising pathway towards addressing complex urban infrastructure challenges while fostering inclusive and resilient urban growth.

The Nigerian urban landscape is characterized by a diverse array of challenges, including inadequate infrastructure, traffic congestion, inadequate housing, and environmental degradation, among others (Adesina, 2012; Amole, 2020). These challenges are further compounded by rapid population growth, unplanned urban sprawl, and limited resources for infrastructure development and maintenance. In this context, the concept of smart cities – urban centres that harness technology, data, and innovation to improve the efficiency, sustainability, and quality of life for residents – holds great potential for transforming Nigeria's urban areas into vibrant, liveable, and sustainable hubs of economic and social activity.

Smart infrastructure lies at the heart of the smart city paradigm, encompassing a range of intelligent systems and technologies designed to enhance the functionality, resilience, and sustainability of urban infrastructure networks (African Development Bank Group, 2019; Olayiwola, 2019). From smart transportation systems and energy-efficient buildings to digital utilities and IoT-enabled services, smart infrastructure offers opportunities to optimize resource use, improve service delivery, and enhance the overall urban experience for residents and businesses alike.

.

2. SMART CITIES AND INFRASTRUCTURE IN NIGERIA: CHALLENGES AND OPPORTUNITIES

2.1 *The Concept of Smart Cities*

The concept of smart cities has gained traction as a potential solution to build more efficient, sustainable, and livable urban environments. Smart cities are urban areas that utilize technology and data to enhance the quality of life for residents, improve the efficiency of urban services, and promote sustainable development (United Nations Economic Commission for Africa, 2017). These cities leverage a wide range of technologies, including IoT sensors, data analytics platforms, and AI algorithms, to collect, analyze, and act on data in real-time. The goal of smart cities is to create interconnected, responsive, and resilient urban ecosystems that can adapt to the needs and

challenges of the modern world. Smart cities leverage technology, data, and innovation to improve the delivery of urban services, enhance resource efficiency, and promote economic development.

Nigeria, the most populous country in Africa, is faced with rapid urbanization. This urban expansion presents both opportunities and challenges, particularly in terms of managing urban infrastructure to meet the needs of its burgeoning urban population. Nigeria's rapid urbanization is driven by factors such as rural-urban migration, natural population growth, and economic development. According to the United Nations, Nigeria's urban population is projected to reach 392 million by 2050, making it one of the fastest-growing urban regions globally (United Nations, 2018). Despite economic growth and development, Nigerian cities face significant infrastructure deficits across various sectors such as; transportation infrastructure, energy infrastructure, water and sanitation infrastructure; Housing and Informal Settlements.

2.2 *Opportunities and Challenges of Smart Cities and Infrastructure in Nigeria*

Transportation infrastructure, including roads, railways, and public transit systems, is inadequate to meet the growing demand for mobility (World Bank, 2020) as traffic congestion is a common issue in major cities such as Lagos, Abuja, and Port Harcourt, leading to productivity losses, air pollution, and road accidents. In the same manner, energy infrastructure in Nigeria is deficient, with frequent power outages and unreliable electricity supply (International Energy Agency, 2020). Despite being a major oil-producing nation, Nigeria struggles to provide consistent and affordable electricity to its citizens, hindering economic productivity and investment. Just like other infrastructures, water and sanitation infrastructure remains a major challenge in Nigerian cities, with millions of people lacking access to clean water and adequate sanitation facilities (World Health Organization, 2019). Informal settlements and peri-urban areas often lack basic water supply systems and sanitation infrastructure, leading to waterborne diseases and environmental pollution. Millions of people live in overcrowded and substandard housing conditions in informal settlements with such informal settlements lacking basic infrastructure of clean water, sanitation, and electricity, leading to health risks, social exclusion, and economic vulnerability. Despite the challenges, Nigeria presents numerous opportunities for the development of smart cities and infrastructure. The country's youthful population, the burgeoning technology sector, and the growing urban middle class create a fertile ground for innovation and investment in smart technologies.

3. THE ROLE OF ARTIFICIAL INTELLIGENCE IN CIVIL ENGINEERING AND INFRASTRUCTURE FOR A SMART AND SUSTAINABLE CITY

Artificial Intelligence (AI) is revolutionizing the field of Civil Engineering and infrastructure by introducing advanced technologies that enhance efficiency, sustainability, data-driven decision-making, and resilience and thereby achieve superior outcomes for sustainable infrastructure development (Mukhopadhyay *et al*., 2019). From optimizing construction processes to managing infrastructure assets, AI offers a wide range of applications that are reshaping the way Civil Engineers plan, design, build, and maintain infrastructure projects. The role of AI in civil engineering and infrastructure for a smart city includes:

3.1 *Predictive Maintenance and Asset Management*

AI-powered predictive maintenance systems analyze vast amounts of data from sensors and IoT devices embedded in infrastructure assets such as bridges, roads, and buildings (Li *et al*., 2019). By monitoring structural health indicators in real-time, AI algorithms can detect potential faults or deterioration early, enabling engineers to schedule timely maintenance interventions. This proactive approach helps prevent costly failures, prolong asset lifespan, and ensure the safety and reliability of critical infrastructure. Some real-world examples include;

- **IBM Maximo Asset Management**: This software integrates AI for predictive maintenance and asset health monitoring, helping identify potential problems with equipment before they occur (Ran *et al*., 2019).
- **GE Predix Platform:** This platform utilizes AI for predictive maintenance in various industries, analyzing sensor data from equipment to predict failures and optimize operations (Cinar *et al*., 2020).
- **Siemens Mind Sphere**: This cloud-based IoT solution integrates AI for predictive maintenance in various infrastructure sectors, including transportation and utilities (Alam, 2021).

3.2. *Construction Process Optimization*

AI algorithms optimize construction processes by analyzing historical project data, simulating various scenarios, and identifying optimal strategies for resource allocation, scheduling, and logistics (Liu *et al*., 2020). Machine learning models can predict project delays, cost overruns, and potential risks, allowing project managers to make informed decisions and adapt plans accordingly. These tools also aid potential Public Private Partnership (PPP) opportunities by providing necessary data to show the viability of such infrastructural investments. Furthermore, AI-powered robotics and automation technologies streamline repetitive tasks on construction sites, improving productivity, safety, and quality control. Some real-world examples are;

- **Autodesk BIM 360 Construct:** This platform integrates AI-powered video analytics for real-time safety monitoring on construction sites.
- **SiteAware:** This company specializes in Digital Construction Verification (DCV) solutions for the civil engineering industry.
- **Oracle Primavera Cloud P6**: This project management platform utilizes AI for predictive analytics and risk management, enabling optimized schedules (Regona *et al*., 2022).
- **Buildots**: This AI-powered construction management platform optimizes schedules and resource allocation through real-time data analysis and progress tracking (Rane, 2023).

3.3 *Structural Health Monitoring and Risk Assessment*

AI enables continuous monitoring of structural health and performance through the analysis of sensor data, satellite imagery, and remote sensing technologies (Abdel-Maguid *et al*., 2020). By detecting anomalies, identifying deterioration patterns, and assessing structural integrity, AI systems provide valuable insights into the condition of infrastructure assets. This information enables engineers to prioritize maintenance interventions, allocate resources efficiently, and mitigate risks associated with aging infrastructure. Some real-world examples include;

- **IBM Maximo Asset Management Platform:** This platform utilizes AI for predictive maintenance, analyzing sensor data from bridges and buildings to predict equipment failures (Cheng *et al*., 2020).
- **Strain Monitoring of Pipelines with Deep Learning:** This cloud-based IoT solution integrates AI for predictive maintenance in various infrastructure sectors, including transportation and utilities (Alam, 2021).

3.4 *Smart Infrastructure Systems*

AI-driven smart infrastructure systems enhance the functionality and efficiency of urban environments by integrating various technologies such as IoT sensors, data analytics, and communication networks (Chen *et al*., 2021). For example, AI-powered traffic management systems optimize traffic flow, reduce congestion, and improve road safety by analyzing real-time traffic data and coordinating signal timings. Similarly, AI-based energy management systems optimize energy consumption, reduce waste, and promote sustainability in buildings, transportation networks, and utility systems.

3.5 *Design Optimization and Simulation*

AI algorithms optimize the design of civil engineering projects by generating innovative solutions, simulating performance scenarios, and optimizing parameters such as material selection, structural configuration, and environmental impact (Yeh *et al*., 2019). Generative design algorithms explore a vast range of design possibilities, considering multiple constraints and objectives, to find optimal solutions that meet project requirements. Additionally, AI-driven simulation tools enable engineers to assess the performance of infrastructure systems under various conditions, such as extreme weather events or seismic loads, ensuring resilience and durability. Further classifications include;

- **Generative Adversarial Networks (GANs)**: These AI models can be used for generative design in infrastructure. One network (generator) creates new design options, while another (discriminator) evaluates them against desired criteria. This iterative process leads to increasingly optimized designs (Baduge *et al*., 2022).
- **Machine Learning (ML) Algorithms**: Various ML algorithms, like support vector machines and random forests, can be used for multi-objective optimization in infrastructure design. These algorithms

can analyze vast datasets and identify designs that excel across multiple factors like cost, performance, and sustainability (Li *et al*., 2022).

- **Building Information Modeling (BIM):** AI can be integrated with BIM platforms to analyze 3D models and identify potential design conflicts or constructability issues early in the design process, leading to more efficient and optimized designs (Pan and Zhang, 2023).

3.6 *Environmental Monitoring and Sustainable Development*

AI plays a crucial role in environmental monitoring and sustainable development by analyzing environmental data, modeling complex systems, and predicting environmental impacts (Shen *et al*., 2020). AI-powered systems monitor air and water quality, analyze ecological patterns, and assess the environmental footprint of infrastructure projects, enabling engineers to minimize negative impacts and promote ecosystem conservation. Furthermore, AI-driven optimization algorithms help optimize resource use, reduce energy consumption, and promote the adoption of renewable energy sources, contributing to the sustainability of civil engineering projects.

4. DISCUSSION

4.1 *Case Studies of Smart City Initiatives in Nigeria*

Several Nigerian cities have embarked on smart city initiatives aimed at leveraging technology to improve urban services and infrastructure. For example, Lagos, the largest city in Nigeria, has implemented various smart transportation solutions to address congestion and improve mobility. These initiatives include the deployment of traffic management systems and digital mapping tools to optimize traffic flow and provide real-time information to commuters (Oluwaseyi and Ademola, 2020). By leveraging AI and IoT technologies, Lagos aims to enhance the efficiency of its transportation network and reduce travel times for residents and commuters.

In addition to Lagos, Abuja, the capital city of Nigeria, is also exploring smart city initiatives to enhance urban services and infrastructure. One of Abuja's key focus areas is energy management, where the city is leveraging AI-powered systems to optimize electricity distribution and reduce energy losses (Oluwaseyi and Ademola, 2020). By analyzing energy consumption patterns and optimizing grid operations, Abuja aims to improve the reliability and sustainability of its energy supply, ultimately benefiting residents, businesses, and the environment. Kwara State also recently acquired a large expanse of land for the establishment of a smart city.

4.2 *Future Trends in Artificial Intelligence application to Smart cities and infrastructural development*

Despite the challenges, the future of AI in smart cities is promising, with continued advancements in technology, policy, and governance. Some key areas for future development and research include:

- Ethical AI: Developing ethical frameworks, regulations, and guidelines to ensure the responsible and equitable use of AI in smart cities (Afolabi and Olajide, 2018).
- Human-Centered Design: Designing AI-powered systems and services that prioritize human needs, preferences, and values, fostering trust, acceptance, and adoption among residents (Caragliu *et al*., 2009).
- Collaboration and Partnerships: Fostering collaboration and partnerships between governments, businesses, academia, and civil society to drive innovation, share best practices, and address common challenges in AI-enabled smart cities (United Nations Economic Commission for Africa, 2017).

5. CONCLUSION AND RECOMMENDATION

In the Nigerian context, the integration of Artificial Intelligence (AI) in Civil Engineering and infrastructure development holds immense potential for addressing the country's pressing urban challenges and driving sustainable development. AI-powered predictive maintenance systems can revolutionize infrastructure management, helping to reduce downtime, optimize resource allocation, and ensure the safety and reliability of critical assets across Nigeria's rapidly growing urban centers. Furthermore, AI-driven construction process optimization can enhance productivity, quality control, and safety on construction sites, crucial for meeting the ambitious infrastructure development goals set by the Nigerian government. By leveraging AI technologies, Nigerian engineers can streamline project delivery, mitigate risks, and accelerate progress on key infrastructure projects, from transportation networks to energy systems. Moreover, AI-enabled structural health monitoring and risk assessment offer valuable tools for maintaining and managing Nigeria's aging infrastructure assets. With proper implementation, AI can help prioritize maintenance interventions, allocate resources effectively, and

ensure the long-term resilience and durability of critical infrastructure systems. By embracing AI-driven innovation, Nigeria has the opportunity to leapfrog traditional development pathways and build a more resilient, efficient, and sustainable infrastructure network for the future.

Some recommended policies, therefore are as follows:

1. The Nigerian government should prioritize investment in AI research and development initiatives aimed at advancing AI technologies relevant to Civil Engineering and infrastructure development.
2. There is a need for responsible and ethical deployment of AI technologies in civil engineering and infrastructure projects with clear framework, guidelines and regulations.
3. The government should invest in capacity building and training programmes to equip engineers, policymakers, and other stakeholders with the necessary skills and knowledge to harness AI technologies effectively.
4. Public-private partnerships (PPPs) should be promoted to facilitate collaboration between government agencies, private sector companies, and research institutions.
5. The government should introduce incentives, such as tax breaks or subsidies, to encourage the adoption of AI technologies in infrastructure projects.
6. To foster innovation and collaboration in AI research and development, the government should establish AI centers of excellence focused on civil engineering and infrastructure.
7. The government should integrate AI considerations into national infrastructure planning processes, ensuring that AI technologies are incorporated into infrastructure projects from the outset.

ACKNOWLEDGEMENT

Firstly, I appreciate the support and guidance of my lecturers, your invaluable guidance, insightful feedback, and unwavering belief in me have been a constant source of motivation. I am deeply grateful for your dedication to my development as a researcher. My appreciation also goes to my colleagues, for their stimulating discussions, collaborative spirit, and willingness to share your expertise.

REFERENCES

Abdel-Maguid, T. I., Khedr, A. A., & Zayed, T. (2020). A Review of Artificial Intelligence Applications in Civil Engineering. Alexandria Engineering Journal, 59(4), 2607-2623.

Adeniran, A. A. (2018). Sustainable Urban Development in Nigeria: Towards a Green City. International Journal of Sustainable Development & World Ecology, 25(1), 68-74. doi:10.1080/13504509.2017.1377010

Adesina, J. O. (2012). The Challenge of Urban Governance in Nigeria. In Urbanisation and Governance in Nigeria (pp. 27-41). African Books Collective.

Afolabi, A. O., & Olajide, O. J. (2018). Sustainable Urban Development in Nigeria: Issues and Challenges. Cogent Social Sciences, 4(1), 1476190. doi:10.1080/23311886.2018.1476190

African Development Bank Group. (2019). African Economic Outlook 2019: Developing Africa's Infrastructure for Enhanced Competitiveness. Retrieved from https://www.afdb.org/en/knowledge/publications/african-economic-outlook

Alam, T. (2021). Cloud-based IoT applications and their roles in smart cities. *Smart Cities*, *4*(3), 1196-1219.

Al-Nasser, A., Mohamed, M. R., & Hussein, Z. (2018). A Review on Smart Cities and Their Sustainable Development. Journal of Engineering and Applied Sciences, 13(5), 1266-1273.

Amole, B. (2020). Smart Cities and Sustainable Development Goals: The Nexus in Nigeria's Urbanization. In Smart Cities, Green Technologies, and Intelligent Transport Systems (pp. 245-257). Springer.

Baduge, S. K., Thilakarathna, S., Perera, J. S., Arashpour, M., Sharafi, P., Teodosio, B. & Mendis, P. (2022). Artificial intelligence and smart vision for building and construction 4.0: Machine and deep learning methods and applications. *Automation in Construction*, *141*, 104440.

Caragliu, A., Del Bo, C., & Nijkamp, P. (2009). Smart Cities in Europe. Journal of Urban Technology, 18(2), 65-82.

Çınar, Z. M., Abdussalam Nuhu, A., Zeeshan, Q., Korhan, O., Asmael, M., & Safaei, B. (2020). Machine learning in predictive maintenance towards sustainable smart manufacturing in industry 4.0. *Sustainability*, *12*(19), 8211.

Chen, Q., Wang, F., Tian, Y., & Xiong, S. (2021). Application of Artificial Intelligence Technology in Civil Engineering. Advances in Civil Engineering, 2021, 1-9.

Cheng, J. C., Chen, W., Chen, K., & Wang, Q. (2020). Data-driven predictive maintenance planning framework for MEP components based on BIM and IoT using machine learning algorithms. *Automation in Construction*, *112*, 103087.

International Energy Agency. (2020). Nigeria Energy Outlook 2020. Retrieved from https://www.iea.org/reports/nigeria-energy-outlook-2020

Li, L., Ma, L., Zuo, J., & Li, H. (2019). Application of Artificial Intelligence in Infrastructure Operation and Maintenance: A Review. Advanced Engineering Informatics, 42, 100988.

Li, P., Xu, T., Wei, S., & Wang, Z. H. (2022). Multi-objective optimization of urban environmental system design using machine learning. *Computers, Environment and Urban Systems*, *94*, 101796.

Liu, Y., Zhang, J., Chen, H., & Hammad, A. W. (2020). Artificial Intelligence in Construction and Civil Engineering: A Review and Future Directions. Advanced Engineering Informatics, 44, 101013.

Mukhopadhyay, A., Yadav, S., & Goel, S. (2019). Review of Artificial Intelligence (AI) in Civil Engineering. Materials Today: Proceedings, 18, 5251-5255.

Oluwaseyi, A. A., & Ademola, O. O. (2020). Leveraging AI in smart cities for sustainable development: A case study of Lagos and Abuja, Nigeria. International Journal of Smart Cities, 2(1), 45-58.

Oluwatobi, S. A. (2019). Urbanization and economic growth nexus in Nigeria: A multivariate approach. Sustainable Cities and Society, 47, 101484. doi:10.1016/j.scs.2019.101484

Onibokun, A. G., & Kumuyi, A. J. (2007). Urbanization and Urban Problems in Nigeria. In Managing the Monster: Urbanisation and Governance in Africa (pp. 233-260). Africa World Press.

Pan, Y., & Zhang, L. (2021). Roles of artificial intelligence in construction engineering and management: A critical review and future trends. *Automation in Construction*, *122*, 103517.

Rane, N. (2023). Integrating Building Information Modelling (BIM) and Artificial Intelligence (AI) for Smart Construction Schedule, Cost, Quality, and Safety Management: Challenges and Opportunities. *Cost, Quality, and Safety Management: Challenges and Opportunities (September 16, 2023)*.

Regona, M., Yigitcanlar, T., Xia, B., & Li, R. Y. M. (2022). Opportunities and adoption challenges of AI in the construction industry: A PRISMA review. *Journal of open innovation: technology, market, and complexity*, *8*(1), 45.

Shen, Z., Zhang, H., Wei, Z., & Liu, Q. (2020). The Application of Artificial Intelligence Technology in Civil Engineering. IOP Conference Series: Earth and Environmental Science, 466(1), 012105.

United Nations. (2018). World Urbanization Prospects: The 2018 Revision, Online Edition. Retrieved from https://population.un.org/wup/

United Nations, Department of Economic and Social Affairs, Population Division. (2018). World Urbanization Prospects: The 2018 Revision, Online Edition. Retrieved from https://population.un.org/wup/

United Nations Economic Commission for Africa. (2017). Economic Report on Africa 2017: Urbanization and Industrialization for Africa's Transformation. Retrieved from https://www.uneca.org/sites/default/files/PublicationFiles/era2017_eng_fin_14march_web.pdf

World Bank. (2018). Nigeria - Urbanization Review: Leveraging the Benefits of Urbanization for Nigeria. Retrieved from https://documents.worldbank.org/en/publication/documents-reports/documentdetail/617031535362753462/nigeria-urbanization-review-leveraging-the-benefits-of-urbanization-for-nigeria

World Bank. (2020). Nigeria - Urbanization Review: Leveraging the Benefits of Urbanization for Nigeria. Retrieved from https://documents.worldbank.org/en/publication/documents-reports/documentdetail/617031535362753462/nigeria-urbanization-review-leveraging-the-benefits-of-urbanization-for-nigeria

World Health Organization. (2019). Progress on household drinking water, sanitation, and hygiene 2000-2017. Special focus on inequalities. Retrieved from https://www.who.int/water_sanitation_health/publications/jmp-report-2019/en/

Yeh, J. R., Wang, X., & He, W. (2019). Artificial Intelligence for Civil Engineering: A Literature Review and Future Research Directions. Automation in Construction, 101, 28